frontiers | Research Topics

Rodent model organisms: human diets and the gut microbiome

Edited by
Ren-You Gan, Naga Betrapally and Hesong Wang

Published in
Frontiers in Microbiology

ISSN 1664-8714
ISBN 978-2-8325-6991-7
DOI 10.3389/978-2-8325-6991-7

Generative AI statement
Any alternative text (Alt text) provided alongside figures in the articles in this ebook has been generated by Frontiers with the support of artificial intelligence and reasonable efforts have been made to ensure accuracy, including review by the authors wherever possible. If you identify any issues, please contact us.

About Frontiers

Frontiers is more than just an open access publisher of scholarly articles: it is a pioneering approach to the world of academia, radically improving the way scholarly research is managed. The grand vision of Frontiers is a world where all people have an equal opportunity to seek, share and generate knowledge. Frontiers provides immediate and permanent online open access to all its publications, but this alone is not enough to realize our grand goals.

Frontiers journal series

The Frontiers journal series is a multi-tier and interdisciplinary set of open-access, online journals, promising a paradigm shift from the current review, selection and dissemination processes in academic publishing. All Frontiers journals are driven by researchers for researchers; therefore, they constitute a service to the scholarly community. At the same time, the *Frontiers journal series* operates on a revolutionary invention, the tiered publishing system, initially addressing specific communities of scholars, and gradually climbing up to broader public understanding, thus serving the interests of the lay society, too.

Dedication to quality

Each Frontiers article is a landmark of the highest quality, thanks to genuinely collaborative interactions between authors and review editors, who include some of the world's best academicians. Research must be certified by peers before entering a stream of knowledge that may eventually reach the public - and shape society; therefore, Frontiers only applies the most rigorous and unbiased reviews. Frontiers revolutionizes research publishing by freely delivering the most outstanding research, evaluated with no bias from both the academic and social point of view. By applying the most advanced information technologies, Frontiers is catapulting scholarly publishing into a new generation.

What are Frontiers Research Topics?

Frontiers Research Topics are very popular trademarks of the *Frontiers journals series*: they are collections of at least ten articles, all centered on a particular subject. With their unique mix of varied contributions from Original Research to Review Articles, Frontiers Research Topics unify the most influential researchers, the latest key findings and historical advances in a hot research area.

Find out more on how to host your own Frontiers Research Topic or contribute to one as an author by contacting the Frontiers editorial office: frontiersin.org/about/contact

Rodent model organisms: human diets and the gut microbiome

Topic editors

Ren-You Gan — The Hong Kong Polytechnic University, China
Naga Betrapally — National Cancer Institute (NIH), United States
Hesong Wang — Southern Medical University, China

Citation

Gan, R.-Y., Betrapally, N., Wang, H., eds. (2025). *Rodent model organisms: human diets and the gut microbiome*. Lausanne: Frontiers Media SA.
doi: 10.3389/978-2-8325-6991-7

Table of contents

frontiers in Microbiology

ORIGINAL RESEARCH
published: 25 February 2022
doi: 10.3389/fmicb.2022.778512

The Impact of Instant Coffee and Decaffeinated Coffee on the Gut Microbiota and Depression-Like Behaviors of Sleep-Deprived Rats

Xinyi Gu[1,2†], Shuyi Zhang[1,2,3†], Weini Ma[1,2], Qixue Wang[1,2], Ying Li[1,2], Chenyi Xia[4], Ying Xu[4], Ting Zhang[1,2], Li Yang[1,2] and Mingmei Zhou[1,2]*

[1] Institute for Interdisciplinary Medicine Sciences, Shanghai University of Traditional Chinese Medicine, Shanghai, China, [2] Shanghai Frontiers Science Center of TCM Chemical Biology, Institute of Interdisciplinary Integrative Medicine Research, Shanghai University of Traditional Chinese Medicine, Shanghai, China, [3] School of Rehabilitation Science, Shanghai University of Traditional Chinese Medicine, Shanghai, China, [4] Department of Physiology, School of Basic Medical Sciences, Shanghai University of Traditional Chinese Medicine, Shanghai, China

OPEN ACCESS

Edited by:
Ekaterina Avershina,
Inland Norway University of Applied Sciences, Norway

Reviewed by:
Silvia Arboleya,
Institute of Dairy Products of Asturias, Spanish National Research Council (CSIC), Spain
Zabdiel Alvarado-Martínez,
University of Maryland, College Park, United States

***Correspondence:**
Mingmei Zhou
zhoumm368@163.com

[†] These authors have contributed equally to this work

Specialty section:
This article was submitted to Microorganisms in Vertebrate Digestive Systems, a section of the journal Frontiers in Microbiology

Received: 21 September 2021
Accepted: 04 January 2022
Published: 25 February 2022

Citation:
Gu X, Zhang S, Ma W, Wang Q, Li Y, Xia C, Xu Y, Zhang T, Yang L and Zhou M (2022) The Impact of Instant Coffee and Decaffeinated Coffee on the Gut Microbiota and Depression-Like Behaviors of Sleep-Deprived Rats. Front. Microbiol. 13:778512. doi: 10.3389/fmicb.2022.778512

Objective: Based on our previous research, chronic paradoxical sleep deprivation (PSD) can cause depression-like behaviors and microbial changes in gut microbiota. Coffee, as the world's most popular drink for the lack of sleep, is beneficial to health and attention and can eliminate the cognitive sequelae caused by poor sleep. The purpose of this study is to investigate the effects of coffee and decaffeinated coffee on PSD rats.

Research Design and Methods: A total of 32 rats were divided into four groups: control group, PSD model group, conventional coffee group, and decaffeinated coffee group. Behavioral tests, including sucrose preference test, open field test, forced swimming test, and tail suspension test, as well as biochemical detection for inflammatory and antioxidant indexes were performed. The effects of coffee and decaffeinated coffee on the gut microbiota of PSD rats were investigated by 16S rRNA gene sequencing.

Results: Coffee and decaffeinated coffee significantly improved the depression-like behaviors. Moreover, the serum levels of interleukin-6 and tumor necrosis factor alpha were decreased in both coffee and decaffeinated coffee groups, as well as the levels of superoxide dismutase and GSH-Px were increased. Gut microbiota analysis revealed that the abundance of *S24-7*, *Lachnospiraceae*, *Oscillospira*, and *Parabacteroides* were significantly increased in PSD rats, while the abundance of *Akkermansia* and *Klebsiella* were significantly decreased. After the treatment of coffee and decaffeinated coffee, the abundance of the above gut microbiota was all restored in different degrees. Coffee had relatively more significant effects on PSD-induced depressive-like behaviors, while the difference between coffee and decaffeinated coffee was not obvious in correcting the disorder of gut microbiota.

Conclusions: These findings have shown that both coffee and decaffeinated coffee are effective for sleep deprivation-induced depression-like behaviors and the dysbiosis of gut microbiota and indicated that caffeine may be not the only key substance of coffee for regulating gut microbiota.

Keywords: coffee, decaffeinated coffee, sleep deprivation, depression, gut microbiota

INTRODUCTION

As the most consumed drink in the world, coffee is second only to water (Butt and Sultan, 2011). In European countries, most adults drink coffee every day (Lopez Garcia et al., 2014). Evidence has been found in recent years that coffee has benefit to the health. People who drink three or four cups of coffee a day have a lower risk of developing type 2 diabetes, which may be due to the presence of green folic acid and caffeine in coffee (George et al., 2008). Moreover, a large amount research reveals that caffeine in the coffee with moderate consumption (three-to-five cups, volume not identified) has the effect of anti-Alzheimer's disease (Mahshad and Mazen, 2017). Caffeine and coffee with a dose of 600 ml/day are helpful to reduce the risk of depression (Grosso et al., 2016). It is said that caffeine and modafinil could improve neuroinflammation and anxiety during sleep deprivation in rats by inhibiting microglial activation (Meetu et al., 2018), while an excessive dose of caffeine (70 mg/kg) showed anxiogenic effect (Kayir and Uzbay, 2006). Drinking coffee also can enhance cognitive function, in which it is believed that coffee has the benefit for attention and can eliminate cognitive sequelae caused by poor sleep (Franke et al., 2014). However, excessive intake of coffee or caffeine can lead to the development of physiological tolerance, and when a habitual caffeine consumer suddenly reduces or ceases taking caffeine, he or she may experience withdrawal symptoms (Hughes et al., 1998; Stachyshyn et al., 2021).

Coffee contains more than 1,000 different compounds including phenolics, diterpenes, and melanoidins (Renouf et al., 2014), of which about 1% is caffeine (Hoelzl et al., 2010; Kim et al., 2017). Studies have proven that caffeine can improve attention measurement and alertness (Haskell et al., 2005; Childs and Wit, 2006). However, excessive caffeine intake can lead to negative health consequences, such as psychomotor agitation, insomnia, headaches, and gastrointestinal discomfort (Wierzejska, 2012). Caffeine and its metabolites pass freely across the placenta into a fetus. Studies have shown that it may bring damage to the fetus by affecting the expression of genes related to cell damage (Abdelkader et al., 2013). Some recent systematic reviews have shown that moderate intake (three cups a day) of various types of coffee can reduce all-cause mortality in healthy people. These benefits may be due to some biologically active compounds instead of caffeine, mainly phenolic acids and diterpenoids, like cafestol and kahweol (Ding et al., 2015; Tsujimoto et al., 2017; Li et al., 2019). Thus, decaffeinated coffee appeared on the market. Decaffeinated coffee contains only a small amount of caffeine, and the International Coffee Organization defines that the content of caffeine is less than 0.3% in decaffeinated coffee. Chlorogenic acid, a kind of phenolic phytochemicals, can represent the principal non-caffeine components in coffee. Decaffeinated coffee with high chlorogenic acid content improves alertness and reduces negative emotions (Camfield et al., 2013). However, these effects of using chlorogenic acid alone are not obvious, considering that it may be the synergistic effect of non-caffeine compounds in coffee (Camfield et al., 2013). To study the effects of coffee on humans, Bunker and McWilliams proposed a criteria in 1979 to define decaffeinated coffee and coffee, using commercial-branded coffee and espresso (caffeine-containing coffee and caffeine-containing coffee 5 mg per cup) (Adan et al., 2008). Studying the impact of coffee or decaffeinated coffee on cognition can better understand daily habits in life and further clarify the benefits of coffee or decaffeinated coffee (Ho and Chung, 2013).

Sleep deprivation has become a health problem in the modern society (Malinalli et al., 2018). Sleep deprivation can be acute or chronic (Jamie et al., 2019). By definition, 24 h without sleep is acute sleep loss, and less than 6 h of sleep per night for 6 nights or more in a row is considered chronic sleep deprivation (Krishnan et al., 2016). The consequences of sleep deprivation are enormous, especially in mental illness (World Health Organization, 2017). Evidence suggests that rapid eye movement sleep changes occur in most patients with mental illness, such as depression (Benca et al., 1992). Furthermore, sleep deprivation may also occur in the same symptoms (Dieter et al., 2019). A study found that the cytokine secretion induced by low-level exposure of immune cells to bacterial cell wall components contributes to normal sleep patterns, while excessive cytokine levels are associated with disrupted sleep (Galland, 2014). At the same time, recent investigations indicated that the alteration of gut microbiome patterns was evident in people with depression (Barandouzi et al., 2020).

Our previous study found that chronic paradoxical sleep deprivation (PSD) could lead to depression-like behaviors, as well as dysbiosis in the host's gut microbiota (Ma et al., 2019). PSD could alter monoamine neurotransmitters such as norepinephrine and serotonin, as well as increase neuro-inflammatory cytokines including IL-1β and TNF-α, microglial activation, and neuronal apoptosis in the brain (Daniele et al., 2017; Mengmei et al., 2017). Sleep deprivation also leads to an accumulation of reactive oxygen species and oxidative stress, specifically in the gut (Alexandra et al., 2020). In addition, some preclinical studies have shown that gut microbiota can affect behaviors and brain conditions through neuroimmunity, neuroendocrine, neural, and humoral pathways (Dinan and Cryan, 2013; Kelly et al., 2016). Coffee has been proven to regulate the gut microbiota (González et al., 2020), which depends more on polyphenols and other non-digestible constituents of coffee like polysaccharides and melanoidins (Kolb et al., 2020). Coffee is the most common beverage used to combat fatigue and fatigue caused by sleep deprivation, while decaffeinated coffee is considered as a healthier alternative to traditional coffee. For the purpose of better understanding the effects of these two beverages on sleep deprivation, we first observed the intervention effect of coffee and decaffeinated coffee on the PSD rat model induced by multi-platform technology, mainly related to depression-related behavioral changes and serum inflammation and oxidative stress indicators. Then, we investigated their impacts on the corresponding alterations in the gut microbiota.

Abbreviations: FST, forced swimming test; GSH-Px, glutathione peroxidase; IL-6, interleukin-6; OFT, open field test; PSD, paradoxical sleep deprivation; SOD, superoxide dismutase; SPT, sucrose preference test; TNF-α, tumor necrosis factor alfa; TST, tail suspension test.

MATERIALS AND METHODS

Materials

Commercial instant coffee powder (200 mg/kg; Nestlé, La Tour-de-Peilz, Switzerland) and decaffeinated coffee powder (200 mg/kg; Nestlé, La Tour-de-Peilz, Switzerland) were dissolved in pure water as previously described (Shin et al., 2010; Turner et al., 2012). Each group was administered by gavage in the same volume (0.5 ml/100 g) once a day. Rats in the control and the model group were given saline.

Animals

A total of 32 inbred-strain male Wistar rats [240 ± 10g, license: SCXK (Hu) 2008-0016] were purchased from Shanghai Sippr-BK Laboratory Animal Co., Ltd. The rats of the same group were housed in animal cages at a density of 4 per cage under standard experimental conditions (room temperature for 24 ± 1°C, relative humidity for 55 ± 15% and 12 h dark/light cycle [07:00–19:00 at 40 w light condition)]. The rats had free access to food and water. Animal welfare and experimental protocols strictly referred to the guide of the care and use of laboratory animals and the ethics and regulations of Shanghai University of Traditional Chinese Medicine. After the rats have been adaptively fed for 1 week, they were randomly divided into four groups as follows: control group (CON), PSD model group (SD), conventional coffee group (CC), and decaffeinated coffee group (DC). Coffee and pure water were administrated on 9:30 a.m. of each day of PSD processing.

Paradoxical Sleep Deprivation Procedure

The modified multi-platform method was used for PSD processing as described (Cheng et al., 2016). The method was based on the loss of muscle tone that characterizes the rapid eye movement sleep condition or paradoxical sleep. Animals would experience a sudden loss of the sleep cycle when falling into the water, and the method is proved to be feasible in the previous study (Machado et al., 2004). The rats were given free access to water and food in a climate-controlled room (24 ± 1°C, 55 ± 15%) on a 12 h light/dark schedule (light on at 07:00–19:00). The box for PSD was sterilized with 75% alcohol every day. The PSD procedure lasted for 7 days.

Behavioral Testing

When the PSD was finished on the morning of the eighth day, the behavioral tests of each group were performed under the conditions of dim light and low noise in the following order. Each test started 30 min after the daily administration of coffee.

Open Field Test

The open field test (OFT) was performed as previously described (Zhai et al., 2015). The test was performed in a quiet room. The apparatus is a self-made rectangular arena (80 cm × 80 cm × 40 cm), with the floor being divided into 25 equal-size squares, and the side walls were black. After the PSD procedure, the rats were set in the center of the arena one by one to explore for 5 min. The following behaviors were recorded: the number of crossing (grid lines crossed with at least three paws) and the total number of grooming and rearing (defined as standing upright with hind legs). Every grooming or rearing was counted as one point alone, every grid crossed was counted as one point, and the behavioral score was the total number of points. The open-field arena was thoroughly cleaned with 70% ethanol at the interval of each test.

Sucrose Preference Test

The sucrose preference test (SPT) was performed as previously described (Zhai et al., 2015). All rats were reared in a single cage during the experiment. The rats were trained to adapt by exposing them to two bottles (one containing 1% sucrose solution and the other containing tap water) for 24 h. Then, the test was performed after 4 h of water deprivation. Two bottles (one with 1% sucrose solution and the other with tap water) were weighed and presented to each rat for 1 h. The position of the two bottles was randomly determined. Sucrose solution and tap water consumption (g) were measured, and the sucrose preference was calculated using the equation: sucrose solution (g)/[sucrose solution (g) + water (g)] × 100%.

Forced Swimming Test

After administration, each rat was placed in a transparent container (50 cm in height, 18 cm in diameter) with water in 30 cm depth (25 ± 1°C). The test lasted 6 min, and the immobility time during the final 4 min was recorded by the person blinded to the purpose of the experiment. The immobility state was defined as the state of rats floating in the water and only keeping the head above the water without struggling or any motions. The test time was from 14:00 to 18:00, and the water was changed after each test.

Tail Suspension Test

Each rat was individually suspended 50 cm above the floor by the tail, using a tape. The test lasted 6 min, and the immobility time during the final 4 min was recorded by the person blinded to the purpose of the experiment. The immobility state was defined as the state only when rats remain completely motionless. The test time was from 14:00 to 18:00.

Sample Collection

After the last sleep deprivation and administration were performed, the rats were individually housed in a metabolic cage, which could separate and collect urine and feces. Fresh feces were collected continuously with sterile operation (Eriksson et al., 2004; Ward and Hubscher, 2012), and stored at −80°C for subsequent analysis. Then rats were sacrificed, and blood was collected from the abdominal aorta. Blood was centrifuged at 4°C at 3,000 r/min for 15 min (Centrifuge 5702R, Eppendorf), and the supernatants were stored at −80°C prior to use.

Biochemical Parameters in Serum

Serum samples were thawed on ice. The levels of interleukin-6 (IL-6), tumor necrosis factor alpha (TNF-α), superoxide dismutase (SOD), and glutathione peroxidase (GSH-Px) in serum samples were detected by commercial enzyme linked immunosorbent assay (ELISA) kits, referring to the instructions provided by the manufacturer (Nanjing Jiancheng Bioengineering Institute, Nanjing, China).

Microbial Community Profiling

The E.Z.N.A.® soil DNA Kit (Omega Bio-Tek, Norcross, GA, United States) was used to extract the microbial community genomic DNA from fecal samples. The microbial DNA regions V3–V4 of the bacterial 16S rRNA gene were amplified with primer pairs 338F (5′-ACTCCTACGGGAGGCAGCAG-3′) and 806R (5′-TACHVGGGTWTCTAAT-3′) (Sinha et al., 2017). The PCR product was extracted from 2% agarose gel and purified using the AxyPrep DNA Gel Extraction Kit (Axygen Biosciences, Union City, CA, United States). Purified amplicons were pooled in equimolar and paired-end sequences on an Illumina MiSeq PE300 platform/NovaSeq PE250 platform (Illumina, San Diego, CA, United States) according to the standard protocols by Majorbio Bio-Pharm Technology Co., Ltd. (Shanghai, China). The raw reads were deposited into the NCBI Sequence Read Archive database (Accession Number: SRP337042; PRJNA762663).

Fastp software ([1]version 0.20.0) and FLASH software ([2]version 1.2.7) were used for the quality control of the original sequencing sequence and splicing (Magoč and Salzberg, 2011; Shifu et al., 2018). UPARSE software ([3]version 7.1) was used to perform an operational taxonomic unit (OTU) clustering of sequences based on 97% similarity, as well as to eliminate chimeras (Stackebrandt and Goebel, 1994; Edgar, 2013). The Venny 2.1[4] was employed to map the Venn diagram of OTUs among four groups. Alpha diversity index (Chao1 index, Ace index, Simpson index, and Shannon index) was based on Mothur 9 (version 1.30.2[5]), and beta diversity was performed based on partial least squares discriminant analysis (PLS-DA) for assessing the clustering patterns on the weighted UniFrac matrices and the ANOSIM function of QIIME 11 (version 1.9.1[6]).

Data Statistical Analysis

All the data were presented as mean ± standard deviation. The statistical analyses were carried out using IBM statistical product and service solutions (SPSS) Statistic Version 21.0 (SPSS; IBM, Armonk, NY, United States). One-way ANOVA test and two tailed Student's *t*-test were used to analyze significant differences between the two groups. A *p*-value of less than 0.05 or 0.01 was considered statistical significance.

RESULTS

Coffee and Decaffeinated Coffee Improved the Depressive-Like Behaviors in PSD Rats

After 7 days of sleep deprivation procedure, as showed in **Figure 1A**, the total behavioral score in the PSD model group was significantly lower than the control group ($P < 0.001$). Conventional coffee significantly increased the total behavioral score ($P < 0.05$), while decaffeinated coffee also increased the score ($P > 0.05$).

The results of SPT showed the effects of coffee and decaffeinated coffee on the changes of sucrose consumption (**Figure 1B**). Compared to the control group, sucrose consumption was significantly reduced in the PSD model group ($P < 0.05$). However, the sucrose consumption was significantly higher after the treatment of conventional coffee and decaffeinated coffee than in the model group ($P < 0.01$, $P < 0.05$).

Chronic PSD remarkably increased immobility time in forced swimming test (FST) and tail suspension test (TST) (**Figures 1C,D**) ($P < 0.05$). The immobility time in the conventional coffee and decaffeinated coffee group was significantly lower than the PSD model group ($P < 0.01$, $P < 0.05$).

Coffee and Decaffeinated Coffee Ameliorate the Level of Inflammatory and Antioxidant Factors in PSD Rats

The effects of conventional coffee and decaffeinated coffee on inflammatory factors and antioxidant factors in the serum of PSD rats were investigated (**Table 1**). Compared with the control group, the levels of IL-6 and TNF-α in PSD rats were significantly increased ($P < 0.001$, $P < 0.01$). IL-6 and TNF-α levels were remarkably decreased after the treatment of conventional coffee ($P < 0.01$, $P < 0.05$), and the level of TNF-α was significantly decreased with the treatment of decaffeinated coffee ($P < 0.05$). Furthermore, the levels of SOD and GSH-Px in the model group were much lower than in the control group ($P < 0.01$, $P < 0.001$). The levels of SOD and GSH-Px were significantly increased with the treatment of conventional coffee ($P < 0.05$, $P < 0.01$), and the level of GSH-Px was significantly increased after the treatment of decaffeinated coffee ($P < 0.05$).

Effects of Coffee and Decaffeinated Coffee on the Gut Microbiota Composition

OTU Classification Statistics

The number of OTUs of each sample, as well as common and unique OTUs, was shown by the Venn diagram (**Supplementary Figure 1**), which could describe sample similarity and overlap intuitively (Cheng et al., 2016). The OTUs alone in each group were as follows: CON group 479; SD group 663; CC group 494; and DC group 465. The total number of OTU in each group was 3,359 (CON), 3.814 (SD), 3,458 (CC), and 3,430 (DC). Therefore, the ratio of the OTU alone in each group to the total OTU was 3.41, 4.72, 3.51, and 3.31%, respectively. A total of 1,343 OTUs were shared among the four groups. The results showed that the out number of the PSD model group increased, while both coffee and decaffeinated coffee treatments could reduce it.

The Diversity of the Gut Microbiota

The Chao1 index, Ace index, Simpson index, and Shannon index were selected to analyze the alpha diversity (**Figure 2**). The

[1]https://github.com/OpenGene/fastp
[2]http://www.cbcb.umd.edu/software/flash
[3]http://drive5.com/uparse/
[4]http://bioinfogp.cnb.csic.es/tools/venny/index.html
[5]https://www.mothur.org/wiki/Download_mothur
[6]http://qiime.org/install/index.html

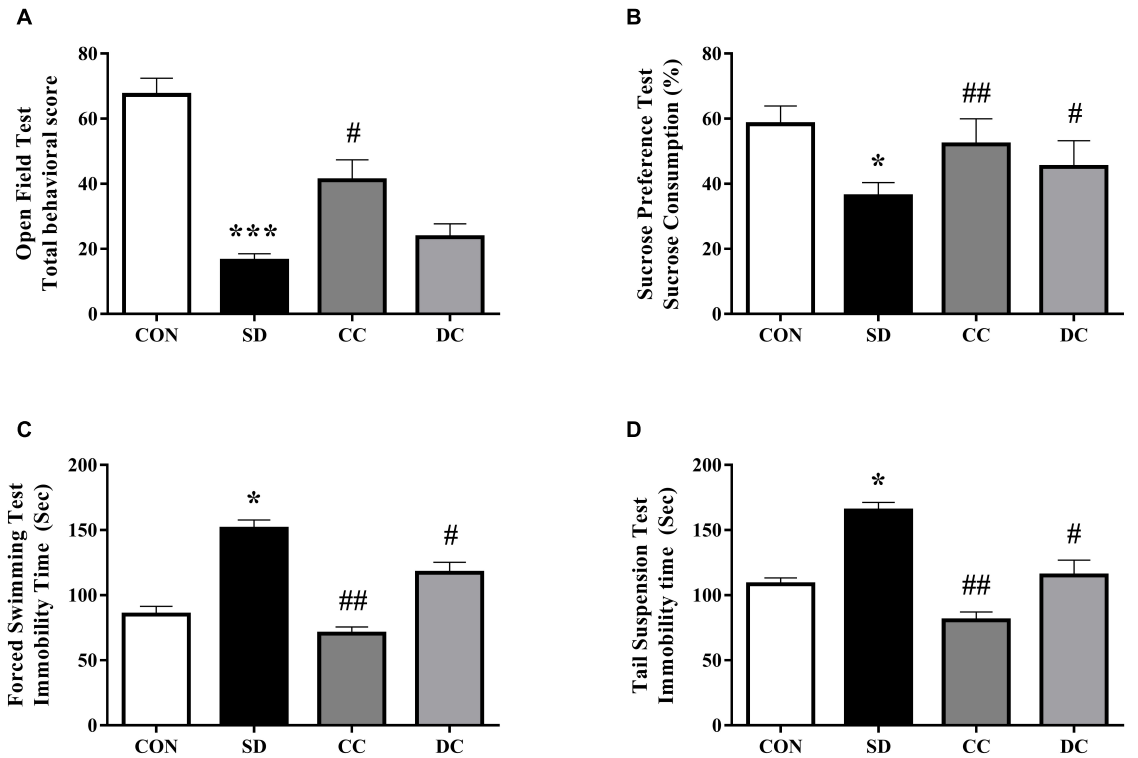

FIGURE 1 | Effects of coffee and decaffeinated coffee on different behaviors in the PSD model. Total behavior score **(A)**, sucrose consumption **(B)**, immobility time of FST **(C)**, immobility time of TST **(D)**. Values were expressed as means ± SEM ($n = 8$). $^{*}P < 0.05$, $^{***}P < 0.001$ significant differences compared to the control group; $^{\#}P < 0.05$, $^{\#\#}P < 0.01$ significant differences compared to the SD group. CON, control group; SD, PSD model group; CC, conventional coffee group; DC, decaffeinated coffee group.

TABLE 1 | Inflammatory and antioxidant factors in the serum.

Parameter	n	CON	SD	CC	DC
IL-6 (pg/ml)	8	4.19 ± 1.04	17.58 ± 3.71***	10.25 ± 3.01##	14.03 ± 2.42
TNF-α (pg/ml)	8	5.07 ± 0.79	12.57 ± 2.67**	8.34 ± 3.16#	9.22 ± 2.66#
SOD (U/ml)	8	156.32 ± 11.61	104.57 ± 13.45**	140.35 ± 15.26#	137.88 ± 16.39
GSH-Px (U/ml)	8	319.23 ± 22.70	167.53 ± 17.13***	217.53 ± 27.35##	193.50 ± 23.62#

Values were expressed as means ± SEM.
***P < 0.01, ***P < 0.001 significant differences compared to the control group; #P < 0.05, ##P < 0.01 significant differences compared to the SD group.*
CON, control group; SD, PSD model group; CC, conventional coffee group; DC, decaffeinated coffee group.

value of Simpson was significantly decreased, and the value of Shannon was significantly increased in the PSD model group compared with the control group ($P < 0.01$, $P < 0.01$). After the administration of conventional coffee, the value of Simpson was significantly increased and the value of Shannon was significantly lower than that in the PSD model group ($P < 0.05$, $P < 0.05$), while those values had no significantly changes with the administration of decaffeinated coffee.

PLS-DA analysis was performed to analyze the beta diversity among the four groups. As shown in **Figure 3**, the composition of the gut microbiota of the control group and the PSD model group was significantly separated and changed. In addition, the composition of the gut microbiota of the conventional coffee group and the decaffeinated coffee group was similar, and both tended to be closer to the control group than the model group. These results indicated that PSD caused disturbances in the gut microbiota. The treatment of conventional coffee and decaffeinated coffee could improve the PSD-induced changes in the gut microbiota, and both had similar therapeutic effects.

Analysis of the Gut Microbiota Composition

At the phylum level, gut microbiota was mainly composed of *Firmicutes*, *Verrucomicrobia*, *Proteobacteria,* and *Bacteroidetes* (**Figure 4A**). Compared with the control group, the abundance of *Firmicutes* and *Bacteroidetes* was remarkably elevated in the model group ($P < 0.05$, $P < 0.001$). After the treatment of conventional coffee, the abundance of *Firmicutes* and *Bacteroidetes* was significantly reduced ($P < 0.05$, $P < 0.001$), and after the treatment of decaffeinated coffee, only the abundance of *Bacteroidetes* had a significant decrease ($P < 0.001$).

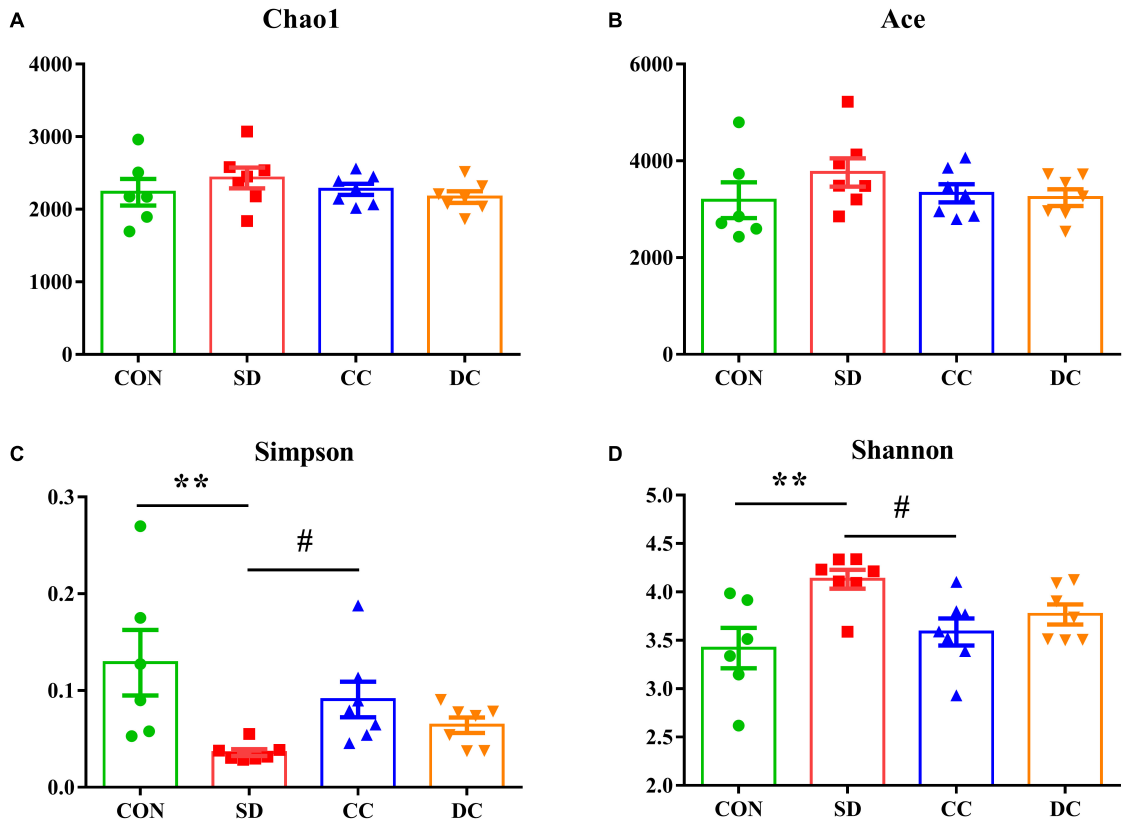

FIGURE 2 | Alpha diversity in each group. Chao1 diversity **(A)**; Ace diversity **(B)**; Simpson diversity **(C)**; Shannon diversity **(D)**. Values were expressed as means ± SEM (n = 6 or 7). $^{**}P < 0.01$ significant differences between the SD group and the control group; $^{\#}P < 0.05$ significant differences of the CC group or DC group as compared to the SD group. CON, control group; SD, PSD model group; CC, conventional coffee group; DC, decaffeinated coffee group.

Moreover, compared with the control group, the abundance of *Verrucomicrobia* was remarkably decreased in the model group ($P < 0.001$). With the treatment of conventional coffee and decaffeinated coffee, the abundance of *Verrucomicrobia* was significantly reversed ($P < 0.001$, $P < 0.01$). After decaffeinated coffee treatment, the abundance was still much lower than the control group ($P < 0.05$). For the abundance of *Proteobacteria*, there was no significant difference between the model group and the control group, and after the administration of conventional coffee and decaffeinated coffee, the abundance was much higher than the model group ($P < 0.05$, $P < 0.05$) and the control group ($P < 0.05$, no statistical significance) (**Figure 4B**).

At the family level, the abundance of *Verrucomicrobiaceae* ($P < 0.001$), *S24-7* ($P < 0.001$), *Ruminococcaceaea* ($P < 0.01$), *Enterobacteriaceae* ($P < 0.001$), *Porphyromonadaceae* ($P < 0.05$), and *Lachnospiraceae* ($P < 0.01$) showed a significant difference between the PSD and normal group (**Figures 5A,B**). Compared with the PSD model group, those relatively abundance except *Porphyromonadaceae* were significantly reversed after the treatment of conventional coffee, and those relatively abundance except *Ruminococcaceae* were significantly reversed after the treatment of decaffeinated coffee (**Figure 5B**).

At the genus level, *Akkermansia* ($P < 0.001$), *S24-7_norank* ($P < 0.001$), *Lachnospiraceae_unclassified* ($P < 0.01$), *Oscillospira* ($P < 0.01$), *Parabacteroides* ($P < 0.05$), and *Klebsiella* ($P < 0.05$) were the differential microbiota of the top six highest contents, between the PSD and normal group (**Figures 6A,B**). After the treatment of conventional coffee, the abundance of *Akkermansia* ($P < 0.001$), *S24-7_norank* ($P < 0.001$), *Lachnospiraceae_unclassified* ($P < 0.01$), *Oscillospira* ($P < 0.05$), and *Klebsiella* ($P < 0.01$) significantly reversed, while the abundance of *Akkermansia* ($P < 0.01$), *S24-7_norank* ($P < 0.01$), *Lachnospiraceae_unclassified* ($P < 0.001$), *Parabacteroides* ($P < 0.05$), and *Klebsiella* ($P < 0.01$) significantly reversed after the treatment of decaffeinated coffee (**Figure 6B**).

DISCUSSION

Chronic sleep deprivation is a stressor that impairs the brain function and causes cognitive impairment, as well as increases oxidative stress and the risk for Alzheimer's disease or depression (McEwen, 2006; Ma et al., 2019). The results of the behavior tests in our study showed the similar depression-like behaviors after PSD induced, and the symptom could be improved in a different extent with the treatment of conventional coffee and decaffeinated coffee (**Figure 1**). It has been reported that caffeinated coffee and caffeine were beneficial to depression-like

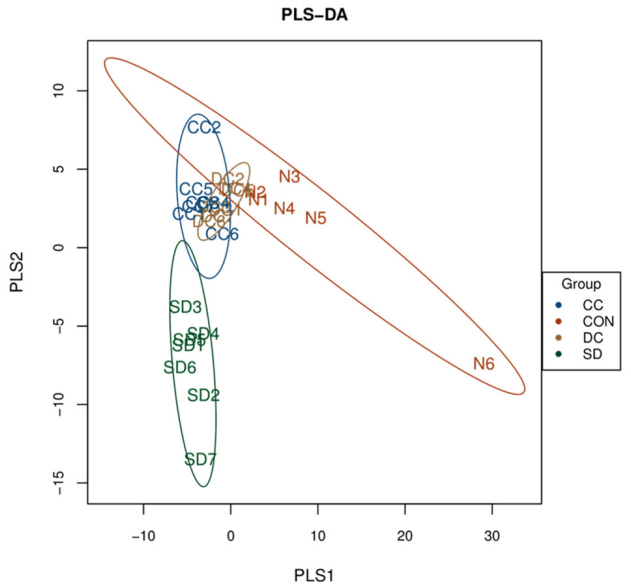

FIGURE 3 | PLS-DA score plots for beta diversity of the microbial community among each group (n = 6 or 7). CON, control group; SD, PSD model group; CC, conventional coffee group; DC, decaffeinated coffee group.

behaviors, while the effect of decaffeinated coffee was not obvious (Paz-Graniel et al., 2020; Xue et al., 2020).

Elevated levels of IL-6 and TNF-α, as well as a negative feedback of SOD and GSH-Px levels in the PSD group (**Table 1**) confirmed that sleep deprivation induced inflammation and oxidative stress. Both IL-6 and TNF-α are the multifunctional cytokines involved in the regulation of the immune response and inflammation, and the production of these pro-inflammatory cytokines could be increased by different stimuli (Akira et al., 1990; Schindler et al., 1990). As one of the stimuli, sleep disturbance was associated with disorders related to inflammation, such as cardiovascular disease, arthritis, diabetes mellitus, and certain cancers (Michael et al., 2015). In addition, evidence suggested that sleep deprivation would promote oxidative stress (Villafuerte et al., 2016). In our study, the levels of IL-6, TNF-α, SOD, and GSH-Px were all reversed after the treatment of conventional coffee and decaffeinated coffee, while the effect of coffee was relatively more significant than that of decaffeinated coffee (**Table 1**). The anti-inflammatory effect of coffee has been widely reported (Yamashita et al., 2012; Erikka et al., 2015). In our study, both in the caffeinated coffee group and the decaffeinated coffee group, a decrease in the levels of pro-inflammatory factors was observed, and the therapeutic effect of caffeinated coffee was more obvious, which indicated that not only caffeine but also the other ingredients in coffee played a role in promoting anti-inflammatory effect, such as chlorogenic acid (Dong et al., 2019). Chlorogenic acid can inhibit protein tyrosine phosphatase 1B to reduce the expression of pro-inflammatory cytokine genes (Giuseppe et al., 2017). Research on the effect of coffee and its biologically active substances such as caffeine, phenolic compounds, diterpenoids, and soluble fiber on oxidative stress is increasing these years (Martini et al., 2016). It has been reported that chronic coffee and caffeine ingestion would increase the activity of SOD, as well as protect the antioxidant system in the brain (Abreu et al., 2011). Light-dark roasted coffee (rich in chlorogenic acid) showed a more significant effect in increasing the level of SOD (Kotyczka et al., 2011). Evidence showed that some diterpenoids (kafestol and kahweol) in coffee could increase the concentration of GSH (Scharf et al., 2001). Furthermore, caffeine also has the exact effect of antioxidant and anti-inflammatory (Daniela et al., 2017; Soohan et al., 2017; Haroon et al., 2019).

Coffee has been confirmed to confer various health benefits, and drinking coffee can alter a host's gut microbiota (Chong et al., 2020). Coffee may partly depend on the modulation of gut microbiota to influence health (González et al., 2020). It has been proven that polyphenols in coffee can change the environment, or they can be catabolized by gut microbiota (Aura, 2008; Couteau et al., 2010). In the microbial community profiling, both caffeinated coffee and decaffeinated coffee could reduce the number of OTUs that increased after PSD induction. Only the Simpson index and Shannon index in alpha diversity index were restored significantly after coffee treatment. In the beta diversity analysis, there was a significant separation between the control group and the model group. With the treatment of coffee and decaffeinated coffee, the composition of the gut microbiota tended to approach the control group, which indicated that both coffee and decaffeinated coffee restored the composition of the gut microbiota of PSD rats. In our results, the levels of *Akkermansia* (Phylum *Verrucomicrobia*) and *Klebsiella* (Phylum *Proteobacteria*) were significantly decreased in the rats with sleep deprivation (**Figure 6B**). As a Gram-negative pathogen, *Klebsiella* could cause a variety of infectious diseases (Guoying et al., 2020) and has the effect of inducing the inflammatory response (Atarashi et al., 2017; Marjolaine et al., 2019). It has been reported that when the *Proteobacteria* increases, intestinal mucus would decrease, resulting in damage to the intestinal barrier and low-grade inflammation (Shin et al., 2015). In our results, sleep deprivation caused an increase in the expression of inflammatory factors, while a decrease in the pro-inflammatory bacteria *Proteobacteria*. This indicated that the inflammation caused by sleep deprivation might be not through the gut microbiota pathway. The decrease of *Akkermansia* is commonly observed in the symptom of sleep deprivation (Heintz-Buschart et al., 2018; Ting et al., 2019). *Akkermansia* is known as a beneficial microbe that is inversely associated with obesity, diabetes, cardiometabolic diseases, and low-grade inflammation (Plovier et al., 2016; Patrice and Willem, 2017). With treatment of conventional coffee and decaffeinated coffee, both levels of *Akkermansia* were increased significantly, and the effect of coffee was more obvious (**Figure 6B**). A study has found that coffee has antibacterial effects and prebiotic function (Nakayama and Oishi, 2013). Compared to caffeine, which is rapidly absorbed and degraded in the upper digestive tract, polyphenols are difficult to be absorbed in the gastrointestinal tract. This caused most of the polyphenols to enter the intestine and affect the gut microbiota and mucosal cells and increase of

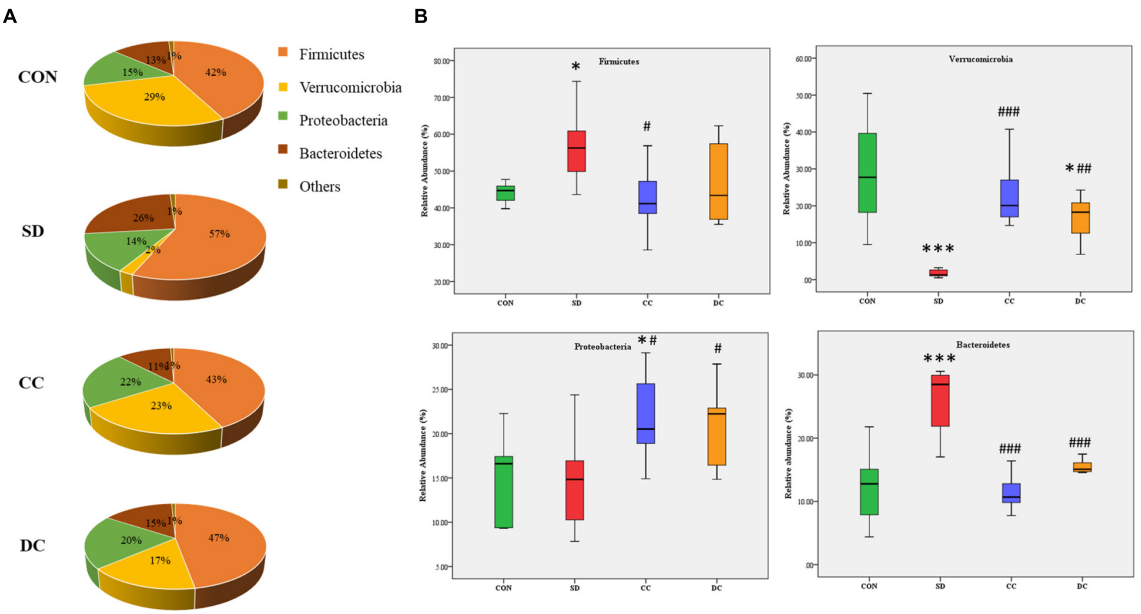

FIGURE 4 | Relative abundances profiling at the phylum level of gut microbiota. **(A)** Pie chart of the relative abundances of gut microbiota in each group; **(B)** the relative abundances of *Firmicutes*, *Verrucomicrobia*, *Proteobacteria*, and *Bacteroidetes*. Values were expressed as means ± SEM ($n = 8$). $^{*}P < 0.05$, $^{***}P < 0.001$ significant differences compared to the control group; $^{\#}P < 0.05$, $^{\#\#}P < 0.01$, $^{\#\#\#}P < 0.001$ significant differences compared to the SD group. CON, control group; SD, PSD model group; CC, conventional coffee group; DC, decaffeinated coffee group.

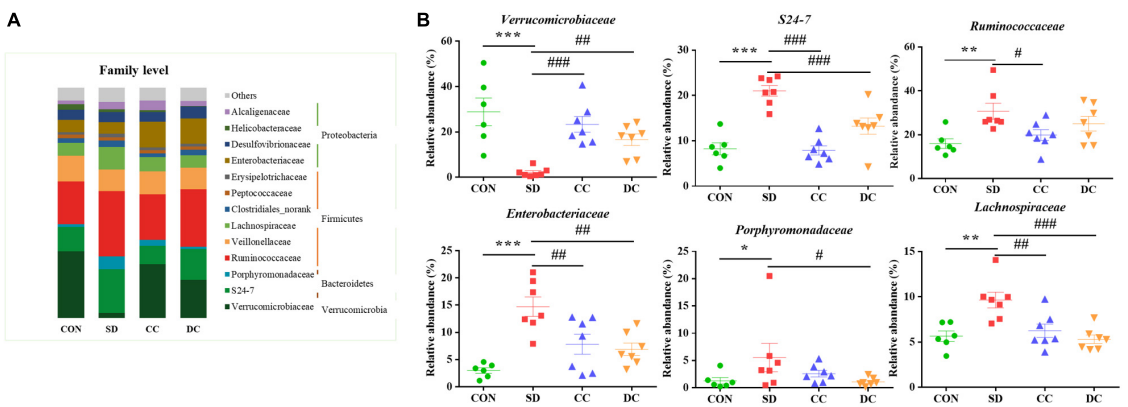

FIGURE 5 | Bacterial taxonomic profiling at the family level of gut microbiota. **(A)** The relative abundance of *Verrucomicrobiaceae*, *S24-7*, *Ruminococcaceaea*, *Enterobacteriaceae*, *Porphyromonadaceae*, and *Lachnospiraceae*; **(B)** values were expressed as means ± SEM ($n = 8$). $^{*}P < 0.05$, $^{**}P < 0.01$, $^{***}P < 0.001$ significant differences compared to the control group; $^{\#}P < 0.05$, $^{\#\#}P < 0.01$, $^{\#\#\#}P < 0.001$ significant differences compared to the SD group. CON: control group; SD: PSD model group; CC: conventional coffee group; DC: decaffeinated coffee group.

the abundance of *Akkermansia* in the intestine (Yuji et al., 2018). A study has shown that tea is rich in polyphenols and caffeine plays a key role in remodeling the disturbed gut microbiota (including *Akkermansia*), which may be a synergistic effect (Xiaoyu et al., 2018).

Our results illustrated that the abundance of *Parabacteroides* (Phylum *Bacteroidetes*) in the PSD group was significantly higher than the normal control. As a kind of Gram-negative bacteria, *Parabacteroides* contains lipopolysaccharide, which is a typical potent endotoxin that can induce strong pro-inflammatory reactions in the host (Kaisa et al., 2020). *Akkermansia* and *Klebsiella*, also Gram-negative bacteria, had lower levels in the PSD group, compared to the normal control, and high levels of inflammatory factors were detected after PSD intervention. These indicated that the inflammatory response might not necessarily be caused by *Parabacteroides*, *Akkermansia*, and *Klebsiella*, but rather be caused by the release of lipopolysaccharide from other types of Gram-negative bacteria or other stress response in the host. In addition, a high level of *Parabacteroides* can be found in patients with depression (Barandouzi et al., 2020),

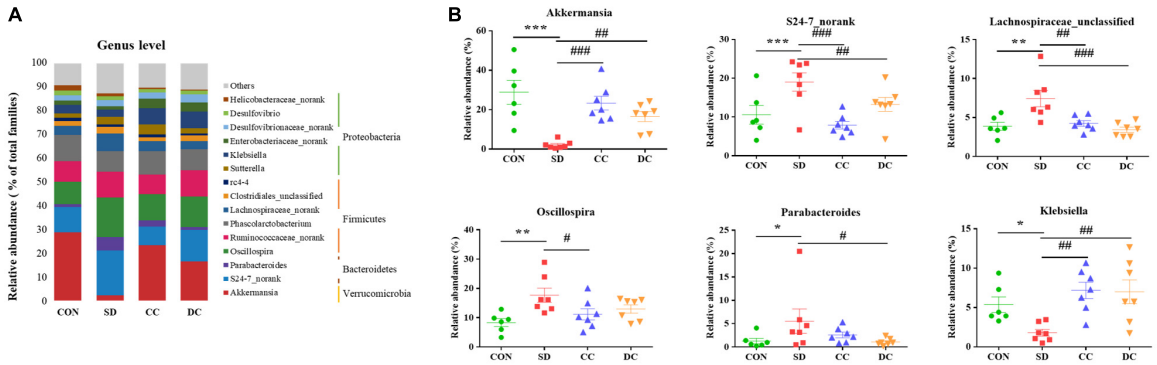

FIGURE 6 | Bacterial taxonomic profiling at the genus level of gut microbiota. **(A)** The relative abundance of *Akkermansia*, *S24-7_norank*, *Lachnospiraceae_unclassified*, *Oscillospira*, *Parabacteroides*, and *Klebsiella*; **(B)** values were expressed as means ± SEM. ($n = 8$). $^{*}P < 0.05$, $^{**}P < 0.01$, $^{***}P < 0.001$ significant differences compared to the control group; $^{\#}P < 0.05$, $^{\#\#}P < 0.01$, $^{\#\#\#}P < 0.001$ significant differences compared to the SD group. CON, control group; SD, PSD model group; CC, conventional coffee group; DC, decaffeinated coffee group.

and our results also showed depression-like behaviors after PSD induced. With the treatment of decaffeinated coffee, the decrease of the level of *Parabacteroides* was relatively more significant than the conventional coffee group. Polyphenols in the decaffeinated green tea and black tea could regulate the abundance of *Parabacteroides* and induced weight loss (Rothenberg et al., 2018). For example, chlorogenic acid can protect intestinal integrity and reduce inflammation by inhibiting the growth of *Bacteroides* and the accumulation of *Bacteroides*-derived lipopolysaccharide (Yan et al., 2020). In addition, evidence has indicated that both caffeinated and decaffeinated coffee have a similar anti-inflammatory effect (Dong et al., 2019), and not only caffeine, but also some phenols including pyrocatechol, chlorogenic acid, and so on, can prevent the inflammatory responses (Hwang et al., 2016; Stefanello et al., 2018; Megumi et al., 2020). Therefore, caffeine and phenols exert anti-inflammatory effects by affecting different gut microbiota.

In our study, the relative abundance of *Lachnospiraceae* (Phylum *Firmicutes*), *S24-7* (Phylum *Bacteroidetes*), and *Oscillospira* (Phylum *Firmicutes*) were significantly increased in the SD group (**Figure 6B**). *Lachnospiraceae* and *S24-7* impact their hosts by producing short-chain fatty acids (SCFAs) (Jennifer et al., 2017; Matthew et al., 2020). In patients with ulcerative coliti, an increase in the level of *Lachnospiraceae* could be observed (Schirmer et al., 2019), which could be explained by the fact that stress increases the abundance of *Lachnospiraceae* (Li et al., 2017). As shown in our study, after the stress of sleep deprivation, the level of *Lachnospiraceae* increased significantly. However, as a butyric acid-producing bacteria, increasing the content of *Lachnospiraceae* also has a beneficial effect to the body (Huws et al., 2011; Dong et al., 2020). *Oscillospira* can be seen in the obese animals, which ferments polysaccharide into SCFAs (Na et al., 2018). In addition, *Oscillospira* is correlated with inflammatory disease (Uri et al., 2017). SCFAs are involved in the regulation of the gut immune system, and the production of the SCFAs is one of the crucial ways that gut microbiota affect the hosts (Jost et al., 2020). Besides, SCFAs play an important role in host defense and immunity, including anti-inflammation and anti-oxidant activities. The increase of these gut microbiota related to fatty acid metabolism indicated that sleep deprivation would lead to metabolism disorders, inflammation, and oxidative stress. After the administration of conventional coffee and decaffeinated coffee, the relative abundance of these gut bacteria decreased in different degrees, and coffee had a relatively more significant effect. Caffeine consumption could attenuate the increase in *Firmicutes*-to-*Bacteroidetes* ratio in high-fat-fed rats (Cowan et al., 2014). Interestingly, some recent studies have now shown that the increase in this ratio has no relation with the presence of high- fat diet but only related to the content of dietary fiber (Dalby et al., 2017; Singh et al., 2020). Moreover, due to lifestyle-associated factors such as diet, physical activity, food additives, and contaminants, the relative abundance of the *Firmicutes* and *Bacteroidetes* varies greatly among individuals (Magne et al., 2020). Caffeine intake is linked to weight loss and the regulation of lipid metabolism, partly through its inhibition of adipogenesis-related factors (Su et al., 2013). It has been reported that some phenols and caffeine were directly associated with *Bacteroides* group levels (González et al., 2020). A study has found that caffeine and chlorogenic acid in coffee have a partially positive effect to the SCFAs in plasma (Kazuchika et al., 2018). The reaction of polyphenols in tea with residual carbohydrates and gut microbiota within the colon produce SCFAs, which enhance lipid metabolism (Rothenberg et al., 2018).

As shown in the previous studies, the differential gut microbiota in our study is commonly seen in patients with depression (Zheng et al., 2016; Cheung et al., 2019). Gut microbiota influences the emotional behavior by affecting the interactions of the gut–brain axis (Emeran et al., 2015), and sleep deprivation would increase the risk of depression (Robert and Hao, 2014). Chronic PSD could bring about depression-like performance, which is proven by our study and previous researches (Ma et al., 2019; Rahmani et al., 2020). In the behavior tests of our study, the effect of coffee to improve depression is more significant than the decaffeinated

coffee. The main difference between the two drinks is the caffeine content. Caffeine is an alkaloid and modulates the dopaminergic activity through nonspecific antagonism against A1/A2 adenosine receptors (Navarro et al., 2018). A moderate intake of caffeine has a stimulating effect on the central nervous system and can improve psychomotor activities (Adan et al., 2008). Furthermore, coffee contains many functional components other than caffeine, such as chlorogenic acid, ferulic acid, nicotinic acid, trigonelline, quinolinic acid, tannic acid, and pyrogallic acid. These compounds have anti-inflammatory or antioxidative effects. Chlorogenic acid and trigonelline, which are present in high amounts in coffee, have an anti-inflammatory effect (Godos et al., 2014), and it has been found that low-grade inflammation seems to be related to the pathogenesis of depression (Sanchez Villegas and Martínez González, 2013). From our results of the treatment with decaffeinated coffee, we know that polyphenols in coffee also can improve depression-like behaviors by affecting the gut microbiota associated with inflammation such as *Akkermansia*, *Klebsiella*, and *Parabacteroides*. On the other hand, it has been suggested that patients with depression have increased oxidative stress and decreased antioxidant defense (Black et al., 2015) and antioxidant is an important aspect of treating depression (Vaváková et al., 2015). Coffee is rich in polyphenols, which not only has an anti-inflammatory effect but also has antioxidant activity (Godos et al., 2014; Martini et al., 2016). In our study, the abundance of the gut microbiota related to oxidative stress such as *S24-7*, *Lachnospiraceae*, and *Oscillospira*, could be revised by both coffee and decaffeinated coffee. Thus, it is demonstrated that the anti-inflammatory and antioxidant effects of polyphenols may be through regulating the gut microbiota, further playing a role in the treatment of depression induced by chronic PSD.

Some limitations must be considered when interpreting our results. The manufacturing procedure of the instant coffee powder we used in the experiment involves the aqueous extraction of soluble coffee components followed by drying to form a soluble powder. Although there are no other food additives, the loss of volatile aroma compounds during concentration through evaporation will lower product quality (Beverly et al., 2020), and at the same time, the results of the study could not fully represent the activity of coffee. In addition, the study lacks the analysis of the components of the samples, although there are other relevant literatures for reference, as well as the analysis of the metabolites of gut microbiota (such as SCFAs), these need to be strengthened in future research to better judge the role of gut microbiota in coffee on sleep deprivation.

CONCLUSION

In this study, 16S rRNA gene sequencing was applied to assess the effects of conventional coffee and decaffeinated coffee on the gut microbial community profiling. Our results revealed that the administration of conventional coffee and decaffeinated coffee ameliorated depression-like behaviors in rats of PSD induced, as well as the changed levels of IL-6, TNF-α, SOD, and GSH-Px. The effect of conventional coffee was relatively obvious than that of decaffeinated coffee. In microbiome analysis, PSD disturbed the composition of gut microbiota, including *Akkermansia*, *S24-7*, *Lachnospiraceae*, *Oscillospira*, *Parabacteroides*, and *Klebsiella*. Both the treatment of conventional coffee and decaffeinated coffee could restore the abundance levels of these gut microbiota. In a word, both coffee and decaffeinated coffee are effective for sleep deprivation-induced depression-like behaviors and the dysbiosis of gut microbiota. It implies that caffeine is not the only key substance of coffee in the regulation of PSD induced gut microbiota disorder.

DATA AVAILABILITY STATEMENT

The datasets presented in this study can be found in online repositories. The names of the repository/repositories and accession number(s) can be found below: https://www.ncbi.nlm.nih.gov/, PRJNA762663.

ETHICS STATEMENT

The animal study was reviewed and approved by Animal Experiment Center, Shanghai University of Traditional Chinese Medicine.

AUTHOR CONTRIBUTIONS

YX, TZ, MZ, CX, and LY accomplished the conception and design of the research. XG, SZ, WM, QW, and YL performed the experiments. XG and SZ prepared the figures. XG, WM, and SZ analyzed and interpreted the data. XG, WM, and YL drafted the manuscript. MZ edited and revised the manuscript. MZ and LY approved final version of the manuscript. All authors read and approved the final manuscript.

FUNDING

This work was supported by Natural Science Foundation of Shanghai, no. 21ZR1460900, and also sponsored by Innovation Project for Undergraduates of Shanghai University of Traditional Chinese Medicine (202110268240).

ACKNOWLEDGMENTS

We would like to thank Jing Song for her efforts in animal experiments and sample analyzation. We would also like to acknowledge the support from the Majorbio Company (Shanghai, China).

SUPPLEMENTARY MATERIAL

The Supplementary Material for this article can be found online at: https://www.frontiersin.org/articles/10.3389/fmicb.2022.778512/full#supplementary-material

REFERENCES

Abdelkader, T. S., Chang, S. N., Kim, T. H., Song, J., Kim, D. S., and Park, J. H. (2013). Exposure time to caffeine affects heartbeat and cell damage-related gene expression of zebrafish *Danio rerio* embryos at early developmental stages. *J. Appl. Toxicol.* 33, 1277–1283. doi: 10.1002/jat.2787

Abreu, R. V., Silva Oliveira, E. M., Moraes, M. F., Pereira, G. S., and Moraes Santos, T. (2011). Chronic coffee and caffeine ingestion effects on the cognitive function and antioxidant system of rat brains. *Pharmacol. Biochem. Behav.* 99, 659–664. doi: 10.1016/j.pbb.2011.06.010

Adan, A., Prat, G., Fabbri, M., and Sànchez-Turet, M. (2008). Early effects of caffeinated and decaffeinated coffee on subjective state and gender differences. *Prog. Neuropsychopharmacol. Biol. Psychiatry* 32, 1698–1703. doi: 10.1016/j.pnpbp.2008.07.005

Akira, S., Hirano, T., Taga, T., and Kishimoto, T. (1990). Biology of multifunctional cytokines: IL 6 and related molecules (IL-1 and TNF). *FASEB J.* 4, 2860–2867.

Alexandra, V., Yosef, K. D., Keishi, N., Elizabeth, A. P., Cindy, L., Michael, E. G., et al. (2020). Sleep loss can cause death through accumulation of reactive oxygen species in the gut. *Cell* 181, 1307–1328.e15. doi: 10.1016/j.cell.2020.04.049

Atarashi, K., Suda, W., Luo, C., Kawaguchi, T., Motoo, I., Narushima, S., et al. (2017). Ectopic colonization of oral bacteria in the intestine drives TH1 cell induction and inflammation. *Science* 358, 359–365. doi: 10.1126/science.aan4526

Aura, A. M. (2008). Microbial metabolism of dietary phenolic compounds in the colon. *Phytochemistry Rev.* 7, 407–429. doi: 10.1007/s11101-008-9095-3

Barandouzi, Z. A., Starkweather, A. R., Henderson, W. A., Gyamfi, A., and Cong, X. S. (2020). Altered composition of gut microbiota in depression: a systematic review. *Front. Psychiatry* 11:541. doi: 10.3389/fpsyt.2020.00541

Benca, R. M., Obermeyer, W. H., Thisted, R. A., and Gillin, J. C. (1992). Sleep and psychiatric disorders. A meta-analysis. *Arch. Gen. Psychiatry* 49, 651–670. doi: 10.1001/archpsyc.1992.01820080059010

Beverly, D., Lopez-Quiroga, E., Farr, R., Melrose, J., Henson, S., Bakalis, S., et al. (2020). Modeling mass and heat transfer in multiphase coffee aroma extraction. *Ind. Eng. Chem. Res.* 59, 11099–11112. doi: 10.1021/acs.iecr.0c01153

Black, C. N., Bot, M., Scheffer, P. G., Cuijpers, P., and Penninx, B. (2015). Is depression associated with increased oxidative stress? A systematic review and meta-analysis. *Psychoneuroendocrinology* 51, 164–175. doi: 10.1016/j.psyneuen.2014.09.025

Butt, M. S., and Sultan, M. T. (2011). Coffee and its consumption: benefits and risks. *Crit. Rev. Food Sci. Nutr.* 51, 363–373. doi: 10.1080/10408390903586412

Camfield, D. A., Silber, B. Y., Scholey, A. B., Nolidin, K., Goh, A., and Stough, C. (2013). A randomised placebo-controlled trial to differentiate the acute cognitive and mood effects of chlorogenic acid from decaffeinated coffee. *PLoS One* 8:e82897. doi: 10.1371/journal.pone.0082897

Cheng, Z., Hu, X., and Sun, Z. (2016). Microbial community distribution and dominant bacterial species analysis in the bio-electrochemical system treating low concentration cefuroxime. *Chem. Eng. J.* 303, 137–144. doi: 10.1016/j.cej.2016.05.131

Cheung, S. G., Goldenthal, A. R., Uhlemann, A. C., Mann, J. J., Miller, J. M., and Sublette, M. E. (2019). Systematic review of gut microbiota and major depression. *Front. Psychiatry* 10:34. doi: 10.3389/fpsyt.2019.00034

Childs, E., and Wit, H. D. (2006). Subjective, behavioral, and physiological effects of acute caffeine in light, nondependent caffeine users. *Psychopharmacology* 185, 514–523. doi: 10.1007/s00213-006-0341-3

Chong, C. W., Wong, L. C., Teh, C. S. J., Ismail, N. H., Chan, P. Q., Lim, C. S., et al. (2020). Coffee consumption revealed sex differences in host endogenous metabolism and gut microbiota in healthy adults. *J. Food Biochem.* 44:e13535. doi: 10.1111/jfbc.13535

Couteau, D., Mccartney, A. L., Gibson, G. R., Williamson, G., and Faulds, C. B. (2010). Isolation and characterization of human colonic bacteria able to hydrolyse chlorogenic acid. *J. Appl. Microbiol.* 90, 873–881. doi: 10.1046/j.1365-2672.2001.01316.x

Cowan, T. E., Palmnäs, M. S., Yang, J., Bomhof, M. R., Ardell, K. L., Reimer, R. A., et al. (2014). Chronic coffee consumption in the diet-induced obese rat: impact on gut microbiota and serum metabolomics. *J. Nutr. Biochem.* 25, 489–495. doi: 10.1016/j.jnutbio.2013.12.009

Dalby, M. J., Ross, A. W., Walker, A. W., and Morgan, P. J. (2017). Dietary uncoupling of gut microbiota and energy harvesting from obesity and glucose tolerance in mice. *Cell Rep.* 21, 1521–1533.

Daniela, M., Valeria, C., Domenico, S., Mattia, P., Michele, B., Salvatore, B., et al. (2017). Beneficial effects of oral pure caffeine on oxidative stress. *J. Clin. Transl. Endocrinol.* 10, 22–27. doi: 10.1016/j.jcte.2017.10.001

Daniele, T., Bruin, P., Rios, E., and Bruin, V. (2017). Effects of exercise on depressive behavior and striatal levels of norepinephrine, serotonin and their metabolites in sleep-deprived mice. *Behav. Brain Res.* 332, 16–22.

Dieter, R., Lukas, B. K., Katharina, W., and Christoph, N. (2019). Sleep, insomnia, and depression. *Neuropsychopharmacology* 45, 74–89. doi: 10.1038/s41386-019-0411-y

Dinan, T. G., and Cryan, J. F. (2013). Melancholic microbes: a link between gut microbiota and depression? *Neurogastroenterol. Motil.* 25, 713–719. doi: 10.1111/nmo.12198

Ding, M., Satija, A., Bhupathiraju, S. N., Hu, Y., Sun, Q., Han, J., et al. (2015). Association of coffee consumption with total and cause-specific mortality in 3 large prospective cohorts. *Circulation* 132, 2305–2315. doi: 10.1161/CIRCULATIONAHA.115.017341

Dong, H., Ane, S. K., Wenjie, M., Yang, H., Fred, K. T., Hongmei, N., et al. (2019). Coffee consumption and plasma biomarkers of metabolic and inflammatory pathways in US health professionals. *Am. J. Clin. Nutr.* 109, 635–647. doi: 10.1093/ajcn/nqy295

Dong, Y., Yan, H., Zhao, X., Lin, R., Lin, L., Ding, Y., et al. (2020). Gu-Ben-Fang-Xiao decoction ameliorated murine msthma in remission stage by modulating microbiota-acetate-tregs axis. *Front. Pharmacol.* 11:549. doi: 10.3389/fphar.2020.00549

Edgar, R. C. (2013). UPARSE: highly accurate OTU sequences from microbial amplicon reads. *Nat. Methods* 10, 996–998. doi: 10.1038/nmeth.2604

Emeran, A. M., Kirsten, T., and Arpana, G. (2015). Gut/brain axis and the microbiota. *J. Clin. Invest.* 125, 926–938. doi: 10.1172/JCI76304

Erikka, L., Meredith, S. S., Barry, I. G., Hormuzd, A. K., Anil, K. C., Britton, T., et al. (2015). Associations of coffee drinking with systemic immune and inflammatory markers. *Cancer Epidemiol. Biomarkers Prev.* 24, 1052–1060. doi: 10.1158/1055-9965.EPI-15-0038-T

Eriksson, E., Royo, F., Lyberg, K., Carlsson, H. E., and Hau, J. (2004). Effect of metabolic cage housing on immunoglobulin A and corticosterone excretion in faeces and urine of young male rats. *Exp. Physiol.* 89, 427–433. doi: 10.1113/expphysiol.2004.027656

Franke, A. G., Bagusat, C., Rust, S., Engel, A., and Lieb, K. (2014). Substances used and prevalence rates of pharmacological cognitive enhancement among healthy subjects. *Eur. Arch. Psychiatry Clin. Neurosci.* 264, 83–90. doi: 10.1007/s00406-014-0537-1

Galland, L. (2014). The gut microbiome and the brain. *J. Med. Food* 17, 1261–1272. doi: 10.1089/jmf.2014.7000

George, S. E., Ramalakshmi, K., and Mohan Rao, L. J. (2008). A perception on health benefits of coffee. *Crit. Rev. Food Sci. Nutr.* 48, 464–486. doi: 10.1080/10408390701522445

Giuseppe, G., Justyna, G., Fabio, G., and Edward, L. G. (2017). Coffee, caffeine, and health outcomes: an umbrella review. *Annu. Rev. Nutr.* 37, 131–156. doi: 10.1146/annurev-nutr-071816-064941

Godos, J., Pluchinotta, F. R., Marventano, S., Buscemi, S., Li Volti, G., Galvano, F., et al. (2014). Coffee components and cardiovascular risk: beneficial and detrimental effects. *Int. J. Food Sci. Nutr.* 65, 925–936. doi: 10.3109/09637486.2014.940287

González, S., Salazar, N., Ruiz-Saavedra, S., Gómez-Martín, M., Los Reyes-Gavilán, C. G., and Gueimonde, M. (2020). Long-term coffee consumption is associated with fecal microbial composition in humans. *Nutrients* 12:1287. doi: 10.3390/nu12051287

Grosso, G., Micek, A., Castellano, S., Pajak, A., and Galvano, F. (2016). Coffee tea, caffeine and risk of depression: a systematic review and dose–response meta-analysis of observational studies. *Mol. Nutr. Food Res.* 60, 223–234. doi: 10.1002/mnfr.201500620

Guoying, W., Guo, Z., Xiaoyu, C., Longxiang, X., and Hongju, W. (2020). The characteristic of virulence, biofilm and antibiotic resistance of *Klebsiella pneumoniae*. *Int. J. Environ. Res. Public Health* 17:6278. doi: 10.3390/ijerph17176278

Haroon, B., Muhammad, I., Waqar, A., Sareer, A., Jong, R. H., and Myeong, O. K. (2019). Caffeine may abrogate LPS-induced oxidative stress and neuroinflammation by regulating Nrf2/TLR4 in adult mouse brains. *Biomolecules* 9:719. doi: 10.3390/biom9110719

Haskell, C. F., Kennedy, D. O., Wesnes, K. A., and Scholey, A. B. (2005). Cognitive and mood improvements of caffeine in habitual consumers and habitual non-consumers of caffeine. *Psychopharmacology* 179, 813–825. doi: 10.1007/s00213-004-2104-3

Heintz-Buschart, A., Pandey, U., Wicke, T., Sixel-Döring, F., Janzen, A., Sittig-Wiegand, E., et al. (2018). The nasal and gut microbiome in Parkinson's disease and idiopathic rapid eye movement sleep behavior disorder. *Mov. Disord.* 33, 88–98. doi: 10.1002/mds.27105

Ho, S. C., and Chung, J. W. (2013). The effects of caffeine abstinence on sleep: a pilot study. *Appl. Nurs. Res.* 26, 80–84. doi: 10.1016/j.apnr.2012.08.004

Hoelzl, C., Knasmüller, S., Wagner, K. H., Elbling, L., Huber, W., Kager, N., et al. (2010). Instant coffee with high chlorogenic acid levels protects humans against oxidative damage of macromolecules. *Mol. Nutr. Food Res.* 54, 1722–1733. doi: 10.1002/mnfr.201000048

Hughes, J. R., McHugh, P., and Holtzman, S. (1998). Caffeine and schizophrenia. *Psychiatr. Serv.* 49, 1415–1417. doi: 10.1176/ps.49.11.1415

Huws, S. A., Kim, E. J., Lee, M. R., Scott, M. B., Tweed, J. K., Pinloche, E., et al. (2011). As yet uncultured bacteria phylogenetically classified as *Prevotella*, Lachnospiraceae incertae sedis and unclassified Bacteroidales, Clostridiales and Ruminococcaceae may play a predominant role in ruminal biohydrogenation. *Environ. Microbiol.* 13, 1500–1512. doi: 10.1111/j.1462-2920.2011.02452.x

Hwang, J. H., Kim, K. J., Ryu, S. J., and Lee, B. Y. (2016). Caffeine prevents LPS-induced inflammatory responses in RAW264.7 cells and zebrafish. *Chem. Biol. Interact.* 248, 1–7. doi: 10.1016/j.cbi.2016.01.020

Jamie, J. C., Caitlin, K. R., Ben, L. Z., Lava, T., Grace, S. R., and David, V. F. (2019). To Sleep, perchance to dream: acute and chronic sleep deprivation in acute care surgeons. *J. Am. Coll. Surg.* 229, 166–174. doi: 10.1016/j.jamcollsurg.2019.03.019

Jennifer, M. M., Dion, L., Wenqing, W., Peter, K. P., Lindsay, E. R., and Krista, A. P. (2017). Navy and black bean supplementation primes the colonic mucosal microenvironment to improve gut health. *J. Nutr. Biochem.* 49, 89–100. doi: 10.1016/j.jnutbio.2017.08.002

Jost, L., Anna, K. K., Petra, V., Gustav, J. D., and Andreas, R. (2020). Distinct patterns of short-chain fatty acids during flare in patients with ulcerative colitis under treatment with mesalamine or a herbal combination of myrrh, chamomile flowers, and coffee charcoal: secondary analysis of a randomized controlled trial. *Eur. J. Gastroenterol. Hepatol.* 32, 175–180. doi: 10.1097/meg.0000000000001582

Kaisa, H., Veera, K., Maiju, S., Tuomas, H., Jolene, R. B., Daniel, J. S., et al. (2020). Isolation of anti-inflammatory and epithelium reinforcing *Bacteroides* and *Parabacteroides* Spp. from a healthy fecal donor. *Nutrients* 12:935. doi: 10.3390/nu12040935

Kayir, H., and Uzbay, I. T. (2006). Nicotine antagonizes caffeine- but not pentylenetetrazole-induced anxiogenic effect in mice. *Psychopharmacology(Berl)* 184, 464–469. doi: 10.1007/s00213-005-0036-1

Kazuchika, N., Syunsuke, W., Jinzhong, X., Ryosuke, N., Hirohisa, O., Takaaki, T., et al. (2018). Effect of coffee or coffee components on gut microbiome and short-chain fatty acids in a mouse model of metabolic syndrome. *Sci Rep.* 8:16173. doi: 10.1038/s41598-018-34571-9

Kelly, J. R., Borre, Y., O' Brien, C., Patterson, E., El Aidy, S., Deane, J., et al. (2016). Transferring the blues: depression-associated gut microbiota induces neurobehavioural changes in the rat. *J. Psychiatr. Res.* 82, 109–118. doi: 10.1016/j.jpsychires.2016.07.019

Kim, S. H., Park, S. Y., Park, Y. L., Myung, D. S., Rew, J. S., and Joo, Y. E. (2017). Chlorogenic acid suppresses lipopolysaccharide-induced nitric oxide and interleukin-1β expression by inhibiting JAK2/STAT3 activation in RAW264.7 cells. *Mol. Med. Rep.* 16, 9224–9232. doi: 10.3892/mmr.2017.7686

Kolb, H., Kempf, K., and Martin, S. (2020). Health effects of coffee: mechanism unraveled? *Nutrients* 12:1842. doi: 10.3390/nu12061842

Kotyczka, C., Boettler, U., Lang, R., Stiebitz, H., Bytof, G., Lantz, I., et al. (2011). Dark roast coffee is more effective than light roast coffee in reducing body weight, and in restoring red blood cell vitamin E and glutathione concentrations in healthy volunteers. *Mol. Nutr. Food Res.* 55, 1582–1586. doi: 10.1002/mnfr.201100248

Krishnan, H. C., Gandour, C. E., Ramos, J. L., Wrinkle, M. C., Sanchez-Pacheco, J. J., and Lyons, L. C. (2016). Acute sleep deprivation blocks short-and long-term operant memory in Aplysia. *Sleep* 39, 2161–2171. doi: 10.5665/sleep.6320

Li, Q., Liu, Y., Sun, X., Yin, Z., Li, H., Cheng, C., et al. (2019). Caffeinated and decaffeinated coffee consumption and risk of all-cause mortality: a dose–response meta-analysis of cohort studies. *J. Hum. Nutr. Diet.* 32, 279–287. doi: 10.1111/jhn.12633

Li, S., Wang, Z., Yang, Y., Yang, S., Yao, C., Liu, K., et al. (2017). Lachnospiraceae shift in the microbial community of mice faecal sample effects on water immersion restraint stress. *AMB Express* 7:82. doi: 10.1186/s13568-017-0383-4

Lopez Garcia, E., Guallar Castillon, P., Leon Muñoz, L., Graciani, A., and Rodriguez Artalejo, F. (2014). Coffee consumption and health-related quality of life. *Clin. Nutr.* 33, 143–149. doi: 10.1016/j.clnu.2013.04.004

Ma, W., Song, J., Wang, H., Shi, F., Zhou, N., Jiang, J., et al. (2019). Chronic paradoxical sleep deprivation-induced depression-like behavior, energy metabolism and microbial changes in rats. *Life Sci.* 225, 88–97. doi: 10.1016/j.lfs.2019.04.006

Machado, R. B., Hipólide, D. C., Benedito-Silva, A. A., and Tufik, S. (2004). Sleep deprivation induced by the modified multiple platform technique: quantification of sleep loss and recovery. *Brain Res.* 1004, 45–51. doi: 10.1016/j.brainres.2004.01.019

Magne, F., Gotteland, M., Gauthier, L., Zazueta, A., Pesoa, S., Navarrete, P., et al. (2020). The Firmicutes/Bacteroidetes ratio: a relevant marker of gut dysbiosis in obese patients? *Nutrients* 12:1474.

Magoč, T., and Salzberg, S. L. (2011). FLASH: fast length adjustment of short reads to improve genome assemblies. *Bioinformatics* 27, 2957–2963. doi: 10.1093/bioinformatics/btr507

Mahshad, K., and Mazen, J. H. (2017). The neuroprotective effects of caffeine in neurodegenerative diseases. *CNS Neurosci. Ther.* 23, 272–290. doi: 10.1111/cns.12684

Malinalli, B. P., Fausto, S. M., Gonzalo, V. P., Fengyang, H., Julio César, A. P., Rafael, B., et al. (2018). Cytokine and microRNA levels during different periods of paradoxical sleep deprivation and sleep recovery in rats. *PeerJ* 13:5567. doi: 10.7717/peerj.5567

Marjolaine, V. D., Sylvie, M., Sophie, G., Thomas, B., Damien, B., Bertrand, E., et al. (2019). Immunomodulatory effects of Lactobacillus plantarum on inflammatory response induced by *Klebsiella pneumoniae*. *Infect. Immun.* 87:e00570-19. doi: 10.1128/iai.00570-19

Martini, D., Del Bo', C., Tassotti, M., Riso, P., Del Rio, D., Brighenti, F., et al. (2016). Coffee consumption and oxidative stress: a review of human intervention studies. *Molecules* 21:979. doi: 10.3390/molecules21080979

Matthew, T. S., Eric, R. L., Emily, F., Thomas, U. M., Claire, E. K., Mergim, G., et al. (2020). Functional and genomic variation between human-derived isolates of Lachnospiraceae reveals inter- and intra-species diversity. *Cell Host Microbe* 28, 134–146.e4. doi: 10.1016/j.chom.2020.05.005

McEwen, B. S. (2006). Sleep deprivation as a neurobiologic and physiologic stressor: allostasis and allostatic load. *Metabolism* 55, 20–23. doi: 10.1016/j.metabol.2006.07.008

Meetu, W., Garima, C., Koustav, R., Surajit, S., Satyanarayan, D., Vishal, J., et al. (2018). Caffeine and modafinil ameliorate the neuroinflammation and anxious behavior in rats during sleep deprivation by inhibiting the microglia activation. *Front. Cell Neurosci.* 12:49. doi: 10.3389/fncel.2018.00049

Megumi, F. T., Yusuke, N., Kenji, T., Mika, T., Yuma, I., Ami, S., et al. (2020). Pyrocatechol, a component of coffee, suppresses LPS-induced inflammatory responses by inhibiting NF-κB and activating Nrf2. *Sci .Rep.* 10:2584. doi: 10.1038/s41598-020-59380-x

Mengmei, Y., Yali, C., Hui, Z., Tinglin, P., Charles, M., Ting, W., et al. (2017). Assessment of mouse cognitive and anxiety-like behaviors and hippocampal inflammation following a repeated and intermittent paradoxical sleep deprivation procedure. *Behav. Brain Res.* 321, 69–78. doi: 10.1016/j.bbr.2016.12.034

Michael, R. I., Tuff, W., Marissa, C., Richard, O., and Elizabeth, C. B. (2015). Sleep loss activates cellular inflammation and signal transducer and activator of transcription (STAT) family proteins in humans. *Brain Behav. Immun.* 47, 86–92. doi: 10.1016/j.bbi.2014.09.017

Na, J., Susan, S. B., Colleen, A. N., Maria, T., Liting, C., Yong, W., et al. (2018). Gut microbiome may contribute to insulin resistance and systemic inflammation in obese rodents: a meta-analysis. *Physiol. Genomics* 50, 244–254. doi: 10.1152/physiolgenomics.00114.2017

Nakayama, T., and Oishi, K. (2013). Influence of coffee (*Coffea arabica*) and galacto-oligosaccharide consumption on intestinal microbiota and the host responses. *FEMS Microbiol. Lett.* 343, 161–168. doi: 10.1111/1574-6968.12142

Navarro, A. M., Abasheva, D., Martínez-González, M. Á, Ruiz-Estigarribia, L., Martín-Calvo, N., Sánchez-Villegas, A., et al. (2018). Coffee consumption and the risk of depression in a middle-aged cohort: the SUN project. *Nutrients* 10:1333. doi: 10.3390/nu10091333

Patrice, D. C., and Willem, M. V. (2017). Next-generation beneficial microbes: the case of *Akkermansia muciniphila*. *Front. Microbiol.* 8:1765. doi: 10.3389/fmicb.2017.01765

Paz-Graniel, I., Babio, N., Becerra-Tomás, N., Toledo, E., Camacho-Barcia, L., Corella, D., et al. (2020). Association between coffee consumption and total dietary caffeine intake with cognitive functioning: cross-sectional assessment in an elderly Mediterranean population. *Eur. J. Nutr.* 60, 2381–2396. doi: 10.1007/s00394-020-02415-w

Plovier, H., Everard, A., Druart, C., Depommier, C., Van Hul, M., Geurts, L., et al. (2016). A purified membrane protein from *Akkermansia muciniphila* or the pasteurized bacterium improves metabolism in obese and diabetic mice. *Nat. Med.* 23, 107–113. doi: 10.1038/nm.4236

Rahmani, M., Rahmani, F., and Rezaei, N. (2020). The brain-derived neurotrophic factor: missing link between sleep deprivation, insomnia, and depression. *Neurochem. Res.* 45, 221–231. doi: 10.1007/s11064-019-02914-1

Renouf, M., Marmet, C., Giuffrida, F., Lepage, M., Barron, D., Beaumont, M., et al. (2014). Dose-response plasma appearance of coffee chlorogenic and phenolic acids in adults. *Mol. Nutr. Food Res.* 58, 301–309. doi: 10.1002/mnfr.201300349

Robert, E. R., and Hao, T. D. (2014). The prospective association between sleep deprivation and depression among adolescents. *Sleep* 37, 239–244. doi: 10.5665/sleep.3388

Rothenberg, D. O., Zhou, C., and Zhang, L. (2018). A review on the weight-loss effects of oxidized tea polyphenols. *Molecules* 23:1176. doi: 10.3390/molecules23051176

Sanchez Villegas, A., and Martínez González, M. A. (2013). Diet, a new target to prevent depression? *BMC Med.* 11:3. doi: 10.1186/1741-7015-11-3

Scharf, G., Prustomersky, S., and Huber, W. W. (2001). Elevation of glutathione levels by coffee components and its potential mechanisms. *Adv. Exp. Med. Biol.* 500, 535–539. doi: 10.1007/978-1-4615-0667-6_82

Schindler, R., Mancilla, J., Endres, S., Ghorbani, R., Clark, S. C., and Dinarello, C. A. (1990). Correlations and interactions in the production of interleukin-6 (IL-6), IL-1, and tumor necrosis factor (TNF) in human blood mononuclear cells: IL-6 suppresses IL-1 and TNF. *Blood* 75, 40–47.

Schirmer, M., Garner, A., Vlamakis, H., and Xavier, R. (2019). Microbial genes and pathways in inflammatory bowel disease. *Nat. Rev. Microbiol.* 17, 497–511. doi: 10.1038/s41579-019-0213-6

Shifu, C., Yanqing, Z., Yaru, C., and Jia, G. (2018). Fastp: an ultra-fast all-in-one FASTQ preprocessor. *Bioinformatics* 34, i884–i890. doi: 10.1093/bioinformatics/bty560

Shin, J. W., Wang, J. H., Kang, J. K., and Son, C. G. (2010). Experimental evidence for the protective effects of coffee against liver fibrosis in SD rats. *J. Sci. Food Agric.* 90, 450–455. doi: 10.1002/jsfa.3838

Shin, N. R., Whon, T. W., and Bae, J. W. (2015). *Proteobacteria*: microbial signature of dysbiosis in gut microbiota. *Trends Biotechnol.* 33, 496–503. doi: 10.1016/j.tibtech.2015.06.011

Singh, R. P., Halaka, D. A., Hayouka, Z., and Tirosh, O. (2020). High-fat diet induced alteration of mice microbiota and the functional ability to utilize fructooligosaccharide for ethanol production. *Front. Cell Infect. Microbiol.* 10:376.

Sinha, R., Abu-Ali, G., Vogtmann, E., Fodor, A. A., Ren, B., Amir, A., et al. (2017). Assessment of variation in microbial community amplicon sequencing by the Microbiome Quality Control (MBQC) project consortium. *Nat. Biotechnol.* 35, 1077–1086. doi: 10.1038/nbt.3981

Soohan, J., Min Hyung, K., Jae Hee, P., Yoonhwa, J., and Kwang Suk, K. (2017). Cellular antioxidant and anti-inflammatory effects of coffee extracts with different roasting levels. *J. Med. Food* 20, 626–635. doi: 10.1089/jmf.2017.3935

Stachyshyn, S., Ali, A., Wham, C., Knightbridge-Eager, T., and Rutherfurd-Markwick, K. (2021). Caffeine consumption habits of New Zealand tertiary students. *Nutrients* 13:1493. doi: 10.3390/nu13051493

Stackebrandt, E., and Goebel, B. M. (1994). Taxonomic note: a place for DNA-DNA reassociation and 16S rRNA sequence analysis in the present species definition in bacteriology. *Int. J. Syst. Bacteriol.* 44, 846–849. doi: 10.1099/00207713-44-4-846

Stefanello, N., Spanevello, R. M., Passamonti, S., Porciúncula, L., Bonan, C. D., Olabiyi, A. A., et al. (2018). Coffee, caffeine, chlorogenic acid, and the purinergic system. *Food Chem. Toxicol.* 123, 298–313. doi: 10.1016/j.fct.2018.10.005

Su, S. H., Shyu, H. W., Yeh, Y. T., Chen, K. M., and Su, S. J. (2013). Caffeine inhibits adipogenic differentiation of primary adipose-derived stem cells and bone marrow stromal cells. *Toxicol. Vitro* 27, 1830–1837. doi: 10.1016/j.tiv.2013.05.011

Ting, G., Zixu, W., Yulan, D., Jing, C., Rutao, L., Xintong, W., et al. (2019). Role of melatonin in sleep deprivation-induced intestinal barrier dysfunction in mice. *J. Pineal. Res.* 67, e12574. doi: 10.1111/jpi.12574

Tsujimoto, T., Kajio, H., and Sugiyama, T. (2017). Association between caffeine intake and all-cause and cause-specific mortality: a population-based prospective cohort study. *Mayo Clin. Proc.* 92, 1190–1202. doi: 10.1016/j.mayocp.2017.03.010

Turner, P. V., Vaughn, E., Sunohara Neilson, J., Ovari, J., and Leri, F. (2012). Oral gavage in rats: animal welfare evaluation. *J. Am. Assoc. Lab. Anim. Sci.* 51, 25–30.

Uri, G., Tom, K., and Henrik, B. N. (2017). Oscillospira and related bacteria-From metagenomic species to metabolic features. *Environ. Microbiol.* 19, 835–841. doi: 10.1111/1462-2920.13658

Vaváková, M., Ďuračková, Z., and Trebatická, J. (2015). Markers of oxidative stress and neuroprogression in depression disorder. *Oxid. Med. Cell Longev.* 2015:898393. doi: 10.1155/2015/898393

Villafuerte, G., Miguel-Puga, A., Rodríguez, E. M., Machado, S., Manjarrez, E., and Arias-Carrión, O. (2016). Sleep deprivation and oxidative stress in animal models: a systematic review. *Oxid. Med. Cell Longev.* 2015:234952. doi: 10.1155/2015/234952

Ward, P. J., and Hubscher, C. H. (2012). Persistent polyuria in a rat spinal contusion model. *J. Neurotrauma.* 29, 2490–2498. doi: 10.1089/neu.2012.2402

Wierzejska, R. (2012). Caffeine-common ingredient in a diet and its influence on human health. *Rocz. Panstw. Zakl. Hig.* 63:141.

World Health Organization (2017). *Depression and Other Common Mental Disorders: Global Health Estimates*. Geneva: WHO.

Xiaoyu, G., Qiuhong, X., Ping, K., Ling, L., Sheng, S., Boyu, X., et al. (2018). Polyphenol-and caffeine-rich postfermented pu-erh tea improves diet-induced metabolic syndrome by remodeling intestinal homeostasis in mice. *Infect. Immun.* 86:e00601-17. doi: 10.1128/iai.00601-17

Xue, D., Shiru, L., Jing, S., Yan, L., and Dongfeng, Z. (2020). Association of coffee, decaffeinated coffee and caffeine intake from coffee with cognitive performance in older adults: national health and nutrition examination survey (NHANES) 2011–2014. *Nutrients* 12:840. doi: 10.3390/nu12030840

Yamashita, K., Yatsuya, H., Muramatsu, T., Toyoshima, H., Murohara, T., and Tamakoshi, K. (2012). Association of coffee consumption with serum adiponectin, leptin, inflammation and metabolic markers in Japanese workers: a cross-sectional study. *Nutr. Diabetes* 2:e33. doi: 10.1038/nutd.2012.6

Yan, Y., Zhou, X., Guo, K., Zhou, F., and Yang, H. (2020). Chlorogenic acid protects against indomethacin-induced inflammation and mucosa damage by decreasing *Bacteroides*-derived LPS. *Front. Immunol.* 11:1125. doi: 10.3389/fimmu.2020.01125

Yuji, N., Kazuhiko, U., and Tomohisa, T. (2018). A next-generation beneficial microbe: *Akkermansia muciniphila*. *J. Clin. Biochem. Nutr.* 63, 33–35. doi: 10.3164/jcbn.18-57

Zhai, X. J., Chen, F., Chen, C., Zhu, C. R., and Lu, Y. N. (2015). LC–MS/MS based studies on the anti-depressant effect of hypericin in the chronic unpredictable mild stress rat model. *J. Ethnopharmacol.* 169, 363–369. doi: 10.1016/j.jep.2015.04.053

Zheng, P., Zeng, B., Zhou, C., Liu, M., Fang, Z., Xu, X., et al. (2016). Gut microbiome remodeling induces depressive-like behaviors through a pathway mediated by the Host's metabolism. *Mol. Psychiatry* 21, 786–796. doi: 10.1038/mp.2016.44

Conflict of Interest: The authors declare that the research was conducted in the absence of any commercial or financial relationships that could be construed as a potential conflict of interest.

Publisher's Note: All claims expressed in this article are solely those of the authors and do not necessarily represent those of their affiliated organizations, or those of the publisher, the editors and the reviewers. Any product that may be evaluated in this article, or claim that may be made by its manufacturer, is not guaranteed or endorsed by the publisher.

frontiers | Frontiers in Microbiology

TYPE Original Research
PUBLISHED 16 December 2022
DOI 10.3389/fmicb.2022.1054097

OPEN ACCESS

EDITED BY
Bruce S. Seal,
Oregon State University–Cascades,
United States

REVIEWED BY
Mohammad Altamimi,
An-Najah National University,
Palestine
Brian B. Oakley,
Western University of Health Sciences,
United States

*CORRESPONDENCE
Matteo Fornai
matteo.fornai@unipi.it

†These authors have contributed equally to this work and share first authorship

SPECIALTY SECTION
This article was submitted to Microorganisms in Vertebrate Digestive Systems, a section of the journal Frontiers in Microbiology

RECEIVED 26 September 2022
ACCEPTED 28 November 2022
PUBLISHED 16 December 2022

CITATION
Panattoni A, Calvigioni M, Benvenuti L, D'Antongiovanni V, Pellegrini C, Di Salvo C, Mazzantini D, Celandroni F, Fornai M, Antonioli L and Ghelardi E (2022) The administration of *Enterococcus faecium* SF68 counteracts compositional shifts in the gut microbiota of diet-induced obese mice.
Front. Microbiol. 13:1054097.
doi: 10.3389/fmicb.2022.1054097

The administration of *Enterococcus faecium* SF68 counteracts compositional shifts in the gut microbiota of diet-induced obese mice

Adelaide Panattoni[1†], Marco Calvigioni[1†], Laura Benvenuti[2], Vanessa D'Antongiovanni[2], Carolina Pellegrini[2], Clelia Di Salvo[2], Diletta Mazzantini[1], Francesco Celandroni[1], Matteo Fornai[2]*, Luca Antonioli[2] and Emilia Ghelardi[1]

[1]Department of Translational Research and New Technologies in Medicine and Surgery, University of Pisa, Pisa, Italy, [2]Department of Clinical and Experimental Medicine, University of Pisa, Pisa, Italy

Microorganisms with probiotic properties are eliciting an increasing interest as coadjuvants in the prevention and treatment of obesity through modulation of the gut microbiota. In this study, a probiotic formulation based on *Enterococcus faecium* SF68 was administered to mice fed with a high-fat diet (HFD) to evaluate its efficacy in reducing body mass gain and in modulating the intestinal bacterial composition. Both stool and ileum samples were collected from untreated and treated mice and absolute abundances of specific *taxa* constituting the gut microbial *consortium* were evaluated. SF68 administration significantly reduced the HFD-induced weight gain. In these animals, the microbial gut composition shifted toward an enrichment in microbes positively correlated with mucus thickness, lower inflammation, lower glycemia levels, and SCFA production (i.e., *Bifidobacterium*, *Akkermansia*, and *Faecalibacterium*), as well as a depletion in bacterial phyla having a key role in obesity (i.e., *Firmicutes*, *Proteobacteria*). Our results demonstrate the efficacy of *E. faecium* SF68 in adjusting the composition of the dysbiotic microbiota of HFD-fed animals, thus ameliorating clinical conditions and exerting anti-obesity effects.

KEYWORDS

probiotics, gut microbiota, *Enterococcus*, obesity, high-fat diet, ileum

Introduction

The administration of probiotics, "live microorganisms which, when administered in adequate amounts, confer a health benefit on the host" (Food and Agricultural Organization of the United Nations and World Health Organization, 2001), is often effective in ameliorating the symptoms of a wide variety of clinical disorders in humans. These include

antibiotic-associated diarrhea (Mekonnen et al., 2020), infectious and *Clostridioides difficile*-associated diarrhea (Sánchez et al., 2017), irritable bowel syndrome (Moayyedi et al., 2010), type 2 diabetes (Ejtahed et al., 2011), inflammatory bowel diseases [e.g., ulcerative colitis (Ganji-Arjenaki and Rafieian-Kopaei, 2018) and obesity (Tenorio-Jiménez et al., 2020)], through countless but poorly investigated mechanisms of action.

Exploiting probiotic microorganisms as coadjuvants in the treatment or prevention of obesity is of clinical relevance. Obesity is a pathological condition that consists of abnormal or excessive fat accumulation, which in turn often drives to other chronic disorders (Cerdó et al., 2019), such as metabolic syndrome, insulin-resistance, and cardiovascular pathologies (Frasca et al., 2017). Moreover, this condition is typically associated with several other biomarkers. Due to aberrant intestinal permeability and mucus thickness, obese patients display high levels of lipopolysaccharide in the bloodstream (Green et al., 2020), a condition known as metabolic endotoxemia, which can lead to a constant state of systemic low-grade inflammation (Cani et al., 2007a). This prolonged inflammatory state contributes to insulin-resistance, triggering the onset of type-2 diabetes and metabolic issues (Cani et al., 2007b). Several studies showed how different probiotic strains were able to improve obesity-related conditions (Yadav et al., 2013; Bagarolli et al., 2017; Ejtahed et al., 2019). By restoring mucus thickness and tight junctions' expression or regulating the production of different cytokines, probiotics can improve the gut barrier integrity and modulate immune functions (Cerdó et al., 2019), as well as stimulate the secretion of satiety-related hormones through the production of short chain fatty acids (SCFAs; Da Silva et al., 2021). Besides these specific mechanisms of action, probiotics can also modulate the gut microbiota composition, thus triggering cascading effects that affect the entire organism (Azad et al., 2018). Considering the severe alteration in the fecal microbiota observed in obese patients, with higher levels of *Firmicutes* (Abenavoli et al., 2019) and *Actinobacteria* (Bibbò et al., 2016) and lower abundances of *Bifidobacterium* and *Akkermansia* (Gérard, 2016) than normal-weight subjects, the administration of probiotics may be considered a potential therapeutic approach aimed at restoring eubiosis of the intestinal flora and counteracting the clinical scenario of obesity.

Previous studies demonstrated the efficacy of selected *Enterococcus* strains in a variety of conditions (i.e., intestinal dysbiosis, metabolic syndrome, high levels of serum cholesterol and triglycerides, and inflammation) due to their recognized ability to secrete propionate and butyrate, hydrolyze bile salts, inhibit the transcription of pro-inflammatory mediators, and modulate the composition of the gut microbiota (Allen et al., 2010; Avram-Hananel et al., 2010; Tarasova et al., 2010; Zhang et al., 2017; Greuter et al., 2020; Mishra and Ghosh, 2020; Huang et al., 2021). Considering the overall positive effects demonstrated in these studies, enterococci seem to be promising candidates for the prevention and treatment of obesity and amelioration of other obesity-related complications.

In this study, *Enterococcus faecium* SF68 was orally administered to mice fed with a high-fat diet (HFD) to evaluate its efficacy in reducing body mass gain, modulating the gut microbiota composition, and restoring a well-balanced intestinal flora. Quantitative analyses were performed to obtain information on the bacterial composition found in both fecal and ileal tissue samples, thus elucidating the role of *E. faecium* SF68 in the interaction with intestinal residing microorganisms and toward amelioration of the obesity condition.

Materials and methods

Experimental design and probiotic administration

In this study, C57BL/6 mice were used as an animal model. Animals were supplied by ENVIGO s.r.l (Italy). Mice were five-week-old and weighed 20 g upon reception. For the duration of the study, mice were housed in cages on a 12-h light cycle, with a room temperature of 22–24°C and 50–60% humidity. Animals were allowed free access to food and water *ad libitum*. They were handled and cared following the European Community Council Directive 2010/63/UE, transposed by the Italian Government. The study was approved by the Italian Ministry of Health (authorization 955/2018-PR). Mice were randomly divided in 4 groups, each constituted of 5 to 10 mice (Figure 1). Two of the four groups were fed with a standard diet (SD, TD.2018), which provided 58% kcal as carbohydrates, 24% kcal as proteins, and 18% kcal as fats (3.1 kcal/g), while the remaining groups were fed with a high-fat diet (HFD, TD.06414), which provided 21.4% kcal as carbohydrates, 18.3% kcal as proteins, and 60.8% kcal as fats (5.1 kcal/g). Both dietary regimes were purchased from ENVIGO s.r.l. Animals belonging to one of the two SD groups were treated with a probiotic formulation based on *Enterococcus faecium* SF68 (SD + SF68), and the same procedure was performed for animals fed with the HFD (HFD + SF68). *E. faecium* SF68 (Cerbios-Pharma SA, Switzerland) is currently available in worldwide commercialized probiotic formulations as a drug. To administer the probiotic formulation, 10^9 CFU of *E. faecium* SF68 were resuspended in 0.15 ml of methocel 3%. Animals received the product daily *via* oral gavage for 4 weeks. After this period, animals were weighed, then anaesthetized and sacrificed to collect feces (withdrawn directly from the sigmoid colon) and ileal samples (tissue and mucus layer deprived of luminal content). All samples were stored separately at −80°C until use.

Genomic DNA extraction from feces and ileal tissue

To perform genomic DNA extraction from fecal and ileal samples, QIAmp PowerFecal Pro DNA Kit (QIAGEN, Germany) and QIAmp DNA Mini Kit (QIAGEN) were used, respectively.

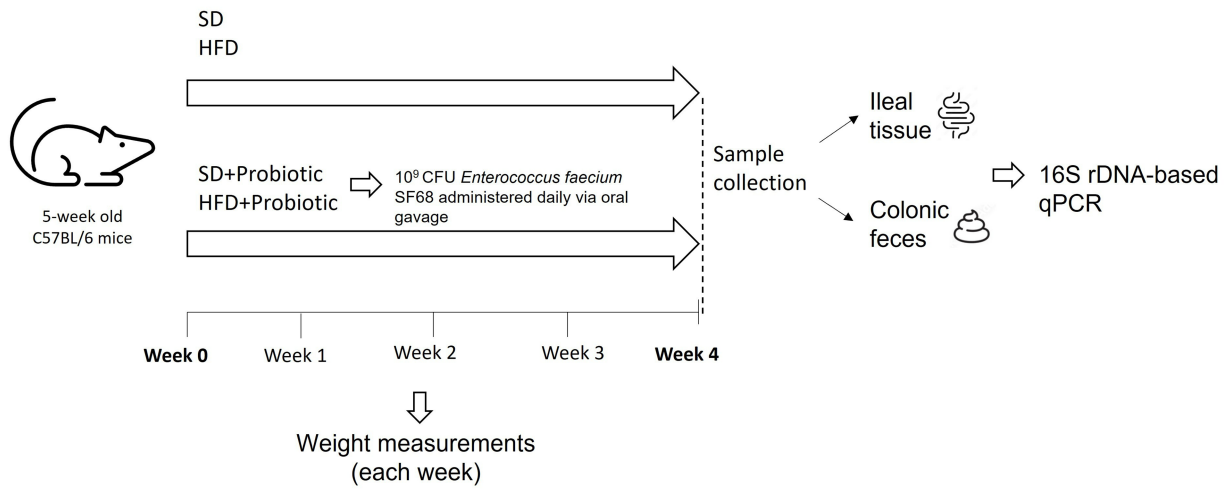

FIGURE 1
Schematic representation of the experimental design.

The extraction procedure was performed following the manufacturer's protocol. Fecal and ileal samples to extract weighed 15 and 25 mg, respectively. DNA concentration was calculated by measuring the optical density at 260 nm (OD260) and DNA purity was estimated by determining the OD260/OD280 ratio with Nanodrop Lite Spectrophotometer (Thermo Fisher Scientific, United States).

Real-Time quantitative PCR

To assess the absolute abundances of total bacteria, and of the main phyla (i.e., *Firmicutes*, *Bacteroidetes*, *Actinobacteria*, *Proteobacteria*) and genera (i.e., *Bacteroides*, *Bifidobacterium*, *Faecalibacterium*, *Lactobacillus*, *Prevotella*) present in both fecal and ileal samples, 16S rRNA gene-based Real-Time qPCR reactions were performed. Quantification of *Akkermansia muciniphila* abundance in ileal samples was also carried out. Primer pairs used in this study, able to specifically anneal to phylum- or genus- specific regions of the gene encoding 16S rRNA, are listed in Tables 1, 2. A degenerate primer pair, used to determine the total bacteria abundance, is also reported (Table 1). PCR reactions were performed using the CFX96 Real-Time System (BioRad, United States), and absolute quantifications were extrapolated using the CFX Manager Software (Biorad). Bacterial quantifications were established using calibration curves, obtained with serial 10-fold dilutions of external standards with known concentration ranging from 10^2 to 10^8 DNA copies/µl. Reactions were carried out in duplicate in a 96-wells plate with a final reaction volume of 20 µl, containing 1 µl of 2.5 ng/µl DNA template, 10 µl of Luna Universal qPCR Master Mix (New England BioLabs, United States), 0.5 µl of each primer (0.25 µM), and 8 µl of sterile water. The amplification conditions were as follows: an initial denaturation step at 95°C for 1 min, followed by 45 cycles of denaturation at 95°C for 15 s, annealing at primers' optimal temperature for 30 s (Tables 1, 2), and extension at 72°C for 10 s (Biagini et al., 2020). To check the amplification specificity, a melting curve analysis was carried out after PCR reactions by increasing the annealing temperature from 65 to 95°C.

Statistical analysis

All data are expressed as mean ± standard deviation. Statistical analyses were carried out with GraphPad Prism 8 (GraphPad Software Inc., United States). For all comparisons (SD vs. HFD; SD vs. SD + SF68; HFD vs. HFD + SF68) statistical significance was set at a p-value of 0.05 and assessed using Student t-tests for unpaired data.

Results

Weight variations in mice

Mice fed with HFD displayed a significant increase in body weight after 3 weeks (29.10 ± 2.56 g, +10.2%, $p = 0.0038$) and 4 weeks (31.60 ± 2.91 g, +20.2%, $p < 0.0001$) of dietary regimen compared to those fed with SD (3 W, 26.40 ± 0.84 g; 4 W: 26.30 ± 0.95 g), thus confirming the efficacy of the dietary regimen in setting up an obesity model (Figure 2). Interestingly, while no statistically significant weight differences were evidenced between SD and SD + SF68 during the entire experimental protocol ($p > 0.05$), mice receiving the probiotic formulation with the concomitant HFD gained less weight than the HFD control group at 2, 3, and 4 weeks (2 W,

TABLE 1 Primer pairs used in this study for the quantification of total bacterial load and microbial phyla.

Investigated bacterial group	Primer name and sequence (5′-3′)	Amplicon length (bp)	Annealing temperature (°C)	References
All bacteria	F: ACTCCTACGGGAGGCAGCAG	200	60	Biagini et al. (2020)
	R: ATTACCGCGGCTGCTGG			
Firmicutes	F: ATGTGGTTTAATTCGAAGCA	126	62	Biagini et al. (2020)
	R: AGCTGACGACAACCATGCAC			
Bacteroidetes	F: CATGTGGTTTAATTCGATGAT	126	62	Biagini et al. (2020)
	R: AGCTGACGACAACCATGCAG			
Actinobacteria	F: CGCGGCCTATCAGCTTGTTG	600	65	Stach et al. (2003)
	R: CCGTACTCCCCAGGCGGGG			
Proteobacteria	F: CATGACGTTACCCGCAGAAGAAG	195	63	Biagini et al. (2020)
	R: CTCTACGAGACTCAAGCTTGC			

TABLE 2 Primer pairs used in this study for the quantification of microbial genera and *Akkermansia muciniphila*.

Investigated bacterial group	Primer name and sequence (5′-3′)	Amplicon length (bp)	Annealing temperature (°C)	References
Akkermansia muciniphila	F: CAGCACGTGAAGGTGGGGAC	329	50	Collado et al. (2007)
	R: CCTTGCGGTTGGCTTCAGAT			
Bacteroides	F: GAGAGGAAGGTCCCCCAC	106	60	Kim et al. (2017)
	R: CGCTACTTGGCTGGTTCAG			
Bifidobacterium	F: CTCCTGGAAACGGGTGG	550	55	Matsuki et al. (2002)
	R: GGTGTTCTTCCCGATATCTACA			
Faecalibacterium	F: GGAGGAAGAAGGTCTTCGG	248	50	Kim et al. (2017)
	R: AATTCCGCCTACCTCTGCACT			
Lactobacillus	F: GAGGCAGCAGTAGGGAATCTTC	126	65	Kim et al. (2017)
	R: GGCCAGTTACTACCTCTATCCTTCTTC			
Prevotella	F: GGTTCTGAGAGGAAGGTCCCC	121	60	Kim et al. (2017)
	R: TCCTGCACGCTACTTGGCTG			

−12.4%, $p = 0.0006$; 3 W: −7.0%, $p = 0.0376$; 4 W: −16.2%, $p = 0.0017$).

Microbiota composition in SD and HFD mice

In fecal samples of HFD-fed mice, significant increases were observed in the total amount of bacteria ($p = 0.0095$), *Firmicutes* ($p = 0.0162$), and *Actinobacteria* ($p = 0.0024$), while *Bacteroidetes* abundance resulted lower ($p = 0.0395$; Figure 3A). At genus level, these animals displayed an increase in *Bifidobacterium* ($p = 0.0007$) and *Faecalibacterium* ($p = 0.0003$), while a decrease was registered in *Bacteroides* ($p = 0.0037$; Figure 3A). The analysis of ileal samples provided different results. *Firmicutes* ($p = 0.0397$) and *Proteobacteria* ($p = 0.0067$) amounts were significantly lower in mice fed with HFD compared to SD and reductions in the absolute abundance of *Lactobacillus* ($p = 0.0363$), *Bacteroides* ($p = 0.0133$), and *Faecalibacterium* ($p = 0.0021$) were also evident in this group of animals (Figure 3B).

Fecal microbiota composition after probiotic treatment in SD- and HFD-fed mice

The administration of *E. faecium* SF68 to SD- and HFD-fed mice caused a significant reduction of the fecal bacterial load (SD + SF68 vs. SD, $p = 0.0275$; HFD + SF68 vs. HFD, $p = 0.0021$), *Firmicutes* (SD + SF68 vs. SD, $p = 0.0318$; HFD + SF68 vs. HFD, $p = 0.0063$), *Bacteroidetes* (SD + SF68 vs. SD, $p = 0.0199$; HFD + SF68 vs. HFD, $p < 0.0001$) and *Proteobacteria* (SD + SF68 vs. SD, $p = 0.0088$; HFD + SF68 vs. HFD, $p = 0.0203$) compared to untreated animals (Figure 4A). An increase in the abundance of *Actinobacteria* was observed in normal weight mice that received the formulation ($p = 0.0001$). Both groups receiving the probiotic displayed a significant increase in the amount of bacteria belonging to the *Bifidobacterium* genus (SD + SF68 vs. SD, $p = 0.0042$; HFD + SF68 vs. HFD, $p = 0.0364$) and a reduction in *Prevotella* (SD + SF68 vs. SD, $p = 0.0008$; HFD + SF68 vs. HFD, $p < 0.0001$) in comparison with SD and HFD controls. A significant reduction was also evidenced in the amount of

Bacteroides in SD + SF68 animals compared to SD controls ($p = 0.0002$).

Ileal microbiota composition after probiotic treatment in SD- and HFD-fed mice

Absolute quantifications of bacteria in ileal samples revealed increased abundance of the phylum *Bacteroidetes* ($p = 0.0092$) and the genus *Faecalibacterium* ($p = 0.0352$) in HFD + SF68 group in comparison with HFD controls (Figure 4B). In addition, an increase in *Lactobacillus* was observed after probiotic treatment in both SD- and HFD-fed mice (SD + SF68 vs. SD, $p = 0.0255$; HFD + SF68 vs. HFD, $p = 0.0004$).

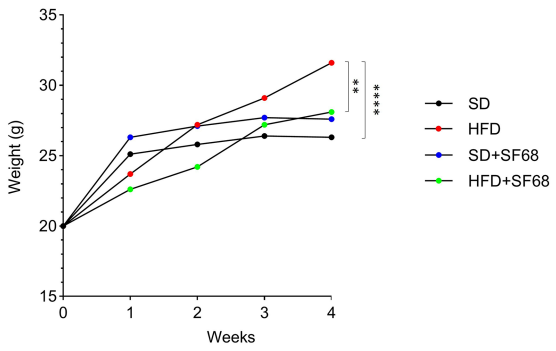

FIGURE 2
Weight variations in groups SD, SD+SF68, HFD, and HFD+SF68 registered weekly up to 4 weeks. **p<0.01; ****p<0.0001.

Akkermansia muciniphila abundance in the ileal mucosa

The amount of *Akkermansia* was significantly lower in obese (HFD) than normal weight (SD) mice ($p = 0.0026$; Figure 5). Notably, a remarkable increase of this microorganism was revealed in HFD + SF68 mice ($4.63 \times 10^2 \pm 3.68 \times 10^2$ of DNA copies/mg of ileum) compared to HFD-fed animals ($7.45 \times 10^{-1} \pm 4.41 \times 10^{-1}$ DNA copies/mg of ileum; $p = 0.0341$; Figure 5).

Discussion

Mice are the most commonly used animals to study obesity after inducing this condition with either monogenic mutations or high-fat diets (Fuchs et al., 2018). High-fat diets have been shown to mimic more faithfully the overall metabolic and physiological alterations observed in obese individuals (Antonioli et al., 2020). For this reason, we selected this procedure to establish a proper experimental model of obesity and to obtain a more representative analysis of the gut microbiota, which was performed on both fecal and ileal samples. In fact, to investigate the entire gut microbiota composition, the analysis of feces alone might not be sufficient (Raoult and Henrissat, 2014; Li et al., 2017), since the microbial community associated with the host's mucus, in particular that residing in the ileal tract, is not adequately represented in the stool. In addition, mucus-associated microorganisms of the upper intestine are actively involved in several physiological processes, such as immune regulation, inflammatory responses (Raoult, 2017), nutrient absorption, particularly of simple

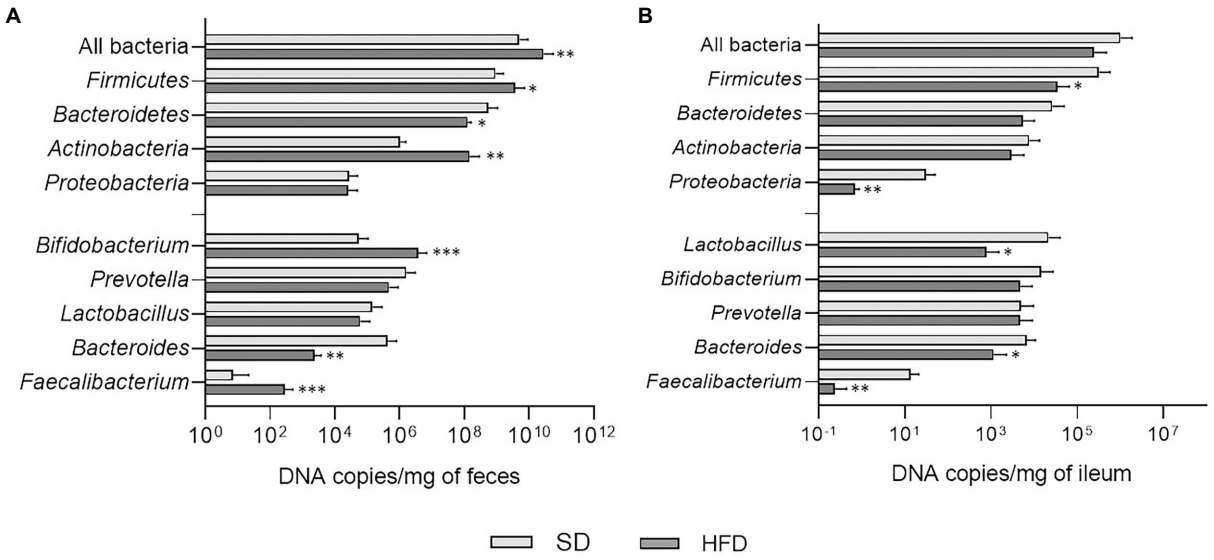

FIGURE 3
(A) Absolute abundances of total bacterial load, phyla, and genera in fecal samples of mice belonging to SD and HFD groups. **(B)** Absolute abundances of total bacterial load, phyla, and genera in ileal samples of mice belonging to SD and HFD groups. *p<0.05; **p<0.01; ***p<0.001.

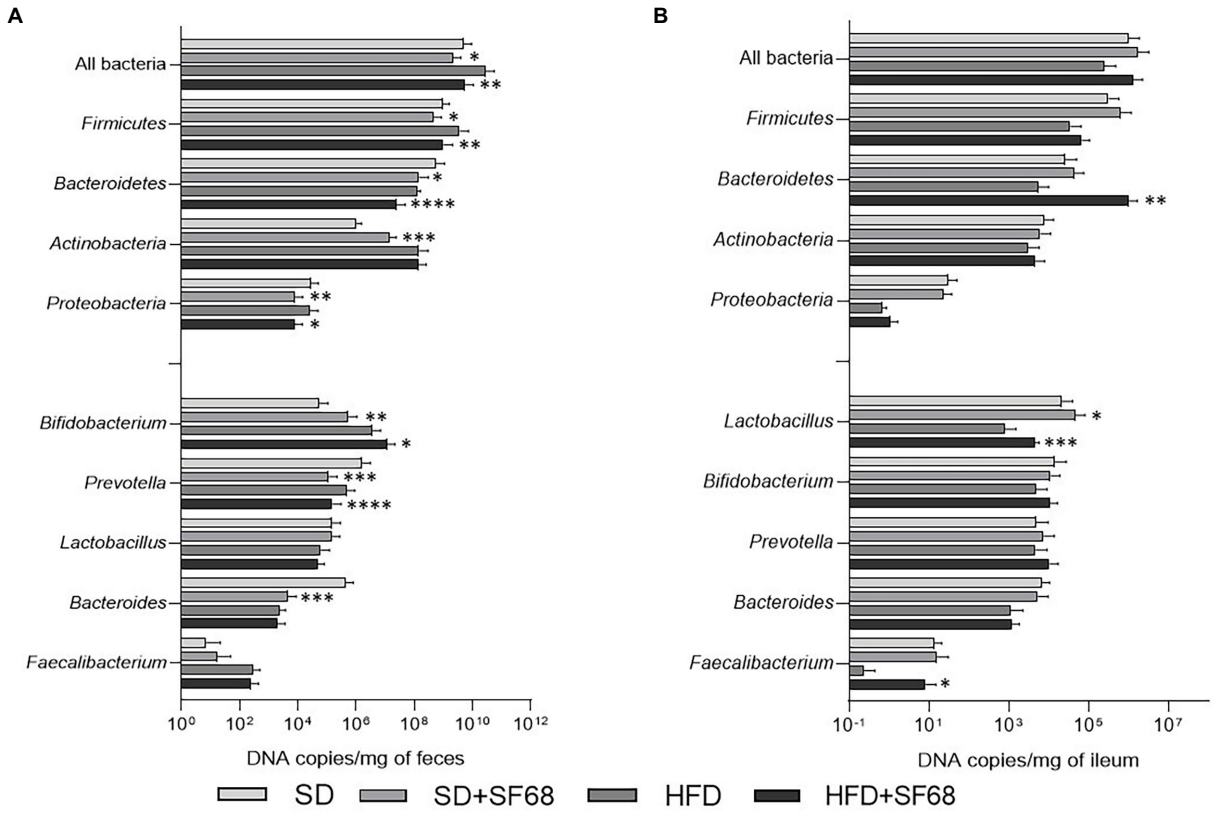

FIGURE 4
(A) Absolute abundances of total bacterial load, phyla, and genera in fecal samples of mice fed with SD or HFD with or without SF68 administration. **(B)** Absolute abundances of total bacterial load, phyla, and genera in ileal samples in both mice fed with SD or HFD with or without SF68 administration. Statistical comparisons were carried out between SD and SD+SF68, and HFD and HFD+SF68. *p<0.05; **p<0.01; ***p<0.001; ****p<0.0001.

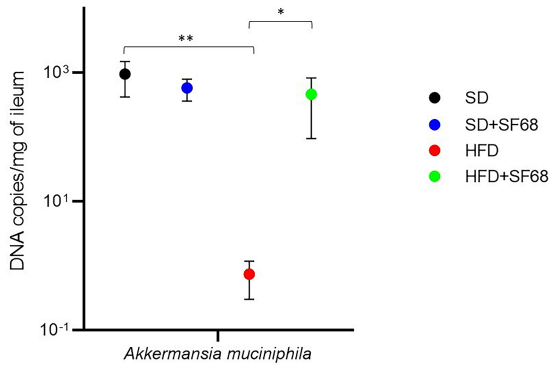

FIGURE 5
Variations in the absolute abundance of *Akkermansia muciniphila* in ileal tissues in both normal weight (SD) and obese (HFD) mice with or without SF68 administration. Statistical comparisons were carried out between SD and SD+SF68, and HFD and HFD+SF68. *p<0.05; **p<0.01.

sugars (Raoult and Henrissat, 2014), and energy intake (Aron-Wisnewsky et al., 2012), which altogether play a key role in the development of obesity.

In our study, mice fed with HFD displayed a remarkable weight gain and substantial variations in their gut microbiota composition, which is usually found dysbiotic in obese individuals (Abenavoli et al., 2019). In particular, obese animals showed an increased fecal abundance of *Firmicutes* and *Actinobacteria*. Previous studies already showed an increase of members belonging to these phyla in fecal samples of obese subjects (Turnbaugh et al., 2006; Clarke et al., 2012; Grigor'eva, 2020). These samples were also demonstrated to contain a higher abundance of bacterial genes commonly associated with obesity and mainly derived from *Actinobacteria* and *Firmicutes* (Turnbaugh et al., 2009). The enrichment in *Firmicutes*, the most abundant phylum in both murine and human gut, has also been associated with increased nutrient absorption, thus suggesting *Firmicutes* as main microbial actors in obesity (Jumpertz et al., 2011).

In accordance with studies performed on obese subjects, which report low intestinal levels of *Bacteroides* being associated with visceral adiposity and obesity (Yin et al., 2022), we observed a reduction in the abundance of *Bacteroides* in both the feces and ileal mucosa of obese mice. We also detected a relevant decrease in *Lactobacillus* and *Faecalibacterium* in ileal samples of obese

mice, consistently with previous studies regarding obesity, non-alcoholic fatty liver disease, and inflammatory bowel diseases (Sokol et al., 2009; Million et al., 2013; Lopez-Siles et al., 2018; Iino et al., 2019). Lactobacilli represent an important component of the microbial community residing in the human gut and exert a variety of beneficial properties (Li et al., 2017; Villmones et al., 2018), which make them the most common probiotics available in the worldwide market (Slattery et al., 2019). On the other hand, *F. prausnitzii*, the unique species belonging to the genus *Faecalibacterium* up to date, is considered a bioindicator for human health (Ferreira-Halder et al., 2017), exerting anti-inflammatory activities (Martín et al., 2015), producing butyrate (Louis and Flint, 2009), and improving the gut barrier function (Carlsson et al., 2013). We can therefore strongly presume that the reduction of *Lactobacillus* and *Faecalibacterium* observed in the HFD group hampered the preservation of a healthy condition in mice. The overall weight gain in HFD mice alongside with the variations we observed in both fecal and ileal microbiota allowed us to assert the robustness of our murine model of obesity.

Since specific *Enterococcus* strains display beneficial effects and satisfactory safety profiles when administered in a variety of pathological conditions in humans (Holzapfel et al., 2018), we wondered whether the oral administration of a probiotic formulation based on *E. faecium* SF68 was able to counteract the excessive weight gain associated with the obesogenic diet and prevent the shift to a dysbiotic gut microbiota. Some strains of *Enterococcus* are known for their ability to lower serum cholesterol (i.e., *E. faecium* CRL 183, M74, and WEFA23) (Foulquié Moreno et al., 2006; Franz et al., 2011; Zhang et al., 2017), exert anti-inflammatory activities (i.e., *E. faecium* M-74 1, *E. durans* M4, and M5) (Avram-Hananel et al., 2010; Franz et al., 2011), increase insulin and leptin sensitivity and reduce adipocyte hypertrophy and fat accumulation (i.e., *E. faecalis* AG5; Mishra and Ghosh, 2020), and directly modulate the intestinal microbial composition (i.e., *E. faecium* L5, and R0026; Tarasova et al., 2010; Huang et al., 2021), thus showing endearing features in the management of obesity (De Carvalho Marchesin et al., 2018; Jiang et al., 2021). *E. faecium* SF68 is a well-known *Enterococcus* probiotic strains contained in commercialized formulations and has been proven to be safe and effective in the treatment of acute diarrhea (Allen et al., 2010; Greuter et al., 2020).

E. faecium SF68 administration to HFD-fed mice resulted in a remarkably lower weight gain. The concurrent variations observed in the intestinal microbiota were altogether encouraging. A reduction of fecal *Firmicutes* abundance was detected in both SD + SF68 and HFD + SF68 mice, thus suggesting an active role of the *Enterococcus* strain in the modulation of *Firmicutes* and in the preservation of an eubiotic state. Interestingly, in fecal samples of both SD- and HFD-fed mice a reduction in *Proteobacteria* after SF68 treatment was also detected. *Proteobacteria* are usually present in small percentages within a healthy gut microbiota. In fact, an association between high abundance of *Proteobacteria* and gut dysbiosis, which often occurs in case of metabolic disorders, intestinal inflammation, and obesity, has been proven (Shin et al., 2015; Litvak et al., 2017).

The abundance of *Bifidobacterium* notably increased in the fecal microbiota of SF68-treated SD- and HFD-fed mice. The correlation between the amount of bifidobacteria and obesity is well-established. A few studies reported higher *Bifidobacterium* abundances to be associated with normal weight conditions (Kalliomäki et al., 2008) and demonstrated that *Bifidobacterium* spp. negatively correlate with endotoxemia and positively correlate with improved glucose tolerance, reduced plasma levels of pro-inflammatory cytokines (Cani et al., 2007b), and higher mucus thickness (Moreira et al., 2012). Additionally, bifidobacteria have been proven to ameliorate obesity-related conditions, for example by reducing cholesterol and glucose levels (Yin et al., 2010; An et al., 2011).

A greater abundance of *Prevotella* in obese individuals (Stanislawski et al., 2019), as well as in patients with hypertension (Dan et al., 2019), has recently been reported. Our finding that *Prevotella* decreased in the fecal samples of both groups of mice after SF68 treatment supports the hypothesis that the reduction of this genus potentially corresponds to an improvement in mice's overall wellbeing. The administration of SF68 also resulted in higher amounts of *Lactobacillus* and *Faecalibacterium* in the ileal mucosa of HFD-fed mice. Besides their aforementioned properties, microbes belonging to *Bifidobacterium*, *Lactobacillus*, and *Faecalibacterium* are additionally able to produce SCFAs. These compounds exert a variety of beneficial effects both at local and systemic level and can therefore ameliorate the clinical characteristics of obese patients (Canfora et al., 2015).

A. muciniphila is well-known for its inverse correlation with obesity, type 2 diabetes, and other metabolic conditions, such as hypercholesterolemia and fatty liver disease (Xu et al., 2020). Conversely, high levels of *Akkermansia* are associated with a better metabolic status, in particular with higher leptin sensitivity, lower fasting blood glucose and insulin resistance, and lower adipocyte size (Dao et al., 2016). Some of the molecular mechanisms of these associations are known. *A. muciniphila* is able to produce SCFAs as a result of mucin degradation (Ottman et al., 2017) and can counteract the onset of obesity by reducing appetite, energy intake, systemic inflammation, and blood pressure, and improve the gut barrier function (Le Blanc et al., 2017; Chambers et al., 2018). Similarly to results obtained in previous studies in which *A. muciniphila* was found to be decreased in obese mice (Everard et al., 2013), we assessed that the HFD-fed group displayed a lower abundance of this microorganism than animals receiving the standard diet. The administration of *E. faecium* SF68 to HFD-fed mice significantly increased *Akkermansia* levels, thus suggesting that the administration of such a probiotic could have a positive impact on the metabolism of mice fed with HFD.

In conclusion, relevant results were obtained when *E. faecium* SF68 was administered to mice fed with a high-fat diet, demonstrating its ability to positively influence the gut microbial community both at luminal and mucosal level and to counteract the weight gain that occurs with an obesogenic diet. Several variations in the microbiota composition were highlighted, such

as the reduction in *Firmicutes* and *Proteobacteria* and the increase in *Bifidobacterium* in fecal samples, as well as an increase in *Faecalibacterium*, *Lactobacillus*, and *Akkermansia* in ileal samples. These findings evidence the potential of *E. faecium* SF68 as a promising approach for the co-treatment and prevention of obesity, also opening new perspectives in the study of the molecular mechanisms underlying its beneficial effect.

Data availability statement

The datasets presented in this study can be found in online repositories. The names of the repository/repositories and accession number(s) can be found at: http://doi.org/10.17632/2syf8c7fsh.1.

Ethics statement

The animal study was reviewed and approved by the Italian Ministry of Health (authorization 955/2018-PR).

Author contributions

MF, LA, and EG: conception and design of the study, validation, formal analysis, and supervision. AP, MC, LB, VD'A, CP, CS, DM, and FC: methodology and investigation. AP and MC: writing – original draft preparation. AP, MC, LB, VD'A, CP, CS, DM, FC, MF, LA, and EG: writing – review and editing. All authors have read and agreed to the published version of the manuscript.

Funding

This study was funded by grants from the University of Pisa (EG) and by Cerbios-Pharma SA (MF and LA).

Conflict of interest

The authors declare that the research was conducted in the absence of any commercial or financial relationships that could be construed as a potential conflict of interest.

Publisher's note

All claims expressed in this article are solely those of the authors and do not necessarily represent those of their affiliated organizations, or those of the publisher, the editors and the reviewers. Any product that may be evaluated in this article, or claim that may be made by its manufacturer, is not guaranteed or endorsed by the publisher.

References

Abenavoli, L., Scarpellini, E., Colica, C., Boccuto, L., Salehi, B., Sharifi-Rad, J., et al. (2019). Gut microbiota and obesity: a role for probiotics. *Nutrients* 11:2690. doi: 10.3390/nu11112690

Allen, S. J., Martinez, E. G., Gregorio, G. V., and Dans, L. F. (2010). Probiotics for treating acute infectious diarrhoea. *Cochrane Database Syst. Rev.* 2010:CD003048. doi: 10.1002/14651858.CD003048.pub3

An, H. M., Park, S. Y., Lee, D. K., Kim, J. R., Cha, M. K., Lee, S. W., et al. (2011). Antiobesity and lipid-lowering effects of *Bifidobacterium* spp. in high fat diet-induced obese rats. *Lipids Health Dis.* 10:116. doi: 10.1186/1476-511X-10-116

Antonioli, L., D'Antongiovanni, V., Pellegrini, C., Fornai, M., Benvenuti, L., di Carlo, A., et al. (2020). Colonic dysmotility associated with high-fat diet-induced obesity: role of enteric glia. *FASEB J.* 34, 5512–5524. doi: 10.1096/fj.201901844R

Aron-Wisnewsky, J., Doré, J., and Clement, K. (2012). The importance of the gut microbiota after bariatric surgery. *Nat. Rev. Gastroenterol. Hepatol.* 9, 590–598. doi: 10.1038/nrgastro.2012.161

Avram-Hananel, L., Stock, J., Parlesak, A., Bode, C., and Schwartz, B. (2010). *E. durans* strain M4-5 isolated from human colonic flora attenuates intestinal inflammation. *Dis. Colon Rectum* 53, 1676–1686. doi: 10.1007/DCR.0b013e3181f4b148

Azad, M. A. K., Sarker, M., Li, T., and Yin, J. (2018). Probiotic species in the modulation of gut microbiota: an overview. *Biomed. Res. Int.* 2018:9478630. doi: 10.1155/2018/9478630

Bagarolli, R. A., Tobar, N., Oliveira, A. G., Araújo, T. G., Carvalho, B. M., Rocha, G. Z., et al. (2017). Probiotics modulate gut microbiota and improve insulin sensitivity in DIO mice. *J. Nutr. Biochem.* 50, 16–25. doi: 10.1016/j.jnutbio.2017.08.006

Biagini, F., Calvigioni, M., Lapomarda, A., Vecchione, A., Magliaro, C., De Maria, C., et al. (2020). A novel 3D in vitro model of the human gut microbiota. *Sci. Rep.* 10:21499. doi: 10.1038/s41598-020-78591-w

Bibbò, S., Ianiro, G., Giorgio, V., Scaldaferri, F., Masucci, L., Gasbarrini, A., et al. (2016). The role of diet on gut microbiota composition. *Eur. Rev. Med. Pharmacol. Sci.* 20, 4742–4749. PMID: 27906427

Canfora, E. E., Jocken, J. W., and Blaak, E. E. (2015). Short-chain fatty acids in control of body weight and insulin sensitivity. *Nat. Rev. Endocrinol.* 11, 577–591. doi: 10.1038/nrendo.2015.128

Cani, P. D., Amar, J., Iglesias, M. A., Poggi, M., Knauf, C., Bastelica, D., et al. (2007a). Metabolic endotoxemia initiates obesity and insulin resistance. *Diabetes* 56, 1761–1772. doi: 10.2337/db06-1491

Cani, P. D., Neyrinck, A. M., Fava, F., Knauf, C., Burcelin, R. G., Tuohy, K. M., et al. (2007b). Selective increases of bifidobacteria in gut microflora improve high-fat-diet-induced diabetes in mice through a mechanism associated with endotoxaemia. *Diabetologia* 50, 2374–2383. doi: 10.1007/s00125-007-0791-0

Carlsson, A. H., Yakymenko, O., Olivier, I., Håkansson, F., Postma, E., Keita, A. V., et al. (2013). *Faecalibacterium prausnitzii* supernatant improves intestinal barrier function in mice DSS colitis. *Scand. J. Gastroenterol.* 48, 1136–1144. doi: 10.3109/00365521.2013.828773

Cerdó, T., García-Santos, J. A., Bermúdez, M. G., and Campoy, C. (2019). The role of probiotics and prebiotics in the prevention and treatment of obesity. *Nutrients* 11:635. doi: 10.3390/nu11030635

Chambers, E. S., Preston, T., Frost, G., and Morrison, D. J. (2018). Role of gut microbiota-generated short-chain fatty acids in metabolic and cardiovascular health. *Curr. Nutr. Rep.* 7, 198–206. doi: 10.1007/s13668-018-0248-8

Clarke, S. F., Murphy, E. F., Nilaweera, K., Ross, P. R., Shanahan, F., O'Toole, P. W., et al. (2012). The gut microbiota and its relationship to diet and obesity: new insights. *Gut Microbes* 3, 186–202. doi: 10.4161/gmic.20168

Collado, M. C., Derrien, M., Isolauri, E., de Vos, W. M., and Salminen, S. (2007). Intestinal integrity and *Akkermansia muciniphila*, a mucin-degrading member of the intestinal microbiota present in infants, adults, and the elderly. *Appl. Environ. Microbiol.* 73, 7767–7770. doi: 10.1128/AEM.01477-07

Da Silva, T. F., Casarotti, S. N., de Oliveira, G. L. V., and Penna, A. L. B. (2021). The impact of probiotics, prebiotics, and synbiotics on the biochemical, clinical, and immunological markers, as well as on the gut microbiota of obese hosts. *Crit. Rev. Food Sci. Nutr.* 61, 337–355. doi: 10.1080/10408398.2020.1733483

Dan, X., Mushi, Z., Baili, W., Han, L., Enqi, W., Huanhu, Z., et al. (2019). Differential analysis of hypertension-associated intestinal microbiota. *Int. J. Med. Sci.* 16, 872–881. doi: 10.7150/ijms.29322

Dao, M. C., Everard, A., Aron-Wisnewsky, J., Sokolovska, N., Prifti, E., Verger, E. O., et al. (2016). *Akkermansia muciniphila* and improved metabolic health during a dietary intervention in obesity: relationship with gut microbiome richness and ecology. *Gut* 65, 426–436. doi: 10.1136/gutjnl-2014-308778

De Carvalho Marchesin, J., Celiberto, L. S., Orlando, A. B., De Medeiros, A. I., Pinto, R. A., Zuanon, J. A. S., et al. (2018). A soy-based probiotic drink modulates the microbiota and reduces body weight gain in diet-induced obese mice. *J. Funct. Foods* 48, 302–313. doi: 10.1016/j.jff.2018.07.010

Ejtahed, H. S., Angoorani, P., Soroush, A. R., Atlasi, R., Hasani-Ranjbar, S., Mortazavian, A. M., et al. (2019). Probiotics supplementation for the obesity management: a systematic review of animal studies and clinical trials. *J. Funct. Foods* 52, 228–242. doi: 10.1016/j.jff.2018.10.039

Ejtahed, H. S., Mohtadi-Nia, J., Homayouni-Rad, A., Niafar, M., Asghari-Jafarabadi, M., Mofid, V., et al. (2011). Effect of probiotic yogurt containing *Lactobacillus acidophilus* and *Bifidobacterium lactis* on lipid profile in individuals with type 2 diabetes mellitus. *J. Dairy Sci.* 94, 3288–3294. doi: 10.3168/jds.2010-4128

Everard, A., Belzer, C., Geurts, L., Ouwerkerk, J. P., Druart, C., Bindels, L. B., et al. (2013). Crosstalk between *Akkermansia muciniphila* and intestinal epithelium controls diet-induced obesity. *Proc. Natl. Acad. Sci. U. S. A.* 110, 9066–9071. doi: 10.1073/pnas.1219451110

Ferreira-Halder, C. V., Faria, A. V. S., and Andrade, S. S. (2017). Action and function of *Faecalibacterium prausnitzii* in health and disease. *Best Pract. Res. Clin. Gastroenterol.* 31, 643–648. doi: 10.1016/j.bpg.2017.09.011

Food and Agricultural Organization of the United Nations and World Health Organization. (2001). *Health and Nutritional Properties of Probiotics in Food Including Powder Milk With Live Lactic Acid Bacteria*. Rome: FAO.

Foulquié Moreno, M. R., Sarantinopoulos, P., Tsakalidou, E., and De Vuyst, L. (2006). The role and application of enterococci in food and health. *Int. J. Food Microbiol.* 106, 1–24. doi: 10.1016/j.ijfoodmicro.2005.06.026

Franz, C. M., Huch, M., Abriouel, H., Holzapfel, W., and Gálvez, A. (2011). Enterococci as probiotics and their implications in food safety. *Int. J. Food Microbiol.* 151, 125–140. doi: 10.1016/j.ijfoodmicro.2011.08.014

Frasca, D., Blomberg, B. B., and Paganelli, R. (2017). Aging, obesity, and inflammatory age-related diseases. *Front. Immunol.* 8:1745. doi: 10.3389/fimmu.2017.01745

Fuchs, T., Loureiro, M. P., Macedo, L. E., Nocca, D., Nedelcu, M., and Costa-Casagrande, T. A. (2018). Animal models in metabolic syndrome. *Rev. Col. Bras. Cir.* 45:e1975. doi: 10.1590/0100-6991e-20181975

Ganji-Arjenaki, M., and Rafieian-Kopaei, M. (2018). Probiotics are a good choice in remission of inflammatory bowel diseases: a meta-analysis and systematic review. *J. Cell. Physiol.* 233, 2091–2103. doi: 10.1002/jcp.25911

Gérard, P. (2016). Gut microbiota and obesity. *Cell. Mol. Life Sci.* 73, 147–162. doi: 10.1007/s00018-015-2061-5

Green, M., Arora, K., and Prakash, S. (2020). Microbial medicine: prebiotic and probiotic functional foods to target obesity and metabolic syndrome. *Int. J. Mol. Sci.* 21:2890. doi: 10.3390/ijms21082890

Greuter, T., Michel, M. C., Thomann, D., Weigmann, H., and Vavricka, S. R. (2020). Randomized, placebo-controlled, double-blind, and open-label studies in the treatment and prevention of acute diarrhea with *Enterococcus faecium* SF68. *Front. Med.* 7:276. doi: 10.3389/fmed.2020.00276

Grigor'eva, I. N. (2020). Gallstone disease, obesity and the *Firmicutes*/*Bacteroidetes* ratio as a possible biomarker of gut dysbiosis. *J. Pers. Med.* 11:13. doi: 10.3390/jpm11010013

Holzapfel, W., Arini, A., Aeschbacher, M., Coppolecchia, R., and Pot, B. (2018). *Enterococcus faecium* SF68 as a model for efficacy and safety evaluation of pharmaceutical probiotics. *Benef. Microbes* 9, 375–388. doi: 10.3920/BM2017.0148

Huang, J., Huang, J., Yin, T., Lv, H., Zhang, P., and Li, H. (2021). *Enterococcus faecium* R0026 combined with *Bacillus subtilis* R0179 prevent obesity-associated hyperlipidemia and modulate gut microbiota in C57BL/6 mice. *J. Microbiol. Biotechnol.* 31, 181–188. doi: 10.4014/jmb.2009.09005

Iino, C., Endo, T., Mikami, K., Hasegawa, T., Kimura, M., Sawada, N., et al. (2019). Significant decrease in *Faecalibacterium* among gut microbiota in non-alcoholic fatty liver disease: a large BMI- and sex-matched population study. *Hepatol. Int.* 13, 748–756. doi: 10.1007/s12072-019-09987-8

Jiang, J., Xiong, J., Ni, J., Chen, C., and Wang, K. (2021). Live combined *B. subtilis* and *E. faecium* alleviate liver inflammation, improve intestinal barrier function, and modulate gut microbiota in mice with non-alcoholic fatty liver disease. *Med. Sci. Monit.* 27:e931143. doi: 10.12659/MSM.931143

Jumpertz, R., Le, D. S., Turnbaugh, P. J., Trinidad, C., Bogardus, C., Gordon, J. I., et al. (2011). Energy-balance studies reveal associations between gut microbes, caloric load, and nutrient absorption in humans. *Am. J. Clin. Nutr.* 94, 58–65. doi: 10.3945/ajcn.110.010132

Kalliomäki, M., Collado, M. C., Salminen, S., and Isolauri, E. (2008). Early differences in fecal microbiota composition in children may predict overweight. *Am. J. Clin. Nutr.* 87, 534–538. doi: 10.1093/ajcn/87.3.534

Kim, M., Park, T., and Yu, Z. (2017). Metagenomic investigation of gastrointestinal microbiome in cattle. *Asian Australas J. Anim. Sci.* 30, 1515–1528. doi: 10.5713/ajas.17.0544

Le Blanc, J. G., Chain, F., Martín, R., Bermúdez-Humarán, L. G., Courau, S., and Langella, P. (2017). Beneficial effects on host energy metabolism of short-chain fatty acids and vitamins produced by commensal and probiotic bacteria. *Microb. Cell Factories* 16:79. doi: 10.1186/s12934-017-0691-z

Li, D., Chen, H., Mao, B., Yang, Q., Zhao, J., Gu, Z., et al. (2017). Microbial biogeography and core microbiota of the rat digestive tract. *Sci. Rep.* 8:45840. doi: 10.1038/srep45840

Litvak, Y., Byndloss, M. X., Tsolis, R. M., and Bäumler, A. J. (2017). Dysbiotic *Proteobacteria* expansion: a microbial signature of epithelial dysfunction. *Curr. Opin. Microbiol.* 39, 1–6. doi: 10.1016/j.mib.2017.07.003

Lopez-Siles, M., Enrich-Capó, N., Aldeguer, X., Sabat-Mir, M., Duncan, S. H., Garcia-Gil, L. J., et al. (2018). Alterations in the abundance and co-occurrence of *Akkermansia muciniphila* and *Faecalibacterium prausnitzii* in the colonic mucosa of inflammatory bowel disease subjects. *Front. Cell. Infect. Microbiol.* 8:281. doi: 10.3389/fcimb.2018.00281

Louis, P., and Flint, H. J. (2009). Diversity, metabolism, and microbial ecology of butyrate-producing bacteria from the human large intestine. *FEMS Microbiol. Lett.* 294, 1–8. doi: 10.1111/j.1574-6968.2009.01514.x

Martín, R., Miquel, S., Chain, F., Natividad, J. M., Jury, J., Lu, J., et al. (2015). *Faecalibacterium prausnitzii* prevents physiological damages in a chronic low-grade inflammation murine model. *BMC Microbiol.* 15:67. doi: 10.1186/s12866-015-0400-1

Matsuki, T., Watanabe, K., Fujimoto, J., Miyamoto, Y., Takada, T., Matsumoto, K., et al. (2002). Development of 16S rRNA-gene-targeted group-specific primers for the detection and identification of predominant bacteria in human feces. *Appl. Environ. Microbiol.* 68, 5445–5451. doi: 10.1128/AEM.68.11.5445-5451.2002

Mekonnen, S. A., Merenstein, D., Fraser, C. M., and Marco, M. L. (2020). Molecular mechanisms of probiotic prevention of antibiotic-associated diarrhea. *Curr. Opin. Biotechnol.* 61, 226–234. doi: 10.1016/j.copbio.2020.01.005

Million, M., Angelakis, E., Maraninchi, M., Henry, M., Giorgi, R., Valero, R., et al. (2013). Correlation between body mass index and gut concentrations of *lactobacillus reuteri*, *Bifidobacterium animalis*, *Methanobrevibacter smithii*, and *Escherichia coli*. *Int. J. Obes.* 37, 1460–1466. doi: 10.1038/ijo.2013.20

Mishra, A. K., and Ghosh, A. R. (2020). Probiotic *Enterococcus faecalis* AG5 mitigated high fat diet induced obesity and produced propionic acid stimulated apoptosis in 3T3-L1 pre-adipocyte. *Life Sci.* 261:118292. doi: 10.1016/j.lfs.2020.118292

Moayyedi, P., Ford, A. C., Talley, N. J., Cremonini, F., Foxx-Orenstein, A. E., Brandt, L. J., et al. (2010). The efficacy of probiotics in the treatment of irritable bowel syndrome: a systematic review. *Gut* 59, 325–332. doi: 10.1136/gut.2008.167270

Moreira, A. P., Texeira, T. F., Ferreira, A. B., Peluzio Mdo, C., and Alfenas Rde, C. (2012). Influence of a high-fat diet on gut microbiota, intestinal permeability and metabolic endotoxaemia. *Br. J. Nutr.* 108, 801–809. doi: 10.1017/S0007114512001213

Ottman, N., Geerlings, S. Y., Aalvink, S., de Vos, W. M., and Belzer, C. (2017). Action and function of *Akkermansia muciniphila* in microbiome ecology, health and disease. *Best Pract. Res. Clin. Gastroenterol.* 31, 637–642. doi: 10.1016/j.bpg.2017.10.001

Raoult, D. (2017). The study of microbiota needs both microbiologists and medical doctors. *Clin. Microbiol. Infect.* 23, 500–501. doi: 10.1016/j.cmi.2017.03.002

Raoult, D., and Henrissat, B. (2014). Are stool samples suitable for studying the link between gut microbiota and obesity? *Eur. J. Epidemiol.* 29, 307–309. doi: 10.1007/s10654-014-9905-4

Sánchez, B., Delgado, S., Blanco-Míguez, A., Lourenço, A., Gueimonde, M., and Margolles, A. (2017). Probiotics, gut microbiota, and their influence on host health and disease. *Mol. Nutr. Food Res.* 61:1600240. doi: 10.1002/mnfr.201600240

Shin, N. R., Whon, T. W., and Bae, J. W. (2015). *Proteobacteria*: microbial signature of dysbiosis in gut microbiota. *Trends Biotechnol.* 33, 496–503. doi: 10.1016/j.tibtech.2015.06.011

Slattery, C., Cotter, P. D., and O'Toole, P. W. (2019). Analysis of health benefits conferred by *Lactobacillus* species from kefir. *Nutrients* 11:1252. doi: 10.3390/nu11061252

Sokol, H., Seksik, P., Furet, J. P., Firmesse, O., Nion-Larmurier, I., Beaugerie, L., et al. (2009). Low counts of *Faecalibacterium prausnitzii* in colitis microbiota. *Inflamm. Bowel Dis.* 15, 1183–1189. doi: 10.1002/ibd.20903

Stach, J. E., Maldonado, L. A., Ward, A. C., Goodfellow, M., and Bull, A. T. (2003). New primers for the class *Actinobacteria*: application to marine and terrestrial environments. *Environ. Microbiol.* 5, 828–841. doi: 10.1046/j.1462-2920.2003.00483.x

Stanislawski, M. A., Dabelea, D., Lange, L. A., Wagner, B. D., and Lozupone, C. A. (2019). Gut microbiota phenotypes of obesity. *NPJ Biofilms Microbiomes* 5:18. doi: 10.1038/s41522-019-0091-8

Tarasova, E., Yermolenko, E., Donets, V., Sundukova, Z., Bochkareva, A., Borshev, I., et al. (2010). The influence of probiotic *Enterococcus faecium* strain L5 on the microbiota and cytokines expression in rats with dysbiosis induced by antibiotics. *Benef. Microbes* 1, 265–270. doi: 10.3920/BM2010.0008

Tenorio-Jiménez, C., Martínez-Ramírez, M. J., Gil, Á., and Gómez-Llorente, C. (2020). Effects of probiotics on metabolic syndrome: a systematic review of randomized clinical trials. *Nutrients* 12:124. doi: 10.3390/nu12010124

Turnbaugh, P. J., Hamady, M., Yatsunenko, T., Cantarel, B. L., Duncan, A., Ley, R. E., et al. (2009). A core gut microbiome in obese and lean twins. *Nature* 457, 480–484. doi: 10.1038/nature07540

Turnbaugh, P. J., Ley, R. E., Mahowald, M. A., Magrini, V., Mardis, E. R., and Gordon, J. I. (2006). An obesity-associated gut microbiome with increased capacity for energy harvest. *Nature* 444, 1027–1031. doi: 10.1038/nature05414

Villmones, H. C., Haug, E. S., Ulvestad, E., Grude, N., Stenstad, T., Halland, A., et al. (2018). Species level description of the human ileal bacterial microbiota. *Sci. Rep.* 8:4736. doi: 10.1038/s41598-018-23198-5

Xu, Y., Wang, N., Tan, H. Y., Li, S., Zhang, C., and Feng, Y. (2020). Function of *Akkermansia muciniphila* in obesity: interactions with lipid metabolism, immune response, and gut systems. *Front. Microbiol.* 11:219. doi: 10.3389/fmicb.2020.00219

Yadav, H., Lee, J. H., Lloyd, J., Walter, P., and Rane, S. G. (2013). Beneficial metabolic effects of a probiotic via butyrate-induced GLP-1 hormone secretion. *J. Biol. Chem.* 288, 25088–25097. doi: 10.1074/jbc.M113.452516

Yin, X. Q., An, Y. X., Yu, C. G., Ke, J., Zhao, D., and Yu, K. (2022). The association between fecal short-chain fatty acids, gut microbiota, and visceral fat in monozygotic twin pairs. *Diabetes Metab. Syndr. Obes.* 15, 359–368. doi: 10.2147/DMSO.S338113

Yin, Y. N., Yu, Q. F., Fu, N., Liu, X. W., and Lu, F. G. (2010). Effects of four *Bifidobacteria* on obesity in high-fat diet induced rats. *World J. Gastroenterol.* 16, 3394–3401. doi: 10.3748/wjg.v16.i27.3394

Zhang, F., Qiu, L., Xu, X., Liu, Z., Zhan, H., Tao, X., et al. (2017). Beneficial effects of probiotic cholesterol-lowering strain of *Enterococcus faecium* WEFA23 from infants on diet-induced metabolic syndrome in rats. *J. Dairy Sci.* 100, 1618–1628. doi: 10.3168/jds.2016-11870

frontiers | Frontiers in Microbiology

TYPE Original Research
PUBLISHED 22 December 2022
DOI 10.3389/fmicb.2022.1051200

OPEN ACCESS

EDITED BY
Giovanni Tarantino,
University of Naples Federico II, Italy

REVIEWED BY
Huizi Tan,
Nanchang University,
China
Naga Betrapally,
National Cancer Institute (NIH),
United States
Anita Y. Voigt,
Jackson Laboratory for Genomic Medicine,
United States

*CORRESPONDENCE
Hongmei Yin
232869043@qq.com
Congwei Gu
gcw081543@swmu.edu.cn

†These authors have contributed equally to this work

SPECIALTY SECTION
This article was submitted to Microorganisms in Vertebrate Digestive Systems, a section of the journal Frontiers in Microbiology

RECEIVED 22 September 2022
ACCEPTED 25 November 2022
PUBLISHED 22 December 2022

CITATION
Yan G, Li S, Wen Y, Luo Y, Huang J, Chen B, Lv S, Chen L, He L, He M, Yang Q, Yu Z, Xiao W, Tang Y, Li W, Han J, Zhao F, Yu S, Kong F, Abbasi B, Yin H and Gu C (2022) Characteristics of intestinal microbiota in C57BL/6 mice with non-alcoholic fatty liver induced by high-fat diet.
Front. Microbiol. 13:1051200.
doi: 10.3389/fmicb.2022.1051200

Characteristics of intestinal microbiota in C57BL/6 mice with non-alcoholic fatty liver induced by high-fat diet

Guangwen Yan[1†], Shuaibing Li[2,3†], Yuhang Wen[2,3†], Yadan Luo[2,3], Jingrong Huang[2,3], Baoting Chen[2,3], Shuya Lv[2,3], Lang Chen[2,3], Lvqin He[2,3], Manli He[2,3], Qian Yang[2,3], Zehui Yu[2,3†], Wudian Xiao[2,3], Yong Tang[3,4], Weiyao Li[5], Jianhong Han[2,3], Fangfang Zhao[5], Shumin Yu[5], Fang Kong[2,3], Benazir Abbasi[6], Hongmei Yin[1*] and Congwei Gu[2,3,5*]

[1]College of Animal Science, Xichang University, Xichang, China, [2]Laboratory Animal Centre, Southwest Medical University, Luzhou, China, [3]Model Animal and Human Disease Research of Luzhou Key Laboratory, Luzhou, China, [4]State Key Laboratory of Quality Research in Chinese Medicine, Macau University of Science and Technology, Taipa, Macao SAR, China, [5]College of Veterinary Medicine, Sichuan Agricultural University, Chengdu, China, [6]College of Veterinary Medicine, Nanjing Agricultural University, Jiangsu, China

Introduction: As a representation of the gut microbiota, fecal and cecal samples are most often used in human and animal studies, including in non-alcoholic fatty liver disease (NAFLD) research. However, due to the regional structure and function of intestinal microbiota, whether it is representative to use cecal or fecal contents to study intestinal microbiota in the study of NAFLD remains to be shown.

Methods: The NAFLD mouse model was established by high-fat diet induction, and the contents of the jejunum, ileum, cecum, and colon (formed fecal balls) were collected for 16S rRNA gene analysis.

Results: Compared with normal mice, the diversity and the relative abundance of major bacteria and functional genes of the ileum, cecum and colon were significantly changed, but not in the jejunum. In NAFLD mice, the variation characteristics of microbiota in the cecum and colon (feces) were similar. However, the variation characteristics of intestinal microbiota in the ileum and large intestine segments (cecum and colon) were quite different.

Discussion: Therefore, the study results of cecal and colonic (fecal) microbiota cannot completely represent the results of jejunal and ileal microbiota.

KEYWORDS

non-alcoholic fatty liver disease, intestinal microbiota, 16S rDNA sequencing, mice, high-fat diet

Introduction

Recently, non-alcoholic fatty liver disease (NAFLD) has become the most common liver disease. In China, NAFLD has replaced Viral Hepatitis B as the most common chronic liver disease (Xiao et al., 2019). In the United States, NAFLD has become one of the main causes of liver transplantation (Gadiparthi et al., 2020). The gut microbiota recently

emerged as a pivotal transducer of environmental influences (i.e., dietary components and drug treatments) to exert protective or detrimental effects on several host tissues and systems, such as the regulation of intermediary metabolism, liver function, and cardiovascular disorders, either directly *via* translocation or indirectly through microbial metabolism or process in metabolic disorders (Lim et al., 2019).

Current research has demonstrated that the gut microbiota structure in patients with fatty liver was significantly different (Aron-Wisnewsky et al., 2020). A study of children reported that the phyla *Bacteroidetes* and *Proteobacteria* were higher in NAFLD, whereas the phylum *Firmicutes* were higher in children who were simply overweight or obese (Schwimmer et al., 2019). It is believed that these changes in intestinal microbiota result from diet and the body (Gao et al., 2020), and changes in the gut microbiota can cause changes in the body's metabolic state (Xu et al., 2020). The liver and the intestine are tightly linked through portal circulation. Consequently, gut microbial-derived products arriving at the liver may have pathogenic implications (Abdou et al., 2016). In recent years, the role of the gut microbiota has been increasingly implicated in modulating risk factors for NAFLD, such as energy homeostasis dysregulation, insulin resistance, increase in intestinal permeability, endogenous production of ethanol, inflammation (innate immunity and inflammasomes), and choline and bile acid (BA) metabolism (He et al., 2016). These factors likely influence the pathogenesis of NAFLD (Aragonès et al., 2019). Gut microbiota-derived factors and short-chain fatty acids (e.g., acetate, propionate, butyrate) can have anti-inflammatory properties, which could prevent the progression of NAFLD, however lactate, ethanol, and trimethyl N-oxide (TMAO) derived from intestinal microbiota can induce a decrease in total bile acid pool size, which in turn can affect Farnesoid X receptor (FXR) signaling and NAFLD (Aron-Wisnewsky et al., 2020).

Currently, feces are the main sample type that is used for gut microbiome research in humans and large animals, and the cecum and feces are the common detection sites in small animals. However, the function and flora of each intestinal segment are different. A major disadvantage of using stool samples to determine the composition of gut microbes is that the fecal microbiota represents only the end of the colon. At the same time, other parts of the gastrointestinal tract, particularly the small intestine, are poorly studied. In research involving NAFLD, the jejunum and ileum microflora were less studied. The small intestine is a hostile environment for microbes to survive due to its short transport time, short digestion enzyme, and bile excretion time. It, therefore, requires a different survival strategy than the colon microbes (Zoetendal et al., 2012). Most microbial species and functions in the fecal community come from coliform bacteria, while only a few microbes are from the small intestine (Chambers et al., 2019). As mentioned above, based on the niche-specific colonization pattern of exogenous flora, donor E. coli microbes may prefer to colonize in the small intestine rather than the large intestine (Li N. et al., 2020). Therefore, whether it is representative to use cecal or fecal (colonic) contents to study intestinal microbiota in the study of NAFLD remains to be shown. In this study, the structural characteristics of intestinal flora in the jejunum, ileum, cecum, and colon (feces) of NAFLD mice were studied to analyze the validity of the cecum and colon as the main sites of intestinal flora research in the pathological state of non-alcoholic fatty liver disease.

Materials and methods

Animal study

Animal feeding and sample collection

Six-week-old specific pathogen-free male C57BL/6 mice (weighting 17–19 g) were purchased from Beijing Weitong Lihua Laboratory Animal Technology Co., LTD and housed at 22 ± 2°C and 50–60% relative humidity in a specific pathogen-free facility maintained on a 12-h light/dark cycle in the Laboratory Animal Center of Southwest Medical University. After 1 week of acclimatization, 20 mice were randomly divided into two groups for 16 weeks: Control (CK) group ($n = 10$, Normal diet, ND) and NAFLD (NA) group ($n = 10$, High fat diet, HFD). The normal diet comprised 65.08 kcal% carbohydrates, 23.07 kcal% proteins, and 11.85 kcal% fats, purchased from HUANYU BIO, while the HFD diet contained 20 kcal% carbohydrates, 20 kcal% proteins, and 60 kcal% fats, which was purchased from Research Diets. The composition of the normal and HFD diet is detailed in Supplementary Table S1. All experimental mice had free access to food and water. The physical activity, consumption of food and water, and excretion of experimental mice were observed daily.

At the end of the prescribed feeding period, all mice were fasted overnight and anesthetized with an intraperitoneal injection of 1% pentobarbital sodium (50 mg/kg body weight). After anesthetization, blood samples were collected from the hearts. After the liver was fixed with 4% paraformaldehyde, the tissue was sectioned and stained with hematoxylin–eosin (HE), Oil Red O (RUIBIO, Y07512), and Masson (Servicebio, G1006). Oil-red O staining is used to stain lipid droplets, and Masson staining is used to degrade collagen. Image Pro Plus software was used to quantitatively analyze the percentage of Oil Red O positive area to total area and the percentage of Masson positive area to total area.

Lkhagva et al. (2021) reported that the microbial composition of the colon and feces was very similar (Suzuki and Nachman, 2016), and the uncertainty of mouse excretion at the time of sampling. We selected colonic contents (formed fecal balls) 1 cm to 1.5 cm from the anus instead of feces. In addition, jejunal contents were 15 cm to 20 cm from the initial pylorus, ileum contents 1 cm to 5 cm from ileocecal valve, and cecal contents below the ileocecal valve selected as jejunum, ileum, and cecum samples, respectively. The contents of the jejunum, ileum, cecum, and colon were placed in liquid nitrogen and tested for the microbiome. The Animal Ethics Committee approved the

experimental protocol of Southwest Medical University (No. of *Animal Ethics* Approval: SWMU2019463).

Biochemical analysis of serum

After anesthetization, blood samples were collected in the morning through cardiac puncture, and were centrifuged at 3500 rpm for 10 min at 4°C. Recovered supernatants were separated into 200 μl tubes and frozen at −80°C. Biochemical indices such as Alanine aminotransferase (ALT), Aspartate aminotransferase (AST), triglyceride (TG), total cholesterol (TC), high-density lipoprotein (HDL), and low-density lipoprotein (LDL) were detected by a fully automatic veterinary biochemical analyzer (Jiangxi Tekang Technology Co., Ltd., TC220).

Microbiota analyses

DNA from the contents of the jejunum, ileum, cecum, and colon were isolated using the Qiagen Gel Extraction Kit (Qiagen, Hilden, Germany). The genomic DNA was amplified using fusion primers (341F, CCTACGGGRBGCASCAG; 806R: GGACTACN NGGGTATCTAAT) targeting the 16S V3-V4 rRNA gene with indexing barcodes. TruSeq® DNA PCR-Free Sample Preparation Kit was used to establish the DNA library, and Qubit and Q-PCR quantified the library. All samples were pooled for sequencing on the Illumina HiSeq™ 2000 Sequencing system according to the manufacturer's specifications.

Raw sequence tags were generated from FLASH (V1.2.7; *FLASH*, 2019[1]; Magoc and Salzberg, 2011). Quality filtering on the basic tags was performed under specific filtering conditions to obtain the high-quality clean labels according to the QIIME (V1.9.1; *Qiime*, 2019[2]; Caporaso et al., 2010) quality-controlled process. Chimera removal, the tags were compared with the reference database (Gold database) using the UCHIME algorithm (*UCHIME*, 2019)[3] to detect chimera sequences. Then the chimera sequences were removed, and the Effective Tags were finally obtained. De novo operational taxonomic units (OTUs) clustering was carried out using the Uparse (V7.0.1001; *Uparse*, 2019[4]; Edgar, 2013), which identifies highly accurate OTUs from amplicon sequencing data with an identity threshold of 97%. Then the OTUs were used to screen effective sequences using Mothur (*Mothur*, 2019[5]; Schloss et al., 2009). The representative sequences of OTUs were used to analyze alpha-diversity (Chao1, Ace, Shannon and Simpson diversity index) based on their relative abundance. A heatmap was generated according to the relative abundance of OTUs by R software (V2.15.3; Gatto et al., 2015). Non-metric multidimensional scaling (NMDS) and Principal Coordinates analysis (PCoA) based on UniFrac distance was performed with Qiime (V1.9.1; *Qiime*, 2019 (see footnote 2); Caporaso et al., 2010). The linear discriminant analysis (LDA) with effect size measurements (LEfSe) was used to identify bacterial indicator groups specialized within the two groups, and species with LDA scores > 4 were considered biological markers. PICRUSt2 (*Picrust*, 2022[6]; Douglas et al., 2020) was used to predict the metabolic pathways of intestinal microbiota and investigate the functional differences in the microbial communities in samples from the four regions. OTUs with an alignment ratio lower than 0.8 were excluded (Langille et al., 2013; Liu et al., 2021).

Statistical analysis

Data of body weight, serum indexes (TC, TG, HDL, LDL, AST, and ALT), and relative abundance of gut microbiota genes in metabolic pathways are presented as mean ± SD. Student's *t*-test was used to determine the significance of the body weight, the relative amount of lipid droplets, the amount of collagen, and serum indexes (TC, TG, HDL, LDL, AST, and ALT). *Wilcox Rank-Sum test* was used to determine the significance of the alpha diversity. *Kruskal-Wallis test* was used to assess the importance of the relative abundance of major bacteria at phylum, family and genus levels and the relative abundance of primary and secondary functional genes in different intestinal segments within the same group. *Wilcox Rank-sum test* was used for the same intestinal segment between the two groups. A value of $p < 0.05$ was considered statistically significant. Statistical analysis was performed with SPSS software (Version 25, SPSS Inc., Chicago, United States).

Results

The animal model of NAFLD was successfully established

Twenty mice were randomly divided into CK and NAFLD groups. The CK group was fed a normal diet (ND), and the NAFLD group was fed a high-fat diet (HFD). After mice were fed HFD for 8 weeks, the body weights of NAFLD mice (31.9 ± 2.67 g) were markedly increased and significantly different from CK mice (27.97 ± 1.70 g; $p = 0.031$; Figure 1A). To produce obvious steatosis of the liver, we fed them the high-fat diet continuously for

1 *FLASH* [Online]. Available: http://ccb.jhu.edu/software/FLASH/ (Accessed 2019).

2 *Qiime* [Online]. Available: http://qiime.org/scripts/split_libraries.html (Accessed 2019).

3 *UCHIME* [Online]. Available: http://drive5.com/uchime/uchime_download.html (Accessed 2019).

4 *Uparse* [Online]. Available: http://drive5.com/uparse/ (Accessed 2019).

5 *Mothur* [Online]. Available: https://mothur.org/CITATION/ (Accessed 2019).

6 *Picrust* [Online]. Available: https://github.com/picrust (Accessed 2019).

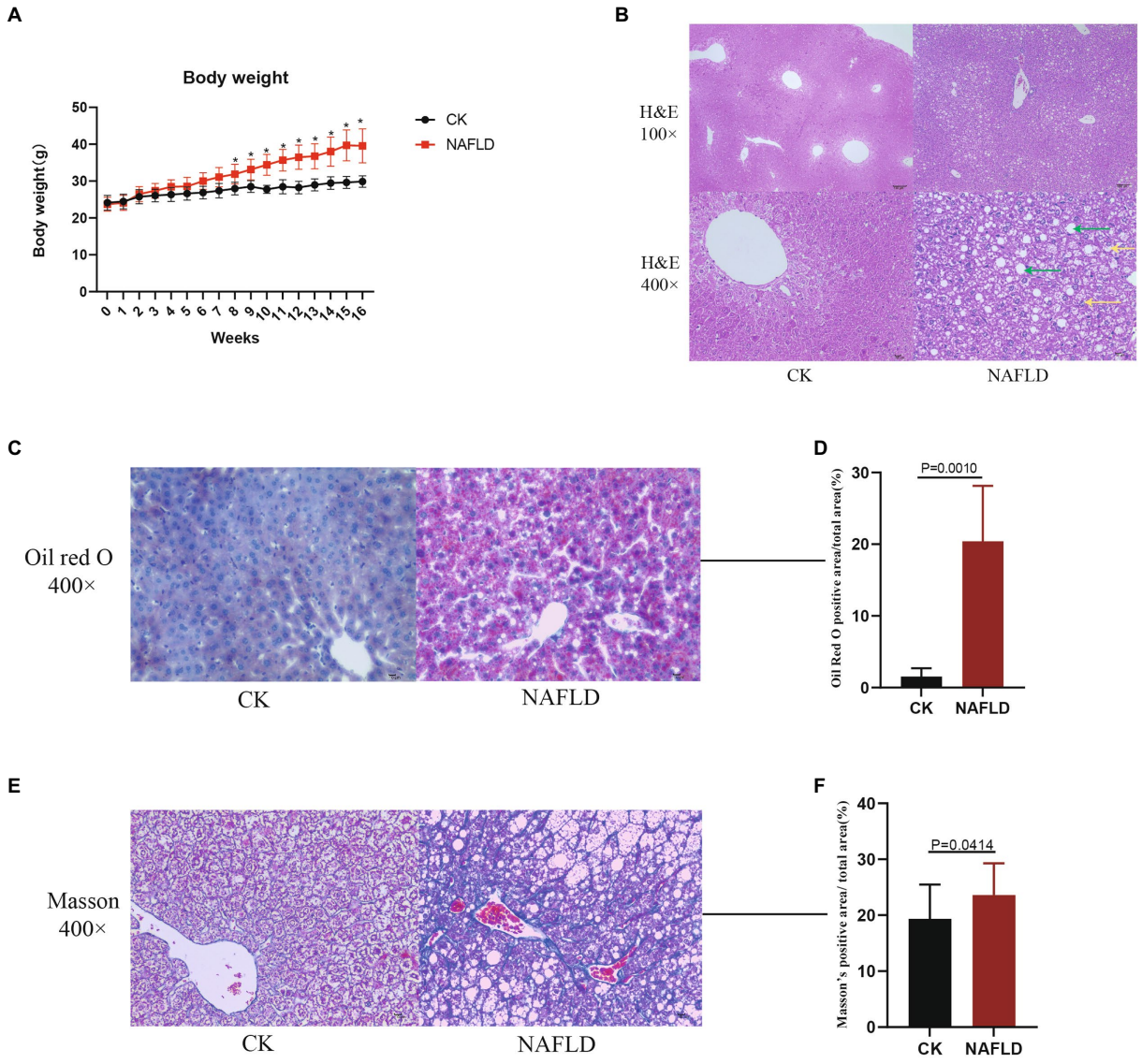

FIGURE 1
The body weight and Histopathology with Control and NAFLD mice. **(A)** Body weight changes in ND or HFD fed mice over 16weeks. **(B)** Representative pictures of hematoxylin and eosin (H&E) staining for liver (100× and 400×), the green arrows indicate hepatic cell steatosis, and the yellow arrows indicate hepatic cell balloon-like changes. **(C,D)** Representative pictures of Oil red O staining for liver (400×) and quantitative analysis of lipid droplets relative amount. **(E,F)** Representative pictures of Masson staining for liver (400×) and quantitative analysis of the relative amount of collagen. Significance was assessed by Student *t-test*.

16 weeks, and the body weight of NAFLD mice reached 39.58 ± 4.61 g, significantly higher than that of the CK group (29.90 ± 1.54 g; $p = 0.033$; Figure 1A).

Liver samples were collected for HE staining, and it was found that hepatic cell vacuolation and steatosis were observed in the liver tissues of NAFLD mice. Some hepatic cells showed obvious balloon-like changes, with different degrees of necrosis accompanied by inflammatory cell infiltration and cracks around the central vein. Pathological changes of hepatic cell necrosis were also observed around the cracks (Figure 1B). In the CK group, the liver cells were polygonal and arranged as hepatic cords, radially distributed around the central vein. There were large and round nuclei in the center of the cells, with uniform cytoplasm, no lipid droplets, and no steatosis or inflammatory cell infiltration (Figure 1B). By Oil Red O staining and calculating the relative amount of lipid droplets, it was found that the number of lipid droplets in the NAFLD group was significantly higher than that in the CK group ($p = 0.0010$; Figures 1C,D). Through Masson staining and the calculation of the relative amount of collagen, it was found that the fibrosis degree of NAFLD mice was significantly higher than that of CK mice, indicating that a certain degree

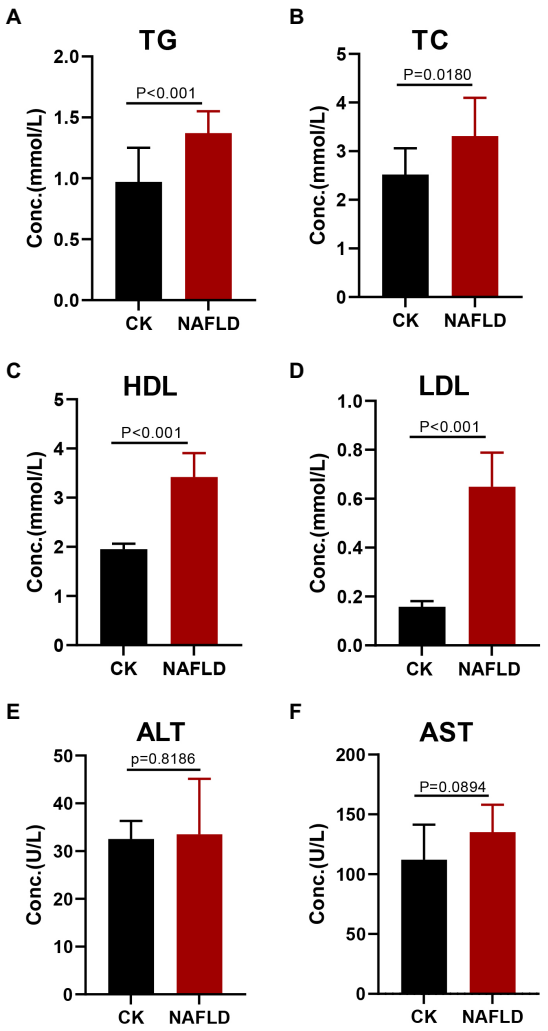

FIGURE 2
Serum lipid profiles and liver function indicators in Control and NAFLD mice. **(A)** Triglycerides (TG), **(B)** Total cholesterol (TC), **(C)** high density lipoprotein (HDL), **(D)** low density lipoprotein (LDL), **(E)** alanine aminotransferase (ALT), and **(F)** aspartate aminotransferase (AST). Significance was assessed by Student *t-test*.

of fibrosis had occurred in the liver of NAFLD mice ($p = 0.0414$; Figures 1E,F).

Serological tests found that the NAFLD mice exhibited increased levels of triglyceride (TG), total cholesterol (TC), high-density lipoprotein (HDL), and low-density lipoprotein (LDL) in the serum ($p < 0.05$; Figures 2A–D), but Alanine aminotransferase (ALT, $p = 0.8186$) and Aspartate aminotransferase (AST, $p = 0.0894$) levels did not change significantly (Figures 2E,F).

The significant increase in body weight of mice in the HFD group, the discovery of hepatocyte steatosis, the rise in the number of lipid droplets, the aggravation of liver tissue fibrosis and the significant increase in serum triglycerides indicated that the HFD diet was successfully used to induce NAFLD model in mice (Lau et al., 2017).

Alpha diversity of intestinal microbiota in CK and NAFLD mice

We used Chao1, ACE, Shannon and Simpson indices to evaluate the alpha diversity of various intestinal sections in normal and NAFLD mice. Microbial diversity was analyzed using the Shannon and Simpson indices, and richness was examined using Chao1 and ACE indices (Figure 3). In CK mice, the Chao1 and ACE indices values in the ileum were significantly higher than in the colon ($p < 0.01$; Figures 3A,B). In NAFLD mice, Chao1 and ACE indices in the ileum also yielded significantly higher values than those in the cecum and colon ($p < 0.01$). The Shannon index and Simpson index values in the jejunum, ileum, cecum, and colon had no significant differences ($p > 0.05$; Figures 3C,D). Compared with CK mice, the Simpson index value of NAFLD mice did not change significantly in the four intestinal segments ($p > 0.05$; Figure 3D). Still, in the ileum and colon, the Chao1, ACE and Shannon index values of NAFLD mice changed significantly ($p < 0.05$; Figures 3A–C). These results indicate that the ileum of CK mice has the highest microbiota diversity, which is substantially higher than that of the colon. The ileum of NAFLD mice has a significantly higher microbiota diversity than the cecum and colon. Compared with CK mice, while the diversity of microbiota in the jejunum and cecum of NAFLD mice did not change significantly, it was considerably greater in the ileum and colon.

Beta diversity of intestinal microbiota in NAFLD mice was changed

Non-metric Multidimensional Scales (NMDS) based on Bray-Curtis distances and Principal Co-ordinate Analysis (PCoA) based on Weighted and Unweighted Unifrac distances were carried out to reveal the differences in the nonlinear and linear bacterial community structure of the samples, respectively. The NMDS and PCoA showed that the distribution regions of jejunum samples from NAFLD mice overlapped with those from CK mice in the two-dimensional coordinate system (Figures 4A,B). However, the distribution regions of the ileum (Figures 4C,D), cecum (Figures 4E,F), and colon (Figures 4G,H) samples from NAFLD mice were separated from those of CK mice.

Although PCoA analysis found that the distribution regions of samples from four different intestinal segments overlapped in both CK mice and NAFLD mice, NMDS analysis showed that the large intestine (cecum and colon) and small intestine (jejunum and ileum) samples from CK mice were shown to be distinct (Figures 5A,B). However, in NAFLD mice, there was significant overlap in the distribution regions of all four intestinal segments. This indicates that following a high-fat diet, the intestinal microbiota structure of the ileum, cecum, and colon of NAFLD mice changes, resulting in the microbiota structure of the large intestine and small intestine, which should be different, sharing more similarities (Figures 5C,D).

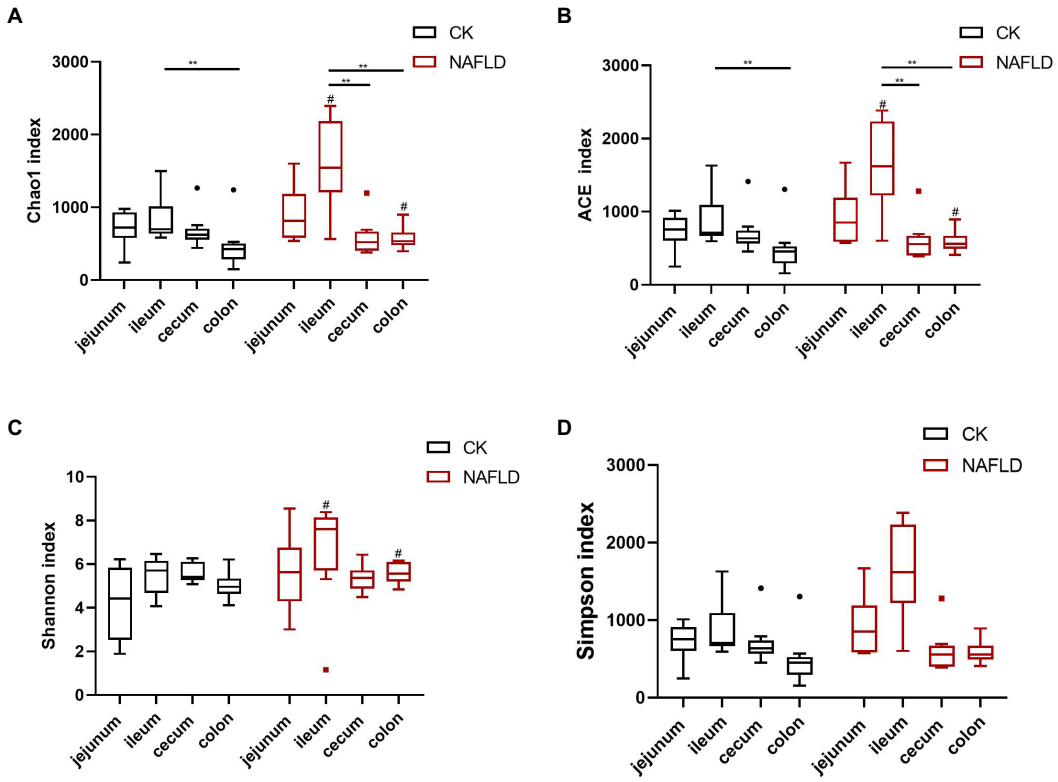

FIGURE 3
Alpha diversity analysis of the bacterial community in the jejunum, ileum, cecum, and colon of Control and NAFLD mice. **(A)** Chao1 index, **(B)** ACE index, **(C)** Shannon index, and **(D)** Simpson index. Significance was assessed by *Wilcox Rank-Sum test*. *indicate significant difference in the different intestinal segments in the CK group and NAFLD group. #indicates the significant difference in the same intestinal segments between CK group and NAFLD group. *or# $p<0.05$; **or## $p<0.01$.

Composition of the intestinal microbiota of CK and NAFLD mice

The observed number of OTUs in the guts of CK and NAFLD mice

Venn graph is used to show the distribution and differences of OTU in four intestinal segments of NAFLD mice and CK mice (Figure 6). The Venn graph showed that in jejunum and ileum, the number of OTUs in the NAFLD group was 1,219 and 1,031 more than in the CK group (Figures 6A,B). In the cecum and colon, the number of OTUs in the NAFLD group was 303 and 76 less than in the CK group (Figures 6C,D). In CK mice and NAFLD mice, the number of OTUs in the ileum was the highest, followed by jejunum and cecum, and the colon was the least (Figures 6E,F). This indicates that after a high-fat diet, the richness of small intestinal (jejunum and ileum) microbiota in NAFLD mice increases, while the richness of the large intestine (cecum and colon) decreases. The richness of the small intestine is more than that of the large intestine, and the richness of ileal microbiota is the most abundant. The jejunum and ileum microbiota had the highest number of common OTUs.

Relative abundance of major bacteria in the intestinal tract of CK and NAFLD mice

We screened the 10 phyla with the highest abundance and displayed the results in a stacked column chart (Figure 7A; Supplementary Table S2). We selected five phyla with the highest abundance using the *Rank Sum test* (Figure 7B; Supplementary Table S2), which accounted for more than 90% of the community abundance at the phylum level. The dominant phyla were *Firmicutes*, *Bacteroidetes*, *Proteobacteria*, *Actinobacteria* and *Verrucomicroibia*. *Firmicutes* were the highest in the jejunum, ileum, and cecum, and *Baceteroidetes* was the highest in the colon. In the gut of CK mice, none of these five phyla differed relative abundance between jejunum and ileum, and only *Fimictutes* differed relative abundance between ileum and cecum ($p<0.05$). However, there are many differences in the relative abundance of microbiota at the phylum level between the small intestine and the large intestine. The relative abundance of *Firmicutes*, *Bacteroidetes*, *Proteobacteria* and *Verrucomicrobia* in the jejunum and ileum is significantly different from that in the colon ($p<0.05$).

In addition, the relative abundance of *Verrucomicrobia* in the jejunum was significantly lower than that in the ileum ($p<0.05$). The relative abundance of *Actinobacteria* in the ileum was

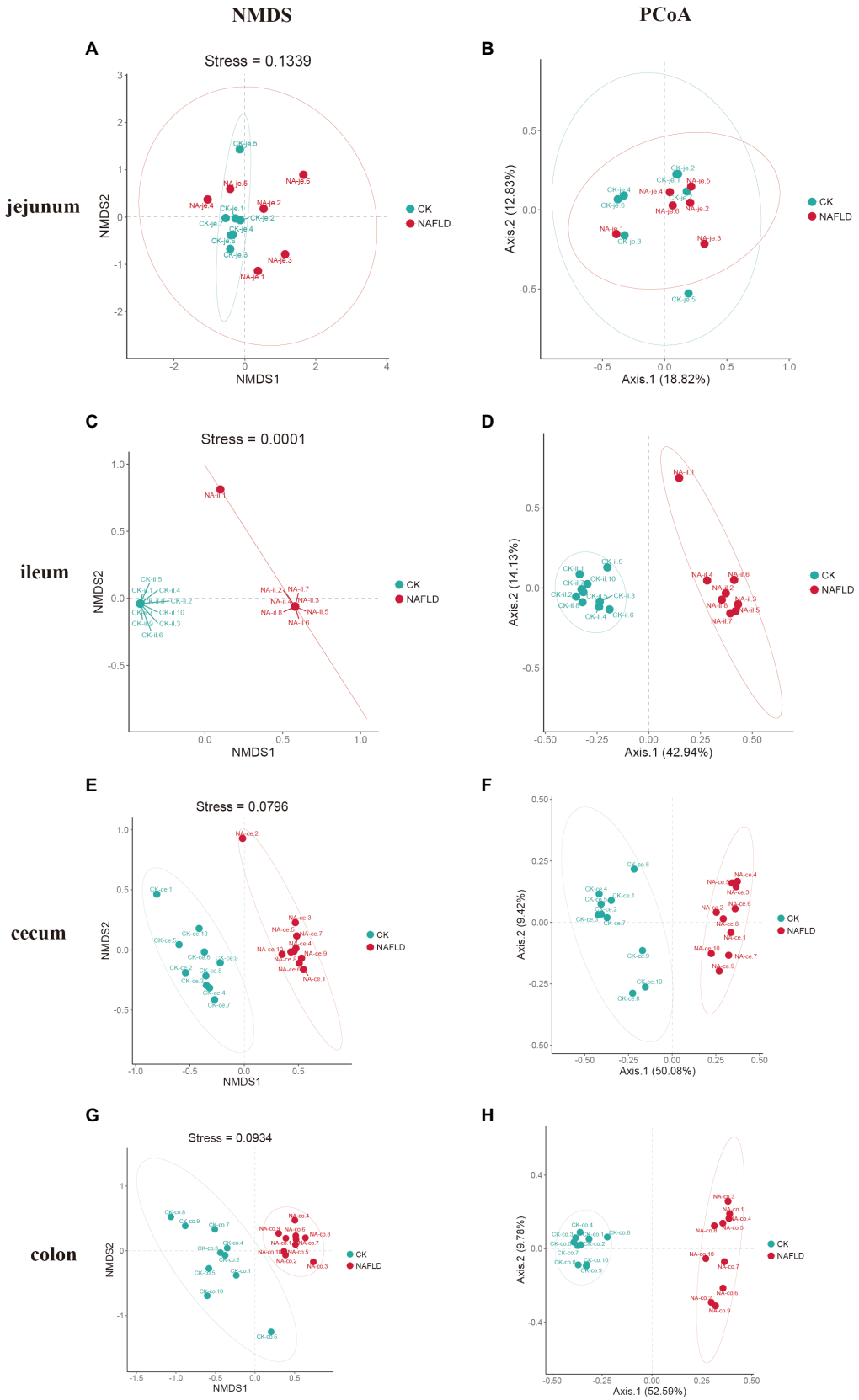

FIGURE 4
Beta diversity analysis of the same intestinal segments between CK group and NAFLD group assessed by NMDS and PCoA based on Bray-Curtis distance. **(A,B)** Jejunum, **(C,D)** ileum, **(E,F)** cecum, and **(G,H)** colon.

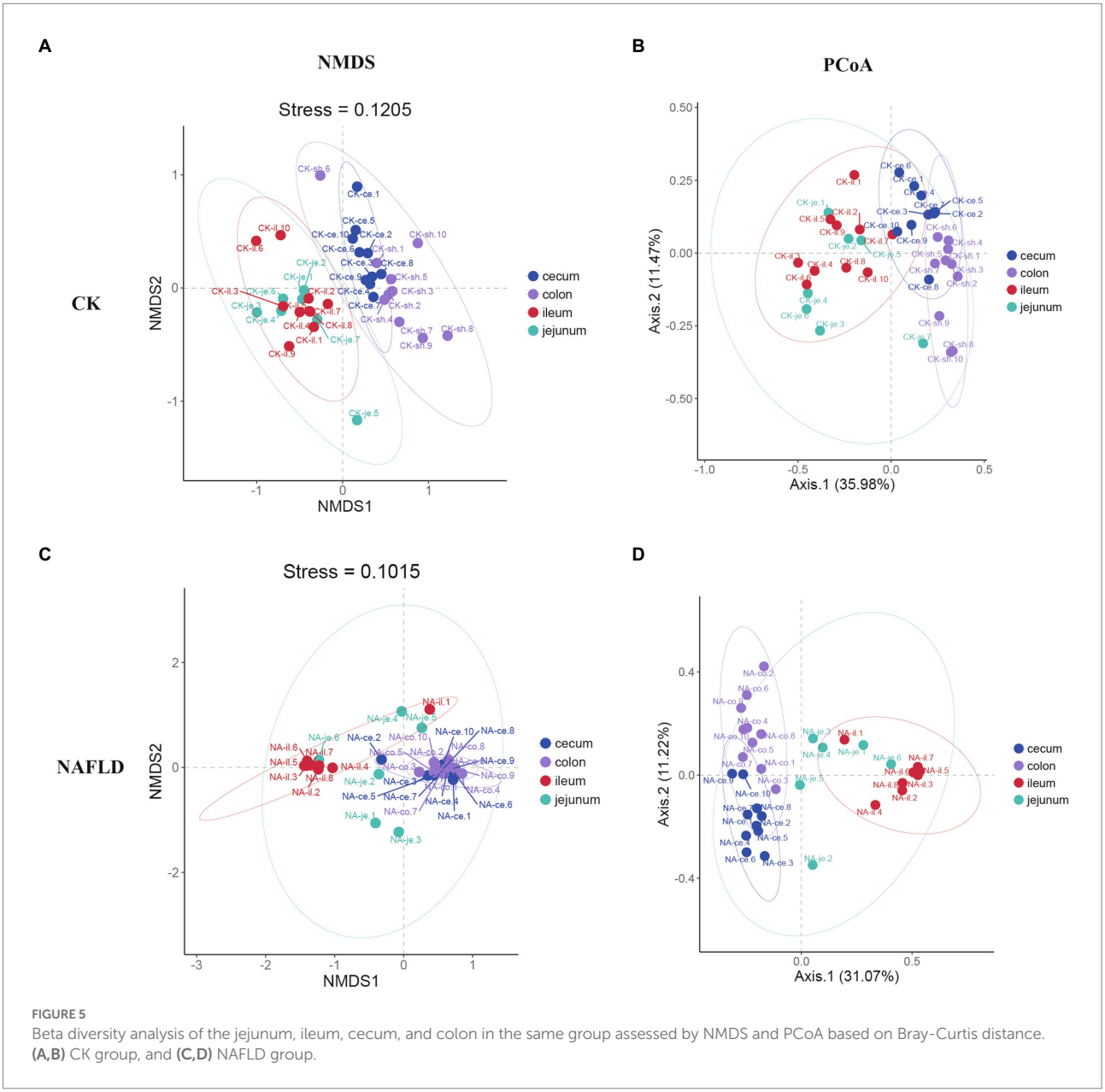

FIGURE 5
Beta diversity analysis of the jejunum, ileum, cecum, and colon in the same group assessed by NMDS and PCoA based on Bray-Curtis distance. **(A,B)** CK group, and **(C,D)** NAFLD group.

substantially higher than that in the cecum and colon ($p < 0.05$). But after the high-fat diet, the differences in the relative abundance of the five phyla became smaller among the four segments. In the intestine of NAFLD mice, *Proteobacteria* showed no difference in relative abundance among four intestinal segments. There was also no difference in the relative abundance of *Firmicutes* between the small and large intestines. Compared with the CK group, after a high-fat diet, there was no significant change in the jejunal microbiota of NAFLD mice. Still, *Firmicutes* significantly decreased, and *Verrucomicrobia* increased dramatically in the ileum ($p < 0.05$). *Firmicutes* and *Proteobacteria* were significantly increased in the cecum and colon ($p < 0.05$), while *Bacteroidetes* and *Verrucomicrobia* were considerably reduced ($p < 0.05$). At the family level, we found the same pattern. After the high-fat diet, the differences in the relative abundance of major families among the four segments became smaller. Compared with CK mice, the relative abundance of bacteria in the jejunum of NAFLD mice was significantly changed in a few cases, only one family. More bacteria in the ileum, cecum and colon had significant changes at the family level. But the family-level bacteria that changed in the cecum and colon and the trends were more similar (Supplementary Figures S1A,B; Supplementary Table S3).

At the genus level, we selected the 10 genera with the highest abundance for the stacked column chart (Figure 8A; Supplementary Table S4), and the relative abundance of these 10 genera accounted for 17–36%. The top 10 genera with the highest relative abundances were plotted in boxplots, and the *Rank Sum test* was performed (Figure 8B; Supplementary Table S4). The results showed that the relative abundance of *Candidatus_Arhromitus* was significantly different between jejunum and ileum

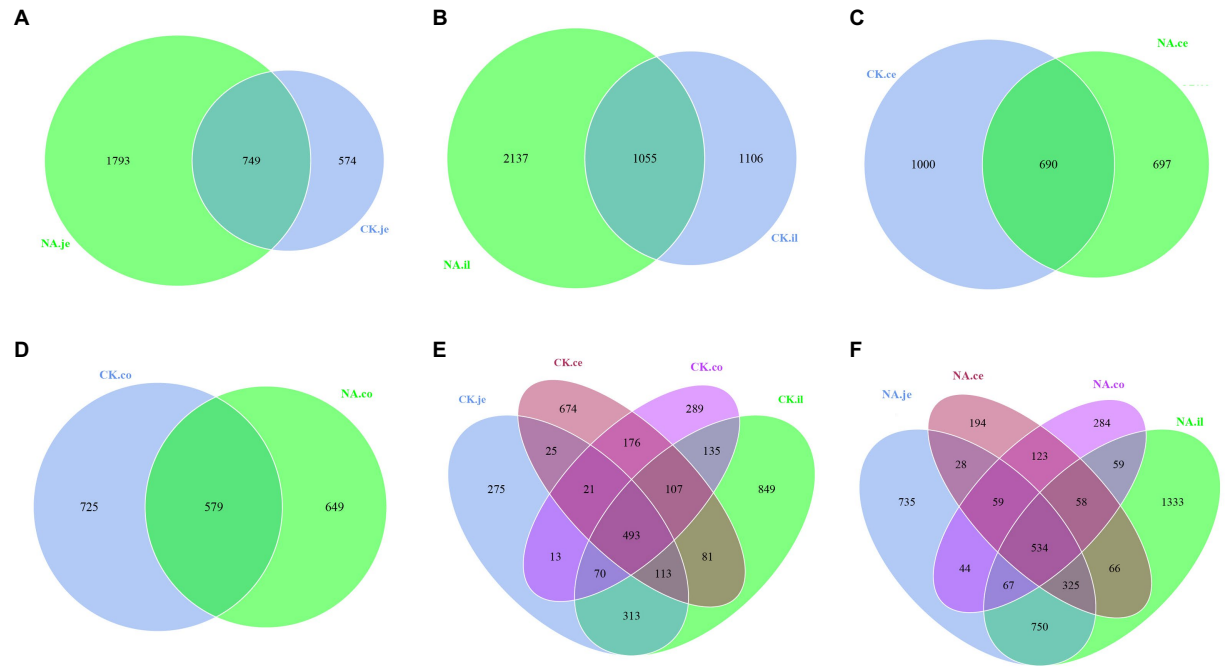

FIGURE 6
Venn diagram based on OTU. **(A)** The jejunum between CK and NAFLD (NA) groups, **(B)** the ileum between CK and NAFLD (NA) groups, **(C)** the cecum between CK and NAFLD (NA) groups, **(D)** the colon between CK and NAFLD (NA) groups, **(E)** the jejunum, ileum, cecum, and colon of CK group, and **(F)** the jejunum, ileum, cecum, and colon of NAFLD (NA) group.

in CK mice ($p < 0.05$). There were no significant differences in the relative abundance of genera between the cecum and colon. There is a large difference between the small and large intestine, *Romboutsia* was significantly different between jejunum and ileum ($p < 0.05$), and *Romboutsia*, *unidentified Enterobacteriaceae*, *Akkermansia* and *Odoribacter* were different between jejunum and colon ($p < 0.05$). There were significant differences between ileum and cecum in seven genera, including *Romboutsia*, *Desulfovibrio*, *Faecallbaculum*, *Lactobacillus*, *Bacteroides*, *Candidatus Arhromitus*, and *Odoribacter* ($p < 0.05$). There were substantial differences between ileum and colon in eight genera, including *Romboutsia*, *unidentified Enterobacteriaceae*, *Allobaculum*, *Akkermansia*, *Desulfovibrio*, *Faecallbaculum*, *Candidatus Arhromitus*, and *Odoribacter* ($p < 0.05$). After the high-fat diet, the differences in microbial abundance between intestinal segments were reduced. The *Romboutsia* has become no significant difference in the jejunum and cecum of NAFLD mice, and *Desulfovibrio* is still significantly different ($p < 0.05$); only *Odoribacter* was significantly different between the jejunum and colon ($p < 0.05$); only five genera, such as *Romboutsia*, *unidentified Enterobacteriaceae*, *Akkermansia*, *Desulfovibrio* and *Odoribacter* showed significant differences between ileum and cecum ($p < 0.05$); Five genera, *Romboutsia*, *unidentified Enterobacteriaceae*, *Allobaculum*, *Desulfovibrio*, and *Odoribacter*, were significantly different between the ileum and colon ($p < 0.05$). Compared with the CK group, only two genera were changed in the jejunum of NAFLD mice, and the relative abundance of *Romboutsia* was significantly increased, and *Allobaculum* was decreased considerably ($p < 0.05$); seven genera changed in the ileum, the relative abundance of *Romboutsia and Candidatus Arhromitus* was improved greatly, while *Allobaculum*, *Akkermansia*, *Desulfovibrio*, *Lactobacillus* and *Odoribacter* were significantly decreased ($p < 0.05$). The relative abundance of 5 genera changed substantially in the cecum, and these 5 genera also changed significantly in the colon ($p < 0.05$). The changing trend was consistent: *Romboutsia* and *Akkermansia* were significantly decreased, while *Allobaculum*, *Desulfovibrio* and *Faecallbaculum* were significantly increased. In addition, three genera in the colon showed significant changes.

These results indicate that the major bacterial compositions of the small intestine (jejunum and ileum) and large intestine (cecum and colon) were quite different. After a high-fat diet, the jejunum's major bacterial compositions had fewer changes. In contrast, the ileum, cecum, and colon had greater changes, and the characteristics of the changes to the major bacterial arrangements of the cecum and colon were closer.

Bacterial taxonomic biomarkers in the intestinal tract of CK and NAFLD mice

Linear discriminant analysis Effect Size (LEfSe) was used to examine the relative abundance of different bacteria taxa (from phylum to genus) in samples from another region (Figures 9, 10). Species with LDA scores >4 were considered biological markers. A comparison between the four different intestinal segments in

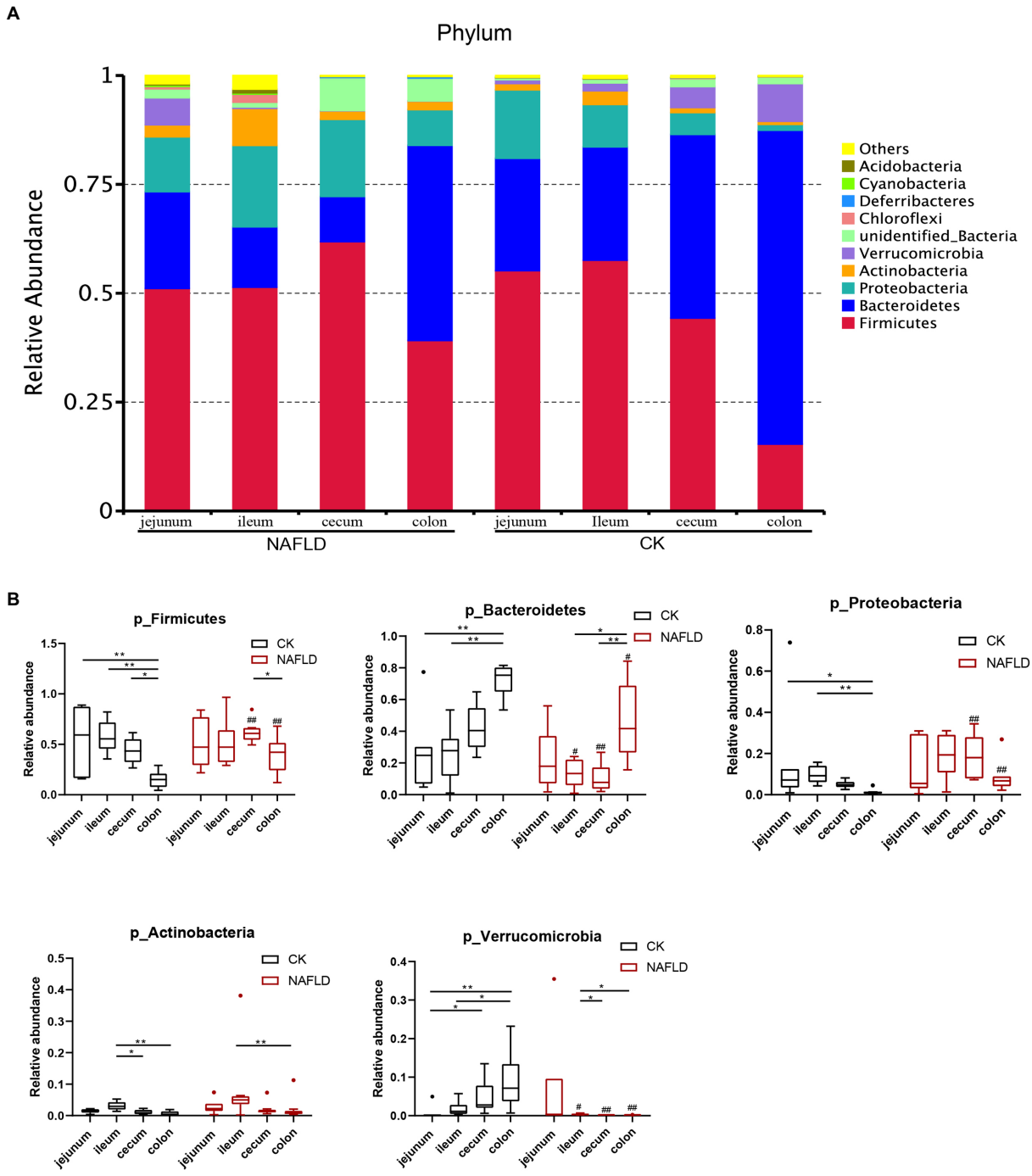

FIGURE 7
Relative abundance of bacteria at phylum level. **(A)** Stacked column graph of the top 10 phyla with the highest relative abundance. **(B)** The box diagram was used to analyze the differences in relative abundance of the five phyla with the highest relative abundance. *Wilcox Rank-sum* test was used to compare the significance of the same intestinal segment between the CK group and the NAFLD group; *Kruskal-wallis test* was used to compare the differences between different intestinal segments in the same group. *indicate significant difference in the different intestinal segments in the CK group and NAFLD group. #indicates the significant difference in the same intestinal segments between CK group and NAFLD group. *or# $p<0.05$; **or## $p<0.01$.

CK mice found only 4 biomarkers in the cecum, up to 22 in the ileum, and 10 in the jejunum and colon (Figure 9A). When comparing the four different intestinal segments in NAFLD mice, the maximum number of biomarkers was 18 in the cecum, 9 in the ileum and colon, and the lowest number was 6 in the jejunum (Figure 9B).

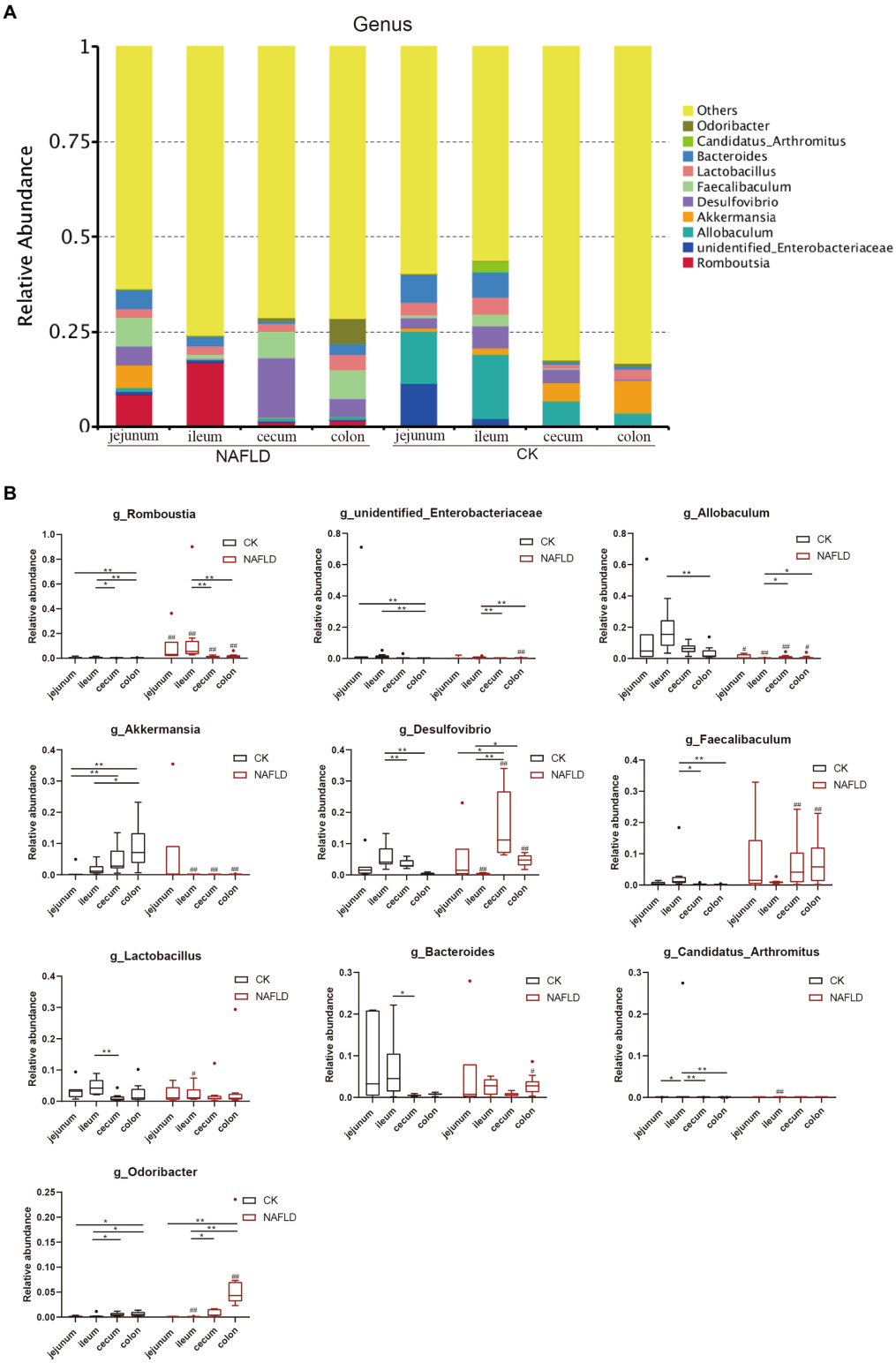

FIGURE 8
Relative abundance of bacteria at genus level. **(A)** Stacked column graph of the top 10 genera with the highest relative abundance. **(B)** The box diagram was used to analyze the differences in relative abundance of the five genera with the highest relative abundance. *Wilcox Rank-sum test* was used to compare the significance of the same intestinal segment between the CK group and the NAFLD group; *Kruskal-wallis test* was used to compare the differences between different intestinal segments in the same group. *indicate significant difference in the different intestinal segments in the CK group and NAFLD group. #indicates the significant difference in the same intestinal segments between CK group and NAFLD group. *or# $p<0.05$; **or## $p<0.01$.

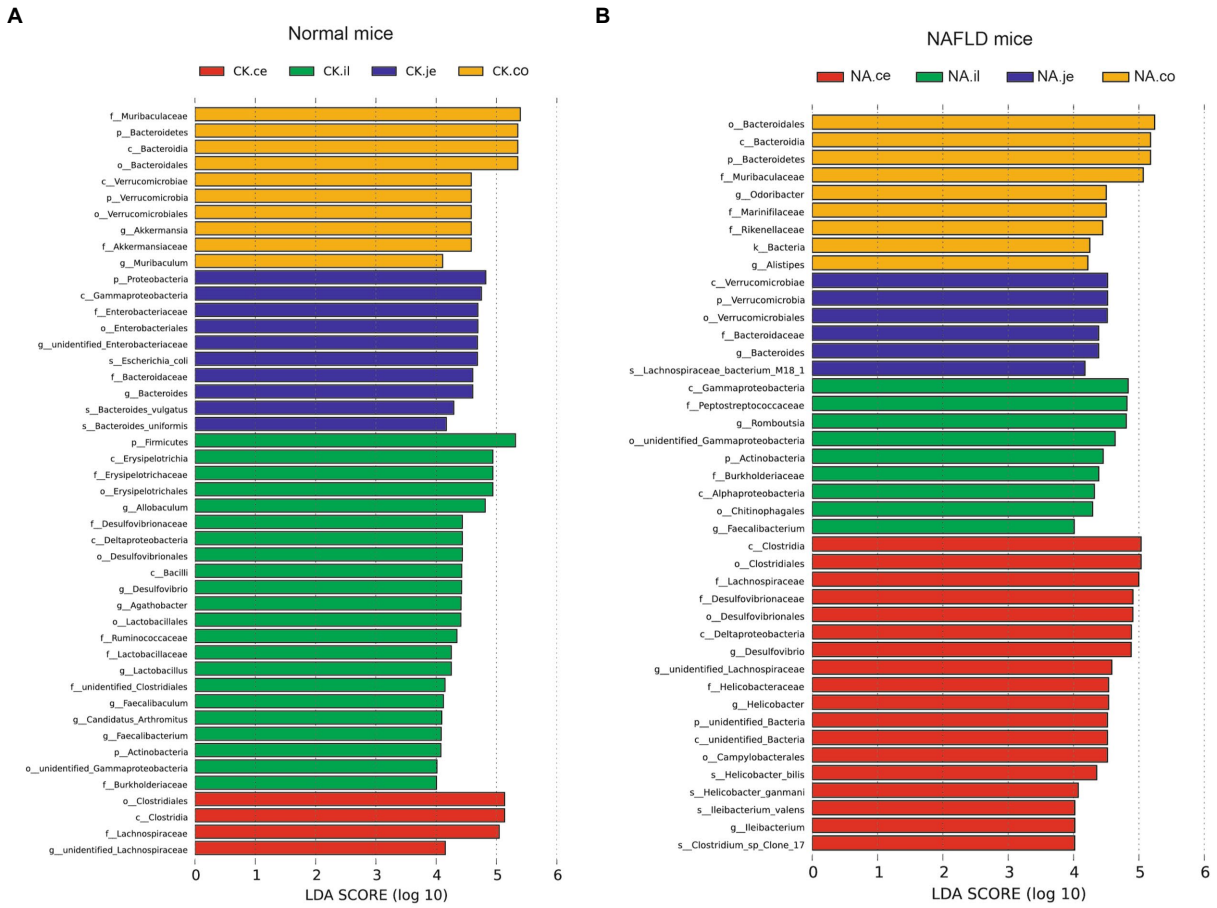

FIGURE 9
Linear discriminant analysis effect size (LEfSe) analysis of microbiota among different intestinal segments in the same group. **(A)** CK group, and **(B)** NAFLD (NA) group (α=0.05, logarithmic Linear Discriminant Analysis (LDA) score threshold=4.0).

While the biomarker of CK mice in the jejunum was *Allobaculum*, those of NAFLD mice were *Peptostreptococcaceae* and *Romboustsia* (Figure 10A). In the ileum, 19 biomarkers were found in CK mice and 8 in NAFLD mice (Figure 10B). In the cecum, there were 10 biomarkers in CK mice and 19 biomarkers in NAFLD mice (Figure 10C). In the colon, 11 biomarkers were found in CK mice and 24 in NAFLD mice (Figure 10D). Compared to CK mice, NAFLD mice had more common biomarkers in the cecum and colon and fewer in the jejunum and ileum. In CK mice, at the genus level, there was one common biomarker, *Allobaculum*, in all four intestinal segments and two in the cecum and colon. In NAFLD mice, at the genus level, five biomarkers in the cecum of NAFLD mice, *Blautia*, *Desulfovibrio*, *Faecalibaculum*, *Helicobacter*, and *unidentified Lachnospiraceae*, were also the biomarkers in the colon. Interestingly, in a previous study, *Blautia*, *Faecalibaculum*, *Helicobacter* and *unidentified Lachnospiraceae* are significantly increased in NAFLD mice (Gu et al., 2022). However, the ileum and large intestine (cecum and colon) shared only a few biomarkers, with only one common biomarker at the genus level.

Predicted function of intestinal microbiota

Based on the 16S rDNA sequence, PICRUSt2 was used to predict the function of intestinal flora, and the relative abundance of metabolic function genes was the highest in the primary function, accounting for about 70%. In the CK group, the colon had a significantly higher relative abundance of metabolic function genes than other intestinal segments but had a lower relative abundance of other primary function genes ($p < 0.05$, Table 1). In NAFLD mice, except for human diseases, other functional genes enriched in the colon were not significantly different from those in the jejunum and ileum ($p > 0.05$, Table 1). Compared with the CK group, there was no significant difference in other metabolic pathways in the jejunum and ileum of NAFLD mice ($p > 0.05$), except that the abundance of genes related to cellular processes in the ileum was significantly increased ($p < 0.05$, Table 1). In the cecum and colon, the abundance of genes related to metabolism was significantly lower in NAFLD mice ($p < 0.05$), along with the abundance of genes related to organismal systems in the cecum ($p < 0.05$, Table 1). However, the abundance of genes

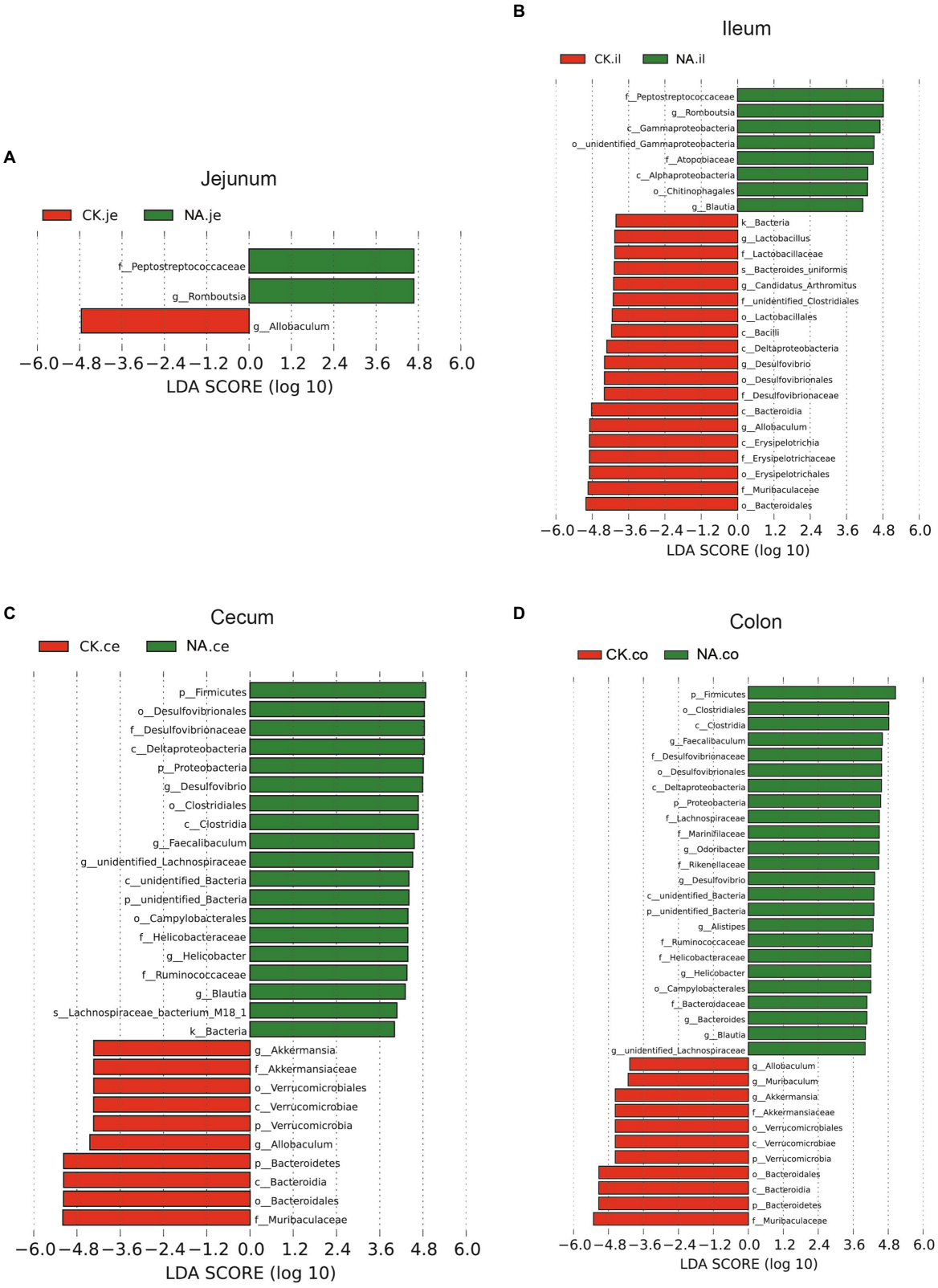

FIGURE 10
LEfSe analysis of intestinal microbiota in the same segment between CK group and NAFLD (NA) group. **(A)** Jejunum; **(B)** Ileum; **(C)** Cecum; **(D)** Colon (α=0.05, logarithmic Linear Discriminant Analysis (LDA) score threshold=4.0).

TABLE 1 Relative abundance of primary functional genes in gut microbiota of normal and NAFLD mice.

Functions	CK-JE	CK-IL	CK-CE	CK-CO	NA-JE	NA-IL	NA-CE	NA-CO
Metabolism	71.87 ± 2.03^{b}	71.72 ± 1.66^{b}	72.97 ± 1.16^{b}	75.78 ± 0.71^{a}	71.76 ± 2.10^{AB}	71.20 ± 1.31^{AB}	69.70 ± 0.69^{A}*	72.59 ± 1.87^{B}*
Genetic Information Processing	12.02 ± 1.52^{ab}	12.19 ± 0.65^{a}	11.49 ± 0.27^{bc}	10.98 ± 0.19^{c}	11.76 ± 0.86	11.53 ± 0.78	12.14 ± 0.50*	11.79 ± 0.80*
Cellular Processes	5.51 ± 1.04^{a}	5.66 ± 0.80^{a}	5.85 ± 0.82^{a}	4.16 ± 0.49^{b}	6.16 ± 1.25^{A}	6.65 ± 0.70^{A}*	7.80 ± 0.81^{B}*	5.77 ± 1.14^{A}*
Human Diseases	5.49 ± 0.9^{a}	5.28 ± 0.24^{a}	5.02 ± 0.11^{ab}	4.82 ± 0.07^{b}	5.30 ± 0.29^{AB}	5.46 ± 0.19^{A}	5.11 ± 0.23^{B}	5.01 ± 0.20^{C}
Environmental Information Processing	2.77 ± 0.8^{ac}	2.81 ± 0.35^{a}	2.38 ± 0.23^{c}	1.83 ± 0.11^{b}	2.63 ± 0.42^{AB}	2.76 ± 0.26^{AB}	3.10 ± 0.27^{A}*	2.44 ± 0.40^{B}*
Organismal Systems	2.34 ± 0.09^{ab}	2.34 ± 0.08^{a}	2.28 ± 0.06^{a}	2.43 ± 0.02^{b}	2.38 ± 0.19^{A}	2.41 ± 0.13^{A}	2.16 ± 0.09^{B}*	2.4 ± 0.11^{A}

1. Lowercase letters, such as a, b, c, are used to indicate significant difference in the relative abundance of functional genes of the microbiota among different intestinal segments in the CK group. Capital letters, such as A, B, C, are used to indicate significant difference in the relative abundance of functional genes of the microbiota among different intestinal segments in NAFLD (NA) group. The presence of identical letters in the superscript of the relative abundance of functional genes indicates no significant differences between groups ($p > 0.05$), while the absence of identical letters indicates significant differences between groups ($p < 0.05$). 2. "*" and "**" indicates the significant difference in the relative abundance of functional genes in the same intestinal microbiota between CK group and NAFLD (NA) group. *$p < 0.05$; **$p < 0.01$.

related to genetic information processing, cellular processes, and environmental information processing was significantly higher in the cecum and colon of NAFLD mice ($p < 0.05$, Table 1).

Among the secondary functional pathways, amino acid metabolism and carbohydrate metabolism were the two secondary metabolic pathways with the highest relative abundance, followed by cofactor and vitamin metabolism. In the CK group, the colon had the lowest relative abundance of amino acid metabolism and carbohydrate metabolism function ($p < 0.05$) and a significantly higher relative abundance of cofactors and vitamin metabolism function than the ileum and cecum ($p < 0.05$, Table 2). However, there was no difference in these functions between the jejunum, ileum, and colon in the NAFLD group ($p > 0.05$), although significant differences were observed in the relative abundance of amino acid metabolism, cofactors and vitamin metabolism between the cecum and the other three intestine segments ($p < 0.05$, Table 2). Compared to CK mice, NAFLD mice had significantly higher levels of amino acid metabolism and carbohydrate metabolism in the cecum and colon ($p < 0.05$), a significantly lower relative abundance of carbohydrate metabolism in the ileum ($p < 0.05$), and significantly higher relative abundance of cofactors and vitamin metabolism in the cecum ($p < 0.05$, Table 2). Changes in the cecum and colon were similar in terms of the relative abundance of functional genes in the microbiota.

Discussion

There have been advances in the study of gut microbes in human health and disease, but all have been inferred from feces, which are easy to sample and are rich in microbes. The cecum is often used as the research focus in small animals, especially rats and mice. It is the fermentation site of undigested food in mice (Jiminez et al., 2015), whereas in humans, the cecum is much smaller, and fermentation occurs in the colon (He et al., 2019). Alteration of the intestinal microbiota of people suffering from obesity (Zhang et al., 2015; Chambers et al., 2019; Sergeev et al., 2020) or NAFLD (Del Chierico et al., 2016; Hrncir et al., 2021) has been recorded. Studies have found that the relative abundance of Escherichia, Dorea, and Peptoniphilus reportedly increased for the gut microbiota of NAFLD patients. At the same time, that of *Anaerosporobacter*, *Coprococcus*, *Eubacterium*, *Faecalibacterium,* and *Prevotella* decreased (Aron-Wisnewsky et al., 2020). Although these changes in the abundance of microbiota in NAFLD patients and NAFLD mice were not consistent, there were still changes in gut bacteria at all taxonomic levels in human or animal models of obesity, fatty liver, and diabetes. Previous studies showed that the relative abundance of *Firmicutes* and *Proteobacteria* increased, while that of *Bacteroidetes* and *Verrucomicrobia* decreased after a high-fat diet in mice (Walker et al., 2014; Araujo et al., 2017; Wang et al., 2018). All these studies used the cecum or feces as subjects.

Our experiment aims to analyze the differences between the cecal and fecal microbiota of NAFLD mice and other intestinal segments and to investigate whether it would be more appropriate to analyze changes in fecal or cecal microbiota instead of whole intestinal microbiota under NAFLD conditions. Consider that at the time of sampling, mice do not necessarily defecate. Since the mouse colon is highly similar to both fecal microbial (Suzuki and Nachman, 2016; Lkhagva et al., 2021) and metabolite (Zeng et al., 2015) composition, we used distal colonic contents (formed fecal balls) instead of feces. Furthermore, the duodenum had too little content to be detected by high-throughput sequencing. Thus only the jejunum, ileum, cecum, and colon were considered in this study.

In our study, serum levels of TG, TC, HDL and LDL in NAFLD mice were significantly increased compared with CK mice. One study reported that *Actinobacteria* was negatively correlated with TC in mouse fecal microorganisms at the phylum level (Li et al., 2019). Among jejunal microorganisms,

TABLE 2 Relative abundance of secondary functional genes in gut microbiota of normal and NAFLD mice.

Functions	CK-JE	CK-IL	CK-CE	CK-CO	NA-JE	NA-IL	NA-CE	NA-CO
Metabolism								
Amino acid metabolism	10.83 ± 1.02^{ab}	10.95 ± 0.45^{a}	10.96 ± 0.23^{a}	10.48 ± 0.12^{b}	10.90 ± 0.33^{A}	10.96 ± 0.42^{A}	11.35 ± 0.22^{B*}	10.89 ± 0.48^{A*}
Biosynthesis of other secondary metabolites	6.14 ± 0.64^{a}	6.29 ± 0.24^{ab}	6.54 ± 0.13^{bc}	6.75 ± 0.10^{c}	6.04 ± 0.35^{AB}	5.75 ± 0.59^{B*}	6.19 ± 0.15^{AB*}	6.48 ± 0.34^{A*}
Carbohydrate metabolism	10.96 ± 0.74^{ab}	11.02 ± 0.30^{a}	10.58 ± 0.25^{b}	10.07 ± 0.13^{c}	10.54 ± 0.61^{AB}	10.15 ± 0.72^{A*}	10.96 ± 0.27^{B*}	10.56 ± 0.37^{AB*}
Chemical structure transformation maps	0.09 ± 0.07^{a}	0.12 ± 0.09^{a}	0.23 ± 0.15^{ab}	0.37 ± 0.25^{b}	0.52 ± 0.67^{B}	0.78 ± 0.46^{B*}	0.02 ± 0.03^{A*}	0.02 ± 0.03^{A*}
Energy metabolism	4.53 ± 0.14^{a}	4.55 ± 0.14^{a}	4.39 ± 0.06^{ab}	4.25 ± 0.07^{b}	4.50 ± 0.20^{B}	4.58 ± 0.13^{AB}	4.73 ± 0.15^{A*}	4.54 ± 0.16^{B*}
Global and overview maps	5.78 ± 0.45^{a}	5.8 ± 0.15^{a}	5.68 ± 0.17^{a}	5.33 ± 0.08^{b}	5.77 ± 0.22^{A}	5.82 ± 0.31^{A}	6.05 ± 0.08^{B*}	5.69 ± 0.23^{A*}
Glycan biosynthesis and metabolism	5.69 ± 2.42^{a}	5.85 ± 1.24^{a}	7.45 ± 1.25^{b}	10.24 ± 0.80^{c}	5.54 ± 2.48^{AB}	3.41 ± 0.60^{C*}	4.04 ± 0.80^{BC*}	6.85 ± 1.96^{A*}
Lipid metabolism	4.34 ± 0.34^{ab}	4.32 ± 0.17^{a}	4.54 ± 0.14^{b}	4.78 ± 0.13^{c}	4.36 ± 0.50^{AB}	4.89 ± 0.40^{C*}	4.07 ± 0.22^{A*}	4.42 ± 0.23^{B*}
Metabolism of cofactors and vitamins	9.48 ± 1.11^{ab}	9.07 ± 0.65^{a}	9.27 ± 0.26^{a}	9.97 ± 0.21^{b}	9.62 ± 0.72^{A}	9.52 ± 0.47^{A}	8.93 ± 0.46^{B}	9.51 ± 0.56^{A*}
Metabolism of other amino acids	7.03 ± 0.51^{ab}	6.96 ± 0.29^{ab}	6.81 ± 0.11^{a}	7.07 ± 0.14^{b}	7.06 ± 0.70^{AB}	7.55 ± 1.11^{B}	6.68 ± 0.21^{A}	7.02 ± 0.44^{AB}
Metabolism of terpenoids and polyketides	2.86 ± 0.37	2.79 ± 0.20	2.75 ± 0.07	2.73 ± 0.07	2.71 ± 0.27^{AB}	2.88 ± 0.20^{A}	2.61 ± 0.19^{B}	2.71 ± 0.20^{AB}
Nucleotide metabolism	1.64 ± 0.13^{a}	1.63 ± 0.05^{a}	1.57 ± 0.03^{b}	1.53 ± 0.03^{b}	1.59 ± 0.14	1.57 ± 0.15	1.61 ± 0.06	1.60 ± 0.09*
Xenobiotics biodegradation and metabolism	2.48 ± 0.81^{ab}	2.37 ± 0.11^{a}	2.22 ± 0.09^{ab}	2.22 ± 0.09^{b}	2.62 ± 0.64^{A}	3.35 ± 0.48^{B*}	2.46 ± 0.27^{A*}	2.28 ± 0.15^{A}
Genetic Information Processing								
Folding, sorting and degradation	3.00 ± 0.28^{a}	2.92 ± 0.10^{ab}	2.81 ± 0.08^{bc}	2.68 ± 0.04^{c}	2.95 ± 0.19^{AB}	3.04 ± 0.16^{A}	3.01 ± 0.08^{AB*}	2.88 ± 0.17^{B*}
Replication and repair	5.53 ± 0.80^{a}	5.65 ± 0.37^{a}	5.32 ± 0.12^{ab}	5.07 ± 0.10^{b}	5.39 ± 0.46	5.18 ± 0.38	5.53 ± 0.31	5.43 ± 0.40*
Transcription	0.32 ± 0.08^{ab}	0.34 ± 0.04^{b}	0.28 ± 0.02^{ac}	0.26 ± 0.01^{c}	0.31 ± 0.04	0.29 ± 0.03	0.32 ± 0.03*	0.30 ± 0.04*
Translation	3.17 ± 0.56^{ab}	3.29 ± 0.22^{a}	3.09 ± 0.08^{ab}	2.98 ± 0.06^{b}	3.13 ± 0.27^{AB}	3.02 ± 0.24^{A}	3.28 ± 0.16^{B*}	3.18 ± 0.23^{AB*}
Cellular Processes								
Cell growth and death	1.89 ± 0.31	1.91 ± 0.05	1.97 ± 0.05	2.02 ± 0.06	1.90 ± 0.15^{A}	1.92 ± 0.14^{A}	1.92 ± 0.03^{A*}	2.03 ± 0.05^{B}
Cell motility	1.86 ± 0.96^{a}	2.12 ± 0.78^{a}	2.26 ± 0.80^{a}	0.6 ± 0.46^{b}	2.59 ± 1.14^{B}	2.97 ± 0.80^{B*}	4.16 ± 0.72^{A*}	2.17 ± 1.12^{B*}
Cellular community – eukaryotes	0.00 ± 0.00	0.00 ± 0.00	0.00 ± 0.00	0.00 ± 0.00	0.00 ± 0.00	0.00 ± 0.00	0.00 ± 0.00	0.00 ± 0.00
Cellular community – prokaryotes	1.46 ± 0.49^{a}	1.32 ± 0.06^{a}	1.26 ± 0.10^{a}	1.05 ± 0.05^{b}	1.36 ± 0.17^{C}	1.50 ± 0.04^{A*}	1.49 ± 0.11^{A*}	1.22 ± 0.11^{B*}
Transport and catabolism	0.30 ± 0.11^{a}	0.31 ± 0.06^{a}	0.37 ± 0.05^{a}	0.49 ± 0.03^{b}	0.31 ± 0.12^{AB}	0.26 ± 0.07^{B}	0.23 ± 0.04^{B*}	0.35 ± 0.09^{A*}
Human Diseases								
Cancer: overview	0.61 ± 0.07	0.58 ± 0.03	0.56 ± 0.01	0.58 ± 0.01	0.58 ± 0.06^{BC}	0.62 ± 0.05^{C}	0.48 ± 0.04^{A*}	0.55 ± 0.06^{B}
Cancer: specific types	0.09 ± 0.05^{b}	0.08 ± 0.01^{b}	0.06 ± 0.01^{ab}	0.06 ± 0.01^{a}	0.09 ± 0.05^{AB}	0.15 ± 0.05^{B*}	0.07 ± 0.01^{A}	0.07 ± 0.01^{A*}

(Continued)

TABLE 2 (Continued)

Functions	CK-JE	CK-IL	CK-CE	CK-CO	NA-JE	NA-IL	NA-CE	NA-CO
Cardiovascular disease	0.17 ± 0.02^{a}	0.16 ± 0.01^{ab}	0.16 ± 0.01^{ab}	0.16 ± 0.01^{b}	0.18 ± 0.03^{AB}*	0.22 ± 0.02^{B}	0.16 ± 0.00^{A}	0.17 ± 0.01^{A}*
Drug resistance: antimicrobial	2.34 ± 0.32^{a}	2.29 ± 0.13^{a}	2.18 ± 0.08^{a}	2.03 ± 0.05^{b}	2.26 ± 0.26	2.13 ± 0.26	2.23 ± 0.15	2.13 ± 0.11*
Drug resistance: antineoplastic	0.78 ± 0.04^{ab}	0.80 ± 0.02^{a}	0.78 ± 0.02^{ab}	0.76 ± 0.01^{b}	0.76 ± 0.06	0.76 ± 0.14	0.76 ± 0.03	0.76 ± 0.03
Endocrine and metabolic disease	0.52 ± 0.06	0.52 ± 0.04	0.49 ± 0.02	0.51 ± 0.01	0.49 ± 0.06	0.48 ± 0.03*	0.45 ± 0.05*	0.49 ± 0.03*
Immune disease	0.16 ± 0.02^{a}	0.15 ± 0.01^{a}	0.16 ± 0.01^{ab}	0.18 ± 0.02^{b}	0.13 ± 0.04^{AB}	0.13 ± 0.04^{AB}	0.12 ± 0.02^{A}*	0.15 ± 0.02^{B}*
Infectious disease: bacterial	0.67 ± 0.45^{a}	0.56 ± 0.08^{a}	0.48 ± 0.04^{ab}	0.45 ± 0.02^{b}	0.56 ± 0.08	0.59 ± 0.11	0.59 ± 0.04*	0.52 ± 0.06*
Infectious disease: parasitic	0.02 ± 0.03^{ab}	0.02 ± 0.01^{a}	0.01 ± 00^{ab}	0.00 ± 0.01^{b}	0.03 ± 0.02^{AB}	0.05 ± 0.01^{B}*	0.02 ± 0.00^{A}*	0.02 ± 0.01^{A}*
Infectious disease: viral	0.02 ± 0.01	0.03 ± 0.01	0.02 ± 0.00	0.02 ± 0.00	0.04 ± 0.03^{AB}	0.07 ± 0.03^{B}*	0.02 ± 0.00^{A}	0.02 ± 0.01^{A}
Neurodegenerative disease	0.10 ± 0.05^{ab}	0.10 ± 0.02^{ab}	0.12 ± 0.02^{a}	0.08 ± 0.01^{b}	0.19 ± 0.08^{A}*	0.25 ± 0.06^{C}*	0.20 ± 0.03^{A}*	0.13 ± 0.04^{B}*
Substance dependence	0.00 ± 0.00	0.00 ± 0.00	0.00 ± 0.00	0.00 ± 0.00	0.00 ± 0.00	0.00 ± 0.00	0.00 ± 0.00	0.00 ± 0.00
Environmental Information Processing								
Membrane transport	1.89 ± 0.69^{ab}	1.92 ± 0.30^{a}	1.54 ± 0.19^{b}	1.09 ± 0.09^{c}	1.70 ± 0.36^{AB}	1.79 ± 0.31^{AB}	2.05 ± 0.23^{A}*	1.58 ± 0.34^{B}*
Signal transduction	0.88 ± 0.13^{a}	0.90 ± 0.07^{a}	0.84 ± 0.05^{a}	0.74 ± 0.04^{b}	0.93 ± 0.12^{AB}	0.96 ± 0.06^{B}	1.05 ± 0.08^{C}*	0.86 ± 0.09^{A}*
Signaling molecules and interaction	0.00 ± 0.00	0.00 ± 0.00	0.00 ± 0.00	0.00 ± 0.00	0.00 ± 0.00	0.00 ± 0.00	0.00 ± 0.00	0.00 ± 0.00
Organismal Systems								
Aging	0.42 ± 0.04^{a}	0.43 ± 0.03^{a}	0.47 ± 0.01^{b}	0.48 ± 0.02^{b}	0.50 ± 0.05^{AB}*	0.52 ± 0.07^{B}	0.48 ± 0.03^{A}	0.48 ± 0.03^{A}
Circulatory system	0.00 ± 0.00	0.00 ± 0.00	0.00 ± 0.00	0.00 ± 0.00	0.00 ± 0.00	0.00 ± 0.00	00.00 ± 0.00	00.00 ± 0.00
Development and regeneration	0.00 ± 0.00	0.00 ± 0.00	0.00 ± 0.00	0.00 ± 0.00	0.00 ± 0.00	0.00 ± 0.00	0.00 ± 0.00	0.00 ± 0.00
Digestive system	0.11 ± 0.07^{ab}	0.12 ± 0.02^{b}	0.06 ± 0.01^{a}	0.08 ± 0.01^{ab}	0.09 ± 0.03^{AB}	0.09 ± 0.040^{AB}	0.07 ± 0.03^{A}	0.10 ± 0.03^{B}*
Endocrine system	0.85 ± 0.10^{a}	0.85 ± 0.07^{a}	0.76 ± 0.02^{b}	0.79 ± 0.02^{b}	0.85 ± 0.09^{BC}	0.91 ± 0.02^{C}*	0.71 ± 0.06^{A}*	0.79 ± 0.06^{B}
Environmental adaptation	0.20 ± 0.02^{ab}	0.21 ± 0.01^{a}	0.20 ± 0.01^{ab}	0.19 ± 0.01^{b}	0.19 ± 0.03^{B}	0.19 ± 0.01^{B}*	0.22 ± 0.01^{A}*	0.21 ± 0.02^{AB}*
Excretory system	0.16 ± 0.09^{a}	0.14 ± 0.04^{a}	0.18 ± 0.03^{a}	0.27 ± 0.03^{b}	0.17 ± 0.09^{A}	0.17 ± 0.05^{A}	0.08 ± 0.03^{B}*	0.19 ± 0.05^{A}*
Immune system	0.29 ± 0.05^{a}	0.29 ± 0.01^{a}	0.29 ± 0.01^{a}	0.27 ± 0.01^{b}	0.29 ± 0.05^{AB}	0.27 ± 0.06^{B}	0.32 ± 0.01^{A}*	0.30 ± 0.02^{AB}*
Nervous system	0.30 ± 0.05^{a}	0.32 ± 0.03^{a}	0.32 ± 0.01^{ab}	0.35 ± 0.01^{b}	0.27 ± 0.04^{A}	0.22 ± 0.02^{B}*	0.27 ± 0.02^{A}*	0.33 ± 0.03^{C}
Sensory system	0.00 ± 0.00	0.00 ± 0.00	0.00 ± 0.00	0.00 ± 0.00	0.00 ± 0.00	0.00 ± 0.00	0.00 ± 0.00	0.00 ± 0.00

1. Lowercase letters, such as a, b, c, are used to indicate significant difference in the relative abundance of functional genes of the microbiota among different intestinal segments in the CK group. Capital letters, such as A, B, C, are used to indicate significant difference in the relative abundance of functional genes of the microbiota among different intestinal segments in NAFLD (NA) group. The presence of identical letters in the superscript of the relative abundance of functional genes indicates no significant differences between groups ($p > 0.05$), while the absence of identical letters indicates significant differences between groups ($p < 0.05$). 2. "*" and "**" indicates the significant difference in the relative abundance of functional genes in the same intestinal microbiota between CK group and NAFLD (NA) group. *$p < 0.05$; **$p < 0.01$.

Erysipelotrichaceae and *Lactobacillaceae* were negatively correlated with TC at the family level (Wang et al., 2021). A study on rats reported that fecal microorganisms *Akkermansia* and *Lactobacillus* were significantly positively associated with TG, TC, and LDL-C and negatively correlated with HDL-C at the genus level (Li R. et al., 2020). In addition, some studies dive into the species level, *Lactobacillus gasseri* and *Lactobacillus taiwanensis* of the fecal microbiota were significantly positively correlated with lipid droplets in the liver (Zeng et al., 2013) and *Desulfovibrio vulgaris* can reduce hepatocyte steatosis and triglyceride accumulation in hepatocytes and liver index (Hong et al., 2021). This indicates intestinal microbiota significantly correlates with serum lipid levels and hepatocyte lesions in NAFLD mice.

At present, research on jejunal microbiota is very rare and limited. Our study found that the alpha diversity (Figure 3) and beta diversity (Figures 4A,B) of the jejunal microbiota of NAFLD

mice were not significantly different from those of CK mice, indicating no significant change in the structure of jejunal microbiota in NAFLD mice after a high-fat diet. In NAFLD mice, the beta diversity in the other three intestinal segments (ileum, cecum, and colon; Figure 4), as well as the alpha diversity in the ileum and colon (Figure 3), were significantly changed. Although, as compared to CK mice, the relative abundance of *Peptostreptococcaceae*, *Romboutsia*, and *Allobaculum* in the jejunum of NAFLD mice had altered considerably, functional prediction analysis showed that the relative abundance of primary functional genes had not changed. Only the relative abundance of two secondary active genes (aging and Cardiovascular disease) had significant changes. This indicates that the changes in the microbiota in the jejunum and the other three intestinal segments are inconsistent. We speculated that jejunal microbiota diversity and composition did not change after a high-fat diet mainly because the jejunum had a strong emptying ability; thus, it remained empty for a long time and had the lowest bacterial abundance. A load of microbial community was estimated to be between 10^4 and 10^7 CFU/ml (Martinez-Guryn et al., 2019). Compared to other intestinal segments, the lumen of the jejunum is more acidic, with a faster transit time and higher gradients of oxygen, antimicrobials (sIgA and AMPs) and bile acids. Conjugated bile acids, probably together with fatty acids, inhibit bacterial growth directly through their pharmacological properties and signaling properties (Wang et al., 2008; Jia et al., 2018; Lema et al., 2020).

From the limited relevant studies in humans, in general, the ileum serves as a major absorption site for nutrients (e.g., B vitamins and residual nutrients that are not absorbed proximal) and reuptake of BA into the liver circulation, with the latter being more influenced by gut microbes (Martinez-Guryn et al., 2019). *Firmicutes* (*Lactobacillus*, *Veillonella*, *Enterococcus*, and *Clostridium*) and *Proteobacteria* (*Enterobacteria*) are the main bacteria in the ileum (Lema et al., 2020). However, some studies suggest that the ileum microbiota appears to be mainly composed of *Bacteroides*, *Clostridium*, *Enterobacteria*, *Lactobacillus*, and *Veillonella* (Martinez-Guryn et al., 2019), while the dominant bacterial phyla in the colon are *Bacteroidetes* (*Bacteroidaceae*, *Prevotellaceae*, etc.) and *Firmicutes* (*Lachnospiraceae* and *Ruminococcaceae*; Lema et al., 2020). Stefania Vaga et al. studied the mucosal flora of five healthy adults from Stockholm. They found that the two phyla with the highest relative abundance in the ileum were *Firmicutes* and *Bacteroides*, consistent with our mouse flora study (Vaga et al., 2020). There was also a study in mice that reported a significant increase in the relative abundance of *Faecalibaculum* in the ileal microbiota of HFD-induced NAFLD mice compared with normal mice (Mu et al., 2020). Our study found that alpha and beta diversity in the ileum of NAFLD mice changed after a high-fat diet, but alpha diversity in the cecum did not change. The *Rank Sum test* results showed that the relative abundance of Firmicutes and Proteobacteria in the ileum did not change after a high-fat diet but increased significantly in the cecum and colon.

Meanwhile, through *rank sum test* and Lefse analysis, it was found that the change trend of characteristic flora and main bacterial composition of ileum was different from that of cecum and colon. Therefore, the changes in the ileum of NAFLD mice were different from those in the large intestine (cecum and colon). The main reason is that the ileum is vastly different from the large intestine in terms of bacterial abundance, diversity, and flora composition. The microbial load in the ileum, estimated at $10^3 \sim 10^8$ CFU/ml, contains both the jejunal microbiota and the large intestine microbiota and is a transition zone between the sparse populations of aerobic microbiota of the jejunum and the very dense populations of strict anaerobic in the colon (Rao and Bhagatwala, 2019). In our study, the number of OTUs in the ileum of CK mice was the largest (Figures 6B,E), which was mainly composed of facultative and obligate anaerobic bacteria (Rao and Bhagatwala, 2019; Shahir et al., 2020; van Kessel et al., 2020). Facultative anaerobic bacteria included *Proteobacteria* and *Lactobacillaceae*, which are equipped to resist the synergistic effect of bile acids and antimicrobial peptides (Tropini et al., 2017).

Additionally, our study found that there were no differences in both alpha and beta diversity between a normal colon and cecum, as well as the relative abundance of major bacteria at phylum, family, and genus levels, indicating that the microbiota of the colon and cecum were highly similar and that the microbiota of both could be substituted for each other during microbiota research and fecal microbiota transplantation. Interestingly, after a high-fat diet, the characteristics of the changes in the abundance of major bacteria were very similar. The functional prediction of intestinal microbiota also showed that the relative abundance of primary and secondary functional genes in cecum and colon was similar. This may be due to the short colon of the mouse, which mainly plays the function of absorbing water and electrolytes as well as transport, and the main fermentation has taken place in the cecum (Brown et al., 2018). However, there are differences in the structure and function of the cecum and colon between humans and mice. In animals, fermentation occurs mainly in the cecum (Brown et al., 2018), while in humans, it occurs primarily in the colon. Human colon microbiota has been studied in greater depth than cecal microbiota. The colon has greater microbial abundance and diversity than the small intestine (jejunum and ileum). Despite its shorter length, food stays in the colon (10 h to several days) longer than it does in the small intestine (1–5 h; Zhuang et al., 2020). The thicker inner and outer layers of mucus (Hansson, 2012) are important barriers to bacteria (an estimated 10^{10} to 10^{12} CFU/ml, including *Firmicutes*, *Bacteroidetes* and other phyla; Jakobsson et al., 2015; Martinez-Guryn et al., 2019). In the colon, the relative abundance of *Butyricicoccus*, *Allobaculum*, *Alloprevotella*, *Lachnospiraceae NK4A136 group*, *Parasutterella*, and *uncultured bacterium Muribaculaceae* decreased, while the relative abundance of *Campylobacter*, *Dubosiella*, *Faecalibaculum* and *Fusobacterium* increased (Mu et al., 2020). In our study,

Bacteroidetes was the main bacteria in the colon of CK mice, with a relative abundance of 72.07%, followed by *Firmicutes* with a relative abundance of 15.36%, and *Verrucomicrobia* with a relative abundance of 8.67% (Supplementary Table S2). At the family level, the bacteria with the highest relative abundance were *Muribaculaceae*, *Akkermansiaceae*, *Lachnospiaceae*, *Erysipelotrichaceae*, and *Lactobacillaeae* (Supplementary Table S3). At the genus level, the five genera with the highest relative abundance were *Akkermansia*, *Allobaculum*, *Muribaculumg*, *Lactobacillus*, and *Parabacteroides* (Supplementary Table S4). Compared with the results of human related studies, was found that in the colon, human and mice have similar bacterial species at the phylum and family level, but have differences at the genus level, which is likely caused by host species. Two studies on cecal microbiota in mice showed a significant increase in the abundance of *Faecalibaculum* in cecal microbiota in NAFLD mice compared with normal mice (Mu et al., 2020; Gu et al., 2022), which was similar to our results.

Conclusion

In conclusion, the structure of jejunal microbiota in NAFLD mice induced by a high-fat diet did not change significantly. In contrast, the intestinal microbiota of the ileum, cecum, and colon (feces) changed significantly. However, the characteristics of the changes in the ileum were substantially different from that of the cecum and colon (feces), and the changes in the cecum and colon (feces) were similar. Therefore, the study results of cecal and colonic (fecal) microbiota cannot completely represent the results of jejunal and ileal microbiota. This is of reference significance for future studies on the role of intestinal microbiota in NAFLD.

Data availability statement

The data presented in the study are deposited in the NCBI-SRA repository (https://www.ncbi.nlm.nih.gov/bioproject/PRJNA877487), accession number PRJNA877487.

Ethics statement

The animal study was reviewed and approved by the Animal Ethics Committee of Southwest Medical University (No. of Animal Ethics Approval: SWMU2019463).

Author contributions

HY and CG: conceptualization. SbL, YW, JrH, BC, WX, and FZ: data curation. YL, BC, SyL, and FK: formal analysis. GY and CG: funding acquisition. SyL, YL, LC, LH, MH, QY, WX, and JhH: investigation. GY, ZY, SY, HY, and CG: methodology. CG: project administration. YL and JrH: resources. ZY and CG: supervision. QY, HY, and CG: validation. YW: visualization. GY, SbL, YW, and BC: writing - original draft. SbL, LH, MH, YT, WL, SY, BA, HY, and CG: writing - review and editing. All authors have read and agreed to the published version of the manuscript.

Funding

This research was funded by the "Applied Basic Research Program of Science and Technology Department of Sichuan Province (2020YJ0399), the Liangshan Science and Technology Bureau (20ZDYF0070), PhD Project of Xichang University (LGLZ201809), and Luzhou Municipal People's Government – Southwest Medical University Technology Strategy Project (2020LZXNYDJ20)."

Conflict of interest

The authors declare that the research was conducted in the absence of any commercial or financial relationships that could be construed as a potential conflict of interest.

Publisher's note

Supplementary material

The Supplementary material for this article can be found online at: https://www.frontiersin.org/articles/10.3389/fmicb.2022.1051200/full#supplementary-material

SUPPLEMENTARY FIGURE S1
Relative abundance of bacteria at family level. **(A)** Stacked column graph of the top 10 families with the highest relative abundance. **(B)** The box diagram was used to analyze the differences in relative abundance of the five families with the highest relative abundance. *Wilcox Rank-sum test* was used to compare the significance of the same intestinal segment between the CK group and the NAFLD group; *Kruskal-wallis test* was used to compare the differences between different intestinal segments in the same group. *indicate significant difference in the different intestinal segments in the CK group and NAFLD group. #indicates the significant difference in the same intestinal segments between CK group and NAFLD group. *or# $p<0.05$; **or## $p<0.01$.

References

Abdou, R. M., Zhu, L., Baker, R. D., and Baker, S. S. (2016). Gut microbiota of nonalcoholic fatty liver disease. *Dig. Dis. Sci.* 61, 1268–1281. doi: 10.1007/s10620-016-4045-1

Aragonès, G., Colom-Pellicer, M., Aguilar, C., Guiu-Jurado, E., Martínez, S., Sabench, F., et al. (2019). Circulating microbiota-derived metabolites: a liquid biopsy? *Int. J. Obes.* 44, 875–885. doi: 10.1038/s41366-019-0430-0

Araujo, J. R., Tomas, J., Brenner, C., and Sansonetti, P. J. (2017). Impact of high-fat diet on the intestinal microbiota and small intestinal physiology before and after the onset of obesity. *Biochimie* 141, 97–106. doi: 10.1016/j.biochi.2017.05.019

Aron-Wisnewsky, J., Vigliotti, C., Witjes, J., Le, P., Holleboom, A. G., Verheij, J., et al. (2020). Gut microbiota and human NAFLD: disentangling microbial signatures from metabolic disorders. *Nat. Rev. Gastroenterol. Hepatol.* 17, 279–297. doi: 10.1038/s41575-020-0269-9

Brown, K., Abbott, D. W., Uwiera, R. R. E., and Inglis, G. D. (2018). Removal of the cecum affects intestinal fermentation, enteric bacterial community structure, and acute colitis in mice. *Gut Microbes* 9, 218–235. doi: 10.1080/19490976.2017.1408763

Caporaso, J. G., Kuczynski, J., Stombaugh, J., Bittinger, K., Bushman, F. D., Costello, E. K., et al. (2010). QIIME allows analysis of high-throughput community sequencing data. *Nat. Methods* 7, 335–336. doi: 10.1038/nmeth.f.303

Chambers, E. S., Byrne, C. S., Morrison, D. J., Murphy, K. G., Preston, T., Tedford, C., et al. (2019). Dietary supplementation with inulin-propionate ester or inulin improves insulin sensitivity in adults with overweight and obesity with distinct effects on the gut microbiota, plasma metabolome and systemic inflammatory responses: a randomised cross-over trial. *Gut* 68, 1430–1438. doi: 10.1136/gutjnl-2019-318424

Del Chierico, F., Nobili, V., Vernocchi, P., Russo, A., De Stefanis, C., Gnani, D., et al. (2016). Gut microbiota profiling of pediatric nonalcoholic fatty liver disease and obese patients unveiled by an integrated meta-omics-based approach. *Hepatology* 65, 451–464. doi: 10.1002/hep.28572

Douglas, G. M., Maffei, V. J., Zaneveld, J. R., Yurgel, S. N., Brown, J. R., Taylor, C. M., et al. (2020). PICRUSt2 for prediction of metagenome functions. *Nat. Biotechnol.* 38, 685–688. doi: 10.1038/s41587-020-0548-6

Edgar, R. C. (2013). UPARSE: highly accurate OTU sequences from microbial amplicon reads. *Nat. Methods* 10, 996–998. doi: 10.1038/nmeth.2604

Gadiparthi, C., Spatz, M., Greenberg, S., Iqbal, U., Kanna, S., Satapathy, S. K., et al. (2020). NAFLD epidemiology, emerging pharmacotherapy, liver transplantation implications and the trends in the United States. *J. Clin. Transl. Hepatol.* 8, 215–221. doi: 10.14218/JCTH.2020.00014

Gao, H., Chi, X., Li, G., Qin, W., Song, P., Jiang, F., et al. (2020). Gut microbial diversity and stabilizing functions enhance the plateau adaptability of Tibetan wild ass (Equus kiang). *Microbiologyopen* 9, 1150–1161. doi: 10.1002/mbo3.1025

Gatto, L., Breckels, L. M., Naake, T., and Gibb, S. (2015). Visualization of proteomics data using R and bioconductor. *Proteomics* 15, 1375–1389. doi: 10.1002/pmic.201400392

Gu, C., Zhou, Z., Yu, Z., He, M., He, L., Luo, Z., et al. (2022). The microbiota and It's correlation with metabolites in the gut of mice with nonalcoholic fatty liver disease. *Front. Cell. Infect. Microbiol.* 12:870785. doi: 10.3389/fcimb.2022.870785

Hansson, G. C. (2012). Role of mucus layers in gut infection and inflammation. *Curr. Opin. Microbiol.* 15, 57–62. doi: 10.1016/j.mib.2011.11.002

He, X., Ji, G., Jia, W., and Li, H. (2016). Gut microbiota and nonalcoholic fatty liver disease: insights on mechanism and application of metabolomics. *Int. J. Mol. Sci.* 17:300. doi: 10.3390/ijms17030300

He, X., Parenti, M., Grip, T., Lönnerdal, B., Timby, N., Domellöf, M., et al. (2019). Fecal microbiome and metabolome of infants fed bovine MFGM supplemented formula or standard formula with breast-fed infants as reference: a randomized controlled trial. *Sci. Rep.* 9:11589. doi: 10.1038/s41598-019-47953-4

Hong, Y., Sheng, L., Zhong, J., Tao, X., Zhu, W., Ma, J., et al. (2021). Desulfovibrio vulgaris, a potent acetic acid-producing bacterium, attenuates nonalcoholic fatty liver disease in mice. *Gut Microbes* 13, 1–20. doi: 10.1080/19490976.2021.1930874

Hrncir, T., Hrncirova, L., Kverka, M., Hromadka, R., Machova, V., Trckova, E., et al. (2021). Gut microbiota and NAFLD: Pathogenetic mechanisms, microbiota signatures, and therapeutic interventions. *Microorganisms* 9:957. doi: 10.3390/microorganisms9050957

Jakobsson, H. E., Rodriguez-Pineiro, A. M., Schutte, A., Ermund, A., Boysen, P., Bemark, M., et al. (2015). The composition of the gut microbiota shapes the colon mucus barrier. *EMBO Rep.* 16, 164–177. doi: 10.15252/embr.201439263

Jia, W., Xie, G., and Jia, W. (2018). Bile acid-microbiota crosstalk in gastrointestinal inflammation and carcinogenesis. *Nat. Rev. Gastroenterol. Hepatol.* 15, 111–128. doi: 10.1038/nrgastro.2017.119

Jiminez, J. A., Uwiera, T. C., Douglas Inglis, G., and Uwiera, R. R. (2015). Animal models to study acute and chronic intestinal inflammation in mammals. *Gut Pathog.* 7:29. doi: 10.1186/s13099-015-0076-y

Langille, M. G., Zaneveld, J., Caporaso, J. G., McDonald, D., Knights, D., Reyes, J. A., et al. (2013). Predictive functional profiling of microbial communities using 16S rRNA marker gene sequences. *Nat. Biotechnol.* 31, 814–821. doi: 10.1038/nbt.2676

Lau, J. K., Zhang, X., and Yu, J. (2017). Animal models of non-alcoholic fatty liver disease: current perspectives and recent advances. *J. Pathol.* 241, 36–44. doi: 10.1002/path.4829

Lema, I., Araujo, J. R., Rolhion, N., and Demignot, S. (2020). Jejunum: the understudied meeting place of dietary lipids and the microbiota. *Biochimie* 178, 124–136. doi: 10.1016/j.biochi.2020.09.007

Li, L., Shi, M., Salerno, S., Tang, M., Guo, F., Liu, J., et al. (2019). Microbial and metabolomic remodeling by a formula of Sichuan dark tea improves hyperlipidemia in apoE-deficient mice. *PLoS One* 14:e0219010. doi: 10.1371/journal.pone.0219010

Li, R., Yao, Y., Gao, P., and Bu, S. (2020). The therapeutic efficacy of Curcumin vs. metformin in modulating the gut microbiota in NAFLD rats: a comparative study. *Front. Microbiol.* 11:555293. doi: 10.3389/fmicb.2020.555293

Li, N., Zuo, B., Huang, S., Zeng, B., Han, D., Li, T., et al. (2020). Spatial heterogeneity of bacterial colonization across different gut segments following inter-species microbiota transplantation. *Microbiome* 8:161. doi: 10.1186/s40168-020-00917-7

Lim, M. Y., Song, E. J., Kang, K. S., and Nam, Y. D. (2019). Age-related compositional and functional changes in micro-pig gut microbiome. *Geroscience* 41, 935–944. doi: 10.1007/s11357-019-00121-y

Liu, W., Wang, Q., Song, J., Xin, J., Zhang, S., Lei, Y., et al. (2021). Comparison of gut microbiota of yaks from different geographical regions. *Front. Microbiol.* 12:666940. doi: 10.3389/fmicb.2021.666940

Lkhagva, E., Chung, H.-J., Hong, J., Tang, W. H. W., Lee, S.-I., Hong, S.-T., et al. (2021). The regional diversity of gut microbiome along the GI tract of male C57BL/6 mice. *BMC Microbiol.* 21:44. doi: 10.1186/s12866-021-02099-0

Magoc, T., and Salzberg, S. L. (2011). FLASH: fast length adjustment of short reads to improve genome assemblies. *Bioinformatics* 27, 2957–2963. doi: 10.1093/bioinformatics/btr507

Martinez-Guryn, K., Leone, V., and Chang, E. B. (2019). Regional diversity of the gastrointestinal microbiome. *Cell Host Microbe* 26, 314–324. doi: 10.1016/j.chom.2019.08.011

Mu, H., Zhou, Q., Yang, R., Zeng, J., Li, X., Zhang, R., et al. (2020). Naringin attenuates high fat diet induced non-alcoholic fatty liver disease and gut bacterial Dysbiosis in mice. *Front. Microbiol.* 11:585066. doi: 10.3389/fmicb.2020.585066

Rao, S. S. C., and Bhagatwala, J. (2019). Small intestinal bacterial overgrowth: clinical features and therapeutic management. *Clin. Transl. Gastroenterol.* 10:e00078. doi: 10.14309/ctg.0000000000000078

Schloss, P. D., Westcott, S. L., Ryabin, T., Hall, J. R., Hartmann, M., Hollister, E. B., et al. (2009). Introducing mothur: open-source, platform-independent, community-supported software for describing and comparing microbial communities. *Appl. Environ. Microbiol.* 75, 7537–7541. doi: 10.1128/AEM.01541-09

Schwimmer, J. B., Johnson, J. S., Angeles, J. E., Behling, C., Belt, P. H., Borecki, I., et al. (2019). Microbiome signatures associated with Steatohepatitis and moderate to severe fibrosis in children with nonalcoholic fatty liver disease. *Gastroenterology* 157, 1109–1122. doi: 10.1053/j.gastro.2019.06.028

Sergeev, I. N., Aljutaily, T., Walton, G., and Huarte, E. (2020). Effects of Synbiotic supplement on human gut microbiota, body composition and weight loss in obesity. *Nutrients* 12:222. doi: 10.3390/nu12010222

Shahir, N. M., Wang, J. R., Wolber, E. A., Schaner, M. S., Frank, D. N., Ir, D., et al. (2020). Crohn's disease differentially affects region-specific composition and Aerotolerance profiles of Mucosally adherent bacteria. *Inflamm. Bowel Dis.* 26, 1843–1855. doi: 10.1093/ibd/izaa103

Suzuki, T. A., and Nachman, M. W. (2016). Spatial heterogeneity of gut microbial composition along the gastrointestinal tract in natural populations of house mice. *PLoS One* 11:e0163720. doi: 10.1371/journal.pone.0163720

Tropini, C., Earle, K. A., Huang, K. C., and Sonnenburg, J. L. (2017). The gut microbiome: connecting spatial organization to function. *Cell Host Microbe* 21, 433–442. doi: 10.1016/j.chom.2017.03.010

Vaga, S., Lee, S., Ji, B., Andreasson, A., Talley, N. J., Agreus, L., et al. (2020). Compositional and functional differences of the mucosal microbiota along the intestine of healthy individuals. *Sci. Rep.* 10:14977. doi: 10.1038/s41598-020-71939-2

van Kessel, S. P., de Jong, H. R., Winkel, S. L., van Leeuwen, S. S., Nelemans, S. A., Permentier, H., et al. (2020). Gut bacterial deamination of residual levodopa

medication for Parkinson's disease. *BMC Biol.* 18:137. doi: 10.1186/s12915-020-00876-3

Walker, A., Pfitzner, B., Neschen, S., Kahle, M., Harir, M., Lucio, M., et al. (2014). Distinct signatures of host-microbial meta-metabolome and gut microbiome in two C57BL/6 strains under high-fat diet. *ISME J.* 8, 2380–2396. doi: 10.1038/ismej.2014.79

Wang, Y. D., Chen, W. D., Moore, D. D., and Huang, W. (2008). FXR: a metabolic regulator and cell protector. *Cell Res.* 18, 1087–1095. doi: 10.1038/cr.2008.289

Wang, H., Guan, L., Li, J., Lai, M., and Wen, X. (2018). The effects of Berberine on the gut microbiota in Apc (min/+) mice fed with a high fat diet. *Molecules* 23:2298. doi: 10.3390/molecules23092298

Wang, R. R., Zhang, L. F., Chen, L. P., Wang, J. Y., Zhang, L., Xu, Y. S., et al. (2021). Structural and functional modulation of gut microbiota by Jiangzhi granules during the amelioration of nonalcoholic fatty liver disease. *Oxidative Med. Cell. Longev.* 2021, 2234695–2234618. doi: 10.1155/2021/2234695

Xiao, J., Wang, F., Wong, N. K., He, J., Zhang, R., Sun, R., et al. (2019). Global liver disease burdens and research trends: analysis from a Chinese perspective. *J. Hepatol.* 71, 212–221. doi: 10.1016/j.jhep.2019.03.004

Xu, X., Lv, J., Guo, F., Li, J., Jia, Y., Jiang, D., et al. (2020). Gut microbiome influences the efficacy of PD-1 antibody immunotherapy on MSS-type colorectal cancer via metabolic pathway. *Front. Microbiol.* 11:814. doi: 10.3389/fmicb.2020.00814

Zeng, H., Grapov, D., Jackson, M. I., Fahrmann, J., Fiehn, O., and Combs, G. F. (2015). Integrating multiple analytical datasets to compare metabolite profiles of mouse colonic-Cecal contents and feces. *Meta* 5, 489–501. doi: 10.3390/metabo5030489

Zeng, H., Liu, J., Jackson, M. I., Zhao, F. Q., Yan, L., and Combs, G. F. Jr. (2013). Fatty liver accompanies an increase in lactobacillus species in the hind gut of C57BL/6 mice fed a high-fat diet. *J. Nutr.* 143, 627–631. doi: 10.3945/jn.112.172460

Zhang, C., Yin, A., Li, H., Wang, R., Wu, G., Shen, J., et al. (2015). Dietary modulation of gut microbiota contributes to alleviation of both genetic and simple obesity in children. *EBioMedicine* 2, 968–984. doi: 10.1016/j.ebiom.2015.07.007

Zhuang, Y., Chai, J., Cui, K., Bi, Y., Diao, Q., Huang, W., et al. (2020). Longitudinal investigation of the gut microbiota in goat kids from birth to Postweaning. *Microorganisms* 8:111. doi: 10.3390/microorganisms8081111

Zoetendal, E. G., Raes, J., van den Bogert, B., Arumugam, M., Booijink, C. C., Troost, F. J., et al. (2012). The human small intestinal microbiota is driven by rapid uptake and conversion of simple carbohydrates. *ISME J.* 6, 1415–1426. doi: 10.1038/ismej.2011.212

frontiers | Frontiers in Microbiology

TYPE Original Research
PUBLISHED 28 July 2023
DOI 10.3389/fmicb.2023.1206909

OPEN ACCESS

EDITED BY
Ren-You Gan,
Singapore Institute of Food and Biotechnology Innovation, Singapore

REVIEWED BY
Ishraq Alim,
Cornell University, United States
Yingli Jing,
Capital Medical University, China

*CORRESPONDENCE
Rizhao Pang
✉ przprz17@126.com
Anren Zhang
✉ anren0124@163.com

†These authors have contributed equally to this work

RECEIVED 16 April 2023
ACCEPTED 04 July 2023
PUBLISHED 28 July 2023

CITATION
Wang J, Zhao X, Zhou R, Wang M, Xiang W, You Z, Li M, Tang R, Zheng J, Li J, Zhu L, Gao J, Li H, Pang R and Zhang A (2023) Gut microbiota and transcriptome dynamics in every-other-day fasting are associated with neuroprotection in rats with spinal cord injury. *Front. Microbiol.* 14:1206909. doi: 10.3389/fmicb.2023.1206909

Gut microbiota and transcriptome dynamics in every-other-day fasting are associated with neuroprotection in rats with spinal cord injury

Junyu Wang[1†], Xiaohua Zhao[2,3†], Ruihan Zhou[2†], Meiyu Wang[4†], Wu Xiang[2], Zilong You[5], Min Li[6], Ruiling Tang[2], Jingqi Zheng[2], Jiayu Li[7], Li Zhu[7], Jiaxin Gao[7], Huaqiang Li[7], Rizhao Pang[2]* and Anren Zhang[6]*

[1]State Key Laboratory of Biotherapy, West China Hospital, Sichuan University, Chengdu, China, [2]Department of Rehabilitation Medicine, General Hospital of Western Theater Command, Chengdu, China, [3]Department of Rehabilitation Medicine, The People's Hospital of Tongliang District, Chongqing, China, [4]Rehabilitation and Wellness Care Centre, Tian Fu College of Swufe, Chengdu, China, [5]Department of Biochemistry and Biophysics, School of Basic Medical Sciences, Peking University, Beijing, China, [6]Department of Rehabilitation Medicine, Shanghai Fourth People's Hospital Affiliated to Tongji University School of Medicine, Shanghai, China, [7]School of Health Preservation and Rehabilitation, Chengdu University of Traditional Chinese Medicine, Chengdu, China

Introduction: Every-other-day fasting (EODF) is a classical intermittent fasting (IF) mode with neuroprotective effects that promotes motor function recovery after spinal cord injury (SCI) in rats. However, its dynamic effects on the gut microbiota and spinal cord transcriptome remain unknown.

Methods: In this study, 16S rRNA sequencing and RNA-seq analysis were used to investigate the effects of ad libitum (AL) and EODF dietary modes on the structural characteristics of rat gut microbiota in rats and the spinal cord transcriptome at various time points after SCI induction.

Results: Our results showed that both dietary modes affected the bacterial community composition in SCI rats, with EODF treatment inducing and suppressing dynamic changes in the abundances of potentially anti-inflammatory and pro-inflammatory bacteria. Furthermore, the differentially expressed genes (DEGs) enriched after EODF intervention in SCI rats were associated with various biological events, including immune inflammatory response, cell differentiation, protein modification, neural growth, and apoptosis. In particular, significant spatiotemporal differences were apparent in the DEGs associated with neuroprotection between the EODF and AL interventions. These DGEs were mainly focused on days 1, 3, and 7 after SCI. The relative abundance of certain genera was significantly correlated with DEGs associated with neuroprotective effects in the EODF-SCI group.

Discussion: Our results showed that EODF treatment may exert neuroprotective effects by modulating the transcriptome expression profile following SCI in rats. Furthermore, gut microbiota may be partially involved in mediating these effects.

KEYWORDS

every-other-day fasting, spinal cord injury, intermittent fasting, gut microbiota, transcriptome, neuroprotection

1. Introduction

Spinal cord injury (SCI) is a highly disabling and traumatic condition without effective treatment options. In recent years, intermittent fasting (IF) has attracted increasing attention because it mediates the energy supply and avoids gastrointestinal damage caused by prolonged fasting (Hatting et al., 2017). Every-other-day fasting (EODF), a classic mode of IF, is a 24-h alternating fasting and feeding dietary pattern shown to exert neuroprotective effects; in studies of neurological diseases, EODF was found to reduce neuro-inflammation secondary to stroke and craniocerebral injury in experimental animals, thus exerting a neuroprotective effect and improving neurological deficits (Varady and Hellerstein, 2007; Davis et al., 2008; Manzanero et al., 2014). EODF-treated rat models of SCI recovered varying levels of motor and sensory function (Plunet et al., 2008, 2010; Jeong et al., 2011). Another study noted that in the SCI rat model, the first 24 h is a very acute phase that may involve changes in most immediate early stress genes; days 3 and 7 represent the peak of delayed apoptosis of neuronal cells; days 10–14 are deemed the subacute phase when tissue inflammation levels have subsided; and the subsequent period is considered the recovery period (Chamankhah et al., 2013). A comparison of two studies that screened for differential genes before and after SCI modeling revealed that the differentially expressed genes (DEGs) caused by SCI were mainly related to stress and immune response, with stress including an inflammatory response and immune response including innate and adaptive immune response; these studies showed that the immune and inflammatory responses continued to spread from the acute phase to the chronic phase, with an intrinsic immune response dominating in the acute phase and an adaptive immune response dominating in the subacute and chronic phases (Chamankhah et al., 2013; Shi et al., 2017). These results suggest that the inflammatory and immune responses are the predominant biological events following SCI. We previously found that EODF exerted significant neuroprotective effects in a rat model of SCI, promoting the recovery of motor function, reducing the inflammatory response in the plane of injury, and inhibiting apoptosis and necrosis (Sun et al., 2018; Li J. J. et al., 2022). However, at the genetic level, the mechanisms by which EODF regulates gene expression levels in distal spinal cord tissue have not been clarified. Furthermore, the biological mechanisms by which EODF exerts its neuroprotective effects in a rat model of SCI treatment are not fully understood.

SCI can disrupt the balance of the gut microbiota (Gungor et al., 2016; Kigerl et al., 2016). The diversity and structural composition of gut microbiota were reduced in SCI patients, suggesting an association between the neurogenic rectum and the gut microbiota (Zhang et al., 2018). SCI has been shown to promote intestinal dysfunction and mucosal permeability, leading to translocation of the gut microbiota (Kigerl et al., 2016). We previously described disturbances in the gut microbiota of patients with SCI and found a correlation in the abundance of certain microbial genera and lymphocyte subpopulations (Pang et al., 2022). Gut microbiota plays key roles in immune, nutritional, and metabolic functions (Ejtahed et al., 2017). Some diet therapies can restore or dramatically alleviate dysfunctions in gut microbiota and are considered a promising approach to preventing and treating global health problems. Increasing evidence indicates that IF has a variety of health benefits for individuals that are healthy (Ali et al., 2021; Su et al., 2021, 2022), obese (Li et al., 2017; Deng et al., 2020; Liu et al., 2021a), or diabetic (Liu et al., 2020), as well as those with cardiovascular disease (Guo et al., 2021; Prisco et al., 2021) hypertension (Maifeld et al., 2021; Shi H. et al., 2021), and neurological disorders (Cignarella et al., 2018; Serger et al., 2022). The beneficial effects of IF are considered to be exerted through the restoration of gut microbiota and metabolite production; however, to the best of our knowledge, the characteristics of gut microbiota in SCI rats treated with EODF have not been reported to date.

To further understand the effects of EODF on the gut microbiota and spine cord tissue transcriptome in SCI rats during the acute, subacute, and recovery phases, we designed the following experiments (Figure 1). We assessed the dynamic changes of gut microbiota in an *ad libitum* diet (AL)-SCI and EODF-SCI group based on the 16S rRNA high-throughput sequencing of fecal samples collected 1 day before and 1, 3, 7, 14, and 28 days after modeling. Furthermore, we assessed the dynamic changes of DEGs in the *ad libitum* diet (AL)-SCI and EODF-SCI groups based on transcriptomic data collected from spinal cord tissues after 1, 3, 7, 14, and 28 days and biological annotation of DEGs through Gene Ontology (GO) and Kyoto Encyclopedia of Genes and Genomes (KEGG) databases to explore the effects of EODF on gene transcription in post-injury spinal cord tissues, particularly on neuroprotection-related DEGs and pathways after SCI. Finally, we used the Spearman's correlation coefficient to identify the gut microbiota associated with neuroprotection-related DEGs. Accordingly, we aimed to describe the characteristics of gut microbiota and DEGs associated with each diet mode and identify the critical bacteria, key DEGs, and main biological events associated with neuroprotection.

2. Materials and methods

2.1. Animal grouping

Healthy male Sprague–Dawley rats (2 months old,130 ± 10 g) were purchased from Chengdu Dashuo Experimental Animal Co., (Chengdu, China). These rats were housed in standard plastic cages (4 animals per cage) in a quiet, clean animal room under temperature control (22 ± 2°C) and a 12-h light–dark cycle (lights were turned on at 8:00 am and turned off at 8:00 pm). To determine the effects of EODF on the gut microbiota of healthy rats, we randomly divided 12 rats into two groups: an experimental group (EODF-Healthy) and a control group (AL-Healthy). To study the effect of EODF on the gut microbiota and spinal cord tissue transcriptome data of SCI rats, we randomly divided 40 successfully modeled SCI rats into the AL-SCI and EODF-SCI groups, in addition, 20 rats were sham-operated as a control group. To study the effect of EODF on the recovery of motor function in SCI rats, we randomly divided 32 successfully modeled SCI rats into AL-SCI and EODF-SCI groups for behavioral analysis, while 16 rats performed sham surgery as a control group.

2.2. SCI and SHAM modeling

An intravenous dose of sodium pentobarbital (45 mg/kg) was used to anesthetize the rats, after which hair was plucked from the back of the neck and the cleared region was cleaned with iodophor.

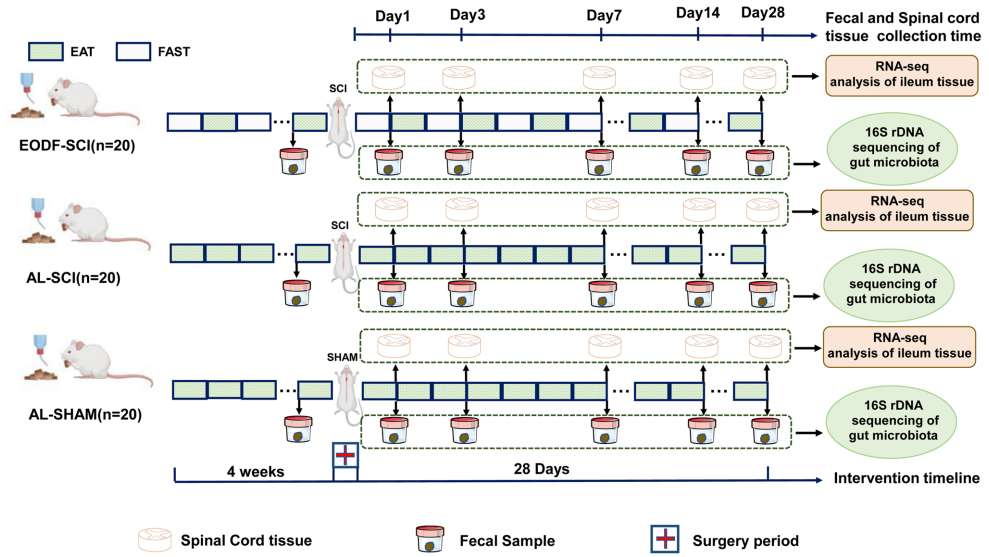

FIGURE 1
Experimental grouping and design.

Beginning at T2 of the thoracic spine, a 3–4 cm incision was made along the head and neck. To properly uncover the C4–C6 vertebral plates of the cervical spine, the surrounding fascia, muscles, and ligaments of the neck had to be dissected apart one by one. It was possible to see the spinal cord, the central vein of the dorsal median sulcus, and both C6 nerve roots after opening the C5 vertebral plate using biting forceps. Special care was taken not to break the dura mater during surgery, which is Located perpendicular to the long axis of the spinal column and above the C6 nerve root. After applying a 70 g closure force with a temporary aneurysm clamp (Yasargil Titanium Mini-Clips, Germany) on the spinal cord epidurally for 30 s, the clamp was withdrawn to a depth ranging from the periphery of the spinal cord to the dorsal median sulcus (C5 half of the spinal cord). For consistency, the same person clamped the spinal cord in every animal used in the experiments. After the incisions had been cleaned and disinfected, the muscles and skin were then sutured together, one layer at a time. The recuperating rats were housed in an incubator until they had totally awoken and were active. Dehydration was avoided by injecting intraperitoneal normal saline (5 mL/animal) for 2 days following surgery. When the injured rat displayed paralysis in the ipsilateral front paw, when the damaged ipsilateral forelimb had difficulties straightening forward and downward when the tail was elevated in the air, or when it fell backward toward the afflicted side when walking, the model was deemed effective (Supplementary Figure S1). In the SHAM-operated group, the steps were the same as those in the SCI group, except that no spinal cord tissue was damaged.

2.3. Behavioral analysis

We referred to a previous method to assess the behavior of SCI rats, whereby the grooming, horizontal ladder, and cylinder rearing tests were used to evaluate the motor function of the affected forelimb in rats (Streijger et al., 2014). Two weeks before modeling, all rats were trained to familiarize them with the behavioral evaluation. Three groups of rats ($n = 16$/group) were tested using these three tests 1 day before surgery, 1 day after surgery, and 1, 2, 4, 6, 8, 10, and 12 weeks after surgery.

2.4. Fecal sample and spine cord tissues collection

Throughout the study, the AL-Healthy group had free access to food and water; whereas, the EODF-Healthy group was fed and fasted every other 24 h. Fecal samples were collected on day 28 after initiating the dietary intervention. Rats in the AL-SCI and AL-SHAM groups had unrestricted access to food and water; whereas, those in the EODF-SCI group began the EODF diet 4 weeks prior to surgery and were fed and fasted every 24 h. In the AL-SCI, AL-SHAM, and EODF-SCI groups, after 1, 3, 7, 14, and 28 days post-operation, rats were euthanized to collect spinal cord tissue. Four rats were randomly selected at each time point. After exposing the spinal cord tissue, approximately 0.5 cm of fresh spinal cord tissue (1 cm in total) was collected cephalad and caudal to the C5 injury area to meet the needs of the test. The surface blood cells were washed off with Phosphate Buffered Saline, placed in a lyophilization tube, labeled, and placed in liquid nitrogen. The entire collection process was carried out in a cold environment. The room temperature was kept below 25°C, and the time between spinal cord tissue release and placement in liquid nitrogen was kept to a minimum of 10 min. After collection, all specimens were quickly frozen in a −80°C refrigerator and stored. Fecal samples were collected 1 days before and 1, 3, 7, 14, and 28 days after modeling, and 0.5–1 g of the central portion of each fecal sample was placed in a germ-free fecal collection tube. To maintain a somewhat anaerobic environment, the tube cap was quickly closed after sample collection. Fecal samples were kept at −80°C until further examination. The rats were in an unfed state when the spinal cord tissue and intestinal feces were collected.

2.5. 16S rRNA sequencing

The Power Fecal DNA Extraction Kit (Qiagen, Hilden, Germany) was used to extract DNA from fecal samples. The 16S rRNA V4 region of each sample was amplified. The relative bands were recovered for 16S rRNA sequencing using a gel recovery kit after electrophoresis of mixed PCR results from the same sample (Qiagen, Hilden, Germany). The primers used were 515F (5′-GTGC CAGCMGCCGC GGTAA-3′) and 806R (5′-GGACTACHVGGGTWT CTAAT-3′; Caporaso et al., 2011; Liu et al., 2017). The sequencing was carried out utilizing the Illumina HiSeq sequencing technology (Illumina, San Diego, CA, United States).

2.6. RNA-seq analysis of spinal cord tissues

Using the protocol provided by the manufacturer of the mirVana™ miRNA ISOlation Kit (Ambion-1561), total RNA was isolated from spinal cord tissue ($n = 4$ per group). The 2100 Bioanalyzer (Agilent Technologies, United States) was used to evaluate total RNA quality, and a NanoDrop ND-2000 (Thermo Scientific, United States) was used for quantification. Libraries for RNA sequencing were made using TruSeq™ RNA Sample Preparation Kits (Illumina, United States) and were quality-checked again with a 2100 Bioanalyzer (Agilent Technologies, United States) before processing on an Illumina HiSeq™ 2500 (Illumina, United States) for sequencing.

2.7. Bioinformatics analysis

2.7.1. Gut microbiome

For the operational taxonomic unit (OTU) analysis, all sequences were classified using UPARSE software version 7.1 (Edgar, 2013). Those with >97% similarity were clustered into one OTU, and then the OTUs were filtered using SSU115.[1] We assessed α diversity according to species richness (ACE and Chao1) and diversity indices (Shannon and Simpson). Principal coordinate analysis (PCoA) was used to examine beta-diversity using the unweighted UniFrac method. The typical OTU sequences were classified using a Bayesian technique for nucleic acid database classification for subsequent taxonomic analysis.

2.7.2. Spinal cord tissue transcriptome

Low-quality bases were removed, and high-quality clean reads were obtained by using the NGS QC Toolkit program for quality control of raw reads. Genomic alignment was performed using the Hisat2 (hierarchical indexing for spliced alignment of transcripts) program (Kim et al., 2015). Transcript expression was calculated using FPKM (fragments per kb per million reads; Roberts et al., 2011) and assessed using Cufflinks software to quantify gene abundance and identify the genes for subsequent analysis. The R language DEseq2 (Love et al., 2014) was used to normalize the number of counts of genes in each sample. After multiplexing the false discovery rate (FDR), $p < 0.05$ and $|\log2(\text{foldchange})| > 0.58$ were DEGs. Functional enrichment of DEGs was analyzed using the Gene Ontology (GO)[2] and Kyoto Encyclopedia of Genes and Genomes (KEGG)[3] databases.

2.8. Statistical analysis

SPSS 19.0 was used for all statistical analyses. We used various methods to test whether the data were normally distributed, including the Shapiro–Wilk test, skewness–kurtosis test, and a graphical method (P–P plot and Q-Q plot), and made our determination based on whether the results of multiple methods were in agreement. If two or more methods showed that the data obeyed the normal-terrestrial distribution, the data were considered to be normally distributed; otherwise, they were considered to be non-normally distributed. Data with a normal distribution and uniform variance were analyzed by one-way ANOVA (LSD method for two-way comparison) or t-test for two independent samples; The Kruskal–Wallis rank–sum test (Dunn's method for two-by-two comparisons and Bonferroni correction for test results) or the Mann–Whitney U test were used if they did not obey a normal distribution or if the variance was not uniform. All graphs were generated using Graphpad Prism9.0 or Chiplot.[4] $p < 0.05$ was chosen as the level of statistical significance.

3. Results

3.1. 16S rRNA gene sequencing results

For all fecal samples collected from the EODF-Healthy, AL-Healthy, AL-SCI, AL-SHAM, and EODF-SCI groups, 2505001raw and 2,467,372 clean reads with an average length of 282 bp were produced by 16S rRNA gene sequencing. Using dilution curves ("abundance curves"), we verified that the amount of sequencing data for each group was sufficient to reflect the species diversity (Supplementary Figure S2).The curves leveled off and reached a plateau for all samples. We concluded that the sequencing depth would cover all species in the samples, and we subsequently clustered the spliced tags into OTUs.

3.2. EODF treatment improves locomotor recovery in SCI (C5 half of the spinal cord) rats

We investigated the effects of EODF on locomotor recovery in rats with SCI (C5 half of the spinal cord). Locomotor recovery was observed during the 12 weeks post-injury in the SCI groups. EODF treatment further significantly increased locomotor function starting from 4 weeks (grooming test), 8 weeks (horizontal ladder test), and 10 weeks (cylinder rearing test) after injury compared to that of the SCI groups. The improvement in grooming test scores, ipsilateral forelimb errors, and contact with ipsilateral forelimb continued until the end of the experiment (Supplementary Figures S1B–D).

1 http://drive5.com/uparse

2 http://geneontology.org/

3 http://www.genome.jp/kegg/

4 https://www.chiplot.online/

3.3. Analysis of the α and β diversity of gut microbiota

First, we compared the effects of EODF and AL on the α diversity of the gut microbiota in healthy rats (Figure 2A). The diversity of gut microbiota in the EODF-Healthy group was significantly higher than that of the AL-Healthy group. However, there was no significant difference in gut microbiota abundance between the two groups. According to the PCoA (Figure 2B), the OTUs of the two groups showed dispersion and aggregation, indicating that β diversity varied between the two groups. We compared the patterns in gut microbiota α diversity between the EODF-SCI, AL-SCI, and AL-SHAM groups on days 0, 1, 3, 7, 14, and 28. As shown in Figures 3A–D, there were significant differences in the Ace, Chao 1, Shannon, and Simpson indices between pre- and post-modeling samples in these three groups. In the EODF-SCI group, ACE and Chao 1 indices decreased exponentially on days 1 and 3 after SCI injury, and recovered gradually until day 28. Shannon and Simpson indices decreased on day 1 after SCI injury, increased gradually until day 3, decreased on day 7, and recovered gradually until day 28. In the AL-SCI group, ACE, Chao 1, Shannon, and Simpson indices increased exponentially on day 3 after SCI injury, and remained stable until day 28. In the AL-SHAM group, ACE, Chao1, Shannon, and Simpson indices increased gradually on day 1 after SCI injury until day 7, decreased exponentially on day 14, and increasing on day 28. These results indicated that the species richness and diversity of the gut microbiota in the three groups had different characteristics.

The α diversity of the bacterial community at each time point was compared between the EODF-SCI, AL-SCI, and AL-SHAM groups. As shown in Figures 3E–H, on day 14 after SCI, the Chao 1 and ACE indices were significantly lower in the EODF-SCI group compared to those in the AL-SCI group, suggesting that EODF intervention reduced the richness of the gut microbiota in SCI rats at that time point. On days 1, 7, and 14 after SCI, the Simpson index was significantly lower in the EODF-SCI group compared to that in the AL-SCI group, suggesting that the EODF intervention reduced the diversity of the gut microbiota of SCI rats in these time points. Furthermore, we observed a significant decrease in the Shannon index in the EODF-SCI group on day 14.

According to the PCoA, days 1, 7, and 14 were clustered together in the EODF-SCI group; days 3, 7, and 14 were clustered in the AL-SCI group; and days 1, 3, and 7 were clustered in the AL-SHAM group (Figures 3I–K). These results indicated that gut microbiota diversity changed over time, and that different dietary interventions had different effects on the β diversity of gut microbiota in rats with SCI.

3.4. Phylum- and genus-level composition of gut microbiota

We explored the effects of the two dietary interventions on the levels of gut microbiota phyla in healthy rats and found no difference between rats in the EODF-Healthy and AL-Healthy rats (Supplementary Figure S3A). *Bacteroidetes* and *Firmicutes* were the dominant phyla in these groupis (Figure 2C). The relative abundances of *Bacteroidetes* and *Firmicutes* in the AL-Healthy group were 58.17 and 36.42%, and those in the EODF-Healthy group were 54.72 and 30.08%, respectively. In the EODF group, the abundance of *Firmicutes* was significantly reduced (30.08%).

To understand the effects of the two dietary interventions on changes in the structure of the gut microbiota in SCI rats, we analyzed the distribution of the gut microbiota at six time points. At the phylum level, the most abundant phyla in the EODF-SCI, AL-SCI, and

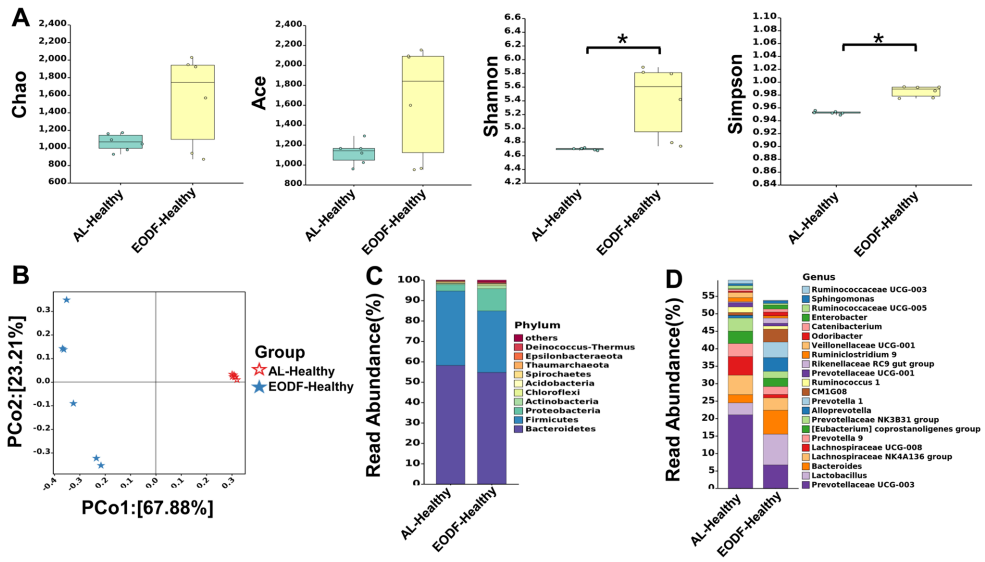

FIGURE 2
Effect of the *ad libitum* diet (AL) and every-other-day fasting (EODF) on gut microbiota diversity and structural composition in healthy rats. **(A)** Chao 1, ACE, Shannon, and Simpson indices assessing the difference in α-diversity between the two healthy groups ($n = 6$/group). Data were analyzed using the Mann–Whitney U test,*$p < 0.05$. **(B)** Principal coordinate analysis assessing the difference in β-diversity between the two healthy groups ($n = 6$). **(C)** Compositional distribution of gut microbiota phyla between the two healthy groups ($n = 6$). **(D)** Compositional distribution of gut microbiota genera between the two healthy groups ($n = 6$).

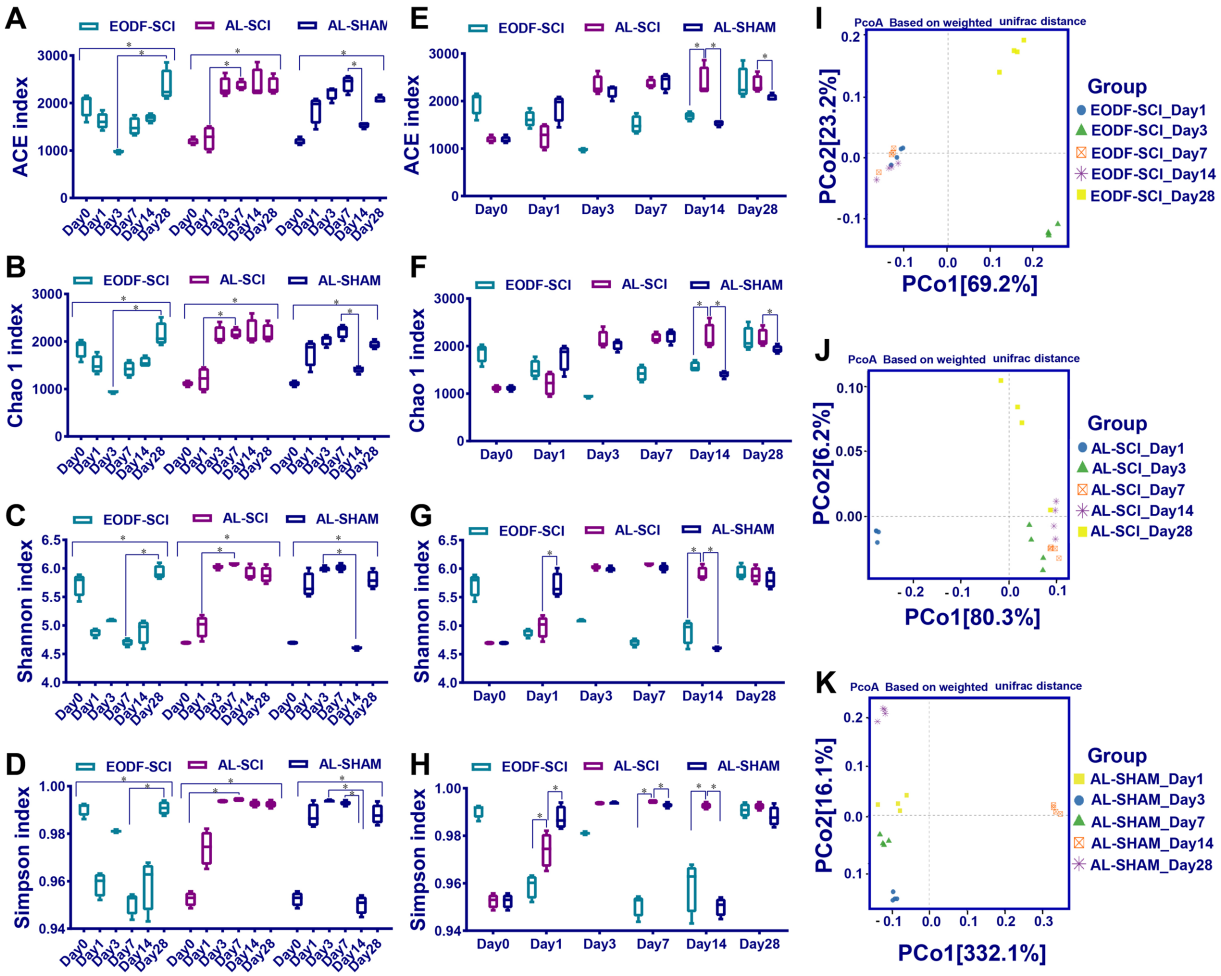

FIGURE 3
Changes in gut microbiota diversity over time. **(A–D)** Chao 1, ACE, Shannon, and Simpson indices assessing α-diversity over time between the EODF-SCI, AL-SCI, and AL-SHAM groups. Data were analyzed using the Kruskal–Wallis test with Dunn *post-hoc* tests. **(E–H)** Chao 1, ACE, Shannon, and Simpson indices assessing α-diversity at the same time points between the EODF-SCI, AL-SCI, and AL-SHAM groups. Data were analyzed using the Mann–Whitney U test. $N = 4$, *indicates that indices were significantly higher ($p < 0.05$). **(I–K)** Principal coordinate analysis assessing β-diversity over time in each group ($n = 4$).

AL-SHAM groups were *Firmicutes* and *Bacteroidetes* (Figures 4A–C). We then used a one-way ANOVA to assess the effect of the two interventions on changes in *Firmicutes* and *Bacteroidetes* abundance at six time points (Figures 4D,E). In the EODF group, the *Bacteroidetes* abundance significantly decreased on day 3 after SCI, then increased on days 7 and 14 post-injury, and finally decreased on day 28; whereas, the *Firmicutes* abundance significantly increased on day 3 after SCI, then decreased on days 7 and 14 post-injury, and finally increased on day 28. In the AL-SCI group, the *Bacteroidetes* abundance gradually decreased on day 1 after SCI, then remained stable on days 3, 7, and 14 after injury, and finally increased slightly on day 28; whereas, *Firmicutes* abundance slowly increased on day 1 after SCI, then remained stable on days 3, 7, 14, and 28 after injury. In the AL-SHAM group, the *Bacteroidetes* abundance decreased significantly on day 1 after SCI, remained stable on days 3 and 7 after injury, increased significantly on day 14, and then decreased on day 28; whereas, the *Firmicutes* abundance increased slightly on day 1 after SCI, then remained stable on days 3, 7, and 14 after injury, and finally increased slightly on day 28.

As represented in Figure 4F, we analyzed the changes in the *Bacteroidetes*/*Firmicutes* ratio. In the AL-SCI group, we found that this ratio decreased significantly on day 1 until day 28 after SCI. This findings suggested that SCI led to time-dependent gut microbial dysbiosis. In the AL-SHAM group, this ratio decreased significantly on days 1, 3, 7, and 28; whereas, in the EODF-SCI group, it only decreased significantly on days 3 and 28 after SCI. Interestingly, we found a significant increase in the *Bacteroidetes*/*Firmicutes* ratio in the EODF-SCI group on days 1, 7, and 14 after injury and a significant decrease on day 28 compared to that in the AL-SCI group (Figure 4G). We further analyzed the differences in the phylum level bacterial populations at the same time point in the EODF-SCI and AL-SCI groups. As shown in Figures 4H–Q, on day 1 after injury, the abundances of *Bacteroidetes*, *Actinobacteria*, *Chloroflexi*, *Acidobacteria*, *Thaumarchaeota*, and *Deinococcus-Thermus* significantly increased, whereas those of *Spirochaetes* and *Epsilonbacteraeota* decreased, compared to those in the AL-SCI group. On day 3 after injury, the abundances of *Proteobacteria*, *Chloroflexi*, and *Acidobacteria* were significantly lower than those in the AL-SCI group. On day 7 after

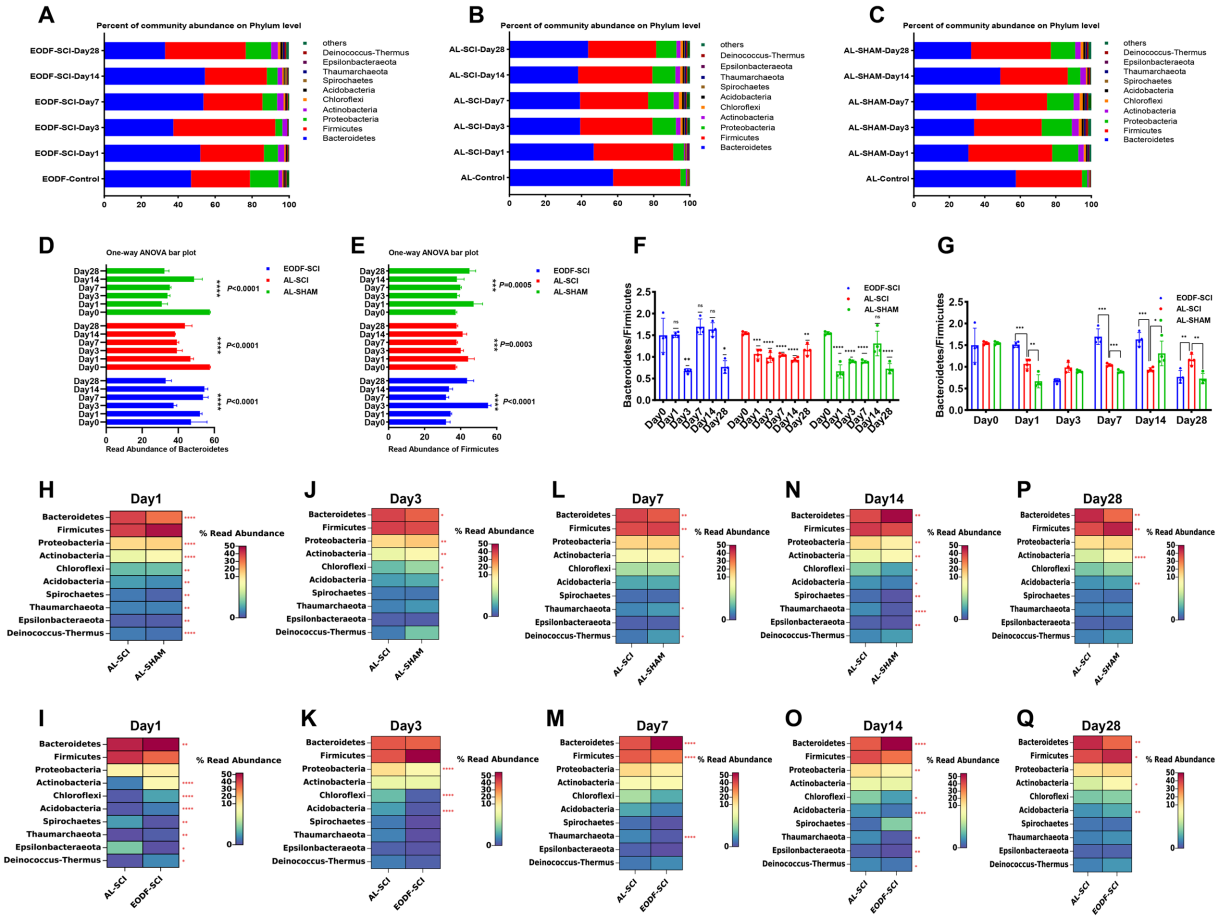

FIGURE 4
Gut microbiota composition at the phylum level. Comparison of the bacterial community composition at the phylum-level and changes over time in the: **(A)** EODF-SCI, **(B)** AL-SCI, **(C)** AL- SHAM groups. Microbial abundance was calculated as a percentage of the total bacterial taxon within each sample. The bar chart shows the average value for each group. Further analysis of the relative abundances of *Bacteroides* and *Firmicutes* over time between the EODF-SCI, AL-SCI, and AL- SHAM group; significance test of the relative abundance of: **(D)** *Bacteroides* and **(E)** *Firmicutes* using one-way ANOVA. **(F)** Comparison of the *Bacteroidetes*/*Firmicutes* ratio at pre-modeling (day 0) and post-modeling (days 1, 3, 7, 14, and 28) using a Student's *t*-test. **(G)** Comparison of the *Bacteroidetes*/*Firmicutes* ratios at the same time points between the EODF-SCI, AL-SCI, and AL-SHAM groups using a Student's *t* test. **(H–P)** Heatmap showing differential bacteria at the phylum level at the same time points between the AL-SCI and AL-SHAM groups using a Student's *t* test. **(I–Q)** Heatmap showing differential bacteria at the phylum level at the same time points between the EODF-SCI and AL-SCI groups using a Student's *t* test. $n = 4$, $^{*}p < 0.05$, $^{**}p < 0.01$, $^{***}p < 0.001$, $^{****}p < 0.0001$.

injury, the *Bacteroidetes* abundance was significantly increased, and the abundances of *Firmicutes* and *Thaumarchaeota* were significantly decreased compared to those in the AL-SCI group. On day 14 after injury, the *Bacteroidetes* abundance was significantly increased, and the abundances of *Proteobacteria*, *Chloroflexi*, *Acidobacteria*, *Thaumarchaeota*, *Epsilonbacteraeota*, and *Deinococcus-Thermus* were significantly decreased compared to those in the AL-SCI group. On day 28 after injury, the abundances of *Firmicutes*, *Actinobacteria*, and *Acidobacteria* increased significantly and that of *Bacteroidetes* decreased significantly compared to those in the AL-SCI group. These findings suggested that EODF appeared to dynamically regulate changes in the gut microbiota of SCI rats.

We compared the differences in gut microbiota between the EODF-Healthy and AL-Healthy groups at the genus level (Supplementary Figure S3B). Compared to the AL-Healthy group, the abundances of the genera *Lactobacillus, Bacteroides, Alloprevotella, Prevotella 1, Rikenel-laceae RC9, Odoribacter, and Catenibacterium* spp. were significantly increased in the EODF-Healthy group, whereas that of *Prevotellaceae UCG-003, Lachnospiraceae NK4A136, Lachnospiraceae UCG-008, Prevotella 9, [Eubacterium] coprostanoligenes, Ruminococcaceae UCG-008, and Ruminococcaceae UCG-003*(among others) was significantly reduced (Figure 2D; Supplementary Table S1).

To understand the effects of the two dietary interventions on structural changes in the gut microbiota of SCI rats, we analyzed the genus-level (top 22) gut microbiota distribution at six time points (Figures 5A–C). We then used a one-way ANOVA to assess the effect of the two interventions on changes in the genus-level (top 22) gut microbiota at six time points (Figures 5D–F). We found no significant difference in the *Veillonellaceae UCG-001* abundance in the EODF-SCI group; however, the abundances of all other bacteria differed significantly in all three groups. We further analyzed the differences in the genus level bacterial populations at the same time point in the EODF-SCI and AL-SCI groups. As shown in Figures 5G–K, on the first day after injury, the abundances of *Lactobacillus, Lachnospiraceae UCG-008, Prevotella9, [Eubacterium]coprostanoligenes group,*

10.3389/fmicb.2023.1206909

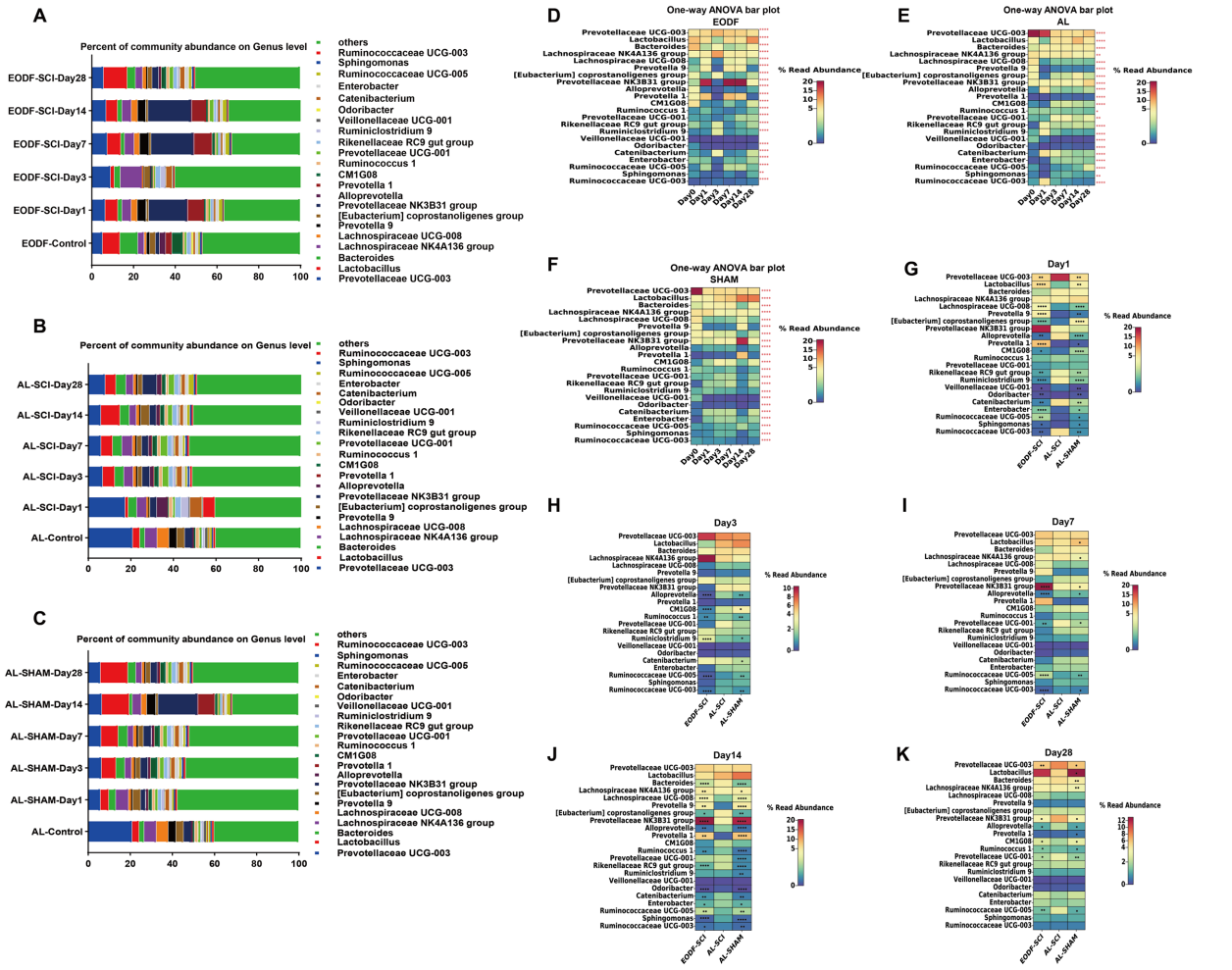

FIGURE 5
Gut microbiota composition at the genus level. Comparison of the bacterial community composition at the genus level and changes over time in the: **(A)** EODF-SCI; **(B)** AL-SCI; **(C)** AL- SHAM groups. Microbial abundance was calculated as a percentage of the total bacterial taxon within each sample. The bar chart shows the average value for each group. Further analysis the relative abundance of genus level over time between the three groups. Significance test of the relative abundances of: **(D)** EODF-SCI, **(E)** AL-SCI, and **(F)** AL-SHAM groups using one-way ANOVA. **(G–K)** Heatmap showing differential bacteria at the genus level at the same time points between three groups using a Student's *t* test. Asterisks in the heat map squares indicate that the EODF-SCI and AL-SHAM groups were significantly different from AL-SCI group. $N = 4$, $^{*}p < 0.05$, $^{**}p < 0.01$, $^{****}p < 0.0001$.

Prevotella1, CM1G08, Odoribacter, Enterobacter, RuminococcaceaeUCG-005, and *Sphingomonas* increased; whereas, the abundances of *Prevotellaceae UCG-003, Alloprevotella, Rikenellaceae RC9 gut group, Ruminiclostridium 9, Veillonellaceae UCG-001, Catenibacterium,* and *Ruminococcaceae UCG-003* decreased, compared to those in the AL-SCI group. On day 3 after injury, the abundance of *Ruminiclostridium 9* increased; whereas, the abundances of *Alloprevotella, CM1G08, Ruminococcus 1, Ruminococcaceae UCG-005,* and *Ruminococcaceae UCG-003* decreased compared to those in the AL-SCI group. On day 7 after injury, the abundances of *Prevotellaceae NK3B31* and *Ruminococcaceae UCG-005 group* increased, whereas those of *Alloprevotella, Prevotellaceae UCG-001,* and *Ruminococcaceae UCG-003* decreased, compared to those of the AL-SCI group. On day 14 after injury, the abundances of *Lachnospiraceae NK4A136 group, Lachnospiraceae UCG-008, Prevotella 9, Prevotella 1, Prevotellaceae NK3B31,* and *Ruminococcaceae UCG-005 group* increased, whereas those of *Bacteroides, [Eubacterium] coprostanoligenes group, Alloprevotella, Ruminococcus 1, Rikenellaceae RC9 gut group, Odoribacter, Catenibacterium, Enterobacter, Sphingomonas,* and *Ruminococcaceae UCG-003* decreased, compared to those of the AL-SCI group. On day 28 after injury, the abundances of *CM1G08* and *Ruminococcus 1* increased, whereas those of *Prevotellaceae UCG-003, Prevotellaceae NK3B31, Alloprevotella, Prevotellaceae UCG-001,* and *Ruminococcaceae UCG-005* decreased, compared to those of the AL-SCI group. These results provide further evidence that EODF intervention led to a dynamic gut microbiota profile in SCI rats that differed from that after AL intervention.

We analyzed the relative abundance and variations of potentially anti-inflammatory genera (including *Prevotella, Lactobacillus, and Lachnospiraceae*) and pro-inflammatory genera (*Bacteroides*), which showed dynamic changes in the AL and EODF groups. On day 1 after SCI, there were significant increases in the abundances of *Lactobacillus*, *Prevotella1*, *Prevotella9*, and *Lachnospiraceae UCG-008* in the EODF-SCI group compared to those in the AL-SCI group. On day 14 after SCI, there were significant increases in the abundances of *Prevotella1, Prevotella9*, and *Lachnospiraceae UCG-008* in the

EODF-SCI group compared to those in the AL-SCI group, However, there was a significant decrease in the *Bacteroide* abundance. These results indicated that EODF treatment induced dynamic changes in the abundance of potentially anti-inflammatory and pro-inflammatory bacteria.

In summary, these results suggested that EODF regulated the relative abundance and variation of gut microbiota, leading to changes in the dynamics of bacteria that differed from those of the AL group.

3.5. Transcriptomic analysis of spinal cord tissue

We completed the sequencing of 60 samples with the reference transcriptome and obtained 452.80 G of clean bases. The distribution of Q30 bases was from 95.19 to 96.62%, and the effective data volume of each sample ranged from 6.30–8.47 G, with an average GC content of 49.50%. Genomic matches were obtained for each sample by comparing the reads to the reference genome, with a 97.40–98.19% match rate. Based on the results of the comparison, a principal component analysis (PCA) was performed on the number of counts of each sample gene (Figure 6A). Comparing the AL-SHAM and AL-SCI groups, on day 1, 2,481 DEGs were significantly regulated, with 935 up-regulated and 1,546 down-regulated (Figure 6B); on day 3, 2055 DEGs were significantly regulated, with 457 up-regulated and 1,598 down-regulated (Figure 6C); on day 7, 2,306 DEGs were significantly regulated, with 501 up-regulated and 1805 down-regulated (Figure 6D); on day 14, 1,422 DEGs were significantly regulated, with 214 up-regulated and 1,208 down-regulated (Figure 6E); and on day 28, 914 DEGs were significantly regulated, with 93 up-regulated and 821 down-regulated (Figure 6F). Comparing the EODF-SCI and AL-SCI groups, on day 1, 250 DEGs were significantly regulated, with 99 up-regulated and 151 down-regulated (Figure 6G); on day 3, 769 DEGs were significantly regulated, with 401 up-regulated and 368 down-regulated (Figure 6H); on day 7, 291 DEGs were significantly regulated, with 123 up-regulated and 168 down-regulated (Figure 6I); on day 14, 128 DEGs were significantly regulated, with 53 up-regulated and 75 down-regulated (Figure 6J); and on day 28, 198 DEGs were significantly regulated, with 66 up-regulated and 132 down-regulated (Figure 6K). These results indicated that SCI modeling caused considerable differences in the transcriptome level in spinal cord tissue. EODF participated in regulating the transcriptome level in spinal cord tissue at different time points, and its trend was significantly different from that of the AL treatment.

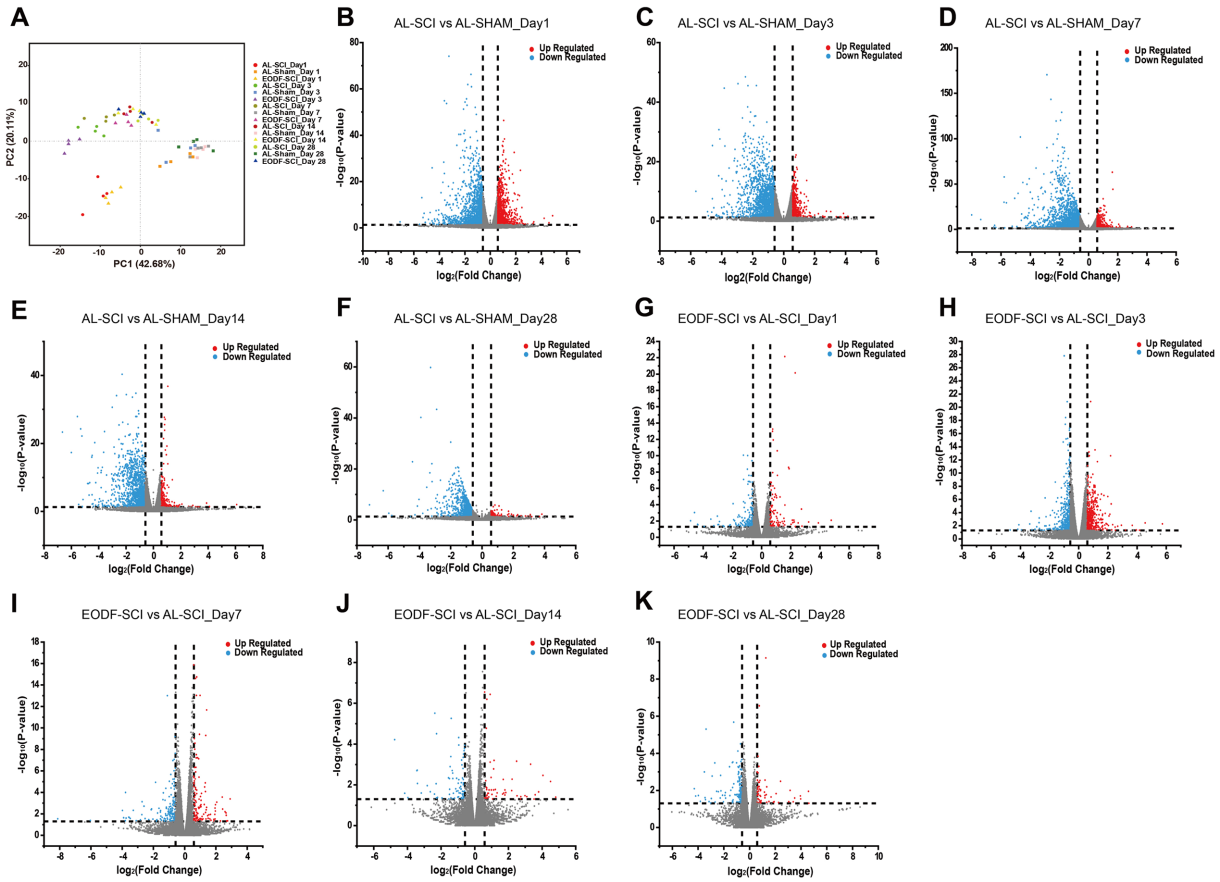

FIGURE 6
Gene transcriptome analysis of spinal cord tissue. **(A)** PCA scores of EODF-SCI, AL-SCI, and AL-SHAM gene counts at different time periods. **(B–F)** DEGs of AL-SHAM vs. AL-SCI in each time period ($p < 0.05$ and $|\log2(\text{foldchange})| > 0.58$). **(G–K)** DEGs of EODF-SCI vs. AL-SCI in each time period ($p < 0.05$ and $|\log2(\text{foldchange})| > 0.58$).

10.3389/fmicb.2023.1206909

3.6. Functional enrichment analysis of DEGs

The function of DEGs was assessed by GO and KEGG enrichment analyses, as demonstrated by the enrichment of the top 20 significant terms and pathways (number of genes >3 per entry). At 1, 3, 7, and 14 days after SCI, the DEGs in the EODF and AL groups were significantly altered by biological events, such as immune inflammatory responses, cell differentiation, and protein modifications (Figures 7A–D), For example, the GO terms "inflammatory response,"

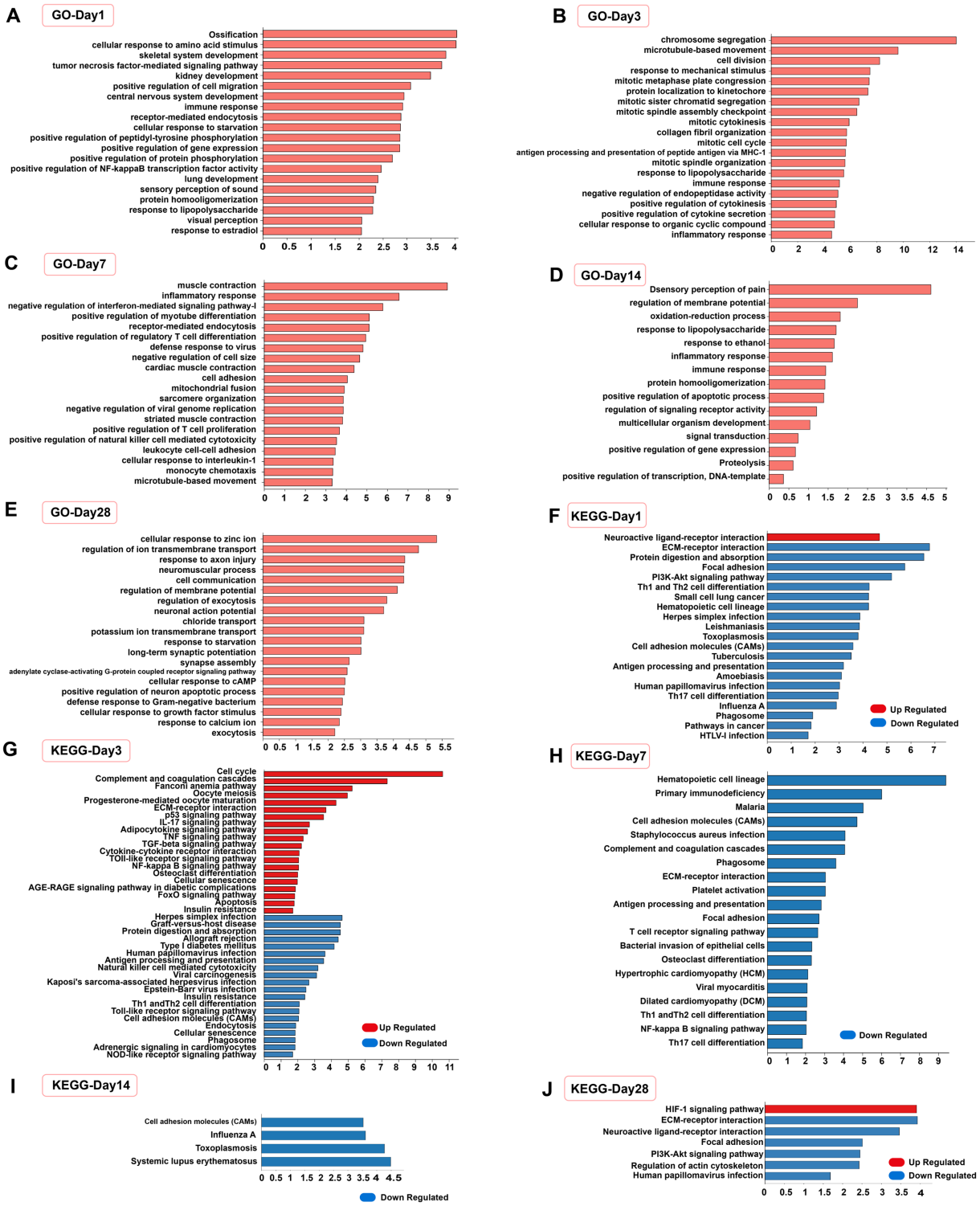

FIGURE 7
Functional analysis of differentially expressed genes. **(A–E)** Top 20 significantly enrichened GO terms in biological process (number of genes >3) of the EODF-SCI group versus the AL-SCI group at different time periods. **(F–J)** Top 20 significantly enriched KEGG pathways of up-regulated and down-regulated DEGs at different time periods.

"immune response," "tumour necrosis factor-mediated signal-ling pathway," "positive regulation of NF-κB transcription factor activity," "lipopolysaccharide response," "positive regulation of regulatory T-cell differen-tiation" and "cellular response to interleukin-1" were all part of the immune inflammatory response; "positive regulation of cell migration," "cell division," "mitotic cell division," "chromosome segregation," "protein localization to kinetochores," and "positive regulation of myotube differentiation" were all associated with cell differentiation; and "positive regulation of peptidyl tyrosine phosphorylation," "positive regulation of protein phosphorylation," "protein homologation" and "negative regulation of endopeptidase activity" were all related to protein modifications. At 28 days, biological events such as the immune inflammatory response were no longer the dominant biological events. In contrast, the terms "response to axon injury," "synapse assembly," "cellular response to growth factor stimulus," and "positive regulation of neuron apoptotic process" suggested possible differences in neuronal differentiation (Figure 7E).

We the performed separate KEGG pathway enrichment analyses for up- and down-regulated DEGs and obtained similar results (Figures 7F–J). The pathways that were enriched at 1, 3, and 7 days after SCI were mainly associated with immune inflammatory responses, including "PI3K-Akt signaling pathway," "NF-kappa B signaling pathway," "P53 signaling pathway," "Th1 and Th2 cell differentiation," "Th17 cell differentiation," "TNF signaling pathway," "Toll-like receptor signaling pathway," "NOD-like receptor signaling pathway," and "FoxO signaling pathway." In addition, at 1 and 3 days after SCI, DEGs were enriched in the "neuroactive ligand-receptor interaction" pathway, representing a collection of all receptors and ligands associated with intra- and extracellular signaling pathways on the plasma membrane. Active biological events occurred 3 days after SCI. In addition to immune inflammation-related pathways, entries in the "TGF-beta signaling pathway" and "apoptosis" were enriched, suggesting differences in biological events, such as nerve growth and apoptosis, after EODF intervention. At 14 days after SCI, DEGs were enriched in cell adhesion molecules, which is a pathway associated with cell adhesion. At 28 days after SCI, the "HIF-1 signaling pathway" was a stress signaling pathway for organisms in a hypoxic state. These results suggested that EODF may have exerted neuroprotective effects by modulating multiple biological events during a 28-day treatment cycle in SCI rats.

3.7. DEGs associated with neuroprotection

The ability of EODF to exert neuroprotective effects in SCI rats was been demonstrated; thus, we sought to determine how EODF regulated gene levels (closely associated with neuroprotection) in SCI rats at 1, 3, 7, 14, and 28 days. Therefore, we further performed an in-depth analysis of the GO and KEGG entries enriched in the EODF-SCI and AL-SCI groups that were associated with neuroprotection (Supplementary Table S2). We used the AL-SHAM group as a baseline, and the DEGs in the entries that were associated with neuroprotection in the EODF-SCI group versus the AL-SCI group are shown in Figures 8A,B, and mainly included: (i) genes with beneficial effects on neuroprotection that are associated with: (1) microglia polarization (*Socs3 and Arg1*); (2) anti-inflammatory effects (*Agtr2, Apoe, C3, Cd36, Gabrb2, Il1rn, Nfkbia,* and *Spp1*); (3) anti-apoptosis (*Bcl2a1*); and (4) nourishing nerves and promoting nerve repair (*Cd4 and Serpine1*); (ii) genes related to nerve injury: (1) pro-inflammatory (*Ccl5, Ccl6, Ccr1, Cebpb, Fosl1, Mapk11, Osm, Sphk1, Tnfrsf25, and Trpm2*); (2) pro-oxidative stress (*Cyba and Sgk1*); (3) pro-inflammatory and induced oxidative stress (*Tlr9*); (4) immune infiltration and activation (*Cd4,Cd14, Cd3d, Cd40, and Cxcl13*); (5) promotion of apoptosis (*C5ar1, Cdk1, Irf3, and Nradd*); and (6) other genes: neurotoxin production (*Kmo*), encodes neurexin U receptor (*Nmur2*) and unknown functional genes (*Thbs1* and *Trhr*). Our results revealed that DEGs associated with neuroprotective effects in both groups were mainly clustered at 1, 3, and 7 days after SCI. Compared to the Al-SCI group, the EODF-SCI group showed predominantly down-regulated DEGs at 1 days, predominantly up-regulated DEGs at 3 days, and predominantly down-regulated DEGs at 7 days. Two DEGs were observed at 14 and 28 days. The above results suggested that the expression levels of DEGs related to neuroprotection at different time points after EODF intervention in SCI rats were significantly different from those in the AL group both spatially and temporally, among which inflammation-related genes accounted for the majority. Therefore, we suggest that EODF may have played an important role in the regulation of inflammation in the acute and subacute phases in SCI rats.

3.8. Association between gut microbiota and neuroprotection-related DEGs

Next, we performed Spearman's correlation analysis of the abundance of gut microbiota in the EODF-SCI group (different genera from the AL-SCI group) with neuroprotection-related DEGs. On day 1, the anti-inflammatory gene *Agtr2* was significantly positively correlated with *Catenibacterium* ($r = 0.985$, $p = 0.015$); and the pro-inflammatory gene *Sgk1* was significantly positively correlated with *CM1G08* ($r = 0.969$, $p = 0.031$) and negatively correlated with *Lachnospiraceae UCG-008* ($r = -0.955$, $p = 0.045$) and *Odoribacter* ($r = -0.992$, $p = 0.008$). The pro-apoptotic gene *Nradd* was significantly positively correlated with *Ruminiclostridium 9* ($r = 0.968$, $p = 0.032$); *Nmur2* was significantly positively correlated with *Alloprevotella* ($r = 0.958$, $p = 0.042$); and *Trhr* was significantly negatively correlated with *[Eubacterium] coprostanoligenes group* ($r = -0.950$, $p = 0.049$; Figure 9A). On day 3, *Socs3* ($r = -0.963$, $p = 0.037$), *Arg1* ($r = -0.992$, $p = 0.008$), and *Ccr1* ($r = -0.981$, $p = 0.018$) were significantly negatively correlated with *Alloprevotella*; *Ruminococcaceae UCG-005* was significantly negatively correlated with *Ccl2* ($r = -0.976$, $p = 0.024$) and significantly positively correlated with *Tnfrsf25* ($r = 0.984$, $p = 0.016$); *Il1rn* was significantly positively correlated with *Ruminococcaceae UCG-003* ($r = 0.959$, $p = 0.041$); and *Fosl1* ($r = -0.987$, $p = 0.013$) and *Ccl5* ($r = -0.967$, $p = 0.033$) were significantly and negatively correlated with *Ruminococcus1* (Figure 9B). On day 7, *Ruminococcaceae UCG-005* was significantly positively correlated with *Cxcl13* ($r = 0.953$, $p = 0.047$), *Cebpb* ($r = 0.955$, $p = 0.045$); *Alloprevotella* was significantly positively correlated with *Cd4* ($r = 0.970$, $p = 0.030$); and *Prevotellaceae NK3B31 group* was significantly negatively correlated with *Cyba* ($r = -0.992$, $p = 0.008$; Figure 9C). However, no genera of DEGs were found to be associated with neuroprotection on days 14 or 28 (Figures 9D,E). The above results suggested that EODF was able to reregulate the abundances of certain gut microbiota that are closely associated with neuroprotective-associated DEGs in SCI rats during the acute and subacute phases of SCI.

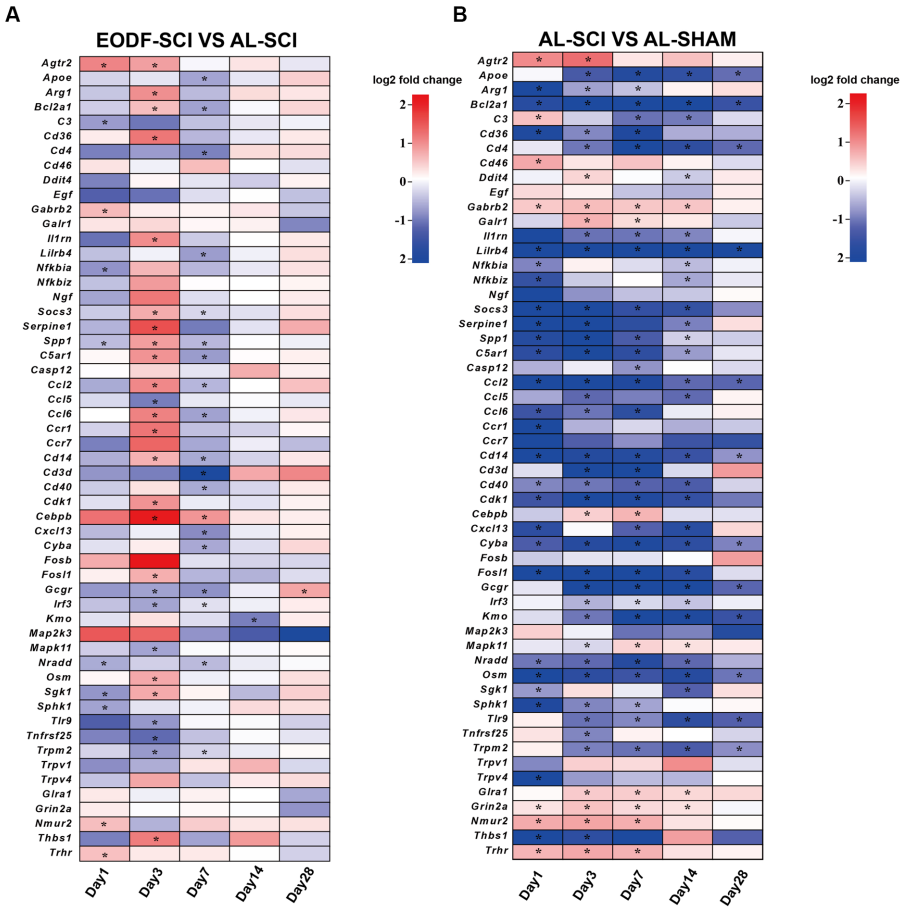

FIGURE 8
DEGs associated with neuroprotection. DEGs associated with neuroprotective effects between: **(A)** the EODF-SCI and AL-SCI groups; and **(B)** the AL-SCI and AL-SHAM groups. log2(foldchange) > 0 indicates up-regulated DEGs, and log2(foldchange) < 0 indicates down-regulated DEGs; *$p < 0.05$.

4. Discussion

EODF, as a dietary intervention therapy, could exert neuroprotective effects and facilitate functional recovery in spinal cord injured rats. We also confirmed that EODF intervention promoted motor function in rats with SCI (C5 half of the spinal cord). However, the effects of EODF treatment on the gut microbiota and the transcriptomic gene expression of spine cord tissues of SCI rats during the acute, subacute, and recovery periods were unknown; therefore, we assessed the long-term effects of EODF treatment on the dynamics changes in gut microbiota and transcriptomic gene expression of spine cord tissues of SCI rats by 16sDNA high-throughput sequencing and RNA transcriptome technology.

Gut microbiota diversity was significantly higher in healthy rats treated with EODF than that in the AL-treated group, based on the Simpson and Shannon indices. Similarly, a recent study found that gut microbiota α diversity was significantly higher in obese mice after a low-fat diet (LFD) combined with IF treatment than with the LFD combined with AL treatment (Deng et al., 2020). By analyzing the α-diversity at each time point in the three groups, our study showed that in the EODF-SCI group, the gut microbiota structure changed dynamically, the abundance of gut microbiota showed a trend of decreasing and then increasing, and its diversity showed a trend of decreasing, then increasing, then decreasing, and finally increasing. In the AL-SCI group, both the abundance and diversity of gut microbiota showed a trend of increasing and then remaining stable. In the AL-SHAM group, both the abundance and diversity of gut microbiota showed a trend of increasing, then decreasing, and finally increasing. We also found that on day 14, the abundance of gut microorganisms was significantly lower in the EODF-SCI group than in the AL-SCI group. On days 1, 7 and 28, the diversity of gut microbiota in the EODF-SCI group was significantly reduced. Analysis of β diversity analysis showed that in the EODF-SCI group, the structure of the gut microbiota differed on days 3 and 28 from that at the other time points; in the AL-SCI group, the structure of the gut microbiota differed from that at the other time points on days 1 and 28; in the AL-SHAM group, the structure of the gut microbiota differed from that at the other time points on days 14 and 28. In the SCI rat models, the most dominant phyla in the EODF-SCI, AL-SCI, and AL-SHAM groups were *Firmicutes* and *Bacteroidetes*. The *Firmicutes/Bacteroidetes* ratio was significantly lower in the EODF-SCI group on days 3 and 28 compared to that in the pre-modeling period (day 0), which differed from the changes in the AL-SCI and AL-SHAM groups. The *Firmicutes/Bacteroidetes* ratio was significantly higher in the EODF-SCI group on days 1, 7, and 14 and significantly lower on day 28 compared to those in the AL-SCI group. *Firmicutes* and *Bacteroidetes*, which account for

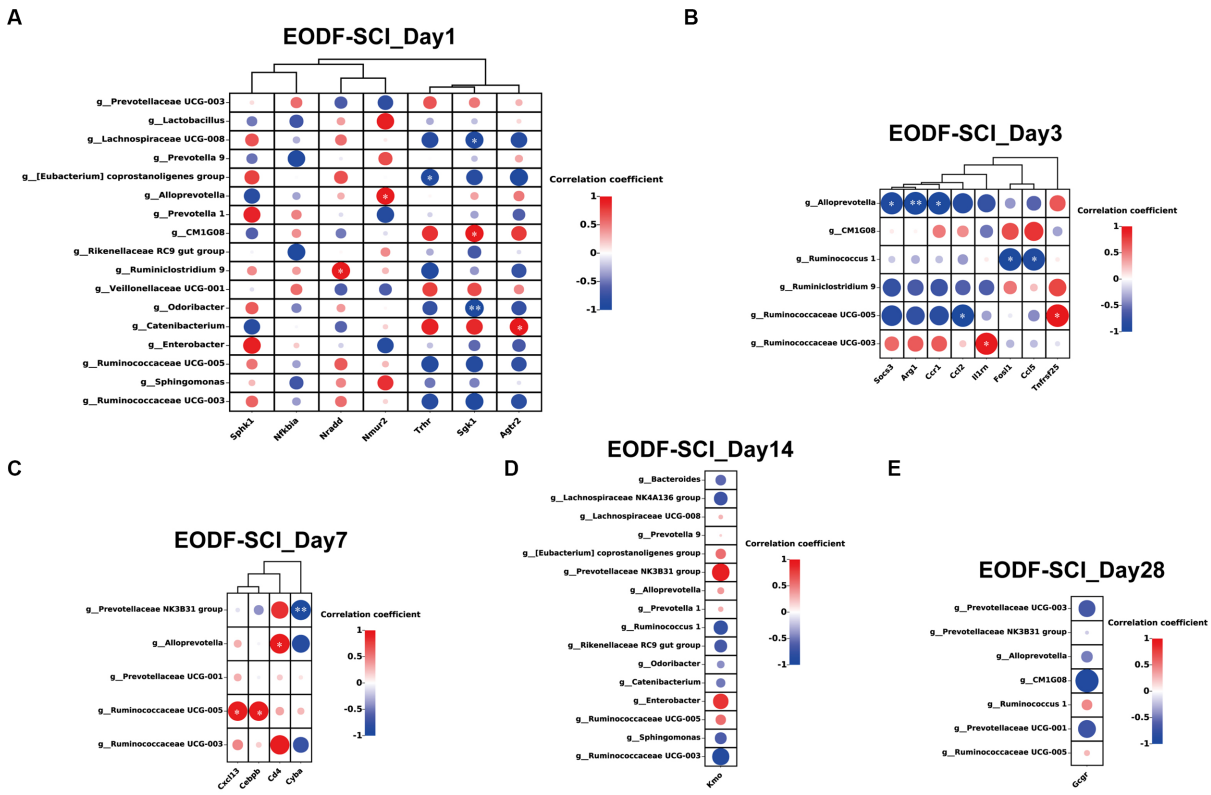

FIGURE 9
Association between gut microbiota (genera with significant differences from the AL-SCI group) and neuroprotection-related DEGs. **(A)** EODF-SCI_Day1; **(B)** EODF-SCI_Day3; **(C)** EODF-SCI_Day7; **(D)** EODF-SCI_Day14; and **(E)** EODF-SCI_Day28. The color gradient illustrates the Spearman's rank correlation coefficient: red indicates a positive correlation and blue indicates a negative correlation. $*p < 0.05$, $**p < 0.01$.

~90% of gut microbiota, have various important functions in host physiology (Rinninella et al., 2019). The *Firmicutes/Bacteroidetes* ratio is crucial for maintaining healthy intestinal homeostasis (Stojanov et al., 2020). In the rat model of SCI, by comparing the abundances of the top 10 ranked phylum level bacteria in the EODF-SCI group with those in the AL-SCI group, we found that the differential bacteria were mainly concentrated on days 1 and 14.

At the genus level, in the EODF group, with the exception of *Veillonellaceae UCG-001*, the abundances of the other bacterial populations changed dynamically at different time points. We analyzed the relative abundances and variations of potentially anti-inflammatory genera (including *Prevotella*, *Lactobacillus*, and *Lachnospiraceae*) and pro-inflammatory genera (*Bacteroides*), which showed dynamic changes in both the AL and EODF groups. On days 1 and 14 after SCI, there was a significant increase in the abundances of *Prevotella1, Prevotella9,* and *Lachnospiraceae UCG-008* in the EODF-SCI group compared to those in the AL-SCI group. Preclinical studies in models of rheumatoid arthritis (Marietta et al., 2016) and experimental acute encephalomyelitis (Mangalam et al., 2017; Shahi, 2019) have shown that oral treatment with this *Prevotella* strain (*P. histicola*) has immunomodulatory effects leading to reduced inflammation development and severity. EDP1815 is prepared from a single strain of *Prevotella* (*P. histicola*). Phase 2 dose-ranging studies in mild and moderate psoriasis [NCT04603027] and a phase 2 study in mild to severe atopic dermatitis [NCT05121480] have been conducted, and these results suggest that EDP1815 has the potential to be used in the treatment of a variety of inflammatory conditions, introducing a new class of drug to the medical community (Itano et al., 2023). *Lachnospiraceae* abundance was decreased in diarrheal children, and supplementing mice with *Lachnospiraceae* reduced obesity-related symptoms and inflammation (Truax et al., 2018; Castro-Mejía et al., 2020). Interestingly, in the present study, on day 1 after SCI, there was a significant increase in the *Lactobacillus* abundance in the EODF-SCI group compared to that in the AL-SCI group. *Lactobacilli* are the most common colonizing bacteria in the gastrointestinal tract of healthy humans and exert beneficial effects by regulating the gut microbiota (Goldstein and Hager, 2015). In addition, *Lactobacillus* exerted neuroprotective effects by rebuilding the microbiota in mice with traumatic brain injury (Ma et al., 2019). A previous study suggests that the *Lactobacillus* app. Cocktail has anti-inflammatory effects on HT-29 cells by modulating the JAK/STAT and NF-κB signaling pathways and that *Lactobacillus* as a dietary supplement may prevent and reduce inflammation-related diseases (Aghamohammad et al., 2022). Anukam et al. found that the *Lactobacillus rhamnosus* and *Lactobacillus reuteri* may help to down-regulate urinary tract infection-related inflammatory factors in patients with SCI (Anukam et al., 2009); in the present study, all five time points after SCI modeling in the EODF-SCI group showed significant reduction in the *Alloprevotella* abundance compared to that in the AL-SCI group. The biological function of *Alloprevotella* is unknown; however, one study suggested that ginkgolide B (GB) is neuroprotective and that GB treatment may exert a neuroprotective effect in AD mice by increasing the *Lactobacillus* abundance and decreasing the abundances of *Alloprevotella, Bacteroidales,* and *Muribaculaceae* (Liu et al., 2021b). On day 14 after SCI, there was a significant decrease in the

Bacteroide abundance in the EODF-SCI group compared to that in the AL-SCI group. Several studies have suggested that *Bacteroides* have potential pro-inflammatory properties (Lindberg et al., 1990; Zhang et al., 2010; Gomez et al., 2012; Munyaka et al., 2016; Ryan et al., 2020). These findings suggested that remodeling of the gut microbiota by EODF treatment may have been beneficial in SCI rats. Particularly on day 1 after SCI in rats (defined as the acute phase), there was a significant increase in the abundances of anti-inflammatory genera in the EODF-SCI group compared to those in the AL-SCI group. We suspect that these beneficial flora may have exerted an anti-inflammatory effect in the acute phase of SCI in rats, and since probiotic products such as *Lactobacillus.app* and *Prevotella.app* are available for purchase, this presents a promising outlook. These probiotics alone, in combination, and in a cocktail, in future studies.

A succession of pathophysiological processes that commence minutes after the original trauma and occur in addition to the primary damage constitute secondary injuries following SCI. They are divided into three phases: acute, subacute, and chronic (Ahuja et al., 2017; Alizadeh et al., 2019; Anjum et al., 2020; Li M. et al., 2022). In humans, the change from the acute to subacute phase often takes place between a few hours and 48 h following the injury. The transition from the acute to the chronic phase, however, is anticipated to take place within 6 months (Ahuja et al., 2017). In contrast, there are three phases of secondary damage in rodents: acute (lasting <24 h), subacute (lasting between 24 h and 7 days), and chronic (lasting >7 days; Li M. et al., 2022). Our transcriptomic data analysis revealed that on days 1, 3, 7, and 14 days after SCI, DEGs between the EODF and AL groups were significantly enriched in entries related to biological events, such as immune response, inflammatory response, cell differentiation, and protein modification. This analysis also showed that at 28 days, entries such as immune and inflammatory responses were no longer significantly enriched, with significantly enriched entries suggesting that major biological events may be associated with neuronal cell differentiation. The results of the KEGG pathway enrichment analysis indicated that the pathways enriched in the EODF and AL groups with DEGs at 1, 3, and 7 days after SCI were mainly associated with immune and inflammatory responses. The studies pointed out that many biological events are involved in different stages of injury after SCI; In the acute phase, the main biological events are associated with immune cell activation, inflammatory response, vascular damage, and oxidative damage;the primary biological occurrences in the subacute period are linked to glial scar formation, reactive astrocyte activation, axonal remodeling, and neuronal death (Alizadeh et al., 2019; Pinchi et al., 2019; Anjum et al., 2020; Zhang et al., 2021). In the acute phase after SCI, the main biological events are associated with neutrophils and microglia, which are immediately activated and secrete inflammatory factors such as interleukin-1β (IL-1β), tumor necrosis factor-alpha (TNF-α) and interleukin 6 (IL-6). The primary biological activities that occur during the subacute phase are linked with monocytes and macrophages entering the spinal cord and releasing pro-inflammatory cytokines, chemokines, and other inflammatory mediators. In both the subacute and chronic stages, the neuroinflammatory response is the response that ultimately causes cell death and tissue degradation, making it an essential component of secondary damage (Hellenbrand et al., 2021). Therefore, we hypothesize that EODF exerts its neuroprotective effects mainly by modulating the immune response and inflammatory response pathways in the early (acute or subacute) phase of SCI.

We further screened the DEGs associated with neuroprotective effects in the AL-SCI and EODF-SCI groups on days 1, 3, 7, 14, 28 days after SCI. and these DEGs were mainly concentrated on days 1, 3, and 7. This further suggested that EODF treatment was able to modulate neuroprotective effects related to DEGs, and that its modulation time was mainly focused on the acute and subacute phases after SCI. These included genes that exert beneficial effects on neuroprotection: (1) *Socs3* and *Arg1* are associated with microglia polarization, with *Socs3* potentially inhibiting microglia polarization and thereby exerting a neuroprotective effect (Wu et al., 2016; Aliena-Valero et al., 2021); *Arg-1* expression presents an association with the M2 phenotype in microglia, and M2-type microglia are considered a beneficial cell type for recovery from neural injury (Li et al., 2021); (2) *Agtr2, Apoe, C3, Cd36, Gabrb2, Il1rn, Nfkbia, and Spp1*, which express proteins thought to be involved in exerting anti-inflammatory effects (Marie et al., 2002; Tukhovskaya et al., 2010; Yeung et al., 2018; Huang et al., 2020; Kisucká et al., 2021; Hou et al., 2022; Kaltschmidt et al., 2022; Li and Jakobs, 2022; Shen et al., 2022); (3) *Bcl2a1*, which exert anti-apoptotic effects (Bedirli et al., 2018); and (4) *Cd4 and Serpine1*, which are involved in nourishing and promote nerve repair (Calenda et al., 2012; Kofke et al., 2018). (i) The DEGs also included genes involved in nerve injury: (1) *Ccl5, Ccl6, Ccr1, Cebpb, Fosl1, Mapk11, Osm, Sphk1, Tnfrsf25,* and *Trpm2*, for which the associated proteins may have been involved in exerting pro-inflammatory effects, including those involved in activating the NF-κB signaling pathway, PI3 kinase/Akt pathway, and CCR1/TPR1/ERK1/2 signaling pathway (Kanno et al., 2005; Li J. et al., 2020; Li M. et al., 2020; Yan et al., 2020; Komori et al., 2022); (2) *Cyba* and *Sgk1*, which promote oxidative stress (Iqbal et al., 2015; Usategui-Martín et al., 2022); (3) *Tlr9*, which are involved in both pro-inflammatory and induction of oxidative stress, and signal activation, and potentially exacerbate neurodegeneration by inducing oxidative stress and inflammation (Dalpke et al., 2002); (4) *Cd4, Cd14, Cd3d, Cd40,* and *Cxcl13*, which promote immune infiltration and activation (Krumbholz et al., 2006; Hernandez et al., 2007; Wang et al., 2022; Daniel et al., 2023) and (5) *C5ar1, Cdk1, Irf3,* and *Nradd*, which promote apoptosis (Wang et al., 2003; Canudas et al., 2004; Solis et al., 2006; Cui et al., 2016; Ding et al., 2021; Shi Y. et al., 2021). (ii) The DEGs also included other genes: (1) Kmo, which expresses proteins that increase the production of toxic kynurenine pathway metabolites in the brain production, such as the neurotoxins 3-hydroxykynurenine and quinolinic acid, and decrease the neuroprotective metabolite kynurenic acid (Chen et al., 2022). Our results revealed that DEGs associated with neuroprotective effects in both groups were mainly clustered on days 1, 3, and 7 after SCI; among them, DEGs related to inflammation accounted for the majority, and the expression levels of DEGs related to neuroprotection were significantly different both temporally and spatially from those in the AL group at different time points after EODF intervention in SCI rats. These results also suggested that EODF may have played an important role in the regulation of immune–inflammation in the acute and subacute phases of SCI rats.

Interestingly, among the DGEs involved in neuroprotection-related genes screened in this study, *Cebpb*, *Socs3*, *Arg1*, *Apoe*, *C3*, *Ccl2,* and *Ccl3* were strongly associated with fasting. Goldstein et al. (2017) found by measuring chromatin accessibility that fasting majorly reorganizes liver chromatin, exposing many fasting-induced enhancers, among which *Cebpb* is one of the key transcription factors regulating the fasting response. c/EBPs are considered constitutive transcription factors, and fasting-related signals glucocorticoids and

glucagon increase the expression and activity of C/EBPβ (the protein encoded by Cebpb), and reducing C/EBPα levels through chromatin regulation impairs gluconeogenesis (Goldstein et al., 2015). In addition, *Socs3* (García et al., 2010; Vendelbo et al., 2015) and *Arg1* (Dai et al., 2022), which have neuroprotective benefits, had increased expression levels under the influence of fasting. *Apoe* is the main apolipoprotein synthesized in the brain in response to injury (Tukhovskaya et al., 2010; Mérian et al., 2023) showed that knocking out *Apoe* increased the susceptibility of mice to cardiovascular disease, and the IF improved glycolipid metabolism in *Apoe*−/− mice. Yamamoto et al. found increased complement C3 levels in a baseline model of cardiac ischemia–reperfusion mice and decreased complement C3 levels in the calorie-restricted group compared to the baseline group (Yamamoto et al., 2016). Liu et al. (2019) performed an 8-week dietary intervention in mice and found that in mice on an IF regime (i.e., continuous fasting for 24 h 3 days per week) IF decreased mRNA levels of macrophage markers (Ccl2 and Ccl3) in inguinal and gonadal adipose and reduced adipose tissue macrophage numbers compared to those in mice on a high-fat diet (HFD, 43% fat). Therefore, the above genes are associated with fasting either by playing a role in the fasting process or as a result of fasting intervention.

Finally, we performed a Spearman's correlation analysis of the DEGs associated with neuroprotection at the gut microbiota abundances (differential genera with those of the AL-SCI group) in the EODF-SCI group. Our results found that EODF was able to regulate the abundance of certain gut microbiota that are closely associated with neuroprotective-associated DEGs in SCI rats during the acute and subacute phases of SCI. Gut microbiota has been shown to play a neuroprotective role in various neurological disorders. Gut microbiota attenuates oxidative stress and inflammatory aspects through its metabolites or the production of secondary metabolites. Moreover, modulation of the gut microbiota with antioxidant and anti-inflammatory probiotics has also shown promising neuroprotective effects (Zhu et al., 2018; Shruti et al., 2022; Solch et al., 2022). Based on this, we hypothesized that the remodeling of the gut microbiota by EODF conferred a neuroprotective effect on the rat model of SCI (Figure 10).

EODF can exert neuroprotective effects and facilitate functional recovery in SCI rats. To allow clinical translation of EODF, we previously conducted a safety study of EODF in patients with SCI (Zheng et al., 2021), and although most of the subjects completed this clinical study, it was found through a post-survey follow-up that this dietary intervention required patients to endure hunger on fasting days, and that many SCI patients and families were less willing to attempt it again. We have also contemplated whether the gut microbiota after EODF intervention could be used as a clinical alternative to EODF. Probiotics have been used to treat urinary tract infections and gastrointestinal discomfort in patients with SCI (Wong et al., 2014). In an animal study, intervention with VSL#3, a medical grade probiotic, was found to improve immune function and promote recovery of motor function in mice with SCI (Laginha et al., 2016). In addition to probiotic intervention, the fecal microbiota transplantation (FMT) approach was also effective in improving motor function and anxiety-like behavior after SCI (Schmidt et al., 2020; Jing et al., 2021, 2022). A recent study demonstrated that EODF intervention can effectively promote axonal regeneration after sciatic nerve compression, and that EODF can exert neuroprotective effects in a mouse model of sciatic nerve injury by means of FMT (Serger et al., 2022). Finally, EODF was found to promote the production of indole-3-propionic acid and affect the metabolism of the organism by increasing the abundance of gut gram-positive *Clostridiales* bacteria, thus achieving the effects of promoting axonal regeneration and accelerating the recovery of sensory function (Serger et al., 2022). Interestingly, They found that both *Clostridiales* bacteria and indole-3-propionic acid supplementation were able to exert similar therapeutic effects as those of EODF. Based on the above study, whether or not the gut microbiota after EODF intervention can protect AL-SCI rats is a very important and clinically translatable scientific question that deserves further study. In the future, the mediating role of gut microbiota can be verified by transplanting the

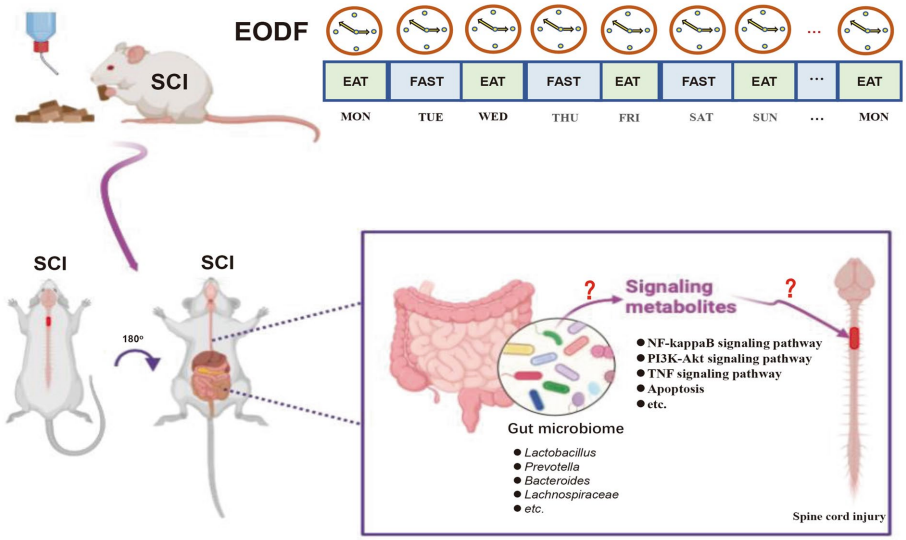

FIGURE 10
Hypothetical model of the mechanism by which EODF-mediated gut microbiota remodeling exerted neuroprotective effects in SCI rats.

healthy rat flora (EODF intervention) into AL-SCI rats by FMT. It is also necessary to conduct an in-depth investigation of the candidate bacteria that are closely related to neuroprotection after EODF intervention to verify whether they can exert similar effects to those of EODF. The findings of our study provide a further basis for treating SCI by targeting the gut microbiota.

5. Conclusion

In this study, we found that EODF could alter the abundance and diversity of the gut microbiota in SCI rats at different time points. Moreover, we revealed characteristic changes in the gut microbiota at various phylogenetic levels. Notably, EODF induced dynamic changes in the abundance of potentially anti-inflammatory and pro-inflammatory bacteria. In addition, spinal cord transcriptome sequencing analysis revealed that: (i) enrichments of DEGs at different time points after EODF intervention in SCI rats compared to that after AL intervention were associated with biological events, such as immune response, inflammatory response, cell differentiation, protein modification, apoptosis, and nerve cell differentiation; (ii) EODF was involved in regulating the levels of DEGs associated with neuroprotection after the onset of SCI, and this expression level was significantly different both spatially and temporally from that of the AL group; (iii) a significant correlation was observed between the relative abundance of certain genera and DEGs associated with neuroprotective effects in spinal cord tissues at different times points in the EODF-SCI group. Although further research is required to elucidate the mechanism underlying the neuroprotective effect of the EODF treatment in SCI rats, by combining the gut microbiota and transcriptome analyses results, we propose that gut microbiota may have been involved in mediating EODF to regulate the transcriptional levels of genes associated with neuroprotective effect in SCI rats, thereby exerting a neuroprotective effect. It should be noted that our study only analyzed the gut microbiota and tissue transcriptome levels. In future studies, a multiomics combination is needed to further explore the specific mechanisms of the neuroprotective effects of EODF in SCI treatment, such as through the combined application of proteomics, metabolomics, single-cell sequencing technology, and genetic engineering.

Data availability statement

The raw sequence data reported in this paper have been deposited in the Genome Sequence Archive (Genomics, Proteomics & Bioinformatics 2021) in National Genomics Data Center (Nucleic Acids Res 2022), China National Center for Bioinformation / Beijing Institute of Genomics, Chinese Academy of Sciences (GSA: CRA011825 and CRA011760) that are publicly accessible at https://ngdc.cncb.ac.cn/gsa.

Ethics statement

The animal study was reviewed and approved by the Western Theater General Hospital Animal Experimentation Ethics Committee (approval number: 2019ky79).

Author contributions

AZ, RP, and JW conceived and designed the study. JW, XZ, RZ, MW, WX, ML, and RT performed the experiments. RP, JW, XZ, RZ, and MW interpreted the results of experiments. JW, XZ, RZ, and MW analyzed the data. JW, RZ, MW, and ZY prepared the figures. JW, RZ, and MW wrote the manuscript. JW, XZ, RZ, MW, JZ, JL, LZ, JG, and HL conducted the literature research. All authors contributed to the article and approved the submitted version.

Funding

This work was supported by the General Program of the National Natural Science Foundation of China (81973927), the Key R&D Program of the Sichuan Department of Science and Technology (2021YFS0133), Sichuan Provincial Administration of Traditional Chinese Medicine Special Research Project on Traditional Chinese Medicine (2020LC0224), and the 2019 Annual Hospital Highland Medicine Research Project (2019ZY03). Projects on the science and technology situation in Tongliang District, Chongqing (2022005, TL2021-06).

Acknowledgments

We would like to thank Editage (www.editage.cn) for English language editing. We thank Chengdu Rhonin Biotechnology Co. for providing amplicon sequencing service of 16SrRNA; We thank Shanghai Ouyi Biomedical Technology Co. for providing transcriptome sequencing service.

Conflict of interest

The authors declare that the research was conducted in the absence of any commercial or financial relationships that could be construed as potential conflicts of interest.

Publisher's note

Supplementary material

The Supplementary material for this article can be found online at: https://www.frontiersin.org/articles/10.3389/fmicb.2023.1206909/full#supplementary-material

References

Aghamohammad, S., Sepehr, A., Miri, S. T., Najafi, S., Pourshafie, M. R., and Rohani, M. (2022). Anti-inflammatory and immunomodulatory effects of Lactobacillus spp. as a preservative and therapeutic agent for IBD control. *Immun Inflamm Dis* 10:e635. doi: 10.1002/iid3.635

Ahuja, C. S., Wilson, J. R., Nori, S., Kotter, M. R. N., Druschel, C., Curt, A., et al. (2017). Traumatic spinal cord injury. *Nat. Rev. Dis. Primers.* 3:17018. doi: 10.1038/nrdp.2017.18

Ali, I., Liu, K., Long, D., and Faisal, S. (2021). Ramadan fasting leads to shifts in human gut microbiota structured by dietary composition. *Front. Microbiol.* 12:642999. doi: 10.3389/fmicb.2021.642999

Aliena-Valero, A., Rius-Pérez, S., Baixauli-Martín, J., Torregrosa, G., Chamorro, Á., Pérez, S., et al. (2021). Uric acid neuroprotection associated to IL-6/STAT3 signaling pathway activation in rat ischemic stroke. *Mol. Neurobiol.* 58, 408–423. doi: 10.1007/s12035-020-02115-w

Alizadeh, A., Dyck, S. M., and Karimi-Abdolrezaee, S. (2019). Traumatic spinal cord injury: an overview of pathophysiology, models and acute injury mechanisms. *Front. Neurol.* 10:282. doi: 10.3389/fneur.2019.00282

Anjum, A., Yazid, M. D., Fauzi Daud, M., Idris, J., Ng, A. M. H., Selvi Naicker, A., et al. (2020). Spinal cord injury: pathophysiology, multimolecular interactions, and underlying recovery mechanisms. *Int. J. Mol. Sci.* 21:7533. doi: 10.3390/ijms21207533

Anukam, K. C., Hayes, K., Summers, K., and Reid, G. (2009). Probiotic *Lactobacillus rhamnosus* GR-1 and *Lactobacillus reuteri* RC-14 may help downregulate TNF-alpha, IL-6, IL-8, IL-10 and IL-12 (p70) in the neurogenic bladder of spinal cord injured patient with urinary tract infections: a two-case study. *Adv. Urol.* 2009:680363, 1–5. doi: 10.1155/2009/680363

Bedirli, N., Bagriacik, E. U., and Yilmaz, G. (2018). Sevoflurane exerts brain-protective effects against sepsis-associated encephalopathy and memory impairment through caspase 3/9 and Bax/Bcl signaling pathway in a rat model of sepsis. *J. Int. Med. Res.* 46, 2828–2842. doi: 10.1177/0300060518773265IF

Calenda, G., Strong, T. D., Pavlovich, C. P., Schaeffer, E. M., Burnett, A. L., Yu, W., et al. (2012). Whole genome microarray of the major pelvic ganglion after cavernous nerve injury: new insights into molecular profile changes after nerve injury. *BJU Int.* 109, 1552–1564. doi: 10.1111/j.1464-410X.2011.10705.x

Canudas, A. M., Jordà, E. G., Verdaguer, E., Jiménez, A., Sureda, F. X., Rimbau, V., et al. (2004). Cyclosporin a enhances colchicine-induced apoptosis in rat cerebellar granule neurons. *Br. J. Pharmacol.* 141, 661–669. doi: 10.1038/sj.bjp.0705664

Caporaso, J. G., Lauber, C. L., Walters, W. A., Berg-Lyons, D., Lozupone, C. A., Turnbaugh, P. J., et al. (2011). Global patterns of 16S rRNA diversity at a depth of millions of sequences per sample. *Proc. Natl. Acad. Sci. U. S. A.* 108, 4516–4522. doi: 10.1073/pnas.1000080107

Castro-Mejía, J. L., O'Ferrall, S., Krych, Ł., O'Mahony, E., Namusoke, H., Lanyero, B., et al. (2020). Restitution of gut microbiota in Ugandan children administered with probiotics (*Lactobacillus rhamnosus GG* and *Bifidobacterium animalis* subsp. *lactis BB-12*) during treatment for severe acute malnutrition. *Gut Microbes* 11, 855–867. doi: 10.1080/19490976.2020.1712982

Chamankhah, M., Eftekharpour, E., Karimi-Abdolrezaee, S., Boutros, P. C., San-Marina, S., and Fehlings, M. G. (2013). Genome-wide gene expression profiling of stress response in a spinal cord clip compression injury model. *BMC Genomics* 14:583. doi: 10.1186/1471-2164-14-583

Chen, Y., Zhang, J., Yang, Y., Xiang, K., Li, H., Sun, D., et al. (2022). Kynurenine-3-monooxygenase (KMO): from its biological functions to therapeutic effect in diseases progression. *J. Cell. Physiol.* 237, 4339–4355. doi: 10.1002/jcp.30876

Cignarella, F., Cantoni, C., Ghezzi, L., Salter, A., Dorsett, Y., Chen, L., et al. (2018). Intermittent fasting confers protection in CNS autoimmunity by altering the gut microbiota. *Cell Metab.* 27, 1222–1235.e6. doi: 10.1016/j.cmet.2018.05.006

Cui, Y., Zhao, D., Sreevatsan, S., Liu, C., Yang, W., Song, Z., et al. (2016). *Mycobacterium bovis* induces endoplasmic reticulum stress mediated-apoptosis by activating IRF3 in a murine macrophage cell line. *Front. Cell. Infect. Microbiol.* 6:182. doi: 10.3389/fcimb.2016.00182

Dai, S., Wei, J., Zhang, H., Luo, P., Yang, Y., Jiang, X., et al. (2022). Intermittent fasting reduces neuroinflammation in intracerebral hemorrhage through the Sirt3/Nrf2/HO-1 pathway. *J. Neuroinflammation* 19:122. doi: 10.1186/s12974-022-02474-2

Dalpke, A. H., Schäfer, M. K. H., Frey, M., and Zimmermann, S. (2002). Immunostimulatory CpG-DNA activates murine microglia. *J. Immunol.* 168, 4854–4863. doi: 10.4049/jimmunol.168.10.4854

Daniel, S., Koniaris Leonidas, G., and Clark, W. (2023). Role of CD14 in human disease. *Immunology* 169, 260–270. doi: 10.1111/imm.13634

Davis, L. M., Pauly, J. R., Readnower, R. D., Rho, J. M., and Sullivan, P. G. (2008). Fasting is neuroprotective following traumatic brain injury. *J. Neurosci. Res.* 86, 1812–1822. doi: 10.1002/jnr.21628

Deng, Y., Liu, W., and Wang, J. (2020). Intermittent fasting improves lipid metabolism through changes in gut microbiota in diet-induced obese mice. *Med. Sci. Monit.* 26:e926789. doi: 10.12659/MSM.926789

Ding, L., Ning, J., Wang, Q., Lu, B., and Ke, H. (2021). Sevoflurane improves nerve regeneration and repair of neurological deficit in brain damage rats via microRNA-490-5p/CDK1 axis. *Life Sci.* 271:119111. doi: 10.1016/j.lfs.2021.119111

Edgar, R. C. (2013). Uparse: highly accurate OTU sequences from microbial amplicon reads. *Nat. Methods* 10, 996–998. doi: 10.1038/nmeth.2604

Ejtahed, H. S., Hasani-Ranjbar, S., and Larijani, B. (2017). Human microbiome as an approach to personalized medicine. *Altern. Ther. Health Med.* 23, 8–9.

García, A. P., Palou, M., Priego, T., Sánchez, J., Palou, A., and Picó, C. (2010). Moderate caloric restriction during gestation results in lower arcuate nucleus NPY- and alphaMSH-neurons and impairs hypothalamic response to fed/fasting conditions in weaned rats. *Diabetes Obes. Metab.* 12, 403–413. doi: 10.1111/j.1463-1326.2009.01174.x

Goldstein, I., Baek, S., Presman, D. M., Paakinaho, V., Swinstead, E. E., and Hager, G. L. (2017). Transcription factor assisted loading and enhancer dynamics dictate the hepatic fasting response. *Genome Res.* 27, 427–439. doi: 10.1101/gr.212175.116

Goldstein, I., and Hager, G. L. (2015). Transcriptional and chromatin regulation during fasting - the genomic era. *Trends Endocrinol. Metab.* 26, 699–710. doi: 10.1016/j.tem.2015.09.005

Goldstein, E. J., Tyrrell, K. L., and Citron, D. M. (2015). Lactobacillus species: taxonomic complexity and controversial susceptibilities. *Clin.Infect.Dis.* 60, S98–S107. doi: 10.1093/cid/civ072

Gomez, A., Luckey, D., Yeoman, C. J., Marietta, E. V., Berg Miller, M. E., Murray, J. A., et al. (2012). Loss of sex and age driven differences in the gut microbiome characterize arthritis-susceptible 0401 mice but not arthritis-resistant 0402 mice. *PLoS One* 7:e36095. doi: 10.1371/journal.pone.0036095

Gungor, B., Adiguzel, E., Gursel, I., Yilmaz, B., and Gursel, M. (2016). Intestinal microbiota in patients with spinal cord injury. *PLoS One* 11:e0145878. doi: 10.1371/journal.pone.0145878

Guo, Y., Luo, S., Ye, Y., Yin, S., Fan, J., and Xia, M. (2021). Intermittent fasting improves cardiometabolic risk factors and alters gut microbiota in patients with metabolic syndrome patients. *J. Clin. Endocrinol. Metab.* 106, 64–79. doi: 10.1210/clinem/dgaa644

Hatting, M., Rines, A. K., Luo, C., Tabata, M., Sharabi, K., Hall, J. A., et al. (2017). Adipose tissue CLK2 promotes energy expenditure during high-fat diet intermittent fasting. *Cell Metab.* 25, 428–437. doi: 10.1016/j.cmet.2016.12.007

Hellenbrand, D. J., Quinn, C. M., Piper, Z. J., Morehouse, C. N., Fixel, J. A., and Hanna, A. S. (2021). Inflammation after spinal cord injury: a review of the critical timeline of signaling cues and cellular infiltration. *J. Neuroinflammation* 18:284. doi: 10.1186/s12974-021-02337-2

Hernandez, M. G., Shen, L., and Rock, K. L. (2007). CD40-CD40 ligand interaction between dendritic cells and CD8+ T cells is needed to stimulate maximal T cell responses in the absence of CD4+ T cell help. *J. Immunol.* 178, 2844–2852. doi: 10.4049/jimmunol.178.5.2844

Hou, J. Y., Cao, G. Z., Tian, L. L., Zhou, R., Zhang, Y., Xu, H., et al. (2022). Integrated transcriptomics and metabolomics analysis reveals that C3 and C5 are vital targets of DuZhi wan in protecting against cerebral ischemic injury. *Biomed. Pharmacother.* 155:113703. doi: 10.1016/j.biopha.2022.113703

Huang, L., Tang, H., Sherchan, P., Lenahan, C., Boling, W., Tang, J., et al. (2020). The activation of phosphatidylser-ine/CD36/TGF-β1 pathway prior to surgical brain injury attenuates neuroinflammation in rats. *Oxidative Med. Cell. Longev.* 2020:4921562. doi: 10.1155/2020/4921562

Iqbal, S., Howard, S., and Lograsso, P. V. (2015). Serum- and glucocorticoid-inducible kinase 1 confers protection in cell-based and inIn VivoNeurotoxin models via the c-Jun N-terminal kinase signaling pathway. *Mol. Cell. Biol.* 35, 1992–2006. doi: 10.1128/MCB.01510-14

Itano, A., Maslin, D., Ramani, K., Mehraei, G., Carpenter, N., Cormack, T., et al. (2023). Clinical translation of anti-inflammatory effects of *Prevotella histicola* in Th1, Th2, and Th17 inflammation. *Front Med (Lausanne).* 10:1070433. doi: 10.3389/fmed.2023.1070433

Jeong, M. A., Plunet, W., Streijger, F., Lee, J. H. T., Plemel, J. R., Park, S., et al. (2011). Intermittent fasting improves functional recovery after rat thoracic contusion spinal cord injury. *J. Neurotrauma* 28, 479–492. doi: 10.1089/neu.2010.1609

Jing, Y., Bai, F., Wang, L., Yang, D., Yan, Y., Wang, Q., et al. (2022). Fecal microbiota transplantation exerts neuroprotective effects in a mouse spinal cord injury model by modulating the microenvironment at the lesion site. *Microbiol. Spectr* 10:e0017722. doi: 10.1128/spectrum.00177-22

Jing, Y., Yu, Y., Bai, F., Wang, L., Yang, D., Zhang, C., et al. (2021). Effect of fecal microbiota transplantation on neurological restoration in a spinal cord injury mouse model: involvement of brain-gut axis. *Microbiome* 9:59. doi: 10.1186/s40168-021-01007-y

Kaltschmidt, B., Helweg, L. P., Greiner, J. F. W., and Kaltschmidt, C. (2022). NF-κB in neurodegenerative diseases: recent evidence from human genetics. *Front. Mol. Neurosci.* 15:954541. doi: 10.3389/fnmol.2022.954541

Kanno, M., Suzuki, S., Fujiwara, T., Yokoyama, A., Sakamoto, A., Takahashi, H., et al. (2005). Functional expression of CCL6 by rat microglia: a possible role of CCL6 in cell-cell communication. *J. Neuroimmunol.* 167, 72–80. doi: 10.1016/j.jneuroim.2005.06.028

Kigerl, K. A., Hall, J. C. E., Wang, L., Mo, X., Yu, Z., and Popovich, P. G. (2016). Gut dysbiosis impairs recovery after spinal cord injury. *J. Exp. Med.* 213, 2603–2620. doi: 10.1084/jem.20151345

Kim, D., Langmead, B., and Salzberg, S. L. (2015). HISAT: a fast spliced aligner with low memory requirements. *Nat. Methods* 12, 357–360. doi: 10.1038/nmeth.3317

Kisucká, A., Bimbová, K., Bačová, M., Gálik, J., and Lukáčová, N. (2021). Activation of neuroprotective microglia and astrocytes at the lesion site and in the adjacent segments is crucial for spontaneous locomotor recovery after spinal cord injury. *Cells* 10:1943. doi: 10.3390/cells10081943

Kofke, W. A., Ren, Y., Augoustides, J. G., Li, H., Nathanson, K., Siman, R., et al. (2018). Reframing the biological basis of neuroprotection using functional genomics: differentially weighted, time-dependent multifactor pathogenesis of human ischemic brain damage. *Front. Neurol.* 9:497. doi: 10.3389/fneur.2018.00497

Komori, R., Matsuo, T., Yokota-Nakatsuma, A., Hashimoto, R., Kubo, S., Kozawa, C., et al. (2022). Regulation of inflammation-related genes through Fosl1 suppression in a levetiracetam-treated pilocarpine-induced status epilepticus mouse model. *Int. J. Mol. Sci.* 23:7608. doi: 10.3390/ijms23147608

Krumbholz, M., Theil, D., Cepok, S., Hemmer, B., Kivisäkk, P., Ransohoff, R. M., et al. (2006). Chemokines in multiple sclerosis: CXCL12 and CXCL13 up-regulation is differentially linked to CNS immune cell recruitment. *Brain* 129, 200–211. doi: 10.1093/brain/awh680

Laginha, I., Kopp, M. A., Druschel, C., Schaser, K. D., Brommer, B., Hellmann, R. C., et al. (2016). Natural killer (NK) cell functionality after human spinal cord injury (SCI): protocol of a prospective, longitudinal study. *BMC Neurol.* 16:170. doi: 10.1186/s12883-016-0681-5

Li, Q. Q., Ding, D. H., Wang, X. Y., Sun, Y. Y., and Wu, J. (2021). Lipoxin A4 regulates microglial M1/M2 polarization after cerebral ischemiareperfusion injury via the notch signaling pathway. *Exp. Neurol.* 339:113645. doi: 10.1016/j.expneurol.2021.113645

Li, S., and Jakobs, T. C. (2022). Secreted phosphoprotein 1 slows neurodegeneration and rescues visual function in mouse models of aging and glaucoma. *Cell Rep.* 41:111880. doi: 10.1016/j.celrep.2022.111880

Li, J. J., Liu, H., Zhu, Y., Yan, L., Liu, R., Wang, G., et al. (2022). Animal models for treating spinal cord injury using bio-materials-based tissue engineering strategies. *Tissue Eng. Part B Rev.* 28, 79–100. doi: 10.1089/ten.TEB.2020.0267

Li, J., Lv, H., and Che, Y. (2020). microRNA-381-3p confers protection against ischemic stroke through promoting angiogenesis and inhibiting inflammation by suppressing CEBPB and Map3k8. *Cell. Mol. Neurobiol.* 40, 1307–1319. doi: 10.1007/s10571-020-00815-4

Li, M., Sun, X., Zhao, J., Xia, L., Li, J., Xu, M., et al. (2020). CCL5 deficiency promotes liver repair by improving inflammation resolution and liver regeneration through M2 macrophage polarization. *Cell. Mol. Immunol.* 17, 753–764. doi: 10.1038/s41423-019-0279-0

Li, G., Xie, C., Lu, S., Nichols, R. G., Tian, Y., Li, L., et al. (2017). Intermittent fasting promotes white adipose browning and decreases obesity by shaping the gut microbiota. *Cell Metab.* 26:801. doi: 10.1016/j.cmet.2017.10.007

Li, M., Yang, X., Sun, N., Tang, R., Wang, W., Huang, X., et al. (2022). Dietary restriction may attenuate the expression of cell death-related proteins in rats with acute spinal cord injury. *World Neurosurg.* 162, e475–e483. doi: 10.1016/j.wneu.2022.03.035

Lindberg, A. A., Weintraub, A., Zähringer, U., and Rietschel, E. T. (1990). Structure–activity relationships in lipopolysaccharides of *Bacteroides fragilis*. *Rev. Infect. Dis.* 12, S133–S141. doi: 10.1093/clinids/12.Supplement_2.S133

Liu, Z., Dai, X., Zhang, H., Shi, R., Hui, Y., Jin, X., et al. (2020). Gut microbiota mediates intermittent-fasting alleviation of diabetes-induced cognitive impairment. *Nat. Commun.* 11:855. doi: 10.1038/s41467-020-14676-4

Liu, B., Page, A. J., Hatzinikolas, G., Chen, M., Wittert, G. A., and Heilbronn, L. K. (2019). Intermittent fasting improves glucose tolerance and promotes adipose tissue remodeling in male mice fed a high-fat diet. *Endocrinol* 160, 169–180. doi: 10.1210/en.2018-00701

Liu, C., Yao, M., Stegen, J. C., Rui, J., Li, J., and Li, X. (2017). Long-term nitrogen addition affects the phylogenetic turnover of soil microbial community in response to moisture pulse. *Sci. Rep.* 7:17492. doi: 10.1038/s41598-017-17736-w

Liu, J., Ye, T., Zhang, Y., Zhang, R., Kong, Y., Zhang, Y., et al. (2021a). Protective effect of Ginkgolide B against cognitive impairment in mice via regulation of gut microbiota. *J. Agric. Food Chem.* 69, 12230–12240. doi: 10.1021/acs.jafc.1c05038

Liu, J., Zhong, Y., Luo, X. M., Ma, Y., Liu, J., and Wang, H. (2021b). Intermittent fasting reshapes the gut microbiota and metabolome and reduces weight gain more effectively than melatonin in mice. *Front. Nutr.* 8:784681. doi: 10.3389/fnut.2021.784681

Love, M. I., Huber, W., and Anders, S. (2014). Moderated estimation of fold change and dispersion for RNA-seq data with DESeq2. *Genome Biol.* 15:550. doi: 10.1186/s13059-014-0550-8

Ma, Y., Liu, T., Fu, J., Fu, S., Hu, C., Sun, B., et al. (2019). *Lactobacillus acidophilus* exerts neuroprotective effects in mice with traumatic brain injury. *J. Nutr.* 149, 1543–1552. doi: 10.1093/jn/nxz105

Maifeld, A., Bartolomaeus, H., Löber, U., Avery, E. G., Steckhan, N., Markó, L., et al. (2021). Fasting alters the gut microbiome and reduces blood pressure and body weight in patients with metabolic syndromes. *Nat. Commun.* 12:1970. doi: 10.1038/s41467-021-22097-0

Mangalam, A., Shahi, S. K., Luckey, D., Karau, M., Marietta, E., Luo, N., et al. (2017). Human gut-derived commensal Bacteria suppress CNS inflammatory and demyelinating disease. *Cell Rep.* 20, 1269–1277. doi: 10.1016/j.celrep.2017.07.031

Manzanero, S., Erion, J. R., Santro, T., Steyn, F. J., Chen, C., Arumugam, T. V., et al. (2014). Intermittent fasting attenuates increases in neurogenesis after ischemia and reperfusion and improves recovery. *J. Cereb. Blood Flow Metab.* 34, 897–905. doi: 10.1038/jcbfm.2014.36

Marie, J. C., Astier, A. L., Rivailler, P., Rabourdin-Combe, C., Wild, T. F., and Horvat, B. (2002). Linking innate and acquired immunity: divergent role of CD46 cytoplasmic domains in T cell-induced inflammation. *Nat. Immunol.* 3, 659–666. doi: 10.1038/ni810

Marietta, E. V., Murray, J. A., Luckey, D. H., Jeraldo, P. R., Lamba, A., Patel, R., et al. (2016). Suppression of inflammatory arthritis by human gut-derived *Prevotella histicola* in humanized mice. *Arthritis Rheumatol.* 68, 2878–2888. doi: 10.1002/art.39785

Mérian, J., Ghezali, L., Trenteseaux, C., Duparc, T., Beuzelin, D., Bouguetoch, V., et al. (2023). Intermittent fasting resolves dyslipidemia and atherogenesis in apolipoprotein E-deficient mice in a diet-dependent manner, irrespective of sex. *Cells* 12:533. doi: 10.3390/cells12040533

Munyaka, P. M., Rabbi, M. F., Khafipour, E., and Ghia, J. E. (2016). Acute dextran sulfate sodium (DSS)-induced colitis promotes gut microbial dysbiosis in mice. *J. Basic Microbiol.* 56, 986–998. doi: 10.1002/jobm.201500726

Pang, R., Wang, J., Xiong, Y., Liu, J., Ma, X., Gou, X., et al. (2022). Relationship between gut microbiota and lymphocyte subsets in Chinese Han patients with spinal cord injury. *Front. Microbiol.* 13:986480. doi: 10.3389/fmicb.2022.986480

Pinchi, E., Frati, A., Cantatore, S., D'Errico, S., Russa, R., Maiese, A., et al. (2019). Acute spinal cord injury: a systematic review investigating mirna families involved. *Int. J. Mol. Sci.* 20:1841. doi: 10.3390/ijms20081841

Plunet, W. T., Lam, C. K., Lee, J. H., Liu, J., and Tetzlaff, W. (2010). Prophylactic dietary restriction may promote functional recovery and increase lifespan after spinal cord injury. *Ann. N. Y. Acad. Sci.* 1198, E1–E11. doi: 10.1111/j.1749-6632.2010.05564.x

Plunet, W. T., Streijger, F., Lam, C. K., Lee, J. H. T., Liu, J., and Tetzlaff, W. (2008). Dietary restriction started after spinal cord injury improves functional recovery. *Exp. Neurol.* 213, 28–35. doi: 10.1016/j.expneurol.2008.04.011

Prisco, S. Z., Eklund, M., Moutsoglou, D. M., Prisco, A. R., Khoruts, A., Weir, E. K., et al. (2021). Intermittent fasting enhances right ventricular function in preclinical pulmonary arterial hypertension. *J. Am. Heart Assoc.* 10:e022722. doi: 10.1161/JAHA.121.022722

Rinninella, E., Raoul, P., Cintoni, M., Franceschi, F., Miggiano, G., Gasbarrini, A., et al. (2019). What is the composition of healthy gut microbiota composition? A changing ecosystem across age, environment, diet, and diseases. *Microorganisms* 7:14. doi: 10.3390/microorganisms7010014

Roberts, A., Trapnell, C., Donaghey, J., Rinn, J. L., and Pachter, L. (2011). Improving RNA-Seq expression estimates by correcting for fragment bias. *Genome Biol.* 12:R22. doi: 10.1186/gb-2011-12-3-r22

Ryan, F. J., Ahern, A. M., Fitzgerald, R. S., Laserna-Mendieta, E. J., Power, E. M., Clooney, A. G., et al. (2020). Colonic microbiota is associated with inflammation and host epigenomic alterations in inflammatory bowel disease. *Nat. Commun.* 11:1512. doi: 10.1038/s41467-020-15342-5

Schmidt, E. K. A., Torres-Espin, A., and Raposo, P. J. F. (2020). Fecal transplant prevents gut dysbiosis and anxiety-like behaviour after spinal cord injury in rats. *PLoS One* 15:e0226128. doi: 10.1371/journal.pone.0226128

Serger, E., Luengo-Gutierrez, L., and Chadwick, J. S. (2022). The gut metabolite indole-3 propionate promotes nerve regeneration and repair. *Nature* 607, 585–592. doi: 10.1038/s41586-022-04884-x

Shahi, S. K. (2019). *Prevotella histicola*, a human gut commensal, is as potent as COPAXONE® in an animal model of multiple sclerosis. *Front. Immunol.* 10:462. doi: 10.3389/fimmu.2019.00462

Shen, L., Chen, D. Y., and Lou, Q. Q. (2022). Angiotensin type 2 receptor pharmacological agonist relieves neurocognitive deficits via reducing neuroinflammation and microglial engulfment of dendritic spines. *J. Neuroimmune Pharmacol.*, 1–17. doi: 10.1007/s11481-022-10054-7

Shi, Y., Chen, X., and Liu, J. (2021). Isoquercetin improves inflammatory response in rats following ischemic stroke. *Front. Neurosci.* 15:555543. doi: 10.3389/fnins.2021.555543

Shi, H., Zhang, B., and Abo-Hamzy, T. (2021). Restructuring the gut microbiota by intermittent fasting lowers blood pressure. *Circ. Res.* 128, 1240–1254. doi: 10.1161/CIRCRESAHA.120.318155

Shi, L. L., Zhang, N., and Xie, X. M. (2017). Transcriptome profile of rat genes in injured spinal cord at different stages by RNA-sequencing. *BMC Genomics* 18:173. doi: 10.1186/s12864-017-3532-x

Shruti, S., Sandeep, K., and Niraj, K. J. (2022). Interplay of gut microbiota and oxidative stress: perspective on neurodegeneration and neuroprotection. *J. Adv. Res.* 38, 223–244. doi: 10.1016/j.jare.2021.09.005

Solch, R. J., Aigbogun, J. O., and Voyiadjis, A. G. (2022). Mediterranean diet adherence, gut microbiota, and Alzheimer's or Parkinson's disease risk: a systematic review. *J. Neurol. Sci.* 434:120166. doi: 10.1016/j.jns.2022.120166

Solis, M., Goubau, D., and Romieu-Mourez, R. (2006). Distinct functions of IRF-3 and IRF-7 in IFN-alpha gene regulation and control of antitumor activity in primary macrophages. *Biochem. Pharmacol.* 72, 1469–1476. doi: 10.1016/j.bcp.2006.06.002

Stojanov, S., Berlec, A., and Štrukelj, B. (2020). The influence of probiotics on the *Firmicutes*/*Bacteroidetes* ratio in the treatment of obesity and inflammatory bowel disease. *Microorganisms* 8:1715. doi: 10.3390/microorganisms8111715

Streijger, F., Lee, J. H., and Duncan, G. J. (2014). Combinatorial treatment of acute spinal cord injury with ghrelin, ibuprofen, C16, and ketogenic diet does not result in improved histologic or functional outcome. *J. Neurosci. Res.* 92, 870–883. doi: 10.1002/jnr.23372

Su, J., Li, F., Wang, Y., Su, Y., Verhaar, A., Ma, Z., et al. (2022). Investigating Ramadan like fasting effects on the gut microbiome of BALB/c mice. *Front. Nutr.* 9:832757. doi: 10.3389/fnut.2022.832757

Su, J., Wang, Y., and Zhang, X. (2021). Xiaofang Zhang remodeling of the gut microbiome during Ramadan-associated intermittent fasting. *Am. J. Clin. Nutr.* 113, 1332–1342. doi: 10.1093/ajcn/nqaa388

Sun, N. Y., Xiong, X. J., and Yu, H. (2018). Every-other-day fasting improved motor functional recovery in rats with clip-compression injury of the spinal cord. *Chin J Tissue Eng Res* 22, 564–569. doi: 10.3969/j.issn.2095-4344.0091

Truax, A. D., Chen, L., and Tam, J. W. (2018). The inhibitory innate immune sensor NLRP12 maintains a threshold against obesity by regulating gut microbiota homeostasis. *Cell Host Microbe* 24, 364–378.e6. doi: 10.1016/j.chom.2018.08.009

Tukhovskaya, E. A., Yukin, A. Y., and Khokhlova, O. N. (2010). COG1410, a novel apolipoprotein-E mimetic, improves functional and morphological recovery in a rat model of focal brain ischemia. *J. Neurosci. Res.* 87, 677–682. doi: 10.1002/jnr.21874

Usategui-Martín, R., Puertas-Neyra, K., and Galindo-Cabello, N. (2022). Retinal neuroprotective effect of mesenchymal stem cells secretome through modulation of oxidative stress, autophagy, and programmed cell death. *Invest. Ophthalmol. Vis. Sci.* 63:27. doi: 10.1167/iovs.63.4.27

Varady, K. A., and Hellerstein, M. K. (2007). Alternate-day fasting and chronic disease prevention: a review of human and animal trials. *Am. J. Clin. Nutr.* 86, 7–13. doi: 10.1093/ajcn/86.1.7

Vendelbo, M. H., Christensen, B., and Grønbæk, S. B. (2015). GH signaling in human adipose and muscle tissue during 'feast and famine': amplification of exercise stimulation following fasting compared to glucose administration. *Eur. J. Endocrinol.* 173, 283–290. doi: 10.1530/EJE-14-1157

Wang, Z., He, Y., and Cun, Y. (2022). Identification of potential key genes for immune infiltration in childhood asthma by data mining and biological validation. *Front. Genet.* 13:957030. doi: 10.3389/fgene.2022.957030

Wang, X., Shao, Z., and Zetoune, F. S. (2003). NRADD, a novel membrane protein with a death domain involved in mediating apoptosis in response to ER stress. *Cell Death Differ.* 10, 580–591. doi: 10.1038/sj.cdd.4401208

Wong, S., Jamous, A., and O'Driscoll, J. (2014). A *Lactobacillus casei* Shirota probiotic drink reduces antibiotic-associated diarrhoea in patients with spinal cord injuries: a randomised controlled trial. *Br. J. Nutr.* 111, 672–678. doi: 10.1017/S0007114513002973

Wu, L. H., Lin, C., and Lin, H. Y. (2016). Naringenin suppresses neuroinflammatory responses through inducing suppressor of cytokine signaling 3 expression. *Mol. Neurobiol.* 53, 1080–1091. doi: 10.1007/s12035-014-9042-9

Yamamoto, T., Tamaki, K., Shirakawa, K., Ito, K., Yan, X., Katsumata, Y., et al. (2016). Cardiac Sirt1 mediates the cardioprotective effect of caloric restriction by suppressing local complement system activation after ischemia-reperfusion. *Am. J. Physiol. Heart Circ. Physiol.* 310, H1003–H1014. doi: 10.1152/ajpheart.00676.2015

Yan, J., Zuo, G., Sherchan, P., Huang, L., Ocak, U., Xu, W., et al. (2020). CCR1 activation promotes neuroinflammation through CCR1/TPR1/ERK1/2 signaling pathway after intracerebral hemorrhage in mice. *Neurotherapeutics* 17, 1170–1183. doi: 10.1007/s13311-019-00821-5

Yeung, R. K., Xiang, Z. H., and Tsang, S. Y. (2018). Gabrb2-knockout mice displayed schizophrenia-like and comorbid phenotypes with interneuron-astrocyte-microglia dysregulation. *Transl. Psychiatry* 8:128. doi: 10.1038/s41398-018-0176-9

Zhang, Y., Yang, S., and Liu, C. (2021). Deciphering glial scar after spinal cord injury. Burns. *Trauma* 9:tkab035. doi: 10.1093/burnst/tkab035

Zhang, C., Zhang, M., and Wang, S. (2010). Interactions between the gut microbiota, host genetics and diet relevant to development of metabolic syndromes in mice. *ISME J.* 4, 232–241. doi: 10.1038/ismej.2009.112

Zhang, C., Zhang, W., and Zhang, J. (2018). Gut microbiota dysbiosis in male patients with chronic traumatic complete spinal cord injury. *J. Transl. Med.* 16:353. doi: 10.1186/s12967-018-1735-9

Zheng, J., Liu, J., and Jiang, Y. (2021). Safety of every-other-day fasting in the treatment of spinal cord injury: a randomized controlled trial. *Am. J. Phys. Med. Rehabil.* 100, 1184–1189. doi: 10.1097/PHM.0000000000001727

Zhu, C. S., Grandhi, R., and Patterson, T. T. (2018). A review of traumatic brain injury and the gut microbiome: insights into novel mechanisms of secondary brain injury and promising targets for neuroprotection. *Brain Sci.* 8:8. doi: 10.3390/brainsci8060113

frontiers | Frontiers in Microbiology

TYPE Original Research
PUBLISHED 07 August 2023
DOI 10.3389/fmicb.2023.1224666

OPEN ACCESS

EDITED BY
Hesong Wang,
Southern Medical University, China

REVIEWED BY
Xiaodan Hui,
University of Louisville, United States
Wenjiang Dong,
Chinese Academy of Tropical Agricultural Sciences, China
Debao Niu,
Guangxi University, China

*CORRESPONDENCE
Gan-Lin Chen
✉ ganlin-chen@163.com;
✉ ganlin-chen@gxaas.net

†These authors have contributed equally to this work

RECEIVED 18 May 2023
ACCEPTED 17 July 2023
PUBLISHED 07 August 2023

CITATION
Zheng F-J, Lin B, Yang Y-X, Fang X-C, Verma KK and Chen G-L (2023) Efficacy and functionality of sugarcane original vinegar on mice. *Front. Microbiol.* 14:1224666. doi: 10.3389/fmicb.2023.1224666

Efficacy and functionality of sugarcane original vinegar on mice

Feng-Jin Zheng[1,2†], Bo Lin[1,2†], Yu-Xia Yang[1,2], Xiao-Chun Fang[1,2], Krishan K. Verma[3] and Gan-Lin Chen[1,2,4*]

[1]Institute of Agro-Products Processing Science and Technology, Guangxi Academy of Agricultural Sciences, Nanning, Guangxi, China, [2]Guangxi Key Laboratory of Fruits and Vegetables Storage-Processing Technology, Nanning, China, [3]Key Laboratory of Sugarcane Biotechnology and Genetic Improvement (Guangxi), Ministry of Agriculture and Rural Affairs, Guangxi Key Laboratory of Sugarcane Genetic Improvement, Sugarcane Research Institute, Guangxi Academy of Agricultural Sciences, Nanning, Guangxi, China, [4]School of Chemistry and Chemical Engineering, Guangxi Minzu University, Nanning, Guangxi, China

Introduction: Due to their bioactive compounds and beneficial health effects, functional foods and plant-based natural medicines are widely consumed. Due to its bioactivities, vinegar is one of them that helps humans. Sugarcane original vinegar (SOV) is a special vinegar made from sugarcane as a raw material through biological fermentation processes.

Methods: The objective of this study was to assess the effects of sugarcane original vinegar on growth performance, immune response, acute oral toxicity, bacterial reverse mutation, mammalian erythrocyte micronucleus, mouse spermatogonial chromosome aberration, mammalian bone marrow cell chromosome aberration changes, and serum characteristics in mice. Distortion parameters were used to assess its safety, and at the same time, the functionality of SOV was monitored during experimentation.

Results: The results show that the SOV has no damage or inhibitory effect on the bone marrow red blood cells of mice and no mutagenic or distortion-inducing effects on the bone marrow cell chromosomes or spermatogonia chromosomes, so it is safe to eat. SOV can improve blood lipids and reduce blood lipid content.

Discussion: The study results provide data basis for the intensive processing of sugarcane and the development of high-value SOV products. Sugarcane original vinegar has a beneficial impact on performance, immune response, and chromosomal aberration. The production application influences the vinegar's quality and, consequently, its health benefits.

KEYWORDS

sugarcane original vinegar,safety, functionality, evaluation, mice

Introduction

Sugarcane vinegar is sweet and sour brewed from sugar crops, i.e., sugarcane, which is prepared by extracting juice from sugarcane mature stems, sterilizing them, and then undergoing alcoholic (Zheng et al., 2018; Luzón-Quintana et al., 2021), acetic acid (Zheng et al., 2016; Huang et al., 2022), and other microbial fermentation processes. It is an advanced type of vinegar product (Chen et al., 2013, 2015, 2023; Yi et al., 2017). Guangxi is the largest sugarcane cultivation and production area in China, accounting for 60% of the total national area and 70% of the total national yield of sugarcane, which plays a major role in the growth and development of Chinese sugar agroindustries (Chen et al., 2020, 2023). The impact on the distribution of heavy metals in the soil has been continuously strengthened, and the content of heavy metals in the soil is increasing day-by-day. Since heavy metals are not degraded by microorganisms, they are not easy to move and accumulate continuously. It causes soil pollution and degrades crop yield and quality (Guga et al., 2023).

Based on previous studies, sugarcane original vinegar (SOV) preserves functional nutrients and nutritional rich values. The major component is acetic acid, and it also contains various organic acids such as oxalic, succinic, and tartaric acids (Chen et al., 2020), as well as flavonoids and phenols. Substances, such as benzoic, ferulic, quinic, chlorogenic, apigenin, kaempferol, caffeic, luteolin, p-coumaric, and other phenolic acids (He et al., 2017), and rich in different kinds of amino acids (Lin et al., 2022) with certain functionality. As an advanced type of vinegar, there are limited studies available on the safety and functional evaluation of sugarcane vinegar. This experiment mainly assesses and analyzes the efficacy and functional mechanisms of sugarcane vinegar to provide for the subsequent intensive processing and utilization of SOV and high-quality products.

Materials and methods

Experimental materials

A total of 220 specific pathogens, healthy Kunming mice, half male and half female (average weight: 18–35 g), were purchased from the Changsha Tianqin Biotechnology Co., Ltd., China [Experimental animal production license number: SCXK (Xiang) 2019-0014, quality certificate number: 430726201100369386, Hunan, China, and experimental animal center of Guangxi Medical University, laboratory animal production license number: SCXK (Gui) 2020-0004, quality certificate number: 0001734, Guangxi, China].

Sugarcane original vinegar (500 ml/bottle) is produced by the Agricultural Products Processing Research Institute of Guangxi Academy of Agricultural Sciences/Guangxi Key Laboratory of New Technology for Fruit and Vegetable Storage and Processing, according to DB 45/T 1536-2017 Guangxi Development and Preparation of Local Standards (Guangxi, China) (Bureau of Quality and Technical Supervision of Guangxi Zhuang Autonomous Region, 2017). Five histidine-deficient strains of *Salmonella typhimurium*, i.e., TA97a, TA98, TA100, TA102, and TA1535, were purchased from the MOLTOX Company, United States.

Mouse feed (basic material) was obtained from the Guangxi Experimental Animal Center, Guangxi Medical University, Nanning, Guangxi, China. High-fat feed (basic feed:lard:egg yolk powder:cholesterol:sodium cholate = 78.8:10:10:1:0.2) was self-made by the Institute of Agricultural Products Processing, Guangxi Academy of Agricultural Sciences/Guangxi Key Laboratory of New Technology for Fruit and Vegetable Storage and Processing.

Ethical approval (GXAAS/AEEIF/00001) was obtained, and animal experiments were performed according to the guidelines of the Animal Care and Use Committee (ACUC) of the Guangxi Academy of Agricultural Sciences, Nanning, Guangxi, China.

Preparation of sugarcane original vinegar

Sugarcane is squeezed by press to obtain sugarcane juice (10–20°Brix). Filter equipment with 75–150 μm diameters (100–200 mesh) was used to filter the squeezed juice to meet the requirement of no impurities, and pasteurization was used to sterilize (sterilization temperature and time: 60–80°C and 20–30 min).

Alcoholic and acetic acid fermentation

Sterilized cane juice was injected using the sterile fermentation equipment, activated fruit wine yeast (0.05–0.10% mass volume active dry yeast) was then added, stirred, and mixed thoroughly; the tank was sealed for fermentation process at an appropriate temperature (30–35°C); and fermentation continued until the volume percentage of alcohol content reached ≥4%.

Amended activated acetic acid bacteria (0.05%—0.10% active acetic acid bacteria in mass volume ratio) are added to the alcohol fermentation mash, stirred well, and mixed thoroughly, and then allowed to ferment to total acid (measured as acetic acid) of ≥3.5 g/100 ml and alcohol concentration of ≤0.1% by volume.

A filter device with a pore size of 0.22–0.45 μm was used and it was then transferred to the aging equipment at room temperature for up to 30 days. Ultra-high temperature instantaneous sterilization (sterilization temperature ≥121°C, sterilization time ≥ 6s) and aseptic filling equipment (Figure 1) were used.

Physical and chemical indicators

The physico-chemical properties of SOV are shown in Table 1.

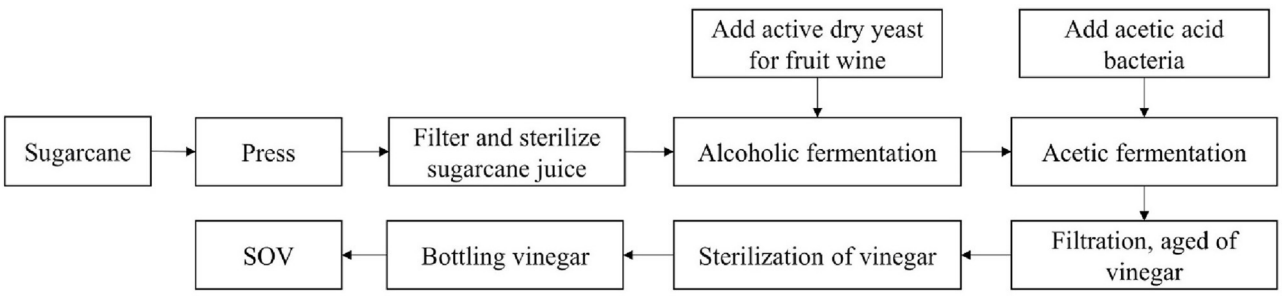

FIGURE 1
Flowchart of sugarcane original vinegar (SOV) fermentation process.

Feeding conditions

The animal experiments were demonstrated in the Toxicology Laboratory of the Guangxi Zhuang Autonomous Region Center for Disease Control and Prevention, and the Experimental animals were raised in a barrier system with a temperature of 22–25°C and a relative humidity of 55%—70% [License number: SYXK (Gui) 2016-0002]. The irradiated animal feed is produced by Beijing Keao Xieli Feed Co., Ltd., China [License number: SCXK (Beijing) 2014-0010].

Analysis of acute oral toxicity in mice

Using Horn's method (Standardization Administration of China, 2014a), 10 mice (18–22 g of body weight) in each group, including male and female (at half capacity of each), were administered different doses including 46,400, 21,500, 10,000, and 4,640 mg/kg BW. Prior to the experiment, the animals were fasted for 4 h with no restriction to drinking water. An amount of 50.0 and 23.2 g of SOV were weighed, respectively; pure water was added to them to prepare 100 ml; and the solutions were mixed well and made up to 500 and 232 mg/ml SOV solutions.

An amount of 46,400 mg/kg BW dose was applied to animals twice at a volume of 0.47 ml/20 g BW (time interval: 4 h), and the 10,000 and 4,640 mg/kg BW doses were 500 and 232 mg/ml, respectively, in a volume of 0.40 ml/20 g BW (vinegar @ 1 time). Observe the toxicity responses of the animals after treatment application. The animals were weighted once a week for up to 2 weeks. At the end of the experiment, the animals were selected for general observation. The acute toxicity of the test substance of SOV was evaluated according to the toxicity classification standard.

Determination of bacterial reverse mutation (Ames)

Five histidine-deficient *S. typhimurium* strains, such as TA97a, TA98, TA100, TA102, and TA1535, were identified with the requirements for the analytical assessment. Five test groups, i.e., 5,000, 1,581, 500, 158, and 50 μg/dish, were set up, as well as a spontaneous reversion control group, a water solvent control group, a dimethyl sulfoxide (DMSO) solvent control group, and a positive mutagen control group. The conditions of the spontaneous back-change control group were the same as those of the sample group, except there was no sample. An amount of 50.0 and 15.81 g of SOV were weighed; each of them was gradually diluted with sterile water according to a specific ratio of 5.0, 0.5, 0.05, 1.581, and 0.158 mg/ml concentration; and then the solutions were sterilized by autoclaving (0.103 MPa, 20 min).

TABLE 1 The physical and chemical properties of sugarcane original vinegar.

Physical and chemical index	Content
Total acid (g/100 ml, citric acid)	3.65
Soluble solids (%)	11.5
Total sugar (g/L, glucose)	4.7
Lead (mg/L) detection limit (5 μg/L)	0.01

Rat liver microsomal enzyme (S9) induced by PCBs was used as an *in vitro* metabolic activation system. According to GB15193.4-2014 (Standardization Administration of China, 2014b), the plate incorporation method was adopted, and 0.1 ml of the test strain enrichment solution, 0.1 ml of the test substance solution, and 0.5 ml of the S9 mixture (when metabolic activation is required) were mixed and poured into the bottom medium plate. For the solvent control, sterilized pure water and DMSO were used to replace the samples, and the remaining conditions were the same as the sample group. Each strain of each group was prepared in three parallel dishes; they were incubated at 37°C for 48 h, and the number of colonies per plate was counted. If the number of reverted mutant colonies in each group of the test substance is upregulated in the dose–response relationship, or at least one strain has a reproducible increase in the number of reverted mutant colonies per plate at one or more doses under the different conditions, or no metabolic activation system is upregulated, that is, a positive mutagenesis test. The whole set of experiments was repeated three times under the same conditions.

Analysis of mammalian erythrocyte micronucleus

A total of 50 Kunming mice were selected randomly (weighing 25–30 g) and divided into five groups, with 10 mice in each group (equally divided as male and female). According to the method of GB15193.5-2014 (Standardization Administration of China, 2014c), the experiment was carried out by oral treatment twice at a specific time interval (24 h). The test dosage, according to the LD_{50} results of the mice, was set at 10,000, 5,000, and 2,500 mg/kg BW for male mice and 7,350, 3,675, and 1,838 mg/kg BW for female mice. We used pure water as a negative control, and 40 mg/kg BW dose of cyclophosphamide (cp) was used as a positive control. An amount of 50.00, 25.00, and 12.50 g of samples were weighed, distilled water (100 ml) was added and mixed thoroughly, and samples of 500, 250, and 125 mg/ml were prepared for male mice. Then, an amount of 36.75, 18.38, and 9.19 g of samples were weighed, pure water (100 ml) was added and mixed thoroughly, and samples of 367.5, 183.8, and 91.9 mg/ml were prepared for female mice; then the animals were given intragastric administration at a volume of 0.4 ml/20 g BW, and an equal volume of distilled water was given to the negative control group. The positive control group was intraperitoneally injected with 4 mg/ml cyclophosphamide solution (prepared with normal saline) at a volume of 0.2 ml/20 g BW. After 24 h of the second sampling, the animals were killed by cervical dislocation, and the sternal bone marrow was diluted with calf serum for smears, dried naturally, fixed with methanol, stained with Gimsa application solution for 10 min, and washed with phosphate buffer solution (pH 6.8). After natural drying, the sample was observed under the optical microscope, polychromatic erythrocytes (PCE) per animal were counted as 2,000, and the micronucleus rate was expressed as the percentage of PCE containing micronuclei. At the same time, by counting and observing the positive staining

of 200 PCE Red blood cells (NCE), the ratio of polychromatic erythrocytes/total erythrocytes (RBC) was calculated.

Analysis of chromosomal aberrations in spermatogonial cells

According to GB 15193.8-2014 (National Standards Administration of China, 2014), 30 Kunming male mice with an average body mass of 25–35 g were selected and randomly divided into five groups, of which 10 were in one group and other four groups had five mice. The three doses of the test groups were 10,000, 5,000, and 2,500 mg/kg BW. Distilled water was applied as a negative control and cyclophosphamide (cp) of 40 mg/kg BW was used as a positive control. Distilled water (40 ml) was added, mixed thoroughly, and made up to different concentrations, i.e., 500, 250, and 125 mg/ml, and the animals were intragastrically applied with a volume of 0.4 ml/20 g BW as a negative control group. The positive control group was applied as a 2 mg/ml cyclophosphamide solution at a volume of 0.4 ml/20 g BW.

The animals in the high concentration were divided into two batches and killed 24 and 48 h after treatment, and the remaining groups were killed 24 h after treatment application. Four hours before treatment, each group was intraperitoneally injected with colchicine at a concentration of 0.5 mg/ml (equivalent dose of 5 mg/kg BW) at a volume of 0.2 ml/20 g BW. The animals were euthanized by cervical dislocation, the testes on both sides were taken, and the testes were placed in 1% trisodium citrate to separate the seminiferous tubules, and then fixed twice in fixative solution (methanol: glacial acetic acid = 3:1), at 60% glacial acetic acid (GAA) to soften and centrifuge. The collected cell suspension was dropped on chilled glass slides, made into 2–3 slices, dried in the air, stained by Giemsa, and examined by an optical microscope. A total of 100 metaphase cells were counted from each animal, the chromosome number and structural changes of spermatogonia were observed, and another 1,000 spermatogonia was observed to determine the mitotic index. The number of cells containing chromosomal structural aberrations and the number of chromosomal aberrations per cell in each animal were observed, and the number and frequency of different types of chromosomal structural aberrations in each group (chromosomal gaps are not included in the aberration rate) were counted.

Determination of mammalian bone marrow cell chromosomal aberration

According to GB 15193.6-2014 (China National Standards Administration Committee, 2014), a one-time exposure method was adopted, and the samples were collected two times. A total of 100 Kunming mice (average body mass of 25–35 g, half male and half female) were selected. According to the LD_{50} results of the mice, the test doses of 10,000, 5,000, and 2,500 mg/kg BW for male mice and 7,350, 3,675, and 1,838 mg/kg BW for female mice were selected. We used distilled water as a negative control and 40 mg/kg BW of cyclophosphamide (cp) as a positive control. At each sampling time, there were five mice of each sex in each group (weighing 50, 25, and 12.50 g). Distilled water (100 ml) was added and mixed thoroughly, and 500, 250, and 125 mg/ml solutions for male mice were prepared, weighing 36.75, 18.38, and 9.19 g. Distilled water (100 ml) was added and mixed thoroughly, and 367.5, 183.8, and 91.9 mg/ml solutions for female mice were prepared. Then, the animals were intragastrically applied with a volume of 0.4 ml/20 g BW. The negative control group was applied as the same volume of distilled water, and the positive control was infused with an equal volume of 2 mg/ml cyclophosphamide solution.

Animals in each group were divided into two subgroups. Subgroup 1 was euthanized 18 h after exposure to collect the first specimen, and subgroup 2 was euthanized 24 h after the animals in subgroup 1 to collect the second sample for analysis. Four hours prior to treatment, each group was intraperitoneally injected with colchicine at a concentration of 0.4 mg/ml (equivalent dose of 4 mg/kg BW) at a volume of 0.2 ml/20 g BW. Animals were euthanized by cervical dislocation; the femur was taken out, and the epiphyses at both ends were cut off. The bone marrow was

TABLE 2 Acute toxicity analytical results of SOV on mice.

Category	Dose group (mg/kg BW)	Number of animals	Body weight (g)				
			0 days	7 days	Body weight gain (%)	14 days	Body weight gain (%)
Male	46,400	5	20.4 ± 1.4	–	–	–	–
	21,500	5	20.4 ± 1.3	25.8 ± 1.1	26.47	29.8 ± 1.2	46.08
	10,000	5	20.1 ± 1.2	25.4 ± 1.1	26.37	29.5 ± 1.2	46.77
	4,640	5	20.4 ± 1.3	26.1 ± 1.5	27.94	30.8 ± 1.8	50.98
Female	46,400	5	20.1 ± 1.5	–	–	–	–
	21,500	5	19.8 ± 1.3	24.5 ± 1.6	23.74	28.2 ± 1.1	42.42
	10,000	5	19.7 ± 1.4	24.3 ± 1.1	23.35	28.3 ± 1.3	43.65
	4,640	5	19.9 ± 1.3	25.3 ± 1.4	27.14	29.5 ± 1.5	48.24

All data are indicated as mean ± SD. LD50: 20,000 mg/kg BW for male mice, 95% credible limit: 12,300–32,400 mg/kg; BW: 14,700 mg/kg BW for female mice, 95% credible limit: 8,620–25,000 mg/kg BW.

TABLE 3 Result findings of the first bacterial reverse mutation test of SOV (mean ± SD).

Dose group (μg/plate)	TA97a		TA98		TA100		TA102		TA1535	
	−S_9	+S_9	−S_9	+S_9	−S_9	+S_9	−S_9	+S_9	−S_9	+S_9
5,000	136.0 ± 28.0	126.3 ± 28.5	39.7 ± 4.2	40.3 ± 0.6	146.7 ± 18.6	160.0 ± 33.2	266.0 ± 29.6	296.0 ± 22.5	25.3 ± 7.1	28.0 ± 6.6
1,581	107.7 ± 11.7	129.7 ± 30.1	35.7 ± 6.4	38.3 ± 3.8	143.0 ± 13.9	169.3 ± 25.5	285.0 ± 11.0	274.0 ± 23.3	18.0 ± 2.7	19.0 ± 1.0
500	132.0 ± 17.4	150.7 ± 47.3	44.3 ± 4.9	45.7 ± 3.8	176.3 ± 24.4	166.7 ± 16.4	293.3 ± 31.9	267.7 ± 31.0	26.3 ± 6.0	21.3 ± 3.5
158	129.0 ± 39.0	139.0 ± 21.4	38.3 ± 5.5	40.7 ± 4.2	172.3 ± 24.5	157.3 ± 31.6	267.0 ± 33.1	278.7 ± 29.0	23.3 ± 5.1	29.7 ± 1.5
50	129.0 ± 38.7	143.3 ± 32.0	40.3 ± 4.9	40.7 ± 5.5	186.0 ± 15.7	178.0 ± 3.0	267.0 ± 16.6	265.3 ± 20.4	23.7 ± 4.2	20.3 ± 6.7
Spontaneous change back	134.3 ± 37.1	135.7 ± 22.5	34.0 ± 2.0	37.0 ± 4.0	149.7 ± 25.6	169.7 ± 42.3	288.0 ± 23.6	300.3 ± 16.9	30.0 ± 3.0	28.0 ± 5.3
Water control	124.3 ± 42.4	140.7 ± 30.6	40.0 ± 1.0	41.7 ± 3.8	154.7 ± 36.9	143.7 ± 13.6	293.7 ± 21.1	289.3 ± 21.9	24.7 ± 3.2	28.7 ± 4.9
DMSO	117.0 ± 21.8	144.7 ± 44.1	35.3 ± 6.1	39.3 ± 4.5	173.3 ± 29.3	169.3 ± 15.5	274.3 ± 35.6	283.0 ± 29.5	32.7 ± 1.2	30.7 ± 3.5
Positive control	2,544.0 ± 94.3	1,724.0 ± 780.1	2,870.7 ± 146.6	4,300.0 ± 191.2	2,940.0 ± 151.2	2,745.3 ± 158.7	757.7 ± 36.6	803.0 ± 28.1	319.7 ± 340.7	141.7 ± 190.1

The above results (number of colonies) are the mean ± standard deviation ($n = 3$).
Positive control: TA97a + S-9, TA98 + S-9, and TA100 + S-9 use 2-aminofluorene (10 μg/dish); TA98–S-9 use daunomycin (6 μg/dish); TA97a–S-9 and TA102–S-9 were treated with dexazone (50 μg/dish). TA100-S-9 and TA1535-S-9 were treated with sodiumazide (1.5 μg/dish). TA102 + S-9 were treated with 1,8-dihydroxyanthraquinone (50 μg/dish) and TA1535 + S-9 adopts cyclophosphamide (200 μg/dish).

TABLE 4 The analytical observations of the second bacterial reverse mutation test of SOV (mean ± SD).

Dose group (μg/dish)	TA97a		TA98		TA100		TA102		TA1535	
	−S_9	+S_9	−S_9	+S_9	−S_9	+S_9	−S_9	+S_9	−S_9	+S_9
5,000	115.7 ± 10.8	130.0 ± 15.6	40.0 ± 4.4	39.0 ± 6.0	171.7 ± 36.9	184.3 ± 10.1	272.0 ± 25.5	270.7 ± 15.5	27.0 ± 3.0	24.3 ± 4.9
1,581	122.0 ± 27.8	151.0 ± 15.1	42.0 ± 3.0	38.3 ± 4.2	147.0 ± 15.5	177.0 ± 18.1	283.0 ± 6.1	287.3 ± 23.2	28.3 ± 6.4	26.0 ± 3.5
500	137.3 ± 27.3	126.0 ± 13.8	40.3 ± 3.5	43.0 ± 2.7	161.0 ± 9.0	155.7 ± 37.1	267.7 ± 25.2	278.7 ± 18.2	23.7 ± 2.5	24.7 ± 4.7
158	130.7 ± 23.6	131.3 ± 25.5	40.7 ± 3.5	42.0 ± 2.7	155.3 ± 27.5	147.3 ± 23.1	282.7 ± 32.5	263.7 ± 20.8	23.7 ± 6.7	26.7 ± 4.0
50	129.7 ± 20.4	160.3 ± 12.5	39.3 ± 4.5	43.7 ± 5.9	166.7 ± 9.1	137.3 ± 0.6	281.7 ± 10.5	252.7 ± 11.5	23.0 ± 3.0	24.0 ± 5.2
Spontaneous change	127.7 ± 13.8	112.0 ± 1.0	35.7 ± 3.1	41.7 ± 5.1	168.0 ± 14.4	132.7 ± 8.7	262.0 ± 29.7	287.7 ± 28.4	21.0 ± 3.0	22.0 ± 5.3
Water control	139.0 ± 28.6	135.7 ± 30.6	42.0 ± 3.6	43.7 ± 4.2	144.0 ± 10.4	138.3 ± 15.0	261.0 ± 18.7	281.7 ± 13.6	31.0 ± 2.0	27.7 ± 6.1
DMSO	126.7 ± 21.7	151.3 ± 21.1	40.0 ± 4.0	36.7 ± 3.8	186.0 ± 16.8	177.7 ± 5.0	288.0 ± 32.8	275.0 ± 17.6	22.7 ± 6.8	29.0 ± 4.6
Positive control	2,570.7 ± 153.7	1,781.3 ± 80.0	2,988.0 ± 137.6	4,104.0 ± 198.9	2,948.0 ± 115.3	2,852.0 ± 108.9	725.7 ± 33.3	819.0 ± 31.2	326.7 ± 29.1	155.3 ± 18.0

The above results (number of colonies) are the mean ± standard deviation of assessed by three plates.

10.3389/fmicb.2023.1224666

TABLE 5 Effect of SOV on the incidence of micronucleus in mouse bone marrow polychromatic erythrocytes (mean ± SD).

Gender	Dose group (mg/kg BW)	Number of animals	Number of tested PCEs (units)	Number of PCEs with micronuclei (units)	Micronucleus rate (%)	Number of tested PCEs (pcs)	Number of NCEs (number)	PCE/RBC (%)
Male	10,000	5	5 × 2,000	16	1.6 ± 0.4	5 × 200	891	0.529 ± 0.015
	5,000	5	5 × 2,000	17	1.7 ± 0.3	5 × 200	888	0.530 ± 0.009
	2,500	5	5 × 2,000	15	1.5 ± 0.4	5 × 200	905	0.525 ± 0.017
	Negative control	5	5 × 2,000	15	1.5 ± 0.4	5 × 200	896	0.528 ± 0.017
	Positive 40 (cp)	5	5 × 2,000	216	21.6 ± 2.7**	5 × 200	1,008	0.498 ± 0.011
Female	7,350	5	5 × 2,000	14	1.4 ± 0.2	5 × 200	896	0.528 ± 0.012
	3,675	5	5 × 2,000	14	1.4 ± 0.4	5 × 200	893	0.528 ± 0.014
	1,838	5	5 × 2,000	17	1.7 ± 0.3	5 × 200	877	0.533 ± 0.008
	Negative control	5	5 × 2,000	14	1.4 ± 0.4	5 × 200	905	0.525 ± 0.005
	Positive 40 (cp)	5	5 × 2,000	208	20.8 ± 2.0**	5 × 200	989	0.503 ± 0.005

PCE/RBC is the ratio of polychromatic erythrocytes to total erythrocytes.

**Indicates a very significant difference at $P < 0.01$ compared with the negative control group.

cp, cyclophosphamide.

TABLE 6 Effects of SOV on chromosomal aberrations in mouse spermatogonia (mean ± SD).

Dose group (mg/kg BW)	Observe the number of cells (pcs)	Chromosome number change		Chromosomal structural changes*								Distorted cell number (units)	Aberrant cell rate (%)	Mitotic index
		Aneuploidy	Polyploid	Fissure	Fracture	Piece	Minute body	Ring	Multiple centromere	Single swap	Unspecified			
10,000 (24 h)	100 × 5	0	21	7	3	0	0	0	0	0	0	24	4.8 ± 0.4	6.9 ± 1.2
10,000 (48 h)	100 × 5	0	20	8	2	0	0	0	0	0	0	22	4.4 ± 1.3	7.5 ± 1.1
5,000	100 × 5	0	16	9	2	0	0	0	0	0	0	18	3.6 ± 0.5	7.6 ± 1.1
2,500	100 × 5	0	20	8	4	0	0	0	0	0	0	24	4.8 ± 0.8	7.8 ± 1.2
Negative control	100 × 5	0	21	8	3	0	0	0	0	0	0	24	4.8 ± 0.8	7.5 ± 1.4
Positive control	100 × 5	0	23	24	20	19	2	1	0	0	0	65	13.0 ± 2.5**	4.4 ± 0.6

*Circular changes of structural changes include centromere and non-centromere. Multiple centromere refers to more than two centromeres, cracks are not included in the number of aberrant cells, and the rate of aberrant cells = number of aberrant cells/number of observed cells × 100.

**Indicates that compared with the negative control group, $P < 0.01$.

10.3389/fmicb.2023.1224666

washed into a centrifuge tube with 5 ml of normal saline and blown to make a cell suspension, centrifuged at 1,000 r/min for 10 min, and the supernatant was discarded. A volume of 0.075 mol/L potassium chloride was added (7 ml) and the cells were mixed gently with a dropper and then placed in a 37°C water bath for hypotonic treatment for 15 min. Next, 2 ml of fixative solution (methanol:glacial acetic acid = 3:1) was added, mixed thoroughly, and centrifuged at 1,000 r/min (10 min), and the supernatant was discarded. A volume of 7 ml of fixative was added, fixed for 15 min, and centrifuged at 1,000 r/min (10 min); the supernatant was discarded; and the whole process was repeated once. The cell suspension was dropped on ice water slides, made into 2–3 slices, dried in the air, stained by Giemsa, and examined by an optical microscope. One hundred metaphase cells were counted for each animal, observed the chromosome number and structural changes of bone marrow cells, and observed another 1,000 bone marrow cells to determine the mitotic index. The number of cells with chromosomal structural aberrations in each animal was recorded. The number of different types of chromosomal structural aberrations in each group was counted (chromosomal gaps were not included in the aberration rate), and the chi-square test was performed on the rate of chromosomal structural aberrations.

Functional verification

A total of 60 28-day-old SPF male mice with similar body mass were selected, fed basal feed for 7 days, then randomly divided as normal saline (control group, MG group, i.e., fed with high-fat feed and gavaged with normal saline) and SOV dosage group (TG, i.e., fed with high-fat feed and gavaged with raw vinegar), weighed once a week, and observed for general characteristics such as mental activity, hair changes, water intake, food intake, and excrement volume. The mice were fed continuously for 8 weeks, and the body mass and serum profile were measured (Li et al., 2020b,c).

Data analysis

The SPSS 13.0 software was used for one-way analysis of variance and pairwise comparison, and the data were expressed as mean ± standard deviation (SD). The significant differences at $P < 0.05$ and $P < 0.01$ levels were analyzed. Graphics were prepared using the Origin 2021 (Origin Lab, Northampton, MA) software.

Results and discussion

Acute oral toxicity

The results of the acute toxicity test for each group are shown in Table 2. After 0.5 h of treatment, it was found that the test animals in the 4,640 mg/kg BW group appeared sluggish, unresponsive, and died, and the death time was after giving the test substance (2–96 h). Autopsies of dead animals showed varying degrees of gastric effusion and flatulence. It may be related to the side effects of vinegar. After vinegar is used, it will change the pH of the local environment in the body. Vinegar can cause the digestive organs to secrete a large amount of digestive juice, and vinegar will corrode the gastrointestinal mucosa and aggravate the development of ulcer disease (Budak et al., 2014; Luo and Xu, 2019). The higher concentration of raw sugarcane vinegar stimulates the digestive organs. At the end of the experimentation, the surviving animals were dissected, and there was no abnormality in the general observation. This is consistent with the research results of our research group's previous research on the effects of SOV on the internal organs of mice fed high-fat diets. There was no difference in the color, size, or character of the organs, and feeding SOV had no adverse effects on the organs of mice (Li et al., 2020a). The median lethal dose (LD_{50}) was carried out due to animal death, and the acute oral toxicity LD_{50} of SOV in male and female mice was 20,000 and 14,700 mg/kg BW, respectively. The LD_{50} of female mice is lower than male mice, and female mice are more sensitive to the test substance than male mice, which is consistent with the acute toxicity study of *Ganoderma leucocontextum* (Deng et al., 2023). According to the acute toxicity dose grading standard and research results in GB15193.3-2014, the acute oral toxicity of raw SOV belongs to the actual non-toxic level, and it is not easy for people with hyperacidity and gastric ulcers to use high concentrations (Younes et al., 2022).

Responses to bacterial reverse mutation

Positive controls such as TA97a+S_{-9}, TA98+S_{-9}, and TA100+S_{-9} used 2-aminofluorene (10 μg/dish); TA98–S_{-9} used daunomycin (6 μg/dish); TA97a–S_{-9} and TA102–S_{-9} adopted dexazone (50 μg/dish); TA100–S_{-9} and TA1535–S_{-9} adopted sodium azide (1.5 μg/dish); TA102+S_{-9} adopted 1, 8-dihydroxyanthraquinone (50 μg/dish); and TA1535+S_{-9} adopted cyclophosphamide (200 μg/dish; Tables 3, 4).

Tables 3, 4 show the number of back-mutant colonies in the SOV bacterial back-mutation test. In the five test strains, such as TA97a, TA98, TA100, TA102, and TA1535, the number of reverted colonies in each concentration and group of sugarcane vinegar did not exceed the number of spontaneous reverted colonies after addition or not of the S9 metabolic activation system. The number of colonies was doubled, and there was no dose–response relationship between the number of back-changing colonies in each dose, indicating that SOV would not induce gene mutations in the test strains, while the positive control group showed obvious mutagenicity and reverse. The number of changed colonies was far more than 2-fold that of the spontaneous back-mutation group. The GB15193.4-2014 standard justified the mutagenesis negative tests, which means that it has no direct effect on the histidine-deficient strains of *S. typhimurium* (TA97a, TA98, TA100, TA102, and TA1535) or indirect mutagenesis.

Impact of mammalian erythrocyte micronucleus

The statistical results of the incidence of polychromatic erythrocyte micronuclei in the bone marrow of the tested animals are shown in Table 5. At different doses of SOV, such

TABLE 7 The effect of the first sampling of raw SOV on chromosomal aberrations in mouse bone marrow cells (mean ± SD).

Gender	Dose group (mg/kg BW)	Observe the number of cells (pcs)	Chromosome number change			Chromosomal structural changes*										Mitotic index
			Aneuploidy	Polyploid	Endoduplication	Fracture	Minute body	Double microsome	Filamentous point ring	Acentric ring	Single swap	Fissure	Non-characteristic type	Aberrant cells (units)	Structural distortion cell rate (%)	
Male	10,000	100 × 5	0	1	0	7	1	0	0	0	0	1	1	9	1.8 ± 0.8	7.6 ± 1.1
	5,000	100 × 5	0	2	0	5	0	0	0	0	0	2	1	6	1.2 ± 0.8	7.3 ± 1.2
	2,500	100 × 5	0	1	0	4	0	0	0	0	1	1	2	7	1.4 ± 1.5	7.9 ± 1.2
	Negative control	100 × 5	0	3	1	6	0	0	1	0	1	3	1	9	1.8 ± 0.8	7.8 ± 1.7
	40 (cp)	100 × 5	0	6	1	72	1	0	1	0	0	38	2	76	15.2 ± 3.3**	4.8 ± 1.1
Female	7,350	100 × 5	0	3	0	5	0	0	1	1	0	1	1	8	1.6 ± 1.1	7.5 ± 1.2
	3,675	100 × 5	0	1	0	5	0	0	0	1	0	1	2	8	1.6 ± 1.5	7.6 ± 1.0
	1,838	100 × 5	0	3	0	3	0	0	1	0	0	3	2	6	1.2 ± 0.8	7.8 ± 1.2
	Negative control	100 × 5	0	1	0	3	0	0	1	1	0	3	1	6	1.2 ± 0.8	8.0 ± 1.3
	40 (cp)	100 × 5	0	8	0	76	0	0	1	1	1	47	3	82	16.4 ± 1.5**	5.0 ± 1.4

*Cracks are not included in the number of structurally aberrant cells, the rate of structurally aberrant cells = the number of structurally aberrant cells/the number of observed cells × 100.

**Indicates that compared with the negative control group, $P < 0.01$.

10.3389/fmicb.2023.1224666

TABLE 8 The effect of the second sampling of raw SOV on the chromosomal aberration of mouse bone marrow cells (mean ± SD).

Gender	Dose group (mg/kg BW)	Observe the number of cells (pcs)	Chromosome number change			Chromosomal structural changes*										Mitotic index
			Aneuploidy	Polyploid	Endoduplication	Fracture	Minute body	Double microsome	Filamentous point ring	Acentric ring	Single swap	Fissure	Non-characteristic type	Aberrant cells (units)	Structural distortion cell rate (%)	
Male	10,000	100 × 5	0	1	0	4	0	0	0	1	0	2	0	5	1.0 ± 0.7	7.5 ± 1.6
	5,000	100 × 5	0	2	0	4	1	0	0	0	0	2	4	9	1.8 ± 1.3	8.0 ± 1.4
	2,500	100 × 5	0	1	0	5	0	0	0	1	0	3	1	7	1.4 ± 1.7	7.9 ± 1.2
	Negative control	100 × 5	0	1	0	3	0	0	0	1	0	1	0	4	0.8 ± 0.8	7.3 ± 1.6
	40 (cp)	100 × 5	0	7	0	70	1	0	0	1	0	38	3	75	15.0 ± 4.1**	4.6 ± 1.3
Female	7,350	100 × 5	0	2	0	4	1	0	0	0	0	0	1	6	1.2 ± 0.8	8.2 ± 1.0
	3,675	100 × 5	0	3	0	4	1	0	0	1	0	1	1	7	1.4 ± 1.3	7.7 ± 1.9
	1,838	100 × 5	0	1	0	5	1	0	0	0	0	2	2	8	1.6 ± 1.5	7.9 ± 1.0
	Negative control	100 × 5	0	1	0	3	1	0	1	0	0	1	1	6	1.2 ± 0.8	7.8 ± 1.1
	40 (cp)	100 × 5	0	6	0	72	1	0	2	1	0	39	3	79	15.8 ± 3.2**	4.9 ± 1.2

*Cracks are not included in the number of structurally aberrant cells, and the rate of structurally aberrant cells = the number of structurally aberrant cells/the number of observed cells × 100.

**Indicates that compared with the negative control group, $P < 0.01$.

10.3389/fmicb.2023.1224666

10.3389/fmicb.2023.1224666

TABLE 9 Effects of SOV on the behavioral state and body weight of mice.

Group	Extremities	Hair	Diet	Drinking water	Stool	Urine	Initial weight after modeling	Final weight	Weight gain
Normal group (CG)	—	—	—	—	—	—	33.40 ± 0.84	37.40 ± 0.84	4.0 ± 0.74
Model group (MG)	—	—	—	—	—	—	36.60 ± 2.22	38.20 ± 3.33	1.90 ± 3.12
Original vinegar group (TG)	—	—	—	—	—	—	35.30 ± 2.45	37.10 ± 4.33	−6.60 ± 1.96**

"—" means normal.
** $P < 0.01$ compared with HF group.

as 10,000, 5,000, and 2,500 mg/kg BW, the micronucleus of polychromatic erythrocyte bone marrow in female and male mice was compared with the negative control group. There was no significant difference in the nuclear rate ($P > 0.05$), and the PCE/RBC values of each dose group were not <20% of the negative control group, and there was no significant difference compared with the negative control group. The difference between the micronucleus rate of the control group (cyclophosphamide) and the negative control group was very significant ($P < 0.01$). According to the procedure of GB 15193.5-2014, within the range of doses, the results of this experiment showed that sugarcane vinegar would not enhance the rate of micronuclei in mammalian polychromatic erythrocytes. No damage or inhibition was detected.

Chromosomal aberration test in mouse spermatogonia

As mentioned in Table 6, compared with the negative control group, there was no significant difference in the number of chromosome aberrations, changes in chromosome structure, or rate of aberrant cells in the spermatogonia of mice in three different dose groups of SOV (10,000, 5,000, and 2,500 mg/kg BW; $P > 0.05$). There was no dose–response relationship or statistical significance among the dose groups. In addition, the mitotic index of the three different dose groups of SOV was not lower than 50% of the negative control group compared with the negative control group. There was no significant difference, but the difference in the chromosomal aberration cell rate between the cyclophosphamide positive control group and the negative control group was more significant ($P < 0.01$). According to the method of GB 15193.8-2014, within the concentration level, the results of this experiment showed that SOV does not have an aberrant effect on spermatogonia chromosomes in mice, and the results are negative.

Mammalian bone marrow cell chromosome aberration test

The bone marrow cell chromosomal aberration test is different from the bone marrow micronucleus test. Cell chromosomal aberration in interphase and prophase, thus directly reflecting the incidence of cell chromosomal aberration and judging whether the test substance has a mutation effect (de Barros et al., 2022; Deng et al., 2023). As mentioned in Tables 7, 8, the first and second sampling time results, SOV in three different dose levels, the number of chromosome aberrations, chromosome structure changes, and aberrant cell rates in bone marrow cells of female and male mice were compared with the negative control group. There was no significant difference ($P > 0.05$), no dose–response relationship between the dose groups, and no statistical significance. In addition, three different dose groups of SOV were administered to female and male mice. The mitotic index of bone marrow cells was not lower than 50% of the negative control group, and there was no

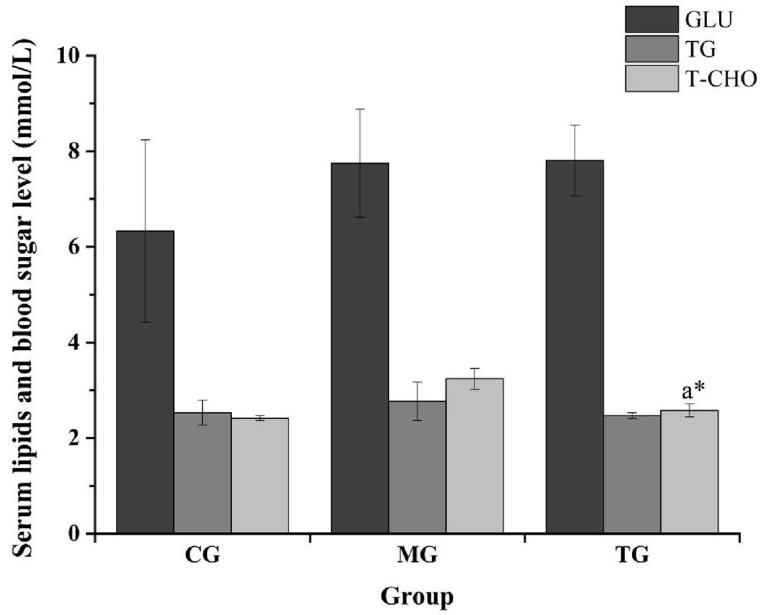

FIGURE 2
Responses of blood glucose and blood lipid levels in different groups. The * symbol indicates significance at $P < 0.05$.

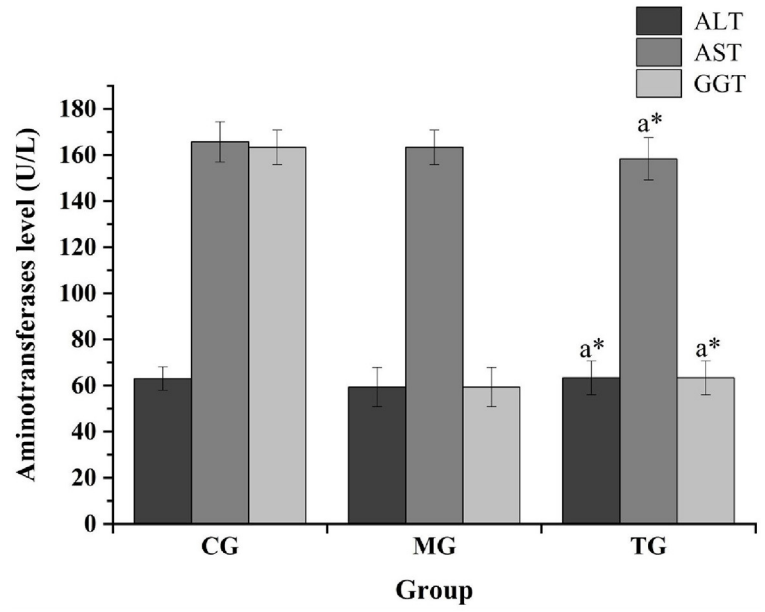

FIGURE 3
Impact of transaminase levels in different groups. The * symbol indicates significance at $P < 0.05$.

significant difference compared with the negative control group. While the difference in the rate of chromosomal structural aberration cells between the cyclophosphamide positive and the negative control groups was significant ($P < 0.01$). According to the method of GB 15193.6-2014, within the dosage range, the results of this experiment showed that the SOV would not have an aberrant effect on the chromosomes of bone marrow cells in mice.

Functional test verification

As shown in Table 9, after continuous observation for 8 weeks, the mental status of the mice in each group was normal for their activities. The mice had smooth fur; a good appetite; a plump body; agile activities; bright eyes; normal urine; no abnormal secretions from the nose, eyes, or mouth; and no adverse conditions. Mice fed a high-fat diet for 4 weeks were fed SOV continuously, and the body

10.3389/fmicb.2023.1224666

TABLE 10 Effects of SOV on serum biochemical indicators in mice.

Group	Normal group (CG)	Model group (MG)	Original vinegar group (TG)	Raw vinegar group changes (TG vs. CG)
ALT/(UL^{-1})	63.00 ± 5.42	59.33 ± 8.39	63.33 ± 7.61*	↑
AST/(U L^{-1})	165.67 ± 8.54	163.33 ± 7.52	158.33 ± 9.31*	↓
GGT/(U L^{-1})	163.33 ± 7.31	59.33 ± 8.64	63.33 ± 7.41*	↓
AST/ALT	3.07 ± 0.37	4.75 ± 0.49	3.31 ± 0.46	↑
TP/(g L^{-1})	67.50 ± 5.48	74.20 ± 3.42	71.60 ± 5.54	↑
ALB/(g L^{-1})	29.90 ± 2.49	29.60 ± 1.91	31.80 ± 0.16	↑
GLB/(g L^{-1})	37.53 ± 8.14	44.57 ± 4.41	39.83 ± 5.61	↑
ALB/GLB	0.81 ± 0.21	0.67 ± 0.18	0.79 ± 0.10	↓
TBIL/(μmol L^{-1})	0.30 ± 0.48	0.70 ± 0.49	1.67 ± 0.60	↑
CREA/(μmol L^{-1})	21.00 ± 0.48	23.00 ± 1.59	22.00 ± 4.51	↑
UA/(μmol L^{-1})	105.30 ± 9.79	94.00 ± 4.93	104.20 ± 8.39*	↓
BUN/(mmol L^{-1})	8.33 ± 0.58	6.67 ± 1.16	7.67 ± 0.56*	↓
GLU/(mmol L^{-1})	6.33 ± 1.91	7.75 ± 1.13	7.81 ± 0.76	↑
TG/(mmol L^{-1})	2.53 ± 0.26	2.77 ± 0.40	2.47 ± 0.06	↓
T-CHO/(mmol L^{-1})	2.42 ± 0.05	3.24 ± 0.22	2.58 ± 0.13*	↑

The ↓, ↑, and * symbols indicate decrease and increase values, and * is statistically significant at $P < 0.05$.

weight of the mice did not increase negatively, indicating that SOV has a weight-loss effect (Younes et al., 2022).

The routine blood analysis of the mice was performed, and the results are shown in Figures 2, 3 and Table 10. Compared with the normal group, the blood indicators of the mice fed the high-fat diet for 4 weeks were different in nine indicators. The degree of increase and the six indicators decline are different degrees. After the high-fat mice were fed with SOV for 4 weeks, compared with the model group MG, the levels of ALT and GCT in the serum of the mice were significantly increased ($P < 0.05$), compared with the normal group CG and the model group MG. The levels of GLU, TG, and T-CHO in mice in the TG group were slightly increased or decreased without significant changes. The levels of CREA, BUN, and UA in serum had no significant changes, which indicated that SOV did not cause kidney damage.

The previous study of our research group found that SOV fermented with sugarcane juice has strong antioxidant activities (Zheng et al., 2015), and SOV can significantly reduce the body mass of mice fed a high-fat diet and can improve blood lipids, reduce blood sugar concentration, and promote fat loss. The effect of reducing blood lipid levels can reduce the levels of triglycerides, total cholesterol, and low-density lipoprotein cholesterol in the plasma of high-fat mice. At the same time, the ability to resist oxidative stress can reduce amylase activity and increase lipase activity, increase the activity of superoxide dismutase (SOD) and glutathione peroxidase (GSH-Px) in plasma and liver, and control the further development of obesity and its complications (Li et al., 2020a,b,c).

Conclusion

Sugarcane vinegar is a healthy and wealthy product with different characteristics, such as antidiabetic, antihyperlipidemic, antimicrobial, and anti-inflammatory effects. Different approaches have unraveled the presence of different bioactive compounds in sugarcane vinegar, which are associated with the raw material used to produce vinegar. The test results showed that SOV products contained some heavy metals; the acute oral toxicity LD_{50} of SOV in male and female mice was 20,000 and 14,700 mg/kg BW, respectively. Oral toxicity is practically non-toxic. The results of genetic toxicity tests (bacterial reverse mutation, mammalian erythrocyte micronucleus, mouse spermatogonial chromosomal aberration, and mouse bone marrow cell chromosomal aberration test) showed that SOV had no damage or inhibitory effect on bone marrow erythrocytes in mice. It has no mutagenic or aberrant effect on the chromosomes of bone marrow cells or spermatogonia in mice. Raw SOV is rich in nutrition, organic acids, flavonoids, phenolic acids, and amino acids. Adhikari et al. (2013) found that SOV has a lipid-lowering effect after drinking it for patients with hyperlipidemia in clinical practice. It has the effect of increasing HDL (Adhikari et al., 2013). For the development and high-value utilization of SOV in the next step, such as the development of high-end products such as SOV beverages, functional SOV powders, and SOV capsules, provide technical direction and safety, and improve the high-quality and sustainable development of the sugarcane industry.

Data availability statement

The original contributions presented in the study are included in the article/supplementary material, further inquiries can be directed to the corresponding author.

Ethics statement

The animal study was reviewed and approved by Ethical approval (GXAAS/AEEIF/00001) was obtained and animal experiments were performed in accordance with the guidelines of the Animal Care and Use Committee (ACUC) of Guangxi Academy of Agricultural Sciences, Nanning, Guangxi, China.

Author contributions

F-JZ, BL, and G-LC conceived and designed the experiment, supervised, and drafted the original manuscript. BL, Y-XY, X-CF, and KKV performed experimental analysis. All authors have read and approved the final manuscript for publication.

Funding

This study was financially supported by the Guangxi Major Science and Technology Program (Grant No. GK-AA22117002), the Opening Project of Guangxi Key Laboratory of Green Processing of Sugar Resources (Grant No. GXTZYKF202208), the Xixiangtang Science and Technology Program of Nanning, Guangxi (Grant No. 2020032101), the Project of Guangxi Agricultural Science and Technology Innovation Alliance (Grant No. GNKM202315), and the Guangxi Academy of Agricultural Sciences Basic Research Business Project (Grant No. GNK2021YT117).

Acknowledgments

We thank the Guangxi Academy of Agricultural Sciences, Nanning, Guangxi, China, for providing the necessary facilities for this study.

Conflict of interest

The authors declare that the research was conducted in the absence of any commercial or financial relationships that could be construed as a potential conflict of interest.

Publisher's note

References

Adhikari, B. K., Gao, M. J., and Meng, X. P. (2013). Effect of sugarcane vinegar on blood lipid level in hyperlipidaemic patients. *China Health Care Nutr.* 5, 554–555.

Budak, N. H., Aykin, E., Seydim, A. C., Greene, A. K., and Guzel-Seydim, Z. B. (2014). Functional properties of vinegar. *J. Food Sci.* 79, R757–R764. doi: 10.1111/1750-3841.12434

Bureau of Quality and Technical Supervision of Guangxi Zhuang Autonomous Region. (2017). *Bureau of Quality and Technical Supervision of Guangxi Zhuang Autonomous Region, DB45/T 1536-2017 Guangxi Local Standard Technical Regulations for Production of Sugarcane Raw Vinegar*.

Chen, G.-L., Zheng, F.-J., Lin, B., Wang, T.-S., and Li, Y.-R. (2013). Preparation and characteristics of sugarcane low alcoholic drink by submerged alcoholic fermentation. *Sugar Tech.* 15, 412–416. doi: 10.1007/s12355-013-0248-3

Chen, G. L., Zheng, F. J., Lin, B., Lao, S. B., He, J., Huang, Z., et al. (2020). Phenolic and volatile compounds in the production of sugarcane vinegar. *ACS Omega* 5, 30587–30595. doi: 10.1021/acsomega.0c04524

Chen, G. L., Zheng, F. J., Lin, B., Yang, Y. X., Fang, X. C., Verma, K. K., et al. (2023). Vinegar: a potential source of healthy and functional food with special reference to sugarcane vinegar. *Front Nutr.* 10, 1145862. doi: 10.3389/fnut.2023.1145862

Chen, G. L., Zheng, F. J., Sun, J., Li, Z. C., Lin, B., and Li, Y. R. (2015). Production and characteristics of high quality vinegar from sugarcane juice. *Sugar Tech.* 17, 89–93. doi: 10.1007/s12355-014-0352-z

China National Standards Administration Committee (2014). *China National Standards Administration Committee, GB 15193.6-2014. Food Safety National Standard Chromosomal Aberration Test of Mammalian Bone Marrow Cells*. Beijing: China Standard Press.

de Barros, M. C., Silva, A. G. B., Souza, T. G. D. S., Chagas, C. A., Machado, J. C. B., Ferreira, M. R. A., et al. (2022). Evaluation of acute toxicity, 28-day repeated dose toxicity, and genotoxicity of *Moringa oleifera* leaves infusion and powder. *J. Ethnopharmacol.* 296, 115504. doi: 10.1016/j.jep.2022.115504

Deng, S., Aga, E. B., Xie, H., Xiong, H., and Ye, B. (2023). Evaluation of the acute toxicity and 28-days subacute toxicity of the alcoholic extract from *Ganoderma leucocontextum*. *Food Sci. Nutr.* 11, 434–442. doi: 10.1002/fsn3.3075

Guga, S., Riao, D., Zhi, F., Sudu, B., Zhang, J., Wang, C., et al. (2023). Dynamic assessment of drought risk of sugarcane in guangxi, china using coupled multi-source data. *Remote Sens.* 15, 1681. doi: 10.3390/rs15061681

He, J., Lao, S., Lin, B., Zheng, F. J., and Chen, G. L. (2017). Simultaneous determination of 11 phenolic compounds in apple cider vinegar and sugarcane vinegar by HPLC-DAD. *Sci. Technol. Food Ind.* 23, 210–213. doi: 10.13386/j.issn1002-0306.2017.23.039

Huang, Z., Fang, X. C., Lin, B., Zheng, F. J., and Chen, G. L. (2022). Comparative analysis of sugarcane vinegar fermented by immobilized acetic acid bacteria on different carriers. *Food Res. Dev.* 43, 131–138. doi: 10.12161/j.issn.1005-6521.2022.10.018

Li, Z. C., Chen, G. L., Zheng, F. J., Sun J., Lin B., and Fang X. C. (2020a). Effects of sugarcane vinegar on body mass, organ coefficient and serum biochemical index of mice fed with high-fat diet. *Chine Brewing* 39, 50–54. doi: 10.11882/j.issn.0254-5071.2020.01.010

Li, Z. C., Chen, G. L., Zheng, F. J., Sun, J., Lin, B., Fang, X., et al. (2020b). Effect of sugarcane vinegar on lipid metabolism and redox state of mice fed high-fat diet. *Food Sci.* 41, 86–90. doi: 10.1111/1750-3841.14967

Li, Z. C., Chen, G. L., Zheng, F. J., Sun, J., Lin, B., Khoo, H. E., et al. (2020c). Effects of sugarcane vinegar supplementation on oxidative stress and weight reduction in hyperlipidaemic mice. *Int. Food Res. J.* 27, 1121–1131.

Lin, B. O., Zheng, F., Fang, X., and Chen, G. (2022). Comparison of amino acids and analysis of nutrition and flavor on sugarcane fermentation products. *Farm. Prod. Process.* 15, 64–69. doi: 10.16693/j.cnki.1671-9646(X)2022.08.015

Luo, D., and Xu, X. (2019). Vinegar could act by gut microbiome. *EBio Med.* 46, 30. doi: 10.1016/j.ebiom.2019.07.061

Luzón-Quintana, L. M., Castro, R., and Durán-Guerrero, E. (2021). Biotechnological processes in fruit vinegar production. *Foods* 10, 945. doi: 10.3390/foods10050945

National Standards Administration of China (2014). *National Standards Administration of China, GB 5193.8-2014. National Food Safety Standard Chromosomal Aberration Test of Mouse Spermatogonia or Spermatocytes*. Beijing: China Standard Press.

Standardization Administration of China (2014a). *Standardization Administration of China, GB15193.3.3-2014. Acute Oral Toxicity Test*. Beijing: China Standard Press.

Standardization Administration of China (2014b). *Standardization Administration of China, GB 5193.4-2014. National Food Safety Standard Bacterial Reverse Mutation Test*. Beijing: China Standard Press.

Standardization Administration of China (2014c). *Standardization Administration of China, GB 15193.5-2014. National Food Safety Standard Mammalian Red Blood Cell Micronucleus Test*. Beijing: China Standards Press.

Yi, L., Huang, T., Li, K., Deng, L., Li, H., Chen, S., et al. (2017). Development of liquid fermented sugarcane vinegar beverage. *Chin. Condiment* 42, 83–88. doi: 10.3969/j.issn.1000-9973.2017.10.018

Younes, M., Aquilina, G., Degen, G. H., Engel, K.-H., Fowler, P. J., Frutos, M. J., et al. (2022). Safety evaluation of buffered vinegar as a food additive. *EFSA J*. 20, e07351. doi: 10.2903/j.efsa.2022.7351

Zheng, F., Chen, G. L., Fang, X. C., Sun, J., Lin, B., Liu, G. M., et al. (2016). Acid fermentation of sugarcane wine by acetic acid bacteria. *Food Ferment. Ind.* 42, 101–107.

Zheng, F. J., Chen, G. L., Meng, Y., Lin, B., and Sun J. (2018). Effects of different dry yeasts on the brewing characteristics of sugarcane juice. *Food Industry Sci. Technol.* 39, 24–28.

Zheng, F. J., Chen, G. L., Meng, Y. H., Sun, J., Lin, B., Fang, X. C., et al. (2015). Antioxidative capacity fermented products from sugarcane juice. *J. Southern Agric.* 46, 475–479. doi: 10.3969/j:issn.2095-1191.2015.3.475

frontiers | Frontiers in Microbiology

TYPE Correction
PUBLISHED 05 September 2023
DOI 10.3389/fmicb.2023.1281182

OPEN ACCESS

APPROVED BY
Frontiers Editorial Office,
Frontiers Media SA, Switzerland

*CORRESPONDENCE
Gan-Lin Chen
ganlin-chen@163.com;
ganlin-chen@gxaas.net

†These authors have contributed equally to this work

RECEIVED 22 August 2023
ACCEPTED 23 August 2023
PUBLISHED 05 September 2023

CITATION
Zheng F-J, Lin B, Yang Y-X, Fang X-C, Verma KK and Chen G-L (2023) Corrigendum: Efficacy and functionality of sugarcane original vinegar on mice. *Front. Microbiol.* 14:1281182. doi: 10.3389/fmicb.2023.1281182

Corrigendum: Efficacy and functionality of sugarcane original vinegar on mice

Feng-Jin Zheng[1,2†], Bo Lin[1,2†], Yu-Xia Yang[1,2], Xiao-Chun Fang[1,2], Krishan K. Verma[3] and Gan-Lin Chen[1,2,4*]

[1]Institute of Agro-Products Processing Science and Technology, Guangxi Academy of Agricultural Sciences, Nanning, Guangxi, China, [2]Guangxi Key Laboratory of Fruits and Vegetables Storage-Processing Technology, Nanning, China, [3]Key Laboratory of Sugarcane Biotechnology and Genetic Improvement (Guangxi), Ministry of Agriculture and Rural Affairs, Guangxi Key Laboratory of Sugarcane Genetic Improvement, Sugarcane Research Institute, Guangxi Academy of Agricultural Sciences, Nanning, Guangxi, China, [4]School of Chemistry and Chemical Engineering, Guangxi Minzu University, Nanning, Guangxi, China

KEYWORDS

sugarcane original vinegar, safety, functionality, evaluation, mice

A corrigendum on
Efficacy and functionality of sugarcane original vinegar on mice

by Zheng, F.-J., Lin, B., Yang, Y.-X., Fang, X.-C., Verma, K. K., and Chen, G.-L. (2023). *Front. Microbiol.* 14:1224666. doi: 10.3389/fmicb.2023.1224666

In the published article, there was a mistake in the keyword "raw sugarcane vinegar".

The correct keyword is "sugarcane original vinegar".

In the published article "Chen et al. 2015b" was cited in the Introduction, first-paragraph, line 5 as "It is an advanced type of vinegar product (Chen et al., 2015a,b, 2023; Yi et al., 2017)".

The correct citation is "It is an advanced type of vinegar product (Chen et al., 2013, 2015, 2023; Yi et al., 2017)".

In the published article, the reference "Chen, G.-L., Zheng, F.-J., Lin, B., Yang, Y.-X., Fang, X.-C., Verma, K. K., et al. (2015b). Research on the production technology of sugarcane vinegar and fruit vinegar beverages. *China Brew.* 34, 154–157" was incorrectly cited.

The correct reference is: "Chen, G.-L., Zheng, F.-J., Lin, B., Wang, T.-S., and Li, Y.-R. (2013). Preparation and characteristics of sugarcane low alcoholic drink by submerged alcoholic fermentation. *Sugar Tech.* 15, 412–416. doi: 10.1007/s12355-013-0248-3".

The authors apologize for this error and state that this does not change the scientific conclusions of the article in any way. The original article has been updated.

Publisher's note

All claims expressed in this article are solely those of the authors and do not necessarily represent those of their affiliated organizations, or those of the publisher, the editors and the reviewers. Any product that may be evaluated in this article, or claim that may be made by its manufacturer, is not guaranteed or endorsed by the publisher.

References

Chen, G.-L., Zheng, F.-J., Lin, B., Wang, T.-S., and Li, Y.-R. (2013). Preparation and characteristics of sugarcane low alcoholic drink by submerged alcoholic fermentation. *Sugar Tech.* 15, 412–416. doi: 10.1007/s12355-013-0248-3

Chen, G. L., Zheng, F. J., Lin, B., Yang, Y. X., Fang, X. C., Verma, K. K., et al. (2023). Vinegar: a potential source of healthy and functional food with special reference to sugarcane vinegar. *Front. Nutr.* 10, 1145862. doi: 10.3389/fnut.2023.1145862

Chen, G. L., Zheng, F. J., Sun, J., Li, Z. C., Lin, B., and Li, Y. R. (2015). Production and characteristics of high quality vinegar from sugarcane juice. *Sugar Tech.* 17, 89–93. doi: 10.1007/s12355-014-0352-z

Yi, L., Huang, T., Li, K., Deng, L., Li, H., Chen, S., et al. (2017). Development of liquid fermented sugarcane vinegar beverage. *Chin. Condiment.* 42, 83–88. doi: 10.3969/j.issn.1000-9973.2017.10.018

frontiers | Frontiers in Microbiology

TYPE Original Research
PUBLISHED 08 August 2023
DOI 10.3389/fmicb.2023.1236583

OPEN ACCESS

EDITED BY
Hesong Wang,
Southern Medical University, China

REVIEWED BY
Krishan K. Verma,
Guangxi Academy of Agricultural Sciences, China
Madalina Preda,
Marius Nasta Institute of Pneumology, Romania
Xingjia Xiang,
Anhui University, China

*CORRESPONDENCE
Gang Liu
✉ liugang8966@163.com
Fan Wang
✉ wangfan1965@126.com

†These authors have contributed equally to this work

RECEIVED 07 June 2023
ACCEPTED 20 July 2023
PUBLISHED 08 August 2023

CITATION
Li X, Feng J, Wang Z, Liu G and Wang F (2023) Features of combined gut bacteria and fungi from a Chinese cohort of colorectal cancer, colorectal adenoma, and post-operative patients. *Front. Microbiol.* 14:1236583. doi: 10.3389/fmicb.2023.1236583

Features of combined gut bacteria and fungi from a Chinese cohort of colorectal cancer, colorectal adenoma, and post-operative patients

Xiaopeng Li[1,2†], Jiahui Feng[3†], Zhanggui Wang[2], Gang Liu[3*] and Fan Wang[1*]

[1]Department of Radiation Oncology, The First Affiliated Hospital of Anhui Medical University, Hefei, China, [2]Department of Radiation Oncology, Anhui No. 2 Provincial People's Hospital, Hefei, China, [3]School of Life Sciences, Anhui Medical University, Hefei, China

Colorectal cancer (CRC) accounts for the third highest morbidity burden among malignant tumors worldwide. Previous studies investigated gut microbiome changes that occur during colorectal adenomas (CRA) progression to overt CRC, thus highlighting the importance of the gut microbiome in carcinogenesis. However, few studies have examined gut microbiome characteristics across the entire spectrum, from CRC development to treatment. The study used 16S ribosomal ribonucleic acid and internal transcribed spacer amplicon sequencing to compare the composition of gut bacteria and fungi in a Chinese cohort of healthy controls (HC), CRC patients, CRA patients, and CRC postoperative patients (PP). Our analysis showed that beta diversity was significantly different among the four groups based on the gut bacterial and fungal data. A total of 51 species of bacteria and 8 species of fungi were identified in the HC, CRA, CRC, and PP groups. Correlation networks for both the gut bacteria and fungi in HC vs. CRA, HC vs. CRC, and HC vs. PP indicated some hub bacterial and fungal genera in each model, and the correlation between bacterial and fungal data indicated that a highly significant negative correlation exists among groups. Quantitative polymerase chain reaction (qPCR) analysis in a large cohort of HC, CRC, CRA, and PP patients demonstrated a significantly increasing trend of *Fusobacterium nucleatum*, *Bifidobacterium bifidum*, *Candida albicans,* and *Saccharomyces cerevisiae* in the feces of CRC patients than that of HC patients ($p < 0.01$). However, the abundance levels of CRA and PP were significantly lower in HC patients than those in CRC patients. Further studies are required to identify the functional consequences of the altered bacterial/fungal composition on metabolism and CRC tumorigenesis in the host.

KEYWORDS

colorectal cancer, colorectal adenomas, feces, biomarker, OTUs

Introduction

Colorectal cancer (CRC) is a common malignancy of the colon and rectum, accounting for approximately 10% of all new cancer cases globally. Moreover, it carries the third highest burden of morbidity among all malignant tumors worldwide (Wong and Yu, 2019; Yang et al., 2019). In China, CRC is the second most common malignancy, with a notably rapid increase in its incidence in recent years (Thanikachalam and Khan, 2019; Guo et al., 2021). The pathogenesis of CRC includes chronic inflammation and the accumulation of

genetic, epigenetic, dietary, and environmental factors; however, the exact etiology of CRC remains underexplored (Song et al., 2015; Plummer et al., 2016; Vacante et al., 2020). Colorectal adenomas (CRA) are defined as benign tumors derived from the colorectal mucosa, with the transformation process referred to as the adenoma-carcinoma sequence. Approximately 60–90% of sporadic CRCs start as premalignant lesions known as CRAs (Kim et al., 2020; Vacante et al., 2020). Surgery, radiation therapy, and chemotherapy remain the main therapeutic strategies, with an average 5-year overall survival rate of approximately 40% (Aguiar et al., 2020; Lohsiriwat et al., 2021). Despite the availability of various methods to screen for CRC, colonoscopy remains the gold standard for accurate diagnosis. However, colonoscopy's invasive and unpleasant nature often causes patients to experience unwanted pain and discomfort, leading to more than half of the preference for non-invasive screening methods.

Despite improvements in imaging technologies, the accurate diagnosis of CRC remains a clinical challenge, and over the past few decades, the gut microbiome has been preferred as a molecular biomarker and non-invasive screening method in humans (Marx, 2014; Sinha et al., 2016; Flemer et al., 2017). The current belief is that gut microbiota dysbiosis and a subsequent inappropriate or altered immune response confer a predisposition to chronic inflammation, which is known to contribute to the development of diseases, including cancer. Several studies have investigated the roles of changes in the gut microbiome in the development of adenomas and carcinomas, highlighting the impact of this process on carcinogenesis (Fearon and Carethers, 2015; Sun et al., 2016; Alhinai et al., 2019; Wong and Yu, 2019; Kim et al., 2020). Indeed, the gut microbiota has recently emerged as a central player linking various risk factors to CRC pathogenesis, and many studies have investigated the changes and its role in adenoma and carcinoma development, highlighting the impact of the gut microbiota on the development of CRA and the subsequent progression to CRC (Round and Mazmanian, 2009; Collins et al., 2011; Kamada et al., 2013; Rooks and Garrett, 2016; Gao et al., 2017; Pickard et al., 2017; Yoshii et al., 2019; Zhang et al., 2019; Kim et al., 2020). Several clinical studies have identified that the abundance and structure of gut microbiota are significantly different between patients with CRA and healthy individuals (Shen et al., 2010; Sanapareddy et al., 2012; Lu et al., 2016). Moreover, it has been reported that patients with CRC have distinct qualitative differences in their gut microbiota compared to healthy controls (HC). Patients with CRC also present with changes in microbial composition, function, and ecology (Chen et al., 2013; Louis et al., 2014; Drewes et al., 2016; Marchesi et al., 2016; Peters et al., 2016; Hibberd et al., 2017; Murphy et al., 2021). Investigations of the impact of CRA endoscopic surgery on the intestinal flora revealed that despite no alterations in the overall microbiome structure after CRA excision, the protective microbiota demonstrated an ascending trend, whereas tumor-associated microbiota exhibited a declining trend (Yu et al., 2017). Thus, the findings of these and other studies suggest that gut microbiota play complex and key roles in CRA and CRC. There is accumulating evidence that the etiology of CRC/CRA is related to the gut microbiota and that gut microbiota composition is a major risk factor for CRC and CRA (Hibberd et al., 2017; Yu et al., 2017; Murphy et al., 2021).

A considerable number of studies have suggested *Fusobacterium nucleatum* (*Fn*), *Bifidobacterium bifidum* (*Bb*), *Candida albicans*, and *Saccharomyces cerevisiae* as potential markers for CRC detection (Sokol et al., 2017; Yu et al., 2017). *Fn* and *Bb* are important gut bacteria in humans; *Fn* has been suggested by a considerable number of studies as a potential marker for CRC detection, and the abundance of this species was significantly increased in CRA and CRC (Yu et al., 2017). *Bb* typically represents the most abundant bacteria in healthy humans, supporting its specific adaptation to the human gut and its implications in terms of supporting host health. Moreover, *Bb* is one of a few probiotic strains that are effective in the treatment of gastrointestinal cancer and its symptoms, and the abundance ratio of *Fn*/*Bb* might favor the progression of CRC (Andresen et al., 2020). Fungal dysbiosis is known to play a role in the development of CRC and is characterized by decreased community diversity in addition to a higher abundance of detrimental fungi, such as *C. albicans* and *S. cerevisiae*. *C. albicans* and *S. cerevisiae* were also revealed to have a close association with gastrointestinal disturbances, and fungal internal transcribed spacer 2 (ITS2) library sequencing revealed the abundance of *S. cerevisiae* decreased, while that of *C. albicans* increased in inflammatory bowel disease (IBD); a shift in the gut microbiota environment was demonstrated by analyzing the correlation between bacteria and fungi (Sokol et al., 2017).

Previous studies have revealed that shifts in gut microbiota may play an important role in the initiation and progression of CRC; however, only a few studies have focused on the "biomarker" characteristics of the gut microbiota during the development of CRC and the treatment process. Therefore, a better understanding of the role of alterations in the gut microbiota is urgently needed to improve diagnostic, therapeutic, and prognostic strategies against CRC. This study aimed to explore the combined data of gut bacterial and fungal profiles in the initiation, progression, and prognosis of CRC and to further screen microbial biomarkers associated with CRC. We profiled the combined data of bacterial and fungal communities of feces in CRC, CRA, postoperative patients (PP), and HC to identify biomarker microbiomes using high-throughput sequencing of the 16S ribosomal ribonucleic acid (rRNA) and ITS gene regions. We also combined multiple data points on bacteria and fungi in CRC and used them for correlation analyses. In addition, we detected variations in the abundance of *Fn*, *Bb*, *C. albicans,* and *S. cerevisiae* in an independent large cohort of patients with CRC, CRA, PP, and HC using quantitative polymerase chain reaction (qPCR). Through these efforts, we aimed to investigate the different gut bacterial and fungal profiles among CRC, CRA, and HC to identify the marker microbiota that likely contributes to CRC development and impact treatment progression.

Materials and methods

Ethics statement

Written oral consent was obtained from each participant before sample collection. All of the methods were performed in accordance with relevant guidelines and regulations, including

any relevant details. Informed consent was obtained from all the patients, and the study was approved by the Institutional Review Board of Anhui No. 2 Provincial People's Hospital.

Study patients

The clinical phenotype was determined by endoscopic and pathological diagnoses. Patients with no abnormalities on colonoscopy were included in the HC group. Additionally, CRA and CRC were diagnosed according to both clinical and pathological criteria, and all CRC subjects had intact colonic lesions at the time of stool collection. Patients who had undergone CRC radical surgery with regular follow-up within 1 month to 3 years after surgery and without relapse were included in the PP group. The inclusion criteria for the four groups were as follows: (a) all participants were older than 40 years at the time of sample collection. (b) Diagnosis of CRC/CRA was defined according to clinical, radiological, endoscopic, and histological criteria and without other diseases. The tumor, node, and metastasis (TNM) classification system was used for staging patients with CRC as having TNM stage II/III disease. (c) None of the patients or HC were treated with antibiotics, colon-cleansing products, or hormones within 1 month. (d) All of the participants had no history of uninterested tract neoplasia or upper gastrointestinal tract surgery. (e) No eating habit changes in the last 4 weeks and no active gastrointestinal tract bleeding in the last 6 months.

Sample collection

A total of 68 fecal samples were collected from 15 CRC patients, 19 CRA patients, 19 PP, and 15 HC for combined gut bacterial and fungal analyses (Supplementary Table 1). An independent cohort of 402 patients consisting of 92 HC patients, 119 CRC patients, 95 CRA patients, and 96 PP was used to detect the abundance variation of *Fn*, *Bb*, *C. albicans,* and *S. cerevisiae* (Supplementary Table 1). All fecal samples were collected at Anhui No. 2 Provincial People's Hospital and the First Affiliated Hospital of Anhui Medical University, China. All patients were asked to maintain a steady diet and lifestyle and to leave fecal samples (>0.5 g) in a germ-free containment. All fresh fecal samples were collected from the patients and placed in a sterile box, which was immediately transported to the lab on ice. All the fecal samples were collected and stored at −20°C within 4 h and −80°C within 24 h for long-term storage.

DNA extraction, amplification, high sequencing, and qPCR analysis

Microbiota sequencing and data analysis are presented in Supplementary Figure 1. Fecal samples (50–100 mg) were weighed using a 2.0 ml centrifuge tube containing glass beads (200 mg) on ice, and deoxyribonucleic acid (DNA) was isolated from fecal samples using a MagPure Soil DNA LQ Kit (Magen, Guangdong, China) according to the manufacturer's instructions. The extracted DNA was diluted to 1 ng/μl and used as the template for PCR amplification. 343F/798R (343F: 5′-TAC GGR AGG CAG CAG-3′; 798R: 5′-AGG GTA TCT AAT CCT-3′) was used to amplify the 16S rRNA gene of gut bacteria, and ITS primers (ITS1F: 5′-CTT GGT CAT TTA GAG GAA GTA A-3′; ITS2: 5′-GCT GCG TTC TTC ATC GAT GC-3′) were used to amplify the ITS gene of gut fungi. Moreover, PCR was performed as described by Allali et al. (2015) and Sokol et al. (2017). The amplified products were then evaluated by 2% agarose gel electrophoresis, purified with Agencourt AMPure XP beads (Beckman Coulter Co., USA), and quantified using the Qubit dsDNA assay kit. The PCR products were sequenced using an Illumina HiSeq platform (PE250) at Shanghai Oebiotech Co., Ltd., China. The raw data were submitted to the Sequence Read Archive of the NCBI database (https://www.ncbi.nlm.nih.gov/sra) under the accession numbers SRR19633851–SRR19633918 and SRR24782233–SRR24782286. The primers for *Fn*, *Bb*, *C. albicans,* and *S. cerevisiae* are listed in Supplementary Table 2. Furthermore, 10 μl SYBR Green II was used as the qPCR system by TAKARA in cooperation with SYBR® Premix Ex TaqTMII (TliRNaseH Plus). Stepone®plus by ABI company was used in qPCR with all the operation and configuration according to the manufacturer's instruction with 40 cycles of 95°C denaturation for 5 s and 60°C annealing and extension for the 30 s in total after 30 s of pre-denaturation at 95°C.

Bioinformatics analysis and potential biomarker identification

Raw sequencing data were provided in the Fastq format. Bioinformatics analysis of bacterial 16S rRNA and fungal ITS gene amplicon pyrosequencing data was performed using the Quantitative Insights Into Microbial Ecology (QIIME v.1.8.0) software pipeline, and the combined raw sequencing data were demultiplexed and filtered. Poor quality (below an average quality score of 30) and short sequences (shorter than 200 bp) of all reads were removed using Trimmomatic software (version 0.35). Clean reads were subjected to primer sequence removal and clustered to generate operational taxonomic units (OTUs) using Vsearch software with a 97% similarity cutoff using USEARCH. Alpha diversity indices (Shannon and Simpson) were calculated using Mothur software. Differences between the bacterial and fungal compositions of the two populations were analyzed based on orthogonal partial least squares-discriminant analysis (OPLS-DA) using the mixOmics package in R (v3.2.1). To identify significant differences among the four groups of gut bacteria/fungi, linear discriminant analysis effect size (LEfSe), which performs a non-parametric factorial Kruskal–Wallis rank-sum test followed by the linear discriminant analysis (LDA) coupled with measurements to assess the effect size of each differentially abundant taxon, was carried out through the LEfSe tool with an LDA of 2.0. Functional predictions were made based on 16S rRNA OTU membership using a phylogenetic investigation of communities by reconstruction of unobserved states (PICRUSt), according to the online protocol (http://picrust.github.io/picrust/). Network analyses were performed to categorize the core fungal taxa using OeBiotech tools available at https://cloud.oebiotech.cn/task/ and the Tutool platform at https://www.cloudtutu.com.

Statistical analysis

Differences in the gut microbial communities between the two groups were analyzed using the non-parametric Kruskal–Wallis rank-sum test. All PCR samples were analyzed in triplicate, and Ct values >5 (Ct_{max} – Ct_{min}) or underdetermined readouts were excluded. The average Ct value from triplicates was calculated, and the relative abundance of the target gut microbiota was based on the Ct value, which was defined as the target Ct value minus the Ct value for 16s rRNA. All values are expressed as mean ± standard deviation. A two-tailed p-value < 0.05 was considered statistically significant. Pairwise multiple comparisons were conducted using analysis of variance (ANOVA), followed by the Bonferroni *post hoc* test. Associations were determined using Spearman's rank correlation. All statistical analyses and associated plots, such as OPLS-DA, pairwise Spearman's correlations, R scores, and p-values, were performed using GraphPad Prism v 7.0 and SPSS 22.0.

Results

Bacterial composition, diversity analysis, and taxonomic alterations

The 16S rRNA gene was amplified and sequenced from 68 fecal samples from four groups, which were designated as HC ($n = 15$, designated sample numbers HC1–15), while the patient groups included CRA ($n = 15$, sample numbers XH1–15), CRC ($n = 19$, sample numbers WC1–19), and PP ($n = 19$, sample numbers ZL1–19). The sequencing results produced 4,933,539 raw reads. After removing low-quality reads, 4,207,009 clean reads corresponding to 8,501 OTUs were retained. Each sample contained an average of 1,283 OTUs (range, 679–2,407 per sample). In total, 2,629 unique OTUs were identified in the four groups: 482 in the HC, 683 in the CRC, 301 in the CRA, and 1,154 in the PP group. Venn analysis revealed 39 unique core OTUs in 68 samples. Gut bacteria from fecal samples collected from HC comprised 27 phyla, 57 classes, 156 orders, 270 families, and 581 genera; those from CRA included 33 phyla, 73 classes, 182 orders, 298 families, and 623 genera; those from CRC included 34 phyla, 82 classes, 198 orders, 321 families, and 660 genera; and those from PP comprised 33 phyla, 88 classes, 213 orders, 351 families, and 727 genera. The dominant bacterial phyla were Bacteroidetes, Firmicutes, and Proteobacteria, accounting for 48.17, 37.35, and 10.40% of the OTUs, respectively (Supplementary Figure 2A). The dominant bacterial classes were the *Bacteroidia*, *Clostridia*, *Gammaproteobacteria*, *Negativicutes*, and *Actinobacteria* (Supplementary Figure 2B). The predominant bacterial orders were *Bacteroidales*, *Oscillospirales*, *Lachnospirales*, *Enterobacterales*, and *Lactobacillales* (Supplementary Figure 2C). The dominant bacterial families were the *Bacteroidaceae*, *Lachnospiraceae*, Prevotellaceae, *Ruminococcaceae*, and *Enterobacteriaceae* (Supplementary Figure 2D). The dominant bacterial genera in the four groups were *Bacteroides*, *Prevotella*, *Faecalibacterium*, *Muribaculaceae*, and *Lachnoclostridium* (Supplementary Figure 2E).

To determine potential shifts in the gut bacterial composition among patients and HC, we compared the alpha and beta diversities among the four groups. However, no changes in alpha diversity (Simpson and Shannon indices) were detected between HC vs. CRC, HC vs. CRA, or HC vs. PP. Moreover, beta diversity comparisons among the samples evaluated by OPLS-DA demonstrated that all CRC samples clustered together, except for CRC2, whereas all HC samples clustered together, except HC8 (Figure 1A). All CRA individuals clustered together, except for CRA1 and CRA2 (Figure 1B), whereas all PP individuals clustered together, except for PP16, PP17, and PP18 (Figure 1C).

High-throughput sequencing data were analyzed to determine which gut bacteria were significantly associated with the HC or patient groups. A total of 51 species of bacteria were identified in the HC, CRA, CRC, and PP groups. *Bacteroides vulgatus*, *Bacteroides plebeius*, *Parabacteroides merdae*, *Romboutsia ilealis*, and *Sutterella wadsworthensis* were the top five most dramatically different species among the four groups. Additionally, LEfSe was used to determine the taxa that most likely revealed differences between CRA/CRC patients and healthy controls, and *Alphaproteobacteria* were increased in the CRA group (Figure 2A). Comparing the HC with CRC groups, *Subdoligranulum* was increased in CRC while *Bacteroides*, *Bacteroidaceae*, *Tannerellaceae* and *Parabacteroides* were increased in HC samples (Figure 2B). Other comparisons revealed that *Firmicutes*, *Bacill*, *Lactobacillales*, *Lactobacillus,* and *Lactobacillaceae* were significantly enriched in the PP group, whereas *Bacteroidales*, *Bacteroidia*, *Bacteroidota*, *Bacteroides,* and *Bacteroidaceae* were more abundant in the HC group than in the PP group (Figure 2C).

In different sample groups, PICRUSt was implemented as a predictive tool for the gut bacterial communities. Overall, 24 Kyoto Encyclopedia of Genes and Genomes (KEGG) orthologs were identified in the KEGG database. Among all samples, PICRUSt analysis indicated that carbohydrate transport and metabolism, transcription, amino acid transport and metabolism, and cell wall/membrane/envelope biogenesis accounted for 11.33, 9.04, 8.42, 7.75, and 6.96% of all functional predictions, respectively (Supplementary Figure 3). Moreover, most of the major functions of the gut bacterial communities in the HC, CRA, CRC, and PP groups (except RNA processing and modification, chromatin structure and dynamics, cell wall/membrane/envelope biogenesis, inorganic ion transport and metabolism, intracellular trafficking, secretion, vesicular transport, defense mechanisms, extracellular structures, and nuclear structure) were significantly different among the four groups.

Fungal composition, diversity analysis, and taxonomic alterations

The ITS gene region was sequenced and analyzed from the same fecal samples, except 15 samples. A total of 54 fecal samples from four designated groups were collected: healthy subjects were designated as HC ($n = 14$, designated sample numbers HC1–14), while the patient groups included CRA ($n = 14$, sample numbers CRA1–14), CRC ($n = 11$, sample numbers CRC1–11), and PP ($n = 15$, sample numbers PP1–15). A total of 4,017,759 reads were retained, and after removing low-quality reads, 3,271,674 clean reads corresponding to 2,970 OTUs were retained. Each sample

10.3389/fmicb.2023.1236583

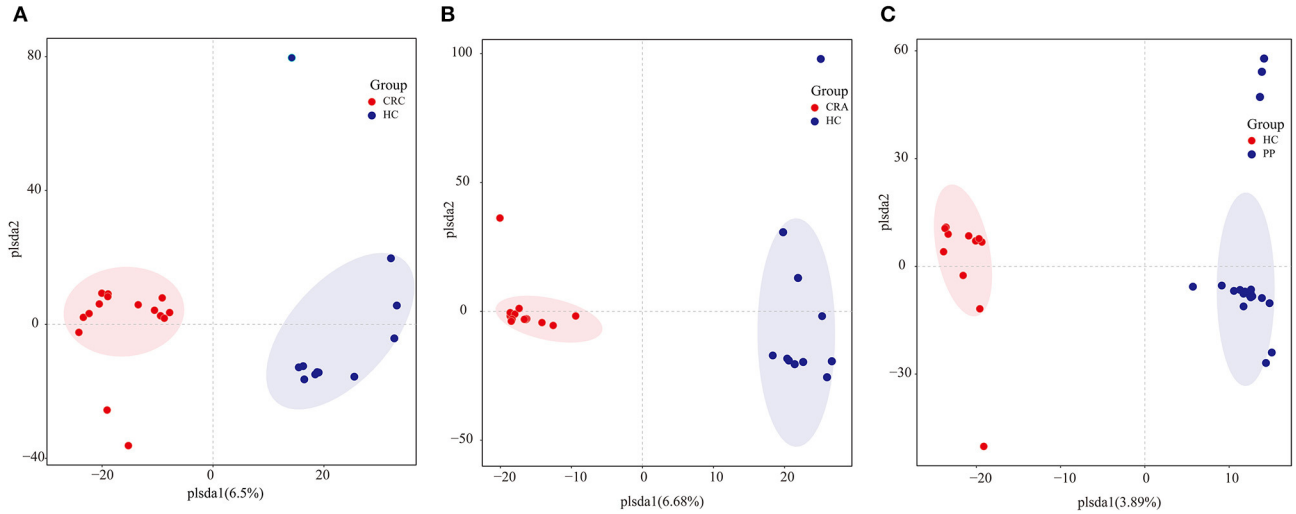

FIGURE 1
Group-wise comparisons by OPLS-DA analysis of the gut bacteria in HC vs. CRC **(A)**, HC vs. CRA **(B)**, and HC vs. PP **(C)**.

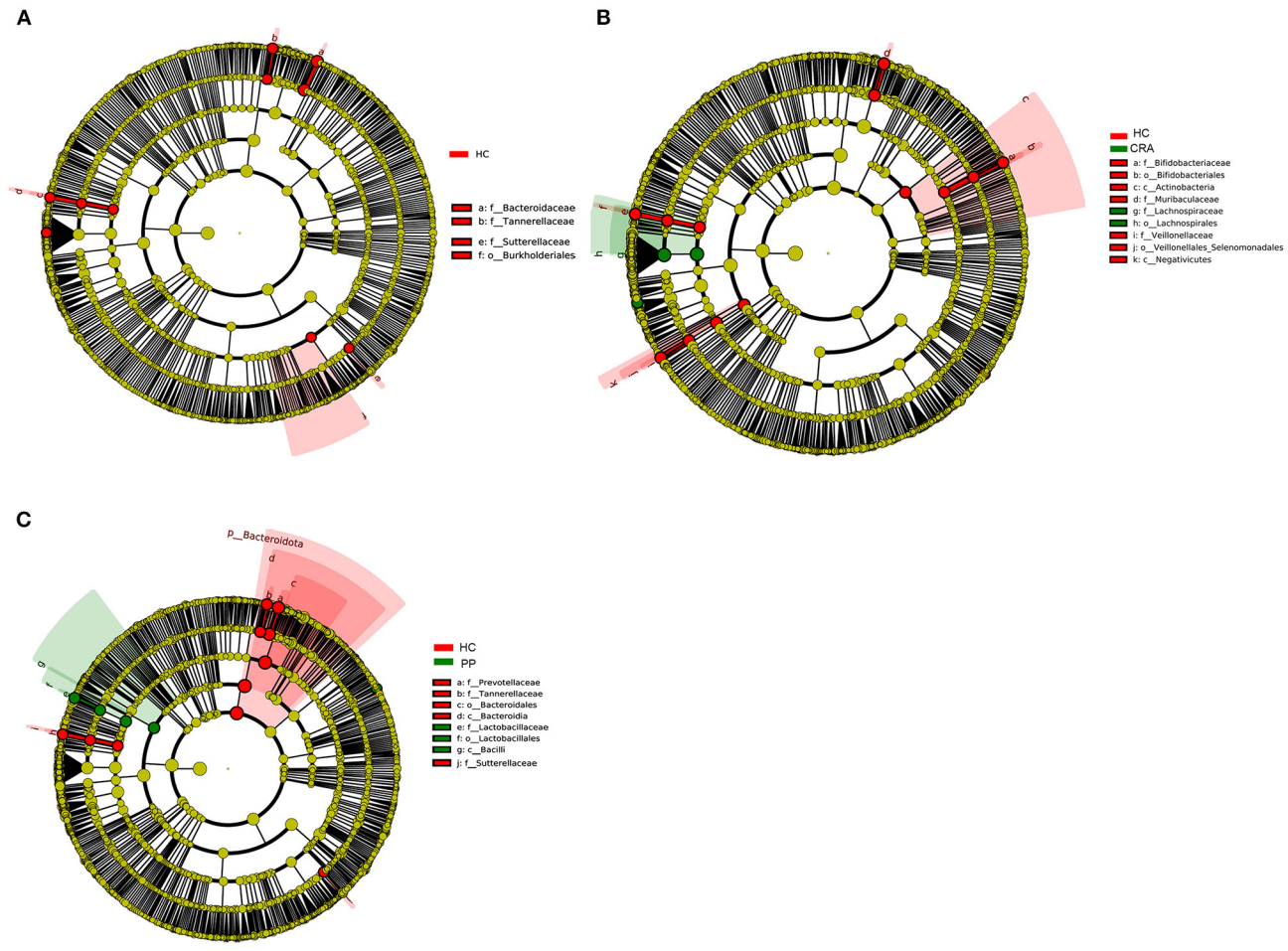

FIGURE 2
The most differentially abundant gut bacterial taxa in HC vs. CRA **(A)**, HC vs. CRC **(B)**, and HC vs. PP **(C)** based on LEfSe analysis, respectively.

10.3389/fmicb.2023.1236583

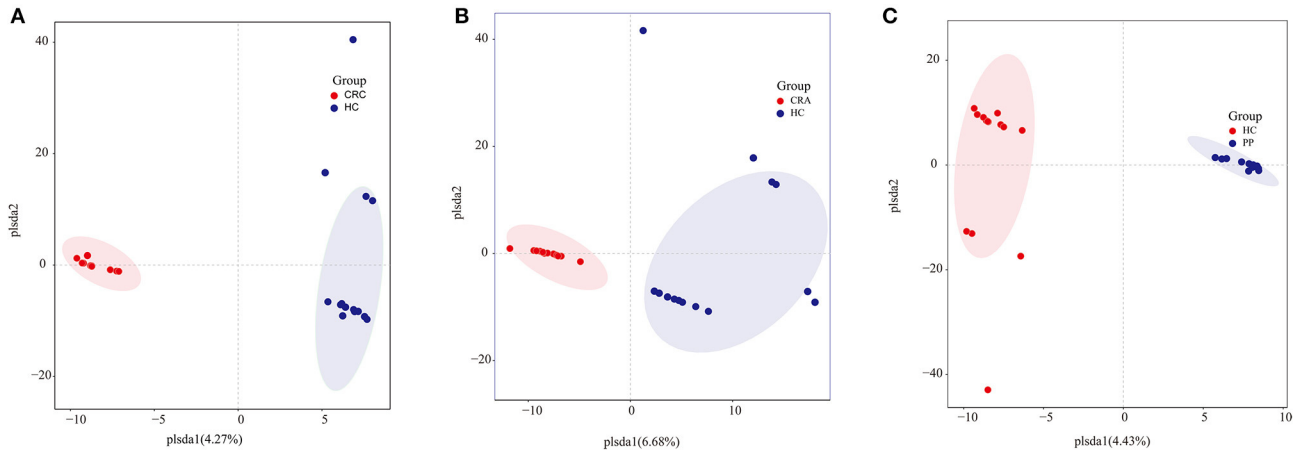

FIGURE 3
Group-wise comparisons by OPLS-DA analysis of the gut fungi in HC vs. CRC **(A)**, HC vs. CRA **(B)**, and HC vs. PP **(C)**.

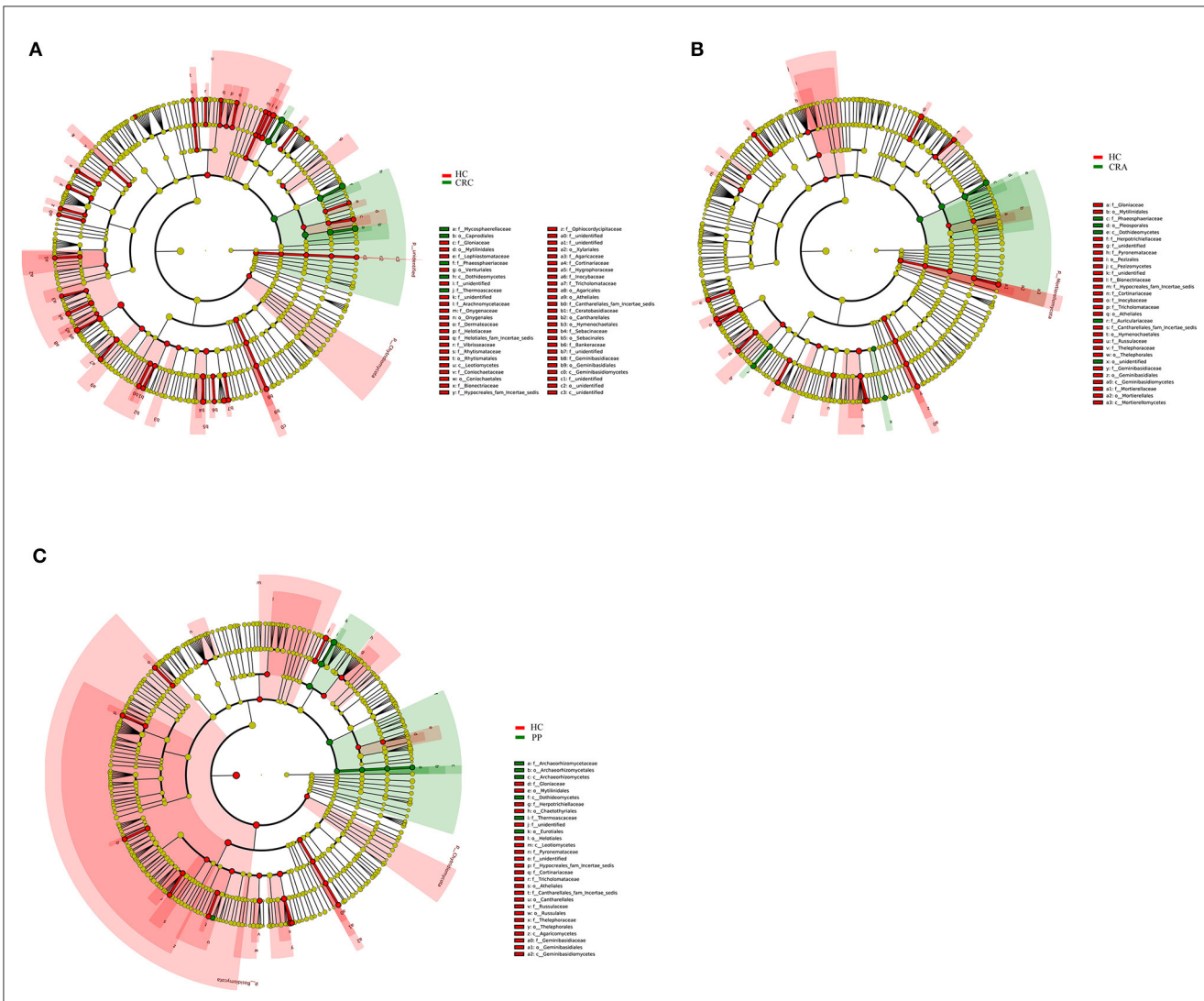

FIGURE 4
The most differentially abundant gut fungal taxa in HC vs. CRA **(A)**, HC vs. CRC **(B)**, and HC vs. PP **(C)** based on LEfSe analysis, respectively.

contained 60,586 ± 9,877 reads (range, 34,481–69,982 per sample), and an average of 55 OTUs (range, 14–311) and 96.5% (mean) were classified as fungal phyla.

Gut fungi from the fecal samples collected from HC comprised 11 phyla, 27 classes, 58 orders, 123 families, and 186 genera; those from CRA included 8 phyla, 20 classes, 41 orders, 71 families, and 89 genera; those from CRC included 8 phyla, 18 classes, 31 orders, 52 families, and 58 genera; and samples collected from PP comprised 8 phyla, 22 classes, 37 orders, 64 families, and 80 genera. The dominant bacterial phyla were *Ascomycota*, *Basidiomycota,* and *Glomeromycota*, accounting for 70.59, 25.29, and 1.22%, respectively (Supplementary Figure 4A). The dominant fungal classes were *Saccharomycetes*, *Agaricomycetes*, *Eurotiomycetes*, *Dothideomycetes,* and *Sordariomycetes* (Supplementary Figure 4B). The main fungal orders identified were *Saccharomycetales*, *Eurotiales*, *Pleosporales*, *Hypocreales*, and *Agaricales* (Supplementary Figure 4C). The main fungal families identified were *Thermoascaceae*, *Nectriaceae*, *Phaeosphaeriaceae*, *Mycosphaerellaceae*, and *Saccharomycetaceae* (Supplementary Figure 4D). The main fungal genera in all four groups were *Candida*, *Byssochlamys*, *Phaeosphaeria*, *Gibberella*, and *Mycosphaerella* (Supplementary Figure 4E).

Similar to gut bacterial alpha diversity, gut fungal alpha diversity was estimated using the observed Simpson and Shannon indices. The alpha diversity of the HC samples was significantly higher than those of the CRC, CRA, and PP samples, as indicated by the number of observed OTUs. The results exhibited no changes in alpha diversity (Simpson and Shannon indices) among the groups, except for the Shannon indices, which demonstrated that alpha diversity differed significantly between HC and CRC and between HC and PP samples. Moreover, individuals from each group were irregularly distributed according to their clade as identified by OPLS-DA (Figures 3A–C).

To explore the variations in fungal community compositions between the two groups, the relative abundances of several taxa were compared among the four groups using LEfSe analysis (Figures 4A–C). High-throughput sequencing data were analyzed to determine which gut fungi were significantly associated with the HC or patient groups. Eight fungal species were identified in the HC, CRA, CRC, and PP groups. *Byssochlamys spectabilis*, *Russula sanguinea*, *Cortinarius bovarius*, *Geminibasidium hirsutum*, and *Tricholoma bonii* were the top five dramatically different fungal species among the four groups.

Network analysis, heatmap, and bacteria-fungi associations

We constructed genus-level correlation networks for both gut bacteria and fungi in the HC vs. CRA, HC vs. CRC, and HC vs. PP groups. The results indicated that *Clavaria*, *Botryotrichum,* and *Olpidium* were the hub fungal genera in each model of the HC vs. CRC (Supplementary Figure 5A). *Cladophialophora* and *Ganoderma* were the hub fungal genera, and *Haemophilus* was the hub bacterial genus in each model of HC vs. CRA (Supplementary Figure 5B). *Ceratobasidium*, *Cutaneotrichosporon*, *Parastagonospor,* and *Saitozyma* were the hub fungal genera, and *Mucispirillum* and *Klebsiella* were the hub bacterial genera in each model of the HC vs. PP (Supplementary Figure 5C).

To investigate the relationship between bacterial and fungal taxa, we analyzed the correlations between the top 20 bacterial genera and the top 20 fungal profiles. Comparison of HC with CRC samples exhibited positive correlations between the abundance of the *Klebsiella* genera with *Cortinarius*, *Sebacina* with *Tricholoma*, *Dialister* with *Inocybe*, *Cutaneotrichosporon* with *Agathobacter*, *Fn* with *Aspergillus*; however, there was no negative correlation (Figure 5A). Comparison of HC with CRA samples identified positive correlations between the abundance of *Mycosphaerella* and *Parasutterella*, *Paraprevotella* and *Archaeorhizomyces*, *Phomopsis* and *Lachnospira*, *Escherichia-Shigella*, *Parasutterella*, *Collinsella,* and *Blautia* (Figure 5B). *Faecalibacterium* was found to be positively correlated with *Gibberella*, *Archaeorhizomyces*, *Russula*, *Geminibasidium*, and *Klebsiella* with *Meyerozyma* (Figure 5C). We calculated the correlations between bacterial and fungal data for HC vs. CRC, HC vs. CRA, and HC vs. PP comparisons. We established a highly significant negative correlation between the bacterial and fungal data for HC vs. CRC ($R = -0.17$, $p = 0.46$) (Figure 5D), with similar results obtained between the bacterial and fungal data for HC vs. CRA ($R = -0.29$, $p = 0.17$; Figure 5E) and HC vs. PP ($R = -0.32$, $p = 0.12$; Figure 5F).

qPCR analysis of some microbial species in HC, CRC, CRA, and PP

The 402 patients in the test cohort consisted of 92 HC, 119 CRC patients, 95 CRA patients, and 96 PP. We discovered that *Fn* demonstrated a significantly increasing trend in the feces of CRC patients compared to that in HC ($p < 0.01$); however, the abundant levels in CRA and PP were significantly lower than those in CRC ($p < 0.05$) (Figure 6A). The relative abundance of *Fn* exhibited a mild increase in CRA and PP, which was higher than that in HC, but lower than that in CRC (Figure 6A). Our results indicated the abundance of *C. albicans* and *S. cerevisiae* in CRC, as described in *Fn* (Figures 6C, D). In our cohort, the relative abundance of *Bb* exhibited different results; it demonstrated a statistically significant difference in CRC compared to HC, CRA, and PP. Compared to healthy controls, the relative abundance of *Bb* in HC was higher than that in CRA, CRC, and PP; however, the relative abundance of *Bb* in CRA and PP was higher than that in HC, but lower than that in CRC (Figure 6B).

Discussion

The incidence of CRC is rising worldwide; sporadic CRC accounts for 95% of all cases, with various pathways, including the adenoma-adenocarcinoma pathway, inflammatory pathway, and *de novo* pathway. Additionally, CRA is regarded as one of the major precancerous lesions of CRC, of which 60–90% arises via the traditional adenoma-carcinoma pathway (Conteduca et al., 2013; Feng et al., 2019; Kim et al., 2020). Genetic and environmental factors play important roles in the pathogenesis of CRC as gut bacteria and fungi contribute to the gut ecosystem through their key roles in host interactions (Bhopal, 2015; Printz, 2015; Yang

10.3389/fmicb.2023.1236583

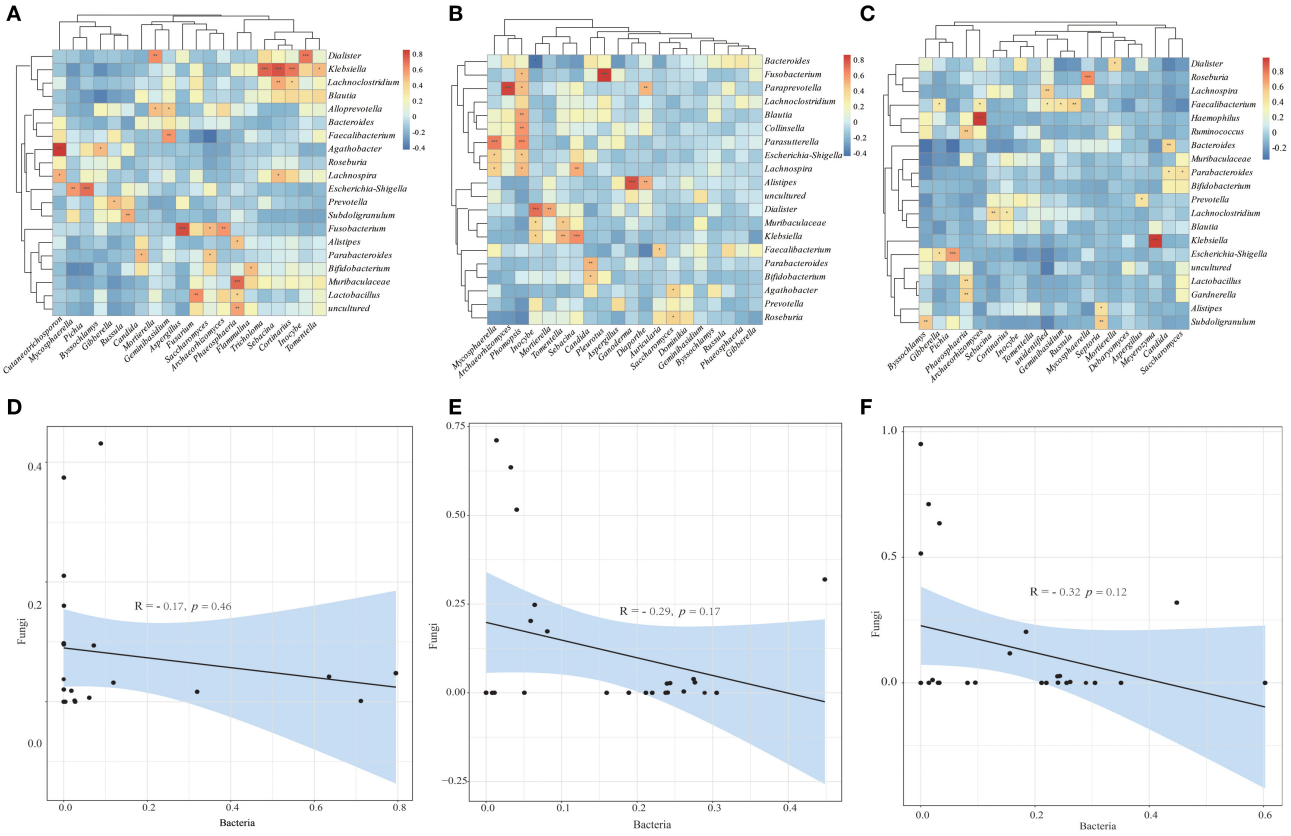

FIGURE 5
Heatmaps illustrating correlations between the top 20 differential bacterial genera and top 20 differential fungal genera in HC vs. CRC **(A)**, HC vs. CRA **(B)**, and HC vs. PP **(C)**, respectively. Correlation between bacterial and fungal data for HC vs. CRC **(D)**, HC vs. CRA **(E)**, and HC vs. PP **(F)**. *$p < 0.05$, **$p < 0.01$, and ***$p < 0.001$. Red: positive correlation; blue: negative correlation.

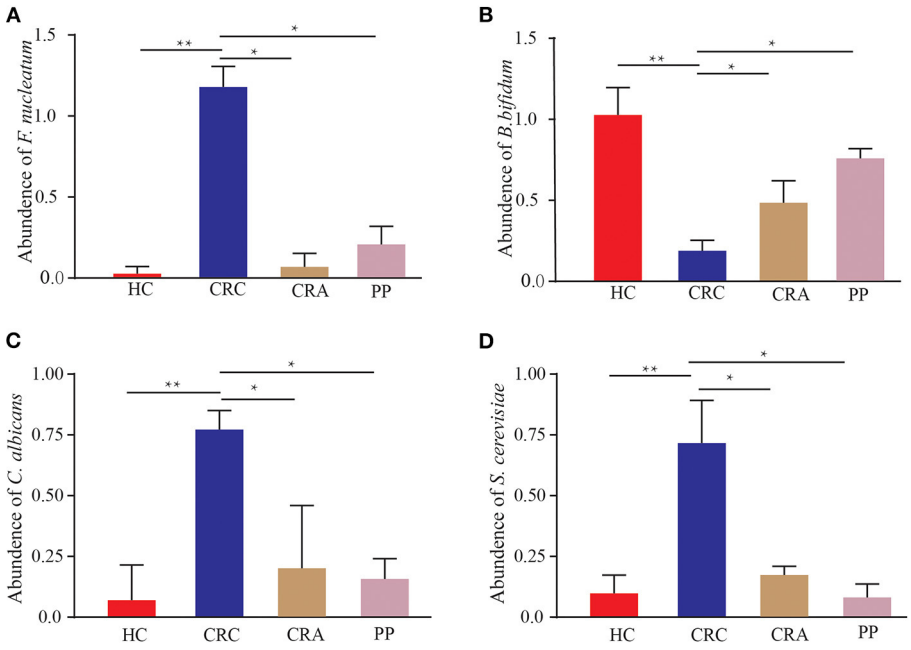

FIGURE 6
The abundance of *Fusobacterium nucleatum* **(A)**, *Bifidobacterium bifidum* **(B)**, *Candida albicans* **(C)**, and *Saccharomyces cerevisiae* **(D)** in HC, CRC, CRA, and PP, respectively. *$p < 0.05$ and **$p < 0.01$.

et al., 2019). Accumulating evidence has revealed that gut dysbiosis is one of the most essential environmental factors in the initiation and progression of CRC, and several studies have indicated that gut bacteria and fungi can act as drivers to initiate precancerous lesions by promoting the accumulation of gene mutations, thereby directly implicating them in the development of CRA and subsequent progression to CRC (Gao et al., 2017; Coker et al., 2019; Liang et al., 2020; Liu et al., 2020). Although colonoscopy is an effective screening tool for CRC diagnosis, it remains unpopular with the subjects being tested. Moreover, studies have increasingly addressed the role of the gut microbiome in CRC since a dysbiotic state has been reported in the gut microbiome of CRA and CRC patients (Allali et al., 2015). Hence, there is an unmet need to develop effective non-invasive examinations to detect the early development of CRC (Feng et al., 2023). High-throughput gene sequencing and metagenomic studies have exhibited decreased overall diversity and increased abundance of certain tumor-promoting bacteria and fungi in tumor tissues (Wang et al., 2012). Our study aimed to test whether the gut microbiome composition of patients with CRC and CRA differs from that of HC. We observed changes in the composition and structure of gut bacteria and fungi in patients with CRC or CRA, similar to previous reports revealing abnormalities in normal bacterial and fungal community composition in the guts of patients with CRC or CRA (Lu et al., 2016; Coker et al., 2019).

The gut microbiome plays complex and key roles in numerous diseases, and a structural imbalance does exist in the gut microbiome of patients. Furthermore, accumulating evidence indicates that the etiology of CRC is related to the gut microbiota (Sheng et al., 2020). Over the last few decades, an increasing number of studies have indicated that the assemblage of the gut microbiota influences the formation and progression of CRC (Geng et al., 2013; Garcia-Castillo et al., 2016; Guthrie et al., 2017). In this study, we investigated the structure of gut bacterial and fungal communities in HC, CRA, CRC, and PP samples. The analysis enabled the elucidation of differences in the guts of CRC, CRA, and PP groups from the HC group. For the bacterial data, alpha diversity analysis did not reveal any difference in the observed species; however, the diversity indicated by the Simpson index in the HC group was higher than that in the CRC group. There was also no significant difference between the CRA and PP groups, which has also been observed in previous studies (Shen et al., 2010; Sanapareddy et al., 2012; Feng et al., 2015; Lu et al., 2016). For fungal data, the Shannon diversity index results established that alpha diversity differed significantly between HC and CRC and between HC and PP. However, beta diversity analyses of HC vs. CRA, HC vs. CRC, and HC vs. PP demonstrated dramatic differences in both bacterial and fungal structures, revealing that the process from CRA to CRC resection had a strong effect on diversity (Shen et al., 2010; Sanapareddy et al., 2012; Feng et al., 2015; Lu et al., 2016). Therefore, this confirmed the perspective that the changes in bacterial and fungal profiles were not entirely elicited by CRA or CRC itself and that bacteria and fungi might play vital roles in CRA or CRC development, while the existing abnormal environment after adenoma resection might also contribute to adenoma recurrence (Yu, 2018). Many studies have confirmed increased microbial diversity in CRC patients compared to HC, suggesting that microbial diversity can be distinguished from HC even when the CRC is excised (Yu, 2018). It was discovered that not only the removal of CRC provided gut microbiota with great alterations but also these alterations encouraged a more normal microbiota, confirming the view that the gut microbial community was not entirely produced by CRC itself and might play a vital role in CRC formation, while the still existing abnormal environment after CRC resection might also lay the groundwork for CRC recurrence (Sze et al., 2017).

Bacteria and fungi are important members of the gut microbial ecosystem that interact with the host, and many factors, such as age, sex, and types of cancer, affect the diversity and composition of the gut mycobiota; however, limited evidence has been proposed that relies on a high-throughput platform to explore the role of bacteria and fungi in CRC development and impact treatment progression (Gao et al., 2017; Rahwa et al., 2020). Some microbial pathogens directly promote CRC progression, and some microbial metabolites may reduce the risk of CRC. Previous research has established that gut bacteria and fungi are greatly altered in patients with the removal of colorectal CRA/CRC, with post-operative gut bacteria characterized by reductions in commensal bacterial species and the growth of detrimental bacterial and fungal strains (Keku et al., 2015; DeGruttola et al., 2016; Yu et al., 2017). In this study, we identified 51 species of bacteria and 8 species of fungi with significantly altered abundance, especially 2 bacterial species (*Fn* and *Bb*) and 2 fungal species (*C. albicans* and *S. cerevisiae*). A considerable number of studies have identified *Fn* as a potential marker for CRC detection, and it is one of the most widely studied bacteria associated with CRC (Yu et al., 2017). As an obligate anaerobic gram-negative bacillus, *Fn* commonly colonizes the oral cavity, and it has also been detected in CRC and CRA (Castellarin et al., 2012). A previous study identified that *Fn* was abundant in tissues of CRC patients with recurrence after chemotherapy and was associated with clinicopathological characteristics. Enriched *Fn* in CRC has an invasive role in colonic epithelial cells. Furthermore, bioinformatic and functional studies have demonstrated that *Fn* promotes colorectal cancer resistance to chemotherapy (Yu et al., 2017). Among the various fecal microbiological tests for CRC diagnosis, qPCR testing for fecal *Fn* abundance exhibits the potential for popularization and may serve as a possible indicator of CRC prognosis (Suehiro et al., 2016). In this study, we discovered that radical surgery may lead to a rapid decline in fecal *Fn* abundance. As for the role of *Fn* in CRC prognosis, it was discovered that CRC patients with higher *Fn* count had a poor prognosis, suggesting its potential value as a non-invasive prognosis indicator for CRC. Some studies have displayed that fecal *Fn* plays a vital part in CRC prognosis and seems to be firmly linked to its treatment response (Flanagan et al., 2014). Despite accumulating achievements in the non-invasive microbial diagnosis of CRC, few studies have investigated cancer prognosis, and most studies are limited to tests relying on *Fn*. Due to the negative correlation between the abundance and survival of *Fn*, it may serve as a promising prognostic indicator for CRC (Mima et al., 2015; Yamaoka et al., 2018). In humans, *Bb* is distributed across seven different ecological niches, including the gastrointestinal tract and oral cavity, and displays notable physiological and genetic features encompassing

adhesion to epithelia as well as the metabolism of host-derived glycans (Turroni et al., 2019). Preclinical reports have displayed that *Bb* can be applied as a biotherapeutic agent in the inhibition or therapy of colorectal cancer through the modification of gut bacteria, and it can play a relevant role in inhibiting colon cancer cell growth, which can be used to prevent some incurable diseases such as cancer (Agah et al., 2019). Previous studies have indicated that the oral consumption of *Bb* probiotics significantly decreased the levels of triglycerides, alkaline phosphatase, low-density lipoprotein, VDR, and LPR gene expression in mouse colon cancer (Tjalsma et al., 2012; Feng et al., 2015; Yang et al., 2019; Kim et al., 2020; Vacante et al., 2020). *C. albicans* has emerged as a major public health problem over the past two decades. The spectrum of diseases caused by *Candida* species ranges from vaginal infections to deep infections in hospitalized patients, which leads to high morbidity and mortality rates and may also play a role in the persistence or worsening of some chronic IBDs (Poulain, 2015). The association between *C. albicans* and cancer has been observed for decades, and most of the current clinical and animal evidence supports *C. albicans* as a member of the oral microbiota that acts as an opportunistic pathogen, along with changes in the epithelium that can predispose individuals to pre-malignancy and/or malignancy (Febriyanti et al., 2022). *S. cerevisiae* is a ubiquitous yeast widely used in industry, and it is also a common colonizer of human mucosae; however, the incidence of invasive infection by these fungi has significantly increased in recent decades (Souza et al., 2013). *S. cerevisiae* has been a key experimental organism for the study of infectious diseases, it has revealed that the abundance of *S. cerevisiae* decreased, while that of *C. albicans* increased in CRC, and a shift in the gut microbiota environment was demonstrated by analyzing the correlation between bacteria and fungi (Coker et al., 2019). We identified CRA-, CRC-, and PP-specific shifts in bacterial and fungal composition by qPCR analysis reflected by the enrichment of *Fn*, *Bb*, *C. albicans,* and *S. cerevisiae.* The shift has been previously highlighted, suggesting that the aforementioned species may constitute "biomarker" bacteria associated with cancer-predisposing CRA or outright CRC.

In conclusion, omics initiatives have reached the forefront of biomedical research by highlighting the significance of biological functions and processes. Thus, multi-omic profiling has yielded important insights into CRC biology by identifying potential biomarkers and therapeutic targets. In this study, the gut bacteria and fungi were altered in affected patients compared to those in normal subjects. Thus, our results identified several gut bacteria and fungi that could act as potential "biomarkers" in the traditional adenoma-carcinoma axis using bacterial and fungal data. However, we acknowledge some limitations to our study. The sample numbers were relatively small; therefore, the putative biomarkers, bacteria/fungi, require further validation. This necessitates alternative, larger cohorts to further validate our findings. However, as no single biomarker screen can provide definitive evidence, the findings of this study make significant contributions to the field. Moreover, diet is an important factor to be considered in associating specific fungi with diseases and may affect their universal application as diagnostic markers. The gut microbiota are significantly influenced by food colonization. Further studies are required to identify the functional consequences of the altered bacterial/fungal composition on metabolism and CRC tumorigenesis in the host.

Data availability statement

The raw data were submitted to the Sequence Read Archive at the NCBI database (https://www.ncbi.nlm.nih.gov/sra) under accession numbers SRR19633851-SRR19633918 and SRR24782233-SRR24782286.

Author contributions

XL, GL, and FW designed the experiments of this manuscript. JF, ZW, and XL conducted the sample collection and data analysis. JF, XL, and GL wrote the manuscript. All authors read and approved the manuscript.

Funding

This research was supported by the Natural Science Foundation for the Higher Education Institutions of Anhui Province of China (Grant No. KJ2021A0246).

Acknowledgments

The authors thank Rick F. Thorne and Prof. Xiaoying Liu for their useful suggestions.

Conflict of interest

The authors declare that the research was conducted in the absence of any commercial or financial relationships that could be construed as a potential conflict of interest.

Publisher's note

Supplementary material

The Supplementary Material for this article can be found online at: https://www.frontiersin.org/articles/10.3389/fmicb.2023.1236583/full#supplementary-material

References

Agah, S., Alizadeh, A. M., Mosavi, M., Ranji, P., Khavari-Daneshvar, H., et al. (2019). More protection of *Lactobacillus acidophilus* than bifidobacterium bifidum probiotics on azoxymethane-induced mouse colon cancer. *Probiotics Antimicrob Proteins*. 11, 857–864. doi: 10.1007/s12602-018-9425-8

Aguiar, S., Oliveira, M. M. D., Mello, C. A. L. D., Calsavara, V. F., and Curado, M. P. (2020). Survival of patients with colorectal cancer in a cancer center. *Arqu. Gastroenterol*. 57, 172–177. doi: 10.1590/s0004-2803.202000000-32

Alhinai, E. A., Walton, G. E., and Commane, D. M. (2019). The role of the gut microbiota in colorectal cancer causation. *Int. J. Molec. Sci*. 20, 5295. doi: 10.3390/ijms20215295

Allali, I., Delgado, S., Marron, P. I., Astudillo, A., Yeh, J. J., et al. (2015). Gut microbiome compositional and functional differences between tumor and non-tumor adjacent tissues from cohorts from the US and Spain. *Gut Microbes*. 6, 161–172. doi: 10.1080/19490976.2015.1039223

Andresen, V., Gschossmann, J., and Layer, P. (2020). Heat-inactivated Bifidobacterium bifidum MIMBb75 (SYN-HI-001) in the treatment of irritable bowel syndrome: a multicentre, randomised, double-blind, placebo-controlled clinical trial. *Lancet Gastroenterol. Hepatol*. 5, 658–666. doi: 10.1016/S2468-1253(20)30056-X

Bhopal, R. S. (2015). Diet and colorectal cancer incidence. *JAMA Internal Med*. 175, 1726–1727. doi: 10.1001/jamainternmed.2015.4016

Castellarin, M., Warren, R. L., Freeman, J. D., Dreolini, L., Krzywinski, M., et al. (2012). *Fusobacterium nucleatum* infection is prevalent in human colorectal carcinoma. *Genome Res*. 22, 299–306. doi: 10.1101/gr.126516.111

Chen, H. M., Yu, Y. N., Wang, J. L., Lin, Y. W., Kong, X., et al. (2013). Decreased dietary fiber intake and structural alteration of gut microbiota in patients with advanced colorectal adenoma. *Am. Clin. Nutr*. 97, 1044–1052. doi: 10.3945/ajcn.112.046607

Coker, O. O., Nakatsu, G., Dai, R. Z., Wu, W. K. K., Wong, S. H., et al. (2019). Enteric fungal microbiota dysbiosis and ecological alterations in colorectal cancer. *Gut*. 68, 654–662. doi: 10.1136/gutjnl-2018-317178

Collins, D., Hogan, A. M., and Winter, D. C. (2011). Microbial and viral pathogens in colorectal cancer. *Lancet Oncol*. 12, 504–512. doi: 10.1016/S1470-2045(10)70186-8

Conteduca, V., Sansonno, D., Russi, S., and Dammacco, F. (2013). Precancerous colorectal lesions. *Int. J. Oncol*. 43, 973–984. doi: 10.3892/ijo.2013.2041

DeGruttola, A. K., Low, D., Mizoguchi, A., and Mizoguchi, E. (2016). Current understanding of dysbiosis in disease in human and animal models. *Infelam. Bowel Dis*. 22, 1137–1150. doi: 10.1097/MIB.0000000000000750

Drewes, J. L., Housseau, F., and Sears, C. L. (2016). Sporadic colorectal cancer: microbial contributors to disease prevention, development and therapy. *Br. J. Cancer*. 115, 273–280. doi: 10.1038/bjc.2016.189

Fearon, E. R., and Carethers, J. M. (2015). Molecular subtyping of colorectal cancer: time to explore both intertumoral and intratumoral heterogeneity to evaluate patient outcome. *Gastroenterology*. 148, 10–13. doi: 10.1053/j.gastro.2014.11.024

Febriyanti, A. N., Yasmin, M. F., Simon, P. T. A., Muhammad, C., Putri, A. V. K., et al. (2022). Role of *Candida albicans* in oral carcinogenesis. *Pathophysiology*. 29, 650–662. doi: 10.3390/pathophysiology29040051

Feng, J., Gong, Z., Sun, Z., L,i, J., Xu, N., et al. (2023). Microbiome and metabolic features of tissues and feces reveal diagnostic biomarkers for colorectal cancer. *Front. Microbiol*. 14, 1034325. doi: 10.3389/fmicb.2023.1034325

Feng, Q., Liang, S., Jia, H., Stadlmayr, A., Tang, L., et al. (2015). Gut microbiome development along the colorectal adenoma-carcinoma sequence. *Nat. Commun*. 6, 6528. doi: 10.1038/ncomms7528

Feng, Z. Q., Cao, J., Nie, Y. Q., Gong, C. H., Wang, H., et al. (2019). Analysis of population-based colorectal cancer screening in Guangzhou, 2011-2015. *Cancer Med*. 8, 2496–2502. doi: 10.1002/cam4.1867

Flanagan, L., Schmid, J., Ebert, M., Soucek, P., Kunicka, T., et al. (2014). *Fusobacterium nucleatum* associates with stages of colorectal neoplasia development, colorectal cancer and disease outcome. *Eur. J. Clin. Microbiol. Infect. Dis*. 33, 1381–1390. doi: 10.1007/s10096-014-2081-3

Flemer, B., Lynch, D. B., Brown, J. M., Jeffery, I. B., Ryan, F. J., et al. (2017).Tumour-associated and non-tumour-associated microbiota in colorectal cancer. *Gut*. 66, 633–643. doi: 10.1136/gutjnl-2015-309595

Gao, R., Gao, Z., Huang, L., and Qin, H. (2017). Gut microbiota and colorectal cancer. *Eur. J. Clin. Microbiol. Infect. Dis*. 36, 757–769. doi: 10.1007/s10096-016-2881-8

Garcia-Castillo, V., Sanhueza, E., McNerney, E., Onate, S. A., and Garcia, A. (2016). Microbiota dysbiosis: a new piece in the understanding of the carcinogenesis puzzle. *J. Med. Microbiol*. 65, 1347–1362. doi: 10.1099/jmm.0.000371

Geng, J., Fan, H., Tang, X., Zhai, H., and Zhang, Z. (2013). Diversified pattern of the human colorectal cancer microbiome. *Gut Pathog*. 5, 2. doi: 10.1186/1757-4749-5-2

Guo, A. J., Wang, F. J., Ji, Q., Geng, H. W., Yan, X., et al. (2021).Proteome analyses reveal S100A11, S100P, and RBM25 are tumor biomarkers in colorectal cancer. *Proteomics Clin. Applic*. 15, 2000056. doi: 10.1002/prca.202000056

Guthrie, L., Gupta, S., Daily, J., and Kelly, L. (2017). Human microbiome signatures of differential colorectal cancer drug metabolism. *NPJ Biofilms. Microbiomes*. 3, 27. doi: 10.1038/s41522-017-0034-1

Hibberd, A. A., Lyra, A., Ouwehand, A. C., and Rolny, P., Lindegren, H., et al. (2017). Intestinal microbiota is altered in patients with colon cancer and modified by probiotic intervention. *BMJ Open Gastroenterol*. 4, e000145. doi: 10.1136/bmjgast-2017-000145

Kamada, N., Chen, G. Y., Inohara, N., and Núñez, G. (2013). Control of pathogens and pathobionts by the gut microbiota. *Nat. Immunol*. 14, 685–690. doi: 10.1038/ni.2608

Keku, T. O., Dula, S., Deveaux, A., Jovov, B., and Han, X. (2015). The gastrointestinal microbiota and colorectal cancer. *Am. J. Physiol. Gastrointest. Liver Physiol*. 308, G351–G363. doi: 10.1152/ajpgi.00360.2012

Kim, M., Vogtmann, E., Ahlquist, D. A., Devens, M. E., Kisiel, J. B., et al. (2020). Fecal metabolomic signatures in colorectal adenoma patients are associated with gut microbiota and early events of colorectal cancer pathogenesis. *Microbiome*. 11, e03186–e03119. doi: 10.1128/mBio.03186-19

Liang, S., Mao, Y., Liao, M., Xu, Y., Chen, Y., et al. (2020). Gut microbiome associated with APC gene mutation in patients with intestinal adenomatous polyps. *Int. J. Biol. Sci*. 16, 135–146. doi: 10.7150/ijbs.37399

Liu,W., Zhang, R., Shu, R., and Yu, J., Li, H., et al. (2020). Study of the relationship between microbiome and colorectal cancer susceptibility using 16S rRNA sequencing. *Biomed. Res. Int*. 2020, 7828392. doi: 10.1155/2020/7828392

Lohsiriwat, V., Lertbannaphong, S., Polakla, B., and Riansuwan, W. (2021). Implementation of enhanced recovery after surgery and its increasing compliance improved 5-year overall survival in resectable stage III colorectal cancer. *Updates Surg*. 73, 2169–2179. doi: 10.1007/s13304-021-01004-8

Louis, P., Hold, G. L., and Flint, H. J. (2014). The gut microbiota, bacterial metabolites and colorectal cancer. *Nat. Rev. Microbiol*. 12, 661–672. doi: 10.1038/nrmicro3344

Lu, Y., Chen, J., Zheng, J., Hu, G., and Wang, J. (2016). Mucosal adherent bacterial dysbiosis in patients with colorectal adenomas. *Scient. Rep*. 6, 26337. doi: 10.1038/srep26337

Marchesi, J. R., Adams, D. H., Fava, F., Hermes, G. D., Hirschfield, G. M., et al. (2016). The gut microbiota and host health: a new clinical frontier. *Gut*. 65, 330–339. doi: 10.1136/gutjnl-2015-309990

Marx, V. (2014). Cell communication: stop the microbial chatter. *Nature*. 511, 493–497. doi: 10.1038/511493a

Mima, K., Nishihara, R., Qian, Z. R., Cao, Y., Sukawa, Y., et al. (2015). *Fusobacterium nucleatum* in colorectal carcinoma tissue and patient prognosi. *Gut*. 65, 1973–1980. doi: 10.1136/gutjnl-2015-310101

Murphy, C. L., Barrett, M., Pellanda, P., Killeen, S., McCourt, M., et al. (2021). Mapping the colorectal tumor microbiota. *Gut Microbes*. 13, 1–10. doi: 10.1080/19490976.2021.1920657

Peters, B. A., Dominianni, C., Shapiro, J. A., Church, T. R., Wu, J., et al. (2016). The gut microbiota in conventional and serrated precursors of colorectal cancer. *Microbiome*. 4, 69. doi: 10.1186/s40168-016-0218-6

Pickard, J. M., Zeng, M. Y., Caruso, R., and Núñez, G. (2017). Gut microbiota: role in pathogen colonization, immune responses and inflammatory disease. *Immunol. Rev*. 279, 70–89. doi: 10.1111/imr.12567

Plummer, M., Martel, C. D., Vignat, J., Ferlay, J., Bray, F., et al. (2016). Global burden of cancers attributable to infections in 2012: a synthetic analysis. *Lancet Global Health*. 4, e609–e616. doi: 10.1016/S2214-109X(16)30143-7

Poulain, D. (2015). *Candida albicans*, plasticity and pathogenesis. *Crit. Rev. Microbiol*. 41, 208–217. doi: 10.3109/1040841X.2013.813904

Printz, C. (2015). Vegetarian diet associated with lower risk of colorectal cancer. *Cancer*. 121, 2667. doi: 10.1002/cncr.29582

Rahwa, T., Daniel, R. G., Lilian, N. R., Marien, I., and de, J., Clara, B., et al. (2020). Growth rate alterations of human colorectal cancer cells by 157 gut bacteria. *Gut Microbes*. 12, 1–20. doi: 10.1080/19490976.2020.1799733

Rooks, M. G., and Garrett, W. S. (2016). Gut microbiota metabolites and host immunity. *Nat. Rev. Immunol*. 16, 341–352. doi: 10.1038/nri.2016.42

Round, J. L., and Mazmanian, S. K. (2009). The gut microbiota shapes intestinal immune responses during health and disease. *Nat. Rev. Immunol*. 9, 313–323. doi: 10.1038/nri2515

Sanapareddy, N., Legge, R. M., Jovov, B., McCoy, A., Burcal, L., et al. (2012). Increased rectal microbial richness is associated with the presence of colorectal adenomas in humans. *ISME J*. 6, 1858. doi: 10.1038/ismej.2012.43

Shen, X. J., Rawls, J. F., Randall, T., Burcal, L., Mpande, C. N., et al. (2010). Molecular characterization of mucosal adherent bacteria and associations with colorectal adenomas. *Gut Microbes*. 1, 138–147. doi: 10.4161/gmic.1.3.12360

Sheng, Q. S., He, K. X., Li, J. J., Zhong, Z. F., Wang, F. X., et al. (2020). Comparison of gut microbiome in human colorectal cancer in paired tumor and adjacent normal tissues. *Onco. Targets Ther*. 13, 635–646. doi: 10.2147/OTT.S218004

Sinha, R., Ahn, J., Sampson, J. N., Shi, J., Yu, G., et al. (2016). Fecal microbiota, fecal metabolome, and colorectal cancer interrelations. *PLoS ONE*. 11, e0152126. doi: 10.1371/journal.pone.0152126

Sokol, H., Leducq, V., Aschard, H., Pham, H. P., Jegou, S., et al. (2017). Fungal microbiota dysbiosis in IBD. *Gut*. 66, 1039–1048. doi: 10.1136/gutjnl-2015-310746

Song, M. Y., Garrett, W. S., and Chan, A. T. (2015). Nutrients, foods, and colorectal cancer prevention. *Gastroenterology*. 148, 1244–1260. doi: 10.1053/j.gastro.2014.12.035

Souza, G. C., de Mattos, O. F., and Severo, L. C. (2013). Infección por Saccharomyces cerevisiae [Saccharomyces cerevisiae infections]. *Rev. Iberoam. Micol.* 30, 205–208. doi: 10.1016/j.riam.2013.03.001

Suehiro, Y., Sakai, K., Nishioka, M., Hashimoto, S., Takami, T., et al. (2016). Highly sensitive stool DNA testing of Fusobacterium nucleatum as a marker for detection of colorectal tumours in a Japanese population. *Ann. Clin. Biochem*. 54, 86–91. doi: 10.1177/0004563216643970

Sun, T., Liu, S. L., Zhou, Y. B., Yao, Z. W., Zhang, D. F., et al. (2016). Evolutionary biologic changes of gut microbiota in an 'adenoma-carcinoma sequence' mouse colorectal cancer model induced by 1, 2-Dimethylhydrazine. *Oncotarget*. 8, 444–457. doi: 10.18632/oncotarget.13443

Sze, M. A., Baxter, N. T., Ruffin, M. T. 4th., Rogers, M. A. M., and Schloss, P. D. (2017). Normalization of the microbiota in patients after treatment for colonic lesions. *Microbiome*. 5, 150. doi: 10.1186/s40168-017-0366-3

Thanikachalam, K., and Khan, G. (2019). Colorectal cancer and nutrition. *Nutrients*. 11, 164. doi: 10.3390/nu11010164

Tjalsma, H., Boleij, A., Marchesi, J. R., and Dutilh, B. E. A. (2012). Bacterial driver-passenger model for colorectal cancer: beyond the usual suspects. *Nat. Rev. Microbiol*. 10, 575–582. doi: 10.1038/nrmicro2819

Turroni, F., Duranti, S., Milani, C., Lugli, G. A., van Sinderen, D., et al. (2019). *Bifidobacterium bifidum*: a key member of the early human gut microbiota. *Microorganisms*. 7, 544. doi: 10.3390/microorganisms7110544

Vacante, M., Ciuni, R., Basile, F., and Biondi, A. (2020). Gut microbiota and colorectal cancer development: a closer look to the adenoma-carcinoma sequence. *Biomedicines*. 8, 489. doi: 10.3390/biomedicines8110489

Wang, T., Cai, G., Qiu, Y., Fei, N., Zhang, M., et al. (2012). Structural segregation of gut microbiota between colorectal cancer patients and healthy volunteers. *ISME J*. 6, 320. doi: 10.1038/ismej.2011.109

Wong, S. H., and Yu, J. (2019). Gut microbiota in colorectal cancer: mechanisms of action and clinical applications. *Nat. Rev. Gastroenterol. Hepatol*. 16, 690–704. doi: 10.1038/s41575-019-0209-8

Yamaoka, Y., Suehiro, Y., Hashimoto, S., Hoshida, T., Fujimoto, M., et al. (2018). *Fusobacterium nucleatum* as a prognostic marker of colorectal cancer in a Japanese population. *J. Gastroenterol.* 2017, 1–8. doi: 10.1007/s00535-017-1382-6

Yang, T. W., Lee, W. H., Tu, S. J., Huang, W. C., Chen, H. M., et al. (2019). Enterotype-based analysis of gut microbiota along the conventional adenoma-carcinoma colorectal cancer pathway. *Scient. Rep*. 9, 10923. doi: 10.1038/s41598-019-45588-z

Yoshii, K., Hosomi, K., Sawane, K., and Kunisawa, J. (2019). Metabolism of dietary and microbial vitamin b family in the regulation of host immunity. *Front. Nutr*. 6, 48. doi: 10.3389/fnut.2019.00048

Yu, S. Y. (2018). *The impact of colorectal neoplasm resection on gut microbiota*. PhD dissertation of Shanghai Jiao Tong University.

Yu, T., Guo, F., Yu, Y., Sun, T., Ma, D., et al. (2017). *Fusobacterium nucleatum* promotes chemoresistance to colorectal cancer by modulating autophagy. *Cell*. 170, 548–563. doi: 10.1016/j.cell.2017.07.008

Zhang, Z., Tang, H., Chen, P., Xie, H., and Tao, Y. (2019). Demystifying the manipulation of host immunity, metabolism, and extraintestinal tumors by the gut microbiome. *Signal Trans. Targ. Ther*. 4, 41. doi: 10.1038/s41392-019-0074-5

frontiers | Frontiers in Microbiology

TYPE Original Research
PUBLISHED 14 August 2023
DOI 10.3389/fmicb.2023.1236847

OPEN ACCESS

EDITED BY
Ren-You Gan,
Agency for Science, Technology and Research, Singapore

REVIEWED BY
Teleky Bernadette-Emoke,
University of Agricultural Sciences and Veterinary Medicine of Cluj-Napoca, Romania
Babak Momeni,
Boston College, United States

*CORRESPONDENCE
Dong Ouyang
✉ xssmt@sina.com.cn
Xiangtao Zheng
✉ vaszhengxiangtao@126.com

RECEIVED 08 June 2023
ACCEPTED 28 July 2023
PUBLISHED 14 August 2023

CITATION
Wu J, Zhang B, Zhou S, Huang Z, Xu Y, Lu X, Zheng X and Ouyang D (2023) Associations between gut microbiota and sleep: a two-sample, bidirectional Mendelian randomization study.
Front. Microbiol. 14:1236847.
doi: 10.3389/fmicb.2023.1236847

Associations between gut microbiota and sleep: a two-sample, bidirectional Mendelian randomization study

Jun Wu[1], Baofu Zhang[1], Shengjie Zhou[2], Ziyi Huang[1], Yindong Xu[1], Xinwu Lu[1,3], Xiangtao Zheng[1]*and Dong Ouyang[1,2]*

[1]Department of Vascular Surgery, The Second Affiliated Hospital of Wenzhou Medical University, Wenzhou, China, [2]Department of Obstetrics and Gynecology, Taizhou Women and Children's Hospital of Wenzhou Medical University, Taizhou, Zhejiang, China, [3]Department of Vascular Surgery, Shanghai Ninth People's Hospital Affiliated to Shanghai Jiao Tong University School of Medicine, Shanghai, China

Introduction: Previous research has reported that the gut microbiota performs an essential role in sleep through the microbiome–gut–brain axis. However, the causal association between gut microbiota and sleep remains undetermined.

Methods: We performed a two-sample, bidirectional Mendelian randomization (MR) analysis using genome-wide association study summary data of gut microbiota and self-reported sleep traits from the MiBioGen consortium and UK Biobank to investigate causal relationships between 119 bacterial genera and seven sleep-associated traits. We calculated effect estimates by using the inverse-variance weighted (as the main method), maximum likelihood, simple model, weighted model, weighted median, and MR-Egger methods, whereas heterogeneity and pleiotropy were detected and measured by the MR pleiotropy residual sum and outlier method, Cochran's Q statistics, and MR-Egger regression.

Results: In forward MR analysis, inverse-variance weighted estimates concluded that the genetic forecasts of relative abundance of 42 bacterial genera had causal effects on sleep-associated traits. In the reverse MR analysis, sleep-associated traits had a causal effect on 39 bacterial genera, 13 of which overlapped with the bacterial genera in the forward MR analysis.

Discussion: In conclusion, our research indicates that gut microbiota may be involved in the regulation of sleep, and conversely, changes in sleep-associated traits may also alter the abundance of gut microbiota. These findings suggest an underlying reciprocal causal association between gut microbiota and sleep.

KEYWORDS

sleep, gut microbiota, Mendelian randomization, instrumental variable, causal relationship

1. Introduction

Sleep disorders have become a global public health issue, affecting approximately 15–30% of adults and causing significant burdens on quality of life, as well as occupational, psychological, and economic well-being (Ohayon, 2002; Morin et al., 2006). In modern society, owing to the negative effects of modern work patterns and screen time, the prevalence of sleep disorders and circadian rhythm disorders is growing (Thomée et al., 2011; Jehan et al., 2017; Murdock et al.,

2017; Harknett et al., 2021; Di et al., 2022). Moreover, recent studies have indicated that insufficient sleep and sleep disturbances are correlated with countless adverse outcomes (Itani et al., 2017; Jike et al., 2018; Sun et al., 2020; Winer et al., 2021; Sun et al., 2022; Han et al., 2023). However, the molecular mechanisms underlying sleep–wake cycles are unclear. Early research focused on the central nervous system's role in sleep regulation and dysregulation (Raven et al., 2018; Van Someren, 2021; Sulaman et al., 2023). However, sleep is not only regulated by the central system but also affected by signals from peripheral tissues. Recently, researchers have focused on specific interactions between circadian rhythm processes and the gut microbiome.

The gut microbiome is a highly complex microbial community that may directly or indirectly participate in the regulation of the sleep–wake cycle through the microbiome–gut–brain axis (Neuman et al., 2015; Sen et al., 2021; Wang et al., 2022). Moreover, dietary composition, rhythms of feeding, and loss of the microbiome influence the composition of the gut cycling transcriptome and the expression of rhythm genes, independently and together (Leone et al., 2015; Zhang et al., 2023). For example, intraperitoneal injection of components of bacterial cell walls or bacteria-derived metabolites, such as lipopolysaccharides, lipoteichoic acid, and butyrate, were found to increase non-REM sleep in mice (Szentirmai and Krueger, 2014; Szentirmai et al., 2019, 2021). Some randomized controlled trials have suggested that *Bifidobacteria* and *Lactobacillaceae* may help enhance sleep quality, especially sleep induction, and relieve subclinical signs of anxiety and depression (Nishida et al., 2019; Ho et al., 2021; Lee et al., 2021). Additionally, sleep disturbances are associated with the disruption of gut bacteria, which results in a dysfunctional colonic barrier and the development of intestinal illnesses (Benedict et al., 2016; Gao et al., 2023). However, owing to the existence of confounding factors, such as lifestyle, diet, and age (Rinninella et al., 2019), and the limitations of experimental ethics, it is difficult to carry out randomized controlled trials (RCT) to uncover the causal association between gut microbiota and sleep. Moreover, previous observational studies were not robust because they contained small numbers of participants and the direction of the effects was difficult to judge. As a result, it is unclear whether gut microbiota and sleep disturbances are causally related.

In genetic epidemiology, Mendelian randomization is a method that involves using genetic variants to compose instrumental variables (IVs) of traits to investigate the causal relationship between traits and outcomes. Since genetic variants are generally randomly assigned at meiosis and are not affected by disease states, MR analysis can minimize common confounding factors, avoid confounding factors measurement error, and overcome reverse causation (Smith and Ebrahim, 2003; Davey Smith and Hemani, 2014).

We conducted a two-sample, bidirectional MR study using single nucleotide polymorphisms (SNPs) from the most recent genome-wide association studies (GWASs) to identify whether gut microbiota affect sleep disturbances and whether such associations are directional.

Abbreviations: MR, Mendelian randomization; OR, Odds ratio; CI, Confidence interval; REM, Rapid eye movement; RCT, Randomized controlled trials; SNP, Single-nucleotide polymorphism; GWAS, Genome-wide association study; MR-PRESS, MR pleiotropy residual sum and outlier; IVW, Inverse-variance weighted; IV, Instrumental variables.

2. Materials and methods

2.1. Description of study design

A two-sample, bidirectional MR design was performed to uncover the possible causal effects of gut microbiota on sleep-related traits (Figure 1). There were three core assumptions that genetic variants had to meet in order to be included as IVs in our study (Swerdlow et al., 2016; Davies et al., 2018): (i) relevance—the relationship between genetic variants and exposure was robust; (ii) independence—the genetic variants were independent of confounding factors affecting exposure and outcome; and (iii) exclusion restriction—the genetic variants influenced the risk of the outcome through exposure rather than other potential pathways. The forward MR analyses considered gut microbiota as the exposure and each sleep phenotype as the outcome. By contrast, reverse MR analyses took each sleep phenotype as the exposure and gut microbiota as the outcome. We used a two-sample MR computational model to investigate if there were bidirectional causal relationships between gut microbiota and sleep traits. Finally, several sensitivity analyses (the heterogeneity test, the pleiotropy test, and leave-one-out analysis) were performed sequentially.

2.2. Data sources

The GWAS summary statistics used in our study were compiled and are shown in Supplementary Table S1. The individuals from the data sources we used for the MR analysis were primarily of European ancestry.

2.2.1. Gut microbiota

GWAS summary data for intestinal bacteria were assessed from the MiBioGen consortium. This consortium conducted the largest GWAS of the intestinal microbiome. The GWAS gathered whole-genome genotyping data from 18,340 participants (24 cohorts) as well as the 16S rRNA genes from participant's fecal microbiomes. Then, using three distinct variable regions (V1-V2, V3-V4, and V4) of the 16S rRNA gene, the study profiled the composition of intestinal microbial species. By performing microbiome trait loci mapping, genetic variants were identified that affected the relative abundance or presence of nine phyla, 16 classes, 20 orders, 35 families, and 131 genera (included 12 unknown genera). Finally, we included 119 genera taxa for our bidirectional MR study.

2.2.2. Sleep-related traits

GWAS summary data for seven sleep-related traits, namely daytime napping ($n = 452{,}633$), daytime sleepiness ($n = 452{,}071$), insomnia ($n = 386{,}533$), sleep duration ($n = 446{,}118$), long sleep duration ($n = 339{,}926$), short sleep duration ($n = 411{,}934$), and chronotype ($n = 403{,}195$) were obtained from United Kingdom Biobank. Sleepiness and napping during the day are recognized as related clinical features of the attenuated arousal continuum (Dashti et al., 2021). Moreover, daytime napping may result from a lack of sleep at night or underlying poor health (Sayón-Orea et al., 2013; Celis-Morales et al., 2017), which makes causal inferences difficult in observational studies. Excessive daytime sleepiness is a main sign of chronic sleep deficiency and several primary sleep disorders; it

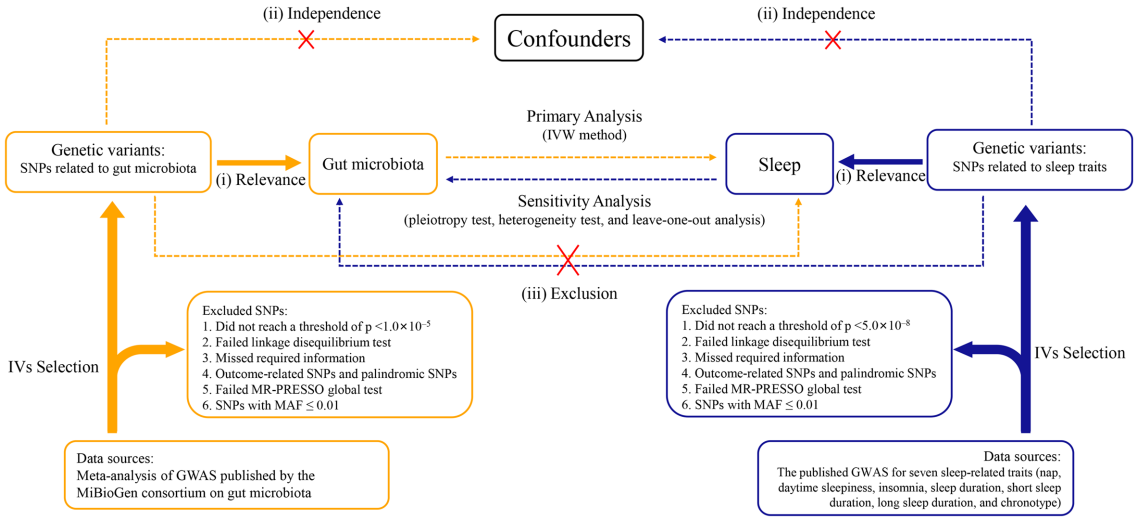

FIGURE 1
Study design of the bidirectional Mendelian randomization study on the associations of gut microbiota and sleep. IVs, instrumental variables. GWAS, genome-wide association studies. SNPs, single nucleotide polymorphisms. MR-PRESSO, Mendelian randomization pleiotropy residual sum and outlier. MAF, minor allele frequency. IVW, inverse variance weighted.

affects 10–20% of the population (Ohayon, 2008; Cohen et al., 2010). Insomnia is a common disorder, and up to 33% of the population experience transient insomnia symptoms at any given time (Morin et al., 2015). Sleep duration, as judged by self-reported data, is traditionally regarded as a continuous variable and divided into two distinct categories: short sleep duration (<7 h/night) and long sleep duration (≥9 h/night). In addition, we excluded extreme cases of sleep duration of less than 3 h or more than 18 h. Chronotype is determined by individual tendencies to sleep earlier or later, often referred to as circadian preference. Chronotype is generally treated as a continuous variable, but to provide interpretable OR in this GWAS study, a binary phenotype was also defined by using the same data field as for chronotype (Jones et al., 2019).

2.3. Selection of instrumental variables

For forward MR analysis, a sufficient number of SNPs need to be included as IVs for subsequent sensitivity analysis and horizontal pleiotropic detection. Therefore, we extracted SNPs closely related to the gut microbiota from the published data, with $p < 1.0 \times 10^{-5}$ as the primary filter. For the reverse MR analysis, SNPs were associated with sleep-related traits and reached the conventional GWAS significance threshold ($p < 5.0 \times 10^{-8}$). Then, to make sure that the IVs applied to exposure were independent, European sample data from the 1,000 Genomes project was used as the reference panel; SNPs in linkage disequilibrium (r2 < 0.001, clumping window = 10,000 kb) were excluded. We extracted SNPs associated with exposure for each outcome, and where exposed SNPs were not available they were discarded. After harmonizing exposure as well as outcome SNPs, we excluded palindromic SNPs, outliers eliminated by the MR pleiotropy residual sum and outlier (MR-PRESSO) global test, and SNPs with minor allele frequency ≤ 0.01.

2.4. Mendelian randomization analysis

For MR analysis, multiple statistical models including inverse-variance weighted (IVW), simple model, weighted model, weighted median, maximum likelihood method, and MR-Egger regression were utilized to estimate the potential bidirectional causal relationships between gut microbiota and sleep traits. We used the random-effects IVW method as the principal statistical method, and the overall estimate obtained by this method is equivalent to weighted linear regression for Wald estimates for each SNP, regardless of intercept (Burgess et al., 2013). However, in the presence of horizontal pleiotropic SNPs, the IVW results would be severely biased (Burgess et al., 2016). Therefore, we used the MR-Egger method, which provides a valid test for causal effects consistent with the IVW method, after excluding SNPs that are directly related to the results or have horizontal pleiotropy (Bowden et al., 2015). The maximum likelihood method, similar to the IVW method, can provide results with a smaller standard error than IVW in the absence of heterogeneity or horizontal pleiotropy (Hartwig et al., 2017). Complementary analyses using the simple model, weighted model, and weighted median method were used as supplements to IVW. The weighted median method gives a credible estimate even if up to half of the results come from invalid SNPs (Bowden et al., 2016). When the largest number of similar individual SNPs causal effect estimates are from efficient SNPs, the weighted model was consistent even if SNPs were invalid (Hartwig et al., 2017). And the simple mode is an unweighted mode of the empirical density function of causal estimation (Hemani et al., 2018).

2.5. Sensitivity analysis

The intercept term of MR-Egger regression was used to determine the presence of pleiotropy. When the intercept term approaches zero, it suggests that there is no horizontal pleiotropy for the SNP used in the bidirectional MR analysis. In addition, we performed the

MR-PRESSO global test to judge horizontal pleiotropy. Furthermore, we used Cochran's Q statistics and funnel plots to assess the heterogeneity of the IVW method. Moreover, to evaluate whether a single SNP impacted the main causal association, we conducted the "leave-one-out" analysis by eliminating each SNP in turn. In order to appraise the strength of IVs, we computed the F-statistic according to the following formula: $F = \frac{R^2 \times (N-1-K)}{(1-R^2) \times K}$. All the bidirectional MR analyses were performed using the two-sample MR (version 0.5.6) R packages in R (version 4.2.2). Finally, when the IVW-derived *p*-value <0.05 and the estimates of all methods were in the same direction, we considered the results of MR analysis to be nominally significant. In addition, taking into account multiple hypothesis testing, we set the *p*-value for Bonferroni correction in the forward MR analysis to 0.05/9 (0.0055) and in the reverse MR analysis to 0.05/119 (4.20×10^{-4}).

3. Results

3.1. Causal effects of gut microbiota on sleep-related traits

Based on the selection criteria of the IVs, we selected 460 SNPs for 42 bacterial taxa to uncover the potential causal associations between gut microbiota and sleep-related traits in the forward MR analysis. rs9393920 (in MR analysis of *Oscillibacter* on sleep duration) and rs736744 (in MR analysis of *Oxalobacter* on daytime sleepiness) were detected as outliers by MR-PRESSO and removed. All the F-statistics of IVs were larger than 10, which indicated weak instrument bias was unlikely. Supplementary Table S2 shows the details of the selected IVs of 42 bacterial taxa, including Beta, standard error, and *p*-values.

As shown in Figure 2 and Supplementary Table S3, genetically predicted abundances of nine genera were associated with daytime napping, 11 genera were associated with daytime sleepiness, seven genera were associated with insomnia, seven genera were associated with sleep duration, five genera were associated with long sleep duration, eight genera were associated with short sleep duration, and six genera were associated with chronotype, according to the estimates of the IVW method.

3.1.1. Daytime napping

The genetic forecast of abundance ratio of *Holdemanella* (OR: 0.989, 95% CI: 0.979–0.998, $p = 0.020$) and *Ruminococcaceae* UCG-002 (OR: 0.990, 95% CI: 0.981–0.999, $p = 0.032$) showed a negative correlation with daytime napping. The genetic forecast of abundance ratio of seven intestinal flora genera was positively correlated with daytime napping, specifically, *Ruminococcus* (*gnavus group*) (OR: 1.010, 95% CI: 1.000–1.019, $p = 0.041$), *Defluviitaleaceae* UCG-011 (OR: 1.011, 95% CI: 1.000–1.021, $p = 0.046$), *Oxalobacter* (OR: 1.011, 95% CI: 1.001–1.021, $p = 0.034$), *Eisenbergiella* (OR: 1.011, 95% CI: 1.001–1.021, $p = 0.040$), *Butyricimonas* (OR: 1.013, 95% CI: 1.001–1.024, $p = 0.035$), *Ruminococcaceae* UCG-013 (OR: 1.015, 95% CI: 1.000–1.029, $p = 0.049$), and *Lachnospiraceae* UCG-010 (OR: 1.017, 95% CI: 1.001–1.034, $p = 0.033$).

3.1.2. Daytime sleepiness

The IVW estimates suggested that the genetic forecast of abundance ratio of 11 intestinal flora genera was positively associated with daytime sleepiness, specifically, *Alloprevotella* (OR: 1.007, 95% CI: 1.000–1.014, $p = 0.048$), *Peptococcus* (OR: 1.009, 95% CI: 1.002–1.015, $p = 0.008$), *Oxalobacter* (OR: 1.014, 95% CI: 1.007–1.021, $p = 2.79E-05$), *Ruminococcus* (*gnavus group*) (OR: 1.010, 95% CI: 1.002–1.018, $p = 0.011$), *Collinsella* (OR: 1.013, 95% CI: 1.000–1.025, $p = 0.045$), *Slackia* (OR: 1.013, 95% CI: 1.001–1.026, $p = 0.006$), *Clostridium sensu stricto 1* (OR: 1.014, 95% CI: 1.002–1.025, $p = 0.021$), *Coprococcus 2* (OR: 1.014, 95% CI: 1.002–1.026, $p = 0.020$), *Coprococcus 3* (OR: 1.018, 95% CI: 1.005–1.031, $p = 0.005$), *Eubacterium* (*eligens group*) (OR: 1.016, 95% CI: 1.003–1.030, $p = 0.021$), and *Butyricimonas* (OR: 1.014, 95% CI: 1.006–1.023, $p = 0.001$).

Moreover, the protective effects of *Coprococcus 3* and *Butyricimonas* on daytime sleepiness were still significant after Bonferroni correction. However, after adjustment for body mass index, the effect of *Alloprevotella* (OR: 1.007, 95% CI: 1.000–1.014, $p = 0.051$) on daytime sleepiness was not nominally significant.

3.1.3. Insomnia

Genetically predicted relative abundance of *Odoribacter* (OR: 0.976, 95% CI: 0.954–1.000, $p = 0.044$) and *Oscillibacter* (OR: 0.985, 95% CI: 0.974–0.996, $p = 0.005$) decreased the risk of insomnia. After Bonferroni correction, the effect of *Oscillibacter* on insomnia risk remained. By contrast, five bacterial taxa increased the risk of insomnia, namely, *Rikenellaceae RC9 gut group* (OR: 1.007, 95% CI: 1.000–1.015, $p = 0.046$), *Prevotella 7* (OR: 1.009, 95% CI: 1.002–1.017, $p = 0.017$), *Marvinbryantia* (OR: 1.014, 95% CI: 1.000–1.029, $p = 0.049$), *Clostridium* (*innocuum group*) (OR: 1.018, 95% CI: 1.005–1.031, $p = 0.006$), and *Lachnoclostridium* (OR: 1.029, 95% CI: 1.007–1.052, $p = 0.009$).

3.1.4. Sleep duration

Alistipes (OR: 0.967, 95% CI: 0.938–0.997, $p = 0.032$) and *Eubacterium* (*hallii group*) (OR: 0.977, 95% CI: 0.959–0.997, $p = 0.022$) showed a negative correlation with sleep duration. By contrast, five intestinal flora genera were positively correlated with sleep duration according to the IVW estimates, namely, *Victivallis* (OR: 1.016, 95% CI: 1.003–1.028, $p = 0.013$), *Anaerofilum* (OR: 1.018, 95% CI: 1.002–1.035, $p = 0.032$), *Oscillibacter* (OR: 1.024, 95% CI: 1.005–1.043, $p = 0.012$), *Lachnospiraceae* UCG-004 (OR: 1.033, 95% CI: 1.004–1.064, $p = 0.026$), and *Odoribacter* (OR: 1.038, 95% CI: 1.001–1.077, $p = 0.043$).

3.1.5. Long sleep duration

The IVW estimates suggested that the genetic forecast of abundance ratio of *Alistipes* (OR: 0.988, 95% CI: 0.980–0.997, $p = 0.011$), *Ruminococcaceae* NK4A214 group (OR: 0.990, 95% CI: 0.983–0.998, $p = 0.009$), and *Butyricimonas* (OR: 0.994, 95% CI: 0.988–1.000, $p = 0.050$) showed a negative correlation with long sleep duration. However, *Slackia* (OR: 1.007, 95% CI: 1.000–1.014, $p = 0.037$) and *Ruminiclostridium 6* (OR: 1.009, 95% CI: 1.001–1.016, $p = 0.020$) were positively correlated with long sleep duration.

3.1.6. Short sleep duration

Coprococcus 1 (OR: 0.987, 95% CI: 0.975–1.000, $p = 0.043$), *Lachnospiraceae* UCG-004 (OR: 0.987, 95% CI: 0.978–0.997,

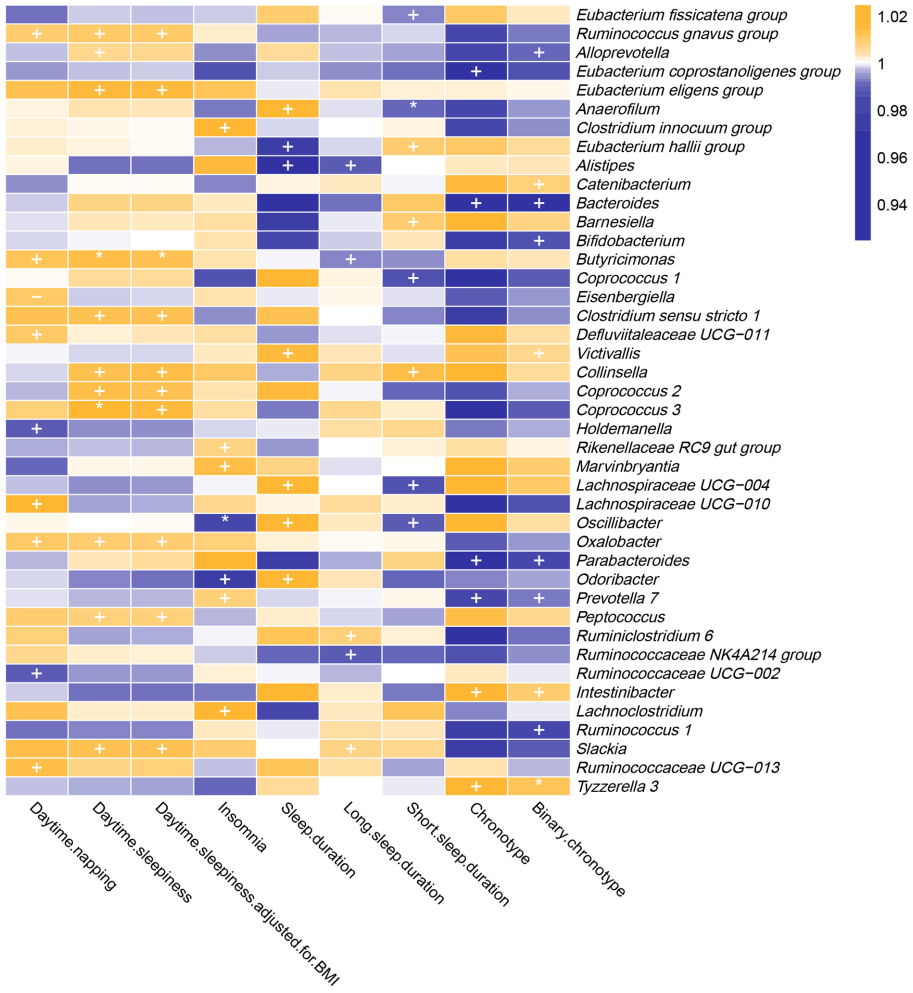

FIGURE 2
In the forward MR analysis, IVW estimates from 42 bacterial genera on seven sleep-associated traits (daytime napping, daytime sleepiness, insomnia, sleep duration, long sleep duration, short sleep duration and chronotype). The color of each block represents the OR of every MR analysis (blue, OR < 1; orange, OR > 1). *p*-values of <0.05 were marked with "+," *p*-values of <0.0055 were marked with "*" and *p*-values of <0.05 with potential pleiotropy were marked with "–".

$p = 0.013$), *Oscillibacter* (OR: 0.990, 95% CI: 0.981–0.998, $p = 0.017$), *Anaerofilum* (OR: 0.991, 95% CI: 0.985–0.997, $p = 0.003$), and *Eubacterium* (*fissicatena group*) (OR: 0.994, 95% CI: 0.988–1.000, $p = 0.041$) showed a negative correlation with short sleep duration. Three genera were positively correlated with short sleep duration, namely, *Eubacterium* (*hallii group*) (OR: 1.010, 95% CI: 1.002–1.018, $p = 0.020$), *Barnesiella* (OR: 1.010, 95% CI: 1.001–1.019, $p = 0.030$), and *Collinsella* (OR: 1.014, 95% CI: 1.001–1.027, $p = 0.037$). Furthermore, the causal link between *Anaerofilum* and short sleep duration was still significant after Bonferroni correction.

3.1.7. Chronotype

The IVW method yielded nominal associations of four intestinal flora genera with chronotype, namely, *Bacteroides* (OR: 0.955, 95% CI: 0.918–0.993, $p = 0.019$), *Parabacteroides* (OR: 0.952, 95% CI: 0.916–0.989, $p = 0.011$), *Eubacterium* (*coprostanoligenes group*) (OR: 0.961, 95% CI: 0.927–0.998, $p = 0.036$), and *Prevotella 7* (OR: 0.982, 95% CI: 0.968–0.997, $p = 0.015$). Genetically predicted relative abundance of *Intestinibacter* (OR: 1.026, 95% CI: 1.003–1.049, $p = 0.025$) and *Tyzzerella 3* (OR: 1.030, 95% CI: 1.009–1.052, $p = 0.006$) had positive causal contributions to chronotype.

After using the binary phenotype of the chronotype, the significant difference of all these associations persisted except for *Eubacterium* (*coprostanoligenes group*) (OR: 0.987, 95% CI: 0.974–1.000, $p = 0.065$). Furthermore, nominal significant effects on chronotype were observed for *Bifidobacterium* (OR: 0.987, 95% CI: 0.977–0.996, $p = 0.006$), *Ruminococcus 1* (OR: 0.986, 95% CI: 0.975–0.998, $p = 0.019$), *Catenibacterium* (OR: 1.009, 95% CI: 1.001–1.017, $p = 0.025$), *Victivallis* (OR: 1.006, 95% CI: 1.000–1.012, $p = 0.032$), and *Alloprevotella* (OR: 0.992, 95% CI: 0.985–1.000, $p = 0.037$). In addition, the influence of *Tyzzerella 3* on chronotype was more significant.

3.1.8. Sensitivity analysis

For the forward MR analysis, *p*-values derived from Cochran's Q were all >0.05, except for estimates of *Clostridium* (*innocuum group*) on insomnia, *Oxalobacter* on daytime napping and daytime sleepiness, *Lachnoclostridium* on insomnia, and *Tyzzerella 3* on chronotype, which showed that there was no significant heterogeneity. Except for

Eisenbergiella, all *p*-values of MR-Egger intercept tests were > 0.05 (Supplementary Table S4), suggesting that no horizontal pleiotropy appeared in forward MR analysis. This was also confirmed by "leave-one-out" analysis and funnel plots (Supplementary Figures S1–S73).

3.2. Causal effects of sleep-related traits on gut microbiota

According to the selection criteria of the IVs, we selected 78 SNPs for daytime napping, 33 SNPs for daytime sleepiness, 34 SNPs for insomnia, 58 SNPs for sleep duration, four SNPs for long sleep duration, 23 SNPs for short sleep duration, and 117 SNPs for chronotype. Details about the selected SNPs are displayed in Supplementary Tables S5–S13. Except for IVs for long sleep duration and short sleep duration, the F-statistics for IVs were larger than 10.

As shown in Figure 3 and Supplementary Table S14, the results of reverse MR analysis indicated that daytime napping was correlated with three bacterial taxa, daytime sleepiness was correlated with eight bacterial taxa, insomnia was correlated with five bacterial taxa, sleep duration was correlated with eight bacterial taxa, long sleep duration was correlated with four bacterial taxa, short sleep duration was correlated with eight bacterial taxa, and chronotype was correlated with five bacterial taxa.

The IVW estimates indicated that daytime napping had causal contribution to the reduction of *Fusicatenibacter* abundance (OR: 0.739, 95% CI: 0.554–0.987, $p = 0.040$), while being positively correlated with *Akkermansia* (OR: 1.530, 95% CI: 1.081–2.166, $p = 0.017$) and *Ruminococcaceae NK4A214 group* (OR: 1.527, 95% CI: 1.115–2.092, $p = 0.008$).

The IVW estimates indicated that daytime sleepiness was negatively correlated with five bacterial taxa, namely, *Oxalobacter* (OR: 0.302, 95% CI: 0.101–0.904, $p = 0.032$), *Slackia* (OR: 0.339, 95% CI: 0.135–0.854, $p = 0.022$), *Coprococcus 3* (OR: 0.541, 95% CI: 0.304–0.962, $p = 0.037$), *Blautia* (OR: 0.555, 95% CI: 0.324–0.950, $p = 0.032$), and *Dorea* (OR: 0.556, 95% CI: 0.322–0.961, $p = 0.035$). In addition, there were suggestive associations between daytime sleepiness with three bacterial taxa, namely, *Dialister* (OR: 2.122, 95% CI: 1.093–4.117, $p = 0.026$), *Flavonifractor* (OR: 2.292, 95% CI: 1.140–4.608, $p = 0.020$), and *Anaerofilum* (OR: 3.688, 95% CI: 1.246–10.916, $p = 0.018$).

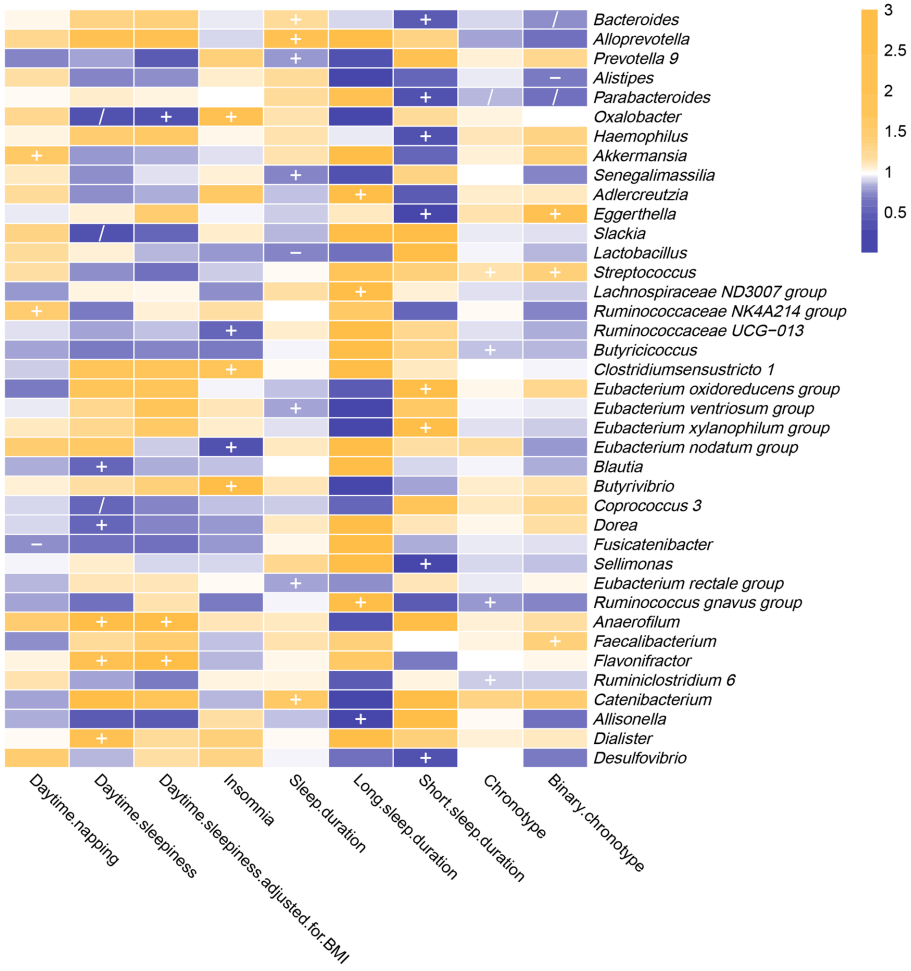

FIGURE 3
In the reverse MR analysis, IVW estimates from seven sleep-associated traits (daytime napping, daytime sleepiness, insomnia, sleep duration, long sleep duration, short sleep duration and chronotype) on 39 bacterial genera. The color of each block represents the OR of every MR analysis (blue, OR < 1; orange, OR > 1). *p*-values of <0.05 were marked with "+," *p*-values <0.05 in both forward and reverse MR analyses were marked with "/" and *p*-values of <0.05 with potential pleiotropy were marked with "–".

However, after additional adjustment for body mass index, the effects of daytime sleepiness on *Slackia*, *Dialister*, *Blautia*, *Dorea*, and *Coprococcus 3* were not significant.

Insomnia was negatively correlated with *Eubacterium* (*nodatum group*) (OR: 0.310, 95% CI: 0.100–0.961, $p = 0.043$) and *Ruminococcaceae UCG-013* (OR: 0.522, 95% CI: 0.345–0.791, $p = 0.002$), while being positively correlated with three bacterial taxa, namely, *Clostridium sensu stricto 1* (OR: 1.708, 95% CI: 1.085–2.687, $p = 0.021$), *Oxalobacter* (OR: 2.434, 95% CI: 1.104–5.369, $p = 0.027$), and *Butyrivibrio* (OR: 2.656, 95% CI: 1.005–7.016, $p = 0.049$).

The results of the IVW method revealed that sleep duration was negatively correlated with five intestinal flora genera, namely, *Senegalimassilia* (OR: 0.709, 95% CI: 0.507–0.991, $p = 0.044$), *Lactobacillus* (OR: 0.726, 95% CI: 0.534–0.988, $p = 0.041$), *Prevotella 9* (OR: 0.776, 95% CI: 0.604–0.998, $p = 0.048$), *Eubacterium* (*ventriosum group*) (OR: 0.786, 95% CI: 0.641–0.964, $p = 0.021$) and *Eubacterium* (*rectale group*) (OR: 0.794, 95% CI: 0.655–0.962, $p = 0.018$). It was positively correlated with three bacterial taxa, namely, *Bacteroides* (OR: 1.225, 95% CI: 1.016–1.477, $p = 0.033$), *Catenibacterium* (OR: 1.649, 95% CI: 1.017–2.672, $p = 0.042$), and *Alloprevotella* (OR: 1.946, 95% CI: 1.104–3.427, $p = 0.021$).

The F-statistic of SNPs for long sleep duration and short sleep duration was less than 10. Therefore, weak instrumental bias could disturb the conclusions of reverse MR analysis (Supplementary Table S15).

Chronotype was negatively correlated with the genetic forecast of abundance ratio of four bacterial taxa, specifically, *Ruminococcus* (*gnavus group*) (OR: 0.781, 95% CI: 0.654–0.933, $p = 0.006$), *Parabacteroides* (OR: 0.858, 95% CI: 0.768–0.957, $p = 0.006$), *Butyricicoccus* (OR: 0.870, 95% CI: 0.782–0.969, $p = 0.011$), and *Ruminiclostridium 6* (OR: 0.884, 95% CI: 0.783–0.998, $p = 0.047$). It was positively correlated with *Streptococcus* (OR: 1.129, 95% CI: 1.011–1.260, $p = 0.031$). However, after using the binary phenotype of the chronotype, the associations of chronotype with *Ruminococcus* (*gnavus group*), *Butyricicoccus*, and *Ruminiclostridium 6* became insignificant. In addition, significant effects of chronotype on *Eggerthella* (OR: 2.124, 95% CI: 1.145–3.941, $p = 0.017$), *Alistipes* (OR: 0.689, 95% CI: 0.489–0.972, $p = 0.034$), *Bacteroides* (OR: 0.736, 95% CI: 0.543–0.997, $p = 0.048$), and *Faecalibacterium* (OR: 1.399, 95% CI: 1.001–1.954, $p = 0.049$) were observed.

For the reverse MR analysis, *p*-values derived from Cochran's Q were all >0.05 (Supplementary Table S15). In other words, there was no evidence of significant heterogeneity. Except for *Fusicatenibacter*, *Lactobacillus*, and *Alistipes*, all *p*-values of MR-Egger intercept tests were > 0.05, suggesting that no horizontal pleiotropy appeared. Furthermore, through funnel plots and "leave-one-out" analysis, we found no causal associations between sleep-related traits and bacterial genera that were primarily driven by any single SNP (Supplementary Figures S74–S123).

4. Discussion

To the best of our knowledge, this is the first bidirectional MR analysis that comprehensively clarifies causal relationships between gut microbiota and sleep-related traits. As shown in Figures 2, 3, our findings indicate that a total of 68 bacterial taxa are causally associated with seven sleep-related traits. Furthermore, 13 bacterial taxa related to sleep-related features in forward MR analysis were regulated by sleep-related traits, including *Alistipes*, *Alloprevotella*, *Anaerofilum*, *Bacteroides*, *Catenibacterium*, *Coprococcus 3*, *Oxalobacter*, *Parabacteroides*, *Ruminiclostridium 6*, *Ruminococcaceae NK4A214 group*, *Ruminococcaceae UCG-013*, *Ruminococcus gnavus group*, and *Slackia*. Nevertheless, the potential causal effects of *Coprococcus 3*, *Oxalobacter*, and *Slackia* on daytime sleepiness, and the potential causal effect of *Parabacteroides* and *Bacteroides* on chronotype in forward MR analysis were not supported by the results of reverse MR analysis. However, these findings did not exclude the possibility that the effects are interactive. Moreover, owing to potential pleiotropy, some causal effects (*Eisenbergiella* on daytime napping, daytime napping on *Fusicatenibacter*, sleep duration on *Lactobacillus*, and binary chronotype on *Alistipes*) were not credible. After excluding the above uncertain causal effects, a total of 40 bacterial taxa had potential causal effects on seven sleep-related traits, which in the other direction may be related to 34 bacterial taxa, and most of the bacterial taxa were of *Bacillota* (Figure 4).

Growing evidence from observational studies indicates that gut microbiota is correlated with sleep-related traits and disorders, and that the absence of gut microbes and their metabolites may alter sleep traits and architecture (Leone et al., 2015; Paulsen et al., 2017; Szentirmai et al., 2019). Szentirmai et al. found that the intestinal microbiome induces non-REM sleep through butyrate-sensitive mechanisms (Szentirmai et al., 2019). Cross-feeding is the central metabolic mechanism of the gut microbiota. *Faecalibacterium* can produce butyrate from acetate and lactate, which are produced by *Bifidobacteria* from fermented carbohydrates. Moreover, the coculture of *Eubacterium hallii group* with *Bifidobacterium* promotes the accumulation of butyrate through cross-feeding (Belenguer et al., 2006). *Butyricimonas*, *Marvinbryantia*, *Holdemanella*, *Intestinibacter*, *Ruminococcaceae NK4A214 group*, *Clostridium sensu stricto 1*, and *Oscillibacter* have also been associated with the production of butyrate, while *Eggerthella* is involved in the depletion of butyrate (Chen et al., 2021; Liu et al., 2022). Consistent with these previous studies, our study found that these butyrate-producing bacteria (*Bifidobacterium*, *Clostridium sensu stricto 1*, *Eubacterium hallii group*, *Holdemanella*, *Intestinibacter*, *Marvinbryantia*, *Oscillibacter*, and *Ruminococcaceae NK4A214 group*) all had a nominally significant causal association with sleep (Figure 5). This finding suggests that these intestinal microbiotas associated with butyrate metabolism are involved in sleep-related regulatory mechanisms (Figure 6). Lipopolysaccharides and peptidoglycans, which are components of bacterial cell walls, are released during the decomposition or division of bacteria and then produce an inflammatory response by activating the expression of proinflammatory factors (Motta et al., 2015; Krueger and Opp, 2016). Previous research has confirmed that these inflammatory responses are related to the sleep that occurs during bacterial infections. However, the butyrate produced by intestinal flora has a strong anti-inflammatory effect and can inhibit inflammation in the colon and liver as well as the expression of inflammatory factors induced by lipopolysaccharides and NF-κB activation (Perez et al., 1998; Thangaraju et al., 2009; D'Souza et al., 2017).

Metabolites of gut microbes such as short-chain fatty acids, butyrate and, acetate may also regulate circadian rhythms by influencing the expression of circadian clock genes (Figure 6). Wang et al. have demonstrated that the gut microbiome modulates the expression of the circadian transcription factor NFIL 3 (Wang et al.,

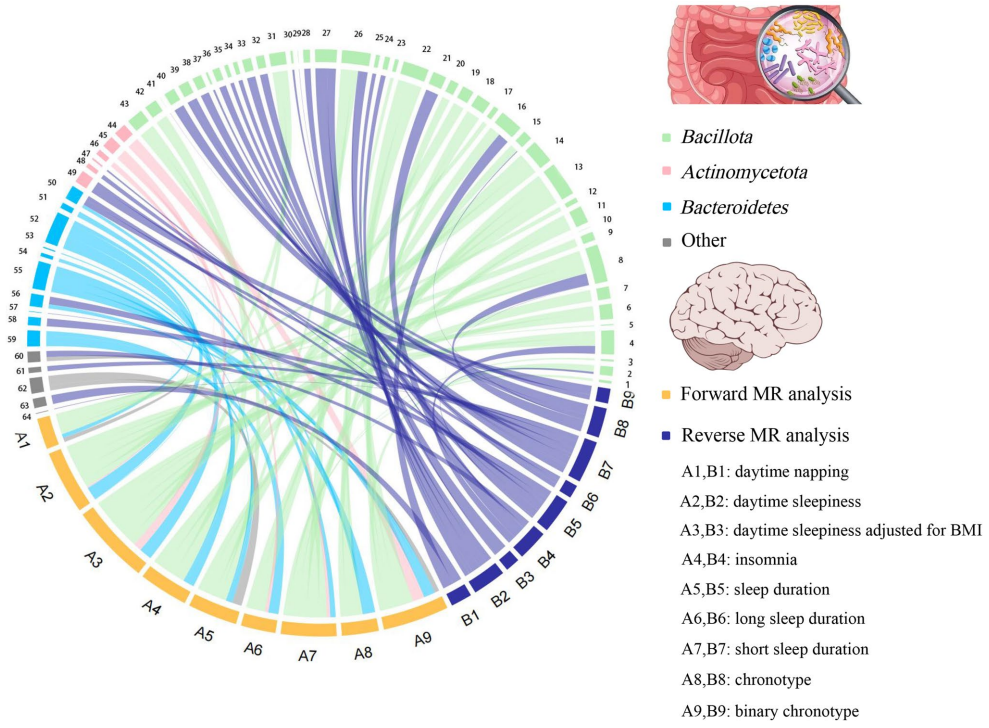

FIGURE 4
The chord plot showed the causal relationships between gut microbiota and sleep. 1: *Eubacterium fissicatena* group; 2: Catenibacterium; 3: Coprococcus 1; 4: Clostridium *sensu stricto* 1; 5: Defluviitaleaceae UCG011; 6: Coprococcus 2; 7: Coprococcus 3; 8: *Ruminococcus gnavus* group; 9: Holdemanella; 10: Marvinbryantia; 11: Lachnospiraceae UCG004; 12: Lachnospiraceae UCG010; 13: Oscillibacter; 14: Peptococcus; 15: Ruminiclostridium 6; 16: Ruminococcaceae NK4A214 group; 17: Ruminococcaceae UCG002; 18: Intestinibacter; 19: Lachnoclostridium; 20: Ruminococcus 1; 21: Ruminococcaceae UCG013; 22: Tyzzerella 3; 23: *Eubacterium coprostanoligenes* group; 24: Blautia; 25: Dorea; 26: Anaerofilum; 27: Flavonifractor; 28: Dialister; 29: Butyrivibrio; 30: *Eubacterium nodatum* group; 31: *Eubacterium eligens* group; 32: *Eubacterium ventriosum* group; 33: *Eubacterium rectale* group; 34: Lachnospiraceae ND3007 group; 35: Allisonella; 36: *Eubacterium oxidoreducens* group; 37: *Eubacterium xylanophilum* group; 38: Sellimonas; 39: Streptococcus; 40: Butyricicoccus; 41: Faecalibacterium; 42: *Clostridium innocuum* group; 43: *Eubacterium hallii* group; 44: Bifidobacterium; 45: Collinsella; 46: Slackia; 47: Senegalimassilia; 48: Adlercreutzia; 49: Eggerthella; 50: Bacteroides; 51: Barnesiella; 52: Butyricimonas; 53: Rikenellaceae RC9 gut group; 54: Odoribacter; 55: Prevotella7; 56: Alloprevotella; 57: Prevotella9; 58: Parabacteroides; 59: Alistipes; 60: Oxalobacter; 61: Haemophilus; 62: Victivallis; 63: Akkermansia; 64: Desulfovibrio.

2017). Furthermore, the absence of gut microbiota and gut microbial metabolites such as butyrate and acetic can led to significant differential expression of hepatic and central circadian clock genes regardless of dietary changes (Leone et al., 2015). An observational study determined that short-chain fatty acids, propionate, and butyrate in feces were associated with nighttime sleep duration in infants (Heath et al., 2020). Another observational study also found that changes in abundance of *Lachnospira*, *Bacteroides*, *Faecalibacterium*, and *Blautia* were significantly associated with sleep quality and disorders (Li et al., 2020), which correspond to our findings. Yu et al. found that after giving mice oral high doses of gamma-aminobutyric acid fermented milk, the relative abundance of *Ruminococcus*, *Allobaculum*, and *Adlercreutzia*, and the levels of short-chain fatty acids increased significantly and sleep time was significantly prolonged (Yu et al., 2020). This result suggests that diet may affect sleep by regulating the intestinal microbiota. These previous studies and our research show that the gut microbiota and its metabolites can participate in the regulation of sleep.

The relative abundance of gut microbiota is unique between individuals, and under healthy conditions, the gut microbiota displays resilience and stability. However, the "healthy" microbiome can be disrupted by changes in age, disease and environmental factors (Hou et al., 2022). Sleep disturbances or circadian rhythm disturbances have also been reported to disrupt the balance of the gut microbiota. Circadian rhythms are essential for maintaining normal physiological functions of the gastrointestinal tract, and circadian rhythm disorders are closely related to certain diseases of the digestive system (Schernhammer et al., 2003; Hoogerwerf et al., 2007; Nojkov et al., 2010). *In vitro* experiments by Summa et al. proved that circadian rhythm disturbance and sleep fragmentation lead to the destruction of the integrity of intestinal barrier function, which in turn increased intestinal permeability (Summa et al., 2013). This increased intestinal permeability may lead to translocations of gut microbiota and its metabolites, which alters the variety and abundance of gut microbiota. Poroyko et al. also demonstrated through *in vitro* experiments that sleep fragmentation can induce selective changes in intestinal flora, such as reducing the abundance of *Bacteroidetes*, *Actinobacteria*, and *Bifidobacteriaceae* (Poroyko et al., 2016). However, the disruption of the integrity of the intestinal barrier caused by sleep disorder may be related to its suppression of melatonin levels (Gao et al., 2019). Gao et al. found that the decrease in the abundance of *Faecalibacterium*, *Bacteroides*, and *Akkermansia* caused by sleep deprivation was associated with decreased levels of melatonin (Gao et al., 2019). Consistent with these conclusions, we also found nominally causal

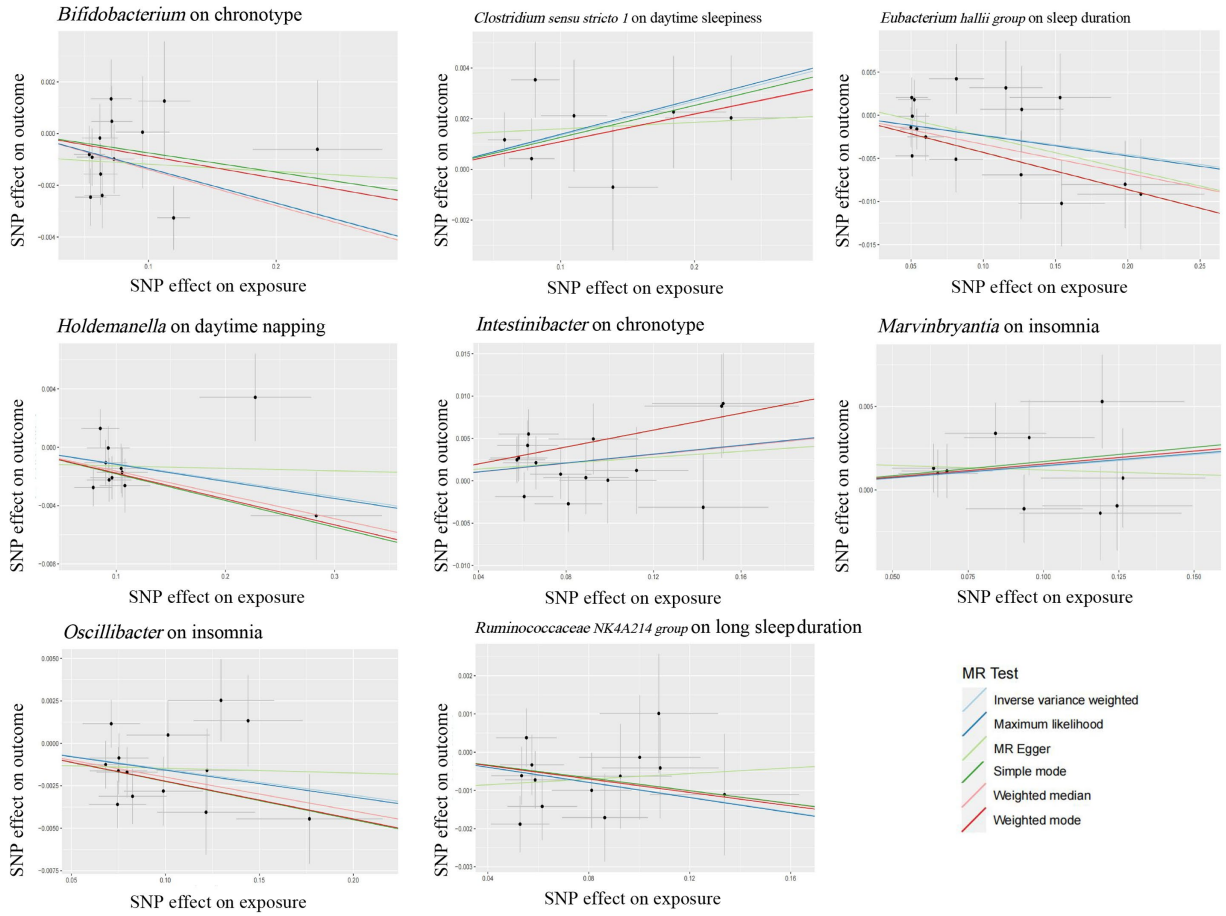

FIGURE 5
Scatter plots for the causal association between several bacteria associated with butyrate-producing and sleep.

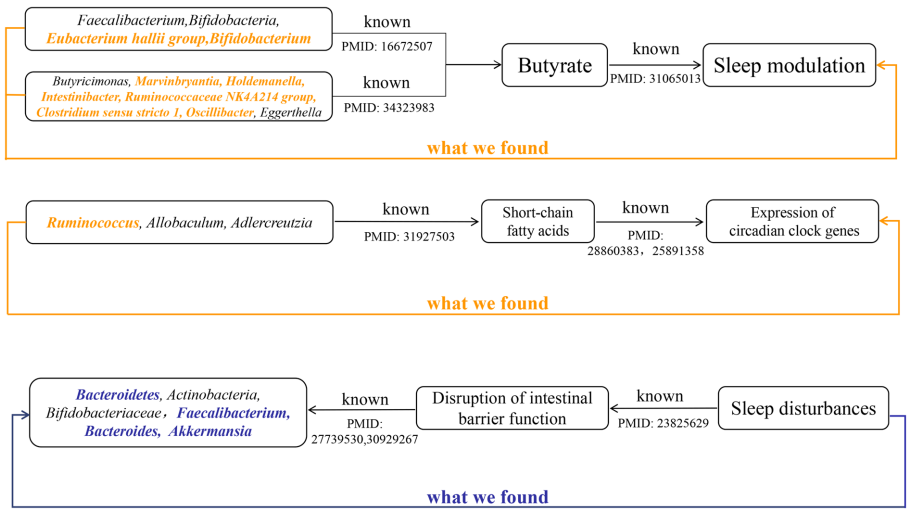

FIGURE 6
The summary of the findings in our study and the existing knowledge in literature about different mechanisms that affect the sleep. Black indicated known evidence, bold orange italics indicated the findings by forward MR analysis, and bold blue italics indicated the findings by reverse MR analysis.

effects of sleep disorder or sleep fragmentation on these bacterial taxa (Figure 6).

The previous studies mentioned above demonstrate that gut microbiota are involved in circadian rhythm regulation and show that circadian rhythm disturbances may cause changes in gut microbiota abundance by damaging the intestinal barrier or inducing changes in melatonin. This is consistent with the results from 13 bacterial taxa found in our study that were both involved in and subject to sleep regulation, which suggests that regulation between gut microbiota and sleep may be bidirectional.

A major advantage of this study was that MR analysis effectively excluded the interference of reverse causation and possible confounding factors in inferring causal effects between gut microbiota and sleep-related traits. The SNPs of the intestinal microbiota came from the largest GWAS meta-analysis available, and the sample sizes were large enough to ensure the strength of the IVs and the robustness of the results. The design of the two-sample MR further avoided bias resulting from overlapping data on exposure and outcome pools. Utilization of various statistical models (such as IVW, weighted median, and maximum likelihood method) as well as sensitivity analyses (such as MR-PRESSO and MR-Egger regression intercept term tests) ensured the confidence of causal effect estimates.

However, our study also had some limitations. First, genus level was the lowest classification level in the data for gut microbiota, which limited the ability to uncover causal relationships between gut microbes and sleep at the species level. Second, the SNPs we utilized in the forward MR analysis did not meet the conventional GWAS threshold ($p < 5 \times 10^{-8}$), but were rescued by Bonferroni correction, which ruled out false positive results to the greatest extent. Third, the participants of gut microbiota and sleep in the GWAS meta-analysis were primarily of European ancestry. The same genetic variant may have different pleiotropic effects in different ethnic populations; therefore, the inference of causal effects derived in our study may not be applicable in non-European populations. Fourth, in the reverse MR analysis, estimates of effects may have been biased by weak IVs because of the small sample size of the GWAS meta-analysis for sleep-related traits. Finally, we applied a number of exclusion criteria to select IVs; however, many internal and external factors affect gut microbes and sleep. Thus, bias resulting from SNPs being associated with potential risk factors cannot be completely ruled out.

In conclusion, this study represents the first bidirectional MR analysis to systematically reveal the causal association between gut microbiota and sleep. Our findings suggest the possible causal effect of 42 bacterial genera on sleep-related traits. Conversely, sleep-related traits may also be involved in the regulation of the abundance of 39 bacterial genera. In addition, 13 of these bacterial genera overlapped, which provides suggestive evidence for a reciprocal role between gut microbiota and sleep. The demonstration of a causal relationship between sleep and gut microbiota provides support for techniques to modify sleep by manipulating the gut microbiome. However, the basic mechanism of gut microbiota on sleep is still unknown, and more research is needed to provide theoretical support for targeted intervention in sleep by regulating specific gut microbiota.

Data availability statement

Publicly available datasets were analyzed in this study. This data can be found at: Summary statistics for the sleep traits are available at: (http://sleepdisordergenetics.org/). Summary statistics for the gut microbiota are available at: (https://mibiogen.gcc.rug.nl/).

Author contributions

DO and JW designed the research. JW, BZ, and SZ collected and analyzed the data and drafted the manuscript. DO, XZ, and XL supervised the study. JW, ZH, and YX were involved in writing the manuscript. All authors contributed to the article and approved the submitted version.

Funding

This work was supported by the National Natural Science Foundation of China (NO. 82271336) and Taizhou "500 Elite Plan" high-level talent project.

Acknowledgments

The data analyzed in this study was provided by MiBioGen consortium and UK Biobank. We gratefully acknowledge their contributing studies and the participants in the corresponding studies without whom this effort would not be possible.

Conflict of interest

The authors declare that the research was conducted in the absence of any commercial or financial relationships that could be construed as a potential conflict of interest.

Publisher's note

Supplementary material

The Supplementary material for this article can be found online at: https://www.frontiersin.org/articles/10.3389/fmicb.2023.1236847/full#supplementary-material

References

Belenguer, A., Duncan, S. H., Calder, A. G., Holtrop, G., Louis, P., Lobley, G. E., et al. (2006). Two routes of metabolic cross-feeding between *Bifidobacterium* adolescentis and butyrate-producing anaerobes from the human gut. *Appl. Environ. Microbiol.* 72, 3593–3599. doi: 10.1128/AEM.72.5.3593-3599.2006

Benedict, C., Vogel, H., Jonas, W., Woting, A., Blaut, M., Schürmann, A., et al. (2016). Gut microbiota and glucometabolic alterations in response to recurrent partial sleep deprivation in normal-weight young individuals. *Mol. Metab.* 5, 1175–1186. doi: 10.1016/j.molmet.2016.10.003

Bowden, J., Davey Smith, G., and Burgess, S. (2015). Mendelian randomization with invalid instruments: effect estimation and bias detection through egger regression. *Int. J. Epidemiol.* 44, 512–525. doi: 10.1093/ije/dyv080

Bowden, J., Davey Smith, G., Haycock, P. C., and Burgess, S. (2016). Consistent estimation in Mendelian randomization with some invalid instruments using a weighted median estimator. *Genet. Epidemiol.* 40, 304–314. doi: 10.1002/gepi.21965

Burgess, S., Butterworth, A., and Thompson, S. G. (2013). Mendelian randomization analysis with multiple genetic variants using summarized data. *Genet. Epidemiol.* 37, 658–665. doi: 10.1002/gepi.21758

Burgess, S., Dudbridge, F., and Thompson, S. G. (2016). Combining information on multiple instrumental variables in Mendelian randomization: comparison of allele score and summarized data methods. *Stat. Med.* 35, 1880–1906. doi: 10.1002/sim.6835

Celis-Morales, C., Lyall, D. M., Guo, Y., Steell, L., Llanas, D., Ward, J., et al. (2017). Sleep characteristics modify the association of genetic predisposition with obesity and anthropometric measurements in 119,679 UK biobank participants. *Am. J. Clin. Nutr.* 105, 980–990. doi: 10.3945/ajcn.116.147231

Chen, Z., Radjabzadeh, D., Chen, L., Kurilshikov, A., Kavousi, M., Ahmadizar, F., et al. (2021). Association of Insulin Resistance and Type 2 diabetes with gut microbial diversity: a microbiome-wide analysis from population studies. *JAMA Netw. Open* 4:e2118811. doi: 10.1001/jamanetworkopen.2021.18811

Cohen, D. A., Wang, W., Wyatt, J. K., Kronauer, R. E., Dijk, D.-J., Czeisler, C. A., et al. (2010). Uncovering residual effects of chronic sleep loss on human performance. *Sci. Transl. Med.* 2:14ra3. doi: 10.1126/scitranslmed.3000458

Dashti, H. S., Daghlas, I., Lane, J. M., Huang, Y., Udler, M. S., Wang, H., et al. (2021). Genetic determinants of daytime napping and effects on cardiometabolic health. *Nat. Commun.* 12:900. doi: 10.1038/s41467-020-20585-3

Davey Smith, G., and Hemani, G. (2014). Mendelian randomization: genetic anchors for causal inference in epidemiological studies. *Hum. Mol. Genet.* 23, R89–R98. doi: 10.1093/hmg/ddu328

Davies, N. M., Holmes, M. V., and Davey Smith, G. (2018). Reading Mendelian randomisation studies: a guide, glossary, and checklist for clinicians. *BMJ* 362:k601. doi: 10.1136/bmj.k601

Di, H., Guo, Y., Daghlas, I., Wang, L., Liu, G., Pan, A., et al. (2022). Evaluation of sleep habits and disturbances among US adults, 2017–2020. *JAMA Netw. Open* 5:e2240788. doi: 10.1001/jamanetworkopen.2022.40788

D'Souza, W. N., Douangpanya, J., Mu, S., Jaeckel, P., Zhang, M., Maxwell, J. R., et al. (2017). Differing roles for short chain fatty acids and GPR43 agonism in the regulation of intestinal barrier function and immune responses. *PLoS One* 12:e0180190. doi: 10.1371/journal.pone.0180190

Gao, T., Wang, Z., Dong, Y., Cao, J., and Chen, Y. (2023). Butyrate ameliorates insufficient sleep-induced intestinal mucosal damage in humans and mice. *Microbiol. Spectr.* 11:e0200022. doi: 10.1128/spectrum.02000-22

Gao, T., Wang, Z., Dong, Y., Cao, J., Lin, R., Wang, X., et al. (2019). Role of melatonin in sleep deprivation-induced intestinal barrier dysfunction in mice. *J. Pineal Res.* 67:e12574. doi: 10.1111/jpi.12574

Han, H., Wang, Y., Li, T., Feng, C., Kaliszewski, C., Su, Y., et al. (2023). Sleep duration and risks of incident cardiovascular disease and mortality among people with type 2 diabetes. *Diabetes Care* 46, 101–110. doi: 10.2337/dc22-1127

Harknett, K., Schneider, D., and Irwin, V. (2021). Improving health and economic security by reducing work schedule uncertainty. *Proc. Natl. Acad. Sci. U. S. A.* 118:e2107828118. doi: 10.1073/pnas.2107828118

Hartwig, F. P., Davey Smith, G., and Bowden, J. (2017). Robust inference in summary data Mendelian randomization via the zero modal pleiotropy assumption. *Int. J. Epidemiol.* 46, 1985–1998. doi: 10.1093/ije/dyx102

Heath, A.-L. M., Haszard, J. J., Galland, B. C., Lawley, B., Rehrer, N. J., Drummond, L. N., et al. (2020). Association between the faecal short-chain fatty acid propionate and infant sleep. *Eur. J. Clin. Nutr.* 74, 1362–1365. doi: 10.1038/s41430-019-0556-0

Hemani, G., Zheng, J., Elsworth, B., Wade, K. H., Haberland, V., Baird, D., et al. (2018). The MR-base platform supports systematic causal inference across the human phenome. *elife* 7:e34408. doi: 10.7554/eLife.34408

Ho, Y.-T., Tsai, Y.-C., Kuo, T. B. J., and Yang, C. C. H. (2021). Effects of *Lactobacillus plantarum* PS128 on depressive symptoms and sleep quality in self-reported insomniacs: a randomized, double-blind, placebo-controlled pilot trial. *Nutrients* 13:2820. doi: 10.3390/nu13082820

Hoogerwerf, W. A., Hellmich, H. L., Cornélissen, G., Halberg, F., Shahinian, V. B., Bostwick, J., et al. (2007). Clock gene expression in the murine gastrointestinal tract: endogenous rhythmicity and effects of a feeding regimen. *Gastroenterology* 133, 1250–1260. doi: 10.1053/j.gastro.2007.07.009

Hou, K., Wu, Z.-X., Chen, X.-Y., Wang, J.-Q., Zhang, D., Xiao, C., et al. (2022). Microbiota in health and diseases. *Signal Transduct. Target. Ther.* 7:135. doi: 10.1038/s41392-022-00974-4

Itani, O., Jike, M., Watanabe, N., and Kaneita, Y. (2017). Short sleep duration and health outcomes: a systematic review, meta-analysis, and meta-regression. *Sleep Med.* 32, 246–256. doi: 10.1016/j.sleep.2016.08.006

Jehan, S., Zizi, F., Pandi-Perumal, S. R., Myers, A. K., Auguste, E., Jean-Louis, G., et al. (2017). Shift work and sleep: medical implications and management. *Sleep Med. Disord.* 1:00008. doi: 10.15406/smdij.2017.01.00008

Jike, M., Itani, O., Watanabe, N., Buysse, D. J., and Kaneita, Y. (2018). Long sleep duration and health outcomes: a systematic review, meta-analysis and meta-regression. *Sleep Med. Rev.* 39, 25–36. doi: 10.1016/j.smrv.2017.06.011

Jones, S. E., Lane, J. M., Wood, A. R., van Hees, V. T., Tyrrell, J., Beaumont, R. N., et al. (2019). Genome-wide association analyses of chronotype in 697,828 individuals provides insights into circadian rhythms. *Nat. Commun.* 10:343. doi: 10.1038/s41467-018-08259-7

Krueger, J. M., and Opp, M. R. (2016). Sleep and microbes. *Int. Rev. Neurobiol.* 131, 207–225. doi: 10.1016/bs.irn.2016.07.003

Lee, H. J., Hong, J. K., Kim, J.-K., Kim, D.-H., Jang, S. W., Han, S.-W., et al. (2021). Effects of probiotic NVP-1704 on mental health and sleep in healthy adults: an 8-week randomized, double-blind, placebo-controlled trial. *Nutrients* 13:2660. doi: 10.3390/nu13082660

Leone, V., Gibbons, S. M., Martinez, K., Hutchison, A. L., Huang, E. Y., Cham, C. M., et al. (2015). Effects of diurnal variation of gut microbes and high-fat feeding on host circadian clock function and metabolism. *Cell Host Microbe* 17, 681–689. doi: 10.1016/j.chom.2015.03.006

Li, Y., Zhang, B., Zhou, Y., Wang, D., Liu, X., Li, L., et al. (2020). Gut microbiota changes and their relationship with inflammation in patients with acute and chronic insomnia. *Nat. Sci. Sleep* 12, 895–905. doi: 10.2147/NSS.S271927

Liu, X., Tong, X., Zou, Y., Lin, X., Zhao, H., Tian, L., et al. (2022). Mendelian randomization analyses support causal relationships between blood metabolites and the gut microbiome. *Nat. Genet.* 54, 52–61. doi: 10.1038/s41588-021-00968-y

Morin, C. M., Drake, C. L., Harvey, A. G., Krystal, A. D., Manber, R., Riemann, D., et al. (2015). Insomnia disorder. *Nat. Rev. Dis. Primers* 1:15026. doi: 10.1038/nrdp.2015.26

Morin, C. M., LeBlanc, M., Daley, M., Gregoire, J. P., and Mérette, C. (2006). Epidemiology of insomnia: prevalence, self-help treatments, consultations, and determinants of help-seeking behaviors. *Sleep Med.* 7, 123–130. doi: 10.1016/j.sleep.2005.08.008

Motta, V., Soares, F., Sun, T., and Philpott, D. J. (2015). NOD-like receptors: versatile cytosolic sentinels. *Physiol. Rev.* 95, 149–178. doi: 10.1152/physrev.00009.2014

Murdock, K. K., Horissian, M., and Crichlow-Ball, C. (2017). Emerging Adults' text message use and sleep characteristics: a multimethod, naturalistic study. *Behav. Sleep Med.* 15, 228–241. doi: 10.1080/15402002.2015.1120203

Neuman, H., Debelius, J. W., Knight, R., and Koren, O. (2015). Microbial endocrinology: the interplay between the microbiota and the endocrine system. *FEMS Microbiol. Rev.* 39, 509–521. doi: 10.1093/femsre/fuu010

Nishida, K., Sawada, D., Kuwano, Y., Tanaka, H., and Rokutan, K. (2019). Health benefits of *Lactobacillus gasseri* CP2305 tablets in young adults exposed to chronic stress: a randomized, double-blind, placebo-controlled study. *Nutrients* 11:1859. doi: 10.3390/nu11081859

Nojkov, B., Rubenstein, J. H., Chey, W. D., and Hoogerwerf, W. A. (2010). The impact of rotating shift work on the prevalence of irritable bowel syndrome in nurses. *Am. J. Gastroenterol.* 105, 842–847. doi: 10.1038/ajg.2010.48

Ohayon, M. M. (2002). Epidemiology of insomnia: what we know and what we still need to learn. *Sleep Med. Rev.* 6, 97–111. doi: 10.1053/smrv.2002.0186

Ohayon, M. M. (2008). From wakefulness to excessive sleepiness: what we know and still need to know. *Sleep Med. Rev.* 12, 129–141. doi: 10.1016/j.smrv.2008.01.001

Paulsen, J. A., Ptacek, T. S., Carter, S. J., Liu, N., Kumar, R., Hyndman, L., et al. (2017). Gut microbiota composition associated with alterations in cardiorespiratory fitness and psychosocial outcomes among breast cancer survivors. *Support Care Cancer* 25, 1563–1570. doi: 10.1007/s00520-016-3568-5

Perez, R. V., Johnson, J., Hubbard, N. E., Erickson, K., Morgan, M., Kim, S., et al. (1998). Selective targeting of Kupffer cells with liposomal butyrate augments portal venous transfusion-induced immunosuppression. *Transplantation* 65, 1294–1298. doi: 10.1097/00007890-199805270-00002

Poroyko, V. A., Carreras, A., Khalyfa, A., Khalyfa, A. A., Leone, V., Peris, E., et al. (2016). Chronic sleep disruption alters gut microbiota, induces systemic and adipose tissue inflammation and insulin resistance in mice. *Sci. Rep.* 6:35405. doi: 10.1038/srep35405

Raven, F., Van der Zee, E. A., Meerlo, P., and Havekes, R. (2018). The role of sleep in regulating structural plasticity and synaptic strength: implications for memory and cognitive function. *Sleep Med. Rev.* 39, 3–11. doi: 10.1016/j.smrv.2017.05.002

Rinninella, E., Raoul, P., Cintoni, M., Franceschi, F., Miggiano, G. A. D., Gasbarrini, A., et al. (2019). What is the healthy gut microbiota composition? A changing ecosystem across age, environment, diet, and diseases. *Microorganisms* 7:14. doi: 10.3390/microorganisms7010014

Sayón-Orea, C., Bes-Rastrollo, M., Carlos, S., Beunza, J. J., Basterra-Gortari, F. J., and Martínez-González, M. A. (2013). Association between sleeping hours and siesta and

the risk of obesity: the SUN Mediterranean cohort. *Obes. Facts* 6, 337–347. doi: 10.1159/000354746

Schernhammer, E. S., Laden, F., Speizer, F. E., Willett, W. C., Hunter, D. J., Kawachi, I., et al. (2003). Night-shift work and risk of colorectal cancer in the nurses' health study. *J. Natl. Cancer Inst.* 95, 825–828. doi: 10.1093/jnci/95.11.825

Sen, P., Molinero-Perez, A., O'Riordan, K. J., McCafferty, C. P., O'Halloran, K. D., and Cryan, J. F. (2021). Microbiota and sleep: awakening the gut feeling. *Trends Mol. Med.* 27, 935–945. doi: 10.1016/j.molmed.2021.07.004

Smith, G. D., and Ebrahim, S. (2003). 'Mendelian randomization': can genetic epidemiology contribute to understanding environmental determinants of disease? *Int. J. Epidemiol.* 32, 1–22. doi: 10.1093/ije/dyg070

Sulaman, B. A., Wang, S., Tyan, J., and Eban-Rothschild, A. (2023). Neuro-orchestration of sleep and wakefulness. *Nat. Neurosci.* 26, 196–212. doi: 10.1038/s41593-022-01236-w

Summa, K. C., Voigt, R. M., Forsyth, C. B., Shaikh, M., Cavanaugh, K., Tang, Y., et al. (2013). Disruption of the circadian clock in mice increases intestinal permeability and promotes alcohol-induced hepatic pathology and inflammation. *PLoS One* 8:e67102. doi: 10.1371/journal.pone.0067102

Sun, X., Liu, B., Liu, S., Wu, D. J. H., Wang, J., Qian, Y., et al. (2022). Sleep disturbance and psychiatric disorders: a bidirectional Mendelian randomisation study. *Epidemiol. Psychiatr. Sci.* 31:e26. doi: 10.1017/S2045796021000810

Sun, J., Wang, M., Yang, L., Zhao, M., Bovet, P., and Xi, B. (2020). Sleep duration and cardiovascular risk factors in children and adolescents: a systematic review. *Sleep Med. Rev.* 53:101338. doi: 10.1016/j.smrv.2020.101338

Swerdlow, D. I., Kuchenbaecker, K. B., Shah, S., Sofat, R., Holmes, M. V., White, J., et al. (2016). Selecting instruments for Mendelian randomization in the wake of genome-wide association studies. *Int. J. Epidemiol.* 45, 1600–1616. doi: 10.1093/ije/dyw088

Szentirmai, É., and Krueger, J. M. (2014). Sickness behaviour after lipopolysaccharide treatment in ghrelin deficient mice. *Brain Behav. Immun.* 36, 200–206. doi: 10.1016/j.bbi.2013.11.017

Szentirmai, É., Massie, A. R., and Kapás, L. (2021). Lipoteichoic acid, a cell wall component of gram-positive bacteria, induces sleep and fever and suppresses feeding. *Brain Behav. Immun.* 92, 184–192. doi: 10.1016/j.bbi.2020.12.008

Szentirmai, É., Millican, N. S., Massie, A. R., and Kapás, L. (2019). Butyrate, a metabolite of intestinal bacteria, enhances sleep. *Sci. Rep.* 9:7035. doi: 10.1038/s41598-019-43502-1

Thangaraju, M., Cresci, G. A., Liu, K., Ananth, S., Gnanaprakasam, J. P., Browning, D. D., et al. (2009). GPR109A is a G-protein-coupled receptor for the bacterial fermentation product butyrate and functions as a tumor suppressor in colon. *Cancer Res.* 69, 2826–2832. doi: 10.1158/0008-5472.CAN-08-4466

Thomée, S., Härenstam, A., and Hagberg, M. (2011). Mobile phone use and stress, sleep disturbances, and symptoms of depression among young adults--a prospective cohort study. *BMC Public Health* 11:66. doi: 10.1186/1471-2458-11-66

Van Someren, E. J. W. (2021). Brain mechanisms of insomnia: new perspectives on causes and consequences. *Physiol. Rev.* 101, 995–1046. doi: 10.1152/physrev.00046.2019

Wang, Y., Kuang, Z., Yu, X., Ruhn, K. A., Kubo, M., and Hooper, L. V. (2017). The intestinal microbiota regulates body composition through NFIL3 and the circadian clock. *Science* 357, 912–916. doi: 10.1126/science.aan0677

Wang, Z., Wang, Z., Lu, T., Chen, W., Yan, W., Yuan, K., et al. (2022). The microbiota-gut-brain axis in sleep disorders. *Sleep Med. Rev.* 65:101691. doi: 10.1016/j.smrv.2022.101691

Winer, J. R., Deters, K. D., Kennedy, G., Jin, M., Goldstein-Piekarski, A., Poston, K. L., et al. (2021). Association of Short and Long Sleep Duration with Amyloid-β Burden and cognition in aging. *JAMA Neurol.* 78, 1187–1196. doi: 10.1001/jamaneurol.2021.2876

Yu, L., Han, X., Cen, S., Duan, H., Feng, S., Xue, Y., et al. (2020). Beneficial effect of GABA-rich fermented milk on insomnia involving regulation of gut microbiota. *Microbiol. Res.* 233:126409. doi: 10.1016/j.micres.2020.126409

Zhang, Y., Li, Y., Barber, A. F., Noya, S. B., Williams, J. A., Li, F., et al. (2023). The microbiome stabilizes circadian rhythms in the gut. *Proc. Natl. Acad. Sci. U. S. A.* 120:e2217532120. doi: 10.1073/pnas.2217532120

frontiers | Frontiers in Microbiology

TYPE Original Research
PUBLISHED 15 August 2023
DOI 10.3389/fmicb.2023.1219763

OPEN ACCESS

EDITED BY
Naga Betrapally,
National Cancer Institute (NIH), United States

REVIEWED BY
Kaijian Hou,
Shantou University, China
Ashley Elizabeth Kates,
University of Wisconsin-Madison, United States

*CORRESPONDENCE
Ting-Li Han
✉ tinglihan@cqmu.edu.cn

†These authors share first authorship

RECEIVED 09 May 2023
ACCEPTED 26 July 2023
PUBLISHED 15 August 2023

CITATION
Shi J, Ma D, Gao S, Long F, Wang X, Pu X, Cannon RD and Han T-L (2023) Probiotic *Escherichia coli* Nissle 1917-derived outer membrane vesicles modulate the intestinal microbiome and host gut-liver metabolome in obese and diabetic mice.
Front. Microbiol. 14:1219763.
doi: 10.3389/fmicb.2023.1219763

Probiotic *Escherichia coli* Nissle 1917-derived outer membrane vesicles modulate the intestinal microbiome and host gut-liver metabolome in obese and diabetic mice

Jun Shi[1,2†], DongXue Ma[1,2†], ShanHu Gao[1,2], Fei Long[1,2], Xin Wang[1,2], XingYu Pu[1,2], Richard D. Cannon[3] and Ting-Li Han[1,2,4*]

[1]State Key Laboratory of Ultrasound in Medicine and Engineering, College of Biomedical Engineering, Chongqing Medical University, Chongqing, China, [2]Chongqing Key Laboratory of Biomedical Engineering, Chongqing Medical University, Chongqing, China, [3]Department of Oral Sciences, Faculty of Dentistry, Sir John Walsh Research Institute, University of Otago, Dunedin, New Zealand, [4]Department of Obstetrics and Gynaecology, The Second Affiliated Hospital of Chongqing Medical University, Chongqing, China

Introduction: Obesity and diabetes are common chronic metabolic disorders which can cause an imbalance of the intestinal flora and gut-liver metabolism. Several studies have shown that probiotics, including *Escherichia coli* Nissle 1917 (EcN), promote microbial balance and metabolic health. However, there are no studies on how EcN outer membrane vesicles (EcN-OMVs) influence the intestinal microflora and affect the metabolic disorders of obesity and diabetes.

Methods: In this study, we evaluated the effects of EcN-OMVs on high-fat diet (HFD)-induced obesity and HFD+streptozotocin (STZ)-induced diabetes.

Results: EcN-OMVs could reduce body weight, decrease blood glucose, and increase plasma insulin in obese mice. Similarly, EcN-OMVs treatment could modify the ratio of *Firmicutes*/*Bacteroidetes* in the gut, elevate intestinal short-chain fatty acid (SCFA)-producing flora, and influence the SCFA content of the intestine. Furthermore, the intestinal metabolites ornithine and fumaric acid, hepatic ω-6 unsaturated fatty acids, and SCFAs were significantly increased after administering EcN-OMVs.

Discussion: Overall, this study showed that EcN-OMVs might act as post-biotic agents that could modulate gut-liver metabolism and ameliorate the pathophysiology of obesity and diabetes.

KEYWORDS

probiotics, *Escherichia coli* Nissle 1917, outer membrane vesicles, diabetes, obesity, gut microbiota, metabolomics

1. Introduction

The incidences of obesity and diabetes are increasing dramatically, the rates are assuming pandemic proportions. It has been estimated that approximately 57.8% of the world's adult population will be obese or overweight by 2030 (Kelly et al., 2008; Meldrum et al., 2017). The global incidence of diabetes has been predicted to increase from 451 million (age 18–99 years) people in 2017 to 693 million cases in 2045 (Cho et al., 2018; Khan et al., 2020). Obesity and diabetes can also cause a variety of associated health problems, such as elevated blood glucose, cardiovascular disease, osteoarthritis, kidney disease, fatty liver, sleep apnoea and intestinal microbial flora disorder (Bluher, 2019; Harding et al., 2019). Therefore, there is an urgent need to discover new prevention and treatment strategies.

Interestingly, a previous study found that the gut microbiota influences nutrient acquisition and energy regulation in the host, as well as the development of obesity, insulin resistance, and diabetes (Durack and Lynch, 2019). Hence, microbiota manipulation through diet changes has been postulated as a promising therapeutic approach. It is increasingly recognized that probiotics can contribute to preventing obesity and alleviating diabetes by manipulating the intestinal microbiota composition and the production of various metabolites (Sommer and Backhed, 2013). Many probiotics have been promoted as pharmaceutical products or dietary supplements to improve obesity, diabetes, and intestinal dysfunction (Sanders et al., 2019; Vallianou et al., 2020). *Escherichia coli* Nissle 1917 (EcN) is a probiotic strain isolated by Alfred Nissle from the stools of a soldier who was not infected during an outbreak of shigellosis, and is used in several probiotic products. EcN is not pathogenic because its lacks virulence factor genes in its genome. It has been reported that EcN colonizes the human gut readily and promotes intestinal homeostasis and microflora balance (Hancock et al., 2010; Scaldaferri et al., 2016; Geervliet et al., 2022).

There is a large amount of evidence indicating that probiotic-mediated effects are mostly achieved indirectly. Studies have shown that almost all Gram-negative, and some Gram-positive, bacteria release nanometer-sized membrane vesicles called extracellular vesicles (EVs) (Ahmadi Badi et al., 2017; Woith et al., 2019). EVs produced by Gram-negative bacteria are derived from the outer membrane and are thus termed as outer membrane vesicles (OMVs). These spherical bilayered phospholipid structures could act as vehicles to mediate gut microbiota-host communication (Kim et al., 2015, 2017). Purified OMVs contain a diverse array of bioactive molecules, such as lipids, proteins, lipopolysaccharides (LPS), phospholipids, and nucleic acids, that could reach host cells, modulate essential biological functions and influence host health (Furuyama and Sircili, 2021). EVs derived from specific bacteria can induce different physiological responses. For example, Raftar and colleagues have shown that *Akkermansia muciniphila* EVs can act as a mucosal delivery vector to reduce the deleterious consequences of obesity in mice. *A. muciniphila* EV treatment caused a significantly greater loss in body weight and fat in HFD mice than treatment with the bacterium itself. Similarly, the same authors found that both *A. muciniphila* and its EVs improved blood glucose and lipid levels in obese mice, and were significantly correlated with intestinal homeostasis (Raftar et al., 2021, 2022). In addition, Qu et al. (2022) have suggested that probiotic-derived vesicles could repair tissue damage associated with the infection by upregulating the levels of anti-inflammatory factors, downregulating pro-inflammatory factors, and regulating cellular biological behaviors. Furthermore, Hu et al. (2020) demonstrated that EcN-OMVs could modulate the functions of host immune cells by stimulating RAW264.7 macrophage proliferation, phagocytic functions, and immune-related enzymatic activities. Another study has shown that EcN-OMVs could ameliorate dextran sodium sulfate-induced mucosal injury and inflammation in the gut, and maintain the intestinal barrier function (Fabrega et al., 2017). However, there is no study investigating the EcN-OMV regulation of metabolic disorder the effect of EcN-OMVs on microbial flora composition in obese and diabetic mice.

In this study, we aimed to investigate the effects of EcN-OMVs on metabolic dysfunctions in mice (obesity and diabetes) by using microbiome and metabolomic approaches. We also studied the mechanism of how EcN-OMVs act as a probiotic-derived therapeutic approach to alleviate obesity and diabetes.

2. Materials and methods

2.1. Bacterial culture

The probiotic *E. coli* strain Nissle 1917 (EcN) was purchased from Biobw (Beijing, China). The bacteria were grown at 37°C in Luria-Bertani (2 g/L, LB) broth with continuous shaking at 180 rpm until the culture reached exponential phase.

2.2. OMV isolation

Outer membrane vesicles (OMVs) were isolated from the EcN culture supernatant as described previously (Fabrega et al., 2016). In brief, the *E. coli* cells were removed from the culture by centrifugation at 5,000×*g* for 30 min at 4°C. Then the supernatant was centrifuged at 10,000×*g* for 30 min at 4°C. The collected supernatant was sequentially filtered through 0.45 μm and 0.22 μm pore size polyethersulfone membranes (Sorfabio, Beijing, China) to remove large particles such as bacterial residues and cellular debris. The filtered supernatant was then ultracentrifuged at 150,000×*g* for 3 h at 4°C to isolate EcN-OMVs. The EcN-OMV pellet was resuspended in sterile phosphate buffered saline (PBS; pH = 7.4). The EcN-OMVs were stored at −80°C for later use.

2.3. Transmission electron microscopy

Isolated OMVs were imaged by transmission electron microscopy (TEM) after negative staining as described by Aguilera et al. (2014). A drop of OMV suspension was placed on Formvar/carbon coated-grids that were previously activated by UV light, for 2 min. Grids were washed with deionized water, stained with 2% uranyl acetate for 1 min, air dried, and evaluated by TEM (Jeol, JEM 1010, Japan).

2.4. NanoSight tracking analysis

A NanoSight NS300 (United Kingdom) optical nanoparticle Brownian motion imager was used to measure the size of OMVs. The number of particles and their movement was recorded for 5 × 60 s (camera level = 11). Particle sizes were quantified by nanotracking analysis (detection threshold = 5) using the NS500 software.

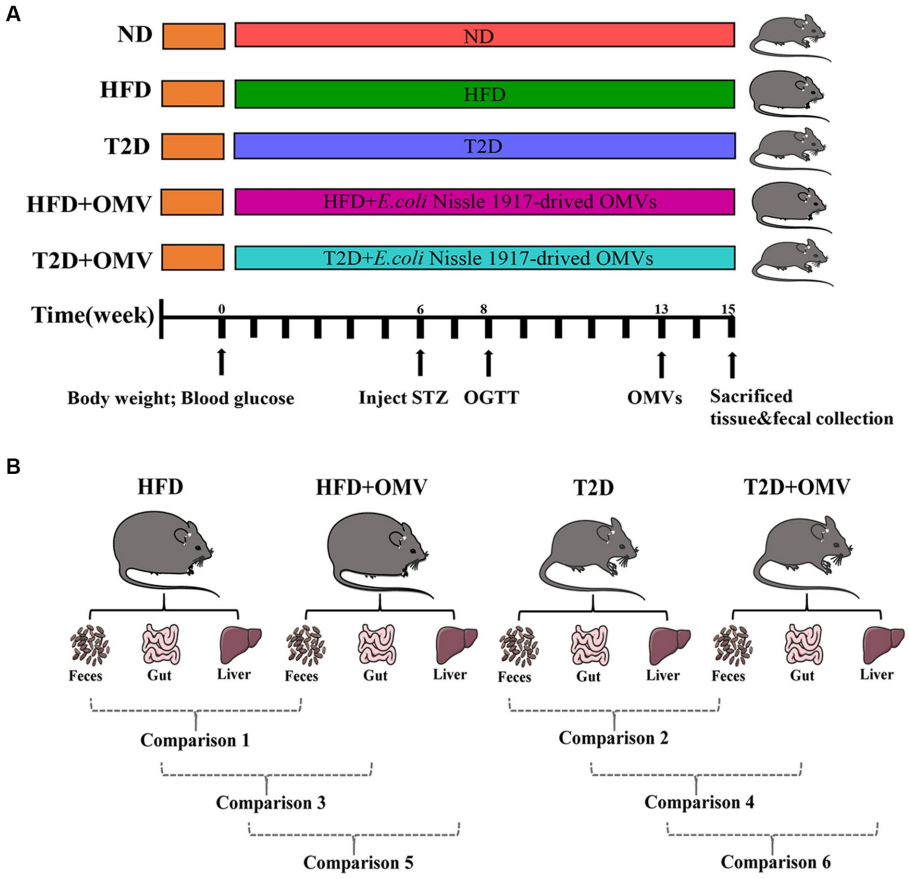

FIGURE 1
(A) Schematic diagram of study design. The important events are indicated on the timeline. There are five experimental groups abbreviated as follows; ND, normal diet; HFD, high-fat diet; T2D (type 2 diabetes), high-fat diet + STZ; HFD + OMV, high-fat diet + OMVs; T2D + OMV, high-fat diet + STZ + OMVs. **(B)** Data comparisons in this study. Comparison 1 compares the fecal metabolites between the HFD + OMV group and the HFD group. Comparison 2 compares the fecal metabolites between the T2D + OMV group and the T2D group. Comparison 3 compares the gut metabolites between the HFD + OMV group and the HFD group. Comparison 4 compares the gut metabolites between the T2D + OMV group and the T2D group. Comparison 5 compares the liver metabolites between the HFD + OMV group and the HFD group. Comparison 6 compares the liver metabolites between the T2D + OMV group and the T2D group.

2.5. Immunoblotting

The OMVs were mixed with SDS–PAGE sample buffer, heated for 5 min at 95°C, and the proteins were separated using 12% SDS-PAGE gels (Beyotime, China) followed by transferring onto 0.45 μm PVDF membranes (Millipore, United States). The membranes were blocked with PBS-0.05% Tween-20 and 5% skimmed milk and incubated with primary antibodies (OMPA and OMPC, Abcam, United States) in 8% BSA solution overnight at 4°C. After washing, the blots were incubated with appropriate secondary antibodies (Beyotime, China) for 1 h at room temperature. Lastly, the blots were visualized using the Genegenome XRQ Chemiluminescence system (Syngen, United Kingdom).

2.6. Establishment of obesity and diabetes mouse models

Mice were raised in accordance with the "Guide for the care and the Use of Laboratory Animals" as promulgated by the Institutional Animal Care and Use Committee (IACUC) of the Chongqing Medical University. The methodology was approved by the Ethics Committee of the Chongqing Medical University. Male C57BL/6J mice (8-weeks-old; approximately 18 g) were obtained from the Experimental Animal Center of Chongqing Medical University. Firstly, all mice were collectively reared adaptively for 2 weeks, and then randomly assigned into five groups: normal diet group (ND), obesity group (HFD), diabetes group (T2D), obesity with EcN-OMVs treatment group (HFD + OMV), and diabetes with EcN-OMVs treatment group (T2D + OMV) (Figure 1A). Moreover, the success rates of the induction mice model in each group were 100, 75, 75, 100, and 100% for ND, HFD, T2D, HFD + OMV, and T2D + OMV, respectively. The ND group was fed with the normal mouse growth diet (20.6% kcal protein, 67.4% kcal carbohydrate, and 12% kcal fat with 3.6 kcal/g), and the other four groups (HFD, T2D, HFD + OMV, T2D + OMV) were fed with the high-fat diet (20% kcal protein, 20% kcal carbohydrate, and 60% kcal fat with 5.24 kcal/g) for a total of 15 weeks. Animal body weight and blood glucose were measured weekly. The diabetic mice (T2D and T2D + OMV) were given 40 mg/kg of streptozotocin (STZ) by intraperitoneal injection for 3 days in the sixth week. The obesity mice (HFD and HFD + OMV) did not receive any other intervention and were maintained on a high-fat diet. All groups were subjected to an oral glucose tolerance test (OGTT) in the eighth week. The experimental design is shown in Figure 1A.

2.7. Gastric gavage with OMVs

After the mouse models were stably established in the 15th week, the treatment groups were given 500 μL of OMVs (17.5 μg protein/500 μL) by gavage every day for 2 weeks, and the same amount of PBS was given to the control group. The 2-weeks OMV treatment was adopted based on previous studies (Fabrega et al., 2017; Chelakkot et al., 2018; Du et al., 2021). The concentration of OMVs was measured using a BCA Protein Assay Kit (Beyotime, Shanghai, China).

2.8. 16S rRNA gene sequencing of gut microbiota

The gut microbiota was analysed by 16S rRNA gene sequencing of the fecal samples of all groups of mice. This was performed by the Chongqing Puroton Institute of Genetic Medicine Co., Ltd.; the main sequencing process was as follows: (1) DNA extraction and PCR amplification: Fecal microbial DNA was extracted using a DNA extraction kit (Qiagen, United States). Universal primers for 16S rRNA (338F and 806R) containing inducers and sequencing adaptors were employed to amplify the V3-V4 gene regions. The sequencing read length for MiSeq was 2 × 300 bp. PCR amplification was performed using a polymerase mix (New England Biolabs). (2) Purification and recovery of amplification products: DNA amplicons were analyzed using 2% agarose gel electrophoresis, and the GeneJET gel recovery kit (Thermo Scientific) was used to recover the amplification products. (3) Quantification of amplification products: the PCR products were quantified using the Quant-iT PicoGreen dsDNA Assay Kit. (4) Preparation of sequencing library: the TruSeq NanoDNA LT Library Prep Kit (Illumina) was used to prepare the sequencing library, and the sequencing libraries were quantified using Qubit. (5) High-throughput sequencing: After performing sequencing library quality control, MiSeq was used to obtain the 16S rRNA sequences. Sequences were binned into OTUs and taxonomy was assigned by QIIME software using Greengenes database (version gg_13_8). All the sequencing data are available in the NCBI Sequence Read Archive database (Citation accession: PRJNA971528).

2.9. Glucose measurement and mouse sample collection

All blood samples were collected from the tail vein, and glucose was measured by the glucose oxidase method using a hand-held OneTouch Ultra glucometer (Sinocare, Beijing, China). To perform the oral glucose tolerance test (OGTT), basal blood glucose levels were first measured after 15 h overnight fasting. A 40% (wt/vol) of glucose solution was then intragastrically administrated at 2 g/kg, and blood glucose levels were measured at 15, 30, 60 and 120 min after the glucose loading. If the glucose level was greater than 599.4 mg/dL, the value of 599.4 mg/dL was recorded. The fecal samples were collected weekly throughout the whole feeding period. Two weeks after the completion of the vesicle gavage intervention, the mice were sacrificed by neck dislocation and samples of liver, gut, and plasma were obtained. The samples for metabolic analysis were frozen at −80°C.

2.10. Histological analyses

Liver and gut biopsies were fixed in 4% formaldehyde/phosphate buffer for 24 h at 4°C, then dehydrated and embedded in paraffin. Tissue sections (5 μm) were stained with hematoxylin and eosin. Light microscopy with Dino-lite digital lens and Dino Capture 2 software (AnMo Electronics Corp., Taiwan) was used for histopathological analysis.

2.11. Short-chain fatty acid (SCFA) quantification by solid phase micro-extraction (SPME) GC–MS

2.11.1. Preparation of mouse fecal samples

A salt solution containing 1.26 g/mL of $(NH_4)_2SO_4/NaH_2PO_4$ in a 3.7:1 ratio and 0.5 mM of internal standard D4-acetic acid was prepared to improve SCFA extraction efficiency and reproducibility. Fecal samples (20 mg) were transferred to a 2 mL screw cap tube with 400 μL of the salt solution and tungsten carbide beads (3 mm diameter). The fecal mixture was homogenized using a TissueLyser II (QIAGEN, United States) and transferred into a 20 mL glass vial with 1.6 mL of the salt solution. The glass vials were placed in the autosampler (PAL RTC 120, Agilent, United States) of the SPME-GC–MS machine until analysis.

2.11.2. SPME-GC–MS analysis

The SPME method used to analyze SCFA was adapted from Nylund et al. (2020). SCFAs were extracted with an SPME fiber on an Agilent Auto-sampler (PAL RTC 120), separated by a 5977A MSD gas chromatograph (Agilent) using a DB-FFAP (30 m × 250 μm id × 0.25 μm, Agilent), and analyzed with a 7890B mass spectrometer (Agilent).

SPME conditions were as follows: DVB/CAR/PDMS fiber (Agilent), agitation temperature 35°C with an extraction time of 30 min. Temperature and desorption time had been preliminarily evaluated and set at 260°C and 5 min, respectively. The fiber post-injection condition was performed at 270°C for 10 min.

The GC conditions were as follows. The volatile compounds were injected into an inlet with a splitless mode at 260°C with 1 mL/min flow rate of helium gas. The GC-oven program was initially held at 35°C for 4 min. Then the temperature was elevated from 35°C to 130°C at a rate of 70°C/min. Then the temperature was ramped at 5°C/min until it reached 155°C. Lastly, the temperature was raised to 240°C at a rate 120°C/min and held for 4 min; the total run time was 15.06 min.

The MS conditions were as follows. The temperatures of auxiliary, MS quadrupole, and MS source were 250°C, 230°C, and 150°C, respectively. The mass range was detected from 30 μm to 550 μm. Scan speed was set to 1.563 μ/s, and the solvent delay was applied until 5.0 min.

2.12. Metabolomic profile by methyl chloroformate derivatization (MCF) based GC–MS analysis

2.12.1. Preparation of fecal, liver, and gut samples

Briefly, fecal and tissue samples were thawed on ice at 4°C and portions (30 mg) transferred from cryotubes to 1.5 mL microcentrifuge tubes. Sodium hydroxide (1 M) and methanol mixture (1:1 v/v; NaOH/MeOH 0.4 mL), two tungsten carbide beads (3 mm diameter),

and 10 µL of D4-alanine (10 mM) were added to each sample followed by 30 s vortex mixing. The samples were homogenized using a TissueLyser II (QIAGEN, United States) at 30 Hz for 1 min. Then the supernatant was isolated by centrifugation at 12,000 rpm (4°C) for 15 min and stored at 4°C prior to derivitization.

2.12.2. OMV sample preparation

Isolated OMVs (500 µL) were concentrated by freeze-drying using a SpeedVac (Labconco, United States) for 4 h at 0.8 HPa. The dried pellets were resuspended in 0.4 mL of NaOH/MeOH and 10 µL of D4-alanine (10 mM) was added followed by 30 s vortex mixing. Then the supernatant was isolated by centrifugation at 12,000 rpm (4°C) for 15 min and stored at 4°C prior to derivitization.

2.12.3. MCF derivitization

To stored supernatants 34 µL of pyridine and 20 µL MCF was added, followed by 30 s of vortex mixing, then another 20 µL of MCF was added followed by 30 s of vortexing. Then, 200 µL of chloroform and 400 µL of sodium bicarbonate (50 mM) were added and the solutions vortexed for 10 s. Subsequently, the aqueous layer was separated from the chloroform layer by centrifugation at 2,000 rpm for 10 min. After centrifugation, the aqueous layer was removed and the remaining chloroform extract was dehydrated by the addition of sodium sulphate (~0.3 g), then transferred to an amber glass GC–MS vial. Negative controls were produced by subjecting an empty microcentrifuge tube to the same processing as the samples.

2.12.4. GC–MS analysis

The GC–MS instrument parameters were set according to Gao et al. (2022). Specifically, the derivatized metabolites were analyzed using an Agilent Intuvo9000 coupled to a MSD5977B with 70 eV of electron impact ionization. The gas capillary column was a BD-1701 (30 m × 250 µm id × 0.25 µm, Agilent). The derivatized samples were injected into a pulsed splitless mode inlet at 290°C with 1 mL/min flow rate of helium gas. The GC-oven program was initially held at 45°C for 2 min. Then the temperature was elevated from 45°C to 180°C at a rate of 9°C/min and held for 5 min. Then the temperature was ramped at a rate of 40°C/min until it reached 220°C and held for 5 min. Then the temperature was raised to 240°C at a rate of 40°C/min and held there for 11.5 min. Lastly, the temperature was raised to 280°C at a rate 80°C/min. The temperatures of the guard chip, auxiliary, MS quadrupole, and MS source were 280°C, 250°C, 230°C, and 150°C, respectively. The mass range was detected from 30 µm to 550 µm. The scan speed was set to 1.563 µ/s and the solvent delay was applied until 5.5 min.

2.13. Data extraction and normalization

Automated Mass Spectral Deconvolution & Identification System software was used for metabolite deconvolution and identification. The metabolites were identified by comparing the MS fragmentation patterns (relative intensity of mass spectra to the most abundant ion) and GC retention time within 0.5 min bins to our in-house MS library built using chemical standards. The MassOmics R-based program was implemented to extract the relative concentration of the metabolites using the peak height of the most abundant reference ion mass. To facilitate quantitative robustness along with minimizing instrumental and human variability, the relative concentrations of the identified compounds were normalized with internal standards (D4-alanine) and then adjusted for either protein concentration or weight of samples for bacterial OMVs or mice samples (fecal, liver, gut).

2.14. Statistical analysis

With regard to the microbiome results, alpha diversity (Simpson, Shannon, and evenness indices), and rarefaction curves were analyzed and plotted using the website https://www.bioincloud.tech/. Phylogenetic beta diversity measures, weighted and unweighted UniFrac distance matrices were calculated using QIIME and visualized with principal coordinate analysis (PCoA). Linear discriminant analysis effect size (LEfSe) analysis was used to identify taxa significantly enriched in the treatment groups. The linear discriminant analysis (LDA) score was computed for taxa differentially abundant between the control group and the treatment group. A taxon at $p < 0.05$ (Kruskal–Wallis test) and $\log_{10}$[LDA] ≥ 2.0 (or ≤ -2.0) were considered significant. The Analysis of Composition of Microbiomes (ANCOM) was performed on QIIME and applied to identify differentially abundant features across the five groups (ND, HFD, T2D, HFD + OMV, and T2D + OMV).

Metabolomic data are presented as the mean ± SEM. The comparisons between two groups were conducted using an unpaired Student's t-test. Comparisons between five groups (ND, HFD, T2D, HFD + OMV, T2D + OMV) were determined using two-way ANOVA followed by Tukey post-hoc analysis. The false discovery rates (FDRs) were calculated using the q-value function in the R program for accounting for multiple comparisons. The important variables in the partial least squares discriminant analysis (PLS-DA) projection were determined using the ropls R-package. $p < 0.05$ with corresponding q-value (FDR) < 0.3 were considered statistically significant. Metabolic pathway activity was predicted based on the Pathway Activity Profiling (PAPi) R-algorithm. Correlations between gut microbiota and metabolites were analyzed by Pearson's correlation using R. Bar graphs and line plots were illustrated using GraphPad Software Prism 9 (GraphPad Software, San Diego, United States). A graphical representation of the significant metabolites was displayed in heat maps using the ggplot2 and complexheatmap R packages.

3. Results

3.1. Identification of EcN-OMVs

The morphology of the OMVs and their size distribution were characterized by transmission electron microscopy (Figure 2A) and nanoparticle tracking analysis (Figure 2C), respectively. We observed that the OMVs were spherical particles with a size range of 20–300 nm, with the most abundant particle size being 211 nm. Furthermore, western blot analysis verified that the isolated OMVs shared several protein markers with probiotic EcN including outer membrane protein A (OMPA) and outer membrane protein C (OMPC) (Figure 2B). These results indicated that OMVs were successfully isolated from the EcN strain.

3.2. Body weight, blood glucose and oral glucose tolerance test (OGTT) of obese and T2D mice prior to OMV intervention

The diabetic-related characteristics of mice prior to 13 weeks of OMV treatment are depicted in Figure 3. Three was a general increase in weight in non-diabetic mice, and the HFD group showed the greatest weight gain (Figure 3A). All groups of mice had similar blood glucose levels until week 6 when, after STZ injection, the blood glucose concentration increased rapidly in the T2D group and reached more than 288 mg/dL (Figure 3C). OGTT measurements at 8 weeks showed that the highest glucose levels were in the T2D group (Figure 3E). Thus, the T2D group displayed typical diabetes symptoms as upon administration of glucose, the concentration rose rapidly and did not return to physiological levels within 2 h.

3.3. Body weight, blood glucose and plasma insulin concentrations of mice after OMV gavage

After gastric gavage feeding with OMVs daily from week 13 to 15, the body weight (Figure 3B) of the OMV treatment groups (HFD + OMV and T2D + OMV) was significantly lower than their corresponding non-OMV groups (HFD and T2D). The blood glucose (Figure 3D) concentrations were significantly lower in the HFD + OMV group but there was no noticeable change for the T2D + OMV group. Similarly, the plasma insulin concentration (Figure 3F) was increased significantly in the HFD + OMV group. Unlike the findings in HFD + OMV mice, the T2D + OMV had no effects on plasma insulin levels. Overall, the OMVs exerted potential preventive effects on obesity and T2D by decreasing body weight, blood glucose, and increasing plasma insulin.

3.4. Histology analysis

To examine the effects of EcN-OMVs on mice in more detail, we assessed the histopathologies of liver and gut tissues. In the liver (Figure 4A), there was an excessive accumulation of lipid droplets in both macrovesicular and microvesicular forms in the HFD and T2D groups compared with the ND group. The lipid droplets were more prominent in the HFD group than in the T2D group. The OMV treatment in the T2D and HFD mice reduced the number of lipid droplets compared with the non-OMV treatment group. Overall, the histopathological examination of the liver samples indicated that EcN-OMVs could prevent HFD and T2D-induced hepatic steatosis.

Since a high-fat diet altered the morphology and integrity of HFD- and T2D-treated mouse liver, we evaluated gut tissue by H&E staining (Figure 4B). Compared with the ND group, the crypt depth and mucous layer thickness was considerably less in the HFD and T2D groups. Nevertheless, no obvious histopathological changes were observed in the OMV treatment groups.

3.5. Overview of differences in the metabolite profiles

A total of 132 distinct metabolites were identified in feces, gut and liver tissue. Three-dimensional partial least squares discriminant analysis (PLS-DA) was performed. We found that the metabolite profiles in feces (Figure 5A), gut (Figure 5B) and liver (Figure 5C) tissue were all clearly segregated among five groups. The metabolites that were unique or shared among different groups were visualized using an Upset plot (Figure 5D). Interestingly, no common metabolites were found among all six comparisons. Ten, fourteen, one, two, two and seven metabolites were unique for comparisons 1–6 (Figure 1B) respectively (Figure 5D). In T2D comparisons, fourteen and seven metabolites fluctuated significantly in the feces (C2) and liver tissue (C6), respectively, with OMV treatment, while the concentrations of two metabolites significantly increased in the gut tissue with OMV treatment (C4). In the comparison of HFD groups, ten and two metabolites were significantly elevated in the feces (C1) and liver tissue (C5), respectively, with OMV treatment, while only one metabolite's concentratin was significantly elevated in the gut tissue (C3) with OMV treatment. Thus, OMV treatment has a greater effect on metabolite changes in feces and liver tissue than in intestinal tissue.

3.6. Characteristic metabolite analysis

Heat maps and volcano plots were used to show differences in the concentrations of specific metabolites in comparisons 1–6 for feces,

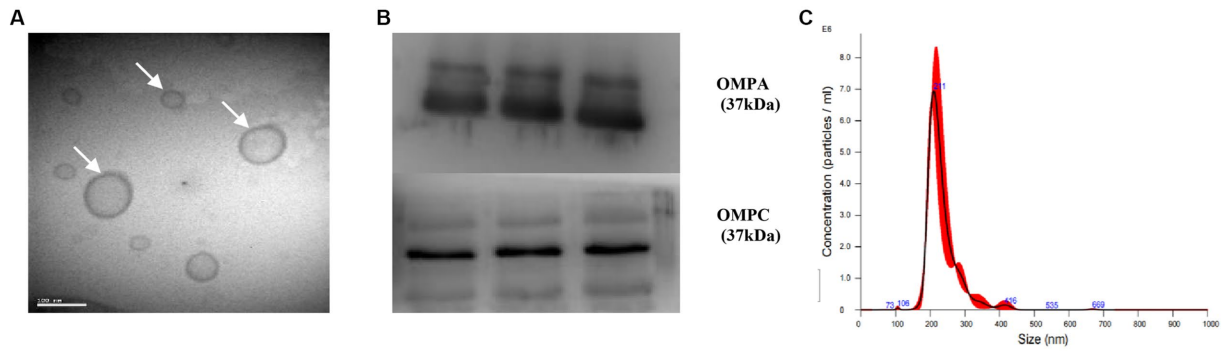

FIGURE 2
Characterization of EcN-OMVs. **(A)** Transmission electron micrograph displaying the morphology of OMVs. **(B)** Western blotting validating OMVs through expression of OMPA and OMPC. **(C)** The size distribution of isolated OMVs measured by nanoparticle tracking analysis.

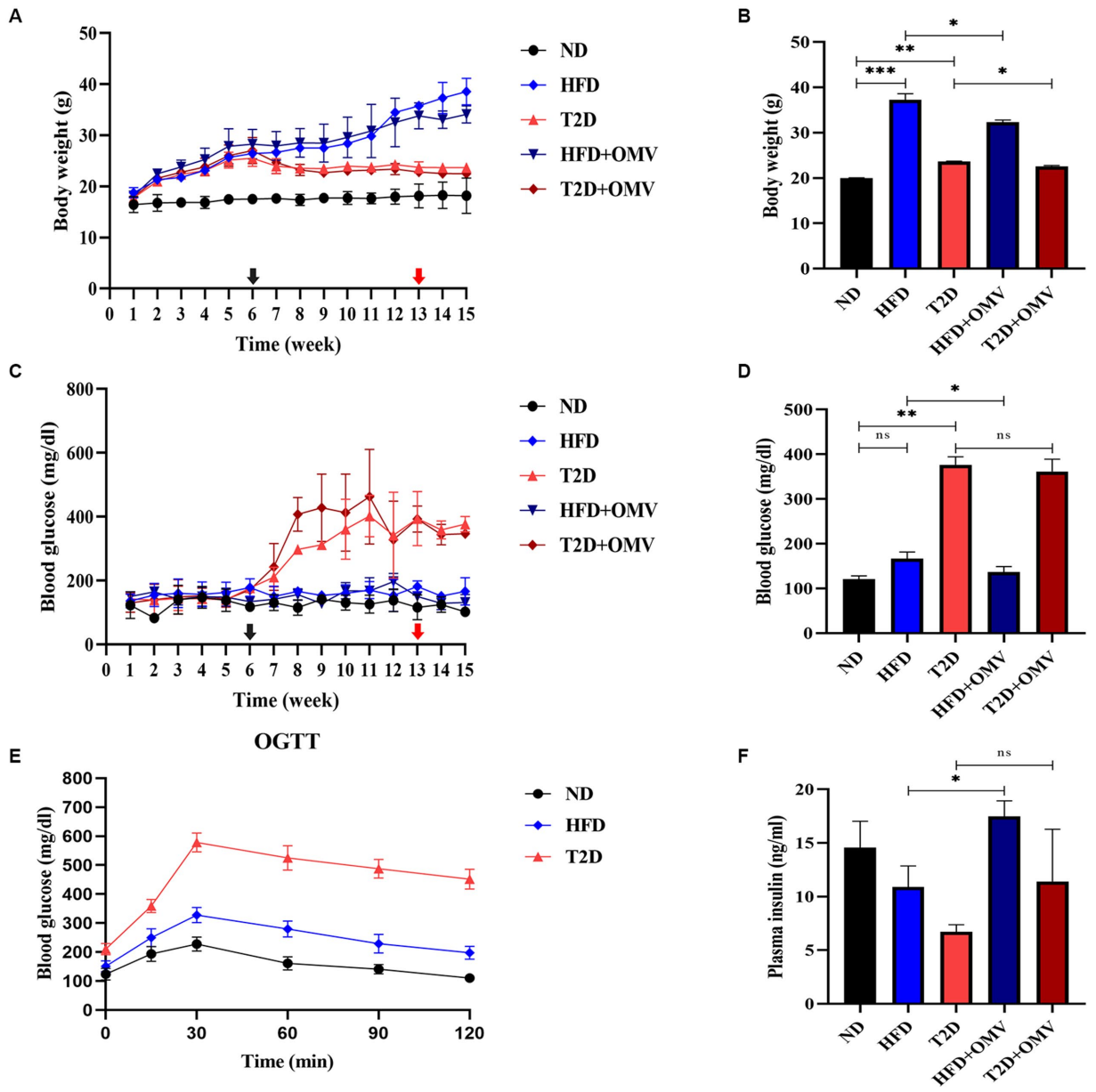

FIGURE 3
The effects of OMVs on body weight **(A,B)**, blood glucose **(C,D)**, and plasma insulin **(F)** in obese (HFD) and T2D mice. The levels of OGTT in normal, obese, and diabetes mice at 8 weeks **(E)**. The black arrow indicates the time of STZ intraperitoneal injection (6 weeks), while the red arrow indicates the time of EcN-OMV intervention (13 weeks). Bar graphs **(B,D,F)** are outcomes after OMV treatments past 13 weeks. Data are presented as the mean ± SD. Statistical analysis was conducted by one-way or two-way ANOVA followed by the *post hoc* Tukey–Kramer test and Student's *t*-test, as appropriate. $^{*}p \leq 0.05$, $^{**}p \leq 0.01$, $^{***}p \leq 0.001$.

gut, and liver tissue (Figures 5E,F). In the fecal metabolome, the concentrations of four metabolites (arachidonic acid, norleucine, alanine, and isoleucine) were elevated, and the concentrations of three SCFAs (3-methyl-pentanoic acid, 3-methyl-valeric acid, and hexanoic acid) were decreased in the OMV group for comparison 1 (FC > 1.5, adjusted $p < 0.05$). For comparison 2, the concentrations of seven metabolites (11-eicosenoic acid, oxidized glutathione, norleucine, creatinine, 11,14-eicosadienoic acid, fumaric acid, and oleic acid) were increased, whilst the concentrations of seven SCFAs (propionic acid, butyric acid, acetic acid, 2-methyl-hexanoic acid, hexanoic acid, 2-methyl-valeric acid, and 3-methyl-valeric acid) were decreased in the OMV group (FC > 1.5, $p < 0.05$). In the gut metabolome, only the concentrations of ornithine and fumaric acid were elevated in the OMV groups for comparison 3 and comparison 4, respectively, (FC > 1.5, $p < 0.05$). In the liver metabolome, the concentrations of unsaturated LCFAs such as 11,14-eicosadienoic acid, 11-eicosenoic acid, 13,16-docosadienoic acid, arachidonic acid, and homo-gamma-linolenic acid were significantly increased in the OMV treatment group for comparison 5. Lastly, the concentrations of sarcosine and succinic acid in the T2D + OMV group were significantly higher than in the T2D group (comparison 6) (FC > 1.5, $p < 0.05$).

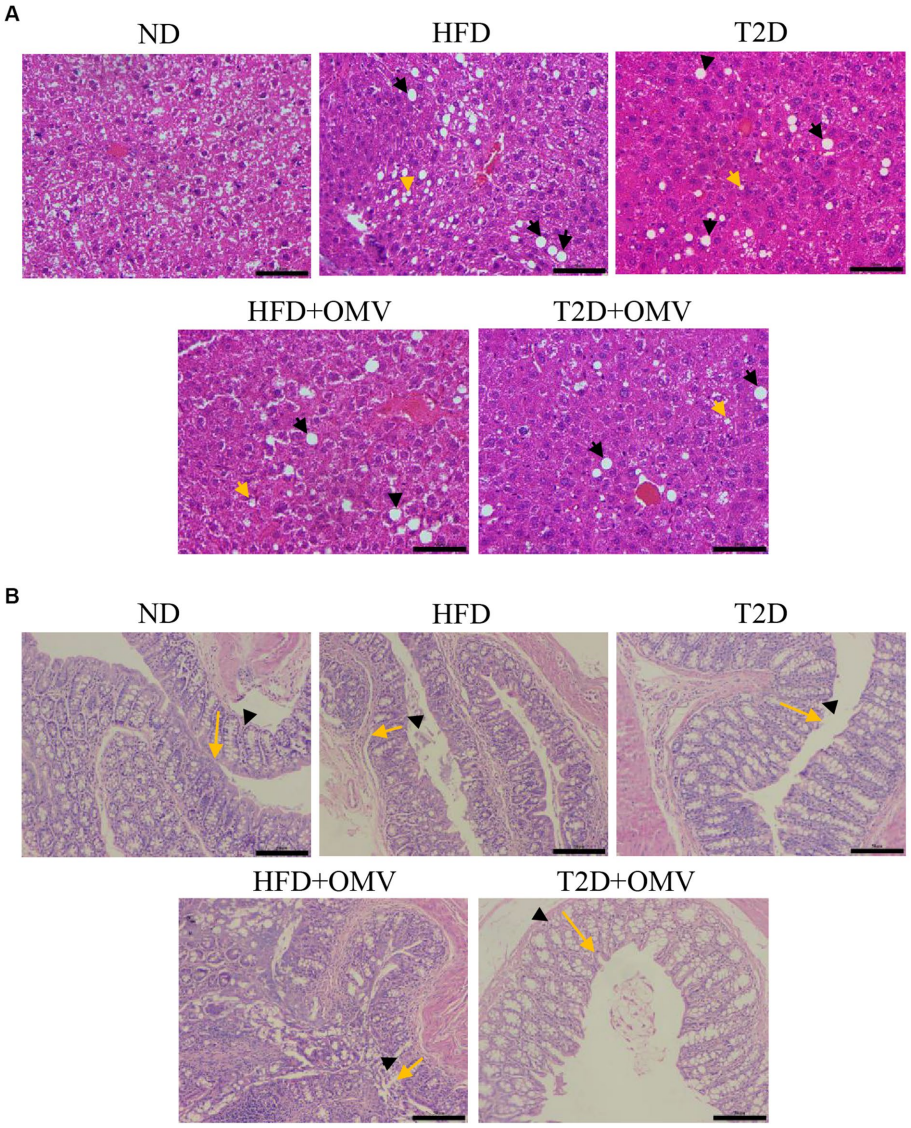

FIGURE 4
The effects of EcN-OMVs on the histopathology of mouse liver and gut tissues. **(A)** Hematoxylin and Eosin (H&E) staining of liver sections (yellow arrows: lipid droplets in microvesicular form, and black arrows: lipid droplets in macrovesicular form, scale bar is 50 μm). **(B)** H&E staining of gut sections (yellow arrows indicate crypt depth, and black arrowheads indicate mucous thickness, scale bar is 50 μm). ND, normal diet; HFD, high-fat diet; T2D (type 2 diabetes), high-fat diet + STZ; HFD + OMV, high-fat diet + OMVs; T2D + OMV, high-fat diet + STZ + OMVs.

3.7. Metabolic pathway enrichment analysis

To further explore the biological role of identified metabolites, we annotated metabolic pathways using the KEGG metabolic framework as shown in Figure 6A. In fecal pathway analysis, comparison 1 indicated four significantly upregulated metabolic pathways including nitrogen metabolism, the phospholipase D signaling pathway, the Foxo signaling pathway, and D-alanine metabolism. Meanwhile, comparison 2 showed that insulin resistance, type II diabetes mellitus, the pentose phosphate pathway, the AMPK signaling pathway, arginine and proline metabolism, and insulin secretion were upregulated, while only the melanogenesis pathway was downregulated in the T2D + OMV group. In gut pathway analysis, comparison 3 indicated that D-arginine and D-ornithine metabolism and the TCA cycle were upregulated, while thyroid hormone synthesis was downregulated in obese mice with OMV intervention. In comparison 4, insulin secretion and the regulation of lipolysis were upregulated, whilst the AMPK signaling pathway was downregulated in the T2D + OMV group. For the liver pathway analysis, comparison 5 indicated six significantly upregulated metabolic pathways including Fc gamma R-mediated phagocytosis, the Fc epsilon RI signaling pathway, arachidonic acid metabolism, the regulation of lipolysis, the GnRH signaling pathway, and aldosterone synthesis. Moreover, comparison 6 identified eight significantly upregulated metabolic pathways including oxidative phosphorylation, the glucagon signaling pathway, propanoate metabolism, pyruvate metabolism, the TCA cycle, arginine and proline metabolism, the cAMP signaling pathway, and the mTOR signaling pathway.

Then we annotated the metabolic pathways most significantly affected in comparisons 1–6, and the results showed that these

10.3389/fmicb.2023.1219763

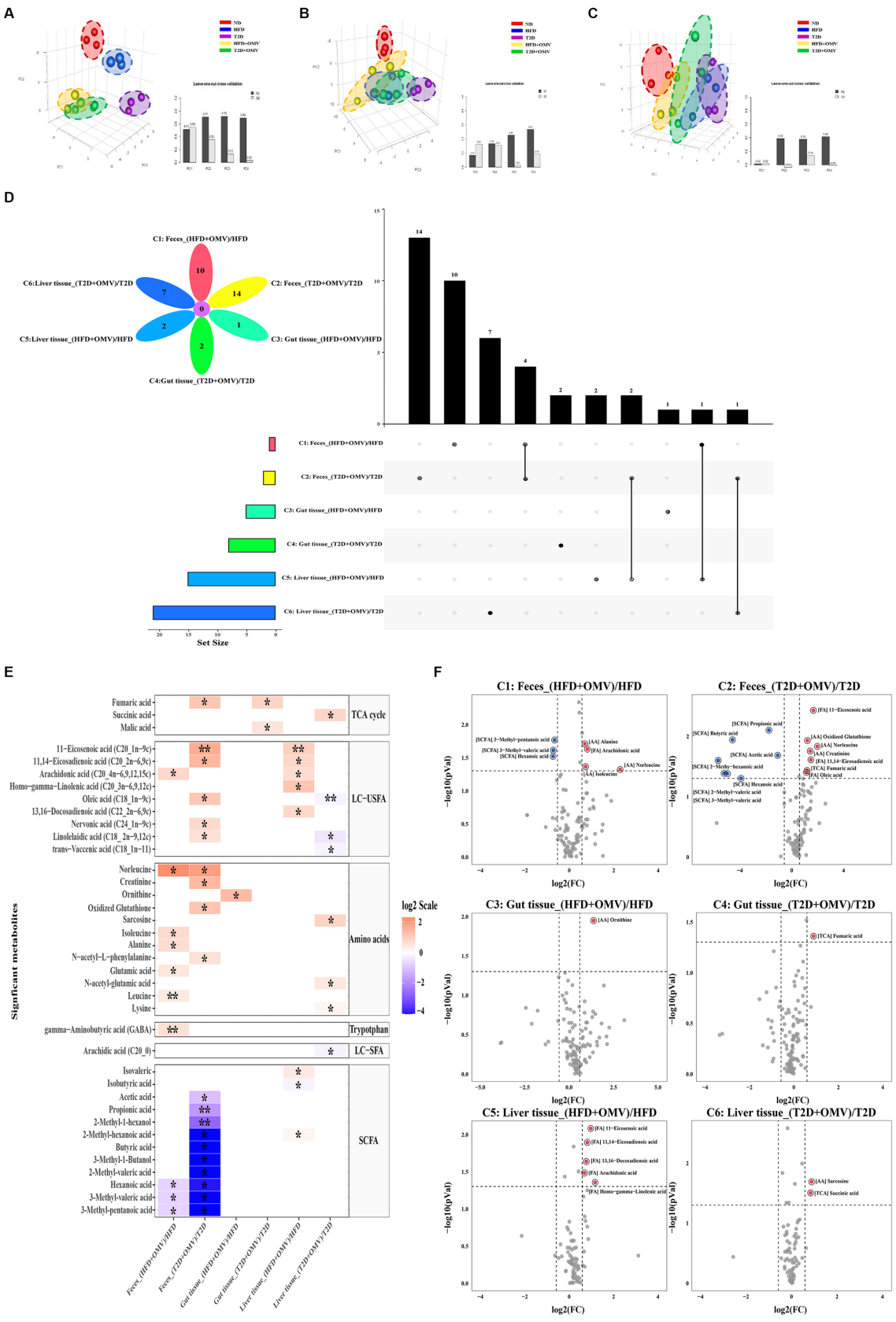

FIGURE 5
Metabolite analysis. Partial least squares discriminant analysis (PLS-DA) of metabolite patterns in **(A)** feces, **(B)** gut tissue, and **(C)** liver tissue. **(D)** Upset plot and Venn diagram of differential (adjusted $p < 0.05$) metabolite levels. The individual or connected dots represent the various intersections of metabolites that were either unique to, or shared among, comparisons, respectively. **(E)** Heatmap of the metabolites detected in feces, gut tissue, and

(Continued)

FIGURE 5 (Continued)
liver tissue showing the ratio of metabolite levels between groups. Red colors indicate higher metabolite concentrations in OMV treatment groups than the corresponding non-OMV treatment groups, while blue colors indicate lower metabolite concentrations in OMV treatment groups than the corresponding non-OMV treatment groups. The relative concentration of metabolites was plotted using a $\log_2$ scale. The significant metabolite differences (adjusted $p < 0.05$, FC > 1.5) are labelled with an asterisk*, and more signficant differences (adjusted $p < 0.001$, FC > 1.5) are labelled with a double asterisk**. **(F)** Volcano plot of the differential ($p < 0.05$, FC > 1.5) metabolite levels between groups. Red dots indicated upregulation, while blue dots indicated downregulation in response to the OMV treatment. HFD, high-fat diet; T2D (type 2 diabetes), high-fat diet + STZ; HFD + OMV, high-fat diet + OMVs; T2D + OMV, high-fat diet + STZ + OMVs.

metabolic pathways involved the 21 most relevant metabolites which included l-glutamate, 4-aminobutanoate, d-alanine, quinolinate, glycine, glutathione disulfide, 5-oxoproline, pyruvate, l-proline, sarcosine, creatinine, l-tyrosine, 2-oxoglutarate, succinate, fumarate, citrate, cis-aconitate, d-alanyl-d-alanine, arachidonate, (r)-3-hydroxybutanoate and l-leucine (Figures 6B–G).

3.8. Gut microbiota data

3.8.1. Gut microbiota in the five groups

Sequencing of the V3-V4 region of the 16S rRNA gene was performed on fecal samples. The alpha diversities of the gut microbiota analyzed using rarefaction curves showed marked differences of microbial species diversity between the five groups (Figure 7A). The gut microbiota diversity of the HFD group and T2D group was lower than that for the ND group. Interestingly, the alpha diversity was lower in the HFD group after OMV treatment, while the alpha diversity was higher in the T2D group after OMV intervention, indicating divergent modulations of the intestinal flora by OMVs. The principal coordinate analysis (PCoA) revealed that the normal diet group were separated from the other four groups (Figure 7B). The significant differences in bacteria among the five groups were shown by LEfSe analysis (Figure 7C). The differentially abundant bacteria were *Sinorhizobium* and *Rhizobiaceae* in the HFD group, but were *Rhizobiales, Acinetobacter and Moraxellaceae* in the HFD + OMV group. Then the differentially abundant bacteria were *Corynebacterium, Corynebacteriaceae, Actinomycetales, Actinobacteria, Aerococcus and Aerococcaceae in the T2D group*, but were *Butyricimonas, Christensenellaceae, SMB53 and Clostridium* in the T2D + OMV group. Finally, *Prevotella*, *Prevotellaceae*, *Clostridium* and *Veillonellaceae* were the markers in the ND group. These findings showed that the OMV treatments were capable of influencing the compositions of intestinal flora in the HFD group and the T2D group.

3.8.2. Gut microbial changes at phylum, family and genus levels

The bacterial composition of the gut contents of the mouse groups was determined at the phylum, family and genus levels by 16S rRNA sequencing (Figures 7D–F).

At the phylum level, *Firmicutes* and *Bacteroidetes* accounted for more than 75% of the bacterial abundance for groups without OMV treatment (Figure 7D). *Firmicutes* accounted for 62.33%, 68.12%, and 84.84% in the ND, T2D, and HFD groups, respectively. *Bacteroidetes* accounted for 21.65%, 8.79%, and 3.36% in the ND, T2D, and HFD groups, respectively. Consistently, analysis of the 16S rRNA data using ANCOM showed that *Firmicutes* and *Bacteroidetes* accounted for the most number of differentially abundant OTUs at the phylum level when compared among HFD vs. ND, T2D vs. ND, HFD + OMV vs. HFD, and T2D + OMV vs. T2D (Table 1). Of note, the *Firmicutes*/*Bacteroidetes* ratios increased in the order of the ND, T2D, and HFD groups. After OMV treatment, the proportion of *Firmicutes* decreased in the HFD + OMV group (55.73%) and the T2D + OMV (60.42%) group. Meanwhile, the proportion of *Bacteroidetes* increased after OMV treatment in the HFD + OMV group (9.02%) and the T2D + OMV group (22.16%). The *Firmicutes*/*Bacteroidetes* ratios for the HFD + OMV group and the T2D + OMV group were similar to the ND group. Therefore, different diets and OMV treatments could alter the composition of the major intestinal microbiota.

At the family level (Figure 7E), *Erysipelotrichaceae*, *Lachnospiraceae*, *Ruminococcaceae*, *Desulfovibrionaceae*, and *Lactobacillaceae* were the most abundant bacterial taxa. Compared with the non-OMV treatment groups (HFD = 46.34%, T2D = 16.86%), *Erysipelotrichaceae* was reduced in the OMV treatment groups (HFD + OMV = 23.41%, T2D + OMV = 10.24%). *Lachnospiraceae* in the OMV treatment groups (HFD + OMV = 9.99%, T2D + OMV = 12.58%) was more abundant than in the groups without OMV treatment (HFD = 7.64%, T2D = 9.59%).

At the genus level (Figure 7F), *Allobaculum*, *Oscillospira*, *Lactobacillus*, *Mucispirillum*, and *Prevotella* were the most abundant genera., *Allobaculum* was reduced in the OMV treatment groups compared with the goups without OMV treatment (HFD = 56.14% vs. HFD + OMV = 26.81%, T2D = 22.80% vs. T2D + OMV = 12.84%). Likewise, *Lactobacillus* had reduced abundance in all OMV treatment groups compared with the goups without OMV treatment (HFD = 20.78% vs. HFD + OMV = 0.60%, T2D = 7.69% vs. T2D + OMV = 4.87%).

3.9. Correlation between stool metabolites and gut microbiota

In order to investigate potential associations between intestinal flora and stool metabolites, Pearson correlation coefficients were determined between shortlisted metabolites (Figure 5E) and dominant gut flora at the phylum, family, and genus levels (Figures 7D–F). Charts of intestinal flora-host metabolites interactions before or after the EcN-OMVs treatment are presented in Figure 8.

At the phylum level before OMVs treatment (Figure 8A), a total of six phyla were positively correlated with 11 differentially abundant metabolites, including *Actinobacteria* with 2-ethyl-1-hexanol, *Firmicutes* with butyric acid, *Spirochaetes* with acetic acid and propionic acid, *Deferribacteres* with six shortlisted metabolites (fumaric acid, alanine, glutamic acid, n-acetyl-L-phenylalanine, 2-methyl hexanoic acid and 2-methyl valeric acid), *Tenericutes* with four shortlisted metabolites (alanine, glutamic acid, leucine, and n-acetyl-l-phenylalanine), and *TM7* with three shortlisted metabolites (alanine, glutamic acid, and n-acetyl-l-phenylalanine). After OMV treatment (Figure 8D), *Bacteroidetes* was significantly negatively

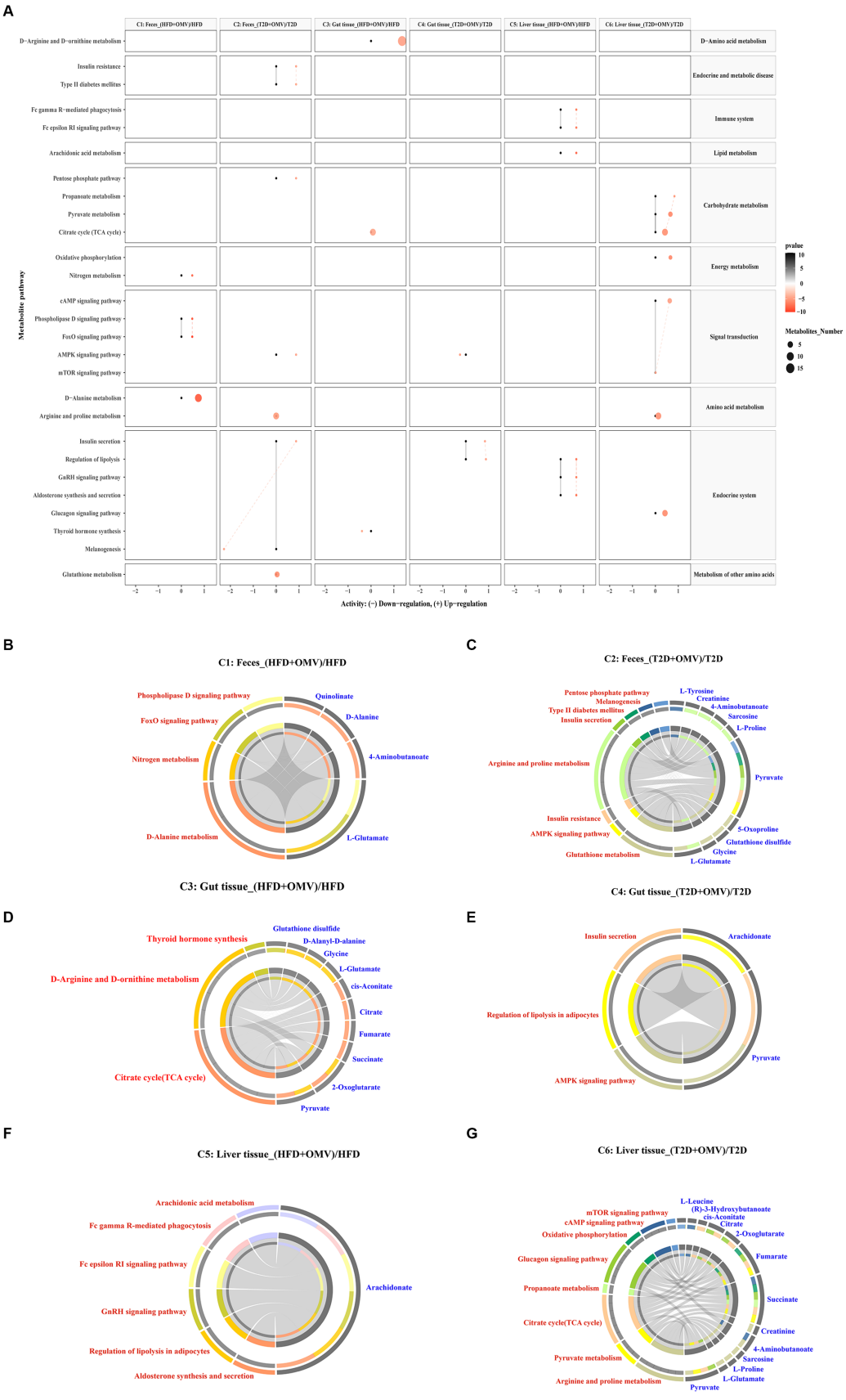

FIGURE 6
Metabolic pathway enrichment. **(A)** Activities of metabolic pathways in feces, gut tissue, and liver tissue for comparisons 1–6. Black dots represent metabolic activities in feces, gut tissue and liver tissue from the HFD group and the T2D group that were adjusted to 0. Red dots represent metabolic

(Continued)

FIGURE 6 (Continued)
activities in feces, gut tissue, and liver tissue from the HFD + OMV group and the T2D + OMV group. The metabolic activities were visualized using a $\log_2$ scale. The dot size indicates the number of metabolites involved in the pathway, and the intensity of the red dot color indicates the significance of *p*-value. **(B–G)** Circos plots display the connectivity of significant metabolites and their pathways in feces for comparison 1 **(B)** and comparison 2 **(C)**. The connectivity between significant metabolites and pathways in the gut tissue for comparison 3 is shown in **(D)** and for comparison 4 is shown in **(E)**. Similarly, comparisons 5 **(F)** and comparison 6 **(G)** show the connectivity between significant metabolites and pathways in the liver tissue. In **(B–G)**, the red text signifies the shortlisted metabolic pathways and the blue text represents the significant metabolites.

correlated with eight differential metabolites (fumaric acid, gamma–aminobutyric acid, alanine, glutamic acid, leucine, n-acetyl-l-phenylalanine, norleucine, and arachidonic acid), while *Deferribacteres* was solely positively correlated with fumaric acid.

At the family level before OMV treatment (Figure 8B), a total of 18 families had significant correlations with 11 differential metabolites. Bacteria such as *Prevotellaceae*, *Deferribacteraceae*, *Peptococcaceae*, *Bradyrhizobiaceae* and *F16* showed positive relationships with nine metabolites (fumaric acid, alanine, glutamic acid, n-acetyl-L-phenylalanine, norleucine, oxidized glutathione, 11,14-eicosadienoic acid, 11-eicosenoic acid, and linolelaidic acid). *Veillonellaceae* showed negative relationships with three differential metabolites (gamma-aminobutyric acid, isoleucine, and leucine). After OMV treatment (Figure 8E), 14 families were correlated with 14 significant metabolites. Bacteria including *Deferribacteraceae*, *Bradyrhizobiaceae*, *Rhizobiaceae*, *Sphingomonadaceae*, *Oxalobacteraceae*, *Helicobacteraceae*, *Enterobacteriaceae,* and *Moraxellaceae* showed positive relationships with eight differential metabolites (fumaric acid, alanine, norleucine, oxidized glutathione, 11,14-eicosadienoic acid, 11-eicosenoic acid, 2-methyhexanoic acid, and 2-methylvaleric acid). *Bacteroidaceae*, *Prevotellaceae*, *S24-7*, *Veillonellaceae,* and *Mogibacteriaceae* showed negative relationships with eight characteristic metabolites (fumaric acid, gamma-aminobutyric acid, alanine, glutamic acid, isoleucine, leucine, n-acetyl-L-phenylalanine, and norleucine).

At the genus level before OMV treatment (Figure 8C), a total of 18 genera were correlated with 20 metabolites. Bacteria like *Mucispirillum*, *Desulfovibrio*, *Blautia*, *Roseburia,* and *Prevotella* showed positive relationships with 11 characteristic metabolites (fumaric acid, alanine, creatinine, glutamic acid, isoleucine, n-acetyl-L-phenylalanine, norleucine, 11,14-eicosadienoic acid, 11-eicosenoic acid, linolelaidic acid, and nervonic acid). *Enterococcus* showed a negative correlation with 3-methylvaleric acid. After OMV treatment (Figure 8F), a total of 13 genera were correlated with 12 differential metabolites. Bacteria including *Vagococcus* and *Acinetobacter* showed positive correlations with two significant metabolites (11,14-eicosadienoic acid and 11-eicosenoic acid). *Coprococcus*, *Prevotella*, *Phascolarctobacterium,* and *Bacteroides* showed negative correlations with five differential metabolites (gamma-aminobutyric acid, glutamic acid, isoleucine, leucine, and arachidonic acid).

4. Discussion

EcN is a probiotic that improves microbiota balance and gastrointestinal homeostasis (Rozanska et al., 2014). OMVs are constitutively produced by Gram-negative bacteria and have an important role in bacteria-host interactions. However, little is known about the influence of probiotic OMVs on host physiology. In this study, we carried out a comparative analysis of the effects of EcN-OMVs on HFD mice and T2D mice to understand the mechanisms underlying effects on obesity and type 2 diabetes. Our findings indicated that administering EcN-OMVs could reduce body weight and blood glucose concentration, and increase plasma insulin levels. Through 16S rRNA gene sequencing analysis, we found that EcN-OMV treatments could modify the ratio of *Firmicutes*/*Bacteroidetes* in the intestine and modulate the relative abundance by increasing beneficial microbiota (*Lachnospiraceae* and *Oscillospira*) and inhibiting the growth of pathobiont bacteria (*Erysipelotrichaceae*). The fecal metabolome showed that EcN-OMVs might regulate SCFA concentrations in the intestinal by reducing the abundance of SCFA-production bacteria. Gut metabolome analysis suggested that EcN-OMVs might influence the intestinal ornithine and fumaric acid levels to mediate the gut ornithine cycle. Liver metabolome analysis revealed that EcN-OMVs might reduce hepatic steatosis in HFD mice by reducing ω-6 unsaturated fatty acid metabolism in the liver. Thus, EcN-OMVs seem to ameliorate the pathophysiologiy of obesity and diabetes by modulating gut-hepatic homeostasis.

4.1. The beneficial effects of EcN-OMVs on obese and T2D mice

Recent reports have confirmed the direct association between gut microbiota-derived OMVs and metabolic diseases, including obesity and diabetes (Nah et al., 2019; Diez-Sainz et al., 2022). Consistent with those studies, we found that oral administration of OMVs led to a significant reduction in body weight and hepatic lipid droplets in both HFD and T2D groups (Figures 3B, 4A). Although no study has investigated the effects of EcN-OMVs on obesity and diabetes, several studies have shown the beneficial outcomes of administering other Gram-negative bacteria on metabolic disorders. Chelakkot et al. (2018) showed that oral administration of *Akkermansia muciniphila* (*A. muciniphila*) OMVs to HFD-fed mice decreased gut barrier permeability, reduced body weight gain, and improved glucose tolerance. Ashrafian et al. (2019) demonstrated that *A. muciniphila* OMVs reduced body weight, lowered adiposity, and ameliorated intestinal inflammation in HFD-induced obese mice. In our study, mice fed with a HFD were prone to the effects of OMVs, including profoundly reduced blood glucose concentrations and elevated plasma insulin levels, with a similar trend in the T2D group. The less significant effect in the T2D group may be due to the fact that the HFD group was only perturbed by the dietary intervention, while the T2D group was administrated STZ in addition, which causes permanent destruction of mouse islet β cells (Szkudelski, 2001; Gheibi et al., 2017). Thus, the EcN-OMV treatment is effective in ameliorating the adverse outcomes caused by a high-fat diet.

10.3389/fmicb.2023.1219763

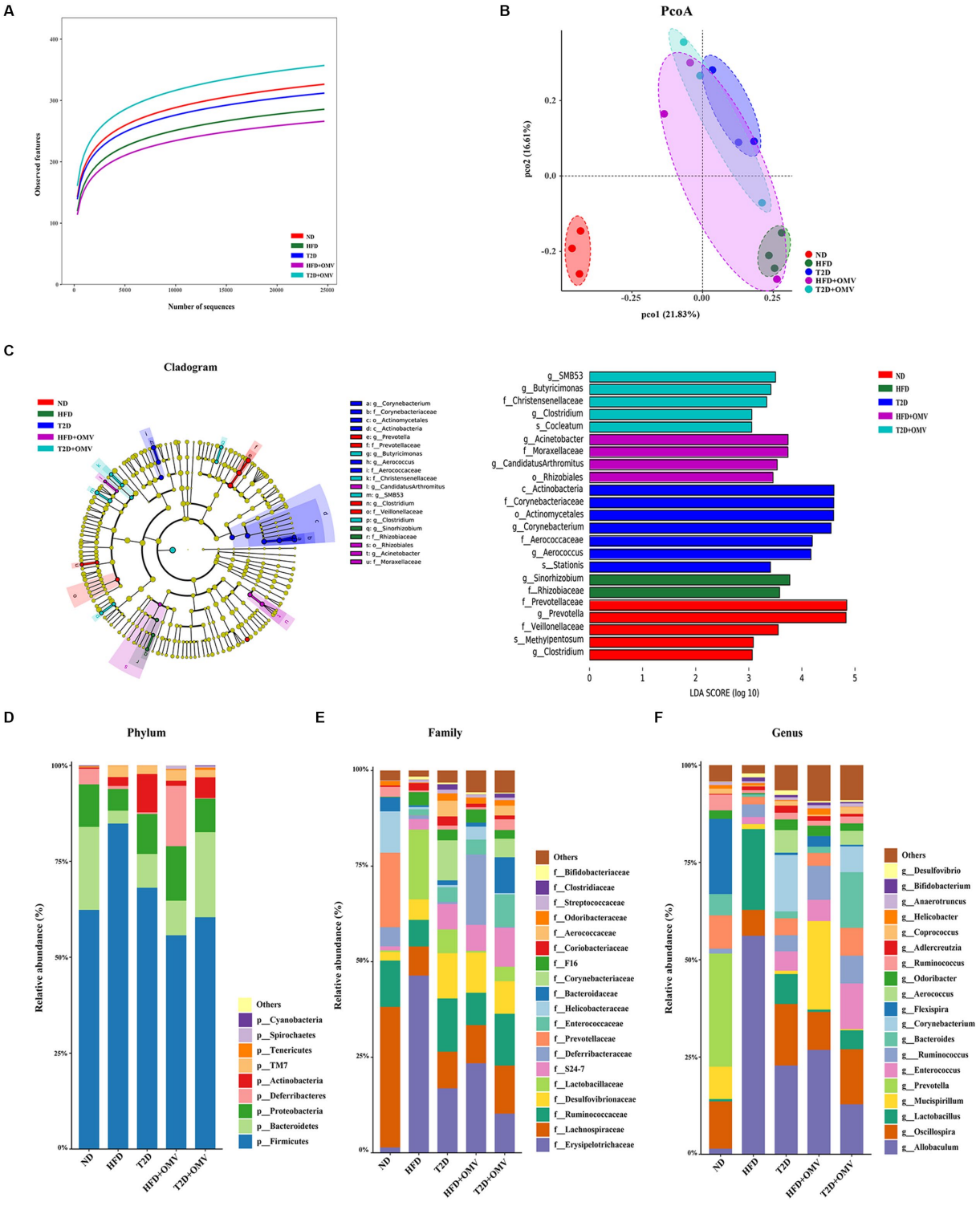

FIGURE 7
Gut microiota. The intestinal microbiota was different in mice in the different groups: normal diet (ND, red), high-fat diet (HFD, green), type 2 diabetes (T2D, blue), high-fat diet+OMVs (HFD+OMV, purple), and type 2 diabetes+OMVs (T2D+OMV, cyan). **(A)** The alpha diversities of gut microbes in the five groups. **(B)** PCoA plots based on bray metrics. **(C)** In the LEfSe cladogram, the inner to outer radiating circles represent the taxonomic level from phylum to species, and the diameter of the circles is proportional to the relative abundance. Species with no significant differences between groups are colored yellow, and species with significant differences are colored according to the group. Only taxa with $p<0.05$ and LDA score ($\log_{10}$) are shown. The relative abundance of species is shown at the **(D)** phylum, **(E)** family and **(F)** genus levels across the five groups. ND, normal diet; HFD, high-fat diet; T2D (type 2 diabetes), high-fat diet+STZ; HFD+OMV, high-fat diet+OMVs; T2D+OMV, high-fat diet+STZ+OMVs.

TABLE 1 Differentially abundant OTUs at the phylum level were identified by ANCOM when comparing mice faeces collected from ND, HFD, T2D, HFD + OMV, and T2D + OMV groups.

HFD vs. ND		T2D vs. ND		HFD + OMV vs. HFD		T2D + OMV vs. T2D	
Number of OTUs considered = 549		Number of OTUs considered = 564		Number of OTUs considered = 425		Number of OTUs considered = 497	
Phylum	Sig	Phylum	Sig	Phylum	Sig	Phylum	Sig
Actinobacteria	19	Actinobacteria	14	Actinobacteria	7	Actinobacteria	4
Bacteroidetes	34	Bacteroidetes	48	Bacteroidetes	10	Bacteroidetes	8
Cyanobacteria	1	Cyanobacteria	1	Deferribacteres	1	Cyanobacteria	1
Firmicutes	161	Firmicutes	171	Firmicutes	37	Firmicutes	33
Proteobacteria	24	Proteobacteria	35	Proteobacteria	6	Proteobacteria	8
TM7	5	TM7	5	Tenericutes	1	Tenericutes	1
Tenericutes	4	Tenericutes	3				
Total	248	Total	277	Total	62	Total	55

The sig represents significantly different OTUs.

4.2. Effects of EcN-OMVs on the gut flora of obese and T2D mice

The gut microbiota plays a crucial role in the modulation of host physiological processes the alterations of which have been strongly associated with the onset and progression of obesity and diabetes (Salgaco et al., 2019; Singer-Englar et al., 2019). Growing evidence suggests that gut microbiota-derived OMVs could be important mediators in gut microbiota-intestinal homeostasis and ultimately influence the pathogenesis of metabolic diseases (Diez-Sainz et al., 2022). Hence, we performed 16S rRNA sequencing of stool samples in order to determine variations in the gut microbiota canused by EcN-OMV administration in obese and diabetic mice.

Our results demonstrated that taxonomic spectra were distinctly different among the five experimental groups from the genus to phylum level (Figures 7D–F), indicating strong perturbations of the intestinal flora and marked regulation by EcN-OMVs. Specifically, at the phylum level before EcN-OMVs treatment with a normal diet, *Bacteroidetes* (B) and *Firmicutes* (F) were the dominant microbes, and the HFD and T2D groups had an increased F/B ratio, due to more *Firmicutes* and less *Bacteroidetes*, which was consistent with previous reports (Vemuri et al., 2018). Coincidentally, this increased F/B ratio has been reported to possibly lead to excessive low-grade inflammation (Wen and Duffy, 2017). Moreover, we found that *Firmicutes* and *Spirochaetes* had positive relationships with inflammatory-related short-chain fatty acids (SCFAs) like acetic acid, butyric acid, and propionic acid (Figure 8A). This result indicated that the HFD reshaped the gut flora such that it produced some proinflammatory SCFAs. After EcN-OMV treatment the F/B ratio at the phylum level decreased in both the HFD and T2D groups. In addition, *Bacteroidetes* abundance showed a negative correlation with metabolites such as arachidonic acid and leucine (Figure 8B). Previous studies have shown that arachidonic acid and its downstream oxylipins play a crucial role in the pathobiology of diabetes mellitus (Das, 2018). In addition, leucine concentrations have been reported to be altered between obese and low BMI humans and contribute to insulin resistance (Newgard et al., 2009). Thus, we postulate that EcN-OMVs might influence intestinal flora composition and subsequently generated anti-inflammatory metabolites that reduce insulin resistance and obesity.

Our study found that two significant bacterial families *Erysipelotrichaceae* and *Lachnospiraceae* which belong to the *Firmicutes* phylum play an important role in ameliorating obesity and diabetes. Firstly, the proportion of *Erysipelotrichaceae* in the HFD and T2D groups was higher than in the ND group prior to EcN-OMV treatment, while it was reduced in both of the high fat-diet groups (HFD + OMV&T2D + OMV) after OMV treatment. Reports documenting a potential role for *Erysipelotrichaceae* in host physiology and disease are increasing. For example, Chen et al. (2018) have shown that an HFD may increase the relative abundance of *Erysipelotrichaceae* in animals and individuals. Spencer et al. (2011) demonstrated that the abundance of *Erysipelotrichaceae* was positively associated with fatty liver in humans. In addition, Zschaler et al. (2014) and Palm et al. (2014) have found that species within the *Erysipelotrichaceae* phylum may have diverse immunogenicity profiles or respond differently to inflammation within the gut. We found that when we instituted a high-fat diet for the HFD and T2D groups, the proportion of *Lachnospiraceae* decreased significantly in comparison with the ND group. A decrease in *Lachnospiraceae* abundance is likely to have negative health implications resulting from the loss of the numerous beneficial functions performed by members of this family. For example, *Lachnospiraceae* can contribute to the microbiota's resistance to colonization by drug-resistant pathogens through the conversion of primary to secondary bile acids, and production of the SCFAs acetate and butyrate (Buffie et al., 2015). Interestingly, the level of *Lachnospiraceae* increased in both the HFD + OMV and T2D + OMV groups after OMV administration. Therefore, the positive regulation of intestinal *Erysipelotrichaceae* and *Lachnospiraceae* levels may be an important mechanism by which EcN-OMVs ameliorate obesity and diabetes.

4.3. Effects of EcN-OMVs on the fecal metabolome of obese and T2D mice

Numerous studies have confirmed that intestinal bacteria-derived SCFA metabolites play an important role in obesity and diabetes. Changes in the microbiota and SCFA profile are profoundly associated with host metabolism. For instance, SCFAs are involved in various physiological functions, including providing energy to intestinal cells, maintaining intestinal mucosal barrier and immune function, and regulating blood sugar and insulin levels (van der Hee and Wells, 2021). Our study found that after instituting a high-fat diet, the abundance of *Firmicutes* in the

10.3389/fmicb.2023.1219763

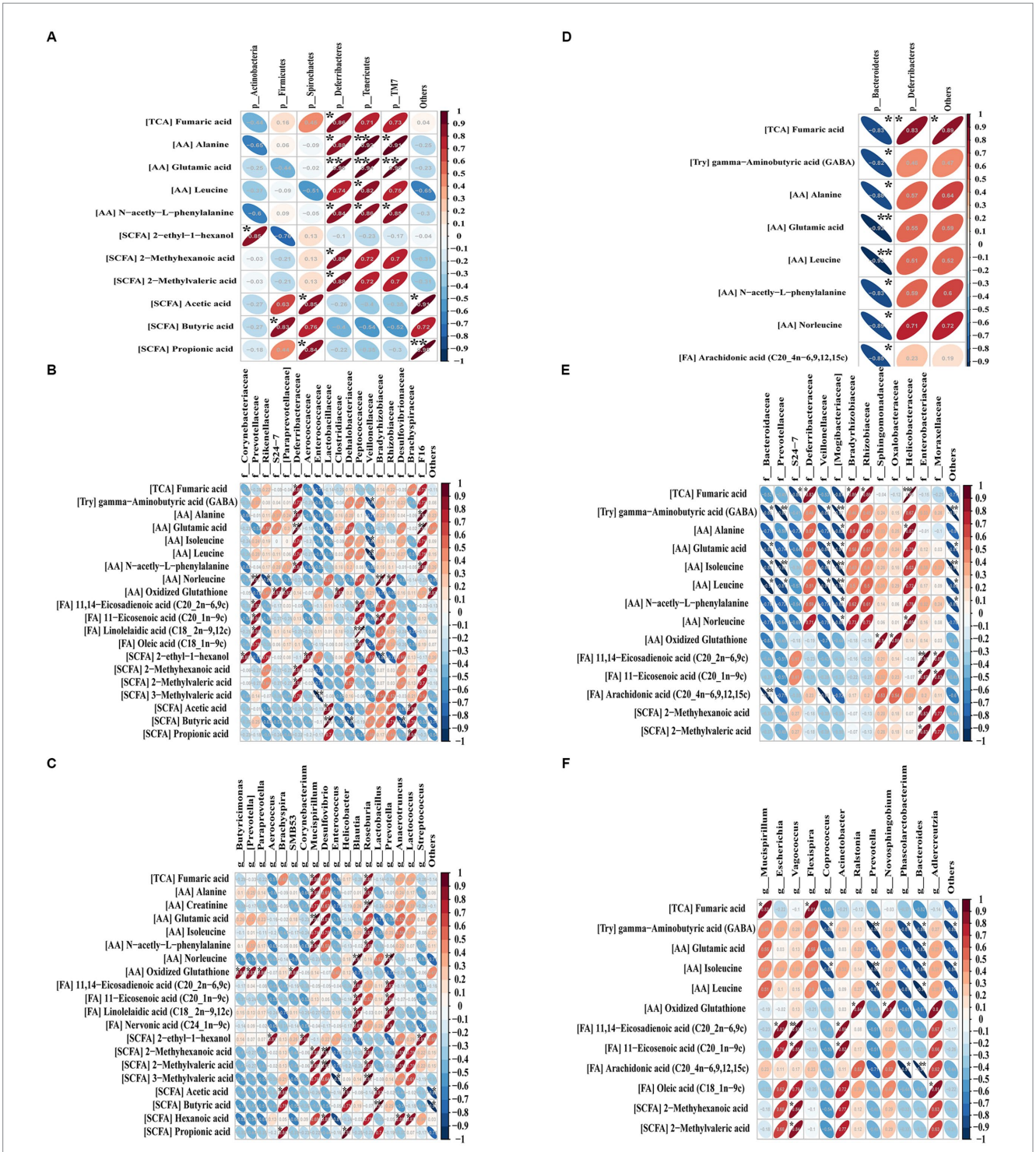

FIGURE 8
Pearson's correlations between the significant metabolites and dominant gut flora at the phylum **(A)**, family **(B)** and genus **(C)** levels before or after **(D–F)** OMV treatment. Blue diagonal down ellipses and red diagonal up ellipses represent negative and positive relationships between metabolites and microbiota, respectively. *$p < 0.05$, **$p < 0.01$, and ***$p < 0.001$.

HFD and T2D mice increased and the abundance of *Bacteroides* decreased. Joseph et al. (2019) have shown that *Firmicutes* and *Bacteroides* are involved in microbial dysbiosis and the development of obesity, and a higher concentration of SCFAs in the feces of overweight children than in healthy children. Gomes et al. (2018) and Iatcu et al. (2021) demonstrated that an imbalance of the intestinal microbiome and a decrease in the amount of SCFA often occurs in patients with obesity or T2D. Qin et al. (2010) suggested that the abundance of SCFA-producing bacteria was decreased in the gut microbiota of T2D patients.

Furthermore, intestinal SCFA levels can be modulated by probiotics, which could help restore intestinal homeostasis. We found that after OMV intervention the abundance of *Bacteroides*, *Lachnospiraceae*, and *Oscillospira* increased in both HFD and T2D groups. Ashrafian et al.

found that the abundance of *Bacteroides* could affect intestinal SCFAs when exposed to *Akkermansia muciniphila* extracellular vesicles. The same authors also reported that the level of *Bacteroides* was negatively correlated with colonic inflammation and proinflammatory cytokines in obese mice (Ashrafian et al., 2021). Byndloss et al. (2017) showed that *Lachnospiraceae* could influence acetate and butyrate production. Yang et al. (2021) demonstrated that *Oscillospira* was negatively associated with obesity and obesity-related chronic inflammatory and metabolic diseases. Meanwhile, Konikoff and Gophna (2016) have shown that *Oscillospira* is also likely to be a genus capable of producing SCFAs dominated by butyrate. In summary, OMVs may alleviate intestinal flora disturbance in obese and diabetic mice caused by a high-fat diet and increase the abundance of SCFA-producing bacteria.

4.4. Effects of EcN-OMVs on the gut metabolome of obese and T2D mice

Among the significant changes ($p < 0.05$, FC > 1.5) in intestinal metabolite concentrations, only ornithine was higher in the HFD + OMV group compared to non-OMV treatment (Figure 5F). Ornithine is a non-essential amino acid synthesized by the enzymatic action of arginase on arginine as part of the urea cycle (Sivashanmugam et al., 2017). Ornithine in the intestine comes from dietary intake (protein-rich food), and endogenous synthesis occurs primarily in the gut microbiota through ornithine synthetases. Notably, Bergen and Wu (2009) suggested that microorganisms play an important role in the intestinal nitrogen cycle, including deaminating ornithine/arginine, hydrolyzing luminal urea, and reabsorbing ammonia. Our study found that arginine and ornithine metabolism was upregulated in gut tissue after OMV administration, the F/B ratio was decreased and the abundance of *Bacteroides* increased significantly. Yoshida et al. (2021) demonstrated that an increased abundance of *Bacteroides* has been negatively associated with obesity. Wexler reported a significant correlation between nitrogen utilization efficiency with the presence of *Bacteroides*. For example, *Bacteroides* could synthesize and degrade amino acids, using them as a nitrogen source to synthesize microbial proteins. It could also undertake several nitrogen metabolic pathways, such as the urea cycle and nitrate metabolism, to regulate the utilization and excretion of nitrogen in the gut (Wexler, 2007). Furthermore, Qi et al. (2019) demonstrated that the modulation of the gut nitrogen cycle through arginine and ornithine could benefit gut mucosal barrier function. Cynober (1994) found that continuous feeding of ornithine to hungry rats can lead to a significantly higher crypt height in the jejunum and ileum and a higher total villous height in the ileum. Ornithine has been shown to maintain the integrity and normal morphology of the intestinal barrier by regulating the secretion of the mucus layer and the proliferation of intestinal epithelial cells. Thus, OMVs might influence the intestinal ornithine level by affecting the gut nitrogen cycle through modulation of microbial metabolism. However, the exact mechanism by which OMVs modulate gut nitrogen metabolism requires further investigation.

In our study, the fumaric acid concentration was significantly higher in the T2D + OMV group than in the T2D group and both the insulin secretion pathway and the lipolysis pathway were upregulated after OMV administration (Figures 5F, 6A). STZ is well known to cause pancreatic β-cell damage and can also inhibit the activity of enzymes that participate in the TCA cycle (Lenzen, 2008). Rojas et al. (2019) found that mice at 12 weeks post-STZ treatment showed an early TCA cycle impairment, and the fumaric acid level was significantly reduced. Some studies have demonstrated that bacterial OMVs contains proteins and enzymes related to the TCA cycle and oxidative phosphorylation process, such as NADH dehydrogenase and ATP synthase (Lee et al., 2007; Aguilera et al., 2014). Furthermore, Qiao et al. (2016) revealed that TCA cycle intermediates (fumaric acid, malic acid, citric acid, and succinic acid) in adipocytes exhibited oscillatory changes over time in response to insulin. Together, these results suggest that EcN-OMVs might alleviate TCA cycle damage caused by STZ by increasing fumaric acid concentrations.

4.5. Effects of EcN-OMVs on the liver metabolome of obese and T2D mice

The liver is a critical hub for numerous physiological processes. These include regulating glucose metabolism and lipid metabolism, and participating in inflammation and immune regulation. In this study, the mice's hepatic metabolome profiles were analyzed prior to, and post, OMV treatment. We found that the concentrations of four omega-6 (ω-6) unsaturated fatty acids (11, 14-eicosadienoic acid, 13, 16 – docosadienoic acid, dihomo-γ-linoleic acid, and arachidonic acid) were significantly increased in the HFD + OMV group. ω-6 fatty acids are a family of essential fatty acids that act as precursors for inflammatory metabolites. In particular, γ-linoleate is converted into dihomo-γ-linoleic acid and then desaturated to arachidonic acid, which subsequently serves as the precursor for the biosynthesis of inflammatory eicosanoids (e.g., prostaglandins) by cyclooxygenase-2 (COX-2). Several studies have demonstrated that SCFAs could inhibit the activity of the COX-2 enzyme (Liu et al., 2016; Kurata et al., 2019). Therefore, we believe that EcN-OMVs might suppress the activity of oxygenases involved in ω-6 unsaturated fatty acid metabolism by increasing SCFA concentrations in the liver, leading to the accumulation of ω-6 unsaturated fatty acids in the liver and reducing inflammation. However, the specific mechanism remains unknown.

Furthermore, SCFAs seem to act as signaling molecules between the gut microbiota and their host. We found that the concentration of 2-methyl-hexanoic acid was significantly changed in both the fecal and hepatic metabolome. den Besten et al. (2015) suggested that SCFAs appear to regulate hepatic lipid and glucose homeostasis in an adenosine monophosphate-activated protein kinase-dependent manner involving peroxisome proliferator-activated receptor-g regulated effects on gluconeogenesis and lipogenesis. Moreover, Chambers et al. (2015) demonstrated that increased SCFA flux through the liver could reduce intrahepatic triglyceride concentrations, likely improving hepatic fat accumulation. Indeed, our results showed the number of liver adipocytes in obese mice significantly decreased, and the intestinal SCFA-producing flora increased after administering EcN-OMVs. Microbiota-derived SCFAs are absorbed in the intestine and transported through the hepatic portal system to modulate liver metabolism. Thus, EcN-OMVs might reduce hepatic steatosis in HFD mice by increasing the concentration of ω-6 unsaturated fatty acids and SCFAs in the liver, and SCFAs are key molecules connecting liver and intestinal metabolomes (Figure 9).

4.6. Limitations

Despite the promising results, several limitations of our research merit discussion. Firstly, EcN has been shown to directly modulate

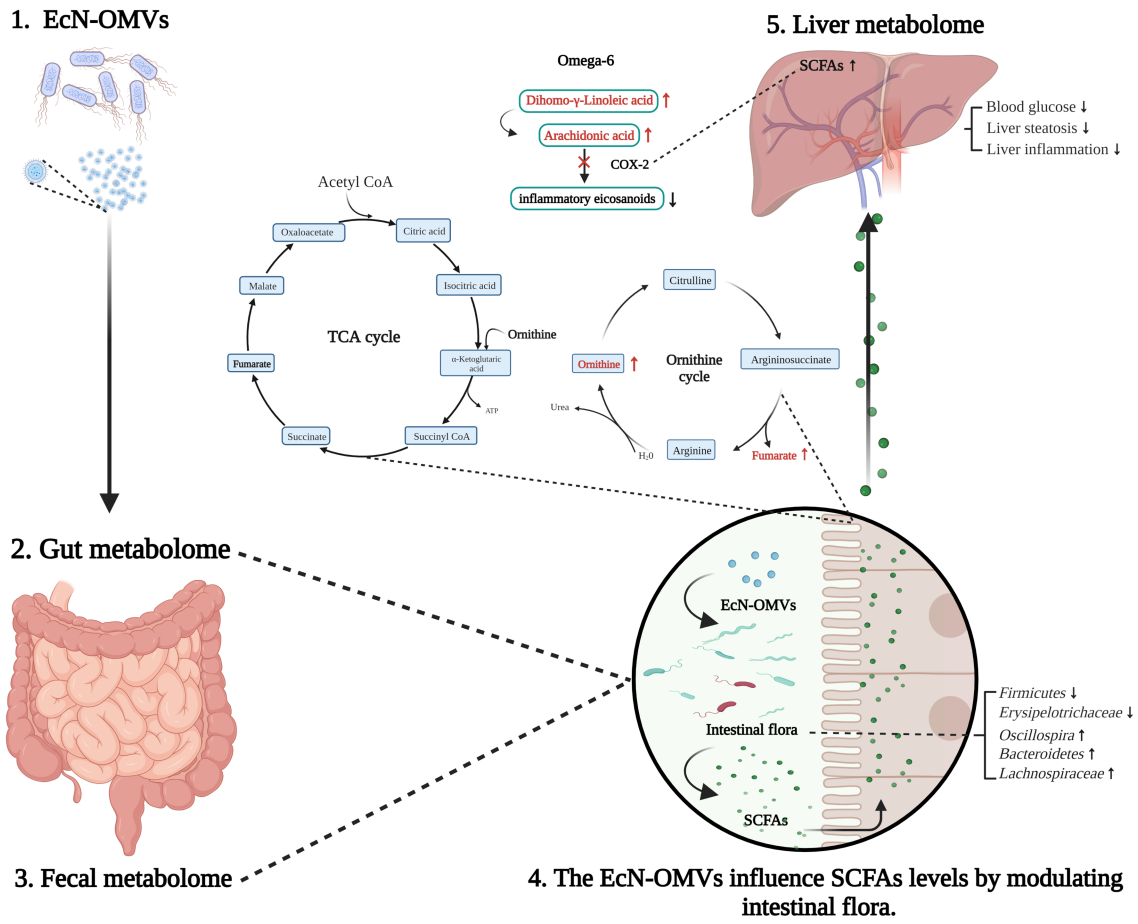

FIGURE 9
Summary of EcN-OMV regulation of the intestinal flora and gut-liver metabolism in obese and diabetic mice. Firstly, EcN-OMV administration modifies the ratio of Firmicutes/Bacteroidetes in the gut. This leads to the elevation of short-chain fatty acid (SCFA)-producing flora and increasing the concentrations of SCFAs in the intestine. Furthermore, intestinal ornithine cycle intermediates such as ornithine and fumaric acid are altered in response to EcN-OMV administration. Then, SCFAs are transported from the intestine to the liver through the hepatic portal vein. Finally, higher hepatic SCFA concentrations may suppress COX2 and subsequently downregulate the ω-6 unsaturated fatty acid metabolism. The upward arrow indicates a higher concentration/upregulation, and the downward arrow indicates a lower concentration/downregulation.

host glucose metabolism and improve postprandial glycemic response in mice (Chavkin et al., 2021). Thus comparisons between EcN and EcN-OMV administrations in obese and diabetic mice should be performed to evaluate their similar or different effects on host glucose metabolism. Secondly, we have isolated EcN-OMVs using the established method of differential ultracentrifugation. Nevertheless, it has been reported that the size-based bacterial OMV separation co-isolated protein contaminants, while size-based tangential flow filtration (TFF) followed by charge-based high-performance anion exchange chromatography (HPAEC) enhances purity (Piroli et al., 2023). Future work should implement orthogonal TTF with HPAEC to purify EcN-OMVs.

5. Conclusion

This is the first study of the effects of EcN-OMVs in obese and diabetic mice based on gut-liver axis metabolomics combined with analysis of the gut microbiome. Overall, our findings have demonstrated that EcN-OMVs can regulate intestinal and liver metabolism by affecting gut microbiota and SCFA concentrations. Thus, this study has laid the foundation for applying EcN-OMVs as a post-biotic agent and potential adjuvant treatment for obesity and diabetes.

Data availability statement

The availability of 16S rRNA gene sequences in this study are deposited in the NCBl Sequence Read Archive database, accession number PRJNA971528.

Ethics statement

The animal studies were approved by Institutional Animal Care and Use Committee (IACUC) of the Chongqing Medical University. The studies were conducted in accordance with the local legislation and institutional requirements. Written informed consent was obtained from the owners for the participation of their animals in this study.

Author contributions

JS contributed to the sample and data collection, performed the statistical analysis, interpreted the results, and wrote the manuscript. DM contributed to interpreting the results and wrote the manuscript. SG, FL, XW, and XP contributed to the samples collection. RC commented on the experimental design and revised the manuscript. T-LH devised the original laboratory study, interpreted the results, supported the writing of the manuscript, directed the project, guarantor of this work and, as such, had full access to all the data in the study and takes responsibility for the integrity of the data and the accuracy of the data analysis. All authors contributed to the article and approved the submitted version.

Funding

This study was supported by the Foundation of State Key Laboratory of Ultrasound in Medicine and Engineering (2023KFKTOO2), Chongqing Science & Technology Commission (cstc2021jcyj-msxmX0213), Chongqing Municipal Education Commission (KJZD-K202100407), and Senior Medical Talents Program of Chongqing for Young and Middle-aged (2022) 15, and the Kuanren Talents Program of the Second Affiliated Hospital of Chongqing Medical University.

Conflict of interest

The authors declare that the research was conducted in the absence of any commercial or financial relationships that could be construed as a potential conflict of interest.

Publisher's note

References

Aguilera, L., Toloza, L., Gimenez, R., Odena, A., Oliveira, E., Aguilar, J., et al. (2014). Proteomic analysis of outer membrane vesicles from the probiotic strain *Escherichia coli* Nissle 1917. *Proteomics* 14, 222–229. doi: 10.1002/pmic.201300328

Ahmadi Badi, S., Moshiri, A., Fateh, A., Rahimi Jamnani, F., Sarshar, M., Vaziri, F., et al. (2017). Microbiota-derived extracellular vesicles as new systemic regulators. *Front. Microbiol.* 8:1610. doi: 10.3389/fmicb.2017.01610

Ashrafian, F., Keshavarz Azizi Raftar, S., Lari, A., Shahryari, A., Abdollahiyan, S., Moradi, H. R., et al. (2021). Extracellular vesicles and pasteurized cells derived from *Akkermansia muciniphila* protect against high-fat induced obesity in mice. *Microb. Cell Factories* 20:219. doi: 10.1186/s12934-021-01709-w

Ashrafian, F., Shahriary, A., Behrouzi, A., Moradi, H. R., Keshavarz Azizi Raftar, S., Lari, A., et al. (2019). *Akkermansia muciniphila*-derived extracellular vesicles as a mucosal delivery vector for amelioration of obesity in mice. *Front. Microbiol.* 10:2155. doi: 10.3389/fmicb.2019.02155

Bergen, W. G., and Wu, G. (2009). Intestinal nitrogen recycling and utilization in health and disease. *J. Nutr.* 139, 821–825. doi: 10.3945/jn.109.104497

Bluher, M. (2019). Obesity: global epidemiology and pathogenesis. *Nat. Rev. Endocrinol.* 15, 288–298. doi: 10.1038/s41574-019-0176-8

Buffie, C. G., Bucci, V., Stein, R. R., McKenney, P. T., Ling, L., Gobourne, A., et al. (2015). Precision microbiome reconstitution restores bile acid mediated resistance to *Clostridium difficile*. *Nature* 517, 205–208. doi: 10.1038/nature13828

Byndloss, M. X., Olsan, E. E., Rivera-Chavez, F., Tiffany, C. R., Cevallos, S. A., Lokken, K. L., et al. (2017). Microbiota-activated PPAR-gamma signaling inhibits dysbiotic Enterobacteriaceae expansion. *Science* 357, 570–575. doi: 10.1126/science.aam9949

Chambers, E. S., Viardot, A., Psichas, A., Morrison, D. J., Murphy, K. G., Zac-Varghese, S. E., et al. (2015). Effects of targeted delivery of propionate to the human colon on appetite regulation, body weight maintenance and adiposity in overweight adults. *Gut* 64, 1744–1754. doi: 10.1136/gutjnl-2014-307913

Chavkin, T. A., Pham, L. D., and Kostic, A. (2021). *E. coli* Nissle 1917 modulates host glucose metabolism without directly acting on glucose. *Sci. Rep.* 11:23230. doi: 10.1038/s41598-021-02431-8

Chelakkot, C., Choi, Y., Kim, D. K., Park, H. T., Ghim, J., Kwon, Y., et al. (2018). *Akkermansia muciniphila*-derived extracellular vesicles influence gut permeability through the regulation of tight junctions. *Exp. Mol. Med.* 50:e450. doi: 10.1038/emm.2017.282

Chen, G., Xie, M., Wan, P., Chen, D., Dai, Z., Ye, H., et al. (2018). Fuzhuan brick tea polysaccharides attenuate metabolic syndrome in high-fat diet induced mice in association with modulation in the gut microbiota. *J. Agric. Food Chem.* 66, 2783–2795. doi: 10.1021/acs.jafc.8b00296

Cho, N. H., Shaw, J. E., Karuranga, S., Huang, Y., da Rocha Fernandes, J. D., Ohlrogge, A. W., et al. (2018). IDF diabetes atlas: global estimates of diabetes prevalence for 2017 and projections for 2045. *Diabetes Res. Clin. Pract.* 138, 271–281. doi: 10.1016/j.diabres.2018.02.023

Cynober, L. (1994). Can arginine and ornithine support gut functions? *Gut* 35, S42–S45. doi: 10.1136/gut.35.1_suppl.s42

Das, U. N. (2018). Arachidonic acid in health and disease with focus on hypertension and diabetes mellitus: a review. *J. Adv. Res.* 11, 43–55. doi: 10.1016/j.jare.2018.01.002

den Besten, G., Bleeker, A., Gerding, A., van Eunen, K., Havinga, R., van Dijk, T. H., et al. (2015). Short-chain fatty acids protect against high-fat diet-induced obesity via a PPARgamma-dependent switch from lipogenesis to fat oxidation. *Diabetes* 64, 2398–2408. doi: 10.2337/db14-1213

Diez-Sainz, E., Milagro, F. I., Riezu-Boj, J. I., and Lorente-Cebrian, S. (2022). Effects of gut microbiota-derived extracellular vesicles on obesity and diabetes and their potential modulation through diet. *J. Physiol. Biochem.* 78, 485–499. doi: 10.1007/s13105-021-00837-6

Du, C., Quan, S., Nan, X., Zhao, Y., Shi, F., Luo, Q., et al. (2021). Effects of oral milk extracellular vesicles on the gut microbiome and serum metabolome in mice. *Food Funct.* 12, 10938–10949. doi: 10.1039/d1fo02255e

Durack, J., and Lynch, S. V. (2019). The gut microbiome: relationships with disease and opportunities for therapy. *J. Exp. Med.* 216, 20–40. doi: 10.1084/jem.20180448

Fabrega, M. J., Aguilera, L., Gimenez, R., Varela, E., Alexandra Canas, M., Antolin, M., et al. (2016). Activation of immune and defense responses in the intestinal mucosa by outer membrane vesicles of commensal and probiotic *Escherichia coli* strains. *Front. Microbiol.* 7:705. doi: 10.3389/fmicb.2016.00705

Fabrega, M. J., Rodriguez-Nogales, A., Garrido-Mesa, J., Algieri, F., Badia, J., Gimenez, R., et al. (2017). Intestinal anti-inflammatory effects of outer membrane vesicles from *Escherichia coli* Nissle 1917 in DSS-experimental colitis in mice. *Front. Microbiol.* 8:1274. doi: 10.3389/fmicb.2017.01274

Furuyama, N., and Sircili, M. P. (2021). Outer membrane vesicles (OMVs) produced by gram-negative Bacteria: structure, functions, biogenesis, and vaccine application. *Biomed. Res. Int.* 2021, 1490732–1490716. doi: 10.1155/2021/1490732

Gao, S., Long, F., Jiang, Z., Shi, J., Ma, D., Yang, Y., et al. (2022). The complex metabolic interactions of liver tissue and hepatic exosome in PCOS mice at young and middle age. *Front. Physiol.* 13:990987. doi: 10.3389/fphys.2022.990987

Geervliet, M., de Vries, H., Jansen, C. A., Rutten, V., van Hees, H., Wen, C., et al. (2022). Effects of *E scherichia coli* Nissle 1917 on the porcine gut microbiota, intestinal epithelium and immune system in early life. *Front. Microbiol.* 13:842437. doi: 10.3389/fmicb.2022.842437

Gheibi, S., Kashfi, K., and Ghasemi, A. (2017). A practical guide for induction of type-2 diabetes in rat: incorporating a high-fat diet and streptozotocin. *Biomed. Pharmacother.* 95, 605–613. doi: 10.1016/j.biopha.2017.08.098

Gomes, A. C., Hoffmann, C., and Mota, J. F. (2018). The human gut microbiota: metabolism and perspective in obesity. *Gut Microbes* 9, 1–18. doi: 10.1080/19490976.2018.1465157

Hancock, V., Vejborg, R. M., and Klemm, P. (2010). Functional genomics of probiotic *Escherichia coli* Nissle 1917 and 83972, and UPEC strain CFT073: comparison of

transcriptomes, growth and biofilm formation. *Mol. Gen. Genomics.* 284, 437–454. doi: 10.1007/s00438-010-0578-8

Harding, J. L., Pavkov, M. E., Magliano, D. J., Shaw, J. E., and Gregg, E. W. (2019). Global trends in diabetes complications: a review of current evidence. *Diabetologia* 62, 3–16. doi: 10.1007/s00125-018-4711-2

Hu, R., Lin, H., Li, J., Zhao, Y., Wang, M., Sun, X., et al. (2020). Probiotic *Escherichia coli* Nissle 1917-derived outer membrane vesicles enhance immunomodulation and antimicrobial activity in RAW264.7 macrophages. *BMC Microbiol.* 20:268. doi: 10.1186/s12866-020-01953-x

Iatcu, C. O., Steen, A., and Covasa, M. (2021). Gut microbiota and complications of Type-2 diabetes. *Nutrients* 14:166. doi: 10.3390/nu14010166

Joseph, N., Vasodavan, K., Saipudin, N. A., Yusof, B. N. M., Kumar, S., and Nordin, S. A. (2019). Gut microbiota and short-chain fatty acids (SCFAs) profiles of normal and overweight school children in Selangor after probiotics administration. *J. Funct. Foods* 57, 103–111. doi: 10.1016/j.jff.2019.03.042

Kelly, T., Yang, W., Chen, C. S., Reynolds, K., and He, J. (2008). Global burden of obesity in 2005 and projections to 2030. *Int. J. Obes.* 32, 1431–1437. doi: 10.1038/ijo.2008.102

Khan, M. A. B., Hashim, M. J., King, J. K., Govender, R. D., Mustafa, H., and Al Kaabi, J. (2020). Epidemiology of type 2 diabetes – global burden of disease and forecasted trends. *J. Epidemiol. Glob. Health* 10, 107–111. doi: 10.2991/jegh.k.191028.001

Kim, O. Y., Lee, J., and Gho, Y. S. (2017). Extracellular vesicle mimetics: novel alternatives to extracellular vesicle-based theranostics, drug delivery, and vaccines. *Semin. Cell Dev. Biol.* 67, 74–82. doi: 10.1016/j.semcdb.2016.12.001

Kim, J. H., Lee, J., Park, J., and Gho, Y. S. (2015). Gram-negative and gram-positive bacterial extracellular vesicles. *Semin. Cell Dev. Biol.* 40, 97–104. doi: 10.1016/j.semcdb.2015.02.006

Konikoff, T., and Gophna, U. (2016). Oscillospira: a central, enigmatic component of the human gut microbiota. *Trends Microbiol.* 24, 523–524. doi: 10.1016/j.tim.2016.02.015

Kurata, N., Tokashiki, N., Fukushima, K., Misao, T., Hasuoka, N., Kitagawa, K., et al. (2019). Short chain fatty acid butyrate uptake reduces expressions of prostanoid EP(4) receptors and their mediation of cyclooxygenase-2 induction in HCA-7 human colon cancer cells. *Eur. J. Pharmacol.* 853, 308–315. doi: 10.1016/j.ejphar.2019.04.014

Lee, E. Y., Bang, J. Y., Park, G. W., Choi, D. S., Kang, J. S., Kim, H. J., et al. (2007). Global proteomic profiling of native outer membrane vesicles derived from *Escherichia coli*. *Proteomics* 7, 3143–3153. doi: 10.1002/pmic.200700196

Lenzen, S. (2008). The mechanisms of alloxan- and streptozotocin-induced diabetes. *Diabetologia* 51, 216–226. doi: 10.1007/s00125-007-0886-7

Liu, R., Li, Y., and Zhang, B. (2016). The effects of konjac oligosaccharide on TNBS-induced colitis in rats. *Int. Immunopharmacol.* 40, 385–391. doi: 10.1016/j.intimp.2016.08.040

Meldrum, D. R., Morris, M. A., and Gambone, J. C. (2017). Obesity pandemic: causes, consequences, and solutions-but do we have the will? *Fertil. Steril.* 107, 833–839. doi: 10.1016/j.fertnstert.2017.02.104

Nah, G., Park, S. C., Kim, K., Kim, S., Park, J., Lee, S., et al. (2019). Type-2 diabetics reduces spatial variation of microbiome based on extracellur vesicles from gut microbes across human body. *Sci. Rep.* 9:20136. doi: 10.1038/s41598-019-56662-x

Newgard, C. B., An, J., Bain, J. R., Muehlbauer, M. J., Stevens, R. D., Lien, L. F., et al. (2009). A branched-chain amino acid-related metabolic signature that differentiates obese and lean humans and contributes to insulin resistance. *Cell Metab.* 9, 311–326. doi: 10.1016/j.cmet.2009.02.002

Nylund, L., Hakkola, S., Lahti, L., Salminen, S., Kalliomaki, M., Yang, B., et al. (2020). Diet, perceived intestinal well-being and compositions of fecal microbiota and short chain fatty acids in oat-using subjects with celiac disease or gluten sensitivity. *Nutrients* 12:2570. doi: 10.3390/nu12092570

Palm, N. W., de Zoete, M. R., Cullen, T. W., Barry, N. A., Stefanowski, J., Hao, L., et al. (2014). Immunoglobulin a coating identifies colitogenic bacteria in inflammatory bowel disease. *Cells* 158, 1000–1010. doi: 10.1016/j.cell.2014.08.006

Piroli, N. H., Reus, L. S. C., Mamczarz, Z., Khan, S., Bentley, W. E., and Jay, S. M. (2023). High performance anion exchange chromatography purification of probiotic bacterial extracellular vesicles enhances purity and anti-inflammatory efficacy. *bioRxiv*. doi: 10.1101/2023.05.01.538917

Qi, H., Li, Y., Yun, H., Zhang, T., Huang, Y., Zhou, J., et al. (2019). Lactobacillus maintains healthy gut mucosa by producing L-ornithine. *Commun. Biol.* 2:171. doi: 10.1038/s42003-019-0424-4

Qiao, Y., Tomonaga, S., Matsui, T., and Funaba, M. (2016). Modulation of the cellular content of metabolites in adipocytes by insulin. *Mol. Cell. Endocrinol.* 424, 71–80. doi: 10.1016/j.mce.2016.01.017

Qin, J., Li, R., Raes, J., Arumugam, M., Burgdorf, K. S., Manichanh, C., et al. (2010). A human gut microbial gene catalogue established by metagenomic sequencing. *Nature* 464, 59–65. doi: 10.1038/nature08821

Qu, M., Zhu, H., and Zhang, X. (2022). Extracellular vesicle-mediated regulation of macrophage polarization in bacterial infections. *Front. Microbiol.* 13:1039040. doi: 10.3389/fmicb.2022.1039040

Raftar, S. K. A., Ashrafian, F., Abdollahiyan, S., Yadegar, A., Moradi, H. R., Masoumi, M., et al. (2022). The anti-inflammatory effects of Akkermansia muciniphila and its derivates in HFD/CCL4-induced murine model of liver injury. *Sci. Rep.* 12:2453. doi: 10.1038/s41598-022-06414-1

Raftar, S. K. A., Ashrafian, F., Yadegar, A., Lari, A., Moradi, H. R., Shahriary, A., et al. (2021). The protective effects of live and pasteurized Akkermansia muciniphila and its extracellular vesicles against HFD/CCl4-induced liver injury. *Microbiol. Spectr.* 9:e0048421. doi: 10.1128/Spectrum.00484-21

Rojas, D. R., Kuner, R., and Agarwal, N. (2019). Metabolomic signature of type 1 diabetes-induced sensory loss and nerve damage in diabetic neuropathy. *J. Mol. Med. (Berl)* 97, 845–854. doi: 10.1007/s00109-019-01781-1

Rozanska, D., Regulska-Ilow, B., Choroszy-Krol, I., and Ilow, R. (2014). The role of *Escherichia coli* strain Nissle 1917 in the gastro-intestinal diseases. *Postepy Hig. Med. Dosw. (Online)* 68, 1251–1256. doi: 10.5604/17322693.1127882

Salgaco, M. K., Oliveira, L. G. S., Costa, G. N., Bianchi, F., and Sivieri, K. (2019). Relationship between gut microbiota, probiotics, and type 2 diabetes mellitus. *Appl. Microbiol. Biotechnol.* 103, 9229–9238. doi: 10.1007/s00253-019-10156-y

Sanders, M. E., Merenstein, D. J., Reid, G., Gibson, G. R., and Rastall, R. A. (2019). Probiotics and prebiotics in intestinal health and disease: from biology to the clinic. *Nat. Rev. Gastroenterol. Hepatol.* 16, 605–616. doi: 10.1038/s41575-019-0173-3

Scaldaferri, F., Gerardi, V., Mangiola, F., Lopetuso, L. R., Pizzoferrato, M., Petito, V., et al. (2016). Role and mechanisms of action of *Escherichia coli* Nissle 1917 in the maintenance of remission in ulcerative colitis patients: an update. *World J. Gastroenterol.* 22, 5505–5511. doi: 10.3748/wjg.v22.i24.5505

Singer-Englar, T., Barlow, G., and Mathur, R. (2019). Obesity, diabetes, and the gut microbiome: an updated review. *Expert Rev. Gastroenterol. Hepatol.* 13, 3–15. doi: 10.1080/17474124.2019.1543023

Sivashanmugam, M., Jaidev, J., Umashankar, V., and Sulochana, K. N. (2017). Ornithine and its role in metabolic diseases: an appraisal. *Biomed. Pharmacother.* 86, 185–194. doi: 10.1016/j.biopha.2016.12.024

Sommer, F., and Backhed, F. (2013). The gut microbiota—masters of host development and physiology. *Nat. Rev. Microbiol.* 11, 227–238. doi: 10.1038/nrmicro2974

Spencer, M. D., Hamp, T. J., Reid, R. W., Fischer, L. M., Zeisel, S. H., and Fodor, A. A. (2011). Association between composition of the human gastrointestinal microbiome and development of fatty liver with choline deficiency. *Gastroenterology* 140, 976–986. doi: 10.1053/j.gastro.2010.11.049

Szkudelski, T. (2001). The mechanism of alloxan and streptozotocin action in B cells of the rat pancreas. *Physiol. Res.* 50, 537–546.

Vallianou, N., Stratigou, T., Christodoulatos, G. S., Tsigalou, C., and Dalamaga, M. (2020). Probiotics, prebiotics, synbiotics, postbiotics, and obesity: current evidence, controversies, and perspectives. *Curr. Obes. Rep.* 9, 179–192. doi: 10.1007/s13679-020-00379-w

van der Hee, B., and Wells, J. M. (2021). Microbial regulation of host physiology by short-chain fatty acids. *Trends Microbiol.* 29, 700–712. doi: 10.1016/j.tim.2021.02.001

Vemuri, R., Shinde, T., Gundamaraju, R., Gondalia, S. V., Karpe, A. V., Beale, D. J., et al. (2018). *Lactobacillus acidophilus* DDS-1 modulates the gut microbiota and improves metabolic profiles in aging mice. *Nutrients* 10:1255. doi: 10.3390/nu10091255

Wen, L., and Duffy, A. (2017). Factors influencing the gut microbiota, inflammation, and type 2 diabetes. *J. Nutr.* 147, 1468S–1475S. doi: 10.3945/jn.116.240754

Wexler, H. M. (2007). Bacteroides: the good, the bad, and the nitty-gritty. *Clin. Microbiol. Rev.* 20, 593–621. doi: 10.1128/CMR.00008-07

Woith, E., Fuhrmann, G., and Melzig, M. F. (2019). Extracellular vesicles-connecting kingdoms. *Int. J. Mol. Sci.* 20:5695. doi: 10.3390/ijms20225695

Yang, J., Li, Y., Wen, Z., Liu, W., Meng, L., and Huang, H. (2021). Oscillospira – a candidate for the next-generation probiotics. *Gut Microbes* 13:1987783. doi: 10.1080/19490976.2021.1987783

Yoshida, N., Yamashita, T., Osone, T., Hosooka, T., Shinohara, M., Kitahama, S., et al. (2021). Bacteroides spp. promotes branched-chain amino acid catabolism in brown fat and inhibits obesity. *iScience* 24:103342. doi: 10.1016/j.isci.2021.103342

Zschaler, J., Schlorke, D., and Arnhold, J. (2014). Differences in innate immune response between man and mouse. *Crit. Rev. Immunol.* 34, 433–454. doi: 10.1615/CritRevImmunol.2014011600

frontiers | Frontiers in Microbiology

TYPE Original Research
PUBLISHED 18 September 2023
DOI 10.3389/fmicb.2023.1214577

OPEN ACCESS

EDITED BY
Ren-You Gan,
Agency for Science, Technology and Research, Singapore

REVIEWED BY
Teng-Gen Hu,
Guangdong Academy of Agricultural Sciences (GDAAS), China
Guoyi Tang,
The University of Hong Kong, Hong Kong SAR, China

*CORRESPONDENCE
Ying Cai
✉ 31650124@qq.com

RECEIVED 30 April 2023
ACCEPTED 07 August 2023
PUBLISHED 18 September 2023

CITATION
Peng X, Yi X, Deng N, Liu J, Tan Z and Cai Y (2023) Zhishi Daozhi decoction alleviates constipation induced by a high-fat and high-protein diet via regulating intestinal mucosal microbiota and oxidative stress. *Front. Microbiol.* 14:1214577. doi: 10.3389/fmicb.2023.1214577

Zhishi Daozhi decoction alleviates constipation induced by a high-fat and high-protein diet via regulating intestinal mucosal microbiota and oxidative stress

Xinxin Peng[1], Xin Yi[2], Na Deng[2], Jing Liu[2], Zhoujin Tan[2] and Ying Cai[2]*

[1]The First Affiliated Hospital of Hunan University of Chinese Medicine, Changsha, China, [2]The Domestic First-Class Discipline Construction Project of Chinese Medicine, Hunan University of Chinese Medicine, Changsha, China

Background: A growing body of evidence has demonstrated that a high-fat and high-protein diet (HFHPD) causes constipation. This study focuses on understanding how the use of Zhishi Daozhi decoction (ZDD) affects the intricate balance of intestinal microorganisms. The insights gained from this investigation hold the potential to offer practical clinical approaches to mitigate the constipation-related issues associated with HFHPD.

Materials and methods: Mice were randomly divided into five groups: the normal (MN) group, the natural recovery (MR) group, the low-dose ZDD (MLD) group, the medium-dose ZDD (MMD) group, and the high-dose ZDD (MHD) group. After the constipation model was established by HFHPD combined with loperamide hydrochloride (LOP), different doses of ZDD were used for intervention. Subsequently, the contents of cholecystokinin (CCK) and calcitonin gene-related peptide (CGRP) in serum, superoxide dismutase (SOD), and malondialdehyde (MDA) in the liver were determined. The DNA of intestinal mucosa was extracted, and 16S rRNA amplicon sequencing was used to analyze the changes in intestinal mucosal microbiota.

Results: After ZDD treatment, CCK content in MR group decreased and CGRP content increased, but the changes were not significant. In addition, the SOD content in MR group was significantly lower than in MLD, MMD, and MHD groups, and the MDA content in MR group was significantly higher than in MN, MLD, and MHD groups. Constipation modeling and the intervention of ZDD changed the structure of the intestinal mucosal microbiota. In the constipation induced by HFHPD, the relative abundance of pathogenic bacteria such as *Aerococcus*, *Staphylococcus*, *Corynebacterium*, *Desulfovibrio*, *Clostridium*, and *Prevotella* increased. After the intervention of ZDD, the relative abundance of these pathogenic bacteria decreased, and the relative abundance of *Candidatus Arthromitus* and the abundance of Tropane, piperidine, and pyridine alkaloid biosynthesis pathways increased in MHD group.

Conclusion: Constipation induced by HFHPD can increase pathogenic bacteria in the intestinal mucosa, while ZDD can effectively relieve constipation, reduce the relative abundance of pathogenic bacteria, and alleviate oxidative stress injury. In addition, high-dose ZDD can increase the abundance of beneficial bacteria, which is more conducive to the treatment of constipation.

KEYWORDS

Zhishi Daozhi decoction, high-fat and high-protein diet, microbial diversity, intestinal mucosal microbiota, constipation

1. Introduction

Constipation is a common and onerous gastrointestinal disease (Dimidi et al., 2017). Its definition includes infrequent defecation, excessive tension, a feeling of incomplete defecation, failure, or excessive time spent on defecation attempts (Sharma and Rao, 2017). Eating habits are one of the important factors that cause constipation. Studies have shown that unhealthy diets, especially HFHPD and low-fiber diets, are important predisposing factors for constipation (Stewart and Schroeder, 2013; Tabbers et al., 2014). In contrast, the intake of dietary fiber and the appropriate amount of water can relieve the symptoms of constipation (Yang et al., 2012). Studies have found that a high-fat diet can cause indigestion, cause constipation, and delay colon transit time by reducing colon mucus in mice (Mukai et al., 2020). Moreover, Liu et al. (2022) found that under a high-fat diet, LOP-induced constipation in mice developed symptoms such as oxidative stress, gastrointestinal hypomotility, and intestinal neurotransmitter disorder. In a study involving older adults and children, high saturated fat intake was closely related to constipation (Lee et al., 2012; Taba Taba Vakili et al., 2015).

Numerous recent studies have shown that constipation is closely related to the intestinal microbiota. The feces in the intestine are stimulated by harmful substances and enrich the harmful bacteria (Zhang X. et al., 2021). Changes in the intestinal microbiota of patients with constipation are generally manifested by a relative decrease in beneficial bacteria and a potential increase in harmful bacteria. These changes may affect intestinal motility and intestinal secretion function by changing the amount of available physiologically active substances in the intestine and the intestinal metabolic environment (Staller et al., 2022). In addition, diet will also change the genetic composition and metabolic activities of the microorganisms living in our bodies. It can be deduced that a high-fat diet has an important relationship with the occurrence of chronic diseases such as constipation (Tan et al., 2021). LOP is a commonly used antidiarrheal in clinics to increase the consistency and hardness of stool to control the symptoms of acute and chronic diarrhea. Thus, LOP is suitable to serve as an inducer combined with HFHPD to establish a constipation animal model (Zhang et al., 2022).

ZDD is a prescription in traditional Chinese medicines derived from Li Dongyuan's Nei Wai Shang Bian Huo Lun and is used for the treatment of constipation and indigestion (Liu F. et al., 2020). Modern pharmacological research shows that ZDD can promote gastric emptying and small intestine propulsion to restore the function of the spleen and stomach transport (Li et al., 2008). This prescription consists of Aurantii Fructus Immaturus (*Citrus aurantium* L.), Rhei Radix et Rhizoma (*Rheum officinale Baill.*), Poria [*Poria cocos* (Schw.) Wolf], Scutellariae Radix (*Scutellaria baicalensis* Georgi), Coptidis Rhizoma (*Coptis chinensis* Franch.), Atractylodis Macrocephalae Rhizoma (*Atractylodes macrocephala* Koidz.), Alismatis Rhizoma [*Alisma orientate* (Sam.) Juzep.], and Massa Medicata Fermentata (Medicated Leaven) (Lin et al., 2020). Among them, Atractylodis Macrocephalae Rhizoma and Poria can improve gastrointestinal hormone secretion and promote gastric emptying. Alismatis Rhizoma has a hypoglycemic effect. Rhei Radix, and Rhizoma can inhibit intestinal water absorption, enhance intestinal peristalsis, and promote defecation. Aurantii Fructus Immaturus can recover intestinal contraction rhythm, improve gastrointestinal excitability, enhance gastrointestinal peristalsis, and relieve gastrointestinal spasms. Massa Medicata Fermentata can increase appetite and maintain the normal digestive function of the body. The combination of these drugs has a definite effect on gastrointestinal infectious inflammation with dyspepsia (Wang et al., 2018; Shen and Tan, 2022). The curative effect of decoction is more obvious than that of pills, and it takes effect faster (Zhu et al., 2022).

However, the relationship between the changes in intestinal mucosal microbiota induced by HFHPD and constipation remains unclear. Therefore, in this study, the constipation model of mice was induced by LOP under the condition of HFHPD. To study the changes in intestinal mucosal microbiota and the levels of gastrointestinal hormones and oxidative stress in mice with HPHFD-induced constipation under the intervention of ZDD.

2. Materials and methods

2.1. Materials

2.1.1. Animals

To exclude the influence of gender on the study, we selected 50 specific-pathogen-free male mice as the research objects (Wu et al., 2022). Mice were purchased from Hunan Slaccas Jingda Laboratory Animal Co., Ltd.

2.1.2. Feed

Self-made high-fat and high-protein feed consists of milk powder (Nestle family nutritious milk powder), flour (Huiyi gluten wheat flour), floss powder (Zhenqiao golden floss), and bean powder (Yonghe sweet soybean milk powder) in a ratio of 1: 1: 1: 2 (He et al., 2019).

The main indexes of nutritional components of growth feed include water, crude protein, crude fiber, crude fat, crude ash, calcium, total phosphorus, lysine, methionine, and cystine. It was provided by the Animal Experiment Center of the Hunan University of Chinese Medicine.

2.1.3. Drugs

ZDD consists of 10 g of Aurantii Fructus Immaturus, 20 g of Rhei Radix et Rhizoma, 6 g of Coptidis Rhizoma, 6 g of Scutellariae Radix, 10 g of Massa Medicata Fermentata, 10 g of Atractylodis Macrocephalae Rhizoma, 6 g of Poria, and 4 g of Alismatis Rhizoma. All these ingredients were purchased from the First Affiliated Hospital of Hunan University of Chinese Medicine. The procedure involved soaking the aforementioned drugs in boiling water for 10 cycles, with each cycle lasting 10 min. The resulting mixture was then filtered and concentrated using a rotary evaporator at 75°C. This process yielded water-based decoctions with varying crude drug concentrations of 0.2, 0.4, and 0.8 g/mL.

LOP capsules was produced by Xian Janssen Pharmaceutical Co., Ltd. (Batch production No. MDJ7007).

2.2. Methods

2.2.1. Grouping of experimental animals

All the mice were fed adaptively at a temperature of 23–25°C and a relative humidity of 50–70% in a clean and quiet environment for 3 days before modeling. The 50 mice were randomly divided into five groups: the normal (MN) group, the natural recovery (MR) group, the low-dose ZDD (MLD) group, the medium-dose ZDD (MMD) group, and the high-dose ZDD (MHD) group. All experiments and procedures involving animals were conducted in accordance with the protocol approved by the Institutional Animal Care and Use Committee of the Hunan University of Chinese Medicine.

2.2.2. Construction of the constipation model

The procedure was divided into two stages. In the first stage, the model mice were fed with HFHPD and gavaged with 50 mg/kg milk twice a day. MN group was fed growth feed and gavaged with an equal dose of sterile water for 7 days (Mai et al., 2018). In the second stage, based on the first stage, the model mice were intraperitoneally injected with 3 mg/kg LOP for 7 days, once a day. MN group ate normally and was intraperitoneally injected with equal doses of normal saline for 7 days (Hajji et al., 2020).

2.2.3. Intervention of ZDD

After the successful model, the model mice were divided into MR, MLD, MMD, and MHD groups. The mice in MLD, MMD, and MHD groups were gavaged with 2.4, 4.7, and 9.4 mg/kg ZDD, respectively, twice a day. MN and MR groups were gavaged with an equal dose of sterile water for 7 days.

2.2.4. General characteristics

At the same time in the morning, the mice were observed and recorded in terms of fur, mental status, activity, fecal traits and odor, perianal cleanliness, and body weight (Li C. R. et al., 2022).

2.2.5. Measurement of CCK and CGRP in serum and MDA and SOD in liver

We selected five mice with consistent fecal characteristics in each group for analysis, and whole blood samples were collected by eyeball extraction. The blood sample was allowed to stand at room temperature for 2 h before being centrifuged at low temperature and high speed (4°C, 3,000 r/min) for 10 min. The supernatant was used for CCK and CGRP content determination. The CCK and CGRP contents of serum were determined by enzyme-linked immunosorbent assay (ELISA). After the mice were killed by cervical dislocation on the aseptic operating platform, the liver was removed, and 0.1 g of liver tissue was collected. Then, 1 mL of normal saline was added to the liver tissue in the ice bath for homogenization, and the mixture was centrifuged at 8,000 g, 4°C for 10 min. The MDA and SOD contents in liver homogenate were determined by ELISA, and the specific operation was carried out according to the instructions of the kit. The MDA kit was provided by Beijing Solarbio Science & Technology Co., Ltd. The CCK, CGRP, and SOD kits were provided by Quanzhou Kenuodi Biotechnology Co., Ltd.

2.2.6. Extraction of intestinal mucosal samples

In each group, five mice were chosen based on consistent fecal characteristics. These mice were euthanized through cervical dislocation on a sterile operating table, and segments spanning from the jejunum to the ileum were collected. After the contents of the bowel segment were extruded, the bowel was cut longitudinally. Then, the residual contents in the intestinal wall were washed with normal saline, and the normal saline on the intestinal wall was sucked dry with filter paper. The intestinal mucosa was scraped off with a cover glass and placed in an EP tube at −80°C for subsequent storage (Zhang et al., 2020).

2.2.7. PCR amplification and illumina Novaseq metagenome sequencing

PCR amplification was conducted using bacteria-specific primers targeting the 16S rRNA V3+V4 region. The primer sequences used were as follows: Forward primer 338F (5′-barcode + ACTCCTACGGGAGGCAGCA-3′) and reverse primer 806R (5′-GGACTACHVGGGTWTCTAAT-3′). The template DNA was pre-denatured at 98°C for 30 s using the PCR instrument, ensuring its completed denaturation for the subsequent amplification cycle. Within each cycle, the template was subjected to a 15-s denaturation step at 98°C, followed by a 30-s primer annealing step at 50°C to ensure optimal primer-template binding. The temperature was then maintained at 72°C for 30 s, facilitating primer extension, DNA synthesis, and completion of a single cycle. This cycle was iterated between 25 an 27 times to accumulate a substantial quantity of amplified DNA fragments. Finally, the product was kept at 72°C for 5 min so that it was completely extended and preserved at 4°C. The amplification results were subjected to 2% agarose gel electrophoresis, and the target fragments were cut out, and then, the target fragments were recovered using the Axygen gel recovery kit. Then, 2 × 250 bp double-ended sequencing was performed on the Illumina NovaSeq machine using the Novaseq 6000 SP Reagent Kit (500 cycles). Sample DNA extraction, amplification, and library sequencing were completed by Shanghai Personalbio Technology Co., Ltd.

2.2.8. Bioinformatics

The 16S rRNA high-throughput sequencing was used to analyze the intestinal mucosal microbiota, and the modified and improved process was used to analyze the biological information of the microbiota. Moreover, 100% sequence similarity was merged to generate characteristic sequence amplicon sequence variants (ASV). The ASV table was used to draw a species accumulation curve, which is used to detect the sequencing depth and evaluate the quality of the sequence data (Qiao et al., 2023). At the same time, various metrics at the ASV level, including Chao 1, observed categories, Shannon, and Simpson indices, were calculated and analyzed based on the ASV table. Beta diversity analysis uses the Bray–Curtis distance to analyze the structural changes of microbial communities between samples and uses non-metric

multidimensional scaling (NMDS) for visualization (Li X. Y. et al., 2022). The linear discriminant analysis (LDA) effect size (LefSe) method is used to detect classification units with rich differences between groups. To evaluate the diagnostic efficiency of different genera selected by LefSe analysis, the statistically significant receiver operating characteristic (ROC) curves of different genera were constructed, and the area under the curve (AUC) was calculated. We calculated the Spearman correlation coefficient, constructed a correlation heat map, and explored the relationship between different microbiota. The metabolic function of microbial microbiota was predicted using PICRUSt2 on the Kyoto Encyclopedia of Genes and Genomes (KEGG) (https://www.kegg.jp/) database (Douglas et al., 2020).

2.2.9. Statistical analysis

SPSS 25.00 software was used for statistical analysis, and the data of each group were expressed as the mean ± standard deviation. GraphPad Prism 9 was used to draw histograms and box charts. If the two groups of data conform to a normal distribution and homogeneity of variance, the ANOVA test is used. The non-parametric test was used if it did not meet the requirements. A P-value of <0.05 was statistically significant.

3. Results

3.1. Effects of different doses of ZDD on the general characteristics of mice with HPHFD-induced constipation

Before modeling, the mice in each group had glossy fur and good autonomous activity. After the modeling was completed, the model mice had withered fur and liked to gather, and their autonomous activity ability was reduced. After the intervention of ZDD, the fur was smooth, and the ability to make independent movements was improved. However, the fur of MR group was yellow, and the mental activity was poor. As can be observed from Figure 1, before modeling (0 d), the weight of mice in each group was similar, and in the first (7 d) and second modeling stages (14 d), the weight of model mice was lower than MN group. However, after the administration of ZDD (21 d), the weights of the mice in the MLD, MMD, and MHD groups increased more than that of the mice in the MR group, though not significantly, and the weight of the mice in the MHD group was closer to that of the mice in the MN group.

Before modeling, the feces of mice in each group were similar in appearance, shaped with moderate hardness, and turned dark brown. After the first stage of modeling, the feces of model mice were shaped but soft, sticky, and yellow. After the second modeling stage, the model mice had feces characterized by a beaded appearance. These feces were sticky and soft and exhibited signs of being incomplete during defecation, requiring more time for the process. After the administration of ZDD, the feces of MLD, MMD, and MHD groups had a moderate level of hardness, which was similar to that of the MN group. However, the feces of the mice in the MR group were harder notably harder than those of the MN group, with a rough, uneven, and dark brown appearance. Given the characteristics of incomplete defecation and the extended duration of the second modeling stage, we believe that the modeling process was successful.

3.2. Effects of different doses of ZDD on the contents of CCK and CGRP in the serum of mice with HPHFD-induced constipation

CCK is secreted by a large number of cells in the central nervous system, duodenum, and jejunum mucosa of mammals. It stimulates the contraction of the gallbladder and relaxation of the sphincter of Oddi to regulate the movement of the small intestine and colon (Wang et al., 2021). Figure 2A shows the CCK content of mice. Though not significantly, the CCK content in MR group was lower than that in MLD, MMD, and MHD groups. In particular, the CCK content in MHD and MN groups was similar. It could be speculated that ZDD had a certain recovery effect on CCK content in constipated mice.

CGRP, mainly distributed in the visceral sensory nerves, inhibits most gastrointestinal movement and is an important neurotransmitter for regulating the function of the digestive tract (Zhang et al., 2018). As shown in Figure 2B, compared to the MR group, the CGRP content in the MLD, MMD, and MHD groups decreased but not significantly. It can be shown that the intestinal peristalsis ability of mice had been restored to some extent after the administration of ZDD.

3.3. Effects of different doses of ZDD on the contents of SOD and MDA in the liver of mice with HPHFD-induced constipation

Oxidative stress has a strong cytotoxic effect on the body, which can damage the intestinal mucosal cells and cause intestinal mucosal dysfunction or induce or aggravate constipation (Xiang et al., 2019; Yi et al., 2023). SOD is an important antioxidant enzyme in the body and can play an antioxidant role (Kim et al., 2021). Figure 2C shows that the SOD content in the mice of the MR groups is significantly lower than that of the MLD, MMD, and MHD groups. At the same time, the SOD content in the MN group is significantly lower than that in the MLD and MHD groups. MDA is one of the products of lipid peroxidation, and its concentration can reflect the degree of cell damage, serving as one of the biomarkers for oxidative stress (Tangvarasittichai, 2015). As shown in Figure 2D, the MDA content in the MR group was significantly higher than that in the MN, MLD, and MHD groups. Combined with the detection results of SOD content, constipation will cause oxidative stress damage to the body, and ZDD has an antioxidant effect.

3.4. Effects of different doses of ZDD on the intestinal mucosal microbiota of mice with HPHFD-induced constipation

The Chao 1 dilution curve (Figure 3A) shows that when the sequencing amount of each sample reaches 2,000, the curve enters a

10.3389/fmicb.2023.1214577

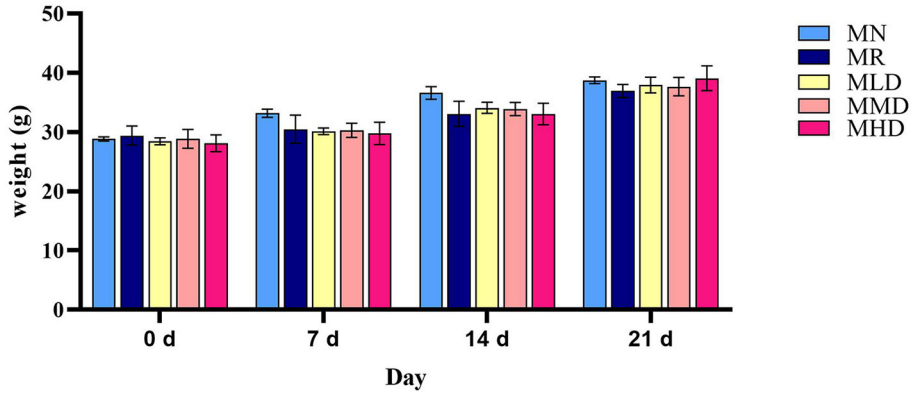

FIGURE 1
Changes of body weight in mice.

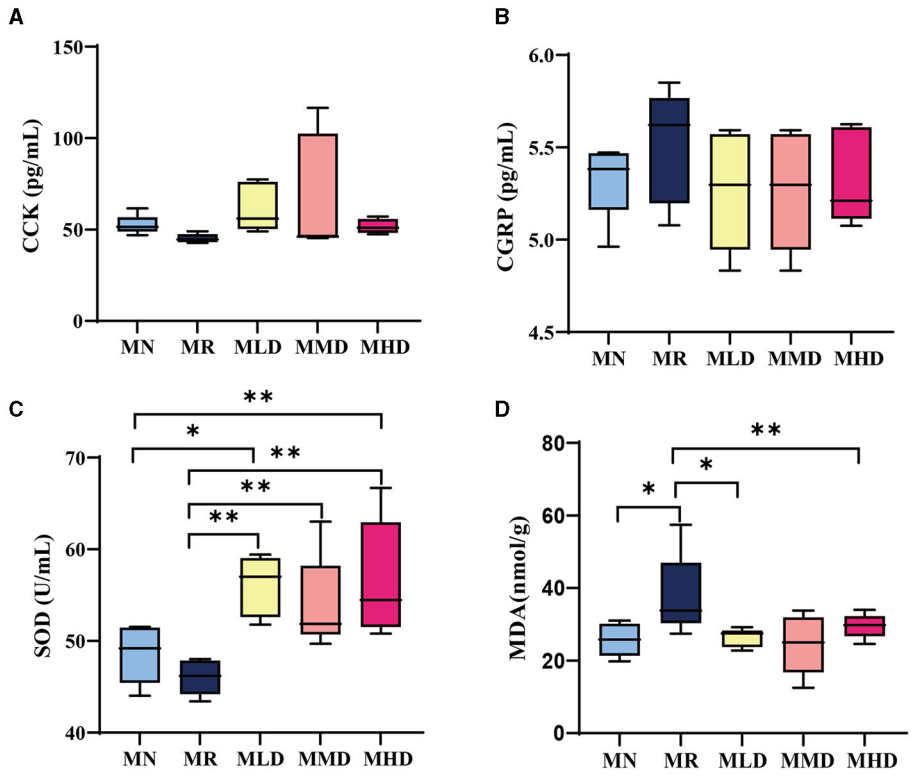

FIGURE 2
Gastrointestinal hormone and oxidative stress level of mice. **(A)** CCK content in serum. **(B)** CGRP content in serum. **(C)** SOD content in the liver. **(D)** MDA content in the liver. $n = 5$, $^{*}p < 0.05$, $^{**}p < 0.01$.

plateau period, and the microbial amount detected in each sample is close to saturation. It shows that the current sequencing depth is enough to reflect the microbial diversity in this sample batch. The total ASV numbers of MN, MR, MLD, MMD, and MHD groups were 209, 290, 415, 184, and 431, respectively. The ASV number of the five groups that generated the intersection was 38 (Figure 3B). It can be seen that MHD group has the largest number of ASVs, which is consistent with the ASV of the MHD group in the Venn diagram above (Figure 3C). Figure 3D shows the Alpha diversity index. Compared with the MN group, the Chao1 indices and observed species had different degrees of increase in the MR, MLD, MMD, and MHD groups. Compared with the MN group, the Shannon and Simpson indices were increased in the MR, MLD, and MMD groups, while the MHD group were decreased, though not significantly, which needs further analysis through the structure of the intestinal microbiota. In NMDS analysis (Figure 3E), there is no intersection between the MN and MR groups, which indicates that constipation induced by HPHFD

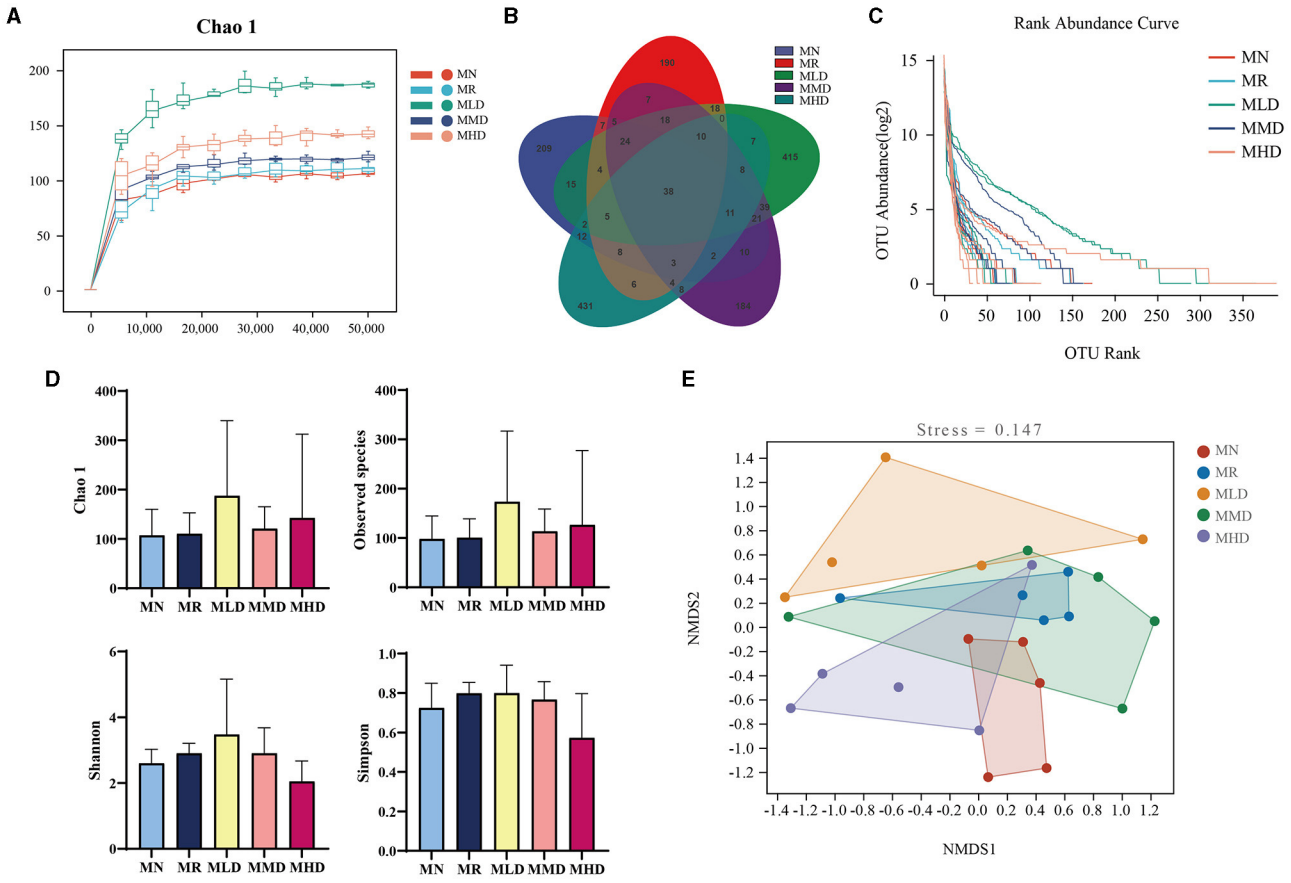

FIGURE 3
Changes in the ASV numbers and diversity of intestinal mucosal microbiota in mice. **(A)** Chao 1 dilution curve. **(B)** Venn diagram. **(C)** Rank abundance distribution curve. **(D)** Alpha diversity indices. **(E)** NMDS analysis.

changes the structure of the intestinal mucosal microbiota. The groups that had the intersection with MN and were closest to the MMD and MHD groups indicated that medium and high doses of ZDD were good for the recovery of the intestinal mucosal microbiota structure.

3.5. Effect of different doses of ZDD on the predominant microbiota in the intestinal mucosa of mice with HPHFD-induced constipation

At the phylum level (Figure 4A), Firmicutes is the dominant phylum in each group, accounting for 98.57, 99.21, 76.87, 90.32, and 96.91% in the MN, MR, MLD, MMD, and MHD groups, respectively, followed by Bacteroidetes, the proportions were 0.61, 0.32, 18.01, 4.82, and 0.13%, respectively. The third was Proteobacteria, with proportions of 0.57, 0.20, 1.49, 2.99, and 1.56%, respectively.

At the genus level (Figure 4B), the dominant bacterium in each group was *Lactobacillus*, and the proportion in the MN, MR, MLD, MMD, and MHD groups was 50.05, 79.53, 56.61, 76.68, and 35.36%, respectively, followed by *Candidatus Arthromitus*, accounting for 47.96, 17.92, 19.11, 13.05, and 61.44% in the MN, MR, MLD, MMD, and MHD groups, respectively. In addition, *Adlercreutzia* was abundant in the MLD and MHD groups, accounting for 3.32% in MLD group and 1.59% in MMD group.

Then, the above species were statistically analyzed (Figure 4C), and the relative abundance of *Streptococcus* in MR group was significantly higher than that in the MHD group ($p < 0.05$) and that of *Staphylococcus* was significantly higher than that in the MHD group ($p < 0.05$) and MN ($p < 0.01$). The abundance of *Succinivibrio* in the MR groups was significantly higher than that in the MLD ($p < 0.05$) and MHD groups ($p < 0.01$), while in the MHD group, it was significantly higher than that in the MMD group ($p < 0.05$). Compared to the MMD group, the relative abundance of *Corynebacterium* in the MR group and *Candidatus Arthromitus* in the MHD group was significantly increased ($p < 0.05$). *Bacillus* in the MN group was significantly higher than that in the MMD ($p < 0.01$) and MHD groups ($p < 0.01$).

3.6. Effects of different doses of ZDD on the intestinal mucosal characteristic microbiota of mice with HPHFD-induced constipation

We selected the LEfSe at a logarithmic LDA threshold of 2.0 to identify microbiota that differed significantly. We

10.3389/fmicb.2023.1214577

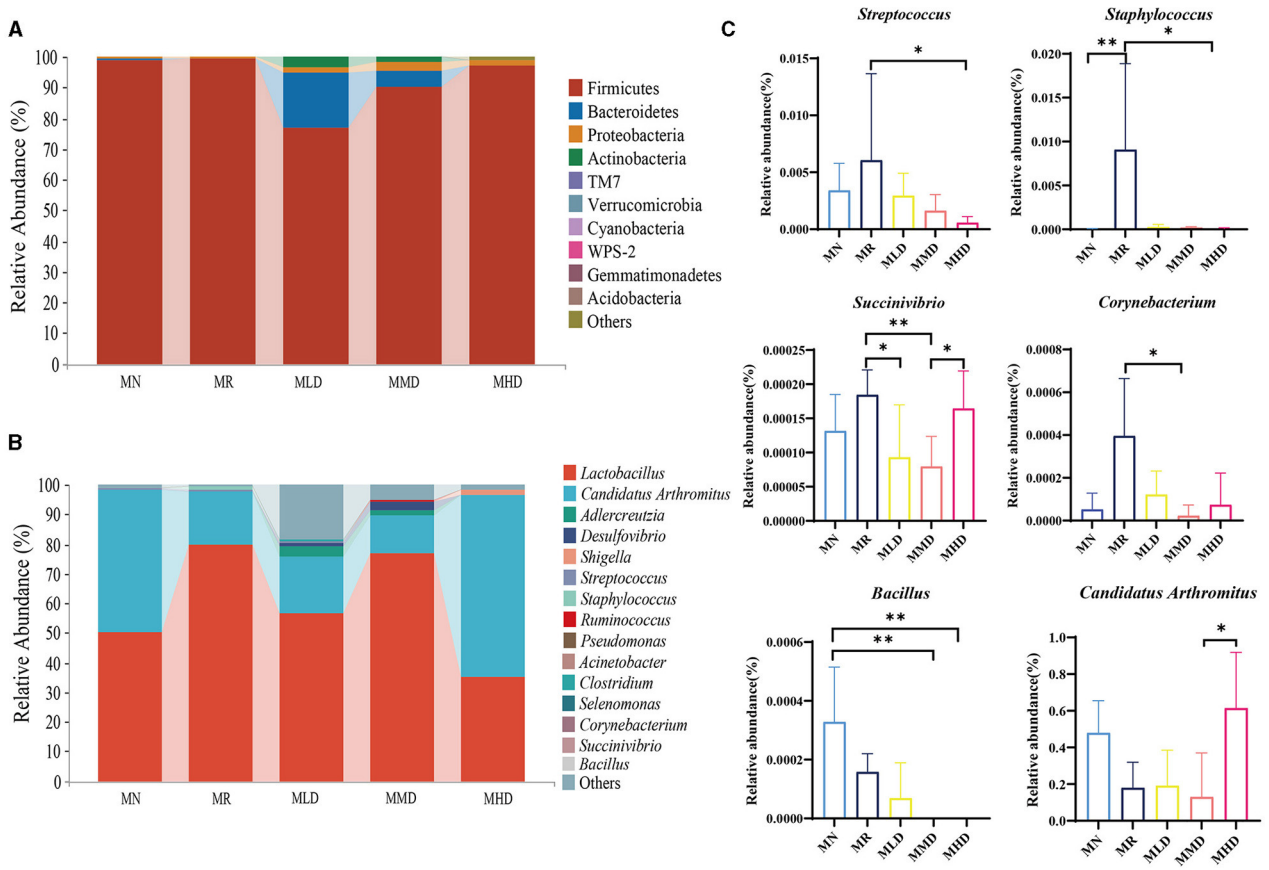

FIGURE 4
Dominant microbiota of intestinal mucosa in mice. **(A)** Phylum level. **(B)** Genus level. **(C)** Differential bacteria in genus level. $n = 5$, $^{*}p < 0.05$, $^{**}p < 0.01$.

mainly analyzed the characteristic bacteria between the MN and MR, MR, and MLD, MR and MMD, MR, and MHD groups. In the LEfSe analysis between the MN and MR groups (Figure 5A), *Lactobacillus*, *Aerococcus*, *Staphylococcus*, and *Corynebacterium* were the characteristic bacteria of the MR group, while *Akkermansia* and *Candidatus Arthromitus* belong to the characteristic bacteria of the MN group. In the LEfSe analysis between the MR and MLD groups (Figure 5B), *Aerococcus* and *Staphylococcus* were mainly enriched in the MR group. In the LEfSe analysis between the MR and MMD groups (Figure 5C), *Succinivibrio*, *Aerococcus*, *Staphylococcus*, *Bacillus*, *Prevotella*, and *Corynebacterium* were characteristic bacteria in the MR group. In the LEfSe analysis between the MR and MHD groups (Figure 5D), the characteristic bacteria of the MR group were *Desulfovibrio*, *Clostridium*, *Streptococcus*, *Lactobacillus*, *Aerococcus*, *Staphylococcus*, *Bacillus*, and *Corynebacterium*, and the characteristic bacteria of the MHD group were *Shigella* and *Candidatus Arthromitus*.

3.7. Analysis of different doses of ZDD on the ROC curve

To further analyze the influence of different doses of ZDD on the correlation between intestinal mucosal microbiota and indexes in constipation mice, we established a random forest model to screen the top eight important bacteria in the MR and MLD, MR and MMD, and MR and MHD groups and conducted ROC analysis on these bacteria. We used an AUC of >0.8 as the standard to verify the accuracy of the diagnosis and the joint evaluation of characteristics. Using ROC analysis, different groups can determine whether they have diagnostic efficacy (Li et al., 2023). In the analysis of the MN and MR groups (Figure 6A), the bacteria with an AUC of >0.8 were *Corynebacterium* (AUC = 0.960), *Akkermansia* (AUC = 0.900), *Aerococcus* (AUC = 0.900), *Lactobacillus* (AUC = 0.880), *Candidatus Arthromitus* (AUC = 0.920), and *Bacillus* (AUC = 0.800). For the analysis involving the MLD and MR groups (Figure 6B), the following bacterial species demonstrated prominent AUC values: *Corynebacterium* (AUC = 0.840), *Aerococcus* (AUC = 0.900), *Bacillus* (AUC = 0.800), and *Succinivibrio* (AUC = 0.840). Similarly, in the assessment of the MMD and MR groups (Figure 6C), specific bacterial species stood out with noteworthy AUC scores: *Prevotella* (AUC = 0.900), *Aerococcus* (AUC = 0.900), *Succinivibrio* (AUC = 0.960), *Corynebacterium* (AUC = 1.000), *Bacillus* (AUC = 1.000). Finally, in the evaluation of the MHD and MR groups (Figure 6D) several bacterial species were characterized by significant AUC values: *Desulfovibrio* (AUC = 0.880), *Aerococcus* (AUC = 0.900), *Shigella* (AUC = 0.900), *Corynebacterium* (AUC = 0.880), *Bacillus* (AUC = 1.000), *Clostridium* (AUC = 1.000), *Lactobacillus* (AUC = 0.880), *Streptococcus* (AUC = 1.000), *Candidatus Arthromitus* (AUC =

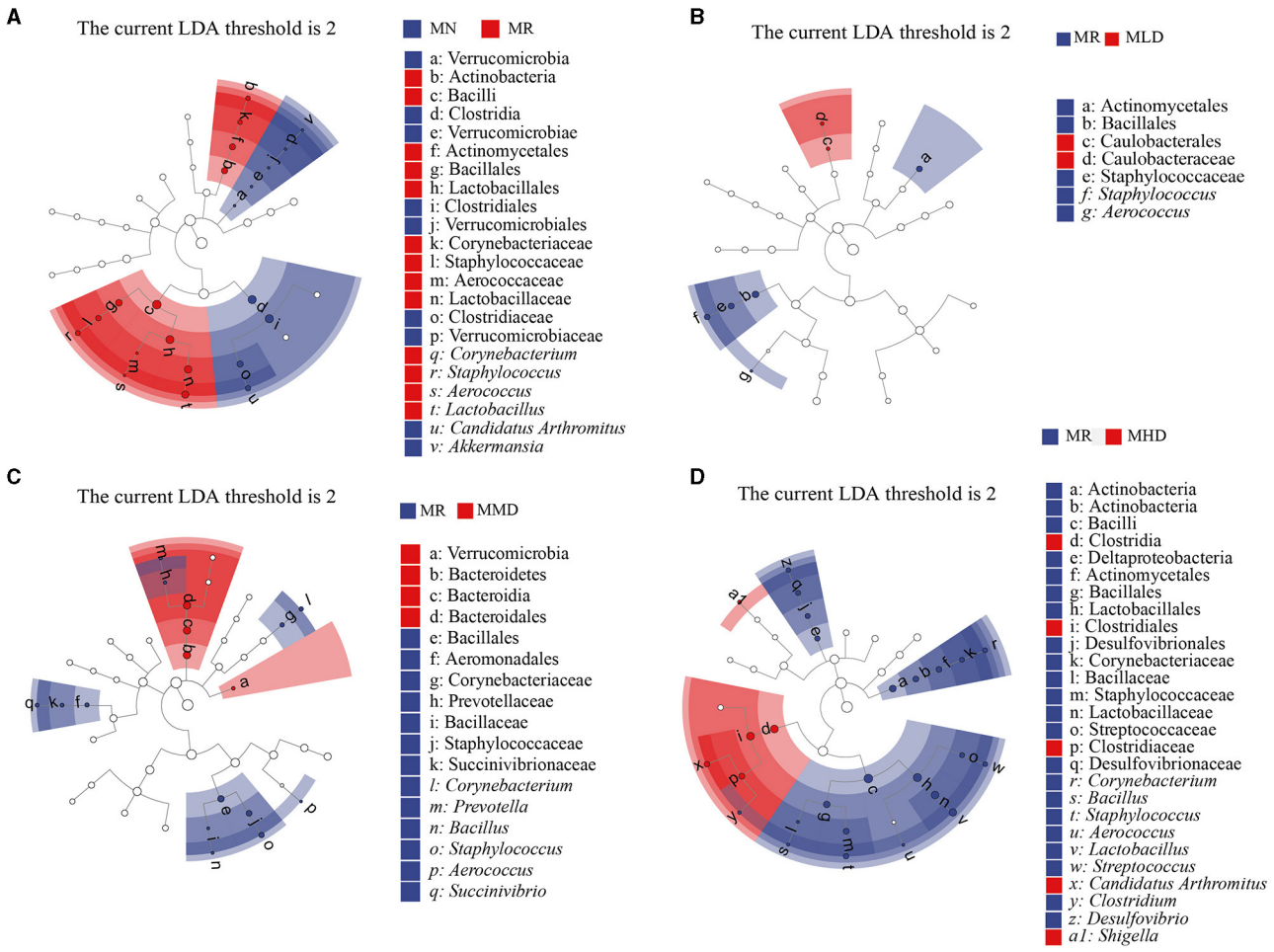

FIGURE 5
Characteristic bacteria of intestinal mucosa in mice. **(A)** MN and MR. **(B)** MR and MLD. **(C)** MR and MMD. **(D)** MR and MHD.

0.880), and *Selenomonas* (AUC = 0.840). Among them, the AUC of *Corynebacterium, Akkermansia, Aerococcus, Bacillus, Succinivibrio, Desulfovibrio, Shigella, Clostridium, Lactobacillus, Selenomonas,* and *Candidatus Arthromitus* was >0.8, and we believe they are diagnostic bacteria.

3.8. Correlation of mice with HPHFD-induced constipation

Then, we selected the top eight characteristic genera in the MR and MLD, MR and MMD, and MR and MHD groups by random forest analysis and directly analyzed the correlation with CCK, CGRP, MDA, and SOD. In the analysis of the top eight characteristic bacteria and related indicators of the MN and MR groups (Figure 7A), *Candidatus Arthromitus* showed a positive correlation with SOD ($p < 0.05$) and a significant negative correlation with the MDA ($p < 0.05$). At the same time, the MDA groups was positively correlated with *Corynebacterium* ($p < 0.05$) and *Aerococcus* ($p < 0.05$). Compared with the MR and MLD groups (Figure 7B), SOD had a significantly negative correlation with *Aerococcus* ($p < 0.05$) and *Bacillus* ($p < 0.01$). Compared with the MR and MMD groups (Figure 7C), *Prevotella* showed a significantly negative correlation with CCK ($p < 0.05$). *Succinivibrio* ($p < 0.05$), *Corynebacterium* ($p < 0.01$), *Aerococcus* ($p < 0.01$), *Bacillus* ($p < 0.01$), and *Prevotella* ($p < 0.01$) were negatively correlated with SOD. There was a significant positive correlation between CGRP and *Streptococcus* ($p < 0.05$). The MDA was positively correlated with *Bacillus* ($p < 0.05$) and *Prevotella* ($p < 0.05$). In the analysis of the top eight characteristic bacteria and related indicators of the MR and MHD groups (Figure 7D), CCK was negatively correlated with *Clostridium* ($p < 0.01$), and *Streptococcus* ($p < 0.05$). SOD was positively correlated with *Shigella* ($p < 0.05$) and negatively correlated with *Bacillus* ($p < 0.01$), *Aerococcus* ($p < 0.01$), *Desulfovibrio* ($p < 0.01$), *Clostridium* ($p < 0.01$), and *Streptococcus* ($p < 0.05$). MDA was negatively correlated with *Shigella* ($p < 0.05$).

3.9. Analysis of different doses of ZDD on the functions of intestinal mucosal microbiota of mice with HPHFD-induced constipation

The functions of the intestinal mucosal microbiota were generally divided into six categories (Figure 8A): organismal

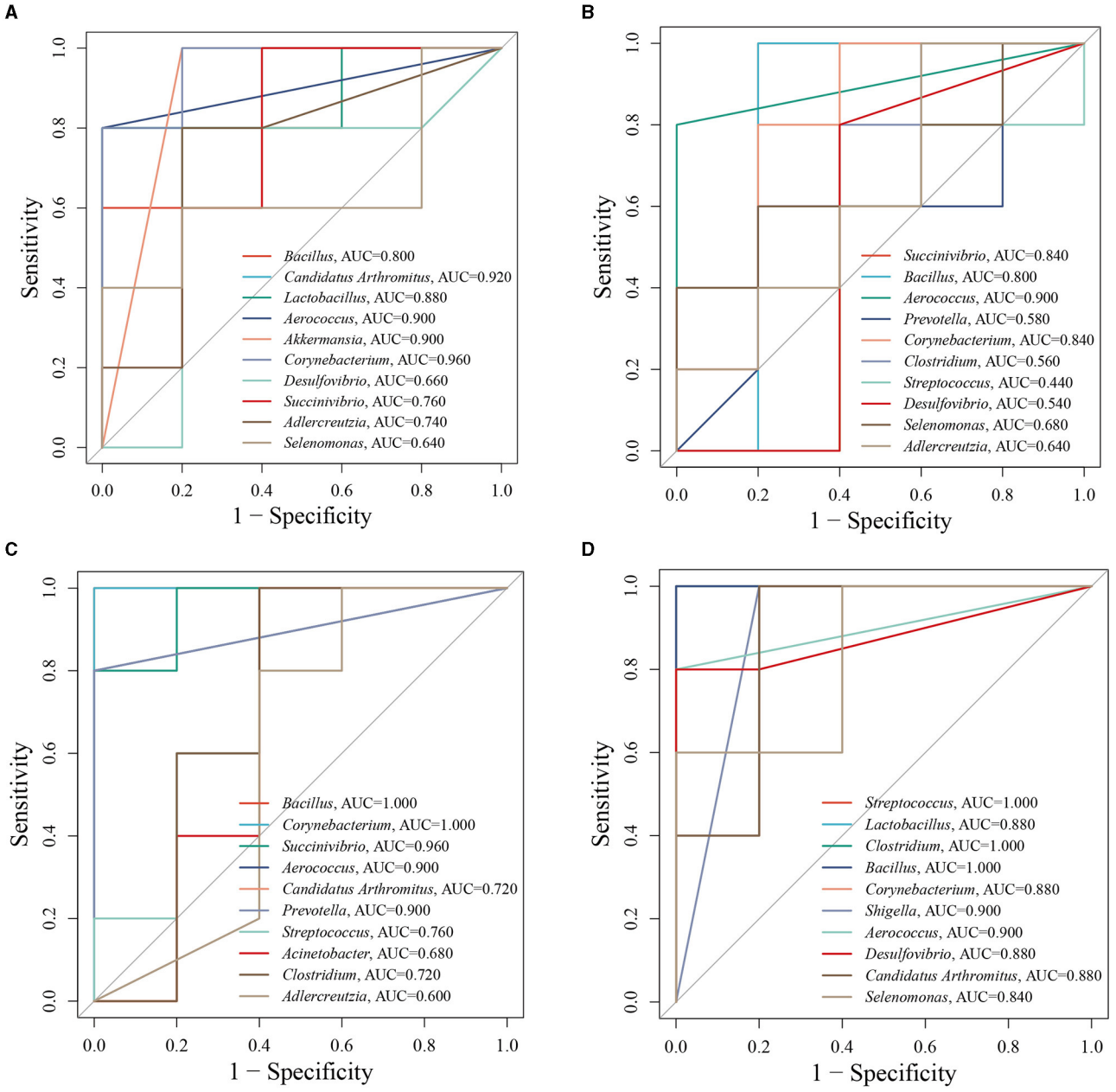

FIGURE 6
ROC curve analysis. **(A)** MN and MR. **(B)** MR and MLD. **(C)** MR and MMD. **(D)** MR and MHD.

systems, metabolism, human diseases, genetic information processing, environmental information processing, and cellular processes. The second level includes 35 sub-functional classes. The abundance of Cell motility, Cell growth, and Cell death was high in the Cellular processes' metabolic pathway. In the realm of Environmental Information Processing, Membrane transport is highly abundant. Translation, Replication and repair, Folding, sorting and degradation exhibit a highly abundant presence in Genetic Information Processing. In addition, Metabolisms of terpenoids and polyketides, Metabolism of other amino acids, Metabolisms of co-factors and vitamins, Lipid metabolism, Carbohydrate metabolism, and Amino acid metabolism are relatively abundant. Further analysis (Figures 8B, C) shows significant upregulation in MN group relative to MR group ($p < 0.05$) and significant downregulation in MR group relative to MHD group ($p < 0.05$) within the abundance of pathways associated with tropone, piperidine, and pyrroline alkaloid biosynthesis.

4. Discussion

Clinically, it has been proven that ZDD can relieve constipation caused by HFHPD. Its mechanism is related to the recovery of intestinal transport function and the transformation of the spleen

10.3389/fmicb.2023.1214577

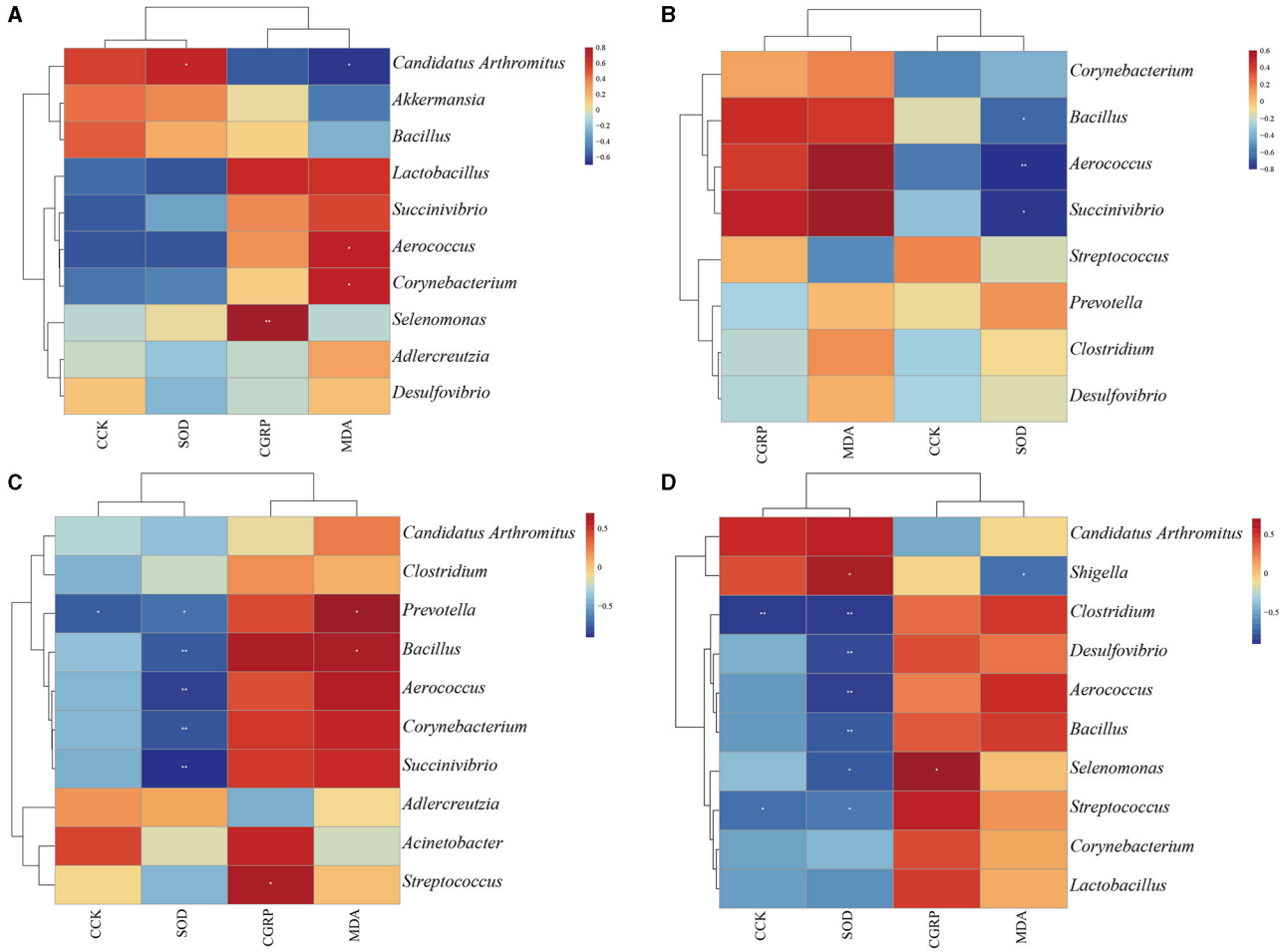

FIGURE 7
Heat maps of correlation between characteristic bacteria, CCK, CGRP, MDA, and SOD. **(A)** MN and MR. **(B)** MR and MLD. **(C)** MR and MMD. **(D)** MR and MHD. $n = 5$, $^{*}P < 0.05$, $^{**}P < 0.01$.

and stomach (Hong and Hong, 2014). This will inevitably interact with the flora in the intestine and participate in the therapeutic mechanism of drugs.

The body weight of the mice fed HFHPD combined with LOP decreased compared to that of MN group. Combined with the fecal characteristics and weight changes of the mice, we considered that HFHPD would lead to constipation, dyspepsia, and less nutrition absorption in mice. After the administration of ZDD, the body weight of mice increased compared with MR group, but it was not significant. Moreover, the body weight of the mice in the MHD group was close to that of mice in the MN group. We speculate that ZDD can relieve dyspepsia caused by HFHPD modeling, with high-dose ZDD having the most prominent effect.

We further analyzed the levels of gastrointestinal hormones and oxidative stress. The results of CCK and CGRP indicated that the intestinal peristalsis of MR group was lower than that of the mice in the MN, MLD, MMD, and MHD groups. The results of the analysis of MDA and SOD showed the presence of oxidative stress damage in constipation mice induced by HFHPD. After the ZDD intervention, the oxidative stress injury in mice was mitigated to a level akin to that observed in the MN group. These findings suggest that ZDD may exert antioxidant properties and yield beneficial effects in counteracting oxidative stress injuries.

Intestinal mucosal symbiotic microbiota is a part of the intestinal mucosal barrier, which means that intestinal mucosal microbiota is more closely related to intestinal epithelial cells and intestinal mucosal function than fecal microbiota (Codling et al., 2010). Therefore, we analyzed the intestinal mucosal microbiota of mice. From the Chao 1 dilution curve analysis, we believe that the experimental samples meet the requirements of microbial diversity analysis. ASV analysis showed that the HFHPD constipation model and the ZDD intervention could alter the intestinal mucosal microbiota in mice. In the grouping of NMDS, the HFHPD model mice and the ZDD intervention changed the intestinal mucosal microbiota structure, and the distance between MMD and MHD groups was closer to MN group. It indicated that medium and high doses of ZDD can restore the intestinal mucosal microbiota's structure. Therefore, by comparing the relative abundance between groups, we can further understand the influence of ZDD on the intestinal microbial environment.

The relative abundance of *Candidatus Arthromitus* in MHD group was higher than that in MMD, and *Candidatus Arthromitus*

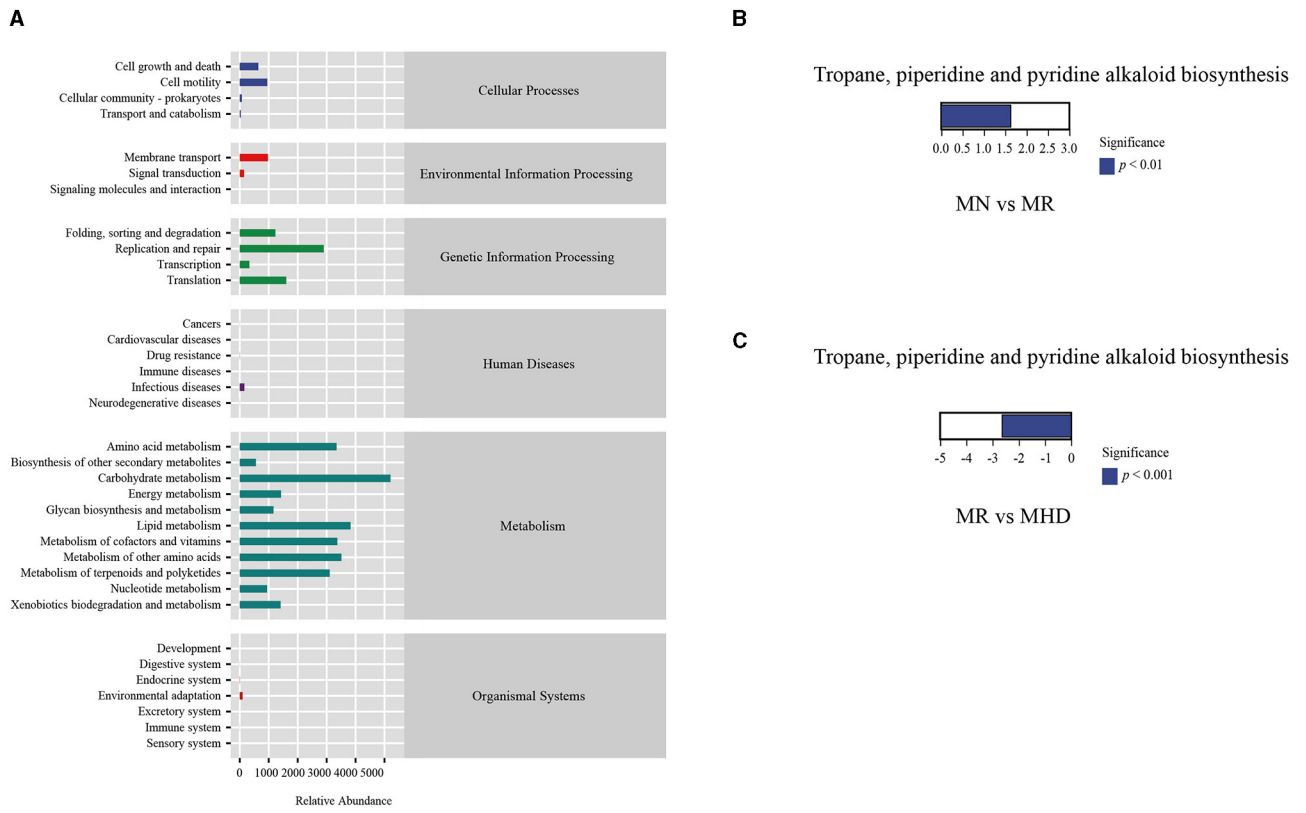

FIGURE 8
Functional prediction analysis. **(A)** KEGG metabolic pathway. **(B)** The differential metabolic pathway between MN and MR. **(C)** The differential metabolic pathway between MR and MHD (up-regulated group vs. control group, the positive horizontal axis in the figure represents up-regulated group compared with the control group, while the negative value is down-regulated).

has a protective effect on the intestine (Ma et al., 2019; Hou et al., 2022). The relative abundance of *Staphylococcus* and *Streptococcus* in MR was significantly higher than that in MHD group. *Staphylococcus* infection can damage the intestinal barrier and the structure of immune organs (Liu G. et al., 2020). *Streptococcus* can cause inflammatory reactions (Batista and Ferreira, 2015; Hashizume-Takizawa et al., 2019). It indicated that HFHPD-induced constipation can increase the relative abundance of pathogenic bacteria. The relative abundance of *Succinivibrio* in MR group was significantly higher than that in the MLD and MMD groups, while that in the MHD group was significantly higher than that in the MMD group. This may be due to the dose-effect relationship of negative feedback formed by high doses of traditional Chinese medicine, which leads to an increase in *Succinivibrio*. It may also be due to the influence of the overall environment. In a high-dose environment, the reproduction of *Succinivibrio* can be promoted by stimulating a certain bacterium. *Succinivibrio* can cause inflammatory reactions (Marquez-Ortiz et al., 2023). *Corynebacterium* was enriched in MR. *Corynebacterium* can not only damage intestinal microbial barrier function but also cause inflammatory reactions (Yang et al., 2022). In addition, *Bacillus* can inhibit the proliferation of harmful bacteria by consuming oxygen in the intestinal tract or secreting antibacterial substances, thereby regulating intestinal microbiota disorders (Père and Etienne, 2007; Aly et al., 2008). However, after ZDD intervention, the relative abundance of *Bacillus* was lower than that in MN group, which may be related to the complex chemical components in the prescription.

We further compared the other groups with MR group by LEfSe analysis and found that MR group was rich in pathogenic bacteria, such as *Aerococcus*, *Corynebacterium*, *Desulfovibrio*, *Clostridium*, and *Prevotella*. Among them, *Aerococcus* is a common harmful bacterium that can lead to an imbalance in the intestinal microbiota (Zheng et al., 2022). *Desulfovibrio* can produce H_2S that is harmful to the human body and has a pro-inflammatory effect (Figliuolo et al., 2017). *Clostridium* can increase the risk of gastrointestinal inflammatory reactions (Wang et al., 2022). *Prevotella* colonization leads to metabolic changes in the microbial population and reduces the production of interleukin-18, thus aggravating intestinal inflammation and potential systemic autoimmune disease (Iljazovic et al., 2021). Therefore, constipation induced by HFHPD can increase the relative abundance of pathogenic bacteria in the intestinal mucosa, and the administration of ZDD can reduce the relative abundance of these pathogenic bacteria and relieve constipation by reducing their proliferation.

As we all know, traditional Chinese medicine prescriptions contain many chemical components, as does ZDD. Experimental studies show that hesperidin and baicalin are anti-inflammatory and anti-bacterial active components in ZDD, which significantly

regulate gastrointestinal movement (Tan et al., 2006; Liu et al., 2023). Hesperidin can selectively remove harmful intestinal microbiota and regulate intestinal microbiota disorders through bacteriostasis, thus affecting intestinal peristalsis. The antibacterial mechanism of hesperidin may be related to its chemical structure, which can coagulate or denature proteins (Guardia et al., 2001). It was found that hesperidin can reduce the relative abundance of harmful bacteria such as *Staphylococcus* and *Desulfovibrio*, which is similar to our experimental results (Mas-Capdevila et al., 2020). Baicalin can regulate the structure of the intestinal microbiota, inhibit gram-negative and positive bacteria, and reduce endotoxin entering the blood and the secretion of inflammatory factors, thus alleviating metabolic inflammation, protecting intestinal epithelial cells from damage, improving intestinal mucosal structure, and promoting intestinal peristalsis (Zhang X. Y. et al., 2021). Our experimental results show that the relative abundance of Gram-positive bacteria such as *Staphylococcus*, *Streptococcus* and Gram-negative bacteria such as *Succinivibrio* decreased to different degrees after different doses of ZDD intervention. Therefore, we speculate that hesperidin and baicalin play a key role in inhibiting harmful bacteria in ZDD.

Among the characteristic bacteria enriched in MR group, it was found that *Corynebacterium*, *Aerococcus*, *Bacillus*, and *Prevotella* were positively correlated with MDA. *Streptococcus* was positively correlated with CGRP. *Succinivibrio*, *Corynebacterium*, *Aerococcus*, *Bacillus*, *Prevotella*, *Clostridium,* and *Streptococcus* were negatively correlated with SOD. *Prevotella*, *Clostridium*, and *Streptococcus* are negatively correlated with CCK. These correlations may be one of the mechanisms of constipation induced by HFHPD. *Candidatus Arthromitus* has a negative correlation with MDA and a positive correlation with SOD, which is similar to the research results of Chen et al. (2023). We speculate that *Candidatus Arthromitus* may relieve constipation by regulating the level of oxidative stress to restore intestinal mucosal dysfunction caused by intestinal mucosal cell damage. In addition, ZDD may reduce the secretion of CGRP to decrease the inhibition of gastrointestinal movement and improve intestinal peristalsis. ZDD can also stimulate intestinal peristalsis and relieve constipation by increasing the secretion of CCK. The mechanism between them needs further study. We also performed functional prediction on intestinal mucosal bacteria and found that, compared with MR group, the abundance of tropone, piperidine, and pyrroline alkaloid biosynthesis pathways was significantly up-regulated in MN and MHD groups. We speculate that tropane, piperidine, and pyridine alkaloid biosynthesis is one of the directions of ZDD to relieve constipation caused by HFHPD.

5. Conclusion

In summary, constipation caused by HFHPD could increase the relative abundance of pathogenic bacteria in the intestinal mucosal microbiota. After the intervention of ZDD, constipation was relieved, and the relative abundance of pathogenic bacteria was reduced. In particular, the high dose of ZDD can not only reduce the oxidative stress damage and increase the relative abundance of beneficial bacteria such as *Candidatus Arthromitus* but also increase the abundance of tropane, piperidine, and pyridine alkaloid biosynthesis, which is of great significance for the treatment of constipation.

Data availability statement

The datasets presented in this study can be found in online repositories. The names of the repository/repositories and accession number(s) can be found below: https://www.ncbi.nlm.nih.gov/, PRJNA 963077.

Ethics statement

The animal study was approved by Animal Care and Use Committee of the Hunan University of Chinese Medicine. The study was conducted in accordance with the local legislation and institutional requirements.

Author contributions

XP: data analysis and writing the original draft. XY and JL: performing animal experiments. ND and ZT: review and editing. YC and ZT: project administration, review, and funding acquisition. All authors contributed to the article and approved the submitted version.

Funding

This research was financially supported by the Natural Science Foundation of Hunan Province (No. 2022JJ40332) and the Domestic First-Class Discipline Construction Project of Chinese Medicine of Hunan University of Chinese Medicine (4901-020000200207).

Conflict of interest

The authors declare that the research was conducted in the absence of any commercial or financial relationships that could be construed as a potential conflict of interest.

Publisher's note

References

Aly, S. M., Abdel-Galil Ahmed, Y., Abdel-Aziz Ghareeb, A., and Mohamed, M. F. (2008). Studies on *Bacillus subtilis* and *Lactobacillus acidophilus*, as potential probiotics, on the immune response and resistance of *Tilapia nilotica* (*Oreochromis niloticus*) to challenge infections. *Fish Shellf. Immunol.* 25, 128–136. doi: 10.1016/j.fsi.2008.03.013

Batista, R. P., and Ferreira, C. R. (2015). *Streptococcus agalactiae* septicemia in a patient with diabetes and hepatic cirrhosis. *Autops Case Rep.* 5, 35–43. doi: 10.4322/acr.2015.028

Chen, Z., Dai, G., Wu, X., Li, L., Tian, Y., and Tan, L. (2023). Protective effects of Fagopyrum dibotrys on oxidized oil-induced oxidative stress, intestinal barrier impairment, and altered cecal microbiota in broiler chickens. *Poult. Sci.* 102, 102472. doi: 10.1016/j.psj.2022.102472

Codling, C., O'Mahony, L., Shanahan, F., Quigley, E. M., and Marchesi, J. R. (2010). A molecular analysis of fecal and mucosal bacterial communities in irritable bowel syndrome. *Dig. Dis. Sci.* 55, 392–397. doi: 10.1007/s10620-009-0934-x

Dimidi, E., Christodoulides, S., Scott, S. M., and Whelan, K. (2017). Mechanisms of action of probiotics and the gastrointestinal microbiota on gut motility and constipation. *Adv Nutr.* 8, 484–494. doi: 10.3945/an.116.014407

Douglas, G. M., Maffei, V. J., Zaneveld, J. R., Yurgel, S. N., Brown, J. R., Taylor, C. M., et al. (2020). PICRUSt2 for prediction of metagenome functions. *Nat. Biotechnol.* 38, 685–688. doi: 10.1038/s41587-020-0548-6

Figliuolo, V. R., Dos Santos, L. M., Abalo, A., Nanini, H., Santos, A., Brittes, N. M., et al. (2017). Sulfate-reducing bacteria stimulate gut immune responses and contribute to inflammation in experimental colitis. *Life Sci.* 189, 29–38. doi: 10.1016/j.lfs.2017.09.014

Guardia, T., Rotelli, A. E., Juarez, A. O., and Pelzer, L. E. (2001). Anti-inflammatory properties of plant flavonoids. Effects of rutin, quercetin and hesperidin on adjuvant arthritis in rat. *Farmaco* 56, 683–687. doi: 10.1016/S0014-827X(01)01111-9

Hajji, N., Wannes, D., Jabri, M. A., Rtibi, K., Tounsi, H., Abdellaoui, A., et al. (2020). Purgative/laxative actions of *Globularia alypum* aqueous extract on gastrointestinal-physiological function and against loperamide-induced constipation coupled to oxidative stress and inflammation in rats. *Neurogastroenterol. Motil.* 32, e13858. doi: 10.1111/nmo.13858

Hashizume-Takizawa, T., Yamaguchi, Y., Kobayashi, R., Shinozaki-Kuwahara, N., Saito, M., and Kurita-Ochiai, T. (2019). Oral challenge with Streptococcus sanguinis induces aortic inflammation and accelerates atherosclerosis in spontaneously hyperlipidemic mice. *Biochem. Biophys. Res. Commun.* 520, 507–513. doi: 10.1016/j.bbrc.2019.10.057

He, Y. S., Tan, Z. J., Li, D. D., and Hui, H. Y. (2019). Effect of Bao-he Pills on intestinal microorganisms and enzyme activity in mice with dyspepsia. *Chin. J. Microecol.* 31, 763–767. doi: 10.13381/j.cnki.cjm.201907004

Hong, Q., and Hong, M. (2014). Clinical application of Citrus Aurantium dredge pill corner. *J. Pract. Tradit. Chin. Int. Med.* 28, 129–130. doi: 10.13729/j.issn.1671-7813.2014.05.67

Hou, C., Xiao, J., Wang, L. M., Wang, X., Fan, Y. H., Ni, Z. J., et al. (2022). Laxative function of fermented fruit and vegetable juice and its effect on gut microbiota. *Food Ferment. Ind.* 48, 111–116. doi: 10.13995/j.cnki.11-1802/ts.031172

Iljazovic, A., Roy, U., Gálvez, E. J. C., Lesker, T. R., Zhao, B., Gronow, A., et al. (2021). Perturbation of the gut microbiome by Prevotella spp. enhances host susceptibility to mucosal inflammation. *Mucosal Immunol.* 14, 113–124. doi: 10.1038/s41385-020-0296-4

Kim, J. E., Choi, Y. J., Lee, S. J., Gong, J. E., Lee, Y. J., Sung, J. E., et al. (2021). Antioxidant activity and laxative effects of tannin-enriched extract of Ecklonia cava in loperamide-induced constipation of SD rats. *PLoS ONE* 16, e0246363. doi: 10.1371/journal.pone.0246363

Lee, H. Y., Kim, J. H., Jeung, H. W., Lee, C. U., Kim, D. S., Li, B., et al. (2012). Effects of *Ficus carica* paste on loperamide-induced constipation in rats. *Food Chem. Toxicol.* 50, 895–902. doi: 10.1016/j.fct.2011.12.001

Li, C. R., Xiao, N. Q., Deng, N., Li, D. D., Tan, Z. J., and Peng, M. J. (2023). Dose of sucrose affects the efficacy of Qiweibaizhu powder on antibiotic-associated diarrhea: association with intestinal mucosal microbiota, short-chain fatty acids, IL-17, and MUC2. *Front. Microbiol.* 14, 1108398. doi: 10.3389/fmicb.2023.1108398

Li, C. R., Zhou, K., Xiao, N. Q., Peng, M. J., and Tan, Z. J. (2022). The Effect of Qiweibaizhu powder crude polysaccharide on antibiotic-associated diarrhea mice is associated with restoring intestinal mucosal bacteria. *Front. Nutr.* 9, 952647. doi: 10.3389/fnut.2022.952647

Li, X. Y., Deng, N., Zheng, T., Qiao, B., Peng, M., Xiao, N. Q., et al. (2022b). Importance of Dendrobium officinale in improving the adverse effects of high-fat diet on mice associated with intestinal contents microbiota. *Front. Nutr.* 9, 957334. doi: 10.3389/fnut.2022.957334

Li, Y., Dong, N. E., and Guo, Y. C. (2008). Effect of Zhishi Daozhi pill on gastric emptying and intestinal propulsion in mice. *J. Chengde Med. Univ.* 2008, 212–213. doi: 10.15921/j.cnki.cyxb.2008.02.014

Lin, L. B., Sun, Y. S., Tang, J., Wang, J., Liu, X. L., and Li, Y. P. (2020). Effect of Chinese medicine on intestinal microecology in patients with functional constipation. *China J. Chin. Med.* 35, 1431–1434. doi: 10.16368/j.issn.1674-8999.2020.07.321

Liu, F., Wei, X. P., and Tang, X. G. (2020). Clinical efficacy of modified Zhishi Daozhi wan on slow transit constipation. *Chin. J. Exp. Tradit. Med. Form.* 26, 92–97. doi: 10.13422/j.cnki.syfjx.20192034

Liu, G., Pang, B., Li, N., Jin, H., Li, J., Wu, W., et al. (2020b). Therapeutic effect of Lactobacillus rhamnosus SHA113 on intestinal infection by multi-drug-resistant Staphylococcus aureus and its underlying mechanisms. *Food Funct.* 11, 6226–6239. doi: 10.1039/D0FO00969E

Liu, J., Wang, S., Yi, R., Long, X., Luo, G., Zhao, X., et al. (2022). LimosiLactobacillus pentosus isolated from mustard relieves drug-induced constipation in mice fed a high-fat diet by modulating enteric neurotransmitter function. *Probiot. Antimicrob. Prot.* 1–11. doi: 10.1007/s12602-022-09991-9

Liu, Y. F., Xiong, Y., Zhao, X. Y., Lai, Y. W., Li, Z. N., and Deng, K. Z. (2023). HPLC determination of 6 component of Aurantii Fructus lmmaturus in Zhishi Daozhi pills and genetic analysis of medicinal materials. *Cent. South Pharm.* 21, 767–771. doi: 10.7539/j.issn.1672-2981.2023.03.035

Ma, H., Xiong, H., Zhu, X., Ji, C., Xue, J., Li, R., et al. (2019). Polysaccharide from Spirulina platensis ameliorates diphenoxylate-induced constipation symptoms in mice. *Int. J. Biol. Macromol.* 133, 1090–1101. doi: 10.1016/j.ijbiomac.2019.04.209

Mai, C. T., Wu, M. M., Qu, C., Wang, C. L., Huang, X. D., Zhang, X. J., et al. (2018). Regulatory effects of Xiao'er Qixingcha on intestinal flora in indigestion model mice. *J. Guangz. Univ. Tradit. Chin. Med.* 35, 881–886. doi: 10.13359/j.cnki.gzxbtcm.2018.05.023

Marquez-Ortiz, R. A., Leon, M., Abril, D., Escobar-Perez, J., Florez-Sarmiento, C., Parra-Izquierdo, V., et al.(2023). Colonoscopy aspiration lavages for mucosal metataxonomic profiling of spondylarthritis-associated gastrointestinal tract alterations. *Sci. Rep.* 13, 7015. doi: 10.1038/s41598-023-33597-y

Mas-Capdevila, A., Teichenne, J., Domenech-Coca, C., Caimari, A., Del Bas, J. M., Escot,é, X., et al. (2020). Effect of hesperidin on cardiovascular disease risk factors: the role of intestinal microbiota on hesperidin bioavailability. *Nutrients* 12, 1488. doi: 10.3390/nu12051488

Mukai, R., Handa, O., Naito, Y., Takayama, S., Suyama, Y., Ushiroda, C., et al. (2020). High-fat diet causes constipation in mice via decreasing colonic mucus. *Dig. Dis. Sci.* 65, 2246–2253. doi: 10.1007/s10620-019-05954-3

Père, M. C., and Etienne, M. (2007). Insulin sensitivity during pregnancy, lactation, and postweaning in primiparous gilts. *J. Anim. Sci.* 85, 101–110. doi: 10.2527/jas.2006-130

Qiao, B., Liu, J., Deng, N., Cai, Y., Bian, Y., Wu, Y. Y., et al. (2023). Gut contents microbiota dysbiosis and dysregulated lipid metabolism in diarrhea caused by high-fat diet in a fatigued state. *Food Funct.* 14, 3880–3892. doi: 10.1039/D3FO00378G

Sharma, A., and Rao, S. (2017). Constipation: pathophysiology and current therapeutic approaches. *Handb. Exp. Pharmacol.* 239, 59–74. doi: 10.1007/164_2016_111

Shen, J. F., and Tan, S. F. (2022). Curative effect of modified Huangqi Jianzhong decoction and Zhishi Xiaopi pills in the treatment of functional dyspepsia with weakness of spleen and stomach. *Chin. For. Med. Res.* 20, 67–70. doi: 10.14033/j.cnki.cfmr.2022.01.019

Staller, K., Olén, O., Söderling, J., Roelstraete, B., Törnblom, H., Song, M., et al. (2022). Chronic constipation as a risk factor for colorectal cancer: results from a nationwide, case-control study. *Clin. Gastroenterol. Hepatol.* 20, 1867–1876.e2. doi: 10.1016/j.cgh.2021.10.024

Stewart, M. L., and Schroeder, N. M. (2013). Dietary treatments for childhood constipation: efficacy of dietary fiber and whole grains. *Nutr. Rev.* 71, 98–109. doi: 10.1111/nure.12010

Taba Taba Vakili, S., Nezami, B. G., Shetty, A., Chetty, V. K., and Srinivasan, S. (2015). Association of high dietary saturated fat intake and uncontrolled diabetes with constipation: evidence from the national health and nutrition examination survey. *Neurogastroenterol. Motil.* 27, 1389–1397. doi: 10.1111/nmo.12630

Tabbers, M. M., DiLorenzo, C., Berger, M. Y., Faure, C., Langendam, M. W., Nurko, S., et al. (2014). Evaluation and treatment of functional constipation in infants and children: evidence-based recommendations from ESPGHAN and NASPGHAN. *J. Pediatr. Gastroenterol. Nutr.* 58, 258–274. doi: 10.1097/MPG.0000000000000266

Tan, R., Dong, H., Chen, Z., Jin, M., Yin, J., Li, H., et al. (2021). Intestinal microbiota mediates high-fructose and high-fat diets to induce chronic intestinal inflammation. *Front. Cell. Infect. Microbiol.* 11, 654074. doi: 10.3389/fcimb.2021.654074

Tan, S. J., Liu, G., Jiang, R., Tang, Q., and Zhang, J. (2006). Determination of hesperidin and baicalin in Zhishidaozhi Wan by HPLC. *Pharm. J. Chin. PLA*. 22, 387–389. doi: 10.3969/j.issn.1008-9926.2006.05.021

Tangvarasittichai, S. (2015). Oxidative stress, insulin resistance, dyslipidemia and type 2 diabetes mellitus. *World J. Diabetes* 6, 456–480. doi: 10.4239/wjd.v6.i3.456

Wang, J., Tian, T. D., Zheng, Z., Li, P., Lu, D. R., Wang, B. L., et al. (2021). Effect and regulation mechanism of Changweishu capsule in the treatment of tumor-related diarrhea and constipation. *Mod. J. Integr. Tradit. Chin. West Med*. 30, 1255–1260+1308. doi: 10.3969/j.issn.1008-8849.2021.12.001

Wang, J., Zhang, S. Y., Sheng, Y. C., and Ao, H. (2018). Research progress on pharmacological Actionof Baizhu in treatment of gastrointestinal diseases. *Chin. Arch. Tradit. Chin. Med*. 36, 2854–2858. doi: 10.13193/j.issn.1673-7717.2018.12.008

Wang, J. L., Ma, X. L., Wang, Y. Z., and Zhu, X. J. (2022). Study on interaction mechanism of gut microbiota and PI3K/AKT/mTOR in rats with gastric precancerous lesions. *J. Pract. Tradit. Chin. Int. Med*. 36, 7–10+143–144. doi: 10.13729/j.issn.1671-7813.Z20211041

Wu, Y., Peng, X. X., Li, X. Y., Li, D. D., Tan, Z. J., and Yu, R. (2022). Sex hormones influence the intestinal microbiota composition in mice. *Front. Microbiol*. 13, 964847. doi: 10.3389/fmicb.2022.964847

Xiang, C., Liu, J., Zhang, Y., and Xu, J. (2019). Effect of modified Simotang on adult functional constipation and intestinal neurotransmitter. *Chin. J. Exp. Tradit. Med. Form*. 25, 150–155. doi: 10.13422/j.cnki.syfjx.20190232

Yang, J., Wang, H. P., Zhou, L., and Xu, C. F. (2012). Effect of dietary fiber on constipation: a meta analysis. *World J. Gastroenterol*. 18, 7378–7383. doi: 10.3748/wjg.v18.i48.7378

Yang, R. B., Gao, Y. B., Ai, S. N., Han, Y. Z., Yin, S. H., Wei, R. J., et al. (2022). The research of the correlation between gut microbiota and type 2-diabetes. *Chin. J. Integr. Tradit. West. Nephrol*. 23, 105–111. doi: 10.3969/j.issn.1009-587X.2022.02.004

Yi, X., Zhou, K., Deng, N., Cai, Y., Peng, X. X., and Tan, Z. J. (2023). Simo decoction curing spleen deficiency constipation was associated with brain-bacteria-gut axis by intestinal mucosal microbiota. *Front. Microbiol*. 14, 1090302. doi: 10.3389/fmicb.2023.1090302

Zhang, C. Y., Shao, H. Q., Peng, X. X., Liu, T. H., and Tan, Z. J. (2020). Microbiotal characteristics colonized in intestinal mucosa of mice with diarrhoea and repeated stress. *3 Biotech* 10, 372. doi: 10.1007/s13205-020-02368-1

Zhang, H., Li, P., He, Y. J., Huang, W. Q., Tang, Y., and Yang, Z. B. (2018). Effects of Qiwei Qingchang capsules on symptoms and the contents of VIP, SP, MOT and CGRP in serum and colon tissue of rats with chronic functional constipation. *China Pharm*. 29, 2170–2174. doi: 10.6039/j.issn.1001-0408.2018.16.03

Zhang, X., Hu, B., Sun, G., Zheng, J., Hu, H., Yang, H., et al. (2022). Plasma metabolomic profiles reveal regulatory effect of chitosan oligosaccharides on loperamide-induced constipation in mice. *J. Pharm. Biomed. Anal*. 211, 114590. doi: 10.1016/j.jpba.2022.114590

Zhang, X., Li, N., Chen, Q., and Qin, H. (2021). Fecal microbiota transplantation modulates the gut flora favoring patients with functional constipation. *Front. Microbiol*. 12, 700718. doi: 10.3389/fmicb.2021.700718

Zhang, X. Y., Liu, J., Ji, N., Feng, J. H., Wang, W. Q., and Jiang, K. (2021). Efficacy and mechanism of qingre lishi prescription in treating children with acute bacterial lower urinary tract infection of bladder damp-heat syndrome. *Chin. J. Exp. Tradit. Med. Form*. 27, 51–57. doi: 10.13422/j.cnki.syfjx.20210724

Zheng, M., Pi, X., Li, H., Cheng, S., Su, Y., Zhang, Y., et al. (2022). Ganoderma spp. polysaccharides are potential prebiotics: a review. *Crit. Rev. Food Sci. Nutr*. 18, 1–19. doi: 10.1080/10408398.2022.2110035

Zhu, X. L., Ye, M. H., Wang, H. B., Yang, M. L., Song, X., and Tong, H. T. (2022). Analysis on the characteristics of YU Jia-yan, a famous doctor from Xujiang area, in the treatment of dyspnea crisis. *Tradit. Chin. Med. J*. 21, 9–11. doi: 10.3389/fonc.2021.714267

frontiers | Frontiers in Microbiology

TYPE Original Research
PUBLISHED 03 October 2023
DOI 10.3389/fmicb.2023.1265425

OPEN ACCESS

EDITED BY
Naga Betrapally,
National Cancer Institute (NIH), United States

REVIEWED BY
Lingyan Ma,
Zhejiang Academy of Agricultural Sciences, China
Jingjing Zhao,
University of Louisville, United States

*CORRESPONDENCE
Wen Sun
✉ sunwen@bucm.edu.cn

†These authors have contributed equally to this work

RECEIVED 22 July 2023
ACCEPTED 13 September 2023
PUBLISHED 03 October 2023

CITATION
Sang X, Li S, Guo R, Yan Q, Liu C, Zhang Y, Lv Q, Wu L, Ma J, You W, Feng L and Sun W (2023) Dynamics and ecological reassembly of the human gut microbiome and the host metabolome in response to prolonged fasting. *Front. Microbiol.* 14:1265425. doi: 10.3389/fmicb.2023.1265425

Dynamics and ecological reassembly of the human gut microbiome and the host metabolome in response to prolonged fasting

Xiaopu Sang[1†], Shenghui Li[2†], Ruochun Guo[2†], Qiulong Yan[3†], Changxi Liu[4†], Yue Zhang[3], Qingbo Lv[3], Lili Wu[4,5,6], Jie Ma[4], Wei You[7], Ling Feng[8] and Wen Sun[4,5,6]*

[1]School of Life Science, Beijing University of Chinese Medicine, Beijing, China, [2]Puensum Genetech Institute, Wuhan, China, [3]Department of Microbiology, College of Basic Medical Sciences, Dalian Medical University, Dalian, China, [4]School of Traditional Chinese Medicine, Beijing University of Chinese Medicine, Beijing, China, [5]Key Laboratory of Health Cultivation of the Ministry of Education, Beijing University of Chinese Medicine, Beijing, China, [6]Beijing Key Laboratory of Health Cultivation, Beijing University of Chinese Medicine, Beijing, China, [7]Beijing Hospital of Traditional Chinese Medicine, Capital Medical University, Beijing, China, [8]Second Affiliated Hospital, Heilongjiang University of Chinese Medicine, Harbin, China

Introduction: Prolonged fasting is an intervention approach with potential benefits for individuals with obesity or metabolic disorders. Changes in gut microbiota during and after fasting may also have significant effects on the human body.

Methods: Here we conducted a 7-days medically supervised water-only fasting for 46 obese volunteers and characterized their gut microbiota based on whole-metagenome sequencing of feces at five timepoints.

Results: Substantial changes in the gut microbial diversity and composition were observed during fasting, with rapid restoration after fasting. The ecological pattern of the microbiota was also reassembled during fasting, reflecting the reduced metabolic capacity of diet-derived carbohydrates, while other metabolic abilities such as degradation of glycoproteins, amino acids, lipids, and organic acid metabolism, were enhanced. We identified a group of species that responded significantly to fasting, including 130 fasting-resistant (consisting of a variety of members of Bacteroidetes, Proteobacteria, and Fusobacteria) and 140 fasting-sensitive bacteria (mainly consisting of Firmicutes members). Functional comparison of the fasting-responded bacteria untangled the associations of taxon-specific functions (e.g., pentose phosphate pathway modules, glycosaminoglycan degradation, and folate biosynthesis) with fasting. Furthermore, we found that the serum and urine metabolomes of individuals were also substantially changed across the fasting procedure, and particularly, these changes were largely affected by the fasting-responded bacteria in the gut microbiota.

Discussion: Overall, our findings delineated the patterns of gut microbiota alterations under prolonged fasting, which will boost future mechanistic and clinical intervention studies.

KEYWORDS

obesity, gut microbiome, metabolome, fasting, dynamics, ecological reassembly

Introduction

Diet intervention is considered an effective method to improve lifespan and slow the progression of various diseases (Carter et al., 2018; Mardinoglu et al., 2018; Tang et al., 2023). Common forms of intervention include caloric restriction (Barquissau et al., 2018), carbohydrate restriction (Harvie et al., 2013), ketogenic diet (Abbasi, 2018), and fasting (Aon et al., 2020; Horne et al., 2020). Caloric and carbohydrate restrictions had been shown to have metabolic benefits, such as reducing body fat and insulin resistance and inducing short-term improvement in plasma glucose and cardiovascular risk (Barquissau et al., 2018; Van Zuuren et al., 2018; Diaz-Ruiz et al., 2021; Mishra et al., 2021), while the ketogenic diet had been proven to decrease triglycerides in the liver and insulin resistance level in individuals with nonalcoholic fatty liver disease (NAFLD) (Luukkonen et al., 2020). As an "unusual" intervention method, fasting had also shown health benefits. Early studies had revealed that intermittent fasting can enhance the antioxidative metabolism and improve neurological symptoms through effects on certain gut microbial taxa in mouse models (Cignarella et al., 2018; Liu et al., 2020). In humans, intermittent fasting can activate white adipose browning to ameliorate obesity (Li et al., 2017), inhibit the proliferation of colorectal cancer (Weng et al., 2020), and improve metabolic abnormalities and healthspan (Etemadifar et al., 2016; Mattson et al., 2017; De Cabo and Mattson, 2019). Also, prolonged fasting (that is, food deprivation for over 2 days) can decrease disease activity in patients with rheumatoid arthritis (RA) (Hafstrom et al., 1988), improved insulin release and maintained glucose tolerance (Solianik et al., 2023; Tripolt et al., 2023), and has potential mood-enhancing and pain-relieving effects in chronic pain patients (Michalsen, 2010). Many of these studies also underscored that further evidence was essential for reducing safety concerns and more accurately defining the impact mechanism of various diet interventions, especially fasting, on human physiology.

In recent studies, increasing evidence indicated that dietary changes are able to alter gut microbial composition and function with profound effects on human health. For example, metabolic patterns of gut microbiota may change in response to seasonal dietary changes of the Hadza of Tanzania (Smits et al., 2017). Gut microbial composition and metabolite profiles can rapidly change to adapt to plant- and animal-based diets (David et al., 2014). Reduced carbohydrate consumption resulted in increased bacterial folate production, which may partially improve multiple metabolic factors, neutralize oxidative stress, and reduce inflammation in patients with NAFLD (Mardinoglu et al., 2018). Food, gut microbiota, and host are the main components of the gut ecosystem, which constitute a diet-microbiome-host interaction network. Previous studies often revealed the associations between the specific dietary substrate and gut microbial taxa or specific host factors, however, the direct interactions between microbiota and host are still underexplored. Human and their gut microbiota are considered as a holobiont and have co-evolved into a diverse and complex system for millions of years (Van de Guchte et al., 2018). A normal gut microbial ecosystem is dynamically balanced, with different bacteria having different niches within the environment. Some bacteria are efficient at breaking down food substrates and providing energy productions [e.g., short-chain fatty acids (SCFAs)] for other bacteria or host cells. Some bacteria can utilize other bacteria or host-derived substances, and these bacteria are most likely food-independent. The dynamic balance of the gut microbiota is considered to be an important factor in human health, and when this balance is disrupted (usually name as "gut dysbiosis"), it may further cause or aggravate a variety of systemic diseases such as inflammatory bowel disease (IBD) (Tomasello et al., 2016; Federici et al., 2022), colorectal cancer (CRC) (Zou et al., 2018), and autoimmune diseases (Kinashi and Hase, 2021; Liang et al., 2022).

Early studies had revealed that intermittent fasting or caloric restriction can enhance the antioxidative metabolism, improve neurological symptoms, and promote anti-tumor immunity through effects on certain gut microbial taxa in mouse models (Cignarella et al., 2018; Liu et al., 2020; Mao et al., 2023). Some studies have also explored the impact of gut microbiota after dietary restrictions on human health (Cignarella et al., 2018; Mardinoglu et al., 2018; Maifeld et al., 2021; Von Schwartzenberg et al., 2021). A randomized human intervention study demonstrated that when gut microbiota from individuals who underwent a very-low-calorie diet intervention were transplanted into mice, the mice experienced a reduction in body weight and adiposity compared to those that had received microbiota before the intervention (Von Schwartzenberg et al., 2021). In a study for obese people with NAFLD, a short-term low-carbohydrate intervention rapidly altered the composition of the gut microbiota (Mardinoglu et al., 2018). This change was accompanied by an enhancement in the folate production of gut microbiota and an increase in folate concentration in the host's blood. This may partly explain how such an intervention improves host lipid metabolism, balances oxidative stress, and reduces inflammation. Overall, although there have been many studies examining the regulatory impact of the gut microbiota on host health during dietary restrictions, most of these findings are derived from research conducted on mice (Cignarella et al., 2018; Liu et al., 2020; Mao et al., 2023). However, it is well-known that there are substantial differences between the gut microbiome of mice and human, and many of these findings require further validation. Currently, there have been only a limited number of studies investigating changes in the gut microbiota in response to dietary restrictions in human. There is still a great deal to explore concerning the complex interaction between the gut microbiota, dietary restriction, and human health.

Based on these backgrounds, we thought that prolonged fasting is a unique model for investigating the direct interaction between gut microbiota and host: when there is no food available, the gut microbiota and host form into a transient new ecosystem. In this study, we analyzed the dynamic and ecological variability of gut microbiota of 46 obese individuals undergoing a 7-days medically supervised water-only fasting procedure combined with specific exercises (collectively called *bigu* in traditional Chinese medicine). Fecal, serum and urine samples were collected from the individuals before fasting, on the 3rd and 7th day during fasting, and on the 7th and 14th day after fasting, and were used for multi-omics analysis by both metagenome and metabolome techniques. These longitudinal datasets were able to identify survival strategies of gut microbiota under extreme nutritional deficiency based on a genome-centric strategy, and to interpret the microbiota-human inter-associations in this transient gut ecosystem.

Results and discussion

Study design, participants, and clinical characteristics

This study included 46 obese volunteers who participated in a 7-days medically supervised water-only fasting procedure and the subsequent recovery phase (3-days low-calorie diet and 4-days

gradually recover to normal diet), with 7-days follow-up (Figure 1A). Fasting led to significant decreases in body weight (body mass index, from 29.6 to 27.5 kg/m^2, $p < 0.001$), waist circumference (from 101.1 ± 10.3 cm to 96.1 ± 10.0 cm, $p < 0.001$), visceral fat rating (from 14.2 to 12.2%, $p < 0.001$), and mean blood pressure (from 98.8 to 92.1 mmHg, $p < 0.001$), along with a considerable decrease of visceral fat rate and metabolic rate (Figure 1B; Supplementary Table S1). Psychological evaluation during fasting revealed that the proportion of struggling participants decreased gradually from the first 3 days (71.4%) to the last day (21.4%), which effectively enhanced their confidence to complete the 7-days fasting procedure (Supplementary Figure S1A).

To further investigate the physiological variation of the volunteers during the whole experimental procedure, we collected the blood and urine specimens from each individual at five timepoints: T0 ($n = 46$), the day before fasting; T1 ($n = 46$) and T2 ($n = 46$), the 3rd and 7th day of fasting; and T3 ($n = 45$) and T4 ($n = 44$), the 7th and 14th day after fasting. Overall, the routine blood, liver, and renal function parameters of the participants had largely changed during the fasting period, however, most of these parameters returned to the original levels at the T3 and T4 timepoints (Supplementary Table S1). Individuals' aspartate transaminase (AST), alkaline phosphatase (ALP), total bilirubin (TBIL), and total bile acids (TBA) deviated from the baseline at T3, but recovered at T4; in particular, their serum creatinine level was significantly decreased at both T3 and T4 (Figure 1C). Similarly, the immune indexes of individuals had been disturbed during fasting and showed no obvious abnormalities at timepoints T3 and T4 (Figure 1D). These results are in agreement with previous studies suggesting the safety of prolonged fasting for humans under careful care (Jiang et al., 2021; Tang et al., 2021), however, the potential benefits of fasting need to be studied further.

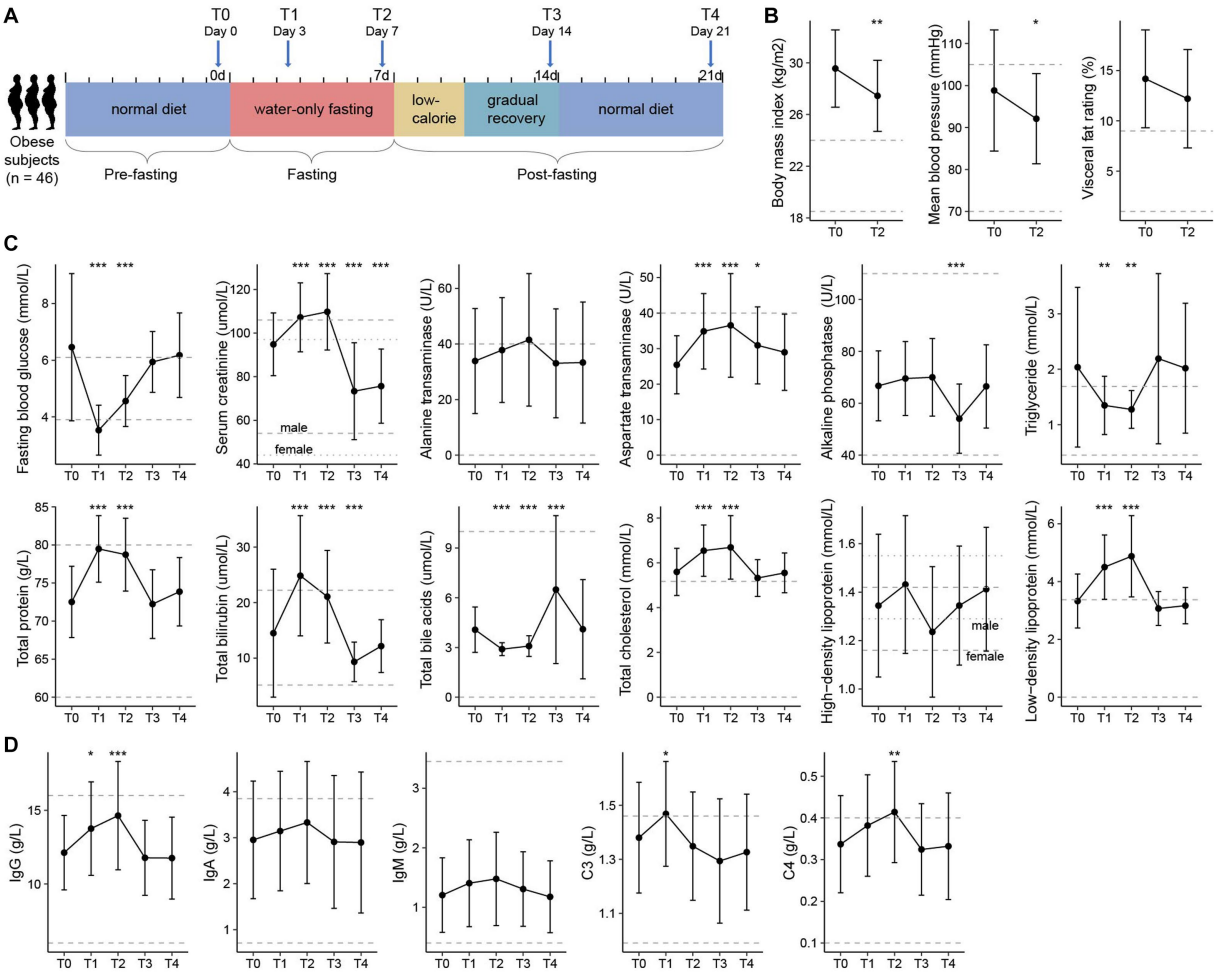

FIGURE 1
Experimental design and clinical characteristics of the participants. **(A)** Flow diagram of the clinical study. Forty-six obese volunteers who met the inclusion criteria were recruited and had finished the whole fasting procedure, including the pre-fasting stage (Day −6 to Day 0), fasting stage (Day 1 to Day 7), and post-fasting stage (Day 8 to Day 21). Clinical data and fecal samples were collected at five timepoints: T0 (Day 0, $n = 46$), T1 (Day 3, $n = 46$), T2 (Day 7, $n = 46$), T3 (Day 14, $n = 45$), and T4 (Day 21, $n = 44$). **(B)** Changes in the body mass index (BMI), visceral fat rating, and mean blood pressure of participants between T0 and T2. **(C)** Changes in the clinical parameters (i.e., routine blood, liver, and renal function parameters) of the participants at five timepoints. **(D)** Changes in the immune indexes of the participants at five timepoints. For **(B–D)**, filled dots represent the average value of the parameters in all individuals, and bars denote the lowest and highest values within 1.5 times the range of the first and third quartiles, respectively. Dotted horizontal lines represent the clinical typical ranges for each parameter. Significance levels compared with samples at T0 (Student's *t*-test): *, $p < 0.05$; **, $p < 0.01$; ***, $p < 0.001$.

Dynamics of the gut microbiota across the fasting procedure

The stool samples of 46 volunteers were collected at the same timepoints (T0-T4; Figure 1A) with their blood and urine specimens. To characterize the dynamics of gut microbiota in response to prolonged fasting, we performed whole-metagenome shotgun sequencing of fecal samples (representing 1,346 Gbp data; Supplementary Table S2) and carried out a metagenomic assembly of single samples and a co-assembly of samples for every individual at five timepoints. A total of 5,263 high-quality metagenomic-assembled genomes (MAGs) (≥90% complete and ≤5% contamination) were produced from the assembled contigs, which could be organized into 433 non-redundant clusters (referring to as "species" in the later text) for the species-level description of the gut microbiome (Jain et al., 2018; Supplementary Tables S3, S4). These species distributed a diverse range of bacterial phyla including Bacteroidetes ($n = 76$), Firmicutes ($n = 204$), Proteobacteria ($n = 30$), Actinobacteria ($n = 18$), Fusobacteria ($n = 5$), Verrucomicrobia ($n = 2$) and Synergistetes ($n = 1$), and an archaeal Euryarchaeota genome. Phylogenetic analysis showed that these species covered the major lineages of human gut microbiota (Supplementary Figure S2); especially, a majority of the species (55.4%) were currently uncultured. In addition, these non-redundant species achieved an average read mapping rate of 83.6% for the original fecal metagenomes (Supplementary Table S2), suggesting their effective representativeness of the gut microbiome.

Using principal coordinates analysis (PCoA) of the gut species profiles, we observed a dramatic alteration of the overall microbial community structure across the experimental procedure (Figure 2A). This change immediately occurred during fasting began (from T0 to T1: *adonis* $R^2 = 18.3\%$, $p < 0.001$), with a similar tendency across all individuals. Inversely, the degree of gut microbiota alteration from 3rd to 7th fasting was little (T1 vs. T2: *adonis* $R^2 = 2.1\%$, $p = 0.018$). When start taking food again, the gut microbiota rapidly recovered, and particularly, the degree of gut microbiota alteration among T0, T3, and T4 was comparatively small (*adonis* $R^2 = 2.4\%$, $p = 0.006$). In addition, the dissimilarity of individuals' gut microbiota during fasting was significantly reduced compared with those at the baseline or after fasting (Figure 2B), in agreement with the observation in PCoA analysis and suggesting that the pattern of gut microbiota alteration may be similar across different individuals.

We estimated the total amount of micrograms in feces using a qPCR analysis of the universal 16S rRNA primers. Consistent with the above findings, this analysis revealed that fasting led to a substantial reduction of bacterial amount (median cells per gram of feces, $T_{0/3/4}$ vs. $T_{1/2} = 6.0\times10^{9}$ vs. 1.1×10^{8}, $p = 1.7\times10^{-20}$), while the bacterial populations among T0, T3, and T4 have not differed (pairwise $p > 0.05$; Figure 2C). Some previous studies had shown that the use of antibiotics eliminated a large number of bacteria and led to a substantial reduction of the microbial diversity of gut microbiota (Chng et al., 2020). Unlike this, we found that both species richness and diversity indexes of the gut microbiota during fasting were approximate to or larger than those at baseline (Figure 2D). A similar increase was also observed in mice practicing intermittent fasting and in overweight women following low-calorie diets (Cignarella et al., 2018; Liu et al., 2020; Von Schwartzenberg et al., 2021). These results suggested that a considerable number of species still survived in the human gut under extreme nutritional deficiency. It should be noted that an increase in the microbiome diversity is generally considered a positive development. This is because higher diversity is often linked to improved health and immune system function, in contrast to lower diversity (Zheng et al., 2020).

Overview of gut microbial functions and ecological patterns during fasting

To investigate the functional dynamics of gut microbiota, we profiled the microbial functions of each sample via the KEGG (The Kyoto Encyclopedia of Genes and Genomes) and Carbohydrate-active enzymes database (CAZy) databases using a genome-centric approach method (Supplementary Table S4). Similar to the phylogenetic composition, PCoA analysis also supported that the functional microbiome is substantially changed during the fasting period and rapidly recovered at the T3 and T4 timepoints (Supplementary Figure S3). We then used the gut metabolic module (GMM) framework (Vieira-Silva et al., 2016) to evaluate the ecological properties of the gut microbiomes during and after fasting. Each GMM is defined as a set of orthologue groups that represent an enzyme-mediated ecological process, such as the degradation of a specific carbohydrate or amino acid, and the metabolism of an active small molecule substance (Vieira-Silva et al., 2016). During the fasting period, the individuals' gut microbiome had remarkedly reduced in the capacity of carbohydrate degradation (Figure 3A). This reduction involved almost all plant-derived polysaccharides, including sucrose, starch, rhamnose, pectin, maltose, fructose, fructan, and arabinoxylan (Figure 3B), which appears to be a direct result of the lack of food. Inversely, almost all other GMMs involved in central metabolism, degradation of glycoproteins, amino acids, lipids, and organic acid metabolism were significantly enhanced in the gut microbiomes during fasting (Figures 3A,B).

The enhancement of central metabolism, especially the pentose phosphate pathway (PPP), during fasting was a typical phenomenon. PPP, a pathway parallel to glycolysis that is involved in the direct oxidation of glucose (Horecker, 2002), is important for generating NADPH, which is an essential cofactor for glutathione- and thioredoxin-dependent enzymes that defend cells against oxidative damage. Since the oxidative stress of the gut environment is profoundly increased during fasting, this pathway might be important for protecting bacteria from oxidative stress. Another noteworthy finding was that, unlike the plant-derived polysaccharides, the degradation of several animal-derived carbohydrates such as lactose and ribose was increased during fasting (Figure 3B). This finding is similar to the metabolic characteristics of gut microbiota of animals during hibernation (Carey et al., 2013; Sommer et al., 2016), suggesting that gut bacteria may be involved in metabolizing host-derived substances. Likewise, the metabolism of mucin, a glycoprotein component of the host intestinal mucosa, was increased during fasting. Similarly, the gut bacteria might also use certain small molecules, such as ethanol, nitrogen, and short-chain fatty acids (i.e., acetate, propionate, and butyrate), as energy sources during fasting, leading to a significant enhancement of the metabolic capacity of these substances. Overall, our findings suggested a substantial ecological reassembly of the human gut microbiome in response to fasting.

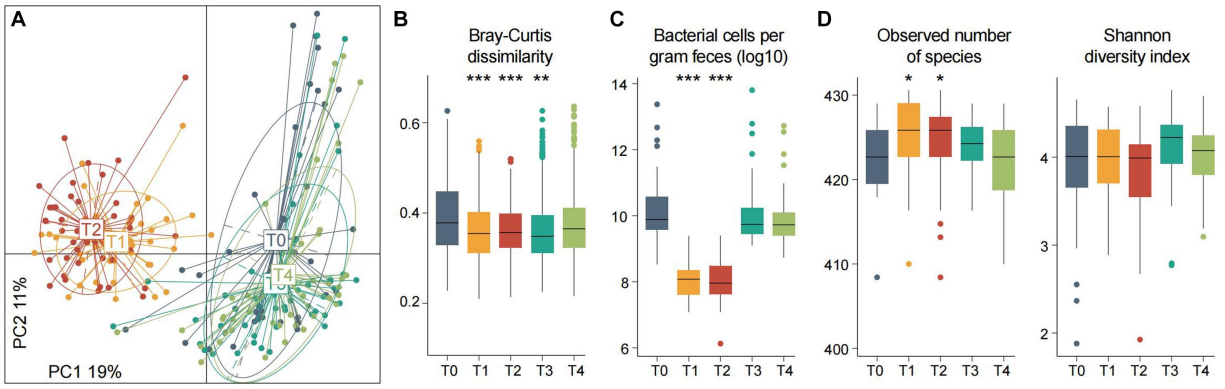

FIGURE 2
Gut microbiota composition and diversity at different timepoints of fasting. **(A)** Principal coordinates analysis (PCoA) of the Bray–Curtis dissimilarity at the species level of fecal samples. Samples are shown at the first and second principal coordinates (PC1 and PC2), and the ratio of variance contributed by these two PCs is shown. Lines connect samples that belonged to the same timepoint, and ellipsoids represent a 95% confidence interval surrounding each timepoint. **(B–D)** Changes of the between-sample Bray–Curtis dissimilarity **(B)** estimated bacterial cell numbers **(C)** and within-sample diversity **(D)** of the participants at five timepoints. Boxes represent the interquartile range between the first and third quartiles and the median (internal line). Whiskers denote the lowest and highest values within 1.5 times the range of the first and third quartiles, respectively; dots represent outlier samples beyond the whiskers. Significance levels compared with samples at T0 (Wilcoxon rank-sum test): *, $p < 0.05$; **, $p < 0.01$; ***, $p < 0.001$.

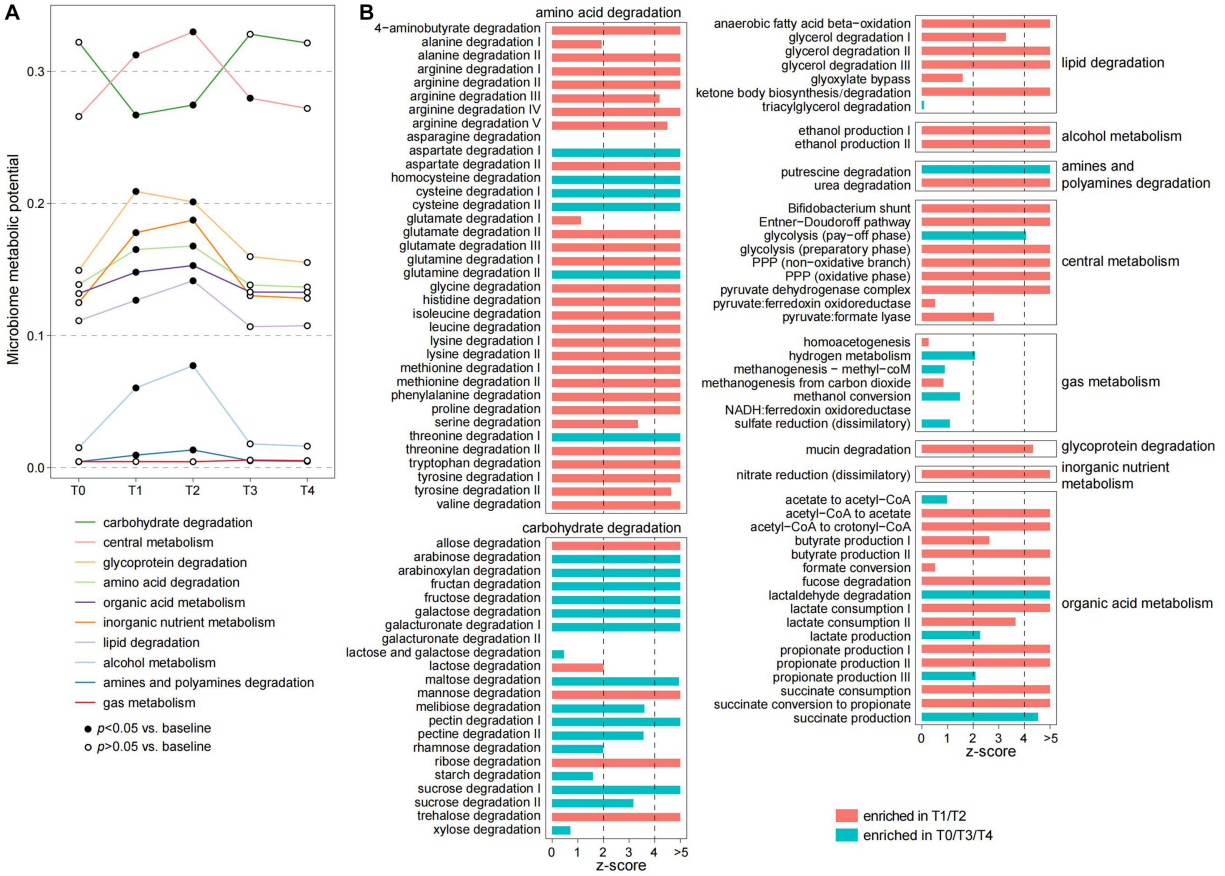

FIGURE 3
Alteration of the ecological pattern of gut microbiota during fasting. **(A)** Changes in the microbiome metabolic potential of the participants at five timepoints. Metabolic potentials of the gut microbiome are evaluated using the gut metabolic module (GMM) framework and grouped into 10 GMM categories. Dots represent the average value of each GMM category in all individuals, and the fitted dots denote a significance level of $p < 0.05$ (Wilcoxon rank-sum test) compared with samples at T0. **(B)** Changes of each GMM during fasting. Barplots indicate the z-score (Wilcoxon rank-sum test) of the comparisons of samples between T1/T2 and T0/T3/T4.

Identification of fasting-resistance and fasting-sensitive bacteria

To identify actively or inactively microbes during fasting, we compared the relative abundance profiles of gut species between the fasting period and non-fasting timepoints. This analysis showed that 270 of 433 species significantly differed in relative abundances between the two stages (Figure 4A; Supplementary Figure S4; Supplementary Table S5), including 130 species that increase during fasting and 140 species decrease. These species were defined as fasting-resistant bacteria (FRBs) and fasting-sensitive bacteria (FSBs), respectively. On average for all individuals, the gross relative abundance of FRBs increased from16.4% at the baseline to 62.6 and 68.7% at T1 and T2, respectively (Figure 4B); considering that the microbial load of feces was substantially reduced during the fasting period, the total cell numbers of these FRBs still decreased to some extent (estimated number of cells per gram of feces, T0 vs. $T_{1/2} = 1.1\times10^{9}$ vs. 6.5×10^{7}, $p = 5.5\times10^{-12}$; Figure 4D). In addition, we calculated the bacterial replication rates of each species to evaluate their growth status and found that the replication rate of FRBs is significantly increased at both T1 and T2 timepoints compared with the baseline ($p < 0.001$; Figure 4C). These results indicated that the FRBs can indeed be activated during fasting. Inversely, the gross relative abundance, estimated number of cells, and replication rate of FSRs were remarkedly reduced during the fasting period (Figures 4B–D).

Taxonomically, the FRBs included members belonged to Firmicutes ($n = 60$), Bacteroidetes ($n = 42$), Proteobacteria ($n = 17$), Fusobacteria ($n = 5$), Actinobacteria ($n = 2$), Synergistetes ($n = 2$), and Verrucomicrobia ($n = 2$); whereas the FSBs were mainly composed by Firmicutes members ($n = 118$), followed by members of Bacteroidetes ($n = 14$), Actinobacteria ($n = 5$), and Proteobacteria ($n = 3$; Figure 4A). At the family and genus levels, we found that the species belonged to *Alistipes*, Marinifilaceae, *Parabacteroides*, Erysipelotrichaceae, *Intestinimonas*, *Lawsonibacter*, and *Faecalicatena* were appeared in the FRBs, while the species belonged to *Prevotella*, Muribaculaceae, *Faecalibacterium*, *Ruminococcus_I*, *Coprococcus*, *Blautia*, *Eubacterium_II*, and *Lachnospira* were FSBs (Figure 4A; Supplementary Table S5). Bacteroidetes are primary degraders of polysaccharides in the human gut (Lapebie et al., 2019), and of these

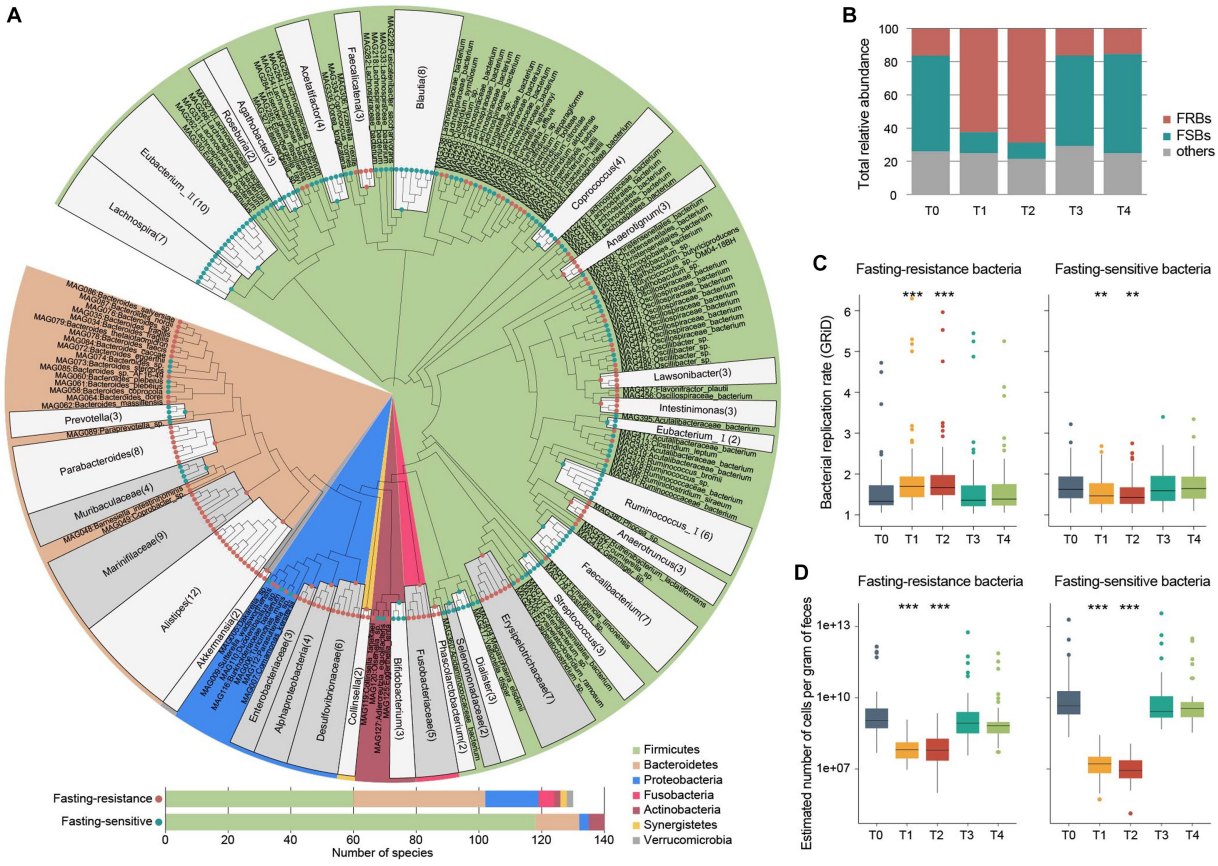

FIGURE 4
Overall representation of the fasting-resistance and fasting-sensitive bacteria. **(A)** Taxonomic characterization of 130 fasting-resistance bacteria (FRBs) and 140 fasting-sensitive bacteria (FSBs). Upper panel, phylogenetic tree showing the taxonomic assignments of the FRBs and FSBs. The adjacent species belonging to the same genus/family are grouped. Bottom panel, barplot showing the number of FRBs and FSBs for each bacterial phylum. **(B)** Total relative abundances of FRBs and FSBs in the gut microbiota at five timepoints. **(C)** Changes in the bacterial replication rate of FRBs (left panel) and FSBs (right panel) of the participants at five timepoints. Boxes represent the interquartile range between the first and third quartiles and the median (internal line). Whiskers denote the lowest and highest values within 1.5 times the range of the first and third quartiles, respectively; dots represent outlier samples beyond the whiskers. **(D)** Changes in the estimated number of cells per gram of feces in FRBs (left panel) and FSBs (right panel) among the participants at five timepoints. Significance levels compared with samples at T0 (Wilcoxon rank-sum test): *, $p < 0.05$; **, $p < 0.01$; ***, $p < 0.001$.

the *Prevotella* members are inclined to plant glycans such as fiber, xylan, starch, and pectin (David et al., 2014; Chen et al., 2017; Fehlner-Peach et al., 2019). Thus, the depletion of *Prevotella* members during fasting is consistent with the findings in the function aspect showing a substantial reduction of the degradation capacity of plant-derived polysaccharides. Firmicutes have the highest species diversity in the gut, and they are involved in a wide variety of important functions in the gut ecosystem, including metabolism/production of amino acids, vitamins, and SCFAs (Dai et al., 2011; Houtman et al., 2022). The higher proportion of FSBs in Firmicutes species during fasting suggested that they are vulnerable to environmental influences. In particular, some fasting-resistance Firmicutes such as Erysipelotrichaceae spp. are potential pathogens associated with human diseases (Kaakoush, 2015). On the other hand, certain Proteobacteria species such as Enterobacteriaceae and Desulfovibrionaceae members are more likely to survive or proliferate in the severe fasting environment (Figure 4A), which may be related to their strong environmental adaptability (David et al., 2014; Walterson and Stavrinides, 2015). For both Bacteroidetes and Firmicutes, we found that the higher bacterial genome size and number of functional orthologs are strongly beneficial to the fasting resistance (Supplementary Figure S5), suggesting that higher metabolic potential is also a strategy for survival during fasting.

Functional characteristics and host dependence of FRBs and FSBs

To elaborate on how the fasting response of gut bacteria is linked to their genomic and functional scopes, we first compared the KEGG and CAZy profiles between FSBs and FRBs using multivariate analyzes. In agreement with previous studies (Forster et al., 2019), the functional composition of gut bacteria was primarily determined by their phylogenetic relationship at the phylum level (effect sizes 36 and 30% for the KEGG and CAZy profiles, respectively, Permutational multivariate analysis of variance (PERMANOVA) $p < 0.001$; Figure 5A; Supplementary Figure S6). Stratification of FSBs and FRBs explained only 7% (PERMANOVA $p < 0.001$) variation in the functional composition. This finding raised us to compare the functional characteristics of FRBs and FSBs within each phylum to reduce the impact of the phylogeny.

Bacteroidetes

We identified 39 modules that significantly enhanced in module abundance (*Number of KEGG orthologs* × *module completion ratio*; see Methods) in the fasting-resistance Bacteroidetes, whereas only 3 modules were enhanced in the FSBs ($q < 0.05$; Figure 5B). The FRB-enhanced modules had more widely participated in amino acid metabolism (e.g., biosynthesis of arginine, polyamine, and ornithine and degradation of methionine), carbohydrate metabolism (mainly involved in PPP), energy metabolism (e.g., methanogenesis), antibiotic resistance and chemotaxis, and some modules involved environmental information processing and metabolism of other substances (e.g., chondroitin, dermatan, tetrahydrobiopterin, and ubiquinone). The higher frequency of PPP modules in FRBs, especially in *Parabacteroides* and *Bacteroides* members, was in agreement with the observations in overall gut microbiota function. And particularly, the PPP product, NAPDH, is a source of multiple sugar molecules that are required for the biosynthesis of nucleic acids and amino acids (Xue et al., 2017; Xu et al., 2018; Zhan et al., 2019), probably linking to the high biosynthesis capacity of arginine, ornithine, ectoine, and nucleotide sugar in fasting-resistance *Bacteroidetes* species. The methanogenesis modules, which may help to promote the carbon cycle in the gut microbiota under malnutrition (Million et al., 2016), were mainly encoded by members of fasting-resistance *Butyricimonas*, *Alistipes*, and *Parabacteroides* spp. Another striking phenomenon is the enhancement of two glycosaminoglycan (GAG) degradation modules (i.e., chondroitin and dermatan sulfate degradation) in FRBs. These modules were mainly encoded by members of *Bacteroides* and *Parabacteroides*. GAG, a type of mucopolysaccharides, is the major component of the extracellular matrix in animals that showed various physiological functions in the human gut (Cartmell et al., 2017; Kawai et al., 2018). This result suggested that, similar to carbohydrates, some bacteria can survive by using proteins from the hosts during the fasting period. Consistent with GAGs, the host glycoprotein mucin was also degraded by fasting-resistance *Parabacteroides* and *Bacteroides*.

Firmicutes

We identified 80 and 25 modules that significantly enhanced in module abundance in the FRBs and FSBs ($q < 0.05$; Figure 5C), respectively. Consistent with the *Bacteroidetes*, the FRB *Firmicutes* also more widely participated in carbohydrate and energy metabolism, especially the central metabolism modules involving to citrate cycle, PPP, Entner-Doudoroff pathway, and De Ley-Doudoroff pathway. Meanwhile, a large proportion (47/80, 58.8%) of FRB-enhanced modules were involved in environmental information processing such as transport system, two-component system, phosphotransferase system (PTS), and multidrug resistance (Supplementary Figure S7). Particularly, some transporters for uptake of plant carbohydrates such as fructose (M00273), ascorbate (M00283), mannose (M00276), and cellobiose (M00275) in gut microbiota were more abundant to be encoded in FRBs (Figure 5C). Compared with the FSBs, the higher capacity of carbohydrate/energy metabolism and environmental information processing in FRBs may involve in greater tolerance to severe oligotrophic environments during fasting. The other FRB-enhanced modules had participated in amino acid metabolism (e.g., degradation of histidine and tryptophan), biosynthesis of secondary metabolites, and nucleotide metabolism, while the FSB-enhanced modules were more widely distributed in sulfur metabolism and biosynthesis of amino acids (e.g., lysine, isoleucine, and methionine), folate, and other substances (e.g., uridine, nucleotide sugar, NAD) (Figure 5C). A notable function that is enriched in the FSBs is folate biosynthesis, for which we found that the major folate producers such as Lachnospiraceae members and *Streptococcus* spp. were sensitive to fasting. These findings were different from the observations in humans with the carbohydrate-restricted diet (Mardinoglu et al., 2018), probably due to differences in intervention patterns between the carbohydrate-restricted diet and our water-only fasting.

Fasting-responded species contribute to serum and urine metabolome changes

To explore the dynamics of the host metabolome across the fasting process, we performed untargeted mass spectrometry (MS) analysis of the serum and urine samples of 46 participants at five timepoints.

10.3389/fmicb.2023.1265425

FIGURE 5
Functional configuration of the fasting-resistance and fasting-sensitive bacteria. **(A)** Principal coordinates analysis (PCoA) of the functional profiles of fasting-resistance bacteria (FRBs) and fasting-sensitive bacteria (FSBs). Bacterial species are shown at the first and second principal coordinates (PC1 and PC2), and the ratio of variance contributed by these two PCs is shown. Species are colored based on their phylogeny at the phylum level (upper panel) or the stratification of FSBs and FRBs (bottom panel). Ellipsoids represent a 95% confidence interval surrounding each phylum. **(B,C)** Heatmap showing the abundances of the differential KEGG modules between FRBs and FSBs belonging to Bacteroidetes **(B)** and Firmicutes **(C)**. Each row represents a KEGG module, and each column represents a species. For **(B)**, the family-level taxonomic assignments of each species are shown. In the heatmap, the displayed modules are those with a Wilcoxon rank-sum test *q*-value of less than 0.05.

The serum and urine metabolomes were profiled based on 1,424 and 1,820 annotated metabolites, respectively, from the MS datasets. PCoA analysis revealed that both the serum and urine metabolomes are substantially altered during the fasting period and could largely recover at the T3 and T4 timepoints (Figure 6A). During the fasting period, 52.0% of serum metabolites and 66.8% of urine metabolites had significant abundances compared with baseline (Supplementary Tables S6, S7). During fasting, benzenoids, lipids and

lipid-like molecules, organic acids and derivatives, and organoheterocyclic compounds were enhanced in individuals' serum, while many of these metabolites were reduced in urine (Supplementary Figure S8).

Furthermore, we carried out an inter-omics analysis to quantify the strength of association between the gut microbiome and serum and urine metabolomes. Univariate analysis identified 37 gut species that independently impact the serum metabolome, as well as 36 gut species that impact the urine metabolome (Figures 6B,C). Several fasting-associated species, such as the fasting-resistance *Odoribacter splanchnicus MAG030*, *Escherichia coli MAG019*, *Bilophila wadsworthia MAG352*, and *Flavonifractor plautii MAG457* and the fasting-sensitive *Fusicatenibacter saccharivorans MAG228*, *Lachnospiraceae bacterium MAG282*, and *Faecalibacterium prausnitzii MAG422* had significant effect sizes on both serum and urine metabolomes, suggesting their importance in shaping the host metabolism homeostasis. Moreover, multivariate analysis showed that the effect of the gut microbiome on metabolic profiles was considerable, as it accounted for 51.2 and 43.7% of the serum and urine metabolome variances, respectively. These findings suggested that the gut microbiota as well as the fasting-responded species appear to be an important determinant of the host metabolic landscape.

Finally, we also assess the association between gut microbial populations and clinical characteristics. Correlation analysis identified 2,195 significant pairwise correlations (Spearman's $|\rho| > 0.35$, $q < 0.05$), involving 224 gut species and 45 clinical characteristics (Supplementary Figure S9). Several fasting-resistance species, such as *Desulfovibrio desulfuricans MAG347*, *Flavonifractor plautii MAG457*, and *Intestinimonas massiliensis MAG458*, exhibited a significant positive correlation with serum immunoglobulin levels, suggesting their importance in the host's immune response during fasting. In addition, the fasting-resistance species fasting-resistance species were frequently positively correlated with indicators like bilirubin, lipoproteins, and creatinine, while the fasting-sensitive species more commonly showed significant positive correlations with indicators such as prealbumin, ApoB100/ApoAI ratio, and fasting blood glucose. These findings suggested that the fasting-responded species may play important roles in influencing various aspects of the host's health.

Conclusion

In summary, the present study investigated the patterns of gut microbiota alterations in a cohort of 46 obese volunteers across a 7-days prolonged fasting and recovery phase. The gut microbial diversity, composition, and estimated bacterial cell number revealed substantial changes during the fasting, with a rapid return to almost original levels after fasting. In terms of microbial function, the ecological pattern of the gut microbiota had also undergone rapid adaptive changes. The capacity of carbohydrate degradation, especially almost all plant-derived polysaccharides (e.g., sucrose, starch, rhamnose, and pectin), were reduced in the gut microbiota during fasting, while other metabolic abilities such as the degradation of glycoproteins, amino acids, lipids, and organic acid metabolism, were enhanced. Moreover, we found that changes in the gut microbiota

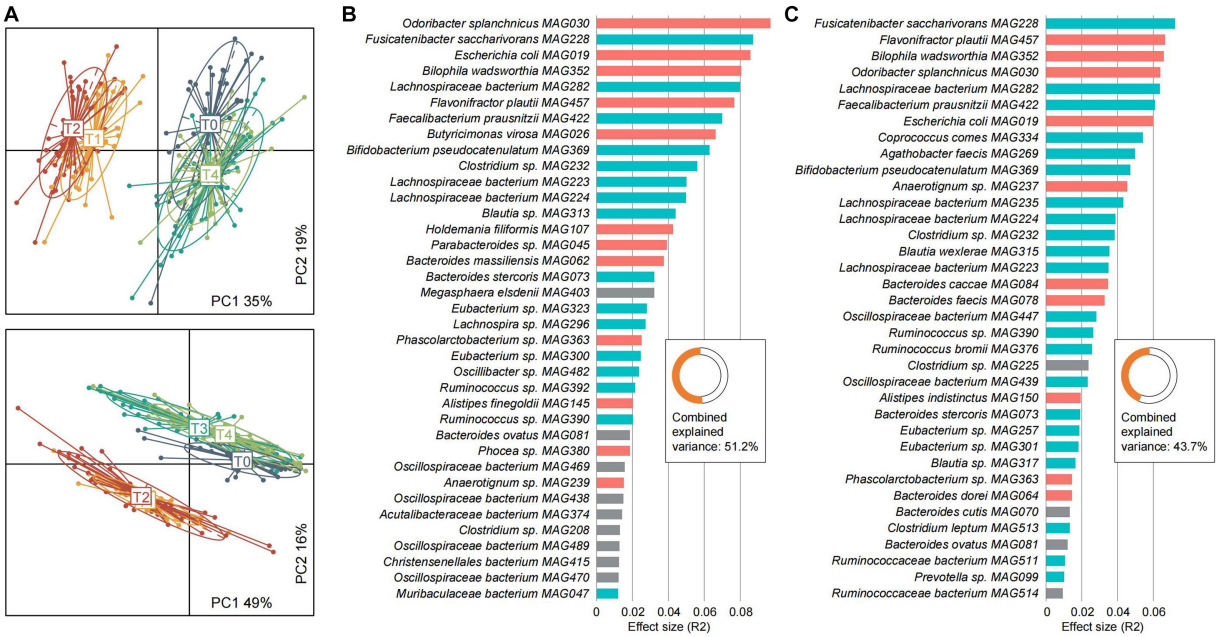

FIGURE 6
Characterization of the serum and urine metabolomes and their associations with gut microbiota. **(A)** Principal coordinates analysis (PCoA) of the serum metabolome (upper panel) and urine metabolome (bottom panel) of all samples. Samples are shown at the first and second principal coordinates (PC1 and PC2), and the ratio of variance contributed by these two PCs is shown. Lines connect samples that belonged to the same timepoint, and ellipsoids represent a 95% confidence interval surrounding each timepoint. **(B,C)** Barplots showing the effect sizes of gut species on the serum **(B)** and urine **(C)** metabolomes. The combined effect sizes of all species are shown in the inset panel. Colors represent the fasting-resistance (red), fasting-sensitive (blue), and other bacteria (gray).

were also, to a large extent, reflected in the serum and urine metabolites, highlighting the important role of the gut microbiota in this procedure. We identified 270 fasting-responded gut species, including 130 FRBs that still have activity (e.g., increase in bacterial replication rate) during fasting and 140 FSBs have been suppressed by fasting. FRBs included many Bacteroidetes members that have been extensively involved in the metabolism of various nutrients, as well as some members of Proteobacteria and Fusobacteria, while the FSBs were mostly Firmicutes members. Functional comparison between FRBs and FSBs untangled the associations of taxon-specific functions (e.g., pentose phosphate pathway modules, antibiotic resistance and chemotaxis, glycosaminoglycan degradation, and folate biosynthesis) with fasting. Together, our findings explained the main responses and strategies for gut bacterium to respond to the extreme nutritional deficiency condition, the results from this study provided guidance for subsequent bacterial ecology (e.g., bacterial cultivation) and clinical intervention (e.g., very low-calorie intake therapy) researches and will enhance our understanding and interpretation of the microbiota-human inter-associations.

Methods

Ethics approval and consent to participate

This study was approved by the Medical Ethics Committee of Beijing University of Chinese Medicine (2017BZHYLL0404). A written informed consent was obtained from each individual. To avoid the potential risk on the participants, we reference the safety and quality standards of an expert panel update of the 2002 consensus guidelines of fasting therapy (Wilhelmi de Toledo et al., 2013).

Study design and sampling

This study was designed as a controlled trial by comparing the differences in participants' physical status before and after the study. Volunteers were recruited between November and December 2016. This study included a 7-days medically supervised water-only fasting procedure, the subsequent recovery phase and follow-up phase (Supplementary Figure S1B). There were five timepoints: T0 (pre-fasting, Day 0), T1 (the 3rd day of fasting, Day 3), T2 (the 7th day of fasting, Day 7), T3 (the 7th day after fasting, Day 14), T4 (the 14th day after fasting, Day 21). The dinner of D0 was supplied only an apple (≤300 kcal). In the fasting period (Day 1 to Day 7), all participants received standard medical care as determined by their individual requirements. Thereafter, participants were allowed unrestricted amounts of natural drinking water (0 kcal, NONGFU SPRING, Guangdong, China), and were advised to drink at least 2.5 L daily. Traditional Chinese meditation and exercises were performed systematically every day. In the recovery period (Day 8-Day 14), participants had a low-calorie diet during the first 3 days, followed by gradually recover to normal diet in the next 4 days. The dietary calories consumed on Day 8, Day 9, and Day 10 were approximately 800 kcal, 1,000 kcal, and 1,200 kcal, respectively. From Day 11 to Day 14, the caloric intake gradually increased to 1,600 kcal. The source of calories was millet, with a caloric value of 360 kcal per 100 g, obtained from the China National Cereals, Oils and Foodstuffs Corporation in Beijing, China. During the follow-up period from Day 15 to Day 21, no intervention was conducted except for a questionnaire survey and telephone return visit.

The inclusion criteria in this trial were: aged from 20 to 70, central obesity (waist circumference: male ≥90 cm, female ≥80 cm), body mass index (BMI) ≥ 25 kg/m^2, or concurrently diagnosed with one of the following three items: (1) elevated triglyceride (TG) level > 1.7 mmoL/L, or treated correspondingly; (2) decreased high-density lipoprotein-cholesterol (HDL-C) level (male <0.9 mmoL/L, female <1.1 mmoL/L), or treated correspondingly; (3) elevated fasting plasma glucose (FPG) (≥ 5.6 mmoL/L), or diagnosed with type 2 diabetes or received appropriate treatment. All participants were volunteered to join fasting and the trial. Exclusion criteria included: patients with type 1 diabetes mellitus, pregnant or lactating women, patients with secondary obesity or severe heart, liver and kidney dysfunction and other serious illness as well as patients undergoing any weight reduction treatment in recent 3 months.

All participants were weighed in light clothing without shoes at the same time in the morning at two time points T0 and T2. Body weight, visceral fat rate and body fate rate were measured by full body sensor body composition monitor and scale (Omron HBF-701). BMI was calculated as weight [kg]/height^2 [m^2]. Waist circumference (WC) was measured at the midpoint between the lower border of the rib cage and the top of the lateral border of the iliac crest by study physicians. Blood pressure was measured in the right arm using the sphygmomanometer (Yuwell, type A) after participants had rested in a seated position for 5 min. Blood and urine samples were collected in the morning after an overnight fast (T0, T3, T4) or during the fasting (T1, T2). Blood samples for clinical were analyzed in 2 h at the hospital. Serum samples were obtained by centrifugation at 3000 rpm for 10 min and immediately stored at −80°C until analysis. Urine samples were stored at −80°C without any preservatives. Feces samples were collected from all participants in the morning at five timepoints (T0-T4) were immediately placed into dry ice containers for transportation to the laboratory and preserved at −80°C until further processing. Adverse events were monitored by standardized questionnaires at T0 and T2 points.

Clinical laboratory tests

Complete blood count was measured using a hematology automated analyzer (Sysmex XE-2100, Sysmex XT-4000i). Serum alanine transaminase (ALT), aspartate transaminase (AST), blood urea nitrogen (BUN), creatinine (CRE), glucose, triglycerides (TG), total cholesterol (TC), high-density lipoprotein cholesterol (HDL-C), and low-density lipoprotein cholesterol (LDL-C), immunoglobulin G (IgG), immunoglobulin A (IgA), immunoglobulin M (IgM), complement component 3 (C3) and complement component 4 (C4) were measured using an autoanalyzer (Hitachi 7,600–110, Beckman AU-680).

Qualitative study

Semi-structured interviews or focus group interviews were conducted among 14 individuals in our study by Qing Dao television

station from D8 to D15, and there were 6 individuals wrote down their experiences during fasting and shared to us at D14. These verbatim transcripts were made and analyzed by two and more coders via NVivo software (version 11) using content analysis method.

Serum and urine metabolomics

LC-HRMS was performed on a Waters UPLC I-class system equipped with a binary solvent delivery manager and a sample manager, coupled with a Waters VION IMS Q-TOF Mass Spectrometer equipped with an electrospray interface (Waters Corporation, Milford, United States).

LC Conditions: Column: Acquity BEH C18 column (100 mm × 2.1 mm i.d., 1.7 μm, Waters, Milford, United States). Solvent: The column was maintained at 50°C and separation was achieved using the following gradient: 1%B–1% B over 0–1.0 min,1%B–20% B over 1.0–5.5 min, 20%B–30%B over 5.5–6.0 min; 30%B–35%B over 6.0–8.5 min; 35%B–70%B over 8.5–10.5 min; 70%B–100%B over 10.5–11.0 min; 100%B–100%B over 11.0–13.0 min;100%B–1%B over13.0–13.1 min; and 13.1–15.0 min holding at 1% B at a flow rate of 0.40 mL/min, where B is acetonitrile (0.1% (v/v) formic acid) and A is aqueous formic acid (0.1% (v/v) formic acid). Injection Volume was 3.00 μL and Column Temperature was set at 50.0°C.

The mass spectrometric data was collected using a Waters VION IMS Q-TOF Mass Spectrometer equipped with an electrospray ionization (ESI) source operating in either positive or negative ion mode. The source temperature and desolvation temperature was set at 120°C and 500°C, respectively, with a desolvation gas flow of 900 L/h. Centroid data was collected from 50 to 1,000 m/z with a scan time of 0.1 s and interscan delay of 0.02 s over a 13 min analysis time.

QC sample was prepared by mixing aliquots of the all samples to be a pooled sample, and then analyzed using the same method with the analytic samples. The QCs were injected at regular intervals (every ten samples) throughout the analytical run to provide a set of data from which repeatability can be assessed.

The UPLC–Q-TOF/MS raw data were analyzed by progenesis QI (Waters Corporation, Milford, United States) software using the following parameters. The parameters used were retention time(RT) range 0.5–14.0 min, mass range 50–1,000 Da, mass tolerance 0.01 Da. Isotopic peaks were excluded for analysis, noise elimination level was set at 10.00, minimum intensity was set to 15% of base peak intensity and, finally, RT tolerance was set at 0.01 min. The Excel file was obtained with three-dimensional data sets including m/z, peak RT and peak intensities, and RT–m/z pairs were used as the identifier for each ion. The resulting matrix was further reduced by removing any peaks with missing value (ion intensity = 0) in more than 60% samples. The internal standard was used for data QC (reproducibility). The positive and negative data were combined to get a combined data set which was imported into SIMCA-P+ 14.0 software package (Umetrics, Umeå, Sweden).

DNA extraction, library construction, and whole-metagenome shotgun sequencing

DNA for metagenomics sequencing was extracted from fecal samples by using the E.Z.N.A.® fecal DNA Kit (Omega Bio-tek, Norcross, GA, United States) according to the manufacturer's protocols. The DNA concentration and purity were quantified with TBS-380 and NanoDrop2000, respectively. DNA quality was examined with the 1% agarose gel electrophoresis system.

DNA was fragmented to an average size of about 300 bp using Covaris M220 (Gene Company Limited, China) for paired-end library construction. Paired-end library was prepared by using the TruSeq™ DNA Sample Prep Kit (Illumina, San Diego, CA, United States). Adapters containing the full complement of sequencing primer hybridization sites were ligated to the Blunt-end fragments. Paired-end sequencing was performed on the Illumina HiSeq4000 platform (Illumina Inc., San Diego, CA, United States) at Majorbio Bio-Pharm Technology Co., Ltd. (Shanghai, China).

Sequencing data quality control

Initial base calling of metagenomic sequencing data was performed using Illumina HiSeq4000 platform with system default parameters. For each metagenomic sample, low-quality paired-end reads were discarded in pair using fastp (Chen et al., 2018) based on any of the following criteria: (1) read with more than 30% bases that be estimated with error rate > 1%; (2) read with ambiguous "N" > 5 bp; (3) read less than 90 bp; (4) read less than 30% low complexity. Furthermore, human genomic DNA reads were identified via Bowtie2 (Langmead and Salzberg, 2012), and were removed if it shared >95% sequence with the human genome reference sequence (GRCh38). The remaining high-quality paired-end reads from metagenomic samples were used for further analysis.

Metagenomic-assembled genomes

For metagenomic samples, we carried out single-sample assembly using MEGAHIT (Li et al., 2015) (option "--k-list 21,41,61,81,101,121,141"), and then assembled contigs longer than 2 kbp in each sample were binned by MetaBAT2 (Kang et al., 2019) with default parameters, leading to 12,291 raw bins of over 200 kbp. In addition, to improve assembly quality, multiple metagenomic samples from the same individual were merged into a new metagenomic sample, and intra-individual assembly and binning were performed based on these merged samples, resulting in 6,800 raw bins of over 200 kbp. The completeness and contamination of all 19,091 raw bins were assessed by CheckM (Parks et al., 2015). For low-quality raw bins with <50% completeness and < 5% contamination, an additional approach was used to improve the quality of these raw bins. Firstly, the taxonomic classification of low-quality raw bins was carried out using the GTDB-Tk toolkit (Chaumeil et al., 2020). Meanwhile, the sequencing depth for each raw bin was defined by mapping the high-quality reads from the corresponding metagenomic sample back to the bin with Bowtie2 (Langmead and Salzberg, 2012) and SAMtools (Li et al., 2009). Lastly, raw bins were merged if they met all of the following criteria: (1) they were recovered from the same metagenomic sample; (2) they had a similar sequencing depth (±10%) and GC content (±2%); (3) they had an identical taxonomic assignment at the species level. The completeness and contamination of merged bins were re-assessed by CheckM (Parks et al., 2015). Finally, we obtained a collection of 5,263 high-quality MAGs (≥90% complete and ≤ 5% contamination). All high-quality MAGs were clustered using dRep

(Olm et al., 2017), leading to a de-replicated database of 433 species-level MAG. The taxonomic classification of these species-level MAGs was carried out using GTDB-Tk (Chaumeil et al., 2020). Phylogenetic analysis was performed using PhyloPhlAn (Asnicar et al., 2020), and visualized by iTOL[1] (Letunic and Bork, 2021).

To generate microbial community profiles, the high-quality paired-end reads of each sample were firstly aligned against the 433 species-level MAGs using Bowtie2 (Langmead and Salzberg, 2012). For the species-level profile, the relative abundance of each MAG was the number of mapped reads for each MAG divided by genomic length and the total number of mapped reads for each sample. For taxonomic profiles of the higher rank levels, the abundance of each taxon was calculated by summing up the relative abundance of MAGs from the same taxon. In addition, we calculated bacterial replication rates of MAGs in each sample to analyze the dynamics of bacterial growth via GRiD (Emiola and Oh, 2018).

Functional analysis

Genes of 433 species-level MAGs were predicted by Prodigal (Hyatt et al., 2010) with option '-p meta'. Functional annotation of the protein-coding genes was performed by assigning the protein sequences to the KEGG (Kyoto Encyclopedia of Genes and Genomes) database (Kanehisa et al., 2016) and using DIAMOND (Buchfink et al., 2015) with options '--evalue 1e-10 --query-cover 50'. Each protein was assigned a KEGG orthologue (KO) with the highest score. Annotation of carbohydrate-active enzymes (CAZymes) was performed by aligning the protein sequence of each MAGs against the CAZy database[2] using DIAMOND (*e*-value <1e-10 and covering >50% of the protein length).

To generate functional profiles of each sample, all putative protein-coding genes were firstly dereplicated by CD-HIT based on nucleotide level similarity >95% and sequence overlap >90%. Then, the high-quality paired-end reads of each sample were aligned against these dereplicated protein-coding genes using Bowtie2. The relative abundance of each gene was the number of mapped reads for each gene divided by gene size and the total number of mapped reads for each sample. For functional profiles, the abundance of each KO (or CAZy family) was calculated as the sum of abundance of genes from the same functional ortholog divided by abundance of all genes with KO (or CAZy family) assignment. In addition, to explore higher-order functions, KOs were assigned into gut metabolic modules (GMMs) (Vieira-Silva et al., 2016), a manually curated metabolic module framework. For GMM profiles of each sample, each GMM abundance was calculated as the median abundance of KOs assigned to the GMM, and then assigned the value of 0 if the number of KOs assigned to this GMM was less than half of total number of KOs in this GMM.

To generate functional profiles of each MAG, each KO (or CAZy family) abundance was calculated as the number of gene from the same functional ortholog in this MAG. KOs were assigned into KEGG modules based on the KEGG website[3] (Kanehisa et al., 2016). To explore higher-order functions of genomes, we calculated the module completion ratio (MCR) of each MAG based on a Boolean algebra-like equation (Takami et al., 2012) using custom scripts.

Statistical analysis

Statistical analyzes were performed on the R platform. The differences of clinical data at five time points were compared based on Student's *t*-test. For the alpha diversities, the Shannon diversity index was calculated via the function 'diversity', and the observed number of species was calculated as the count of unique species-level MAGs in each sample. The Bray-Curtis distance between samples was evaluated based on species-level profiles by the function 'vegdist'. (PCoA) based on Bray-Curtis distance was performed using the function 'pcoa', and normal confidence ellipses were computed using the function 'stat_ellipse' with parameters: geom of polygon and level of 0.8. PERMANOVA analysis was performed using the function 'adonis', and *adonis* R (Mardinoglu et al., 2018) was adjusted using the function 'RsquareAdj'. Statistical significance between two groups was assessed using the Wilcoxon rank-sum test via the function 'wilcox.test'. For comparisons involving multiple groups, the Kruskal-Wallis test was employed, and calculations were conducted using the 'kruskal.test' function. The *p*-values obtained were adjusted into q values using the Benjamini-Hochberg method via the function 'p.adjust'. To evaluate the impact of each bacterium on the metabolome, the 'adonis' function was used to estimate the "one-to-all" effect size (R^2) between the relative abundance of each MAG and the overall metabolic profiles. For correlation analysis between gut microbiota and clinical characteristics, we calculated the Spearman Rank Correlation Coefficient using the 'cor.test' function with the 'method = spearman' option, and then adjusted the p-values to q-values using the Benjamini-Hochberg method via the 'p.adjust' function.

Data visualization was implemented using the function 'ggplot2'.

qPCR detection for bacteria counts from original feces

To count the total bacterial load in feces, we performed relative quantification analysis by quantitative PCR (ABI StepOne, United States) (Alavi et al., 2020). The standard curves were prepared using two internal reference strains (Use *Lactococcus lactis* NZ9000 to represent Gram-positive bacteria and *Escherichia coli* BL21 to represent Gram-negative bacteria). The bacterial genome DNA extracted from 5 mL of liquid medium was used as a reference sample, and total DNA extracted from 170 mg corresponding host feces was used as a test sample. The number of internal reference strains was determined using CFU counting by solid plates before bacterial genome extraction. Consistent with the reference (Alavi et al., 2020), universal primers used in the article listed below (forward: CTCCTACGGGAGGCAGCAG; reverse: TTACCGCGGCTGCTGGCAC). PCR enzymes and chemicals were used according to the manufacturer's instructions (Innovgene, China). Each reaction was performed in triplicate. A 25 μL reaction system contained 1 μL of template DNA or sterile double distilled water (negative control), 12.5 μL of SYBR Premix (Innovgene, China), 0.5 μL of forward primer, 0.5 μL of reverse primer, and 10.5 μL of water. Amplifications were performed with the following reaction procedures: 1 cycle of predenaturation at 95°C for 3 min, followed by 39 cycles of denaturation

1 https://itol.embl.de/
2 http://www.cazy.org/
3 https://www.kegg.jp

at 95°C for 10 s and annealing at 55°C for 30 s. The total bacterial amount in test feces was calculated using the $2^{-\triangle\triangle C(T)}$ method (Alavi et al., 2020). For each fecal sample, we also estimated the bacterial amount of the fasting-resistance and fasting-sensitive bacteria, respectively. This was calculated as the sum of the relative abundances of all bacteria within each group divided by the total bacterial amount quantified for that sample using qPCR.

Data availability statement

The data presented in the study are deposited in the National Center for Biotechnology Information Sequence Read Achieve (NCBI-SRA) repository, accession number PRJNA433058.

Ethics statement

The studies involving humans were approved by Medical Ethics Committee of Beijing University of Chinese Medicine. The studies were conducted in accordance with the local legislation and institutional requirements. The participants provided their written informed consent to participate in this study.

Author contributions

XS: Conceptualization, Writing – original draft. SL: Data curation, Formal analysis, Methodology, Writing – original draft. RG: Data curation, Formal analysis, Methodology, Writing – original draft. QY: Data curation, Writing – original draft. CL: Conceptualization, Writing – original draft. YZ: Data curation, Methodology, Writing – original draft. QL: Methodology, Writing – original draft. LW: Data curation, Writing – original draft. JM: Data curation, Methodology, Writing – original draft. WY: Data curation, Writing – original draft. LF: Data curation, Investigation, Writing – original draft. WS: Conceptualization, Writing – original draft.

Funding

The authors declare financial support was received for the research, authorship, and/or publication of this article. This study was supported by the funding from Beijing University of Chinese Medicine (Nos. 5050071720001 and 2180072120049) and Beijing Social Science Fund Project (No. 21DTR047).

Acknowledgments

We would like to acknowledge Anlong Xu for technical help and Bin Su for her help and enthusiastic support.

Conflict of interest

The authors declare that the research was conducted in the absence of any commercial or financial relationships that could be construed as a potential conflict of interest.

Publisher's note

Supplementary material

The Supplementary material for this article can be found online at: https://www.frontiersin.org/articles/10.3389/fmicb.2023.1265425/full#supplementary-material

References

Abbasi, J. (2018). Interest in the ketogenic diet grows for weight loss and type 2 diabetes. *JAMA* 319, 215–217. doi: 10.1001/jama.2017.20639

Alavi, S., Mitchell, J. D., Cho, J. Y., Liu, R., Macbeth, J. C., and Hsiao, A. (2020). Interpersonal gut microbiome variation drives susceptibility and resistance to cholera infection. *Cells* 181, 1533–1546.e13. doi: 10.1016/j.cell.2020.05.036

Aon, M. A., Bernier, M., Mitchell, S. J., di Germanio, C., Mattison, J. A., Ehrlich, M. R., et al. (2020). Untangling determinants of enhanced health and lifespan through a multi-omics approach in mice. *Cell Metab.* 32:100-116 e104. doi: 10.1016/j.cmet.2020.04.018

Asnicar, F., Thomas, A. M., Beghini, F., Mengoni, C., Manara, S., Manghi, P., et al. (2020). Precise phylogenetic analysis of microbial isolates and genomes from metagenomes using PhyloPhlAn 3.0. *Nat. Commun.* 11, 1–10. doi: 10.1038/s41467-020-16366-7

Barquissau, V., Léger, B., Beuzelin, D., Martins, F., Amri, E. Z., Pisani, D. F., et al. (2018). Caloric restriction and diet-induced weight loss do not induce Browning of human subcutaneous white adipose tissue in women and men with obesity. *Cell Rep.* 22, 1079–1089. doi: 10.1016/j.celrep.2017.12.102

Buchfink, B., Xie, C., and Huson, D. H. (2015). Fast and sensitive protein alignment using DIAMOND. *Nat. Methods* 12, 59–60. doi: 10.1038/nmeth.3176

Carey, H. V., Walters, W. A., and Knight, R. (2013). Seasonal restructuring of the ground squirrel gut microbiota over the annual hibernation cycle. *Am. J. Phys. Regul. Integr. Comp. Phys.* 304, R33–R42. doi: 10.1152/ajpregu.00387.2012

Carter, S., Clifton, P. M., and Keogh, J. B. (2018). Effect of intermittent compared with continuous energy restricted diet on glycemic control in patients with type 2 diabetes: a randomized noninferiority trial. *JAMA Netw. Open* 1:e180756. doi: 10.1001/jamanetworkopen.2018.0756

Cartmell, A., Lowe, E. C., Baslé, A., Firbank, S. J., Ndeh, D. A., Murray, H., et al. (2017). How members of the human gut microbiota overcome the sulfation problem posed by glycosaminoglycans. *Proc. Natl. Acad. Sci.* 114, 7037–7042. doi: 10.1073/pnas.1704367114

Chaumeil, P.-A., Mussig, A. J., Hugenholtz, P., and Parks, D. (2020). GTDB-Tk: a toolkit to classify genomes with the genome taxonomy database. *Bioinformatics* 36, 1925–1927. doi: 10.1093/bioinformatics/btz848

Chen, T., Long, W., Zhang, C., Liu, S., Zhao, L., and Hamaker, B. R. (2017). Fiber-utilizing capacity varies in *Prevotella*–versus Bacteroides-dominated gut microbiota. *Sci. Rep.* 7:2594. doi: 10.1038/s41598-017-02995-4

Chen, S., Zhou, Y., Chen, Y., and Gu, J. (2018). fastp: an ultra-fast all-in-one FASTQ preprocessor. *Bioinformatics* 34, i884–i890. doi: 10.1093/bioinformatics/bty560

Chng, K. R., Ghosh, T. S., Tan, Y. H., Nandi, T., Lee, I. R., Ng, A. H. Q., et al. (2020). Metagenome-wide association analysis identifies microbial determinants of post-antibiotic ecological recovery in the gut. *Nat. Ecol. Evol.* 4, 1256–1267. doi: 10.1038/s41559-020-1236-0

Cignarella, F., Cantoni, C., Ghezzi, L., Salter, A., Dorsett, Y., Chen, L., et al. (2018). Intermittent fasting confers protection in CNS autoimmunity by altering the gut microbiota. *Cell Metab.* 27, 1222–1235. doi: 10.1016/j.cmet.2018.05.006

Dai, Z.-L., Wu, G., and Zhu, W.-Y. (2011). Amino acid metabolism in intestinal bacteria: links between gut ecology and host health. *Front. Biosci.* 16, 1768–1786. doi: 10.2741/3820

David, L. A., Maurice, C. F., Carmody, R. N., Gootenberg, D. B., Button, J. E., Wolfe, B. E., et al. (2014). Diet rapidly and reproducibly alters the human gut microbiome. *Nature* 505, 559–563. doi: 10.1038/nature12820

De Cabo, R., and Mattson, M. P. (2019). Effects of intermittent fasting on health, aging, and disease. *N. Engl. J. Med.* 381, 2541–2551. doi: 10.1056/NEJMra1905136

Diaz-Ruiz, A., Rhinesmith, T., Pomatto-Watson, L. C. D., Price, N. L., Eshaghi, F., Ehrlich, M. R., et al. (2021). Diet composition influences the metabolic benefits of short cycles of very low caloric intake. *Nat. Commun.* 12:6463. doi: 10.1038/s41467-021-26654-5

Emiola, A., and Oh, J. (2018). High throughput in situ metagenomic measurement of bacterial replication at ultra-low sequencing coverage. *Nat. Commun.* 9:4956. doi: 10.1038/s41467-018-07240-8

Etemadifar, M., Sayahi, F., Alroughani, R., Toghianifar, N., Akbari, M., and Nasr, Z. (2016). Effects of prolonged fasting on fatigue and quality of life in patients with multiple sclerosis. *Neurol. Sci.* 37, 929–933. doi: 10.1007/s10072-016-2518-9

Federici, S., Kredo-Russo, S., Valdés-Mas, R., Kviatcovsky, D., Weinstock, E., Matiuhin, Y., et al. (2022). Targeted suppression of human IBD-associated gut microbiota commensals by phage consortia for treatment of intestinal inflammation. *Cells* 185, 2879–2898.e24. doi: 10.1016/j.cell.2022.07.003

Fehlner-Peach, H., Magnabosco, C., Raghavan, V., Scher, J. U., Tett, A., Cox, L. M., et al. (2019). Distinct polysaccharide utilization profiles of human intestinal *Prevotella copri* isolates. *Cell Host Microbe* 26, 680–690. doi: 10.1016/j.chom.2019.10.013

Forster, S. C., Kumar, N., Anonye, B. O., Almeida, A., Viciani, E., Stares, M. D., et al. (2019). A human gut bacterial genome and culture collection for improved metagenomic analyses. *Nat. Biotechnol.* 37, 186–192. doi: 10.1038/s41587-018-0009-7

Hafstrom, I., Ringertz, B., Gyllenhammar, H., Palmblad, J., and Harms-Ringdahl, M. (1988). Effects of fasting on disease activity, neutrophil function, fatty acid composition, and leukotriene biosynthesis in patients with rheumatoid arthritis. *Arthritis Rheum.* 31, 585–592. doi: 10.1002/art.1780310502

Harvie, M., Wright, C., Pegington, M., McMullan, D., Mitchell, E., Martin, B., et al. (2013). The effect of intermittent energy and carbohydrate restriction v. daily energy restriction on weight loss and metabolic disease risk markers in overweight women. *Br. J. Nutr.* 110, 1534–1547. doi: 10.1017/S0007114513000792

Horecker, B. L. (2002). The pentose phosphate pathway. *J. Biol. Chem.* 277, 47965–47971. doi: 10.1074/jbc.X200007200

Horne, B. D., Grajower, M. M., and Anderson, J. L. (2020). Limited evidence for the health effects and safety of intermittent fasting among patients with type 2 diabetes. *JAMA* 324:341. doi: 10.1001/jama.2020.3908

Houtman, T. A., Eckermann, H. A., Smidt, H., and de Weerth, C. (2022). Gut microbiota and BMI throughout childhood: the role of firmicutes, bacteroidetes, and short-chain fatty acid producers. *Sci. Rep.* 12, 1–13. doi: 10.1038/s41598-022-07176-6

Hyatt, D., Chen, G. L., LoCascio, P. F., Land, M. L., Larimer, F. W., and Hauser, L. J. (2010). Prodigal: prokaryotic gene recognition and translation initiation site identification. *BMC Bioinformatics* 11, 1–11. doi: 10.1186/1471-2105-11-119

Jain, C., Rodriguez, R. L., Phillippy, A. M., Konstantinidis, K. T., and Aluru, S. (2018). High throughput ANI analysis of 90K prokaryotic genomes reveals clear species boundaries. *Nat. Commun.* 9:5114. doi: 10.1038/s41467-018-07641-9

Jiang, Y., Yang, X., Dong, C., Lu, Y., Yin, H., Xiao, B., et al. (2021). Five-day water-only fasting decreased metabolic-syndrome risk factors and increased anti-aging biomarkers without toxicity in a clinical trial of normal-weight individuals. *Clin. Transl. Med.* 11:e502. doi: 10.1002/ctm2.502

Kaakoush, N. O. (2015). Insights into the role of Erysipelotrichaceae in the human host. *Front. Cell. Infect. Microbiol.* 5:84. doi: 10.3389/fcimb.2015.00084

Kanehisa, M., Sato, Y., Kawashima, M., Furumichi, M., and Tanabe, M. (2016). KEGG as a reference resource for gene and protein annotation. *Nucleic Acids Res.* 44, D457–D462. doi: 10.1093/nar/gkv1070

Kang, D. D., Li, F., Kirton, E., Thomas, A., Egan, R., An, H., et al. (2019). MetaBAT 2: an adaptive binning algorithm for robust and efficient genome reconstruction from metagenome assemblies. *PeerJ* 7:e7359. doi: 10.7717/peerj.7359

Kawai, K., Kamochi, R., Oiki, S., Murata, K., and Hashimoto, W. (2018). Probiotics in human gut microbiota can degrade host glycosaminoglycans. *Sci. Rep.* 8, 1–13. doi: 10.1038/s41598-018-28886-w

Kinashi, Y., and Hase, K. (2021). Partners in leaky gut syndrome: intestinal dysbiosis and autoimmunity. *Front. Immunol.* 12:673708. doi: 10.3389/fimmu.2021.673708

Langmead, B., and Salzberg, S. L. (2012). Fast gapped-read alignment with bowtie 2. *Nat. Methods* 9, 357–359. doi: 10.1038/nmeth.1923

Lapebie, P., Lombard, V., Drula, E., Terrapon, N., and Henrissat, B. (2019). Bacteroidetes use thousands of enzyme combinations to break down glycans. *Nat. Commun.* 10:2043. doi: 10.1038/s41467-019-10068-5

Letunic, I., and Bork, P. (2021). Interactive tree of life (iTOL) v5: an online tool for phylogenetic tree display and annotation. *Nucleic Acids Res.* 49, W293–W296. doi: 10.1093/nar/gkab301

Li, H., Handsaker, B., Wysoker, A., Fennell, T., Ruan, J., Homer, N., et al. (2009). The sequence alignment/map format and SAMtools. *Bioinformatics* 25, 2078–2079. doi: 10.1093/bioinformatics/btp352

Li, D., Liu, C. M., Luo, R., Sadakane, K., and Lam, T. W. (2015). MEGAHIT: an ultra-fast single-node solution for large and complex metagenomics assembly via succinct de Bruijn graph. *Bioinformatics* 31, 1674–1676. doi: 10.1093/bioinformatics/btv033

Li, G., Xie, C., Lu, S., Nichols, R. G., Tian, Y., Li, L., et al. (2017). Intermittent fasting promotes white adipose Browning and Decreases obesity by shaping the gut microbiota. *Cell Metab.* 26:801. doi: 10.1016/j.cmet.2017.10.007

Liang, W., Enée, E., Andre-Vallee, C., Falcone, M., Sun, J., and Diana, J. (2022). Intestinal cathelicidin antimicrobial peptide shapes a protective neonatal gut microbiota against pancreatic autoimmunity. *Gastroenterology* 162, 1288–1302.e16. doi: 10.1053/j.gastro.2021.12.272

Liu, Z., Dai, X., Zhang, H., Shi, R., Hui, Y., Jin, X., et al. (2020). Gut microbiota mediates intermittent-fasting alleviation of diabetes-induced cognitive impairment. *Nat. Commun.* 11:855. doi: 10.1038/s41467-020-14676-4

Luukkonen, P. K., Dufour, S., Lyu, K., Zhang, X. M., Hakkarainen, A., Lehtimäki, T. E., et al. (2020). Effect of a ketogenic diet on hepatic steatosis and hepatic mitochondrial metabolism in nonalcoholic fatty liver disease. *Proc. Natl. Acad. Sci. U. S. A.* 117, 7347–7354. doi: 10.1073/pnas.1922344117

Maifeld, A., Bartolomaeus, H., Löber, U., Avery, E. G., Steckhan, N., Markó, L., et al. (2021). Fasting alters the gut microbiome reducing blood pressure and body weight in metabolic syndrome patients. *Nat. Commun.* 12:1970. doi: 10.1038/s41467-021-22097-0

Mao, Y.-Q., Huang, J. T., Zhang, S. L., Kong, C., Li, Z. M., Jing, H., et al. (2023). The antitumour effects of caloric restriction are mediated by the gut microbiome. *Nat. Metab.* 5, 96–110. doi: 10.1038/s42255-022-00716-4

Mardinoglu, A., Wu, H., Bjornson, E., Zhang, C., Hakkarainen, A., Räsänen, S. M., et al. (2018). An integrated understanding of the rapid metabolic benefits of a carbohydrate-restricted diet on hepatic steatosis in humans. *Cell Metab.* 27:559-571 e555. doi: 10.1016/j.cmet.2018.01.005

Mattson, M. P., Longo, V. D., and Harvie, M. (2017). Impact of intermittent fasting on health and disease processes. *Ageing Res. Rev.* 39, 46–58. doi: 10.1016/j.arr.2016.10.005

Michalsen, A. (2010). Prolonged fasting as a method of mood enhancement in chronic pain syndromes: a review of clinical evidence and mechanisms. *Curr. Pain Headache Rep.* 14, 80–87. doi: 10.1007/s11916-010-0104-z

Million, M., Tidjani Alou, M., Khelaifia, S., Bachar, D., Lagier, J. C., Dione, N., et al. (2016). Increased gut redox and depletion of anaerobic and methanogenic prokaryotes in severe acute malnutrition. *Sci. Rep.* 6, 1–11. doi: 10.1038/srep26051

Mishra, A., Mirzaei, H., Guidi, N., Vinciguerra, M., Mouton, A., Linardic, M., et al. (2021). Fasting-mimicking diet prevents high-fat diet effect on cardiometabolic risk and lifespan. *Nat. Metab.* 3, 1342–1356. doi: 10.1038/s42255-021-00469-6

Olm, M. R., Brown, C. T., Brooks, B., and Banfield, J. F. (2017). dRep: a tool for fast and accurate genomic comparisons that enables improved genome recovery from metagenomes through de-replication. *ISME J.* 11, 2864–2868. doi: 10.1038/ismej.2017.126

Parks, D. H., Imelfort, M., Skennerton, C. T., Hugenholtz, P., and Tyson, G. W. (2015). CheckM: assessing the quality of microbial genomes recovered from isolates, single cells, and metagenomes. *Genome Res.* 25, 1043–1055. doi: 10.1101/gr.186072.114

Smits, S. A., Leach, J., Sonnenburg, E. D., Gonzalez, C. G., Lichtman, J. S., Reid, G., et al. (2017). Seasonal cycling in the gut microbiome of the Hadza hunter-gatherers of Tanzania. *Science* 357, 802–806. doi: 10.1126/science.aan4834

Solianik, R., Židonienė, K., Eimantas, N., and Brazaitis, M. (2023). Prolonged fasting outperforms short-term fasting in terms of glucose tolerance and insulin release: a randomised controlled trial. *Br. J. Nutr.* 1:10. doi: 10.1017/S0007114523000557

Sommer, F., Ståhlman, M., Ilkayeva, O., Arnemo, J. M., Kindberg, J., Josefsson, J., et al. (2016). The gut microbiota modulates energy metabolism in the hibernating brown bear *Ursus arctos*. *Cell Rep.* 14, 1655–1661. doi: 10.1016/j.celrep.2016.01.026

Takami, H., Taniguchi, T., Moriya, Y., Kuwahara, T., Kanehisa, M., and Goto, S. (2012). Evaluation method for the potential functionome harbored in the genome and metagenome. *BMC Genomics* 13:699. doi: 10.1186/1471-2164-13-699

Tang, L., Li, L., Bu, L., Guo, S., He, Y., Liu, L., et al. (2021). Bigu-style fasting affects metabolic health by modulating taurine, glucose, and cholesterol homeostasis in healthy Young adults. *J. Nutr.* 151, 2175–2187. doi: 10.1093/jn/nxab123

Tang, D., Tang, Q., Huang, W., Zhang, Y., Tian, Y., and Fu, X. (2023). Fasting: from physiology to pathology. *Adv. Sci.* 10:e2204487. doi: 10.1002/advs.202204487

Tomasello, G., Mazzola, M., Leone, A., Sinagra, E., Zummo, G., Farina, F., et al. (2016). Nutrition, oxidative stress and intestinal dysbiosis: influence of diet on gut microbiota in inflammatory bowel diseases. *Biomed. Pap. Med. Fac. Univ. Palacky Olomouc Czech Repub.* 160, 461–466. doi: 10.5507/bp.2016.052

Tripolt, N. J., Hofer, S. J., Pferschy, P. N., Aziz, F., Durand, S., Aprahamian, F., et al. (2023). Glucose metabolism and Metabolomic changes in response to prolonged fasting in individuals with obesity, type 2 diabetes and non-obese people—a cohort trial. *Nutrients* 15:511. doi: 10.3390/nu15030511

Van de Guchte, M., Blottière, H. M., and Doré, J. (2018). Humans as holobionts: implications for prevention and therapy. *Microbiome* 6, 1–6. doi: 10.1186/s40168-018-0466-8

Van Zuuren, E. J., Fedorowicz, Z., Kuijpers, T., and Pijl, H. (2018). Effects of low-carbohydrate- compared with low-fat-diet interventions on metabolic control in people with type 2 diabetes: a systematic review including GRADE assessments. *Am. J. Clin. Nutr.* 108, 300–331. doi: 10.1093/ajcn/nqy096

Vieira-Silva, S., Falony, G., Darzi, Y., Lima-Mendez, G., Garcia Yunta, R., Okuda, S., et al. (2016). Species-function relationships shape ecological properties of the human gut microbiome. *Nat. Microbiol.* 1:16088. doi: 10.1038/nmicrobiol.2016.88

Von Schwartzenberg, R. J., Bisanz, J. E., Lyalina, S., Spanogiannopoulos, P., Ang, Q. Y., Cai, J., et al. (2021). Caloric restriction disrupts the microbiota and colonization resistance. *Nature* 595, 272–277. doi: 10.1038/s41586-021-03663-4

Walterson, A. M., and Stavrinides, J. (2015). Pantoea: insights into a highly versatile and diverse genus within the Enterobacteriaceae. *FEMS Microbiol. Rev.* 39, 968–984. doi: 10.1093/femsre/fuv027

Weng, M. L., Chen, W. K., Chen, X. Y., Lu, H., Sun, Z. R., Yu, Q., et al. (2020). Fasting inhibits aerobic glycolysis and proliferation in colorectal cancer via the Fdft1-mediated AKT/mTOR/HIF1alpha pathway suppression. *Nat. Commun.* 11:1869. doi: 10.1038/s41467-020-15795-8

Wilhelmi de Toledo, F., Buchinger, A., Burggrabe, H., Hölz, G., Kuhn, C., Lischka, E., et al. (2013). Fasting therapy-an expert panel update of the 2002 consensus guidelines. *Complement. Med. Res.* 20, 434–443. doi: 10.1159/000357602

Xu, J. Z., Yang, H. K., and Zhang, W. G. (2018). NADPH metabolism: a survey of its theoretical characteristics and manipulation strategies in amino acid biosynthesis. *Crit. Rev. Biotechnol.* 38, 1061–1076. doi: 10.1080/07388551.2018.1437387

Xue, J., Balamurugan, S., Li, D. W., Liu, Y. H., Zeng, H., Wang, L., et al. (2017). Glucose-6-phosphate dehydrogenase as a target for highly efficient fatty acid biosynthesis in microalgae by enhancing NADPH supply. *Metab. Eng.* 41, 212–221. doi: 10.1016/j.ymben.2017.04.008

Zhan, M., Kan, B., Dong, J., Xu, G., Han, R., and Ni, Y. (2019). Metabolic engineering of *Corynebacterium glutamicum* for improved L-arginine synthesis by enhancing NADPH supply. *J. Ind. Microbiol. Biotechnol.* 46, 45–54. doi: 10.1007/s10295-018-2103-8

Zheng, D., Liwinski, T., and Elinav, E. (2020). Interaction between microbiota and immunity in health and disease. *Cell Res.* 30, 492–506. doi: 10.1038/s41422-020-0332-7

Zou, S., Fang, L., and Lee, M.-H. (2018). Dysbiosis of gut microbiota in promoting the development of colorectal cancer. *Gastroenterol. Rep.* 6, 1–12. doi: 10.1093/gastro/gox031

frontiers | Frontiers in Microbiology

TYPE Original Research
PUBLISHED 03 November 2023
DOI 10.3389/fmicb.2023.1283453

OPEN ACCESS

EDITED BY
Naga Betrapally,
National Cancer Institute (NIH), United States

REVIEWED BY
Babu Roshan Padmanabhan,
University Hospitals Cleveland Medical Center, United States
Mian Adnan Kakakhel,
China Three Gorges University, China

*CORRESPONDENCE
Binghui Wang
✉ wangbh@kust.edu.cn
Xueshan Xia
✉ oliverxia2000@aliyun.com

RECEIVED 26 August 2023
ACCEPTED 06 October 2023
PUBLISHED 03 November 2023

CITATION
Shah T, Hou Y, Jiang J, Shah Z, Wang Y, Li Q, Xu X, Wang Y, Wang B and Xia X (2023) Comparative analysis of the intestinal microbiome in *Rattus norvegicus* from different geographies.
Front. Microbiol. 14:1283453.
doi: 10.3389/fmicb.2023.1283453

Comparative analysis of the intestinal microbiome in *Rattus norvegicus* from different geographies

Taif Shah[1], Yutong Hou[1], Jinyong Jiang[2], Zahir Shah[3], Yuhan Wang[4], Qian Li[1], Xiang Xu[2], Yixuan Wang[4], Binghui Wang[1]* and Xueshan Xia[1,5]*

[1]Faculty of Life Science and Technology, Kunming University of Science and Technology, Kunming, Yunnan, China, [2]Yunnan International Joint Laboratory of Vector Biology and Control & Yunnan Provincial Key Laboratory of Vector-Borne Diseases Control and Research of Yunnan Institute of Parasitic Diseases, Yunnan, China, [3]College of Veterinary Sciences, The University of Agriculture, Peshawar, Pakistan, [4]Research Institute of Forest Protection, Yunnan Academy of Forestry and Grassland, Kunming, Yunnan, China, [5]School of Public Health, Kunming Medical University, Kunming, Yunnan, China

Rat species *Rattus norvegicus*, also known as the brown street rat, is the most abundant mammal after humans in urban areas, where they co-exist with humans and domestic animals. The reservoir role of *R. norvegicus* of zoonotic pathogens in cities among rodent-borne diseases that could endanger the lives of humans and other mammals. Therefore, understanding the normal microbiome of *R. norvegicus* is crucial for understanding and preventing zoonotic pathogen transmission to humans and animals. We investigated the intestinal microbiome of free-living *R. norvegicus* collected from the Ruili, Nujiang, and Lianhe regions of Yunnan, China, using 16S rRNA gene sequence analysis. Proteobacteria, followed by Firmicutes, and Bacteroidetes were abundant in the intestines of *R. norvegicus*; however, bacterial compositions varied significantly between samples from different locations. Following a similar trend, Gammaproteobacteria, Bacilli, and Clostridia were among the top bacterial classes in most intestinal samples. The situation differed slightly for the Lianhe and Nujiang samples, although Phyla Bacteroidota and Spirochaetota were most prevalent. The Alpha diversity, Chao1, and Simpson indexes revealed microbial richness among the *R. norvegicus* samples. A slight variation was observed among the samples collected from Ruili, Nujiang, and Lianhe. At species levels, several opportunistic and zoonotic bacterial pathogens, including *Lactococcus garvieae*, *Uruburuella suis*, *Bartonella australis*, *Clostridium perfringens*, *Streptococcus azizii*, *Vibrio vulnificus*, etc., were revealed in the *R. norvegicus* intestines, implying the need for a regular survey to monitor and control rodent populations. In conclusion, we explored diverse microbial communities in *R. norvegicus* intestines captured from different regions. Further, we identified several opportunistic and potential bacterial pathogens, which still need to be tested for their underlying pathogenesis. The findings of our current study should be considered a warning to the health authorities to implement rat control and surveillance strategies globally.

KEYWORDS

***Rattus norvegicus*, Yunnan, intestines, microbiome, pathogens**

Introduction

Microbial communities, including archaea, bacteria, and fungi, coexist with the mammalian digestive tract, regulating host homeostasis, physiology, and immune function (Le Roy et al., 2019). Host-microbiome relationships are maintained throughout the host's lifetime and are thus important for our understanding of life. Hosts and microbiome associations can benefit from the association in various ways (Brahe et al., 2016). Perturbations to these relationships in humans and animals have resulted in changes in the microbial structures (Pickard et al., 2017) that further influence host functions, leading to dysbiosis and increased susceptibility to disorders, including obesity, inflammatory bowel disease, autoimmune disorders, etc. (Brahe et al., 2016; Larabi et al., 2020). This raises several concerns for wild animal conservation initiatives regarding how changes in the natural environment may influence intestinal microbiome community compositions. Little research has been conducted on the microbiome communities along the gastrointestinal tract of wild animals, particularly rodents (Anders et al., 2021). So far, no study has looked into the intestinal microbial community compositions of free-living *R. norvegicus* from the Ruili, Nujiang, and Lianhe regions of Yunnan Province, China.

Rodent models have become crucial in studying the gastrointestinal tract microbiome compositions, particularly in the intestines. Due to limitations in human research, the rat was the first mammalian species domesticated for scientific purposes. *R. norvegicus* is a social animal that is large enough to be easily grasped and is regarded as one of the best rodent pets due to its calm nature. So far, scientists have frequently used different rat models, including diseased or genetically altered models, to understand host–microbe interactions (Fritz et al., 2013). Obesity, chronic respiratory disease, and tumors are common in older *R. norvegicus*, but their biological system is similar to that of mice, making them ideal for microbiome research (Franklin and Ericsson, 2017). In addition, rats' physiological parameters are closely related to those of humans (Franklin and Ericsson, 2017). In contrast, mice have different living environments and immune systems from those observed in humans (Fritz et al., 2013).

Microbiome community compositions vary from individual to individual. The phyla Firmicutes and Bacteroidetes dominate the gut region of captive and wild rodents, accounting for approximately >80% of their abundance (Bensch et al., 2023). In contrast, the human microbiota mainly comprises Actinobacteria, Proteobacteria, Verrucomicrobia, Fusobacteria, Tenericutes, Spirochetes, etc. (Hillman et al., 2017). A comparative microbiome analysis in the guts of humans, mice, rats, and non-human primates revealed that the beta diversity of humans and non-human primates showed high similarity (Nagpal et al., 2018). In contrast, Prevotella and Clostridiales were abundant in rats, while Clostridiales and Oscillospira were abundant in mice. Furthermore, humans had more Bacteroides, Ruminococcaceae, and Clostridiales than rats and mice (Nagpal et al., 2018). A similar study reports obvious differences in the intestinal microbiome of two different Kunming mouse models, HFA-KM and HFA-C57BL/6J (Zhang et al., 2014). Genus *Clostridium* dominated HFA-KM, whereas *Blautia* dominated HFA-C57BL/6J, implying that genotype differences may shape rodent intestinal microflora diversity. Another study revealed abundant Bacteroidetes, Firmicutes, and Proteobacteria along the digestive tract of healthy rats, whereas *Lactobacillus* and *Alistipes* primarily dominated the gut regions. It has also been shown that the upper digestive tract segments had more bacterial diversity than the lower. At the same time, large intestines had diverse and richer microbial profiles; however, microbial diversity in the gastric and duodenum is comparable (Li et al., 2017).

According to the available literature, wild rats are reservoirs for various pathogens that can severely threaten public health due to their close interactions with humans and domestic animals (Easterbrook et al., 2007; Shah et al., 2023). *R. norvegicus* is prevalent in urban environments and threatens public health through its destructive behavior. In a very recent study, we reported several opportunistic and pathogenic bacteria, including *Bordetella*, *Clostridium*, *Corynebacterium*, *Empedobacter*, *Helicobacter*, *Limosilactobacillus*, *Macrococcus*, *Neisseria zaloph*, *Porphyromonas*, *Pseudomonas*, *Rahnella*, *Ralstonia*, *Rhodococcus*, *Rickettsiella*, *Streptococcus*, etc. in the free-living urban *R. norvegicus* (Shah et al., 2023). *R. norvegicus* is also reported to be a host for a large number of blood-sucking ectoparasites, such as Polyplax lice, fleas, fur mites, mesostigmatid mites, etc., in the West Indies (Thille et al., 2019). Another study investigated free-living *R. norvegicus* for the presence of zoonotic viruses, parasites, and bacteria in Maryland, United States (Easterbrook et al., 2007). They detected antibodies in *R. norvegicus* against the *hepatitis E virus*, the *Seoul virus*, *Bartonella elizabethae*, *Leptospira interrogans*, and *Rickettsia typhi*. Due to the presence of many zoonotic pathogens, *R. norvegicus* may seriously threaten the lives of humans and other mammals.

Laboratory rats have been helpful animal models for studying intestinal microbiota for the last decade. However, more researchers have focused on studying microbial community profiles in the gut samples of laboratory rats (Fritz et al., 2013; Nagpal et al., 2018) and fewer on wild rats (Gurbanov et al., 2022). Therefore, we designed this study to investigate microbial community compositions in the intestines of this important rodent. We report diverse microbial profiles in the intestines of *R. norvegicus* collected from three different regions of Yunnan Province. We also revealed several opportunistic and zoonotic pathogens, highlighting the medical importance of these free-living rodents for public health.

Materials and methods

Study site selection and sampling

We captured 10 free-living adult rat species (*R. norvegicus*) from three different municipalities (i.e., two from Ruili, four from Nujiang, and four from Lianhe) in Yunnan Province using mousetrap cages between January 2023 and July 2023. The animal trap locations included dense vegetation near residential areas and farmland. All the trapped *R. norvegicus* were anesthetized with cervical dislocation, after which they were dissected. A total of 10 intestinal samples (one from each animal) were collected aseptically and stored at −80°C until further processing.

The experiment was conducted according to the guidelines for using laboratory animals, Faculty of Life Science and Technology, Kunming University of Science and Technology, Kunming, Yunnan Province of China (protocol no. 16048).

Microbial DNA extraction

Genomic DNA was extracted from each intestinal tissue sample using the TIANamp Bacterial DNA Mini Kit (TIANGEN Bio., Co., Ltd., Beijing, China) following company protocol. Briefly, the tissue samples in the Eppendorf tubes were centrifuged, and the supernatant was discarded. The pellet was dissolved in GA buffer (200 μL), Proteinase K enzyme (20 μL), and 95% ethanol (220 μL), followed by brief centrifugation. After centrifugation, the solution was transferred to the column tube and then centrifuged. The effluent was discarded, and PW buffer (600 μL) was added to the column tube for centrifugation. The column tube was placed back onto a 1.5 mL Eppendorf tube before adding TE buffer (100 μL). Centrifugation was performed after holding the tube for two mins at room temperature, and DNA-containing effluent was collected. The extracted DNA integrity and purity were determined using agarose gel and a NanoDrop Spectrophotometer (Thermo Fisher, United States).

Bacterial 16S rDNA gene sequencing and analysis

The Illumina 16S rDNA gene amplicon was used to prepare the sequencing samples. The variable V3-V4 region of the 16S rDNA gene was amplified for microbial profiling with PCR-specific primers: 338F (5′ACTCCTACGGGAGGCAGCA3′) and 806R (5′GGACTACHVGGGTWTCTAAT3′). The PCR reaction contained a 25 μL mixture, including 10 μL of PCR Mix (Thermo Fisher, United States), 2 μL of template gDNA, 0.5 μL of each forward and reverse primer, and 12 μL of ddH_2O. The conditions set for the PCR machine were: initial denaturation at 95°C for 3 min, followed by 32 cycles of denaturation at 94°C for 15 s, annealing at 55°C for 30 s, extension at 72°C for 30 s, and final extension at 72°C for 7 min. The PCR-amplified product was confirmed on a 1.5% agarose gel (470 bp) and purified using the QIAquick Gel Extraction Kit (Qiagen, Germany). Sequencing libraries were made with the Illumina Library Prep Kit (Illumina, United States), following company protocol, and their quality was evaluated with a Qubit 2.0 Fluorometer (Thermo Fisher, United States) before sequencing on an Illumina HiSeq 2000 sequencer. According to the Illumina quality filtering protocol, low-quality reads containing adaptors, primer dimers, reads shorter than 230 bp, and sequences with low-quality scores (≤ Q20 score) were removed. Qualified reads were trimmed using the Illumina pipeline version 2.6, following company guidelines.

The quality reads in each sample were clustered using the Mothur algorithm and the UPARSE drive5 pipeline, and OTUs were defined by clustering 97% of the identity sequences. We screened each OTU representative sequence for microbial taxonomy annotation. The Silva database 138 and the Mothur algorithm were used to annotate and differentiate Ruili, Nujiang, and Lianhe data at various taxonomic levels. We summarized the OTU relative abundance after normalizing it using the sample with the fewest sequences by standard sequence number. After normalizing, we examined the relative abundance of alpha and beta diversity indexes.

Evaluating the alpha diversity index

In the phyloseq package, the Alpha Diversity Index (Chao1, ACE, and Simpson) was calculated using cumulative sum-scaling normalized values. ANOVA and post-hoc Tukey tests were used for alpha diversity indices to determine significant differences between groups. The cleaned data was converted into relative abundance. Good coverage was chosen to describe the depth of the sequencing.

Evaluating the beta diversity index

We used the beta diversity index to compare the similarity of various samples. The beta diversity was calculated based on the two methods (weighted and unweighted UniFrac). Principal Component Analysis (PCA) and Principal Coordinate Analysis (PCoA) were used to reduce the original variable dimensions and to visualize complex, multi-dimensional data, apart from showing the relationships among microbial community structures. First, we calculated a distance matrix between samples using weighted or unweighted UniFrac methods, which were then transformed into orthogonal axes. PCoA demonstrated the highest variation factor, followed by the second, third, and so on. Then, Adonis analysis was performed to observe location-wise variations in the microbial structures. USEARCH software was used for significant difference analysis.

Statistical analysis

Analyses in this study are reported as the standard error of the mean (SEM), and differences in relative bacterial abundance between groups were examined using Mann–Whitney sum rank tests. Data with a p-value ($p < 0.05$) were considered statistically significant.

Results

Bacterial composition in the *Rattus norvegicus* intestines

All the intestinal tissues collected from the free-living urban *R. norvegicus* were subjected to microbial profile analyses. A total of 1,229,810 raw reads (pair-end sequences) were generated for all the samples, with an average of 122,981 reads for each sample. After sequence assembly and quality control filtering (removing primer dimers and ambiguous and low-quality reads), 1,106,641 cleaned tags were obtained with an average Q30 score of >93%, which were used for subsequent analysis (Supplementary Table S1). The Chao1 diversity index curves for all the intestinal tissues reached a certain sequencing level, whereas the Simpson curves failed to level off (Supplementary Figure S1). These findings suggest that the abundance community structure has already been captured, though more microbial phenotypes can be explored with deeper sequencing in the future.

Clean tags from each *R. norvegicus* intestinal tissue were combined to generate an Operational Taxonomic Unit (OTU) for identifying differential microbial taxonomy levels. Clustering at 97% identity

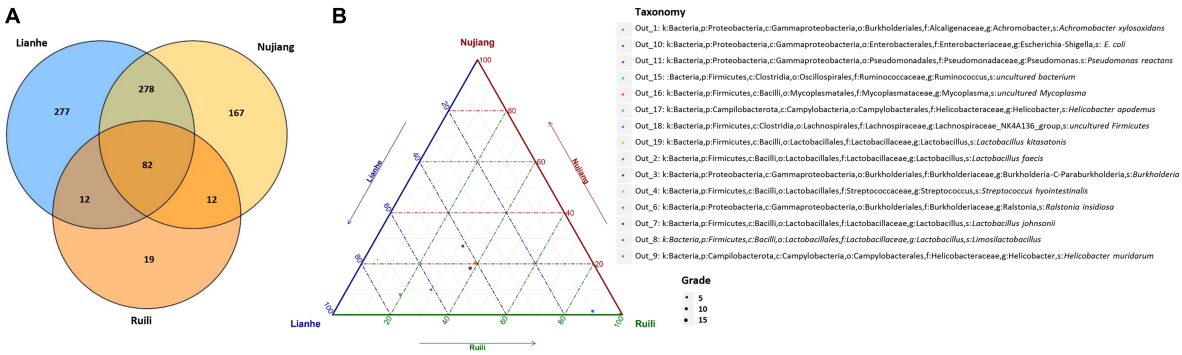

FIGURE 1
Clean tags from each *R. norvegicus* specimen were combined to generate OTUs for identifying differential microbial taxonomy levels. **(A)** The Venn diagram shows that among the 847 distinct OTUs, 19 were exclusive to the Ruili, 167 Nujiang, and 277 Lianhe groups, while 82 OTUs were shared. All these OTUs were then annotated to identify differential microbial taxonomy levels. **(B)** The top 15 OUTs abundance with different taxonomy levels.

produced 847 distinct OTUs, of which 19 OTUs were exclusive to the Ruili, 167 Nujiang, and 277 Lianhe areas, while 82 OTUs were shared among them (Figure 1A). All these OTUs were then annotated into 104 families, 168 genera, and 17 phyla. OTUs deep analysis revealed medically important opportunistic and highly pathogenic bacteria, including *Acinetobacter bereziniae* (OTU_227), *Bartonella australis* (OTU_23), *Burkholderia singularis* (OTU_1403), *Citrobacter koseri* (OTU_63), *Clostridium perfringens* (OTU_469), *Streptococcus hyointestinalis* (OTU_4), *Rickettsiella agriotidis* (OTU_1119), *Corynebacterium camporealensis* (OTU_805), *Mycoplasma haemomuris* (OTU_1089), *Corynebacterium pseudotuberculosis* (OTU_489), *Enterobacter cancerogenus* (OTU_32), *Streptococcus azizii* (OTU_139), *Streptococcus caballi* (OTU_240), *Pseudomonas mendocina* (OTU_269), *Vibrio vulnificus* (OTU_121), *Enterococcus faecalis* (OTU_189), *Escherichia coli* (OTU_10 and OTU_1436), etc., implying that rodents and their associated pathogens should be monitored regularly public health safety. However, the underlying pathogenic mechanisms of these bacteria need further investigation. The details about the OTU analysis and bacterial abundance at different taxonomic levels are shown in Figure 1B and Supplementary Table S2.

According to the relative abundance, Class Gammaproteobacteria, Bacilli, and Clostridia were the highest among the three groups (Figure 2). Following a similar trend, Gammaproteobacteria, Bacilli, and Clostridia were among the top bacterial classes in most samples (Supplementary Figure S2). The situation differed slightly for the Lianhe and Nujiang samples, although Phyla Bacteroidota and Spirochaetota were most prevalent. In contrast, the phylum Campilobacterota and Fusobacteriota were abundant in samples from Ruili. Overall, the highest number of phyla was reported in the Nujiang group (Figure 3A). Rhizobiales, Campylobacterales, and Mycoplasmatales were the richest order among the samples from Ruili, whereas Lactobacillales, Actinomycetales, and Desulfovibrionales were abundant in the Nujiang group (Figure 3B). Family-level classification showed Rhizobiaceae, Helicobacteraceae, and Mycoplasmataceae had the highest abundance in the Ruili group, whereas Lactobacillaceae, Bacteroidaceae, Bacillaceae, etc., were richest in the Nujiang group. Overall, the highest level of family abundance was reported in the Lianhe group and the lowest in the Ruili group (Figure 3C). Moreover, Genus *Helicobacter* and

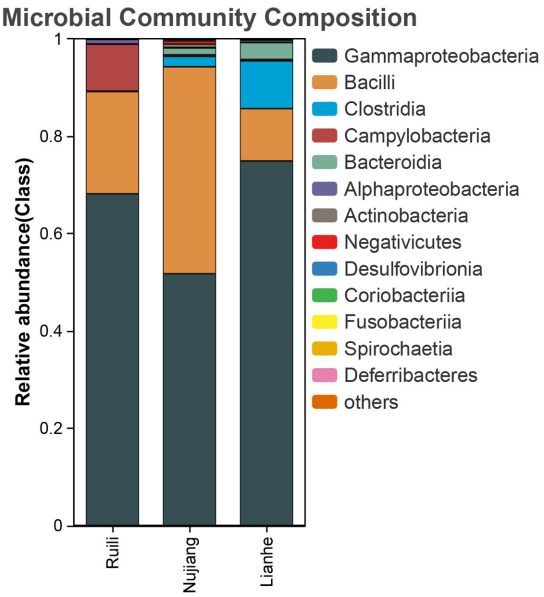

FIGURE 2
The top 14 relative abundance microbial class in the intestines of *R. norvegicus* collected from Ruili, Nujiang, and Lianhe regions.

Mycoplasma were abundant in the Ruili group, whereas *Lactobacillus*, *Bacillus*, *Escherichia-Shigella*, etc., were richest in the Nujiang group (Figure 3D). The detailed values of the various taxonomic groups among the three groups are shown in Supplementary Table S3.

Bacterial diversity analysis

The Alpha Diversity Index determined microbial diversity and richness differences among the *R. norvegicus* intestinal samples from various locations. The Chao1 and Simpson indexes revealed the richness of the bacterial community among the three groups. Both the Chao1 and Simpson indexes changed similarly across the three groups. Compared to Ruili, samples from Nujiang and Lianhe were the highest,

10.3389/fmicb.2023.1283453

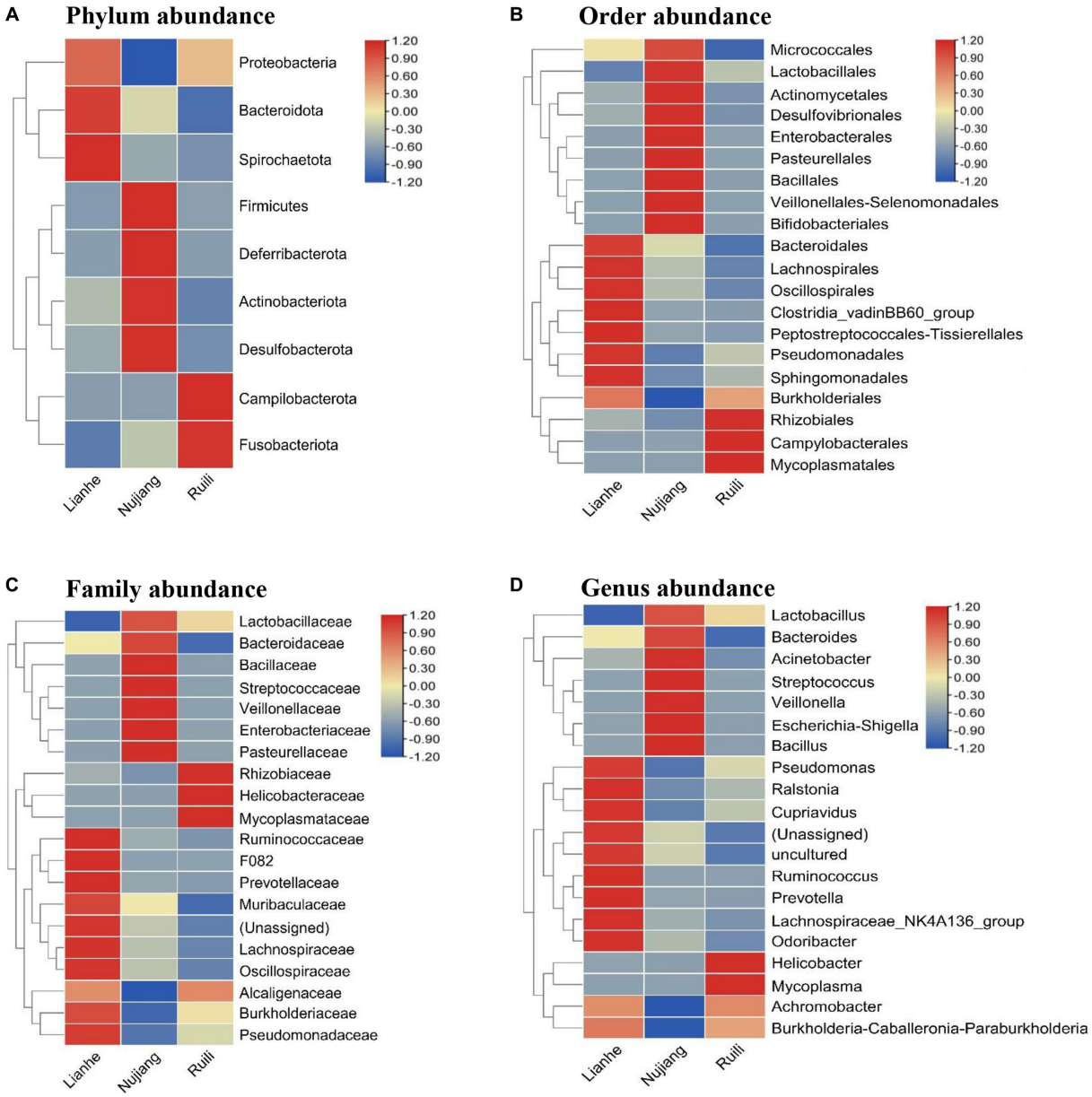

FIGURE 3
The relative microbial abundance at different taxonomic levels in the intestines of *R. norvegicus* collected from Lianhe, Nujiang and Ruili regions. **(A)** Microbial abundance at phylum level, **(B)** Microbial abundance at order level, **(C)** Microbial abundance at family level, and **(D)** Microbial abundance at genus level.

with significantly more bacterial abundance (Figure 4A). The Simpson index revealed the highest bacterial abundance in the Nujiang group, followed by Lianhe and Ruili (Figure 4B). Compared to the other eight samples, the Chao1 diversity index revealed the highest bacterial richness in the sample (J04) from the Lianhe region. In contrast, samples H03 and P04 from Nujiang had almost no difference in bacterial richness (Supplementary Figure S3A). Moreover, the Simpson diversity index revealed bacterial community richness and evenness among samples from different demographics. Samples from Lianhe (L04) and Nujiang (N02) showed the highest bacterial richness (Supplementary Figure S3B). In contrast, sample J04 from the Lianhe had less bacterial richness compared to others in the same group.

Variation in the bacterial communities

Two distance metrics (Bray-Curtis and Euclidean) estimate microbial variation among different intestinal samples. A significant difference was observed in the *R. norvegicus* intestinal microbial communities among the three locations. PCoA visualized variation among the intestinal microbial community at various study sites. Using the Bray-Curtis distance, two PCoA plots coordinate percentage variation, i.e., PCoA1 (46.2.8%) and PCoA2 (19.6%) among the intestinal samples (Figure 5A). A slight variation was observed between the samples from different regions. In addition, the Euclidean distance metric estimates two PCoA

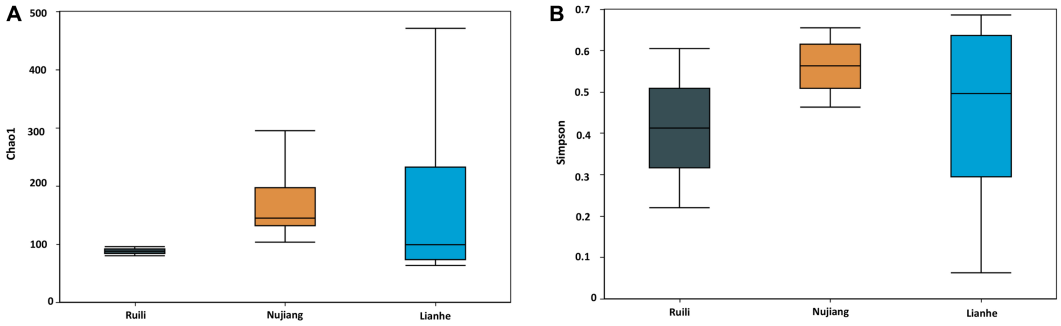

FIGURE 4
Chao 1 and Simpson indices represent the microbial abundance of different groups. **(A)** The Nujiang group had a significantly higher microbial species abundance than the Ruili and Lianhe. **(B)** The same pattern was observed for the Simpson indices, where Nujiang had higher bacterial richness and evenness compared to the other two groups.

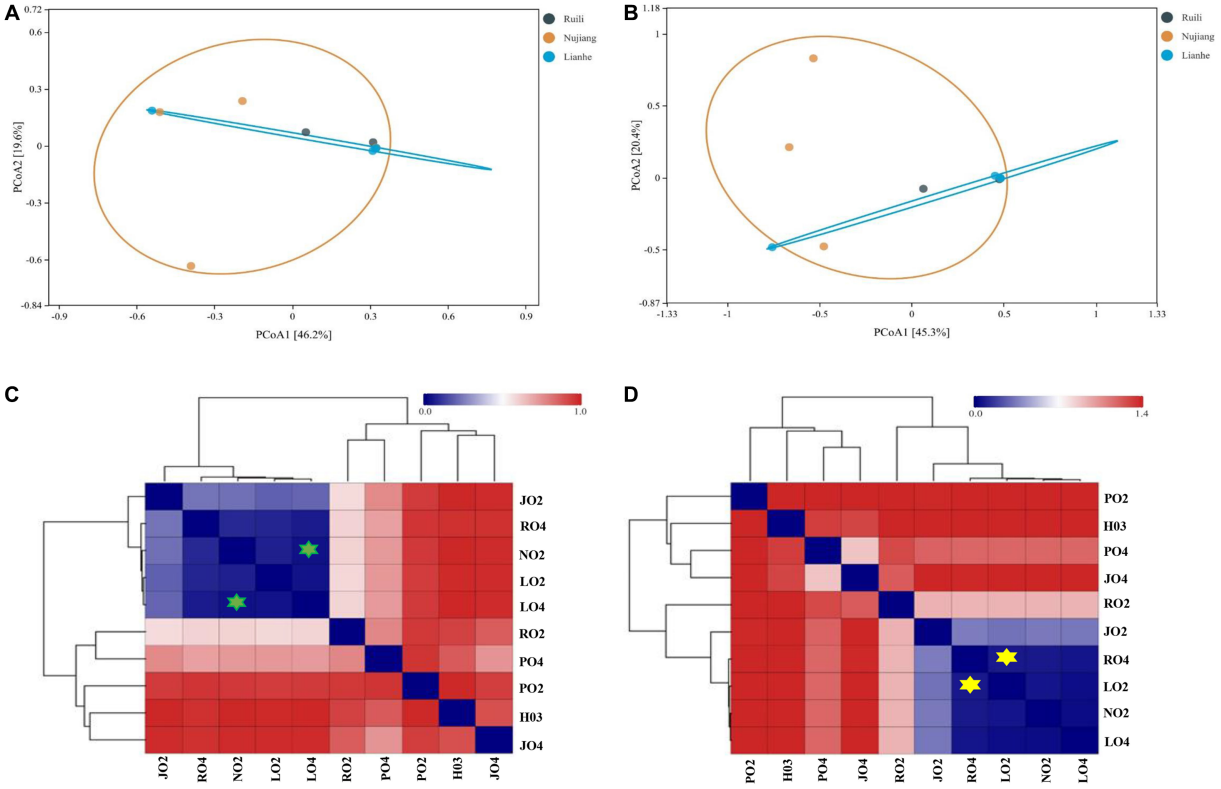

FIGURE 5
Principal Coordinate Analysis (PCoA) showing microbial differences in the intestines of *R. norvegicus* collected from Ruili, Nujiang, and Lianhe regions. **(A)** Microbial differences was determined using Bray Curtis distances matrix and **(B)** Euclidean distances matrix between samples from different locations. **(C)** Heatmap showing Bray Curtis distances between intestinal microbial communities **(D)** and Euclidean distances between *R. norvegicus* intestinal microbial communities.

plots for percentage variation: PCoA1 (45.3%) and PCoA2 (20.4%) among the intestinal samples (Figure 5B), implying that the variation may be attributed to differences in geographical locations. Heatmaps based on Bray-Curtis and Euclidean distances showed microbial variation among different intestinal samples. According to Bray-Curtis distance, the most similar lowest microbial difference was 0.0337, observed between samples N02 (Nujiang) and L04 (Lianhe), shown with green stars (Figure 5C), followed by 0.035 between L02 and L04 (samples from Lianhe), and 0.062 between L02 (Lianhe) and N02 (Nujiang), etc. (Supplementary Table S4). In addition, Euclidean distance showed similarity in the *R. norvegicus* intestinal microbial communities. The lowest difference (0.069) was observed between samples R04 (Ruili) and L02 (Lianhe), highlighted with yellow stars (Figure 5D), followed by R04 (Ruili) and N02 (Nujiang), suggesting that bacterial communities in these intestinal tissues were evolutionary similar. The detailed values of Euclidean distances are shown in Supplementary Table S5.

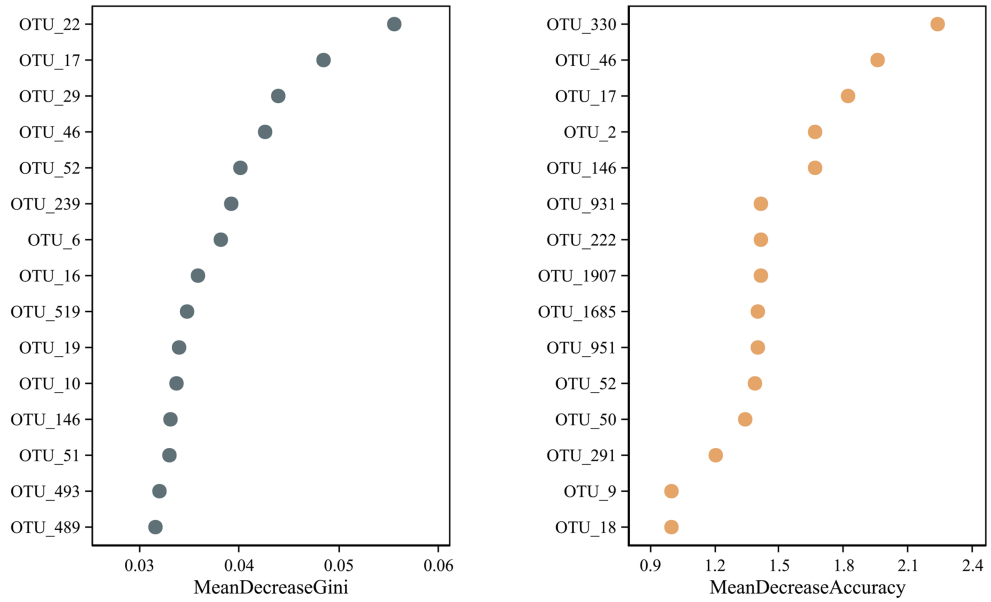

FIGURE 6
A random forest test identified fifteen potential OTU biomarkers in the intestines of *R. norvegicus*. The mean decrease in accuracy and the mean reduction in the Gini coefficient showed potential microbial OTU biomarkers in the *R. norvegicus* intestinal samples.

Identification of potential OTU biomarkers

A random forest test identified potential microbial OTU biomarkers in the *R. norvegicus* intestinal samples. A random forest model cross-validation curve revealed 15 important OTU biomarkers (Supplementary Table S6). The mean decrease in accuracy and mean reduction in the Gini coefficient showed some important OTU distributions (Figure 6), validating potential microbial biomarkers in the *R. norvegicus* intestinal samples.

Identification of potential bacterial pathogens

We screened and identified several opportunistic and potential bacterial pathogens in the intestines of *R. norvegicus* collected from the Ruili, Nujiang, and Lianhe regions. These pathogens were *Acinetobacter bereziniae*, associated with blood, urinary tract, and lung infections in humans. *Bartonella australis* was known to cause anemia syndrome and deaths in eastern grey kangaroos, whereas *Burkholderia singularis* causes cystic fibrosis in humans. *Citrobacter koseri* causes meningoencephalitis and multiple brain abscesses in humans. *Clostridium perfringens* is a famous anaerobic bacterial pathogen causing food poisoning, diarrhea, and gas gangrene in humans. Bacterial pathogens, *Corynebacterium camporealensis* and *Corynebacterium pseudotuberculosis,* are reportedly responsible for mastitis in sheep and necrotizing lymphadenitis in other animals. *Streptococcus azizii* and *Streptococcus caballi* cause meningoencephalitis, ventriculitis in mice, and laminitis in horses, respectively. *Pseudomonas mendocina* was associated with spinal infection in humans, whereas *Vibrio vulnificus* was linked with cholera in humans. *Enterococcus faecalis* and *E. coli* cause nosocomial infections and diarrhea in humans (Table 1).

Discussion

Captive *R. norvegicus* is a preferred model in biomedical research for studying physiological parameters, behavior, and human diseases (Smith et al., 2019). The first *R. norvegicus* genomic sequence was published in 2004 (Gibbs et al., 2004) and yielded insights into mammalian evolution. It was the third sequenced genome after the human and the mouse. However, the rat intestinal microbiome has not been thoroughly studied, and our understanding of the microbial spatial structure remains limited. According to the authors, no previous study has investigated microbial community compositions and potential bacterial pathogens in the intestines of *R. norvegicus* collected from different regions of Yunnan Province. Therefore, we used high-throughput 16S rRNA gene sequencing to explore the intestinal microbial diversity of free-living *R. norvegicus*.

Our findings show that the intestinal microbiome of free-living urban *R. norvegicus* from the Ruili, Nujiang, and Lianhe regions was dominated by the phyla Proteobacteria and Firmicutes. The alpha and beta diversity compositions within groups differed significantly, which could be attributed to differences in sampling times, body sizes, and genders of the animals used. The gap between the Ruili, Nujiang, and Lianhe groups was more remarkable than within a group. Researchers have found significant differences in the bacterial compositions of *R. norvegicus* intestinal samples (He et al., 2020). In our study, Proteobacteria and Firmicutes were the two most abundant phyla in the intestines of *R. norvegicus*, which were consistent with previous findings from laboratory rats (Li et al., 2017), revealing a similar microbial profile in wild-type and laboratory rats; the phenomenon might be attributed to the host microbiota tropism. In addition, Lactobacillus constitutes a major component of the human intestines (Vemuri et al., 2018).

We found Lactobacillus abundance in the *R. norvegicus* intestines, consistent with the findings of He et al. (2020), who

TABLE 1 Shows some medically important bacterial pathogens with known pathogenesis.

Bacterial pathogens (this study)	Ruili	Nujiang	Lianhe	Disease descriptions	Reference database
Acinetobacter bereziniae	1.5	1.8	13.3	Opportunistic pathogens target blood, urinary tract, and lung in humans	BV-BRC
Bacillus thuringiensis	0.5	481	1.5	Opportunistic pathogen of animals (other than insects) causing necrosis and pulmonary infections	VFDB
Bartonella australis	729.5	0.8	0.5	Anemia syndrome and deaths of eastern grey kangaroos	BV-BRC
Burkholderia singularis	0	0	0.5	Cause meningoencephalitis and cystic fibrosis in humans	BV-BRC
Citrobacter koseri	301.5	41.5	2.8	Meningoencephalitis, multiple brain abscesses in humans	BV-BRC
Clostridium perfringens	2.5	6	4.5	Food poisoning, diarrhea, and gas gangrene in humans	VFDB
Corynebacterium camporealensis	3	0	0	Associated with mastitis in sheep	BV-BRC
Corynebacterium pseudotuberculosis	0	7.3	0	Necrotizing lymphadenitis in animals	VFDB
Desulfovibrio fairfieldensis	0	0	1.3	Damage intestinal epithelial barrier and activate intrinsic inflammation in humans	BV-BRC
Enterococcus faecalis	45	19.2	26.5	Nosocomial infection in humans	VFDB
Escherichia coli	60	16456.8	225.3	Cause diarrhea in humans	VFDB
Mycoplasma haemomuris	3.5	0	0	Cause anemia in rats and mice	BV-BRC
Pseudomonas mendocina	0	0.5	10.5	Cause spinal infection in humans	VFDB
Streptococcus azizii	4.5	15	30.8	Meningoencephalitis and ventriculitis in mice	BV-BRC
Streptococcus caballi	0	22.8	0	Associated with laminitis in horses	BV-BRC
Vibrio vulnificus	0	42.8	0	Intestinal disease (cholera) in humans	VFDB

The digits in the regional columns (i.e., Ruili, Nujiang, and Lianhe) represent the relative abundance of bacterial pathogens. VFDB: Virulence Factors of Pathogenic Bacteria Database (http://www.mgc.ac.cn/VFs/search_VFs.htm). BV-BRC: Bacterial and Viral Bioinformatics Resource Center (https://www.bv-brc.org/view/Bacteria/2)/EIsource.

report abundant Lactobacillus in human guts, implying that *R. norvegicus* could be a possible experimental model for studying disease-related microbial alterations in humans (He et al., 2020). Firmicutes are the most common phylum in human digestive tracts, with Streptococcaceae being the most common family (Vemuri et al., 2018; Jiang et al., 2019). We discovered that the family Streptococcaceae was common within Firmicutes in *R. norvegicus* intestines, implying that the microbial composition of *R. norvegicus* and humans is strikingly similar. We found that the family Streptococcaceae was common within the phylum Firmicutes in the intestines, suggesting a remarkable similarity between *R. norvegicus* and the human microbiome structures.

R. norvegicus is a commensal synanthropic pest mammal species that lives primarily in forests and feeds on invertebrates. The rapid increase in human populations and industrialization have resulted in significant reductions in *R. norvegicus* natural habitats. As a result, this mammal is transforming into a commensal rodent, increasing opportunities for human-animal interaction and potential pathogen transmission to humans and other domestic mammals. *R. norvegicus* lives and feeds closer to humans, which may be a source of infectious diseases through cross-species transmission.

Our study annotated more sequences for notarizing, opportunistic, and highly pathogenic bacteria, particularly *S. azizii*, *S. ferus*, *S. caballi*, *Peptostreptococcus anaerobius*, *S. hyointestinalis*, *Peptostreptococcus anaerobius*, etc., in the *R. norvegicus* intestines. Therefore, effective disease prevention and rodent control measures should be taken at the animal-human interface. A better surveillance system is advised to further aid in the early detection of disease in humans and other domestic animals. The anaerobic spore-forming bacterium *Clostridium perfringens*, which was discovered in the guts of *R. norvegicus*, has been linked to acute gastrointestinal problems, necrotizing enterocolitis, and myonecrosis in humans (Yao and Annamaraju, 2023). Another *Clostridium celatum* isolated from human feces has been known to cause severe human infections (Agergaard et al., 2016). *Lactococcus lactis* subsp. hordniae identified in our study was previously involved in serious diseases such as endocarditis, peritonitis, and intra-abdominal infections in humans (Lahlou et al., 2023). A bacterial species, *Lactococcus garvieae*, appears to correlate with seasonal aquaculture outbreaks in humans (Wang et al., 2007). *Mycoplasma haemomuris* is a gram-negative extracellular obligate parasite of rat erythrocytes. This bacterial infection has been shown to affect tumor kinetics, reticuloendothelial function, erythrocyte shelf life, interferon production, and host response to viral and protozoal infections (Otto et al., 2015). We identified two genus *Escherichia-Shigella* in the *R. norvegicus* intestines, reportedly responsible for human gastrointestinal disorders (Belotserkovsky and Sansonetti, 2018). The commensal species *Neisseria subflava* identified in our current study is a rare cause of invasive diseases like meningitis, endocarditis, bacteremia, pericarditis, and septic arthritis in humans (Uwamino et al., 2017). *S. azizii* (associated with meningoencephalitis in newborn weanling C57BL/6 mice) was

named in honor of American microbiologist Aziz, who provided many years of his life supporting Memorial Sloan Kettering Cancer Center in New York, United States (Braden et al., 2015). *Corynebacterium* species are facultative intracellular bacilli that can cause pneumonia and lower respiratory tract infections (Marques da Silva et al., 2021). The *Corynebacterium pseudotuberculosis* reported in this study is known for causing caseous lymphadenitis in ruminants, mastitis in dairy cattle, lymphangitis in horses, and edema in buffaloes (Marques da Silva et al., 2021). These findings indicate that *R. norvegicus* may transmit potential infectious pathogens to humans and other mammals via contaminated food and water. A study found a high prevalence of Bartonella in the blood of *R. norvegicus*, indicating that these rodents may transmit infectious diseases, particularly Bartonellosis and rat-bite fever, to humans and domestic animals (Hsieh et al., 2010). We identified *Bartonella australis* in the *R. norvegicus* intestines, indicating that Bartonella may pass from the rodent via excrement. In Guangdong Province, China, in 2019, a patient who had been bitten by a wild rat one week prior to the onset of rat-bite fever (caused by *Streptobacillus moniliformis*) symptoms (Mai et al., 2019). We also identified the same bacterial species, *Streptobacillus moniliformis*, in the *R. norvegicus* intestines, indicating a risk of transmitting the same pathogen to humans in light of the possibility that rat-bite fever could be transmitted by *R. norvegicus*, suggesting strict disease prevention strategies regarding pathogen transmission (Mai et al., 2019).

Our current study has several limitations. The first limitation of this study was that we did not identify the age and gender of the free-living urban rat species *R. norvegicus*, even though age and gender may affect microbial community structures in the intestines of these important rodents. Second, the sample size in our current study was small, so more samples are needed to investigate the diverse microbial community compositions in each segment of the digestive tract. Third, we did not examine how season, age, gender, diet, etc., affect microbiome profiles; thus, larger sample sizes in future studies should confirm our findings.

Conclusion

In conclusion, we reported the intestinal microbial compositions of free-living *R. norvegicus*. We also revealed pathogenic bacteria in the intestinal samples of *R. norvegicus*, raising the possibility of these important rodents being exposed to humans and animals. Although intestinal samples cannot represent the entire microbiome of the digestive tract, future research must ensure sampling from every segment of the digestive tract to explore deep microbial profiles and their role in gut dysbiosis and disease progression.

Data availability statement

The datasets presented in this study can be found in online repositories. The names of the repository/repositories and accession number(s) can be found below: NCBI – SRP463903.

Ethics statement

The animal study was approved by the experiment was comconducted according to the guidelines for the use of laboratory animals, Faculty of Life Science and Technology, Kunming University of Science and Technology, Yunnan, China (protocol no. 16048). The study was conducted in accordance with the local legislation and institutional requirements.

Author contributions

TS: Conceptualization, Writing – original draft, Writing – review & editing. YH: Writing – original draft. JJ: Writing – original draft. ZS: Writing – original draft. YuW: Writing – original draft. QL: Writing – original draft. XiX: Writing – original draft. YiW: Writing – original draft. BW: Conceptualization, Writing – original draft. XuX: Writing – original draft, Conceptualization, Funding acquisition, Supervision, Writing – review & editing.

Funding

The author(s) declare financial support was received for the research, authorship, and/or publication of this article. This study was supported by Yunnan Key R&D Program (grant no. 202103AQ100001), Yunnan Major Scientific and Technological Projects (grant no. 202202AG050013), Yunnan Province Basic Research Program Projects (grant no. 202101AS070028), and Active Monitoring and Early Warning of Major Terrestrial Wildlife Diseases in Yunnan Province and Construction of a Primary Laboratory (grant no. 2022GF218Y-04).

Conflict of interest

The authors declare that the research was conducted in the absence of any commercial or financial relationships that could be construed as a potential conflict of interest.

Publisher's note

Supplementary material

The Supplementary material for this article can be found online at: https://www.frontiersin.org/articles/10.3389/fmicb.2023.1283453/full#supplementary-material

References

Agergaard, C. N., Hoegh, S. V., Holt, H. M., and Justesen, U. S. (2016). Two serious cases of infection with *Clostridium celatum* after 40 years in hiding? *J. Clin. Microbiol.* 54, 236–238. doi: 10.1128/jcm.01938-15

Anders, J. L., Moustafa, M. A. M., Mohamed, W. M. A., Hayakawa, T., Nakao, R., and Koizumi, I. (2021). Comparing the gut microbiome along the gastrointestinal tract of three sympatric species of wild rodents. *Sci. Rep.* 11:19929. doi: 10.1038/s41598-021-99379-6

Belotserkovsky, I., and Sansonetti, P. J. (2018). Shigella and Enteroinvasive *Escherichia Coli*. *Curr. Top. Microbiol. Immunol.* 416, 1–26. doi: 10.1007/82_2018_104

Bensch, H. M., Tolf, C., Waldenström, J., Lundin, D., and Zöttl, M. (2023). Bacteroidetes to Firmicutes: captivity changes the gut microbiota composition and diversity in a social subterranean rodent. *Anim. Microbiome* 5:9. doi: 10.1186/s42523-023-00231-1

Braden, G. C., Arbona, R. R., Lepherd, M., Monette, S., Toma, A., Fox, J. G., et al. (2015). A novel α-hemolytic Streptococcus species (Streptococcus azizii sp. nov.) associated with meningoencephalitis in Naïve weanling C57BL/6 mice. *Comp. Med.* 65, 186–195.

Brahe, L. K., Astrup, A., and Larsen, L. H. (2016). Can we prevent obesity-related metabolic diseases by dietary modulation of the gut microbiota? *Adv. Nutr.* 7, 90–101. doi: 10.3945/an.115.010587

Easterbrook, J. D., Kaplan, J. B., Vanasco, N. B., Reeves, W. K., Purcell, R. H., Kosoy, M. Y., et al. (2007). A survey of zoonotic pathogens carried by Norway rats in Baltimore, Maryland, USA. *Epidemiol. Infect.* 135, 1192–1199. doi: 10.1017/s0950268806007746

Franklin, C. L., and Ericsson, A. C. (2017). Microbiota and reproducibility of rodent models. *Lab. Anim. (NY)* 46, 114–122. doi: 10.1038/laban.1222

Fritz, J. V., Desai, M. S., Shah, P., Schneider, J. G., and Wilmes, P. (2013). From meta-omics to causality: experimental models for human microbiome research. *Microbiome* 1:14. doi: 10.1186/2049-2618-1-14

Gibbs, R. A., Weinstock, G. M., Metzker, M. L., Muzny, D. M., Sodergren, E. J., Scherer, S., et al. (2004). Genome sequence of the Brown Norway rat yields insights into mammalian evolution. *Nature* 428, 493–521. doi: 10.1038/nature02426

Gurbanov, R., Kabaoğlu, U., and Yağcı, T. (2022). Metagenomic analysis of intestinal microbiota in wild rats living in urban and rural habitats. *Folia Microbiol. (Praha)* 67, 469–477. doi: 10.1007/s12223-022-00951-y

He, W. Q., Xiong, Y. Q., Ge, J., Chen, Y. X., Chen, X. J., Zhong, X. S., et al. (2020). Composition of gut and oropharynx bacterial communities in Rattus norvegicus and *Suncus murinus* in China. *BMC Vet. Res.* 16:413. doi: 10.1186/s12917-020-02619-6

Hillman, E. T., Lu, H., Yao, T., and Nakatsu, C. H. (2017). Microbial ecology along the gastrointestinal tract. *Microbes Environ.* 32, 300–313. doi: 10.1264/jsme2.ME17017

Hsieh, J. W., Tung, K. C., Chen, W. C., Lin, J. W., Chien, L. J., Hsu, Y. M., et al. (2010). Epidemiology of Bartonella infection in rodents and shrews in Taiwan. *Zoonoses Public Health* 57, 439–446. doi: 10.1111/j.1863-2378.2009.01234.x

Jiang, Q., Zhou, X., Cheng, L., and Li, M. (2019). The adhesion and invasion mechanisms of streptococci. *Curr. Issues Mol. Biol.* 32, 521–560. doi: 10.21775/cimb.032.521

Lahlou, W., Bourial, A., Maaouni, T., Bensaad, A., Bensahi, I., Sabry, M., et al. (2023). *Lactococcus lactis* endocarditis and liver abscess in an immunocompetent patient: a case report and review of the literature. *J. Med. Case Rep.* 17:115. doi: 10.1186/s13256-022-03676-1

Larabi, A., Barnich, N., and Nguyen, H. T. T. (2020). New insights into the interplay between autophagy, gut microbiota and inflammatory responses in IBD. *Autophagy* 16, 38–51. doi: 10.1080/15548627.2019.1635384

Le Roy, T., Lécuyer, E., Chassaing, B., Rhimi, M., Lhomme, M., Boudebbouze, S., et al. (2019). The intestinal microbiota regulates host cholesterol homeostasis. *BMC Biol.* 17:94. doi: 10.1186/s12915-019-0715-8

Li, D., Chen, H., Mao, B., Yang, Q., Zhao, J., Gu, Z., et al. (2017). Microbial biogeography and Core microbiota of the rat digestive tract. *Sci. Rep.* 7:45840. doi: 10.1038/srep45840

Mai, W., Chen, S., Chen, D., Zhu, X., and Wang, R. (2019). One case of rat bite fever caused by *Streptobacillus moniliformis*. *China Trop. Med.* 19, 192–194.

Marques da Silva, W., Seyffert, N., Silva, A., and Azevedo, V. (2021). A journey through the *Corynebacterium pseudotuberculosis* proteome promotes insights into its functional genome. *PeerJ* 9:e12456. doi: 10.7717/peerj.12456

Nagpal, R., Wang, S., Solberg Woods, L. C., Seshie, O., Chung, S. T., Shively, C. A., et al. (2018). Comparative microbiome signatures and short-chain fatty acids in mouse, rat, non-human primate, and human feces. *Front. Microbiol.* 9:2897. doi: 10.3389/fmicb.2018.02897

Otto, G. M., Franklin, C. L., and Clifford, C. B. (2015). "Chapter 4 – biology and diseases of rats" in *Laboratory animal medicine (third edition)*. eds. J. G. Fox, L. C. Anderson, G. M. Otto, K. R. Pritchett-Corning and M. T. Whary (Boston: Academic Press), 151–207.

Pickard, J. M., Zeng, M. Y., Caruso, R., and Núñez, G. (2017). Gut microbiota: role in pathogen colonization, immune responses, and inflammatory disease. *Immunol. Rev.* 279, 70–89. doi: 10.1111/imr.12567

Shah, T., Wang, Y., Wang, Y., Li, Q., Zhou, J., Hou, Y., et al. (2023). A comparative analysis of the stomach, gut, and lung microbiomes in *Rattus norvegicus*. *Microorganisms* 11:2359. doi: 10.3390/microorganisms11092359

Smith, J. R., Bolton, E. R., and Dwinell, M. R. (2019). The rat: a model used in biomedical research. *Methods Mol. Biol.* 2018, 1–41. doi: 10.1007/978-1-4939-9581-3_1

Thille, K. N., Rametta, N. F., Fitzpatrick, D. M., Springer, C. C., Tiwari, K., Pinckney, R. D., et al. (2019). Ectoparasites of brown rats (*Rattus norvegicus*) in Grenada, West Indies. *Vet. World* 12, 1390–1394. doi: 10.14202/vetworld.2019.1390-1394

Uwamino, Y., Sugita, K., Iwasaki, E., Fujiwara, H., Nishimura, T., Hasegawa, N., et al. (2017). The first case report of acute cholangitis and bacteremia due to *Neisseria subflava*. *Intern. Med.* 56, 221–223. doi: 10.2169/internalmedicine.56.7482

Vemuri, R., Gundamaraju, R., Shastri, M. D., Shukla, S. D., Kalpurath, K., Ball, M., et al. (2018). Gut microbial changes, interactions, and their implications on human lifecycle: an ageing perspective. *Biomed. Res. Int.* 2018, 4178607–4178613. doi: 10.1155/2018/4178607

Wang, C. Y., Shie, H. S., Chen, S. C., Huang, J. P., Hsieh, I. C., Wen, M. S., et al. (2007). *Lactococcus garvieae* infections in humans: possible association with aquaculture outbreaks. *Int. J. Clin. Pract.* 61, 68–73. doi: 10.1111/j.1742-1241.2006.00855.x

Yao, P. Y., and Annamaraju, P. (2023). "*Clostridium perfringens* infection" in *StatPearls* (Treasure Island (FL)) companies. Disclosure: Pavan Annamaraju declares no relevant financial relationships with ineligible companies. Available at: https://europepmc.org/books/n/statpearls/article-87627/?extid=31082016&src=med (Accessed October 22, 2023).

Zhang, X., Zeng, B., Liu, Z., Liao, Z., Li, W., Wei, H., et al. (2014). Comparative diversity analysis of gut microbiota in two different human flora-associated mouse strains. *Curr. Microbiol.* 69, 365–373. doi: 10.1007/s00284-014-0592-x

frontiers | Frontiers in Microbiology

TYPE Original Research
PUBLISHED 06 December 2023
DOI 10.3389/fmicb.2023.1322910

OPEN ACCESS

EDITED BY
Naga Betrapally,
National Cancer Institute (NIH), United States

REVIEWED BY
Jayesh Jagannath Ahire,
Dr. Reddy's Laboratories (India), India
Ramesh Kothari,
Saurashtra University, India
Corina-Diana Ceapa,
National Autonomous University of Mexico, Mexico

*CORRESPONDENCE
Yan Zeng
✉ yanzeng@sicau.edu.cn
Xueqin Ni
✉ xueqinni@foxmail.com
Dong Zeng
✉ zend@sicau.edu.cn

†These authors have contributed equally to this work and share first authorship

RECEIVED 17 October 2023
ACCEPTED 13 November 2023
PUBLISHED 06 December 2023

CITATION
Chen B, Zhou Y, Duan L, Gong X, Liu X, Pan K, Zeng D, Ni X and Zeng Y (2023) Complete genome analysis of *Bacillus velezensis* TS5 and its potential as a probiotic strain in mice. *Front. Microbiol.* 14:1322910. doi: 10.3389/fmicb.2023.1322910

Complete genome analysis of *Bacillus velezensis* TS5 and its potential as a probiotic strain in mice

Benhao Chen[1,2†], Yi Zhou[1,2†], Lixiao Duan[1,2†], Xuemei Gong[1,2], Xingmei Liu[1,2], Kangcheng Pan[1,2], Dong Zeng[1,2*], Xueqin Ni[1,2*] and Yan Zeng[1,2*]

[1]Animal Microecology Institute, College of Veterinary Medicine, Sichuan Agricultural University, Chengdu, China, [2]Engineering Research Center of Southwest Animal Disease Prevention and Control Technology, Ministry of Education of the People's Republic of China, Chengdu, China

Introduction: In recent years, a large number of studies have shown that *Bacillus velezensis* has the potential as an animal feed additive, and its potential probiotic properties have been gradually explored.

Methods: In this study, Illumina NovaSeq PE150 and Oxford Nanopore ONT sequencing platforms were used to sequence the genome of *Bacillus velezensis* TS5, a fiber-degrading strain isolated from Tibetan sheep. To further investigate the potential of *B. velezensis* TS5 as a probiotic strain, in vivo experiments were conducted using 40 five-week-old male specific pathogen-free C57BL/6J mice. The mice were randomly divided into four groups: high fiber diet control group (H group), high fiber diet probiotics group (HT group), low fiber diet control group (L group), and low fiber diet probiotics group (LT group). The H and HT groups were fed high-fiber diet (30%), while the L and LT groups were fed low-fiber diet (5%). The total bacteria amount in the vegetative forms of *B. velezensis* TS5 per mouse in the HT and LT groups was 1×10^9 CFU per day, mice in the H and L groups were given the same volume of sterile physiological saline daily by gavage, and the experiment period lasted for 8 weeks.

Results: The complete genome sequencing results of *B. velezensis* TS5 showed that it contained 3,929,788 nucleotides with a GC content of 46.50%. The strain encoded 3,873 genes that partially related to stress resistance, adhesion, and antioxidants, as well as the production of secondary metabolites, digestive enzymes, and other beneficial nutrients. The genes of this bacterium were mainly involved in carbohydrate metabolism, amino acid metabolism, vitamin and cofactor metabolism, biological process, and molecular function, as revealed by KEGG and GO databases. The results of mouse tests showed that *B. velezensis* TS5 could improve intestinal digestive enzyme activity, liver antioxidant capacity, small intestine morphology, and cecum microbiota structure in mice.

Conclusion: These findings confirmed the probiotic effects of *B. velezensis* TS5 isolated from Tibetan sheep feces and provided the theoretical basis for the clinical application and development of new feed additives.

KEYWORDS

probiotic, *Bacillus velezensis* TS5, complete genome, cellulose, digestive enzyme activity

1 Introduction

The International Scientific Association for Probiotics and Prebiotics (ISAPP) defined probiotics as "live microorganisms that, when administered in adequate amounts, confer a health benefit on the host" (Hill et al., 2014). Probiotics are commonly used to improve host health and maintain the balance of intestinal flora. Commonly used bacterial probiotics are derived mainly from *Lactobacillus*, *Bifidobacterium*, and *Bacillus* (Vera-Santander et al., 2023). Among them, *Bacillus* probiotics have sporulation ability and are more suitable for processing, storage, and survival through the gastrointestinal tract (Lu et al., 2022). Many studies have reported that *Bacillus* can interact with the host at multiple levels, such as secreting antibacterial substances and a variety of digestive enzymes, improving the structure of intestinal flora, regulating immunity, etc., thus exerting its probiotic properties (Du et al., 2018; Hu et al., 2018; Zou et al., 2022; Iqbal et al., 2023). All of these properties and their long shelf life make *Bacillus* direct feeding microbials (DFM) strains and their endospores an ideal feed supplement (Bahaddad et al., 2023). Probiotics strains of *Bacillus* benefit the health of piglets and broilers and help reduce the misuse of direct antibiotics in feed (Luise et al., 2022). In addition, the research results by Bahaddad et al. (2023) also confirmed that *Bacillus* can be used as a direct feed microbial addition for monogastric animals.

Bacillus velezensis was first and identified in the river Velez in Málaga, southern Spain (Ruiz-García et al., 2005). This strain is easy to isolated and cultured, and it exists widely in nature, making it a potential probiotic candidate. Due to the absence of toxigenic potential and aminoglycoside production capacity, *Bacillus velezensis* was recommended for Qualified Presumption of Safety (QPS) status in 2020 by European Food Safety Authority (EFSA) (Koutsoumanis et al., 2020). Previous studies have reported the usefulness of *Bacillus velezensis* as a probiotic in the aquaculture (Zhang et al., 2019; Wu et al., 2021; Monzón-Atienza et al., 2022), and it has the potential to promote plant growth and inhibit plant pathogenic fungi (Tzipilevich et al., 2021; Dong et al., 2023; Thanh Tam et al., 2023). Khalid et al. (2021) reviewed the potential properties of *Bacillus velezensis* as a probiotic in the animal feed industry, which is expected to become a candidate probiotic in this industry. Complete genome sequence analysis can effectively identify potential characteristics of probiotics and enhance our understanding of the relationship between genotype and phenotype (Huang et al., 2022). It has been shown that the genomes of *Bacillus velezensis* from different sources, such as spontaneously fermented coconut water (Dhanya Raj et al., 2023), fermented kimchi (Heo et al., 2021), and soil (Pereira et al., 2019), have been well characterized, revealing the reasons for its probiotic properties. In addition, an increasing number of studies suggest that probiotics require animal functional experiments to verify their probiotic properties. Among these experiments, rodents such as mice (Cao et al., 2023), rats (Elkholy et al., 2023), and rabbits (Hou et al., 2023) are the most widely used in clinical practice.

The *Bacillus velezensis* TS5 isolated from Tibetan sheep feces is a potential probiotic strain with *in vitro* probiotic properties. This study aimed to analyze the complete genome sequencing information of this strain and evaluate its digestive promotion and antioxidant effects on mice, including its effects on growth performance, blood routine, small intestine morphology, antioxidant capacity, intestinal digestive enzyme activity, and cecum microbiota.

2 Materials and methods

2.1 Bacterial strains

The *Bacillus velezensis* TS5 strain was isolated from Tibetan sheep feces and provided by the Animal Microecology Research Center of Sichuan Agricultural University. The bacteria is stored in the Chinese Typical Culture Preservation Center (CCTCC NO: M2023345).

2.2 Complete genome sequencing and analysis of bacterial

The genomic DNA of *Bacillus velezensis* TS5 was extracted using the TIANamp Bacteria DNA kit (DP302). The quality and concentration of the extracted DNA were determined using 1% agarose gel electrophoresis and a nucleic acid quantizer. The second and third generations of complete genome sequencing for strain TS5 were conducted using the Illumina NovaSeq PE150 and Oxford Nanopore ONT sequencing platforms, respectively. Libraries were constructed from the samples and sequenced to obtain second-generation data. Quality control of the raw data was performed using FastQC (Patel and Jain, 2012). The third-generation single-molecule sequencing data was assembled using Unicycle and Flye software to obtain contig sequences. To correct the second-generation high-quality data for the third-generation contig results, pilon (Walker et al., 2014) software was used. Finally, the contigs were spliced to obtain a complete sequence.

To construct a phylogenetic tree of multiple site sequence fragments of isolated strains and standard strains, AutoMLST webserver and MEGA X software were used (Alanjary et al., 2019). Additionally, the GGDC (The Genome to Genome Distance Calculator) webserver (Meier-Kolthoff et al., 2022) and the Average Nucleotide Identity (ANI) calculator software (Yoon et al., 2017) on the EzBioCloud platform were utilized to analyze the DNA-DNA Hybridization (DDH) and ANI between strain TS5 and the standard strain. To predict gene islands in the genome of *Bacillus velezensis* TS5, Island Viewer 4 was utilized (Bertelli et al., 2017). Secondary metabolites analysis was performed on genomic data of isolated strains using anti SMASH 6.0 (Blin et al., 2021). Bacterial genomic information was annotated in the Gene Ontology (GO) (Conesa and Götz, 2008), Kyoto Encyclopedia of Genes and Genomes (KEGG) (Moriya et al., 2007), evolutionary genealogy of genes: Non-supervised Orthologous Groups (eggNOG) (Galperin et al., 2015), Swiss-Prot (Pedruzzi et al., 2015), and Carbohydrate-Active Enzymes Database (CAZy) (Lombard et al., 2014) using various tools. Mining candidate genes related to probiotic properties in the genome of *Bacillus velezensis* TS5 based on the above annotation results. The CGView software was then employed to draw a genome circle diagram (Stothard and Wishart, 2005), while the genome sequences were uploaded to the NCBI database with an accession number of CP125654.1.

The BLAST software was used to predict the presence of antibiotic resistance related genes in the genome of *Bacillus velezensis* TS5 in the Comprehensive Antibiotic Resistance Database (CARD) (McArthur et al., 2013). The BLAST alignment parameter *E*-value was set to $1e^{-6}$, and the consistency of amino acid sequences was above 45%. The ratio of sequence alignment length to sequence length was not less than 70%. The ResFinder 4.1 was used to identify the acquired antibiotic resistance genes (Verschuuren et al., 2022). The BLAST software was used to compare the protein sequences encoded by genes with the amino acid sequences (Set A) in the Virulence Factors of Pathogenic Bacteria (VFDB) database to predict the virulence factor related genes in the genome of *Bacillus velezensis* TS5 (Altschul et al., 1990; Chen et al., 2016). The BLAST alignment parameter *E*-value was set to $1e^{-5}$, and the consistency of amino acid sequences was over 60%. The ratio of the length of the sequence alignment to the length of the corresponding virulence factor related gene sequence was not less than 70%, and the gap length of the alignment was less than 10% of the sequence alignment length. The Virulence Finder (V2.0.3) was used to predict the presence of virulence genes in the genome of *Bacillus velezensis* TS5 (Joensen et al., 2014).

2.3 Animal experimental design

A total of 40 five-week-old male specific pathogen free C57BL/6J mice (weighing 18 ± 1 g) were purchased from Beijing Sibeifu Biotechnology Co., Ltd (China). The mice were randomly divided into four groups: high fiber diet control group (H group), high fiber diet probiotics group (HT group), low fiber diet control group (L group), and low fiber diet probiotics group (LT group), 10 mice per group. Mice in the H and HT groups were fed a high-fiber diet containing 30% cellulose, while those in the L and LT groups were fed a low-fiber diet containing 5% cellulose. Each mouse in the HT and LT groups received 0.2 mL vegetative form of *Bacillus velezensis* TS5 solution at a concentration of 5×10^9 CFU/mL per day, while those in the H and L groups were given 0.2 mL of sterile saline (0.9%). The experimental period was 8 weeks, during which the mental and eating state of the mice were observed every day, and the morbidity, mortality, and feed consumption were recorded. The body weight of each mouse was also recorded regularly every week. The mouse experiments were carried out in the Animal Microecology Research Center of Sichuan Agriculture University, and all experimental procedures adhered to the guidelines for the feeding and use of experimental animals approved by the Committee of Sichuan Agriculture University (SYXKchuan2019-187).

2.4 Blood routine testing

At the conclusion of the experimental, blood was collected from the mouse eyeball using tweezers and placed in an anticoagulation tube containing Ethylene Diamine Tetraacetie Acid (EDTA). The content of white blood cells, neutrophils, lymphocytes, monocyte, red blood cells, platelets, and hemoglobin content were immediately measured by a fully automated blood analyzer (BC-5000 Vet, Mindray medical international limited).

2.5 HE staining

The jejunum, ileum, liver, kidney and testes tissues of three mice in each group were washed with PBS (pH 7.4) solution and fixed with 4% Paraformaldehyde solution. The tissues were then dehydrated, embedded, sectioned, stained with hematoxylin and eosin, and sealed. The tissues sections were observed under a microscope and photographed. Villus height, crypt depth and villus/crypt (V/C) ratio of the small intestinal tissue were measured and analyzed.

2.6 Liver antioxidant testing

Mouse livers were subjected to liquid nitrogen freezing and stored at −80°C for subsequent analysis. The activity of liver catalase (CAT), dismutase (SOD), malondialdehyde (MDA), glutathione peroxidase (GSH Px), and total antioxidant capacity (T-AOC) were determined using ammonium molybdate (A007-1-1), water-soluble tetrazolium salt-1 (WST-1) (A001-3), colorimetry (A003-2), dithiodinitrobenzoic acid (A005-1), and 2,2′-Azino-bis(3-ethylbenzothiazoline-6-sulfonic acid) (ABTS) (A015-2-1) methods, respectively. The test kits were obtained from Nanjing Jiancheng Biotechnology Research Institute and the procedures followed the instructions provided by the kit.

2.7 Detection of intestinal digestive enzyme activity

Weighed 0.10 g of intestinal contents and added 0.9 mL of sterile normal saline (0.9%). Homogenized the mixture and centrifuged it at 8000 rpm for 10 min at 4°C. After collecting the supernatant, added 9 mL of sterile normal saline (0.9%) and mixed the resulting solution as crude enzyme solution.

The activities of β-glucosidase, endoglucanase, exoglucanase, filter paper enzyme, and xylanase were determined using 1% salicylic solution, 1% sodium carboxymethyl cellulose solution, 0.05 g absorbent cotton, 0.05 g starch free filter paper, and 1% xylan solution as enzyme reaction substrates [23], respectively. The activities of cellulase and hemicellulase were measured by incubating 0.5 mL of crude enzyme solution and a special substrate in citrate acid buffer (pH 4.8) at 50°C for 30 min (Budihal et al., 2016). The reducing sugar formed after incubation was estimated by the 3, 5-dinitrosalicylic acid method (Miller, 1959). The enzyme activity unit (U) represents the amount of enzyme that produce 1 μg of reducing sugar from a 1.0 g sample hydrolyzing the substrate for 1.0 min. The mass of reducing sugar of the measuring and blank control was recorded as A1 and A0, respectively. The activities of cellulase and hemicellulose were calculated using the following formula:

$$X = \frac{(A \times 1000 \times n)}{(V \times t)} \quad (1)$$

In formula (1), X represents the activity of cellulase and hemicellulose, expressed in U/g. A represents the yield of reducing sugar (A1-A0), expressed in mg. 1000 is the conversion factor, 1 mmol = 1000 μmol. "n" represents the dilution ratio of

the crude enzyme solution in mL. V represents the volume of crude enzyme solution in mL. "t" represents the reaction time expressed in minutes.

The determination of protease activity was performed using a modified method as described in reference (Ramkumar et al., 2018). Casein was dissolved in a phosphoric acid buffer solution at pH 7.5 to produce a 2% casein solution as the reaction substrate. A mixture of 1.0 mL crude enzyme solution and 1.0 mL casein solution was incubated in a water bath at 40°C for 20 min, followed by the addition of 2.0 mL of 0.4 mol/L trichloroacetic acid solution. The mixture was then centrifuged at 8000 rpm for 10 minutes at 4°C. After discarding the supernatant, 1.0 mL of the resulting supernatant was added to a new test tube. After adding 5.0 mL of 0.4 mol/L Na_2CO_3 and 1.0 mL of folin phenol reagent to the reaction mixture, the solution was cooled to room temperature after a water bath at 40°C for 20 min. A blank control tube containing 1.0 mL of crude enzyme solution was boiled for 10 minutes to inactivate it. Then, 2.0 mL of 0.4 mol/L trichloroacetic acid solution and 1.0 mL of casein solution were added to both the measuring tube and the blank control tube, following the same procedure as before. The absorbance of the resulting solution at the wavelength of 660 nm was measured using an enzymoscope, and a linear equation was used to calculate the L-tyrosine standard curve. The mass of L-tyrosine in the measuring and blank control tubes was recorded as B1 and B0, respectively. Under standard assay conditions, the amount of enzyme required to release 1 μmol of tyrosine per minute from hydrolyzing casein is considered as the unit of protease activity (U). The formula for calculating protease activity is as follows:

$$X = \frac{(B \times V \times n)}{(t \times V')} \quad (2)$$

In equation (2), X represents protease activity, expressed in U/g. B represents the stands for L-tyrosine production (B1-B0) in μg. V is the volume of the reaction solution in mL. "n" represents the dilution ratio of the crude enzyme solution. "t" is the reaction time, expressed in min. V' is the volume of the crude enzyme solution in mL.

The amylase activity was determined using the improved method as described in reference (Yao et al., 2019). To perform the assay, 1.0 mL of crude enzyme solution and 1.0 mL of a 2% soluble starch solution were combined and mixed. After a 30-min water bath at 60°C, 2.0 mL of DNS solution was added. The mixture was then subjected to a boiling water bath for 10 min and cooled to a constant volume of 25 mL with distilled water. A blank control tube containing 1.0 mL of crude enzyme solution was boiled for 10 min to inactivate the enzyme. The remaining steps were the same as those used in the determination tube. The absorbance of the 520 nm wavelength was measured using an enzyme standard instrument, and the results were used to calculate the maltose standard curve equation. The mass of maltose in the measuring and blank control tubes was recorded as C1 and C0, respectively. A unit of amylase activity (U) was defined as the amount of enzyme required to hydrolyze soluble starch per minute to release 1 μmol maltose under standard assay conditions. The activity of amylase was calculated using the following formula:

$$X = \frac{(C \times 1000 \times n)}{(V \times t \times 342)} \quad (3)$$

In equation (3), X represents the activity of amylase, measured in U/g. C represents the yield of Maltose (C1-C0), measured in mg. 1000 is the conversion factor, with 1 mmol equivalent to 1000 μmol. "n" represents the dilution ratio of the crude enzyme solution. V is the volume of crude enzyme solution, measured in mL. "t" represents the reaction time, measured in minutes. Finally, 342 is relative molecular weight of maltose.

The lipase activity was determined using an improved method as described in reference (Joseph et al., 2012). To perform the assay, 100 μL p-nitrophenol palmitate solution (10 mmol/L), 700 μL of Tris HCl (pH 8.8) buffer solution, and 200 μL of crude enzyme solution were added to a centrifuge tube in sequence and mixed. After a 20-min incubation at 37°C water bath, 1.0 mL of 0.5 mol/L trichloroacetic acid solution was added and mixed well before standing for 5 min to complete the reaction. Next, 3 mL of 0.5 mol/L NaOH solution was added to mix well. As a blank control, 200 μL of distilled water was used instead of the crude enzyme solution, and the remaining steps were the same as those used in the determination tube. The absorbance of the 410 nm wavelength was measured using an enzyme standard instrument, and the results were used to calculated the standard cure equation for p-Nitrophenol. The mass of p-Nitrophenol in the measuring and blank control tubes was recorded as D1and D0, respectively. A unit of lipase activity (U) was defined as the amount of enzyme required to release 1 mol of p-nitrophenol from the p-nitrophenol palmitate per minute under standard assay conditions. The activity of lipase was calculated using the following formula:

$$X = \frac{(D \times V \times n)}{(t \times V')} \quad (4)$$

In equation (4), X represents the lipase activity, measured in U/g. D represents the generation amount of p-nitrophenol (D1-D0), measured in μmol. V denotes the final volume of the reaction solution, measured in mL. "n" is the dilution ratio of the crude enzyme solution. "t" represents the reaction time, measured in min. V' represents the volume of crude enzyme solution, measured in mL.

2.8 16S rRNA gene sequencing of cecal contents

The cecal contents were analyzed for total bacterial DNA using the Magnetic Soil and Stool DNA Kit (DP712). The purity and concentration of the extracted DNA were determined by Agilent 5400 agarose gel electrophoresis. Primers 515F (5′-GTGCCAGCMGCCGCGGTAA-3′) and 806R (5′-GGACTACHVGGGTWTCTAAT-3′) were used to amplify V4 region of the 16S rRNA gene in the bacterial DNA. The amplified products were detected using 2% agarose gel electrophoresis. DNA sequencing library was constructed with DNA library preparation kit and quantified using Qubit and qPCR. Finally, the Novaseq6000 system from Beijing Novogene Bioinformatics Technology Co., Ltd., was used for sequencing.

The original sequencing data was first filtered, followed by OTU clustering/denoising and species classification analysis to generate a species abundance spectrum for OTU and other classification levels. The OTU species abundance spectrum after

data homogenization was then analyzed for OTU abundance and diversity index, as well as the statistical analysis of species annotation and community structure at different classification levels. R software's pheatmap package was used to draw a correlation heat map between cecal digestive enzyme activity and flora, in order to identify microbial flora or species with strong correlation with cecal digestive enzyme activity.

2.9 Statistical analysis

The results were presented as mean ± SD and were evaluated using a student's *t*-test. The statistical analysis showed that $P < 0.05$ was considered significant, while $P < 0.01$ was considered extremely significant. The phenotypic data was presented using GraphPad Prism (version 9.0, GraphPad Software Inc, San Diego, CA, USA).

3 Results

3.1 Complete genome information of *Bacillus velezensis* TS5

The genome of *Bacillus velezensis* TS5 is a circular chromosome with a total length of 3, 929, 788 bp and an average GC-content of 46.50% (Table 1). It contains 3873 protein-coding sequences, accounting for 88.59% of the total length, along with 82 ncRNAs, 86 tRNAs, and 27 rRNAs (Table 1). And its genome lacks CRISPRs. From inside to outside, the diagrammatic of the genome circle shows that the first circle represents scale, the second circle represents GC Skew, the third circle represents GC-content, the fourth and seventh circles represent COG to which each CDS belongs, the fifth and sixth circles represent the positions of CDS, tRNA, and rRNA on the genome (Figure 1A). Phylogenetic analysis based on multi-site sequence fragment analysis revealed strain TS5 and standard strain *Bacillus velezensis* SQR9 (NCBI login number: NZ_CP006890.1) to be part of the same branch (Figure 1B). The DDH and ANI homology indices were calculated between strain TS5 and 11 standard strains, and the results showed that strain TS5 had the highest homology with standard strain *Bacillus velezensis* SQR9 (DDH = 97.76%, ANI = 98.81%). These values meet the requirements for the same species of microorganisms, with a DDH greater than 95% and an ANI greater than 70%.

TABLE 1 Genome assembly and annotation of *Bacillus velezensis* TS5.

Types	Numbers	Genome percentage
Genome length	3929788 bp	/
Chromosome	1	/
Plasmid	0	/
GC-content	/	46.50%
Total number of protein coding genes	3873	/
The total length of protein coding genes	3481215 bp	88.59%
5S rRNA	9	0.03 %
16S rRNA	9	0.35 %
23S rRNA	9	0.67 %
tRNA	86	0.17 %
ncRNA	82	0.32 %
CRISPRs	0	/

The genome of *Bacillus velezensis* TS5 has been annotated with 136 genes in the carbohydrate active enzymes database (CAZy) (Figure 1C). The data revealed that 46 genes related to glycoside hydrolase (GHs) accounted for 33.82%, while 38 genes related to glycosyl transferases (GTs), represented 27.94%. Additionally, 27 genes related to carbohydrate esterases (CEs) made up 19.85%, and 15 genes related to carbohydrate binding modules (CBMs), accounted for 11.03%. Seven genes related to auxiliary activities (AAs) were found, representing 5.15%, while three genes related to polysaccharide lyases (PLs), accounted for 2.21%. These findings suggest that the metabolic activity of *Bacillus velezensis* TS5 is primarily focused on the breakdown of food substances.

Bacillus velezensis TS5 was found to contain 14 cellulase genes, including Beta-glucosidase, Exo-beta-1,4-glucanase, Glucan 1,3-beta-glucosidase, Glucan 1,4-beta-glucosidase, Exo-1,3-1,4-glucanase, Endo-1,3(4)-beta-glucanase, and Endoglucanase. These proteins encoded by cellulase genes belong the GH1, GH3, GH16, GH30, and GH51 families (Table 2). In addition, 43 hemicellulase genes were identified, such as Alpha-L-arabinofuranosidase, Xylan 1,4-beta-xylosidase, Alpha-galactosidase, Alpha-glucuronidase, Xylanase, Xyloglucanase, Beta-mannanase, Beta-1,3-xylanase, Beta-xylosidase, Endo-beta-1,6-galactanase, Endo-beta-1,4-galactanase, Alpha-1,6-mannanase, and Acetyl xylan esterase. The proteins encoded by these genes belong to the GH3, GH4, GH11, GH16, GH26, GH30, GH43, GH51, GH53, GH76, CE1, CE3, CE4, CE6, CE7, and CE12 families (Table 2). The results of the annotation suggest that *Bacillus velezensis* TS5 has the potential to degrade both cellulose and hemicellulose. This finding is significant for applications in biotechnology and industrial processes that require efficient degradation of plant cell wall polysaccharides.

In total, 2,163 KEGG annotation genes were identified in the genome of *Bacillus velezensis* TS5 (Figure 1D). These genes were assigned to six different signaling pathway levels. The distributing of these genes among various categories was as follows: 1333 genes related to metabolism, 290 genes related to environmental information processing, 207 genes related to genetic information processing, 160 genes related to cellular processes, 96 genes related to human diseases, and 67 genes related to biological system. Among the metabolism-related genes, the main annotations included carbohydrate metabolism (375), amino acid metabolism (285), metabolism of cofactors and vitamins (151), energy metabolism (129), lipid metabolism (85), nucleotide metabolism (84), metabolism of other amino acids (51), biosynthesis of other secondary metabolites (50), xenobiotics biodegradation and metabolism (47), metabolism of terpenoids and polyketides (44) and glycine biosynthesis and metabolism (32). These findings suggest that *Bacillus velezensis* TS5 has strong abilities in carbohydrates and proteins metabolism, which could be valuable for applications in various industries such as food production and biotechnology.

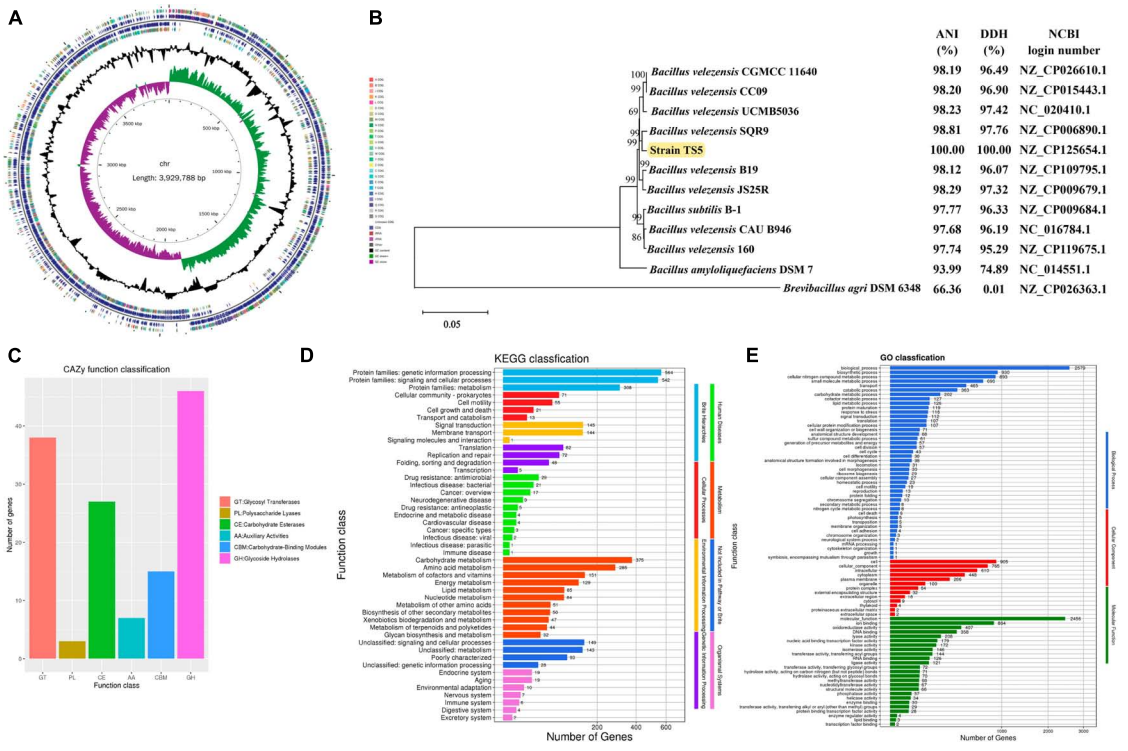

FIGURE 1
Genome analysis results of *Bacillus velezensis* TS5. **(A)** Genomic map of *B. velezensis* TS5. **(B)** Phylogenetic tree of *B. velezensis* TS5 based on genomic sequence. **(C)** Functional annotation of CAZy databases of *B. velezensis* TS5. **(D)** Functional annotation of KEGG databases of *B. velezensis* TS5. **(E)** Functional annotation of GO databases of *B. velezensis* TS5.

Bacillus velezensis TS5 was analyzed for functional prediction using the GO database, and the genic functions were divided into three categories: biological processes, cellular components, and molecular functions (Figure 1E). The majority of genes were assigned to various biological processes, including biosynthesis (2579), biosynthetic process (930), cellular nitrogen compound metabolic process (893), small molecule metabolic process (696), transport (465), catabolic process (363), carbohydrate metabolic process (202), cofactor metabolic process (127), lipid metabolic process (126), protein maturation (119), response to stress (116), signal transduction (112), translation (107), and cellular protein modification process (107). In addition, *Bacillus velezensis* TS5 was found to have a diverse range of cellular components and molecular functions. In terms of cellular components, most genes were associated with cell (905), cellular component (765), intracellular (610), cytoplasm (448), plasma membrane (286), and organelle (100). This suggests that *Bacillus velezensis* TS5 has the potential to perform various cellular processes within its cells. In terms of molecular function, the majority of genes were associated with molecular function (2456), ion binding (864), oxidoreductase activity (407), DNA binding (358), lyase activity (208), nucleic acid binding transcription factor activity (179), kinase activity (172), isomerase activity (146), transferase activity and transferring acyl groups (144), RNA binding (126), and ligase activity (121). These findings suggest that *Bacillus velezensis* TS5 has the ability to perform a wide range of molecular functions within its cells.

The genome of *Bacillus velezensis* TS5 was searched for multiple gene clusters related to the synthesis of antibacterial metabolites using the antiSMASH tool (Table 3). The identified gene clusters include Butirosin, Macroactin, Bacillaene, Difficidin, Bacilliactin, and Bacilysin, which have known antibacterial abilities. Additionally, Fengytin has been previously identified as having antifungal abilities, while Surfactin has various potentials such as antibacterial, antifungal, and antiviral properties. These findings suggest that *Bacillus velezensis* TS5 may have a diverse range of natural products with antimicrobial activities.

Based on gene annotation results, the genome of *Bacillus velezensis* TS5 identified numerous genes that function as probiotic markers, such as acid tolerance, bile salt tolerance, adhesion, antioxidant, and digestive enzyme (Supplementary Tables 1, 2). These probiotic genes are an important prerequisite for *Bacillus velezensis* TS5 to exert probiotic functions. In addition, compared with the CARD database, the results showed that the genome alignment of *Bacillus velezensis* TS5 identified 40 genes related to antibiotic resistance, 22 genes related to antibiotic target, and 3 genes related to antibiotic biosynthesis (Supplementary Table 3). However, there were no acquired resistance genes found in the genome of *Bacillus velezensis* TS5 by using the ResFinder tool to compare the resistance genes. Comparing the genome sequence of *Bacillus velezensis* TS5 with the VFDB database, only a few virulence genes related to motility, adhesion, stress survival, immune modulation, and nutritional/metabolic factor were detected in the genome data of *Bacillus velezensis* TS5 (Supplementary Table 4). However, there were no virulence genes found in the genome of *Bacillus velezensis* TS5 using the Virulence finder tool.

TABLE 2 Cellulase and hemicellulase genes in the genome of *Bacillus velezensis* TS5.

Classification	CAZy	Count	Enzyme classification	EC numbers	Gene ID[a]
Cellulose- related	GH1	3	Beta-glucosidase	EC 3.2.1.21	gene1168 gene1935 gene3634
	GH1	3	Exo-beta-1,4-glucanase	EC 3.2.1.74	gene1168 gene1935 gene3634
	GH3	1	Beta-glucosidase	EC 3.2.1.21	gene184
	GH3	1	Glucan 1,3-beta-glucosidase	EC 3.2.1.58	gene184
	GH3	1	Glucan 1,4-beta-glucosidase	EC 3.2.1.74	gene184
	GH3	1	Exo-1,3-1,4-glucanase	EC 3.2.1.-	gene184
	GH16	1	Endo-1,3(4)-beta-glucanase	EC 3.2.1.6	gene3677
	GH30	1	Beta-glucosidase	EC 3.2.1.21	gene1935
	GH51	2	Endoglucanase	EC 3.2.1.4	gene2588 gene2610
Hemicellulose-related	GH3	1	Alpha-L-arabinofuranosidase	EC 3.2.1.55	gene184
	GH3	1	Xylan 1,4-beta-xylosidase	EC 3.2.1.37	gene184
	GH4	4	Alpha-galactosidase	EC 3.2.1.22	gene2762 gene2097 gene791 gene3619
	GH4	4	Alpha-glucuronidase	EC 3.2.1.139	gene2097 gene2762 gene3619 gene791
	GH11	1	Xylanase	EC 3.2.1.8	gene3426
	GH16	1	Xyloglucanase	EC 3.2.1.151	gene3677
	GH26	1	Beta-mannanase	EC 3.2.1.78	gene3638
	GH26	1	Beta-1,3-xylanase	EC 3.2.1.32	gene3638
	GH30	1	Beta-xylosidase	EC 3.2.1.37	gene1935
	GH30	1	Endo-beta-1,6-galactanase	EC:3.2.1.164	gene1935
	GH43	1	Beta-xylosidase	EC 3.2.1.37	gene1812
	GH43	1	Beta-1,3-xylosidase	EC 3.2.1.-	gene1812
	GH43	1	Alpha-L-arabinofuranosidase	EC 3.2.1.55	gene1812
	GH43	1	Xylanase	EC 3.2.1.8	gene1812
	GH51	2	Alpha-L-arabinofuranosidase	EC 3.2.1.55	gene2588 gene2610
	GH53	1	Endo-beta-1,4-galactanase	EC 3.2.1.89	gene1162
	GH76	1	Alpha-1,6-mannanase	EC 3.2.1.101	gene3847
	CE1	6	Acetyl xylan esterase	EC 3.1.1.72	gene1064 gene1144 gene123 gene1931 gene2924 gene825
	CE3	2	Acetyl xylan esterase	EC 3.1.1.72	gene1987 gene406
	CE4	7	Acetyl xylan esterase	EC 3.1.1.72	gene770 gene932 gene1437 gene1641 gene165 gene2407 gene3657
	CE6	1	Acetyl xylan esterase	EC 3.1.1.72	gene2425
	CE7	1	Acetyl xylan esterase	EC 3.1.1.72	gene314
	CE12	2	Acetyl xylan esterase	EC 3.1.1.72	gene2406 gene2712

Gene ID[a]: In this study, a total of 3873 genes were obtained in the genome of *Bacillus velezensis* TS5. Each gene was assigned a unique identification number, ranged from "Gene 1" to "Gene 3873", according to its position within the genome sequence.

3.2 Results on the probiotic functions of *Bacillus velezensis* TS5 in mice

The results of the study showed that mice in the probiotic group (HT and LT groups) had slower weight growth compared to the control group (H and L groups), as depicted in Figures 2A, B. Additionally, mice on the high fiber diet (H and HT groups) consumed more feed than those on the low fiber diet (L and LT groups), while the probiotic group (HT and LT groups) had lower feed consumption than the control group (H and L groups) (Figure 2C). The organ index results for mice were presented in Figure 2D. The spleen index of the HT group was significantly higher than that of the H group ($P < 0.05$), but there was no significant difference in other organ indices (heart, liver, lungs, kidneys, and testes) ($P > 0.05$). There was also no significant difference in all organ indices (heart, liver, spleen, lungs, kidneys, and testes) between the LT group and L group ($P > 0.05$).

The blood routine results of the mice are presented in Table 4, and it can be seen that the control group (H and L groups)

TABLE 3 Secondary metabolites gene clusters determined by antiSMASH analysis in *Bacillus velezensis* TS5 genome.

Cluster	Type	Most similar known cluster	Length (bp)	Function	Similarity (%)
1	NRPS	Surfactin	63977	Multiple	82
2	PKS-like	Butirosin	41244	Antibacterial	7
3	Terpene	/	17408	/	/
4	Lanthipeptide class II	/	28888	/	/
5	TransAT-PKS	Macrolactin H	87835	Antibacterial	100
6	TransAT-PKS	Bacillaene	100565	Antibacterial	100
7	NRPS	Fengycin	134310	Antifungal	100
8	Terpene	/	21883	/	/
9	T3PKS	/	41100	/	/
10	TransAT-PKS	Difficidin	93792	Antibacterial	100
11	NRPS	Bacillibactin	51791	Antibacterial	100
12	other	Bacilysin	41418	Antibacterial	100

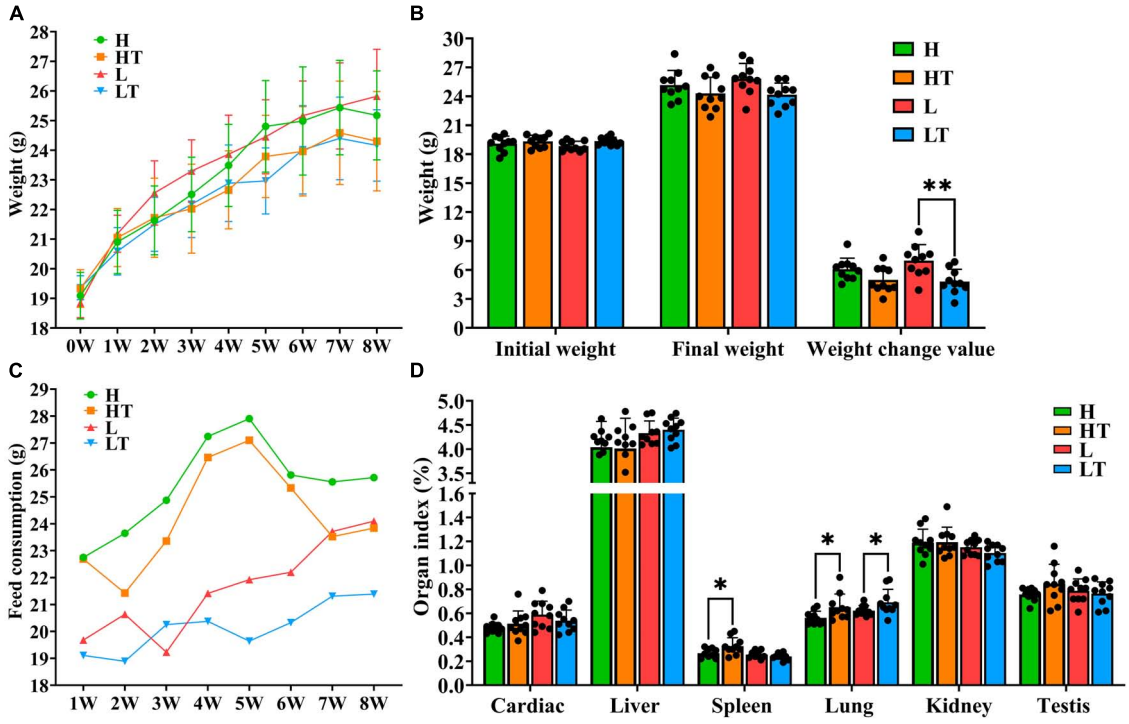

FIGURE 2
Mouse growth indicators. **(A,B)** Body weight changes in mice. **(C)** Consumption of mice feed. **(D)** Organ index of mice. "*" indicates a significant difference ($P < 0.05$), "**" indicates a significant difference ($P < 0.01$).

had normal blood routine indicators. In contrast, the hemoglobin content in the blood of the HT group mice was found to be significantly higher than that of the H group ($P < 0.05$), while the hemoglobin content in the blood of the LT group mice was also significantly higher than that of the L group ($P < 0.05$). The other blood routine indicators of the probiotic group (HT and LT groups) were within the normal range, with only slightly increases in hemoglobin content compared to the reference value. This increase may be attributed to a reduction in water consumption by the mice, leading to an increase in blood concentration.

The tissues of the jejunum and ileum from all mice were found to be intact, with clear structure and no obvious pathological changes (Figures 3A–H). The results of measuring the length of intestinal villi and the depth of crypts (Figures 3I, J) revealed that the height of jejunal and ileal villi in the HT group were significantly longer than that in the H group ($P < 0.0001$), while the depth of jejunal and ileal crypts in the LT group was significantly lower than that in the L group ($P < 0.05$). Additionally, the ratio of villi length to crypt depth in the HT group was significantly higher than that in the H group ($P < 0.01$), while it was also significantly higher in

TABLE 4 Blood routine results of mice.

Parameter	H group	HT group	L group	LT group	Reference value
Leukocyte (10^9/L)	6.08 ± 2.42	6.46 ± 2.21	7.01 ± 2.77	9.38 ± 1.92	0.80-10.60
Neutrophils (10^9/L)	0.74 ± 0.28^{b}	0.90 ± 0.26^{b}	0.89 ± 0.43^{b}	1.32 ± 0.27^{a}	0.23-3.60
Lymphocyte (10^9/L)	4.94 ± 1.99	5.21 ± 1.99	6.04 ± 2.31	8.20 ± 1.77	0.60-8.90
Monocyte (10^9/L)	0.21 ± 0.10	0.14 ± 0.05	0.18 ± 0.11	0.24 ± 0.11	0.04-1.40
Erythrocyte (10^{12}/L)	9.98 ± 1.38	10.65 ± 0.69	9.54 ± 1.11	10.36 ± 0.85	6.50-11.50
Hemoglobin (g/L)	162.75 ± 19.85^{ab}	174.33 ± 9.71^{a}	156.38 ± 18.81^{b}	170 ± 13.84^{a}	110-165
Platelet (10^9/L)	1017.22 ± 278.09	1151.91 ± 217.84	868.33 ± 350.26	1023 ± 133.88	400-1600

Peer data shows significant differences using different letters ($P < 0.05$), while the same or no letters indicate no significant differences ($P > 0.05$).

the LT group compared to the L group ($P < 0.01$). These findings suggest that *Bacillus velezensis* TS5 not only did not cause any damage to the jejunum and ileum of mice, but also improved their intestinal morphology by increasing villus length and decreasing crypt depth.

The pathological section results of mouse liver, kidney, and testes (Figure 4) revealed that in each group of mice, the central vein and portal area could be seen in the liver under microscope. The structure of lobules of liver was normal, with no swelling of necrosis of hepatocytes observed, and they were arranged in strips. No abnormality was found in the kidney, and the capillaries of the renal corpuscle in the renal cortex showed no abnormal changes. The morphology of the tubular wall cells was normal, and the boundaries of the renal vesicles were clear. The results of testicular sections indicated that the size of seminiferous tubules in each group of mice was essentially the same, and all levels of spermatogenic cells in the tubules were arranged neatly. Sperm were present in the tubules, and the interstitial tissue was normal without congestion or bleeding, indicating a normal tissue morphology and structure.

The results of the anti-oxidation analysis of mouse liver showed that the Catalase (CAT) activity in the probiotic groups (HT and LT groups) was higher than that in their respective control groups (L and LT groups), but the difference was not significant ($P > 0.05$) (Figure 5A). In addition, the activities of Superoxide dismutase (SOD) in the HT group were significantly higher than those in the H group ($P < 0.001$), and the activities of SOD in the LT group were significantly higher than those in the L group ($P < 0.05$) (Figure 5B). Furthermore, the activities of Glutathione peroxidase (GSH Px) in the LT group were significantly higher than those in the L group ($P < 0.01$) (Figure 5C). The content of Malondialdehyde (MDA) in the HT group was also lower than that in the H group ($P < 0.01$) (Figure 5D). Finally, the total antioxidant capacity (T-AOC) in the probiotic group (HT and LT groups) was significantly higher than that in their respective control groups (L and LT groups) ($P < 0.01$) (Figure 5E). These findings suggest that *Bacillus velezensis* TS5 enhances the antioxidant capacity of the mouse liver and has a positive impact on the immune system to a certain extent.

The results of the enzyme activity in mice cecum contents are shown in Figure 6. The activities of β glucosidase ($P < 0.0001$), endoglucanase ($P < 0.0001$), exoglucanase ($P < 0.05$), filter paper enzyme ($P < 0.001$), xylanase ($P < 0.0001$) and lipase activity ($P < 0.01$) in the HT group were significantly higher than those in the H group. Similarly, the activities of β glucosidase ($P < 0.0001$), filter paper enzyme ($P < 0.0001$), xylanase ($P < 0.05$), protease ($P < 0.05$) and lipase ($P < 0.05$) in the LT group were significantly higher than those in the L group. These findings indicated that *Bacillus velezensis* TS5 can enhance the activities of β glucosidase, filter paper enzyme, xylanase and lipase in the mice cecum, thereby facilitating intestinal nutrient digestion.

The results of the digestive enzyme activity in mice's whole intestinal contents are depicted in Figure 7. The cecum exhibited higher activities of cellulase activities (including β glucosidase, endoglucanase, exoglucanase, and filter paper enzyme activities) compared to other intestinal segments. Additionally, the colon had relatively high activities of xylanase and lipase. It is noteworthy that the activities of protease and amylase gradually decreased from the foregut to the hindgut, with the highest levels observed in the duodenum. These findings suggest that *Bacillus velezensis* TS5 has the ability to increase digestive enzyme activity throughout the entire intestinal tract of mice, particularly in the cecum, colon, and duodenum.

The Chao1 index results of Alpha diversity (Figure 8A) showed that the species richness of cecal bacteria in the probiotic group (HT and LT groups) was higher than that of the respective control groups (H and L groups), but the difference was not statistically significant ($P > 0.05$). The observed OTU index (Figure 8B) also indicated that the microbial diversity in the cecum of the HT group mice was higher than that of the H group mice ($P > 0.05$), while the microbial diversity in the cecum of the LT group mice was lower than that of the L group mice ($P > 0.05$). The principal coordinate analysis (PCoA) results of beta diversity showed (Figure 8C) that the samples of the high fiber diet group (H and HT groups) and the low fiber diet group (L and LT groups) were gathered together and separated from each other, indicating that there was a significant difference in species diversity between the two groups. The petal plot (Figure 8D) further revealed that there were 532 common

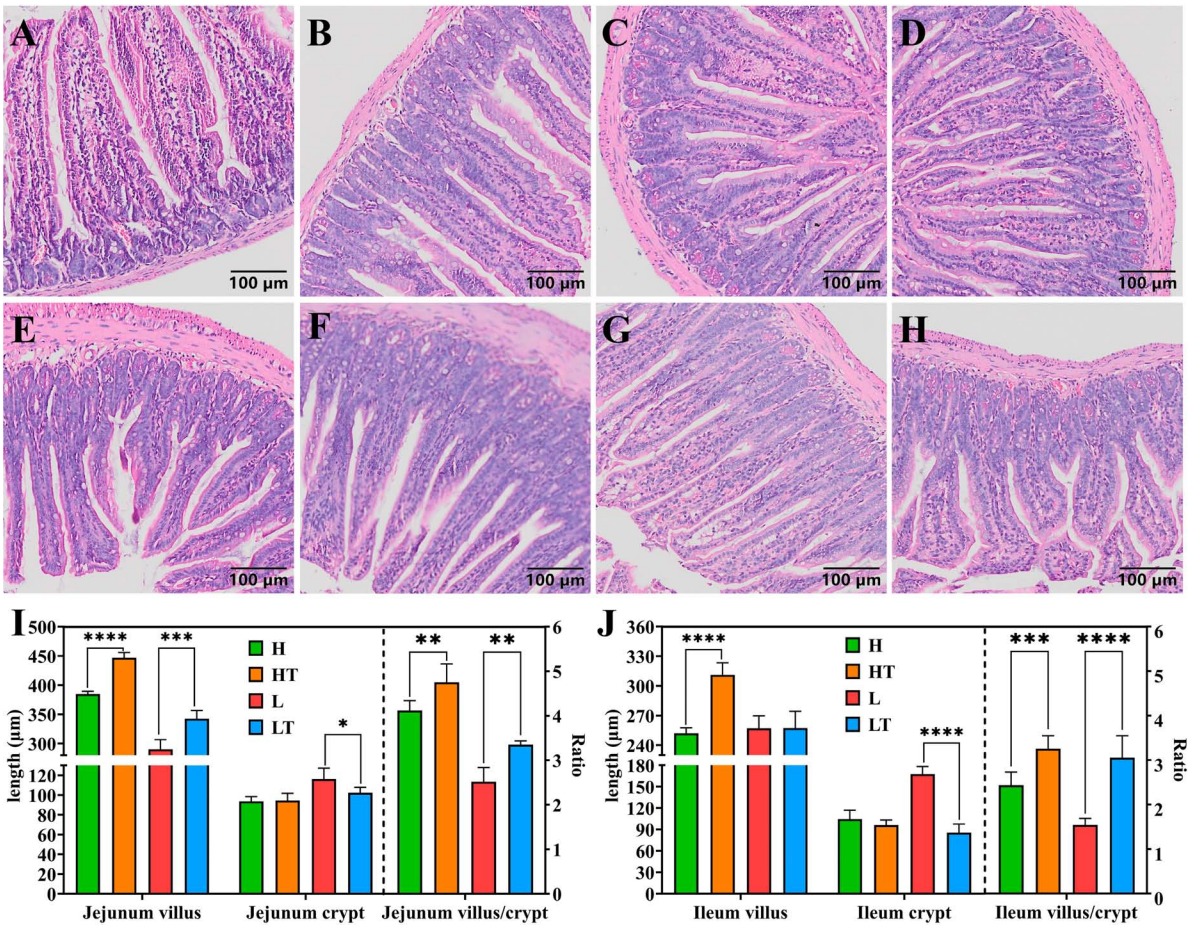

FIGURE 3
HE staining results of mice jejunum and ileum. **(A–D)** Pathological section results of the jejunum in groups H, HT, L, and LT (100×). **(E–H)** Pathological section results of the ileum in groups H, HT, L, and LT (100×). **(I)** The villus length, crypt depth and the ratio of villus length to crypt depth in jejunum. **(J)** The villus length, crypt depth and the ratio of villus length to crypt depth in ileum. "*" indicates a significant difference ($P < 0.05$), "**" indicates a significant difference ($P < 0.01$), "***" indicates a significant difference ($P < 0.001$), "****" indicates a significant difference ($P < 0.0001$).

OTUs in all four groups, with the number of unique OTUs in the cecal contents of mice in the H, HT, L, and LT groups being 407, 608, 293, and 574, respectively. Notably, the number of OTUs in the cecum of mice in the probiotic group (HT and LT groups) was higher than that of the corresponding control groups (H and L groups), indicating that *Bacillus velezensis* TS5 had a positive impact on increasing the diversity of the cecal microbiota in mice.

The results of the phylum level analysis (Figures 8E, F) revealed that Firmicutes, Bacteroidota, Verrucomicrobiota, Campilobacterota, and Desulfobacteria were the most dominant phyla in the cecum of all four groups of mice. Comparing the H group with the HT group, the abundance of Verrucomicrobiota, Campylobacter and Desulfobacteria was lower in the HT group, while the abundance of Firmicutes and Bacteroidota was higher. Conversely, when comparing the L group with the LT group, there was a decrease in the abundance of Firmicutes, Campylobacter, and Desulfobacteria, and an increase in the abundance of Bacteroidota and Verrucomicrobiota in the LT group. At the genus level (Figures 8G, H), the comparison between the H group and the HT group showed an increase in the abundance of *unspecified_Muribaaculaceae*, *Lactobacillus*, *Clostridia_UCG_014*, and *Muribaculum*, while a decrease in the abundance of *Helicobacter*, *Unspecified_Desulfovibrionacea, and Colidextribacter*. In contrast, when comparing the L group with the LT group, there was an increase in the abundance of *Unspecified_Muribaculaceae, Clostridia_UCG_014*, and *Muribaculum*, while a decreased in the abundance of *Helicobacter*, *Unspecified_ Desulfovibrionaceae, and Colidextribacter* in the LT group.

The correlation analysis between the phylum level microbiota and digestive enzyme activities was presented in Figure 8I. The results showed that the activities of exoglucanase (E3), filter paper enzyme (E4), protease (E6), and amylase (E7) were positively correlated with the abundances of Deferribactere, Campilobacterota, and Desulfobacterota, but negatively correlated with Bacteroidota. On the other hand, the activities of xylanase (E5) and lipase (E8) were positively correlated with Bacteroidota, and negatively correlated with the abundance of Deferribactere, Campilobacterota, and Desulfobacterota. The correlation analysis between the genus level microbiota and digestive enzyme activities was shown in Figure 8J. The results indicated that the activity of exoglucanase (E3) was positively correlated with the abundance of *Mucispirillum*, *Lachnoclostridium*, *Tuzzerella*,

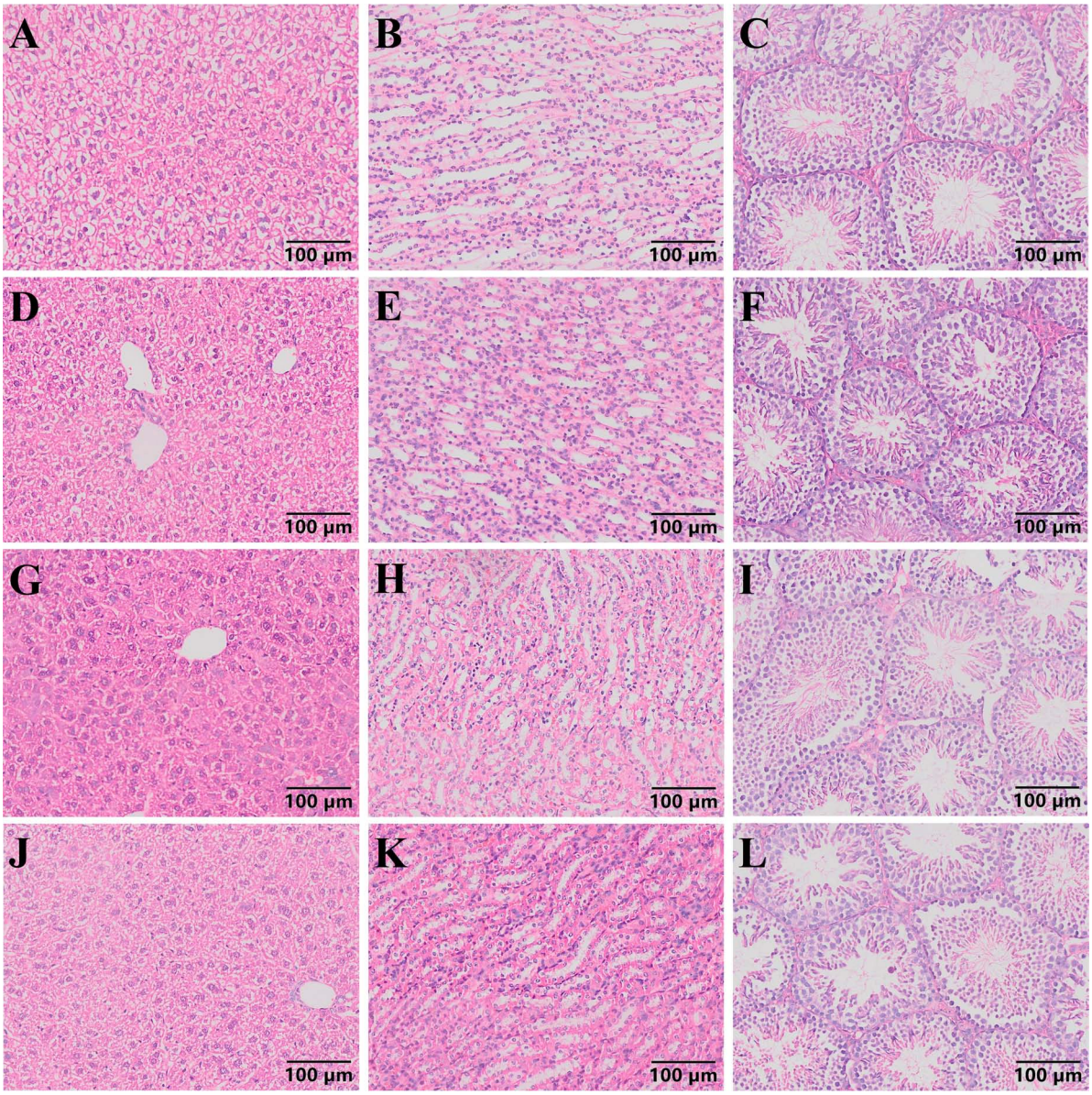

FIGURE 4
Pathological section results of mouse liver, kidney and testis (100 ×). **(A–C)** Pathological sections of liver, kidney, and testicles in group H mice. **(D–F)** Pathological sections of liver, kidney, and testicles in group HT mice. **(G–I)** Pathological sections of liver, kidney, and testicles in group L mice. **(J–L)** Pathological sections of liver, kidney, and testicles in group LT mice.

and *Bilophila*, while negatively correlated with the abundance of *Muribaculaceae*, *Bifidobacterium*, *Dubosiella*, *Gordonibacter*, and *Lachnospiraceae_UCG_009*. The activity of filter paper enzyme (E4) was positively correlated with the abundance of Bilophila, and significantly negatively correlated with the abundance of *Dubosiella* and *Lachnospiraceae_UCG_009*. The activity of protease (E6) was negatively correlated with *Dubosiella* and *Gordonibacter*. Additionally, the activity of xylanase (E5) was positively correlated with the abundance of *Muribaculaceae* and *Muribaculum*, while negatively correlated with the abundance of *Helicobacter* and *Acetatifactor*. Interestingly, the bacterial microbiota that were positively correlated with the activities of exoglucanase, filter paper enzyme, protease, and amylase were negatively correlated with the activities of xylanase and lipase, and vice versa, respectively.

4 Discussion

4.1 Complete genome sequencing analysis provides probiotic potential for *Bacillus velezensis* TS5

Genomic analysis can reveal the presence of genes encoding probiotic properties such as acid and bile tolerance, epithelial adhesion, and production of antibacterial substances (Kapse et al., 2019; Pereira et al., 2019; Soni et al., 2021). The genome sequence analysis of *Bacillus velezensis* TS5 also identified several stress-resistant genes including *DnaK*, *OppA*, *Eno*, *nhaC*, *nhaX*, and *nhaK* (**Supplementary Table 1**). These findings are consistent

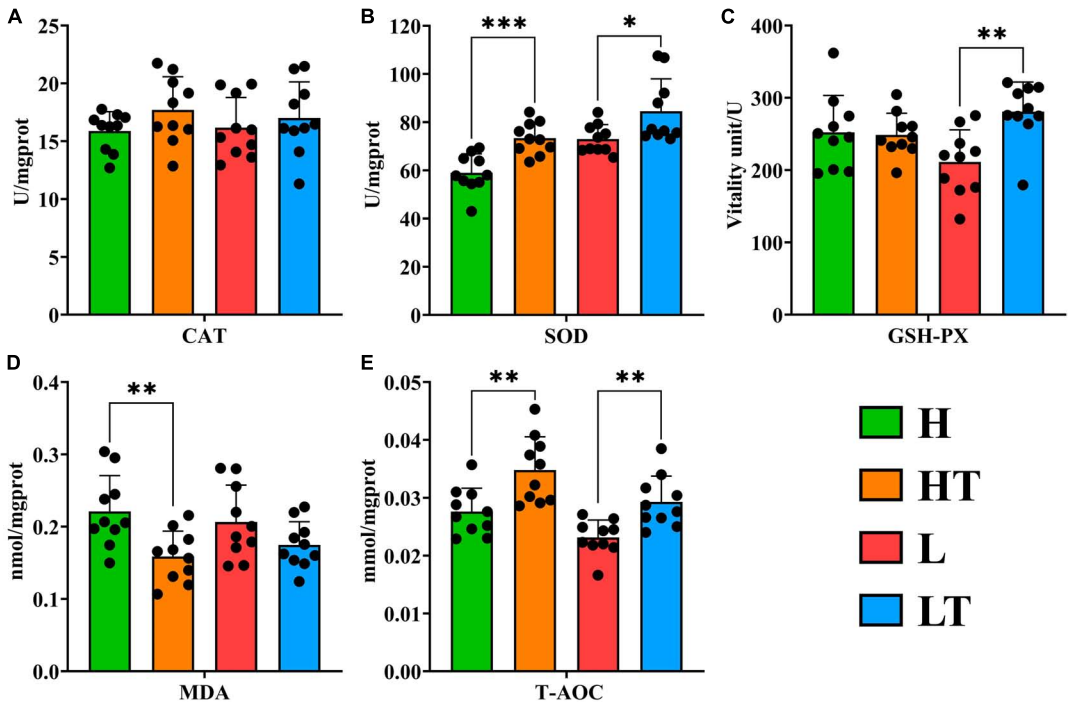

FIGURE 5
Antioxidant test results of liver in mice. **(A)** CAT in mouse liver. **(B)** SOD in mouse liver. **(C)** GSH-PX in mouse liver. **(D)** MDA in mouse liver. **(E)** T-AOC in mouse liver. "*" indicates a significant difference ($P < 0.05$), "**" indicates a significant difference ($P < 0.01$), "***" indicates a significant difference ($P < 0.001$).

with previous studies which have reported the presence of bile salt tolerance genes (*DnaK*, *OppA*, and *Eno*) in probiotic *Bacillus velezensis* FS26 (Sam-On et al., 2023). The Na/H antiporter (*nhaC*, *nhaX*) and universal stress proteins (*nhaK*) play a crucial role in Na resistance and pH homeostasis, allowing the bacteria to survive in acidic conditions (Fujisawa et al., 2005). Moreover, our results indicate that *B. velezensis* TS5 is capable of producing antimicrobial compounds and exhibiting broad-spectrum antimicrobial activity.

The genome of *Bacillus velezensis* TS5 contains three genes, lipoprotein signal peptidase (*LspA* gene), glutamine binding periplasmic protein (*GlnH* gene), and elongation factor Tu (*Tuf* gene), which are also known as mucus adhesion domain protein (MucBPs) (**Supplementary Table 1**). These proteins play a grucial role in host adhesion, automatic aggregation, and/or coaggregation with pathogenic bacteria (Sam-On et al., 2023). The findings are consistent with previous studies which have reported the presence of similar MucBPs (*LspA*, *GlnH*, and *Tuf* genes) in probiotic *Bacillus velezensis* FS26 (Sam-On et al., 2023).

Probiotics have been widely acknowledged for their ability to enhance the host's antioxidant capacity by activating antioxidant related pathways or increasing the activity of antioxidant enzymes (Xu et al., 2019; Zhao et al., 2021). For instance, glutathione peroxidase (*bsaA*) is known to protect cells from oxidative stress by reducing hydrogen peroxide to water (Lubos et al., 2011). Previous studies have also reported the presence of multiple genes encoding catalase and peroxidase in the genome of *Bacillus subtilis* DE111, a safe commercial probiotic (Mazhar et al., 2022). In this study, we found that *Bacillus velezensis* TS5 contains multiple genes encoding both glutathione peroxidase, catalases, peroxidases, and thioredoxin which further validated its antioxidant properties (**Supplementary Table 1**).

The process of decomposing carbohydrates such as cellulose, proteoglycans, and starch into mono or oligo saccharides that can be absorbed by intestinal epithelium requires the essential CAZymes (Shang et al., 2022). The GH family enzymes play a crucial role in this process by hydrolyzing glycosidic bonds (Roth et al., 2017). In *Bacillus velezensis* TS5, 11 GH family members were identified, including GH1, GH3, GH16, GH30, and GH51 that encoded cellulase, while GH1 and GH3 were primarily β-glucosidases (Suzuki et al., 2013). These enzymes coordinately degrade cellulose, while other GH family members could also degrade hemicellulose. For instance, GH3, GH4, GH11, GH16, GH26, GH30, GH43, GH51, GH53, and GH76 could degrade hemicellulose. Among them, GH26 was mainly composed of β-1,4 mannanases that could hydrolyze mannan, galactomannan, and glucomannan (Taylor et al., 2005). Additionally, GH43 was an important member of xylan degradation (Zanphorlin et al., 2019), while GH51 could dissociate arabinogalactan and arabinomannan in cell walls promoting the degradation of pectin (Im et al., 2012). GH53 had been reported as an endo-1,4-β-galactanase and had the ability to hydrolyze 1,4-β-D-galactoside bonds (Sakamoto et al., 2013). In addition, carbohydrate esterases related to xylan decomposition were identified in *Bacillus velezensis* TS5, including CE1, CE3, CE4, CE6, CE7, and CE12. Among these, CE3, CE4, and CE7 were acetyl xylan esterases that could promote the dissolution of xylan (Zhang et al., 2011). The abundance of cellulase and hemicellulase genes further indicated that *Bacillus velezensis* TS5 has the potential to degrade both cellulose and hemicellulose.

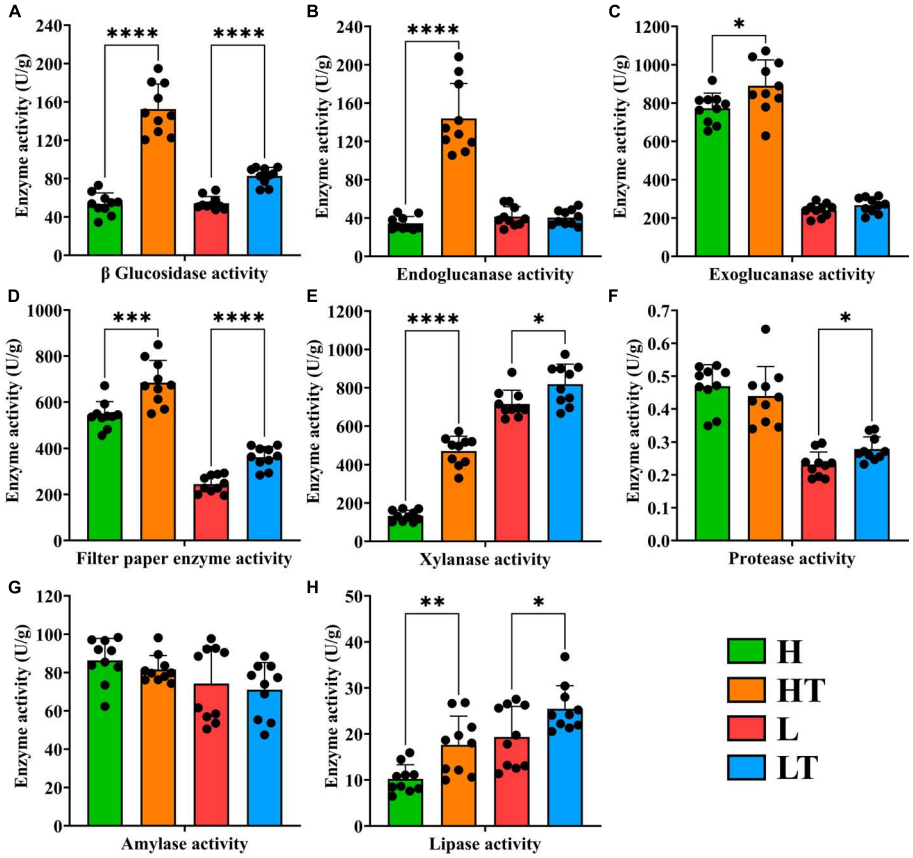

FIGURE 6
Digestive enzyme activity of cecum contents in mice. **(A)** β glucosidase activity. **(B)** Endoglucanase activity. **(C)** Exoglucanase activity. **(D)** Filter paper enzyme activity. **(E)** Xylanase activity. **(F)** Protease activity. **(G)** Amylase activity. **(H)** Lipase activity. "*" indicates a significant difference ($P < 0.05$), "**" indicates a significant difference ($P < 0.01$), "***" indicates a significant difference ($P < 0.001$), "****" indicates a significant difference ($P < 0.0001$).

These findings suggest that *Bacillus velezensis* TS5 is a promising candidate for the degradation of complex carbohydrates in various industrial applications.

Proteases, amylases, and lipases are enzymes that can decompose proteins, carbohydrates, and lipids into amino acids, aldehydes, amines, free fatty acids, organic acids, and esters (Heo et al., 2021). *Bacillus velezensis* TS5 was found to possess 21 protease or peptidase genes (**Supplementary Table 2**), which suggest that it has the ability to degrade proteins. In addition, *Bacillus velezensis* TS5 also encoded seven α-amylase gene and five lipases and esterases genes (**Supplementary Table 2**). These findings suggest that *Bacillus velezensis* TS5 has the potential to promote nutrient digestion. A study indicated that the cellulase and phytase secreted by *Bacillus velezensis* LB-Y-1 contribute to the release of nutrients in Arbor Acres broiler chickens feed (Li et al., 2023). The protease and amylase secreted by *Bacillus velezensis* LB-Y-1 enhanced the intestinal digestibility of broilers, thereby promoting nutrient digestion.

Bacterial resistance can be divided into two categories: one is inherent resistance that develops during the formation of microorganisms and usually does not transfer, and the other is acquired resistance with high levels of transfer potential (Holzapfel et al., 2018). The acquired resistance genes in probiotic strains are considered a major threat to the spread of drug resistance between different bacterial species (Fu et al., 2022). There were no acquired resistance genes found in the genome of *Bacillus velezensis* TS5, indicated a lower risk of spreading resistance. Although the analysis of the *Bacillus velezensis* TS5 genome against the VFDB revealed the presence of some putative virulence genes, they could not be considered really harmful. Genes encoding hemolysin A (hlyA), cytolysin (cyl), enterotoxins haemolysin BL (Hbl), non-hemolytic enterotoxin (Nhe), and cytotoxin K (CytK), which are well-known potential virulence factors, were missing in *Bacillus velezensis* TS5 (Schoeni and Wong, 2005; Dietrich et al., 2021). In addition, no truly toxic toxin coding genes were found in the genome of *Bacillus velezensis* TS5. More importantly, we have demonstrated the safety of *Bacillus velezensis* TS5 through mice experiments.

4.2 The probiotic function in mice is an important prerequisite for *Bacillus velezensis* TS5 to become a potential digestive probiotic

Recently, high-fiber feeds such as wheat bran, rapeseed meal, and cottonseed meal have been increasingly utilized in monogastric animal feed production (Shang et al., 2022). However, these high fiber contents present a challenge for monogastric animals to digest,

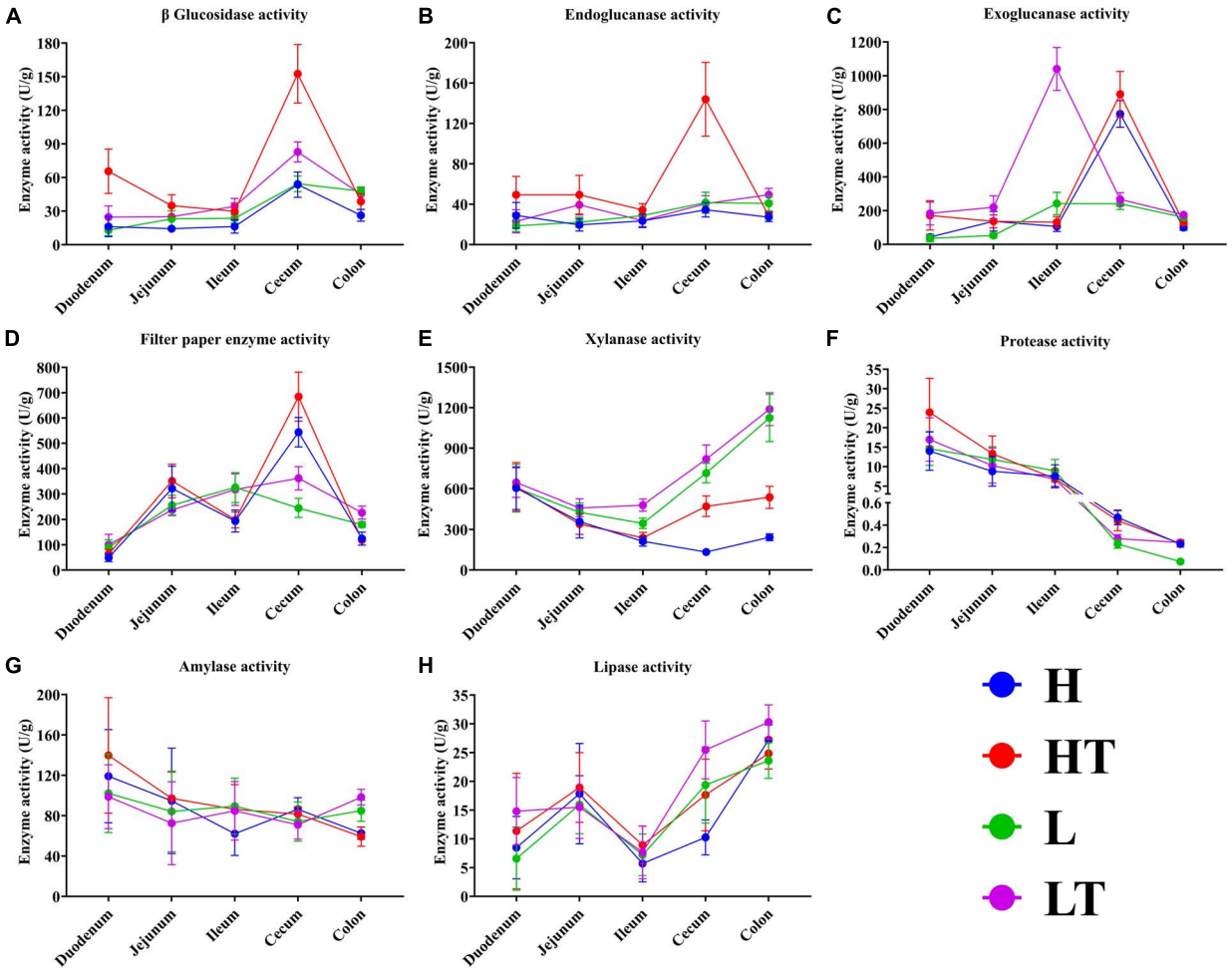

FIGURE 7
Digestive enzyme activities of whole intestinal contents in mice. **(A)** β glucosidase activity. **(B)** Endoglucanase activity. **(C)** Exoglucanase activity. **(D)** Filter paper enzyme activity. **(E)** Xylanase activity. **(F)** Protease activity. **(G)** Amylase activity. **(H)** Lipase activity.

resulting in the wasteful consumption of limited feed resources. A high-fiber diet can lead to an increase in chyme emptying rate, which residence time of chyme in the gastrointestinal tract, decreased the contact between digestive enzymes and chyme, and ultimately lowers the digestibility of nutrients (Jha and Leterme, 2012). Therefore, enhancing the degradation of fiber components in feed is an effective approach to improve feed digestibility. Previous studies have demonstrated that incroporating probiotics, such as *Bacillus*, into animal feed can promote digestion and absorption, thereby enhancing feed utilization and production performance (Manhar et al., 2016; Mahoney et al., 2020; Khalid et al., 2021). Soni et al. (2021) supplemented *Bacillus velezensis* ZBG17 to the broiler diet, resulting in a significantly improvement in the feed utilization rate and humoral immunity response of broilers. Genomic analysis of this bacterium revealed that it lacked genes related to safety hazards, demonstrating its potential as a direct feeding microorganism in the poultry industry. Li et al. (2020) isolated a strain of *Bacillus velezensis* JT3-1 with potent antibacterial activity from yak feces, which improve the growth performance of calves and alleviated calf diarrhea to some extent. Although numerous studies suggested that *Bacillus velezensis* is a promising probiotic, its probiotic properties still require further exploration. Therefore, in this study, we established two distinct cellulose diets for mice and administered gavage *Bacillus velezensis* TS5 for an entire 8-week period, with the aim of investigating the *in vivo* probiotic properties of *Bacillus velezensis* TS5.

Probiotics are live microorganisms that have beneficial effects on the host by colonizing the gut and modifying the composition of certain gut microbiota (Gupta and Garg, 2009). A previous study examined the probiotic potential of *Bacillus licheniformis* (named D1 and D2) and *Bacillus pumilus* (named X1 and X2) isolated from yak intestines, and the results showed that supplementation with these probiotics increased daily weight gain and reduced feed conversion rate in mice (Zeng et al., 2022). Yang et al. (2023) reported that *Bacillus subtilis* BS-Z15 can regulate the gut microbiota of mice through its metabolites to reduce weight gain. In this study, we found that *Bacillus velezensis* TS5 slowed down the weight gain of mice, which was not affected by the cellulose content in the feed (high fiber or low fiber feed). Moreover, *Bacillus velezensis* TS5 increased the diversity and richness of the cecal microbiota in mice and altered the content of certain microbiota (increased the content of Bacteroides and reduced the content of Campylobacter and Desulfobacteria). Previous research has shown that the main function of the Bacteroidetes phylum is to degrade

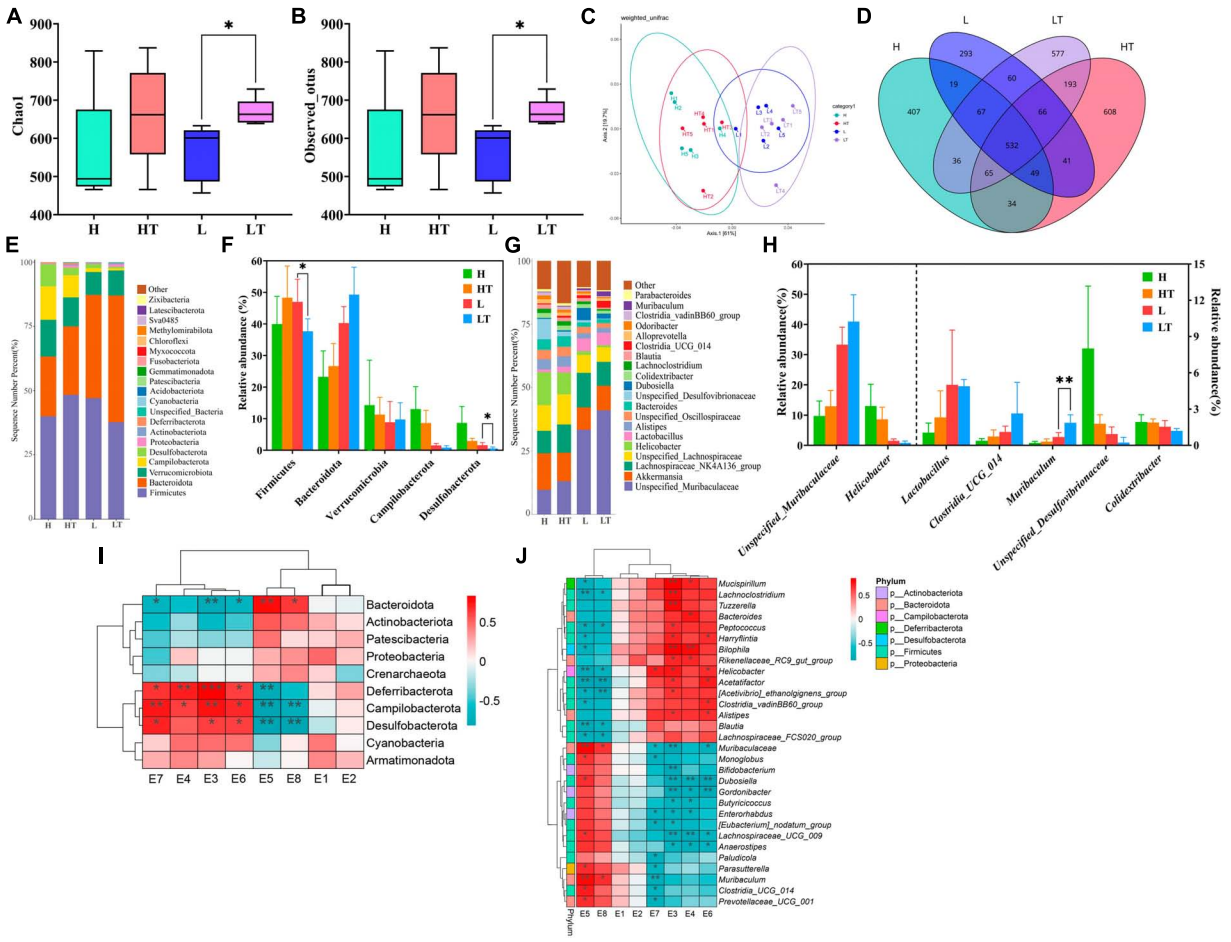

FIGURE 8
Results and analysis of 16S rRNA amplification and sequencing in the mice cecum. **(A)** Box plot of Chao1's diversity index. **(B)** Box plot of observed OTU's diversity index. **(C)** Principal co-ordinates analysis (PCoA) with weighted unifrac of microbiota. **(D)** Venn diagram of the cecal microbiota. **(E)** Histogram of the top 20 phylum level microbiota in relative abundance. **(F)** Histogram of relative abundance of dominant bacterial phyla in the cecum. **(G)** Histogram of the top 20 genus level microbiota in relative abundance. **(H)** Histogram of relative abundance of dominant bacterial genera in the cecum. **(I)** Thermogram of correlation between cecal digestive enzyme activity and phylum level microbiota. **(J)** Thermogram of correlation between cecal digestive enzyme activity and genus level microbiota. E1-E8 represents the activities of β-glucosidase, endoglucanase, exoglucanase, filter paper enzyme, xylanase, protease, amylase, and lipase, respectively. "*" indicates a significant difference ($P < 0.05$), "**" indicates a significant difference ($P < 0.01$).

carbohydrates and proteins and participate in lipid metabolism (Yang et al., 2023). At the genus level, *Bacillus velezensis* TS5 increased the abundance of *Lactobacillus* in the mice's cecum, which is consistent with the findings reported by Donaldson et al. (2016) and Yang et al. (2023) that there is an association between increased abundance of beneficial gut bacteria, such as *Lactobacillus* and *Bifidobacterium* and weight loss. This indicated that *Bacillus velezensis* TS5 regulated weight gain in mice by altering the intestinal bacterial structure, which could potentially prevent obesity in human.

Previous research has demonstrated that supplementing probiotics helps maintain the balance of gut microbiota in the host, while also increasing the number of beneficial bacteria and reducing the colonization of harmful bacteria in the intestinal tract (Baldwin et al., 2018; Li et al., 2019a; Fuerniss et al., 2022). The cecum, a significant fermentation site in mice, contains a rich microbial community. Previous studies have shown that *Bacillus velezensis* isolated from Tibetan yaks can enhance the gut microbiota of mice (Li et al., 2019c). In this study, oral administration of *Bacillus velezensis* TS5 decreased the relative abundance of potential harmful bacteria such as *Helicobacter*, *Unspecified_Desulfovibrionaceae*, and *Colidextribacter* in the cecum and improved the composition of the mice's cecum microbiota to a certain extent.

The small intestine is a vital part of the animal body for absorption, and research has shown that probiotic supplementation can enhance this process by increasing the length of intestinal villus and reducing the depth of crypts. In this study, the pathological sections showed that the jejunum and ileum tissues in mice appeared healthy with no apparent lesions (**Figure 3**). By evaluating the villus length and crypt depth of these regions, it was discovered that the V/C values of the probiotic group were significantly higher than those of the control group ($P < 0.01$). This demonstrates that *Bacillus velezensis* TS5 promotes nutrient absorption and improves intestinal morphology in mice.

Previous research has reported that probiotics can enhance antioxidant capacity by increasing the activity of antioxidant enzymes in the host body (Wang et al., 2017). Li et al. (2019b) found that *Bacillus velezensis* BV2 could increase SOD and GSH-PX activity in the liver of mice, reduce MDA content, and increase T-AOC, thereby improving the antioxidant capacity of mice. In this study, the results showed that compared to the control group, the probiotic group increased the activity of CAT, SOD, and GSH-Px in the mouse liver, decreased the MDA content, and increased T-AOC. This suggests that *Bacillus velezensis* TS5 has the potential to improve the antioxidant capacity of mice.

During intestinal colonization, probiotics can metabolize and produce extracellular digestive enzyme such as protease, lipase, and cellulase, which can further improve the digestive capacity of the host. *Bacillus* may be the most important source of proteases due to their ability to produce a large number of neutral and alkaline proteolytic enzymes with significant characteristics, such as high stability under extreme temperatures, pH, organic solvents, detergents, and oxidizing compounds (Contesini et al., 2018). Li et al. (2019b) found that *Bacillus velezensis* BV2 enhanced the growth of small intestine (duodenum, jejunum, and ileum) in mice by increasing α-amylase, lipase, and trypsin activities. Jang et al. (2023) reported that supplementing red sea bream (Pagrus major) with *Bacillus sp.* PM8313 significantly increased trypsin and lipase activity in the anterior midgut. In this study, we measured the activity of digestive enzymes in the intact intestinal contents of mice. Our results showed that *Bacillus velezensis* TS5 promoted nutrient digestion by increasing the activities of β glucosidase, filter paper enzyme, xylanase and lipase in the mice's cecum (**Figure 6**). Furthermore, the activity of other intestinal contents was also increased to varying degrees (**Supplementary Figures 1–4**).

5 Conclusion

In summary, the genomic and *in vivo* studies of *Bacillus velezensis* TS5 isolated from Tibetan sheep provided valuable insights into its efficacy as a probiotic in mice study. The genome mining of *Bacillus velezensis* TS5 identified numerous genes that function as probiotic markers in terms of host intestinal adhesion, antioxidant, production of antibacterial substances and digestive enzyme, as well as acid and bile salt tolerance. Animal experiments demonstrated that *Bacillus velezensis* TS5 can improve the activity of intestinal digestive enzymes and liver antioxidant capacity in mice, as well as the morphology of small intestine and cecum microbiota structure. These findings provided a theoretical basis for the clinical application and development of *Bacillus velezensis* TS5 as a new feed additive.

Data availability statement

The raw data of the bacterial complete genome and the 16S rRNA sequencing data are deposited in the NCBI repository, with the accession numbers CP125654.1 and PRJNA1028384, respectively.

Ethics statement

The animal study was approved by the Animal Ethical and Welfare Committee of Sichuan Agricultural University [SYXK (Chuan) 2019-187]. The study was conducted in accordance with the local legislation and institutional requirements.

Author contributions

BC: Data curation, Methodology, Validation, Visualization, Writing – original draft, Software. YiZ: Software, Visualization, Writing – original draft. LD: Data curation, Investigation, Writing – original draft. XG: Data curation, Investigation, Software, Writing – original draft. XL: Investigation, Validation, Writing – original draft. KP: Methodology, Software, Writing – review and editing. DZ: Writing – review and editing, Project administration, Supervision. XN: Writing – review and editing, Conceptualization, Methodology. YaZ: Funding acquisition, Methodology, Project administration, Supervision, Writing – review and editing.

Funding

The author(s) declare financial support was received for the research, authorship, and/or publication of this article. This work was supported by funding from the Sichuan Natural Science Foundation Project (2022NSFSC1771), China.

Conflict of interest

The authors declare that the research was conducted in the absence of any commercial or financial relationships that could be construed as a potential conflict of interest.

Publisher's note

All claims expressed in this article are solely those of the authors and do not necessarily represent those of their affiliated organizations, or those of the publisher, the editors and the reviewers. Any product that may be evaluated in this article, or claim that may be made by its manufacturer, is not guaranteed or endorsed by the publisher.

Supplementary material

The Supplementary Material for this article can be found online at: https://www.frontiersin.org/articles/10.3389/fmicb.2023.1322910/full#supplementary-material

References

Alanjary, M., Steinke, K., and Ziemert, N. (2019). AutoMLST: an automated web server for generating multi-locus species trees highlighting natural product potential. *Nucleic Acids Res.* 47, W276–W282. doi: 10.1093/nar/gkz282

Altschul, S. F., Gish, W., Miller, W., Myers, E. W., and Lipman, D. J. (1990). Basic local alignment search tool. *J. Mol. Biol.* 215, 403–410.

Bahaddad, S. A., Almalki, M. H. K., Alghamdi, O. A., Sohrab, S. S., Yasir, M., Azhar, E. I., et al. (2023). *Bacillus* species as direct-fed microbial antibiotic alternatives for monogastric production. *Probiotics Antimicrob. Proteins* 15, 1–16. doi: 10.1007/s12602-022-09909-5

Baldwin, S., Hughes, R. J., Hao Van, T. T., Moore, R. J., and Stanley, D. (2018). At-hatch administration of probiotic to chickens can introduce beneficial changes in gut microbiota. *PLoS One* 13:e0194825. doi: 10.1371/journal.pone.0194825

Bertelli, C., Laird, M. R., Williams, K. P., Lau, B. Y., Hoad, G., Winsor, G. L., et al. (2017). IslandViewer 4: expanded prediction of genomic islands for larger-scale datasets. *Nucleic Acids Res.* 45, W30–W35. doi: 10.1093/nar/gkx343

Blin, K., Shaw, S., Kloosterman, A. M., Charlop-Powers, Z., Van Wezel, G. P., Medema, M. H., et al. (2021). antiSMASH 6.0: improving cluster detection and comparison capabilities. *Nucleic Acids Res.* 49, W29–W35. doi: 10.1093/nar/gkab335

Budihal, S. R., Agsar, D., and Patil, S. R. (2016). Enhanced production and application of acidothermophilic *Streptomyces* cellulase. *Bioresour. Technol.* 200, 706–712. doi: 10.1016/j.biortech.2015.10.098

Cao, F., Jin, L., Gao, Y., Ding, Y., Wen, H., Qian, Z., et al. (2023). Artificial-enzymes-armed *Bifidobacterium longum* probiotics for alleviating intestinal inflammation and microbiota dysbiosis. *Nat. Nanotechnol.* 18, 617–627. doi: 10.1038/s41565-023-01346-x

Chen, L., Zheng, D., Liu, B., Yang, J., and Jin, Q. (2016). VFDB 2016: hierarchical and refined dataset for big data analysis–10 years on. *Nucleic Acids Res.* 44, 694–697. doi: 10.1093/nar/gkv1239

Conesa, A., and Götz, S. (2008). Blast2GO: a comprehensive suite for functional analysis in plant genomics. *Int. J. Plant Genomics* 2008:619832.

Contesini, F. J., Melo, R. R., and Sato, H. H. (2018). An overview of *Bacillus* proteases: from production to application. *Crit. Rev. Biotechnol.* 38, 321–334. doi: 10.1080/07388551.2017.1354354

Dhanya Raj, C. T., Suryavanshi, M. V., Kandaswamy, S., Ramasamy, K. P., and James, R. A. (2023). Whole genome sequence analysis and in-vitro probiotic characterization of *Bacillus velezensis* FCW2 MCC4686 from spontaneously fermented coconut water. *Genomics* 115:110637. doi: 10.1016/j.ygeno.2023.110637

Dietrich, R., Jessberger, N., Ehling-Schulz, M., Märtlbauer, E., and Granum, P. E. (2021). The food poisoning toxins of *Bacillus cereus*. *Toxins (Basel)* 13:98.

Donaldson, G. P., Lee, S. M., and Mazmanian, S. K. (2016). Gut biogeography of the bacterial microbiota. *Nat. Rev. Microbiol.* 14, 20–32.

Dong, H., Gao, R., Dong, Y., Yao, Q., and Zhu, H. (2023). *Bacillus velezensis* RC116 inhibits the pathogens of bacterial wilt and fusarium wilt in tomato with multiple biocontrol traits. *Int. J. Mol. Sci.* 24:8527. doi: 10.3390/ijms24108527

Du, W., Xu, H., Mei, X., Cao, X., Gong, L., Wu, Y., et al. (2018). Probiotic *Bacillus* enhance the intestinal epithelial cell barrier and immune function of piglets. *Benef. Microbes* 9, 743–754. doi: 10.3920/BM2017.0142

Elkholy, S. E., Maher, S. A., Abd El-Hamid, N. R., Elsayed, H. A., Hassan, W. A., Abdelmaogood, A. K. K., et al. (2023). The immunomodulatory effects of probiotics and azithromycin in dextran sodium sulfate-induced ulcerative colitis in rats via TLR4-NF-κB and p38-MAPK pathway. *Biomed. Pharmacother.* 165:115005.

Fu, X., Lyu, L., Wang, Y., Zhang, Y., Guo, X., Chen, Q., et al. (2022). Safety assessment and probiotic characteristics of *Enterococcus lactis* JDM1. *Microb. Pathog.* 163:105380. doi: 10.1016/j.micpath.2021.105380

Fuerniss, L. K., Kreikemeier, K. K., Reed, L. D., Cravey, M. D., and Johnson, B. J. (2022). Cecal microbiota of feedlot cattle fed a four-species *Bacillus* supplement. *J. Anim. Sci.* 100:skac258. doi: 10.1093/jas/skac258

Fujisawa, M., Kusumoto, A., Wada, Y., Tsuchiya, T., and Ito, M. (2005). NhaK, a novel monovalent cation/H+ antiporter of *Bacillus subtilis*. *Arch. Microbiol.* 183, 411–420. doi: 10.1007/s00203-005-0011-6

Galperin, M. Y., Makarova, K. S., Wolf, Y. I., and Koonin, E. V. (2015). Expanded microbial genome coverage and improved protein family annotation in the COG database. *Nucleic Acids Res.* 43, 261–269. doi: 10.1093/nar/gku1223

Gupta, V., and Garg, R. (2009). Probiotics. *Indian J. Med. Microbiol.* 27, 202–209.

Heo, S., Kim, J. H., Kwak, M. S., Sung, M. H., and Jeong, D. W. (2021). Functional annotation genome unravels potential probiotic *Bacillus velezensis* Strain KMU01 from traditional Korean fermented kimchi. *Foods* 10:563. doi: 10.3390/foods10030563

Hill, C., Guarner, F., Reid, G., Gibson, G. R., Merenstein, D. J., Pot, B., et al. (2014). Expert consensus document. The international scientific association for probiotics and prebiotics consensus statement on the scope and appropriate use of the term probiotic. *Nat. Rev. Gastroenterol. Hepatol.* 11, 506–514.

Holzapfel, W., Arini, A., Aeschbacher, M., Coppolecchia, R., and Pot, B. (2018). *Enterococcus faecium* SF68 as a model for efficacy and safety evaluation of pharmaceutical probiotics. *Benef. Microbes* 9, 375–388. doi: 10.3920/BM2017.0148

Hou, X., Dai, P., Song, X., Long, X., Gao, J., and Chai, T. (2023). Understanding the effect of compound probiotics on the health of rabbits and its mechanisms through metagenomics. *Probiotics Antimicrob. Proteins* doi: 10.1007/s12602-023-10072-8

Hu, S., Cao, X., Wu, Y., Mei, X., Xu, H., Wang, Y., et al. (2018). Effects of probiotic *Bacillus* as an alternative of antibiotics on digestive enzymes activity and intestinal integrity of piglets. *Front. Microbiol.* 9:2427. doi: 10.3389/fmicb.2018.02427

Huang, K., Shi, W., Yang, B., and Wang, J. (2022). The probiotic and immunomodulation effects of *Limosilactobacillus reuteri* RGW1 isolated from calf feces. *Front. Cell. Infect. Microbiol.* 12:1086861. doi: 10.3389/fcimb.2022.1086861

Im, D. H., Kimura, K., Hayasaka, F., Tanaka, T., Noguchi, M., Kobayashi, A., et al. (2012). Crystal structures of glycoside hydrolase family 51 α-L-arabinofuranosidase from *Thermotoga maritima*. *Biosci. Biotechnol. Biochem.* 76, 423–428.

Iqbal, S., Begum, F., Rabaan, A. A., Aljeldah, M., Al Shammari, B. R., Alawfi, A., et al. (2023). Classification and multifaceted potential of secondary metabolites produced by *Bacillus subtilis* group: a comprehensive review. *Molecules* 28:927. doi: 10.3390/molecules28030927

Jang, W. J., Lee, K. B., Jeon, M. H., Lee, S. J., Hur, S. W., Lee, S., et al. (2023). Characteristics and biological control functions of *Bacillus* sp. PM8313 as a host-associated probiotic in red sea bream (*Pagrus major*) aquaculture. *Anim. Nutr.* 12, 20–31. doi: 10.1016/j.aninu.2022.08.011

Jha, R., and Leterme, P. (2012). Feed ingredients differing in fermentable fibre and indigestible protein content affect fermentation metabolites and faecal nitrogen excretion in growing pigs. *Animal* 6, 603–611. doi: 10.1017/S1751731111001844

Joensen, K. G., Scheutz, F., Lund, O., Hasman, H., Kaas, R. S., Nielsen, E. M., et al. (2014). Real-time whole-genome sequencing for routine typing, surveillance, and outbreak detection of verotoxigenic *Escherichia coli*. *J. Clin. Microbiol.* 52, 1501–1510. doi: 10.1128/JCM.03617-13

Joseph, B., Shrivastava, N., and Ramteke, P. W. (2012). Extracellular cold-active lipase of *Microbacterium luteolum* isolated from *Gangotri glacier*, western Himalaya: isolation, partial purification and characterization. *J. Genet. Eng. Biotechnol.* 10, 137–144.

Kapse, N. G., Engineer, A. S., Gowdaman, V., Wagh, S., and Dhakephalkar, P. K. (2019). Functional annotation of the genome unravels probiotic potential of *Bacillus coagulans* HS243. *Genomics* 111, 921–929. doi: 10.1016/j.ygeno.2018.05.022

Khalid, F., Khalid, A., Fu, Y., Hu, Q., Zheng, Y., Khan, S., et al. (2021). Potential of *Bacillus velezensis* as a probiotic in animal feed: a review. *J. Microbiol.* 59, 627–633. doi: 10.1007/s12275-021-1161-1

Koutsoumanis, K., Allende, A., Alvarez-Ordóñez, A., Bolton, D., Bover-Cid, S., Chemaly, M., et al. (2020). Update of the list of QPS-recommended biological agents intentionally added to food or feed as notified to EFSA 11: suitability of taxonomic units notified to EFSA until September 2019. *EFSA J.* 18:e05965.

Li, A., Jiang, X., Wang, Y., Zhang, L., Zhang, H., Mehmood, K., et al. (2019a). The impact of *Bacillus subtilis* 18 isolated from Tibetan yaks on growth performance and gut microbial community in mice. *Microb. Pathog.* 128, 153–161. doi: 10.1016/j.micpath.2018.12.031

Li, A., Wang, Y., Pei, L., Mehmood, K., Li, K., Qamar, H., et al. (2019c). Influence of dietary supplementation with *Bacillus velezensis* on intestinal microbial diversity of mice. *Microb. Pathog.* 136:103671. doi: 10.1016/j.micpath.2019.103671

Li, A., Wang, Y., Li, Z., Qamar, H., Mehmood, K., Zhang, L., et al. (2019b). Probiotics isolated from yaks improves the growth performance, antioxidant activity, and cytokines related to immunity and inflammation in mice. *Microb. Cell Fact.* 18:112. doi: 10.1186/s12934-019-1161-6

Li, C., Li, S., Dang, G., Jia, R., Chen, S., Deng, X., et al. (2023). Screening and characterization of *Bacillus velezensis* LB-Y-1 toward selection as a potential probiotic for poultry with multi-enzyme production property. *Front. Microbiol.* 14:1143265. doi: 10.3389/fmicb.2023.1143265

Li, Y., Li, X., Jia, D., Liu, J., Wang, J., Liu, A., et al. (2020). Complete genome sequence and antimicrobial activity of *Bacillus velezensis* JT3-1, a microbial germicide isolated from yak feces. *3 Biotech* 10:231. doi: 10.1007/s13205-020-02235-z

Lombard, V., Golaconda Ramulu, H., Drula, E., Coutinho, P. M., and Henrissat, B. (2014). The carbohydrate-active enzymes database (CAZy) in 2013. *Nucleic Acids Res.* 42, D490–D495.

Lu, S., Na, K., Li, Y., Zhang, L., Fang, Y., and Guo, X. (2022). *Bacillus*-derived probiotics: metabolites and mechanisms involved in bacteria-host interactions. *Crit. Rev. Food Sci. Nutr.* 1–14. doi: 10.1080/10408398.2022.2118659

Lubos, E., Loscalzo, J., and Handy, D. E. (2011). Glutathione peroxidase-1 in health and disease: from molecular mechanisms to therapeutic opportunities. *Antioxid. Redox Signal.* 15, 1957–1997. doi: 10.1089/ars.2010.3586

Luise, D., Bosi, P., Raff, L., Amatucci, L., Virdis, S., and Trevisi, P. (2022). *Bacillus* spp. probiotic strains as a potential tool for limiting the use of antibiotics, and

improving the growth and health of pigs and chickens. *Front. Microbiol.* 13:801827. doi: 10.3389/fmicb.2022.801827

Mahoney, R., Weeks, R., Zheng, T., Huang, Q., Dai, W., Cao, Y., et al. (2020). Evaluation of an industrial soybean byproduct for the potential development of a probiotic animal feed additive with *Bacillus* species. *Probiotics Antimicrob. Proteins* 12, 1173–1178. doi: 10.1007/s12602-019-09619-5

Manhar, A. K., Bashir, Y., Saikia, D., Nath, D., Gupta, K., Konwar, B. K., et al. (2016). Cellulolytic potential of probiotic *Bacillus Subtilis* AMS6 isolated from traditional fermented soybean (*Churpi*): an in-vitro study with regards to application as an animal feed additive. *Microbiol. Res.* 186–187, 62–70. doi: 10.1016/j.micres.2016.03.004

Mazhar, S., Khokhlova, E., Colom, J., Simon, A., Deaton, J., and Rea, K. (2022). *In vitro* and *in silico* assessment of probiotic and functional properties of *Bacillus subtilis* DE111(®). *Front. Microbiol.* 13:1101144. doi: 10.3389/fmicb.2022.1101144

McArthur, A. G., Waglechner, N., Nizam, F., Yan, A., Azad, M. A., Baylay, A. J., et al. (2013). The comprehensive antibiotic resistance database. *Antimicrob. Agents Chemother.* 57, 3348–3357.

Meier-Kolthoff, J. P., Carbasse, J. S., Peinado-Olarte, R. L., and Göker, M. (2022). TYGS and LPSN: a database tandem for fast and reliable genome-based classification and nomenclature of prokaryotes. *Nucleic Acids Res.* 50, D801–D807. doi: 10.1093/nar/gkab902

Miller, G. L. (1959). Use of dinitrosalicylic acid reagent for determination of reducing sugar. *Anal. Biochem.* 31, 426–428.

Monzón-Atienza, L., Bravo, J., Fernández-Montero, Á, Charlie-Silva, I., Montero, D., Ramos-Vivas, J., et al. (2022). Dietary supplementation of *Bacillus velezensis* improves *Vibrio anguillarum* clearance in European sea bass by activating essential innate immune mechanisms. *Fish Shellfish Immunol.* 124, 244–253. doi: 10.1016/j.fsi.2022.03.032

Moriya, Y., Itoh, M., Okuda, S., Yoshizawa, A. C., and Kanehisa, M. (2007). KAAS: an automatic genome annotation and pathway reconstruction server. *Nucleic Acids Res.* 35, W182–W185.

Patel, R. K., and Jain, M. (2012). NGS QC Toolkit: a toolkit for quality control of next generation sequencing data. *PLoS One* 7:e30619. doi: 10.1371/journal.pone.0030619

Pedruzzi, I., Rivoire, C., Auchincloss, A. H., Coudert, E., Keller, G., De Castro, E., et al. (2015). HAMAP in 2015: updates to the protein family classification and annotation system. *Nucleic Acids Res.* 43, 1064–1070. doi: 10.1093/nar/gku1002

Pereira, J. Q., Ritter, A. C., Cibulski, S., and Brandelli, A. (2019). Functional genome annotation depicts probiotic properties of *Bacillus velezensis* FTC01. *Gene* 713:143971. doi: 10.1016/j.gene.2019.143971

Ramkumar, A., Sivakumar, N., Gujarathi, A. M., and Victor, R. (2018). Production of thermotolerant, detergent stable alkaline protease using the gut waste of *Sardinella longiceps* as a substrate: optimization and characterization. *Sci. Rep.* 8:12442. doi: 10.1038/s41598-018-30155-9

Roth, C., Weizenmann, N., Bexten, N., Saenger, W., Zimmermann, W., Maier, T., et al. (2017). Amylose recognition and ring-size determination of amylomaltase. *Sci. Adv.* 3:e1601386. doi: 10.1126/sciadv.1601386

Ruiz-García, C., Béjar, V., Martínez-Checa, F., Llamas, I., and Quesada, E. (2005). *Bacillus velezensis* sp. nov., a surfactant-producing bacterium isolated from the river Vélez in Málaga, southern Spain. *Int. J. Syst. Evol. Microbiol.* 55, 191–195. doi: 10.1099/ijs.0.63310-0

Sakamoto, T., Nishimura, Y., Makino, Y., Sunagawa, Y., and Harada, N. (2013). Biochemical characterization of a GH53 endo-β-1,4-galactanase and a GH35 exo-β-1,4-galactanase from *Penicillium chrysogenum*. *Appl. Microbiol. Biotechnol.* 97, 2895–2906.

Sam-On, M. F. S., Mustafa, S., Mohd Hashim, A., Yusof, M. T., Zulkifly, S., Malek, A. Z. A., et al. (2023). Mining the genome of *Bacillus velezensis* FS26 for probiotic markers and secondary metabolites with antimicrobial properties against aquaculture pathogens. *Microb. Pathog.* 181:106161. doi: 10.1016/j.micpath.2023.106161

Schoeni, J. L., and Wong, A. C. (2005). *Bacillus cereus* food poisoning and its toxins. *J. Food Prot.* 68, 636–648.

Shang, Z., Liu, S., Duan, Y., Bao, C., Wang, J., Dong, B., et al. (2022). Complete genome sequencing and investigation on the fiber-degrading potential of *Bacillus amyloliquefaciens* strain TL106 from the tibetan pig. *BMC Microbiol.* 22:186. doi: 10.1186/s12866-022-02599-7

Soni, R., Keharia, H., Bose, A., Pandit, N., Doshi, J., Rao, S. V. R., et al. (2021). Genome assisted probiotic characterization and application of *Bacillus velezensis* ZBG17 as an alternative to antibiotic growth promoters in broiler chickens. *Genomics* 113, 4061–4074. doi: 10.1016/j.ygeno.2021.10.012

Stothard, P., and Wishart, D. S. (2005). Circular genome visualization and exploration using CGView. *Bioinformatics* 21, 537–539. doi: 10.1093/bioinformatics/bti054

Suzuki, K., Sumitani, J., Nam, Y. W., Nishimaki, T., Tani, S., Wakagi, T., et al. (2013). Crystal structures of glycoside hydrolase family 3 β-glucosidase 1 from *Aspergillus aculeatus*. *Biochem. J.* 452, 211–221.

Taylor, E. J., Goyal, A., Guerreiro, C. I., Prates, J. A., Money, V. A., Ferry, N., et al. (2005). How family 26 glycoside hydrolases orchestrate catalysis on different polysaccharides: structure and activity of a *Clostridium thermocellum* lichenase, CtLic26A. *J. Biol. Chem.* 280, 32761–32767. doi: 10.1074/jbc.M506580200

Thanh Tam, L. T., Jähne, J., Luong, P. T., Phuong Thao, L. T., Nhat, L. M., Blumenscheit, C., et al. (2023). Two plant-associated *Bacillus velezensis* strains selected after genome analysis, metabolite profiling, and with proved biocontrol potential, were enhancing harvest yield of coffee and black pepper in large field trials. *Front. Plant Sci.* 14:1194887. doi: 10.3389/fpls.2023.1194887

Tzipilevich, E., Russ, D., Dangl, J. L., and Benfey, P. N. (2021). Plant immune system activation is necessary for efficient root colonization by auxin-secreting beneficial bacteria. *Cell Host Microbe* 29, 1507–1520.e4. doi: 10.1016/j.chom.2021.09.005

Vera-Santander, V. E., Hernández-Figueroa, R. H., Jiménez-Munguía, M. T., Mani-López, E., and López-Malo, A. (2023). Health benefits of consuming foods with bacterial probiotics, postbiotics, and their metabolites: a review. *Molecules* 28:1230. doi: 10.3390/molecules28031230

Verschuuren, T., Bosch, T., Mascaro, V., Willems, R., and Kluytmans, J. (2022). External validation of WGS-based antimicrobial susceptibility prediction tools, KOVER-AMR and ResFinder 4.1, for *Escherichia coli* clinical isolates. *Clin. Microbiol. Infect.* 28, 1465–1470. doi: 10.1016/j.cmi.2022.05.024

Walker, B. J., Abeel, T., Shea, T., Priest, M., Abouelliel, A., Sakthikumar, S., et al. (2014). Pilon: an integrated tool for comprehensive microbial variant detection and genome assembly improvement. *PLoS One* 9:e112963. doi: 10.1371/journal.pone.0112963

Wang, Y., Wu, Y., Wang, Y., Xu, H., Mei, X., Yu, D., et al. (2017). Antioxidant properties of probiotic bacteria. *Nutrients* 9:521.

Wu, Z., Qi, X., Qu, S., Ling, F., and Wang, G. (2021). Dietary supplementation of *Bacillus velezensis* B8 enhances immune response and resistance against *Aeromonas veronii* in grass carp. *Fish Shellfish Immunol.* 115, 14–21. doi: 10.1016/j.fsi.2021.05.012

Xu, R., Aruhan, Xiu, L., Sheng, S., Liang, Y., Zhang, H., et al. (2019). Exopolysaccharides from *Lactobacillus buchneri* TCP016 attenuate LPS- and d-GalN-induced liver injury by modulating the gut microbiota. *J. Agric. Food Chem.* 67, 11627–11637. doi: 10.1021/acs.jafc.9b04323

Yang, J., Ning, H. C., Zhang, Q., Yue, J. Q., Cao, X. Y., Li, J. Y., et al. (2023). Effects of *Bacillus subtilis* BS-Z15 on intestinal microbiota structure and body weight gain in mice. *Probiotics Antimicrob. Proteins* 15, 706–715. doi: 10.1007/s12602-021-09897-y

Yao, D., Su, L., Li, N., and Wu, J. (2019). Enhanced extracellular expression of *Bacillus stearothermophilus* α-amylase in *Bacillus subtilis* through signal peptide optimization, chaperone overexpression and α-amylase mutant selection. *Microb. Cell Fact.* 18:69.

Yoon, S. H., Ha, S. M., Lim, J., Kwon, S., and Chun, J. (2017). A large-scale evaluation of algorithms to calculate average nucleotide identity. *Antonie Van Leeuwenhoek* 110, 1281–1286.

Zanphorlin, L. M., De Morais, M. A. B., Diogo, J. A., Domingues, M. N., De Souza, F. H. M., Ruller, R., et al. (2019). Structure-guided design combined with evolutionary diversity led to the discovery of the xylose-releasing exo-xylanase activity in the glycoside hydrolase family 43. *Biotechnol. Bioeng.* 116, 734–744. doi: 10.1002/bit.26899

Zeng, Z., Zhang, J., Li, Y., Li, K., Gong, S., Li, F., et al. (2022). Probiotic potential of *Bacillus licheniformis* and *Bacillus pumilus* isolated from Tibetan Yaks, China. *Probiotics Antimicrob. Proteins* 14, 579–594. doi: 10.1007/s12602-022-09939-z

Zhang, D., Gao, Y., Ke, X., Yi, M., Liu, Z., Han, X., et al. (2019). *Bacillus velezensis* LF01: *in vitro* antimicrobial activity against fish pathogens, growth performance enhancement, and disease resistance against streptococcosis in Nile tilapia (*Oreochromis niloticus*). *Appl. Microbiol. Biotechnol.* 103, 9023–9035. doi: 10.1007/s00253-019-10176-8

Zhang, J., Siika-Aho, M., Tenkanen, M., and Viikari, L. (2011). The role of acetyl xylan esterase in the solubilization of xylan and enzymatic hydrolysis of wheat straw and giant reed. *Biotechnol. Biofuels* 4:60. doi: 10.1186/1754-6834-4-60

Zhao, M., Chen, C., Yuan, Z., Li, W., Zhang, M., Cui, N., et al. (2021). Dietary *Bacillus subtilis* supplementation alleviates alcohol-induced liver injury by maintaining intestinal integrity and gut microbiota homeostasis in mice. *Exp. Ther. Med.* 22:1312. doi: 10.3892/etm.2021.10747

Zou, X. Y., Zhang, M., Tu, W. J., Zhang, Q., Jin, M. L., Fang, R. D., et al. (2022). *Bacillus subtilis* inhibits intestinal inflammation and oxidative stress by regulating gut flora and related metabolites in laying hens. *Animal* 16:100474. doi: 10.1016/j.animal.2022.100474

frontiers | Frontiers in Microbiology

TYPE Original Research
PUBLISHED 06 December 2023
DOI 10.3389/fmicb.2023.1320567

OPEN ACCESS

EDITED BY
Ren-You Gan,
Agency for Science, Technology and Research, Singapore

REVIEWED BY
Samara Paula Mattiello,
University of Tennessee Southern, United States
Hoi Leong Xavier Wong,
Hong Kong Baptist University, Hong Kong SAR, China

*CORRESPONDENCE
Jun-peng Yao
✉ yjpcdtcm@163.com
Ying Li
✉ liying@cdutcm.edu.cn

†These authors have contributed equally to this work and share first authorship

RECEIVED 12 October 2023
ACCEPTED 06 November 2023
PUBLISHED 06 December 2023

CITATION
Li Y-q, Yan X-y, Xiao X-j, Ma P-t, Wang S-q, Liu H-l, Zhang W, Chen M, Yao J-p and Li Y (2023) The gut microbiome and metabolites are altered and interrelated in patients with functional constipation.
Front. Microbiol. 14:1320567.
doi: 10.3389/fmicb.2023.1320567

The gut microbiome and metabolites are altered and interrelated in patients with functional constipation

Yan-qiu Li[1†], Xiang-yun Yan[1†], Xian-jun Xiao[2†], Pei-tao Ma[1], Si-qi Wang[1], Hui-lin Liu[1], Wei Zhang[1], Min Chen[3], Jun-peng Yao[1*] and Ying Li[1*]

[1]Acupuncture and Tuina School, Chengdu University of Traditional Chinese Medicine, Chengdu, Sichuan, China, [2]School of Health Preservation and Rehabilitation, Chengdu University of Traditional Chinese Medicine, Chengdu, Sichuan, China, [3]Anorectal Department, Hospital of Chengdu University of Traditional Chinese Medicine, Chengdu, Sichuan, China

Introduction: Gut microbiota and metabolites have been identified to contribute to the pathogenesis of functional constipation (FC); however, the underlying mechanism(s) have not been elucidated, and the relationship between the gut microbiota and metabolites in FC has received limited attention in the literature.

Methods: 16S rDNA sequencing and non-targeted metabolomic detection based on liquid chromatography-mass spectrometry (LC–MS/MS) technologies were combined to analyze the altered gut microbiome and metabolic profile of fecal samples from FC patients and healthy individuals (healthy control; HC).

Results: The richness and diversity of gut microbiota significantly ($p < 0.01$) increased in FC patients. Compared to the HC group, 18 genera, including *Intestinibacter*, *Klebsiella*, and *Akkermansia*, exhibited statistically significant changes ($p < 0.05$). Metabolic analysis showed that metabolic profiles were also markedly altered with 79 metabolites, such as (-)-caryophyllene oxide, chenodeoxycholic acid, and biliverdin, indicating significant inter-group differences ($p < 0.05$). Besides, the primary bile acid biosynthesis, as well as the metabolic profile of porphyrin and chlorophyll, were the most dominant enriched pathways (FDR < 0.01), in which chenodeoxycholic acid and biliverdin were significantly enriched, respectively. Correlation analysis demonstrated a strong relationship between 10 genera and 19 metabolites ($r > 0.6$, FDR < 0.05), and notably, *Intestinibacter* showed a negative correlation with biliverdin (FDR < 0.001), which highlighted the interplay of the gut microbiota and metabolites in the pathogenesis of FC.

Conclusion: Our research describes the characteristics of the gut microbiota and metabolic profiles and the correlation between the gut microbiota and metabolites in FC patients. This may contribute to the understanding of the underlying mechanisms involved in FC pathogenesis and may provide novel insights into therapeutic interventions.

KEYWORDS

functional constipation, gut microbiota, fecal metabolites, correlation analysis, clinical trial

Introduction

Functional constipation (FC) is an incurable gastrointestinal disorder characterized by recurrent reduced bowel movements, straining, and hard feces (Lacy et al., 2016). It is estimated that ~11.7% of the global population suffers from FC, and it is more prevalent in women (Barberio et al., 2021). In addition to paying for expensive medical care (Johanson and Kralstein, 2007), patients tend to face lower quality of life (Koloski et al., 2013) and higher risks of severe diseases such as colorectal cancer (Sumida et al., 2019). Moreover, the absence of targeted therapeutic interventions is attributed to the intricate and yet poorly understood pathophysiology of FC. Currently, laxatives are a favorable choice for alleviating relative symptoms of FC (Liu et al., 2016). However, frequent usage of laxatives can result in drug dependence and a cathartic colon; therefore, a laxative is not a satisfactory therapy for FC patients (Yao et al., 2022). Therefore, there is a perceived need to perform further research into the mechanism of FC, with the aim of enhancing the efficacy of treatment strategies.

The gut microbiome, resident in the intestinal tract of humans, establishes a mutualistic and symbiotic relationship with the host and can influence the physiology and pathology of the intestine (Reigstad and Kashyap, 2013). Although the mechanism of FC caused by gut microbiota is not well-known, researchers have reached an agreement that restoring the balance of gut microbiota can be beneficial for patients with FC (Wu et al., 2023). It has been shown that the manipulation of the gut microbiome has the potential to decrease the presence of inflammation factors and alleviate inflammatory reactions (Fontaine et al., 2015; Stein, 2021). Additionally, this manipulation has shown promise in restoring the integrity of the intestinal mucosal barrier and promoting regular movement of the intestinal tract (Fu et al., 2021). Besides, studies have discovered that *Bifidobacterium longum* and *Lacticaseibacillus rhamnosus* could soften stools and relieve the symptoms of FC (Lai et al., 2023). Therefore, FC management can be facilitated by analyzing the features of gut microbiota and elucidating the mechanism of FC mediated by the gut microbiome.

Gut metabolites, produced by the gut microbiota and host, help maintain gut microenvironment stability and physiological function. Correspondingly, the presence of aberrant gut metabolites can lead to impaired functioning of the gut microbiota and contribute to the development of several intestinal disorders. Studies have revealed that short-chain fatty acids (SCFAs), the common metabolites produced by the gut microbiota, can provide energy for intestinal epithelial cells and promote the contraction of intestinal smooth muscle to improve intestinal movement (Wang et al., 2019). Bile acids, crucial metabolites present in the human gut, possess the ability to modulate gut motility and impede the excessive proliferation of the gut microbiome, hence preserving the integrity of the gut mucosal barrier (Hofmann and Eckmann, 2006; Bunnett Nigel, 2014). Researchers have reported that regulating the abundance of these metabolites helps to improve the relative symptoms of FC (Liu et al., 2022; Jeong et al., 2023).

In short, dysregulation of the gut microbiota and associated metabolites constitutes significant elements in the development of FC and needs additional research. However, the available literature has mainly explored the pathogenesis of FC in terms of the gut microbiota, while the interaction of the microbiome and metabolites in the development of FC has been less reported. Therefore, we employed a combination of 16S rDNA sequencing and non-targeted metabolomic detection based on liquid chromatography-mass spectrometry (LC–MS/MS) technologies to analyze the alterations of the gut microbiome and metabolites in FC patients and explore the interactions of the differential gut microbiome and metabolites, with the ultimate goal of providing more support for future research on the mechanism and treatment of FC.

Methods

Recruitment and sample collection

Twenty-one FC patients were recruited from January 2022 to October 2022. Patients were diagnosed according to the Rome IV diagnostic criteria and recruited at the outpatient of the Affiliated Hospital of Chengdu University of Traditional Chinese Medicine (Sichuan Province, China). The inclusion criteria of patients were as follows: (1) diagnosed with FC by physicians according to the Rome IV criteria; (2) aged 18 to 60 years old; (3) not taking any drugs for FC for at least 1 week before recruitment; (4) maintaining regular eating habits and no extreme diets like vegetarian food; and (5) not suffering from severe anxiety, depression, or other psychological illness. In addition, 21 healthy individuals were mainly enrolled online (WeChat platform). We used online questionnaires and face-to-face communication to screen healthy individuals with the following requirements: (1) aged 18–60 years old; (2) complete spontaneous bowel movements (CSBMs) once a day and 6–7 times a week; (3) a fecal trait score of 4 according to Bristol scoring criteria; (4) defecation without abdominal pain or other discomforts; (5) not suffering from intestinal disorders or other diseases that can affect the intestinal flora; and (6) no extreme diets like vegetarian food. All FC patients and healthy individuals were to be excluded if they (1) received any probiotics or antibiotics or other therapies that may disturb the gut microbiota within a month before stool sample collection; (2) had any other diseases with gastrointestinal involvement; (3) had serious primary diseases such as progression cancer, severe cardiovascular diseases, or cognitive dysfunction, or were unable to cooperate; and (4) were pregnant or lactating women. Finally, written informed consent from all participants was obtained. This study was approved by Sichuan Provincial Commission of Traditional Chinese Medicine Regional Ethics Review (approval ID: 2021KL-023) and registered on the Chinese Clinical Trial Registry (ChiCTR2100048831). Fresh stool samples of all participants were collected in sterile stool containers and immediately transferred to the −80°C freezer.

DNA extraction and 16s rDNA sequencing

The sodium dodecyl sulfate (SDS) method was used to extract DNA from the fecal samples, and the quality and concentration of DNA were tested by agarose gel electrophoresis. Subsequently, the DNA was diluted to 1 ng/μl with sterile water. PCR amplification was performed on the 16S V3–V4 region. Specific primers with

barcode, Phusion® High Fidelity PCR Master Mix with GC Buffer (New England Biolabs), and high-efficiency, high-fidelity enzymes were selected for PCR to ensure amplification efficiency and accuracy. The PCR products were detected by 2% agarose gel electrophoresis, and equal amounts of samples were mixed according to the PCR product concentration, and then the PCR products were detected again. After that, the strips were recovered with an adhesive recovery kit (Qiagen). The Next® Ultra™ The IIDNA Library Preparation Kit (New England Biolabs) was used for library construction, which was subjected to test the Qubit and Q-PCR quantification. After the library was qualified, NovaSeq6000 was used for machine sequencing.

16s rDNA sequencing result analysis

After gaining the effective tags, the DADA2 module in QIIME2 software was used for noise reduction and filtering out sequences to obtain the final ASVs (Amplicon Sequence Variants) and feature table. Subsequently, the classify sklearn module in QIIME2 software was used to compare the obtained ASVs with the database to get species information for each ASV. According to the SILVA (v132) database, effective sequences were clustered into operational taxonomic units (OTUs) with 97% consistency, and the species annotation analysis was performed. The QIIME2 software (Version 1.9.1) was used to calculate the alpha diversity, including the Chao1 index, Shannon index, and Simpson index, and generate the rarefaction curve. An independent sample *t*-test was used to compare the inter-group difference of indices between the two groups, and Graphpad Prism software (Version 8) was used to generate a bar graph. R package (version 4.3.0) was used to perform the principal coordinates analysis (PCoA). The linear discriminant analysis (LDA) effect size (LEfSe) software was used to analyze and screen out the significantly differential microbiome, and the differential microbiome with LDA-value > 3 was selected. Finally, Spearman's correlation analysis was used to explore the correlation between clinical parameters of FC and differential microbiome [significance threshold was FDR (false discovery rate) < 0.05].

Fecal metabolome profiling

Metabolites were extracted from fecal samples after pretreatment. Fecal metabolites profiling was performed using the untargeted metabolomics approach through LC-MS/MS technology, which combined ultra-performance liquid chromatography (UHPLC) with high-resolution mass spectrometry. The chromatographic column was selected for the chromatographic conditions, the chromatographic column temperature remained at 45°C mobile phase, and the flow rate was kept at 0.2 mL/min. The mass spectrum condition was set as the ESI source, and the signal acquisition was collected in both positive and negative ion scanning modes. The mobile phase consisted of 0.1% formic acid (A) and methyl alcohol (B) in positive ion mode, while the mobile phase was 5 mM ammonium acetate (pH9.0) and methyl alcohol (B) in negative ion mode. The scanning range was set to m/z 100–1,500. The raw data files were imported into the Compound Discoverer 3.1 (Thermo Fisher) software to further perform qualitative and quantitative analysis.

LC-MS/MS metabolic analysis

Using SIMCA software (version 14.1), the orthogonal partial least-squares discriminant analysis (OPLS-DA) was performed to compare the differences between the two groups. The variable importance in projection (VIP) value of the first principal component, fold change, and *p*-value of *t*-test were calculated to screen out the significantly differential metabolites. Using the R package (version 4.3.0), volcano plots were generated to demonstrate the differential metabolites with fold change > 2, VIP value > 1.5, and $p < 0.05$. Kyoto Encyclopedia of Genes and Genomes (KEGG) pathway enrichment analysis was conducted to evaluate the relationship between the differential metabolites and different metabolic pathways via the MetaboAnalyst platform (https://www.metaboanalyst.ca/MetaboAnalyst/). Spearman's correlation analysis and Mantel test were used to explore the correlation between differential metabolites and clinical parameters of FC (significance threshold was FDR < 0.05).

Statistical analysis

Statistical analysis was performed using SPSS software (version 25.0), SIMCA software (version 14.1), GraphPad Prism software (version 8), and R package (version 4.3.0). Continuous variables with homogeneity of normal variance were expressed as mean ± SD and an independent sample *t*-test was used to compare the difference between the two groups, but the Wilcoxon rank-sum test was used for normal variables with unequal variances. Generally, $p < 0.05$ was considered statistically significant, and the Benjamini-Hochberg (BH) method was used to calculate the adjusted FDR *p*-value.

Moreover, Spearman's correlation analysis was used to explore the correlation between the differential gut microbiome and differential metabolites (significance threshold was FDR < 0.05). Through Random Forest analysis, the receiver operating characteristic curve (ROC) was drawn, and the area under the curve (AUC) was calculated to evaluate the discriminatory accuracy of the differential genera and differential metabolites.

Results

Characteristics of participants

In total, 21 patients with FC and 21 HC were enrolled in this study. The demographic and clinical presentation data are presented in Table 1. The average age and body mass index ($p > 0.05$) were balanced across the two groups, and no significant difference was found. Similarly, they had no significant difference in gender distribution. Compared to the HC group, fewer CSBMs per week, lower levels of bristol stool form scale (BSFS), and higher levels of straining during defecation were identified in the FC group ($p < 0.01$), and all these were the dominant manifestations of FC.

TABLE 1 Demographic and clinical presentation data of participants.

Variables		FC group	HC group	*p*-value
Age (means ± SD)		32.71 ± 9.62	27.90 ± 7.58	0.08
Gender, n	Female	21	21	-
	Male	0	0	
Body mass index (means ± SD)		20.67 ± 2.57	21.60 ± 2.39	0.27
Disease course (months) (means ± SD)		132.29 ± 73.79	-	-
CSBMs/week (means ± SD)		0.71 ± 0.78	7.48 ± 1.66	8.77×10^{-18}
BSFS (means ± SD)		2.74 ± 0.84	4.10 ± 0.40	5.09×10^{-6}
Straining during defecation (means ± SD)		1.04 ± 0.33	0.12 ± 0.21	3.29×10^{-8}
PAC-QOL index (means ± SD)		2.57 ± 0.61	1.14 ± 0.09	7.02×10^{-9}
SAS index (means ± SD)		42.26 ± 6.96	27.16 ± 6.58	3.57×10^{-7}
SDS index (means ± SD)		43.33 ± 8.88	27.89 ± 5.63	2.06×10^{-6}

Besides, the self-assessment of constipation quality of life (PAC-QOL) index, self-rating anxiety scale (SAS) index, and self-rating depression scale (SDS) index were much higher in the FC group than in the HC group ($p = 7.02 \times 10^{-9}$, $p = 3.57 \times 10^{-7}$, $p = 2.06 \times 10^{-6}$, respectively).

Alterations of the gut microbiome community associated with FC

Annotated with the SILVA (v132) database, a total of 5,077 OTUs were obtained with 97% similarity. A rarefaction curve based on observed species suggested the gut microbial richness was high in the FC group (Figure 1A). Additionally, the alpha diversity indices, including the Chao1 index, Shannon index, and Simpson index, also indicated that the microbial diversity in the FC group was significantly high ($p < 0.01$) (Figure 1B). The principal coordinates analysis (PCoA) showed a significant difference in beta diversity between the two groups, and ANOISM analysis revealed that the gut microbial community in the FC group changed appreciably ($R = 0.357$, $p < 0.005$) (Figure 1C).

The gut microbial structure at the phylum level in these two groups was analyzed, and the top 10 dominant taxa are presented in Figure 1D. Specifically, *Firmicutes* and *Bacteroidota* were the dominant taxa at the phylum level in these two groups, and there was no significant inter-group difference ($p > 0.05$). Among the 10 dominant phyla, the abundance of *Verrucomicrobiota* increased markedly in the FC group ($p < 0.01$). The significant differential genera between these two groups at the genus level are shown in Figure 1E. We noticed that *Eubacterium_coprostanoligenes_group*, *Oscillospiraceae_UCG-002*, *Eubacterium_ruminantium_group*, *Akkermansia*, *Klebsiella*, *Parabacteroides*, and *Lachnospiraceae_UCG-010* ($p < 0.001$) were significantly enriched in the FC group, while *ML635J-40_aquatic_group* was significantly enriched in the HC group ($p = 0.001$).

LEfSe analysis was conducted to further identify the key differential genera between the two groups, and 30 differential genera with LDA value > 3 were finally identified (Figures 2A, B). Further, 18 genera were identified to be the significantly differential microbiota through the *t*-test analysis ($p < 0.05$) (Supplementary Table S1). The dominant genera with higher abundance in the FC group were *Eubacterium_coprostanoligenes_group*, *Intestinibacter*, *Klebsiella*, *Eubacterium_ruminantium_group*, *Colidextribacter,* and *Akkermansia*. While *Gilliamella*, *ML635J_40_aquatic_group,* and *Parabacteroides* had higher abundance in the HC group.

To further investigate the associations between the gut microbiota and manifestations of FC, mantel tests were performed to demonstrate the correlation between the 18 differential genera and clinical indicators (Figure 2C). The result showed that these 18 genera were all significantly correlated with clinical parameters of FC (FDR < 0.05), and 15 genera were significantly correlated with CSBMs and BSFS, among which *Intestinibacter*, *Klebsiella*, *Eubacterium_coporstanoligenes_group,* and *Colidextribacter* enriched in the FC group were negatively correlated with CSBMs, BSFS, and PAC-QOL, and positively correlated with the course of FC, straining, SDS and SAS. *ML635J_40_aquatic_group* and *Gilliamella* showed the opposite correlation tendency (Supplementary Table S2). Besides, we could notice that 13 genera were significantly correlated with all these clinical indicators, suggesting these genera could not only have an impact on gut function but also the emotional state.

The potential function of the gut microbiome in the progress of FC

Besides, PICRUST was utilized to predict the potential function of the differential gut microbiota in FC. The result indicated that the differential gut microbiota could exert an effect on the energy metabolism, metabolism of cofactors and vitamins, lipid metabolism, and biosynthesis of other secondary metabolites ($p < 0.05$) (Figure 2D). After *p*-value adjustment, lipid metabolism and metabolism of cofactors and vitamins were still significant (FDR < 0.05) (Supplementary Table S3), which indicated that the change in the gut microbiome might have altered the lipid metabolism and metabolism of cofactors and vitamins in the progress of FC.

Alterations of fecal metabolites profiling associated with FC

To identify characteristic metabolites between the two groups, untargeted metabolomics was performed, and forty-two fecal samples (FC, $n = 21$, HC, $n = 21$) were analyzed. OPLS-DA score plots displayed that the fecal metabolites differed significantly

10.3389/fmicb.2023.1320567

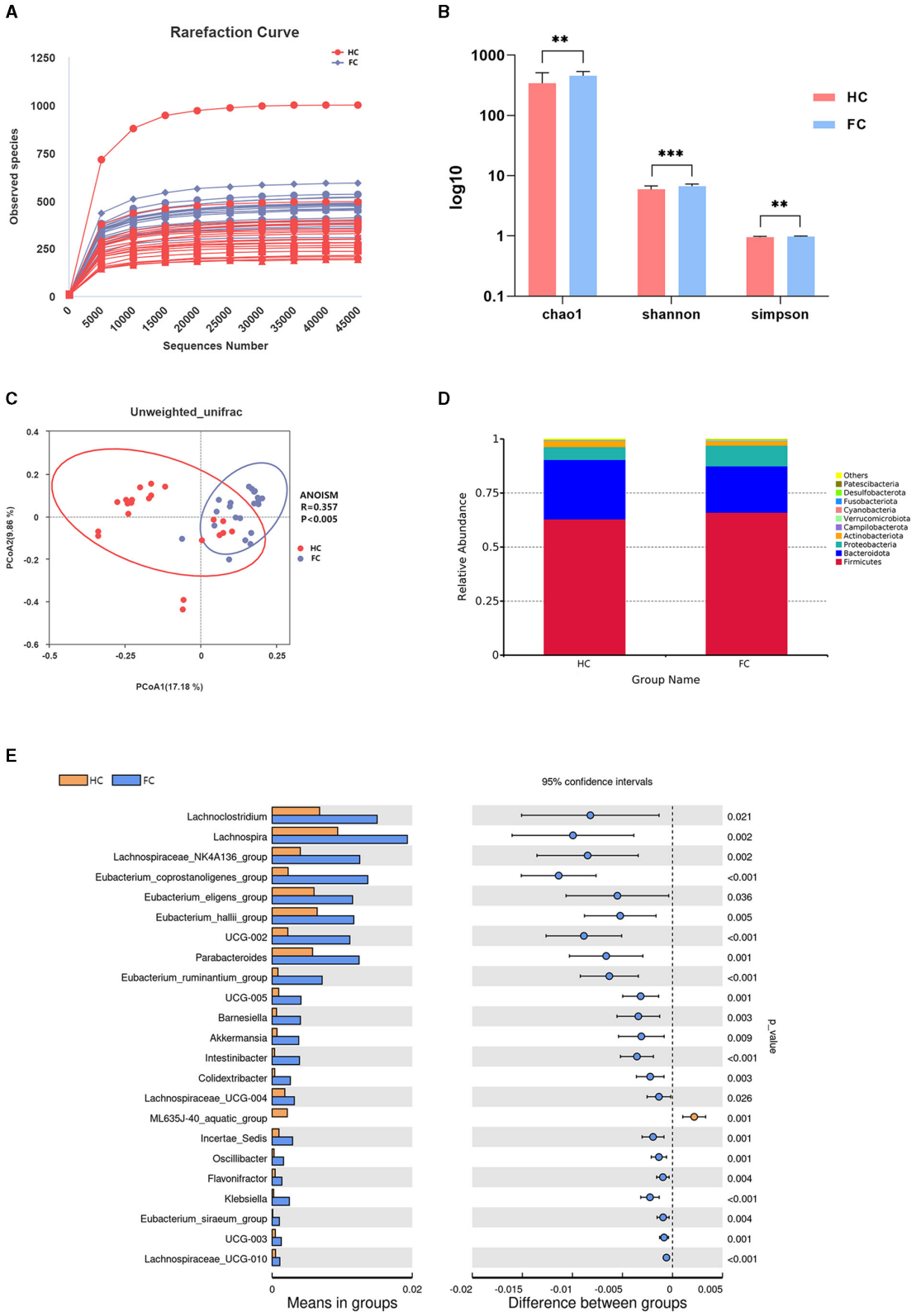

FIGURE 1
(A) Rarefaction curve. Each curve represents a sample. The nearly smooth curves indicate that sequencing samples are adequate. **(B)** Inter-group differences of alpha diversity indices, including the Chao1 index, Shannon index, and Simpson index. $^{***}p < 0.001$, $^{**}p < 0.01$. **(C)** PCoA plot showing the difference in the fecal microbial composition between the two groups. The abscissa and ordinate represent the two main components with the greatest contribution to explaining the inter-group difference. **(D)** Relative abundance of the microbiome at the phylum level of the two groups. **(E)** Differential microbiome of the FC and HC groups at the genus levels.

10.3389/fmicb.2023.1320567

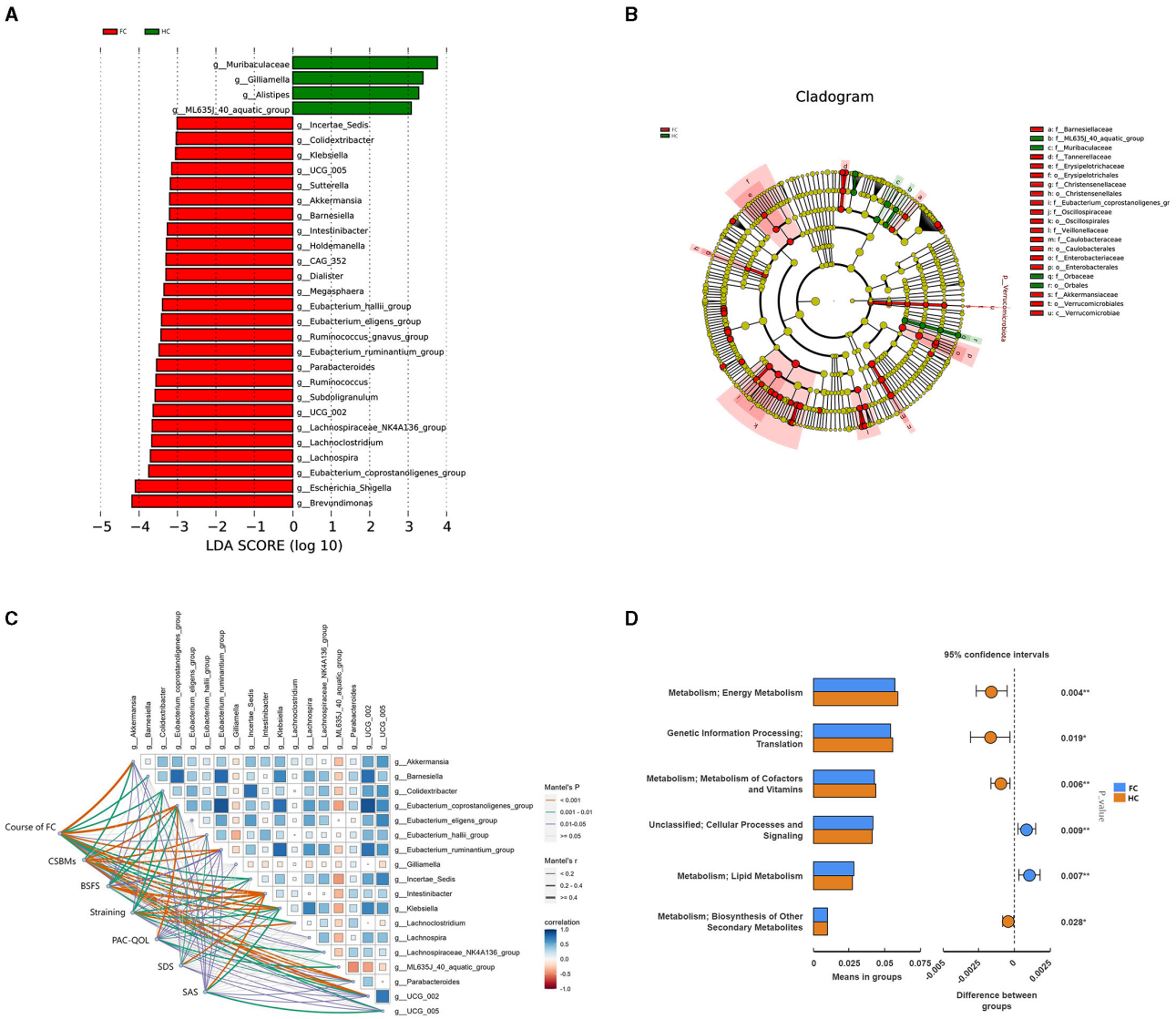

FIGURE 2
(A) LDA score diagram and the significantly differential genera. The color represents groups, and the length of the histogram represents the LDA score. The higher the score, the more significant difference in the differential microbiome. **(B)** Phylogenetic tree in the cladogram of differential taxa. Different colors represent different groups and different microbiota at different levels. **(C)** Pairwise comparisons of the gut genera with Spearman's correlation coefficient and the correlation between genera and clinical parameters with the Mantel test. The edge width represents Spearman's r-value for the corresponding distance correlations, and the color represents the statistical significance. Blue represents a positive correlation, and red represents a negative correlation. **(D)** PICRUST result indicating the potential function of differential microbiota. Red represents the HC group, and blue represents the FC group.

between the two groups in both positive and negative ion modes (Figures 3A, B). The 200 permutation test results verified that the OPLS-DA models were not overfitting (Figures 3C, D).

A total of 1,725 metabolites were identified, including 1,202 in positive ion mode and 523 in negative ion mode. Significantly differential metabolites between the two groups were screened by variable importance of projection (VIP) value, fold change, and *p*-value of *t*-test (fold change $>$ 2, VIP value $>$ 1.5, and $p < 0.05$ or fold change $<$ 0.5, VIP value $>$ 1.5, and $p < 0.05$). The results are shown in the volcano plots (Figures 3E, F). There were 42 markedly up-regulated metabolites and 39 markedly down-regulated metabolites in total (Supplementary Table S4). (-)-Caryophyllene oxide, 11-deoxy prostaglandin F1α, 3-(4-pyridyl methylidene) chroman-4-one, biliverdin, and chenodeoxycholic acid had higher abundance in the HC group, while glutaric acid, pipecolic acid, N-(2,4-Dimethylphenyl) formamide, and prostaglandin E2 had higher abundance in the FC group.

We then correlated the differential metabolites with clinical indicators to determine the association between differential fecal metabolites and the development of FC. The result showed that there were 78 differential metabolites significantly correlated with clinical parameters of FC (Supplementary Figure S1), and 57 metabolites were identified to be the main correlated differential metabolites with clinical parameters ($r > 0.5$, FDR < 0.05) (Supplementary Table S5). We could notice that N-(2,3-dihydro-1,4-benzodioxin-6-yl)-2,5-dimethyl-3-furamide,

10.3389/fmicb.2023.1320567

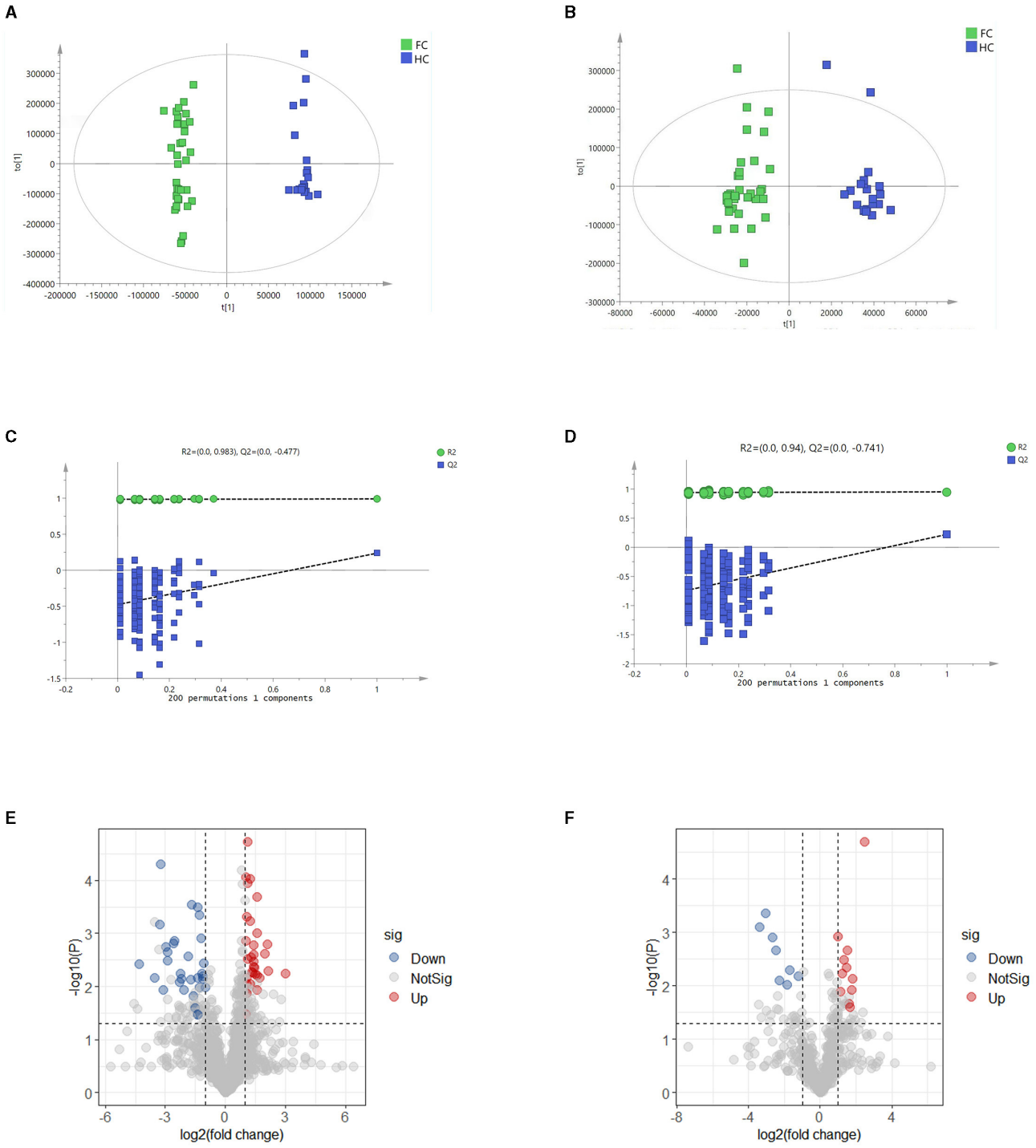

FIGURE 3
(A, B) OPLS-DA score plots in positive and negative ion models, respectively. The abscissa represents the difference between groups, and the ordinate represents the difference within groups. **(C, D)** Validation models through 200 permutation tests in positive and negative ion models, respectively. R2 and Q2 are the intercept values of the fitted lines on the ordinate, respectively, and represent the reliability and overfitting degree of the model. **(E, F)** Volcano plots in positive and negative models, respectively, indicate the discrimination of fecal metabolites between the two groups. The ordinate shows the -log10 (p-value), and the abscissa is the log2 (fold change) value. The screening threshold of significantly differential metabolites was fold change > 2, VIP value > 1.5, and p-value < 0.05 or fold change < 0.5, VIP value > 1.5, and p < 0.05. Every dot represents a kind of metabolite, and the blue ones represent the significantly down-regulated metabolites, while the red dots represent the significantly up-regulated metabolites. The gray dots represent the metabolites that have no significant difference between the two groups.

norverapamil, pipecolic acid, soyasaponin I, and biliverdin had the most significant correlations with FC. Besides, metabolites abundant in the HC group, such as biliverdin, guggulsterone, and chenodeoxycholic acid were positively correlated with CSBMs and BSFS, while metabolites enriched in the FC group such as 2-(3,5-dimethyl-1H-pyrazol-4-yl)-5-methoxy benzoic acid,

prostaglandin E2, norverapamil were negatively associated with CSBMs and BSFS, and positively associated with straining.

Annotation of differential metabolites through KEGG pathway enrichment analysis

Differential metabolites were further explored through the KEGG pathway enrichment analysis. It was found that differential metabolites were mainly involved in the primary bile acid biosynthesis, sphingolipid metabolism, arachidonic acid metabolism, porphyrin and chlorophyll metabolism, retinol metabolism, arginine and proline metabolism, cysteine and methionine metabolism, arginine biosynthesis alanine, aspartate, and glutamate metabolism (FDR < 0.05) (Figure 4A). Ten metabolites enriched in the above-mentioned pathways and seven significantly altered metabolites are further illustrated in Figure 4B, which exhibited a lower abundance of all-trans-13,14-Dihydroretinol, and a higher abundance of biliverdin, chenodeoxycholic acid, phytosphingosine, S-adenosylmethionine, prostaglandin E2, and agmatine in FC patients.

Correlation analysis between differential gut microbiota and fecal metabolites

To assess the interactions between gut microbiota and metabolites, we correlated the 18 differential genera and 57 differential metabolites (Figure 5A). Then, we constructed a correlation network graph to demonstrate the main interactions of microbiota and microbiome ($r > 0.6$, FDR < 0.05) (Figure 5B). We can observe that there were complex correlations between differential genera and metabolites. *Intestinibacter* was positively correlated with norverapamil ($r = 0.665$, FDR < 0.001) and negatively correlated with biliverdin ($r = -0.625$, FDR < 0.001). Besides, *Eubacterium_coprostanoligenes_group*, *Oscillospiraceae_UCG-005*, *Oscillospiraceae_UCG-002,* and *Eubacterium_ruminantium_group* appeared to be the core differential microbiota. These were found to be negatively correlated with (-)-caryophyllene oxide and glycerophospho-N-palmitoyl ethanolamine, which were the metabolites enriched in the HC group. On the other hand, they were positively correlated with N-Acetyl-L-tyrosine and 1-(4-methyl-2-morpholino-1,3-thiazol-5-yl) ethan-1-one, which were the differential metabolites enriched in the FC group. *Lachnoclostridium* was negatively correlated with guggulsterone ($r = -0.641$, FDR < 0.001) (Supplementary Table S6).

Function prediction analysis of differential microbiota and metabolites associated with FC

Subsequently, we calculated the AUC values of the differential genera and metabolites. Figure 5C illustrates the differential genera and metabolites with Spearman's r-value > 0.6. The result shows that the combinations of these genera and metabolites had great potential in distinguishing FC patients from HCs with an AUC-value > 0.907 [generally, an AUC value > 0.85 is thought to be a very good value for prediction (Gong et al., 2020)], indicating that the interplay of these genera and metabolites was vital pathogenesis of FC and worthy of further exploration. Besides, we calculated the AUC-values of these 10 genera and 19 metabolites to further identify the key genera or metabolites. It was observed that most differential microbiota had better predictive functions than differential metabolites (Supplementary Tables S7, S8); in particular, *Intestinibacter*, *Eubacterium_coprostanoligenes_group*, *Klebsiella*, *Colidextribacter,* and *Eubacterium_ruminantium_group* with AUC-values ≥ 0.9 had the highest discrimination ability.

Discussion

Functional constipation (FC) is a refractory condition that significantly impacts the wellbeing of individuals and diminishes their overall quality of life. Accumulated evidence shows that the alteration of gut microbiota and metabolites is crucial to the pathogenesis of FC. However, the contribution of gut microbiota and associated metabolites to the pathogenesis of FC has not been elucidated. In this study, we recruited 21 patients with FC and 21 healthy individuals to examine the alterations in the gut microbiome and fecal metabolites among FC patients and evaluate the association between the interaction of distinct gut microbiota and fecal metabolites with the progression of FC.

We found that the richness and diversity of gut microbiome significantly differed between patients with FC and healthy individuals, suggesting that gut microbiome dysbiosis occurred in the development of FC. *Intestinibacter*, *Eubacterium_coprostanoligenes_group*, *Klebsiella*, *Akkermansia*, *Eubacterium_ruminantium_group*, *Oscillospiraceae_UCG-005*, and *Oscillospiraceae_UCG-002* altered significantly and might be the core genera in the pathogenesis of FC.

Intestinibacter, *Klebsiella,* and *Akkermansia*, recognized as potential pathogens, were shown to be enriched in FC patients, which was consistent with previous research (Cao et al., 2017; Zeyue et al., 2022; Chen et al., 2023). *Intestinibacter* (Forbes et al., 2018; Xiang et al., 2023) and *Klebsiella* (Gevers et al., 2014; Li et al., 2022) were reported to have a close relationship with inflammatory responses in intestinal disorders; therefore, we speculated that the increased abundance of *Intestinibacter* and *Klebsiella* could disrupt the gut function by exerting intestinal inflammation, thus resulting in FC. *Akkermansia* can excessively degrade the mucin, causing dysfunction of the intestinal barrier and accumulation of harmful substances, ultimately leading to the development of intestinal disorders (Zhang et al., 2016). The *Eubacterium_coprostanoligenes_group*, *Eubacterium_ruminantium_group*, *Oscillospiraceae_UCG-002,* and *Oscillospiraceae_UCG-005* possess the ability to metabolize dietary fiber through fermentation processes and produce SCFAs which have been associated with various positive effects on gastrointestinal (Mukherjee et al., 2020; Hu et al., 2023) and mental health (Liang et al., 2022; Zhao et al., 2022). However, these genera had a higher abundance in the FC group. Furthermore, we

10.3389/fmicb.2023.1320567

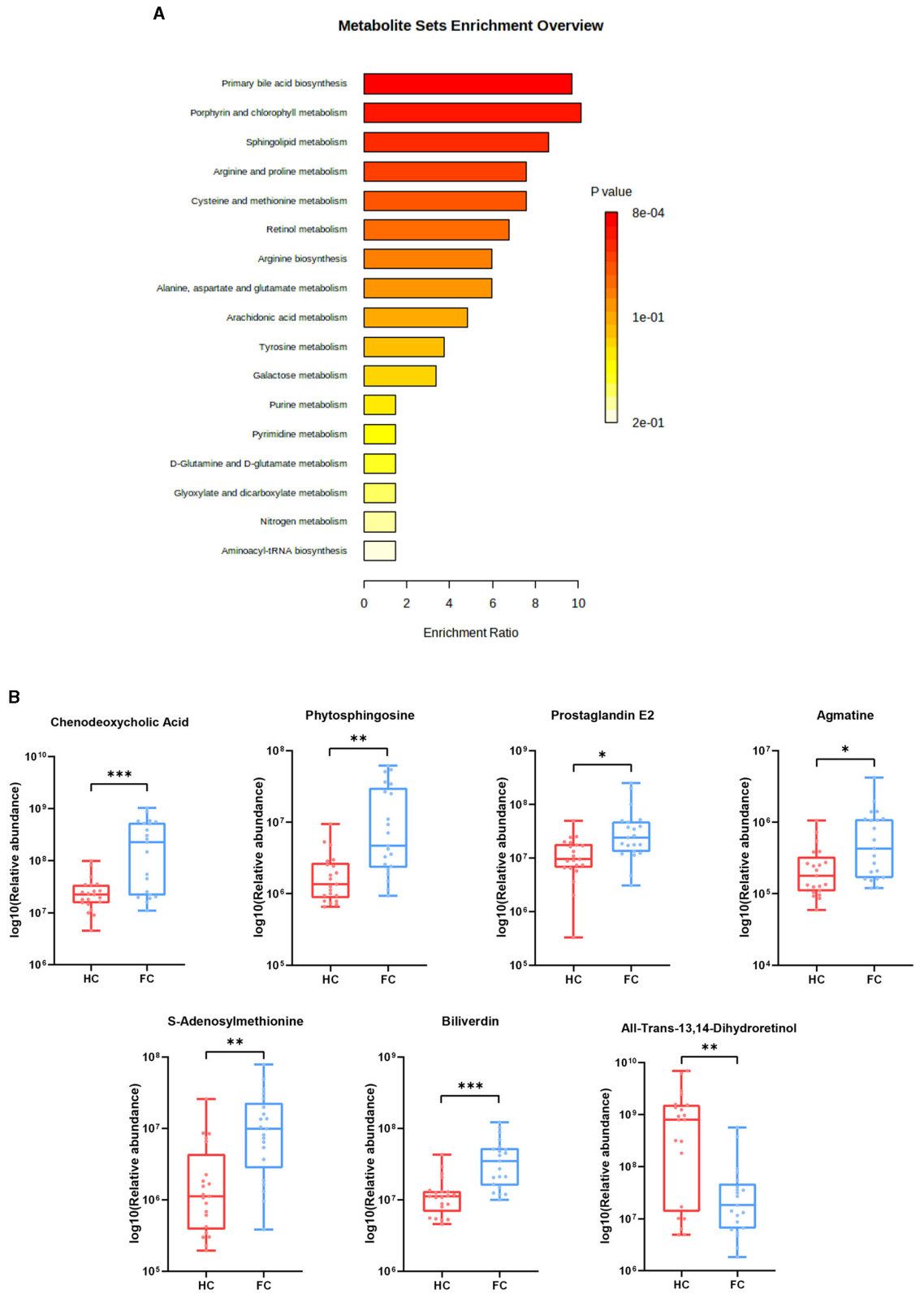

FIGURE 4
(A) Pathway enrichment bar plot of differential metabolites. The abscissa represents enrichment radio, and the ordinate represents enrichment pathways. **(B)** Seven differential metabolites were enriched in the pathways. ***$p < 0.001$, **$p < 0.01$, *$p < 0.05$.

10.3389/fmicb.2023.1320567

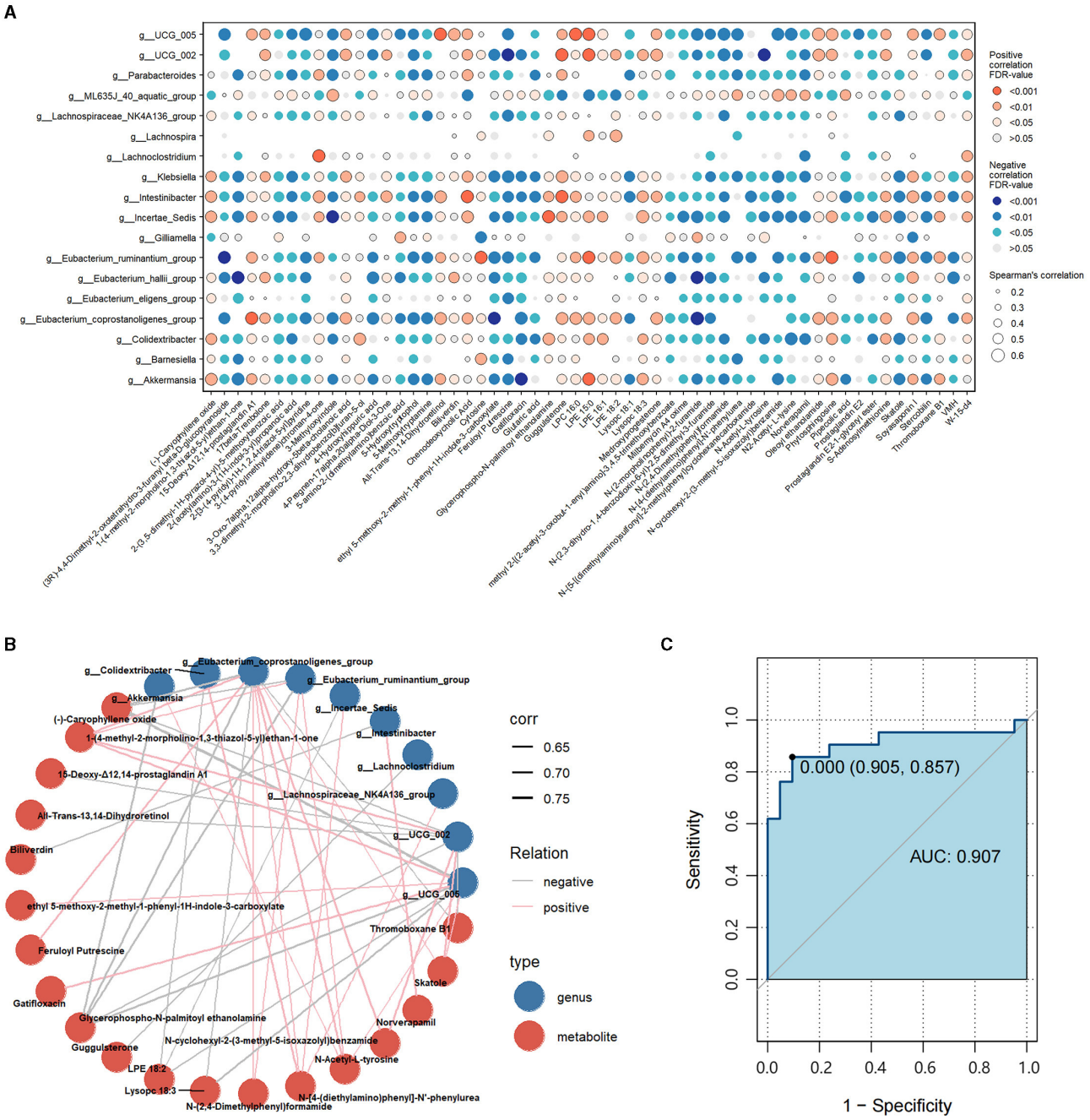

FIGURE 5
(A) Correlations between differential genera and differential metabolites. Red represents a positive correlation, and blue represents a negative correlation. The size of each dot represents the significant degree of correlation. **(B)** Correlation network graph of the differential genera and metabolites with Spearman's *r*-value > 0.6. Blue dots represent the differential genera, and red dots represent differential metabolites. Pink lines represent positive correlations, while gray lines represent negative correlations. The width of the line is proportional to the absolute value of the *r*-value. **(C)** ROC curves of the combination of the differential genera and metabolites with Spearman's *r*-value > 0.6.

found significant negative correlations between these genera and CSBMs, BSFS, and PAC-QOL and positive correlations between these genera and straining, SAS, and SDS, which suggest that these genera have a detrimental impact on the development of FC.

The aforementioned genera underwent substantial modifications and played a crucial role in diagnostics. They may serve as a key avenue for investigating the mechanism of FC and hold promise as potential therapy targets for FC in the future. In particular, *Intestinibacter* had the best diagnostic efficacy for FC, with the highest AUC = 0.975, and is expected to be a clinical diagnostic biomarker for FC. The findings from PICRUST and KEGG pathway enrichment analysis suggested that the alteration in the gut microbiome could influence the metabolism of lipids, cofactors, and vitamins, which leads us to hypothesize that such effects may arise from the interplay between differential metabolites and the gut microbiome.

In the analysis of metabolites, we discovered the alteration in fecal metabolites in FC patients. Primary bile acid production and porphyrin and chlorophyll metabolism were two of the most important metabolic processes where the differentiated metabolites were engaged. Among the metabolites implicated in these two pathways, chenodeoxycholic acid and biliverdin exhibited differential metabolic pathways. Chenodeoxycholic Acid can modulate the gastrointestinal secretory process and maintain normal defecation (Bazzoli et al., 1983). Consistent with previous research (Wong Banny et al., 2011), chenodeoxycholic acid was found to have a higher abundance in FC patients and was positively correlated with CSBMs, BSFS, and PAC-QOL, while being negatively correlated with straining, SAS, SDS, and the course of FC. Biliverdin was enriched in the HC group and showed a negative correlation with the pathogenesis of FC in our research. Researchers have reported that biliverdin could reduce pro-inflammatory mediators and relieve inflammatory responses (Wegiel et al., 2009; Bonelli et al., 2012). Besides, biliverdin can be reduced into bilirubin, which can alleviate immune inflammatory responses (Vitek et al., 2023) and is thought to be an effective prognostic biomarker for advanced colorectal cancer (Khoei et al., 2020).

Additionally, five notable differential metabolites were involved in other significant pathways. Phytosphingosine was enriched in the HC group and demonstrated a negative correlation with the development of FC. Studies indicated the strong anti-inflammatory activity of phytosphingosine *in vitro* and discovered that it could suppress the inflammatory responses in colitis mice (Montenegro-Burke et al., 2021). Similar to phytosphingosine, agmatine can also inhibit inflammatory responses. Moreover, agmatine has the potential to improve mood disorders (Freitas et al., 2016). In our study, agmatine was enriched in the HC group and was negatively associated with SDS and SAS. Thus, we assumed that agmatine may provide an explanation for the co-occurrence of anxiety or depression in individuals with FC. S-Adenosylmethionine (SAM), a type of bioactive substance involved in various biochemical reactions in the body (Pascale Rosa et al., 2022), had a higher abundance in the HC group. In this study, a positive correlation was observed between SAM and FC pathogenesis. It is possible that the gut microbiome has a self-balancing mechanism at play; however, further studies are needed to verify this assumption. Prostaglandin E2, involved in the arachidonic acid metabolism, can not only regulate the gut inflammatory response and promote the repair of intestinal mucosa but also regulate the expression of aquaporin 3 to regulate intestinal fluid metabolism (Na et al., 2021). In our study, increased levels of prostaglandin E2 were found among FC patients, and we thought that it may be attributed to a mechanism of self-regulation throughout the progression of FC.

In light of the intricate biological dynamics within the human gut, we conducted an analysis to establish the connections between the varied composition of microbiota and metabolites. In the correlation network, *Intestinibacter* was strongly negatively correlated with biliverdin. *Eubacterium_coprostanoligenes_group*, *Oscillospiraceae-UCG_005*, *Oscillospiraceae-UCG_002,* and *Eubacterium_ruminantium_group* were all negatively correlated with (-)-caryophyllene oxide and glycerophospho-N-palmitoyl ethanolamine, and positively correlated with 1-(4-methyl-2-morpholino-1,3-thiazol-5-yl) ethan-1-one. The abundance of (-)-caryophyllene oxide and glycerophospho-N-palmitoyl ethanolamine, which have been identified as metabolites with potential benefits in anti-inflammatory responses, was decreased in FC patients (Park et al., 2011; Li et al., 2021; Su et al., 2022). Conversely, the concentration of 1-(4-methyl-2-morpholino-1,3-thiazol-5-yl) ethan-1-one was observed to be elevated in the FC group. Despite the limited research on 1-(4-methyl-2-morpholino-1,3-thiazol-5-yl) ethan-1-one, our findings indicate its significant negative association with CSBMs and PAC-QOL. This suggests a potential interaction between 1-(4-methyl-2-morpholino-1,3-thiazol-5-yl) ethan-1-one and the gut microbiome, which may influence both the physiological functioning of the intestinal tract and the psychological wellbeing of patients.

In summary, our study found a complex and close relationship between significantly differential genera and metabolites. These altered genera and metabolites were reported to be related to inflammatory reactions; therefore, we speculated that these genera and their related metabolic profiles might mediate the occurrence of intestinal inflammation, affecting the integrity of intestinal mucosa and intestinal contractile function, thus resulting in FC. Biliverdin can reduce the release of pro-inflammatory factors in the gut of septic rats and improve intestinal contractility (Nakao et al., 2004). Besides, research has reported that biliverdin can be used in inflammatory bowel disease (Berberat et al., 2005). Therefore, biliverdin has the potential to be another therapy for FC by regulating intestinal microbiota and improving the relief of inflammatory reactions in the gut. However, this hypothesis still needs to be verified in future large-sample studies. Additionally, (-)-caryophyllene oxide, glycerophospho-N-palmitoyl ethanolamine, N-[4-(diethylamino)phenyl]-N'-phenylurea, and 1-(4-methyl-2-morpholino-1,3-thiazol-5-yl)ethan-1-one are the most correlated metabolites in the correlation network and might exert a more comprehensive and extensive regulation on the disordered gut microbiota, which are also worth further exploration.

Despite the rigorous adherence to scheduling and implementation in this clinical trial, there were several limitations in this study. Due to the small sample size, the results may be limited for generalization; thus, trials with larger sample sizes are required to verify the suggested associations. Besides, it is well-known that the composition of gut microbiota varies across different age groups. However, the sample size of our research was not sufficient to conduct in-depth research on the differences in the gut microbiota related to aging. Therefore, exploring the changes in the gut microbiota of FC patients at different ages is one of the feasible research directions that may improve clinical treatment. Moreover, it is worth mentioning that we did not confirm the causal relationship between the gut microbiota, metabolites, and clinical parameters in this research, and more studies are needed to further explore this in the future.

Conclusion

In conclusion, our research demonstrates the characteristics of the gut microbiota and metabolic profiles in FC patients. Investigating the underlying mechanism of FC can yield valuable insights for the improvement of FC treatment strategies. Future

research should aim to validate the interaction between the gut microbiota and metabolites in the development of FC. These endeavors may facilitate the discovery of novel therapeutic interventions for individuals affected by FC.

Data availability statement

The data presented in the study are deposited in the National Library of Medicine (https://submit.ncbi.nlm.nih.gov/) repository, accession number: PRJNA1031121.

Ethics statement

The studies involving humans were approved by Sichuan Provincial Commission of Traditional Chinese Medicine Regional Ethics Review (Approval ID: 2021KL-023). The participants provided their written informed consent to participate in this study.

Author contributions

Y-qL: Formal analysis, Methodology, Software, Writing – original draft. X-yY: Data curation, Formal analysis, Software, Writing – review & editing. X-jX: Data curation, Formal analysis, Methodology, Writing – review & editing. P-tM: Methodology, Resources, Writing – review & editing. S-qW: Methodology, Resources, Writing – review & editing. H-lL: Methodology, Resources, Writing – review & editing. WZ: Resources, Validation, Writing – review & editing. MC: Resources, Validation, Writing – review & editing. J-pY: Conceptualization, Project administration, Writing – review & editing. YL: Conceptualization, Funding acquisition, Project administration, Writing – review & editing.

Funding

The author(s) declare financial support was received for the research, authorship, and/or publication of this article. This study was supported by a grant from the National Natural Science Foundation of China (NO.82074554).

Conflict of interest

The authors declare that the research was conducted in the absence of any commercial or financial relationships that could be construed as a potential conflict of interest.

Publisher's note

All claims expressed in this article are solely those of the authors and do not necessarily represent those of their affiliated organizations, or those of the publisher, the editors and the reviewers. Any product that may be evaluated in this article, or claim that may be made by its manufacturer, is not guaranteed or endorsed by the publisher.

Supplementary material

The Supplementary Material for this article can be found online at: https://www.frontiersin.org/articles/10.3389/fmicb.2023.1320567/full#supplementary-material

References

Barberio, B., Judge, C., Savarino, E. V., and Ford, A. C. (2021). Global prevalence of functional constipation according to the Rome criteria: a systematic review and meta-analysis. *Lancet Gastroenterol. Hepatol.* 6, 3800856. doi: 10.2139/ssrn.3800856

Bazzoli, F., Malavolti, M., Petronelli, A., Barbara, I., and Roda, E. (1983). Treatment of constipation with chenodeoxycholic acid. *J. Int. Med. Res.* 11, 120–123. doi: 10.1177/030006058301100211

Berberat, P. O., Rahim, Y. I., Yamashita, K., Warny, M. M., Csizmadia, E., Robson, S. C., et al. (2005). Heme oxygenase-1-generated biliverdin ameliorates experimental murine colitis. *Inflamm. Bowel Dis.* 11, 350–359. doi: 10.1097/01.MIB.0000164017.06538.8a

Bonelli, M., Savitskaya, A., Steiner, C.-W., Rath, E., Bilban, M., Wagner, O., et al. (2012). Heme oxygenase-1 end-products carbon monoxide and biliverdin ameliorate murine collagen induced arthritis. *Clin. Exp. Rheumatol.* 30, 73–78.

Bunnett Nigel, W. (2014). Neuro-humoral signalling by bile acids and the TGR5 receptor in the gastrointestinal tract. *J. Physiol.* 592, 2943–2950. doi: 10.1113/jphysiol.2014.271155

Cao, H., Liu, X., An, Y., Zhou, G., Liu, Y., Xu, M., et al. (2017). Dysbiosis contributes to chronic constipation development via regulation of serotonin transporter in the intestine. *Sci. Rep.* 7, 8. doi: 10.1038/s41598-017-10835-8

Chen, E., Mahurkar-Joshi, S., Liu, C., Jaffe, N., Labus, J., Dong, T., et al. (2023). The association between a mediterranean diet and symptoms of irritable bowel syndrome. *Clin Gastroenterol Hepatol.* 162, S939. doi: 10.1016/j.cgh.2023.07.012

Fontaine, C. A., Skorupski, A. M., Vowles, C. J., Anderson, N. E., Poe, S. A., and Eaton, K. A. (2015). How free of germs is germ-free? Detection of bacterial contamination in a germ free mouse unit. *Gut Microbes* 6, 1054596. doi: 10.1080/19490976.2015.1054596

Forbes, J. D., Chen, C.-Y., Knox, N. C., Marrie, R.-A., El-Gabalawy, H., de Kievit, T., et al. (2018). A comparative study of the gut microbiota in immune-mediated inflammatory diseases-does a common dysbiosis exist? *Microbiome* 6, 221. doi: 10.1186/s40168-018-0603-4

Freitas, A., Neis, V., and Rodrigues, A. L. S. (2016). Agmatine, a potential novel therapeutic strategy for depression. *Eur. Neuropsychopharmacol.* 26, 1885–1899. doi: 10.1016/j.euroneuro.2016.10.013

Fu, R., Li, Z., Zhou, R., Li, C., Shao, S., and Li, J. (2021). The mechanism of intestinal flora dysregulation mediated by intestinal bacterial biofilm to induce constipation. *Bioengineered* 12, 6484–6498. doi: 10.1080/21655979.2021.1973356

Gevers, D., Kugathasan, S., Denmsen, L. A., Baeza, Y. V., Treuren, W. Y., Ren, B., et al. (2014). The treatment-naive microbiome in new-onset crohn's disease. *Cell Host Microbe* 15, 382–392. doi: 10.1016/j.chom.2014.02.005

Gong, C. G., Song, R. S., and Jin, S. (2020). Pulmonary fibrosis alters gut microbiota and associated metabolites in mice: an integrated 16S and metabolomics analysis. *Life Sci.* 264, 118616. doi: 10.1016/j.lfs.2020.118616

Hofmann, A. F., and Eckmann, L. (2006). How bile acids confer gut mucosal protection against bacteria. *Proc. Natl. Acad. Sci. USA.* 103, 4333–4334. doi: 10.1073/pnas.0600780103

Hu, S., Ma, Y., Xiong, K., Wang, Y., Liu, Y., Sun, Y., et al. (2023). Ameliorating effects of vitamin K2 on dextran sulfate sodium-induced ulcerative colitis in mice. *Int. J. Mol. Sci*. 24. doi: 10.3390/ijms24032986

Jeong, J., Ganesan, R., Jin, Y., Park, H. J., Min, B. H., Jeaong, M. K., et al. (2023). Multi-strain probiotics alleviate loperamide-induced constipation by adjusting the microbiome, serotonin, and short-chain fatty acids in rats. *Front. Microbiol*. 14, 1174968. doi: 10.3389/fmicb.2023.1174968

Johanson, J. F., and Kralstein, J. (2007). Chronic constipation: a survey of the patient perspective. *Aliment. Pharmacol. Ther*. 25, 599–608. doi: 10.1111/j.1365-2036.2006.03238.x

Khoei, N. S., Jenab, M., Murphy, N., Banbury, B. L., Carreras-Torres, R., Viallon, V., et al. (2020). Circulating bilirubin levels and risk of colorectal cancer: serological and Mendelian randomization analyses. *BMC Med*. 18, 1703. doi: 10.1186/s12916-020-01703-w

Koloski, N. A., Jones, M., Wai, R., Gill, R. S., Byles, J., and Talley, N. J. (2013). Impact of persistent constipation on health-related quality of life and mortality in older community-dwelling women. *Am. J. Gastroenterol*. 108, 137. doi: 10.1038/ajg.2013.137

Lacy, B. E., Mearin, F., Chang, L., Chey, W. D., Lembo, A. J., Simren, M., et al. (2016). Bowel disorders. *Gastroenterology*. 150, 1393–1407. doi: 10.1053/j.gastro.2016.02.031

Lai, H., Li, Y., He, Y., Chen, F., Mi, B., Li, J., et al. (2023). Effects of dietary fibers or probiotics on functional constipation symptoms and roles of gut microbiota: a double-blinded randomized placebo trial. *Gut Microbes* 15, 2197837. doi: 10.1080/19490976.2023.2197837

Li, J., Gao, Q., Ma, Y., Deng, Y., Li, S., Shi, N., et al. (2022). Causality of opportunistic pathogen klebsiella pneumoniae to hypertension development. *Hypertension (Dallas, Tex:* 1979). 79, 2743–2754. doi: 10.1161/HYPERTENSIONAHA.122.18878

Li, W.-X., Qian, P., Guo, Y.-T., Gu, L., Jurat, J., Bai, Y., et al. (2021). Myrtenal and β-caryophyllene oxide screened from Liquidambaris Fructus suppress NLRP3 inflammasome components in rheumatoid arthritis. *BMC Complem. Med. Therap*. 21. doi: 10.1186/s12906-021-03410-2

Liang, S., Sin, Z. Y., Yu, J., Zhao, S., Xi, Z., Bruzzone, R., et al. (2022). Multi-cohort analysis of depression-associated gut bacteria sheds insight on bacterial biomarkers across populations. *Cellul. Mol. Life Sci.* 80, 2. doi: 10.1007/s00018-022-04650-2

Liu, X., Li, M., Jian, C., Wei, F., Liu, H., Li, K., et al. (2022). *Astragalus* polysaccharide alleviates constipation in the elderly via modification of gut microbiota and fecal metabolism. *Rejuvenation Res*. 25, 275–290. doi: 10.1089/rej.2022.0039

Liu, Z., Yan, S., Wu, J., He, L., Li, N., Dong, G., et al. (2016). (2022). Acupuncture for chronic severe functional constipation: a randomized trial. *Ann. Intern. Med*. 165, 761–769. doi: 10.7326/M15-3118

Montenegro-Burke, J. R., Kok, B. P., Guijas, C., Domingo-Almenara, X., Moon, C., Galmozzi, A., et al. (2021). Metabolomics activity screening of T cell-induced colitis reveals anti-inflammatory metabolites. *Sci. Signal*. 14, 6584. doi: 10.1126/scisignal.abf6584

Mukherjee, A., Lordan, C., Ross, R. P., and Cotter, P. D. (2020). Gut microbes from the phylogenetically diverse genus Eubacterium and their various contributions to gut health. *Gut Microbes* 12. doi: 10.1080/19490976.2020.1802866

Na, Y. R., Jung, D., Stakenborg, M., Jang, H., Gu, G. J., Jeong, M. R., et al. (2021). Prostaglandin E(2) receptor PTGER4-expressing macrophages promote intestinal epithelial barrier regeneration upon inflammation. *Gut* 70, 2249–2260. doi: 10.1136/gutjnl-2020-322146

Nakao, A., Otterbein, L. E., Overhaus, M., Sarady, J. K., Tsung, A., Kimizuka, K., et al. (2004). Biliverdin protects the functional integrity of a transplanted syngeneic small bowel. *Gastroenterology* 127, 595–606. doi: 10.1053/j.gastro.2004.05.059

Park, K. R., Nam, D., Yun, H. M., Lee, S-G., Jang, H., Sethi, G., et al. (2011). β-Caryophyllene oxide inhibits growth and induces apoptosis through the suppression of PI3K/AKT/mTOR/S6K1 pathways and ROS-mediated MAPKs activation. *Cancer Lett*. 312, 178–188. doi: 10.1016/j.canlet.2011.08.001

Pascale Rosa, M., Simile Maria, M., Calvisi Diego, F., Feo, C., and Feo, F. (2022). S-Adenosylmethionine: from the discovery of its inhibition of tumorigenesis to its use as a therapeutic agent. *Cells* 11, 409. doi: 10.3390/cells11030409

Reigstad, C. S., and Kashyap, P. C. (2013). Understanding the impact of gut microbiota on host biology. *Neurogastroenterol. Motil*. 25, 358–372. doi: 10.1111/nmo.12134

Stein, J. M. (2021). Fecal microbiota transplantation modulates the gut flora favoring patients with functional constipation. *Front. Microbiol*. 12, 700718. doi: 10.3389/fmicb.2021.700718

Su, L., Zeng, Y., Li, G., Chen, J., and Chen, X. (2022). Quercetin improves high-fat diet-induced obesity by modulating gut microbiota and metabolites in C57BL/6J mice. *Phytotherapy research: PTR* 36. doi: 10.1002/ptr.7575

Sumida, K., Molnar, M. Z., Potukuchi, P. K., Thomas, F., Lu, J., Yamagata, K., et al. (2019). Constipation and risk of death and cardiovascular events. *Atherosclerosis* 281, 114–120. doi: 10.1016/j.atherosclerosis.2018.12.021

Vitek, L., Hinds Terry, D., Stec David, E., and Tribelli, C. (2023). The physiology of Bilirubin: health and disease equilibrium. *Trends Mol. Med*. 29. doi: 10.1016/j.molmed.2023.01.007

Wang, X., Yang, B., Yin, J., Wei, W., and Chen, J. D. Z. (2019). Electroacupuncture via chronically implanted electrodes improves gastrointestinal motility by balancing sympathovagal activities in a rat model of constipation. *Am. J. Physiol. Gastrointest. Liver Physiol*. 316, G797–G805. doi: 10.1152/ajpgi.00018.2018

Wegiel, B., Baty, C. J., Gallo, D., Csizmadia, E., Scott, J. R., Akhavan, A., et al. (2009). Cell surface biliverdin reductase mediates biliverdin-induced anti-inflammatory effects via phosphatidylinositol 3-kinase and Akt. *J. Biol. Chem*. 284, 21369–21378. doi: 10.1074/jbc.M109.027433

Wong Banny, S., Camilleri, M., Mckinzie, S., Burton, D., Graffner, H., Zinsmeister, A. R. (2011). Effects of A3309, an ileal bile acid transporter inhibitor, on colonic transit and symptoms in females with functional constipation. *Am. J. Gastroenterol*. 106, 2154–2164. doi: 10.1038/ajg.2011.285

Wu, L., Yuan, Q., Wu, L., Xia, H. H.-X., Zhong, M., Liu, T., et al. (2023). Efficacy of washed microbiota transplantation for therapeutic targets of refractory functional constipation and the influencing factors: a single-center, retrospective, 24-week follow-up study. *BMC Gastroenterol*. 23, 7. doi: 10.1186/s12876-023-02929-7

Xiang, Y., Zhang, C., Wang, J., Cheng, Y., Wang, L., Tong, Y., et al. (2023). Identification of host gene-microbiome associations in colorectal cancer patients using mendelian randomization. *J. Transl. Med*. 21, 9. doi: 10.1186/s12967-023-04335-9

Yao, J., Yan, X., Chen, L., Li, Y., Zhang, L., Chen, M., et al. (2022). Efficacy and microRNA-gut microbiota regulatory mechanisms of acupuncture for severe chronic constipation: study protocol for a randomized controlled trialand#13. *Front. Med*. 9, 906403. doi: 10.3389/fmed.2022.906403

Zeyue, Y. U., Liyu, H., Zongyuan, L. I., Jianhui, S., Hongying, C., Hairu, H., et al. (2022). Correlation between slow transit constipation and spleen Qi deficiency, and gut microbiota: a pilot study. *J. Tradit. Chinese Med*. 42, 353–363. doi: 10.19852/j.cnki.jtcm.20220408.002

Zhang, Z., Wu, X., Cao, S., Wang, L., Wang, D., Yang, H., et al. (2016). Caffeic acid ameliorates colitis in association with increased Akkermansia population in the gut microbiota of mice. *Oncotarget* 7, 9306. doi: 10.18632/oncotarget.9306

Zhao, H., Gao, X., Liu, Z., Zhang, L., Fang, X., Sun, J., et al. (2022). Sodium alginate prevents non-alcoholic fatty liver disease by modulating the gut–liver axis in high-fat diet-fed rats. *Nutrients* 14, 4846. doi: 10.3390/nu14224846

frontiers | Frontiers in Microbiology

TYPE Original Research
PUBLISHED 14 December 2023
DOI 10.3389/fmicb.2023.1256748

OPEN ACCESS

EDITED BY
Hesong Wang,
Southern Medical University, China

REVIEWED BY
Yu Pi,
Chinese Academy of Agricultural Sciences, China
Naresh Chandra Bal,
KIIT University, India

*CORRESPONDENCE
Peishi Yan
✉ yanps@hotmail.com

RECEIVED 11 July 2023
ACCEPTED 13 November 2023
PUBLISHED 14 December 2023

CITATION
Li J, Cui Z, Wei M, Almutairi MH and Yan P (2023) Omics analysis of the effect of cold normal saline stress through gastric gavage on LPS induced mice.
Front. Microbiol. 14:1256748.
doi: 10.3389/fmicb.2023.1256748

Omics analysis of the effect of cold normal saline stress through gastric gavage on LPS induced mice

Jing Li[1], Zhihao Cui[1], Ming Wei[1], Mikhlid H. Almutairi[2] and Peishi Yan[1]*

[1]College of Animal Science and Technology, Nanjing Agricultural University, Nanjing, China, [2]Department of Zoology, College of Science, King Saud University, Riyadh, Saudi Arabia

Cold stress is a significant environmental stimulus that negatively affects the health, production, and welfare of animals and birds. However, the specific effects of cold stimulation combined with lipopolysaccharide (LPS) on the mouse intestine remain poorly understood. Therefore, we designed this research to explore the effect of cold stimulation + LPS on mice intestine via microbiome and microbiota sequencing. Forty-eight mice were randomly divided into four experimental groups (n = 12): Control (CC), LPS-induced (CL), cold normal saline-induced (MC) and LPS + cold normal saline-induced (ML). Our results showed body weight was similar among different groups of mice. However, the body weight of mice in groups CC and CL were slightly higher compared to those in groups MC and ML. The results of gene expressions reflected that CL and ML exposure caused gut injury and barrier dysfunction, as evident by decreased *ZO-1*, *OCCLUDIN* ($P < 0.01$), and *CASPASE-1* ($P < 0.01$) expression in the intestine of mice. Moreover, we found that cold stress induced oxidative stress in LPS-challenged mice by increasing malondialdehyde (MDA) accumulation and decreasing the antioxidant capacity [glutathione peroxidase (GSH-Px), superoxide dismutase (SOD), total and antioxidant capacity (T-AOC)]. The cold stress promoted inflammatory response by increased IL-1β in mice treated with cold normal saline + LPS. Whereas, microbiome sequencing revealed differential abundance in four phyla and 24 genera among the mouse groups. Metabolism analysis demonstrated the presence of 4,320 metabolites in mice, with 43 up-regulated and 19 down-regulated in CC vs. MC animals, as well as 1,046 up-regulated and 428 down-regulated in ML vs. CL animals. It is Concluded that cold stress enhances intestinal damage by disrupting the balance of gut microbiota and metabolites, while our findings contribute in improving management practices of livestock in during cold seasons.

KEYWORDS

cold stress, LPS, mice, microbiome, metabolism

Introduction

Cold stress is an important environmental stimulation factor to animals and human beings in cold regions and during wintertime in other regions, which bring negative effects on health, production and welfare of animals and birds (Wei et al., 2018; Liu et al., 2022). Previous studies found that cold stimulation effect the productivity, oxidative resistance and immune dysfunction (Li et al., 2020; Liu et al., 2022). The enteric canal is a useful organ for nutrient absorption and regulation of immune function (Lee et al., 2018), and this organ is sensitive to stressors like cold stimulation, which cause inflammation reactions, oxidative stress, and intestinal injury in animals (Fu et al., 2013; Zhao et al., 2013). Many intestinal pathogens are related to stress like inflammatory bowel disease and injury (Lee et al., 2018). Water is important for body health and physiological activities, but it is reported that weaned piglets drinking warm (30°C) water has a better feed-to-weight ratio than those drinking cold (13°C) water (Zhang et al., 2020), which implied that low-temperature drinking water is a cold stress factor. Lipopolysaccharide (LPS) is a pathogenic component derived from gram-negative bacteria, which produce an immune response and lead to injury through oxidative damage (Meng et al., 2022). LPS is widely used to induce enteric canal inflammation and oxidative damage in different animals (Hassan et al., 2021; Feng et al., 2023).

Gut microbiota comprises of trillions of microorganisms, such as archaea, parasites, fungi, viruses, and bacteria (Naibaho et al., 2021; Ruigrok et al., 2023). These microorganisms contribute to the absorption and metabolism of nutrition, protect against pathogens, and is helpful to develop host's immune system (Nishida et al., 2018). Gut dysbiosis is commonly linked with intestinal diseases like irritable bowel syndrome (Nishino et al., 2018), inflammatory bowel disease (Matsuoka and Kanai, 2015), and salmonellosis (Aljahdali et al., 2020). Previous studies have confirmed an intestinal imbalance in LPS-induced animals (Chen et al., 2022; Ruan et al., 2022; Wang et al., 2022).

Lipopolysaccharide is known as a major activator of the inflammatory response, it binds to toll-like receptor 4 (TLR4), activates nuclear factor kappa B (NF-κB) and enhances the inflammation through the production of pro-inflammatory cytokines and injury to endothelial cells (Joo et al., 2016). In rat and rabbit animal models, LPS-induced systemic inflammation is depend on several factors including ambient temperature and LPS dose (Romanovsky et al., 2005). At a low temperature (cold stress), low doses of LPS causes fever and several sequential, while at neutral temperature even high doses of LPS cause low fever and less detrimental effects (Romanovsky et al., 2005; Rudaya et al., 2005).

Thus, we hypothesized that exposure to cold temperature is a factor that aggravates inflammation. To evaluate this hypothesis, we investigated the effect of cold stress on the severity of inflammatory responses due to LPS in mouse model. Therefore, we examined the impact of cold stress and LPS on the mouse intestine via microbiome and microbiota sequencing.

Materials and methods

Animals, experimental design and sample collection

A total of 48 four-week-old ICR mice (24 males and 24 females) with a middle weight of 18 ± 2.2 g was purchased from Qinglongshan Animal Breeding (Nanjing, China). After 3-day of acclimatization period, mice were randomly divided into four groups: control group (CC), LPS-induced group (CL), cold normal saline-induced group (MC), and LPS + cold normal saline-induced group (ML) as shown in **Figure 1**. Mice in group CC and CL were administered room temperature normal saline (25°C) by gavage from day 4th to 31st, while LPS was administered only in CL group on 32nd day. Whereas, mice in group MC and ML were administered cold normal saline (4°C) at a dosage of 0.5 mL per mouse every 2 h for four times daily to induce cold stress from day 4th to 31st, while LPS was administered only in ML group on 32nd day. On day 32nd, mice in groups CL and ML were infected with 20 mg/kg LPS (Solarbio life science, China) according to previous study (Chen et al., 2022). All the groups were kept and reared on same ambient temperature at 25°C throughout the experimental period from day 1st to 32nd. After 1-day of LPS administration on 33rd day, the mice in all the groups were euthanized to collect serum, heart, liver, kidney, lung, spleen, stomach, jejunum, ileum, cecum, colon, and rectum. The mice were provided the Pellet diet and water *ad libitum* throughout the experimental, and daily body weights and diarrhea were also recorded.

Hematoxylin and eosin staining

Tissue samples including the spleen, stomach, jejunum, ileum, cecum, and colon, were collected from mice of all the groups and fixed in 4% paraformaldehyde for 24 h and subjected to H&E staining. The tissues fixed in the formalin were processed further to observe the histopathological lesions by following the routinely used procedures like dehydrations, embedding, sectioning, mounting and staining. Thick sections of the tissues about 4–5 μm were cut and stained by the Hematoxylin and Eosin staining techniques. The histological sections were examined using a CX23 microscope (Olympus Co., Tokyo, Japan). The villus height and crypt depth of each selected mouse were measured following the methods described by Chen et al. (2022).

Antioxidant indexes, NO, and cytokine levels examination

The serums obtained from mice were kept at −20°C for further assays. For the antioxidant capacity indexes, superoxide dismutase, glutathione peroxidase, total anti-oxidation capacity, NO, and malondialdehyde were measured using commercially available kits following the manufacturer's instructions (Nanjing Jiancheng Bioengineering Research Institute Co., Ltd., China).

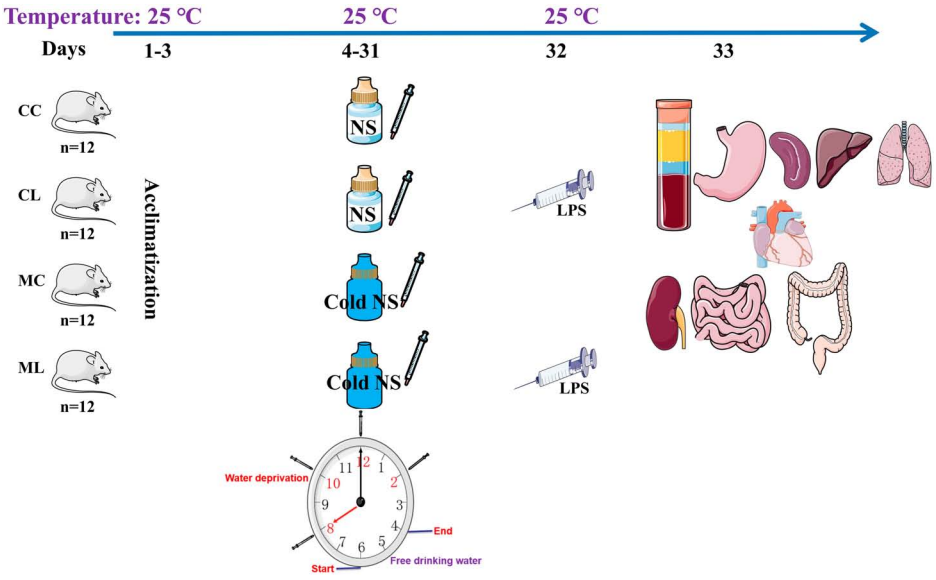

FIGURE 1
Research design diagram of the present experiment.

Tumor necrosis factor (TNF-α), interleukin 1 beta (IL-1β), interleukin-6 (IL-6) and IL-10 were detected in the blood serum of mice through specific kits (Solarbio life science, China).

Gut microbiome analysis

Mice rectums of all the groups (CC, CL, MC, and ML) were used to extract genomic DNA (gDNA) by employing the GenElute^{TM} Microbiome DNA Purification Kit (Sigma-Aldrich, Germany), following the manufacturers instructions. The concentration and integrity of the DNA products were surveyed via NanoDrop 2000 spectrophotometer (Thermo Scientific, USA) and agarose gel electrophoresis. The targeting regions of the microbial 16S rRNA (V3-V4) gene were amplified using the forward primer 338F (5′-ACTCCTACGGGAGGCAGCAG-3′) and the reverse primer 806R (5′-GGACTACHVGGGTWTCTAAT-3′). Subsequently, amplicon sequencing of the ICR animals was conducted using the Illumina platform at Bioyi Biotechnology Co., Ltd., as described in previous studies (Chen et al., 2022; Dong et al., 2023). Following sequencing, Trimmomatic, Cutadapt, QIIME2, and DADA2 were utilized to generate accurate and reliable data for subsequent bioinformatic analysis (Edgar, 2013; Callahan et al., 2016; Bolyen et al., 2019). High-quality sequences with a similarity threshold of 97% were clustered into operational taxonomic units (OTUs) using USEARCH (Edgar, 2013) and assigned taxonomic annotations by aligning them with the SILVA database (Bolyen et al., 2019). A Venn map was constructed to identify the shared OTUs among the groups following the previous method (Chen and Boutros, 2011). The annotation of the microbial communities was visually displayed using KRONA software as outlined by Ondov et al. (2011). Alpha diversity metrics, including Chao1, Ace, Shannon, Simpson, and PD_whole_tree, were calculated to assess the individual microbial diversity. Beta diversity analysis, including Principal Component Analysis, Principal Coordinates Analysis, Non-Metric Multi-Dimensional Scaling, Unweighted Pair-group Method with Arithmetic Mean, and heat maps were performed to examine the variation in microbial communities across samples. These analyses were carried out using QIIME2 and R software as described by Bolyen et al. (2019). To uncover distinctive bacteria among the groups, we utilized various statistical methods and tools including analysis of variance, Wilcoxon rank-sum test, ternary phase diagram, Linear discriminant analysis Effect Size, Metastats, and statistical analysis of Metagenomic Profiles (White et al., 2009; Segata et al., 2011; Parks et al., 2014). Network analysis was performed using R to explore potential correlations among bacterial taxa. Additionally, the prediction of microbiota functional potential was conducted using PICRUSt2, targeting the Kyoto Encyclopedia of Genes and Genomes and Cluster of Orthologous Groups databases (Kanehisa and Goto, 2000; Langille et al., 2013).

Metabolomics analysis

Metabolites from rectum samples (n = 6) of each group were extracted and subjected to metabolomics analysis via LC/MS (Dunn et al., 2011; Wang et al., 2016). Raw data processing and annotation were performed using MassLynx and Progenesis QI software (Wang et al., 2016). Spearman rank correlation and PCA were conducted to ensure the validity of current results. The annotation of metabolites was carried out using the KEGG, HMDB, and Lipidmaps databases (Fahy et al., 2007; Wishart et al., 2018).

Venn diagrams, PCA, and OPLS-DA were performed to investigate the variation between and within the groups (Chen et al., 2020). Remarkable differences in metabolomics among the mice groups were identified based on the variable importance in projection (VIP) values (>1) combined with statistical significance (P < 0.05). The differential metabolomics was described using multiple methods, including bar charts illustrating fold differences,

volcano plots, cluster heatmaps, correlation graphs, z-score diagrams, radar charts and violin plots.

qRT-PCR analysis

RNA extraction was performed from jejunum and ileum tissues of all the animals using Trizol reagent (Life Technologies, USA), and then the quality and quantity of RNA products were inspected via gel electrophoresis and Nanodrop 2000 (Thermo Fisher Scientific, China). The cDNA synthesis was carried out using Invitrogen^{TM} kits (Thermo Fisher Scientific, USA), followed by RT-PCR analysis using 2X SYBR Green Fast qPCR Mix (ABclonal, China). The analysis was conducted using the StepOnePlus^{TM} RT-PCR System (Applied Biosystems, USA). Three independently repeated reactions were performed for each mouse sample, and the relative quantification of genes was determined by using $2^{-\Delta\Delta CT}$ method. The primers information is shown in **Table 1**.

Statistical analysis

Analysis of variance (ANOVA) and Student's *t*-test were employed to analyze the data. The statistical analysis was conducted using IBM SPSS software (version 26.0). The data are presented as means ± standard deviation (SD), and $P < 0.05$ was considered statistically significant.

Results

The effects of LPS on mice body weights, organ indexes, and intestines damage

Similar body weight was observed in mice among all the experimental groups. However, the mice in groups CC and CL had slightly higher body weights compared to the mice in groups MC and ML (**Figure 2A**) but the difference is not significant ($P > 0.05$). Similarly, there was no prominent difference ($P > 0.05$) in the organ index between mouse groups (**Figure 2B**). Histopathological analysis revealed that LPS administration in groups CL and ML severely damaged the integrity of intestinal villi and gastric epithelium. The villus length was obviously shorter ($p < 0.05$) and crypt depth was observably longer ($p < 0.05$) in these mice, especially in animals in ML (**Supplementary Figure 1**).

Additionally, the spleens of LPS-induced mice showed enlarged red pulps and increased leukomonocytes (**Figure 3**).

The effects of cold normal saline stress on LPS induced mice on antioxidant indexes, NO and cytokine levels in serum

The antioxidant indexes, including T-AOC, GSH-Px, and SOD were significantly ($P < 0.05$) lower in mice challenged with LPS and prolonged cold stress exposure compared with other groups. Conversely, the MDA level was markedly higher ($P < 0.01$) in mice particularly in the group treated with cold normal saline + LPS. Whereas, the level of nitric oxide (NO) and interleukin-10 (IL-10) were examined in different groups but the differences were non-significant ($P > 0.05$) in all the groups. However, the cytokines TNF-α and IL-6 ($P < 0.01$) were expressed higher significantly ($P < 0.05$) in mice challenged with LPS and prolonged cold stress exposure compared with other groups. Furthermore, IL-1β level was similar between groups CC and CL, but it was significantly ($P < 0.05$) elevated in mice treated with cold normal saline + LPS (**Figure 4**).

The effects of cold normal saline stress on LPS induced mice on related genes' expressions

The expression levels of *ZO-1*, *OCCLUDIN*, and *CLAUDIN* in the jejunum were significantly ($P < 0.05$) decreased in mice challenged with LPS and cold stress as compared to other groups.

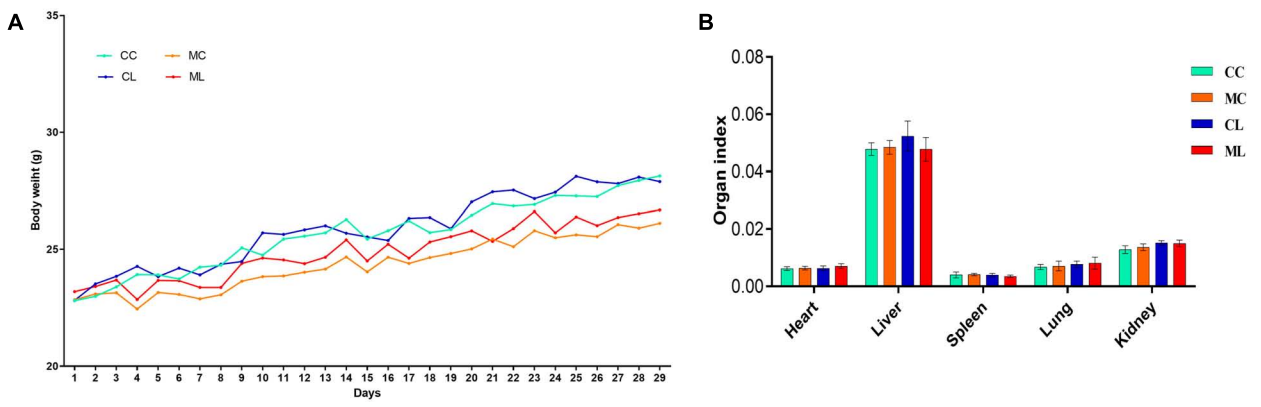

FIGURE 2
Effects of LPS on mice body weights **(A)** and organ indexes **(B)**. Scale bar 50 μm. Data were presented as the mean ± SEM ($n = 3$).

10.3389/fmicb.2023.1256748

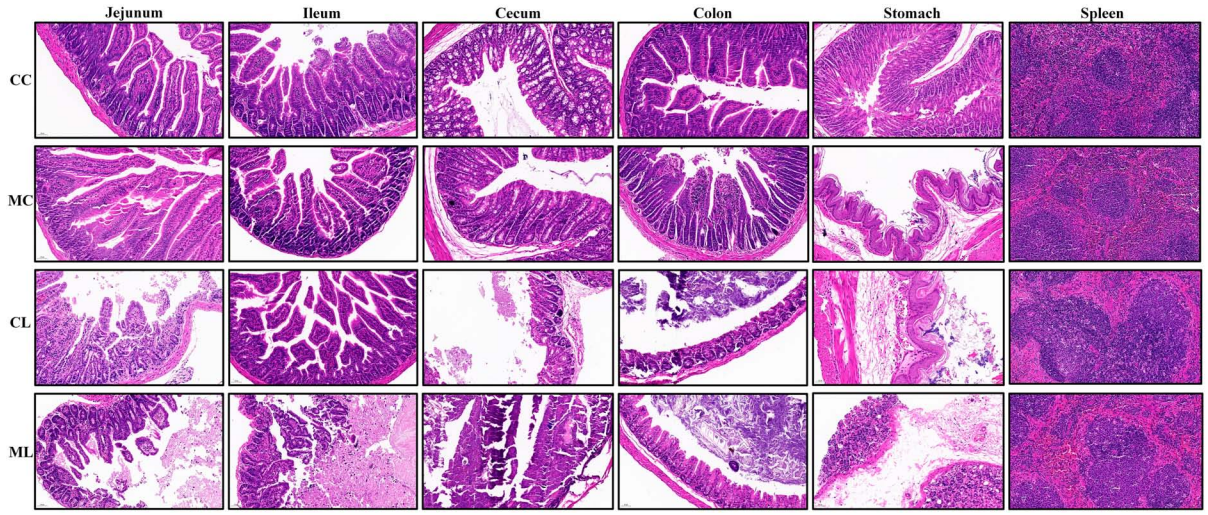

FIGURE 3
LPS caused damages in intestines, stomach and spleen in mice.

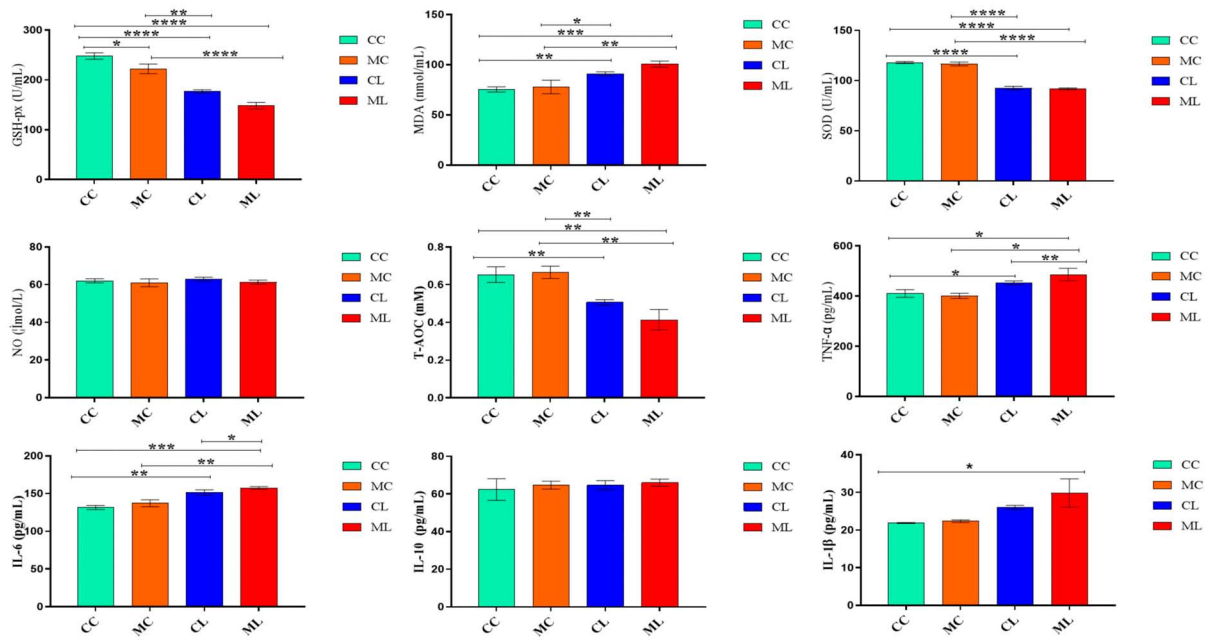

FIGURE 4
The effects of LPS on antioxidant indexes, NO and cytokine levels in serum. Significance is presented as *$p < 0.05$, **$p < 0.01$, ***$p < 0.001$, and ****$p < 0.0001$; data are presented as the mean ± SEM ($n = 6$).

Conversely, the expression levels of *CASPASE-1* and *NLRP3* were significantly increased ($P < 0.05$) in CL and ML groups compared with CC and MC groups (Figure 5A). Similar results were observed in the ileum in which *ZO-1*, *OCCLUDIN* and *CLAUDIN* expressions were significantly ($P < 0.05$) decreased in CL and ML groups compared with CC and MC groups. Whereas, the expression levels of *CASPASE-1* and *NLRP3* were significantly increased ($P < 0.05$) in mice challenged with LPS and prolonged cold stress exposure as compared to CC and MC groups (Figure 5B).

The effects of LPS on the structure and diversity of animal gut microbiota

A total of 1,781,514 and 1,775,898 raw and clean reads, respectively were obtained from the current mice samples. Each group had more than 75,339, 48,262, 49,246, and 60,260 non-chimeric reads (Table 2). The number of data reads in group MC was noticeably ($P < 0.05$) lower compared to the CC group (Figure 6A). In total, 9,228 operational taxonomic units (OTUs) were identified in the mice, with 246 OTUs shared among the groups. Group CL shared 434 to 486 OTUs, while group ML shared

10.3389/fmicb.2023.1256748

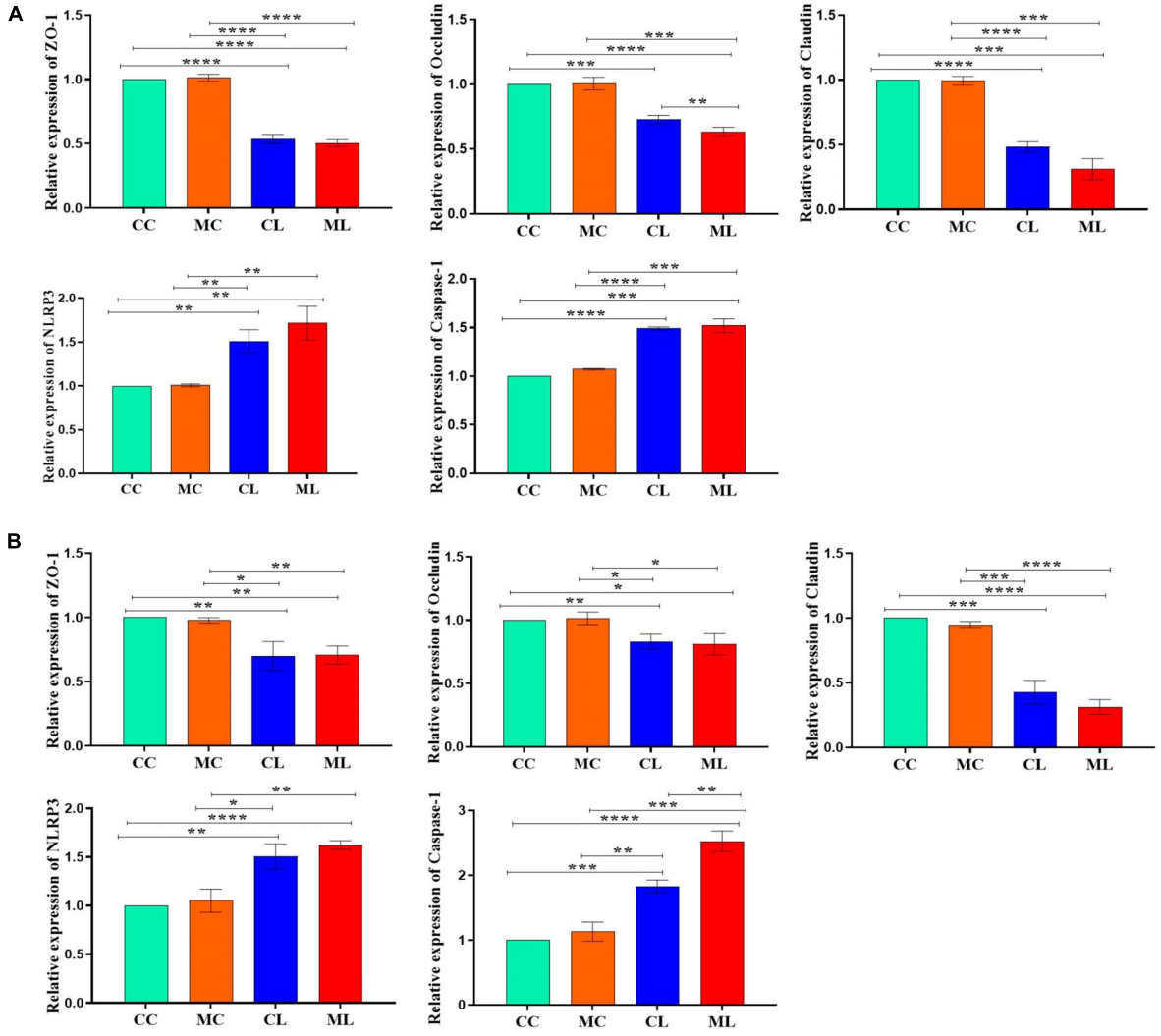

FIGURE 5
Relative expression analysis of ZO-1, Occludin, Claudin, Caspase-1 and NLRP3 via qRT-PCR, **(A)** jejunum, **(B)** ileum. Significance is presented as $*p < 0.05$, $**p < 0.01$, $***p < 0.001$, and $****p < 0.0001$; data are presented as the mean ± SEM ($n = 3$).

TABLE 1 **Primers used in the present study.**

Genes	Primer sequence	Product size (bp)	Tm (°C)
Occludin	F: 5′–TGCTTCATCGCTTCCTTAGTAA–3′ R: 5′–GGGTTCACTCCCATTATGTACA–3′	155	54
ZO-1	F:5′– CTGGTGAAGTCTCGGAAAAATG–3′ R: 5′–CATCTCTTGCTGCCAAACTATC–3′	97	54
NLRP3	F: 5′–CATCAATGCTGCTTCGACAT–3′ R: 5′–TCAGTCCCACACACAGCAAT–3′	118	56
CLAUDIN	F: 5′–AGATACAGTGCAAAGTCTTCGA–3′ R:5′– CAGGATGCCAATTACCATCAAG–3′	86	54
CASPASE-1	F: 5′–TGCCCTCATTATCTGCAACA–3′ R: 5′–GATCCTCCAGCAGCAACTTC–3′	95	56
B-*ACTIN*	F:5′– CTACCTCATGAAGATCCTGACC–3′ R: 5′–CACAGCTTCTCTTTGATGTCAC–3′	90	54

459 to 518 OTUs with the other groups (Figure 6B). Alpha diversity analysis indicated that Shannon ($P < 0.05$) and Simpson ($P < 0.05$) indices in ML were memorably lower than those in MC (Table 3; Figure 6C). Beta diversity analysis showed that the samples in groups MC, CL, and ML clustered closely together on PCA. The distance between groups CC and MC was short based on PCoA,

10.3389/fmicb.2023.1256748

TABLE 2 Statistical analysis of mouse samples sequencing data.

Sample ID	Raw reads	Clean reads	Denoised reads	Merged reads	Non-chimeric reads
CC1	76,318	76,123	75,965	75,831	75,339
CC2	79,710	79,546	79,475	79,303	78,613
CC3	79,832	79,616	79,578	79,366	79,162
CC4	77,558	77,319	77,215	77,014	76,930
CC5	79,901	79,684	79,532	79,277	79,101
CC6	80,020	79,836	79,786	79,539	79,337
CL1	79,896	79,677	79,665	79,642	79,598
CL2	79,979	79,759	79,562	79,207	78,628
CL3	79,762	79,572	79,442	78,964	77,710
CL4	78,135	77,868	77,722	77,692	77,198
CL5	48,593	48,397	48,317	48,283	48,262
CL6	75,015	74,752	74,608	74,581	74,351
MC1	69,957	69,784	69,717	69,510	69,293
MC2	49,502	49,343	49,332	49,248	49,246
MC3	79,983	79,724	79,614	79,486	79,179
MC4	60,134	59,844	59,775	59,576	58,688
MC5	57,577	57,410	57,218	57,083	56,915
MC6	79,811	79,609	79,548	79,459	79,417
ML1	68,956	68,759	68,704	68,659	68,575
ML2	80,034	79,783	79,615	79,425	79,139
ML3	69,063	68,761	68,676	68,581	68,439
ML4	71,884	71,593	71,344	71,308	71,240
ML5	60,568	60,321	60,288	60,277	60,260
ML6	119,326	118,818	118,780	118,552	118,308

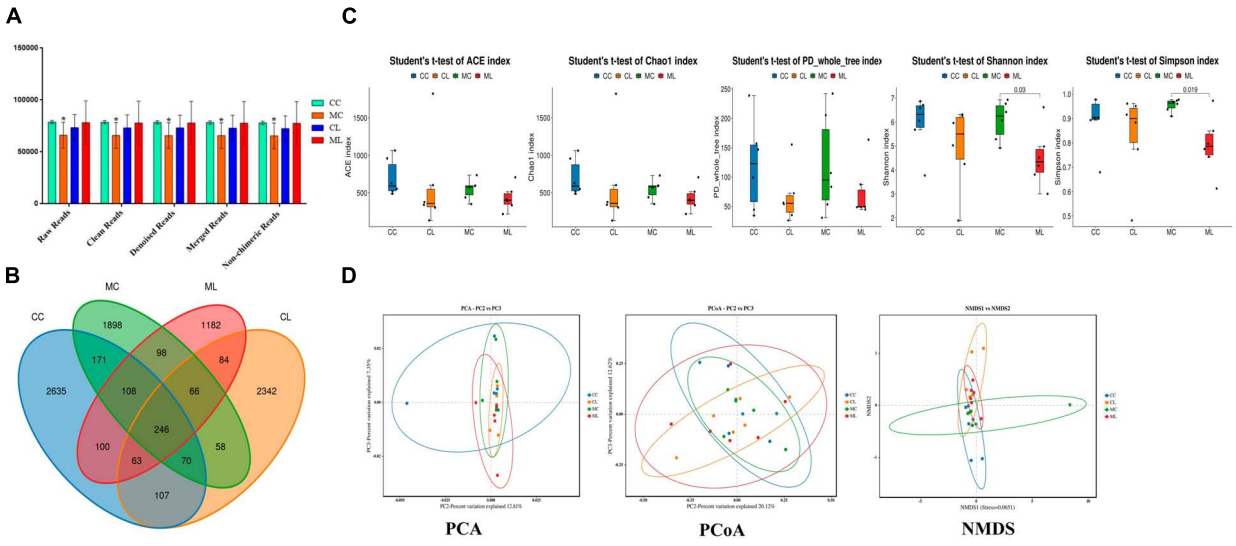

FIGURE 6
Effects of LPS on the structure and diversity of animal gut microbiota. **(A)** Sequencing data statistical analysis, **(B)** Length distribution of sequencing data, **(C)** Rank abundance curve, **(D)** Alpha diversity index analysis. Significance is presented as $*p < 0.05$, $**p < 0.01$, $***p < 0.001$, and $****p < 0.0001$; data are presented as the mean ± SEM ($n = 6$).

TABLE 3 Statistical analysis of Alpha diversity index.

Sample	Feature	ACE	Chao1	Simpson	Shannon	PD_whole_tree	Coverage
CC1	627	629.1382	627.4912	0.9033	6.0561	99.0368	0.9999
CC2	485	486.3673	485.0938	0.9778	6.576	44.2971	0.9999
CC3	547	553.6486	549.7755	0.6798	3.7706	146.8667	0.9998
CC4	955	959.9665	955.6791	0.8934	5.6838	238.9361	0.9998
CC5	1061	1064.7711	1061.7258	0.9034	6.7134	157.1504	0.9999
CC6	517	520.0825	517.56	0.9772	6.8684	34.4298	0.9999
CL1	127	131.8703	128.2	0.4822	1.8885	26.0812	0.9999
CL2	1822	1823.9508	1822.1186	0.8838	6.2684	155.4129	0.9999
CL3	601	602.635	601.0971	0.9508	6.315	35.2559	0.9999
CL4	375	377.0643	375.5	0.9611	5.9666	54.0704	0.9999
CL5	304	304.5632	304.0435	0.7741	4.2534	72.4377	1
CL6	339	339.9516	339.375	0.9157	5.0324	56.0789	0.9999
MC1	589	591.3971	589.5385	0.9733	6.7646	106.8593	0.9999
MC2	350	350.6995	350.1765	0.9668	6.0784	53.4059	0.9999
MC3	728	736.0014	729.6132	0.9773	6.9336	242.2064	0.9998
MC4	439	439.3646	439	0.9374	5.2844	30.5536	1
MC5	594	595.7274	594.4773	0.9601	6.4219	83.3632	0.9999
MC6	569	571.886	569.3218	0.9094	4.9192	205.6026	0.9999
ML1	406	408.5056	406.6222	0.7965	4.1665	87.3503	0.9999
ML2	514	514.5357	514.0323	0.9729	6.6193	49.4554	1
ML3	393	393.525	393.0357	0.7429	4.5134	48.9056	1
ML4	332	333.5886	332.2857	0.8489	4.9739	44.7464	0.9999
ML5	216	217.5451	217.1538	0.7749	3.8148	48.7069	0.9999
ML6	705	708.6438	707.0192	0.6129	3.0064	163.7069	0.9999

while groups CL and ML were close to each other based on NMDS (Figure 6D).

The effect of LPS on intestinal microbiota in different taxa

At the phylum level, the ruling phyla in CC mice were Firmicutes (53.53%), Campylobacterota (20.01%), and Bacteroidota (12.91%), the ruling phyla in MC mice were Firmicutes (59.70%), Bacteroidota (11.6%) and Proteobacteria (9.96%), in CL animals were Proteobacteria (38.02%), Firmicutes (27.58%) and Bacteroidota (16.41%), while ruling phyla in ML animals were Proteobacteria (40.05%), Bacteroidota (19.40%) and Firmicutes (18.35%) (Figure 7A and Table 4). At the class level, the top three most abundant classes were Clostridia (32.23%), Bacilli (20.90%) and Campylobacteria (20.24%) in group CC, Gammaproteobacteria (36.90%), Bacilli (17.59%) and Bacteroidia (16.57%) in group CL, Clostridia (33.18%), Bacilli (26.2%) and Bacteroidia (11.19%) in group MC, while Gamma proteobacteria (42.66%), Bacteroidia (17.52%) and Campylobacteria (12.9%) in group ML (Figure 7B). At the order level, the main orders in group CC were Lachnospirales (25.56%), Campylobacterales (20.24%) and Lactobacillales (16.66%), in group CL were Enterobacterales (35.71%), Bacteroidales (16.32%) and Lactobacillales (12.73%), in group MC were Lachnospirales (24.62%), Lactobacillales (20.68%) and Bacteroidales (11.03%), and in group ML were Enterobacterales (41.02%), Bacteroidales (17.84%) and Campylobacterales (12.90%) (Figure 7C). At the family level, Lachnospiraceae (25.56%), Helicobacteraceae (20.21%) and Lactobacillaceae (16.19%) were mainly found in CC animals, Enterobacteriaceae (32.39%), Lactobacillaceae (10.28%) and Lachnospiraceae (8.78%) were primary families in CL mice, Lachnospiraceae (24.61%), Lactobacillaceae (18.61%) and Helicobacteraceae (7.66%) were mainly detected in MC animals, and Enterobacteriaceae (38.44%), Helicobacteraceae (12.90%) and Lactobacillaceae (5.12%) were principally examined in ML mice (Figure 7D). At the genus level, the staple genera were *Helicobacter* (20.21%), *Lactobacillus* (15.34%) and Lachnospiraceae_NK4A136_group (13.30%) in CC mice, *Escherichia_Shigella* (30.88%), *Helicobacter* (7.60%) and Bacteroides (5.91%) in CL animals, *Lactobacillus* (16.39%), unclassified_Lachnospiraceae (12.04%) and Lachnospiraceae_NK4A136_group (9.19%) in MC mice, *Escherichia_Shigella* (38.39%), *Helicobacter* (12.90%) and unclassified_Muribaculaceae (6.97%) in CL animals (Figure 7E). At species level, unclassified_*Helicobacter* (20.21%), unclassified_Lachnospiraceae_NK4A136_group (11.35%) and

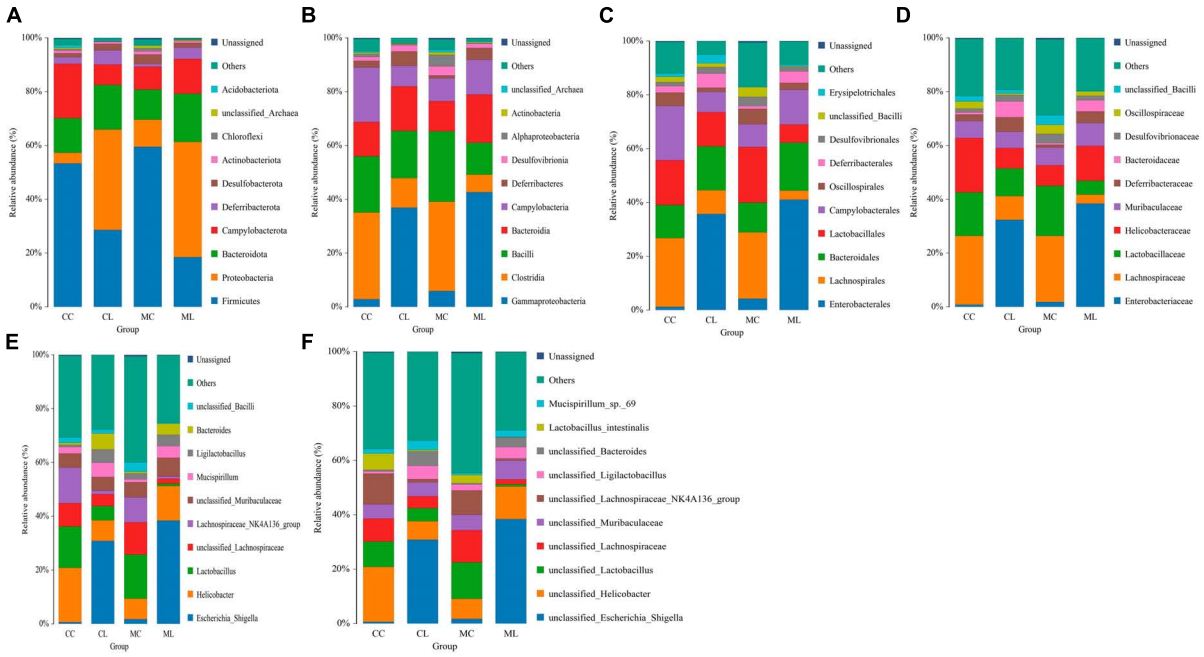

FIGURE 7
The effect of LPS on intestine microbiota in different taxa. **(A)** Phylum, **(B)** Class, **(C)** Order, **(D)** Family, **(E)** Genus, and **(F)** Species.

unclassified_*Lactobacillus* (9.30%) were mainly uncovered in mice in CC group, unclassified_*Escherichia_Shigella* (30.88%), unclassified_*Helicobacter* (6.75%) and unclassified_Bacteroides (5.28%) were revealed in mice in CL group, unclassified_*Lactobacillus* (13.38%), unclassified_Lachnospiraceae (11.82%) and unclassified_Lachnospiraceae_NK4A136_group (8.97%) were tested in mice in MC group, while unclassified_*Escherichia_Shigella* (38.39%), unclassified_*Helicobacter* (12.05%) and unclassified_Muribaculaceae (6.97%) were examined in mice in group ML (Figure 7F). Phylogenetic tree distribution analysis to top 80 abundant OTUs found that the abundance of g__Lachnospiraceae_NK4A136_group (ASV39), s__uncultured_*Clostridiales_bacterium* (ASV29), g__Lachnospiraceae_NK4A136_group (ASV9), g__Lachnospiraceae_NK4A136_group (ASV75), f__Lachnospiraceae (ASV52), s__Lachnospiraceae_bacterium_DW59 (ASV77), g__*Roseburia* (ASV57), g__*Anaerotruncus* (ASV33), g__*Candidatus_Arthromitus* (ASV56), s__*Lactobacillus_intestinalis* (ASV7), g__*Helicobacter* (ASV5), g__*Helicobacter* (ASV38), g__*Helicobacter* (ASV24) and *Alloprevotella* (ASV36) decreased, especially in LPS induced mice, while g__*Enterococcus* (ASV67), g__Ligi*lactobacillus* (ASV6), g__Ligi*lactobacillus* (ASV64), s__*Malacoplasma_muris* (ASV18), s__*Mucispirillum*_sp._69 (ASV14), g__*Mucispirillum* (ASV12), g__Rodentibacter (ASV17), g__*Escherichia_Shigella* (ASV22), g__*Escherichia_Shigella* (ASV23), g__*Escherichia_Shigella* (ASV1), g__*Helicobacter* (ASV4), s__*Helicobacter_ganmani* (ASV40), g__*Parabacteroides* (ASV26), f__Muribaculaceae (ASV42), f__Muribaculaceae (ASV70), f__Muribaculaceae (ASV61), f__Muribaculaceae (ASV43), g__Bacteroides (ASV20), g__Bacteroides (ASV30), g__Bacteroides (ASV63), g__Bacteroides (ASV41) and g__Bacteroides (ASV74) increased in LPS challenged animals (Figure 8A). Krona species annotation showed that the main genera were unclassified__*Helicobacter* (20%), unclassified__Lachnospiraceae_NK4A136_group (11%), unclassified__Lachnospiraceae (9%) and unclassified__*Lactobacillus* (9%) in CC mice, unclassified__*Escherichia_Shigella* (31%), unclassified__*Helicobacter* (7%), unclassified__Bacteroides (5%), unclassified__Muribaculaceae (5%), unclassified__Ligi*lactobacillus* (5%) and unclassified__*Lactobacillus* (5%) in mice in CL, and unclassified__*Escherichia_Shigella* (38%), unclassified__*Helicobacter* (12%) and unclassified__Muribaculaceae (7%) (Figure 8B).

Marker bacteria in microbiota of mice among different groups

We first performed LEfSe analysis and found that o__Enterobacterales, C__Gammaproteobacteria, p__Proteobacteria, f__Enterobacteriaceae, s__unclassified_*Escherichia_Shigella*, g__*Escherichia_Shigella*, p__*Firmicutes*, c__*Clostridia*, o__Oscillospirales, f__Oscillospiraceae, s__unclassified_Bacteroides and g__Lachnospiraceae_NK4A136_group were biomakers in mice (Figure 9).

Then we used metastats analysis and revealed that compared with CC mice, the abundance of UCG_005 ($P < 0.001$), Family_XIII_001 ($P < 0.05$), UBA1819 ($P < 0.05$), *Parasutterella* ($P < 0.05$), *Intestinimonas* ($P < 0.05$) and Pantoea ($P < 0.05$) were lower in MC mice, while *Acetatifactor* ($P < 0.01$), *Lactococcus* ($P < 0.01$), Incertae_Sedis ($P < 0.01$), Atopostipes

TABLE 4 Statistical analysis of reads in different taxa.

Sample	Kingdom	Phylum	Class	Order	Family	Genus	Species
CC1	75,261	75,071	75,065	75,017	73,860	50,526	3,060
CC2	78,503	78,481	78,481	75,954	75,584	59,422	21,274
CC3	79,042	78,171	77,975	77,567	76,968	69,792	4,558
CC4	76,730	74,151	74,087	70,185	68,418	62,388	21,170
CC5	79,000	77,285	77,116	76,573	74,843	62,087	9,946
CC6	79,231	79,207	79,207	76,259	75,909	53,918	10,070
CL1	79,534	79,518	79,518	78,718	78,711	78,335	1,631
CL2	78,409	77,824	77,656	77,138	75,770	63,363	5,955
CL3	77,559	77,544	77,537	74,000	73,939	55,710	11,246
CL4	77,148	77,095	77,093	76,728	76,137	58,235	9,729
CL5	48,233	48,076	48,072	48,023	47,866	43,122	7,841
CL6	74,338	74,165	74,158	72,903	72,781	65,317	13,959
MC1	69,208	68,879	68,877	68,188	66,961	45,445	4,970
MC2	49,218	49,120	49,099	48,978	48,718	31,895	1,332
MC3	79,011	77,206	77,199	75,244	73,489	50,675	6,446
MC4	58,545	58,506	58,499	58,410	58,203	35,689	13,450
MC5	56,852	56,633	56,604	51,276	50,820	33,578	5,152
MC6	79,300	76,213	76,179	69,964	69,301	65,916	21,261
ML1	68,498	68,182	68,179	67,834	67,615	63,701	3,528
ML2	79,092	79,038	79,038	78,779	78,204	50,708	12,429
ML3	68,404	68,342	68,339	68,109	67,847	57,078	4,400
ML4	71,201	71,136	71,133	70,866	70,771	59,408	4,200
ML5	60,238	60,175	60,175	60,030	59,914	57,902	10,959
ML6	118,175	116,506	116,470	115,923	115,416	113,662	10,614

($P < 0.05$), 2013Ark19i ($P < 0.05$), Blvii28_sludge_group ($P < 0.05$), *Candidatus_Caldatribacterium* ($P < 0.05$), *Comamonas* ($P < 0.05$), *Ponticaulis* ($P < 0.05$), Tepidisphaera ($P < 0.05$), unclassified_11_24 ($P < 0.05$), unclassified_Euzebyaceae ($P < 0.05$), unclassified_Halobacterota ($P < 0.05$) and unclassified_Mariniliaceae ($P < 0.05$) were higher. The abundance of *Oscillibacter* ($P < 0.001$), *Peptococcus* ($P < 0.001$), *Colidextribacter* ($P < 0.01$), Family_XIII_001 ($P < 0.01$), unclassified_Peptococcaceae ($P < 0.01$), *Tyzzerella* ($P < 0.01$), *Novosphingobium* ($P < 0.01$), *Candidatus_Arthromitus* ($P < 0.01$), *Polynucleobacter* ($P < 0.05$), *Bacillus* ($P < 0.05$), *Serratia* ($P < 0.05$), UCG_005 ($P < 0.05$), unclassified_Enterobacteriaceae ($P < 0.05$) and Pantoea ($P < 0.05$) were lower in group CL, while *Escherichia_Shigella* ($P < 0.01$), *Streptococcus* ($P < 0.01$), *Enterococcus* ($P < 0.01$), Bacteroides ($P < 0.01$), Acetatifactor ($P < 0.01$) and Rodentibacter ($P < 0.05$) were higher. Compared with mice in group CC, genera of *Peptococcus* ($P < 0.001$), unclassified_Ruminococcaceae ($P < 0.001$), Lachnospiraceae_UCG_001 ($P < 0.001$), *Roseburia* ($P < 0.01$), *Novosphingobium* ($P < 0.01$), Family_XIII_UCG_001 ($P < 0.01$), UCG_005 ($P < 0.01$), *Tyzzerella* ($P < 0.01$), unclassified_Lachnospiraceae ($P < 0.01$), unclassified_Comamonadaceae ($P < 0.01$), *Oscillibacter* ($P < 0.01$), unclassified_Peptococcaceae ($P < 0.01$), *Colidextribacter* ($P < 0.01$), unclassified_Cyanobacteriales ($P < 0.01$) and *Bacillus* ($P < 0.01$) were lower in group ML, while *Escherichia_Shigella* ($P < 0.001$), Providencia ($P < 0.01$), *Enterococcus* ($P < 0.01$) and *Staphylococcus* ($P < 0.01$) were higher. Whereas, compared with MC mice, the abundance of unclassified_Peptococcaceae ($P < 0.01$), *Colidextribacter* ($P < 0.01$), Incertae_Sedis ($P < 0.01$), Serralia ($P < 0.01$), *Oscillibacter* ($P < 0.01$), *Candidatus_Arthromitus* ($P < 0.01$), *Chujaibacter* ($P < 0.05$), *Prevotella_7* ($P < 0.05$), *Candidatus_Saccharimonas* ($P < 0.05$), *Peptococcus* ($P < 0.05$), unclassified_Oscillospiraceae ($P < 0.05$), *Runella* ($P < 0.05$), 2013Ark19i ($P < 0.05$), *Anaeromyxobacter* ($P < 0.05$) and Blvii28_wastewater_sludge_group ($P < 0.05$) were lower in CL mice, while *Escherichia_Shigella* ($P < 0.01$), *Mucispirillum* ($P < 0.01$), *Erysipelatoclostridium* ($P < 0.01$), Bacteroides ($P < 0.01$), Parabacteroides ($P < 0.05$), were higher. Similarly, compared with mice in group MC, the abundance of RB41 ($P < 0.001$), unclassified_Peptococcaceae ($P < 0.01$), unclassified_Sphingomonadaceae ($P < 0.01$), *Candidatus_Solibacter* ($P < 0.01$), unclassified_Lachnospiraceae ($P < 0.01$), *Peptococcus* ($P < 0.01$), *Acetatifactor* ($P < 0.05$), *Serratia* ($P < 0.05$), *Prevotella_7* ($P < 0.05$), *Sphingomonas* ($P < 0.05$), *Chujaibacter* ($P < 0.05$), unclassified_Sphingomonadaceae ($P < 0.05$), *Prevotella* ($P < 0.05$)

10.3389/fmicb.2023.1256748

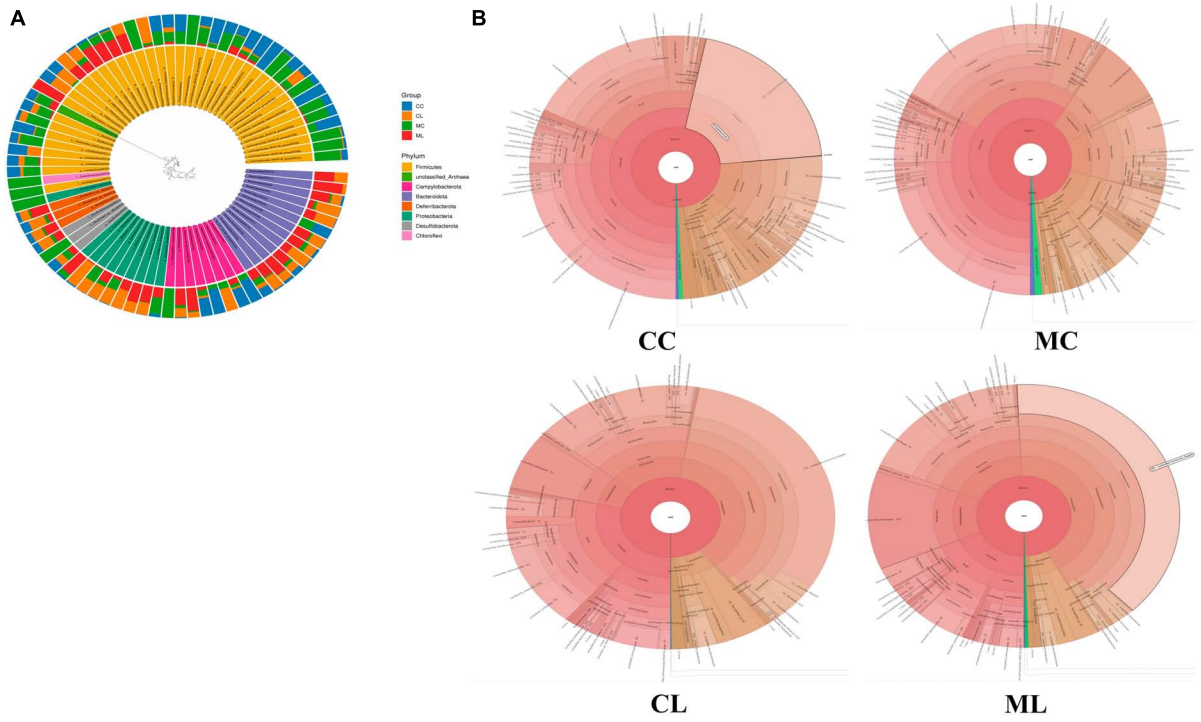

FIGURE 8
Microbiota composition analysis of mouse gut microbiota. **(A)** Phylogenetic tree distribution map, **(B)** Krona species annotation diagram.

and unclassified_Gemmatimonadaceae ($P < 0.05$) were lower in group ML, while *Escherichia_Shigella* ($P < 0.001$), *Providencia* ($P < 0.01$), *Enterorhabdus* ($P < 0.01$), *Yaniella* ($P < 0.05$), Bacteroides ($P < 0.05$) and UCG_005 ($P < 0.05$) were higher. Compared with mice in CL group, the abundance of Streptococcus ($P < 0.01$), *Bacillus* ($P < 0.01$), ASF356 ($P < 0.05$), Aclinospica ($P < 0.05$), *Aliidiomarina* ($P < 0.05$), *Asticcacaulis* ($P < 0.05$), BC19_17_termte_group ($P < 0.05$), *Candidatus*_Fritschea ($P < 0.05$), *Castellaniella* ($P < 0.05$), Cytophaga ($P < 0.05$) and *Elusimicrobium* ($P < 0.05$) were lower in ML mice, while *Staphylococcus* ($P < 0.01$), *Providencia* ($P < 0.01$), *Yaniella* ($P < 0.01$), *Aeromonas* ($P < 0.01$), Facklamia ($P < 0.01$), uncultured_Muribaculaceae_bacterium ($P < 0.05$), *Aerococcus* ($P < 0.05$), *lgnavigranum* ($P < 0.05$) and *Jeotgalicoccus* ($P < 0.05$) were higher (Figure 10).

Likewise, we compared the abundance of bacteria among the four groups at the phylum and genus levels. The results showed that the phylum Deferribacterota was significantly higher in CL mice compared to MC animals ($P < 0.05$). Firmicutes was markedly lower in group CL ($P < 0.05$) and ML ($P < 0.05$) compared to group MC, and it was also significantly lower than that in group CC ($P < 0.05$). Gemmatimonadota in ML animals was dramatically lower compared to MC animals ($P < 0.05$). Proteobacteria in CL mice showed a significantly higher abundance compared to CC ($P < 0.01$) and MC ($P < 0.05$) animals, respectively. Similar results were observed in ML mice, with a significantly higher abundance of Proteobacteria in ML compared to CC ($P < 0.01$) and MC ($P < 0.05$) (Figure 11A). At the genus level, the abundance of Acetatifactor in CL mice was significantly higher than in CC animals ($P < 0.05$). *Candidatus_Solibacter* ($P < 0.05$) and unclassified_Sphingomonadaceae ($P < 0.05$) in CL mice were notably higher compared to ML mice. *Colidextribacter* in MC mice was significantly lower than that in CC ($P < 0.05$) and CL ($P < 0.05$) animals. *Erysipelatoclostridium* ($P < 0.05$) and Mucispirillum ($P < 0.05$) in MC animals was markedly higher than that in CL mice. *Escherichia_Shigella* was higher in MC animals than CC ($P < 0.05$) and CL mice ($P < 0.05$). Similarly, this genus was obviously higher found in group ML than groups CC ($P < 0.01$) and CL ($P < 0.05$). Family_XIII_UCG_001 in group CC was higher than group MC ($P < 0.05$) and ML ($P < 0.05$), respectively. Incertae_Sedis ($P < 0.05$) and Serratia ($P < 0.05$) was significantly higher in mice in CL than that in MC. Lachnospiraceae_UCG_001 ($P < 0.05$), *Novosphingobium* ($P < 0.05$), *Roseburia* ($P < 0.05$) and unclassified_Comamonadaceae ($P < 0.05$) in CC mice was notably higher than ML mice, respectively. *Oscillibacter* in CC animals was significantly higher than MC ($P < 0.01$) and ML ($P < 0.05$) groups. *Peptococcus* was discovered higher in group CC than group MC ($P < 0.05$) and ML ($P < 0.01$). Similarly, it was observably higher in CL mice than ML mice ($P < 0.05$). *Providencia* was obviously higher in ML mice than animals in other groups ($P < 0.05$). RB41 was higher in CL groups than ML ($P < 0.01$). *Tyzzerella* in group CC was higher than group MC ($P < 0.05$) and ML ($P < 0.05$). *Staphylococcus* in mice in group ML was significantly higher than it in group MC ($P < 0.05$), while *Streptococcus* in mice in group ML was significantly lower than group MC ($P < 0.05$). UCG_005 in mice in CC was markedly higher than animals in group CL ($P < 0.01$) and ML ($P < 0.05$).

10.3389/fmicb.2023.1256748

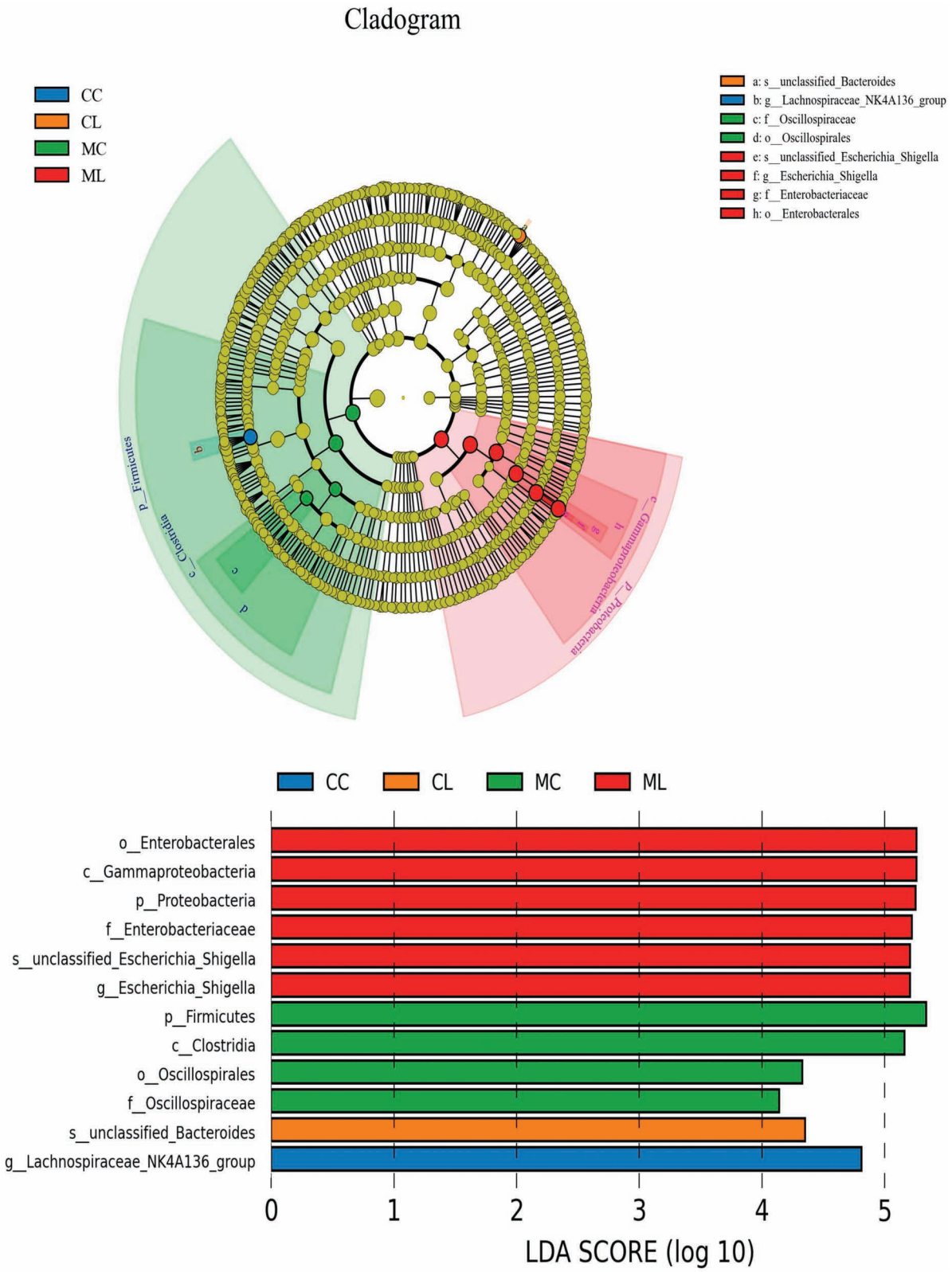

FIGURE 9
Marker microbiota analysis of mice in different groups via LEfSe analysis.

The abundance of unclassified_Lachnospiraceae in group ML was significantly lower than it in group CC ($P < 0.05$) and CL ($P < 0.05$). Unclassified_Peptococcaceae in CC animals was markedly higher than MC animals ($P < 0.05$), similarly it was higher in CL mice than MC ($P < 0.05$) and ML ($P < 0.05$) (Figure 11B).

10.3389/fmicb.2023.1256748

LPS changed microbiota function in mice among different groups

Function prediction via Picrust2 showed that obviously different functions of KEGG level of organismal systems ($P < 0.05$), genetic information processing ($P < 0.05$) and metabolism ($P < 0.05$) were examined between CC and ML mice (Table 5). Phenotypic analysis bugbase revealed that Contains_Mobile_Elements ($P < 0.05$), Gram_Negative ($P < 0.05$) and Gram_Positive were observably higher in ML mice, Facultatively_Anaerobic ($P < 0.05$), Potentially_Pathogenic ($P < 0.05$) and Stress_Tolerant ($P < 0.05$) were significantly higher in mice in CL and ML (Table 6). Tax4Fun analysis found that glycan biosynthesis and metabolism (GBD) ($P < 0.01$), circulatory system ($P < 0.01$), translation

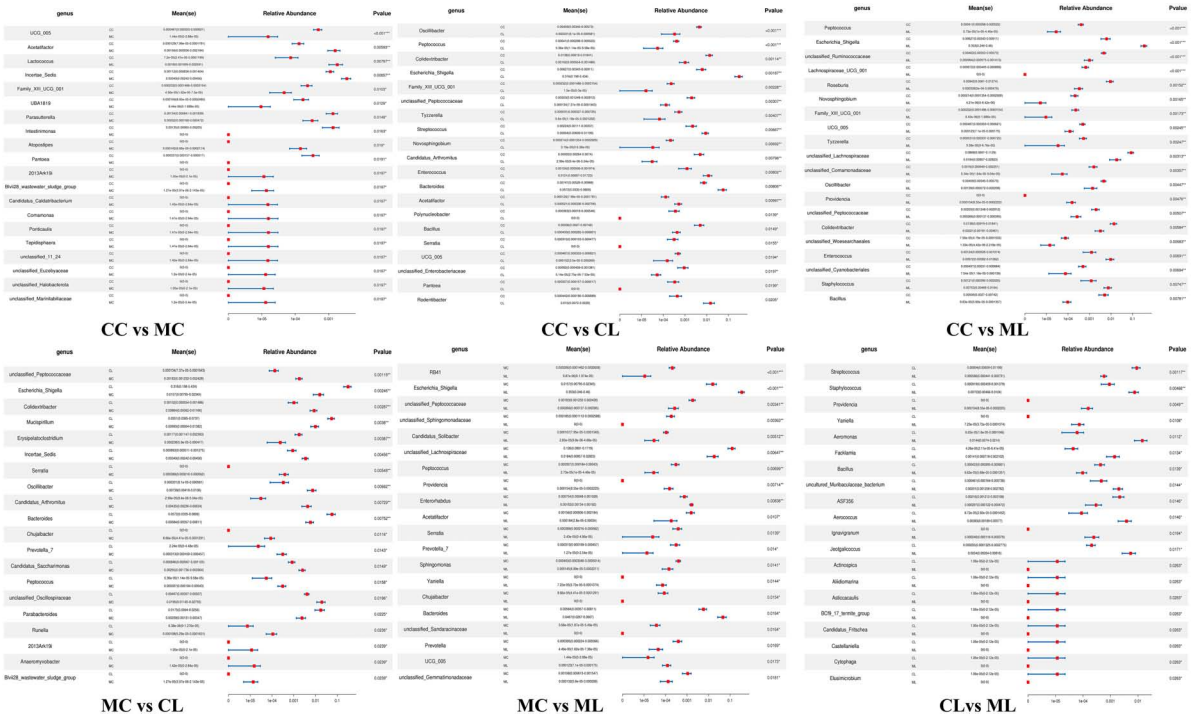

FIGURE 10
Marker microbiota analysis of mice in different groups via metastats.

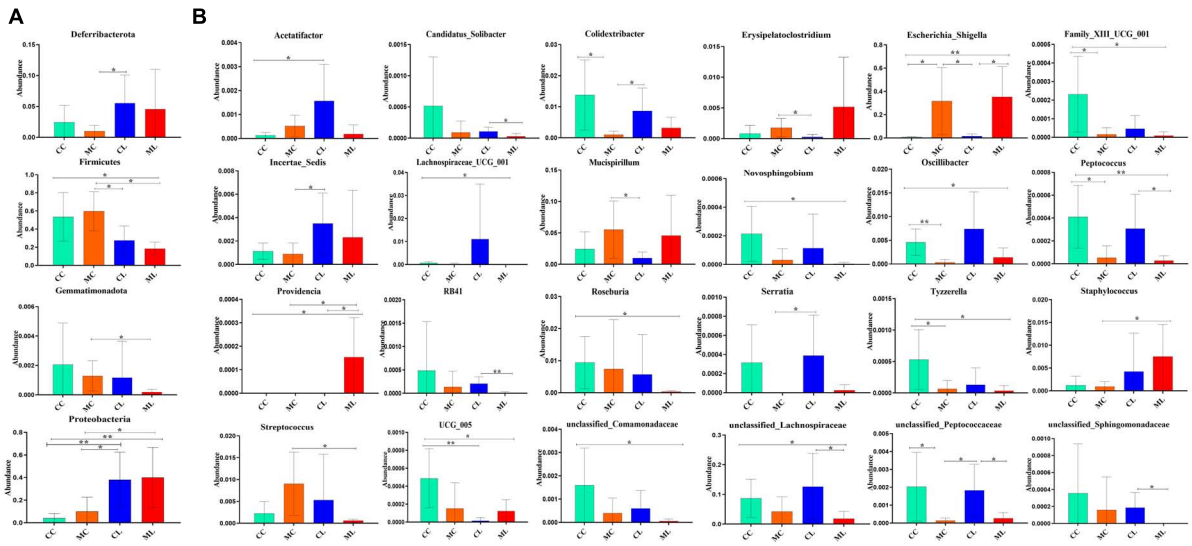

FIGURE 11
Distinguished microbiota analysis of mice in different groups. **(A)** Phylum, **(B)** Genus. Significance is presented as $*p < 0.05$, $**p < 0.01$; data are presented as the mean ± SEM ($n = 6$).

($P < 0.05$), transcription ($P < 0.05$), folding, sorting and degradation (FSD) ($P < 0.05$), replication and repair (RR) ($P < 0.05$), and endocrine and metabolic diseases (EMDs) in CL animals were obviously lower than mice in CC, while metabolism of other amino acids ($P < 0.05$), cellular community-prokaryotes ($P < 0.05$) and signal transduction ($P < 0.05$) were significantly higher. Compared with mice in group CC, metabolism of other amino acids ($P < 0.01$), infectious diseases: bacterial ($P < 0.05$) and metabolism of terpenoids and polyketides ($P < 0.05$) were observably higher, while translation ($P < 0.01$), transcription ($P < 0.05$), GBD ($P < 0.05$), FSD ($P < 0.05$), RR ($P < 0.05$), and circulatory system ($P < 0.05$) were lower (Figure 12A). FAPROTAX analysis showed that nitrate reduction ($P < 0.05$) and chemoheterotrophy ($P < 0.05$) in CL and ML were memorably lower than CC, while nitrate reduction ($P < 0.01$), human pathogens all ($P < 0.05$), mammal gut ($P < 0.05$) and human gut ($P < 0.05$) were significantly higher in ML. Compared with animals in MC, nitrate reduction ($P < 0.01$), human pathogens ($P < 0.05$) and mammal gut ($P < 0.05$) were obviously higher in animals in ML group (Figure 12B).

TABLE 5 Comparing KEGG level 1 function of mice microbiota in different groups via picrust2.

Class 1	CC	MC	CL	ML
Organismal systems	1.29 ± 0.06	1.30 ± 0.04	1.35 ± 0.04	1.37 ± 0.05*
Cellular processes	3.73 ± 0.39	3.68 ± 0.61	3.44 ± 0.18	3.53 ± 0.24
Human diseases	2.77 ± 0.40	2.73 ± 0.25	2.96 ± 0.26	3.04 ± 0.22
Genetic information processing	8.84 ± 0.87	8.83 ± 1.34	7.93 ± 0.65	7.60 ± 0.63*
Environmental information processing	7.27 ± 0.83	7.45 ± 0.0.40	7.52 ± 0.86	7.33 ± 0.82
Metabolism	76.10 ± 0.63	76.00 ± 0.81	76.80 ± 0.97	77.13 ± 0.57*

Data are presented as the mean ± std.dev ($n = 6$), significance is presented as $^*p < 0.05$.

TABLE 6 Comparing phenotypic analysis of mice microbiota in different groups via bugbase prediction.

Phenotypes	CC	MC	CL	ML
Aerobic	37.76 ± 29.96	31.33 ± 14.09	21.06 ± 11.56	26.67 ± 20.41
Anaerobic	52.61 ± 33.35	59.77 ± 22.80	44.30 ± 20.85	38.31 ± 24.41
Contains_Mobile_Elements	0.32 ± 0.34^a	1.58 ± 2.14^a	23.67 ± 24.27^a	23.04 ± 15.89^b
Facultatively_Anaerobic	7.70 ± 9.35^a	7.53 ± 9.23^a	32.57 ± 20.47^b	33.28 ± 21.12^b
Forms_Biofilms	0.64 ± 0.70	0.42 ± 0.55	4.95 ± 7.71	0.94 ± 0.93
Gram_Negative	46.75 ± 27.30^a	44.81 ± 26.25^a	69.34 ± 16.51^a	76.68 ± 8.18^b
Gram_Positive	53.25 ± 27.30^a	55.19 ± 26.25^a	30.66 ± 16.51^a	23.32 ± 8.18^b
Potentially_Pathogenic	0.87 ± 0.86^a	1.71 ± 2.14^a	27.73 ± 21.69^b	23.14 ± 15.91^b
Stress_Tolerant	1.05 ± 1.05^a	3.52 ± 3.67^a	29.99 ± 20.34^b	25.32 ± 16.90^b

Data are presented as the mean ± std.dev ($n = 6$), significance is presented as different letters when $p < 0.05$.

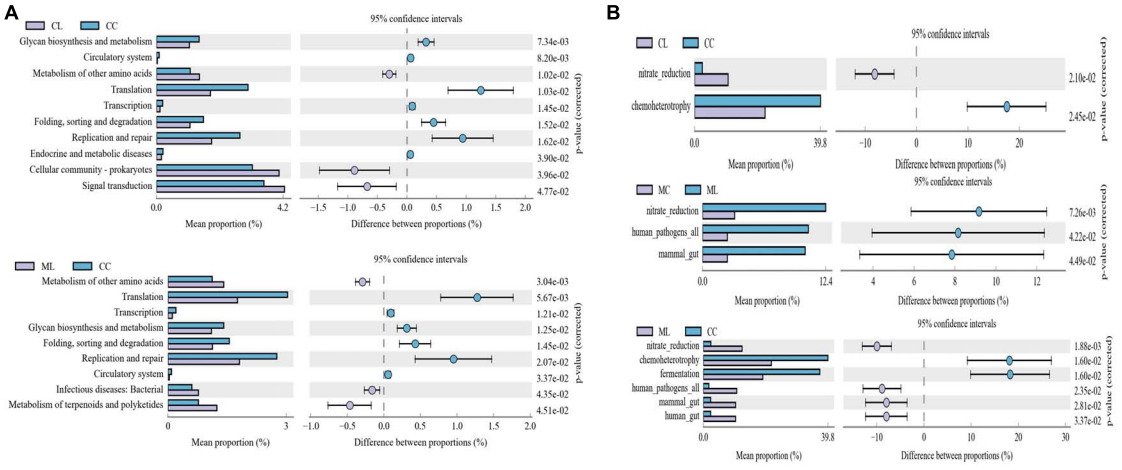

FIGURE 12
Potential Function prediction analysis of mouse microbiota. **(A)** Tax4Fun, **(B)** FAPROTAX.

10.3389/fmicb.2023.1256748

LPS and cold normal saline changed metabolites in mice among different groups

Out of 4,320 metabolites, 2,181 and 2,139 were in positive and negative ion mode, respectively in mice in our study. Those metabolites were mainly annotated to amino acid metabolism and lipid metabolism via KEGG (Figure 13A), lipids and lipid-like molecules and organic acids and derivatives via HMDB (Figure 13B), and fatty acyls and glycerolipids via LIPID MAPS (Figure 13C). Compared with CC mice, there were 43 up-regulated and 19 down-regulated metabolites in MC animal, 410 up-regulated and 968 down-regulated metabolites in CL animal, while 213 up-regulated and 128 down-regulated metabolites in CL animals. Compared with group MC, there were 205 up-regulated and 792 down-regulated metabolites in CL animal, whereas 182 up-regulated and 103 down-regulated metabolites in ML animals. Compared with CL group, there were 1,046 up-regulated and 428 down-regulated metabolites in ML animals (Figure 14). Venn map showed that there were no shared differential metabolites among mice groups (Figure 15). Z-score analysis of top 30 differential metabolites in animals showed

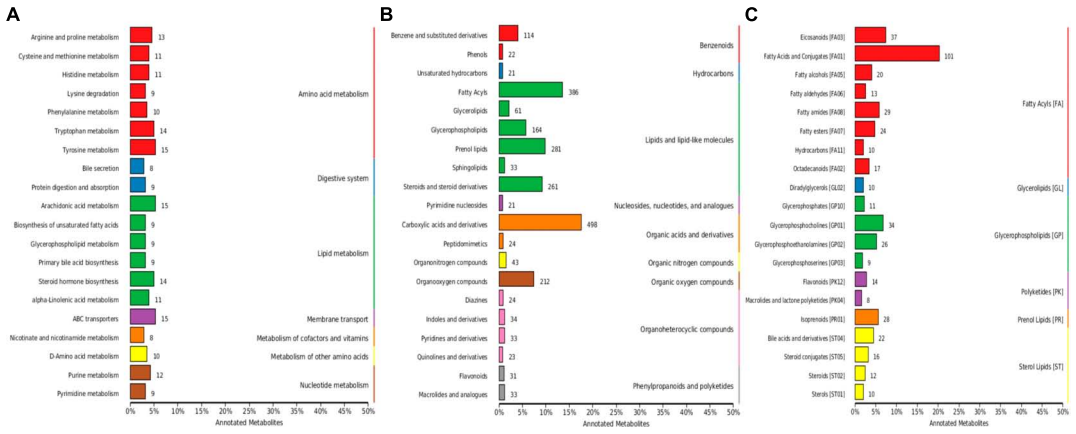

FIGURE 13
Metabolites annotation of mice. **(A)** KEGG, **(B)** HMDB, and **(C)** LIPID MAPS.

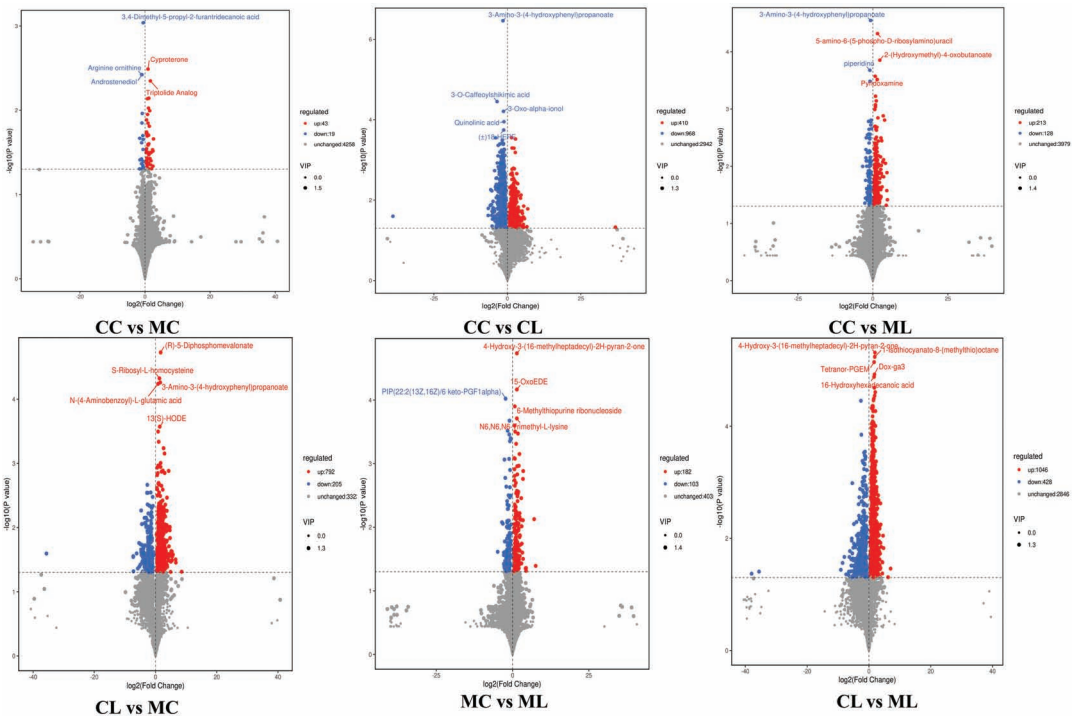

FIGURE 14
Volcano plot of differential metabolites in mice.

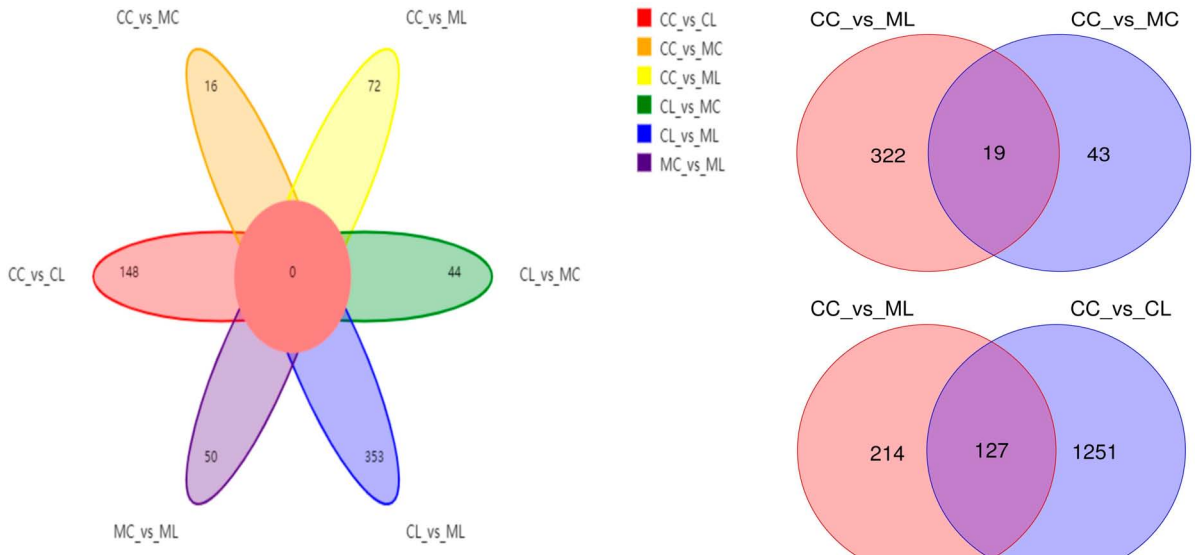

FIGURE 15
Venn map of differential metabolites among different mice groups.

that the abundance of metabolites in mice treated with ice-cold normal saline decreased with red balls mainly distributed in MC and ML sides, while LPS challenging could increase the abundance of metabolites with more red balls in the CL sides (**Supplementary Figure 2**). To further reveal the marker metabolites between mice groups, we examined metabolites between CC vs. MC and CC vs. ML. The results showed that compared with mice in group CC, neg_3481 ($P < 0.05$), neg_457 ($P < 0.01$), neg_7126 ($P < 0.05$), pos_771 ($P < 0.05$), pos_715 ($P < 0.05$), neg_539 ($P < 0.05$), neg_4796 ($P < 0.05$), pos_1504 ($P < 0.05$), pos_3391 ($P < 0.05$), neg_6883 ($P < 0.05$) and pos_4916 ($P < 0.05$) were obviously higher in group MC and ML, while neg_6324 ($P < 0.05$) and pos_783 ($P < 0.05$) were significantly lower in group MC and ML. The abundance of neg_6169 ($P < 0.05$) and neg_6271 ($P < 0.05$) were observably lower in MC than CC, while higher in ML. The abundance of neg_1751 ($P < 0.01$), neg_87 ($P < 0.01$), pos_699 ($P < 0.05$) and pos_4607 ($P < 0.05$) in MC were markedly higher ($P < 0.05$) than CC, while lower in ML (**Supplementary Figure 3**). Whereas, comparing of metabolites in mice in CC indicated that 127 shared differential metabolites in group CL and ML, with 94 lower abundant metabolites and 33 higher abundant metabolites (**Table 7**).

Correlation analysis of gut microbiota and inflammatory cytokines in mice

Correlation analysis showed that *Enterococcus* and *Escherichia_Shigella* were both positively related to TNF-α, IL-1β and IL-6, while Lachnospiraceae_UCG_001 and unclassified_Lachnospiraceae were negatively related to these inflammatory cytokines. Bacteroides was positively related to TNF-α, Parateroides was positively related to IL-10, TNF-α and IL-1β, and unclassified_Muribaculaceae was positively related to IL-10, while *Colidextribacter* and Lachnospiraceae_NK4A136_group were negatively related to IL-1β and IL-6 (**Supplementary Figure 4**).

Discussion

During the winter period or in cold areas, cold water can induce stress in animals. When it is combined with factors such as feed supplements, social factors and environmental stresses, it can significantly impair the function of the digestive system in animals, and lead to growth performance disorders (Yin et al., 2014; Oraby et al., 2021; Rehman et al., 2021). In this study, we aimed to investigate the impact of cold stimulus combined with LPS on mice. Our findings revealed that the mice treated with cold normal saline exhibited a slightly lower body weight. This observation is consistent with previous studies conducted on pigs in which different temperature water treatments influenced the body weight (Zhang et al., 2020). Pathological analysis revealed that cold stress had minimal impact on the integrity of intestinal villi and gastric epithelium, while LPS significantly destroyed the villi. These findings are congrant with previous studies conducted on cold-stressed broilers (Su et al., 2018) and LPS-challenged hens (Feng et al., 2023).

Furthermore, the cytokines TNF-α and IL-6 were significantly more expressed in mice challenged with LPS and cold normal saline stress compared to other groups. Whereas, IL-1β level was similar between groups CC and CL, but it was significantly elevated in mice treated with cold normal saline + LPS. Previous study reported that chronic cold exposure upregulated IL6 and TNFα level in the blood of mice (Bal et al., 2017). Our findings are in line with their results in which cold normal saline stress increase the expression of TNF-α and IL-6.

TABLE 7 Comparing of differential metabolites among different mice groups.

ID	CC	CL	ML
neg_1198	33.07 ± 17.46^{a}	135.20 ± 74.40^{b}	72.99 ± 28.02^{b}
neg_1556	3836.96 ± 315.62^{b}	2990.18 ± 622.50^{a}	2987.65 ± 661.52^{a}
neg_1598	6562.27 ± 3649.38^{b}	1409.85 ± 958.93^{a}	1897.95 ± 959.68^{a}
neg_1683	164.84 ± 87.20^{b}	35.87 ± 23.49^{a}	31.38 ± 21.59^{a}
neg_1745	127.60 ± 27.63^{c}	50.20 ± 27.30^{a}	82.88 ± 13.63^{b}
neg_1751	27.41 ± 12.37^{b}	8.13 ± 7.14^{a}	9.98 ± 7.01^{a}
neg_1790	213.76 ± 19.45^{c}	75.04 ± 17.08^{a}	126.06 ± 10.16^{b}
neg_1819	33.69 ± 31.76^{a}	82.37 ± 26.70^{b}	217.30 ± 142.44^{b}
neg_1830	758.31 ± 184.44^{b}	391.08 ± 172.60^{a}	396.48 ± 122.24^{a}
neg_2058	11.35 ± 9.14^{a}	28.81 ± 10.51^{b}	40.49 ± 22.07^{b}
neg_2088	6140.61 ± 2537.07^{b}	2008.73 ± 470.76^{a}	2125.20 ± 798.61^{a}
neg_2352	754.67 ± 1084.69^{a}	3595.94 ± 1739.60^{b}	3417.12 ± 2193.03^{b}
neg_3041	161.69 ± 62.16^{b}	77.94 ± 39.70^{a}	241.30 ± 46.43^{c}
neg_3305	738.85 ± 111.02^{b}	458.96 ± 129.22^{a}	462.15 ± 96.80^{a}
neg_335	194.08 ± 29.05^{b}	86.22 ± 26.31^{a}	120.24 ± 25.24^{a}
neg_336	273.50 ± 108.99^{b}	44.32 ± 25.33^{a}	117.69 ± 79.59^{a}
neg_3439	105.94 ± 140.46^{a}	493.43 ± 238.22^{b}	320.37 ± 124.28^{b}
neg_3667	4.79 ± 9.70^{a}	68.50 ± 48.74^{b}	71.84 ± 26.57^{b}
neg_3765	1514.62 ± 509.87^{b}	530.18 ± 192.89^{a}	812.15 ± 258.59^{a}
neg_3801	24414.46 ± 8231.70^{b}	9737.90 ± 5857.18^{a}	12475.74 ± 5106.68^{a}
neg_381	520.97 ± 131.36^{c}	89.03 ± 19.11^{a}	218.78 ± 90.63^{b}
neg_3954	23780.12 ± 7905.96^{c}	8040.20 ± 4143.39^{a}	13795.74 ± 2672.11^{b}
neg_406	17735.61 ± 5578.39^{c}	2080.01 ± 339.00^{a}	7906.46 ± 3804.20^{b}
neg_4452	6984.31 ± 2014.20^{b}	4174.15 ± 1406.84^{a}	4244.05 ± 582.62^{a}
neg_471	296.71 ± 69.52^{b}	167.78 ± 41.54^{a}	211.55 ± 44.99^{a}
neg_4774	1014.78 ± 378.38^{c}	195.90 ± 143.81^{a}	563.30 ± 209.31^{b}
neg_478	884.96 ± 264.79^{c}	286.06 ± 71.49^{a}	547.49 ± 176.05^{b}
neg_4796	517.57 ± 192.50^{a}	1256.56 ± 602.77^{b}	1693.47 ± 746.30^{b}
neg_485	8061.86 ± 2603.25^{c}	730.48 ± 561.39^{a}	4198.18 ± 2243.77^{b}
neg_4878	2368.18 ± 856.82^{c}	497.93 ± 208.63^{a}	1153.53 ± 402.62^{b}
neg_4939	14443.58 ± 3996.24^{c}	3704.55 ± 1851.07^{a}	6653.47 ± 2168.27^{b}
neg_4970	169.74 ± 43.30^{a}	1131.30 ± 668.86^{b}	2004.70 ± 954.91^{b}
neg_508	1019.59 ± 261.38^{b}	513.35 ± 180.02^{a}	628.64 ± 184.37^{a}
neg_5089	2002.32 ± 1269.18^{a}	6585.82 ± 3665.93^{b}	10566.29 ± 5215.02^{b}
neg_5210	4117.40 ± 1611.32^{c}	666.28 ± 314.09^{a}	1701.79 ± 707.80^{b}
neg_5222	158435.10 ± 46708.06^{c}	45323.48 ± 21375.06^{a}	96036.72 ± 28872.87^{b}
neg_5224	371.72 ± 126.98^{b}	121.36 ± 73.08^{a}	190.93 ± 86.04^{a}
neg_5253	547.70 ± 124.64^{c}	163.79 ± 76.62^{a}	342.35 ± 153.65^{b}
neg_5329	448.83 ± 70.37^{b}	299.41 ± 91.80^{a}	339.57 ± 79.46^{a}
neg_5399	31.22 ± 29.09^{a}	127.88 ± 80.19^{b}	571.94 ± 292.91^{c}
neg_5406	11726.23 ± 4434.50^{b}	3089.03 ± 798.86^{a}	4195.31 ± 742.53^{c}
neg_5572	20.51 ± 18.20^{a}	83.47 ± 30.47^{b}	112.16 ± 70.99^{b}
neg_5592	2307.16 ± 1094.87^{a}	4817.65 ± 1244.49^{b}	4163.16 ± 874.03^{b}
neg_574	4833.78 ± 2092.78^{c}	572.14 ± 95.36^{a}	1962.32 ± 1287.23^{b}
neg_577	2607.41 ± 1131.95^{b}	331.70 ± 158.62^{a}	650.89 ± 428.41^{a}
neg_578	492.53 ± 131.40^{b}	146.92 ± 56.56^{a}	236.18 ± 122.00^{a}
neg_581	2669.57 ± 1179.95^{b}	467.98 ± 76.42^{a}	1103.83 ± 713.88^{a}
neg_601	494.69 ± 120.96^{b}	155.81 ± 62.66^{a}	283.54 ± 148.32^{a}
neg_6173	291.47 ± 62.71^{a}	549.08 ± 158.00^{b}	743.58 ± 187.45^{b}
neg_6221	21.03 ± 13.82^{a}	63.75 ± 12.91^{b}	106.48 ± 60.37^{b}
neg_6242	1423.83 ± 674.37^{a}	11954.68 ± 8368.04^{b}	3864.34 ± 2024.83^{b}
neg_6324	4399.15 ± 1060.33^{b}	1688.54 ± 788.53^{a}	2732.95 ± 963.99^{a}
neg_6362	1253.77 ± 257.68^{b}	555.29 ± 238.83^{a}	690.29 ± 268.98^{a}
neg_6432	2462.59 ± 572.13^{b}	1117.27 ± 492.70^{a}	1325.89 ± 533.48^{a}
neg_6522	2584.38 ± 1399.82^{b}	888.98 ± 791.94^{a}	695.70 ± 300.39^{a}
neg_6581	13.00 ± 11.83^{a}	167.00 ± 100.66^{b}	64.13 ± 33.06^{b}
neg_6582	892.06 ± 701.20^{a}	7449.60 ± 4601.59^{b}	3956.39 ± 2164.10^{b}
neg_671	26968.05 ± 13838.66^{c}	2798.41 ± 782.76^{a}	8661.32 ± 5462.16^{b}
neg_674	4851.40 ± 1084.60^{b}	2278.15 ± 482.32^{a}	2862.09 ± 853.62^{a}
neg_6765	21.76 ± 27.96^{a}	299.10 ± 219.90^{b}	479.13 ± 393.34^{b}
neg_6823	1346.85 ± 758.51^{a}	4833.82 ± 2452.01^{b}	3830.03 ± 1958.09^{b}
neg_6913	137886.28 ± 97522.72^{b}	11193.54 ± 7971.42^{a}	21812.49 ± 28529.04^{a}
neg_7013	6143.66 ± 906.40^{a}	53349.97 ± 24038.65^{b}	39412.50 ± 25899.05^{b}
neg_830	63.66 ± 13.48^{b}	44.98 ± 5.54^{a}	41.65 ± 8.49^{a}
neg_836	19475.29 ± 8469.42^{b}	1143.80 ± 568.40^{a}	1143.80 ± 568.40^{a}
neg_85	25.29 ± 17.46^{a}	74.76 ± 24.70^{b}	57.46 ± 8.44^{b}
neg_88	131.02 ± 30.28^{b}	38.22 ± 24.16^{a}	64.16 ± 23.64^{a}
neg_928	4758.94 ± 1151.76^{b}	2315.88 ± 396.22^{a}	2618.04 ± 450.70^{a}
neg_929	3861.78 ± 1502.59^{b}	657.04 ± 152.17^{a}	785.12 ± 370.81^{a}
neg_934	375.91 ± 87.21^{b}	244.99 ± 46.84^{a}	223.38 ± 46.87^{a}
neg_962	2387.74 ± 872.87^{b}	347.79 ± 158.42^{a}	691.30 ± 332.90^{a}
pos_101	35.26 ± 13.70^{b}	9.01 ± 9.04^{a}	16.66 ± 11.67^{a}
pos_111	179.65 ± 33.57^{b}	127.09 ± 38.49^{a}	270.18 ± 41.82^{c}
pos_120	162.89 ± 28.43^{b}	104.68 ± 42.31^{a}	226.26 ± 27.28^{c}
pos_1241	1612.74 ± 384.75^{b}	639.20 ± 277.29^{a}	667.70 ± 589.61^{a}
pos_135	21.76 ± 8.64^{b}	6.16 ± 4.75^{a}	8.53 ± 4.91^{a}
pos_137	55.49 ± 14.07^{b}	34.73 ± 14.12^{a}	75.85 ± 13.45^{c}
pos_1527	1433.16 ± 369.76^{b}	960.75 ± 187.49^{a}	897.95 ± 267.67^{a}
pos_1678	3732.37 ± 2687.22^{a}	9030.32 ± 3598.49^{b}	9951.02 ± 4849.47^{b}
pos_190	1270.08 ± 274.45^{b}	478.72 ± 268.87^{a}	661.93 ± 181.21^{a}
pos_305	28.68 ± 17.86^{b}	4.67 ± 5.39^{a}	62.10 ± 23.63^{c}
pos_318	1515.25 ± 645.48^{b}	146.11 ± 73.63^{a}	305.24 ± 210.36^{a}
pos_3262	523.14 ± 225.11^{c}	59.23 ± 21.70^{a}	158.94 ± 85.34^{b}
pos_3412	176.14 ± 70.73^{c}	25.76 ± 10.59^{a}	86.33 ± 43.74^{b}
pos_355	83.47 ± 35.41^{c}	6.09 ± 6.91^{a}	40.96 ± 15.82^{b}

TABLE 7 (Continued)

ID	CC	CL	ML
pos_4053	183.61 ± 91.59^{a}	394.88 ± 64.95^{b}	448.39 ± 186.59^{b}
pos_461	45.02 ± 5.04^{b}	24.97 ± 16.66^{a}	22.40 ± 6.90^{a}
pos_4633	588.10 ± 152.55^{b}	290.05 ± 142.60^{a}	221.15 ± 82.51^{a}
pos_482	776.77 ± 369.55^{c}	19.85 ± 22.17^{a}	298.62 ± 243.72^{b}
pos_498	600.32 ± 275.63^{b}	146.84 ± 71.72^{a}	260.20 ± 174.62^{a}
pos_5000	2707.16 ± 1052.65^{b}	1434.77 ± 553.10^{a}	4528.64 ± 1449.18^{c}
pos_5165	243.17 ± 122.32^{a}	705.73 ± 214.14^{b}	2681.04 ± 861.58^{c}
pos_5199	151.46 ± 88.02^{a}	275.60 ± 84.50^{b}	596.29 ± 252.17^{c}
pos_5239	25.00 ± 37.13^{a}	146.34 ± 86.50^{b}	114.10 ± 52.48^{b}
pos_5265	304.55 ± 102.30^{c}	106.81 ± 33.47^{a}	166.58 ± 41.40^{b}
pos_5266	146.16 ± 47.13^{b}	57.87 ± 15.77^{a}	78.94 ± 17.50^{a}
pos_5268	97.19 ± 26.85^{b}	37.01 ± 11.62^{a}	41.00 ± 18.13^{a}
pos_5269	2801.55 ± 1037.16^{b}	1304.27 ± 459.16^{a}	1537.39 ± 439.94^{a}
pos_5424	1729.51 ± 604.11^{b}	604.74 ± 392.17^{a}	886.82 ± 409.98^{a}
pos_5531	948.73 ± 281.52^{b}	516.96 ± 261.90^{a}	435.77 ± 95.40^{a}
pos_5899	542.57 ± 196.19^{a}	3892.82 ± 2543.66^{b}	3370.83 ± 2021.23^{b}
pos_598	140361.16 ± 43082.17^{a}	24809.18 ± 14315.74^{b}	24809.18 ± 14315.74^{b}
pos_6025	185.22 ± 47.41^{b}	105.43 ± 44.50^{a}	118.67 ± 37.25^{a}
pos_6064	733.73 ± 209.51^{a}	1235.90 ± 230.23^{b}	2146.20 ± 762.14^{c}
pos_609	195.47 ± 97.71^{c}	14.30 ± 10.57^{a}	72.67 ± 43.36^{b}
pos_6099	1577.45 ± 454.01^{a}	15237.29 ± 11320.29^{c}	12216.60 ± 4648.55^{b}
pos_6146	6115.40 ± 2305.52^{c}	1324.47 ± 415.27^{a}	3094.72 ± 536.07^{b}
pos_619	5394.04 ± 1664.79^{b}	1136.21 ± 756.32^{a}	2773.09 ± 1707.43^{a}
pos_620	39.25 ± 12.09^{b}	8.36 ± 4.46^{a}	13.10 ± 12.97^{a}
pos_621	773.71 ± 247.55^{b}	129.33 ± 69.45^{a}	309.73 ± 232.69^{a}
pos_6249	2768.17 ± 778.71^{c}	877.96 ± 414.92^{a}	1831.54 ± 423.24^{b}
pos_6405	809.69 ± 229.70^{a}	1882.51 ± 609.71^{b}	1635.54 ± 407.97^{b}
pos_6646	1872.51 ± 694.98^{b}	708.78 ± 365.46^{a}	877.43 ± 198.16^{a}
pos_6725	276.60 ± 76.67^{b}	128.63 ± 97.98^{a}	155.60 ± 57.67^{a}
pos_6889	10388.01 ± 2876.39^{c}	2620.05 ± 1556.63^{a}	5667.42 ± 2170.47^{b}
pos_6961	248.79 ± 97.16^{b}	89.13 ± 49.15^{a}	425.01 ± 141.92^{c}
pos_7617	519.30 ± 84.38^{a}	2461.45 ± 1081.21^{b}	2790.60 ± 1801.86^{b}
pos_762	179.67 ± 55.39^{b}	61.29 ± 24.87^{a}	52.46 ± 45.29^{a}
pos_7698	13132.79 ± 4950.31^{a}	21968.14 ± 6396.33^{b}	34126.43 ± 10518.70^{b}
pos_7749	584.61 ± 112.35^{b}	392.79 ± 137.82^{a}	911.55 ± 72.67^{c}
pos_783	227.54 ± 90.95^{b}	33.10 ± 28.85^{a}	94.55 ± 72.67^{a}
pos_8045	685.39 ± 148.84^{b}	406.45 ± 103.18^{a}	886.37 ± 115.58^{c}
pos_806	243.82 ± 118.45^{b}	23.22 ± 28.23^{a}	69.21 ± 114.87^{a}
pos_8108	540.46 ± 117.12^{b}	314.67 ± 116.01^{a}	784.02 ± 94.97^{c}
pos_8112	7987.51 ± 1358.04^{b}	5198.31 ± 1640.70^{a}	10436.67 ± 1341.77^{c}
pos_832	9894.85 ± 3939.77^{b}	1387.88 ± 561.12^{a}	3719.36 ± 3176.71^{a}
pos_99	79.63 ± 16.18^{b}	30.53 ± 19.93^{a}	35.69 ± 19.49^{a}

Data are presented as the mean ± std.dev ($n = 6$), significance is presented as different letters when $p < 0.05$.

To explore the potential mechanisms, we detected the gene expressions of tight junction proteins in small intestine (jejunum and ileum). Among them OCCLUDIN is recognized as important component of intestinal permeability (Chen et al., 2015, 2022). Whereas, relative gene expression confirmed that significant differences were detected in the expression levels of *OCCLUDIN* and *CASPASE-1* in mice in the CL and ML groups. The expression of *OCCLUDIN* is in line with a study on inflammatory bowel disease in humans (Chen et al., 2015), while expression of *CLAUDIN* is in line with He et al. (2022). Additionally, slight differences in *CLAUDIN* and *NLRP3* were observed between mice in the CL and ML groups. Previous studies found that the activation of *Caspase-1* by *NLRP3* cause inflammation reaction (Sho and Xu, 2019; He et al., 2022).

Moreover, our study assessed the antioxidant indexes, NO levels, and cytokine levels in the serum of various groups in mice. Our findings revealed that cold stress reduced the antioxidant capacity in LPS-challenged mice by lowering the level of T-AOC, GSH-Px, and SOD, and increasing the level of MDA. Additionally, cold stress promoted an inflammatory response, as evidenced by higher levels of IL-1β in mice treated with cold normal saline + LPS. Previous studies have mentioned that the expression of antioxidant is disturbed in different inflammatory conditions (Sho and Xu, 2019; Aziz et al., 2021; Murtaza et al., 2021). Gut microbiome analyzing showed that cold stress led to a decrease in data numbers in the MC group, as well as a reduction in the Shannon and Simpson indexes in the ML group. Moreover, cold stress increased the beta diversities of PCA, PCoA, and NMDS.

To further investigate the distinguished bacteria influenced by cold stress and LPS, we conducted LEfSe analysis and identified 12 biomarkers (o__Enterobacterales, C__Gammaproteobacteria, p__Proteobacteria, f__Enterobacteriaceae, s__unclassified_*Escherichia_Shigella*, g__*Escherichia_Shigella*, p__Firmicutes, c__*Clostridia*, o__Oscillospirales, f__Oscillospiraceae, s__unclassified_Bacteroides and g__Lachnospiraceae_NK4A136_group) in different mouse groups, which was partly in line with the results in cold stress treated rates (Sun et al., 2023). Among them higher abundance of pathogenic s__unclassified_*Escherichia_Shigella* and g__*Escherichia_Shigella* were found in mice in ML, which inferred that cold stress could promote the colonization of harmful bacteria in LPS induced mice. When compared with CC mice, the abundance of 20, 20, and 19 genera were obviously different with MC, CL, and MC animals, respectively. Compared with MC mice, the abundance of 20 and 20 genus were prominently different with mice in CL and ML groups, respectively. There were different 20 genus between CL and ML. Further analysis revealed significant differences in the abundance of 4 phyla and 24 genera were among the mouse groups. Notably, the abundance of *Candidatus_Solibacter* in the ML group was lower compared to the other groups, particularly the CL group. Previous studies have reported a positive correlation between *Candidatus Solibacter*, *Peptococcus*, and antioxidant capacity (Peng et al., 2021; Kong et al., 2022), which is suggesting that the decreased abundance of these genera in the MC and ML groups may indicate reduced oxidative resistance in animals exposed to cold stress.

Additionally, *Escherichia_Shigella* is a genus known to cause mucosal inflammation and has been found in abundant in

mice with ulcerative colitis and individuals with Crohn's disease (Jialing et al., 2020; Ma et al., 2022). The higher abundance of this genus observed in mice in the MC and ML groups, particularly in the ML animals, is consistent with previous studies (Chen et al., 2022). This finding suggests that cold stress may exacerbate intestinal inflammation in mice. On the other hand, lower abundances of Family_XIII_UCG_001, Lachnospiraceae_UCG_001, *Novosphingobium*, RB41, and *Tyzzerella* have been previously reported in chronic colitis mice (Huangfu et al., 2021; Xu et al., 2021), Crohn's disease patients (Jiang et al., 2022), ulcerative colitis mice (Wang et al., 2019), heat stress-induced rabbits (Shi et al., 2022) and Alzheimer patients (Kaiyrlykyzy et al., 2022), respectively. These findings are consistent with the observations in the MC and ML groups of the current study, which indicated that cold stress may have a negative impact on mice by reducing the abundance of these four genera.

The proportion of Mucispirillum was higher in cold stressed mice, which was in agreement with findings in colitis mouse (Li et al., 2022). Providencia is an opportunistic pathogenic genera known to cause acute enteric infection (Ovchinnikova et al., 2013), and its higher abundance has been previously reported in diarrheal dogs (Herstad et al., 2021). The increased abundance of this pathogenic genus may contribute to intestinal injury in mice. *Staphylococcus* is also a pathogenic genera threatening public health (Hoveida et al., 2019), which may infer that this genera negatively affect animals in the current study.

Previous studies found that unclassified_Lachnospiraceae, Unclassified_Peptococcaceae and unclassified_Sphingomonadaceae were negatively associated with the pathogenesis of type 2 diabetes (Kim et al., 2022), pulmonary fibrosis (Li et al., 2022), and mastitis in camel, respectively. These findings are consistent with the decreased abundance of these three genera observed in the cold-stressed animals in the current study. *Roseburia* is a promising probiotic genus known to improve the gut ecosystem (Sanders et al., 2019; Seo et al., 2020). The lower abundance of *Roseburia* in the MC and ML groups may indicate that cold stress contributes to damage by reducing the presence of this genus.

Cold stress and LPS induction also had an impact on the metabolites in mice. We detected a total of 4,320 metabolites, with 43 up-regulated and 19 down-regulated metabolites in the CC vs. MC animal comparison. Similarly, in the comparison of ML vs. CL animals, we observed 1,046 up-regulated and 428 down-regulated metabolites. Z-score analysis further confirmed the changes in metabolites induced by cold stress. Among these metabolites, there were 19 that showed significant changes between CC vs. MC and CC vs. ML groups. These metabolites include (neg_3481, neg_457, neg_7126, pos_771, pos_715, neg_539, neg_4796, pos_1504, pos_3391, neg_6883, pos_4916, neg_6324, pos_783, neg_6169, neg_6271, neg_1751, neg_87, pos_699, and pos_4607). The alterations in these metabolites, induced by cold stress and LPS, ultimately led to changes in microbiota function.

There are many reports in which it is mentioned that systemic LPS treatment in mice severely impact whole body temperature as well as induce thermogenesis proteins in the skeletal muscle (Bal et al., 2021). In our study, LPS treatment is probably is not systemic, that's why there were no noticeable induction of thermogenesis proteins in the skeletal muscle. This may be a limitation of present study.

Conclusion

In conclusion, we investigated the impact of cold stress on LPS-induced mice and observed that cold stress exacerbated intestinal damage by disrupting the balance of gut microbiota and altering its metabolites. These findings have important implications for improving the feeding and management practices of livestock in cold regions or during cold periods.

Data availability statement

The data presented in this study are deposited in the NCBI database under BioProject accession number PRJNA972973 (https://www.ncbi.nlm.nih.gov/bioproject/PRJNA972973/).

Ethics statement

All the experiment operations were under the instructions and approval of Laboratory Animals Research Centre of Jiangsu, China and the Ethics Committee of Nanjing Agricultural University. The study was conducted in accordance with the local legislation and institutional requirements.

Author contributions

JL: Data curation, Formal analysis, Investigation, Methodology, Writing—original draft, Writing—review and editing. ZC: Data curation, Investigation, Methodology, Formal analysis, Writing—review and editing. MW: Data curation, Investigation, Methodology, Writing—review and editing. MA: Formal analysis, Validation, Writing—review and editing. PY: Conceptualization, Funding acquisition, Project administration, Supervision, Validation, Visualization, Writing—review and editing.

Funding

The author(s) declare financial support was received for the research, authorship, and/or publication of this article. This study was supported by the Public Welfare Industry (Agriculture) Scientific Research Projects (201303145) and the National Natural Science Foundation of China (31501930).

Acknowledgments

The authors extend their appreciation to the Researchers Supporting Project number (RSP2023R191), King Saud University, Riyadh, Saudi Arabia.

Conflict of interest

The authors declare that the research was conducted in the absence of any commercial or financial relationships that could be construed as a potential conflict of interest.

Publisher's note

All claims expressed in this article are solely those of the authors and do not necessarily represent those of their affiliated organizations, or those of the publisher, the editors and the reviewers. Any product that may be evaluated in this article, or claim that may be made by its manufacturer, is not guaranteed or endorsed by the publisher.

Supplementary material

The Supplementary Material for this article can be found online at: https://www.frontiersin.org/articles/10.3389/fmicb.2023.1256748/full#supplementary-material

SUPPLEMENTARY FIGURE 1
Comparing of villus height and crypt depth in mice in different groups. **(A)** jejunum, **(B)** ileum, **(C)** colon. Significance is presented as $*p < 0.05$, $**p < 0.01$, $***p < 0.001$, and $****p < 0.0001$; data are presented as the mean ± SEM ($n = 3$).

SUPPLEMENTARY FIGURE 2
Z-score analysis of top 30 differential metabolites among different mice groups.

SUPPLEMENTARY FIGURE 3
Comparing of differential metabolites among different mice groups.

SUPPLEMENTARY FIGURE 4
Analysis of the correlation between gut microbiota and inflammatory cytokines in mice.

References

Aljahdali, N. H., Sanad, Y. M., Han, J., and Foley, S. L. (2020). Current knowledge and perspectives of potential impacts of *Salmonella enterica* on the profile of the gut microbiota. *BMC Microbiol.* 20:353. doi: 10.1186/s12866-020-02008-x

Aziz, S., Abdullah, S., Anwar, H., Latif, F., and Mustfa, W. (2021). Effect of engineered nickel oxide nano particles on antioxidant enzymes in fresh water fish, Labeo rohita. *Pak. Vet. J.* 41, 424–428. doi: 10.29261/pakvetj/2021.044

Bal, N. C., Gupta, S. C., Pant, M., Sopariwala, D. H., Gonzalez-Escobedo, G., Turner, J., et al. (2021). Is upregulation of sarcolipin beneficial or detrimental to muscle function? *Front. Physiol.* 12:633058. doi: 10.3389/fphys.2021.633058

Bal, N. C., Maurya, S. K., Pani, S., Sethy, C., Banerjee, A., Das, S., et al. (2017). Mild cold induced thermogenesis: Are BAT and skeletal muscle synergistic partners? *Biosci. Rep.* 37:BSR20171087. doi: 10.1042/BSR20171087

Bolyen, E., Rideout, J. R., Dillon, M. R., Bokulich, N. A., Abnet, C. C., Al-Ghalith, G. A., et al. (2019). Reproducible, interactive, scalable and extensible microbiome data science using QIIME 2. *Nat. Biotechnol.* 37, 852–857. doi: 10.1038/s41587-019-0209-9

Callahan, B. J., Mcmurdie, P. J., Rosen, M. J., Han, A. W., Johnson, A. J. A., and Holmes, S. P. (2016). DADA2: high-resolution sample inference from Illumina amplicon data. *Nat. Methods* 13, 581–583. doi: 10.1038/nmeth.3869

Chen, C., Luo, F., Wu, P., Huang, Y., Das, A., Chen, S., et al. (2020). Metabolomics reveals metabolite changes of patients with pulmonary arterial hypertension in China. *J. Cell. Mol. Med.* 24, 2484–2496. doi: 10.1111/jcmm.14937

Chen, H., and Boutros, P. C. (2011). VennDiagram: a package for the generation of highly-customizable Venn and Euler diagrams in R. *BMC Bioinformatics* 12:35. doi: 10.1186/1471-2105-12-35

Chen, J., Tellez, G., Richards, J. D., and Escobar, J. (2015). Identification of potential biomarkers for gut barrier failure in broiler chickens. *Front. Vet. Sci.* 2:14. doi: 10.3389/fvets.2015.00014

Chen, X., Kong, Q., Zhao, X., Zhao, C., Hao, P., Irshad, I., et al. (2022). Sodium acetate/sodium butyrate alleviates lipopolysaccharide-induced diarrhea in mice via regulating the gut microbiota, inflammatory cytokines, antioxidant levels, and NLRP3/Caspase-1 signaling. *Front. Microbiol.* 13:1036042. doi: 10.3389/fmicb.2022.1036042

Dong, H., Chen, X., Zhao, X., Zhao, C., Mehmood, K., Kulyar, M. F., et al. (2023). Intestine microbiota and SCFAs response in naturally *Cryptosporidium*-infected plateau yaks. *Front. Cell. Infect. Microbiol.* 13:1105126. doi: 10.3389/fcimb.2023.1105126

Dunn, W. B., Broadhurst, D., Begley, P., Zelena, E., Francis-Mcintyre, S., Anderson, N., et al. (2011). Procedures for large-scale metabolic profiling of serum and plasma using gas chromatography and liquid chromatography coupled to mass spectrometry. *Nat. Protoc.* 6, 1060–1083. doi: 10.1038/nprot.2011.335

Edgar, R. C. (2013). UPARSE: highly accurate OTU sequences from microbial amplicon reads. *Nat. Methods* 10, 996–998. doi: 10.1038/nmeth.2604

Fahy, E., Sud, M., Cotter, D., and Subramaniam, S. (2007). LIPID MAPS online tools for lipid research. *Nucleic Acids Res.* 35, W606–W612. doi: 10.1093/nar/gkm324

Feng, J., Li, Z., Ma, H., Yue, Y., Hao, K., Li, J., et al. (2023). Quercetin alleviates intestinal inflammation and improves intestinal functions via modulating gut microbiota composition in LPS-challenged laying hens. *Poult. Sci.* 102:102433. doi: 10.1016/j.psj.2022.102433

Fu, J., Liu, C., Zhang, Z., Xing, M., and Xu, S. (2013). Influence of inflammatory pathway markers on oxidative stress induced by cold stress in intestine of quails. *Res. Vet. Sci.* 95, 495–501. doi: 10.1016/j.rvsc.2013.05.006

Hassan, M., Ali, A., Wajid, M., Ahmad, A., Saleemi, M. K., Sarwar, Y., et al. (2021). Purification and antigenic detection of lipopolysaccharides of *Salmonella enterica* serovar Typhimurium isolate from Faisalabad, Pakistan. *Pak. Vet. J.* 41, 434–438. doi: 10.29261/pakvetj/2021.046

He, Y., Li, Z., Xu, T., Luo, D., Chi, Q., Zhang, Y., et al. (2022). Polystyrene nanoplastics deteriorate LPS-modulated duodenal permeability and inflammation in mice via ROS drived-NF-κB/NLRP3 pathway. *Chemosphere* 307:135662. doi: 10.1016/j.chemosphere.2022.135662

Herstad, K. M. V., Trosvik, P., Haaland, A. H., Haverkamp, T. H. A., Muinck, E. J., and Skancke, E. (2021). Changes in the fecal microbiota in dogs with acute hemorrhagic diarrhea during an outbreak in Norway. *J. Vet. Intern. Med.* 35, 2177–2186. doi: 10.1111/jvim.16201

Hoveida, L., Halaji, M., Rostami, S., and Mobasherizadeh, S. (2019). Biofilm-producing ability of *Staphylococcus* spp isolated from different foodstuff products. *Ann. Ig.* 31, 140–147. doi: 10.7416/ai.2019.2266

Huangfu, L., Cai, X., Yang, J., Wang, H., Li, Y., Dai, Z., et al. (2021). Irisin attenuates inflammation in a mouse model of ulcerative colitis by altering the intestinal microbiota. *Exp. Ther. Med.* 22:1433. doi: 10.3892/etm.2021.10868

Jialing, L., Yangyang, G., Jing, Z., Xiaoyi, T., Ping, W., Liwei, S., et al. (2020). Changes in serum inflammatory cytokine levels and intestinal flora in a self-healing dextran sodium sulfate-induced ulcerative colitis murine model. *Life Sci.* 263:118587. doi: 10.1016/j.lfs.2020.118587

Jiang, J., Chen, L., Chen, Y., and Chen, H. (2022). Exclusive enteral nutrition remodels the intestinal flora in patients with active Crohn's disease. *BMC Gastroenterol.* 22:212. doi: 10.1186/s12876-022-02293-y

Joo, S. Y., Park, M. J., Kim, K. H., Choi, H. J., Chung, T. W., Kim, Y. J., et al. (2016). Cold stress aggravates inflammatory responses in an LPS-induced mouse model of acute lung injury. *Int. J. Biometeorol.* 60, 1217–1225.

Kaiyrlykyzy, A., Kozhakhmetov, S., Babenko, D., Zholdasbekova, G., Alzhanova, D., Olzhayev, F., et al. (2022). Study of gut microbiota alterations in Alzheimer's dementia patients from Kazakhstan. *Sci. Rep.* 12:15115. doi: 10.1038/s41598-022-19393-0

Kanehisa, M., and Goto, S. (2000). KEGG: kyoto encyclopedia of genes and genomes. *Nucleic Acids Res.* 1, 27–30.

Kim, K., Lee, S., Park, S. C., Kim, N. E., Shin, C., Lee, S. K., et al. (2022). Role of an unclassified Lachnospiraceae in the pathogenesis of type 2 diabetes: a longitudinal study of the urine microbiome and metabolites. *Exp. Mol. Med.* 54, 1125–1132. doi: 10.1038/s12276-022-00816-x

Kong, L., Wang, Z., Xiao, C., Zhu, Q., and Song, Z. (2022). Glycerol monolaurate attenuated immunological stress and intestinal mucosal injury by regulating the

gut microbiota and activating AMPK/Nrf2 signaling pathway in lipopolysaccharide-challenged broilers. *Anim. Nutr.* 10, 347–359. doi: 10.1016/j.aninu.2022.06.005

Langille, M. G. I., Zaneveld, J., Caporaso, J. G., Mcdonald, D., Knights, D., Reyes, J. A., et al. (2013). Predictive functional profiling of microbial communities using 16S rRNA marker gene sequences. *Nat. Biotechnol.* 31, 814–821. doi: 10.1038/nbt.2676

Lee, Y. S., Lee, S. H., Gadde, U. D., Oh, S. T., Lee, S. J., and Lillehoj, H. S. (2018). Allium hookeri supplementation improves intestinal immune response against necrotic enteritis in young broiler chickens. *Poult. Sci.* 97, 1899–1908. doi: 10.3382/ps/pey031

Li, Q., Wu, W., Fang, X., Chen, H., Han, Y., Liu, R., et al. (2022). Structural characterization of a polysaccharide from bamboo (*Phyllostachys edulis*) shoot and its prevention effect on colitis mouse. *Food Chem.* 387:132807. doi: 10.1016/j.foodchem.2022.132807

Li, S., Li, J., Liu, Y., Li, C., Zhang, R., and Bao, J. (2020). Effects of intermittent mild cold stimulation on mRNA expression of immunoglobulins, cytokines, and toll-like receptors in the small intestine of broilers. *Animals* 10:1492. doi: 10.3390/ani10091492

Liu, X., Li, S., Zhao, N., Xing, L., Gong, R., Li, T., et al. (2022). Effects of acute cold stress after intermittent cold stimulation on immune-related molecules, intestinal barrier genes, and heat shock proteins in broiler ileum. *Animals* 12:3260. doi: 10.3390/ani12233260

Ma, X., Lu, X., Zhang, W., Yang, L., Wang, D., Xu, J., et al. (2022). Gut microbiota in the early stage of Crohn's disease has unique characteristics. *Gut Pathog.* 14:46. doi: 10.1186/s13099-022-00521-0

Matsuoka, K., and Kanai, T. (2015). The gut microbiota and inflammatory bowel disease. *Semin. Immunopathol.* 37, 47–55. doi: 10.1007/s00281-014-0454-4

Meng, M., Huo, R., Wang, Y., Ma, N., Shi, X., Shen, X., et al. (2022). Lentinan inhibits oxidative stress and alleviates LPS-induced inflammation and apoptosis of BMECs by activating the Nrf2 signaling pathway. *Int. J. Biol. Macromol.* 222, 2375–2391. doi: 10.1016/j.ijbiomac.2022.10.024

Murtaza, S., Khan, J. A., Aslam, B., and Faisal, M. N. (2021). Pomegranate peel extract and quercetin possess antioxidant and hepatoprotective activity against concanavalin A-induced liver injury in mice. *Pak. Vet. J.* 41, 197–202. doi: 10.29261/pakvetj/2020.097

Naibaho, F. G., Hartanto, A., Bintang, M., Jamilah, I., Priyani, N., and Putra, E. D. (2021). GC-MS analysis and antimicrobial activity of the aqueous extract from the bulbs of Allium chinense G. Don. cultivated in North Sumatra, Indonesia. *Asian J. Agric. Biol.* 2021:201912562. doi: 10.35495/ajab.2019.12.562

Nishida, A., Inoue, R., Inatomi, O., Bamba, S., Naito, Y., and Andoh, A. (2018). Gut microbiota in the pathogenesis of inflammatory bowel disease. *Clin. J. Gastroenterol.* 11, 1–10. doi: 10.1007/s12328-017-0813-5

Nishino, K., Nishida, A., Inoue, R., Kawada, Y., Ohno, M., Sakai, S., et al. (2018). Analysis of endoscopic brush samples identified mucosa-associated dysbiosis in inflammatory bowel disease. *J. Gastroenterol.* 53, 95–106. doi: 10.1007/s00535-017-1384-4

Ondov, B. D., Bergman, N. H., and Phillippy, A. M. (2011). Interactive metagenomic visualization in a Web browser. *BMC Bioinformatics* 12:385. doi: 10.1186/1471-2105-12-385

Oraby, M. I., Baraka, T. A., and Rakha, G. H. (2021). Impact of cadmium intoxication on health status, rumen and blood constituents in Egyptian Ossimi sheep. *Int. J. Vet. Sci.* 10, 102–106.

Ovchinnikova, O. G., Rozalski, A., Liu, B., and Knirel, Y. A. (2013). O-antigens of bacteria of the genus providencia: structure, serology, genetics, and biosynthesis. *Biochemistry (Mosc)* 78, 798–817. doi: 10.1134/S0006297913070110

Parks, D. H., Tyson, G. W., Hugenholtz, P., and Beiko, R. G. (2014). STAMP: statistical analysis of taxonomic and functional profiles. *Bioinformatics* 30, 3123–3124. doi: 10.1093/bioinformatics/btu494

Peng, S., Wang, X., Wang, Y., Lv, T., Zhao, H., Wang, Y., et al. (2021). Effects of dietary *Bacillus* and non-starch polysaccharase on the intestinal microbiota and the associated changes on the growth performance, intestinal morphology, and serum antioxidant profiles in ducks. *Front. Microbiol.* 12:786121. doi: 10.3389/fmicb.2021.786121

Rehman, A., Hassan, F., Qamar, R., and Rehman, A. U. (2021). Application of plant growth promoters on sugarcane (*Saccharum officinarum* L.) budchip under subtropical conditions. *Asian J. Agric. Biol.* 2021:202003202. doi: 10.35495/ajab.2020.03.202

Romanovsky, A. A., Almeida, M. C., Aronoff, D. M., Ivanov, A. I., Konsman, J. P., Steiner, A. A., et al. (2005). Fever and hypothermia in systemic inflammation: recent discoveries and revisions. *Front. Biosci.* 10:2193–2216. doi: 10.2741/1690

Ruan, D., Wu, S., Fouad, A. M., Zhu, Y., Huang, W., Chen, Z., et al. (2022). Curcumin alleviates LPS-induced intestinal homeostatic imbalance through reshaping gut microbiota structure and regulating group 3 innate lymphoid cells in chickens. *Food Funct.* 13, 11811–11824. doi: 10.1039/D2FO02598A

Rudaya, A. Y., Steiner, A. A., Robbins, J. R., Dragic, A. S., and Romanovsky, A. A. (2005). Thermoregulatory responses to lipopolysaccharide in the mouse: dependence on the dose and ambient temperature. *Am. J. Physiol. Regul. Integr. Comp. Physiol.* 289, R1244–R1252.

Ruigrok, R., Weersma, R. K., and Vich, V. A. (2023). The emerging role of the small intestinal microbiota in human health and disease. *Gut Microbes* 15:2201155. doi: 10.1080/19490976.2023.2201155

Sanders, M., Merenstein, D., Reid, G., Gibson, G., and Rastall, A. R. A. (2019). Probiotics and prebiotics in intestinal health and disease: from biology to the clinic. *Nat. Rev. Gastroenterol. Hepatol.* 16, 605–616.

Segata, N., Izard, J., Waldron, L., Gevers, D., Miropolsky, L., Garrett, W. S., et al. (2011). Metagenomic biomarker discovery and explanation. *Genome Biol.* 12:R60. doi: 10.1186/gb-2011-12-6-r60

Seo, B., Jeon, K., Moon, S., Lee, K., Kim, W., Jeong, H., et al. (2020). *Roseburia* spp. abundance associates with alcohol consumption in humans and its administration ameliorates alcoholic fatty liver in mice. *Cell Host Microbe* 27, 25–40.e6. doi: 10.1016/j.chom.2019.11.001

Shi, Y., Tang, L., Bai, X., Du, K., Wang, H., Jia, X., et al. (2022). Heat stress altered the vaginal microbiome and metabolome in rabbits. *Front. Microbiol.* 13:813622. doi: 10.3389/fmicb.2022.813622

Sho, T., and Xu, J. (2019). Role and mechanism of ROS scavengers in alleviating NLRP3-mediated inflammation. *Biotechnol. Appl. Biochem.* 66, 4–13. doi: 10.1002/bab.1700

Su, Y., Zhang, X., Xin, H., Li, S., Li, J., Zhang, R., et al. (2018). Effects of prior cold stimulation on inflammatory and immune regulation in ileum of cold-stressed broilers. *Poult. Sci.* 97, 4228–4237. doi: 10.3382/ps/pey308

Sun, L., Wang, X., Zou, Y., He, Y., Liang, C., Li, J., et al. (2023). Cold stress induces colitis-like phenotypes in mice by altering gut microbiota and metabolites. *Front. Microbiol.* 14:1134246. doi: 10.3389/fmicb.2023.1134246

Wang, C., Li, W., Wang, H., Ma, Y., Zhao, X., Zhang, X., et al. (2019). *Saccharomyces boulardii* alleviates ulcerative colitis carcinogenesis in mice by reducing TNF-α and IL-6 levels and functions and by rebalancing intestinal microbiota. *BMC Microbiol.* 19:246. doi: 10.1186/s12866-019-1610-8

Wang, J., Zhang, T., Shen, X., Liu, J., Zhao, D., Sun, Y., et al. (2016). Serum metabolomics for early diagnosis of esophageal squamous cell carcinoma by UHPLC-QTOF/MS. *Metabolomics* 12:116. doi: 10.1007/s11306-016-1050-5

Wang, Y., Xiao, H., Liu, Y., Tong, Q., Yu, Y., Qi, B., et al. (2022). Effects of Bu Shen Hua Zhuo formula on the LPS/TLR4 pathway and gut microbiota in rats with letrozole-induced polycystic ovary syndrome. *Front. Endocrinol.* 13:891297. doi: 10.3389/fendo.2022.891297

Wei, H., Zhang, R., Su, Y., Bi, Y., Li, X., Zhang, X., et al. (2018). Effects of acute cold stress after long-term cold stimulation on antioxidant status, heat shock proteins, inflammation and immune cytokines in broiler heart. *Front. Physiol.* 9:1589. doi: 10.3389/fphys.2018.01589

White, J. R., Nagarajan, N., and Pop, M. (2009). Statistical methods for detecting differentially abundant features in clinical metagenomic samples. *PLoS Comput. Biol.* 5:e1000352. doi: 10.1371/journal.pcbi.1000352

Wishart, D. S., Feunang, Y. D., Marcu, A., Guo, A. C., Liang, K., Vázquez-Fresno, R., et al. (2018). HMDB 4.0: the human metabolome database for 2018. *Nucleic Acids Res.* 46, D608–D617. doi: 10.1093/nar/gkx1089

Xu, H., Huang, H., Liu, Y., Zhu, J., Zhou, Y., Chen, H., et al. (2021). Selection strategy of dextran sulfate sodium-induced acute or chronic colitis mouse models based on gut microbial profile. *BMC Microbiol.* 21:279. doi: 10.1186/s12866-021-02342-8

Yin, J., Wu, M. M., Xiao, H., Ren, W. K., Duan, J. L., Yang, G., et al. (2014). Development of an antioxidant system after early weaning in piglets2. *J. Anim. Sci.* 92, 612–619. doi: 10.2527/jas.2013-6986

Zhang, Z., Li, Z., Zhao, H., Chen, X., Tian, G., Liu, G., et al. (2020). Effects of drinking water temperature and flow rate during cold season on growth performance, nutrient digestibility and cecum microflora of weaned piglets. *Animals* 10:1048. doi: 10.3390/ani10061048

Zhao, F., Zhang, Z., Yao, H., Wang, L., Liu, T., Yu, X., et al. (2013). Effects of cold stress on mRNA expression of immunoglobulin and cytokine in the small intestine of broilers. *Res. Vet. Sci.* 95, 146–155. doi: 10.1016/j.rvsc.2013.01.021

frontiers | Frontiers in Microbiology

TYPE Original Research
PUBLISHED 11 January 2024
DOI 10.3389/fmicb.2023.1323877

OPEN ACCESS

EDITED BY
Ren-You Gan,
Agency for Science, Technology and Research, Singapore

REVIEWED BY
Youyou Lu,
Huazhong Agricultural University, China
Jingjing Meng,
University of Miami, United States

*CORRESPONDENCE
Fang Zeng
✉ zengfang@cdutcm.edu.cn
Ying Li
✉ liying@cdutcm.edu.cn

†These authors have contributed equally to this work and share first authorship

RECEIVED 18 October 2023
ACCEPTED 12 December 2023
PUBLISHED 11 January 2024

CITATION
Yao J, Yan X, Li Y, Chen Y, Xiao X, Zhou S, Zhang W, Wang L, Chen M, Zeng F and Li Y (2024) Altered gut microbial profile is associated with differentially expressed fecal microRNAs in patients with functional constipation.
Front. Microbiol. 14:1323877.
doi: 10.3389/fmicb.2023.1323877

Altered gut microbial profile is associated with differentially expressed fecal microRNAs in patients with functional constipation

Junpeng Yao[1†], Xiangyun Yan[1†], Yanqiu Li[1†], Yaoyao Chen[1], Xianjun Xiao[2], Siyuan Zhou[3], Wei Zhang[1], Lu Wang[1], Min Chen[4], Fang Zeng[1*] and Ying Li[1*]

[1]Acupuncture and Tuina School, Chengdu University of Traditional Chinese Medicine, Chengdu, Sichuan, China, [2]School of Health Preservation and Rehabilitation, Chengdu University of Traditional Chinese Medicine, Chengdu, Sichuan, China, [3]Teaching Affairs Office, Chengdu University of Traditional Chinese Medicine, Chengdu, Sichuan, China, [4]Department of Colorectal Disease, Hospital of Chengdu University of Traditional Chinese Medicine, Chengdu, China

While dysbiosis within the intestinal ecosystem has been associated with functional constipation (FC), the mechanisms underlying the interactions between FC and the microbiome remain poorly elucidated. Recent investigations suggested that host microRNAs (miRNAs) can modulate bacterial growth and influence the composition of the gut microbiome. To explore the connection between gut microbiota and fecal miRNAs in FC patients, we initially employed 16S rRNA sequencing to assess the gut microbial landscape in 30 FC patients and 30 healthy controls (HCs). The α-diversity within the FC group exhibited some alterations, and the β-diversity significantly differed, signifying distinctive variations in gut microbiota composition between FC patients and HCs. Subsequently, we identified 44 differentially expressed (DE) miRNAs in feces from FC patients and HCs. Through correlation analysis between DE miRNAs and FC-associated microbiota, we detected an interaction involving nine DE miRNAs (*miR-205-5p*, *miR-493-5p*, *miR-215-5p*, *miR-184*, *miR-378c*, *miR-335-5p*, *miR-514a-3p*, *miR-141-3p*, and *miR-34c-5p*) with seven bacterial genera (*Oscillibacter*, *Escherichia.Shigella*, *UCG.002*, *Lachnospiraceae_NK4A136_group*, *Lachnospiraceae_UCG.010*, *Eubacterium_ruminantium_group* and *Megamonas*), as evidenced by a co-occurrence network. Further, a comprehensive panel of seven diagnostic biomarkers (*Oscillibacter*, *Escherichia.Shigella*, *UCG.002*, *miR-205-5p*, *miR-493-5p*, *miR-215-5p,* and *Lachnospiraceae_NK4A136_group*) demonstrated robust discriminatory capacity in predicting FC status when integrated into a random forest model (AUC = 0.832, 95% CI: 65.73–98.88). Microbiomes correlating with DE miRNAs exhibited enrichment in distinct predicted metabolic categories. Moreover, miRNAs correlated with FC-associated bacteria were found to be enriched in signaling pathways linked to colonic contractility, including Axon guidance, PI3K-Akt signaling pathway,

MAPK signaling pathway, and Hippo signaling pathway. Our study offers a comprehensive insight into the global relationship between microbiota and fecal miRNAs in the context of FC, presenting potential targets for further experimental validation and therapeutic interventions.

KEYWORDS

functional constipation, gut microbiota, microRNA, 16S rRNA, microRNA sequencing

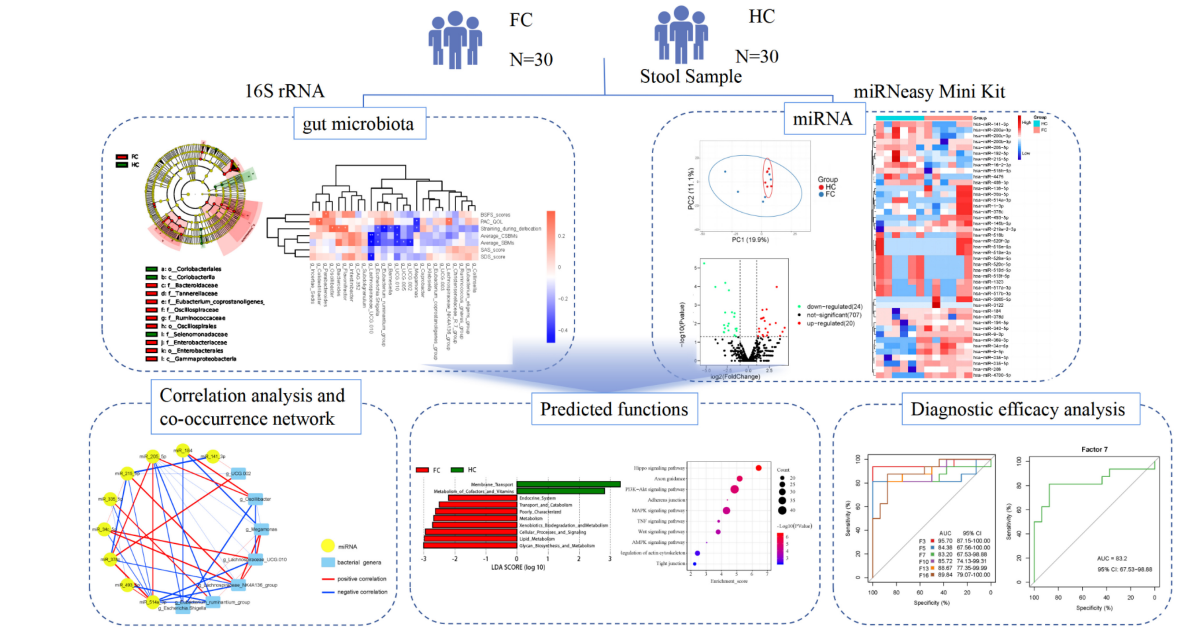

GRAPHICAL ABSTRACT

Highlights

- This study suggested functional constipation (FC) patients display distinct microbial profiles and identified 26 potential FC-associated bacteria.
- This study identified unique fecal miRNA patterns in FC patients.
- Correlations were found between the abundance of seven bacterial genera and nine fecal miRNAs.
- This study might shed light on a novel underlying mechanism by which miRNAs can selectively recruit microbes by orchestrating glycan biosynthesis and enhancing axon guidance in the enteric nervous system.

1 Introduction

Functional constipation (FC) is characterized by chronic and non-organic causes of constipation, excluding cases associated with irritable bowel syndrome, structural abnormalities, or metabolic disorders (Black et al., 2020). FC is a prevalent functional bowel disorder on a global scale, with an incidence of approximately 17.5% in the Americas and the Asia Pacific region, 8.75% in Europe, and ranging from 3 to 17% in China (Palsson et al., 2020). While FC does not pose an immediate threat to life, its substantial disease burden cannot be underestimated. Prolonged constipation may contribute to the development of colon cancer, and straining during defecation can increase the risk of cardiovascular and cerebrovascular events in affected individuals (Power et al., 2013; Dong et al., 2023). Moreover, certain metabolites produced by gut bacteria can influence brain function (Morais et al., 2021). As the precise pathophysiological mechanisms underlying FC remain incompletely understood, current treatment approaches primarily focus on symptom management. However, long-term reliance on laxatives can lead to adverse reactions such as laxative dependence, melanosis coli, and electrolyte imbalances (Bharucha and Lacy, 2020; Shah et al., 2021; Sharma et al., 2021). Therefore, investigating the pathogenesis of FC and enhancing treatment efficacy hold substantial clinical significance.

The intestinal microbial ecosystem represents the largest and most vital microbial ecosystem of the organism, playing a pivotal role in activating and sustaining intestinal physiological functions (Jia et al., 2018; Fan and Pedersen, 2021). Research by Parthasarathy et al. (2016) has revealed alterations in the gut microbiota composition of patients with constipation. Notable changes include significant reductions in the populations of beneficial bacteria such as *Lactobacillus* and *Bifidobacterium*, alongside significant increases in the abundance of pathogenic bacteria like *Enterobacter* and *Escherichia coli* (Parthasarathy et al., 2016). Functional studies have demonstrated that the gut microbiota of patients with

FC can modulate the levels of 5-hydroxytryptamine (5-HT) in the intestinal tract by influencing the expression of tryptophan hydroxylase-2 (TPH2). This modulation, in turn, impacts local neural activity within the intestinal tract, regulating intestinal secretion and motility (Bhattarai et al., 2018). Additionally, there is a significant increase in bacteria involved in the metabolism of butyric acid and bile acids within the gut microbiota of FC patients (Fan et al., 2022). These findings collectively underscore an intricate interplay between gut microorganisms and the host in individuals with constipation, although the precise key regulatory elements governing this interaction remain elusive.

MicroRNAs (miRNAs), which have been highly conserved throughout evolution, represent a class of endogenous, non-coding single-stranded RNAs approximately 22 nucleotides in length (Yao et al., 2022). They exert a post-transcriptional level of control by negatively regulating the expression of target genes through complementary binding with specific sequences on mRNAs (Hong et al., 2021). Mazzone et al. (2020) identified 13 significantly up-regulated miRNAs in the colon mucosa of FC patients. Additionally, in animal experiments, miR-129 was observed to be markedly overexpressed in colon tissues in an FC mouse model, and it was found to influence the distribution and function of Interstitial Cells of Cajal (ICC) through negative regulation of the N-acetylgalactosaminyltransferase-like 1/transforming growth factor-β1 signaling pathway (Wang et al., 2022). All these studies suggested that miRNAs are involved in the pathophysiology of FC and have the potential to be a non-invasive marker for the diagnosis and assessment of FC. Recent findings by Liu et al. (2016) further revealed that miRNAs in intestinal epithelial cells and Hopx-positive cells could enter the gut microbiota to modulate and regulate the transcription of microbiota-related genes, providing insight into how host cells can regulate microbial communities. However, our understanding of the role of miRNAs in the interplay between the host and gut microbiota in the context of FC remains limited.

To deepen our comprehension of the gut microbiota structure in FC and elucidate the relationship between gut microbiota and fecal miRNAs, this study first employed 16S rDNA sequencing and small RNA sequencing techniques to analyze the gut microbiota structure and fecal miRNA expression profiles. Subsequently, correlation analyses were conducted between the identified miRNAs and gut microbiota, and a random forest model was constructed to assess the collective diagnostic potential of these biomarkers. Finally, pathway analysis was employed to predict the biological functions of these miRNAs and gut microbiota. To the best of our knowledge, this study represents the first attempt to investigate the associations between miRNA expression and the microbiome within the context of FC.

2 Results

2.1 Information of cohort FC patients and healthy subjects

A total of 30 subjects with a clinical diagnosis of FC (age, 30.00 [8.50]; sex, male: female, 3:27) and 30 healthy individuals (age, 29.50 [18.00]; sex, male: female, 4:26) were recruited from February of 2022 to December of 2022 (**Table 1**). There was no statistical difference in age, gender, and body mass index between the two groups (p-value > 0.05), indicating these characteristics are matched. Defecation frequency and BSFS scores were statistically decreased (p-value < 0.01), while the defecation difficulties and PAC-QOL scores were significantly increased in FC patients when compared to the healthy individuals (p-value < 0.01).

2.2 Alterations of gut microbiota composition in FC patients based on 16S rRNA data

The rarefaction curves and species accumulation boxplots were generated from ASVs, with 97% identity achieved in all samples (**Supplementary Figure 1**). This indicated that the testing samples were sufficient and the amount of data were reasonable for the investigation of fecal microbiota. The FC group and the healthy control (HC) group displayed 2,870 and 1,632 unique ASVs, respectively. A total of 919 ASVs were shared by both groups (**Figure 1A**). Taking the genus level as an example, there was a difference in the relative abundance of species between the FC group and the HC group. *Bacteroides* and *Parabacteroides* were significantly increased, while *Megamonas* were decreased in the FC group (p-value < 0.01 or 0.05) (**Figure 1B**). The results of seven indexes in α-diversity analysis are shown in **Table 2**, **Supplementary Figure 2**, and **Figures 1C, D**. It is indicated that the α-diversity of gut microbiota in FC patients was richer than HCs, there were significant differences in the 6 indexes (p-value < 0.01 or 0.05), except for the goods coverage index. The PCoA and NMDS were performed to investigate the extent of the similarity of the microbial communities in the two cohorts based on unweighted UniFrac distance metrics (**Figures 1E, F**). These analyses indicated that the microbiota composition of the FC group clusters was more heterogeneous and significantly different from that of the HC group.

To identify microbes with significantly different relative abundance in the two cohorts, a t-test was carried out (**Figure 2A**). As compared with HCs, the abundance of 22 genera, including *Bacteroides* (p = 0.007) and *Parabacteroides* (p = 0.003) were significantly increased, while the abundance of *Megamonas* (p = 0.021) and *Collinsella* (p = 0.042) were decreased in FC patients (**Figure 2A**). Meanwhile, LEfSe analysis identified 29 significantly different microbes between the two groups, the LDA distribution diagram analysis (LDA > 3.5) showed a clear alteration of the microbiota characterized by higher *CAG_352*, *Subdoligranulum*, *UCG_002*, *Lachnospira*, *Parabacteroides*, *Lachnospiraceae_NK4A136_group*, *Eubacterium_coprostanoligenes_group*, *Escherichia_Shigella*, and *Bacteroides* levels in FC group (**Figures 2B, C**). However, *Megamonas* levels were significantly decreased in FC patients (**Figures 2B, C**).

2.3 Sequencing analysis revealed differentially expressed miRNAs between the two groups

Through miRNA high-throughput sequencing analysis, 1,844 miRNAs were obtained from all samples, including 1,047 known

TABLE 1 Demographics and characteristics of study cohort.

	Healthy subjects	FC patients	*p*-value
Subjects (n)	30	30	N/A
Age (years)	30.00 [8.50]	29.50 [18.00]	0.50
Sex, male/female	3/27	4/26	0.50
Body mass index (kg/m^2)	21.51 ± 2.09	20.94 ± 2.49	0.34
Disease duration (months)	N/A	121.00 [111.75]	N/A
Average of CSBMs per week (n)	7.00 [0.00]	1.50 [3.00]	< 0.001
Average of SBMs per week (n)	7.00 [1.00]	2.00 [2.25]	< 0.001
Straining during defecation	0.00 [0.19]	1.00 [0.08]	< 0.001
BSFS scores	4.09 ± 0.40	2.91 ± 1.14	< 0.001
PAC-QOL scale	1.13 ± 0.09	2.50 ± 0.62	< 0.001
Self-rating depression scale	34.92 ± 8.08	40.38 ± 9.02	0.292
Self-rating anxiety scale	34.38 [11.25]	38.75 [12.50]	0.004

FC, functional constipation; CSBMs, complete spontaneous bowel movements; SBMs, spontaneous bowel movements; BSFS, Bristol stool form scale; PAC-QOL, patient-assessment of constipation quality of life.

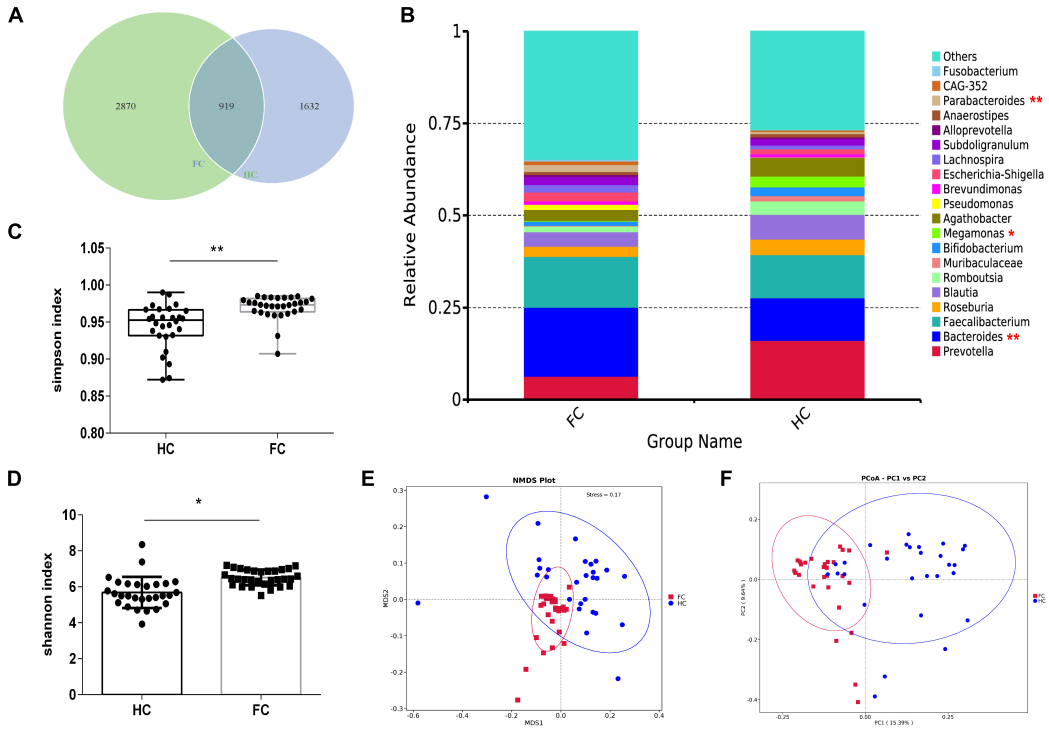

FIGURE 1
The shift of gut microbiota in FC patients and HCs based on the 16S rDNA data. **(A)** Venn diagram of the observed ASVs in FC and HC. **(B)** The relative abundance between two groups at the level of genus (Top 20). **(C,D)** Difference analysis of Shannon and Simpson index between the FC and HC groups. **(E,F)** PCoA and NMDS of the microbiota based on the unweighted UniFrac distance metrics. ANOSIM, $R = 0.3742$, $p = 0.004$. *$p < 0.05$ and **$p < 0.01$ are indicated.

miRNAs and 797 newly predicted miRNAs. After alignment of miRNA sequence data against the human miRNA database (miRBase v21),[1] principal component analysis (PCA) visualized the sample distribution in a two-dimensional scatter plot, the contribution of PC1 and PC2 to the overall variance in the data set is 19.9 and 11.1%, respectively (Figure 3A). These data indicated that the overall miRNA expression pattern was distinguished according to the presence of FC.

The fecal miRNAs differentially expressed between patients with FC and HCs were determined according to a statistical criterion of *p-value* < 0.05, log2FoldChange (log2FC) ≥ 1 and CPM ≥ 1. A total of 44 significantly different miRNAs were

1 http://www.mirbase.org/

TABLE 2 α-diversity indices comparing FC patients to healthy subjects.

α -diversity index	Healthy subjects	FC patients	*p*-value
Chao1	278.88 [110.40]	366.17 [146.17]	<0.001
Dominance	0.05 [0.04]	0.03 [0.02]	<0.001
Goods coverage	1.00 ± 0.00	1.00 [0.00]	0.309
Observed otus	278.50 [110.00]	364.00 [142.00]	<0.001
Pielou_e	0.69 ± 0.07	0.76 ± 0.04	0.022
Shannon	5.68 ± 0.87	6.51 ± 0.44	0.030
Simpson	0.95 [0.04]	0.97 [0.02]	<0.001

FC, functional constipation. Pielou_e and Shannon index were tested by *t*-test; Chao1, Dominance, Goods coverage, Observed_otus and Simpson index were tested by *Wilcoxon Mann-Whitney U* test.

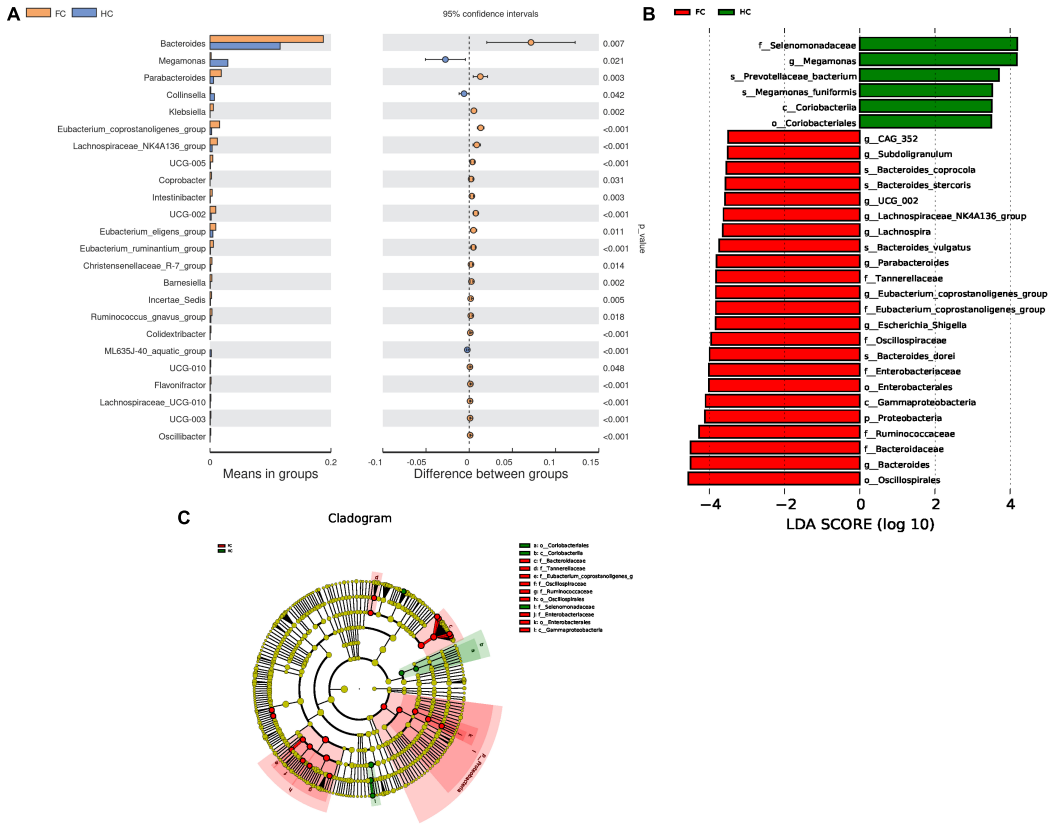

FIGURE 2
Differential microbes in FC patients and HCs. **(A)** The bar plots of the relative abundance of differential genera based on *t*-test. **(B)** LDA scores for the bacterial taxa are differentially abundant between groups (LDA > 3.5). Green bars indicate taxa with enrichment in FC, and red bars indicate taxa with enrichment in HC. **(C)** Evolutionary cladograms generated by LEfSe indicate differences in the bacterial taxa between groups. Green bars indicate taxa with enrichment in FC, and red bars indicate taxa with enrichment in HC.

identified, with 20 upregulated and 24 downregulated in FC group compared to HC group (Figure 3B). The heatmap of the 44 different miRNAs of the FC and HC groups is shown in Figure 3C.

2.4 The preliminary screening results of the differential expressed miRNAs and constipated-associated gut microbiota

In terms of sequencing results, miRNAs with extremely low signals (base mean = 0) were not selected. As shown in Tables 3, 4, the top 10 differentially expressed (DE) miRNAs with higher enrichment in FC patients include *miR-4700-5p*, *miR-493-5p*, *miR-514a-3p*, *miR-369-3p*, *miR-335-5p*, *miR-34c-5p*, *miR-378d*, *miR-335-3p*, *miR-378c*, and *miR-184* (Table 3); meanwhile, *miR-4476*, *miR-215-5p*, *miR-526a-5p*, *miR-520c-5p*, *miR-518*, *miR-141-3p*, *miR-205-5p*, and *miR-517* were observed at higher enrichment in healthy controls (Table 4).

Correlation analysis can help measure the closeness of significant gut microbiota to clinical indicators. With reference to the results of LEfSe analysis (Figures 2B, C) and relative abundance differences between groups (Figure 2A), 26

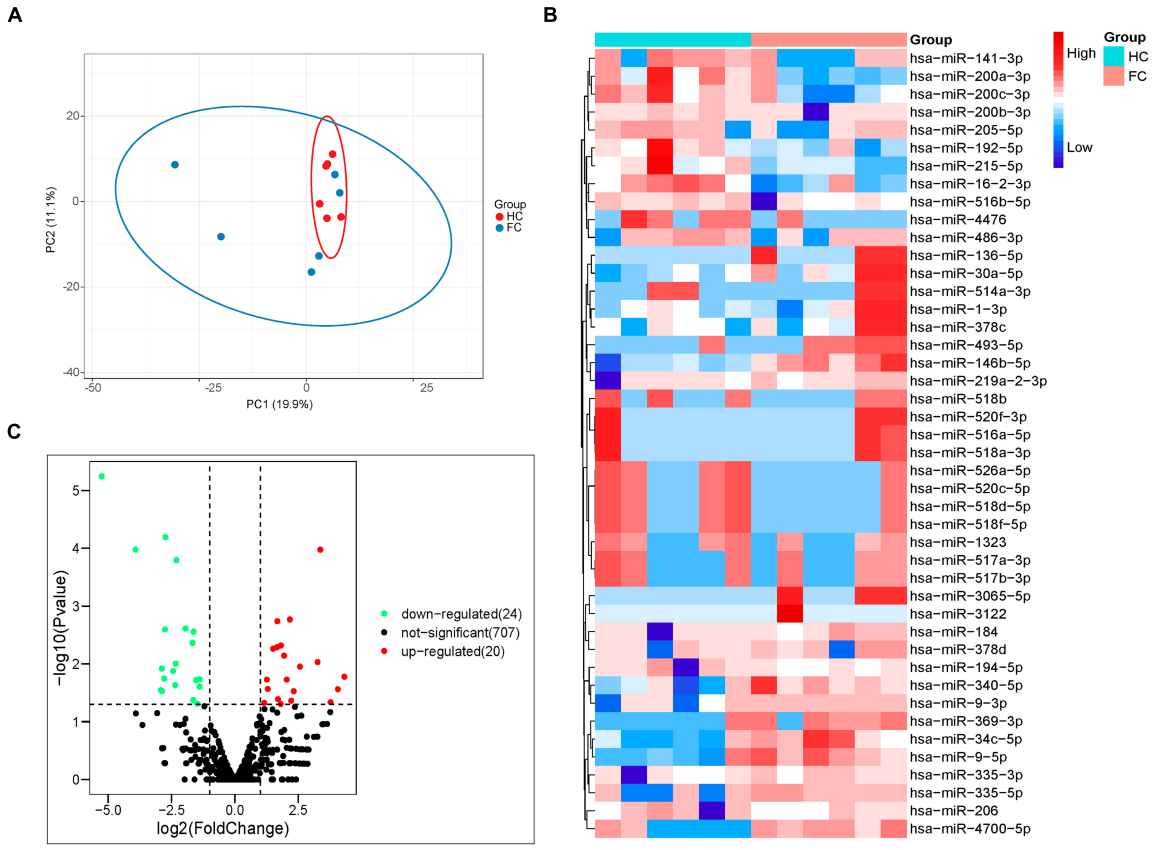

FIGURE 3
Analysis of fecal miRNAs in FC patients and HCs by the next generation RNA sequencing. **(A)** PCA of differential miRNAs distinguishes two cohorts. **(B)** Volcano plot showing differential expression of miRNAs. Differential miRNAs expression is shown by red (upregulated) versus blue (downregulated) intensity. The Y-axis depicts a 2.0-fold up or down change, while the X-axis represents a *p*-value of 0.05. **(C)** Heatmap of differentially expressed miRNAs; 20 upregulated and 24 downregulated miRNAs are presented.

TABLE 3 Top 10 upregulated fecal miRNAs in FC patients compare with HCs.

Mature_ID	baseMean_HC	baseMean_FC	log2FoldChange	*p*-value
hsa-miR-4700-5p	71.815615350	693.827634690	3.366860705	0.000105565
hsa-miR-493-5p	16.704200050	173.056229683	3.258242335	0.009301524
hsa-miR-514a-3p	49.673742633	253.023384167	2.560963284	0.011150233
hsa-miR-369-3p	26.175798417	188.508430743	2.31652355	0.029673918
hsa-miR-335-5p	55.940851755	269.550745500	2.219740171	0.043330153
hsa-miR-34c-5p	214.96979333	1041.70131158	2.16592952	0.001705622
hsa-miR-378d	118.96303679	446.120967775	2.041749259	0.018700679
hsa-miR-335-3p	177.38402455	733.078402583	1.939176065	0.007201004
hsa-miR-378c	431.04086138	1420.23373135	1.814298629	0.004796602
hsa-miR-184	85.769245733	297.110001637	1.802566638	0.049538533

different gut genera were preliminary screened. The results of Spearman's correlation analysis between these bacterial genera and constipated-manifestations are shown in **Supplementary Table 2** and **Figure 4**, including *Lachnospiraceae_NK4A136_group*, *Megamonas*, *Lachnospiraceae_UCG.010*, *Escherichia.Shigella*, *Eubacterium_ruminantium_group*, *Barnesiella*, *UCG.010*, *UCG.005*, *UCG.002*, *Colidextribacter*, *Parabacteroides*, *Oscillibacter*, *Bacteroides* and *Flavonifractor* (*FDR*-corrected $p < 0.05$).

2.5 The correlation analysis and co-occurrence network construction among the DEMs and FC-associated microbiomes

Subsequently, correlation analysis between the DE miRNAs and FC-associated gut microbiota was performed (**Figure 5A**;

TABLE 4 Top 10 downregulated fecal miRNAs in FC patients compare with HCs.

Mature_ID	baseMean_HC	baseMean_FC	log2FoldChange	*p*-value
hsa-miR-4476	704.389441	22.493451	5.26066761917007	0.000000569
hsa-miR-215-5p	16319.510613	1085.697440	3.92030432655696	0.000105701
hsa-miR-526a-5p	101.571103228	4.142552805	2.92188708907852	0.02845614
hsa-miR-520c-5p	101.571103228	4.142552805	2.92188708907852	0.02845614
hsa-miR-518f-5p	101.571103228	4.142552805	2.92188708907852	0.02845614
hsa-miR-518d-5p	101.571103228	4.142552805	2.92188708907852	0.02845614
hsa-miR-141-3p	316.647900822	42.55817459	2.7580489273887	0.002529715
hsa-miR-205-5p	853.539032167	98.04627931	2.7422651145099	0.0000063907
hsa-miR-517b-3p	231.263391800	25.04197379	2.44023464326948	0.013306236
hsa-miR-517a-3p	231.263391800	25.04197379	2.44023464326948	0.013306236

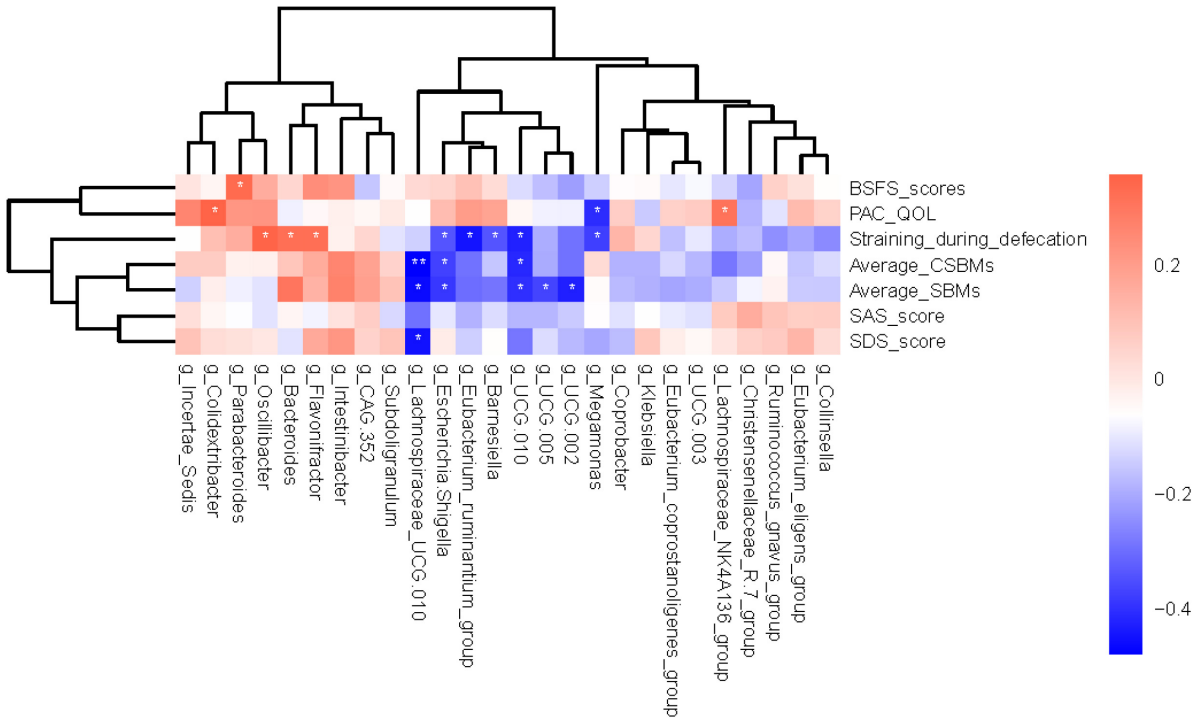

FIGURE 4
Heatmap showing bacterial genera that were significantly correlated with the constipated-indicators. Blue indicates negative correlations, and red indicates positive correlations. The color depth was related to the absolute value of the correlation coefficient. **FDR*-corrected $p < 0.05$ and ***FDR*-corrected $p < 0.01$ are indicated.

Supplementary Table 3). The correlations clearly show a distinct pattern based on the enrichment of miRNAs, 11 miRNAs that have statistically significant positive or negative correlations with 9 microflora (*FDR*-corrected $p < 0.05$).

Then, a co-occurrence network was constructed to visualize the relationships between these miRNAs and their correlated bacteria (Figure 5B; Supplementary Figure 3). The network showing the interconnection between these miRNAs and bacterial genera, which consists of 20 nodes and 43 edges with the average degree of connexions at 4.30 (The detailed information can be found in Supplementary Tables 4, 5).

Interestingly, *miR-205-5p* was inversely associated with *Escherichia.Shigella*, *Megamonas*, *Lachnospiraceae_NK4A136_group*, *Eubacterium_ruminantium_group* and *Lachnospiraceae_UCG.010*, while positively interacted with *miR-514a-3p*, *miR-378c* and *Oscillibacter*. Furthermore, *miR-514a-3p* expression was negatively associated with *miR-335-5p*, *miR-34c-5p*, *miR-215-5p*, *Lachnospiraceae_NK4A136_group*, *Eubacterium_ruminantium_group* and *Lachnospiraceae_UCG.010*, and was positively associated with *miR-378c*. Additionally, an interaction among *miR-34c-5p*, *Eubacterium_ruminantium_group*, *miR-215-5p*, *Lachnospiraceae_NK4A136_group* and *Lachnospiraceae_UCG.010* was also observed. In the same way, *Escherichia.Shigella* abundance was negative related to *miR-184* and *Oscillibacter*, and was positive related to the abundance of *Megamonas*. Experimental validations are required to investigate these correlations.

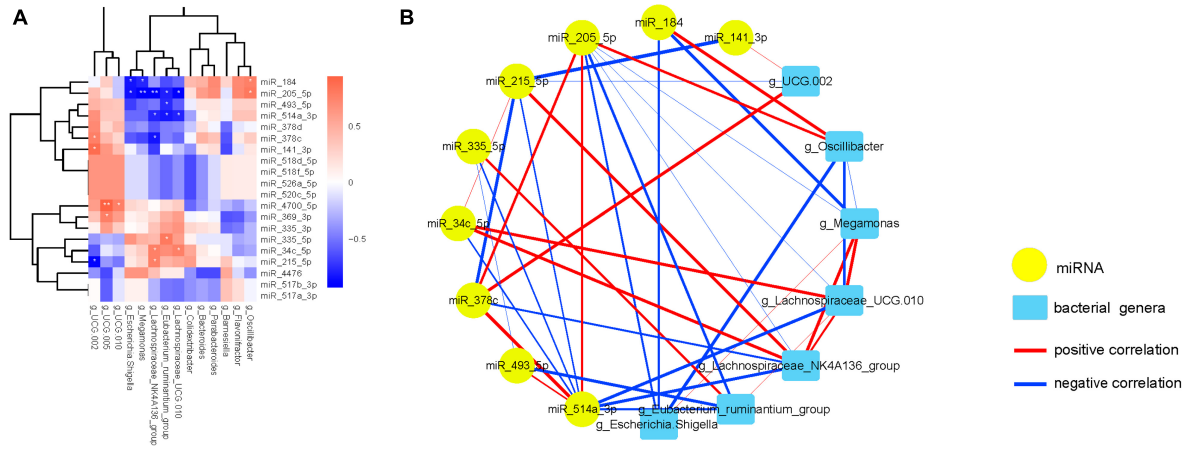

FIGURE 5
FC-associated microbiomes significantly correlated with most significantly DE miRNAs. **(A)** The heatmap shows the 20 most significantly DEMs correlated with FC-associated microbiomes. Positive correlations are shown in red, and negative correlations are shown in blue. **(B)** Interaction network showing the 11 DEMs and their correlated bacteria. Each node presents a miRNA or bacteria. Edge thickness represents the magnitude of the correlation, with red indicating positive correlation and with blue indicating negative correlation. **FDR*-corrected $p < 0.05$ and ***FDR*-corrected $p < 0.01$ are indicated.

Moreover, the expression of *miR-4700-5p* was positive related to *UCG.010* and *UCG.005*, and the expression of *miR-369-3p* was positive related to the abundance of *UCG.005* (Supplementary Figure 3).

2.6 Predicted functions of microbiomes correlated with DE miRNAs

To confirm the findings of the analysis of the interaction between certain gut microbiota and miRNAs, bioinformatics predictions were conducted. The KEGG information corresponding to the ASVs was obtained using PICRUSt software (Figure 6). Meanwhile, all the KEGG pathways based on level 2 were disrupted in FC, relative to HC group (Figure 6A). There were significant differences in carbohydrate metabolism ($p = 0.021$), energy metabolism ($p = 0.039$), translation ($p = 0.007$), metabolism of cofactors and vitamins ($p = 0.006$), cellular processes and signaling ($p < 0.001$), lipid metabolism ($p < 0.001$) and cell growth and death ($p = 0.017$) between two groups (Figure 6B). The LEfSe analysis results based on the prediction of KEGG pathway are shown in Figure 6C. The differential microbiomes in the FC group were closely related to glycan biosynthesis and metabolism, lipid metabolism, cellular processes and signaling, xenobiotics biodegradation and metabolism, metabolism, transport and catabolism, and endocrine system (Figure 6C).

2.7 Predicted functions of miRNAs correlated with FC-associated microbiomes

Then, we investigate the function of miRNAs correlated with FC-associated microbiomes. We hypothesized that if these bacteria affect FC through modulating miRNA expression, then miRNAs that are significantly correlated with the bacteria should show enrichment in constipation-related genes and pathways. The target genes of the miRNAs can be found in Supplementary Figure 4 and Supplementary Table 6, while the MF, CC, and BP analysis of the target genes of the miRNAs are shown in Figure 7A. The top 5 statistically significantly enriched BP terms were Axon development ($-\text{Log}_{10}$ p-value = 9.628), Muscle tissue development ($-\text{Log}_{10}$ p-value = 11.67), Regulation of nervous system development ($-\text{Log}_{10}$ p-value = 8.63), Epithelial cell proliferation ($-\text{Log}_{10}$ p-value = 7.88), and Cell-cell adhesion via plasma-membrane adhesion molecules ($-\text{Log}_{10}$ p-value = 13.57). Then, we predicted the functions of miRNAs by assigning pathways to the miRNA targets using the KEGG database. As shown in Figure 7B, the top 5 significantly enriched KEGG pathways were the PI3K-Akt signaling pathway ($-\text{Log}_{10}$ p-value = 4.86), MAPK signaling pathway ($-\text{Log}_{10}$ p-value = 4.33), Hippo signaling pathway ($-\text{Log}_{10}$ p-value = 6.43), Axon guidance ($-\text{Log}_{10}$ p-value = 5.19), and Regulation of actin cytoskeleton ($-\text{Log}_{10}$ p-value = 2.43). Overall, the results of the GO and KEGG analyses indicate that fecal miRNAs correlated with FC-associated bacteria are involved in the regulation of colonic smooth muscle contractility and motility in FC patients.

2.8 Diagnostic efficacy analysis of associated DE miRNAs and microbiota in patients with FC

To further explore the potential diagnostic biomarkers, the ROC curve and AUC index were drawn for statistical analysis. The random-forest model was applied to construct the diagnostic prediction model based on the correlation analysis results between the DE miRNAs and FC-associated microbiomes. The AUC and these indicators are shown in Table 5 and Figure 8A, which were regarded as potential diagnostic features. After comprehensive consideration of

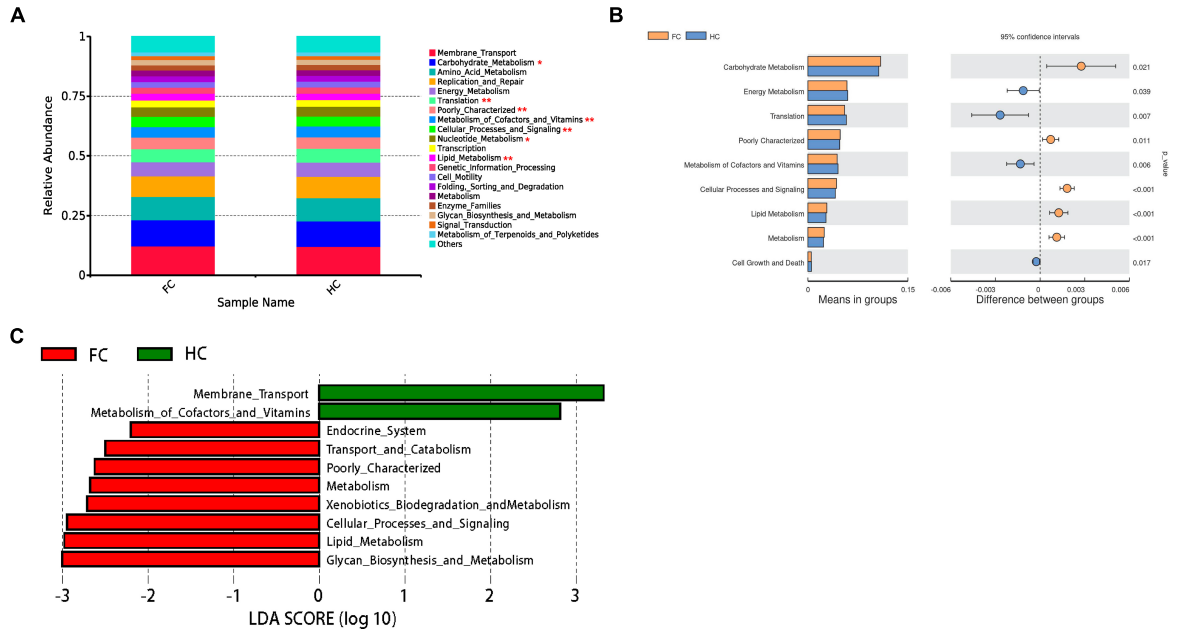

FIGURE 6
PICRUSt analyses of the microbiomes correlated with DE miRNAs. **(A)** The average abundance of KEGG pathway differentially enriched in HC and FC according to level 2. **(B)** The bar plots of the relative functional abundance between groups based on *Wilcoxon rank-sum* test. **(C)** LDA scores for the KEGG functions showed different abundances between HC and FC. Only taxa with LDA > 2.0 are shown.

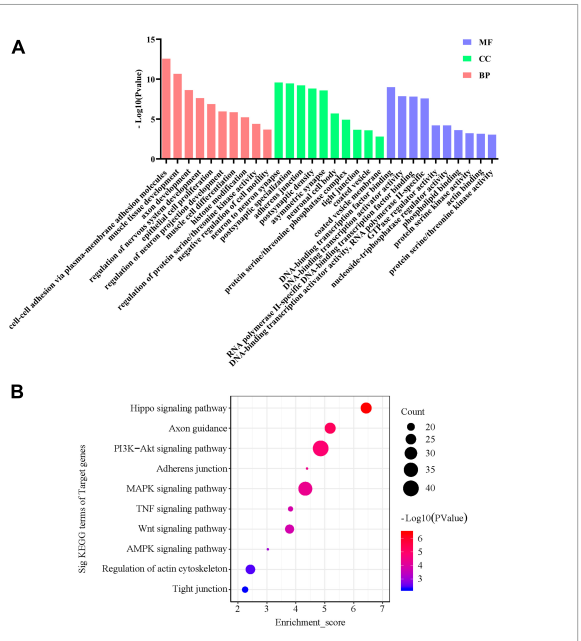

FIGURE 7
GO and KEGG signaling pathway analyses of the differentially expressed miRNAs correlated with FC-associated microbiomes. **(A)** Gene Ontology designations and **(B)** KEGG pathways were generated via DAVID database. Only terms with $-\text{Log}_{10}$ *p*-value > 2 are presented.

the AUCs and random-forest scores (**Figures 8B, C**), seven potential diagnostic biomarkers (including *Oscillibacter*, *Escherichia.Shigella*, *UCG.002*, *miR-205-5p*, *miR-493-5p*, *miR-215-5p,* and *Lachnospiraceae_NK4A136_group*) were screened out and showed a strong diagnostic ability to predict FC status with AUC = 0.832 (95% CI: 65.73–98.88). On the whole, combined use of these diagnostic features may accurately discriminate against FC patients and healthy populations.

3 Discussion

This study employed a prospective cohort design, enrolling healthy individuals as controls and individuals diagnosed with FC as participants. Through 16S rDNA and miRNA sequencing, the initial investigation revealed substantial discrepancies in the composition of the gut microbiota between FC patients and the healthy controls. Specifically, *Oscillibacter*, *Escherichia.Shigella*, *UCG.002*, *Lachnospiraceae_NK4A136_group*, *Lachnospiraceae_UCG.010*, and *Eubacterium_ruminantium_group* exhibited elevated relative abundance in the FC patients compared to the healthy controls, while the relative abundance of *Megamonas* was notably reduced in the FC patients. Furthermore, we identified 44 DE miRNAs in the fecal samples when comparing FC patients with healthy subjects. Among these miRNAs, *miR-493-5p*, *miR-184*, *miR-378c*, *miR-335-5p*, *miR-514a-3p*, and *miR-34c-5p* were significantly up-regulated in the FC patients, while *miR-205-5p*, *miR-215-5p*, and *miR-141-3p* were significantly down-regulated. Moreover, network analysis unveiled interactions among the aforementioned DE miRNAs and seven dominant bacterial genera. The incorporation of these correlated miRNAs with bacterial genera in diagnosis models demonstrated robust diagnostic performance, introducing a novel approach for detecting FC through the lens of gut microbiota-miRNA interactions. Additionally, functional analysis revealed that miRNAs strongly

TABLE 5 AUCs and importance of associated DE miRNAs and bacterial genera for the diagnosis of FC.

Features	AUCs	Random_forest score	*p*-value
Oscillibacter	0.99609375	47.60270751	0.0074308
Escherichia.Shigella	0.94140625	34.70327863	0.00000116
UCG.002	0.962890625	31.1279629	0.001357407
miR-205-5p	0.8203125	24.75648229	0.023738515
miR-493-5p	0.83203125	19.68565209	0.019342821
miR-215-5p	0.77734375	14.4763298	0.007411587
Lachnospiraceae_NK4A136_group	0.83203125	13.79572187	0.00000792
miR-184	0.798828125	13.14203929	0.001180187
Lachnospiraceae_UCG.010	0.8359375	12.04186135	0.001971689
miR-378c	0.734375	9.666136448	0.637159684
miR-335-5p	0.775390625	8.321658334	0.294937957
miR-514a-3p	0.6015625	7.031576587	0.037125322
miR-141-3p	0.734375	6.669248571	0.003933245
Megamonas	0.548828125	5.710350377	0.001074839
miR-34c-5p	0.7421875	5.304328568	0.020979493
Eubacterium_ruminantium_group	0.71484375	1.881095259	0.0000204

associated with the gut microbiota were enriched in pathways related to axon guidance, hinting at a potential contribution of axon guidance mechanisms to the pathogenesis of FC.

The gut microbiota, constituting the largest microbial ecosystem within the human body, plays a pivotal role in numerous metabolic processes (Yan et al., 2022). Beyond its primary role in digestion and absorption, the gut microbiota serves various functions, including the promotion of intestinal motility, establishment of immune defenses, protection against pathogen infiltration and tumor development, and maintenance of overall growth, metabolism, and intestinal equilibrium (Pan et al., 2022; Xiao and Kashyap, 2022). Any perturbation or dysregulation of the microbial composition can lead to metabolic disruptions. Our findings demonstrated significant alterations in the structure, abundance, and co-occurrence patterns of gut microbiota in FC patients in comparison to healthy subjects, aligning with similar microbial shifts observed in prior research studies (Parthasarathy et al., 2016; Tigchelaar et al., 2016; Xie et al., 2021; Nikolaieva et al., 2022).

The biggest innovative finding of this study is that miRNAs likely mediate host-microbiome communication in the context of FC. Notably, an intricate interplay was observed involving *miR-205-5p*, the relative abundance of six distinct intestinal bacteria (*Oscillibacter*, *Escherichia.Shigella*, *Megamonas*, *Lachnospiraceae_NK4A136_group*, *Eubacterium_ruminantium_group*, and *Lachnospiraceae_UCG.010*), and two specific miRNAs (*miR-514a-3p* and *miR-378c*). Chen et al. (2022b) previously demonstrated that *miR-205-5p* exhibited reduced expression in gastric cancer (GC) cells and its up-regulation exerted inhibitory effects on GC cell proliferation. *Escherichia.Shigella*, a relatively uncommon pathogenic bacterium within the human microbiota and a member of the Enterobacteriaceae family, can modulate the onset and progression of constipation by producing docosapentaenoic acid, which in turn reduces gastrointestinal motility (Chen et al., 2022a). *Oscillibacter*, *Lachnospiraceae_NK4A136_group*, and *Lachnospiraceae_UCG.010* fall under the category of short-chain fatty acids (SCFAs) producing bacteria (Zhang X. et al., 2023). The SCFAs have a direct impact on enterocytes, prompting the expression of TPH1. This, in turn, promotes the synthesis of colonic 5-HT, thereby enhancing intestinal motility (Reigstad et al., 2015). *Eubacterium_ruminantium_group*, on the other hand, participates in downstream bacterial lipopolysaccharide metabolic pathways. It interacts with the toll-like receptor 4 and activates the molecule myeloid differentiation factor 88/nuclear factor-κB pathway in immune cells, ultimately leading to the secretion of pro-inflammatory cytokines such as interleukin-6, interleukin-1, and tumor necrosis factor-α, thereby exacerbating the inflammatory response (Kanauchi et al., 2006; Lu et al., 2022). Meanwhile, *Megamonas* is considered a probiotic bacterium with potential contributions to maintaining an anti-inflammatory milieu through the regulation of the balance between regulatory T cells and T helper cell 17 (Shimizu et al., 2019; Yang et al., 2023).

MiR-514a-3p displayed associations with the abundance of three specific intestinal bacteria (*Lachnospiraceae_NK4A136_group*, *Eubacterium_ruminantium_group*, and *Lachnospiraceae_UCG.010*), in addition to four miRNAs (*miR-378c*, *miR-335-5p*, *miR-34c-5p*, and *miR-215-5p*). While direct correlations of *miR-514a-3p*, *miR-378c*, and *miR-335-5p* with FC have not been reported, their known functions and their potential relevance to FC pathogenesis offer valuable avenues for future investigation. Previous studies have indicated that *miR-514a-3p* and *miR-335-5p* may contribute to the proliferation, migration, and phenotypic switch of vascular smooth muscle cells (VSMCs) (Ma J. et al., 2022; Ma R. et al., 2022). Additionally, *miR-514a-3p* was identified as a novel tumor suppressor, with functional assays demonstrating its capacity to inhibit cell proliferation by targeting the epidermal growth factor receptor in clear cell renal

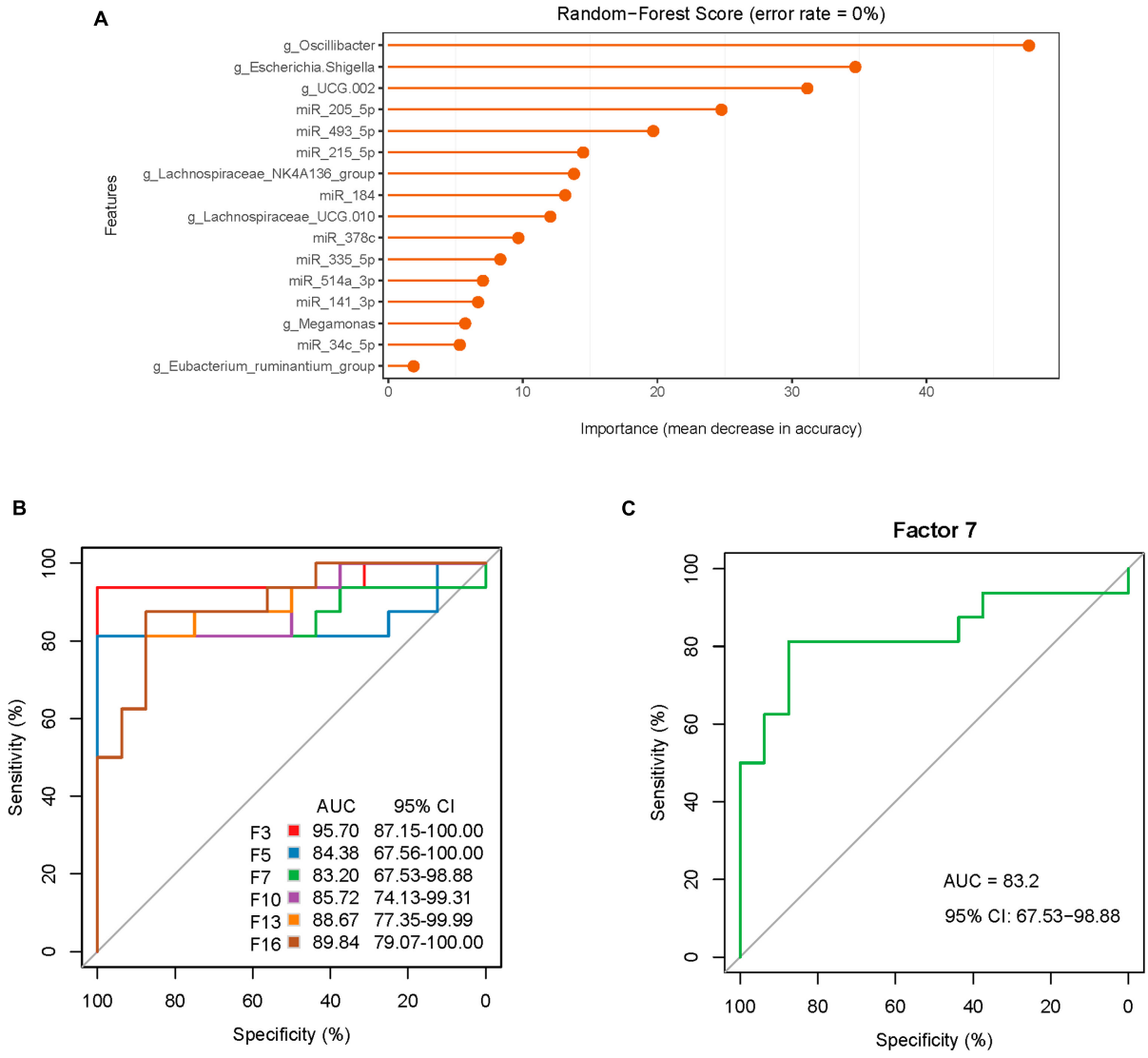

FIGURE 8
Random forest model prediction of diagnostic efficacy of associated DE miRNAs and microbiota between FC patients and healthy controls. **(A)** The importance of associated features from the model with the highest accuracy. **(B)** The random forest model displaying the classification for FC and HCs employing 3, 5, 7, 10, 13, and 16 different genera or miRNAs. **(C)** The random forest model used 7 different genera or miRNAs.

cell carcinoma (Ke et al., 2017). Additionally, *miR-378c* has shown a promising value as a diagnostic and prognostic indicator for gastric cancer (Zhang et al., 2021). Notably, *miR-378c* can promote phenotypic modulation of VSMCs within atherosclerotic lesions by directly targeting the sterile alpha motif domain containing 1 (Tian et al., 2021).

Furthermore, a connection involving *miR-34c-5p*, *Eubacterium_ruminantium_group*, *miR-215-5p*, *Lachnospiraceae_NK4A136_group*, and *Lachnospiraceae_UCG.010* was also identified. Xu et al. (2021) demonstrated that M1 macrophage-derived exosomal *miR-34c-5p* could target the tyrosine kinase receptor/stem cell factor signaling pathway. This regulation influenced the expression profile of ICC in colonic tissues, ultimately restoring intestinal motility in an FC rat model. Additionally, Yao et al. (2020) investigated the role of *miR-215-5p* in the regulation of inflammation, suggesting its potential relevance to FC-related research. Furthermore, Cai et al. (2019) found that *miR-215-5p* might modulate cell autophagy by targeting the phosphoinositide 3-kinase/protein kinase B/mammalian target of rapamycin signaling pathway and the reactive oxygen species/mitogen-activated protein kinase signaling pathway. Given the established correlation between cell autophagy and the initiation and progression of FC (Wang et al., 2022), this association holds particular significance. In summary, these identified interactions within the present study provide valuable insights for further exploration and validation in animal models to elucidate their directional causality.

Although we recruited patients without severe anxiety, included FC patients still showed significantly higher SAS scores. The relationship between anxiety and FC is complex and multifaceted. Studies have shown that people with anxiety are more likely to experience gastrointestinal symptoms, including constipation; on the other hand, the embarrassment of living with FC can also exacerbate feelings of anxiety (Liu et al., 2021;

Shiha et al., 2021). The gut microbiota has emerged as a key player in the bidirectional communication between the gut and the brain, known as the gut-brain axis (Margolis et al., 2021). Emerging evidence suggests that disturbances in the gut-brain axis may contribute to the development of both anxiety and FC (Jin et al., 2020; Westfall et al., 2021). Studies in animals have demonstrated that perturbations in the gut microbiota can lead to anxiety-like behaviors (Tao et al., 2024), while clinical research in humans has suggested that alterations in the gut microbiota may be associated with anxiety disorders (Wei et al., 2023). The gut microbiota could influence gut-brain axis through several mechanisms, including the production of serotonin and gamma-aminobutyric acid (Zhang W. et al., 2023), modulation of the immune response (Li et al., 2023), and regulation of the hypothalamic-pituitary-adrenal axis (Tsilimigras et al., 2018). In light of these findings, future studies could explore whether fecal miRNAs could be utilized as a potential target for modifying the gut microbiota to help manage anxiety and FC.

Currently, the etiology and pathogenesis of FC remain elusive and are primarily associated with aberrations in gastrointestinal motility, chronic intestinal inflammatory responses, diminished mechanosensitivity in the intestine, and abnormal brain-gut interactions (Wald, 2016; Vriesman et al., 2020). Intriguingly, functional predictions arising from this investigation have unveiled a significant enrichment of axon guidance pathways in miRNAs closely intertwined with the gut microbiota. Of note, glycans play pivotal roles in transmitting axonal signals, and enzymes responsible for glycan modifications finely regulate the information conveyed to axons, which can subsequently be interpreted by glycan-binding proteins (Sakamoto et al., 2021; Abad-Rodríguez et al., 2023). Enhanced glycan production may, in turn, augment the recruitment of certain bacteria (Kudelka et al., 2020). Consequently, these findings might shed light on a novel underlying mechanism by which miRNAs can selectively recruit particular microbes by orchestrating glycan biosynthesis and enhancing axon guidance function in the nervous system, ultimately retarding intestinal transit. Nevertheless, this mechanism warrants further comprehensive exploration.

Given the incomplete understanding of FC's precise pathophysiology and the absence of specific biomarkers, FC is typically diagnosed based on clinical symptoms, often in conjunction with procedures such as enteroscopy (Aziz et al., 2020; Black et al., 2020). The diagnosis is confirmed after ruling out other organic gastrointestinal disorders, which can be challenging and may lead to misdiagnosis or undiagnosis (Sharma et al., 2021; Chiarioni et al., 2023; Sun et al., 2023). In this study, a combined diagnostic approach employing seven diagnostic biomarkers (*Oscillibacter*, *Escherichia.Shigella*, *UCG.002*, *miR-205-5p*, *miR-493-5p*, *miR-215-5p,* and *Lachnospiraceae_NK4A136_group*) yielded an impressive AUC value of 83.20%. This signifies a high predictive accuracy and holds significant promise for clinical application (Ren et al., 2019). This study introduces a novel diagnostic method for FC from the perspective of miRNA-gut microbiota interactions. Moreover, this non-invasive, cost-effective, and convenient fecal sample-based diagnosis provides an expedited and valuable clinical tool.

Nonetheless, several limitations warrant acknowledgment in this study. Firstly, the relatively small clinical sample size in this study may limit the detection of subtle miRNA expression differences between groups. Secondly, the study does not directly validate the causal relationships between these miRNAs and bacterial genera. Future study should consider isolating differentiated strains to verify its relevance with miRNAs. Thirdly, predictions derived from bioinformatics may not always precisely mirror real biological systems. Despite these constraints, the study's elucidation of potential interactions between fecal miRNAs and the gut microbiota underscores their critical relevance for future inquiries into the pathogenesis of constipation.

4 Materials and methods

4.1 Ethics statement

The study was approved by the Ethics Committee of the Affiliated Hospital of Chengdu University of Traditional Chinese Medicine (Approval No. 2021KL-023). All subjects signed an informed consent form. All of them received a case report form and a fecal collection kit.

4.2 Study subject recruitment

A total of 30 patients with FC and 30 healthy volunteers were enrolled in the study. All patients with FC were recruited from the Outpatient Clinic of Anorectal and Digestive Departments of the Affiliated Hospital of Chengdu University of Traditional Chinese Medicine from February 2022 to December 2022. All patients with constipation were diagnosed by the specialist of the Anorectal or Digestive Department prior to enrollment. Inclusion criteria: patients aged 18–60 years regardless of gender; patients who met the Rome IV criteria (Palsson et al., 2020) for the diagnosis of FC and had a history of constipation for at least half a year; patients with a frequency of complete spontaneous bowel movements (CSBMs) $\leq$ 2 times per week, which lasted for more than 3 months (Yao et al., 2022); patients without special eating habits (vegetarian, vegan diet, or related to particular religious or social traditions) and mental disorders such as severe anxiety and depression [self-rating anxiety scale (SAS) or self-rating depression scale (SDS) standard score $<$ 75 points]; the patients with exertion in defecation and dry stool at baseline [Bristol stool form scale (BSFS) $\leq$ 3 points]; patients who had no medication history for constipation, including intestinal microecologics, probiotics preparation, etc. Exclusion criteria: patients with a history of abdominal or anorectal surgery; patients with irritable bowel syndrome and organic or drug-induced constipation; patients with constipation secondary to endocrine, metabolic, or neurogenic constipation; patients with heart, liver, kidney damage or cognitive dysfunction, aphasia, or unable to cooperate with sampling and treatment; patients with other primary diseases caused by gut microbiota disorder (diabetes, obesity, migraine, etc.); pregnant or lactating patients, or patients with a pregnancy plan within the next 3 months. The health volunteers were mainly from society and online (WeChat Official Account and Moments). Inclusion criteria for healthy volunteers: aged 18–60 years regardless of gender; all subjects underwent a physical examination to ensure good physical health;

no record of antibiotics, probiotics, yogurt, and other fermented dairy products during the baseline period; subjects not enrolled in other clinical studies, and signed the informed consent form. Exclusion criteria: following the special diet for other reasons (vegetarian, vegan diet, or related to particular religious or social traditions) were excluded; subjects with mental disorders such as severe anxiety and depression; subjects during pregnancy or lactation; subjects who cannot cooperate with blood and fecal sample collection.

The baseline clinical data of each subject, including gender, age, course of the disease, gastrointestinal symptoms, medication history, allergic history, and lifestyle habits (such as water intake and exercise level) was recorded by the investigator. The quality of life of all subjects was assessed using Patient-Assessment of Constipation Quality of Life (PAC-QOL), and the psychological and emotional disorders of patients were evaluated with SAS and SDS.

4.3 Fecal sample collection and storage

In the week before sampling, participants were instructed to maintain their regular diet (with no special changes compared with the previous); 72 h before sampling, participants were instructed to avoid intense physical activities such as running; and 24 h before sampling, it is mandatory to refrain from consuming coffee, chocolate, or any other caffeinated foods. Patients received the teaching video, as well as detailed written and oral instructions on how to collect feces using the Longsee fecal microbial genome protection solution kit (Guangdong Nanxin Medical Technology Co., Ltd.). The collection of two tubes of feces is required for the detection of gut microbiome and fecal miRNAs. Because it is difficult for FC patients to collect feces, the collection site could be chosen at home or in the hospital according to the specific situation. About 300 mg of formed stool from the middle section is collected, and then immediately transferred to a −80°C refrigerator in the hospital or temporarily frozen in the refrigerator at home. It should be quickly transferred to the researchers within 24 h for further sequencing analysis.

4.4 DNA isolation and 16S rRNA gene sequencing

The genomic DNA was extracted from the samples using CTAB- or SDS-based method, and then the purity and concentration of the DNA were detected by agarose gel electrophoresis. An appropriate amount of sample DNA was placed into a centrifuge tube and diluted to 1 ng/μL with sterile water. With the diluted genomic DNA as the template, PCR amplification was performed targeting the V3-V4 region of 16S rRNA using specific Barcode-tagged primers. The primer sequences of the 16S V34 region were as follows: forward (F): CCTAYGGGRBGCASCAG; R: GGACTACNNGGGTATCTAAT. The library was constructed using TruSeq® DNA PCR-Free Sample Preparation Kit, and the constructed library was sequenced on the computer using the Illumina Hiseq platform (NovaSeq6000, China). All Effective Tags were clustered using the Uparse algorithm (Uparse v7.0.1001),[2] and the obtained sequences were clustered into Amplicon Sequence Variants (ASVs) at 97% Identity (default). The Mothur method and SILVA138.1[3] SSUrRNA database were employed for species annotation and analysis of ASVs sequences (threshold value set at 0.8∼1).

4.5 Analysis of species diversity, community structure, and differential microbes

The parameters Observed-species, Chao1, Shannon, Simpson, ACE, Goods-coverage, and PD_whole_tree were calculated using Qiime software (Version 1.9.1) to evaluate the α-diversity of the gut microbiota. The rank abundance curve, and species accumulation curve were plotted with R software (Version 4.2.1), and the difference in α-diversity between groups was analyzed with R software. The Unifrac distance was calculated using Qiime software (Version 1.9.1). Principal coordinate analysis (PCoA) and non-metric multi-dimensional scaling (NMDS) maps were plotted using R software to evaluate the β-diversity. The PCoA analyses were conducted with the ade4 package and ggplot2 package of R software, and NMDS analysis was done using the vegan package of R software. LEfSe analysis was performed with LEfSe software, and a linear discriminant analysis (LDA) score of 3.5 was set as the default screening value. The ANOSIM function of the vegan package in the R program was employed for ANOSIM analysis. The species showing significant differences between groups were subjected to a *t*-test and the graphs were drawn using R software.

4.6 MicroRNA extraction and sequencing

Fecal samples from six patients with FC and six healthy subjects were selected using stratified random sampling with the age as the stratifying variable to minimize the potential for any bias or confounding factors (Verhoef et al., 2014; Kho et al., 2016) (demographic characteristics of these subjects can be found in **Supplementary Table 1**). The total RNA was extracted from samples using the miRNeasy Mini Kit (Qiagen, Hilden, Germany). The purity and concentration of total RNA in the samples were determined by NanoDrop ND1000 (Agilent Technologies, Inc., CA). The miRNA sequencing was performed with the Illumina HiSeq 2000 sequencing system. The total RNA of all samples was used to construct the miRNA sequencing library, including the following steps: (1) 3'-linker connection; (2) 5′-linker connection; (3) cDNA synthesis; (4) PCR amplification; (5) Selection of a PCR amplification fragment with a size of about 135–155 bp (corresponding to a small RNA of 15 to 35 nt). The library was denatured into single-stranded DNA molecules, captured on Illumina flow cells (Illumina, San Diego, CA), and amplified into clusters *in situ*, followed by 51 cycles of final sequencing on Illumina NextSeq according to the manufacturer's instructions. The expression profiles of miRNAs were statistically compared to the

2 http://www.drive5.com/uparse/
3 http://www.arb-silva.de/

known genomes and obtained by the software miRdeep2. The mean value of counts per million reads (CPM) ≥ 1 was set as the threshold value of miRNA expression in each group, and the miRNAs that met the criteria were considered to be expressed in the subgroup and then subjected to statistical analysis.

4.7 Correlation analysis and co-occurrence network construction

Correlations among the frequency of completely autonomous defecation in a week, fecal trait scores, degree of defecation difficulty, PAC-QOL, SDS, SAS, gut bacterial genus, and differentially expressed microRNAs were analyzed using Spearman's correlation coefficient. During the Spearman correlation analysis, the Spearman correlation coefficient values for species and environmental factors were first calculated with the corr.test function from the psych package in R software and then tested statistically for significance. The results were then visualized with the pheatmap function from the pheatmap package.

After obtaining the matrix of correlation coefficients between genus and miRNAs, the screening criteria were set as follows: (a) the weakly-correlated connections were removed with a cutoff value (>0.6) as the threshold; (b) node self-connections were filtered out; (c) connections with a node abundance less than 0.005% were removed; According to the filtered correlation coefficient values, a co-occurrence network was constructed using Cytoscape Version 3.9.1 software[4] with bacterial genus or miRNAs as nodes and values as edges.

4.8 Random forest analysis

Random forest is a classical machine learning model based on the classification tree algorithm that classifies the data into training and testing sets, and then the classification function can be continuously trained with the training set to achieve the optimal classification performance, which is validated using the testing set. Random forest analysis was performed using the Random Forest package in R software, and the significant species were screened with Random-Forest scores. Afterward, the performance of each model was cross-validated (default 10-fold). Receiver operating characteristic (ROC) curves were drawn, and the area under the curve (AUC) was calculated to evaluate the diagnostic performance of the model.

4.9 Functional annotation of bacterial genus and microRNAs

For the gut bacterial genus, the functional gene compositions of the target bacteria were analyzed using PICRUSt software, Kyoto Encyclopedia of Genes and Genomes (KEGG) pathway data corresponding to ASVs were obtained, and functional differences were analyzed. For the differentially expressed microRNAs, we first performed target gene prediction with the multimiR package in R software. The target genes of the differentially expressed miRNAs were then mapped to individual nodes of the Gene Ontology (GO) database, and the number of genes in each node was counted. Subsequently, Fisher's exact test was used to identify significantly enriched GO terms in the target genes of the differentially expressed miRNAs. Through this analysis, the molecular function (MF), cellular component (CC), and biological process (BP) of miRNA target genes were analyzed to reveal their biological functions. Finally, with KEGG Pathway as a unit, Fisher's exact test was applied to identify the pathways significantly enriched by the target genes of the differentially expressed miRNAs, to identify the dominating signal transduction pathways and biochemical metabolic pathways in which they were involved.

4.10 Data analysis

SPSS 23.0 software was adopted for statistical analysis of the difference between the two groups of clinical parameters. The gender ratio was examined using 2×2 chi-square text. The normality of all data was tested by the Shapiro–Wilk test, with $p > 0.05$ indicating normal distribution, and the homogeneity of variance was examined using one-way analysis of variance (ANOVA) with $p > 0.05$ deemed as an equal variance. The continuous variables obeying normal distribution and equal variance were represented by $\overline{x} \pm S$, and compared between the two groups by the independent sample t-test; otherwise, the continuous variables were represented as median (M), interquartile range (IQR), and *Wilcoxon Mann-Whitney U* test was employed for their comparison between the two groups. All sequenced data were analyzed with R software. All statistical results were considered statistically significant with $p < 0.05$.

5 Conclusion

In summary, this comprehensive study highlights notable disruptions in the gut microbiota composition in individuals affected by FC. Furthermore, our investigation unveiled dozens of fecal miRNAs that are differentially regulated in FC patients. Notably, we identified interactions between the abundance of seven specific bacterial genera and the expression of nine fecal miRNAs, strongly implicating fecal miRNAs as potential mediators of the host-microbiome interplay in FC. This work provides a first systems-level map of the association between microbes and fecal miRNAs in FC, and subsequent investigations should consider isolating differentiated strains to verify their causal relevance with miRNAs.

Data availability statement

The datasets presented in this study can be found in online repositories. The names of the repository/repositories and accession number(s) can be found below: NCBI, PRJNA1048321.

4 http://www.cytoscape.org

Ethics statement

The study was approved by the Ethics Committee of the Affiliated Hospital of Chengdu University of Traditional Chinese Medicine (Approval No. 2021KL-023). All subjects signed an informed consent form. The studies were conducted in accordance with the local legislation and institutional requirements. The participants provided their written informed consent to participate in this study.

Author contributions

JY: Formal analysis, Writing—original draft. XY: Formal analysis, Writing—original draft. YQL: Formal analysis, Writing—review and editing. YC: Project administration, Writing—review and editing. XX: Methodology, Writing – review and editing. SZ: Validation, Writing—review and editing. WZ: Validation, Writing—review and editing. LW: Project administration, Writing—review and editing. MC: Project administration, Writing—review and editing. FZ: Conceptualization, Writing—review and editing. YL: Conceptualization, Writing—review and editing.

Funding

The author(s) declare financial support was received for the research, authorship, and/or publication of this article. This study was supported by grants from the National Natural Science Foundation of China (grant numbers: 82074554 and 82274652). The funder of the study had no role in study design, data collection, data analysis, data interpretation, or writing of the manuscript.

Acknowledgments

We would like to thank all the subjects who consented to participate in this study. We would also like to thank all the physicians, nurses, and staff from the Laboratory Department of the Hospital of Chengdu University of Traditional Chinese Medicine for help in sample collecting. We acknowledge NuoheZhiyuan Biotechnology Co., Ltd., for the assistance with the data analysis. They were not compensated for their contributions.

Conflict of interest

The authors declare that the research was conducted in the absence of any commercial or financial relationships that could be construed as a potential conflict of interest.

Publisher's note

All claims expressed in this article are solely those of the authors and do not necessarily represent those of their affiliated organizations, or those of the publisher, the editors and the reviewers. Any product that may be evaluated in this article, or claim that may be made by its manufacturer, is not guaranteed or endorsed by the publisher.

Supplementary material

The Supplementary Material for this article can be found online at: https://www.frontiersin.org/articles/10.3389/fmicb.2023.1323877/full#supplementary-material

References

Abad-Rodríguez, J., Brocca, M., and Higuero, A. (2023). Glycans and carbohydrate-binding/transforming proteins in axon physiology. *Adv. Neurobiol.* 29, 185–217.

Aziz, I., Whitehead, W., Palsson, O., Törnblom, H., and Simrén, M. (2020). An approach to the diagnosis and management of Rome IV functional disorders of chronic constipation. *Expert Rev. Gastroenterol. Hepatol.* 14, 39–46. doi: 10.1080/17474124.2020.1708718

Bharucha, A. E., and Lacy, B. E. (2020). Mechanisms, evaluation, and management of chronic constipation. *Gastroenterology* 158, 1232–1249.e3.

Bhattarai, Y., Williams, B. B., Battaglioli, E. J., Whitaker, W. R., Till, L., Grover, M., et al. (2018). Gut microbiota-produced tryptamine activates an epithelial G-protein-coupled receptor to increase colonic secretion. *Cell Host Microbe* 23, 775–785.e5. doi: 10.1016/j.chom.2018.05.004

Black, C. J., Drossman, D. A., Talley, N. J., Ruddy, J., and Ford, A. C. (2020). Functional gastrointestinal disorders: Advances in understanding and management. *Lancet* 396, 1664–1674.

Cai, J., Yang, J., Liu, Q., Gong, Y., Zhang, Y., Zheng, Y., et al. (2019). Mir-215-5p induces autophagy by targeting PI3K and activating ROS-mediated MAPK pathways in cardiomyocytes of chicken. *J. Inorg. Biochem.* 193, 60–69. doi: 10.1016/j.jinorgbio.2019.01.010

Chen, X., Qiu, T., Wang, Y., Xu, L., Sun, J., Jiang, Z., et al. (2022a). *Shigella* species variant is causally linked to intractable functional constipation. *J. Clin. Invest.* 132:e150097. doi: 10.1172/JCI150097

Chen, X., Zhang, L., Geng, J., Chen, Z., and Cui, X. (2022b). MiR-205-5p functions as a tumor suppressor in gastric cancer cells through downregulating FAM84B. *J. Oncol.* 2022:8267891. doi: 10.1155/2022/8267891

Chiarioni, G., Lambiase, C., Whitehead, W., Rettura, F., Morganti, R., Popa, S., et al. (2023). Difficult defecation in constipated patients: Diagnosis by minimally invasive diagnostic tests. *Dig. Liver Dis.* [Online ahead of print]. doi: 10.1016/j.dld.2023.06.004

Dong, Q., Chen, D., Zhang, Y., Xu, Y., Yan, L., and Jiang, J. (2023). Constipation and cardiovascular disease: A two-sample Mendelian randomization analysis. *Front. Cardiovasc. Med.* 10:1080982. doi: 10.3389/fcvm.2023.1080982

Fan, Y., and Pedersen, O. (2021). Gut microbiota in human metabolic health and disease. *Nat. Rev. Microbiol.* 19, 55–71.

Fan, Y., Xu, C., Xie, L., Wang, Y., Zhu, S., An, J., et al. (2022). Abnormal bile acid metabolism is an important feature of gut microbiota and fecal metabolites in patients with slow transit constipation. *Front. Cell Infect. Microbiol.* 12:956528. doi: 10.3389/fcimb.2022.956528

Hong, Y., Ren, X., Liu, W., Sun, K., Chen, B., Liu, B., et al. (2021). miR-128 participates in the pathogenesis of chronic constipation by regulating the p38α/M-CSF inflammatory signaling pathway. *Am. J. Physiol. Gastrointest. Liver Physiol.* 321, G436–G447.

Jia, W., Xie, G., and Jia, W. (2018). Bile acid-microbiota crosstalk in gastrointestinal inflammation and carcinogenesis. *Nat. Rev. Gastroenterol. Hepatol.* 15, 111–128.

Jin, X., Guan, Y., Bai, H., Liu, Y., and Lv, X. (2020). Effects of sEA on slow transit constipation through the microbiota-gut-brain axis in rats. *Evid. Based Complement. Alternat. Med.* 2020:8828846. doi: 10.1155/2020/8828846

Kanauchi, O., Fukuda, M., Matsumoto, Y., Ishii, S., Ozawa, T., Shimizu, M., et al. (2006). *Eubacterium limosum* ameliorates experimental colitis and metabolite of microbe attenuates colonic inflammatory action with increase of mucosal integrity. *World J. Gastroenterol.* 12, 1071–1077. doi: 10.3748/wjg.v12.i7.1071

Ke, X., Zeng, X., Wei, X., Shen, Y., Gan, J., Tang, H., et al. (2017). MiR-514a-3p inhibits cell proliferation and epithelial-mesenchymal transition by targeting EGFR in clear cell renal cell carcinoma. *Am. J. Transl. Res.* 9, 5332–5346.

Kho, A., Sharma, S., Davis, J., Spina, J., Howard, D., McEnroy, K., et al. (2016). Circulating MicroRNAs: Association with lung function in Asthma. *PLoS One* 11:e0157998. doi: 10.1371/journal.pone.0157998

Kudelka, M., Stowell, S., Cummings, R., and Neish, A. (2020). Intestinal epithelial glycosylation in homeostasis and gut microbiota interactions in IBD. *Nat. Rev. Gastroenterol. Hepatol.* 17, 597–617. doi: 10.1038/s41575-020-0331-7

Li, F., Wang, Y., and Zheng, K. (2023). Microglial mitophagy integrates the microbiota-gut-brain axis to restrain neuroinflammation during neurotropic herpesvirus infection. *Autophagy* 19, 734–736. doi: 10.1080/15548627.2022.2102309

Liu, J., Lv, C., Wu, D., Wang, Y., Sun, C., Cheng, C., et al. (2021). Subjective taste and smell changes in conjunction with anxiety and depression are associated with symptoms in patients with functional constipation and irritable bowel syndrome. *Gastroenterol. Res. Pract.* 2021:5491188. doi: 10.1155/2021/5491188

Liu, S., da Cunha, A., Rezende, R., Cialic, R., Wei, Z., Bry, L., et al. (2016). The host shapes the gut microbiota via fecal MicroRNA. *Cell Host Microbe* 19, 32–43.

Lu, H., Xu, X., Fu, D., Gu, Y., Fan, R., Yi, H., et al. (2022). Butyrate-producing *Eubacterium rectale* suppresses lymphomagenesis by alleviating the TNF-induced TLR4/MyD88/NF-κB axis. *Cell Host Microbe* 30, 1139–1150.e7.

Ma, J., Liu, J., Li, T., and Ren, J. (2022). Hsa_circ_0030042 facilitates the proliferation and migration of vascular smooth muscle cells via the miR-514a-3p/FOXO1 Axis. *J. Endovasc. Ther.* 29, 611–622. doi: 10.1177/15266028211057086

Ma, R., Zhang, D., Song, Y., Kong, J., Mu, C., Shen, P., et al. (2022). miR-335-5p regulates the proliferation, migration and phenotypic switching of vascular smooth muscle cells in aortic dissection by directly regulating SP1. *Acta Biochim. Biophys. Sin.* 54, 961–973. doi: 10.3724/abbs.2022081

Margolis, K., Cryan, J., and Mayer, E. (2021). The microbiota-gut-brain axis: From motility to mood. *Gastroenterology* 160, 1486–1501.

Mazzone, A., Strege, P., Gibbons, S., Alcaino, C., Joshi, V., Haak, A., et al. (2020). microRNA overexpression in slow transit constipation leads to reduced Na1.5 current and altered smooth muscle contractility. *Gut* 69, 868–876. doi: 10.1136/gutjnl-2019-318747

Morais, L. H., Schreiber, H. L., and Mazmanian, S. K. (2021). The gut microbiota-brain axis in behaviour and brain disorders. *Nat. Rev. Microbiol.* 19, 241–255.

Nikolaieva, N., Sevcikova, A., Omelka, R., Martiniakova, M., Mego, M., and Ciernikova, S. (2022). Gut Microbiota-MicroRNA interactions in intestinal homeostasis and cancer development. *Microorganisms* 11:107. doi: 10.3390/microorganisms11010107

Palsson, O. S., Whitehead, W., Törnblom, H., Sperber, A. D., and Simren, M. (2020). Prevalence of Rome IV functional bowel disorders among adults in the United States, Canada, and the United Kingdom. *Gastroenterology* 158, 1262–1273.e3.

Pan, R., Wang, L., Xu, X., Chen, Y., Wang, H., Wang, G., et al. (2022). Crosstalk between the gut microbiome and colonic motility in chronic constipation: Potential mechanisms and microbiota modulation. *Nutrients* 14:3704. doi: 10.3390/nu14183704

Parthasarathy, G., Chen, J., Chen, X., Chia, N., O'Connor, H. M., Wolf, P. G., et al. (2016). Relationship between microbiota of the colonic mucosa vs feces and symptoms, colonic transit, and methane production in female patients with chronic constipation. *Gastroenterology* 150, 367–379.e1.

Power, A. M., Talley, N. J., and Ford, A. C. (2013). Association between constipation and colorectal cancer: Systematic review and meta-analysis of observational studies. *Am. J. Gastroenterol.* 108, 894–903.

Reigstad, C., Salmonson, C., Rainey, J., Szurszewski, J., Linden, D., Sonnenburg, J., et al. (2015). Gut microbes promote colonic serotonin production through an effect of short-chain fatty acids on enterochromaffin cells. *FASEB J.* 29, 1395–1403. doi: 10.1096/fj.14-259598

Ren, Z., Li, A., Jiang, J., Zhou, L., Yu, Z., Lu, H., et al. (2019). Gut microbiome analysis as a tool towards targeted non-invasive biomarkers for early hepatocellular carcinoma. *Gut* 68, 1014–1023. doi: 10.1136/gutjnl-2017-315084

Sakamoto, K., Ozaki, T., Suzuki, Y., and Kadomatsu, K. (2021). Type IIa RPTPs and Glycans: Roles in axon regeneration and synaptogenesis. *Int. J. Mol. Sci.* 22:5524. doi: 10.3390/ijms22115524

Shah, E. D., Staller, K., Nee, J., Ahuja, N. K., Chan, W. W., Lembo, A., et al. (2021). Evaluating the impact of cost on the treatment algorithm for chronic idiopathic constipation: Cost-effectiveness analysis. *Am. J. Gastroenterol.* 116, 2118–2127. doi: 10.14309/ajg.0000000000001403

Sharma, A., Rao, S. S. C., Kearns, K., Orleck, K., and Waldman, S. (2021). Review article: Diagnosis, management and patient perspectives of the spectrum of constipation disorders. *Aliment Pharmacol. Ther.* 53, 1250–1267.

Shiha, M., Asghar, Z., Thoufeeq, M., Kurien, M., Ball, A., Rej, A., et al. (2021). Increased psychological distress and somatization in patients with irritable bowel syndrome compared with functional diarrhea or functional constipation, based on Rome IV criteria. *Neurogastroenterol. Motil.* 33:e14121.

Shimizu, J., Kubota, T., Takada, E., Takai, K., Fujiwara, N., Arimitsu, N., et al. (2019). Relative abundance of *Megamonas* hypermegale and Butyrivibrio species decreased in the intestine and its possible association with the T cell aberration by metabolite alteration in patients with Behcet's disease (210 characters). *Clin. Rheumatol.* 38, 1437–1445. doi: 10.1007/s10067-018-04419-8

Sun, G., Trzpis, M., Ding, H., Gao, X., Broens, P., and Zhang, W. (2023). Co-occurrence of fecal incontinence with constipation or irritable bowel syndrome indicates the need for personalized treatment. *Neurogastroenterol. Motil.* 35:e14633.

Tao, Y., Zhou, H., Li, Z., Wu, H., Wu, F., Miao, Z., et al. (2024). TGR5 deficiency-induced anxiety and depression-like behaviors: The role of gut microbiota dysbiosis. *J. Affect. Disord.* 344, 219–232. doi: 10.1016/j.jad.2023.10.072

Tian, S., Cao, Y., Wang, J., Bi, Y., Zhong, J., Meng, X., et al. (2021). The miR-378c-Samd1 circuit promotes phenotypic modulation of vascular smooth muscle cells and foam cells formation in atherosclerosis lesions. *Sci. Rep.* 11:10548. doi: 10.1038/s41598-021-89981-z

Tigchelaar, E., Bonder, M., Jankipersadsing, S., Fu, J., Wijmenga, C., and Zhernakova, A. (2016). Gut microbiota composition associated with stool consistency. *Gut* 65, 540–542.

Tsilimigras, M., Gharaibeh, R., Sioda, M., Gray, L., Fodor, A., and Lyte, M. (2018). Interactions between stress and sex in microbial responses within the microbiota-gut-brain axis in a mouse model. *Psychosom. Med.* 80, 361–369. doi: 10.1097/PSY.0000000000000572

Verhoef, V., Bosgraaf, R., van Kemenade, F., Rozendaal, L., Heideman, D., Hesselink, A., et al. (2014). Triage by methylation-marker testing versus cytology in women who test HPV-positive on self-collected cervicovaginal specimens (PROHTECT-3): A randomised controlled non-inferiority trial. *Lancet Oncol.* 15, 315–322. doi: 10.1016/S1470-2045(14)70019-1

Vriesman, M., Koppen, I., Camilleri, M., Di Lorenzo, C., and Benninga, M. (2020). Management of functional constipation in children and adults. *Nat. Rev. Gastroenterol. Hepatol.* 17, 21–39.

Wald, A. (2016). Constipation: Advances in diagnosis and treatment. *JAMA* 315, 185–191.

Wang, H., Ren, B., Pan, J., Fu, S., Liu, C., and Sun, D. (2022). Effect of miR-129-3p on autophagy of interstitial cells of Cajal in slow transit constipation through SCF C-kit signaling pathway. *Acta Biochim. Pol.* 69, 579–586. doi: 10.18388/abp.2020_5877

Wei, S., Mai, Y., Hu, L., Zheng, R., Zheng, D., Chen, W., et al. (2023). Altered gut microbiota in temporal lobe epilepsy with anxiety disorders. *Front. Microbiol.* 14:1165787. doi: 10.3389/fmicb.2023.1165787

Westfall, S., Caracci, F., Estill, M., Frolinger, T., Shen, L., and Pasinetti, G. (2021). Chronic stress-induced depression and anxiety priming modulated by gut-brain-axis immunity. *Front. Immunol.* 12:670500. doi: 10.3389/fimmu.2021.670500

Xiao, Y., and Kashyap, P. (2022). Microbially derived polyunsaturated fatty acid as a modulator of gastrointestinal motility. *J. Clin. Invest.* 132:e161572. doi: 10.1172/JCI161572

Xie, L., Xu, C., Fan, Y., Li, Y., Wang, Y., Zhang, X., et al. (2021). Effect of fecal microbiota transplantation in patients with slow transit constipation and the relative mechanisms based on the protein digestion and absorption pathway. *J. Transl. Med.* 19:490. doi: 10.1186/s12967-021-03152-2

Xu, S., Zhai, J., Xu, K., Zuo, X., Wu, C., Lin, T., et al. (2021). M1 macrophages-derived exosomes miR-34c-5p regulates interstitial cells of Cajal through targeting SCF. *J. Biosci.* 46:90.

Yan, X., Yao, J., Li, Y., Zhang, W., Xi, M., Chen, M., et al. (2022). Global trends in research on miRNA-microbiome interaction from 2011 to 2021: A bibliometric analysis. . *Front. Pharmacol.* 13:974741. doi: 10.3389/fphar.2022.974741

Yang, J., Wang, L., Liu, H., Xu, H., Liu, F., Song, H., et al. (2023). Dysregulation of Ruminococcaceae and *Megamonas* could be predictive markers for rapid progression of mild cognitive impairment. *Microb Pathog.* 183:106272. doi: 10.1016/j.micpath.2023.106272

Yao, J., Yan, X., Chen, L., Li, Y., Zhang, L., Chen, M., et al. (2022). Efficacy and MicroRNA-gut microbiota regulatory mechanisms of acupuncture for severe chronic constipation: Study protocol for a randomized controlled trial. *Front. Med.* 9:906403. doi: 10.3389/fmed.2022.906403

Yao, Y., Xu, K., Sun, Y., Tian, T., Shen, W., Sun, F., et al. (2020). MiR-215-5p inhibits the inflammation injury in septic H9c2 by regulating ILF3 and LRRFIP1. *Int. Immunopharmacol.* 78:106000. doi: 10.1016/j.intimp.2019.106000

Zhang, L., Zou, L., and Sun, P. (2021). Relationship between miR-378c and YY1 expression in patients with gastric cancer and the clinicopathological features. *Cell Mol. Biol. Lett.* 26:12. doi: 10.1186/s11658-021-00256-x

Zhang, W., Guo, Y., Cheng, Y., Yao, W., and Qian, H. (2023). Neuroprotective effects of polysaccharide from Sparassis crispa on Alzheimer's disease-like mice: Involvement of microbiota-gut-brain axis. *Int. J. Biol. Macromol.* 225, 974–986. doi: 10.1016/j.ijbiomac.2022.11.160

Zhang, X., Yu, D., Wu, D., Gao, X., Shao, F., Zhao, M., et al. (2023). Tissue-resident Lachnospiraceae family bacteria protect against colorectal carcinogenesis by promoting tumor immune surveillance. *Cell Host Microbe* 31, 418–432.e8. doi: 10.1016/j.chom.2023.01.013

frontiers | Frontiers in Microbiology

TYPE Original Research
PUBLISHED 16 January 2024
DOI 10.3389/fmicb.2023.1292082

OPEN ACCESS

EDITED BY
Hesong Wang,
Southern Medical University, China

REVIEWED BY
Guiyang Zhang,
Anhui Medical University, China
Youyou Lu,
Huazhong Agricultural University, China

*CORRESPONDENCE
Feiyan Dai
dfy1995026@163.com

†These authors have contributed equally to this work and share first authorship

RECEIVED 11 September 2023
ACCEPTED 22 November 2023
PUBLISHED 16 January 2024

CITATION
Wang K, Li G, Yang Z, Yang F, Sun Y, Duan G, Sun W, Zhou K, He J and Dai F (2024) Compound Chinese medicine (F1) improves spleen deficiency diarrhea by protecting the intestinal mucosa and regulating the intestinal flora.
Front. Microbiol. 14:1292082.
doi: 10.3389/fmicb.2023.1292082

Compound Chinese medicine (F1) improves spleen deficiency diarrhea by protecting the intestinal mucosa and regulating the intestinal flora

Kang Wang[1†], Guanzong Li[2†], Zhi Yang[3†], Fumei Yang[1], Yulin Sun[4], Gang Duan[1], Wang Sun[1], Ke Zhou[1], Jun He[1] and Feiyan Dai[1*]

[1]College of Veterinary Medicine, Yunnan Agricultural University, Kunming, China, [2]College of Veterinary Medicine, South China Agricultural University, Guangzhou, China, [3]Animal Disease Prevention and Control Center of Chuxiong, Chuxiong, China, [4]Veterinarian, Kunming Technical Contract Accreditation and Registration Station, Kunming, China

Compound Chinese medicine (F1) is a traditional prescription in Chinese medicine that is commonly used to treat spleen deficiency diarrhea (SDD). It has demonstrated remarkable effectiveness in clinical practice. However, the precise mechanism by which it exerts its antidiarrheal effect is still unclear. This study aimed at investigating the antidiarrheal efficacy and mechanism of F1 on senna-induced secretory diarrhea (SDD). Senna was utilized to induce the development of a mouse model of senna-induced secretory diarrhea (SDD) in order to observe the rate of diarrhea, diarrhea index, blood biochemistry, and histopathological changes in the small intestine. Additionally, the levels of sodium and hydrogen exchange protein 3 (NHE3) and short-chain fatty acids (SCFAs) were determined using enzyme-linked immunosorbent assay (ELISA). The impact of F1 on the senna-induced SDD mouse models was evaluated by monitoring changes in the gut microbiota through 16S rRNA (V3-V4) sequencing. The results demonstrated that F1, a traditional Chinese medicine, effectively increased the body weight of SDD mice and reduced the incidence of diarrhea and diarrhea index. Additionally, F1 restored liver and kidney function, reduced the infiltration of inflammatory cells in intestinal tissue, and promoted the growth of intestinal villi. Furthermore, F1 was found to enhance the expression of NHE3 and SCFAs. It also increased the abundance of Firmicutes and Lactobacillus species, while decreasing the abundance of Proteobacteria and Shigella.

KEYWORDS

compound Chinese medicine, SDD, intestinal mucosa, intestinal flora, regulate

1 Introduction

Spleen deficiency diarrhea is a prevalent gastrointestinal syndrome in clinical practice (Ma et al., 2019; Shi et al., 2019). It is primarily caused by congenital endowment deficiency or prolonged illness, leading to weakness in the spleen and stomach, impaired digestion, and diarrhea (Mei et al., 2022). Some literature has pointed out that the irritable bowel syndrome caused by weak spleen and stomach is as high as 57.5% (Zhu et al., 2016). The spleen functions optimally in a dry environment. However, when the spleen and stomach are weak, they struggle

to digest and metabolize food, resulting in the formation of a cold and humid environment that further exacerbates the symptoms of spleen deficiency (Su et al., 2021). The symptoms include diarrhea with loose stools, weight loss, and dull fur. Based on the pathogenesis characteristics of the deficiency of spleen yang, the treatment focuses on the principle of regulating spleen and stomach (Wu, 1998). Chinese herbal medicine, as a significant component of complementary and alternative medicine, has gained considerable acceptance in clinical treatment. It is noteworthy that data reveals that 61.6% of patients suffering from digestive diseases have sought the benefits of traditional Chinese medicine (Tan et al., 2020). In clinical practice, the commonly used treatments are Sijunzi Decoction, Shengmai Yin, Shenling Baizhu San, etc., combined with spicy or bitter Chinese medicine to invigorate the spleen and eliminate dampness (Yu et al., 2016; Gan et al., 2017; You et al., 2020; Chen et al., 2022).

According to modern medicine, the concept of the 'spleen' involves the functions of multiple systems such as digestion, endocrine, and immunity (Lewis et al., 2019; Willard-Mack et al., 2019; Li et al., 2021). Traditional Chinese medicine considers the intestine to be an important component of spleen function. Recent medical research has also found a close association between small intestinal bacterial overgrowth (SIBO), gastrointestinal digestive dysfunction, intestinal inflammation, decreased immune function, and intestinal flora disorders (Brown et al., 2022; Banaszak et al., 2023; Li et al., 2023). The intestinal mucosal epithelium acts as a selective barrier that protects the host from harmful substances while allowing nutrient absorption (Turner, 2009; Fa et al., 2016). Disruption of this barrier can result in increased permeability, inflammation, reduced NHE3 activity, and other pathological changes, ultimately leading to diarrhea (Peritore-Galve et al., 2023). In recent years, there have been increasing reports on the potential of traditional Chinese medicine to improve the health of the intestinal mucosa (An et al., 2022). For instance, berberine has been found to protect the intestinal mucosal barrier function by reducing intestinal macrophage infiltration and the inflammatory response (Li et al., 2020; Dong et al., 2022). Additionally, Poria polysaccharide has shown promising results in reducing intestinal mucosal injury and inflammation in mice, thereby improving intestinal barrier function (Xu et al., 2023).

The intestinal flora and the animal immune system have a mutually beneficial relationship, known as the 'flora-host' symbiotic relationship (Zhou et al., 2020). The active involvement of the intestinal flora and its metabolites in maintaining the balance of the intestinal immune system has a positive impact on preventing and controlling intestinal diseases, and it also plays an essential role in regulating animal health (Liu et al., 2022). When the dynamic balance of the intestinal microecosystem is disrupted, the intestinal flora becomes imbalanced, leading to various diseases both inside and outside the intestine (Hu and Yang, 2022; Liu et al., 2022). Traditional Chinese medicine has gained significant attention and research from experts and scholars due to its influence on the intestinal flora and its ability to regulate bodily functions (Che et al., 2022; Li et al., 2022). Since Chinese herbal medicines are typically consumed orally, their active ingredients directly interact with the intestinal flora, thereby influencing the structure of the intestinal flora and its metabolites. Cang Zhu Compound has been shown to regulate the structure of intestinal flora, improving the intestinal microenvironment (Ma et al., 2019). Additionally, Huo Xiang Zhengqi oral liquid has been found to promote beneficial bacteria in the intestinal flora and inhibit the growth of pathogenic bacteria, effectively alleviating symptoms of wet spleen and stomach in rats. Research has also highlighted the close relationship between traditional Chinese medicine and the regulation of intestinal flora metabolites, such as short-chain fatty acids, amino acids, bile acids, indole, and its derivatives (Feng et al., 2018; Sun et al., 2022; Li et al., 2023). Therefore, maintaining a balanced intestinal flora and regulating microbial metabolites have emerged as new avenues of study in understanding the mechanism of action of traditional Chinese medicine.

This study aims to investigate the antidiarrheal effect of F1 and explore its curative potential in the treatment of SDD. The specific mechanisms involved, including the regulation of intestinal microbiota and the maintenance of intestinal barrier function, will be elucidated. The findings of this study will provide a theoretical reference for the clinical application of F1.

2 Materials and methods

2.1 Experimental consumables

Experimental Chinese medicine pieces such as Codonopsis, Largehead Atractylodes Rhizome, Poria, Dried Ginger, Yam, Rhizome of Szechuan Lovage, Knotweed, Fortune Eupatorium Herb, Herba Lycopi, Coptis chinensis Franch, Divine Comedy, Senna, etc.

Mouse sodium hydrogen exchange factor 3 (NHE3) ELISA detection kit, mouse short-chain fatty acid (SCFA) ELISA detection kit, 4% paraformaldehyde. 4% paraformaldehyde,Absolute ethanol (AR grade), xylene (AR grade), hematoxylin stain, eosin stain, hydrochloric acid (AR grade), neutral gum.

2.2 Laboratory animals

ICR mice: 50, 25 male and 25 females; Weight: 20 ± 2 g; From the Laboratory Animal Center of Yunnan University.

2.3 Preparation of compound Chinese medicine preparation F1 and senna

F1: Baishu 20 g, Poria 12 g, Codonopsis 15 g, Dried Ginger 20 g, Yam 20 g, Chuanxiong 15 g, Knotweed 10 g, Peran 10 g, Zeeland 10 g, Coptis 6 g, Divine Comedy 12 g. The ingredients were mixed and crushed in the specified proportions. The resulting mixture was then passed through a 120 mesh sieve and sealed for storage. For preparation, 200 g of the powder was soaked in 2000 mL of warm water for 2 h and boiled for 1 h. The chemical solution was filtered using 8 layers of gauze, and the resulting filtrate was evaporated and concentrated at 60°C under reduced pressure until the volume reached 400 mL. This crude drug solution had a concentration of 500 mg/mL and was stored at 4°C for future use.

Senna aqueous solution was prepared as follows: 30 g of senna was soaked in 100 mL of warm water for 1 h and then boiled for 15 min. After filtration through 8 layers of gauze, the solution was centrifuged at 5000 r/min for 5 min. The supernatant volume was adjusted to 50 mL, resulting in a concentration of 600 mg/mL. The solution was stored at 4°C for future use.

2.4 Establishment and treatment of SDD mouse model

After adapting 50 mice for 5 days, they were randomly divided into two groups: the experimental group and the control group. Both groups were managed with the same feeding protocol. In the experimental group, each mouse was orally administered 0.5 mL of senna water extract twice a day for 7 days, following a 5-h fasting period before each administration. The control group received the same volume of normal saline. Throughout this period, the clinical manifestations of the mice were observed, and the diarrhea rate and diarrhea index were calculated as the primary indicators for evaluating the diarrhea models.

After successful modeling, three mice were randomly chosen from the experimental group for sampling and dissection (recorded as sdd); Subsequently, twenty mice were selected for treatment with F1 (denoted as f1). Each mouse received a dosage of 1 mg/g Chinese medicine solution through oral gavage, based on their body weight. The administration was conducted once in the morning and once in the evening, continuously for five days. The control group (recorded as nc), received normal feeding without any additional treatment.

2.5 Sample collection and processing

After successful modeling and drug treatment, three mice were randomly selected from each group. One milliliter of blood was collected from the heart using ordinary blood collection tubes. The collected blood was allowed to stand for 4 h and then centrifuged at 4000 r/min for 8 min to separate the serum. The serum was transferred to a 2 mL centrifuge tube and stored at −20°C. Simultaneously, the mice were dissected after their necks were broken, and the small intestinal tissues and spleen were collected and stored in 4% paraformaldehyde at 4°C. The contents of the small intestine were also collected and stored by freezing them with liquid nitrogen.

2.6 Clinical status monitoring of mice

The study recorded the appearance of coat, behavioral activity, mental state, appetite (feed consumption), fecal morphology, weight change, and death of mice. Additionally, the number of effective treatments, cases of cure, deaths, and recurrences were recorded for each treatment group. The effective rate, cure rate, mortality rate, and recurrence rate were then calculated for each group.

2.7 Blood biochemical detection of mice

The levels of alanine aminotransferase (ALT), aspartate aminotransferase (AST), serum total protein (TP), albumin (ALB), urea (UREA), creatinine (CREA), and other components were measured using a veterinary automatic blood biochemistry analyzer.

2.8 Determination of spleen and intestinal injury repair in mice

The spleen and intestinal tissues were dehydrated, trimmed, embedded, sectioned, stained, and sealed after paraformaldehyde fixation. They were then subjected to microscopic examination. The BA210 digital trinocular microcamera system was used to capture slice images. Each section was observed at low magnification to identify any tissue lesions. Specific lesions were further examined using 100x and 400x pictures. The extent of the lesion was determined using a four-stage grading approach. Additionally, the height of intestinal villi, crypt depth, and muscle thickness were measured using the line tool.

2.9 NHE3 and SCFAs expression

The expression of serum NHE3 and SCFAs was determined using the bianti-antibody sandwich ELISA method by creating a linear regression model based on the creating of the standarded curve.

2.10 Detection of intestinal microbial diversity in mice

The intestinal contents of mice were frozen using liquid nitrogen and then sent to Beijing Baimeike Biotechnology Co., Ltd. for next-generation sequencing of the 16S rRNA V3-V4 region to analyze the intestinal bacteria.

2.11 Data statistics and analysis

Preliminary statistical collation of data was performed using Excel 2019, followed by statistical analysis using GraphPad Primim 8.0.2. The results were represented as mean ± standard error. A significant difference was denoted by $p < 0.05$, indicated by "*," while a greater difference was denoted by $p < 0.01$, represented by "**." Gut microbiome analysis was conducted using BMKCloud.[1]

3 Results

3.1 Treatment results

Table 1 presents the number of treatments and cures, indicating that the effective rate reaches 95% after 5 days of treatment and the cure rate reaches 95% after 6 days. Additionally, the recurrence rate and mortality rate during this period are low.

1 www.biocloud.net

TABLE 1 Statistics of treatment results of spleen deficiency and diarrhea in mice.

	Significant number	Efficient	Number of cures	Cure rate	Number of deaths	Mortality	Number of recurrences	Relapse rate
1d	8	40%	0	0	0	0	0	0
2d	11	55%	7	35%	0	0	0	0
3d	15	75%	12	60%	1	5%	0	0
4d	17	85%	15	75%	0	0	1	11.11%
5d	19	95%	18	90%	0	0	0	0
6d	19	95%	19	95%	0	0	0	0
7d	19	95%	19	95%	0	0	0	0

TABLE 2 Results of blood biochemical test results of mice in each group of spleen deficiency and diarrhea.

Project		sdd	F1	nc
ALT	U/L	115.2000 ± 14.2700	26.08 ± 5.4610	23.0800 ± 2.8420
AST	U/L	188.3000 ± 2.6360	160.6000 ± 6.7540	155.3000 ± 7.6210
ALP	U/L	179.2000 ± 19.9500	217.0000 ± 11.9100	234.3000 ± 18.8800
UREA	mmol/L	14.2700 ± 1.8300	11.8400 ± 0.7727	8.7630 ± 0.2089
CREA-S	μmol/L	14.7700 ± 0.9228	11.8400 ± 0.7727	8.6440 ± 0.2100
TPII	g/L	44.6900 ± 2.9180	52.3600 ± 1.4360	50.2800 ± 0.9495
TG	mmol/L	1.8500 ± 0.0319	0.6160 ± 0.0594	0.6260 ± 0.0474
TC	mmol/L	1.7030 ± 0.1803	1.7780 ± 0.0788	1.9520 ± 0.2225
CHE	U/L	4,716 ± 227.3000	6,504 ± 301.1000	5,194 ± 185.7000
Glu-G	mmol/L	3.2700 ± 0.3536	8.066 ± 0.2623	6.8100 ± 0.4811
Ca	mmol/L	1.9450 ± 0.0578	2.1240 ± 0.0628	2.0150 ± 0.1550
P	mmol/L	2.8150 ± 0.2374	2.6500 ± 0.1102	3.4750 ± 0.1950

3.2 Blood biochemical results

The blood biochemistry of mice in each treatment group was analyzed using a veterinary automatic blood biochemistry instrument, and the results were statistically analyzed (Table 2 and Figure 1). The levels of ALT, TG, UREA, and crea-S in the sdd group were significantly higher than those in the nc group ($p < 0.01$). Additionally, the levels of AST were significantly higher than those in the nc group ($p < 0.05$), while the Glu-G levels were significantly lower ($p < 0.01$). Following F1 treatment, the liver and kidney function indexes of mice showed a recovery, with the exception of slightly higher levels of CREA-S, CHE, and Glu compared to the nc group. However, there was no significant difference in other indexes ($p > 0.05$).

3.3 Histoscopy observation and pathology of lesions

3.3.1 Repair of spleen damage

One patient in the sdd group exhibited lymphocyte necrosis in the splenic nodule of albidon, along with cytosolic lysis of necrotic cells. Additionally, there was solid shrinkage and disintegration of nuclei, resulting in the phenomenon commonly referred to as 'full of stars' (Figure 2A). In another case, there was an increase in cell components in the pulp, as well as the presence of lobulated nuclei or rod-shaped nuclei neutrophils (Figure 2B). Mild extramedullary hematopoiesis was observed in one case, with an increased number of naïve granulocytes in the tissue (Figure 2C). Following F1 treatment, the spleen tissue membrane remained intact, and there was no proliferation of the membrane or splenic trabecular fibrous connective tissue. The demarcation between white pulp and red pulp was clear, and there was no hyperplasia or atrophy observed in the white pulp splenic nodule, with no significant decrease in the number of cells. No obvious proliferation or decrease of various cellular components was noted in the red medullary, and the spleen and blood sinuses formed a network without any signs of congestion or inflammatory cell infiltration.

3.3.2 Damage to the intestines

In one case from the sdd group, a minor amount of inflammatory cell infiltration was observed, primarily consisting of lymphocytes with oval nuclei. There was no notable inflammatory cell infiltration or hyperplasia in the outer membrane layer. No other significant pathological changes were observed after treatment (see Figure 3).

3.4 Intestinal tissue measurement

After measurement (Table 3 and Figure 4), the height of intestinal villi was found to be significantly lower in the sdd group compared to

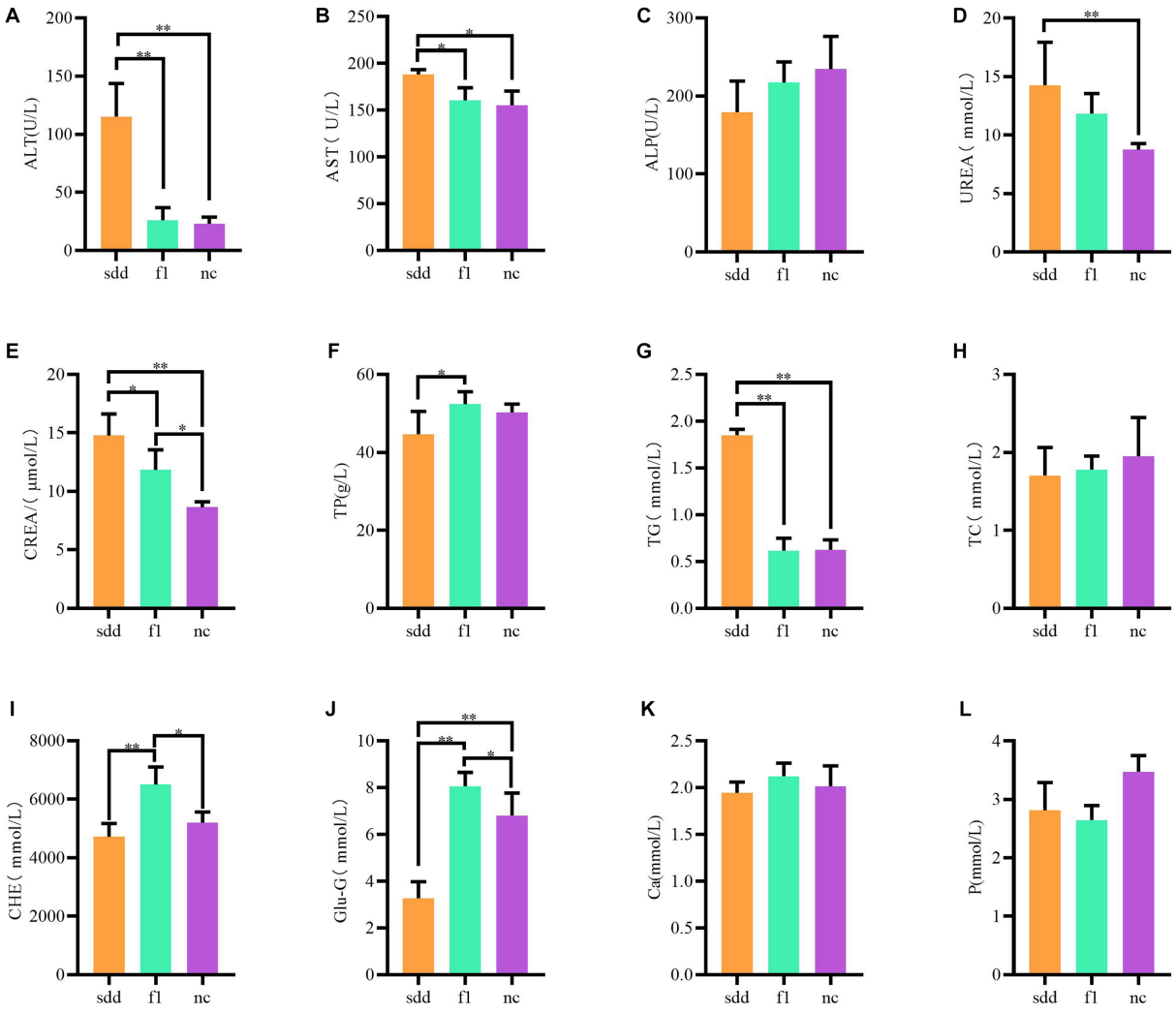

FIGURE 1
Analysis of differences in blood biochemical tests in mice. **(A–L)** Represents a histogram of 12 different blood biochemical indicators; All abscissa indicates grouping information (orange for sdd group, green for fl group, purple for nc group); Ordinates represent numeric values.

both the f1 group and the nc group ($p < 0.01$). However, there was no significant difference in the height of intestinal villi between the f1 group and the nc group ($p > 0.05$). The crypt depth in the sdd group was significantly higher than that in the f1 group and the nc group ($p < 0.01$), while there was no significant difference in crypt depth between the F1 group and the nc group ($p > 0.05$). Additionally, the muscular layer in the sdd group was significantly higher than that in the nc group ($p < 0.01$) and also higher than that in the F1 group, although the difference between the f1 group and the nc group was not significant ($p > 0.05$).

3.5 NHE3 and SCFAs expression

The serum NHE3 content in the sdd group was significantly lower than that in the f1 and nc groups ($p < 0.01$), and the f1 group was significantly lower than that in the nc group ($p < 0.01$) (Table 4 and Figure 5A).

There was no significant difference in serum SCFAs content between the three groups ($p > 0.05$), but the f1 content was the highest (Table 4 and Figure 5B).

3.6 Intestinal flora sequencing results

3.6.1 Sequencing data quality assessment

A total of 719,228 pairs of Reads were obtained from the three sequencing groups. After double-ended Reads quality control and splicing, a total of 714,143 CleanReads were generated (Table 5). There were no significant differences observed in RawReads, CleanReads, DenoisedReads, MergedReads, Non-chimericReads, and ASVs between the three groups ($p > 0.05$).

3.6.2 Species distribution analysis

At the phylum level, the dominant community composition of the intestinal colony in the three groups of mice was Firmicutes. sdd

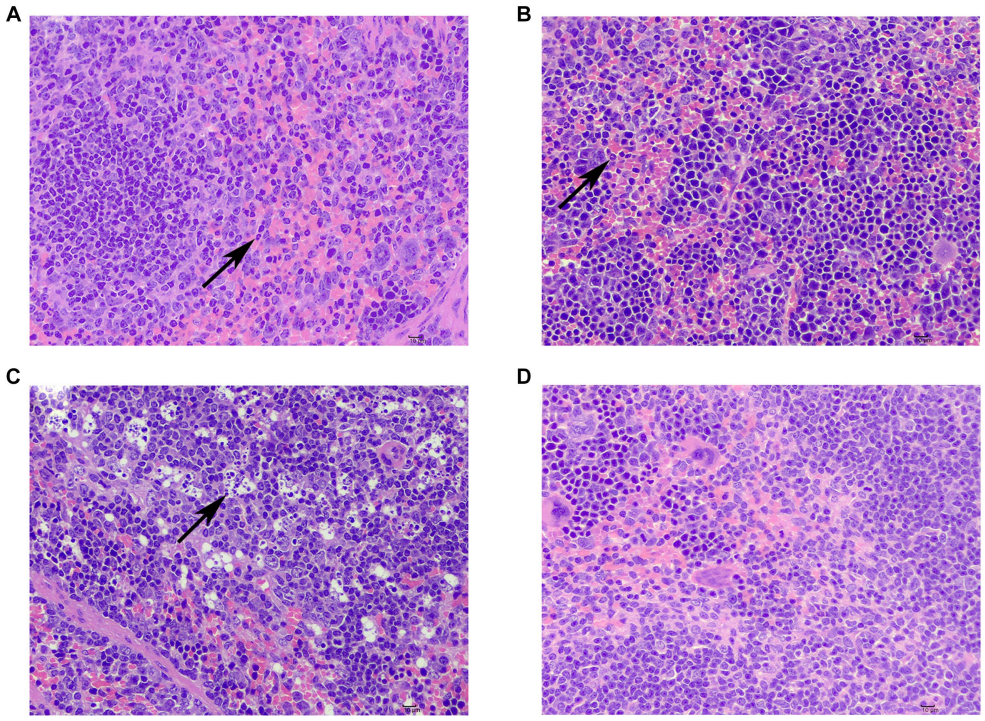

FIGURE 2
Spleen injury and repair in mice. **(A)** Lymphocyte necrosis in the splenic nodule of albilopulp (↑); **(B)** neutrophilia within the white pulp (↑); **(C)** increased number of naïve granulocytes in tissues (↑); **(D)** No obvious abnormalities were seen.

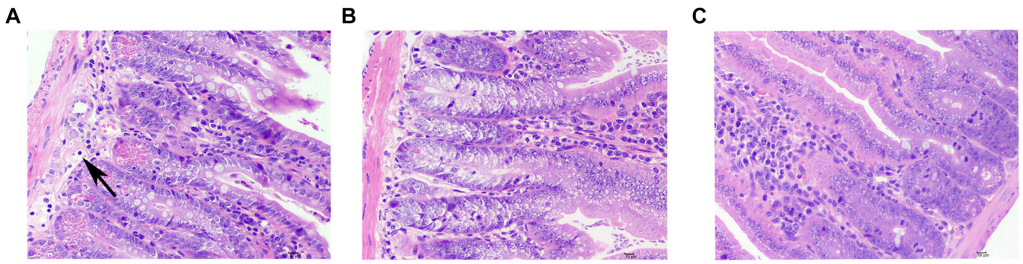

FIGURE 3
Pathological slides of small bowel injuries. **(A)** Typical lesions in the sdd group, inflammatory cell infiltration (↑). **(B)** f1 group showed no obvious pathological changes, and one was randomly selected as a representative picture. **(C)** No obvious pathological changes were seen in the nc group, and one was randomly selected as a representative picture.

showed approximately 20% less Firmicutes and approximately 20% more Proteobacteria compared to f1 and nc (Figure 6A).

At the class level, the dominant community composition of the intestinal flora in the three groups of mice was Bacilli. sdd showed approximately 20% less Bacilli than f1 and nc, while Gammaproteobacteria increased by approximately 20% (Figure 6B).

At the order level, the dominant community composition of the intestinal flora in the three groups of mice was Lactobacillales. sdd exhibited a decrease of approximately 16% in Lactobacillales and approximately 22% in Enterobacterales compared to nc (Figure 6C).

At the family level, the dominant community composition of the intestinal flora in the three groups of mice was Lactobacillaceae. sdd showed a decrease of approximately 13% in Lactobacillaceae and approximately 22% in Enterobacteriaceae compared to nc (Figure 6D).

At the genus level, the intestinal colony community composition of the three groups of mice was predominantly composed of Lactobacillus. However, there were variations in the species composition and proportion among the groups. In comparison to the nc group, the sdd group exhibited a decrease of approximately 22% in lactobacillaceae, an increase of around 21% in Escherichia_Shigella, and a rise of about 9% in Ligilactobacillus (Figure 6E).

3.6.3 Alpha diversity analysis

The sample Alpha diversity index was evaluated using the QIIME2 2020.6 software (Figure 7). There were no significant differences ($p > 0.05$) observed between the six indexes of Ace, Chao1, Simpson, Shannon, Coverage, and PD_whole_tree. However, the Ace, Chao1, and PD_whole_tree indices were highest in the f1 group, followed by

TABLE 3 Small intestinal tissue measurement data of mice with spleen deficiency and diarrhea.

Project		sdd	F1	nc
Intestinal villi height	μm	250.9 ± 14.09	438.3 ± 11.74	482.0 ± 7.237
Crypt depth	μm	116.5 ± 3.580	88.25 ± 3.669	88.50 ± 3.190
Muscular layer thickness	μm	34.82 ± 2.182	27.05 ± 2.060	26.20 ± 1.453

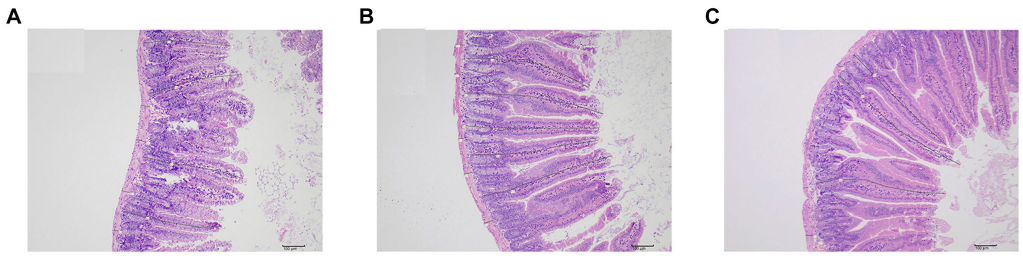

FIGURE 4
Small intestinal tissue measurements. **(A)** Representative figure of intestinal villi height, crypt depth and muscular thickness measurement in sdd group. **(B)** Representative figure of intestinal villi height, crypt depth and muscular thickness measurement in fl group. **(C)** Representative figure of intestinal villi height, crypt depth and muscular thickness measurement in nc group.

the sdd group, and lowest in the nc group. Group nc exhibited the largest Simpson and Shannon indices.

4 Discussion

The compound traditional Chinese medicine preparation has shown significant effectiveness in treating spleen deficiency and diarrhea in mice. The treatment demonstrated a faster effect, with 40% of mice showing significant improvement after just 1 day of medication. By the fifth day, the cure rate reached 90%, with the exception of one weaker mouse that unfortunately died midway. All the remaining mice were successfully cured after a six-day medication period. The mice with spleen deficiency and diarrhea exhibited much higher levels of serum ALT, AST, TG, UREA, CREA-S, etc., compared to the normal group of mice. In particular, ALT levels were almost five times higher than normal, and Glu levels were significantly lower than those in the control group. These findings indicate that long-term administration of senna not only leads to spleen deficiency and diarrhea in mice but also causes damage to the liver and kidney function. However, after 7 days of treatment with the compound traditional Chinese medicine preparations, the liver and kidney function indexes returned to normal, with no significant difference compared to the normal group, except for slightly higher levels of CREA-S, CHE, and Glu. From the perspective of serum biochemical indexes, the presence of spleen deficiency and diarrhea is accompanied by some degree of liver and kidney function damage. Although structural damage cannot be confirmed without pathological sections and urine sediment examination, the study demonstrates that the compound traditional Chinese medicine preparation not only promotes the recovery of liver and kidney function in mice with spleen deficiency and diarrhea, but also increases serum total protein and blood glucose levels.

The spleen, as the largest secondary immune organ, plays a crucial role in disease development. It is responsible for the transport and localization of lymphocytes in the splenic microenvironment, allowing them to scan antigen-presenting cells (Lewis et al., 2019). Lymphocyte necrosis and disintegration can result in weakened immunity. This compound traditional Chinese medicine has been found to have a reparative effect on spleen damage, thereby enhancing the immune function of mice.

In this study, we observed intestinal paraffin sections and performed HE staining before and after treatment and recovery. We also measured and compared the numerical values of intestinal villi and crypts. These observations provided a more intuitive understanding that the compound Chinese medicine can promote the regeneration of intestinal villi and repair damaged mucosa. However, further research and exploration are needed to determine whether this compound TCM preparation can promote the proliferation and differentiation of intestinal stem cells and tufted mesenchymal cells, facilitate the regeneration of wound-associated epithelial (WAE) cells (Quirós and Nusrat, 2019), or increase the secretion of Hh ligand by pseudo-multilayer intestinal epithelium and the expression of myosin II-related genes. It is important to note that compound traditional Chinese medicine preparations have a complex composition and exhibit multi-action and multi-target characteristics.

Spleen deficiency and diarrhea in mice were found to have significantly lower serum NHE3 levels compared to normal groups. Previous studies have shown that excessive stimulation of bacterial heat-stable enterotoxin STa, along with cGMP accumulation and an increase in protein kinase A, strongly inhibits NHE3. Additionally, certain viral infections causing diarrhea can also inhibit NHE3 protein (Weiglmeier et al., 2010). It has also been research discovered that Jin-PiY-in can reduce the expression of GLP-1, reduce the ubiquitination and phosphorylation of NHE3, regulate the expression of NHE3, at least partly improve ion transport in the intestinal epithelium, and improve the imbalance of electrolyte absorption, thus significantly reducing the diarrhea symptoms (Ma et al., 2023). In this study, the level of NHE3 improved after treatment with compound traditional Chinese medicine preparations, indicating that promoting

the expression of NHE3 protein may be one of the mechanisms by which these preparations treat spleen deficiency and diarrhea.

For mice with spleen deficiency and diarrhea, the intestinal flora exhibited significant changes in the abundance of Firmicutes and Proteobacteriaces. Specifically, there was a notable decrease of approximately 22% in the abundance of Lactobacillus, while the abundance of Shigella increased by approximately 21%. Although some changes were observed in other phyla and genus, they were relatively minor in magnitude. These findings provide evidence that spleen deficiency leads to a compromised defense qi, resulting in susceptibility to external pathogens. Consequently, the intestinal micro-ecosystem loses its self-stable state, leading to damage to the

TABLE 4 Mouse NHE3 /detection results.

		sdd	f1	nc
NHE3	ng/mL	15.95 ± 0.3955	19.48 ± 0.4236	23.80 ± 0.4512
SCFAs	ng/mL	80.74 ± 3.085	90.15 ± 6.520	88.10 ± 3.114

TABLE 5 Sequencing data quality.

Project	Unit	Outcome		
		sdd	f1	nc
RawReads	Strip	79,878 ± 113.5	79,939 ± 52.92	79,925 ± 70.97
CleanReads	Strip	79,310 ± 106.7	79,373 ± 61.61	79,365 ± 62.27
DenoisedReads	Strip	77,977 ± 326.0	77,297 ± 405.5	76,600 ± 1,061
MergedReads	Strip	76,210 ± 1,018	74,733 ± 837.3	73,250 ± 2,265
Non-chimericReads	Strip	68,534 ± 2079	66,639 ± 530.0	62,802 ± 2,989
OTU_Num		436.0 ± 184.5	465.0 ± 105.5	379.7 ± 53.82
Seqs_Num		68,521 ± 2074	66,624 ± 529.7	62,771 ± 3,010

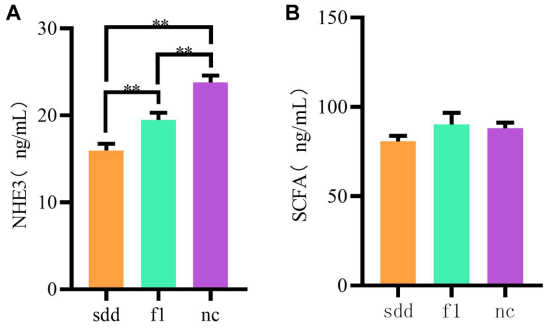

FIGURE 5
Mouse serum NHE3 and SCFAs expression. **(A)** Is a histogram of serum NHE3 expression, and **(B)** is a histogram of serum SCFA expression. The abscissa coordinates are all grouping information (orange indicates sdd group, green indicates fl group, purple nc indicates blank control,); The ordinate represents the expressed numerical value.

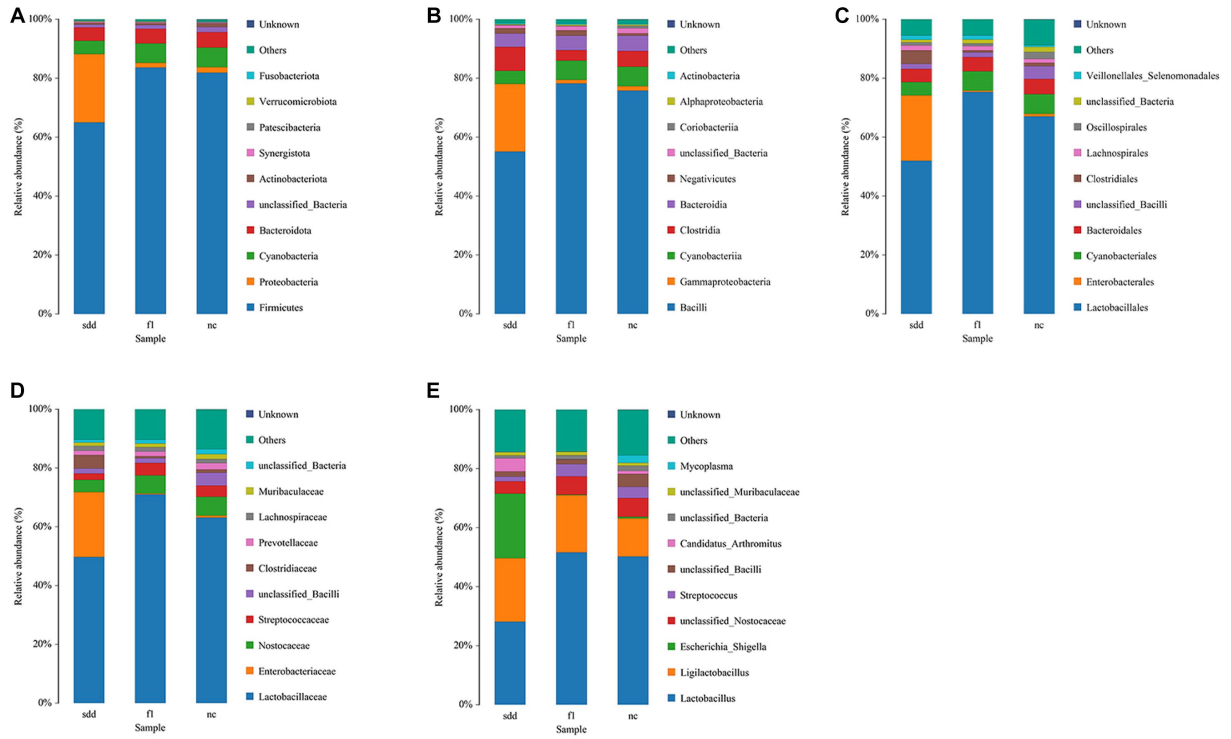

FIGURE 6
Distribution of intestinal microbial community composition in mice. **(A–E)** Represent the histogram of the structure of the intestinal colonies of the three groups of mice from the phylum to the genus level. The abscissa is grouped information; The ordinate represents the composition percentage; Different color legends represent different flora information.

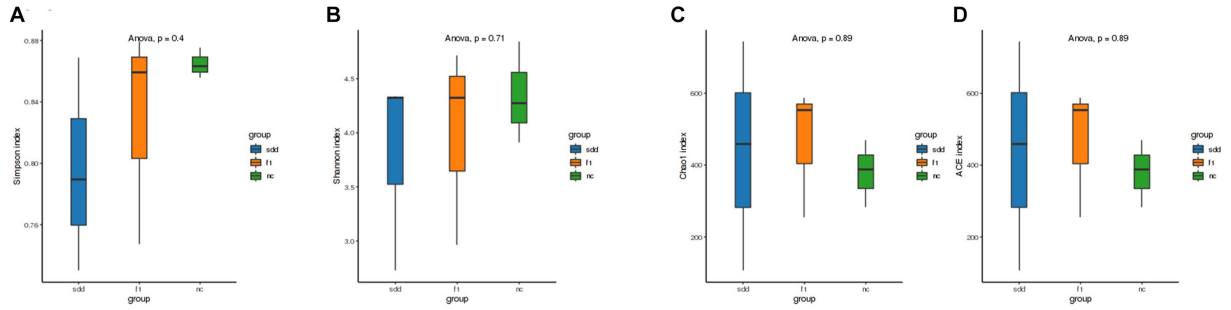

FIGURE 7
Analysis of alpha diversity of mouse intestinal flora. **(A–D)** Represents the four index difference analysis charts of Simpson, Shannon, Chaol, and Ace in three groups. The abscissa is grouped information; Ordinates represent numeric values; Different color legends represent different groups.

intestinal mucosal barrier and immune function disorders. Following treatment with compound traditional Chinese medicine preparations, the abundance of Lactobacillus under the phylum Firmicutes reached 51.6%, while the abundance of Shigella under the phylum Proteobacteria decreased to 0.2%. Overall, the flora structure and composition were nearly identical to those of the normal groups.The study indicated that the compound traditional Chinese medicine preparation effectively increased the abundance of intestinal firmicutes and Lactobacillus in mice with spleen deficiency and diarrhea. This, in turn, led to an increase in the abundance of beneficial bacteria while inhibiting the growth and reproduction of pathogenic bacteria like Shigella. The compound also demonstrated the ability to promote the restoration of homeostasis in the intestinal flora and repair the biological barrier of the intestinal mucosa.

In this experiment, the serum SCFAs content of mice was quantitatively analyzed by double anti-sandwich enzyme-linked immunoassay, and the dysbacteriosis of the mice was caused by spleen deficiency and diarrhea, and the SCFAs level was lower than that of the blank control group. Decreased biosynthesis of SCFAs affects the barrier function of the intestine and increases the translocation of intestinal wall endotoxins, thereby triggering chronic inflammation and disruption of glucose and lipid metabolism in the body (Xiong et al., 2022). The SCFAs of mice cured by the compound TCM preparation were slightly higher than those in the control group, indicating that the compound TCM preparation had a certain promoting effect on SCFAs, but only the total SCFAs were measured and analyzed, and the specific components were not determined, resulting in no significant difference. Due to the low concentration and lack of standardization of SCFAs, which are difficult to measure clinically, veterinary clinical research on SCFAs remains a challenge.

5 Conclusion

The compound traditional Chinese medicine preparation F1 is involved in the treatment of spleen deficiency and diarrhea by regulating the body's sodium and hydrogen exchange proteins, intestinal mucosa, intestinal flora, and metabolites.

Data availability statement

The original contributions presented in the study are publicly available. This data can be found at: https://figshare.com/10.6084/m9.figshare.24460048.

Ethics statement

The animal study was approved by Ethical Review Committee of Laboratory Animal Welfare of Yunnan University. The study was conducted in accordance with the local legislation and institutional requirements.

Author contributions

FD, KW, and GL Conceptualization, Methodology, Visualization, Validation, Analysis, and Writing - draft. ZY, FY, YS, GD, WS, KZ, and JH Writing - review & revision. All authors contributed to the article and approved the submitted version.

Funding

The author(s) declare financial support was received for the research, authorship, and/or publication of this article. This work was supported by "Rural Revitalization - Dairy Goat Industry Science and Technology Mission in Shilin County, Yunnan Province" Project (Project No: 202104BI090017).

Conflict of interest

The authors declare that the research was conducted in the absence of any commercial or financial relationships that could be construed as a potential conflict of interest.

Publisher's note

References

An, J., Liu, Y., Wang, Y., Fan, R., Hu, X., Zhang, F., et al. (2022). The role of intestinal mucosal barrier in autoimmune disease: a potential target. *Front. Immunol.* 13:871713. doi: 10.3389/fimmu.2022.871713

Banaszak, M., Górna, I., Woźniak, D., Przysławski, J., and Drzymała-Czyż, S. (2023). Association between gut Dysbiosis and the occurrence of SIBO, LIBO, SIFO and IMO. *Microorganisms* 11:573. doi: 10.3390/microorganisms11030573

Brown, G., Hoedt, E. C., Keely, S., Shah, A., Walker, M. M., Holtmann, G., et al. (2022). Role of the duodenal microbiota in functional dyspepsia. *Neurogastroenterol. Motil.* 34:e14372. doi: 10.1111/nmo.14372

Che, Q., Luo, T., Shi, J., He, Y., and Xu, D. L. (2022). Mechanisms by which traditional Chinese medicines influence the Intestinal Flora and Intestinal barrier. *Front. Cell. Infect. Microbiol.* 12:863779. doi: 10.3389/fcimb.2022.863779

Chen, J., Shen, B., and Jiang, Z. (2022). Traditional Chinese medicine prescription Shenling BaiZhu powder to treat ulcerative colitis: clinical evidence and potential mechanisms. *Front. Pharmacol.* 13:978558. doi: 10.3389/fphar.2022.978558

Dong, Y., Fan, H., Zhang, Z., Jiang, F., Li, M., Zhou, H., et al. (2022). Berberine ameliorates DSS-induced intestinal mucosal barrier dysfunction through microbiota-dependence and Wnt/β-catenin pathway. *Int. J. Biol. Sci.* 18, 1381–1397. doi: 10.7150/ijbs.65476

Fa, U., Bl, P., and Jm, H. (2016). "Alimentary system" in *Jubb, Kennedy & Palmer's Pathology of Domestic Animals*. ed. M. Grant Maxie, *Volume 2*.

Feng, W., Ao, H., and Peng, C. (2018). Gut microbiota, short-chain fatty acids, and herbal medicines. *Front. Pharmacol.* 9:1354. doi: 10.3389/fphar.2018.01354

Gan, D., Xu, A., Du, H., and Ye, Y. (2017). Chinese classical formula Sijunzi decoction and chronic atrophic gastritis: evidence for treatment approach? *Evid. Based Complement. Alternat. Med.* 2017:9012929. doi: 10.1155/2017/9012929

Hu, X., and Yang, F. (2022). Analysis of the therapeutic effect of Changyanning on intestinal Flora in inflammatory bowel disease. *Contrast Media Mol. Imaging* 2022, 3757763–3757768. doi: 10.1155/2022/3757763

Lewis, S. M., Williams, A., and Eisenbarth, S. C. (2019). Structure and function of the immune system in the spleen. *Sci. Immunol.* 4:eaau6085. doi: 10.1126/sciimmunol.aau6085

Li, H., Feng, C., Fan, C., Yang, Y., Yang, X., Lu, H., et al. (2020). Intervention of oncostatin M-driven mucosal inflammation by berberine exerts therapeutic property in chronic ulcerative colitis. *Cell Death Dis.* 11:271. doi: 10.1038/s41419-020-2470-8

Li, J., Li, D., Chen, Y., Chen, W., Xu, J., and Gao, L. (2023). Gut microbiota and aging: traditional Chinese medicine and modern medicine. *Clin. Interv. Aging* 18, 963–986. doi: 10.2147/cia.S414714

Li, H., Liu, Z. L., Lu, L., Buffet, P., and Karniadakis, G. E. (2021). How the spleen reshapes and retains young and old red blood cells: a computational investigation. *PLoS Comput. Biol.* 17:e1009516. doi: 10.1371/journal.pcbi.1009516

Li, B., Tao, X., Sheng, L., Li, Y., Zheng, N., and Li, H. (2022). Divergent impacts on the gut microbiome and host metabolism induced by traditional Chinese medicine with cold or hot properties in mice. *Chin. Med.* 17:144. doi: 10.1186/s13020-022-00697-2

Liu, M., Yan, J., Wu, Y., Zhu, H., Huang, Y., and Wu, K. (2022). The impact of herbal medicine in regulating intestinal flora on female reproductive disorders. *Front. Pharmacol.* 13:1026141. doi: 10.3389/fphar.2022.1026141

Ma, J. X., Chen, T., Xue, H., Zhang, M., Li, Z. Y., Li, X., et al. (2023). Jian-pi-yin decoction attenuates lactose-induced chronic diarrhea in rats by regulating GLP-1 and reducing NHE3 ubiquitination and phosphorylation. *Heliyon* 9:e17444. doi: 10.1016/j.heliyon.2023.e17444

Ma, S., Jiang, Y., Zhang, B., Pang, J., Xu, X., Sun, J., et al. (2019). Comparison of the modulatory effect on intestinal microbiota between raw and bran-fried Atractylodis Rhizoma in the rat model of spleen-deficiency syndrome. *Int. J. Environ. Res. Public Health* 16:3183. doi: 10.3390/ijerph16173183

Mei, L., Wang, F., Yang, M., Liu, Z., Wang, L., Chen, Q., et al. (2022). Studies on the mechanism of the volatile oils from Caoguo-4 decoction in regulating spleen deficiency diarrhea by adjusting intestinal microbiota. *Oxidative Med. Cell. Longev.* 2022:5559151. doi: 10.1155/2022/5559151

Peritore-Galve, F. C., Kaji, I., Smith, A., Walker, L. M., Shupe, J. A., Washington, M. K., et al. (2023). Increased intestinal permeability and downregulation of absorptive ion transporters Nhe3, Dra, and Sglt1 contribute to diarrhea during Clostridioides difficile infection. *Gut Microbes* 15:2225841. doi: 10.1080/19490976.2023.2225841

Quirós, M., and Nusrat, A. (2019). Contribution of wound-associated cells and mediators in orchestrating gastrointestinal mucosal wound repair. *Annu. Rev. Physiol.* 81, 189–209. doi: 10.1146/annurev-physiol-020518-114504

Shi, K., Qu, L., Lin, X., Xie, Y., Tu, J., Liu, X., et al. (2019). Deep-fried Atractylodis Rhizoma protects against spleen deficiency-induced diarrhea through regulating intestinal inflammatory response and gut microbiota. *Int. J. Mol. Sci.* 21:124. doi: 10.3390/ijms21010124

Su, Y., Qin, W., Wu, L., Yang, B., Wang, Q., Kuang, H., et al. (2021). A review of Chinese medicine for the treatment of psoriasis: principles, methods and analysis. *Chin. Med.* 16:138. doi: 10.1186/s13020-021-00550-y

Sun, Q., Xin, X., An, Z., Hu, Y., and Feng, Q. (2022). Therapeutic potential of natural plants against non-alcoholic fatty liver disease: targeting the interplay between gut microbiota and bile acids. *Front. Cell. Infect. Microbiol.* 12:854879. doi: 10.3389/fcimb.2022.854879

Tan, N., Gwee, K. A., Tack, J., Zhang, M., Li, Y., Chen, M., et al. (2020). Herbal medicine in the treatment of functional gastrointestinal disorders: a systematic review with meta-analysis. *J. Gastroenterol. Hepatol.* 35, 544–556. doi: 10.1111/jgh.14905

Turner, J. R. (2009). Intestinal mucosal barrier function in health and disease. *Nat. Rev. Immunol.* 9, 799–809. doi: 10.1038/nri2653

Weiglmeier, P. R., Rösch, P., and Berkner, H. (2010). Cure and curse: *E. coli* heat-stable enterotoxin and its receptor guanylyl cyclase C. *Toxins (Basel)* 2, 2213–2229. doi: 10.3390/toxins2092213

Willard-Mack, C. L., Elmore, S. A., Hall, W. C., Harleman, J., Kuper, C. F., Losco, P., et al. (2019). Nonproliferative and proliferative lesions of the rat and mouse Hematolymphoid system. *Toxicol. Pathol.* 47, 665–783. doi: 10.1177/0192623319867053

Wu, X. N. (1998). Current concept of spleen-stomach theory and spleen deficiency syndrome in TCM. *World J. Gastroenterol.* 4, 2–6. doi: 10.3748/wjg.v4.i1.2

Xiong, R. G., Zhou, D. D., Wu, S. X., Huang, S. Y., Saimaiti, A., Yang, Z. J., et al. (2022). Health benefits and side effects of short-chain fatty acids. *Foods* 11:2863. doi: 10.3390/foods11182863

Xu, H., Wang, S., Jiang, Y., Wu, J., Chen, L., Ding, Y., et al. (2023). Poria cocos polysaccharide ameliorated antibiotic-associated diarrhea in mice via regulating the homeostasis of the gut microbiota and intestinal mucosal barrier. *Int. J. Mol. Sci.* 24:1423. doi: 10.3390/ijms24021423

You, Y., Luo, L., You, Y., Lin, Y., Hu, H., Chen, Y., et al. (2020). Shengmai yin formula modulates the gut microbiota of spleen-deficiency rats. *Chin. Med.* 15:114. doi: 10.1186/s13020-020-00394-y

Yu, W., Lu, B., Zhang, H., Zhang, Y., and Yan, J. (2016). Effects of the Sijunzi decoction on the immunological function in rats with dextran sulfate-induced ulcerative colitis. *Biomed. Rep.* 5, 83–86. doi: 10.3892/br.2016.678

Zhou, B., Yuan, Y., Zhang, S., Guo, C., Li, X., Li, G., et al. (2020). Intestinal Flora and Disease mutually shape the regional immune system in the intestinal tract. *Front. Immunol.* 11:575. doi: 10.3389/fimmu.2020.00575

Zhu, J.-J., Liu, S., Su, X.-L., Wang, Z.-S., Guo, Y., Li, Y.-J., et al. (2016). Efficacy of Chinese herbal medicine for diarrhea-predominant irritable bowel syndrome: a meta-analysis of randomized, double-blind, placebo-controlled trials. *Evid. Based Complement. Alternat. Med.* 2016, 1–15. doi: 10.1155/2016/4071260

frontiers | Frontiers in Microbiology

TYPE Original Research
PUBLISHED 27 February 2024
DOI 10.3389/fmicb.2024.1344992

OPEN ACCESS

EDITED BY
Ren-You Gan,
Technology and Research, Singapore

REVIEWED BY
Yeshi Yin,
Hunan University of Science and Engineering, China
Yong Yang,
Qingdao Agricultural University, China

*CORRESPONDENCE
Zhong-Hong Wu
✉ wuzhh@cau.edu.cn

†These authors have contributed equally to this work and share first authorship

RECEIVED 27 November 2023
ACCEPTED 05 February 2024
PUBLISHED 27 February 2024

CITATION
He S, Zhang K-H, Jin Q-Y, Wang Q-J, Huang J, Li J-J, Guo Y, Liu P, Liu Z-Y, Liu D, Geng S-X, Li Q, Li M-Y, Liu M and Wu Z-H (2024) The effects of ambient temperature and feeding regimens on cecum bacteria composition and circadian rhythm in growing rabbits.
Front. Microbiol. 15:1344992.
doi: 10.3389/fmicb.2024.1344992

The effects of ambient temperature and feeding regimens on cecum bacteria composition and circadian rhythm in growing rabbits

Shuai He[1†], Ke-Hao Zhang[1†], Qiong-Yu Jin[1], Qiang-Jun Wang[1,2], Jie Huang[1], Jun-Jiao Li[1,3], Yao Guo[1], Peng Liu[1], Zhong-Ying Liu[1], Dan Liu[1], Shi-Xia Geng[1], Qin Li[1], Ming-Yong Li[4], Man Liu[4] and Zhong-Hong Wu[1*]

[1]State Key Laboratory of Animal Nutrition and Feeding, College of Animal Science and Technology, China Agricultural University, Beijing, China, [2]College of Animal Science and Technology, Anhui Agricultural University, Hefei, China, [3]Handan Livestock Technology Extension Station, Handan, China, [4]National Rabbit Industry Technology System Qingdao Comprehensive Experimental Station, Qingdao, China

Seasonal environmental shifts and improper eating habits are the important causes of diarrhea in children and growing animals. Whether adjusting feeding time at varying temperatures can modify cecal bacterial structure and improve diarrhea remains unknown. Three batches growing rabbits with two groups per batch were raised under different feeding regimens (fed at daytime vs. nighttime) in spring, summer and winter separately, and contents were collected at six time points in 1 day and used 16S rRNA sequencing to investigate the effects of feeding regimens and season on the composition and circadian rhythms of cecum bacteria. Randomized forest regression screened 12 genera that were significantly associated with seasonal ambient temperature changes. Nighttime feeding reduced the abundance of the conditionally pathogenic bacteria *Desulfovibrio* and *Alistipes* in summer and *Campylobacter* in winter. And also increases the circadian rhythmic Amplicon Sequence Variants in the cecum, enhancing the rhythm of bacterial metabolic activity. This rhythmic metabolic profile of cecum bacteria may be conducive to the digestion and absorption of nutrients in the host cecum. In addition, this study has identified 9 genera that were affected by the combination of seasons and feeding time. In general, we found that seasons and feeding time and their combinations affect cecum composition and circadian rhythms, and that daytime feeding during summer and winter disrupts the balance of cecum bacteria of growing rabbits, which may adversely affect cecum health and induce diarrhea risk.

KEYWORDS

growing rabbit, feeding regimens, cecal bacteria, seasonal variations, diarrhea

1 Introduction

Diarrhea is one of the most common diseases in children. Diarrhea in children seriously damages intestinal health and hinders growth and development (Mensah and Tomkins, 2003; Hanieh et al., 2021). Many epidemiological studies have shown that the occurrence of diarrhea in children and growth animals is directly related to seasonal rotations and climate change (Rowland, 1986; Windeyer et al., 2014; Uibel et al., 2022). In addition, the use of electronic products in children at night impairing sleep quality and increasing nocturnal eating behavior, thus impairing intestinal health (Afonso et al., 2022; Lepley et al., 2022). Numerous studies have ascribed the cause of seasonal diarrhea to environmental conditions influencing the variability of digestive tract bacteria, but are limited to stool samples that do not fully represent the bacterial composition of the intestinal lumen (Wen et al., 2018; Eybpoosh et al., 2021). Similarly, variations in feeding time and durations of light exposure also disrupted the rest rhythms and impacted the growth performance of developing animals (Schanbacher and Crouse, 1980; Robert et al., 1991). Disrupted rest rhythms lead to the accumulation of Reactive Oxygen Species (ROS) in the animal's gut, causing oxidative stress and increasing the risk of death (Vaccaro et al., 2020). It remains unclear whether meal time that clash with their natural activity rhythms can disturb the balance of the cecal bacteria and heighten the risk of diarrhea, especially during periods when children and growing animals are more prone to it.

Ambient temperature possesses sufficient phenotypic plasticity mediated through gut bacteria. The same species was shaped with differential digestive characteristics at different ambient temperatures (Li et al., 2018). Cold exposure altered intestinal flora and enhanced nutrient absorption, insulin sensitivity, and white fat browning in mice (Chevalier et al., 2015). The cold environment also reshaped the gut bacteria to increase thermogenesis (Bo et al., 2019). In addition, Animals exhibit dysbiosis of the gut bacteria and remarkable changes in metabolites that damage the intestinal barrier in heat-stressed environments (Hu et al., 2022; Xia et al., 2022). Repeated hot and cold environmental temperature domestication in Mongolian gerbils alters intestinal bacteria and drives the development of host-adapted metabolic activity (Khakisahneh et al., 2020).

Light exposure has also been reported to be an upstream signal of structural variation in gut bacteria (Wu et al., 2018; Wei et al., 2020). Coordination of photoperiod with feeding time controls oscillations of gut bacteria through fluctuations in antimicrobial peptides (Talbot et al., 2020; Brooks et al., 2021; Heddes et al., 2022). Ambient light cues can also be translated into group III innate lymphocyte signaling in the gut, which plays a role in shaping and regulating the intestinal bacterial community (Godinho-Silva et al., 2019).

The suprachiasmatic nucleus (SCN) of animals in the field environment orchestrate foraging and resting behavior during the light-dark phase transition. Inverting the light and dark phases of ingestion in growing animals presents a challenge to the SCN in orchestrating whole-body rhythmic activity. The light/dark cycle regulates the rhythm of animal activity/rest by affecting the loop from the animal's SCN to the sympathetic nerves (Scheer et al., 2005). Increased sympathetic activity in the early stages of animal wakefulness promotes enhanced thermoregulation (Guo et al., 2021). Seasonal Rotation caused by the Earth's revolution are important regulators of the clock mechanism, integrating changes in the timing of light and ambient temperature (Arendt, 2012). Environmental temperature changes are most pronounced during the turnover of seasons, causing a shift in the thermoneutral zone and changing the metabolic intensity for the animal SCN activity of the animals (Liao et al., 2022). Daytime feeding in rodents alters the oscillatory rhythm of bile acids in the circulation (Eggink et al., 2017), which subsequently interferes with the thermogenesis and thermoregulation of brown fat G protein-coupled bile acid receptor 1 (TGR5) (Watanabe et al., 2006).

In the livestock industry, although intelligent feeding systems were introduced in the animal rearing process, the rational parameters of feeding regimens were predominantly set according to the workers' timetable, ignoring the activity/rest phase of the animals. For rabbits in particular, daytime feeding contradicts their nocturnal activity. Daytime feeding of nocturnal animals causes bacterial imbalance and damages intestinal health (Voigt et al., 2014). The cecum bacterial community of rabbits is considered to be an important basis for maintaining digestive health and promoting animal growth (Combes et al., 2013). The symbiotic relationship between bacteria and host involves the regulation of intestinal physiological, immune and metabolic activities (Yoo et al., 2020). Numerous fecal transplantation experiments have shown that specific intestinal bacteria can improve intestinal disease and alter the metabolic profile and health of recipient animals (Allegretti et al., 2020; Craven et al., 2020; Leong et al., 2020). Factors such as food structure and environmental conditions can alter the composition and function of intestinal bacteria (Claesson et al., 2012; Deng et al., 2020). The intestinal bacterial structure of rabbits in the growing stage is exceptionally unstable, and the superimposition of weaning, cage transport and feed stress often triggers diarrhea, causing the most serious animal losses (Zhuang et al., 2022). Children, comparable to growing rabbits, are also characterized by immature gut development and gut bacterial instability (Lu et al., 2009). The disruption of intestinal bacterial homeostasis triggers the occurrence of diarrhea in a large number of children (Di Biase et al., 2021). Seasonal changes in environmental temperature and humidity are also important factors impacting the balance of the gut bacterial community in growing animals and children (Oakley et al., 2018; Chong et al., 2021). Therefore, identifying feeding regimens that enhance the stability and resilience of the gut bacteria under different seasonal environmental conditions can be an effective strategy for providing a healthy diet for children and contribute to efficient livestock production.

We have previously found that feeding growing rabbits during the day in summer can alter the cecum bacterial structure and increase the risk of diarrhea (Wang et al., 2021). In rabbit production, the use of open shed not only saves the farmer's capital investment, but also provides sufficient sunlight and natural air for rabbits and enhances animal welfare (Rahman et al., 2018). Compared to closed rabbit sheds, rabbits survive in open sheds with greater fluctuations in light intensity, light hours and temperature, more closely resembling real seasonal environmental variations. In order to investigate the effects of ambient temperature and feeding regimens on cecum composition and circadian rhythm.

This study combined 16S rRNA amplification, high-throughput sequencing, PICRUSt prediction and random forest to achieve multi-time points sample collection, analyze the differences in cecum bacterial composition and potential function of rabbits growing in open sheds, identify bacterial fluctuation characteristics associated with feeding time and look for bacteria associated with seasonal environmental temperature. Thus, this study provides a scientific basis for evaluating feeding regimens and environmental regulation in growing rabbits. This also provides important clues to assess the impact of seasonal diarrhea and disturbances in the timing of eating on cecal health in children.

2 Materials and methods

2.1 Growing rabbit feeding management

In the experiment, a total of 648 weaned rabbits of similar age (35 days old) and body weight (0.91 ± 0.10 kg) were selected in summer (July–August), spring (April–May), and winter (December-February) with 216 rabbits in each season. And 216 rabbits were randomly divided into two groups (daytime feeding, DF and night-restricted feeding, NRF) of 108 rabbits per group per season, and reared in an open rabbit shed with rolling plastic curtain in a commercial rabbit farm in Qingdao China. The plastic curtain was fully opened in summer. In spring and winter the plastic curtain was used to keep warm. When the temperature drops at night, the curtains were closed and were partly opened during the daytime when the temperature rises. The DF and NRF groups dropped feed before dawn and before dark, respectively, and both groups collected residual feed before dawn the following day. The DF feed delivery time was 7:00 am, 6:00 am, and 6:30 am in winter, summer and spring, respectively, and NRF feed were delivered at 5:00 pm, 7:00, pm and 6:30 pm. Both DF and NRF surplus food were collected at 7:00 am in winter, 6:00 am in summer and 6:30 am in spring (**Figure 1A**). The feed formulation and nutrient composition are shown in **Supplementary Table 1**.

2.2 Ambient temperature recording

The test was conducted using an automatic temperature and humidity recorder (Apresy179-TH, Apresy Precision Optoelectronics Co., Ltd., accuracy ± 0.3°C, ± 3% RH, respectively) to continuously record the temperature and humidity in the house, and the data were automatically recorded once every 10 min. In the analysis of the relationship between ambient temperature and cecum bacterial abundance, the temperature values at the moment of slaughter and at the closest distance were recorded as the room temperature at which the growing rabbits were kept.

2.3 Mortality and diarrhea

Death and diarrhea were recorded daily during each season of the experiment in the DF and NRF groups, respectively, cumulative mortality and diarrhea rates were calculated in 7-days increments.

2.4 Growth rabbit cecum contents collection

Growing rabbits were reared until 84 days of age, rabbits were euthanized by cervical dislocation at an interval of 4 h. The contents of the cecum of 36 rabbits were collected from each of the DF and NRF each season. The specific sampling operation was as follows: six collection time points (7:00, 11:00, 15:00, 19:00, 23:00, 3:00) were set to collect mid-cecum contents, six rabbits per time point as biological replicates, and stored at −80°C, for subsequent genomic DNA isolation.

2.5 DNA extraction and sequencing for cecum bacteria

Genomic DNA was extracted from cecum contents using the Power Soil DNA Isolation Kit (MOBIO Laboratories, Carlsbad, CA, USA) according to the manufacturer's instructions. Forward primer 5′-ACTCCTACGGGAGGCAGCA-3′ and reverse primer 5′- GGACTACHVGGGTWTCTAAT-3′ were used to amplify the V3-V4 region of the 16SrRNA gene with a specific barcode. High-throughput sequencing was performed using Illumina HiSeq for the 2500 PE250 platform (Illumina, San Diego, CA, USA).

2.6 Bioinformatics analysis

Raw reads were uploaded to Quantitative Insights into Microbial Ecology (QIIME2) software, and fastq files were quality filtered, trimmed, denoised, and merged using the DADA2 package packaged with QIIME2. Clean reads were then feature-classified using DADA2 to filter out amplicon sequence variants (ASVs) with relative abundance <0.005%. The classification annotation of ASVs was based on the SILVA132 database using the naive Bayes classifier. In addition, sequence data was refined to a depth of 29675 sequences per sample to perform bacterial α and β diversity calculations. In the β diversity analysis, Principal Coordinates Analysis (PCoA) was performed based on unweighted UniFrac distances, and analysis of similarities (ANOSIM) tested for statistically significant differences between groups. In addition, we used linear discriminant analysis Linear Discriminant Analysis (LDA) to select thresholds (LDA > 3.0) and Linear discriminant analysis Effect Size (LEfSe) to select biomarkers in different groups. simca (version 13.0) was used for partial least squares discriminant analysis (Partial least squares Discriminant Analysis, PLS-DA).

Phylogenetic Investigation of Communities by Reconstruction of Unobserved States 2 [PICRUSt2 (2.3.0)] from the BMKCloud[1] was used to predict differences in bacterial function between a single season specific time point and the remaining five time point sets.

The relative abundance of bacterial taxa in the cecum of growing rabbits at the genus level and the corresponding ambient temperature were regressed using the default parameters implemented in the R algorithm (R package randomForest

1 http://www.biocloud.net

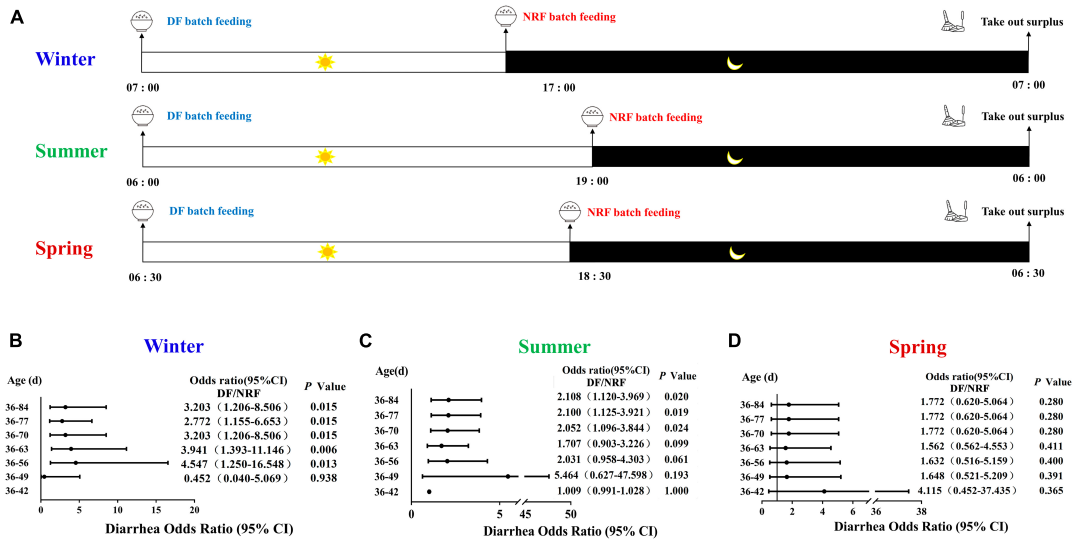

FIGURE 1
Design of animal feeding regimens and cumulative diarrhea rate of growing rabbits. **(A)** Design of rabbits feeding regimens in spring, summer and winter. Feeding time change the risk of cumulative diarrhea occurring in **(B)** winter; in **(C)** summer, results from our previous study (Wang et al., 2021); in **(D)** spring.

ntree = 1000, using the default mtry of p/3, where p is the number of taxonomic units of the class). A random forest classifier was used to analyze the relationship between bacteria with relative abundance greater than 0.1% and temperature variation. The list of taxa ordered by feature importance from the random forest is determined over 100 iterations. The number of tagged taxa is determined by 10-fold cross-validation using the rfcv() function in the R package "randomForest," repeated five times.

2.7 Jonckheere-Terpstra-Kendall cycle (JTK_Cycle) analysis

The non-parametric Jonckheere-Terpstra-Kendall cycle (JTK_Cycle) was used to analyze the significance, amplitude and phase of the 24-h cecal bacterial rhythms (Hughes et al., 2010). The relative abundance values of microorganisms sequenced at six time points during the day and night were entered into the corresponding R program of JTK_Cycle to obtain the corresponding rhythmic parameters such as period, phase and amplitude.

2.8 Statistical analysis

The cumulative incidence of diarrhea and death was evaluated using the ratio (OR), and the chi-square test was calculated at 95% confidence intervals (95% CI). The Wilcoxon rank sum test was used to analyze the differences in non-parametric data between the two groups. For all other data, *t*-test was used to compare the differences between the two groups, and two-way ANOVA was used to analyze the interaction between cecum bacterial composition and seasonal variation, feeding regimens, and seasonal variation and feeding regimens interactions, using SPSS 20.0 software (SPSS, Inc., Chicago, IL, USA) for statistical analysis. In addition, Spearman's rho non-parametric correlations and *P*-values (false discovery rate corrected *P*-values) were calculated using the Psych package.[2] Data plots were generated by Prism 7.0 software (GraphPad software, Inc., La Jolla, CA, USA).

3 Results

A total of 17,199,561 pairs of Reads were sequenced from 216 samples. A total of 12,628,568 Clean Reads were generated after double-ended Reads were quality controlled and spliced, generating at least 41,695 Clean Reads per sample and an average of 58,466 Clean Reads. Each cecum content sample had sufficient ASVs to reflect the maximum level of bacterial diversity, indicating sufficient sequencing depth (**Supplementary Figure 1**).

3.1 Seasonal variations induce alterations in bacterial composition

Both the Shannon-Wiener diversity index (Shannon) and Abundance-based Coverage Estimator (ACE) indices were used to reflect the diversity of the cecum bacteria of rabbits grown in different seasons. Cecum bacterial α diversity was significantly higher in spring than in other seasons ($P < 0.05$) (**Figure 2A**). The ACE index of cecum bacteria was significantly higher in winter-grown rabbits than in other seasons ($P < 0.05$) (**Supplementary Figure 2**). Overall, the cecum bacterial diversity of growing rabbits was higher in spring than in other seasons, and the bacterial community richness was higher in winter than

2 https://cran.r-project.org/web/packages/psych/index.html

in other seasons. The weighted UniFrac was used to calculate the distance of cecum contents samples in different seasons. Analysis of Similarities (ANOSIM) analysis indicated that intergroup differences were significantly greater than the intra-group differences in different seasons. The PCoA analysis showed that the *R*-values were all greater than 0 ($P = 0.001$). PLS-DA, Non-metric Multidimensional Scaling (NMDS) and PCoA all clearly classified cecum bacteria into three different groups in different seasons, indicating significant differences in the cecum bacterial structure of growing rabbits reared in different seasons (**Figure 2B** and **Supplementary Figures 2B, C**). The top 10 dominant phyla in 84-day-old growing rabbits were composed of Phylum *Firmicutes*, *Bacteroidetes*, *Verrucomicrobia*, *Proteobacteria*, *Tenericutes*, *Cyanobacteria*, *uncultured_bacterium_k_Bacteria*, *Actinomycetes*, *Epsilonbacteraeota*, and *Patescibacteria* were the top 10 bacterial phyla in terms of abundance (**Figure 2C**). The overall composition was mainly composed of *Firmicutes* and *Bacteroidetes*, which together accounted for more than 80% of the bacterial composition of the rabbit cecum. In addition, the relative abundance of bacteria at the level of 20 genera was higher than 1% (**Figure 2D**).

To further explore the seasonal rotation of cecum bacteria composition for growing rabbits, linear discriminant analysis effect size analysis (LDA > 3) and Wilcoxon rank-sum test was performed on the bacteria in different seasons. The iconic winter genera are *Campylobacter*, *Anaerovorax*, *Butyricimonas*, *Akkermansia*, and *Roseburia*. The iconic summer genera are *dgA-11_gut_group*, *Alistipes*, *Synergistes*, *Desulfovibrio*, *Bacteroides*, *uncultured_bacterium_f_Rikenella*. The iconic spring genera are *Erysipelotrichaceae_UCG-004*, *Blautia*, and *Lachnospiraceae_NK4A136_group* (**Figure 2E**).

3.2 Dietary regimens alter the composition and circadian rhythms of cecal bacteria

There was no difference between DF and NRF in the comparison of bacterial α diversity either in winter or spring (**Figure 3A**). PLS-DA results classified NRF and DF cecum bacteria into 2 groups in winter and spring. Thus different feeding regimens altered the structure of cecum bacteria β diversity (**Figure 3B**). The Wilcoxon rank-sum tests were performed in winter and spring. Compared to DF, NRF significantly increased the abundance of *Lentisphaerae* phylum in winter and decreased the abundance of *Cyanobacteria* and *Patescibacteria* phylum in spring (**Supplementary Figure 3**). LDA effect size analysis at genus level (LDA > 3) showed that *Ruminococcaceae_NK4A214_group* and *uncultured_bacterium_o_Izimaplasmatales* were significantly enriched in DF group in winter ($P < 0.05$). In spring, *Ruminococcaceae_NK4A214_group*, *Bacteroides*, and *Ruminococcus_1* were significantly enriched in NRF group ($P < 0.05$). *Ruminococcaceae_V9D2013*, *Ruminococcaceae_UCG_2013*, *Ruminococcaceae_UCG_011*, *bacterium_f_Clostridiales_vadinBB60*, and *Akkermansia* were significantly enriched in DF group ($P < 0.05$) (**Figure 3C**).

The sequenced cecal bacterial relative abundance data were analyzed by JTK to reflect the diurnal fluctuation of bacteria. In winter, 23 ASVs in DF group had circadian rhythm, accounting for 1.05% out of the total ASVs, and 57 ASVs in NRF group had circadian rhythm, accounting for 2.60% out of the total ASVs (ADJ. $P < 0.05$) (**Figure 4A**). Venn diagram analysis showed that most of the rhythmic ASVs were unique at different feeding regimens, and only two were rhythmic in both DF group and NRF group (**Figure 4B**). Radar and heat maps showed that the peak values of ASVs in DF group were mainly distributed at all-time points during the day, while those in the NRF group were mainly distributed at all-time points during the night (**Figure 4C**). The rhythmic ASVs of DF and NRF groups mainly belong to *Firmicutes*, *Bacteroidetes*, *Actinobacteria*, and *Proteobacteria*. Some ASVs in NRF group also came from *Actinobacteria*, *Cyanobacteria*, and *Tenericutes* (**Figure 4D**).

In spring, 57 ASVs in DF group had circadian rhythm, accounting for 2.60% out of the total ASVs, and 43 ASVs in NRF group had circadian rhythm, accounting for 1.96% out of the total ASVs (ADJ. $P < 0.05$). Most of the rhythmic ASVs were unique at different feeding regimens, and only five were rhythmic in both DF group and NRF group. The peak value of ASVs in the DF group was mainly distributed before and after dark, while that in the NRF group was mainly distributed before feeding at night. The rhythmic ASVs mainly belong to *Firmicutes*, *Proteobacteria*, and *Actinobacteria* in DF group. NRF group mainly belonged to *Firmicutes*, *Bacteroidetes*, *Tenericutes*, *uncultured_bacterium_k_Bacteria*, *Proteobacteria*, and *Actinobacteria* (**Supplementary Figures 4A–D**).

3.3 Interactive effects of season and feeding regimens on cecum bacterial composition

Seasonal rotation changes bacterial structure, and feeding time also changes cecum bacterial composition and diurnal oscillations. Therefore, we performed seasonal and feeding regimens interaction analyses for bacteria with relative abundance greater than 0.5% in either season (**Supplementary Table 2**). The results of the interaction between season and feeding regimens showed that *Ruminococcus_1* was higher in spring than in summer and winter, and NRF was higher than DF. In total, we found that bacterial abundance in nine genera was influenced by seasons, feeding patterns, and the interaction of season and feeding regimens. These included *Alistipes*, *Ruminococcaceae_UCG-013*, *Synergistes*, *[Eubacterium]_coprostanoligenes_group*, *uncultured_bacterium_f_Clostridiales_vadinBB60_group*, *uncultured_bacterium_f_Rikenellaceae*, *uncultured_bacterium_o_Bacteroidales*, and *uncultured_bacterium_o_Izimaplasmatales* (**Supplementary Figures 5A, B**).

3.4 Correlation between cecum bacterial changes and diarrheal incidences

We counted the number of diarrhea occurrences throughout the feeding period and found that there was no significant difference in the risk of cumulative diarrhea between the DF and NRF groups until 49 days of age in winter growing rabbits ($P > 0.05$), and between 49 and 84 days of age, the risk of

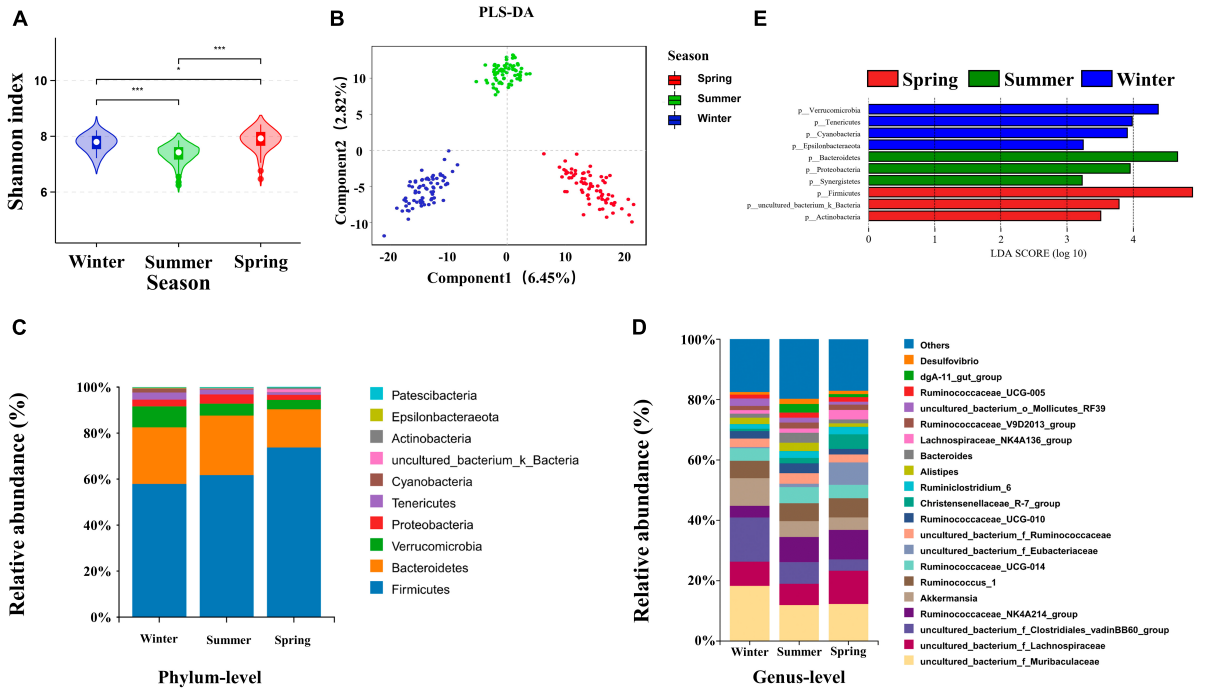

FIGURE 2
Effects of seasons on cecum bacterial structure of growing rabbits. **(A)** Shannon analysis of cecum bacteria, * represents $P < 0.05$ and *** represents $P < 0.001$. **(B)** PLS-DA analysis of the cecal bacteria. The taxonomic composition of cecum bacteria at the **(C)** phylum level (top 10, according to relative abundance) and **(D)** genus level (top 20) under different seasons. **(E)** LEfSe analysis at the genus level (LDA > 3).

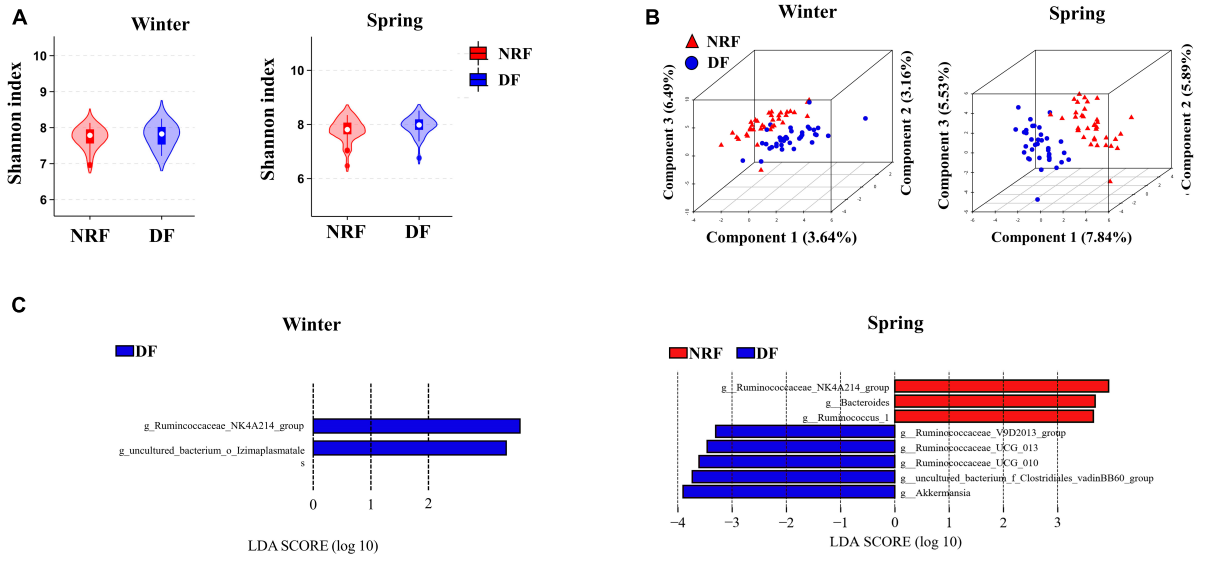

FIGURE 3
Comparison of bacterial structure under different feeding methods in winter and spring. **(A)** Shannon analysis of cecum bacteria, **(B)** PLS-DA analysis of the cecal bacteria and **(C)** LEfSe analysis at the genus level (LDA > 3).

cumulative diarrhea was significantly higher in the DF group than in the NRF group ($P < 0.05$) (Figure 1B). The cumulative risk of developing diarrhea was significantly higher in the DF group of growing rabbits than in the NRF group between 63 and 84 days of age during summer growing rabbit rearing ($P < 0.05$) (Figure 1C). There was no significant difference in the cumulative risk of occurrence of diarrhea between the DF and NRF groups of growing rabbits during the entire trial period of spring growing rabbit feeding ($P > 0.05$) (Figure 1D). The comparison of total diarrhea cases and death cases in seasonal feeding practice showed that the incidence and death of diarrhea in open shed rabbits were significantly related to the season (Supplementary Table 3). The number of diarrhea in summer growing rabbits was significantly higher than in winter and spring in both the DF and NRF feed

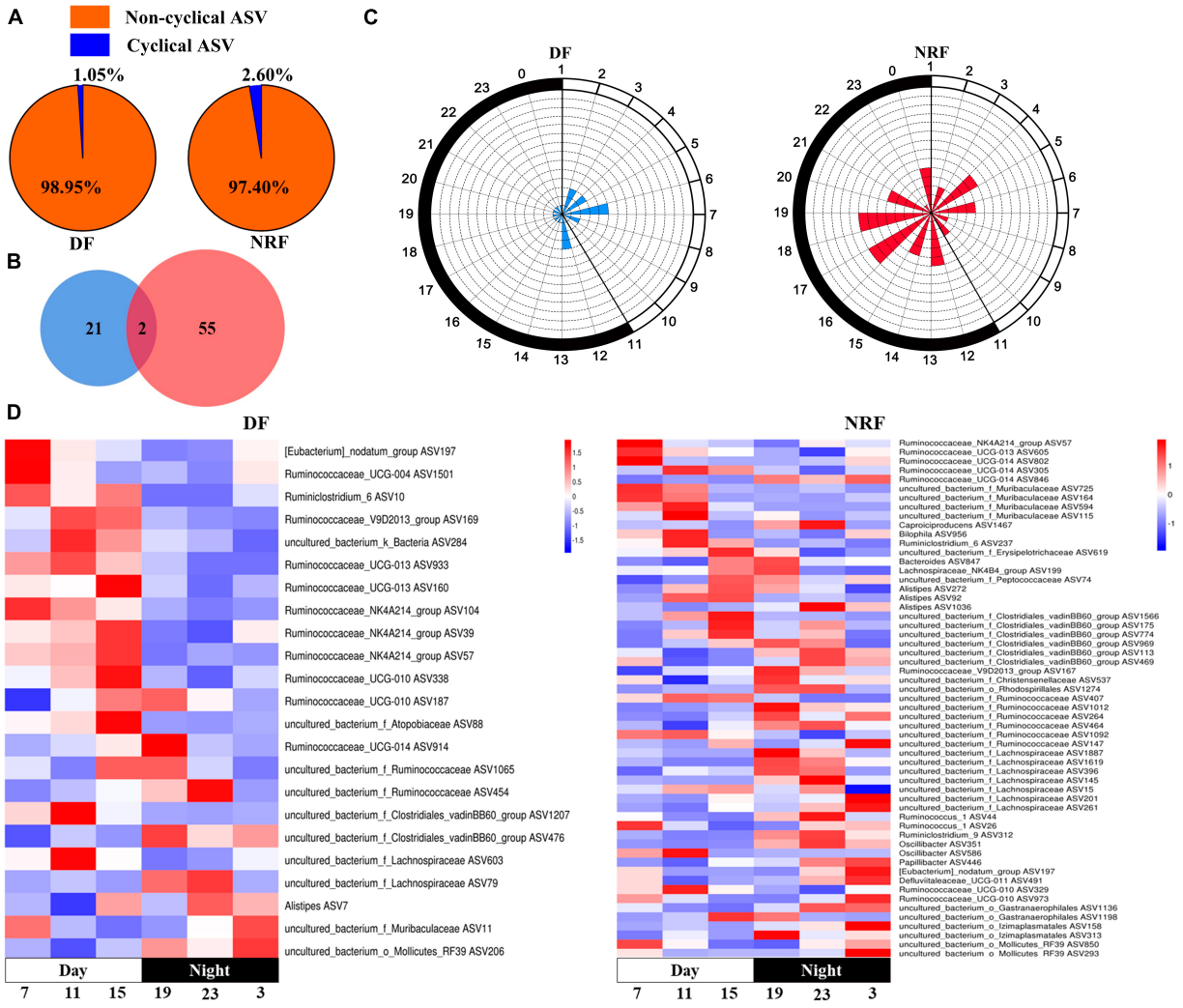

FIGURE 4
Cecal rhythmic ASVs in DF and NRF growing rabbits in winter. **(A)** Pie chart showing the proportion of rhythmic and non-rhythmic ASVs in cecum. **(B)** Venn diagram showing the number and overlapping number of rhythmic ASVs in DF group and NRF group. **(C)** A radar chart is used to display the abundance peak time of ASVs throughout the day, in which blue represents the DF group, red represents the NRF group, and the fill represents the number of rhythmic ASVs at that time point, and the time when the rhythmic ASVs peak appeared. Using JTK analysis and prediction, the radius of the dashed concentric circles represents the number of ASVs, the minimum radius unit of the dashed concentric circles represents the number of 1, and the black and white shadows on the edge of the radar map represent night and day. **(D)** Heat map showing the trend of rhythmic ASVs in growing rabbits DF group and NRF group throughout the day.

regimens ($P < 0.001$). The number of spring growing rabbits mortalities was significantly lower than in winter and summer in both the DF and NRF feed regimens. The number of mortalities was significantly lower in the winter DF group than in the summer ($P < 0.01$), while NRF reduced the number of summer mortalities resulted in no difference between winter and summer ($P > 0.05$).

We found a high tendency of diarrhea in summer. Considering that cecal bacteria are closely prioritized to cecal physiological functions, we sought to analyze the variation in cecum bacterial composition and rhythms caused by summer. We analyzed the composition at the genus level in different seasons and found that *Uncultured_bacterium_f_Barnesiellacea*, *Parabacteroides*, *Desulfovibrio*, *dgA-11_gut_group*, *Synergistes*, and *Alistipes* were significantly higher in the intestine of summer-grown rabbits compared to spring and winter ($P < 0.05$), *Escherichia-Shigella* abundance was higher in summer compared to the other two seasons. *Marvinbryantia*, *Tyzzerella_3*, and *Blautia* were significantly higher ($P < 0.05$) and *Alistipes*, *Bilophila*, and *Campylobacter* were significantly lower ($P < 0.05$) in the cecum of spring-grown rabbits than in summer and winter. Winter growth rabbits intestinal *Campylobacter*, *Akkermansia*, *Roseburia*, and *Erysipelotrichaceae_UCG-004* were significantly higher than summer and spring (Supplementary Figure 6).

Bifactorial analysis of season and feeding regimens showed that seasonal changes could significantly affect the cecum bacterial structure of growing rabbits (Supplementary Table 2). Ambient temperature was used to represent a characteristic with distinct seasonal variation. Therefore, the daily ambient temperature recorded in the rabbit shed during feeding trials completed in different seasons was used to explore seasonal bacterial variation (Supplementary Figure 7).

The results of the Multivariate Regression Trees (MRT) analysis showed that the differences in environmental temperature in the house during the three seasons could classify the bacteria into three groups (**Figure 5A**). Random forest regression models of temperature and bacterial abundance across seasons explained 84.36% of the total variance, indicating a strong association between cecum bacterial variation and seasonally induced temperature changes. To reveal important bacterial taxa associated with environmental temperature changes in the house as biomarker taxa, the cross-validation error was minimized when 9 important marker taxa were used by 10-fold cross-validation, however, the number of classes against the cross-validation error curve was stable when 9–14 marker taxa were used, i.e., the desired regression results could be obtained, therefore, we selected 12 classes as the biomarker model in the taxa (**Figure 5B**). The top 12 bacterial taxa of the growing rabbit cecum bacteria with temperature, these genera belong to the phyla *Firmicutes*, *Bacteroidetes*, *Cyanobacteria*, *uncultured_bacterium_k_Bacteria*, *Proteobacteria*, and *Actinomycetes*. The relative abundance of cecum *uncultured_bacterium_f_Barnesiellacea*, *dgA-11_gut_group*, and *Subdoligranulum* was positively correlated with ambient temperature and was higher in the summer temperature range The relative abundance of *uncultured_bacterium_f_Atopobiaceae*, *Ruminococcaceae_NK4A214_group*, *uncultured_bacterium_k_Bacteria*, *uncultured_bacterium_f_Eubacteriaceae*, *Blautia*, and *uncultured_bacterium_f_Erysipelotrichaceae* was higher in the spring temperature interval. The *Anaerovorax*, *uncultured_bacterium_f_Clostridiales_vadinBB60_group*, and *uncultured_bacterium_o_Gastranaerophilales* had higher relative abundance in the temperature interval in winter (**Figure 5C**).

To explore the role of rhythmic changes in cecum bacteria, we used PICRUSt2 for functional prediction of cecum bacteria in each season. The biosynthesis potential of 2-Oxocarboxylic acid metabolism, phenylalanine, tyrosine, tryptophan, amino acid, secondary metabolite, and antibiotic biosynthesis was higher at 7:00 am than at the rest of the day during winter NRF feeding, and the intensity of cysteine and methionine metabolism, 2-Oxocarboxylic acid metabolism, was at its lowest level of the day at 11 pm. In winter DF feeding, only the ATP-binding cassette transporter (ABC transporter) was higher at 7:00 pm than at the rest of the day (**Figure 6A** and **Supplementary Figure 8A**). During spring NRF feeding, processes such as carbon metabolism and protein biosynthesis peak at 3:00 am at night. In contrast, starch and sucrose, alanine, aspartate and glutamate, amino acid and nucleotide metabolism, amino acid-tRNA biosynthesis, and the pentose phosphate pathway reach their troughs at this time of day. Starch and sucrose metabolism reached its highest value and Oxidative phosphorylation, glycine, serine and threonine metabolism, and pyruvate metabolism reached their lowest level at 7:00 pm. In the predicted model of cecum bacterial function under DF feeding in spring, gluconeogenesis/glycolysis was lower than the rest of the time at 3 am at night, and biosynthesis of amino acids reached the lowest level at 7:00 am. The peak of the day and the strongest ribosomal activity at 3:00 pm (**Figure 6B** and **Supplementary Figure 8B**).

4 Discussion

Daytime feeding is often used in rabbit production, which is inconsistent with their activity rhythms. We had introduced nighttime feeding in the summer to compare the differences in cecal bacterial composition with daytime feeding regimens (Wang et al., 2021). Now we also examined whether this alteration in cecal bacterial composition caused by feeding regimens was preserved in different seasonal environments.

In this study, the gut bacteria were clearly separated in the three seasons, indicating that there were significant differences in the cecum bacterial structure of growing rabbits under the three seasons. The environmental temperature is vital for the regulation of the animal's thermal balance. In this study, the average temperature difference between summer and spring reached 5°C, and the average temperature difference between spring and winter reached 13°C. *Actinomycetes* have the function of maintaining a stable intestinal bacterial structure in response to intestinal anti-inflammation (Doaa et al., 2016), while *Proteobacteria* can result in reduced intestinal bacteria diversity and induce inflammatory processes, a phylum directly related to irritable bowel syndrome (Pittayanon et al., 2019). Therefore, the lower abundance of *Proteobacteria* and higher abundance of *Actinomycetes* observed in the spring suggest a healthier gastrointestinal environment. This supports the hypothesis that a well-balanced cecum bacteria composition is instrumental in diminishing the incidence of diarrhea and mortality. At the genus level, the relative abundance of *Blautia*, *Marvinbryantia*, and *Tyzzerella-3* was higher in spring than in the other two seasons. *Blautia* has been shown to modulate host health and attenuate metabolic syndrome (Liu et al., 2021). *Marvinbryantia* facilitates fiber breakdown, aids in the digestion of the cecum and replenishes energy (Gao et al., 2022). Related studies have reported that both *Tyzzerella-3* and *Marvinbryantia* are associated with the synthesis of SCFA (Short Chain Fatty Acids), and their elevated abundance implies an increase in the ability to maintain the intestinal barrier (Zhang et al., 2020; Gao et al., 2022). The potential pathogens *Desulfovibrio* and *Alistipes*, the diarrhea causative agent *Escherichia-Shigella* (Nataro and Kaper, 1998), were significantly higher in relative abundance in summer than in the other two seasons. *Desulfovibrio* reduces sulfate to produce H_2S, which poisons intestinal epithelial cells and can cause intestinal sensitivity and leaky gut (Kushkevych et al., 2019). The relative abundance of intestinal *Alistipes* is significantly elevated in patients in stressful environments or suffering from chronic fatigue syndrome (Nagy-Szakal et al., 2017). The winter and summer seasons may raise stress levels due to the effects of unsuitable long-term ambient temperatures, while daytime feeding disturbs daytime rest in rabbits, causing constant stress, and may be an important contributor to elevated *Alistipes* abundance. *Alistipes* produces sulfonolipid, which induce cecal inflammation (Parker et al., 2020). Feeding time determines the circadian rhythm of the serotonin substrate tryptophan, which *Alistipes* hydrolyzes to indole, interfering with serotonin availability (Cussotto et al., 2021). Thus, *Alistipes* may reduce the availability of serotonin, upstream of melatonin synthesis, thereby reducing melatonin production and affecting gut health by influencing the intestinal clearance of ROS. However, the *dgA-11_gut_group* and *uncultured_bacterium_f_Barnesiellacea* involving in amino acid

10.3389/fmicb.2024.1344992

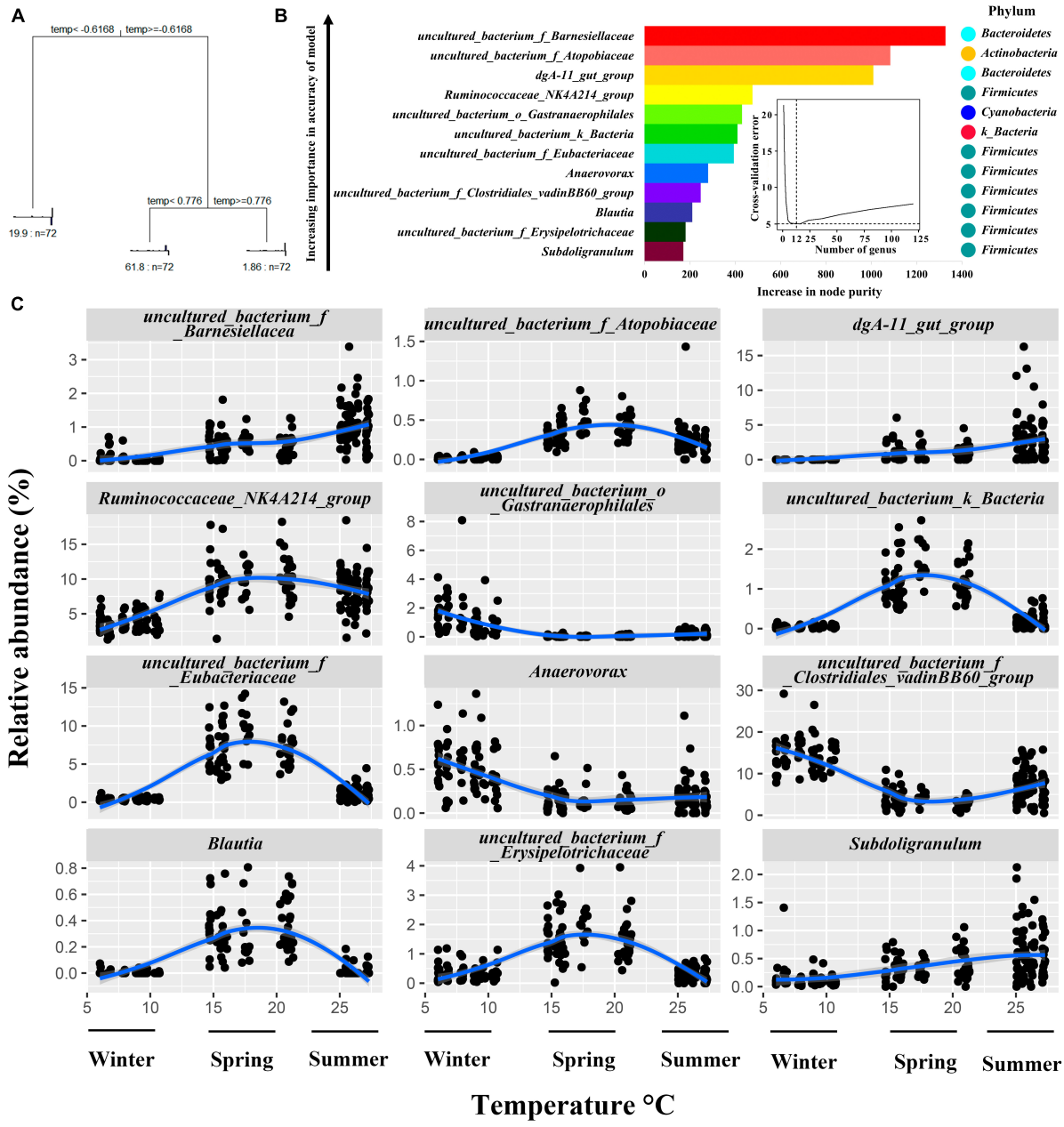

FIGURE 5
Relationship between relative abundance changes of growing rabbits cecum bacteria at the genus level and seasonal environmental temperature changes. **(A)**. MRT Analysis: correlating shed temperature with cecal bacterial genera abundance in growing rabbits. **(B)** Random Forest Analysis: assessing correlations between cecal bacteria genera variability and shed temperature in growing rabbits. **(C)** Top 12 Cecal bacteria Genera: examining temperature-dependent variations in growing rabbits' shed environment.

transport and metabolism, energy production and conversion (Sun et al., 2020), and protection of the intestinal barrier increases significantly during the summer. The abundance of *Bilophila*, which produces acetic, succinic, and sulfides and promotes inflammation, and *Campylobacter*, which produces endotoxins and induces severe diarrhea in animals (Rauws et al., 1988; Natividad et al., 2018). And the number of *Akkermansia*, *Roseburia*, and *Erysipelotrichaceae_UCG-004*, which have protective effects, also increased. Overall, different bacteria show differential sensitivity to such environmental changes. Growing rabbits in open shed growing rabbits have a healthier cecum bacterial community composition in spring than in winter and summer. Environmental factors during the winter and summer seasons may contribute to dysbiosis of cecum bacterial homeostasis and the increased abundance of harmful bacteria, which may be the potential cause of the increased risk of diarrhea.

And how do seasons affect the composition of cecum bacteria in growing rabbits? Of note, recent studies on giant pandas, forest and alpine musk deer point to structural and functional variation in gut bacteria due to seasonal turnover-induced changes in food types (Jiang et al., 2021; Huang et al., 2022). However, the type of feed we have supplied to growing rabbits has been consistent over the past

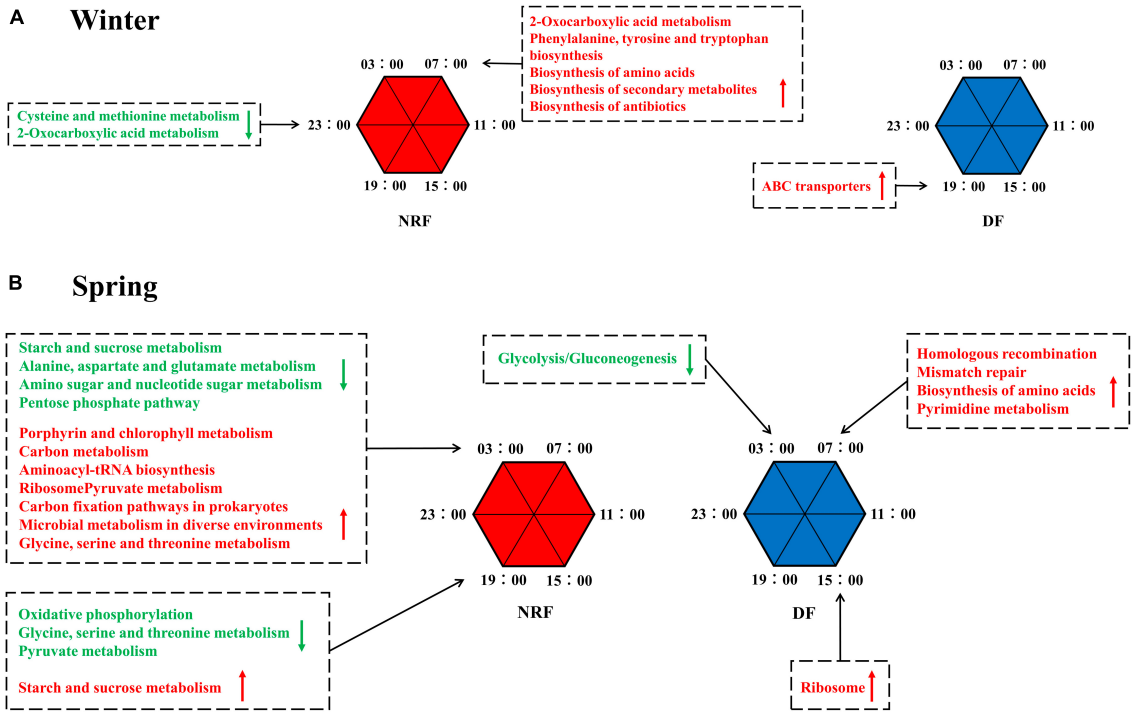

FIGURE 6
PICRUSt predicted the diurnal metabolic potential of cecum bacteria for different feeding regimens in **(A)** winter, in **(B)** spring. Green font means that the metabolic process described at that time point is weaker than the other five time points. The opposite is indicated in red font.

three seasons (**Supplementary Table 1**). Similar to the results of a previous environmental acclimatization trial with Chinese giant salamanders, 10% of the changes in the gut bacterial community were also caused by differences in ambient temperature, even though the type of feed did not change (Zhu et al., 2021). Our study found that the abundance of cecal bacteria varies with the ambient temperature (**Figure 5**). It is possible that variations in ambient temperature and humidity resulting from seasonal changes may impact the growth of foodborne bacteria, despite consistent exposure durations to air (Rowland, 1986).

Temperature changes occurring as a result of seasonal rotation are an important driver of bacterial variation in the cecum of growing rabbits, after a bifactorial analysis of feeding time and seasonal differences as well as MRT analysis. The variance explained by the random forest model of ambient temperature and changes in cecum bacterial abundance of growing rabbits in each season was 84.36%, indicating a strong correlation between cecum bacterial abundance and ambient temperature changes. Season specific dominant genera such as *Blautia*, *dgA-11_gut_group*, and *uncultured_bacterium_f_Barnesiellaceae* are also marker bacteria for environmental temperature changes. Therefore, we consider changes in beneficial and harmful bacterial composition mediated by seasonal temperature changes as potential factors affecting cecum health and risk of diarrheal mortality in growing rabbits.

Regular living and rhythmic time-restricted feeding can maintain the balance of gut bacterial abundance in adult humans and animals, reducing the risk of metabolic disease and intestinal inflammation (Asher and Sassone-Corsi, 2015; Voigt et al., 2016). Our study points out that changes in feeding time affect the composition of gut bacteria. Among the top 10 phyla in terms of relative abundance in winter, the NRF group contained a significantly higher abundance of *Lentisphaerae* than that of DF. The presence of more *Lentisphaerae* in the gut of healthy subjects compared to patients with non-alcoholic fatty liver disease (NAFLD) (Jiang et al., 2015) and juvenile idiopathic arthritis (Tejesvi et al., 2016) suggests a potential protective effect of this phylum on organismal health. The *Cyanobacteria* and *Patescibacteria* phylum were significantly higher in the spring DF group. The relative abundance of these two phyla was increased in the gut of patients with ankylosing spondylitis and accompanied by a more severe organismal inflammatory signal (Liu et al., 2022). Suggesting that the DF feeding may form a potentially pro-inflammatory bacterial structure.

Gut bacterial communities follow natural circadian rhythms, and this diurnal fluctuation alters the schedule of the host's metabolic profile (Thaiss et al., 2014). Ambient light cues can be transformed into enteric group 3 innate lymphoid cell (ILC3) signals, shaping intestinal metabolism (Godinho-Silva et al., 2019) and affecting the expression of antimicrobial peptide circadian rhythms (Brooks et al., 2021). Our results point to changes in feeding time affecting the circadian rhythm of cecum bacteria, which is consistent with previous research on feeding rhythms guiding bacterial oscillations (Thaiss et al., 2014). Summer NRF rabbits had a maximum of 4% cecal rhythm bacteria (Wang et al., 2021) and a minimum of 1.05% bacteria in DF in winter exhibited significant circadian rhythms, much lower than in adult rats (15%) and humans (10%) (Thaiss et al., 2014). The bacterial structure was further influenced by the growth phase of animals (Wang et al., 2019) and greater fluctuations in circadian ambient temperature (Grant et al., 2021). NRF raises the proportion of rhythmic bacteria

in summer and winter. The results predicted by PICRUSt showed that NRF allowed peaks or troughs of bacterial metabolic activity to be enriched at nocturnal rabbit activity time phases. Similar to Palomba's findings, changing the feeding regime affected the relative abundance and function of gut bacteria (Palomba et al., 2021). However, we dynamically recorded circadian rhythms of bacterial abundance and metabolic activity under different feeding regimes in growing rabbits. We consider that the period of the day with the highest bacterial abundance may perform more intense biological functions. Thus, NRF groups that showed more bacterial rhythmicity were enriched for richer digestive, metabolic, and immune pathways at specific time points. It may facilitate the digestion and absorption of food in animals.

The interaction of season and feeding regimens influenced the relative abundance of cecal bacteria. Seasonal and feeding time interactions were significantly associated with changes in the relative abundance of the SCFA production-associated bacterium *Ruminococcus_1*. *Ruminococcus_1* abundance of daytime feeding in spring was not significantly different among the three seasons, whereas switching to nighttime feeding significantly increased *ruminococcus_1* abundance and which was higher in spring than in winter and summer (**Supplementary Figure 7**). Although we have not been able to determine the exact reason for the interaction of season and feeding time on bacteria, the pairing of feeding time and different seasons predicts a diverse combination of nutritional and environmental signals. We can make two speculations. On the one hand, because of the differences in feeding time and seasons, we hypothesize that these bacteria are sensitive to both seasonal light time, light intensity, or ambient temperature, as well as to some of the nutrient signals that synchronize feeding behavior (e.g., bile acids, leptin, and insulin). And on the other hand, combinations with season and feeding time may cause nutrients favored by specific bacteria to be enriched, thus promoting bacterial proliferation.

Compared to DF, the NRF group of potentially conditionally pathogenic bacteria involving *Alistipes*, *uncultured_bacterium_f_Rikenellaceae* (Sun et al., 2017), and *Synergistes* (Borsanelli et al., 2018) showed a consistent downward trend compared to DF, while seasonal differences interfered with the magnitude of the changes. In particular, NRF decreased the most dramatically in potentially pathogenic bacteria during summer, suggesting that summer night-restricted feeding may be more beneficial for cecum health than DF.

Combined with our previous summer results (Wang et al., 2021), it was surprising that different feeding time under different seasonal environmental conditions changed the structure of the cecum microbiome community, but there was no specific pathway of bacterial community change. Alternatively, some more drastic factors during the seasonal change masked the effect of feeding time. How exactly do feeding time conditions and seasonal ambient temperatures interfere with the composition of cecum bacteria? Multiple levels of neural signaling, hormonal transmission, activity rhythms and thermoregulation may be involved in this regulatory process. Animals differ in the intensity of SCN activity in the active phase vs. the resting phase, with differences in output nerve conduction and hormone levels. Feeding time conditions that are contrary to the animal's activity rhythms can interfere with sympathetic nerve activity and alter the circadian oscillations in body temperature (Guo et al., 2021). Long-term training in feeding patterns can stimulate the deviation of feeding phase from the active period (Chung et al., 2017). The disturbance of feeding and activity rhythm will lead to the destruction of intestinal smooth muscle contraction rhythm (Rao et al., 2001) and the accumulation of ROS in the intestinal cavity (Vaccaro et al., 2020), thus disrupting bacterial homeostasis (Ballard and Towarnicki, 2020). The secretion of melatonin is low in the day and high in the night, and the length of sunshine in different seasons also regulates the rhythm of melatonin for a long time (Adamsson et al., 2016). Studies have reported that melatonin targets enzymes that regulate bile acid synthesis (Pathak et al., 2013). The liver is infiltrated by relatively high concentrations of melatonin at night, and food entrainment placed during the day or night will alter the rhythm of bile acid synthesis and circulation patterns. Intestinal bacteria can perform bile acid biotransformation reactions, and the composition and abundance of intestinal bacteria are in turn influenced by bile acids (Cai et al., 2022). The results of the random forest reveal that 10/12 of the genera that vary with seasonal environmental temperature are from the phyla *Bacteroidetes*, *Firmicutes*, and *Actinobacteria*. These phyla are involved in the production of bile salt hydrolases and alter the structure of bile acids (Jia et al., 2021). Therefore, the seasonal variation of bacterial abundance may be attributed to the differences in hormone entrainment caused by the intensity and duration of seasonal rotation light.

The metabolic rate of the animal organism fluctuates with the turnover of seasons (Zhu and Wang, 2015; Nord et al., 2021). Intestinal bacteria are hidden "organs" involved in regulating host metabolism, energy balance and immune response (Muszer et al., 2015; de Vos et al., 2022). The processes of food digestion, absorption, and nutrient conversion consume energy and release heat, which affect the animal's body temperature and energy balance (Chan and Hsieh, 2022). The thermal effect of this food accounts for 5 to 15 percent of the total energy expenditure (Okla et al., 2017) and does not change with ambient temperature (DeRuisseau et al., 2004). The ambient temperatures we recorded suggest that growing rabbits may be subjected to heat and cold stress at midday in summer and at night in winter, respectively (**Supplementary Figure 8**). Compared to spring, the abundance of potentially harmful bacteria increases in summer and winter, the abundance of short-chain fatty acid-producing bacteria decreases, the cecal barrier weakened, and the cecal immune response process activated with greater intensity. The immune response depends on energy availability (Wolowczuk et al., 2008), and changing the timing of feeding under conditions of diurnal ambient temperature fluctuations profoundly interferes with the dynamic processes regulating the balance of energy intake and consumption. Feeding growing rabbits during the hotter daylight days of summer exacerbates the heat stress response by overlapping the food-induced heat production with the thermal environmental periods of the day. Feeding growing rabbits on colder winter nights ensures that the increased energy expenditure due to increased cold-induced thermogenesis is rapidly compensated by caloric intake (Louis-Sylvestre, 1987).

Compared with NRF, DF violates the activity rhythm of growing rabbits, which may disrupt cecal peristaltic rhythm, accumulate ROS, and destroy bacterial balance. It also partially eliminated the regulation of intestinal liver circulation by high concentration of melatonin in dietary stage. Feeding during the day destroys the balance of intestinal microflora, reduces the bacteria

that oscillate in circadian rhythm, reduces the characteristics of circadian metabolism, and weakens the function of bacteria to assist host digestion and absorption of nutrients. In particular, daytime feeding in summer causes heat increment effects of food to be distributed during hotter daytime hours, exacerbating the heat stress response (Guo et al., 2021). Daytime feeding keeps the increased heat of the food away from the colder winter nights and does not alleviate cold stress. Therefore, daytime feeding has an impact on the circadian rhythm and diurnal oscillation of cecal bacteria in growing rabbits. This feeding regimen may disrupt digestive coordination and immune response between the host and cecal bacteria due to energy distribution imbalances in high and low temperature environments, exacerbating cold and heat stress responses, thereby increasing the risk of diarrhea.

5 Conclusion

In this study, we systematically and comprehensively analyzed the effects of season and feeding time on the composition of rabbit cecum bacteria. This study found a significant correlation between cecum bacteria and seasonal ambient temperature. It also showed that nighttime feeding significantly decreased the abundance of the harmful bacteria in summer and winter, increased the number of cecum bacteria genera with diurnal oscillations, and enhanced the circadian rhythm of bacterial metabolic activity. In general, different seasons and feeding time interacted to influence the composition and circadian rhythms of cecum bacteria. We suggest that synchronization of nutrient signals altered by foraging activity with the light-dark cycle is particularly important for the dynamic balance of the cecum bacteria. Seasonal and feeding time "mismatches" can lead to imbalances in gut bacteria, disrupting their balance and natural rhythms, which may increase the risk of diarrhea.

Data availability statement

The datasets presented in this study can be found in online repositories. The names of the repository/repositories and accession number(s) can be accessed at https://www.ncbi.nlm.nih.gov/sra, registration number PRJNA632844.

Ethics statement

The animal studies were approved by the China Agricultural University Laboratory Animal Welfare and Animal Experimental Ethical Committee. The studies were conducted in accordance with the local legislation and institutional requirements. Written informed consent was obtained from the owners for the participation of their animals in this study.

Author contributions

SH: Methodology, Visualization, Formal analysis, Writing – original draft, Writing – review and editing. K-HZ: Methodology, Investigation, Data curation, Writing – review and editing. Q-YJ: Methodology, Formal analysis, Visualization, Writing – review and editing. Q-JW: Conceptualization, Methodology, Formal analysis, Visualization, Writing – review and editing. JH: Data curation, Investigation, Writing – review and editing. J-JL: Data curation, Investigation, Writing – review and editing. YG: Investigation, Conceptualization, Writing – review and editing. PL: Investigation, Conceptualization, Writing – review and editing. Z-YL: Investigation, Conceptualization, Writing – review and editing. DL: Investigation, Data curation, Writing – review and editing. S-XG: Investigation, Data curation, Writing – review and editing. QL: Investigation, Data curation, Writing – review and editing. M-YL: Investigation, Conceptualization, Data curation, Writing – review and editing. ML: Investigation, Conceptualization, Data curation, Writing – review and editing. Z-HW: Conceptualization, Funding acquisition, Supervision, Writing – review and editing.

Funding

The author(s) declare financial support was received for the research, authorship, and/or publication of this article. This work was supported by the National Key Research and Development Program of China (No. 2022YFD1301104) and the earmarked fund for China Agriculture Research System (grant number CARS-43-D-2).

Acknowledgments

We thank to Dr. Feng Zhu of the College of Animal Science and Technology, China Agricultural University, for directing the analysis of bacteria. We also thank to Yu-Pei Hu, Chun-Yan Yao, Wei Fu, and Yu Zhang for their assistance with sample collection.

Conflict of interest

The authors declare that the research was conducted in the absence of any commercial or financial relationships that could be construed as a potential conflict of interest.

Publisher's note

Supplementary material

The Supplementary Material for this article can be found online at: https://www.frontiersin.org/articles/10.3389/fmicb.2024.1344992/full#supplementary-material

References

Adamsson, M., Laike, T., and Morita, T. (2016). Annual variation in daily light exposure and circadian change of melatonin and cortisol concentrations at a northern latitude with large seasonal differences in photoperiod length. *J. Physiol. Anthropol.* 36:6. doi: 10.1186/s40101-016-0103-9

Afonso, A., Jacinto, G., Infante, P., and Engana, T. (2022). Primary school children's sleep habits: Association with socioeconomic factors and physical activity habits. *Children* 9:965. doi: 10.3390/children9070965

Allegretti, J. R., Kassam, Z., Mullish, B. H., Chiang, A., Carrellas, M., Hurtado, J., et al. (2020). Effects of fecal microbiota transplantation with oral capsules in obese patients. *Clin. Gastroenterol. Hepatol.* 18, 855–863. doi: 10.1016/j.cgh.2019.07.006

Arendt, J. (2012). Biological rhythms during residence in polar regions. *Chronobiol. Int.* 29, 379–394. doi: 10.3109/07420528.2012.668997

Asher, G., and Sassone-Corsi, P. (2015). Time for food: The intimate interplay between nutrition, metabolism, and the circadian clock. *Cell* 161, 84–92. doi: 10.1016/j.cell.2015.03.015

Ballard, J. W. O., and Towarnicki, S. G. (2020). Mitochondria, the gut microbiome and ROS. *Cell Signal.* 75:109737. doi: 10.1016/j.cellsig.2020.109737

Bo, T. B., Zhang, X. Y., Wen, J., Deng, K., Qin, X. W., and Wang, D. H. (2019). The microbiota-gut-brain interaction in regulating host metabolic adaptation to cold in male Brandt's voles (*Lasiopodomys brandtii*). *ISME J.* 13, 3037–3053. doi: 10.1038/s41396-019-0492-y

Borsanelli, A. C., Lappin, D. F., Viora, L., Bennett, D., Dutra, I. S., Brandt, B. W., et al. (2018). Microbiomes associated with bovine periodontitis and oral health. *Vet. Microbiol.* 218, 1–6. doi: 10.1016/j.vetmic.2018.03.016

Brooks, J. F. II, Behrendt, C. L., Ruhn, K. A., Lee, S., Raj, P., Takahashi, J. S., et al. (2021). The microbiota coordinates diurnal rhythms in innate immunity with the circadian clock. *Cell* 184, 4154–4167. doi: 10.1016/j.cell.2021.07.001

Cai, J., Sun, L., and Gonzalez, F. J. (2022). Gut microbiota-derived bile acids in intestinal immunity, inflammation, and tumorigenesis. *Cell Host Microbe* 30, 289–300. doi: 10.1016/j.chom.2022.02.004

Chan, P. C., and Hsieh, P. S. (2022). The role and regulatory mechanism of brown adipose tissue activation in diet-induced thermogenesis in health and diseases. *Int. J. Mol. Sci.* 23:9448. doi: 10.3390/ijms23169448

Chevalier, C., Stojanovic, O., Colin, D. J., Suarez-Zamorano, N., Tarallo, V., Veyrat-Durebex, C., et al. (2015). Gut microbiota orchestrates energy homeostasis during cold. *Cell* 163, 1360–1374. doi: 10.1016/j.cell.2015.11.004

Chong, K. C., Chan, E. Y. Y., Lee, T. C., Kwok, K. L., Lau, S. Y. F., Wang, P., et al. (2021). A 21-year retrospective analysis of environmental impacts on paediatric acute gastroenteritis in an affluent setting. *Sci. Total Environ.* 764:142845. doi: 10.1016/j.scitotenv.2020.142845

Chung, S., Lee, E. J., Cha, H. K., Kim, J., Kim, D., Son, G. H., et al. (2017). Cooperative roles of the suprachiasmatic nucleus central clock and the adrenal clock in controlling circadian glucocorticoid rhythm. *Sci. Rep.* 7:46404. doi: 10.1038/srep46404

Claesson, M. J., Jeffery, I. B., Conde, S., Power, S. E., O'Connor, E. M., Cusack, S., et al. (2012). Gut microbiota composition correlates with diet and health in the elderly. *Nature* 488, 178–184. doi: 10.1038/nature11319

Combes, S., Fortun-Lamothe, L., Cauquil, L., and Gidenne, T. (2013). Engineering the rabbit digestive ecosystem to improve digestive health and efficacy. *Animal* 7, 1429–1439. doi: 10.1017/S1751731113001079

Craven, L., Rahman, A., Nair Parvathy, S., Beaton, M., Silverman, J., Qumosani, K., et al. (2020). Allogenic fecal microbiota transplantation in patients with nonalcoholic fatty liver disease improves abnormal small intestinal permeability: A randomized control trial. *Am. J. Gastroenterol.* 115, 1055–1065. doi: 10.14309/ajg.0000000000000661

Cussotto, S., Walsh, J., Golubeva, A. V., Zhdanov, A. V., Strain, C. R., Fouhy, F., et al. (2021). The gut microbiome influences the bioavailability of olanzapine in rats. *EBioMedicine* 66:103307. doi: 10.1016/j.ebiom.2021.103307

de Vos, W. M., Tilg, H., Van Hul, M., and Cani, P. D. (2022). Gut microbiome and health: Mechanistic insights. *Gut* 71, 1020–1032. doi: 10.1136/gutjnl-2021-326789

Deng, L., Xu, H. C., Liu, P., Wu, S. Z., Shi, Y. C., Lv, Y. W., et al. (2020). Prolonged exposure to high humidity and high temperature environment can aggravate influenza virus infection through intestinal flora and Nod/RIP2/NF-kappa B signaling pathway. *Vet. Microbiol.* 251:108896. doi: 10.1016/j.vetmic.2020.108896

DeRuisseau, L. R., Parsons, A. D., and Overton, J. M. (2004). Adaptive thermogenesis is intact in B6 and A/J mice studied at thermoneutrality. *Metabolism* 53, 1417–1423. doi: 10.1016/j.metabol.2004.06.007

Di Biase, A. R., Marasco, G., Ravaioli, F., Dajti, E., Colecchia, L., Righi, B., et al. (2021). Gut microbiota signatures and clinical manifestations in celiac disease children at onset: A pilot study. *J. Gastroen Hepatol.* 36, 446–454. doi: 10.1111/jgh.15183

Doaa, M., Dalia, M., and Ahmed, F. S. (2016). Gut bacterial microbiota in psoriasis: A case control study. *Afr. J. Microbiol. Res.* 10, 1337–1343. doi: 10.5897/ajmr2016.8046

Eggink, H. M., Oosterman, J. E., de Goede, P., de Vries, E. M., Foppen, E., Koehorst, M., et al. (2017). Complex interaction between circadian rhythm and diet on bile acid homeostasis in male rats. *Chronobiol. Int.* 34, 1339–1353. doi: 10.1080/07420528.2017.1363226

Eybpoosh, S., Mostaan, S., Gouya, M. M., Masoumi-Asl, H., Owlia, P., Eshrati, B., et al. (2021). Frequency of five *Escherichia Coli* pathotypes in Iranian adults and children with acute diarrhea. *PLoS One* 16:e0245470. doi: 10.1371/journal.pone.0245470

Gao, Q., Sun, G., Duan, J., Luo, C., Yangji, C., Zhong, R., et al. (2022). Alterations in gut microbiota improve SCFA production and fiber utilization in Tibetan pigs fed alfalfa diet. *Front. Microbiol.* 13:969524. doi: 10.3389/fmicb.2022.969524

Godinho-Silva, C., Domingues, R. G., Rendas, M., Raposo, B., Ribeiro, H., da Silva, J. A., et al. (2019). Light-entrained and brain-tuned circadian circuits regulate ILC3s and gut homeostasis. *Nature* 574, 254–258. doi: 10.1038/s41586-019-1579-3

Grant, C. V., Loman, B. R., Bailey, M. T., and Pyter, L. M. (2021). Manipulations of the gut microbiome alter chemotherapy-induced inflammation and behavioral side effects in female mice. *Brain Behav. Immun,* 95, 401–412. doi: 10.1016/j.bbi.2021.04.014

Guo, Y., Wang, Q. J., Zhang, K. H., Yao, C. Y., Huang, J., Li, Q., et al. (2021). Night-restricted feeding improves locomotor activity rhythm and modulates nutrient utilization to accelerate growth in rabbits. *Faseb J.* 35:e21166. doi: 10.1096/fj.202001265RR

Hanieh, S., Mahanty, S., Gurruwiwi, G., Kearns, T., Dhurrkay, R., Gondarra, V., et al. (2021). Enteric pathogen infection and consequences for child growth in young Aboriginal Australian children: A cross-sectional study. *BMC Infect. Dis.* 21:9. doi: 10.1186/s12879-020-05685-1

Heddes, M., Altaha, B., Niu, Y., Reitmeier, S., Kleigrewe, K., Haller, D., et al. (2022). The intestinal clock drives the microbiome to maintain gastrointestinal homeostasis. *Nat. Commun.* 13:6068. doi: 10.1038/s41467-022-33609-x

Hu, C., Patil, Y., Gong, D., Yu, T., Li, J., Wu, L., et al. (2022). Heat stress-induced dysbiosis of porcine colon microbiota plays a role in intestinal damage: A fecal microbiota profile. *Front. Vet. Sci.* 9:686902. doi: 10.3389/fvets.2022.686902

Huang, G., Wang, L., Li, J., Hou, R., Wang, M., Wang, Z., et al. (2022). Seasonal shift of the gut microbiome synchronizes host peripheral circadian rhythm for physiological adaptation to a low-fat diet in the giant panda. *Cell Rep.* 38:110203. doi: 10.1016/j.celrep.2021.110203

Hughes, M. E., Hogenesch, J. B., and Kornacker, K. (2010). JTK_CYCLE: An efficient nonparametric algorithm for detecting rhythmic components in genome-scale data sets. *J. Biol. Rhythms* 25, 372–380. doi: 10.1177/0748730410379711

Jia, B., Park, D., Chun, B. H., Hahn, Y., and Jeon, C. O. (2021). Diet-related alterations of gut bile salt hydrolases determined using a metagenomic analysis of the human microbiome. *Int. J. Mol. Sci.* 22:3652. doi: 10.3390/ijms22073652

Jiang, F., Gao, H., Qin, W., Song, P., Wang, H., Zhang, J., et al. (2021). Marked seasonal variation in structure and function of gut microbiota in forest and alpine musk deer. *Front. Microbiol.* 12:699797. doi: 10.3389/fmicb.2021.699797

Jiang, W., Wu, N., Wang, X., Chi, Y., Zhang, Y., Qiu, X., et al. (2015). Dysbiosis gut microbiota associated with inflammation and impaired mucosal immune function in intestine of humans with non-alcoholic fatty liver disease. *Sci. Rep.* 5:8096. doi: 10.1038/srep08096

Khakisahneh, S., Zhang, X. Y., Nouri, Z., and Wang, D. H. (2020). Gut microbiota and host thermoregulation in response to ambient temperature fluctuations. *mSystems* 5:e00514-20. doi: 10.1128/mSystems.00514-20

Kushkevych, I., Dordevic, D., and Vitezova, M. (2019). Toxicity of hydrogen sulfide toward sulfate-reducing bacteria Desulfovibrio piger Vib-7. *Arch. Microbiol.* 201, 389–397. doi: 10.1007/s00203-019-01625-z

Leong, K. S. W., Jayasinghe, T. N., Wilson, B. C., Derraik, J. G. B., Albert, B. B., Chiavaroli, V., et al. (2020). Effects of fecal microbiome transfer in adolescents with obesity: The gut bugs randomized controlled trial. *JAMA Netw Open* 3:e2030415. doi: 10.1001/jamanetworkopen.2020.30415

Lepley, T., Schwager, Z., and Khalid, Z. (2022). Identification and management of night eating syndrome in the adolescent and young adult population. *Prim Care Companion CNS Disord.* 24:21r03062. doi: 10.4088/PCC.21r03062

Li, H., Qu, J., Li, T., Wirth, S., Zhang, Y., Zhao, X., et al. (2018). Diet simplification selects for high gut microbial diversity and strong fermenting ability in high-altitude pikas. *Appl. Microbiol. Biotechnol.* 102, 6739–6751. doi: 10.1007/s00253-018-9097-z

Liao, S., Tan, S., Jiang, M., Wen, J., Liu, J., Cao, J., et al. (2022). Temperature determines the shift of thermal neutral zone and influences thermogenic capacity in striped hamsters. *Integr. Zool.* 18, 353–371. doi: 10.1111/1749-4877.12678

Liu, B., Ding, Z., Xiong, J., Heng, X., Wang, H., and Chu, W. (2022). Gut microbiota and inflammatory cytokine changes in patients with ankylosing spondylitis. *Biomed. Res. Int.* 2022:1005111. doi: 10.1155/2022/1005111

Liu, X., Mao, B., Gu, J., Wu, J., Cui, S., Wang, G., et al. (2021). Blautia-a new functional genus with potential probiotic properties? *Gut. Microbes* 13, 1–21. doi: 10.1080/19490976.2021.1875796

Louis-Sylvestre, J. (1987). Adaptation of food ingestion to energy expenditure. *Reprod. Nutr. Dev.* 27, 171–188.

Lu, L., Khan, A., and Walker, W. A. (2009). ADP-ribosylation factors regulate the development of CT signaling in immature human enterocytes. *Am. J. Physiol. Gastrointest. Liver Physiol.* 296, G1221–G1229. doi: 10.1152/ajpgi.90686.2008

Mensah, P., and Tomkins, A. (2003). Household-level technologies to improve the availability and preparation of adequate and safe complementary foods. *Food Nutr. Bull.* 24, 104–125. doi: 10.1177/156482650302400106

Muszer, M., Noszczynska, M., Kasperkiewicz, K., and Skurnik, M. (2015). Human microbiome: When a friend becomes an enemy. *Arch. Immunol. Ther. Exp.* 63, 287–298. doi: 10.1007/s00005-015-0332-3

Nagy-Szakal, D., Williams, B. L., Mishra, N., Che, X., Lee, B., Bateman, L., et al. (2017). Fecal metagenomic profiles in subgroups of patients with myalgic encephalomyelitis/chronic fatigue syndrome. *Microbiome* 5:44. doi: 10.1186/s40168-017-0261-y

Nataro, J. P., and Kaper, J. B. (1998). Diarrheagenic *Escherichia coli*. *Clin. Microbiol. Rev.* 11, 142–201. doi: 10.1128/CMR.11.1.142

Natividad, J. M., Lamas, B., Pham, H. P., Michel, M. L., Rainteau, D., Bridonneau, C., et al. (2018). Bilophila wadsworthia aggravates high fat diet induced metabolic dysfunctions in mice. *Nat. Commun.* 9:2802. doi: 10.1038/s41467-018-05249-7

Nord, A., Metcalfe, N. B., Page, J. L., Huxtable, A., McCafferty, D. J., and Dawson, N. J. (2021). Avian red blood cell mitochondria produce more heat in winter than in autumn. *Faseb J.* 35:e21490. doi: 10.1096/fj.202100107R

Oakley, B. B., Vasconcelos, E. J. R., Diniz, P., Calloway, K. N., Richardson, E., Meinersmann, R. J., et al. (2018). The cecal microbiome of commercial broiler chickens varies significantly by season. *Poult. Sci.* 97, 3635–3644. doi: 10.3382/ps/pey214

Okla, M., Kim, J., Koehler, K., and Chung, S. (2017). Dietary factors promoting brown and beige fat development and thermogenesis. *Adv. Nutr.* 8, 473–483. doi: 10.3945/an.116.014332

Palomba, A., Tanca, A., Abbondio, M., Sau, R., Serra, M., Marongiu, F., et al. (2021). Time-restricted feeding induces Lactobacillus- and Akkermansia-specific functional changes in the rat fecal microbiota. *NPJ Biofilms Microbiomes* 7:85. doi: 10.1038/s41522-021-00256-x

Parker, B. J., Wearsch, P. A., Veloo, A. C. M., and Rodriguez-Palacios, A. (2020). The genus alistipes: Gut bacteria with emerging implications to inflammation, cancer, and mental health. *Front. Immunol.* 11:906. doi: 10.3389/fimmu.2020.00906

Pathak, P., Li, T., and Chiang, J. Y. (2013). Retinoic acid-related orphan receptor alpha regulates diurnal rhythm and fasting induction of sterol 12alpha-hydroxylase in bile acid synthesis. *J. Biol. Chem.* 288, 37154–37165. doi: 10.1074/jbc.M113.485987

Pittayanon, R., Lau, J. T., Yuan, Y., Leontiadis, G. I., Tse, F., Surette, M., et al. (2019). Gut microbiota in patients with irritable bowel syndrome-A systematic review. *Gastroenterology* 157, 97–108. doi: 10.1053/j.gastro.2019.03.049

Rahman, S. U., Wang, X., and Yu, L. (2018). Observations on biotic parameters of angora rabbit breed under controlled conditions in different housing systems. *Vet. World* 11, 88–92. doi: 10.14202/vetworld.2018.88-92

Rao, S. S., Sadeghi, P., Beaty, J., Kavlock, R., and Ackerson, K. (2001). Ambulatory 24-h colonic manometry in healthy humans. *Am. J. Physiol. Gastrointest. Liver Physiol.* 280, G629–G639. doi: 10.1152/ajpgi.2001.280.4.G629

Rauws, E. A., Langenberg, W., Houthoff, H. J., Zanen, H. C., and Tytgat, G. N. (1988). Campylobacter pyloridis-associated chronic active antral gastritis. A prospective study of its prevalence and the effects of antibacterial and antiulcer treatment. *Gastroenterology* 94, 33–40.

Robert, S., Matte, J. J., and Girard, C. L. (1991). Effect of feeding regimen on behavior of growing-finishing pigs supplemented or not supplemented with folic acid. *J. Anim. Sci.* 69, 4428–4436. doi: 10.2527/1991.69114428x

Rowland, M. G. (1986). The Gambia and Bangladesh: The seasons and diarrhoea. *Dialogue Diarrhoea* 26:3.

Schanbacher, B. D., and Crouse, J. D. (1980). Growth and performance of growing-finishing lambs exposed to long or short photoperiods. *J. Anim. Sci.* 51, 943–948. doi: 10.2527/jas1980.514943x

Scheer, F. A., Pirovano, C., Van Someren, E. J., and Buijs, R. M. (2005). Environmental light and suprachiasmatic nucleus interact in the regulation of body temperature. *Neuroscience* 132, 465–477. doi: 10.1016/j.neuroscience.2004.12.012

Sun, T., Liu, S., Zhou, Y., Yao, Z., Zhang, D., Cao, S., et al. (2017). Evolutionary biologic changes of gut microbiota in an 'adenoma-carcinoma sequence' mouse colorectal cancer model induced by 1, 2-Dimethylhydrazine. *Oncotarget* 8, 444–457. doi: 10.18632/oncotarget.13443

Sun, X., Shen, J., Liu, C., Li, S., Peng, Y., Chen, C., et al. (2020). L-Arginine and N-carbamoylglutamic acid supplementation enhance young rabbit growth and immunity by regulating intestinal microbial community. *Asian Australas J. Anim. Sci.* 33, 166–176. doi: 10.5713/ajas.18.0984

Talbot, J., Hahn, P., Kroehling, L., Nguyen, H., Li, D., and Littman, D. R. (2020). Feeding-dependent VIP neuron-ILC3 circuit regulates the intestinal barrier. *Nature* 579, 575–580. doi: 10.1038/s41586-020-2039-9

Tejesvi, M. V., Arvonen, M., Kangas, S. M., Keskitalo, P. L., Pirttila, A. M., Karttunen, T. J., et al. (2016). Faecal microbiome in new-onset juvenile idiopathic arthritis. *Eur. J. Clin. Microbiol. Infect. Dis.* 35, 363–370. doi: 10.1007/s10096-015-2548-x

Thaiss, C. A., Zeevi, D., Levy, M., Zilberman-Schapira, G., Suez, J., Tengeler, A. C., et al. (2014). Transkingdom control of microbiota diurnal oscillations promotes metabolic homeostasis. *Cell* 159, 514–529. doi: 10.1016/j.cell.2014.09.048

Uibel, D., Sharma, R., Piontkowski, D., Sheffield, P. E., and Clougherty, J. E. (2022). Association of ambient extreme heat with pediatric morbidity: A scoping review. *Int. J. Biometeorol.* 66, 1683–1698. doi: 10.1007/s00484-022-02310-5

Vaccaro, A., Kaplan Dor, Y., Nambara, K., Pollina, E. A., Lin, C., Greenberg, M. E., et al. (2020). Sleep loss can cause death through accumulation of reactive oxygen species in the gut. *Cell* 181, 1307–1328. doi: 10.1016/j.cell.2020.04.049

Voigt, R. M., Forsyth, C. B., Green, S. J., Engen, P. A., and Keshavarzian, A. (2016). Circadian rhythm and the gut microbiome. *Int. Rev. Neurobiol.* 131, 193–205. doi: 10.1016/bs.irn.2016.07.002

Voigt, R. M., Forsyth, C. B., Green, S. J., Mutlu, E., Engen, P., Vitaterna, M. H., et al. (2014). Circadian disorganization alters intestinal microbiota. *PLoS One* 9:e97500. doi: 10.1371/journal.pone.0097500

Wang, Q., Fu, W., Guo, Y., Tang, Y., Du, H., Wang, M., et al. (2019). Drinking Warm Water Improves Growth Performance and Optimizes the Gut Microbiota in Early Postweaning Rabbits during Winter. *Animals* 9:346. doi: 10.3390/ani9060346

Wang, Q. J., Guo, Y., Zhang, K. H., Zhang, L., Geng, S. X., Shan, C. H., et al. (2021). Night-restricted feeding improves gut health by synchronizing microbe-driven serotonin rhythm and eating activity-driven body temperature oscillations in growing rabbits. *Front. Cell Infect. Microbiol.* 11:771088. doi: 10.3389/fcimb.2021.771088

Watanabe, M., Houten, S. M., Mataki, C., Christoffolete, M. A., Kim, B. W., Sato, H., et al. (2006). Bile acids induce energy expenditure by promoting intracellular thyroid hormone activation. *Nature* 439, 484–489. doi: 10.1038/nature04330

Wei, L., Yue, F., Xing, L., Wu, S., Shi, Y., Li, J., et al. (2020). Constant light exposure alters gut microbiota and promotes the progression of steatohepatitis in high fat diet rats. *Front. Microbiol.* 11:1975. doi: 10.3389/fmicb.2020.01975

Wen, H., Yin, X., Yuan, Z., Wang, X., and Su, S. (2018). Comparative analysis of gut microbial communities in children under 5 years old with diarrhea. *J. Microbiol. Biotechnol.* 28, 652–662. doi: 10.4014/jmb.1711.11065

Windeyer, M. C., Leslie, K. E., Godden, S. M., Hodgins, D. C., Lissemore, K. D., and LeBlanc, S. J. (2014). Factors associated with morbidity, mortality, and growth of dairy heifer calves up to 3 months of age. *Prev. Vet. Med.* 113, 231–240. doi: 10.1016/j.prevetmed.2013.10.019

Wolowczuk, I., Verwaerde, C., Viltart, O., Delanoye, A., Delacre, M., Pot, B., et al. (2008). Feeding our immune system: Impact on metabolism. *Clin. Dev. Immunol.* 2008:639803. doi: 10.1155/2008/639803

Wu, G., Tang, W., He, Y., Hu, J., Gong, S., He, Z., et al. (2018). Light exposure influences the diurnal oscillation of gut microbiota in mice. *Biochem. Biophys. Res. Commun.* 501, 16–23. doi: 10.1016/j.bbrc.2018.04.095

Xia, B., Wu, W., Fang, W., Wen, X., Xie, J., and Zhang, H. (2022). Heat stress-induced mucosal barrier dysfunction is potentially associated with gut microbiota dysbiosis in pigs. *Anim. Nutr.* 8, 289–299. doi: 10.1016/j.aninu.2021.05.012

Yoo, J. Y., Groer, M., Dutra, S. V. O., Sarkar, A., and McSkimming, D. I. (2020). Gut microbiota and immune system interactions. microorganisms. *Microorganisms* 8:1587. doi: 10.3390/microorganisms8122046

Zhang, X. Y., Chen, J., Yi, K., Peng, L., Xie, J., Gou, X., et al. (2020). Phlorizin ameliorates obesity-associated endotoxemia and insulin resistance in high-fat diet-fed mice by targeting the gut microbiota and intestinal barrier integrity. *Gut Microbes* 12, 1–18. doi: 10.1080/19490976.2020.1842990

Zhu, L., Zhu, W., Zhao, T., Chen, H., Zhao, C., Xu, L., et al. (2021). Environmental temperatures affect the gastrointestinal microbes of the Chinese giant salamander. *Front. Microbiol.* 12:543767. doi: 10.3389/fmicb.2021.543767

Zhu, W. L., and Wang, Z. K. (2015). Seasonal changes in body mass, serum leptin levels and hypothalamic neuropeptide gene expression in male Eothenomys olitor. *Comp. Biochem. Physiol. A Mol. Integr. Physiol.* 184, 83–89. doi: 10.1016/j.cbpa.2015.02.011

Zhuang, J., Zhou, T., Bai, S., Zhao, B., Wu, X., and Chen, Y. (2022). Effects of restricted feeding on growth performance, intestinal immunity, and skeletal muscle development in new zealand rabbits. *Animals* 12:160. doi: 10.3390/ani12020160

frontiers | Frontiers in Microbiology

TYPE Original Research
PUBLISHED 07 March 2024
DOI 10.3389/fmicb.2023.1271835

OPEN ACCESS

EDITED BY
Ren-You Gan,
Agency for Science, Technology and Research, Singapore

REVIEWED BY
Beihui He,
Zhejiang Chinese Medical University, China
Connie W. Woo,
The University of Hong Kong, Hong Kong SAR, China

*CORRESPONDENCE
Lei Xiao
✉ 13956999018@126.com
Jiatao Liu
✉ liujiatao@ahmu.edu.cn

†These authors have contributed equally to this work

RECEIVED 13 August 2023
ACCEPTED 11 October 2023
PUBLISHED 07 March 2024

CITATION
Zhu M, Cheng Y, Tang Y, Li S, Rao P, Zhang G, Xiao L and Liu J (2024) Nanoparticles alleviate non-alcoholic steatohepatitis via ER stress sensor-mediated intestinal barrier damage and gut dysbiosis.
Front. Microbiol. 14:1271835.
doi: 10.3389/fmicb.2023.1271835

Nanoparticles alleviate non-alcoholic steatohepatitis via ER stress sensor-mediated intestinal barrier damage and gut dysbiosis

Manman Zhu[1†], Yong Cheng[2†], Yue Tang[2], Shuojiao Li[3], Peng Rao[2], Guiyang Zhang[4], Lei Xiao[1*] and Jiatao Liu[1*]

[1]Department of Pharmacy, The First Affiliated Hospital of Anhui Medical University, Hefei, Anhui, China, [2]School of Pharmacy, Anhui Medical University, Hefei, Anhui, China, [3]Department of Pharmacy, Anhui University of Chinese Medicine, Hefei, Anhui, China, [4]Department of Pharmacology, School of Basic Medical Sciences, Anhui Medical University, Hefei, Anhui, China

Introduction: The gut microbiota plays an important role in the development of non-alcoholic steatohepatitis (NASH), but the underlying mechanism is unclear. It has been found that the transcription factor XBP1s plays an important role in regulating inflammation and lipid metabolism and maintaining the integrity of intestinal barrier. However, whether XBP1s modulates the development of NASH by regulating the integrity of the intestinal barrier and altering the composition of the gut microbiota remains unknown.

Methods: Mice fed with a fat-, fructose-, cholesterol-rich (FFC) diet for 24 weeks successfully established the NASH model, as demonstrated by significant hepatic steatosis, inflammation, hepatocyte injury and fibrosis. The profile of gut microbiota dynamically changed with the different stages of NAFLD via 16S rDNA sequencing the feces from mice fed with FFC diet for 0, 12, or 24 weeks or NASH mice treated with siRNA-loaded folic acid-modified TPGS (hereafter named FT@XBP1).

Results: NASH mice had significantly higher abundance of Firmicutes, Blautia and Bacteroides, and lower abundance of Bifidobacterium and GCA-900066575. FT@XBP1 supplementation had a significantly attenuated effect on FFC diet-induced weight gain, hepatic fat accumulation, dyslipidemia, inflammatory cytokines, ER stress and fibrosis. In particularly, FT@XBP1 modulates the composition of the intestinal flora; for example, NASH mice demonstrated higher abundance of Blautia and Bacteroides, and lower abundance of Actinobacteriota, Muribaculaceae and Bifidobacterium, which were partially restored by FT@XBP1 treatment. Mechanistically, FT@XBP1 increased the expression of ZO-1 in the intestine and had the potential to restore intestinal barrier integrity and improve antimicrobial defense to alleviate enterogenic endotoxemia and activation of inflammatory signaling pathways.

Discussion: Regulation of the key transcription factor XBP1s can partially restore the intestinal microbiota structure, maintain the integrity of intestinal mucosal barrier, and prevent the progression of NASH, providing new evidence for treating NASH.

KEYWORDS

non-alcoholic steatohepatitis, endoplasmic reticulum stress, X-box binding protein 1, gut microbiota, lipopolysaccharide

Background

The incidence of non-alcoholic fatty liver disease (NAFLD) is increasing year by year, with a global prevalence of ~25.24%, and it has become an important public health problem worldwide (Friedman et al., 2018; Younossi et al., 2018). NAFLD consists of a series of liver diseases, including non-alcoholic simple fatty liver (NAFL), non-alcoholic steatohepatitis (NASH) and NASH-associated cirrhosis. Approximately 25% of patients with NAFL can progress to NASH, which in turn may further develop into fibrosis, cirrhosis, and ultimately hepatocellular carcinoma (Huang et al., 2021). However, the precise mechanism of NAFL progression to NASH is still not fully understood, and there are no effective therapeutic interventions in the clinic. Therefore, in-depth study of the molecular mechanism of NAFL progression to NASH and an exploration of potential therapeutic targets are of great theoretical and practical value.

In recent years, the role of intestinal flora in the development of NAFL/NASH has received more and more attention. Early studies have found that intestinal flora can release some harmful substances to promote the progression of NAFL to NASH. For example, Gram-negative bacteria in humans can release lipopolysaccharide (LPS), which activates Kupffer cells and exacerbates inflammation in the liver (Seki et al., 2001). Clinical studies have found a significant positive correlation between endotoxemia and the severity of pathological lesions in NAFL, suggesting that LPS may play a crucial role in the transformation of NAFL into NASH (Vespasiani-Gentilucci et al., 2018). Carvalho et al. (2012) found that inhibition of bacterial overgrowth significantly reduced circulating levels of LPS and improved the insulin signaling and glucose tolerance in high-fat-fed mice, suggesting that increased intestinal permeability and elevated circulating LPS levels may play an indispensable role in the progression of NAFLD. In addition, one study found that the abundance of intestinal ethanol-producing bacteria was significantly increased in patients with NASH, along with significantly higher plasma levels of ethanol (Zhu et al., 2013). *In vivo* and *in vitro* studies have also found that endogenous ethanol not only promotes hepatocellular triglyceride deposition, but also promotes the production of reactive oxygen radicals and liver inflammation (Wang et al., 2021). The above results suggest that gut flora plays a vital role in the onset and progression of NAFL/NASH, but there are still several gaps that need to be filled in terms of their mode of action and specific mechanisms.

A variety of stresses can lead to the accumulation of unfolded and/or misfolded proteins in the endoplasmic reticulum (ER), resulting in ER stress and the subsequently unfolded protein reaction (UPR). The intestinal epithelium, a key barrier and messenger between the intestinal environment and the host immune system, which is susceptible to ER stress (Adolph et al., 2012). Chen et al. (2022) found that the induction of ER stress in intestinal mucosal epithelial cells could significantly disrupt the intestinal mucosal barrier and result in enteric dysbacteriosis, whereas the inhibition of ER stress with Pterostilbene significantly reversed these effects. A Winnie mouse model carrying a single missense mutation in the Muc2 mucin gene, characterized by reduced goblet cells and mucus layer and increased epithelial permeability, provided important evidence to elucidate that protein misfolding and the associated UPR pathway in secretory cells are major trigger for colitis (Das et al., 2013). Importantly, Winnie mice responded to anti-inflammatory agents, namely, glucocorticoids (Das et al., 2013), and azathioprine (Oancea et al., 2017), accompanied by a reduction in ER stress and UPR activation, a restoration of mature mucin production, and an amelioration of goblet cells failure. Notably, ER stress in the intestinal epithelium induces a series of adverse cellular responses, including redox imbalance, impaired autophagic fluxes, uncontrolled inflammatory responses, and apoptosis, which are involved in intestinal barrier dysfunction pathogenesis (Holczer et al., 2015; Vancamelbeke and Vermeire, 2017). However, some researchers have also found that the alleviation of protein misfolding and restoration of ER homeostasis can also lead to intestinal inflammation (Yoshida et al., 2001). Although both secretory cell ER stress and intestinal flora dysbiosis can trigger inflammation, the relative roles of the two in driving colitis progression remain unclear. Therefore, therapeutic strategies targeting ER stress may hold promise for mitigating intestinal barrier damage and intestinal disease. Nanoparticles can be synthesized in short steps and often use polyethylene glycol (PEG) and polycaprolactone (PCL) FDA approved polymers with high drug loading capacities to resolve these challenges, and effective in specific drug delivery, diagnosis and therapy in clinic (Verma et al., 2021).

IRE1α-XBP1 is the most evolutionarily conserved UPR pathway, and is closely associated with insulin resistance, dyslipidemia, hepatic steatosis and NAFLD inflammation (Lebeaupin et al., 2018). Following ER stress, the ribonucleic acid endonuclease activity of IRE1α cleaves X-box binding protein 1 (XBP1) mRNA to produce splice osomal XBP1 mRNAs (XBP1s). XBP1s is a key transcription factor of ER stress and is involved in the constitutive maintenance of core genes of ER in almost all cells as well as in the transcriptional regulation of a range of condition-specific target genes (Shaffer et al., 2004; Acosta-Alvear et al., 2007). It is also required for the development and survival of the secretory cell. Kaser et al. (2008) found that XBP1 deficiency in intestinal epithelial cells (IECs) resulted in spontaneous enterocolitis and increased the susceptibility of IECs to colitis secondary to Paneth cell defects and IBD inducers. Interestingly, single-nucleotide polymorphisms (SNPs) in the XBP1 gene significantly increase the risk of Crohn's disease and ulcerative colitis (Kaser et al., 2008). Most importantly, Chen et al. (2021) reported that HFD-fed mice exhibited a reduced abundance of tight junction proteins (claudin-1, claudin-4, ZO-1, and occludin), while ER stress-associated proteins, such as p-IRE1α and BIP, was activated, and Gly supplementation improved the intestinal mucosal barrier in HFD-induced obese mice by reducing ER stress-related signaling. Therefore, the present study was proposed to explore whether XBP1s plays an important role in preventing the progression of NASH via modulating dysbacteriosis and intestinal barrier damage by constructing *Xbp1* siRNA loading TPGS nano-micelles (hereafter named FT@XBP1).

Materials and methods

Fabrication of FT@XBP1

Rhodamine B (RhB) isothiocyanate DMSO solution (0.266 mg/ml, 500 μl) was added into the enzyme-free aqueous solutions

[1.65 mg/ml, 1 ml, *n*(RhB): *n*(si*Xbp1*) = 2:1] and shaken well. $NaHCO_3$ solution (0.1 ml, 1 M) was added to adjust pH to 8.0 and then stirred overnight. The mixture was dialyzed using deionized H_2O (9 L, three times) and lyophilized to obtain rhodamine B modified si*Xbp1* (RhB-si*Xbp1*), and then stored at −20°C. Folic acid modified TPGS delivery system was prepared as follow. Briefly, the functional FA-TPGS@RhB-si*Xbp1* (herein called FT@XBP1) was synthesized by the cross-linking effect [*n*(FA-TPGS): *n*(si*Xbp1*) = 5:1]. Firstly, FA-TPGS (2.24 mg), RhB-si*Xbp1* and 1,4 dioxane (2 ml) were added into a penicillin bottle. The samples were sonicated for 20 min and then assembled using a micro flow meter (7 ml ultrapure water, 2 h with rapid stirring). And the nanocarriers were dialyzed after assembly. Then products were lyophilized for 24 h and stored at −20°C for further characterizations.

Mice and treatment

Male C57BL/6J mice at the age of 5–7 weeks (18–20 g) were purchased from Gem Pharmatech corporation (Jiangsu, China). Mice were housed in specific pathogen-free (SPF) conditions and fed with either a chow diet (CD) or a fat-, fructose- and cholesterol-rich (FFC) diet for 12 and 24 weeks, respectively, to obtain the different stages of NAFLD, and NASH mouse models were established by feeding an FFC diet for 24 weeks. Mice in the NASH group were randomly divided into two subgroups (FFC and FFC + FT@XBP1) at the beginning of 20 weeks. FT@XBP1 were injected intravenously (2 OD, 0.05 nM, 100 μl) every 3 days for 4 weeks through the tail vein.

The body weights were recorded once a week during the experiments. Fecal samples were collected from each mouse at week of 0, 12 and 24, and quickly placed into liquid nitrogen for 15 min and then stored at −80°C for 16S rDNA gene sequencing. Mice were euthanized after 12 and 24 weeks of FFC diet feeding, and blood samples were collected by removing the eyeballs, allowing them to clot for at least 30 min at room temperature, and then centrifuged at 3,000 rpm for 10 min to collect the serum, which was stored at −80°C. The liver was isolated and weighed; then, a portion of the liver tissue was fixed in a 4% paraformaldehyde solution and embedded in paraffin. Another portion of the liver tissue was quickly frozen in liquid nitrogen and embedded in an optimal cutting temperature compound (OCT) for frozen sectioning; the remaining liver tissue was cut into small pieces and quickly placed into liquid nitrogen for further RNA and protein extraction. The epididymal fat tissue was isolated, weighed, and stored at −80°C. The colon tissue was isolated and washed with physiological saline to remove intestinal contents before being quickly placed in liquid nitrogen and stored at −80°C in a freezer. All animal experiments were performed according to procedures approved by the Laboratory Animal Ethics Committee of Anhui Medical University (LLSC20221000).

Liver and intestinal tissue histopathological analysis

Mouse hepatic and intestinal samples were fixed in 4% paraformaldehyde for 12 h and embedded in paraffin. Paraffin-embedded samples were sectioned and then subjected to hematoxylin and eosin (H&E) staining for the assessment of liver and intestine histopathology. Liver tissue embedded in OCT was sectioned into 8–10 μm slices, and Oil Red O staining was performed on these frozen sections to measure the hepatic steatosis according to manufacturer's protocol. Masson's trichrome staining and Sirius red staining were performed on 4-μm paraffin-embedded liver tissue sections to evaluate the degree of liver fibrosis according to the manufacturer's protocol. The NAFLD activity score (NAS) was calculated from the grade of steatosis, inflammation, and ballooning as previously reported (Kleiner et al., 2005). In brief, steatosis was quantified as 0 (<5%), 1 (5%−33%), 2 (>33%−66%), and 3 (>66%) based on the percentage of liver cells containing fat droplets. Lobular inflammation was scored as 0 (no foci), 1 (<2 foci), 2 (2–4 foci), and 3 (>4 foci) according to the inflammation foci per 200×field. Ballooning degeneration was scored as 0 (none), 1 (few), and 2 (many) according to the number of ballooning hepatocytes. The hepatic and intestinal histology and NAS were independently evaluated by two pathologists who were blinded to the sample groups.

Immunofluorescence assay

Fresh liver tissues were embedded with OCT and cut into 8–10 μm slices. Then, the sections were washed with PBS and blocked with 2% BSA at room temperature for 1 h. The sections were then co-incubated with various primary antibodies at 4°C overnight in a light-avoiding environment. Subsequently, the sections were washed using PBS twice and co-incubated with a secondary antibody at 37°C in dark for 1 h. Finally, the sections were washed with PBS and stained with DAPI for 5 min, and photographed using a fluorescence microscope.

Detection of serum lipopolysaccharide and serum parameters

Serum alanine aminotransferase (ALT), aspartic transaminase (AST) and total cholesterol (TC) in mice were detected using an Mindray BS-430 automated biochemical analyzer. The levels of hepatic triglycerides (TG) and lipopolysaccharides (LPSs) in mouse serum were detected according to the manufacturer's instructions (ADS Bio, Jiangsu, China).

16s rDNA gene sequencing and bioinformatics analysis

The feces of seven mice were collected for 16S rDNA sequencing analysis. In brief, total bacterial genomic DNAs were

extracted using MagPure Soil DNA LQ Kit (D6356-02, Magen) following the manufacturer's instructions. The quality of the DNA was verified using agarose gel and quantified using a NanoDrop 2000c spectrophotometer (Thermo Fisher Scientific, United States), and then stored at −20°C until further processing. The diluted DNA was used as template for the PCR amplification of bacterial 16S rDNA genes with the bar-coded primers and Takara Ex Taq (Takara). The primers were 343F (5′-TACGGRAGGCAGCAG-3′) and 798R (5′-AGGGTATCTAATCCT-3′). Amplicon quality was visualized using gel electrophoresis, purified with AMPure XP beads (Agencourt), and amplified for another round of PCR. After being purified with the AMPure XP beads again, the final amplicon was quantified using a Qubit dsDNA assay kit. Equal amounts of purified amplicon were pooled for subsequent sequencing.

The 16S amplicon sequencing and analysis were conducted by OE biotech Co., Ltd. (Shanghai, China). In brief, raw sequencing data were in FASTQ format. Paired-end reads were then preprocessed using Cut adapt software to detect and cut off the adapter. After trimming, paired-end reads were filtered for low-quality sequences, denoised, merged and detect, and the chimera reads were cut off using DADA2 with the default parameters of QIIME2 (2020.11). Finally, the software outputs the representative reads and the ASV abundance table. The representative read of each ASV was selected using QIIME2 package. All representative reads were annotated and blasted against Silva database Version 138 (or Unite; 16S rDNA) using q2-feature-classifier with the default parameters.

RNA extraction and qRT-PCR

Approximately 1 ml of TRIzol (R0016, Beyotime Biotechnology, China) was added to 20 mg of liver tissues and the total RNA was extracted according to the manufacturer's instructions. The total RNA (1 μg) was reverse-transcribed into cDNA using PrimeScript™RT Master Mix (RR036Q, Takara Bio, Japan). Real-time quantitative polymerase chain reaction (qRT-PCR) was performed using the QuantiNova SYBR Green PCR Kit (208054, QIAGEN, Germany) and the Light Cycler® 96 Real-time PCR System (Roche, Switzerland), with the β-actin gene as the internal control. The relative expression of each gene mRNA was calculated using the $2^{-\Delta\Delta Ct}$ method. Detailed information about the sequence used in this study is listed in Supplementary Table 1.

Western blot analysis

Approximately 5 mg of liver or colon tissues were weighed and added to 1 ml of protein lysis buffer containing 1% PMSF (protease inhibitor). The mixture was homogenized using a mini-bead beater for 30 s, then lysed on ice for 30 min, and centrifugated at 12,000 rpm for 10 min to collect the protein supernatant. The total protein concentration was quantified using the BCA assay kit before mixing with 5× loading buffer and boiling for 10 min in boiling water. Next, 20–30 μg of each sample was added to the polyacrylamide gel and subjected to electrophoresis, then, the protein was transferred onto PVDF membrane, and blocked with 5% milk at room temperature for 2 h. After washing, the membrane was incubated overnight with corresponding primary antibodies (such as β-actin, XBP1s, Col1αI, and α-SMA, all diluted at 1:1,000). Finally, the membrane was incubated with secondary antibodies and visualized using an Image Quant LAS 4000 chemiluminescence imaging system. Detailed information about the antibodies used in this study is shown in Supplementary Table 2.

Statistical analysis

Statistical analysis was performed using SPSS 16.0, and all data were presented as mean ± standard deviation (SD). The differences between two groups were analyzed using Two-tailed Student's *t*-test, while one-way ANOVA was used to analyze the differences between more than two groups. Bonferroni's *post hoc* test was used for multiple comparisons. A *p*-value of <0.05 was considered to be statistically significant.

Results

FFC diet induces NASH and liver injury

To mimic the different stages of NAFLD in humans, the two groups of mice were fed a high-fat, high-sugar, and high-cholesterol (FFC) diet for 12 and 24 weeks, while control mice were given a chow diet (CD) feeding (Figure 1A). Body weights were measured once a week, as shown in Figures 1B–D. After 12 weeks of FFC dietary (hereafter named FFC_12W) intervention, the body weight increased significantly compared with that in the CD group, and FFC dieting for 24 weeks (hereafter named FFC_24W) increased the body weight even more ($p < 0.05$). Consistently, we found that the liver weight and the liver index (liver-to-weight ratio) were significantly higher than those in the CD diet group (Figures 1E, F, $p < 0.01$). The levels of serum alanine aminotransferase (ALT) and aspartate aminotransferase (AST) were also significantly elevated in mice fed with FFC diet (Figure 1G). HE staining showed that FFC_24W significantly increased fatty deposits in the liver, as demonstrated by macrovesicular and microvesicular steatosis, massive infiltration of inflammatory cells in the central venous area and the confluent area, and significant ballooning and fat accumulation in some hepatocytes compared with mice fed with CD or FFC_12W (Figure 1H). Oil red O staining further confirmed that hepatic steatosis was significantly increased in FFC-fed mice compared to the CD group and was more pronounced in the FFC_24W group (Figure 1I). In addition, we found that the contents of hepatic TG (Figure 1J) in the FFC_24W group were significantly higher than in the FFC_12W group (217.20 ± 7.94 nmol/mg vs. 77.30 ± 8.13 nmol/mg, $p < 0.001$). Similarly, the levels of serum triglyceride (Figure 1K), hepatic steatosis (Figure 1L) and significant ballooning (Figure 1M) in some hepatocytes compared with mice fed with CD or FFC_12W were also significantly increased in the FFC_24W group. Taken together, our results suggested that mice fed with FFC dieting for 24 weeks caused significant fat deposition and injury in the liver.

10.3389/fmicb.2023.1271835

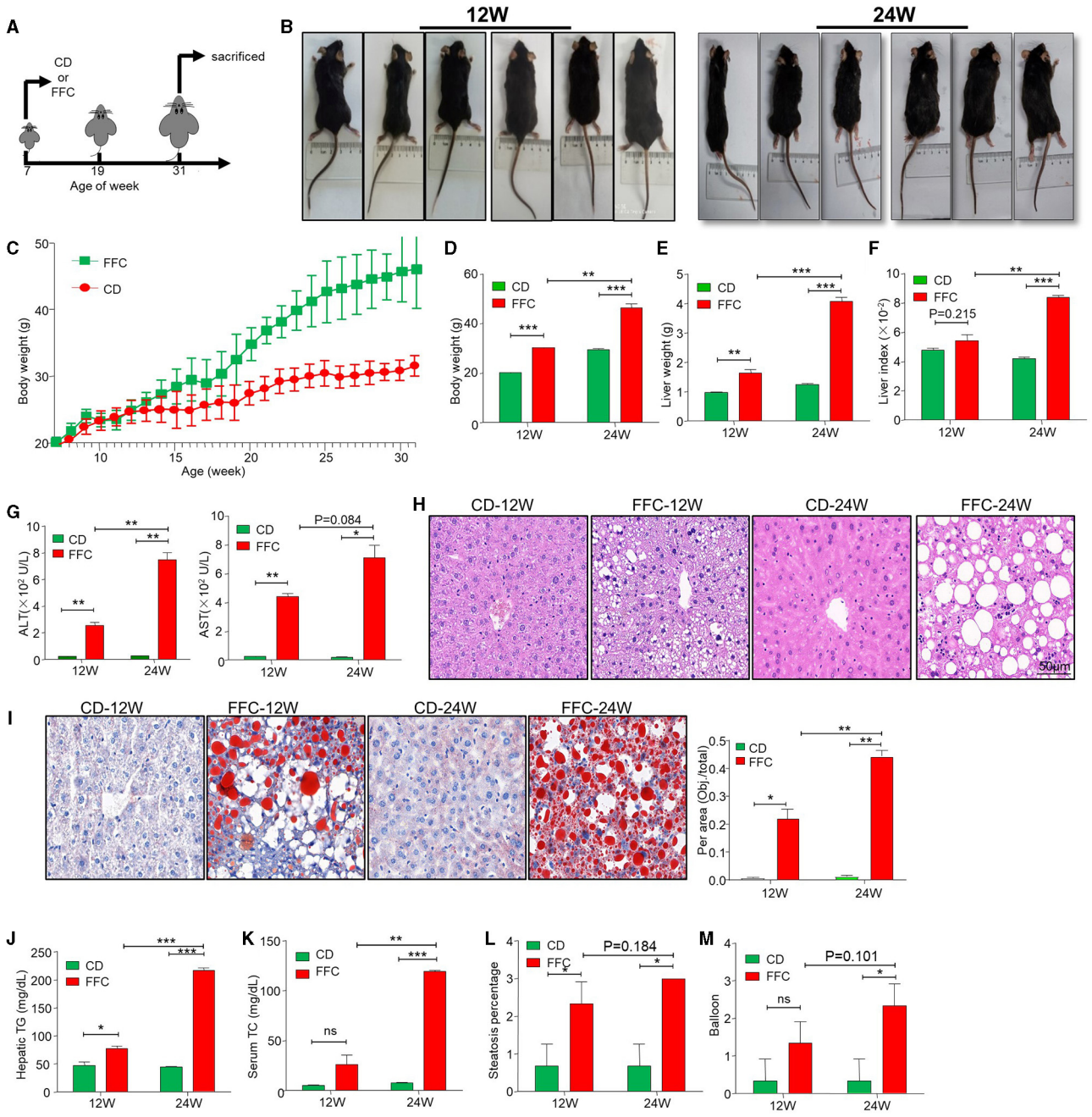

FIGURE 1
FFC diet exacerbated hepatic steatosis and NASH formation in mice. **(A)** Schematic overview of experimental design. **(B)** Images of mice fed with chow- (CD) or FFC- diet for 12 or 24 weeks. Body weights (C, D), liver weights **(E)**, liver/body weight ratio **(F)**, and serum ALT and AST **(G)** in mice fed on CD or FFC diet for 12 and 24 weeks. **(H)** H&E, **(I)** Oil red O staining and **(J)** hepatic TG of hepatic tissues from CD or FFC diet-fed mice for 12 and 24 weeks (scale bar = 50 μm). FFC diet increased the levels of serum TC **(K)**, and aggravated hepatic steatosis **(L)** and balloon **(M)**. Data are presented as the means ± SD (error bar) with $*p < 0.05$, $**p < 0.01$, and $***p < 0.001$ vs. indicated group ($n = 3$ for each group). FFC, high-fat high-cholesterol; ALT, alanine transaminase; AST, aspartate transaminase; CD, chow diet.

FFC diet promotes liver fibrosis in NASH model

Fibrosis is a serious consequence secondary to chronic liver injury and inflammation and a risk factor for NASH worsening. In the current study, we used Sirius and Masson staining to determine hepatic collagen deposition and found that collagen deposition and pericellular fibrosis were significantly increased in the livers of FFC-fed mice compared to CD-fed mice (Figure 2A). The NAS was used for the quantitative evaluation of unique NASH-identified lesions. We found that both the FFC_24W and FFC_12W groups significantly increased NAS as demonstrated by hepatic steatosis, pronounced inflammation and balloon-like degeneration compared to mice in the CD group, and mice in the FFC_24W

group showed higher NAS than those in the FFC_12W group (Figure 2B). The fibrosis index was calculated based on Masson and Sirius staining, and as shown in Figure 2C, FFC dietary feeding significantly elevated the fibrosis index compared to CD group, but there was no significant difference between the FFC_24W and FFC_12W groups ($p = 0.23$). Immuno-blotting assays also revealed that the expression levels of both α-SMA and Col1αI protein (two fibrosis-related markers) in liver tissues were significantly higher in FFC_24W group compared with the normal group (Figure 2D).

Inflammatory cell infiltration is another major pathological feature of NAFLD (Sacks et al., 2018). Therefore, we examined the mRNA levels of several inflammatory factors using liver tissues via qRT-PCR assay, and we found that FFC feeding significantly increased the expression of pro-inflammatory factors *Il-6*, *Il-1β*, and *Tnf-α* and anti-inflammation factor *Il-10* compared to mice fed with CD diet (Figure 2E). Moreover, the levels of pro-inflammatory factors (*Il-6, Il-1β*, and *Tnf-α*) were significantly elevated in FFC_24W group compared with the FFC_12W group, but there was no significant difference between the FFC_24W and FFC_12W groups in *Il-10* levels. Similarly, FFC_24W significantly increased lobular inflammation compared to mice in FFC_12W and CD groups (Figure 2F). These results suggested that FFC dietary feeding increased hepatic inflammation and promoted the progression of NASH.

Dynamic changes of intestinal flora in the development of NASH

To assess the dynamic changes of the gut microbiota at different stages of NAFLD, next-generation sequencing was used to sequence the V3–V4 region of the gut bacterial 16S rDNA gene in the feces of mice from the CD, FFC_12W and FFC_24W groups ($n = 7$). A total of 1,680,254 raw reads were obtained, and 131,178 high-quality reads were filtered, from which a total of 5,070 ASVs were clustered based on 99% sequence similarity. Observed-species rarefaction curves (Supplementary Figure 1A) and Shannon (Supplementary Figure 1B) showed that the current sequencing depth was sufficient to capture the majority of gut microbiota in all samples.

As shown in Supplementary Figure 2A, the ACE index, and Chao1 index were higher in the FFC diet group compared to the CD group, and the Shannon index and Chao1 index were higher in the FFC_24W group compared to the FFC_12W group, but there was no statistical significance among the three groups. According to the relative abundance of ASVs, principal component analysis (PCA) and Bray-Curtis distance-based principal coordinate analysis (PCoA) were used to analyze the structural changes in the gut microbiota in each sample, and the results showed that the gut microbiota of FFC-fed mice were completely separated from that of CD-fed mice (Supplementary Figures 2B, C). In addition, PCoA (Supplementary Figure 2C) similarity analyses showed that there was a complete separation of the gut flora in the FFC_12W and FFC_24W group ($p = 0.001$).

The relative abundance of gut microbiota in each group at the phylum and genus levels is shown in Figures 3A, B. At the phylum level, the gut microbiota composition in the FFC_12W group, compared to the CD group, significantly changed, as shown by a higher abundance of Campilobacterota (0.07% vs. 1.09%, $p < 0.001$), Desulfobacterota (4.1% vs. 8.4%, $p < 0.001$), Actinobacteria (3.6% vs. 13.1%, $p < 0.01$) and Firmicutes (17.2% vs. 47.9%, $p < 0.01$), whereas the abundance of Bacteroidota (76.1% vs. 25.7%, $p < 0.001$) significantly decreased (Figure 3C). The relative abundance of Firmicutes (25.7% vs. 56.1%, $p > 0.05$) was further upregulated in the FFC_24W group compared to the FFC_12W group, whereas the relative abundance of Actinobacteriota (13.1% vs. 2.1%, $p < 0.001$) was significantly lowered (Figure 3C).

At the genus level, the relative abundance of Blautia (0.05% vs. 6.68%, $p < 0.001$), Faecalibaculum (0.61% vs. 8.33%, $p < 0.001$), Bacteroides (0.60% vs. 7.37%, $p < 0.001$), Bifidobacterium (2.94% vs. 8.53%, $p < 0.05$), Parabacteroides (0.07% vs. 3.83%, $p < 0.001$), Erysipelatoclostridium (0.02% vs. 3.81%, $p < 0.01$), GCA-900066575 (0.10% vs. 4.66%, $p < 0.01$), and Rikenellaceae_RC9_gut_group (0.26% vs. 3.86%, $p < 0.001$) in the FFC_12W group was significantly increased compared to CD group; however, the relative abundance of Muribaculaceae was significantly reduced (70.89% vs. 9.34%, $p < 0.001$; Figure 3D). In comparison with the FFC_12W group, the abundance of Blautia (6.68% vs. 6.88%, $p > 0.05$) and Bacteroides (7.37% vs. 7.61%, $p > 0.05$) was further increased, while the relative abundance of two intestinal probiotics, Bifidobacterium (8.53% vs. 0.63%, $p < 0.001$) and GCA-900066575 (4.66% vs. 1.63%, $p < 0.01$) was significantly decreased (Figure 3D).

FT@XBP1 ameliorated hepatic injury and fibrosis in the NASH model

ER stress plays an important role in the occurrence and development of NAFLD (Zheng et al., 2022). We used an immunoblotting assay to detect the expression of ER stress-related proteins, and found that GRP78, ATF6, PERK, IRE1a, and XBP1s in the liver of FFC diet-fed mice were significantly upregulated compared to CD mice (Figure 4A, Supplementary Figure 3A). Moreover, ER stress downstream transcription factor XBP1s was more significantly upregulated than other ER stress markers (Figure 4A). In addition, we used immunofluorescence (IF) assays to confirm that XBP1s expression was higher in the liver tissue of FFC diet-induced NASH mice than in CD-fed mice (Supplementary Figure 3B), suggesting that XBP1s may play an important role in NASH progression. Thus, we used folate to modify TPGS and incorporate *Xbp1* siRNA (FT@XBP1) to knock down XBP1 and found that the body weight (Figure 4B), and liver weight (Figure 4C) were significantly reduced in mice treated with FT@XBP1 than in mice fed with FFC diet, but had no effect on the liver-to-weight ratio compared with FFC diet-fed mice (Figure 4D). We also found that FT@XBP1 could significantly reduce epididymal fat in mice fed with FFC diet (Figure 4E). Moreover, FFC diet-induced mice had high levels of serum alanine transaminase (ALT) and aspartate aminotransferase (AST) in comparison with mice with the CD diet, and FT@XBP1 treatment remarkably decreased ALT and AST levels (Figure 4F). Most interestingly, we also found that FT@XBP1 treatment could

10.3389/fmicb.2023.1271835

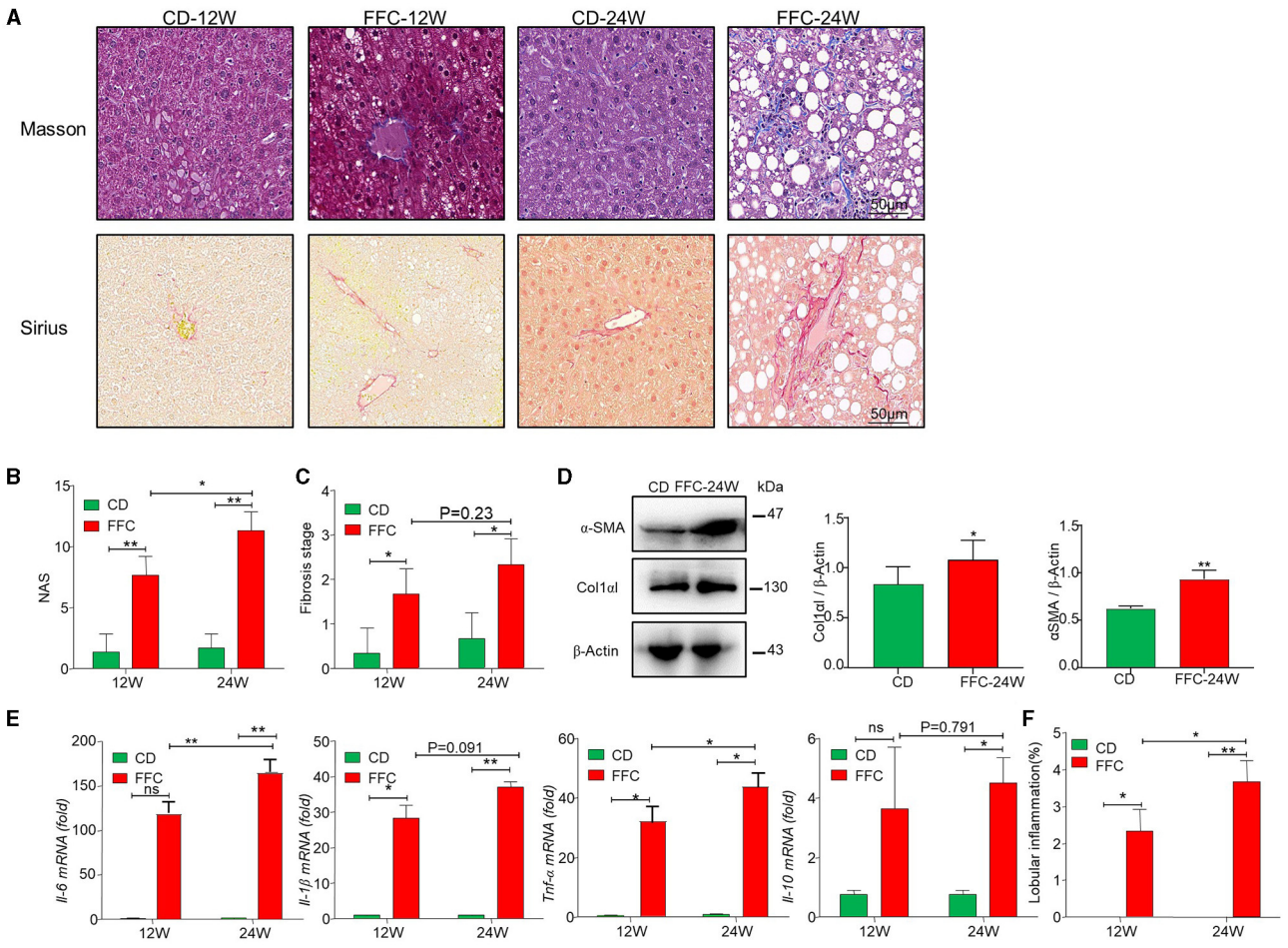

FIGURE 2
FFC diet promoted fibrosis in NASH mice model. **(A)** Representative Masson (upper panel) and Sirius red (lower panel) staining images (scale bar = 50 μm), and NAS **(B)** and fibrosis stages **(C)** of liver tissues from mice in the CD and FFC group ($n = 3$). **(D)** The expression of fibrotic proteins of α-SMA and Col1αI in liver tissues, and semi-quantitatively analyzed the band intensity ($n = 3$). **(E)** Inflammatory factors *Il-6*, *Il-1β*, *Tnf-α*, and *Il-10* in hepatic tissues of FFC fed mice or relative controls were measured using qRT-PCR, and **(F)** the lobular inflammation was calculated ($n = 3$ for each group). Data are presented as the means ± SD (error bar) with $*p < 0.05$ and $**p < 0.01$ vs. indicated group ($n = 3$ for each group). NAS, NAFLD activity score.

significantly reduce FFC diet-induced serum TC and hepatic TG compared to mice fed with FFC diet (Figure 4G).

We also investigated the role of XBP1s on liver injury, lipid accumulation, inflammatory cells infiltration, collagen deposition, and fibrosis using HE staining, Oil red staining, Masson staining, and Sirius staining, respectively. We found that XBP1 deficiency largely attenuated FFC diet-induced liver injury (Figure 4H) and steatohepatitis-related parameters in mice, for example intrahepatic ballooning (Figures 4H–J) and steatosis percentage (Figure 4K), which relieved lipid accumulation and improved liver histology. As previously reported, inflammatory cell infiltration plays a vital role in NASH progression. Interestingly, a decrease in lobular inflammation was also noted in FT@XBP1-treated mice compared to FFC-fed mice (Figure 4L).

As fibrosis is a vital risk for the deterioration of NASH to hepatic fibrosis, we determined collagen deposition in the liver tissues using Masson and picrosirius red staining (Figure 4M). Most interestingly, we found that the livers of mice fed with FFC diet demonstrated an evident increase in collagen deposition and pericellular fibrosis compared with CD-fed mice, and these pathological changes were significantly reversed by treating mice with FT@XBP1 (Figure 4M). The NAS score was used for the quantitative evaluation of unique NASH-identified lesions. As shown in Figure 4N, the FFC diet significantly increased NAS compared with the CD diet, whereas FT@XBP1 treatment remarkably reduced NAS compared with mice fed with an FFC diet, as demonstrated by evidently reduced lobular inflammation and steatosis. Consistently, we found that FT@XBP1 treatment remarkably reduced the fibrosis stage (Figure 4O). In addition, indicators of hepatic fibrosis, such as Col1αI and α-SMA, were significantly reduced in mice treated with FT@XBP1 compared with FFC diet-fed mice, as demonstrated by Western blot analysis (Figure 4P). These results suggested that FT@XBP1 treatment ameliorated steatohepatitis and fibrosis in response to FFC diet-induced NASH.

10.3389/fmicb.2023.1271835

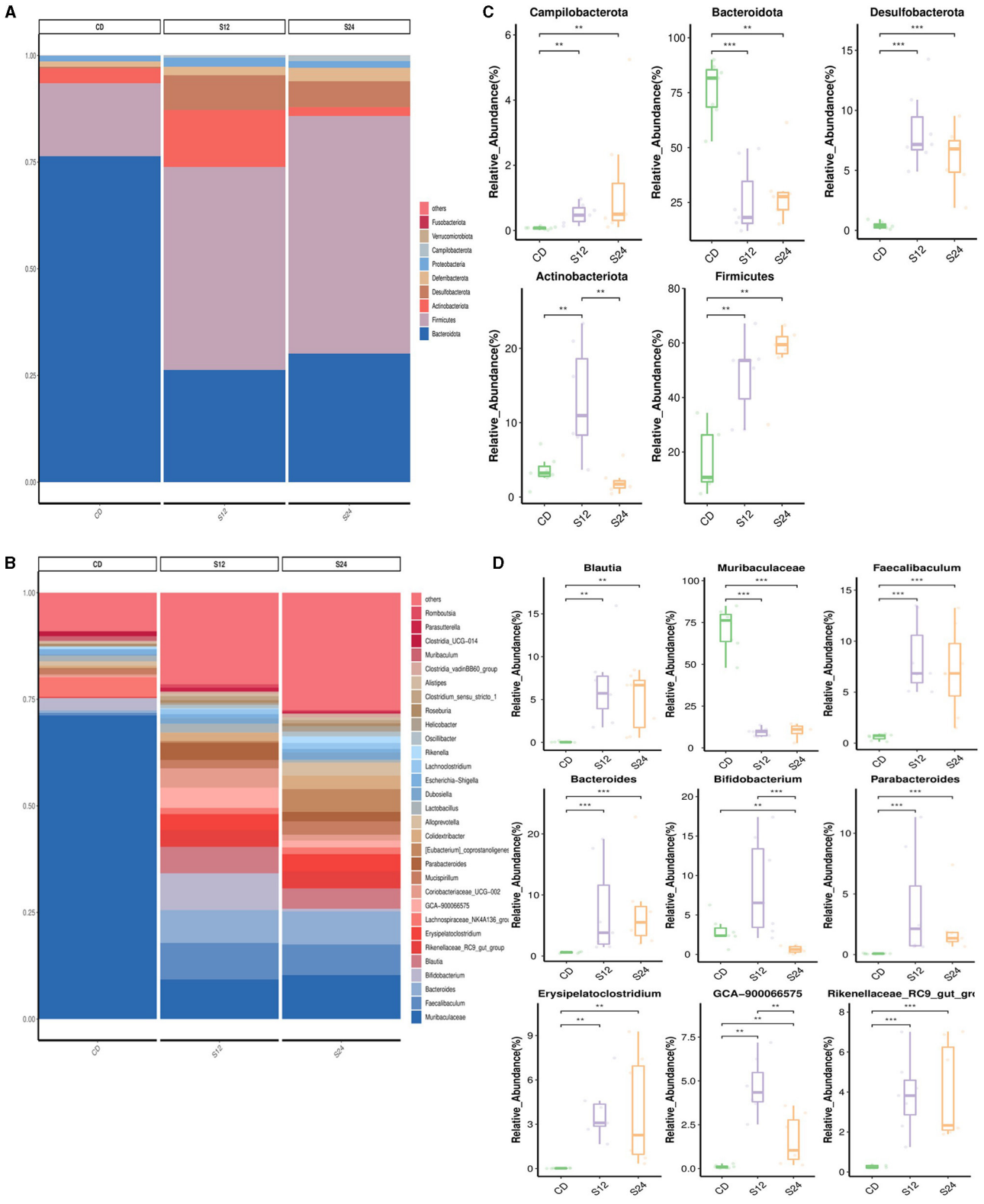

FIGURE 3
The alteration in the gut microbiome associated with FFC diet. Relative abundance of bacterial communities from mice at the different stages of NASH at the phylum **(A)** and genus level **(B)**. Comparison of average abundance of specific gut bacteria from CD diet or FFC-diet for 12 or 24 weeks at the phylum **(C)** and genus level **(D)**. Data are presented as the means ± SD (error bar) with $^{**}p < 0.01$, and $^{***}p < 0.001$ vs. indicated group ($n = 7$).

10.3389/fmicb.2023.1271835

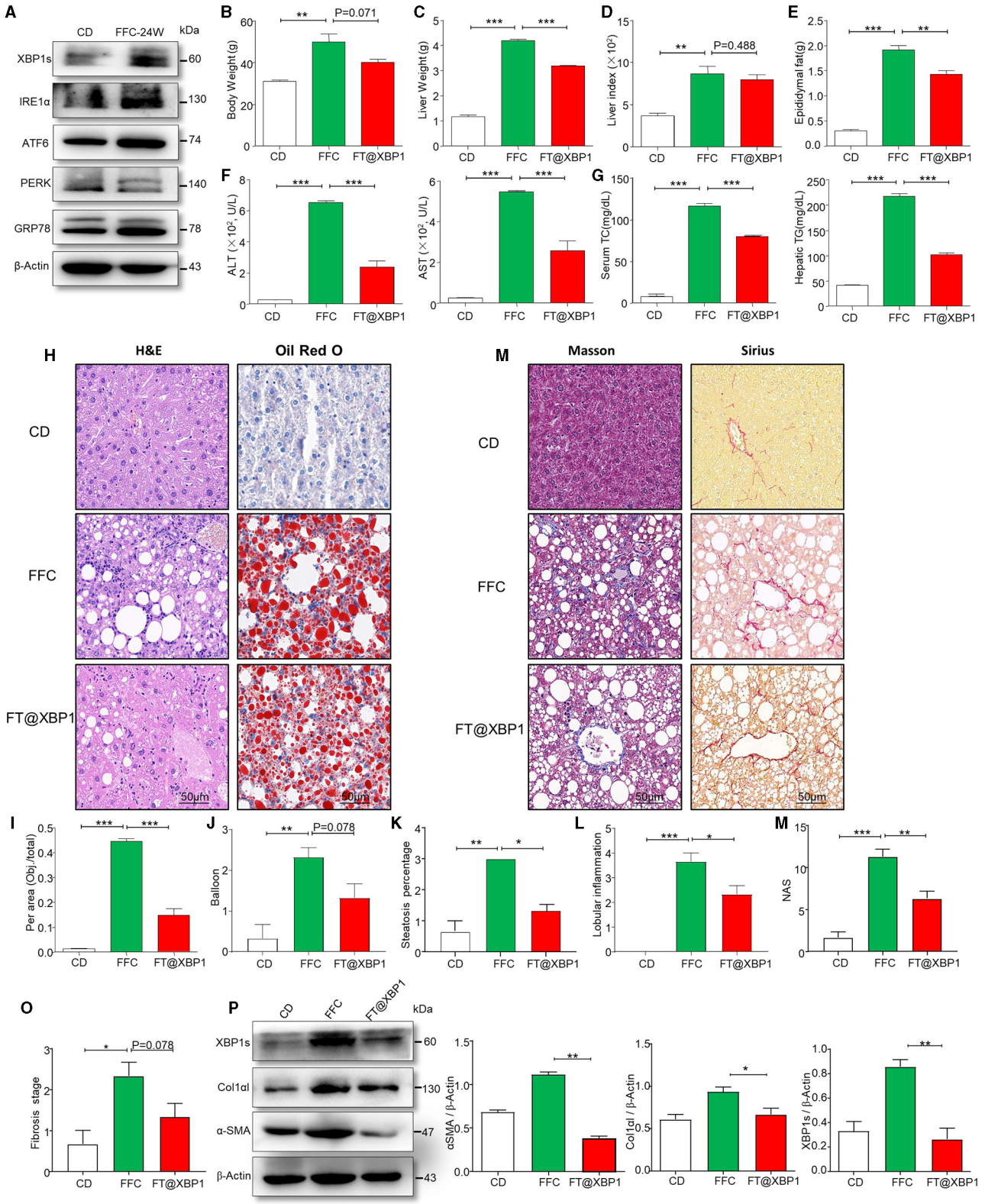

FIGURE 4
FT@XBP1 alleviated liver injury, steatosis and fibrosis in NASH mice. **(A)** Western blot analysis determined the expression of XBP1s, IRE1α, ATF6, PERK, and GRP78 in liver tissues from FFC diet induced NASH mice. **(B)** Body weights, **(C)** liver weights, **(D)** liver/body weight ratio, **(E)** epididymal fat, **(F)** serum ALT and AST, **(G)** and serum TC and hepatic TG in FFC-fed or chow-fed mice, and FFC-fed mice treated with FT@XBP1. **(H)** Representative images of H&E (left panel), Oil red O staining (right panel) in hepatic tissues from mice fed with FFC diet and FFC-fed mice treated with FT@XBP1, and **(I)** semi-quantitative analyzed the staining intensity of Oil red O staining (scale bar = 50 μm). FT@XBP1 treatment alleviated FFC diet induced **(J)** balloon, **(K)** steatosis percentage and **(L)** lobular inflammation. **(M)** Representative images of Masson (left panel), Sirius (right panel) staining in hepatic tissues from mice fed with the FFC diet and FFC-fed mice treated with FT@XBP1 (scale bar = 50 μm). FT@XBP1 treatment decreased **(N)** NAS and **(O)** fibrosis stages, and **(P)** decreased the expression of XBP1s, α-SMA and Col1αI in liver tissues and semi-quantitative analysis of figure **(P)**. Data are presented as the means ± SD (error bar) with $*p < 0.05$, $**p < 0.01$, and $***p < 0.001$ vs. indicated group ($n = 3$ for each group).

10.3389/fmicb.2023.1271835

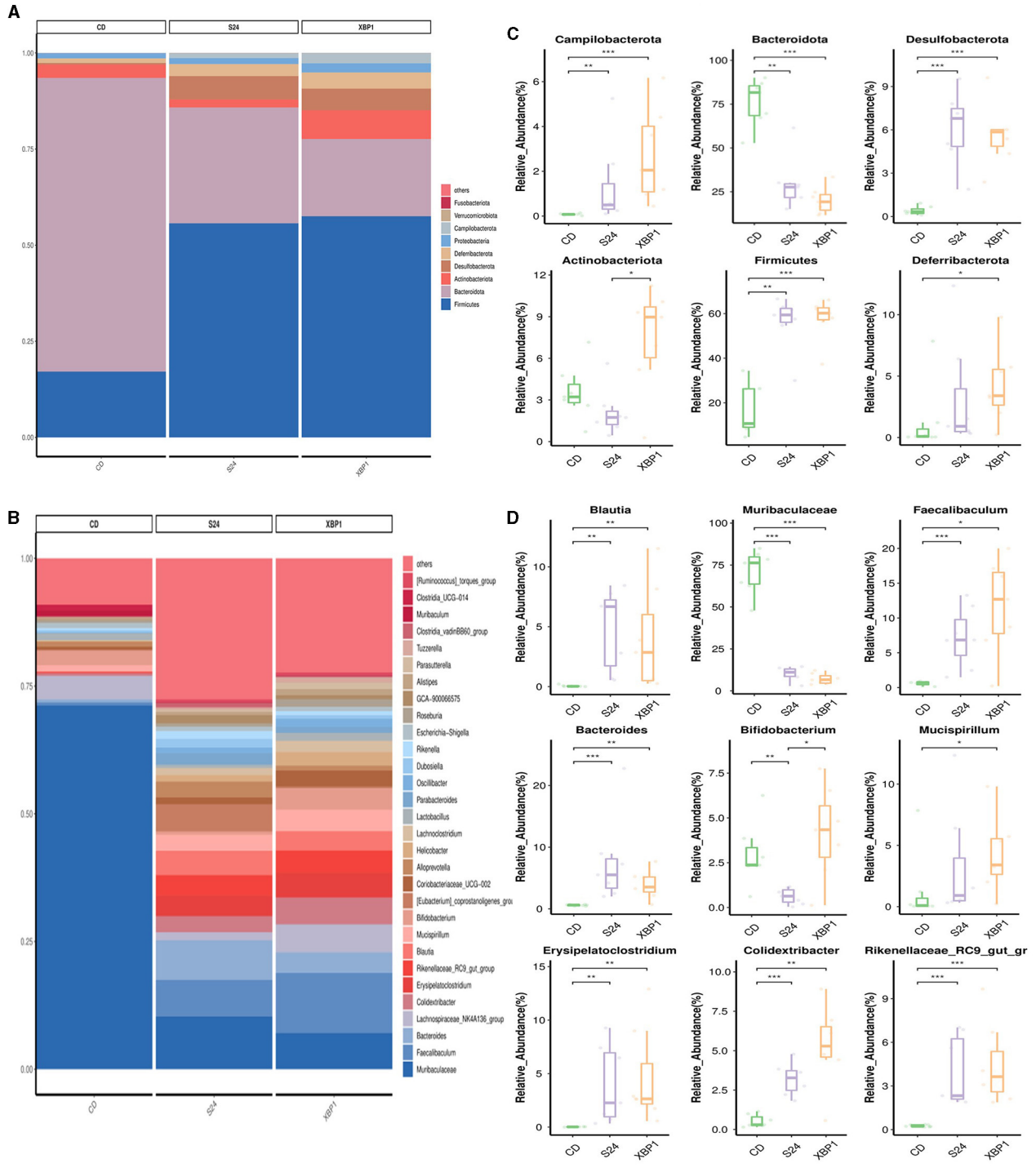

FIGURE 5
FT@XBP1 treatment partially restored the gut microbiome in FFC induced NASH model. Relative abundance of bacterial communities from mice at the phylum **(A)** and genus species level **(B)** in FFC diet fed mice or mice treated with FT@XBP1. Comparison of average abundance of specific gut bacteria from FFC diet fed mice or mice treated with FT@XBP1 at the phylum **(C)** and genus level **(D)**. Data are presented as the means ± SD (error bar) with $*p < 0.05$, $**p < 0.01$, and $***p < 0.001$ vs. indicated group ($n = 7$).

FT@XBP1 partially restored the dysbiosis of the gut microbiota in NASH mice

To explore the effect of FT@XBP1 treatment on the diversity of gut microbiota in NASH mice, the V3–V4 regions of the intestinal bacterial 16S rDNA genes from CD, FFC_24W, and FFC diet in combination with FT@XBP1 (120 mg/kg) treatment were sequenced using the next-generation sequencing. A total of 1,681,217 raw reads were obtained, and 1,303,526 high-quality reads were filtered, of which a total of 4,997

10.3389/fmicb.2023.1271835

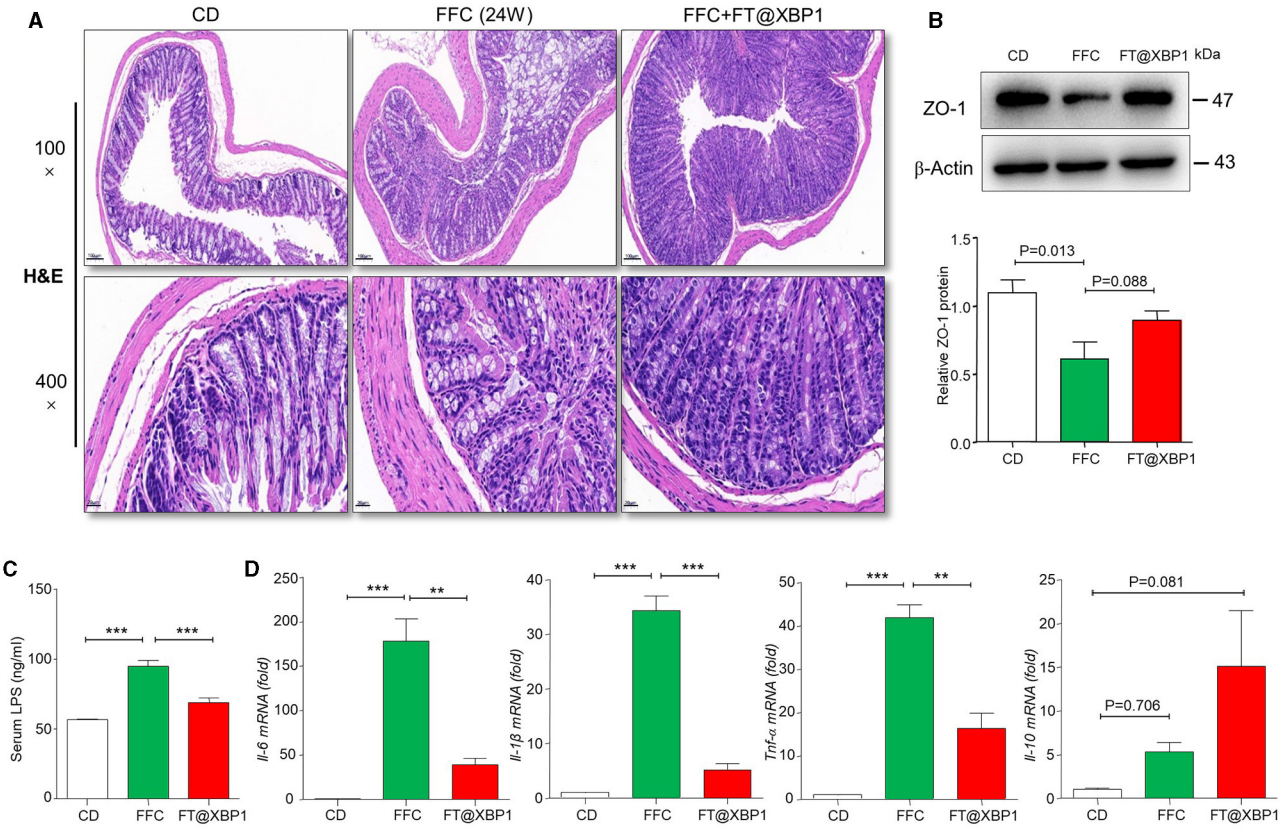

FIGURE 6
FT@XBP1 protected against intestinal barrier disruption and reduced serum LPS and inflammatory cytokines in NASH mice. **(A)** H&E staining of mouse intestinal tissue from CD, FFC and FT@XBP1 treatment group (scale bar = 50/20 μm). **(B)** Western blot analysis the expression of ZO-1 in colon tissues, and semi-quantitative analyzed. **(C)** FT@XBP1 treatment reduced the levels of serum LPS and **(D)** the inflammatory factors *Il-6*, *Il-1β*, *Tnf-α*, and *Il-10* in hepatic tissues in NASH mice. Data are presented as the means ± SD (error bar) with $^{**}p < 0.01$, and $^{***}p < 0.001$ vs. indicated group ($n = 3$ for each group).

differential ASVs were clustered based on 99% sequence similarity. Observed-species rarefaction curves (Supplementary Figure 4A) and Shannon (Supplementary Figure 4B) reached a plateau, indicating that the current sequencing depth was reasonable and sufficient to capture most of the gut microbes in the samples. As shown in Supplementary Figure 5A, the Shannon index and Simpson index were slightly elevated in the FFC_24W and FT@XBP1 treatment groups, while the ACE index and Chao1 index were slightly reduced compared to the chow diet group but did not reach a statistically significant difference. Beta diversity represents the difference in the composition of microbial communities between samples. In the current study, PCA (Supplementary Figure 5B) and PCoA (Supplementary Figure 5C) similarity analyses were used to observe the similarity of the species composition between samples. It was found that the gut microbiota of FFC-fed mice was completely separated from that of CD-fed mice ($p = 0.001$), but the gut microbiota of the FFC-fed mice was not completely separated from the FT@XBP1 treatment group, suggesting that FT@XBP1 treatment could partially restore the composition of the intestinal microbiota in NASH mice.

The relative abundance of intestinal bacteria in each group at the phylum and genus levels is shown in Figures 5A, B. As shown in Figure 5C, at the phylum level, the relative abundance of Campilobacterota (0.07% vs. 1.33%, $p < 0.001$), Desulfobacterota (0.41% vs. 6.12%, $p < 0.001$) and Firmicutes (17.22% vs. 56.12%, $p < 0.01$) in the FFC_24W group was significantly increased compared with the CD group, while the relative abundance of Bacteroidota (76.06% vs. 29.53%, $p < 0.01$) and Actinobacteriota (3.57% vs. 2.09%, $p > 0.05$) was decreased significantly. FT@XBP1 treatment further increased the relative abundance of Campilobacterota (0.07% vs. 2.69%, $p > 0.05$) and Deferribacterota (1.35% vs. 3.21%, $p < 0.05$), but decreased the abundance of Desulfobacterota (6.12% vs. 5.66%, $p > 0.05$) compared to the FFC_24W group. Interestingly, we found that FT@XBP1 treatment significantly reversed FFC feeding induced decreases in Actinobacteriota abundance (2.09% vs. 7.42%, $p < 0.05$).

At the genus level (Figure 5D), FFC diet feeding significantly increased the relative abundance of Blautia (0.05% vs. 4.80%, $p < 0.01$), Faecalibaculum (0.61% vs. 7.20%, $p < 0.001$), Bacteroides (0.60% vs. 7.61%, $p < 0.001$), Erysipelatoclostridium (0.02% vs. 3.96%, $p < 0.01$), Colidextribacter (0.53% vs. 3.19%, $p < 0.001$) and Rikenellaceae_RC9_gut_group (0.26% vs. 3.99%, $p < 0.001$) compared to CD-fed mice, while the relative abundance of Muribaculaceae (70.89% vs. 10.22%, $p < 0.001$) and Bifidobacterium (2.94% vs. 0.63%, $p < 0.01$)

was significantly decreased. FT@XBP1 treatment could further increase the abundance of Faecalibaculum (7.20% vs. 11.65%, $p > 0.05$), Rikenellaceae_RC9_gut_group (3.99% vs. 4.45%, $p > 0.05$) and Colidextribacter (3.19% vs. 5.29%, $p > 0.05$), while decreased the abundance of Muribaculaceae (10.22% vs. 7.09%, $p > 0.05$) compared to the FFC_24W group. More importantly, FT@XBP1 treatment not only effectively reversed the FFC_24W-induced decrease in intestinal probiotic Bifidobacterium (0.63% vs. 4.17%, $p < 0.05$), but also increased the intestinal abundance of Mucispirillum (3.21% vs. 4.25%, $p > 0.05$). These suggest that FT@XBP1 may prevent the progression of NASH by regulating the composition of gut microbiota.

In addition, we obtained functional annotations and relative abundance information of the gut microbiota in each group, and cluster analysis was performed according to the level of functional difference. As shown in Supplementary Figure 6, FFC diet feeding for 24 weeks showed significant activation of glycosaminoglycan degradation, glycosphingolipid biosynthesis-ganglio series, phenylpropanoid biosynthesis, sphingolipid metabolism and various types of N-glycan biosynthesis pathway, whereas FT@XBP1 treatment showed an opposite trend. Furthermore, we found that the apoptosis, ferroptosis and lysosome pathways were activated after 24 weeks of FFC dietary feeding, while FT@XBP1 treatment significantly inhibited the activation of these pathways. These results suggested that FT@XBP1 may play a vital role in the prevention of NASH progression by restoring the dysbiosis of the gut microbiota.

FT@XBP1 ameliorates intestinal barrier dysfunction in NASH

Intestinal mucosal homeostasis plays a vital role in maintaining the normal physiological activities of the organism, and intestinal mucosal barrier damage and increased intestinal epithelial permeability are often accompanied by the progression of NASH (Albillos et al., 2020). Thus, we first stained the mouse colonic mucosa using H&E staining, and found that FFC feeding significantly increased the degree of colonic epithelial barrier disruption (Figure 6A). Furthermore, the apical and crypt areas of colonic tissues showed significant structural disruption and disorganization, with intermediate deletions, while, the integrity of the colon barrier was found to be intact after 4-week intervention with FT@XBP1, which indicated that FT@XBP1 could ameliorate FFC diet-induced Intestinal mucosal barrier disruption (Figure 6A). Subsequently, we used immunoblotting assay to detect the expression level of epithelial tight junction protein 1 (zonula occludens-1, ZO-1), and found that the protein level of ZO-1 was significantly lower in FFC diet group compared with that of the CD diet group (Figure 6B). Furthermore, FT@XBP1 treatment induced a certain recovery of the ZO-1 protein compared with FFC group (Figure 6B), but there was no statistical difference ($p = 0.088$). To further understand the mechanism of FT@XBP1 on FFC-induced NAFLD progression, we examined the plasma endotoxin levels and found that plasma LPS levels were significantly elevated in the FFC dietary group compared with the CD group, whereas FT@XBP1 treatment obviously reversed this effect (Figure 6C). In addition, qRT-PCR assays showed that FT@XBP1 treatment significantly decreased the levels of inflammatory factors *Il-6*, *Il-1β*, and *Tnf-α* (Figure 6D), but the levels of *Il-10* were elevated to some extent compared with FFC diet mice ($p = 0.081$). Therefore, our results suggest that XBP1s plays an important role in maintaining intestinal mucosal homeostasis by regulating the expression of tight junction proteins, which together reduce the penetration of intestinal-sourced endotoxins into the circulation and then alleviate liver inflammation to prevent the progression of NASH.

Discussion

The pathogenesis of NAFLD is complex, and the traditional "two-hit" hypothesis is not sufficient to fully explain the pathogenesis of NASH, especially for non-obese individuals (Wang et al., 2016), because there is evidence that TG is not hepatotoxic in mice with steatohepatitis (Yamaguchi et al., 2007). However, the accumulation of other lipids, such as free fatty acids, diacylglycerol, cholesterol, ceramides, and phospholipids, in the liver can induce ER stress, mitochondrial dysfunction, and oxidative stress, ultimately leading to liver inflammation and fibrosis (Feldstein et al., 2004; Tilg and Moschen, 2010). Recently, some researchers put forward a "multiple parallel hit model" (Tilg and Moschen, 2010; Papatheodoridi and Cholongitas, 2018), with intestinal flora disturbance and the related enterogenic endotoxemia possibly being the key "hit" leading to persistent liver injury and NAFLD progression (Poeta et al., 2017). NAFLD patients are often associated with varying degrees of intestinal flora disturbance and translocation, which manifests as decreased abundance of Bacteroidetes and an increased relative abundance of Firmicutes at the phylum level. Meanwhile, Gram-negative bacteria in the gut are overpopulated, while the abundance of Gram-positive bacteria such as Bifidobacterium and Lactobacillus are decreased significantly, and intestinal bacteria and LPS could translocate into the portal vein system, which results in enterogenic endotoxemia and persistent inflammatory injury in the liver (Zhu et al., 2013; Shen et al., 2017). Schnabl and Brenner (2014) found that mice lacking intestinal flora were resistant to the development of diet-induced liver steatosis; however, replenishing flora via fecal microbiota transplantation (FMT) can promote the development of NAFLD in these mice, and liver steatosis can be improved after application of probiotics and antibiotics. In the current study, we found that FFC diet significantly increased the relative abundance of Firmicutes and decreased the abundance of Bacteroidota compared to mice fed with chow diet at the phylum level. Meanwhile, we found that FFC diet increased the abundance of Blautia and Bacteroides, while the abundance of intestinal probiotics, such as Bifidobacterium and GCA-900066575, was significantly decreased at the genus level (Figure 3D). These results suggest that the development of NASH is accompanied by a disturbance of the intestinal flora.

Recently, the role of the intestinal mucosal barrier and inflammatory response in the development of NAFLD has been a high concern (Takaki et al., 2013; Tripathi et al., 2018). Dysbacteriosis and intestinal endotoxemia (IETM) are important causes of liver inflammation and NAFLD. The normal intestinal mucosal barrier can prevent the translocation and invasion of

enterogenic pathogenic factors, such as intestinal bacteria and endotoxins (Brandl et al., 2017). However, in some pathological conditions, intestinal mucosal barrier integrality is impaired, and harmful substances such as bacterial DNA, lipopolysaccharide (LPS), and ethanol can enter the liver through the portal vein, thus promoting the progression of NASH (Pierantonelli et al., 2017; Longo et al., 2020). Germ-free animals transplanted with fecal from NAFLD patients demonstrated significant hepatic steatosis, multifocal necrosis, and inflammatory cell infiltration in the liver, accompanied by increased levels of serum LPS and inflammatory cytokines (such as IL-6 and MCP-1) and the disturbance of intestinal flora, indicating that the occurrence of NAFLD is closely related to intestinal flora disturbance (Chiu et al., 2017). In this study, we found that FFC diet not only impaired the integrity of intestinal mucosal barrier and decreased the levels of ZO-1 protein but also significantly increased the levels of several pro-inflammatory factors (such as IL6, IL-1β, and TNF-α) and plasma LPS compared to chow diet mice. These results suggest that high-fat diet may lead to enterogenic endotoxemia by altering the structure of the intestinal flora and aggravating liver inflammation, thus accelerating the progression of NASH.

The endoplasmic reticulum (ER) plays an essential role in protein folding and maturation, in addition to other metabolic processes. ER stress has been observed in nearly all chronic liver diseases and is distinguished by the activation of three UPR pathways. Guo et al. (2018) reported increased mRNA expression of ER stress markers, including BiP, activating transcription factor 4 (ATF4), and c/EBP-homologous protein (CHOP), in mice fed an HFD diet. Consistently, mice fed with the FFC diet demonstrated higher levels of ER stress-related proteins, including GRP78, PERK, ATF6, IRE1α and XBP1s, and IRE1α-XBP1s pathway was significantly elevated compared to other ER stress markers (Figure 4A). Dysregulation of the ER stress response has been implicated in intestinal inflammation associated with inflammatory bowel disease (IBD), a chronic condition characterized by changes in the mucosa and alteration of the gut microbiota (McGovern et al., 2010). However, the exact relationship between ER stress and gut microbes is largely unclear. In the current study, we found that FT@XBP1 treatment could not only significantly inhibit liver lipid accumulation and collagen deposition in the FFC diet fed mice but also improve high-fat-induced intestinal barrier dysfunction, as demonstrated by the restoration the integrity of the intestinal barrier (Figure 6A) and increased levels of ZO-1 protein expression (Figure 6B), which partially restored intestinal flora structure, reduced endotoxemia and alleviated liver inflammation. Similarly, Laudisi et al. (2019) demonstrated that mice fed a maltodextrin (MDX)-enriched diet exhibited an activated ER stress response in intestinal epithelial cells and an exacerbated intestinal inflammation, while treatment of mice with TUDCA prevented mucin-2 depletion and attenuated colitis in MDX-fed mice. Most interestingly, Grey et al. (2022) found that ERN2 was required for microbiota-induced goblet cell maturation and mucus barrier assembly in the colon, and mice lacking Ern2 had a dysbiotic microbial community. The secretory capacity of the gut epithelium, especially mucin and antimicrobial protein production, likely demands the maintenance of ER proteostasis (Kaser et al., 2008). These results suggested that ER stress transcription factor XBP1s evolved on mucosal surfaces to mediate crosstalk between gut microbes and the mucus barrier required for normal homeostasis and host defense. However, several pieces of evidence suggested that *Xbp1* deletion in mouse intestinal epithelial cells resulted in Paneth and goblet cell apoptosis, spontaneous ileal inflammation, and increased sensitivity to dextran sodium sulfate (DSS)-induced colitis (Kaser et al., 2008).

In summary, our study showed that the inhibition of XBP1s by FT@XBP1 could restore the integrity of the intestinal mucosal barrier and intestinal flora disturbance and inhibit LPS translocation, which subsequently reduces liver inflammation and lipid deposition and prevents NASH progression. However, this study inevitably has some limitations. First, this study established NASH model by feeding animals with FFC (high fat, high fructose and high cholesterol) diets. It was found that the progression of NASH induced by FFC diet was related to intestinal flora disturbance and the integrity of intestinal mucosal barrier, but the exact relationship was not fully understood. Second, intravenously administrated FT@XBP1 exerted its effect mainly by targeting the key transcription factor XBP1s, however, whether it affects the integrity of the intestinal mucosal barrier and regulates liver inflammation to indirectly restore intestinal microflora homeostasis in NASH is worthy of further study. Finally, the role of other downstream signaling pathways of ER stress in intestinal flora disturbance and the progression of NASH is also worth further investigation.

Data availability statement

Data relating with the current paper are available upon reasonable request to the corresponding author. The 16S rDNA sequencing data was store in the SRA database (PRJNA1030503), with the following link https://www.ncbi.nlm.nih.gov/sra/.

Ethics statement

The animal study was approved by the Laboratory Animal Ethics Committee of Anhui Medical University (LLSC20221000). The study was conducted in accordance with the local legislation and institutional requirements.

Author contributions

MZ: Data curation, Writing – original draft, Formal analysis, Investigation, Methodology, Validation. YC: Investigation, Methodology, Writing – original draft, Project administration. YT: Methodology, Writing – original draft, Data curation, Formal analysis, Resources. SL: Data curation, Formal analysis, Methodology, Resources, Writing – review & editing. PR: Data curation, Formal analysis, Methodology, Writing – review & editing. GZ: Data curation, Formal analysis, Methodology, Writing – review & editing. LX: Writing – review & editing, Conceptualization, Funding acquisition, Resources, Supervision,

Writing – original draft. JL: Conceptualization, Funding acquisition, Writing – original draft, Writing – review & editing, Data curation.

Funding

The author(s) declare financial support was received for the research, authorship, and/or publication of this article. This study was supported by the National Nature and Science Foundation of China (grant no. 82072687), Natural Science Research Project of Anhui Educational Committee (grant no. KJ2020A0177), and the Natural Science Foundation of Anhui Province (grant no. 2008085MH257).

Acknowledgments

The authors thank Prof. Meijuan Zheng and the Center for Scientific Research of Anhui Medical University for their valuable help in our experiment.

Conflict of interest

The authors declare that the research was conducted in the absence of any commercial or financial relationships that could be construed as a potential conflict of interest.

Publisher's note

Supplementary material

The Supplementary Material for this article can be found online at: https://www.frontiersin.org/articles/10.3389/fmicb.2023.1271835/full#supplementary-material

References

Acosta-Alvear, D., Zhou, Y., Blais, A., Tsikitis, M., Lents, N. H., Arias, C., et al. (2007). XBP1 controls diverse cell type- and condition-specific transcriptional regulatory networks. *Mol. Cell* 27, 53–66. doi: 10.1016/j.molcel.2007.06.011

Adolph, T. E., Niederreiter, L., Blumberg, R. S., and Kaser, A. (2012). Endoplasmic reticulum stress and inflammation. *Dig. Dis.* 30, 341–346. doi: 10.1159/000338121

Albillos, A., de Gottardi, A., and Rescigno, M. (2020). The gut-liver axis in liver disease: pathophysiological basis for therapy. *J. Hepatol.* 72, 558–577. doi: 10.1016/j.jhep.2019.10.003

Brandl, K., Kumar, V., and Eckmann, L. (2017). Gut-liver axis at the frontier of hostmicrobial interactions. *Am. J. Physiol. Gastrointest. Liver Physiol.* 312, G413–G419. doi: 10.1152/ajpgi.00361.2016

Carvalho, B. M., Guadagnini, D., Tsukumo, D. M. L., Schenka, A. A., Latuf-Filho, P., Vassallo, J., et al. (2012). Modulation of gut microbiota by antibiotics improves insulin signalling in high-fat fed mice. *Diabetologia* 55, 2823–2834. doi: 10.1007/s00125-012-2648-4

Chen, J., Yang, Y., Yang, Y., Dai, Z., Kim, I. H., Wu, G., et al. (2021). Dietary supplementation with glycine enhances intestinal mucosal integrity and ameliorates inflammation in C57BL/6J mice with high-fat diet-induced obesity. *J. Nutr.* 151, 1769–1778. doi: 10.1093/jn/nxab058

Chen, Y., Zhang, H., Li, Y., Ji, S., Jia, P., Wang, T., et al. (2022). Pterostilbene prevents tunicamycin-induced intestinal barrier damage by targeting endoplasmic reticulum stress, oxidative stress, autophagy, and gut microbiota. *J. Agric. Food Chem.* 70, 13661–13675. doi: 10.1021/acs.jafc.2c06041

Chiu, C. C., Ching, Y. H., Li, Y. P., Liu, J. Y., Huang, Y. T., Huang, Y. W., et al. (2017). Nonalcoholic fatty liver disease is exacerbated in high-fat diet-fed gnotobiotic mice by colonization with the gut microbiota from patients with nonalcoholic steatohepatitis. *Nutrients* 9:1220. doi: 10.3390/nu9111220

Das, I., Png, C. W., Oancea, I., Hasnain, S. Z., Lourie, R., Proctor, M., et al. (2013). Glucocorticoids alleviate intestinal ER stress by enhancing protein folding and degradation of misfolded proteins. *J. Exp. Med.* 210, 1201–1216. doi: 10.1084/jem.20121268

Feldstein, A. E., Werneburg, N. W., Canbay, A., Guicciardi, M. E., Bronk, S. F., Rydzewski, R., et al. (2004). Free fatty acids promote hepatic lipotoxicity by stimulating TNF-alpha expression via a lysosomal pathway. *Hepatology* 40, 185–194. doi: 10.1002/hep.20283

Friedman, S. L., Neuschwander-Tetri, B. A., Rinella, M., and Sanyal, A. J. (2018). Mechanisms of NAFLD development and therapeutic strategies. *Nat. Med.* 24, 908–922. doi: 10.1038/s41591-018-0104-9

Grey, M. J., De Luca, H., Ward, D. V., Kreulen, I. A., Bugda Gwilt, K., Foley, S. E., et al. (2022). The epithelial-specific ER stress sensor ERN2/IRE1b enables hostmicrobiota crosstalk to affect colon goblet cell development. *J. Clin. Invest.* 132:e153519. doi: 10.1172/JCI153519

Guo, X., Tang, R., Yang, S., Lu, Y., Luo, J., Liu, Z., et al. (2018). Rutin and its combination with inulin attenuate gut dysbiosis, the inflammatory status and endoplasmic reticulum stress in paneth cells of obese mice induced by high-fat diet. *Front. Microbiol.* 9:2651. doi: 10.3389/fmicb.2018.02651

Holczer, M., Márton, M., Kurucz, A., Bánhegyi, G., and Kapuy, O. A. (2015). Comprehensive systems biological study of autophagy-apoptosis crosstalk during endoplasmic reticulum stress. *Biomed Res. Int.* 2015:319589. doi: 10.1155/2015/319589

Huang, D. Q., El-Serag, H. B., and Loomba, R. (2021). Global epidemiology of NAFLD-related HCC: trends, predictions, risk factors and prevention. *Nat. Rev. Gastroenterol. Hepatol.* 18, 223–238. doi: 10.1038/s41575-020-00381-6

Kaser, A., Lee, A. H., Franke, A., Glickman, J. N., Zeissig, S., Tilg, H., et al. (2008). XBP1 links ER stress to intestinal inflammation and confers genetic risk for human inflammatory bowel disease. *Cell* 134, 743–756. doi: 10.1016/j.cell.2008.07.021

Kleiner, D. E., Brunt, E. M., Van Natta, M., Behling, C., Contos, M. J., Cummings, O. W., et al. (2005). Design and validation of a histological scoring systemfor nonalcoholic fatty liver disease. *Hepatology* 41, 1313–1321. doi: 10.1002/hep.20701

Laudisi, F., Di Fusco, D., Dinallo, V., Stolfi, C., Di Grazia, A., Marafini, I., et al. (2019). The food additive maltodextrin promotes endoplasmic reticulum stress-driven mucus depletion and exacerbates intestinal inflammation. *Cell Mol. Gastroenterol. Hepatol.* 7, 457–473. doi: 10.1016/j.jcmgh.2018.09.002

Lebeaupin, C., Vallée, D., Hazari, Y., Hetz, C., Chevet, E., Bailly-Maitre, B., et al. (2018). Endoplasmic reticulum stress signalling and the pathogenesis of non-alcoholic fatty liver disease. *J. Hepatol.* 69, 927–947. doi: 10.1016/j.jhep.2018.06.008

Longo, L., Tonin Ferrari, J., Rampelotto, P. H., Hirata Dellavia, G., Pasqualotto, A., Oliveira, P. C., et al. (2020). Gut dysbiosis and increased intestinal permeability drive microRNAs, NLRP-3 inflammasome and liver fibrosis in a nutritional model of nonalcoholic steatohepatitis in adult male sprague dawley rats. *Clin. Exp. Gastroenterol.* 13, 351–368. doi: 10.2147/CEG.S262879

McGovern, D. P., Gardet, A., Törkvist, L., Goyette, P., Essers, J., Taylor, K. D., et al. (2010). Genome-wide association identifies multiple ulcerative colitis susceptibility loci. *Nat. Genet.* 42, 332–337. doi: 10.1038/ng.549

Oancea, I., Movva, R., Das, I., Aguirre de Cárcer, D., Schreiber, V., et al. (2017). Colonic microbiota can promote rapid local improvement of murine colitis by thioguanine independently of T lymphocytes and host metabolism. *Gut* 66, 59–69. doi: 10.1136/gutjnl-2015-310874

Papatheodoridi, M., and Cholongitas, E. (2018). diagnosis of non-alcoholic fatty liver disease (NAFLD): current concepts. *Curr. Pharm. Des.* 24, 4574–4586. doi: 10.2174/1381612825666190117102111

Pierantonelli, I., Rychlicki, C., Agostinelli, L., Giordano, D. M., Gaggini, M., Fraumene, C. et al. (2017). Lack of NLRP3-inflammasome leads to gut-liver axis derangement, gut dysbiosis and a worsened phenotype in a mouse model of NAFLD. *Sci. Rep*. 7:12200. doi: 10.1038/s41598-017-11744-6

Poeta, M., Pierri, L., and Vajro, P. (2017). Gut-liver axis derangement in nonalcoholic fatty liver disease. *Children* 4:66. doi: 10.3390/children4080066

Sacks, D., Baxter, B., Campbell, B. C. V., Carpenter, J. S., Cognard, C., Dippel, D., et al. (2018). Multisociety consensus quality improvement revised consensus statement for endovascular therapy of acute ischemic stroke. *Int. J. Stroke* 13, 612–632. doi: 10.1016/j.jvir.2017.11.026

Schnabl, B., and Brenner, D. A. (2014). Interactions between the intestinal microbiome and liver diseases. *Gastroenterology* 146, 1513–1524. doi: 10.1053/j.gastro.2014.01.020

Seki, E., Tsutsui, H., Nakano, H., Tsuji, N., Hoshino, K., Adachi, O., et al. (2001). Lipopolysaccharide-induced IL-18 secretion from murine Kupffer cells independently of myeloid differentiation factor 88 that is critically involved in induction of production of IL-12 and IL-1beta. *J. Immunol.* 166, 2651–2657. doi: 10.4049/jimmunol.166.4.2651

Shaffer, A. L., Shapiro-Shelef, M., Iwakoshi, N. N., Lee, A. H., Qian, S. B., Zhao, H., et al. (2004). XBP1, downstreamof Blimp-1, expands the secretory apparatus and other organelles, and increases protein synthesis in plasma cell differentiation. *Immunity* 21, 81–93. doi: 10.1016/j.immuni.2004.06.010

Shen, F., Zheng, R. D., Sun, X. Q., Ding, W. J., Wang, X. Y., Fan, J. G., et al. (2017). Gut microbiota dysbiosis in patients with non-alcoholic fatty liver disease. *Hepatobiliary Pancreat Dis. Int.* 16, 375–381. doi: 10.1016/S1499-3872(17)60019-5

Takaki, A., Kawai, D., and Yamamoto, K. (2013). Multiple hits, including oxidative stress, as pathogenesis and treatment target in non-alcoholic steatohepatitis (NASH). *Int. J. Mol. Sci.* 14, 20704–20728. doi: 10.3390/ijms141020704

Tilg, H., and Moschen, A. R. (2010). Evolution of inflammation in nonalcoholic fatty liver disease: the multiple parallel hits hypothesis. *Hepatology* 52, 1836–1846. doi: 10.1002/hep.24001

Tripathi, A., Debelius, J., Brenner, D. A., Karin, M., Loomba, R., Schnabl, B., et al. (2018). The gut-liver axis and the intersection with the microbiome. *Nat. Rev. Gastroenterol. Hepatol.* 15, 397–411. doi: 10.1038/s41575-018-0011-z

Vancamelbeke, M., and Vermeire, S. (2017). The intestinal barrier: a fundamental role in health and disease. *Expert Rev. Gastroenterol. Hepatol.* 11, 821–834. doi: 10.1080/17474124.2017.1343143

Verma, P., Srivastava, A., Srikanth, C. V., and Bajaj, A. (2021). Nanoparticle-mediated gene therapy strategies for mitigating inflammatory bowel disease. *Biomater Sci.* 9, 1481–1502. doi: 10.1039/D0BM01359E

Vespasiani-Gentilucci, U., Gallo, P., and Picardi, A. (2018). The role of intestinal microbiota in the pathogenesis of NAFLD: starting points for intervention. *Arch. Med. Sci.* 14, 701–706. doi: 10.5114/aoms.2016.58831

Wang, B., Jiang, X., Cao, M., Ge, J., Bao, Q., Tang, L., et al. (2016). Altered fecal microbiota correlates with liver biochemistry in nonobese patients with non-alcoholic fatty liver disease. *Sci. Rep*. 6:32002. doi: 10.1038/srep32002

Wang, R., Tang, R., Li, B., Ma, X., Schnabl, B., Tilg, H., et al. (2021). Gut microbiome, liver immunology, and liver diseases. *Cell. Mol. Immunol.* 18, 4–17. doi: 10.1038/s41423-020-00592-6

Yamaguchi, K., Yang, L., McCall, S., Huang, J., Yu, X. X., Pandey, S. K., et al. (2007). Inhibiting triglyceride synthesis improves hepatic steatosis but exacerbates liver damage and fibrosis in obese mice with nonalcoholic steatohepatitis. *Hepatology* 45, 1366–1374. doi: 10.1002/hep.21655

Yoshida, H., Matsui, T., Yamamoto, A., Okada, T., and Mori, K. (2001). XBP1 mRNA is induced by ATF6 and spliced by IRE1 in response to ER stress to produce a highly active transcription factor. *Cell* 107, 881–891. doi: 10.1016/S0092-8674(01)00611-0

Younossi, Z., Anstee, Q. M., Marietti, M., Hardy, T., Henry, L., Eslam, M., et al. (2018). Global burden of NAFLD and NASH: trends, predictions, risk factors and prevention. *Nat. Rev. Gastroenterol. Hepatol.* 15, 11–20. doi: 10.1038/nrgastro.2017.109

Zheng, W., Sun, Q., Li, L., Cheng, Y., Chen, Y., Lv, M., et al. (2022). Role of endoplasmic reticulum stress in hepatic glucose and lipid metabolism and therapeutic strategies for metabolic liver disease. *Int. Immunopharmacol.* 113:109458. doi: 10.1016/j.intimp.2022.109458

Zhu, L., Baker, S. S., Gill, C., Liu, W., Alkhouri, R., Baker, R. D., et al. (2013). Characterization of gut microbiomes in nonalcoholic steatohepatitis (NASH) patients: a connection between endogenous alcohol and NASH. *Hepatology* 57, 601–609. doi: 10.1002/hep.26093

frontiers | Frontiers in Microbiology

TYPE Original Research
PUBLISHED 29 April 2024
DOI 10.3389/fmicb.2024.1356176

OPEN ACCESS

EDITED BY
Ren-You Gan,
Singapore Institute of Food and Biotechnology Innovation, Singapore

REVIEWED BY
Gabriel Vasconcelos Pereira,
University of Michigan, United States
Naheed Mojgani,
Razi Vaccine and Serum Research Institute, Iran

*CORRESPONDENCE
Dongmei Pei
✉ Peidm1111@hotmail.com

†These authors have contributed equally to this work and share first authorship

RECEIVED 15 December 2023
ACCEPTED 08 April 2024
PUBLISHED 29 April 2024

CITATION
Lu J, Gong X, Zhang C, Yang T and Pei D (2024) A multi-omics approach to investigate characteristics of gut microbiota and metabolites in hypertension and diabetic nephropathy SPF rat models.
Front. Microbiol. 15:1356176.
doi: 10.3389/fmicb.2024.1356176

A multi-omics approach to investigate characteristics of gut microbiota and metabolites in hypertension and diabetic nephropathy SPF rat models

Jinjing Lu[1†], Xiaoying Gong[2†], Chenlu Zhang[3†], Tengfei Yang[1] and Dongmei Pei[1*]

[1]Department of Health Management, Shengjing Hospital of China Medical University, Shenyang, China, [2]Department of Critical Care Unit, Shengjing Hospital of China Medical University, Shenyang, China, [3]Department of Neurosurgery, Shengjing Hospital of China Medical University, Shenyang, China

Background: Imbalance in intestinal microbiota caused by microbial species and proportions or metabolites derived from microbes are associated with hypertension, as well as diabetic nephropathy. However, the involvement of the intestinal microbiota and metabolites in hypertension and diabetic nephropathy comorbidities (HDN) remains to be elucidated.

Methods: We investigated the effects of intestinal microbiota on HDN in a rat model and determined the abundance of the intestinal microbiota using 16S rRNA sequencing. Changes in fecal and serum metabolites were analyzed using ultra-high-performance liquid chromatography-mass spectrometry.

Results: The results showed abundance of *Proteobacteria* and *Verrucomicrobia* was substantially higher, whereas that of *Bacteroidetes* was significant lower in the HDN group than in the sham group. *Akkermansia*, *Bacteroides*, *Blautia*, *Turicibacter*, *Lactobacillus*, *Romboutsia, and Fusicatenibacter* were the most abundant, and *Prevotella, Lachnospiraceae_NK4A136_group*, and *Prevotella_9* were the least abundant in the HDN group. Further analysis with bile acid metabolites in serum showed that *Blautia* was negatively correlated with taurochenodeoxycholic acid, taurocholic acid, positively correlated with cholic acid and glycocholic acid in serum.

Conclusions: These findings suggest that the gut microbiota and metabolites in feces and serum substantially differed between the HDN and sham groups. The F/B ratio was higher in the HDN group than in the sham group. *Blautia* is potentially associated with HDN that correlated with differentially expressed bile acid metabolites, which might regulate the pathogenesis of HDN *via* the microorganism–gut–metabolite axis.

KEYWORDS

multi-omics, intestinal microbiota, metabolites, hypertension, diabetic nephropathy

1 Introduction

Diabetes mellitus (DM) is a metabolic disorder that is characterized by chronic hyperglycemia due to an absolute or relatively insufficient amount of secreted insulin. The estimated global prevalence of diabetes among people aged 20–79-years during 2021 was ~10.5% (536.6 million people) and is expected to reach 12.2% (783.2 million people)

by 2045 (Sun et al., 2022). Diabetic nephropathy (DN) is a prevalent microvascular complication of diabetes and the leading cause of end-stage renal disease (ESRD) in developed countries and developed regions of China (Ma, 2018; Johansen et al., 2021). Approximately 40% of DM patients will eventually develop DN (Chen et al., 2023).

Hypertension affect ~1.5 billion (Murray and Lopez, 2013) people worldwide. Patients with diabetes have a high prevalence of hypertension (Sabuncu et al., 2021) and those with hypertension are also at increased risk of developing diabetes (Izzo et al., 2009). Since patients with both DN and hypertension are more prone to develop macrovascular (Yen et al., 2022) and microvascular complications (Brownrigg et al., 2016) that lead to a poor prognosis, understanding the underlying mechanisms is crucial.

Changes to the intestinal microbiota caused by microbial species and proportions or metabolites derived from microbes are associated with increased susceptibility to diseases (Gentile and Weir, 2018). Intestinal microbiota disorders play important roles in DM (Wu et al., 2023), DN (Zhao et al., 2023), chronic kidney disease, ESRD (Luo et al., 2023), and in DM progression to DN and subsequent ESRD (Mao et al., 2023). However, the underlying mechanisms of how intestinal flora affects DN remain uncertain.

The intestinal microbiota plays a key role in the development of hypertension (Lucas et al., 2023). However, a disordered intestinal microbiota in DN is inconsistent with hypertension. For instance, the ratio of abundance of *Firmicutes* to *Bacteroidetes* (F/B) is significantly decreased in DN (Li et al., 2020), whereas that in the intestinal contents of patients with hypertension is increased (Yang et al., 2015). These findings suggest a complex mechanism between intestinal microbiota functions and derived metabolites in DN and comorbid hypertension.

16S rDNA amplicon sequencing technology has become an important means of studying the composition and structure of microbial communities in environmental samples. Untargeted metabolomics aims to detect as many metabolites as possible in biological samples for the purpose of discovery, reflecting the overall metabolite information to the greatest extent possible, LC-MS/MS technology is used. To delve into this aspect further, in this study, we aimed to investigate changes and crucial regulatory roles of gut microbiota and their metabolites in the DN and comorbid hypertension, by feeding rats with a high-carbohydrate high-fat diet, inducing diabetes in them by injecting streptozotocin (STZ), unilaterally ligating the renal arteries, and applying non-targeted metabolomics and 16S rRNA gene sequencing. The results showed abundance of *Proteobacteria* and *Verrucomicrobia* was substantially higher, whereas that of *Bacteroidetes* was significant lower in the HDN group than in the sham group. *Akkermansia*, *Bacteroides*, *Blautia*, *Turicibacter*, *Lactobacillus*, *Romboutsia, and Fusicatenibacter* were the most abundant, and *Prevotella, Lachnospiraceae_NK4A136_group*, and *Prevotella_9* were the least abundant in the HDN group. Further analysis with bile acid metabolites in resum showed that *Blautia* was negatively correlated with taurochenodeoxycholic acid, taurocholic acid, positively correlated with cholic acid and glycocholic acid in serum.

2 Materials and methods

2.1 Animals

A total of 26 six-week-old SPF Sprague-Dawley rats weighing 200 g were selected for studies (Beijing Huafukang Biotechnology Co. Ltd., Beijing, China). The rats were randomly assigned to either a group with hypertension and diabetic nephropathy (HDN) or a sham group ($n = 14$ per group). We induced HDN model by feeding the rats with a high-calorie high-carbohydrate diet for 24 weeks. The purified diets were produced by Trophic Animal Feed High-Tech Co., Ltd. (Nantong, China). The diet formulas are shown in Supplementary Table 1. The HDN group was anesthetized before undergoing unilateral renal artery ligation. We intraperitoneally injected 30 mg/kg of streptozotocin into the HDN group on postoperative day (POD) 7. The sham group was fed with a standard diet (Trophic Animal Feed High-Tech Co. Ltd, Nantong, China). This group was also anesthetized and underwent an abdominal incision, and suturing; however, the renal arteries were not clipped. The sham group was intraperitoneally injected with 0.1 mol/L sodium citrate buffer (pH 4.2) on POD 7. Fasting blood glucose (FBG) was evaluated in tail tip blood and measured using an Accu-Chek Advantage glucometer (Roche Diagnostics GmbH, Mannheim, Germany). Blood pressure (BP) was determined using a tail-cuff. Rats with FBG >16.7 mmol/L and BP >140 mmHg were considered as successful models. The Institutional Animal Care and Use Committee of Shengjing Hospital of China Medical University (Shenyang, China) approved the animal experiments (2023PS1422K).

2.2 Sample collection

All rats were anesthetized with isoflurane before the blood was collected from the orbital venous plexus. Serum (≥ 1.5 mL) obtained by centrifugation at 300 × g was stored at −80°C. Colon contents were collected and immediately frozen with liquid nitrogen after sampling and stored at −80°C.

2.3 Sequencing and analysis of 16s rDNA amplicons

The purity and concentration of extracted DNA from colon contents were detected using 2% agarose gel Electrophoresis. A library was then constructed from 1 ng/μL of DNA using TruSeq® DNA PCR-Free Sample Preparation Kits (Illumina, California -San Diego, USA). The library was quantified using Qubit and Q-PCR, then sequenced using a NovaSeq 6000 System (Novogene, Sacramento, CA). Filtered sequences were clustered into operational taxonomic units (OTUs) using the UPARSE-OTU algorithm, then species annotation was analyzed using Mothur and classified using the small subunit ribosomal (SSUr) RNA database. Changes in intestinal flora were analyzed using QIIME v.1.9.1 and R v. 3.5.2 (R Foundation for Statistical Computing, Vienna, Austria).

2.4 Sample processing and analysis

Metabolites were extracted from thawed serum samples using 80% methanol buffer. Serum was incubated on ice for 5 min followed by centrifugation at 15000 *g*, 4°C for 20 min. The supernatants were transferred to 96-well plates, dried under nitrogen and stored at −80°C. Thawed fecal samples (100 mg) were extracted using 80% methanol, centrifuged at 15000 *g*, 4°C for 20 min, then supernatants were stored at −80°C.

2.5 UHPLC-MS/MS

UHPLC-MS/MS analyses were performed using a Vanquish UHPLC system (ThermoFisher, Germany) coupled with an Orbitrap Q ExactiveTMHF-X mass spectrometer (Thermo Fisher, Germany) in Novogene Co., Ltd. (Beijing, China). Samples processed previously were injected onto a Hypesil Gold column (100 × 2.1 mm, 1.9 μm) using a 17-min linear gradient at a flow rate of 0.2 mL/min. The eluents for the positive polarity mode were eluent A (0.1% FA in Water) and eluent B (Methanol).The eluents for the negative polarity mode were eluent A (5 mM ammonium acetate, pH 9.0) and eluent B (Methanol).The solvent gradient was set as follows: 2% B, 1.5 min; 2%−100% B, 3 min; 100% B, 10 min;100%−2% B, 10.1 min;2% B, 12 min. Q ExactiveTM HF-X mass spectrometer was operated in positive/negative polarity mode with spray voltage of 3.5 kV, capillary temperature of 320°C, sheath gas flow rate of 35 psi and aux gas flow rate of 10 L/min, S-lens RF level of 60, Aux gas heater temperature of 350°C.

2.6 Metabolite analysis

The metabolites were annotated using the Encyclopedia of Genes and Genomes (KEGG), the Human Metabolome Database (HMDB), and the Lipid Metabolites and Pathways Strategy (LIPIDMaps) (https://www.lipidmaps.org/). Principal components analysis (PCA) and partial least squares discriminant analysis (PLS-DA) proceeded using metaX® (https://metaxsoft.com). Statistically significant metabolite parameters comprised fold change (FC) $\geq$ 2 or $\leq$ 0.5, variable importance in projection (VIP) $>$ 1, $p < 0.05$, then volcano plots of metabolites were plotted based on log2 FC and –log10p. Differential metabolites were visualized using clustering heat maps. Correlations among differential metabolites were calculated using Pearson coefficients. Results with $p < 0.05$ were considered to be significantly different.

2.7 Statistical analysis

Continuous variables are presented as means ± standard error of mean (SEM). Between-group differences were analyzed using Student *t*-tests. Relationships between species and metabolites were analyzed using Spearman rank correlations. All data were analyzed using SPSS 21 (IBM Corp., Armonk, NY, USA) and R v. 3.5.2.

3 Results

3.1 Evaluation of HDN model

Fasting blood glucose (FBG) levels were increased in HDN compared with sham rats (Figure 1A). The urinary albumin to creatinine ratio (UACR) was significantly increased in rats with HDN compared with sham rats (Figure 1B). These ratios are sensitive indicators for early diagnoses of renal damage in diabetes; Changes in UACR precede those of blood urea nitrogen and creatinine, indicating impaired glomerular filtration function. Moreover, BP was significantly elevated in the HDN rats (Figure 1C), confirming successful establishment of the model.

3.2 Gut microbial profiles

The gut microbiota notably differed between the HDN and sham rats. The quality control effective rate 81.71%, with 67,665 quality-control-validated data points, among 81,631 valid data points. We obtained 3,092 OTUs with 97% identity, then annotated them using the Silva138 database (https://www.arb-silva.de/). We annotated 1260 (40.75%) OTUs at the genus level. We identified the top-five most abundant microbiota at the phylum level using a Sankey map (Supplementary Figure 1A). Rarefaction curves indicated that the current sequencing depth adequately reflected microbial diversity (Supplementary Figures 1B, C). Rank abundance curves indicated the richness and evenness of species (Supplementary Figures 1D, E). Box plots of biodiversity and community surveys show species richness (Supplementary Figure 1F).

Alpha diversity analysis revealed significant differences in goods coverage, as well as the Shannon and Simpson indices between the HDN and sham groups (Figures 2A–C). Principal coordinate (PCoA) and principal component (PCA), analyses and non-metric multidimensional scaling (NMDS) for beta diversity, revealed differences between the groups and significant divergence in the composition and abundance of the gut microbiota (Figures 2D–F). Supplementary Table 1 shows the alpha diversity indexes (Shannon, Simpson, chao1, ACE, goods coverage, PD_whole_tree) of the samples (data volume selected during homogenization: cutoff = 46,210, at a consistency threshold of 97%).

3.3 Changes in composition of gut microflora associated with HDN

The abundance of *Proteobacteria* and *Verrucomicrobiota* increased, whereas that of *Bacteroidetes* was lower at the phylum level in the HDN group, compared with the sham group. Supplementary Figures 2A, B show that at the pylum level, *Verrucomicrobiota* was significantly increased in the HDN group, *Bacteroidetes* was decreased in the HDN group. At the genus

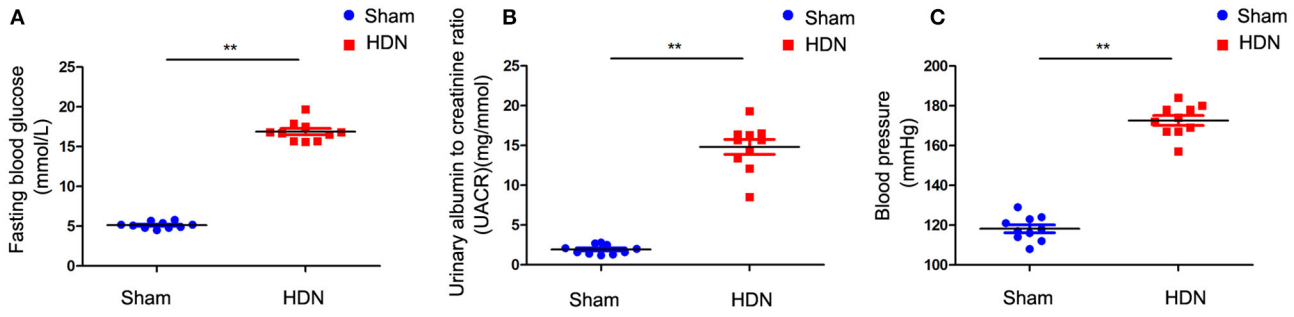

FIGURE 1
Evaluation of diabetic nephropathy-hypertension (HDN) model rats. Evaluation of **(A)** fasting blood glucose, **(B)** urinary albumin to creatinine ratios, and **(C)** blood pressure. Data are expressed as means ± SEM (n =10; $^{**}P < 0.01$).

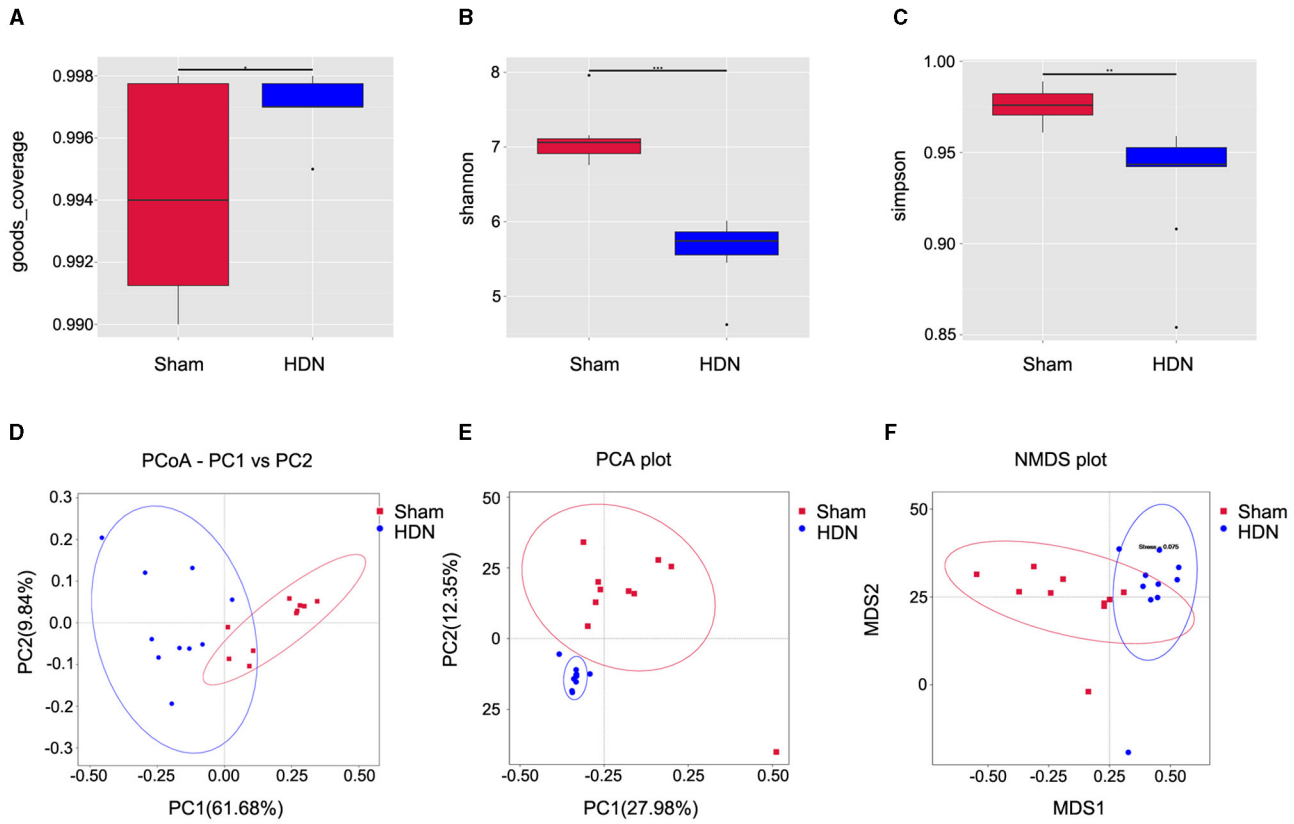

FIGURE 2
Relative bacterial richness and evenness in two groups of samples. **(A)** Good coverage of each sample library. Higher values represent a higher probability of sequence detection. **(B)** Shannon index estimates of microbial diversity. **(C)** Simpson index estimates of diversity. Assessment of gut microbiota using **(D)** PCoA (PC1 = 61.68%, PC2 = 9.84%), **(E)** PCA (PC1 = 27.98%, PC2 = 12.35%) and **(F)** NMDS analysis. Red: sham group; blue: HDN group. HDN, hypertension and diabetic nephropathy; NDMS, non-metric multidimensional scaling; PCA, principal component analysis; PCoA, principal coefficient analysis.

level, *Akkermansia*, *Bacteroidetes* and *Blautia* were increased in the HDN group. The abundance of *Proteobacteria* was higher in the HDN group than in the sham group. The trend was similar in the HDN and sham groups for *Verrucomicrobiota*; however, *Bacteroidetes* were less abundant in the HDN group (Figures 3A, B). The abundance of *Verrucomicrobiota* (P = 0.0167) was significantly more, whereas *Bacteroidetes* (P = 0.001), *Gemmatimonadota* (P = 0.042), *Myxococcota* (P = 0.048), *Gemmatimonadetes* (P = 0.025), and *Elusimicrobia* (P = 0.004) were less abundant in the HDN group (Supplementary Table 2). Supplementary Table 3 shows that 114 genera significantly differed between the groups. The relative prevalence of species at the phylum level was determined using the unweighted pair group method with arithmetic (UPGMA) (Figure 3C). The *Firmicutes/Bacteroidetes* (F/B) ratio is associated with multiple diseases (Li et al., 2020). We found a higher F/B ratio in the HDN group (Figure 3D). We further investigated relationships among microbiota from the phylum to the genus

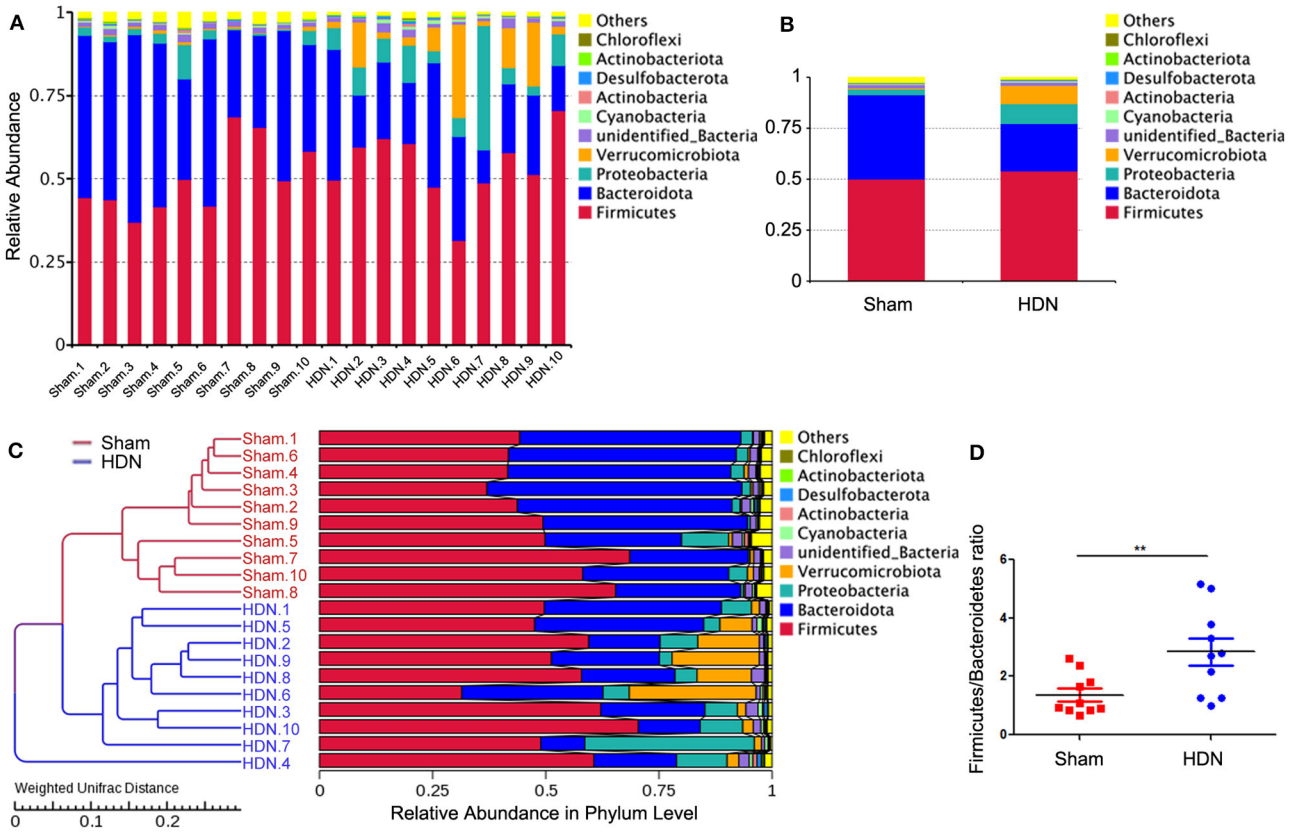

FIGURE 3
Changes in gut microflora phyla associated with HDN. Data are expressed as means ± SEM. **(A, B)** Proportions of gut microflora phyla in HDN and sham groups assessed using microbial taxa assignment. **(C)** Left, UPGMA cluster tree; right, distribution map of relative species abundance at phylum level. **(D)** Changes in *Firmicutes*/*Bacteroidetes* ratios in HDN and sham groups (n =10 each). $^{**}P < 0.01$. HDN, hypertension and diabetic nephropathy; UPGMA, Unweighted Pair Group Method with Arithmetic Mean.

level using linear discriminant analysis (LDA) Effect Size (LEfSe) (Figures 4A, B).

Figure 5A shows a cluster heat map of the relative abundance of 35 genera. The overall abundance of OTUs was higher in the HDN group than in the sham group (18 vs. 17; Figure 5B). Collectively, the significant difference in abundance of microbes was sufficient to distinguish healthy from HDN rats, fed with high-carbohydrate high-fat diet.

3.4 Metabolomics analysis of fecal and serum samples from HDN and sham rats

The gut microbiome has effects on fecal metabolites (Wikoff et al., 2009). We investigated differences in fecal and serum metabolites between the groups using non-targeted metabolomics and LC-MS.

The fecal metabolites were separated in the groups (Figure 6A), indicating that HDN caused changes in fecal biomarkers. Volcano plots of 544 fecal metabolites identified by LC-MS showed that 43 and 226 of 269 fecal metabolites were significantly upregulated and downregulated, respectively (Figure 6B). Compared with the sham group, The top 10 downregulated fecal metabolites in the HDN group comprised fatty acid esters of hydroxy fatty acids (FAHFA; 18:2/20:4), acyl GlcADG (12:0-12:0-18:2), alpha-ketoglutaric acid, 2-ketohexanoic acid, 4-methylvaleric acid, dodecanedioic acid, 4-hydroxybenzoic acid, xanthosine, ursolic acid, and 3-methyladipic acid (Supplementary Table 4).

Orthogonal projections to latent structures with discriminant analysis (OPLS-DA) of serum metabolite profiles revealed good separation in the groups, suggesting that HDN altered serum biomarkers (Figure 6C). Volcano plots revealed that among 182 of 501 serum metabolites, 79 and 103 were significantly upregulated and downregulated, respectively, in the HDN group (Figure 6D). The top 10 differential downregulated metabolites in the HDN group were dihydroroseoside, equol, taurochenodeoxycholic acid (sodium salt), myricetin, taurochenodeoxycholic acid, 18-β-glycyrrhetinic acid, sulfaquinoxaline, calcitriol, 3-(2-naphthyl)-D-alanine, and taurocholic acid (Supplementary Table 5).

3.5 Differences between HDN and sham groups by multi-level analysis

Among differential metabolic pathways involved in HDN development identified using KEGG analysis, 69 regulated

10.3389/fmicb.2024.1356176

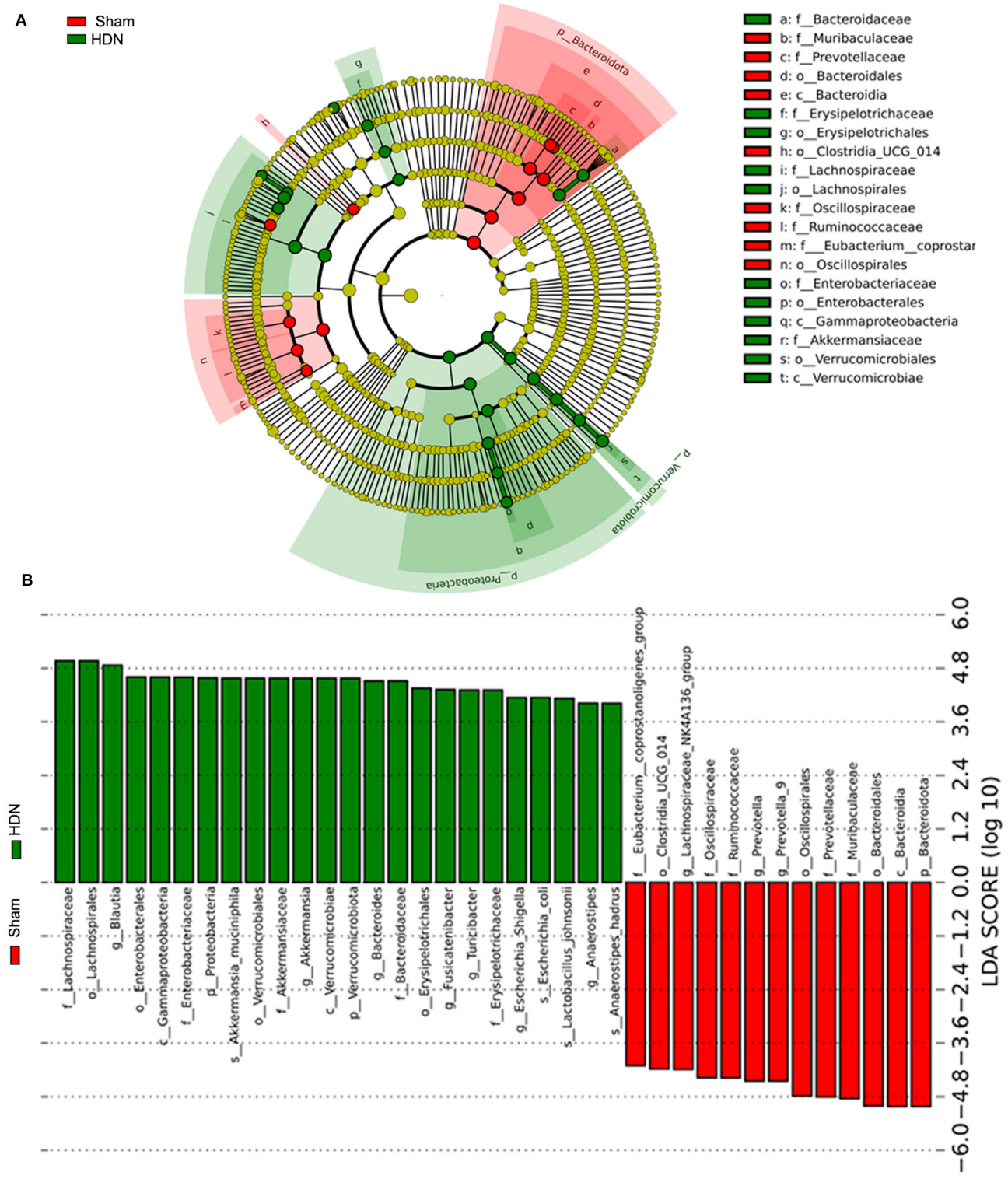

FIGURE 4
Findings of LEfSe. **(A)** Cladogram shows phylogenetic distribution of microbiota in sham and HDN groups. **(B)** Histogram of LDA scores shows effective size and rank of differentially abundant taxa. Green and red, HDN and sham groups, respectively ($n = 10$; LDA score > 4.0). HDN, hypertension and diabetic nephropathy; LDA, linear discriminant analysis; LEfSe, linear discriminant analysis effect size.

synthesis of fecal metabolites (Supplementary Table 6). Biosynthesis of unsaturated fatty acid pathways were significantly relevant to fecal metabolic alterations (Figure 7A). Among the fecal metabolites, stearic, palmitic, docosanoic, arachidonic, docosapentaenoic, arachidic, and docosahexaenoic acids represented the biosynthesis of unsaturated fatty acids pathway.

FIGURE 5
Cluster heat map of relative abundance of 35 genera. **(A)** Thirty-five OTUs are distributed at the phylum and genera levels. **(B)** Heat map shows relative abundance of differential OTUs between HDN and sham groups. Data were compared using Wilcoxon rank sum tests. Z-transformation is shown from low (blue) to high (red) abundance. HDN, hypertension and diabetic nephropathy; OTUs, operational taxonomic units.

A heat map revealed many correlations between gut microbial genera and distinct metabolites, as shown in Figure 7B, *Blautia*, *Fusicatenibacter* and *Bacteroides* was negatively correlated with Docosapentaenoic acid, Docosahexaenoic acid, Arachidonic acid, Palmitic acid, Arachidic acid, Stearic acid and Docosanoic Acid; *Prevotella* was positively correlated with above metabolites. The

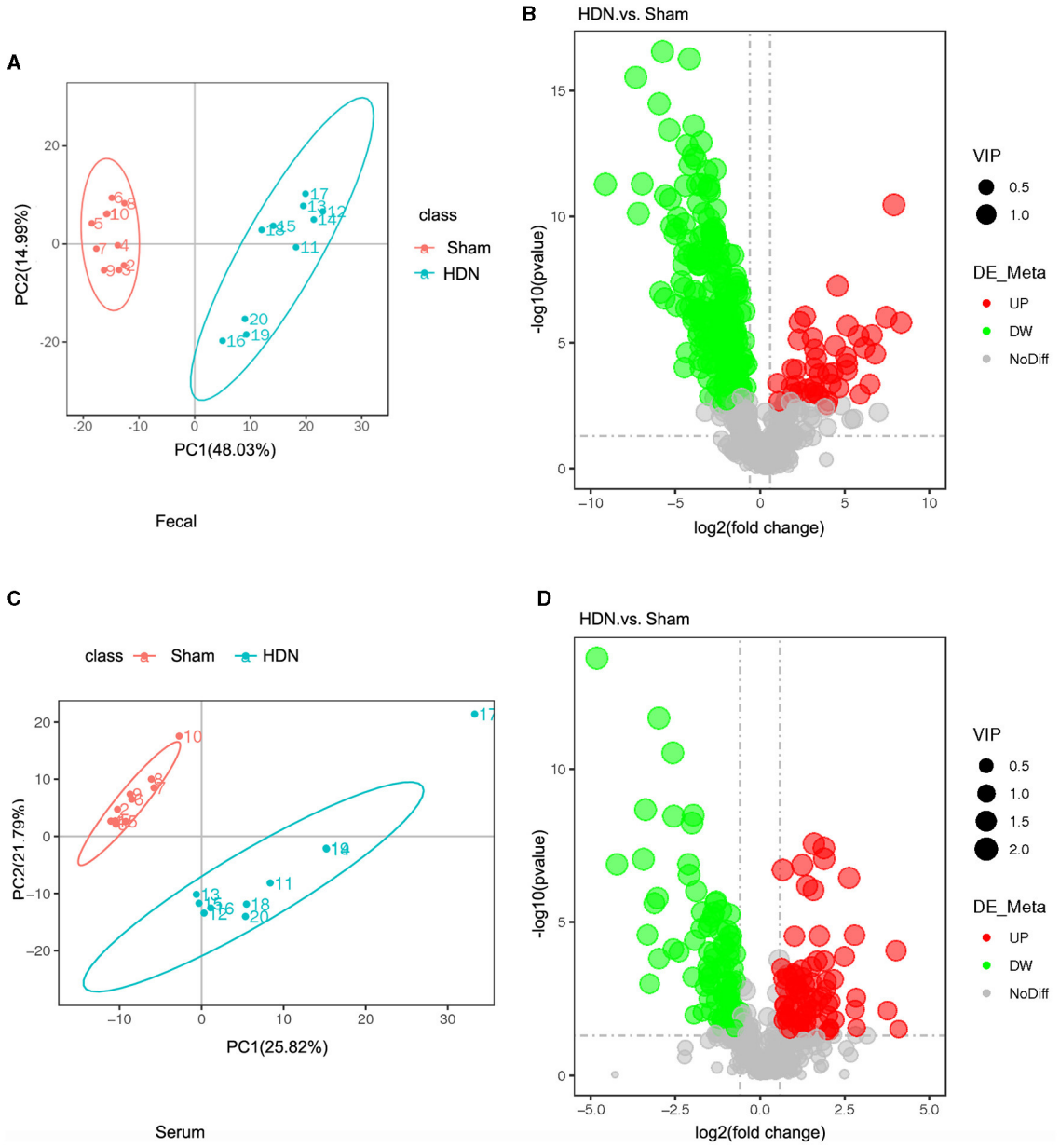

FIGURE 6
Fecal and serum metabolites differed between HDN and sham rats. **(A)** OPLS-DA scores and **(B)** volcano plot of fecal metabolites. **(C)** OPLS-DA scores and **(D)** volcano plot of serum metabolite (VIP > 1; $|P_{corr}| \geq 0.5$). HDN, hypertension and diabetic nephropathy; OPLS-DA, Orthogonal Projections to Latent Structures with Discriminant Analysis; VIP, variable importance in projection.

findings of fecal metabolomic and 16S analyses showed that docosahexaenoic acid ($r = -0.811$), palmitic acid ($r = -0.818$), stearic acid ($r = -0.813$) negatively correlated with the prevalence *Blautia* (Supplementary Table 7).

The KEGG analysis revealed 36 pathways that participated in serum metabolite synthesis (Supplementary Table 8). The cholesterol metabolism and primary bile acid biosynthesis pathways were significantly associated with serum metabolic alterations (Figure 8A). Among serum metabolites, taurochenodeoxycholic, taurocholic, and glycocholic acids represented the cholesterol metabolism pathway, and taurochenodeoxycholic, taurocholic, cholic, and glycocholic acids represented the primary bile acid biosynthesis pathway. Bile acids change the abundance of the microbiota by promoting the proliferation of bile-metabolizing bacteria and inhibiting the proliferation of bile-sensitive bacteria (Sayin et al., 2013). The microbiota can also regulate bile acid synthesis (Abenavoli et al., 2019). Therefore, we further analyzed relationships between the microbiota and bile acids. A heat map shows correlations between serum metabolites and gut microbial genera (Figure 8B). Taurochenodeoxycholic acid correlated negatively with the prevalence of *Blautia* ($r = -0.815$), and taurochenodeoxycholic acid correlated positively with Lachnospiraceae ($r = 0.831$) and *Prevotella* ($r = 0.832$) (Supplementary Table 9).

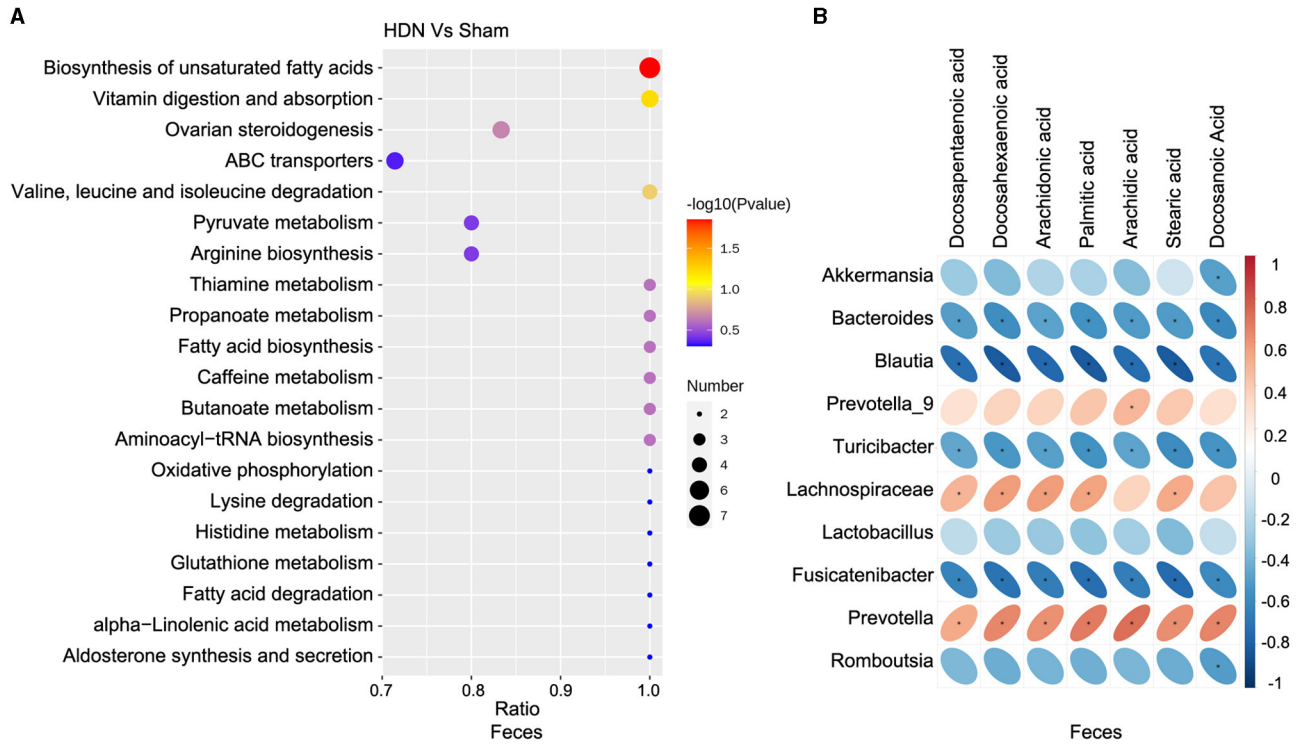

FIGURE 7
Correlations between microbiota and fecal metabolites. **(A)** Fecal metabolic changes in most relevant KEGG pathways. **(B)** Positive (red) and negative (blue) correlations between microbiota and fecal metabolites. *$P < 0.05$. KEGG, Kyoto Encyclopedia of Genes and Genomes.

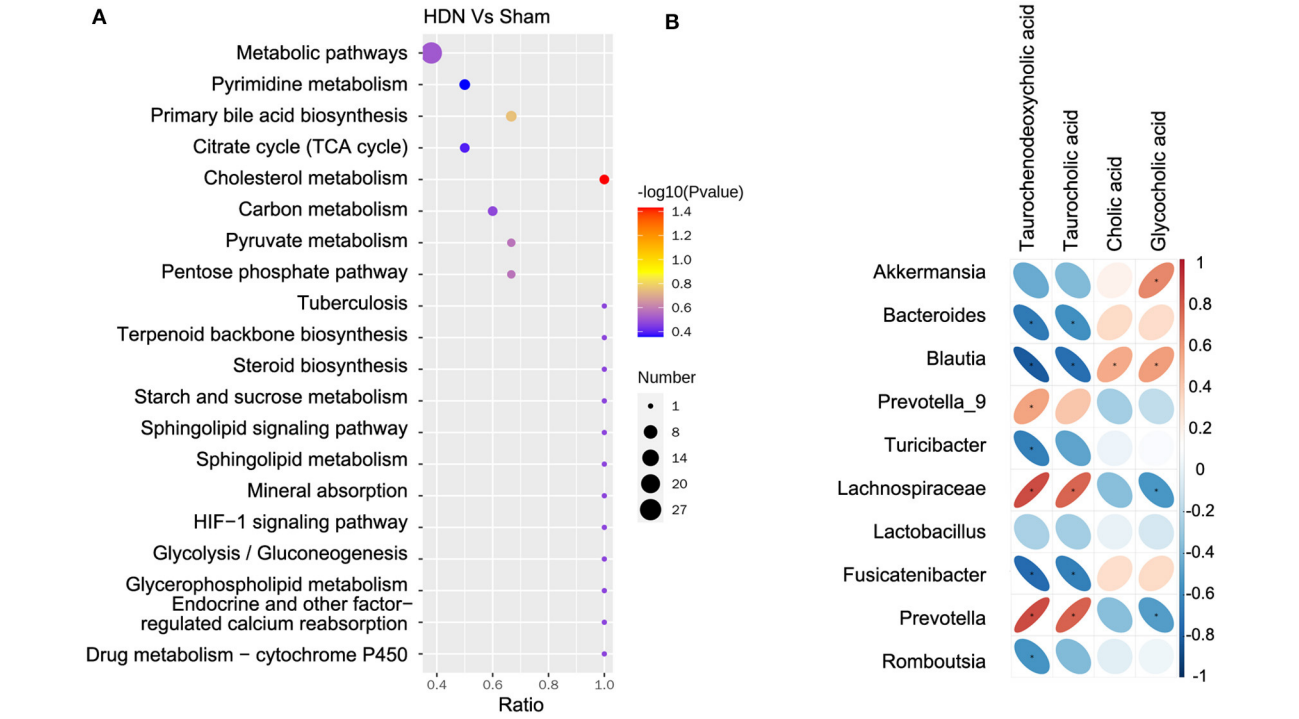

FIGURE 8
Correlations between microbiota and serum metabolites. **(A)** Serum metabolite changes in most relevant KEGG pathways. **(B)** Positive (red) and negative (blue) correlations between microbiota and serum metabolites. *$P < 0.05$. KEGG, Kyoto Encyclopedia of Genes and Genomes.

4 Discussion

In the current research, we compared changes in the composition and function of gut microbiota in HDN and sham rats using 16S rRNA gene sequencing, we further explored the relationship and function between microbiota and metabolites. Our results indicate that the metabolic spectrum, composition, and structure of the gut microbiota significantly differed between HDN and sham rats. The F/B ratio was notably higher in the HDN group than in the sham group. The abundance of *Proteobacteria* and *Verrucomicrobia* was substantially higher, whereas that of *Bacteroidetes* was significant lower in the HDN group than in the sham group. *Akkermansia*, *Bacteroides*, *Blautia*, *Turicibacter*, *Lactobacillus*, *Romboutsia, and Fusicatenibacter* were the most abundant, and *Prevotella, Lachnospiraceae_NK4A136_group*, and *Prevotella_9* were the least abundant in the HDN group. Further analysis with bile acid metabolites in serum showed that *Blautia* was negatively correlated with taurochenodeoxycholic acid, taurocholic acid, positively correlated with cholic acid and glycocholic acid in serum.

The F/B ratio is an indicator that typically reflects the dysbiosis of gut microbiota in various metabolic diseases, changes in this ratio can lead to a range of illnesses (Abenavoli et al., 2019). The F/B ratio was notably higher in the HDN group than in the sham group. *Bacteroidetes* was significant lower in the HDN group than in the sham group. Consistent with our results, the abundance of *Bacteroides* is decreased in patients with T2DM (Yamaguchi et al., 2016), and *Bacteroides* supplementation improves insulin resistance in diabetic mice (Yang et al., 2017). *Bacteroides* is a protective bacterium that plays a crucial role in glucose metabolism. *Bacteroidetes* produces short chain fatty acids, enhancing the function of the intestinal barrier (Chen et al., 2021).Short chain fatty acids, especially butyric acid, can activate GPR43, PPAR-γ, RASS system (Maslowski et al., 2009; Bolognini et al., 2016; Stino and Smith, 2017; Wysocki et al., 2017), lack of *Bacteroidetes* may promote the occurrence and development of HDN by activating GPR43, PPAR-γ, RASS system.

Proteobacteria are frontline responders that are sensitive to environmental factors such as diet (Shin et al., 2015). Excessive *Proteobacteria* growth is associated with inflammatory bowel disease and metabolic syndrome (Lavelle et al., 2015). Our findings on *Proteobacteria* was substantially higher are consistent with those of a meta-analysis of 578 patients with diabetic kidney disease (DKD) and 444 healthy persons (Wang et al., 2022), which revealed an enriched relative abundance of Proteobacteria in patients with DKD compared with healthy individuals.

We also found enriched abundance of *Akkermansia muciniphila* (phylum *Verrucomicrobia*) in the HDN group, *Akkermansia* aids in the development and preservation of the intestinal mucus layer, improves the functionality of the intestinal barrier, inhibits the proliferation of detrimental bacteria, and diminishes the concentration of intestinal endotoxins, thus protecting intestinal health (Zheng et al., 2023). *Akkermansia* reduces the risk of obesity, diabetes, enteritis, colon cancer and other diseases (Li et al., 2023; Zheng et al., 2023). However, the abundance of *A. muciniphila* is increased in experimental animals and humans with CKD (Lakshmanan et al., 2021), accompanied by an increase in indoxyl sulfate and p-cresyl sulfate (pCS). *A. muciniphila* in renal hypertension caused by CKD enhances the progression of renal hypertension by promoting inflammation (Lau et al., 2018). The inflammatory response is more active in renal hypertension (Rodriguez-Iturbe and Johnson, 2010), which might increase the abundance of *A. muciniphila*. Salt retention, endothelial dysfunction, volume overload, and abnormal hormone levels might results in HDN (Ku et al., 2019), these may increase mucus foraging in intestinal mucus layer. Besides that, in our HDN rat model, lack of fiber diet may lead to increased mucus foraging and increasing *Akkermansia* relative abundance.

Blautia was significantly more abundant in the HDN group, in direct proportion to various bile acids (BAs). *Blautia* is involved in converting primary to secondary Bas (Vojinovic et al., 2019). BAs exert toxic effects on the liver, kidney, intestine, stomach, and cardiovascular endothelial cells (Perez and Briz, 2009). BAs also regulating the activation of farnesoid X receptor (FXR), G protein-coupled 5 receptor, vitamin D receptor and pregnane X receptor (Wahlstrom et al., 2016). FXR, interacts with bile acids, haspotential protective effects on inflammatory and fibrotic damage in the CKD (Glastras et al., 2015). Researchers have used the FXR/TGR5 agonist int-767 to treat db/db mice, which can improve proteinuria, prevent podocyte damage, mesangial dilation, and renal tubulointerstitial fibrosis (Wang et al., 2018). In rats, taurochenodeoxycholic acid acts as an agonist of FXR in rats (Parks et al., 1999), cholic acid has an antagonistic effect on FXR, and the gut microbiota of mice benefits FXR signaling by reducing cholic acid (Sayin et al., 2013). In the present study, serum cholic acid was increased in HDN, which is positively correlated with the *Blautia* microbiota in feces, whereas taurochenodeoxycholic acid was decreased in HDN, negatively correlated with the *Blautia* microbiota in feces, suggesting that *Blautia* promotes HDN progression through the FXR signaling pathway regulated by bile acid metabolism. *Blautia* regulates the pathogenesis of HDN via the microorganism - gut - metabolite axis.

5 Conclusions

A disordered intestinal microbiota is closely associated with HDN. The F/B ratio was significantly increased in the HDN group, compared with the sham group. The most abundant bacteria in HDN were *Akkermansia*, *Bacteroides*, *Blautia*, *Turicibacter*, *Lactobacillus*, *Fusicatenibacter*, and *Romboutsia*; the least abundant flora were *Prevotella_9, Lachnospiraceae_NK4A136_group*, and *Prevotella*. Among them, *Blautia* is an important inducer of HDN. *Blautia* was negatively correlated with taurochenodeoxycholic acid, taurocholic acid, positively correlated with cholic acid, and glycocholic acid in serum, which might regulate pathogenesis through the microorganism – gut – metabolite axis. However, the present study has a limitation. It is the relatively small sample size of the study. Our finding of a correlation between intestinal microbiota and metabolites in HDN might pave the way toward therapy targeting the intestinal microbiota of patients with HDN.

Data availability statement

The data presented in the study are deposited in the figshare repository, accession number is 10.6084/m9.figshare.25623453.

Ethics statement

The animal study was approved by the Institutional Animal Care and Use Committee of Shengjing Hospital of China Medical University (Shenyang, China). The study was conducted in accordance with the local legislation and institutional requirements.

Author contributions

DP: Writing – review & editing, Writing – original draft, Supervision, Funding acquisition, Conceptualization. JL: Writing – review & editing, Writing – original draft, Methodology, Funding acquisition, Formal analysis, Conceptualization. XG: Writing – review & editing, Writing – original draft, Formal analysis, Data curation. CZ: Data curation, Supervision, Writing – original draft, Writing – review & editing. TY: Writing – review & editing, Writing – original draft, Methodology, Investigation, Formal analysis.

Funding

The author(s) declare financial support was received for the research, authorship, and/or publication of this article. This work was supported by Supporting the Liaoning Province Applied Basic Research Program (no. 2022JH2/101500060), High Quality Development Science and Technology Fund Project of China Medical University (2023020779-JH2/202), Liaoning Province Education Science Planning Project (no. JG21DB544), and 345 Talent Project of Shengjing Hospital of China Medical University (no. M0681).

Conflict of interest

The authors declare that the research was conducted in the absence of any commercial or financial relationships that could be construed as a potential conflict of interest.

Publisher's note

All claims expressed in this article are solely those of the authors and do not necessarily represent those of their affiliated organizations, or those of the publisher, the editors and the reviewers. Any product that may be evaluated in this article, or claim that may be made by its manufacturer, is not guaranteed or endorsed by the publisher.

Supplementary material

The Supplementary Material for this article can be found online at: https://www.frontiersin.org/articles/10.3389/fmicb.2024.1356176/full#supplementary-material

References

Abenavoli, L., Scarpellini, E., Colica, C., Boccuto, L., Salehi, B., Sharifi-Rad, J., et al. (2019). Gut microbiota and obesity: a role for probiotics. *Nutrients* 11:2690. doi: 10.3390/nu11112690

Bolognini, D., Tobin, A. B., Milligan, G., and Moss, C. E. (2016). The pharmacology and function of receptors for short-chain fatty acids. *Mol. Pharmacol.* 89, 388–398. doi: 10.1124/mol.115.102301

Brownrigg, J. R., Hughes, C. O., Burleigh, D., Karthikesalingam, A., Patterson, B. O., Holt, P. J., et al. (2016). Microvascular disease and risk of cardiovascular events among individuals with type 2 diabetes: a population-level cohort study. *Lancet Diab. Endocrinol.* 4, 588–597. doi: 10.1016/S2213-8587(16)30057-2

Chen, X., Dai, W., Li, H., Yan, Z., Liu, Z., He, L., et al. (2023). Targeted drug delivery strategy: a bridge to the therapy of diabetic kidney disease. *Drug Deliv.* 30:2160518. doi: 10.1080/10717544.2022.2160518

Chen, Y., Zhou, J., and Wang, L. (2021). Role and mechanism of gut microbiota in human disease. *Front. Cell Infect Microbiol.* 11:625913. doi: 10.3389/fcimb.2021.625913

Gentile, C. L., and Weir, T. L. (2018). The gut microbiota at the intersection of diet and human health. *Science* 362, 776–780. doi: 10.1126/science.aau5812

Glastras, S. J., Wong, M. G., Chen, H., Zhang, J., Zaky, A., Pollock, C. A., et al. (2015). FXR expression is associated with dysregulated glucose and lipid levels in the offspring kidney induced by maternal obesity. *Nutr. Metab.* 12:40. doi: 10.1186/s12986-015-0032-3

Izzo, R., de Simone, F., Chinali, G., Iaccarino, M., Trimarco, G., Rozza, V., et al. (2009). Insufficient control of blood pressure and incident diabetes. *Diabetes Care* 32, 845–850. doi: 10.2337/dc08-1881

Johansen, K. L., Chertow, G. M., Foley, R. N., Gilbertson, D. T., Herzog, C. A., Ishani, A., et al. (2021). US renal data system 2020 annual data report: epidemiology of kidney disease in the United States. *Am. J. Kidney Dis.* 77, A7–A8. doi: 10.1053/j.ajkd.2021.01.002

Ku, E., Lee, B. J., Wei, J., and Weir, M. R. (2019). Hypertension in CKD: core curriculum 2019. *Am. J. Kidney Dis.* 74, 120–131. doi: 10.1053/j.ajkd.2018.12.044

Lakshmanan, A. P., Al, Z. M., Ali, B. H., and Terranegra, A. (2021). The influence of the prebiotic gum acacia on the intestinal microbiome composition in rats with experimental chronic kidney disease. *Biomed. Pharmacother.* 133:110992. doi: 10.1016/j.biopha.2020.110992

Lau, W. L., Vaziri, N. D., Nunes, A., Comeau, A. M., Langille, M., England, W., et al. (2018). The phosphate binder ferric citrate alters the gut microbiome in rats with chronic kidney disease. *J. Pharmacol. Exp. Ther.* 367, 452–460. doi: 10.1124/jpet.118.251389

Lavelle, A., Lennon, G., O'Sullivan, O., Docherty, N., Balfe, A., Maguire, A., et al. (2015). Spatial variation of the colonic microbiota in patients with ulcerative colitis and control volunteers. *Gut* 64, 1553–1561. doi: 10.1136/gutjnl-2014-307873

Li, J., Yang, G., Zhang, Q., Liu, Z., Jiang, X., Xin, Y., et al. (2023). Function of Akkermansia muciniphila in type 2 diabetes and related diseases. *Front. Microbiol.* 14:1172400. doi: 10.3389/fmicb.2023.1172400

Li, Y., Su, X., Gao, Y., Lv, C., Gao, Z., Liu, Y., et al. (2020). The potential role of the gut microbiota in modulating renal function in experimental diabetic nephropathy murine models established in same environment. *Biochim. Biophys. Acta Mol. Basis Dis.* 1866:165764. doi: 10.1016/j.bbadis.2020.165764

Lucas, S. E., Walton, S. L., Mirabito, C. K., Mileto, S. J., Lyras, D., Denton, K. M., et al. (2023). Antihypertensives and antibiotics: impact on intestinal dysfunction and hypertension. *Hypertension* 80, 1393–1402. doi: 10.1161/HYPERTENSIONAHA.122.20073

Luo, M., Cai, J., Luo, S., Hong, X., Xu, L., Lin, H., et al. (2023). Causal effects of gut microbiota on the risk of chronic kidney disease: a Mendelian randomization study. *Front. Cell Infect Microbiol.* 13:1142140. doi: 10.3389/fcimb.2023.1142140

Ma, R. (2018). Epidemiology of diabetes and diabetic complications in China. *Diabetologia* 61, 1249–1260. doi: 10.1007/s00125-018-4557-7

Mao, Z. H., Gao, Z. X., Liu, D. W., Liu, Z. S., and Wu, P. (2023). Gut microbiota and its metabolites - molecular mechanisms and management strategies in diabetic kidney disease. *Front. Immunol.* 14:1124704. doi: 10.3389/fimmu.2023.1124704

Maslowski, K. M., Vieira, A. T., Ng, A., Kranich, J., Sierro, F., Yu, D., et al. (2009). Regulation of inflammatory responses by gut microbiota and chemoattractant receptor GPR43. *Nature* 461, 1282–1286. doi: 10.1038/nature08530

Murray, C. J., and Lopez, A. D. (2013). Measuring the global burden of disease. *N. Engl. J. Med.* 369, 448–457. doi: 10.1056/NEJMra1201534

Parks, D. J., Blanchard, S. G., Bledsoe, R. K., Chandra, G., Consler, T. G., Kliewer, S. A., et al. (1999). Bile acids: natural ligands for an orphan nuclear receptor. *Science* 284, 1365–1368. doi: 10.1126/science.284.5418.1365

Perez, M. J., and Briz, O. (2009). Bile-acid-induced cell injury and protection. *World J. Gastroenterol.* 15, 1677–1689. doi: 10.3748/wjg.15.1677

Rodriguez-Iturbe, B., and Johnson, R. J. (2010). The role of renal microvascular disease and interstitial inflammation in salt-sensitive hypertension. *Hypertens. Res.* 33, 975–980. doi: 10.1038/hr.2010.148

Sabuncu, T., Sonmez, A., Eren, M. A., Sahin, I., Corapcioglu, D., Ucler, R., et al. (2021). Characteristics of patients with hypertension in a population with type 2 diabetes mellitus. Results from the Turkish Nationwide SurvEy of Glycemic and Other Metabolic Parameters of Patients with Diabetes Mellitus (TEMD Hypertension Study). *Prim Care Diab.* 15, 332–339. doi: 10.1016/j.pcd.2020.11.001

Sayin, S. I., Wahlstrom, A., Felin, J., Jantti, S., Marschall, H. U., Bamberg, K., et al. (2013). Gut microbiota regulates bile acid metabolism by reducing the levels of tauro-beta-muricholic acid, a naturally occurring FXR antagonist. *Cell Metab.* 17, 225–235. doi: 10.1016/j.cmet.2013.01.003

Shin, N. R., Whon, T. W., and Bae, J. W. (2015). Proteobacteria: microbial signature of dysbiosis in gut microbiota. *Trends Biotechnol.* 33, 496–503. doi: 10.1016/j.tibtech.2015.06.011

Stino, A. M., and Smith, A. G. (2017). Peripheral neuropathy in prediabetes and the metabolic syndrome. *J. Diabetes Investig.* 8, 646–655. doi: 10.1111/jdi.12650

Sun, H., Saeedi, P., Karuranga, S., Pinkepank, M., Ogurtsova, K., Duncan, B.B., et al. (2022). IDF Diabetes Atlas: Global, regional and country-level diabetes prevalence estimates for 2021 and projections for 2045. *Diabetes Res. Clin. Pract.* 183:109119. doi: 10.1016/j.diabres.2021.109119

Vojinovic, D., Radjabzadeh, D., Kurilshikov, A., Amin, N., Wijmenga, C., Franke, L., et al. (2019). Relationship between gut microbiota and circulating metabolites in population-based cohorts. *Nat. Commun.* 10:5813. doi: 10.1038/s41467-019-13721-1

Wahlstrom, A., Sayin, S. I., Marschall, H. U., and Backhed, F. (2016). Intestinal crosstalk between bile acids and microbiota and its impact on host metabolism. *Cell Metab.* 24, 41–50. doi: 10.1016/j.cmet.2016.05.005

Wang, X. X., Wang, D., Luo, Y., Myakala, K., Dobrinskikh, E., Rosenberg, A. Z., et al. (2018). FXR/TGR5 dual agonist prevents progression of nephropathy in diabetes and obesity. *J. Am. Soc. Nephrol.* 29, 118–137. doi: 10.1681/ASN.2017020222

Wang, Y., Zhao, J., Qin, Y., Yu, Z., Zhang, Y., Ning, X., et al. (2022). The specific alteration of gut microbiota in diabetic kidney diseases-a systematic review and meta-analysis. *Front. Immunol.* 13:908219. doi: 10.3389/fimmu.2022.908219

Wikoff, W. R., Anfora, A. T., Liu, J., Schultz, P. G., Lesley, S. A., Peters, E. C., et al. (2009). Metabolomics analysis reveals large effects of gut microflora on mammalian blood metabolites. *Proc. Natl. Acad. Sci. U. S. A.* 106, 3698–3703. doi: 10.1073/pnas.0812874106

Wu, J., Yang, K., Fan, H., Wei, M., and Xiong, Q. (2023). Targeting the gut microbiota and its metabolites for type 2 diabetes mellitus. *Front. Endocrinol.* 14:1114424. doi: 10.3389/fendo.2023.1114424

Wysocki, J., Ye, M., Khattab, A. M., Fogo, A., Martin, A., David, N. V., et al. (2017). Angiotensin-converting enzyme 2 amplification limited to the circulation does not protect mice from development of diabetic nephropathy. *Kidney Int.* 91, 1336–1346. doi: 10.1016/j.kint.2016.09.032

Yamaguchi, Y., Adachi, K., Sugiyama, T., Shimozato, A., Ebi, M., Ogasawara, N., et al. (2016). Association of intestinal microbiota with metabolic markers and dietary habits in patients with type 2 diabetes. *Digestion* 94, 66–72. doi: 10.1159/000447690

Yang, J. Y., Lee, Y. S., Kim, Y., Lee, S. H., Ryu, S., Fukuda, S., et al. (2017). Gut commensal Bacteroides acidifaciens prevents obesity and improves insulin sensitivity in mice. *Mucosal. Immunol.* 10, 104–116. doi: 10.1038/mi.2016.42

Yang, T., Santisteban, M. M., Rodriguez, V., Li, E., Ahmari, N., Carvajal, J. M., et al. (2015). Gut dysbiosis is linked to hypertension. *Hypertension* 65, 1331–1340. doi: 10.1161/HYPERTENSIONAHA.115.05315

Yen, F. S., Wei, J. C., Chiu, L. T., Hsu, C. C., and Hwu, C. M. (2022). Diabetes, hypertension, and cardiovascular disease development. *J. Transl. Med.* 20:9. doi: 10.1186/s12967-021-03217-2

Zhao, H., Yang, C. E., Liu, T., Zhang, M. X., Niu, Y., Wang, M., et al. (2023). The roles of gut microbiota and its metabolites in diabetic nephropathy. *Front. Microbiol.* 14:1207132. doi: 10.3389/fmicb.2023.1207132

Zheng, T., Hao, H., Liu, Q., Li, J., Yao, Y., Liu, Y., et al. (2023). Effect of extracelluar vesicles derived from akkermansia muciniphila on intestinal barrier in colitis mice. *Nutrients* 15:22. doi: 10.3390/nu15224722

frontiers | Frontiers in Microbiology

TYPE Original Research
PUBLISHED 26 June 2024
DOI 10.3389/fmicb.2024.1421209

OPEN ACCESS

EDITED BY
Ren-You Gan,
Agency for Science, Technology and Research, Singapore

REVIEWED BY
Liew Pui Pui Winnie,
University of Putra Malaysia, Malaysia
Ruheea Taskin Ruhee,
Waseda University, Japan

*CORRESPONDENCE
Yuhua Yang
✉ yangyuhua20230808@163.com

RECEIVED 22 April 2024
ACCEPTED 30 May 2024
PUBLISHED 26 June 2024

CITATION
Yang X, Wang Y and Yang Y (2024) Impact of *Pediococcus pentosaceus* YF01 on the exercise capacity of mice through the regulation of oxidative stress and alteration of gut microbiota. *Front. Microbiol.* 15:1421209. doi: 10.3389/fmicb.2024.1421209

Impact of *Pediococcus pentosaceus* YF01 on the exercise capacity of mice through the regulation of oxidative stress and alteration of gut microbiota

Xiaoguang Yang[1], Yeni Wang[2] and Yuhua Yang[3]*

[1]School of Physical Education, Yan'an University, Yan'an, Shaanxi, China, [2]Ministry of Sports, Xiamen Institute of Technology, Xiamen, Fujian, China, [3]Department of Social Sports Management, College of Humanities and Law, Beijing University of Chemical Technology, Beijing, China

Using treadmill training, this study replicated human exercise conditions and triggered exercise-induced fatigue in mice to examine the potential of *Pediococcus pentosaceus* YF01 in delaying this fatigue by regulating oxidative stress and its impact on the exercise capacity and gut microbiota of mice. The exercise capacity of mice was tested by conducting exhaustion tests, determining histopathological changes in mouse tissues, detecting the levels of serum biochemical markers, and evaluating the mRNA expression levels of relevant genes. YF01 prolonged the exhaustion time of mice, increased the serum levels of oxidative stress-related markers T-AOC, CAT, and GSH, as well as GLU and LA levels in the mice. YF01 decreased the levels of hepatic-related markers AST and ALT, as well as exercise-related markers LDH, BUN, UA, and CRE in the mice. YF01 upregulated the mRNA expression of MyHc I, SIRT1, and PGC in muscle tissues, as well as SOD1, SOD2, and CAT in both liver and muscle tissues. YF01 also downregulated the mRNA expression of MyHc IIa, MyHc IIb, and MyHc IIx in muscle tissues. Furthermore, YF01 increased the abundance of beneficial bacteria such as *Lactobacillus* and *Lachnospiraceae* in the gut microbiota of mice. In conclusion, *P. pentosaceus* YF01 may affect the exercise capacity of mice by modulating oxidative stress levels, thereby offering novel ideas for developing of sports science and human health.

KEYWORDS

***Pediococcus pentosaceus*, gut microbiota, oxidative stress, exercise capacity, lactic acid bacteria**

1 Introduction

The benefits of exercise for physical and mental health are well-known (Begdache et al., 2020; Das and Gailey, 2022). Exercise has become increasingly crucial because of the advancement of society and the improvement of living standards. Research on exercise capacity has consistently attracted considerable attention. Physical exercise is extensively

recognized as an effective means of maintaining physical health and helps in strengthening the body, improving immunity, enhancing cardiovascular and respiratory functions, etc. (Fiuza-Luces et al., 2018; Shao et al., 2021). Furthermore, doping is prohibited among professional athletes (Morente-Sanchez and Zabala, 2013). Therefore, long-term intake of certain foods, such as probiotics, to improve exercise capacity is a more feasible approach. The mouse treadmill model is commonly used in experiments to evaluate the exercise ability, endurance, and coordination of mice (Cai et al., 2018). We used a mouse treadmill model to simulate human exercise training and explore the impact of *Pediococcus pentosaceus* on exercise capacity.

Oxidative stress significantly influences exercise capacity during physical activity (McLeay et al., 2017). It damages proteins, lipids, and DNA by inducing an imbalance in the cellular redox state, characterized by increased levels of reactive oxygen species (ROS) (Lushchak, 2014). Excessive oxidative stress accelerates cellular aging and causes a decline in organ function, thereby affecting the normal metabolism and exercise capacity of the body (Liguori et al., 2018). While performing physical exercise or other forms of activity, an individual's body is in a high-intensity metabolic state, which elevates cellular oxidative stress levels (Powers and Jackson, 2008). As the physical activity escalates, the level of cellular oxidative stress also increases, which may induce excess ROS production, thereby harming the cells and body (He et al., 2016). On the other hand, moderate oxidative stress promotes the body's adaptation to continuous exercise, improves exercise performance, and augments physical endurance (Simioni et al., 2018). Therefore, a balance in oxidative stress must be maintained for good human health.

Pediococcus pentosaceus is a lactic acid bacteria (LAB) commonly used for producing fermented foods such as kimchi, sauerkraut, and certain types of sourdough bread (Qi et al., 2021). This LAB is known to produce lactic acid, which contributes to food preservation and fermentation (Nanasombat et al., 2017). It is used as a probiotic in various dairy products and supplements because of its potential health benefits, including promoting gut health and boosting the immune system (Erten et al., 2014; Pan et al., 2021). Different *P. pentosaceus* strains may exhibit diverse characteristics and applications in food fermentation and probiotic use. This LAB can modulate oxidative stress levels. *P. pentosaceus* decreased ROS production by affecting the cellular redox equilibrium, thus alleviating the adverse effects of oxidative stress on the body (Kim et al., 2019). Nevertheless, the impact of *P. pentosaceus* on physical performance has not been exhaustively examined. Therefore, this study investigates *P. pentosaceus* YF01 to determine if it affects exercise capacity in mice by modulating oxidative stress.

The intestine is an important organ for maintaining health balance, and there is a close connection between the gut microbiota of mice and their exercise performance. Certain intestinal microbiota can produce excitatory neurotransmitters that promote exercise performance, such as norepinephrine and dopamine, providing energy to intestinal epithelial cells (Bao et al., 2019). Other studies have indicated that there is a close and coordinated relationship between gut microbiota and host metabolism, energy utilization, and storage (Nicholson et al., 2012). Hence, maintaining a healthy gut microbiota may help improve exercise performance. Adjusting diet, supplementing with probiotics, or other methods to promote a balance in gut microbiota can assist in improving metabolic status, enhancing immune function, and consequently improving exercise performance.

Through experimental observation and data analysis on mice, we elucidated the specific mechanisms through which YF01 affects oxidative stress levels and exercise performance in mice. The study findings will contribute to the understanding of the role of oxidative stress during exercise, thereby offering a scientific basis for identifying new strategies for augmenting exercise performance and maintaining good health. By exploring the potential application of YF01 as an oxidative stress modulator in exercise, we intend to contribute to sports science development and provide novel insights and theoretical foundations for human health.

2 Materials and methods

2.1 Strain preparation

This study used LAB isolated and purified from fermented kimchi in Sangou Village, Dawan Town, Yubei, Chongqing, as the experimental strain. The 16S rDNA analysis revealed that this strain belonged to *P. pentosaceus*, with Gram staining unveiling its colony morphology. China General Microbiological Culture Collection Center (CGMCC, Beijing) has preserved it as *P. pentosaceus* YF01 with preservation number 29920. Before conducting the subsequent experiments, the preserved strain was reactivated by inoculating 2% inoculum in MRS liquid medium for 16–24 h at 37°C.

2.2 Tolerance of the experimental strain in artificial gastric fluid

To prepare the artificial gastric fluid, 0.2% NaCl and 0.35% pepsin were used (Beijing Solarbio Biotechnology Co. Ltd., Beijing, China), with the pH of the fluid adjusted to 3.0 with 1 mol/L HCl after preparation. The solution was filtered through a 0.22-μm filter. Subsequently, a 5 ml sample of the activated bacterial culture was centrifuged at 3,000 rpm at room temperature for 10 min. The bacterial cells were collected after discarding the supernatant. They were then washed twice with sterile physiological saline. The cells were resuspended in 5 ml of physiological saline and adjusted to achieve a concentration of 1×10^8 colony-forming units (CFU)/ml. A 0-h time point sample was prepared by mixing the experimental bacterial suspension with the artificial gastric fluid at a 1:9 volumetric ratio. This mixture was shaken well, and 2 ml of the mixture was added to a 5 ml centrifuge tube. In the next step, the remaining 8 ml samples were shaken vertically at 37°C and at 50 rpm for 3 h in a constant-temperature air bath. Using 10-fold dilutions of the samples collected at 0 and 3 h, we determined the viable cell count. After the dilutions were plated on the MRS solid medium and incubated at 37°C for 48 h, CFUs were counted using the plate counting method (Pan et al., 2021). The survival rate was calculated using the following formula: Survival rate (%) = Number of viable cells at 3 h (CFU/ml) / Number of viable cells at 0 h (CFU/ml) × 100.

2.3 Evaluation of growth efficiency of an experimental strain in bile salts

Bacterial cultures were inoculated into an MRS-THIO medium containing varying levels of bovine bile salts at a 2% rate. A control medium with 0.00% bovine bile salts in MRS-THIO was also used. For 24 h, the cultures were incubated at 37°C in a constant-temperature incubator. At 600 nm, a spectrophotometer was used to measure the absorbance (OD) of the cultures in media with different concentrations (Pan et al., 2021). The growth efficiency at different bile salt concentrations was calculated as follows: Growth efficiency (%) = Absorbance of medium containing bile salts at 600 nm / Absorbance of blank medium at 600 nm × 100.

2.4 Detection of the hydroxyl radical scavenging rate of experimental bacterial strain

A 5 ml activated bacterial culture was centrifuged in a 10 ml centrifuge tube for 10 min at 3,000 rpm. After the supernatant was discarded, bacterial cells were collected, washed twice with sterile physiological saline, resuspended in 5 ml of physiological saline, and adjusted to attain a concentration of 1×10^8 CFU/ml. The experiment was conducted according to the instructions provided in the hydroxyl radical scavenging rate detection kit (Leagene, Beijing, China).

2.5 Detection of the DPPH radical scavenging rate of the experimental bacterial strain

The activated bacterial culture was adjusted to 1×10^8 CFU/ml, and the experiment was conducted following the DPPH radical scavenging rate detection kit (Leagene).

2.6 Animal model

Forty Kunming mice (gender: male, age: 5 weeks, weight: 20 ± 2 g) were purchased from Chongqing Enswell Biotechnology Co., Ltd. All mice were housed in a temperature-controlled room (temperature: 25°C ± 2°C, relative humidity: 50% ± 5%, 12-h light/dark cycles), and were provided a standard mouse diet (Jiangsu Xietong Pharmaceutical Bio-engineering Co., Ltd., Jiangsu, China) and water *ad libitum*. A 1-week adaptation period was followed by 2 days of bedding replacement. The mice were randomly divided into four groups, each consisting of 10 mice: normal, control, Vc, and YF01. The experiment lasted for 29 days (Figure 1). In the first week, all mice received daily gavage treatment. The normal and control groups were gavaged with 0.1 ml/10 g of 0.9% saline. The Vc group received 0.1 ml/10 g of 200 mg/Kg Vitamin C (Vc) solution, as a positive control. The YF01 group received 0.1 ml/10 g of a 1.0×10^9 CFU/ml *P. pentosaceus* YF01 solution. In the second week, the mice underwent a 6-day adaptation training on a treadmill set at a 0° slope with a speed controlled at 10 m/min for 10 min per day. Gavage treatment was administered before each exercise/training session. In the third week, a 2-week endurance training was conducted on a 5° slope for 10 min per training session, with an acceleration of 1 m/min and a maximum speed of 10 m/min. Training was conducted for 6 days/week, with 1 rest day, followed by fasting for 16–24 h after the last gavage. In the fifth week (day 29), the exhaustion test was conducted, with its protocol including treadmill running at 0°, 10 m/min for 15 min; 5°, 10 m/min for 15 min; and 10°, 10 m/min until exhaustion, defined as the mouse being willing to endure electric shocks over 3 s for five times (1 mA current), or staying on the electrical grid for 5 s continuously. The exhaustion time was recorded when the mice reached exhaustion. After exhaustion, blood was immediately collected from the eye socket of the mice, and the liver and muscle tissues of the mice were isolated for further use. The Animal Ethics Committee of Beijing University of Chemical Technology approved all animal experiments.

2.7 H&E staining

Approximately half of the right liver lobe and half of the muscle tissues of the mice were excised, rinsed with saline solution, and fixed in a tissue fixative. After the tissues were rehydrated with ethanol, they were soaked in xylene and ethanol for approximately 30 min, embedded in paraffin, sectioned using a microtome, and mounted on glass slides. The cell morphology was analyzed using an optical microscope (BX43F, Olympus Co., Tokyo, Japan) after the cytoplasm was stained with hematoxylin and eosin (H&E) dyes (Pan et al., 2020).

2.8 Mice serum index detection

For later use, the mouse serum was centrifuged for 10 min at 4°C and 4,000 rpm, collected, and stored at −80°C. Following the manufacturer's recommended protocol, appropriate biochemical assay kits were used to determine the serum levels of total antioxidant capacity (T-AOC), catalase (CAT), glutathione (GSH), aspartate aminotransferase (AST), alanine aminotransferase (ALT), total protein (TP), albumin (Alb), glucose (GLU), LA, lactate dehydrogenase (LDH), blood urea nitrogen (BUN), uric acid (UA), and creatinine (CRE).

2.9 Real-time quantitative PCR

A SYBR Green assay was performed to determine mRNA expression in the mouse liver and skeletal muscle tissues. Approximately 100 mg of tissues were homogenized. Total RNA was extracted from the tissues by using the TRIzol reagent (ABclonal Technology Co., Ltd., Wuhan, China). Using a spectrophotometer (Allsheng Co., Hangzhou, China), the RNA concentration was measured. RNA was reverse transcribed with Hifair™ II 1st Strand cDNA Synthesis SuperMix for qPCR to obtain cDNA templates. Subsequently, amplification was performed using the StepOnePlus™ Real-Time PCR System

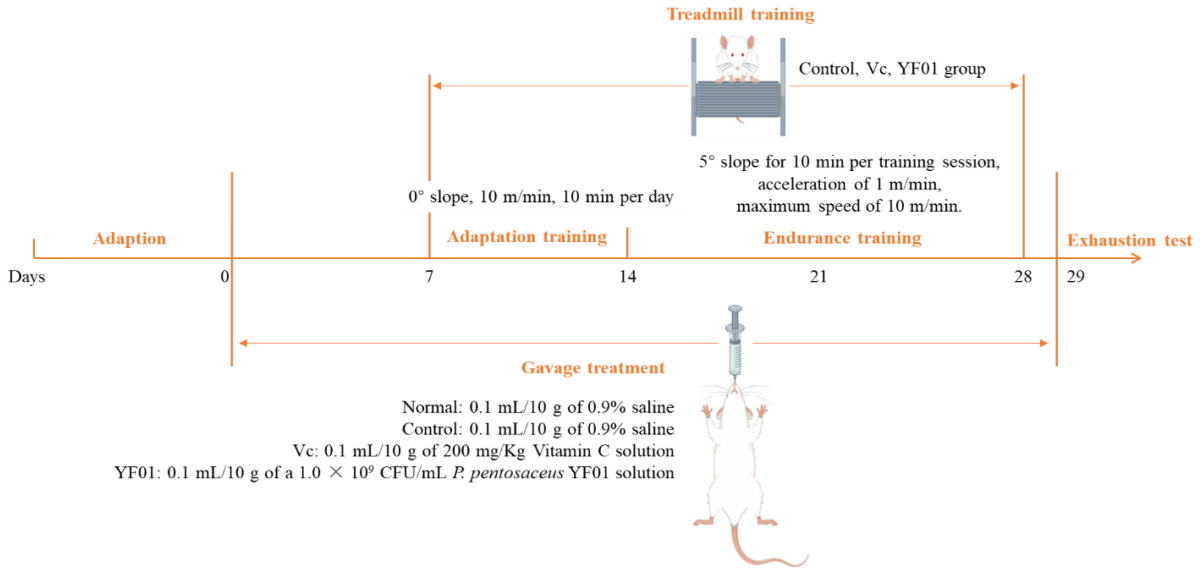

FIGURE 1
Timeline of the experiment.

(Thermo Fisher Scientific Inc., Waltham, MA, USA) comprising 10 μl SYBR Green PCR Master Mix, 1 μl of each primer, 1 μl of cDNA template, and 7 μl of DEPC. The cycling conditions were set as follows: 95°C for 3 min; 40 cycles of 95°C for 5 s, and 60°C for 30 s. The gene expression levels were determined by calculating the relative expression levels of each gene by using the $2^{-\Delta\Delta CT}$ method. This calculation included ββ-actin as the internal reference gene and CT representing the cycle threshold. Table 1 lists primer sequences used in this study.

TABLE 1 Primer names and sequences.

Gene name	Primer sequence
SOD1	F: 5′-AACCAGTTGTGTTGTCAGGAC-3′ R: 5′-CCACCATGTTTCTTAGAGTGAGG-3′
SOD2	F: 5′-CAGACCTGCCTTACGACTATGG-3′ R: 5′-CTCGGTGGCGTTGAGATTGTT-3′
CAT	F: 5′-GGAGGCGGGAACCCAATAG-3′ R: 5′-GTGTGCCATCTCGTCAGTGAA-3′
MycH I	F: 5′-ACTGTCAACACTAAGAGGGTCA-3′ R: 5′-TTGGATGATTTGATCTTCCAGGG-3′
MycH II a	F: 5′-TAAACGCAAGTGCCATTCCTG-3′ R: 5′-GGGTCCGGGTAATAAGCTGG-3′
MycH II b	F: 5′-CTTTGCTTACGTCAGTCAAGGT-3′ R: 5′-AGCGCCTGTGAGCTTGTAAA-3′
MycH II x	F: 5′-GCGAATCGAGGCTCAGAACAA-3′ R: 5′-GTAGTTCCGCCTTCGGTCTTG-3′
SIRT I	F: 5′-ATGACGCTGTGGCAGATTGTT-3′ R: 5′-CCGCAAGGCGAGCATAGAT-3′
PGC	F: 5′-TATGGAGTGACATAGAGTGTGCT-3′ R: 5′-CCACTTCAATCCACCCAGAAAG-3′
β-actin	F: 5′-ATGGAGCCGGACAGAAAAGC-3′ R: 5′-TGGGAGGTGTCAACATCTTCTT-3′

2.10 Gut microbiota analysis

The mouse fecal samples were extracted for genomic DNA using the magnetic bead method and the Soil and Fecal Genomic DNA Extraction Kit (TIANGEN BIOTECH CO., LTD., Beijing, China). Subsequently, 1% agarose gel electrophoresis was performed to assess the purity and concentration of the DNA. An appropriate amount of sample DNA was taken in a centrifuge tube and diluted with sterile water to a concentration of 1 ng/μl. All PCR mixtures were prepared by adding 15 μl of Phusion™ High-Fidelity PCR Master Mix (New England Biolabs), 0.2 μM primers (16S V4 region primers 515F and 806R), and 10 ng of genomic DNA template. The PCR amplification included an initial denaturation at 98°C for 1 min, followed by 30 cycles of denaturation at 98°C for 10 s, annealing at 50°C for 30 s, and extension at 72°C for 30 s, with a final extension at 72°C for 5 min. The PCR products were analyzed by electrophoresis on a 2% agarose gel. Qualified PCR products underwent magnetic bead purification, quantified using enzymatic methods, and pooled in equimolar concentrations based on the PCR product concentration. After thorough mixing, the PCR products were subjected to another round of electrophoresis on a 2% agarose gel. Target bands were purified using a universal DNA purification kit (TIANGEN). Library construction was carried out using the NEBNext® Ultra™ II FS DNA PCR-free Library Prep Kit (New England Biolabs). The constructed libraries were quantified with Qubit and Q-PCR, and after passing quality control, PE 250 sequencing was performed on the NovaSeq 6000 platform.

Split each sample data from the raw data based on the Barcode sequence and PCR amplification primer sequence. After trimming the Barcode and primer sequences, the reads of each sample were assembled using FLASH (Version 1.2.11[1])

1 http://ccb.jhu.edu/software/FLASH/

(Magoc and Salzberg, 2011), resulting in the assembled sequences as the Raw Tags. The assembled Raw Tags were subjected to rigorous filtering using fastp software (Version 0.23.1) to obtain high-quality Clean Tags (Bokulich et al., 2013). After the aforementioned processing, the Tags obtained need to undergo the removal of chimeric sequences. The Tags sequences are aligned with species annotation databases (Silva database[2] for 16S/18S, Unite database[3] for ITS) to detect chimeric sequences and ultimately remove them to obtain the Effective Tags (Edgar et al., 2011).

2.11 Data analysis

The averages of serum and tissue indices of each mouse were calculated from three or more parallel experiments. Data were analyzed using IBM SPSS 22 statistical software. Results are expressed as mean ± standard deviation. One-way ANOVA, followed by Duncan's multiple range test, was used to determine differences between the mean values of each group. Differences with a p-value of <0.05 were considered statistically significant.

3 Results

3.1 Biological morphology of the strain

YF01 exhibited opaque milky-white circular colonies on MRS solid culture medium, with smooth and raised surfaces and neat edges (Figure 2A). Gram staining revealed that YF01 was gram-positive (Figure 2B), and no spore production was noted.

3.2 *In vitro* bioactivity testing of the strain

The experimental results (Table 2) demonstrated that the viability of the experimental strain *P. pentosaceus* YF01 in the artificial gastric juice was 90.11% ± 2.44%, and the viabilities in 0.30%, 0.50%, and 1.00% bile salts were 27.22% ± 0.42%, 23.91% ± 0.21%, and 16.16% ± 0.18%, respectively. Additionally, the hydroxyl radical scavenging rate of YF01 was 19.24% ± 0.33%, and 14.73% ± 0.98% for the DPPH radical scavenging rate. Based on the high viability of YF01 in gastric acid and bile salts, the experimental strain was considered to have the potential for good survival in the gastrointestinal tract. The free radical scavenging rates also indicated the potential developability of the functional properties of the experimental strain. Subsequently, animal experiments were conducted for further verification.

3.3 Mouse weight and organ index

During the experimental period, the mouse weight changed (Figure 3). From the third week, all exercised mice lost weight at a slower rate than the normal mice. However, no significant difference in weight gain was noted between the groups. The heart, liver, kidneys, spleen, and testis of mice exhibited no significant difference in weight (Table 3). However, the muscle tissue of mice from the Vc and YF01 groups exhibited significant increases. This indicated that YF01 has no toxic effects, and long-term exercise may inhibit abnormal weight gain and enhance muscle development.

3.4 Mouse exhaustion time

The exhaustion time of mice typically reflects their anti-fatigue ability and endurance. The shortest exhaustion time of 2,998.32 ± 139.11 s was noted in the control group,

TABLE 2 *In vitro* activity of *Pediococcus pentosaceus* YF01.

In vitro activity	%
Survival rate at pH 3.0	90.11 ± 2.44
Growth efficiency in 0.3% bile salt	27.22 ± 0.42
Growth efficiency in 0.5% bile salt	23.91 ± 0.21
Growth efficiency in 1.0% bile salt	16.16 ± 0.18
Hydroxyl free radical scavenging capacity	19.24 ± 0.33
DPPH scavenging activity	14.73 ± 0.98

2 https://www.arb-silva.de/
3 https://unite.ut.ee/

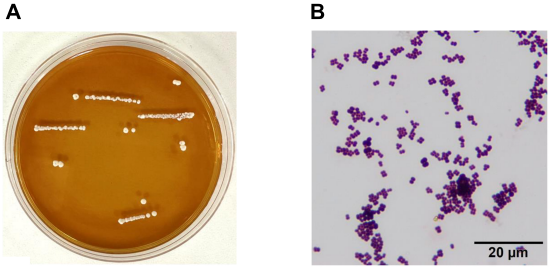

FIGURE 2
Morphological characteristics of *Pediococcus pentosaceus* YF01. **(A)** intuitive observation, **(B)** gram staining observation.

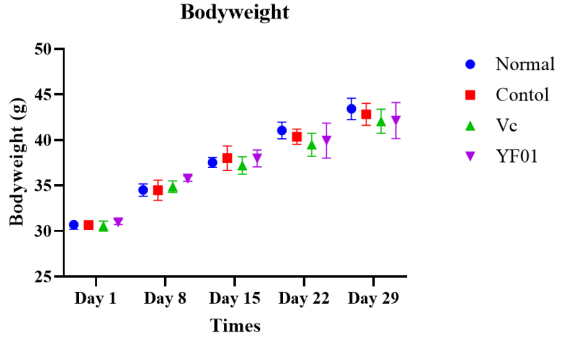

FIGURE 3
Bodyweight of mice. Normal, gavaged with 0.1 ml/10 g of 0.9% saline; Control, gavaged with 0.1 ml/10 g of 0.9% saline; Vc, gavaged with 0.1 ml/10 g of a 200 mg/Kg Vc solution; YF01, gavaged with 0.1 ml/10 g of a 1.0×10^9 CFU/ml *Pediococcus pentosaceus* YF01 solution.

TABLE 3 Tissue index of mice.[1]

Group	Heart	Liver	Kidney	Spleen	Muscle	Testis
Normal	0.45 ± 0.01^{a}	3.94 ± 0.10^{ab}	1.27 ± 0.06^{b}	0.32 ± 0.01^{a}	2.42 ± 0.09^{b}	0.60 ± 0.01^{a}
Control	0.45 ± 0.01^{a}	3.79 ± 0.04^{b}	1.27 ± 0.07^{b}	0.33 ± 0.02^{a}	2.49 ± 0.15^{b}	0.54 ± 0.02^{b}
Vc	0.44 ± 0.02^{a}	3.79 ± 0.09^{a}	1.29 ± 0.07^{b}	0.33 ± 0.03^{a}	2.74 ± 0.43^{ab}	0.55 ± 0.02^{b}
YF01	0.46 ± 0.03^{a}	4.01 ± 0.20^{b}	1.41 ± 0.01^{a}	0.32 ± 0.04^{a}	2.85 ± 0.17^{a}	0.54 ± 0.02^{b}

[1]Normal, gavaged with 0.1 ml/10 g of 0.9% saline; Control, gavaged with 0.1 ml/10 g of 0.9% saline; Vc, gavaged with 0.1 ml/10 g of a 200 mg/Kg Vc solution; YF01, gavaged with 0.1 ml/10 g of a 1.0×10^{9} CFU/ml *Pediococcus pentosaceus* YF01 solution. Means with the different letters (a–b) are significantly different ($p < 0.05$) using Duncan's multiple range test.

whereas the exhaustion times in the Vc and YF01 groups were 4,139.64 ± 220.44 s and 3,562.92 ± 239.02 s, respectively (Table 4). These results of exhaustion time suggest that the intake of Vc and YF01 can augment the endurance of mice.

3.5 Histological analysis of mouse tissues

Figure 4 presents the histological sections of mouse liver and muscle tissues. In normal liver tissues, the hepatocyte structure was intact, with clear, large, and round nuclear structures. The hepatic lobule structure was largely intact in the control group, but the hepatocyte arrangement was irregular, with scattered cells exhibiting reduced volume, increased cytoplasm density, concentrated nuclei, and fragmented nuclear membranes. Occasional cell shrinkage and nuclear condensation were observed in the liver tissues of the Vc group. Compared with the normal group, the YF01 group exhibited the most similar liver tissue structure. On visualizing the H&E-stained sections of muscle tissues, we noted that exercise fatigue in the control group mice resulted in muscle inflammation and damage, characterized by changes in muscle fibers, including blurred muscle bundle borders, irregular arrangement of muscle fibers, interstitial diffusion, increased gaps, connective tissue proliferation, and infiltration of inflammatory cells. When supplemented through food, Vc or YF01 helps in improving these conditions by reducing inflammation infiltration and narrowing the gaps between muscle fibers. In conclusion, YF01 exhibited a beneficial reparative effect on the livers and muscles of mice treated with YF01.

3.6 Mouse serum levels of oxidative stress markers T-AOC, CAT, and GSH

According to Figure 5, mouse serum levels of oxidation-related indicators. The control group had the lowest levels of the oxidation indicators T-SOD, CAT, and GSH. Serum levels of T-SOD, CAT, and GSH significantly increased in the Vc and YF01 groups ($p < 0.05$) compared with the control group. Moreover, neither the Vc group nor the YF01 group exhibited significant differences in oxidation-related indicators ($p > 0.05$). The above results indicate that YF01 has a good inhibitory effect on oxidative stress caused by exercise fatigue.

TABLE 4 Exercise exhaustion time of mice.[1]

Group	Times (s)
Control	$2{,}998.32 \pm 139.11^{c}$
Vc	$4{,}139.64 \pm 220.44^{a}$
YF01	$3{,}562.92 \pm 239.02^{b}$

[1]Normal, gavaged with 0.1 ml/10 g of 0.9% saline; Control, gavaged with 0.1 ml/10 g of 0.9% saline; Vc, gavaged with 0.1 ml/10 g of a 200 mg/Kg Vc solution; YF01, gavaged with 0.1 ml/10 g of a 1.0×10^{9} CFU/ml *Pediococcus pentosaceus* YF01 solution. Means with the different letters (a–c) are significantly different ($p < 0.05$) using Duncan's multiple range test.

3.7 Mouse serum levels of liver-related indicators

Serum AST and ALT levels were the highest in the control group (Figure 6). Both Vc and YF01 groups exhibited significant reductions in AST and ALT levels compared to the control group ($p < 0.05$), whereas the normal group ($p > 0.05$) exhibited no significant differences. Regarding TP and Alb, no significant differences were noted between the groups ($p > 0.05$). This indicates that exercise fatigue may cause liver damage without affecting protein synthesis or secretion, and YF01 improves exercise fatigue-induced liver damage.

3.8 Mouse serum levels of exercise performance-related indicators

As shown in Figure 7, the control group had the lowest GLU and LA levels, whereas it had the highest LDH, BUN, UA, and CRE levels ($p < 0.05$). The intake of Vc and YF01 effectively alleviated the decrease in GLU levels and the increase in LDH, BUN, UA, and CRE levels. The YF01 group exhibited serum GLU, UA, and CRE levels closest to those of the normal group, with no significant differences in LDH and BUN levels compared with the Vc group ($p > 0.05$). A higher LA level was noted in the YF01 group than in the Vc group ($p < 0.05$). Thus, YF01 can effectively inhibit exercise fatigue-induced changes in mouse serum-related performance indicators as well as augment endurance in mice.

3.9 Liver tissue oxidation-related gene expression levels in mice

The normal group expressed the highest SOD1, SOD2, and CAT levels, whereas the control group expressed the lowest levels ($p < 0.05$, Figure 8). The YF01 mice had similar expression levels of SOD1 and CAT as the normal mice, with no significant differences

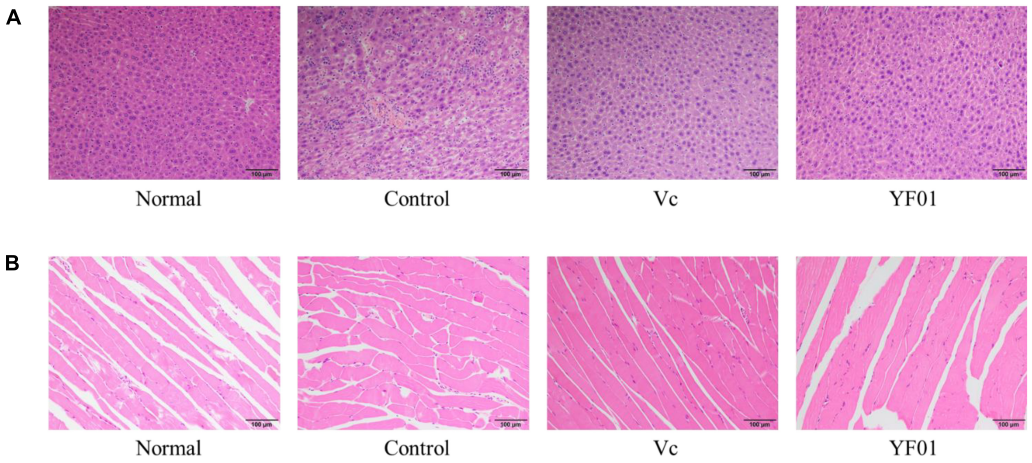

FIGURE 4
Liver **(A)** and muscle **(B)** morphology of mice. Normal, gavaged with 0.1 ml/10 g of 0.9% saline; Control, gavaged with 0.1 ml/10 g of 0.9% saline; Vc, gavaged with 0.1 ml/10 g of a 200 mg/Kg Vc solution; YF01, gavaged with 0.1 ml/10 g of a 1.0×10^9 CFU/ml *Pediococcus pentosaceus* YF01 solution.

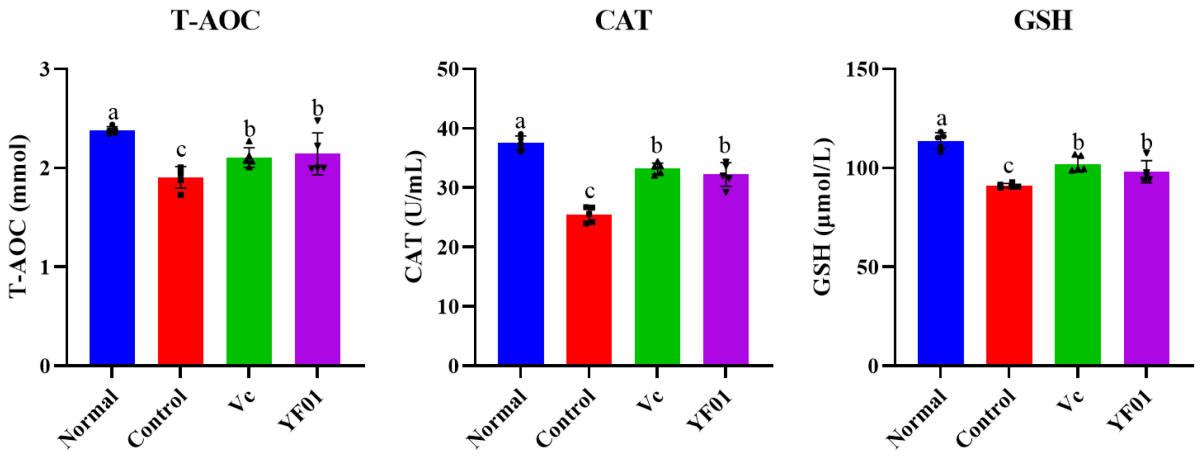

FIGURE 5
Serum levels of oxidant-related indices of mice. Normal, gavaged with 0.1 ml/10 g of 0.9% saline; Control, gavaged with 0.1 ml/10 g of 0.9% saline; Vc, gavaged with 0.1 ml/10 g of a 200 mg/Kg Vc solution; YF01, gavaged with 0.1 ml/10 g of a 1.0×10^9 CFU/ml *Pediococcus pentosaceus* YF01 solution. Means with the different letters (a–c) above the bars are significantly different ($p < 0.05$) using Duncan's multiple range test.

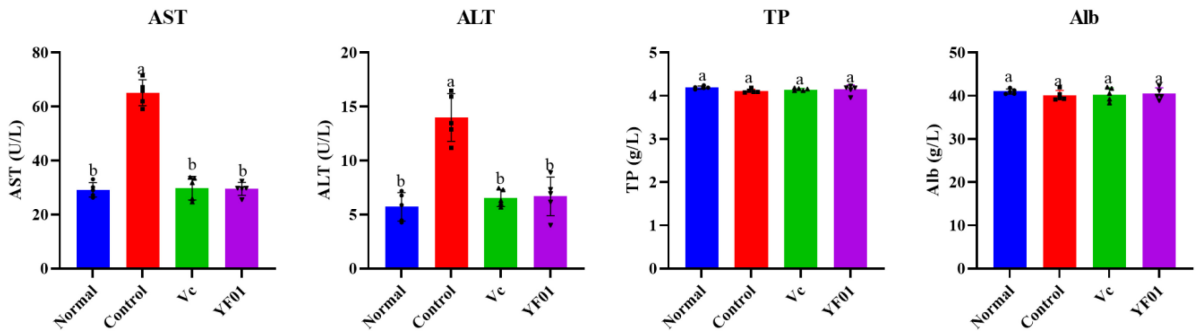

FIGURE 6
Serum levels of liver function related indices of mice. Normal, gavaged with 0.1 ml/10 g of 0.9% saline; Control, gavaged with 0.1 ml/10 g of 0.9% saline; Vc, gavaged with 0.1 ml/10 g of a 200 mg/Kg Vc solution; YF01, gavaged with 0.1 ml/10 g of a 1.0×10^9 CFU/ml *Pediococcus pentosaceus* YF01 solution. Means with the different letters (a–b) above the bars are significantly different ($p < 0.05$) using Duncan's multiple range test.

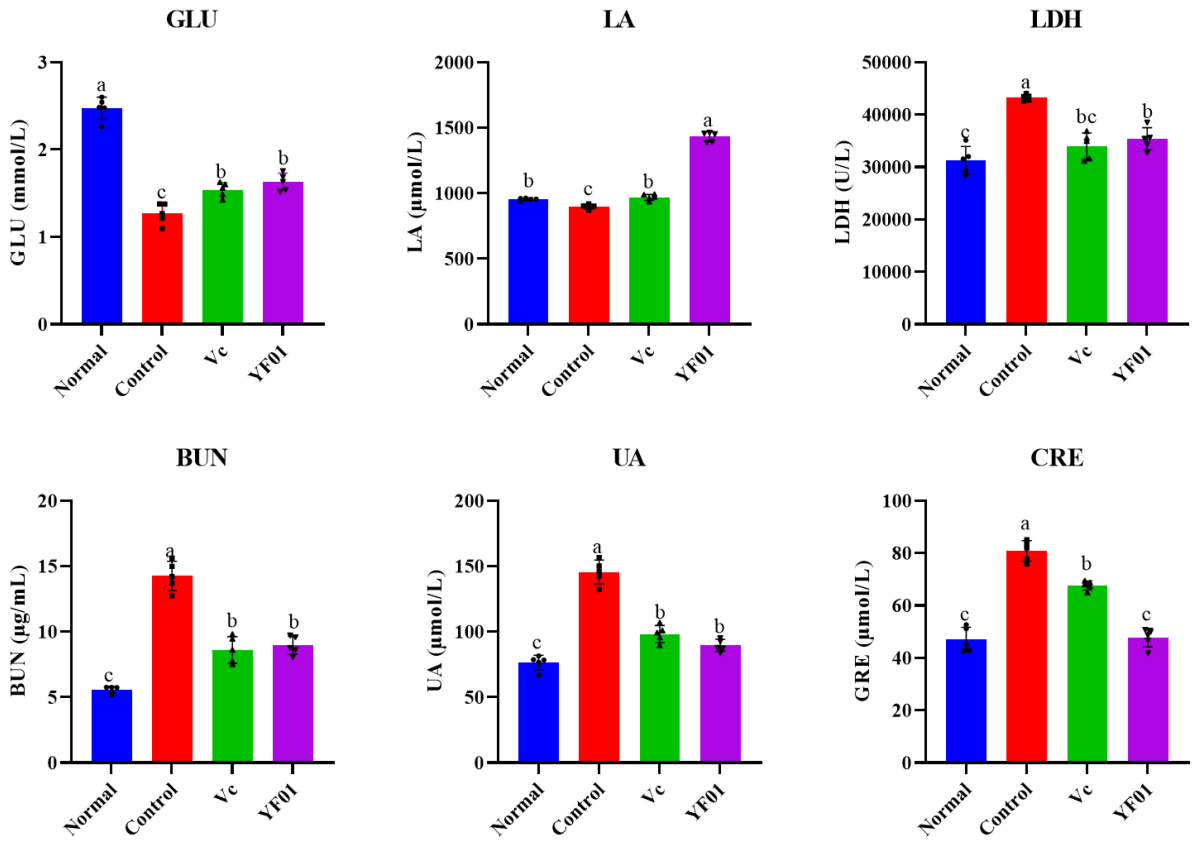

FIGURE 7
Indices related to physical performance in mice serum. Normal, gavaged with 0.1 ml/10 g of 0.9% saline; Control, gavaged with 0.1 ml/10 g of 0.9% saline; Vc, gavaged with 0.1 ml/10 g of a 200 mg/Kg Vc solution; YF01, gavaged with 0.1 ml/10 g of a 1.0×10^9 CFU/ml *Pediococcus pentosaceus* YF01 solution. Means with the different letters (a–c) above the bars are significantly different ($p < 0.05$) using Duncan's multiple range test.

from the Vc mice ($p < 0.05$). Vc and YF01 groups had similar SOD2 expression levels ($p > 0.05$). The inhibitory effect of YF01 on exercise-induced oxidative damage in the mouse liver tissue was significant.

3.10 Muscle mRNA expression levels of genes related to oxidation and exercise performance

Figure 9A presents the mRNA expression levels of oxidation-related genes in the mouse muscle tissue. Similar to the mouse liver tissue, SOD1, SOD2, and CAT expression was the highest in the normal group, whereas it was the lowest in the control group ($p < 0.05$). In the YF01 group, SOD1, SOD2, and CAT expression levels were 18, 10, and 7 times higher than those in the control group. Figure 9B shows the mRNA expression levels for genes related to exercise performance. The normal group exhibited the highest levels of MyHc IIa, MyHc IIb, MyHc IIx, SIRT1, and PGC, with the YF01 group ranking below the control group and the Vc group showing the lowest levels. In contrast, the mRNA expression level of MyHc I is opposite. These results indicate that dietary supplementation with Vc and YF01 can effectively prevent oxidative damage and contribute to improving exercise performance in mice.

3.11 Effects of exercise and *P. pentosaceus* YF01 on intestinal microbial communities

By sequencing, we evaluated the effects of exercise and *P. pentosaceus* YF01 on the intestinal microbial community of mice. The results (Figures 10A–C) showed that there were differences in the gut microbiota between the four groups, with all four groups having shared and unique OTU, with 900 OTUs in the Normal group, 1085 OTUs in the Control group, and 935 OTUs in the Vc group, the YF01 group has 898 OTUs, and different samples have 409 common OTUs. Subsequently, comparisons were made at the phylum and genus levels, and it was found that the relative abundance of *Firmicutes* in the YF01 group was higher at the phylum level; at the genus level, the relative abundance of *Bacteroides* was reduced in all exercise groups (Con, Vc, and YF01 group), and the relative abundance of *Helicobacter*, *Saccharimonas*, and *Colidextribacter* was higher in the YF01 group, while the relative abundance of *Alistipes* was higher in the Con group and YF01 group.

In addition, the relative abundance heat map results (Figures 11A–C) show that at the phylum level (Figure 11A), Desulfobacterota, Firmicutes, Patescibacteria, and Deferribacterota are more abundant in the YF01 group than in other groups. At the genus level (Figure 11B), the contents of *Bacteroides*, *Rikenellaceae*,

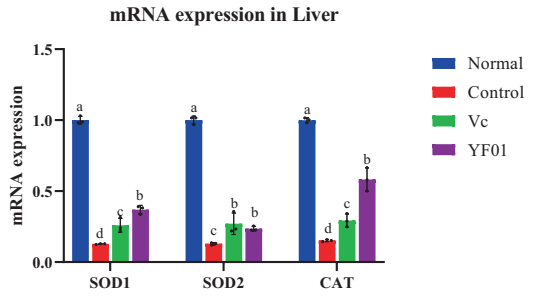

FIGURE 8
Expression levels of oxidation-related genes mRNA in mice liver tissues. Normal, gavaged with 0.1 ml/10 g of 0.9% saline; Control, gavaged with 0.1 ml/10 g of 0.9% saline; Vc, gavaged with 0.1 ml/10 g of a 200 mg/Kg Vc solution; YF01, gavaged with 0.1 ml/10 g of a 1.0×10^9 CFU/ml *Pediococcus pentosaceus* YF01 solution. Means with the different letters (a–d) above the bars are significantly different ($p < 0.05$) using Duncan's multiple range test.

Parabacteroides, and *Enterorhabdus* as well as GCA-900066575 from the Lachnospiraceae family were more in the Normal group than in the exercise group; *Alloprevotella*, *Anaeroplasma,* and *Prevotellaceae* were most abundant in the VC group; *Ruminococcus*, *Candidatus_Saccharimonas*, *Colidextribacter,* and *Helicobacter* were most abundant in the YF01 group; and *Odoribacter* and *Alistipes* were most abundant in the Con group. At the species level (Figure 11C), *Lactobacillus*, *Lachnospiraceae,* and *Burkholderiales bacterium* were most abundant in the YF01 group.

3.12 Principal component analysis and alpha diversity analysis

Principal component analysis (PCA) analysis results (Figure 12A) showed that no significant differences were found between the groups, but it was found that the intestinal microbial diversity increased in the exercise group, among which the microbial community composition of the Vc group and the YF01 group was the most similar. In addition, the shannon index (Figure 12B) reflects that the YF01 group has the highest community diversity and a relatively even distribution of species.

3.13 Differential microbial screening

Linear discriminant analysis Effect Size (LEfSe) analysis (linear discriminant analysis effect size method) was used to determine the characteristic microorganisms of each group, and the relationship between different microbial groups from the

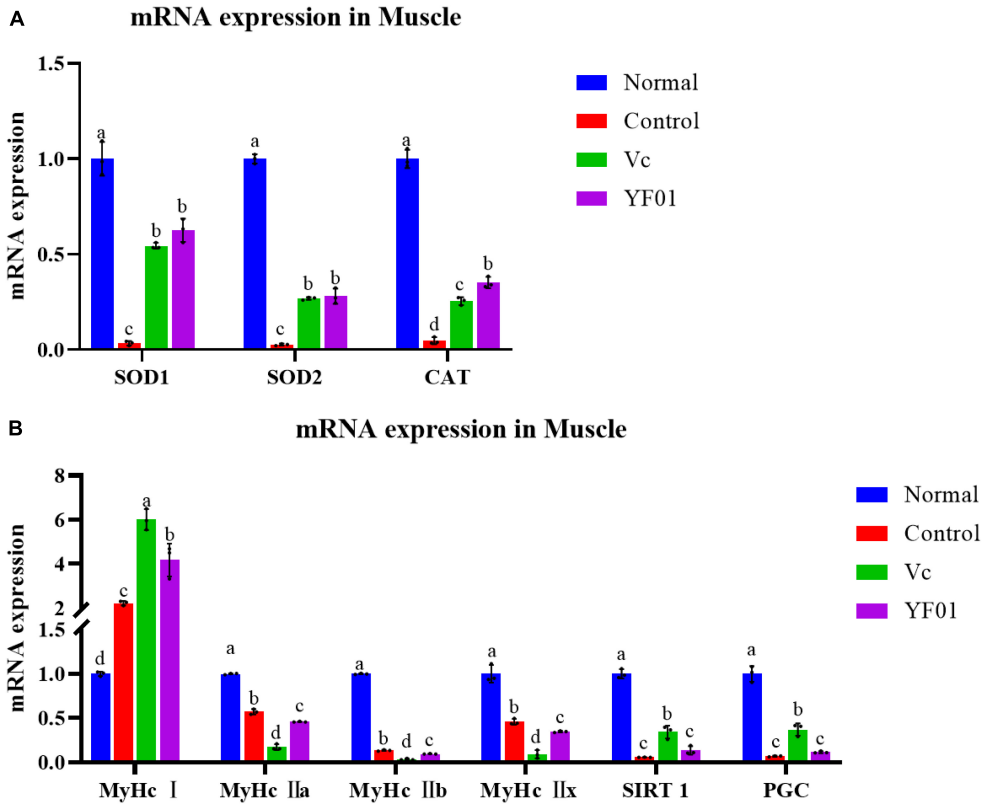

FIGURE 9
Expression levels of genes related to oxidation **(A)** and physical performance **(B)** in mice muscle tissues. Normal, gavaged with 0.1 ml/10 g of 0.9% saline; Control, gavaged with 0.1 ml/10 g of 0.9% saline; Vc, gavaged with 0.1 ml/10 g of a 200 mg/Kg Vc solution; YF01, gavaged with 0.1 ml/10 g of a 1.0×10^9 CFU/ml *Pediococcus pentosaceus* YF01 solution. Means with the different letters (a–d) above the bars are significantly different ($p < 0.05$) using Duncan's multiple range test.

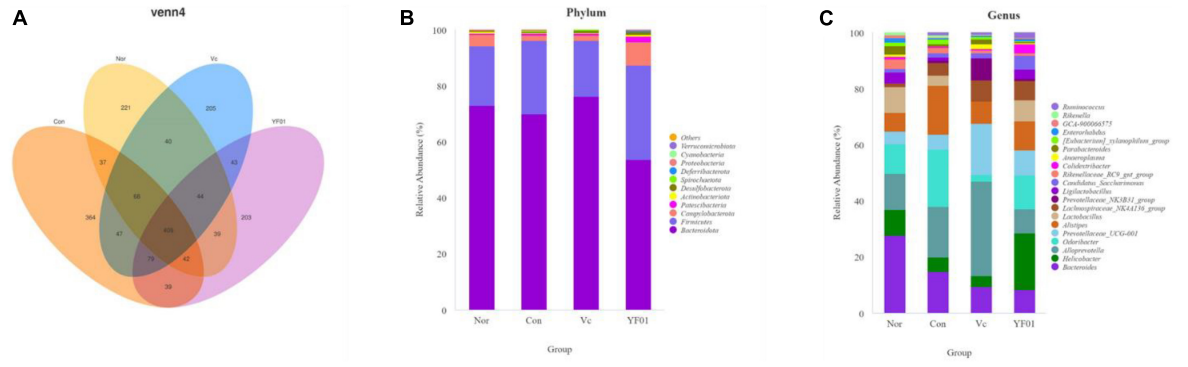

FIGURE 10
Venn analysis among each group and comparison of dominant phylum and genus in different groups. **(A)** Venn diagrams of bacterial OTUs. **(B)** At the phylum level, the horizontal coordinate represents the group and the vertical coordinate represents the percent of community abundance. **(C)** At the genus level.

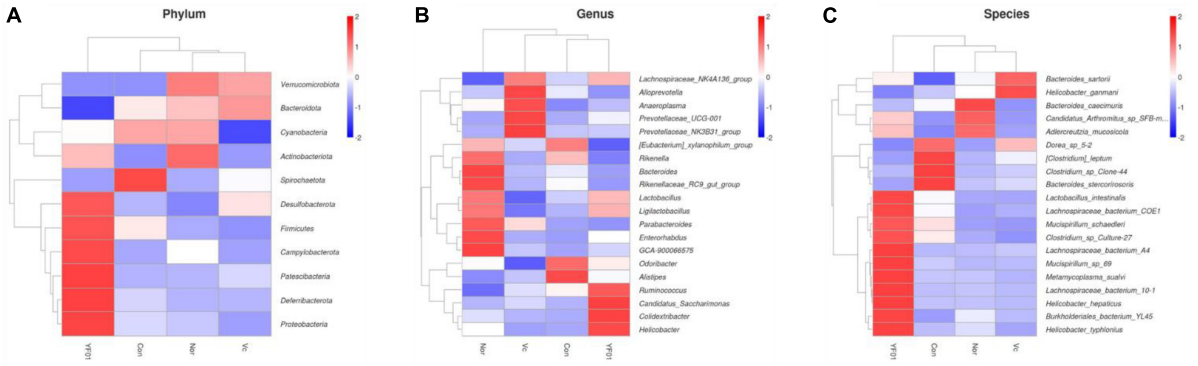

FIGURE 11
A relative abundance heat map showing significant inter-group differences at different levels. **(A)** At the phylum level. **(B)** At the genus level. **(C)** At the species level.

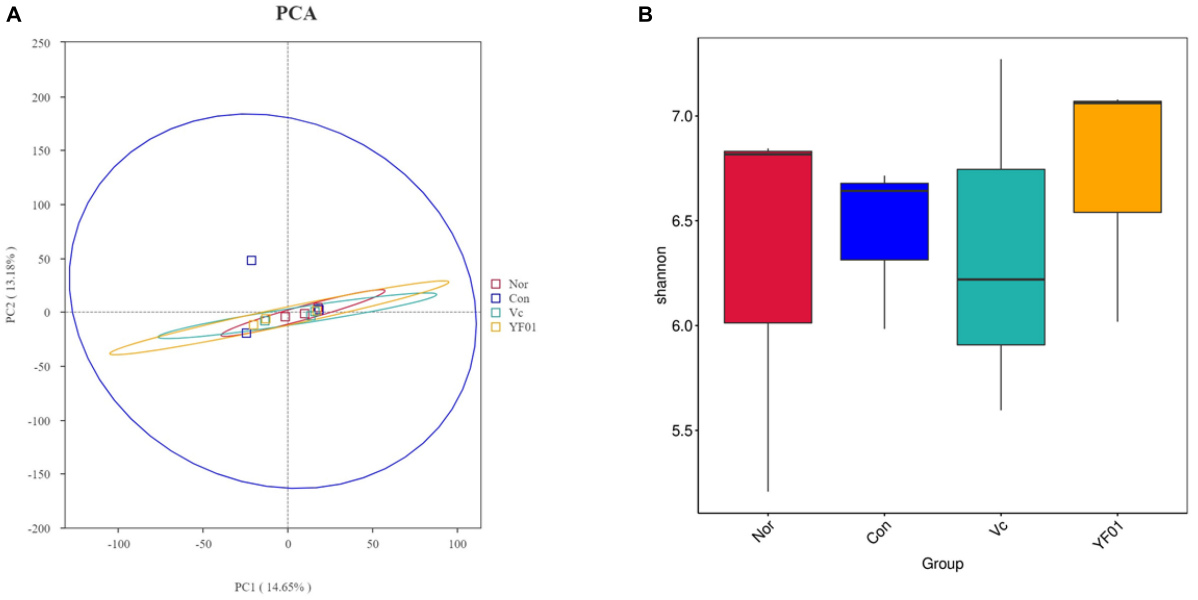

FIGURE 12
Principal component analysis and alpha diversity analysis. **(A)** Principal component analysis. **(B)** Shannon diversity index.

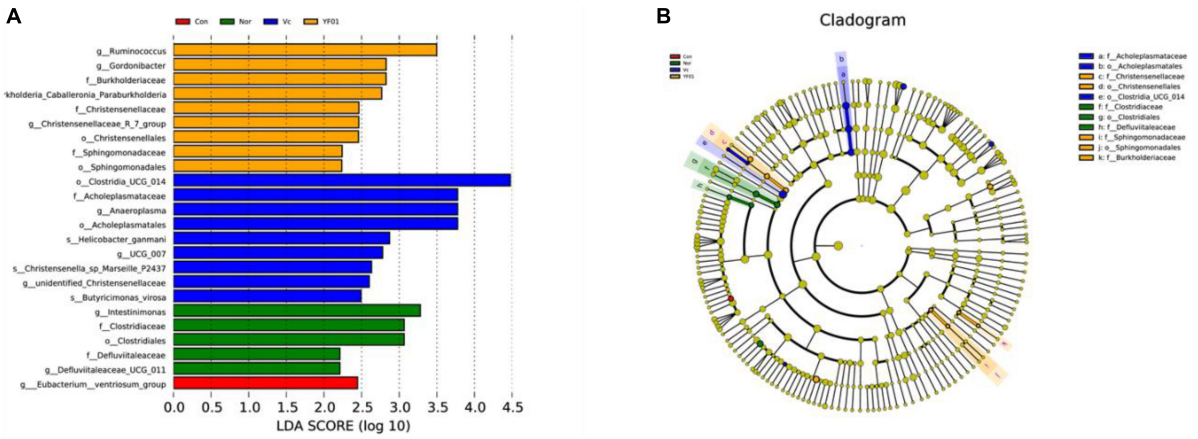

FIGURE 13
Linear discriminant analysis Effect Size (LEfSe) of different groups, LDA = 2. **(A)** Bar plot of LDA scores distribution. **(B)** Phylogenetic tree.

phylum to the species level (LDA = 2) was displayed in a cladogram (Figures 13A, B). The results showed that in the control group, the relative abundance of *Eubacterium* was higher; in the normal group, the relative abundance of *Intestinimonas*, *Clostridiaceae*, *Clostridiales,* and *Defluviitaleaceae* was higher. In the VC group, relative abundance of *Clostridia*, *Acholeplasmataceae*, *Anaeroplasma*, *Acholeplasmatales*, *Helicobacter*, UCG 007, *Christensenella* sp. *Marseille*, unidentified *Christensenellaceae*, and *Butyricimonas virosa* was higher; in the YF01 group, the relative abundance of *Ruminococcus*, *Gordonibacter*, Burkholderiaceae, *kholderia Caballeronia Paraburkholderia*, *Christensenellaceae*, *Christensenellales*, *Sphingomonadaceae,* and *Sphingomonadales* is higher. These bacteria with higher relative abundance can be used as biomarkers for further research. Among the four groups, there were 11 OTUs with significant differences at different levels from phylum to species.

4 Discussion

Exercise-induced fatigue is a symptom commonly associated with sports and physical activities. It can lead to adverse effects such as muscle pain and physical exhaustion (Wan et al., 2017). Oxidative stress, a physiological response characterized by excessive ROS generation within cells, plays a crucial role in exercise-induced fatigue (Moir et al., 2023). Oxidative stress leads to cellular oxidative damage. High-intensity exercises increase the body's oxidative stress levels, resulting in muscle fatigue and damage (Debold, 2015). Probiotics are beneficial bacteria believed to protect against oxidative stress (Lee and Kang, 2022). Moreover, probiotics can help the body to recover from oxidative stress and promote muscle repair. Therefore, supplementing probiotics may help reduce exercise-induced fatigue and improve exercise performance (Jager et al., 2019). In this study, *P. pentosaceus* YF01 exhibited good *in vitro* resistance and effectively scavenged oxygen free radicals, thereby reducing exercise-induced damage due to free radicals and enhancing exercise performance.

A probiotic's survival rate in the artificial gastric fluid and the presence of different bile salt concentrations is a crucial indicator of its ability to colonize the gastrointestinal tract (Bezkorovainy, 2001). Additionally, the *in vitro* antioxidant capacity of probiotics represents their *in vivo* antioxidant capacity. Probiotics with strong *in vitro* antioxidant capacity also exhibit good abilities to scavenge oxygen free radicals *in vivo* (Noureen et al., 2019). In the present study, the YF01 strain demonstrated excellent *in vitro* resistance and a good capacity to scavenge oxygen free radicals, which lays the foundation for its antioxidant mechanisms *in vivo*.

Exercise, particularly high-intensity and prolonged exercise, increases metabolism, which increases the demand for oxygen and oxygen-free radical-induced oxidative stress reactions (Kawamura and Muraoka, 2018). Oxygen free radicals damage nucleic acids, proteins, and lipids, thereby triggering a series of physiological responses including liver and muscle damage (Muriel, 2009; Kıran et al., 2023). The liver, a crucial metabolic organ, is susceptible to oxidative stress (Cichoz-Lach and Michalak, 2014). During exercise, the liver performs the task of clearing metabolic waste and toxins, thereby making the liver cells vulnerable to oxygen-free radical-induced oxidative stress and causing liver damage (Muriel, 2009). An impaired liver function can affect metabolite clearance and synthesis, thereby influencing the body's physiological functions (Yan et al., 2014). Muscles are executors of exercise, and muscle tissue is also susceptible to the effects of oxidative stress that occurs during exercise (Kozakowska et al., 2015). Oxidative stress can cause damage, such as lipid peroxidation of muscle cell membranes and protein oxidation, impairing the muscle structure and function, which ultimately results in muscle fatigue and damage (Steinbacher and Eckl, 2015). Additionally, oxidative stress may trigger inflammatory reactions in the muscle, exacerbating muscle damage and repair processes (Kozakowska et al., 2015). In an exercise-induced fatigue model, mouse livers suffered oxidative damage, whereas probiotics alleviated this phenomenon (Liu et al., 2021). This study also yielded similar results, the liver and muscle tissues of mice suffered inflammatory damage after exercise, and YF01 effectively alleviated these phenomena, which indicated that YF01 suppressed the liver and muscle damage caused by exercise-induced oxidative stress.

The body has several antioxidant defense systems that help cope with oxidative stress. These include T-AOC, SOD1, SOD2, GSH, and CAT, among others (Surai et al., 2019). Using T-AOC, a key indicator of the antioxidant system, the overall body's ability to respond to oxidative stress can be assessed (Huang et al., 2022). Cells use GSH as an antioxidant molecule that neutralizes ROS and participates in redox reactions (Lushchak, 2012). SOD1, SOD2, and CAT are vital antioxidant enzymes. SOD1 and SOD2 can eliminate intracellular superoxide radicals, while CAT can degrade harmful oxidants such as hydrogen peroxide, thereby reducing the oxygen-free radical-induced damage (Shields et al., 2021). These antioxidant enzymes play crucial roles in exercise, protecting the cells from oxidative damage and maintaining the oxidative balance within the cells. In this study, exercise-induced fatigue in mice increased the generation of free radicals in the serum, and liver and muscle tissues, and a series of oxidative stress reactions were triggered. *P. pentosaceus* YF01 boosts antioxidant enzyme activity in mice, thereby improving their ability to eliminate free radicals and defend against lipid peroxidation.

Time to exhaustion is a notable indicator for assessing exercise-induced fatigue. It reflects the endurance and persistence of muscles during fatigue (Pageaux and Lepers, 2016). Various factors, including muscle fiber types, expression of exercise-related proteins, and regulation, influence this indicator. In general, a longer time to exhaustion indicates greater endurance. The impact of exercise on metabolic products in the body has always interested researchers, including blood biochemical indicators such as GLU, LA, LDH, BUN, UA, and CRE. These indicators may change during exercise, thereby indicating the body's regulation of energy and metabolic products during physical activity. GLU is the main energy source in the human body. During exercise, the liver releases glycogen and transports GLU to muscles for energy supply. At the same time, the demand for GLU by muscle cells increases, and the GLU concentration possibly increases to meet the muscle's energy metabolism needs (Richter and Hargreaves, 2013). On the other hand, LA, a product of glycolysis, accumulates rapidly during high-intensity exercise, thereby increasing the LA concentration. An increase in the lactate threshold indicates augmented endurance (Ghosh, 2004). LDH is involved in the release of lactate metabolism enzymes, which is crucial for lactate production and elimination (Gupta, 2022). BUN indicates the formation of the metabolic product urea nitrogen, which increases during exercise. It is chiefly influenced by amino acid metabolism in the body (Sokal et al., 2013). UA and CRE are metabolic waste products, and various factors affect their concentrations, including muscle metabolism, water balance, and kidney function. During exercise, UA and CRE concentrations may change because of increased muscle metabolism and water loss, reflecting the effect of muscle metabolism and exercise load on the kidneys (Golino et al., 2021; Gherghina et al., 2022). The study findings indicate that *P. pentosaceus* YF01 administration significantly increases the time to exhaustion in running mice and effectively alleviates the effects of exercise-induced fatigue on various biochemical markers, including GLU, LA, LDH, BUN, UA, and CRE. This reflects the positive role of YF01 in regulating the balance of energy and metabolic products during physical activity in mice.

The bulk of muscles is composed of fast-twitch fibers (Type II) and slow-twitch fibers (Type I). As slow-twitch fibers contain heavy myosin chains (MyHc I), they exhibit endurance qualities, which provides them the ability to offer a prolonged energy supply. Fast-twitch fibers are further divided into MyHc IIa, MyHc IIb, and MyHc IIx, and each of them has a different contraction speed and endurance performance (Talbot and Maves, 2016). Sirtuin 1 (SIRT1) and peroxisome proliferator-activated receptor gamma coactivator (PGC), as crucial regulatory proteins in cells, are associated with the regulation of cellular energy metabolism and time to exhaustion (Canto and Auwerx, 2009). SIRT1 is involved in regulating the cellular metabolic balance and oxidative stress response. It thus is crucial for the cell's adaptive capacity to exercise (Radak et al., 2020). PGC is involved in regulating muscle mitochondrial biogenesis and exercise performance, and thus, it influences time to exhaustion and muscle endurance (Lira et al., 2010). During exercise-induced fatigue, muscle fibers undergo continuous intense exercise loading, which results in the depletion of energy reserves, LA accumulation, and oxidative stress. This negative impact possibly interferes with the expression and activity of MyHc I, MyHc IIa, MyHc IIb, and MyHc IIx in the muscle and disrupts the regulatory functions of SIRT1 and PGC, thereby influencing muscle endurance and exercise performance. The study findings indicate that *P. pentosaceus* YF01 by regulating muscle fibers, this probiotic enhances the body's overall exercise capacity, particularly in terms of endurance and recovery rate.

Intestinal microbiota plays a crucial role in human health, including influencing exercise capacity through various pathways. Intestinal flora can directly affect nerve transmission and regulate muscle movement and coordination by synthesizing and decomposing neurotransmitters such as dopamine and glutamate (Wu et al., 2020). Research has also found that the composition and interactions of intestinal flora may affect muscle quality, function, and energy metabolism by altering the gut microbiota, known as the gut-muscle axis (Ticinesi et al., 2019). Additionally, intestinal microbiota responds to endurance exercise by adaptively regulating various biological functions, including energy metabolism, inflammatory response, stress resistance, and oxidative stress, thereby playing a role in exercise regulation (Li et al., 2022). Our study revealed that the intake of *P. pentosaceus* YF01 increased the abundance of beneficial bacterial groups such as *Firmicutes*, *Lactobacillus*, *Lachnospiraceae*, and *B. bacterium* Y45 in the mouse intestines, which may be a potential reason for improving the mice's exercise performance.

5 Conclusion

In the present study, a mouse exercise-induced fatigue model was established. Using this model, we demonstrated that *P. pentosaceus* YF01 regulates oxidative stress in mice so as to enhance their antioxidant capacity, thus preventing damage due to exercise-induced fatigue and augmenting the exercising capacity. According to the experimental results, YF01 exhibited good *in vitro* resistance; reduced liver and muscle damage; prolonged the time to exhaustion in running mice; and increased serum T-AOC, CAT, GSH, GLU, and LA levels in mice and liver/muscle mRNA expression of SOD1, SOD2, and CAT. In addition, YF01 upregulated MyHc I, SIRT1, and PGC mRNA expression levels in the muscle tissue, whereas decreased serum AST, ALT, LDH, BUN, UA, and CRE levels and downregulated MyHc IIa, MyHc IIb, and MyHc IIx mRNA expression levels. And YF01 promoted the abundance of beneficial bacteria such as *Lactobacillus* and

Lachnospiraceae in the gut microbiota of mice. In summary, this study demonstrated that *P. pentosaceus* YF01 can effectively mitigate exercise-induced fatigue through the by regulating oxidative stress response and muscle fiber expression. We also elucidated the action mechanism of YF01, thereby providing a basis for the mitigation of exercise-induced fatigue and enhancement of exercise performance by using food-derived antioxidants.

Data availability statement

The original contributions presented in this study are included in the article/Supplementary material, further inquiries can be directed to the corresponding author.

Ethics statement

The animal study was approved by the Beijing University of Chemical Technology. The study was conducted in accordance with the local legislation and institutional requirements.

Author contributions

XY: Writing – original draft. YW: Writing – original draft. YY: Writing – review & editing.

Funding

The author(s) declare that no financial support was received for the research, authorship, and/or publication of this article.

Conflict of interest

The authors declare that the research was conducted in the absence of any commercial or financial relationships that could be construed as a potential conflict of interest.

Publisher's note

All claims expressed in this article are solely those of the authors and do not necessarily represent those of their affiliated organizations, or those of the publisher, the editors and the reviewers. Any product that may be evaluated in this article, or claim that may be made by its manufacturer, is not guaranteed or endorsed by the publisher.

Supplementary material

The Supplementary Material for this article can be found online at: https://www.frontiersin.org/articles/10.3389/fmicb.2024.1421209/full#supplementary-material

References

Bao, T., Li, Y., Xie, J., Jia, Z., and Chen, W. (2019). Systematic evaluation of polyphenols composition and antioxidant activity of mulberry cultivars subjected to gastrointestinal digestion and gut microbiota fermentation. *J. Funct. Foods* 58, 338–349.

Begdache, L., Sadeghzadeh, S., Derose, G., and Abrams, C. (2020). Diet, exercise, lifestyle, and mental distress among young and mature men and women: A repeated cross-sectional study. *Nutrients* 13:248.

Bezkorovainy, A. (2001). Probiotics: Determinants of survival and growth in the gut. *Am. J. Clin. Nutr.* 73, 399S–405S.

Bokulich, N. A., Subramanian, S., Faith, J. J., Gevers, D., Gordon, J. I., Knight, R., et al. (2013). Quality-filtering vastly improves diversity estimates from illumina amplicon sequencing. *Nat. Methods* 10, 57–59.

Cai, X., Yuan, Y., Liao, Z., Xing, K., Zhu, C., Xu, Y., et al. (2018). alpha-Ketoglutarate prevents skeletal muscle protein degradation and muscle atrophy through PHD3/ADRB2 pathway. *FASEB J.* 32, 488–499.

Canto, C., and Auwerx, J. (2009). PGC-1alpha, SIRT1 and AMPK, an energy sensing network that controls energy expenditure. *Curr. Opin. Lipidol.* 20, 98–105.

Cichoz-Lach, H., and Michalak, A. (2014). Oxidative stress as a crucial factor in liver diseases. *World J. Gastroenterol.* 20, 8082–8091.

Das, A., and Gailey, S. (2022). Green exercise, mental health symptoms, and state lockdown policies: A longitudinal study. *J. Environ. Psychol.* 82:101848.

Debold, E. P. (2015). Potential molecular mechanisms underlying muscle fatigue mediated by reactive oxygen and nitrogen species. *Front. Physiol.* 6:239. doi: 10.3389/fphys.2015.00239

Edgar, R. C., Haas, B. J., Clemente, J. C., Quince, C., and Knight, R. (2011). Uchime improves sensitivity and speed of chimera detection. *Bioinformatics* 27, 2194–2200.

Erten, H., Ağirman, B., GündüZ, C. P. B., Çarşanba, E., Sert, S., Bircan, S., et al. (2014). "Importance of yeasts and lactic acid bacteria in food processing," in *Food processing: Strategies for quality assessment*, eds A. Malik, Z. Erginkaya, S. Ahmad, and H. Erten (New York, NY: Springer).

Fiuza-Luces, C., Santos-Lozano, A., Joyner, M., Carrera-Bastos, P., Picazo, O., Zugaza, J. L., et al. (2018). Exercise benefits in cardiovascular disease: Beyond attenuation of traditional risk factors. *Nat. Rev. Cardiol.* 15, 731–743.

Gherghina, M. E., Peride, I., Tiglis, M., Neagu, T. P., Niculae, A., and Checherita, I. A. (2022). Uric acid and oxidative stress-relationship with cardiovascular, metabolic, and renal impairment. *Int. J. Mol. Sci.* 23:3188.

Ghosh, A. K. (2004). Anaerobic threshold: Its concept and role in endurance sport. *Malays. J. Med. Sci.* 11, 24–36.

Golino, G., Danzi, V., and De Rosa, S. (2021). "Serum creatinine, muscle mass, and nutritional status in intensive care," in *Biomarkers and bioanalysis overview*, ed. C. F. Nunes (London: IntechOpen).

Gupta, G. S. (2022). The lactate and the lactate dehydrogenase in inflammatory diseases and major risk factors in Covid-19 patients. *Inflammation* 45, 2091–2123.

He, F., Li, J., Liu, Z., Chuang, C. C., Yang, W., and Zuo, L. (2016). Redox mechanism of reactive oxygen species in exercise. *Front. Physiol.* 7:486. doi: 10.3389/fphys.2016.00486

Huang, F., Shen, X., Zhang, Y., Vuong, A. M., and Yang, S. (2022). Postprandial changes of oxidative stress biomarkers in healthy individuals. *Front. Nutr.* 9:1007304. doi: 10.3389/fnut.2022.1007304

Jager, R., Mohr, A. E., Carpenter, K. C., Kerksick, C. M., Purpura, M., Moussa, A., et al. (2019). International society of sports nutrition position stand: Probiotics. *J. Int. Soc. Sports Nutr.* 16:62.

Kawamura, T., and Muraoka, I. (2018). Exercise-induced oxidative stress and the effects of antioxidant intake from a physiological viewpoint. *Antioxidants (Basel)* 7:119.

Kim, J. S., Kim, J. H., Palaniyandi, S. A., Lee, C. C., You, J. W., Yang, H., et al. (2019). Yak-Kong soybean (Glycine max) fermented by a novel *Pediococcus pentosaceus*

inhibits the oxidative stress-induced monocyte-endothelial cell adhesion. *Nutrients* 11:1380.

Kıran, T. R., Otlu, O., and Karabulut, A. B. (2023). Oxidative stress and antioxidants in health and disease. *J. Lab. Med.* 47, 1–11.

Kozakowska, M., Pietraszek-Gremplewicz, K., Jozkowicz, A., and Dulak, J. (2015). The role of oxidative stress in skeletal muscle injury and regeneration: Focus on antioxidant enzymes. *J. Muscle Res. Cell Motil.* 36, 377–393.

Lee, J. Y., and Kang, C. H. (2022). Probiotics alleviate oxidative stress in H(2)O(2)-exposed hepatocytes and t-Bhp-induced C57bl/6 Mice. *Microorganisms* 10:234.

Li, Y., Wang, S., Quan, K., Ma, D., Zhang, H., Zhang, W., et al. (2022). Co-administering yeast polypeptide and the probiotic, *Lacticaseibacillus casei* Zhang, significantly improves exercise performance. *J. Funct. Foods* 95:105161.

Liguori, I., Russo, G., Curcio, F., Bulli, G., Aran, L., Della-Morte, D., et al. (2018). Oxidative stress, aging, and diseases. *Clin. Interv. Aging* 13, 757–772.

Lira, V. A., Benton, C. R., Yan, Z., and Bonen, A. (2010). Pgc-1alpha regulation by exercise training and its influences on muscle function and insulin sensitivity. *Am. J. Physiol. Endocrinol. Metab.* 299, E145–E161.

Liu, D., Liu, D. C., Fan, H., and Wang, Y. (2021). *Lactobacillus fermentum* Cqpc08 attenuates exercise-induced fatigue in mice through its antioxidant effects and effective intervention of Galactooligosaccharide. *Drug Des. Dev. Ther.* 15, 5151–5164.

Lushchak, V. I. (2012). Glutathione homeostasis and functions: Potential targets for medical interventions. *J. Amino Acids* 2012:736837.

Lushchak, V. I. (2014). Free radicals, reactive oxygen species, oxidative stress and its classification. *Chem. Biol. Interact.* 224, 164–175.

Magoc, T., and Salzberg, S. L. (2011). FLASH: Fast length adjustment of short reads to improve genome assemblies. *Bioinformatics* 27, 2957–2963.

McLeay, Y., Stannard, S., Houltham, S., and Starck, C. (2017). Dietary thiols in exercise: Oxidative stress defence, exercise performance, and adaptation. *J. Int. Soc. Sports Nutr.* 14:12.

Moir, H. J., Maciejczyk, M., Maciejczyk, M., Aidar, F. J., and Arazi, H. (2023). Editorial: Exercise-induced oxidative stress and the role of antioxidants in sport and exercise. *Front. Sports Act. Liv.* 5:1269826. doi: 10.3389/fspor.2023.1269826

Morente-Sanchez, J., and Zabala, M. (2013). Doping in sport: A review of elite athletes' attitudes, beliefs, and knowledge. *Sports Med.* 43, 395–411.

Muriel, P. (2009). Role of free radicals in liver diseases. *Hepatol. Int.* 3, 526–536.

Nanasombat, S., Treebavonkusol, P., Kittisrisopit, S., Jaichalad, T., Phunpruch, S., Kootmas, A., et al. (2017). Lactic acid bacteria isolated from raw and fermented pork products: Identification and characterization of catalase-producing *Pediococcus pentosaceus*. *Food Sci. Biotechnol.* 26, 173–179.

Nicholson, J. K., Holmes, E., Kinross, J., Burcelin, R., Gibson, G., Jia, W., et al. (2012). Host-gut microbiota metabolic interactions. *Science* 336, 1262–1267.

Noureen, S., Riaz, A., Arshad, M., and Arshad, N. (2019). In vitro selection and in vivo confirmation of the antioxidant ability of *Lactobacillus brevis* MG000874. *J. Appl. Microbiol.* 126, 1221–1232.

Pageaux, B., and Lepers, R. (2016). Fatigue induced by physical and mental exertion increases perception of effort and impairs subsequent endurance performance. *Front. Physiol.* 7:587. doi: 10.3389/fphys.2016.00587

Pan, Y., Ning, Y., Hu, J., Wang, Z., Chen, X., and Zhao, X. (2021). The preventive effect of *Lactobacillus plantarum* ZS62 on DSS-induced IBD by regulating oxidative stress and the immune response. *Oxid. Med. Cell Longev.* 2021:9416794.

Pan, Y., Wang, H., Tan, F., Yi, R., Li, W., Long, X., et al. (2020). *Lactobacillus plantarum* KFY02 enhances the prevention of CCl4-induced liver injury by transforming geniposide into genipin to increase the antioxidant capacity of mice. *J. Funct. Foods* 73:104128.

Powers, S. K., and Jackson, M. J. (2008). Exercise-induced oxidative stress: Cellular mechanisms and impact on muscle force production. *Physiol. Rev.* 88, 1243–1276.

Qi, Y., Huang, L., Zeng, Y., Li, W., Zhou, D., Xie, J., et al. (2021). *Pediococcus pentosaceus*: Screening and application as probiotics in food processing. *Front. Microbiol.* 12:762467. doi: 10.3389/fmicb.2021.762467

Radak, Z., Suzuki, K., Posa, A., Petrovszky, Z., Koltai, E., and Boldogh, I. (2020). The systemic role of SIRT1 in exercise mediated adaptation. *Redox Biol.* 35:101467.

Richter, E. A., and Hargreaves, M. (2013). Exercise, GLUT4, and skeletal muscle glucose uptake. *Physiol. Rev.* 93, 993–1017.

Shao, T., Verma, H. K., Pande, B., Costanzo, V., Ye, W., Cai, Y., et al. (2021). Physical activity and nutritional influence on immune function: An important strategy to improve immunity and health status. *Front. Physiol.* 12:751374. doi: 10.3389/fphys.2021.751374

Shields, H. J., Traa, A., and Van Raamsdonk, J. M. (2021). Beneficial and detrimental effects of reactive oxygen species on lifespan: A comprehensive review of comparative and experimental studies. *Front. Cell Dev. Biol.* 9:628157. doi: 10.3389/fcell.2021.628157

Simioni, C., Zauli, G., Martelli, A. M., Vitale, M., Sacchetti, G., Gonelli, A., et al. (2018). Oxidative stress: Role of physical exercise and antioxidant nutraceuticals in adulthood and aging. *Oncotarget* 9, 17181–17198.

Sokal, P., Jastrzebski, Z., Jaskulska, E., Sokal, K., Jastrzebska, M., Radziminski, L., et al. (2013). Differences in blood urea and creatinine concentrations in earthed and unearthed subjects during cycling exercise and recovery. *Evid. Based Complement. Alternat. Med.* 2013:382643.

Steinbacher, P., and Eckl, P. (2015). Impact of oxidative stress on exercising skeletal muscle. *Biomolecules* 5, 356–377.

Surai, P. F., Kochish, I. I., Fisinin, V. I., and Kidd, M. T. (2019). antioxidant defence systems and oxidative stress in poultry biology: An update. *Antioxidants (Basel)* 8:235.

Talbot, J., and Maves, L. (2016). Skeletal muscle fiber type: Using insights from muscle developmental biology to dissect targets for susceptibility and resistance to muscle disease. *Wiley Interdiscip. Rev. Dev. Biol.* 5, 518–534.

Ticinesi, A., Nouvenne, A., Cerundolo, N., Catania, P., Prati, B., Tana, C., et al. (2019). Gut microbiota, muscle mass and function in aging: A focus on physical frailty and sarcopenia. *Nutrients* 11:1633.

Wan, J. J., Qin, Z., Wang, P. Y., Sun, Y., and Liu, X. (2017). Muscle fatigue: General understanding and treatment. *Exp. Mol. Med.* 49:e384.

Wu, W., Kong, Q., Tian, P., Zhai, Q., Wang, G., Liu, X., et al. (2020). Targeting gut microbiota dysbiosis: Potential intervention strategies for neurological disorders. *Engineering* 6, 415–423.

Yan, J., Li, S., and Li, S. (2014). The role of the liver in sepsis. *Int. Rev. Immunol.* 33, 498–510.

frontiers | Frontiers in Microbiology

TYPE Original Research
PUBLISHED 29 August 2024
DOI 10.3389/fmicb.2024.1428308

OPEN ACCESS

EDITED BY
Naga Betrapally,
National Cancer Institute (NIH), United States

REVIEWED BY
Yuqing Feng,
China Agricultural University, China
Denglang Zou,
Qinghai Normal University, China

*CORRESPONDENCE
Jinrong Wang
✉ Wangjr@haut.edu.cn

RECEIVED 06 May 2024
ACCEPTED 15 August 2024
PUBLISHED 29 August 2024

CITATION
Gan L, Zhao Y, Zhang Z, Zhao C, Li J, Jia Q, Shi Y, Wang P, Guo L, Qiao H, Cui Y and Wang J (2024) The impact of high polymerization inulin on body weight reduction in high-fat diet-induced obese mice: correlation with cecal *Akkermansia*. *Front. Microbiol.* 15:1428308. doi: 10.3389/fmicb.2024.1428308

The impact of high polymerization inulin on body weight reduction in high-fat diet-induced obese mice: correlation with cecal *Akkermansia*

Liping Gan, Yifeng Zhao, Zongbao Zhang, Chenkai Zhao, Jiake Li, Qingyu Jia, Yusu Shi, Peng Wang, Linna Guo, Hanzhen Qiao, Yaoming Cui and Jinrong Wang*

School of Bioengineering, Henan University of Technology, Zhengzhou, China

Obesity presents a significant public health challenge, demanding effective dietary interventions. This study employed a high-fat diet-induced obesity mouse model to explore the impacts of inulin with different polymerization degrees on obesity management. Our analysis reveals that high-degree polymerization inulin (HDI) exhibited a significantly higher oil binding capacity and smaller particle size compared to low-degree polymerization inulin (LDI) ($p < 0.05$). HDI was more effective than LDI in mitigating body weight gain in high-diet induced obese mice, although neither LDI nor HDI affected blood sugar levels when compared to the high-fat diet control group ($p < 0.05$). Both HDI and LDI administrations reduced liver weight and enhanced brown adipose tissue thermogenesis compared to the high-fat diet induced control group ($p < 0.05$). Additionally, HDI suppressed hepatic lipogenesis, resulting in a further reduction in liver triglycerides compared to the high-fat diet-induced obese mice ($p < 0.05$). Notably, HDI improved gut health by enhancing intestinal morphology and modulating gut microbiota structure. HDI administration notably increased the relative abundance of cecal *Akkermansia*, a gut microbe associated with improved metabolic health, while LDI showed limited efficacy ($p < 0.05$ and $p > 0.05$, respectively). These findings underscore the importance of the structural properties of inulin in its potential to combat obesity and highlight the strategic use of inulin with varying polymerization degrees as a promising dietary approach for obesity management, particularly in its influence on gut microbiota composition and hepatic lipid metabolism regulation.

KEYWORDS

inulin, polymerization degree, obesity, gut microbiota, high fat diet, *Akkermansia*

Introduction

Obesity has emerged as a global health crisis over the past few decades, with rates tripling worldwide in the last half-century (Prillaman, 2023). This surge in obesity has brought with it a myriad of health complications, including fatty liver disease, type 2 diabetes (T2D), etc., contributing to decreased life expectancy and imposing substantial economic burdens on both

individuals and societies (Eliby, 2022). While lifestyle modifications aimed at reducing calorie intake and increasing energy expenditure are commonly advocated for obesity prevention and treatment, their long-term efficacy remains limited (Bluher, 2019). Although several FDA-approved drugs for obesity treatment exist, their effectiveness varies among individuals, and there is a paucity of research on their safety and efficacy in adolescents and children (Prillaman, 2023). Hence, the pursuit of safe and effective dietary interventions, particularly those involving dietary fiber, has gained considerable attention.

Inulin, a widely studied dietary fiber, has gained prominence in recent research as an effective dietary intervention to combat obesity and related disorders in both adults and children (Al-Abdullatif and Azzam, 2023; Singh et al., 2018; Visuthranukul et al., 2022). Its appeal lies, in part, in its extraction from readily available sources like chicory and Jerusalem artichokes, which are rich in inulin with relatively simple fructose-based compositions. However, it is important to note that commercial inulin products, particularly those derived from chicory, encompass various types classified based on their polymerization degree (DP). This raises a crucial question: do all types of inulin yield identical anti-obesity effects?

Previous studies have explored the anti-obesity potential of inulin with varying DP, yielding mixed results. Some studies have reported that combining high-fat diets with high DP inulin led to reductions in body and liver weight in mice, whereas low DP inulin yielded no such effects (Du et al., 2020). Conversely, other researchers, utilizing different degrees of polymerized inulin in conjunction with high fat diet (HFD), found no impact on body and liver weight compared to HFD-fed mice (Li et al., 2020). These disparities in findings may be attributed to differences in experimental conditions and the metabolic status of the subjects, particularly the latter.

Crucially, inulin as a fermentable dietary fiber, exerts its anti-obesity properties by profoundly influencing the composition of the intestinal microbiota. The gut microbiome plays a pivotal role in host energy metabolism and is a promising target for weight management due to its intricate connection with obesity. Dysbiosis of the intestinal microbiota is a well-documented consequence of obesity, and it can significantly impact the host's physical condition (Delannoy-Bruno et al., 2021). Furthermore, the DP of inulin can have varying effects on microbiota. Although several studies have evaluated the impact of inulin with different DP on gut microbiota, many of these studies initiated interventions with high-fat diets and inulin from the start of the study, using mice of normal weight (Du et al., 2020; Hu et al., 2021; Li et al., 2020; Zhu et al., 2019). Given the fact that there are significant differences in gut microbiota and metabolic status between obese and lean individuals, administering inulin combined with a high-fat diet to mice with normal weight may not accurately reflect the effects of inulin on obese individuals. Therefore, further investigation is required to understand the effects and mechanisms of inulin on obese individuals. Additionally, while some studies assessed changes in colonic microbiota following inulin intervention, others utilized fecal samples (Li et al., 2020; Zhu et al., 2017). It is important to explore the effects of various DP of inulin specifically on cecal microbiota, as the cecum serves as the primary microbial fermentation site in mice.

The structural properties of different polymerized inulin types may offer insights into whether they uniformly affect obesity and its underlying mechanisms. In this study, we induced obesity in mice using a high-fat diet and subsequently administered inulin treatment, comparing the properties of inulin with varying DP both *in vitro* and *in vivo*. The study involved in-depth assessments of gut microbiota, liver health, and body weight in response to different polymerized inulin treatments. By examining these critical aspects, we sought to shed light on the potential applications of inulin as a dietary intervention for individuals dealing with obesity and overweight conditions.

Materials and methods

Inulin

Low DP inulin (LDI, Orafti P95, purity = 97.8%, 4 < DP <6) and high DP inulin (HDI, Orafti HP, purity = 100%, DP ≥ 23 units) used in this study were sourced from Beneo (Mannheim, Germany). These specific types of inulin were selected based on their purities and DP to ensure accurate and reliable results. Inulin was incorporated into the mice's feed as part of the experimental procedure.

Morphological analysis of inulin in the current experiment

The microstructure and morphology of the inulin used in this experiment were examined using a scanning electron microscope (SEM, SU8200, Hitachi, Japan) operated at an accelerating voltage of 3 kV and magnifications of 100×, 500×, and 1,000×. Approximately 0.1 g of inulin powder was affixed to the SEM stub, followed by sputter coating with gold. Subsequently, images were captured using the SEM.

To assess the particle size of the inulin powder, the diameters of 6–8 particles were measured from three images taken at different perspectives, utilizing magnifications of 500× and 1,000× for LDI and HDI, respectively. This analysis was conducted using Fiji (ImageJ-win64).

Oil absorption capacity

The absorption capacity of inulin for oils was determined using a modified version of the method described by Jeddou et al. (2016). In brief, a reaction system was prepared in a pre-weighed centrifuge tube, where 0.5 g of HDI or LDI were mixed with 10 mL of corn oil. The oil absorption capacity was calculated using the following formula:

Oil Absorption Capacity (g oil/g polysaccharide) = [(weight of the tube contents after draining – weight of the dried polysaccharide) / weight of the dried polysaccharide].

The effects of inulin with different degree of polymerization on bacteria *in vitro*

The effects of inulin on *Lactobacillus rhamnosus* (ATCC 9595), *L. plantarum* (CICC 24936), and *L. reuteri* (CICC 6119), which were routinely cultivated in either liquid or solid MRS medium, were detected. For evaluating the inhibitory effects of inulin on Opportunistic pathogen, we utilized *Escherichia coli ETEC* (CICC 10667) and

Staphylococcus aureus (CICC AB 91093), which were also routinely grown in either liquid or solid LB medium. After inoculating approximately 1×10^6 CFU/mL of each of the five bacterial strains in MRS or LB liquid medium, with and without 8% HDI or LDI, the cultures were incubated at 37°C for 24 h. Three replicates were conducted for each treatment and each bacterial strain. After the 24 h incubation period, the optical density of the liquid medium was measured at 600 nm. Subsequently, each bacterial culture was appropriately diluted for colony counting on agar plates.

Fourier transform infrared spectroscopy of inulin powder

In this experiment, inulin samples with varying DP were subjected to Fourier Transform Infrared Spectroscopy (FTIR) using the Nicolet iS20 instrument from Thermo Scientific, United States. The absorption spectra were recorded across a frequency range spanning from 400 to 4,000 nm. For each analysis, a portion of the inulin powder was carefully positioned on the attenuated total reflectance (ATR) section of the spectrometer. Over 64 scans were conducted, each at a resolution of 4 cm^{-1}, and the resulting spectra were averaged to obtain a representative spectrum.

Animals and treatment

The animal protocols utilized in this study received approval from and were conducted in accordance with the Animal Care and Use Committee of Biological Engineering, Henan University of Technology (no. HAUTETHI-2022-1099).

A total of 32 healthy male C57BL/6 J mice, aged 5 weeks and with similar body weights, were procured from the laboratory animal center of Zhengzhou University for the purpose of this study. These mice were accommodated in the animal facility at Henan University of Technology. Following a one-week acclimatization period, the mice were randomly divided into four groups, each comprising eight mice, ensuring that there were no significant weight discrepancies between the groups. The mice were housed in pairs within cages and were provided with either a low-fat diet (10% of energy from fat, TP 23302) or a high-fat diet (60% of energy from fat, TP 23302), both obtained from Trophic Animal Feed High-Tech Co., Ltd., China. The treatment groups consisted of the following: high-fat diet control group (HFD), Low-fat diet control group (LFD), High-fat diet with LDI treatment group (HFD + LDI), High-fat diet with HDI treatment group (HFD + HDI). To explore the effects of inulin with different degrees of polymerization (DP) in obese mice, we first induced obesity in the mouse model. For the initial 4 weeks, the LFD group was fed a low-fat diet, while the other three groups received the same basal high-fat diet (ingredients listed in Supplementary Table S1). Subsequently, the HFD + LDI and HFD + HDI groups were administered diets containing 8% LDI or HDI, respectively, added to the basal high-fat diet. The HFD group received a diet with 8% microcrystalline cellulose added, while the LFD group continued on the low-fat diet for 6 weeks. The dosage of inulin used in this experiment is based on previous research evaluating the effects of fiber on high-fat diet- induced mice (Patnode et al., 2019).

All mice were housed in a controlled environment maintained at a temperature of 20–25°C, with a relative humidity of 60%, under a 12-h light–dark cycle. They were given unrestricted access to food and clean water. High-fat food was stored in the refrigerator to preserve its quality, and water bottles were cleaned weekly, with fresh water replenished every 3 days. Body weights of individual mice and feed intake per cage were recorded on a weekly basis. After 10 weeks of treatment, the mice were euthanized via cervical dislocation for sample collection, which included cecal contents, intestines, liver, white adipose tissue, and brown adipose tissue. White adipose tissue was collected using the method described by (Tan et al., 2018). Briefly, the mouse was pinned on its back on a pad, and the abdominal skin was cut without disturbing the muscle or membranes. The exposed adipose tissue on both sides of the skin was abdominal subcutaneous fat (ASF), which was collected and weighed on an analytical balance. The abdominal muscle was then cut to expose the abdominal organs. The fat around the reproductive organs (epididymal fat, EF) was carefully collected and weighed on both sides. The gut was removed to expose the kidneys, and the adipose tissue surrounding the kidneys (perirenal fat, PF) was collected and weighed after removing the adrenal glands. Brown adipose tissue, located at the junction of the back and neck (Lee et al., 2022), was also collected and weighed.

Oral glucose tolerance test of the mice

In order to assess the disposal of an orally administered glucose load over time in mice subjected to various treatment regimens, the OGTT method was employed in this study, as previously described by (Nagy and Einwallner, 2018).

Briefly, at the conclusion of the ninth week, the mice were transferred to fresh bedding and subjected to an overnight fast lasting 12 h, during which they retained access to drinking water. Subsequently, a small drop of blood sample (~3 μL) was obtained by carefully removing 1 mm from the tail tip for the measurement of basal blood glucose levels using a glucometer (Yuehao I 720, Yuwell, Jiangsu, China). Following the basal measurement, a glucose solution (1 g glucose/kg body weight) was administered directly into the stomach of each mouse via a feeding needle. At time intervals of 15, 30, 60, 90, and 120 min after the administration of glucose, blood glucose levels were measured using the glucometer for each individual mouse.

mRNA expression detected by quantitative real-time (qRT)-PCR

Total RNA was extracted from liver and brown adipose tissue using Freezol (R711, Vazyme, Nanjing, China) according to the manufacturer's instructions. The quality and quantity of the RNA were assessed using a NanoDrop 2000. The PrimeScript RT reagent kit with gDNA eraser (TaKaRa, Dalian, China) was used for the reverse transcription according to the manufacturer's instructions. qRT-PCR was performed in duplicate on a PCR System (qTOWER^3, Analytik Jena, Germany) with the Universal SYBR qPCR Master Mix (Vazyme, Nanjing, China). The primer sequences used to detect the gene expression are listed in Supplementary Table S2. Gene expression was normalized to the expression of the housekeeping gene beta-actin using comparative $2^{-\Delta\Delta CT}$ method, as described previously (Livak and Schmittgen, 2001).

Hematoxylin and eosin (H&E) staining and Oil Red O staining

The small intestinal segments and liver, which were fixed in 4% paraformaldehyde, underwent a series of ethanol dehydration steps before being embedded in paraffin. Subsequently, the tissues were sectioned to a thickness of 8 μm and subjected to hematoxylin and eosin staining. Microscopic images of the liver and intestine tissues were acquired using a microscope (RVL-110-G, Echo Laboratories, United States), and villus height and crypt depth of the small intestine were measured based on magnified images.

For Oil Red O staining, the liver samples underwent a series of dehydration steps in different concentration of sucrose solutions, were then embedded in Optimum Cutting Temperature, quick-frozen in liquid nitrogen, and stored at −80°C overnight prior to sectioning in a cryostat (CM1850 UV, Leica Biosystems, United States). Oil Red O staining was performed in accordance with the procedure outlined by Cui et al. (2017). Following staining, photographs of the stained tissues were captured using a microscope (RVL-110-G, Echo Laboratories, United States).

Triglycerides contents detection in the liver

The triglycerides contents in the liver of the mice were detected using the triglycerides kit (BC0625, Solarbio Life Sciences, Beijing, China) according to the manufacturer's instructions.

Pyrosequencing of cecal microbiota

DNA samples were extracted from cecal digesta using QIAamp DNA Stool Mini Kits (Qiagen Inc., Hilden, Germany) following the manufacturer's instructions. Subsequently, gel electrophoresis was performed to assess the concentration and purity of the DNA samples. Amplification of microbial 16S rRNA gene sequences was achieved using universal primers designed for the V3-V4 region. The resulting PCR products were subjected to analysis through 2% gel electrophoresis and subsequently purified using the QIAquick Gel Extraction Kit (Qiagen Inc., Hilden, Germany).

Pyrosequencing for 16S rRNA was conducted utilizing the Illumina Novaseq platform (Illumina, San Diego, United States). All procedures were carried out by Biomarker Technologies (Beijing, China). Following quality filtering via Cutadapt (Version 1.9.1) and the removal of chimeric sequences using the UCHIME algorithm (version 8.1), clean reads were obtained. Subsequently, the clean reads were clustered into operational taxonomic units (OTUs) using USEARCH (version 10.0) with a similarity threshold exceeding 97%. These OTUs were then subjected to taxonomy-based analysis using the RDP algorithm in conjunction with the Greengenes database (version 13.5).

Statistical analysis

Statistical significance was assessed utilizing Student's *t*-test, one-way ANOVA, or two-way ANOVA for comparisons involving multiple groups. For pairwise comparisons between two groups, the Tukey *post-hoc* test was employed. Data analysis was conducted using Excel or Prism 8. A significance threshold of $p < 0.05$ was applied to determine statistical significance.

Results

Morphology of inulin with different molecular weights under SEM

The morphology of inulin with various DP is illustrated in Figures 1A,B. Inulin sourced from chicory presents itself as spherical particles, albeit with some variation in particle size even within a single type of inulin. There were notable distinctions when comparing the two types of inulin, the variant with LDI (Figure 1B) exhibits larger particle sizes than the inulin with HDI (Figure 1A).

Upon magnification of the inulin particles by 1,000 times, it becomes evident that the average particle size of LDI is approximately five times greater than that of HDI (Figures 1A,B, Supplementary Table S3). It is worth noting that while LDI is readily soluble in water, HDI is virtually insoluble in cold to warm water but can be dissolved in hot water.

Fourier transform infrared spectroscopy of inulin powder

The specificity of carbohydrates arises from the geometry of the O-H groups and the configuration of C-O, C-C, and C-H bonds within the carbon backbone (Coates, 2000). As depicted in Figure 1C, HDI inulin exhibited similar infrared spectra to LDI. Both types of inulin display characteristic band spectra around 3,385, 2,934, and 1,648 cm^{-1}, corresponding to O-H stretching, C-H stretching, and O-H deformation, respectively. In accordance with the FTIR analysis conducted by Akram and Garud (2020) and Chikkerur et al. (2020), vibrations within the spectral range of 1,500–900 cm^{-1} primarily result from C-H, O-H, C-O-C bending, C-O-C, and C-O stretching modes within oligo- and polysaccharides.

Although the peak intensity differs between the two types of inulin (see Supplementary Table S4), their peak positions in the spectral range of 1,500 to 900 cm^{-1} remain similar (Figure 1C). Of particular note is the presence of more peaks in the spectrum of LDI compared to HDI within the spectral range of 600–900 cm^{-1}, particularly at 781.48 cm^{-1}, representing CH_2 bending (Coates, 2000). The similarity in peak positions at 3386, 2,934, and 1,647 cm^{-1} between LDI and HDI inulin suggests that similar functional groups are present in both.

Oil binding capacity two types of inulin *in vitro*

The oil holding capacity is a critical characteristic and a technological property closely associated with the chemical structure of polysaccharides. As depicted in Figure 1D, HDI exhibits a significantly greater oil binding capacity ($p = 0.0078$, 2.123 vs. 1.494 g/g) compared to LDI.

Body weight and plasma glucose levels of the mice during the experiment

The experimental outline for each group is illustrated in Figure 2A. Following 4 weeks of high-fat diet treatment, mice in the

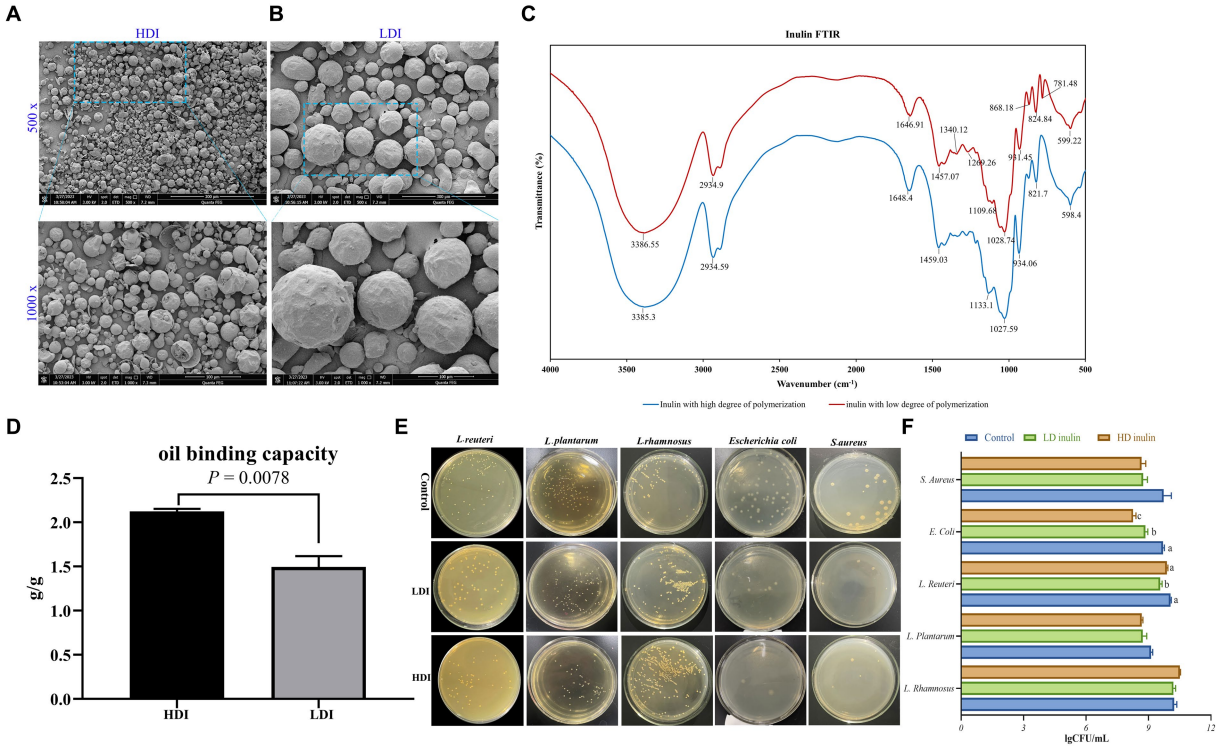

FIGURE 1
Characterization of low-degree polymerized inulin (LDI) and high-degree polymerized inulin (HDI). **(A)** Scanning electron microscopy (SEM) images of HDI, with 500× magnification in the upper panel and 1,000× magnification in the lower panel; **(B)** SEM images of LDI, with 500 × magnification in upper panel and 1,000 × in the lower panel; **(C)** Fourier transform infrared (FTIR) spectrum of LDI and HDI; **(D)** oil binding capacity of HDI and LDI inulin; **(E,F)** effects of LDI and HDI on the growth of *L. rhamnosus, L. plantarum, L. reuteri, E. coli,* and *S. aureus in vitro*.

high-fat diet group exhibited significantly higher body weights compared to those on the low-fat diet ($p < 0.05$, Figure 2C). By the fourth week, the body weights of mice in the various high-fat diet groups were statistically similar ($p > 0.05$). Subsequently, after administering inulin with different DP to the high-fat diet mice for 6 weeks, significant reductions in body weight were observed in both the LDI ($p < 0.05$) and HDI ($p < 0.001$) inulin groups. Furthermore, the body weight of mice in the HFD + HDI group was significantly lower than that in the HFD + LDI group ($p < 0.05$). Despite the reductions in body weight induced by the addition of inulin to the HFD groups, the body weight in these groups remained higher than that of the LFD group ($p < 0.001$, see Figures 2B,D).

High-fat diet consumption significantly increased the weight of ASF, EF, and PF in mice ($p < 0.001$, Figure 2E) when compared to mice in LFD. Mice in the HFD + HDI group experienced reductions in ASF, EF, and PF contents by approximately 37, 34, and 32%, respectively, when compared to mice in the HFD group. However, there were minimal differences between mice in the HFD and HFD + LDI groups concerning fat contents.

Plasma glucose levels of the mice are depicted in Figure 2F. High-fat diet consumption elevated fasting blood glucose levels in comparison to the LFD group. Moreover, blood glucose levels had not returned to baseline even 120 min after oral administration of glucose. Supplementation with inulin of different polymerization degrees did not ameliorate this phenomenon. Notably, mice in the HFD, HFD + LDI, and HFD + HDI groups exhibited higher area under the curve (AUC) values than mice in the LFD group, suggesting that the addition of inulin had minimal effects on blood glucose levels (Figure 2G).

Inulin reduces lipid content in the liver of HFD-induced mice

As demonstrated in Figure 3B, mice in the HFD group exhibited a significant increase in liver weight compared to mice in the LFD group ($p = 0.001$). Notably, both HFD + HDI and HFD + LDI resulted in reduced liver weight when compared with the HFD group ($p < 0.05$). This reduction in liver weight may be attributed to the decreased triglyceride content in the liver, as illustrated in Figures 3A,C.

High-fat diet consumption led to fat accumulation in the liver, as evident in H&E and Oil Red O staining in Figure 3A. Furthermore, compared to the HFD + HDI, HFD + LDI, and LFD groups, the livers of mice in the HFD group exhibited greater immune cell infiltration, as indicated by the arrowheads in Figure 3A, indicative of increased liver inflammation. However, supplementation with high- and low-DP inulin effectively reduced the size of lipid droplets and inflammation in the liver.

To elucidate the mechanisms underlying the reduction of fat accumulation in both liver and adipose tissues by inulin, we assessed the genes related to fat metabolism in both brown adipose tissue and the

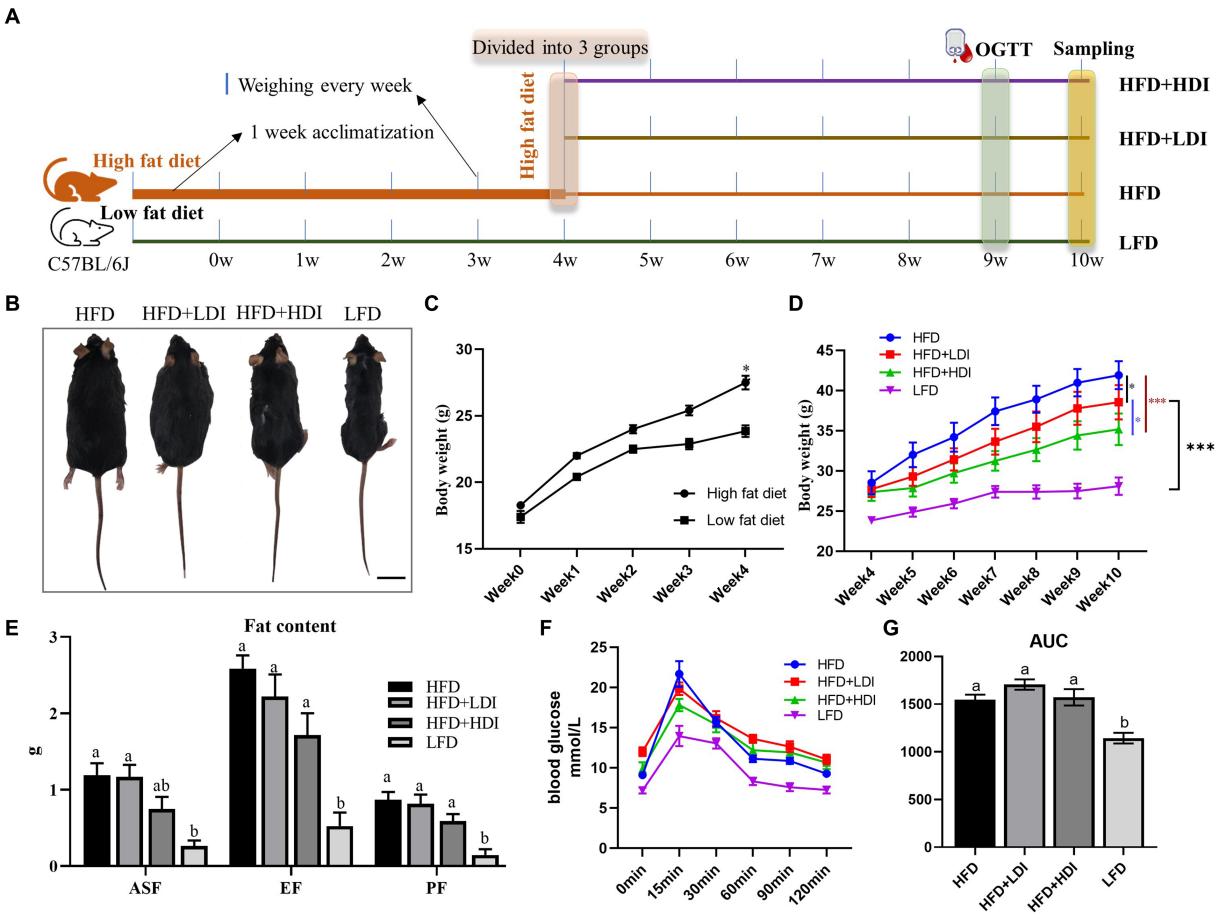

FIGURE 2
Effects of different polymerization degrees of inulin on body weight and glucose tolerance in obese mice. **(A)** Experimental design of the animal study. **(B)** Representative images of mice in each treatment group at the end of the study. **(C)** Changes in body weight of mice after 4 weeks of high-fat diet treatment (n = 24 in the high-fat diet group, n = 8 in the low-fat diet group). **(D)** Changes in body weight of mice during the 5th to 10th weeks (n = 8). **(E)** Fat contents of mice in different treatment groups (n = 8). ASF, abdominal subcutaneous fat; EF, epididymal fat; PF, perirenal fat; **(F)** Glucose levels during the oral glucose tolerance test (OGTT). After an overnight fast, glucose (mg/dL) levels were measured in the fasting state and at 15, 30, 60, 90, and 120 min after administering glucose solution orally via gavage (1 g glucose/kg) (n = 8). **(G)** Glucose area under the curve (AUC) during OGTT of mice in different treatment groups. Results are mean ± SEM. *p < 0.05, **p < 0.01, ***p < 0.001. Within each panel, different letters indicate significant changes at p < 0.05. Statistical analysis in **(D)** was performed using two-way ANOVA and Tukey's *post-hoc* test, while in other cases, one-way ANOVA and Tukey's *post-hoc* test were applied.

liver of mice subjected to different treatment regimens. As presented in Figures 4A,B, the weight of brown adipose tissue in the LFD group significantly decreased compared to that in the HFD mice (p<0.05). Furthermore, mice fed both LDI and HDI inulin exhibited similar brown adipose tissue weights to those in the HFD groups (p>0.05). Concurrently, the mRNA expression of uncoupling protein 1 (*UCP-1*) in brown adipose tissue was significantly higher in the HFD+LDI, HFD+HDI, and LFD groups than in the HFD group (p<0.05).

Eight mRNA expressions related to hepatic lipid metabolism were examined in this study (Figures 4C–J), with only two genes—peroxisome proliferator-activated receptor γ (*PPARγ*, Figure 4D) and sterol regulatory element-binding protein 1 (*SREBP1*, Figure 4E)—being reduced by inulin administration. In contrast, five genes were influenced by dietary fat content, including reduced mRNA expression of *PPARγ* and *SREBP1* and increased mRNA expression of *LPIN*, stearoyl-coenzyme A desaturase 1 (*SCD1*), and PPARγ coactivator 1α (*PGC1α*) by the LFD compared to the HFD group (p<0.05).

Different polymerization degrees of inulin improve the intestinal health of obese mice

Figure 5A displays the results of H&E staining of the small intestine in mice subjected to various treatment regimens. High-fat diet consumption induced atrophy of the small intestinal villi, resulting in reduced villus height in both the ileum and jejunum of the mice (p<0.05) in comparison to mice in LFD group. Notably, the administration of HDI significantly increased the V/C ratio in the duodenum, jejunum, and ileum (p<0.05, Figures 5B–D) of the mice when compared to those in the HFD groups. Furthermore, LDI also elevated the V/C ratio in the duodenum and ileum in comparison to

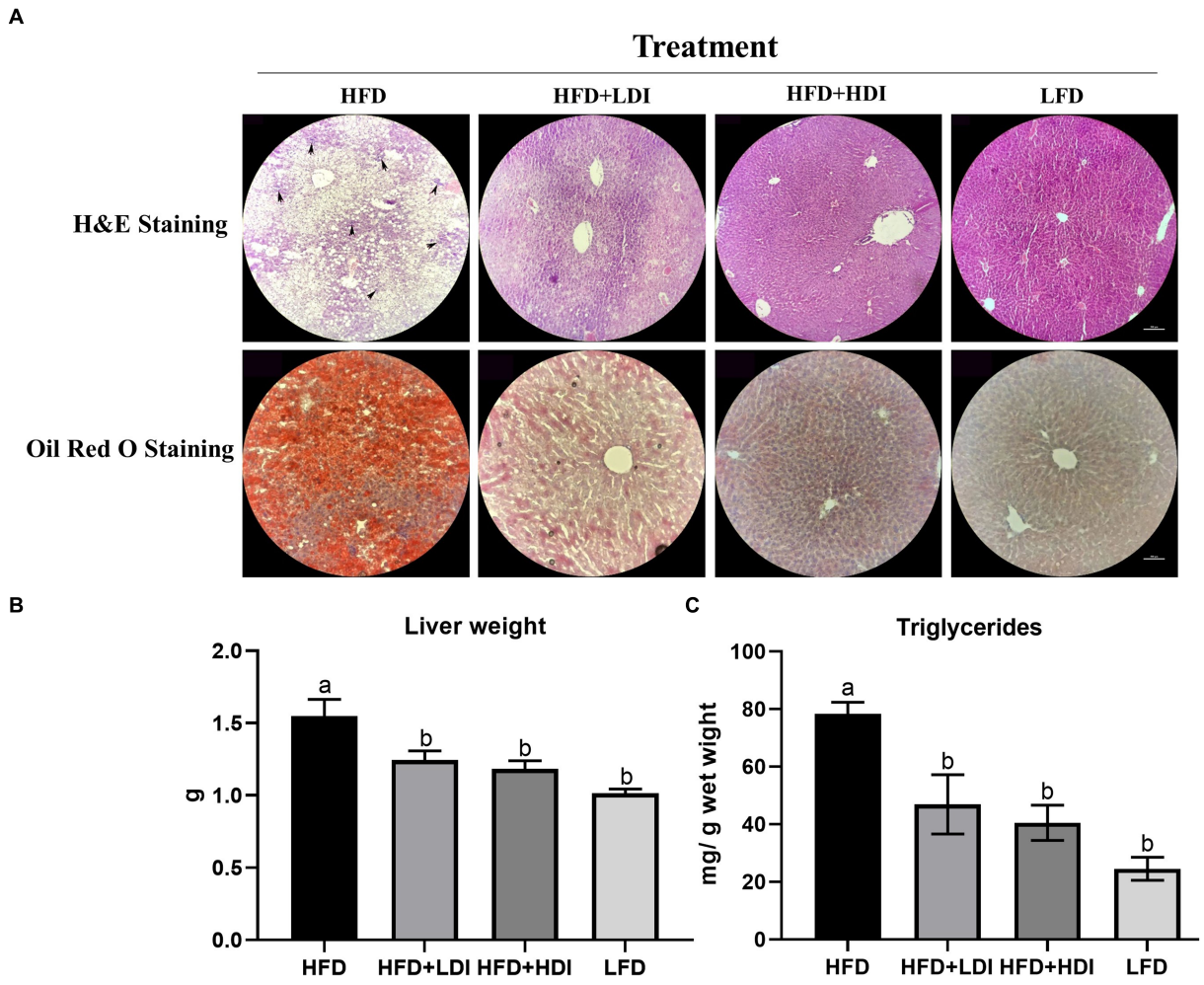

FIGURE 3
Effects of different polymerization degrees of inulin on liver health of high-fat diet and low-fat diet mice. **(A)** Hematoxylin and eosin (H&E) staining and Oil Red O staining of the liver of mice in different treatment groups. The arrowheads indicate inflammatory cell infiltration. **(B)** Liver weight of mice in different treatment groups. **(C)** Triglyceride levels in different treatment groups ($n = 8$). Within each panel, groups without a common letter indicate significant differences at $p < 0.05$. Scale bar, 500 μm.

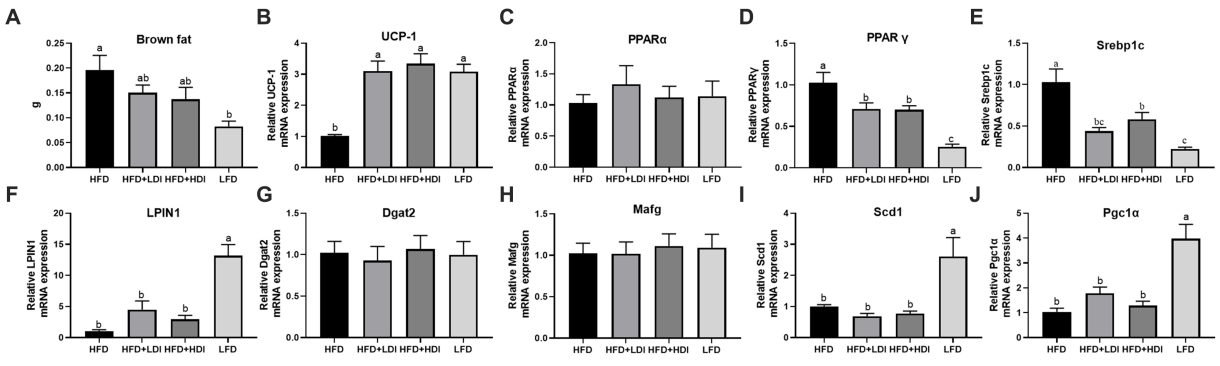

FIGURE 4
Effects of different polymerization degrees of inulin on gene expression in brown tissue and liver of high-fat diet mice. **(A,B)** Weight of brown fat tissue in different treatment groups. **(B)** Uncoupling protein 1 (UCP-1) gene expression in brown fat tissues. **(C-J)** Hepatic gene expression of PPARα, PPARγ, Srebp1, LPIN1, Dgat2, Mafg, Scd1, and Pgc1α ($n = 8$). Within each panel, groups without a common letter indicate significant differences at $p < 0.05$. HFD, high fat diet; HFD + HDI, high fat diet with high polymerized degree inulin; HFD + LDI, high fat diet with low polymerized degree inulin; LFD, low fat diet.

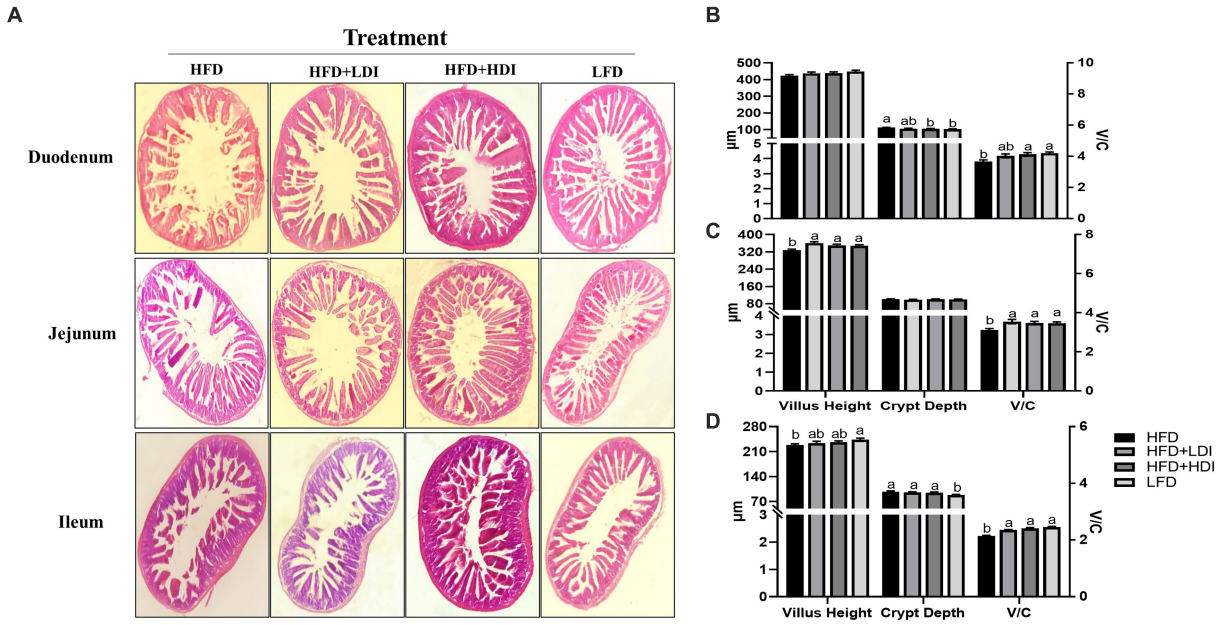

FIGURE 5
Effects of different polymerization degrees of inulin on intestinal health of high-fat diet-induced obese mice. **(A)** Morphology of duodenum, jejunum, and ileum in mice with different treatments. **(B–D)** Villus height, crypt depth, and the ratio of villus height to crypt depth (V/C) of duodenum, jejunum, and ileum, respectively, in mice with different treatments ($n = 8$). Within each panel, groups without a common letter indicate significant differences at $p < 0.05$. HFD, high fat diet; HFD + HDI, high fat diet with high polymerized degree inulin; HFD + LDI, high fat diet with low polymerized degree inulin; LFD, low fat diet.

mice in the HFD groups ($p < 0.05$). The supplementation of inulin effectively enhanced the morphology of the intestine in high-fat diet-induced obese mice.

The effects of inulin on the microbiota both *in vitro* and *in vivo*

As depicted in Figures 1E,F, the supplementation of inulin led to a significant reduction in the abundance of *E. coli* when compared to the basic LB control medium ($p < 0.001$). Notably, HDI inulin exhibited a more potent inhibitory effect on *E. coli* than LDI inulin ($p = 0.03$).

Furthermore, the inclusion of inulin in the LB medium demonstrated a tendency to reduce the abundance of *S. aureus* ($p = 0.059$). The supplementation of 8% inulin had minimal impact on the growth of *L. plantarum* and *L. rhamnosus*. However, it was observed that the addition of 8% LDI inulin significantly reduced the abundance of *L. reuteri* ($p = 0.019$), whereas HDI had no discernible effect on *L. reuteri*.

To investigate the impact of inulin on cecal microbiota in obese mice, we employed sequencing of the bacterial 16S rRNA V3 + V4 region. Following data processing, a total of 331 operational taxonomic units (OTUs) were clustered and generated, guided by the principle of over 97% similarity, based on 1,139,609 sequencing reads. The sequencing depth was sufficient to encompass (>99%) all OTUs present in the cecum digesta, providing a nearly comprehensive representation of the overall microbial species richness, as evidenced by rarefaction and ranked abundance (Supplementary Figure S1).

Differential analysis of α-diversity metrics among groups revealed a significant impact of dietary fat on cecal microbial richness. This was indicated by lower Chao1 and ACE indices in mice from the HFD, HFD + LDI, and HFD + HDI groups compared to those in the LFD treatment group ($p = 0.021$ and 0.015, respectively; Figures 6A,B). Importantly, the supplementation of inulin did not restore microbial richness in the ceca of the mice. Intriguingly, mice administered HDI inulin exhibited lower cecal microbiota diversity, as evidenced by reduced Shannon and Simpson indices compared to those in the HFD and HFD + LDI groups ($p = 0.0089$ and 0.0044, respectively; Figures 6C,D).

For a deeper exploration of beta diversity within cecal microbiota across different treatment groups, we conducted principal components analysis (PCA) and principal coordinates analysis (PCoA) of OTUs in each sample. As illustrated in Figures 6E,F, the bacterial communities of mice in the HFD + HDI group were distinct from those in the HFD and LFD groups. Additionally, ANOSIM analysis on OTUs and other taxonomic levels revealed that the differences between inter-group compositions were more significant than those within the same group, with $p < 0.05$ (Supplementary Figure S2).

Figure 7 presents the relative abundance of cecal microbiota in mice, focusing on phylum and family levels (more than 0.5%) and genus and species levels (more than 1%). The dominant phyla in the cecum of mice were Bacteroidetes and Firmicutes, accounting for 87.7, 82.5, 68.1, and 86.9% in the HFD, HFD + LDI, HFD + HDI, and LFD groups, respectively (Figure 7A). Interestingly, the abundance of Verrucomicrobiota in the cecum of mice in the HFD + HDI group was notably higher than that in other groups ($p = 0.009$, Figure 7A and Supplementary Table S5).

At the family level, the most dominant bacterial families in the cecal contents of the mice from different treatment groups were Lachnospiraceae, Muribaculaceae, Erysipelotrichaceae, Bacteroidaceae, and Akkermansiaceae, collectively accounting for approximately 66%

10.3389/fmicb.2024.1428308

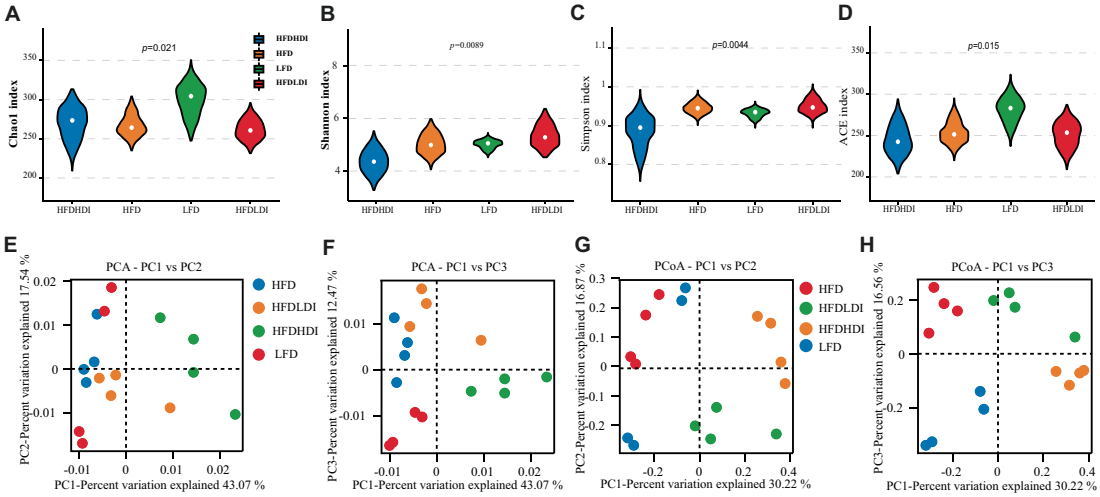

FIGURE 6
Effects of different polymerization degrees of inulin on the diversity of cecal microbiota in mice with different treatment groups. **(A–D)** Chao1 index, Shannon index, Simpson index, and ACE index of cecal microbiota. **(E,F)** Principal component analysis (PCA) at PC1 and PC2, and PC1 and PC3 of cecal microbiota of the mice. **(G,H)** Principal coordinates analysis (PCoA) at PC1 and PC2, and PC1 and PC3 of cecal microbiota ($n = 4$). HFD, high fat diet; HFD + HDI, high fat diet with high polymerized degree inulin; HFD + LDI, high fat diet with low polymerized degree inulin; LFD, low fat diet.

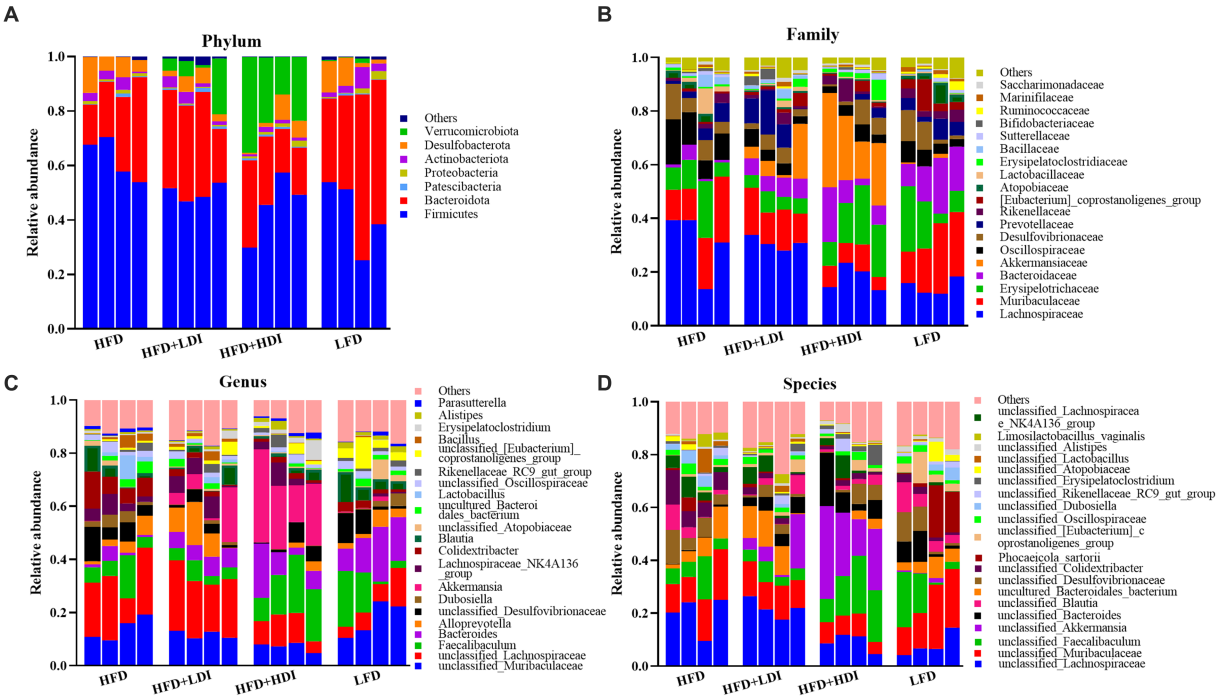

FIGURE 7
Relative abundance of cecal microbiota at phylum **(A)**, family **(B)**, genus **(C)**, and species **(D)** levels in mice under different treatments ($n = 4$).

of the bacterial abundance at the family level (Figure 7B). The abundance of Akkermansiaceae, a member of the Verrucomicrobiota phylum, was significantly higher in mice from the HFD group compared to other treatment groups ($p = 0.021$, Supplementary Table S5).

The abundance of cecal bacteria at the genus and species levels also reflected differences in microbiota composition among all treatments. The increased abundance of the *Akkermansia* genus ($p = 0.013$, Figure 7C and Supplementary Table S5) and *unclassified_Akkermansia* species ($p = 0.017$, Figure 7D and Supplementary Table S5) in the HFD + HDI group aligns with the increased presence of the Verrucomicrobiota phylum and the Akkermansiaceae family.

Identification of microbiota composition in different treatments and correlation analysis

To further unveil the microbiota with statistically significant differences between different groups, we employed Linear Discriminant Analysis Effect Size (LEfSe) analysis. The cladogram in Figure 8A illustrates the biomarkers in different treatment groups of mice at various taxonomic levels. Additionally, Figure 8B provides a detailed representation of microbiota with LDA scores exceeding 4. At the phylum level, Verrucomicrobiales emerged as the highly abundant microbiota in the HFD + HDI group, while Firmicutes prevailed as the highly abundant microbiota in the HFD group. On the gene level, *Bacteroides*, *unclassified_Lachnospiraceae*, *Akkermansia*, and *Colidextribacter* were identified as highly enriched in the cecal microbiota of mice in the LFD, HFD + LDI, HFD + HDI, and HFD groups, respectively.

To delve deeper into the relationships between these microbiota in different treatments and their potential functions in mice, Spearman correlation analysis was conducted between microbiotas that are distinguishably distributed across different treatment groups and various indexes related to mouse body weight. As depicted in Figure 9A, in the correlation analysis across the four treatment groups, the microbiota in the LFD group, notably Bacteroides, exhibited a strong positive association with gene expression of *UCP1* and *LPIN1*. Conversely, it displayed a highly negative association with body weight, liver weight, liver TG contents, and gene expression of *PPARγ* ($p < 0.01$). In contrast, microbiota highly abundant in the HFD group, such as Lachnospirales, Lachnospiraceae, and *Colidextribacter*, displayed a strong positive correlation with body weight ($p < 0.05$). However, Firmicutes, Oscillospiraceae, and *Colidextribacter* exhibited a highly negative correlation with gene expression of *UCP1* ($p < 0.05$). The microbiota that was notably abundant in the HFD + HDI group, such as Verrucomicrobiota and *Akkermansia*, exhibited a strong correlation with *UCP1* and a negative correlation with *Scd1* gene expression ($p < 0.05$).

Furthermore, Spearman correlation analysis was conducted among the high-fat diet treatment groups (HFD, HFD + LDI, and HFD + HDI) to examine possible associations of microbiota in the inulin treatment group with other indexes. As shown in Figure 9B, biomarker microbiota in the HFD + HDI group, including *Erysipelatoclostridium*, Verrucomicrobiota, and *Akkermansia*, demonstrated strong negative associations with body weight, liver weight, and liver TG contents ($p < 0.05$). These same microbiota were also positively associated with *UCP1* ($p < 0.05$). Conversely, Oscillospiraceae and *Colidextribacter* in the HFD group displayed strong positive associations with body weight, liver weight, *PPARγ*, and hepatic TG contents, while showing a negative association with *UCP1* gene expression ($p < 0.05$) (Figure 10).

Discussion

The biochemical functionality of inulin is intricately linked to its structural attributes. Consequently, comprehending the characteristics and functional traits of inulin with varying polymerization becomes imperative for their multifaceted applications across diverse conditions. The DP, often referred to as chain length, wields substantial influence over the biological functions of inulin. In our investigation, we observed that HDI exhibited near-insolubility in water at 25°C, while LDI readily dissolved in water. This observation aligns with prior research findings that have consistently demonstrated a decrease in inulin solubility as the DP increases (Mensink et al., 2015). A closer examination of their morphology revealed that LDI powder exhibited a larger apparent particle size than HDI. The solubility of inulin is closely related to its molecular conformation and DP (Barclay et al., 2010). LDI is more flexible and can adopt a range of conformations and orientations. This flexibility is reflected in the additional peak observed in the FTIR spectra at 781.49 cm^{-1}, which corresponds to the hydroxyl functional group. The increased flexibility of LDI may result in different vibrational modes of the OH group, leading to the observed extra peak. Moreover, the presence of hydrophilic functional groups and the flexibility of LDI enhance its ability to form hydrogen bonds and other molecular interactions (Mensink et al., 2015), partially explaining its solubility. In contrast, HDI consists of a larger number of fructose units, forming an extensive hydrogen-bonding network that creates a nearly crystalline structure. This can result in a more rigid and extended molecular configuration, limiting its flexibility and interactions with other molecules. Consequently, water molecules have difficulty penetrating and surrounding HDI molecules, leading to their limited solubility. Additionally, inulin is known to exhibit intermolecular forces (French, 1989), which may further stabilize the structure of HDI and reduce its affinity for water. The larger particle size observed in LDI may be attributed to the tendency of shorter chains to agglomerate. Furthermore, due to the presence of hydrophilic groups in LDI, exposure to air may cause water molecules to interact with the hydrophilic groups on the surface of LDI, causing it to swell and appear larger when observed under a microscope.

Many polysaccharides and dietary fibers are characterized by their oil binding capacity, a property that plays a crucial role in delaying the digestion and absorption of dietary fats. This delay in fat absorption can contribute to the prevention of obesity (You et al., 2022). Consequently, inulin's ability to bind to dietary oils can slow down the digestion and absorption of fats, potentially leading to increased fat excretion. This mechanism may explain the reduction in body weight observed in high-fat diet-induced obese mice following inulin administration. Furthermore, it is worth noting that HDI exhibits a higher oil binding capacity than LDI. This difference in oil binding capacity could account for the superior effects of HDI in reducing body weight compared to LDI. This observation aligns with a study conducted by Han et al. (2013), which demonstrated that inulin with an average DP of 24 significantly increased cecal total lipid contents when compared to a cellulose-HFD in rats (Han et al., 2013).

Given that inulin is primarily fermented by intestinal microbiota rather than being absorbed by the host animal, we conducted *in vitro* experiments to examine the effects of inulin on certain bacteria. In our study, we found that inulin had the capacity to inhibit the growth of the pathogenic bacteria *E. coli*. Notably, this inhibitory ability increased with DP, which can be attributed to *E. coli*'s inability to utilize either long or short inulin as a carbon source due to the absence of crucial inulin degradation enzyme β-fructofuranosidases (Cockburn and Koropatkin, 2016). Additionally, HDI has been reported to form a stable gel in water (Bchir et al., 2019), which could potentially hinder nutrients uptake by *E. coli*.

Obesity is a significant risk factor in the development of T2D (Nagy and Einwallner, 2018). In our study, a high-fat diet indeed induced higher fasting blood glucose levels and impaired glucose tolerance, and these effects could not be reversed by the addition of

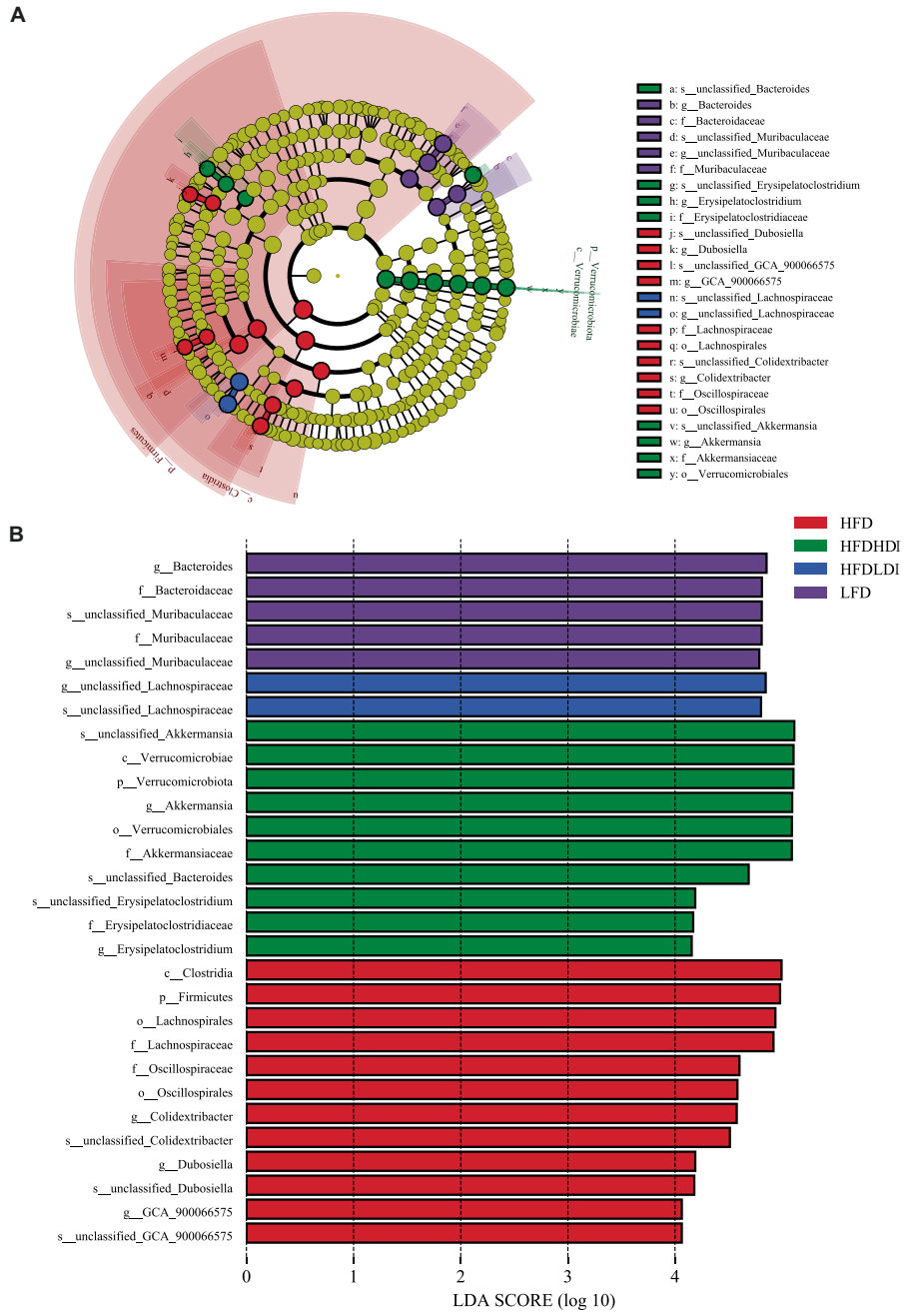

FIGURE 8
Dominant bacteria in the cecum of mice under different treatments. **(A)** Cladograms representing the LEfSe results for different treatment groups. **(B)** LDA scores of gut microbiota in different groups. HFD, high fat diet; HFD + HDI, high fat diet with high polymerized degree inulin; HFD + LDI, high fat diet with low polymerized degree inulin; LFD, low fat diet.

inulin. The impact of inulin on insulin resistance is a topic of debate, with varying results reported in both animal experiments and human clinical trials (Han et al., 2013; Shao et al., 2020). This controversy is especially apparent in obese individuals, as insulin resistance may not be improved by inulin supplementation (Rao et al., 2019). It is noteworthy that obese mice exhibit a distinct composition of intestinal microbiota compared to lean mice, potentially accounting for the different effects on insulin resistance in obese and lean subjects. In our study, inulin was added 4 weeks after starting the high-fat diet, which differs from some other studies where inulin was supplemented from the beginning of the diet (Li et al., 2021), thus better reflecting its effects in obese individuals. Our findings suggest that glucose metabolism in the current study was not significantly influenced by inulin treatment, indicating that the observed changes in body weight due to inulin were not likely caused by alterations in glucose absorption.

To better understand why inulin reduced the body weight of high-fat diet-induced obese mice, we investigated the weight of white adipose tissue and brown adipose tissue. While there were no statistically significant differences among mice in the HFD + LDI, HFD + HDI, and HFD treatment groups, both LDI

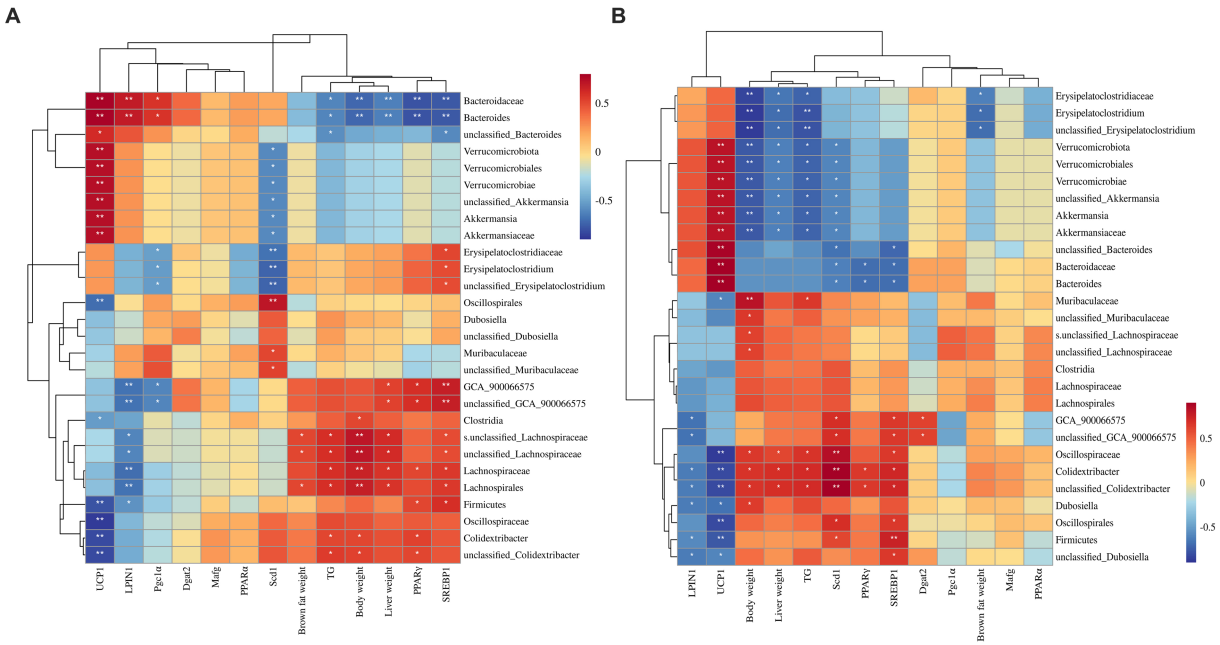

FIGURE 9
Correlation between biomarker microbiota and other fat-synthesis related parameters. **(A)** Spearman's correlation conducted using all treatment group data, including the low-fat diet group. **(B)** Spearman's correlation conducted using data from the three high-fat diet groups. $*p < 0.05$, $**p < 0.01$.

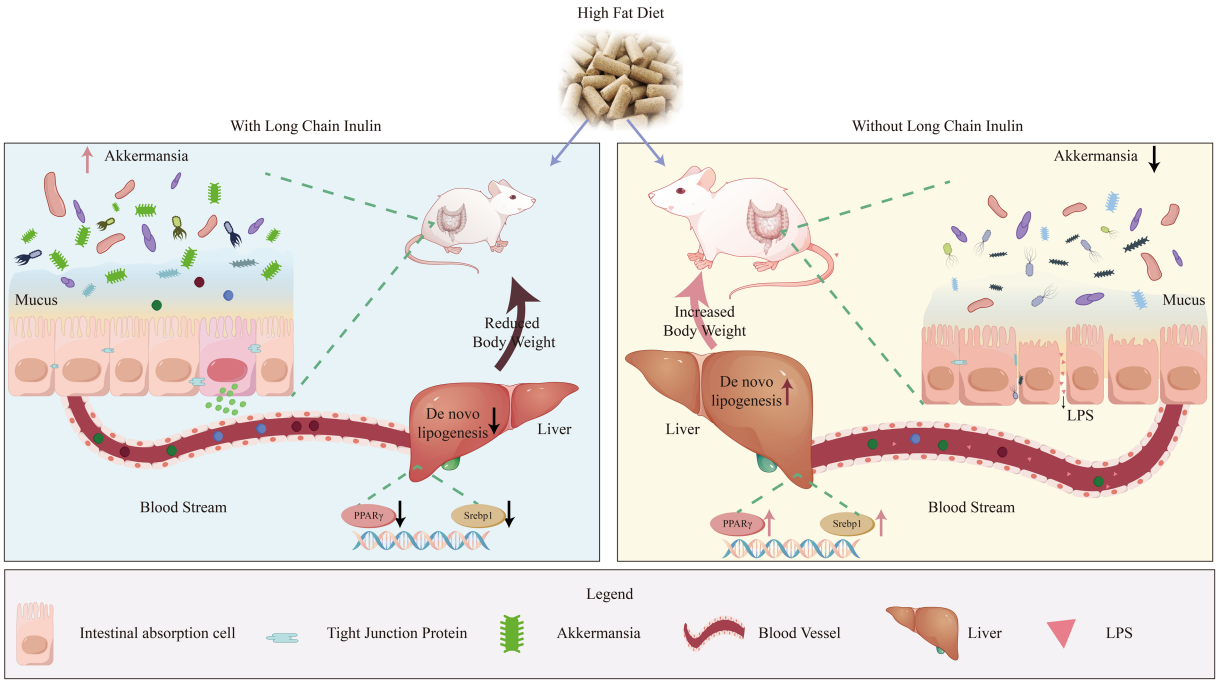

FIGURE 10
Long-chain inulin reduces body weight in high-fat dietinduced obese mice by inhibiting liver lipogenesis and modulating cecal microbiota composition, particularly increasing the abundance of Akkermansia.

and HDI administration resulted in some reduction in white adipose tissue. UCP1 is responsible for thermogenesis in brown adipose tissue, which increases energy expenditure (Iwen et al., 2008). Notably, both LDI and HDI inulin increased the gene expression of *UCP1* in brown adipocytes by 200%, suggesting that LDI and HDI inulin could enhance energy expenditure in high-fat

diet-induced obese mice, contributing to the observed reduction in body weight.

Furthermore, in our study, both LDI and HDI had a significant impact on the liver of obese mice when compared to white adipose tissues. These inulin treatments resulted in a reduction in lipid content in the liver, consistent with the observed decrease in liver weight, with HDI showing more pronounced effects. Triglycerides in the liver can originate from 3 main sources: uptake of fatty acids from the plasma (released by lipolysis), *de novo* synthesis of fatty acids, and dietary fat delivered by chylomicron remnants (Jensen-Urstad and Semenkovich, 2012). Since high-fat diet-induced insulin resistance was evident in our study, as indicated by high fasting blood glucose levels and reduced glucose tolerance, it is unlikely that the reduction in liver triglycerides was due to increased uptake of fatty acids from the plasma. As mentioned previously, inulin administration led to increased fecal fat excretion, which may have contributed to the reduction in dietary fatty acid uptake by the liver. Hepatic lipid metabolism is regulated by a dynamic transcriptional network, with nuclear receptors, particularly PPARs, playing a pivotal role. Srebp-1, highly expressed in the liver, regulates genes responsible for lipogenesis in response to insulin stimulation (Zhu et al., 2021).

Our results showed that HFD mice had the highest expression of the *Srebp1* gene, followed by inulin-administered mice and the LFD group. This pattern of gene expression correlates with the triglyceride contents in the treatment groups. Since *Srebp1* is regulated by insulin, the observed changes in its expression suggest that both LDI and HDI could improve insulin resistance caused by a high-fat diet. The reduced expression of *Srebp1* by LDI and HDI subsequently inhibited hepatic lipogenesis, leading to decreased hepatic triglyceride levels. The PPARα signaling pathway plays a crucial role in various metabolic processes, including fatty acid oxidation and ketone body synthesis. On the other hand, PPARγ is a key regulator of adipocyte differentiation, promoting adipogenesis and weight gain. Increased expression of *PPARγ* has been observed in patients with fatty liver disease (Skat-Rørdam et al., 2019). In our study, consistent with previous research, mice in the LFD group exhibited the lowest expression of the *PPARγ* gene, which was associated with the lowest hepatic triglyceride content. The addition of inulin inhibited the upregulation of *PPARγ* expression induced by the high-fat diet, resulting in reduced fat accumulation in the liver. Furthermore, overexpression of *PPARγ* has been reported to increase inflammation in the liver (Lee et al., 2018), which aligns with our findings of increased inflammation in the liver of HFD mice. Additionally, high-fat diet-induced elevation of *PPARγ* levels has been associated with increased expression of *Srebp-1*, a regulator of downstream lipogenic genes that enhances hepatic lipogenesis. Therefore, the high expression of PPARγ in the HFD group may have induced the activation of Srebp-1 and, in turn, increased hepatic lipogenesis. Besides regulating Srebp-1, PPARγ can directly target fat-specific protein, which is involved in both lipogenesis and fatty acid uptake in the liver. Thus, the high expression of PPARγ and Srebp-1 may have contributed to fat accumulation in the liver of HFD mice, while the reduced expression of these genes in LDI and HDI treatment groups implied a reduced capacity for lipid synthesis in the liver, consistent with the observed decrease in hepatic triglyceride content.

Obesity leads to defects in the mucus layer, characterized by increased penetrability and reduced mucus growth rate (Schroeder et al., 2020), which may result in the increased leakage of inflammatory substances into the body and contribute to increased inflammation in the liver, as observed in the HFD group of mice. Notably, the addition of HDI improved villus morphology in obese mice, suggesting a potential positive effect on certain aspects of intestinal function. Furthermore, gut microbiota plays a crucial role in maintaining intestinal health, and fiber consumption, such as inulin, is typically associated with increased diversity in intestinal microbiota in both animals and humans. Interestingly, in our study, the inclusion of inulin, especially HDI, significantly decreased the α diversity of cecal microbiota in high-fat diet-induced obese mice. This finding aligns with previous research that has also reported decreased α diversity in response to inulin supplementation, even at different doses and dietary contexts (Hutchinson et al., 2023; Le Bastard et al., 2020; Li et al., 2021). High-fat diets have been shown to reduce microbial richness, the richness did not fully recover with HDI or LDI administration in our study. Moreover, the diversity within individual samples significantly decreased with HDI inulin administration. It is important to note that interpretations of α diversity can vary depending on the calculation method used, and the significance or value of these metrics may not always be straightforward (Koutoukidis et al., 2022; Shade, 2017).

Examining the relative abundance of intestinal microbiota revealed an increase in the abundance of Verrucomicrobiota at the phylum level and *Akkermansia* at the genus level in the HDI inulin group. This led to increased dominance within the microbial community, potentially resulting in reduced evenness and, consequently, decreased diversity (as indicated by reduced Shannon and Simpson index) in the HFD + HDI group.

The increased abundance of *Akkermansia* in the cecum of obese mice due to the addition of HDI is of particular interest, as *Akkermansia muciniphila* is considered a potential health-promoting bacterium (Shin et al., 2014). Administrating *Akkermansia* to HFD-induced obese mice could strengthen the tight junction and mucus barrier (Li et al., 2024). Previous studies have shown that high-fat diets tend to decrease the abundance of *Akkermansia* in the microbiota of mice compared to low-fat diets, making its increase through dietary intervention a valuable finding (Wang et al., 2020). It is worth noting that the impact of inulin on *Akkermansia* abundance can be influenced by various factors, including diet composition and the interactions among different microbial species. For instance, some studies have reported that inulin supplementation, especially in the context of high-fat diets, can increase the abundance of *Akkermansia* (Pérez-Monter et al., 2022). The mechanisms behind these changes in *Akkermansia* abundance are complex and may involve factors such as the influence of HDI on the gut mucosal layer, potential cross-feeding interactions with other bacteria, or the HDI's effects on the overall gut microbiota composition. Interestingly, another biomarker genus, *Erysipelatoclostridium*, was positively correlated with *Akkermansia* in the HFD + HDI group. *Erysipelatoclostridium* has been associated with anti-inflammatory properties in obese mice (Roager et al., 2019; van Trijp et al., 2020) and was found to increase during *in vitro* fermentation experiments with human small intestinal microbiota.

Overall, these findings suggest that dietary interventions with HDI may have a positive impact on gut microbiota composition, particularly with regard to the abundance of beneficial bacteria like *Akkermansia*, which could contribute to improved host health. Further research is needed to fully understand the complex interactions within the gut microbiota and how dietary factors like inulin can influence these interactions and promote health.

The correlations between specific gut microbiota and various metabolic and health parameters in response to inulin treatment provide valuable insights into the complex interplay between diet, gut

microbiota, and host health. In the HFD group, the biomarker microbiota like *Colidextribacter*, Lachnospiraceae, Lachnospirales, and Dubosiella exhibited strong positive correlations with factors associated with obesity and fatty liver, such as body weight, triglycerides, *PPARγ*, and *Srebp1*. These correlations suggest that these microbiota may contribute to the development of obesity and its associated metabolic complications. The negative correlation with *UCP1* further highlights their potential role in reduced energy expenditure. Conversely, in the HFD + HDI group, the biomarker microbiota *Akkermansia* and *Erysipelatoclostridium* displayed positive correlations with *UCP1*, indicating a potential role in promoting energy expenditure. This is consistent with the observed reduction in body weight in this group. Gut microbiota plays vital roles in alleviating steatotic liver through reducing hepatic PPARγ and related lipogenesis genes (Murakami et al., 2016). The negative correlations with factors like body weight, *PPARγ*, and *Srebp1* in our experiment further suggest that these microbiota may play a role in reducing fat accumulation and improving liver health. The role of SCFA produced by gut microbiota, especially *Akkermansia*, is highlighted as a potential mechanism for improving liver health and reducing hepatic *PPARγ* expression. Additionally, aside from the potential metabolites that regulate hepatic *PPARs* expression and other lipid metabolic genes, *A. muciniphila* has been reported to mitigate inflammatory factors, thus reducing hepatic lipogenesis (Ghaderi et al., 2022). These findings suggest that the microbiota's metabolites, influenced by dietary fiber such as inulin, can have significant effects on host health. The variations in outcomes observed in different studies using inulin with varying DP and different dietary conditions underscore the complexity of the gut microbiota-host interaction (Yamaguchi et al., 2021). The individual's baseline health status, along with diet and specific inulin properties, can all contribute to different responses in gut microbiota composition and metabolic outcomes.

Conclusion

Overall, our experiment highlights the potential benefits of HD inulin in managing body weight, ameliorating liver health issues, and modulating the composition and structure of cecal microbiota in obese mice (Figure 10). The observed effects of HDI in promoting the abundance of *Akkermansia* in the intestines of obese mice are noteworthy, as previous research has demonstrated the beneficial effects of certain *Akkermansia* species supplementation on both liver and intestinal health. Additionally, the limited effects of LDI on cecal *Akkermansia* may suggest that the differing impacts of different DP of inulin on obese individuals largely originate from their effects on the intestinal *Akkermansia*. If HDI administration yields similar effects to those of prebiotic supplementation, it could offer a more practical approach for alleviating fatty liver disease and managing body weight, given the ease of handling dietary fiber compared to live bacteria.

Furthermore, while our study demonstrated the enrichment of *Akkermansia*, it did not directly link this to improvements in intestinal and hepatic health. Further investigation is warranted to provide more robust evidence and to explore the mechanisms through which HD inulin could enrich *Akkermansia*. Additionally, more studies should be conducted to elucidate the specific metabolites responsible for these potential effects. Since inulin fiber is primarily utilized by intestinal bacteria, it is essential to identify the metabolites produced by these bacteria and their mechanisms of action. Additionally, conducting fecal bacteria translocation experiments in HFD-induced mice could provide further insights into the role of the microbiota in mediating the effects of inulin supplementation. These future investigations will contribute to a more comprehensive understanding of the mechanisms underlying the beneficial effects of HDI inulin on host health.

Data availability statement

The original contributions presented in the study are publicly available. This data can be found here: https://www.ncbi.nlm.nih.gov/, accession number PRJNA1151349.

Ethics statement

The animal study was approved by the Animal Care and Use Committee of Biological Engineering, Henan University of Technology. The study was conducted in accordance with the local legislation and institutional requirements.

Author contributions

LGa: Conceptualization, Data curation, Supervision, Writing – original draft. YZ: Data curation, Investigation, Writing – original draft. ZZ: Data curation, Investigation, Writing – original draft. CZ: Data curation, Investigation, Writing – original draft. JL: Data curation, Investigation, Writing – original draft. QJ: Data curation, Investigation, Writing – original draft. YS: Data curation, Investigation, Writing – original draft. PW: Methodology, Writing – review & editing. LGu: Methodology, Writing – review & editing. HQ: Methodology, Writing – review & editing. YC: Methodology, Writing – review & editing. JW: Supervision, Writing – review & editing.

Funding

The author(s) declare that financial support was received for the research, authorship, and/or publication of this article. This research was funded by the National Natural Science Foundation of China (grant no. 32202696), the National Key Research and Development Program of China (grant no. 2022YFD1300604), the scientific research startup project of Henan University of Technology (grant no. 31401405), and the Cultivation Program for young key teachers in Henan University of Technology (grant no. 21421255).

Acknowledgments

The authors thank all the teachers and students on the "Feed Safety and Nutrition Quality" team for their contributions in helping us to collect the samples of the mice.

Conflict of interest

The authors declare that the research was conducted in the absence of any commercial or financial relationships that could be construed as a potential conflict of interest.

Publisher's note

All claims expressed in this article are solely those of the authors and do not necessarily represent those of their affiliated organizations, or those of the publisher, the editors and the reviewers. Any product that may be evaluated in this article, or claim that may be made by its manufacturer, is not guaranteed or endorsed by the publisher.

Supplementary material

The Supplementary material for this article can be found online at: https://www.frontiersin.org/articles/10.3389/fmicb.2024.1428308/full#supplementary-material

References

Akram, W., and Garud, N. (2020). Optimization of inulin production process parameters using response surface methodology. *Future J. Pharm. Sci.* 6, 1–9. doi: 10.1186/s43094-020-00087-1

Al-Abdullatif, A., and Azzam, M. M. (2023). Effects of hot arid environments on the production performance, carcass traits, and fatty acids composition of breast meat in broiler chickens. *Life* 13:1239. doi: 10.3390/life13061239

Barclay, T., Ginic-Markovic, M., Cooper, P., and Petrovsky, N. (2010). Inulin—a versatile polysaccharide with multiple pharmaceutical and food chemical uses. *J. Excipients Food Chem.* 1, 27–50.

Bchir, B., Sadin, N., Ronkart, S. N., and Blecker, C. (2019). Effect of powder properties on the physicochemical and rheological characteristics of gelation inulin–water systems. *Colloid Polym. Sci.* 297, 849–860. doi: 10.1007/s00396-019-04510-9

Bluher, M. (2019). Obesity: global epidemiology and pathogenesis. *Nat. Rev. Endocrinol.* 15, 288–298. doi: 10.1038/s41574-019-0176-8

Chikkerur, J., Samanta, A. K., Kolte, A. P., Dhali, A., and Roy, S. (2020). Production of short chain Fructo-oligosaccharides from inulin of chicory root using fungal Endoinulinase. *Appl. Biochem. Biotechnol.* 191, 695–715. doi: 10.1007/s12010-019-03215-7

Coates, J. (2000). Interpretation of infrared spectra, a practical approach in, Encyclopedia of Analytical Chemistry, John Wiley and Sons Ltd. Chichester. Eds. Meyers, R. A. and McKelvy, M. L. 10815-10837. doi: 10.1002/9780470027318.a5606

Cockburn, D. W., and Koropatkin, N. M. (2016). Polysaccharide degradation by the intestinal microbiota and its influence on human health and disease. *J. Mol. Biol.* 428, 3230–3252. doi: 10.1016/j.jmb.2016.06.021

Cui, A., Hu, Z., Han, Y., Yang, Y., and Li, Y. (2017). Optimized analysis of in vivo and in vitro hepatic steatosis. *J. Vis. Exp.* 121:e55178. doi: 10.3791/55178

Delannoy-Bruno, O., Desai, C., Raman, A. S., Chen, R. Y., Hibberd, M. C., Cheng, J., et al. (2021). Evaluating microbiome-directed fibre snacks in gnotobiotic mice and humans. *Nature* 595, 1–5. doi: 10.1038/s41586-021-03671-4

Du, H., Zhao, A., Wang, Q., Yang, X., and Ren, D. (2020). Supplementation of inulin with various degree of polymerization ameliorates liver injury and gut microbiota Dysbiosis in high fat-fed obese mice. *J. Agric. Food Chem.* 68, 779–787. doi: 10.1021/acs.jafc.9b06571

Eliby, D. (2022). How can we combat the obesity epidemic? *J. Health Design* 7, 490–493. doi: 10.21853/JHD.2022.156

French, A. D. (1989). Chemical and physical properties of Fructans. *J. Plant Physiol.* 134, 125–136. doi: 10.1016/S0176-1617(89)80044-6

Ghaderi, F., Sotoodehnejadnematalahi, F., Hajebrahimi, Z., Fateh, A., and Siadat, S. D. (2022). Effects of active, inactive, and derivatives of *Akkermansia muciniphila* on the expression of the endocannabinoid system and PPARs genes. *Sci. Rep.* 12:10031. doi: 10.1038/s41598-022-13840-8

Han, K., Tsuchihira, H., Nakamura, Y., Shimada, K., Ohba, K., Aritsuka, T., et al. (2013). Inulin-type Fructans with different degrees of polymerization improve lipid metabolism but not glucose metabolism in rats fed a high-fat diet under energy restriction. *Dig. Dis. Sci.* 58, 2177–2186. doi: 10.1007/s10620-013-2631-z

Hu, Y., He, J., Zheng, P., Mao, X., Huang, Z., Yan, H., et al. (2021). Prebiotic inulin as a treatment of obesity related nonalcoholic fatty liver disease through gut microbiota: a critical review. *Crit. Rev. Food Sci. Nutr.* 63, 1–11. doi: 10.1080/10408398.2021.1955654

Hutchinson, N. T., Wang, S. S., Rund, L. A., Caetano-Silva, M. E., Allen, J. M., Johnson, R. W., et al. (2023). Effects of an inulin fiber diet on the gut microbiome, colon, and inflammatory biomarkers in aged mice. *Exp. Gerontol.* 176:112164. doi: 10.1016/j.exger.2023.112164

Iwen, K. A. H., Senyaman, O., Schwartz, A., Drenckhan, M., Meier, B., Hadaschik, D., et al. (2008). Melanocortin crosstalk with adipose functions: ACTH directly induces insulin resistance, promotes a pro-inflammatory adipokine profile and stimulates UCP-1 in adipocytes. *J. Endocrinol.* 196, 465–472. doi: 10.1677/JOE-07-0299

Jeddou, K. B., Chaari, F., Maktouf, S., Nouri-Ellouz, O., Helbert, C. B., and Ghorbel, R. E. (2016). Structural, functional, and antioxidant properties of water-soluble polysaccharides from potatoes peels. *Food Chem.* 205, 97–105. doi: 10.1016/j.foodchem.2016.02.108

Jensen-Urstad, A. P. L., and Semenkovich, C. F. (2012). Fatty acid synthase and liver triglyceride metabolism: housekeeper or messenger? *Biochim. Biophys. Acta* 1821, 747–753. doi: 10.1016/j.bbalip.2011.09.017

Koutoukidis, D. A., Jebb, S. A., Zimmerman, M., Otunla, A., Henry, J. A., Ferrey, A., et al. (2022). The association of weight loss with changes in the gut microbiota diversity, composition, and intestinal permeability: a systematic review and meta-analysis. *Gut Microbes* 14:2020068. doi: 10.1080/19490976.2021.2020068

Le Bastard, Q., Chapelet, G., Javaudin, F., Lepelletier, D., Batard, E., and Montassier, E. (2020). The effects of inulin on gut microbial composition: a systematic review of evidence from human studies. *Eur. J. Clin. Microbiol. Infect. Dis.* 39, 403–413. doi: 10.1007/s10096-019-03721-w

Lee, S.-Y., Oh, H. R., Kim, Y.-H., Bae, S.-H., Lee, Y., Lee, Y.-S., et al. (2022). Cerenkov luminescence imaging of interscapular brown adipose tissue using a TSPO-targeting PET probe in the UCP1 ThermoMouse. *Theranostics* 12, 6380–6394. doi: 10.7150/thno.74828

Lee, Y. K., Park, J. E., Lee, M., and Hardwick, J. P. (2018). Hepatic lipid homeostasis by peroxisome proliferator-activated receptor gamma 2. *Liver Res.* 2, 209–215. doi: 10.1016/j.livres.2018.12.001

Li, Z., Nie, Q., and Nie, S.-P. (2024). Comprehensive insights: Unraveling the mechanisms of gut commensals in glucose metabolism regulation. *Sci. China Life Sci.* 67, 414–417. doi: 10.1007/s11427-023-2455-y

Li, L., Wang, Y., Zhu, L., Liu, Z., Ye, C., and Qin, S. (2020). Inulin with different degrees of polymerization protects against diet-induced endotoxemia and inflammation in association with gut microbiota regulation in mice. *Sci. Rep.* 10:978. doi: 10.1038/s41598-020-58048-w

Li, L., Zhang, L., Zhou, L., Jin, M., and Xu, L. (2021). Chain length-dependent inulin alleviates diet-induced obesity and metabolic disorders in mice. *Food Sci. Nutr.* 9, 3470–3482. doi: 10.1002/fsn3.2283

Livak, K. J., and Schmittgen, T. D. (2001). Analysis of relative gene expression data using real-time quantitative PCR and the $2^{-\Delta\Delta CT}$ method. *Methods* 25, 402–408. doi: 10.1006/meth.2001.1262

Mensink, M. A., Frijlink, H. W., Van Der Voort Maarschalk, K., and Hinrichs, W. L. J. (2015). Inulin, a flexible oligosaccharide I: review of its physicochemical characteristics. *Carbohydr. Polym.* 130, 405–419. doi: 10.1016/j.carbpol.2015.05.026

Murakami, M., Tognini, P., Liu, Y., Eckel-Mahan, K. L., Baldi, P., and Sassone-Corsi, P. (2016). Gut microbiota directs PPARγ-driven reprogramming of the liver circadian clock by nutritional challenge. *EMBO Rep.* 17, 1292–1303. doi: 10.15252/embr.201642463

Nagy, C., and Einwallner, E. (2018). Study of in vivo glucose metabolism in high-fat diet-fed mice using oral glucose tolerance test (OGTT) and insulin tolerance test (ITT). *J. Vis. Exp.* 131:56672. doi: 10.3791/56672

Patnode, M. L., Beller, Z. W., Han, N. D., Cheng, J., Peters, S. L., Terrapon, N., et al. (2019). Interspecies competition impacts targeted manipulation of human gut bacteria by Fiber-derived glycans. *Cell* 179, 59–73. doi: 10.1016/j.cell.2019.08.011

Pérez-Monter, C., Álvarez-Arce, A., Nuño-Lambarri, N., Escalona-Nández, I., Juárez-Hernández, E., Chávez-Tapia, N. C., et al. (2022). Inulin improves diet-induced hepatic steatosis and increases intestinal Akkermansia genus level. *Int. J. Mol. Sci.* 23:991. doi: 10.3390/ijms23020991

Prillaman, M. (2023). Four key questions on the new wave of anti-obesity drugs. *Nature* 620, 28–30. doi: 10.1038/d41586-023-02445-4

Rao, M., Gao, C., Xu, L., Jiang, L., Zhu, J., Chen, G., et al. (2019). Effect of inulin-type carbohydrates on insulin resistance in patients with type 2 diabetes and obesity: a systematic review and meta-analysis. *J. Diabetes Res.* 2019:e5101423. doi: 10.1155/2019/5101423

Roager, H. M., Vogt, J. K., Kristensen, M., Hansen, L. B. S., Ibrügger, S., Mærkedahl, R. B., et al. (2019). Whole grain-rich diet reduces body weight and systemic low-grade inflammation without inducing major changes of the gut microbiome: a randomised cross-over trial. *Gut* 68, 83–93. doi: 10.1136/gutjnl-2017-314786

Schroeder, B. O., Birchenough, G. M. H., Pradhan, M., Nyström, E. E. L., Henricsson, M., Hansson, G. C., et al. (2020). Obesity-associated microbiota contributes to mucus layer defects in genetically obese mice. *J. Biol. Chem.* 295, 15712–15726. doi: 10.1074/jbc.RA120.015771

Shade, A. (2017). Diversity is the question, not the answer. *ISME J.* 11:118. doi: 10.1038/ismej.2016.118

Shao, T., Yu, Q., Zhu, T., Liu, A., Gao, X., Long, X., et al. (2020). Inulin from Jerusalem artichoke tubers alleviates hyperglycaemia in high-fat-diet-induced diabetes mice through the intestinal microflora improvement. *Br. J. Nutr.* 123, 308–318. doi: 10.1017/S0007114519002332

Shin, N.-R., Lee, J.-C., Lee, H.-Y., Kim, M.-S., Whon, T. W., Lee, M.-S., et al. (2014). An increase in the *Akkermansia* spp. population induced by metformin treatment improves glucose homeostasis in diet-induced obese mice. *Gut* 63, 727–735. doi: 10.1136/gutjnl-2012-303839

Singh, A., Zapata, R. C., Pezeshki, A., Reidelberger, R. D., and Chelikani, P. K. (2018). Inulin fiber dose-dependently modulates energy balance, glucose tolerance, gut microbiota, hormones and diet preference in high-fat-fed male rats. *J. Nutr. Biochem.* 59, 142–152. doi: 10.1016/j.jnutbio.2018.05.017

Skat-Rørdam, J., Højland Ipsen, D., Lykkesfeldt, J., and Tveden-Nyborg, P. (2019). A role of peroxisome proliferator-activated receptor γ in non-alcoholic fatty liver disease. *Basic Clin. Pharmacol. Toxicol.* 124, 528–537. doi: 10.1111/bcpt.13190

Tan, P., Pepin, É., and Lavoie, J. L. (2018). Mouse adipose tissue collection and processing for RNA analysis. *J. Visualized Exp.* 131:57026. doi: 10.3791/57026

van Trijp, M. P. H., Rösch, C., An, R., Keshtkar, S., Logtenberg, M. J., Hermes, G. D. A., et al. (2020). Fermentation kinetics of selected dietary fibers by human small intestinal microbiota depend on the type of fiber and subject. *Mol. Nutr. Food Res.* 64:2000455. doi: 10.1002/mnfr.202000455

Visuthranukul, C., Chamni, S., Kwanbunbumpen, T., Saengpanit, P., Chongpison, Y., Tepaamorndech, S., et al. (2022). Effects of inulin supplementation on body composition and metabolic outcomes in children with obesity. *Sci. Rep.* 12:13014. doi: 10.1038/s41598-022-17220-0

Wang, B., Kong, Q., Li, X., Zhao, J., Zhang, H., Chen, W., et al. (2020). A high-fat diet increases gut microbiota biodiversity and energy expenditure due to nutrient difference. *Nutrients* 12:3197. doi: 10.3390/nu12103197

Yamaguchi, A., Teratani, T., Chu, P., Suzuki, T., Taniki, N., Mikami, Y., et al. (2021). Hepatic adenosine triphosphate reduction through the short-chain fatty acids–peroxisome proliferator-activated receptor γ–uncoupling protein 2 Axis alleviates immune-mediated acute hepatitis in inulin-supplemented mice. *Hepatol. Commun.* 5, 1555–1570. doi: 10.1002/hep4.1742

You, Y., Song, H., Yan, C., Ai, C., Tong, Y., Zhu, B., et al. (2022). Dietary fibers obtained from *Caulerpa lentillifera* prevent high-fat diet-induced obesity in mice by regulating the gut microbiota and metabolite profiles. *Food Funct.* 13, 11262–11272. doi: 10.1039/D2FO01632J

Zhu, C., Huang, M., Kim, H.-G., Chowdhury, K., Gao, J., Liu, S., et al. (2021). SIRT6 controls hepatic lipogenesis by suppressing LXR, ChREBP, and SREBP1. *Biochim. Biophys. Acta (BBA) Mol. Basis Dis.* 1867:166249. doi: 10.1016/j.bbadis.2021.166249

Zhu, Z., Huang, Y., Luo, X., Wu, Q., He, J., Li, S., et al. (2019). Modulation of lipid metabolism and colonic microbial diversity of high-fat-diet C57BL/6 mice by inulin with different chain lengths. *Food Res. Int.* 123, 355–363. doi: 10.1016/j.foodres.2019.05.003

Zhu, L., Qin, S., Zhai, S., Gao, Y., and Li, L. (2017). Inulin with different degrees of polymerization modulates composition of intestinal microbiota in mice. *FEMS Microbiol. Lett.* 364:fnx075. doi: 10.1093/femsle/fnx075

frontiers | Frontiers in Microbiology

TYPE Original Research
PUBLISHED 29 August 2024
DOI 10.3389/fmicb.2024.1420103

OPEN ACCESS

EDITED BY
Hesong Wang,
Southern Medical University, China

REVIEWED BY
Kaijian Hou,
Shantou University, China
Sidharth Prasad Mishra,
University of South Florida, United States

*CORRESPONDENCE
Zhaohui Fang
✉ fangzhaohui1111@163.com

RECEIVED 22 April 2024
ACCEPTED 29 July 2024
PUBLISHED 29 August 2024

CITATION
Zhao J and Fang Z (2024) Alterations of the gut microbiota and metabolites by ShenZhu TiaoPi granule alleviates hyperglycemia in GK rats.
Front. Microbiol. 15:1420103.
doi: 10.3389/fmicb.2024.1420103

Alterations of the gut microbiota and metabolites by ShenZhu TiaoPi granule alleviates hyperglycemia in GK rats

Jindong Zhao[1,2] and Zhaohui Fang[1,2]*

[1]Department of Endocrinology, The First Affiliated Hospital of Anhui University of Chinese Medicine, Hefei, Anhui, China, [2]Center for Xin'an Medicine and Modernizatison of Traditional Chinese Medicine of IHM, The First Affiliated Hospital of Anhui University of Chinese Medicine, Hefei, Anhui, China

ShenZhu TiaoPi granule (STG) is a compound prescription that is used in Chinese medicine for the treatment of type 2 diabetes mellitus (T2DM). Previous studies have indicated a hypoglycaemic effect, but the underlying mechanism remains unclear. Goto-Kakizaki (GK) rats were used to establish an in vivo T2DM model (Mod). The metformin (Met) and STG treatment time was 12 weeks. Fasting blood glucose (FBG) and insulin levels and the area under the glucose curve (GAUC) were measured. Intestinal pathology and permeability were observed. Microbial diversity analysis and metabolomics were used to investigate the underlying mechanisms. Compared with the Con group, the T2DM Mod group presented significant differences in weight, FBG, GAUC, and homeostasis model assessment–insulin resistance (HOMA-IR) indices ($p < 0.01$). Met and STG improved these indicators ($p < 0.01$). The pathological morphology and zonula occludens 1 protein levels in the intestines of the Mod group of rats were altered, leading to increases in the lipopolysaccharide (LPS) and interleukin-1β (IL-1β) levels. In the Met and STG groups, the intestinal conditions improved, and the LPS and IL-1β levels significantly decreased ($p < 0.01$). Changes in the gut microbiota and metabolites occurred in the Mod group. In the STG group, the abundance of Intestinimonas increased, and the abundance of Eubacterium coprostanoligenes decreased significantly ($p < 0.05$). Moreover, STG also altered 2-deoxyglucose, beta-muricholic acid and dioxolithocholic acid production. In addition, the main metabolic pathways affected by STG were bile acid biosynthesis and cholesterol metabolism. Intestinimonas, D-maltose_and_alpha-lactose may be potential biomarkers for the effects of STG. STG alleviates hyperglycaemia via the gut microbiota and metabolites in GK rats.

KEYWORDS

type 2 diabetes mellitus, alleviating hyperglycemia, gut microbiota, gut metabolites, ShenZhu TiaoPi granule

Introduction

Type 2 diabetes mellitus (T2DM) is a metabolic disease characterized by elevated blood glucose levels due to a complex combination of genetic and environmental factors (Chen and Wang, 2021; Laffel et al., 2023). Good glycemic control has a profound effect on the occurrence, development and regression of T2DM and its acute and chronic complications

(Wang et al., 2018). In modern daily life, unhealthy dietary structures and exercise patterns have accelerated the rising trend of T2DM and its rejuvenation, seriously jeopardizing human health (Fujihara et al., 2023).

The intestinal flora is an important internal environment in the body, and a decrease in beneficial bacteria and an increase in pathogenic bacteria in the intestinal tract can lead to the abnormal function of organs, tissues and cells of the body, which can contribute to an imbalance in glucose metabolism (Chen and Wang, 2021). Intestinal metabolites are important signaling factors, energy substrates, nutritional sensors and metabolic regulators involved in the development of T2DM (Swann et al., 2011; Jia et al., 2018).

T2DM belongs to the category of "Xiao Ke" in Chinese medicine. The etiology and pathogenesis of T2DM are qi and yin deficiency. Among them, qi and yin are highly energetic and important substances in the human body. Qi and yin deficiency syndrome can manifest as thirst, increased diet, increased frequency of urination, and weight loss, among other symptoms. Chinese medicine has clinical efficacy in the prevention and treatment of T2DM (Bai et al., 2019). Shenzhu Tiaopi granule (STG) tonifies qi and nourishes yin. Clinical studies have shown that STG can lower blood glucose levels, alleviate dry mouth, thirst, and fatigue, and reduce the frequency of urination (Fang et al., 2014; Zhang et al., 2023). These changes are associated with improved hepatic insulin resistance (Yin et al., 2021). However, whether STG affects the gut flora or metabolites is unclear. The present study was conducted using GK rats with T2DM to further explore the effects of STG in regulating blood glucose levels by affecting the intestinal flora and metabolites and to explore the possible mechanisms of action to provide an effective prescription for alleviating hyperglycaemia in individuals with T2DM and to facilitate scientific research on the prevention and treatment of T2DM by traditional Chinese medicine.

Materials and methods

Animals and experimental design

Fifteen-to sixteen-week-old male GK rats were obtained from Changzhou Cavens Model Animal Co., Ltd. (Changzhou, China; certificate no. 202145537). Male Wistar rats of the same age were obtained from Sipeifu (Beijing) Biotechnology Co., Ltd. (Beijing, China; certificate no. 110324210106676238). The rats were acclimated in a specific pathogen-free laboratory. The rats were provided standard chow and water *ad libitum*. The temperature was maintained at 22 ± 2°C with 50–70% humidity on a 12/12 h light/dark cycle.

After acclimation for 1 week, 32 GK rats with high fasting blood glucose (FBG) levels (≥ 11.1 mmol/L) were randomly divided into three groups ($n = 8$). The T2DM model group (Mod) received distilled water intragastrically. Metformin (Met) obtained from Sino-American Shanghai Squibb Pharmaceuticals Ltd. (Shanghai, China) was administered by oral gavage at 100 mg/kg/d to the Met group. The STG group was orally gavaged with 21 g/kg/d STG. Wistar rats in the control (Con) group received distilled water via oral gavage. The course of treatment was 12 weeks.

Weight and blood glucose measurements

Weight and FBG levels were measured once every 2 weeks. FBG levels were measured as follows: after 12 h of fasting, blood was collected from the tail vein of the rats, and FBG levels were measured using a Roche ACCU-CHEK Performa glucometer (Basel, Switzerland).

After 12 h of fasting, each rat was administered 2.0 g/kg of 50% dextrose by gavage, and blood glucose levels were measured using a blood glucose meter after blood was collected from the tail tip for oral glucose tolerance test (OGTT) measurements before and 15, 30, 60, 90, and 120 min after gavage.

The area under the glucose curve (GAUC) was calculated as 0.5 × (FPG + glucose for 30 min) × 30 + 0.5 × (glucose for 30 min + glucose for 60 min) × 30 + 0.5 × (glucose for 60 min + glucose for 120 min) × 60 (Gu et al., 2019). The GAUC is reported in min-mmol/L.

Sample collection and biochemical analysis

The rats were weighed and anaesthetized deeply via an intraperitoneal injection of 30 mg/kg pentobarbital sodium (Merck, United States). Blood samples were collected in non-heparinized tubes and centrifuged at 4,000 rpm for 10 min at 4°C. The contents were removed by separating and dissecting the ileum. The serum and ileum contents were stored in Eppendorf tubes at −80°C. The fasting insulin (FIns, American Laboratory Products Company, New Hampshire, United States), interleukin-1β (IL-1β, Abbkine Scientific Co., Ltd., WuHan, China), and lipopolysaccharide (LPS, MyBiosource, Inc., Santiago, United States) concentrations were analyzed using enzyme-linked immunosorbent assay kits according to the manufacturers' instructions.

The homeostasis model assessment–insulin resistance (HOMA-IR) score was calculated as the FIns level (miu/L) × FBG level (mmol/L)÷22.5 (Hu et al., 2022).

Histology

The ileum was washed with phosphate-buffered saline, fixed in a tube containing a 4% paraformaldehyde solution for 24 h, embedded in paraffin wax, sliced into 4 μm sections, and stained with hematoxylin and eosin. Intestinal zonula occludens 1 (ZO-1) protein levels were observed through immunofluorescence staining to evaluate the defense barrier function of the intestinal mucosa. Images were captured using a Nikon Eclipse Ci-L microscope (Tokyo, Japan; 200× magnification).

16S sequencing of the gut microbiome and metabolomic profiling

Total ileal bacterial DNA was extracted using a MagPure Stool DNA KF kit B (Guangzhou Magen Biotechnology Co., Ltd., Guangzhou, China) according to the manufacturer's instructions. Approximately 30 ng of DNA was used to generate amplicons with an Agencourt AMPure XP kit (Beckman Coulter, California). After PCR amplification of the full-length 16S rDNA, the qualified library was sequenced on the HiSeq 2,500 platform, which targets the V4 region (California, America) (Zhang et al., 2020). The raw

data were filtered to generate high-quality clean reads. Tags were generated using Fast Length Adjustment of Short Reads (v1.2.11). Clustering was performed according to 97% sequence similarity to determine the abundance of operational taxonomic units (OTUs) in the gut microbiota via USEARCH (v7.0.1090) (Zhu et al., 2020).

After the ileal samples were crushed, an HM400 standard curve was generated, and the samples were subjected to derivatization, dilution and other steps prior to analysis. The resulting supernatant was subjected to liquid chromatography–mass spectrometry on a QTRAP 6500 + SCIEX instrument (Massachusetts, America) (Peng et al., 2023). The chromatographic column used was a BEH C18 column (2.1 mm × 10 cm, 1.7 μm, Waters, Massachusetts, America). The ion source was an electrospray ionization (ESI)+/ESI-system. The parameters for the integration of each multiple-reaction monitoring transition and manual inspection were determined with HMQuant software (BGI Shenzhen, Guangdong, China) (Li et al., 2023). The concentration was calculated according to the integrated peak area of the target index (Bai et al., 2023).

Statistics and analysis

The data were analyzed using one-way analysis of variance followed by the least significant difference test or Dunnett's T3 test. Partial least squares discriminant analysis (PLS-DA) and principal component analysis (PCA) were used to display classification changes with R software (v3.1.1), mixOmics, and the ade4 package. A Venn diagram and heatmap were constructed with the R software (v3.1.1) Venn diagram and gplots packages. The Kyoto Encyclopedia of Genes and Genomes (KEGG) pathways were predicted using PICRUSt2 v2.2.0-b and R (v3.4.10). ImageGP was used for the intergroup pathway analysis. Significantly enriched metabolite pathways were identified using the MetaboAnalyst platform.[1] An analysis of functional differences was performed using the Wilcoxon test. The data were analyzed using the Microbial Amplification Subsystem[2] and the Gene Denovo Cloud Platform.[3] SPSS 23.0 (New York, United States) and GraphPad Prism 5.0 (San Diego, United States) were used for analyses. An analysis of the receiver operating characteristic (ROC) curves of metabolites is a common method for screening potential biomarkers. The area under the curve (AUC) was calculated using R software (version 4.2.1). When a single factor was used, the pROC package was used to perform the ROC curve analysis, and the results were visualized via ggplot2. Before conducting the joint factor analysis, the data were cleaned, and a multifactor logistic regression model was constructed using a generalized linear model. The model continued the analysis with the same process as before. $p < 0.05$ were considered to indicate statistical significance.

Results

Effects of STG on weight and blood glucose-related indicators

Compared with the Con group, the Mod group presented significant reductions in weight at weeks 5, 7, 9, 11, and 13 ($p < 0.05$ or $p < 0.01$). Compared with those in the Mod group, the weight changes in the Met and STG groups were not significantly different ($p > 0.05$). Compared with that in the Met group, the weight change in the STG group was non-significant ($p > 0.05$), as shown in Figure 1A.

1 https://www.metaboanalyst.ca/
2 https://meta.bgi.com/microbe/login
3 https://www.omicshare.com/

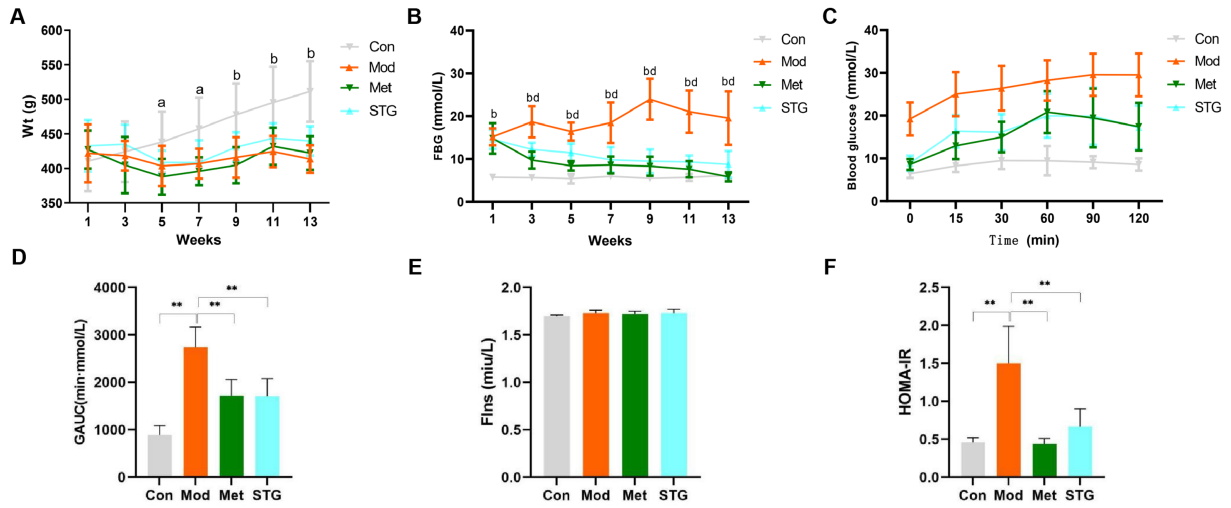

FIGURE 1
Effects of STG on weight and glucose metabolism-related indicators in rats. **(A)** Comparison of weight. **(B)** Comparison of FBG levels. **(C)** Comparison of blood glucose levels obtained with the OGTT. **(D)** Comparison of the GAUC obtained with the OGTT. **(E)** Comparison of FIns levels. **(F)** Comparison of HOMA-IR. The data are presented as the means ± standard deviations; $n = 8$ rats in the four groups. a = Mod group vs. Con group, $p < 0.05$; b = Mod group vs. Con group, $p < 0.01$; d = Met or STG group vs. Mod group, $p < 0.01$; Con, control; Mod, T2DM model; Met, metformin; STG, Shenzhu Tiaopi granule; T2DM, type 2 diabetes mellitus; Wt, weight; FBG, fasting blood glucose; GAUC, area under the glucose curve; FIns, fasting insulin; HOMA-IR, homeostasis model assessment–insulin resistance. 1, Acclimation for 1 week; 3, the second week after the drug intervention; 5, the fourth week after the drug intervention; 7, the sixth week after the drug intervention; 9, the eighth week after the drug intervention; 11, the tenth week after the drug intervention; and 13: the twelfth week after the drug intervention. $^{**}p < 0.01$.

Compared with the Con group, the Mod group presented a significant increase in FBG levels at weeks 1, 3, 5, 7, 9, 11, and 13 ($p < 0.01$). Compared with those in the Mod group, the FBG levels in the Met and STG groups decreased significantly ($p < 0.01$). Compared with that in the Met group, the FBG level in the STG group did not change significantly ($p > 0.05$) (Figure 1B). Compared with that in the Con group, the GAUC in the Mod group was significantly greater ($p < 0.01$). Compared with that of the Mod group, the GAUC of the Met and STG groups decreased significantly ($p < 0.01$). Compared with that in the Met group, the GAUC of the STG group did not change significantly ($p > 0.05$) (Figures 1C,D).

No significant difference in the FIns level was observed between the Mod group and the Con group ($p > 0.05$). Compared with that in the Mod group, no significant changes in the FIns levels were observed in the Met and STG groups ($p > 0.05$). Compared with the Con group, the Mod group presented a significant increase in HOMA-IR ($p < 0.01$). Compared with the Mod group, the HOMA-IR index was significantly lower in the Met and STG groups ($p < 0.01$). Compared with those in the Met group, FIns levels and the HOMA-IR in the STG group did not change significantly ($p > 0.05$) (Figures 1E,F).

Effects of STG on inflammatory indicators and the pathological morphology of the intestine

Compared with those in the Con group, the LPS and IL-1β levels in the Mod group were significantly higher ($p < 0.01$). Compared with those in the Mod group, the LPS and IL-1β levels were significantly lower in the Met and STG groups ($p < 0.05$ or $p < 0.01$) (Figures 2A,B).

Compared with the Con group, a decrease in the length of the intestinal villi, an increase in the degree of necrotic shedding of epithelial cells, solidification of the cell nuclei, a smaller volume of intestinal crypts, unclear demarcation, and a small number of cup-shaped cells were observed in the ileum of the Mod group. Compared with the Mod group, the length of the intestinal villi, extent of necrotic shedding of epithelial cells, volume of intestinal crypts, and number of cup-shaped cells were greater in the Met and STG groups (Figure 2C). In addition, the expression of Zo-1 tended to decrease in the Mod group compared with the Con group, whereas Zo-1 protein expression increased in the Met and STG groups (Figure 2D).

Effects of STG on the gut microbiota community

A total of 148,472 clean reads were obtained, providing a total of 1,136 OTUs. Notably, 9 unique OTUs were identified in the STG group, 13 unique OTUs in the Met group, 20 unique OTUs in the Mod group and 18 unique OTUs in the Con group (Figure 3A). PLS-DA indicated that the clustering of the gut microbiota differed among the four groups. The gut microbiota structure of the mice in the STG treatment group clearly shifted to that of the Con group (Figure 3B). The community

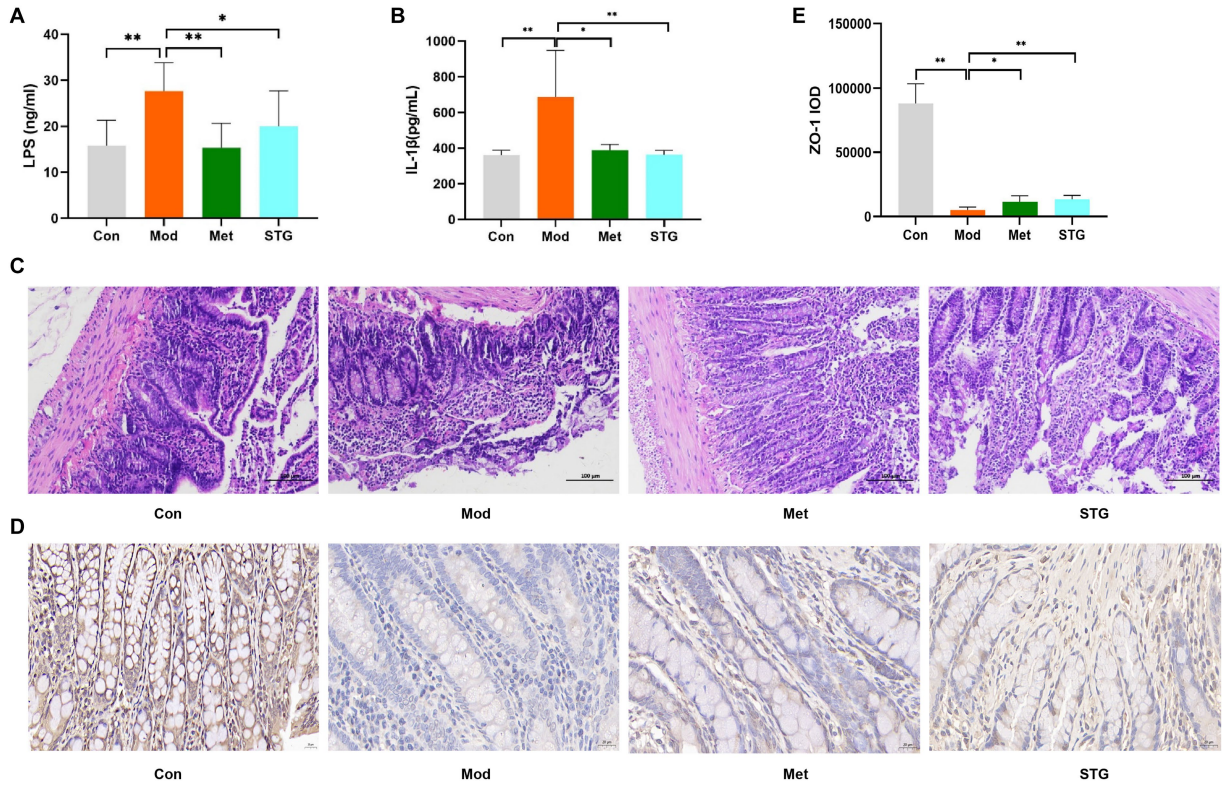

FIGURE 2
Effects of STG on inflammatory indicators and intestinal pathological morphology in rats. **(A)** Comparison of LPS levels. **(B)** Comparison of IL-1β levels. **(C)** Comparison of HE staining of the ileum. **(D)** Comparison of Zo-1 immunohistochemical staining in the ileum. **(E)** Comparison of the ileal Zo-1 IOD. The data are presented as the means ± standard deviations; $n = 8$ rats in the four groups. Con, control; Mod, T2DM model; Met, metformin; STG, Shenzhu Tiaopi granule; T2DM, type 2 diabetes mellitus; LPS, lipopolysaccharide; IL-1β, interleukin-1β; IOD, integrated optical density. Pathology images are shown separately 200 and 400 × magnification in (**C** and **D**); scale bar, 100 μm and 20 μm in (**C** and **D**). *$p < 0.05$ and **$p < 0.01$.

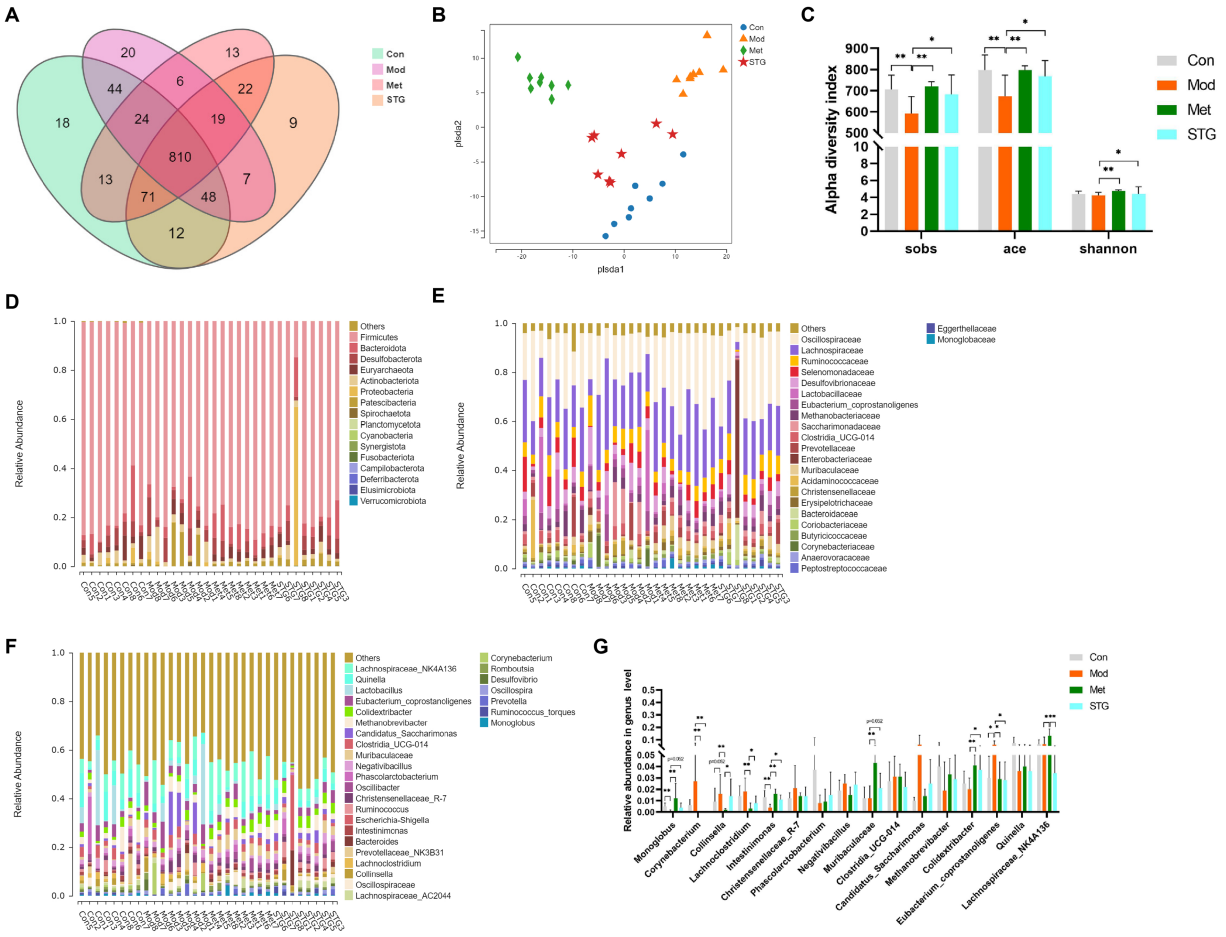

FIGURE 3
Comparison of the gut microbiota structure. **(A)** Comparison of the OTUs. **(B)** Comparison of the gut microbiota structure using PLS-DA. **(C)** Comparison of alpha diversity. **(D)** Composition at the phylum level. **(E)** Composition at the family level. **(F)** Composition at the genus level. **(G)** Comparison of the relative abundance at the genus level. The data are presented as the means ± standard deviations; $n = 8$ rats in the four groups. OTUs, operational taxonomic units; PLS-DA, partial least squares discriminant analysis. Con, control; Mod, T2DM model; Met, metformin; STG, Shenzhu Tiaopi granule; T2DM, type 2 diabetes mellitus. *$p < 0.05$ and **$p < 0.01$.

richness estimated by the Sobs and ACE indices was significantly lower in the Mod group than in the Con group ($p < 0.01$). Compared with those in the Mod group, the Sobs and ACE indices were significantly higher in the Met and STG groups ($p < 0.05$ or $p < 0.01$). Although no differences in the Shannon index were observed between the Mod and Con groups, the Shannon index was significantly higher in the Met and STG groups than in the Mod group ($p < 0.05$ or $p < 0.01$) (Figure 3C).

The intestinal bacterial composition of each sample at the phylum and family levels is listed in Figures 3D,E. The main components were not significantly different among the four groups ($p > 0.05$). The composition of each sample at the genus level is listed in Figure 3F.

Compared with those in the Con group, the *Monoglobus* and *Intestinimonas* abundances in the Mod group were significantly lower ($p < 0.01$). Compared with those in the Mod group, the abundances of these bacteria were significantly greater in the Met group ($p < 0.01$). In the STG groups, the abundance of *Intestinimonas* increased ($p < 0.05$). Compared with the Con group, the Mod group presented a significant increase in the abundance of *Eubacterium coprostanoligenes* ($p < 0.05$). Compared with that in the Mod group, the abundance of *Eubacterium coprostanoligenes* was significantly lower in the Met and STG groups ($p < 0.05$) (Figure 3G).

Correlation analysis of the gut microflora with baseline data

At the genus level, the clustering heatmap revealed that the Met group was closest to the Con group, followed by the STG group and finally the Mod group (Figure 4A). FBG, HOMA-IR, and IL-1β levels were significantly negatively correlated with *Intestinimonas* abundance ($p < 0.01$). Moreover, the LPS level was significantly positively correlated with *Collinsella* abundance ($p < 0.01$), as shown in Figure 4B. A cladogram showing the relationships among taxa at the phylum, class, order, family, and genus levels was generated using Linear discriminant analysis (LDA) effect size analysis. *Dermabacteraceae*, *Carnobacteriaceae*, *Gemellaceae*, *Staphylococcaceae* and *Beijerinckiaceae* had significant effects on the Mod group. *Muribaculaceae*, *Clostridiaceae*, *Clostridiales*, *Lachnospiraceae*, *Lachnospirales*, *Monoglobaceae* and *Monoglobales* had significant effects on the Met group. *Peptococcaceae*, *Peptococcales*, *Anaerovoracaceae*, *Fusobacteriaceae*, *Fusobacteriales*, *Fusobacteria*, *Enterobacteriaceae* and *Enterobacterales* had significant effects on the STG group (Figure 4C). The components of the gut microbiota with an LDA score > 4 were defined as unique. At the genus level, *Actinobacteriota* and *Lachnoclostridium* were significantly enriched in the Mod group ($p < 0.01$).

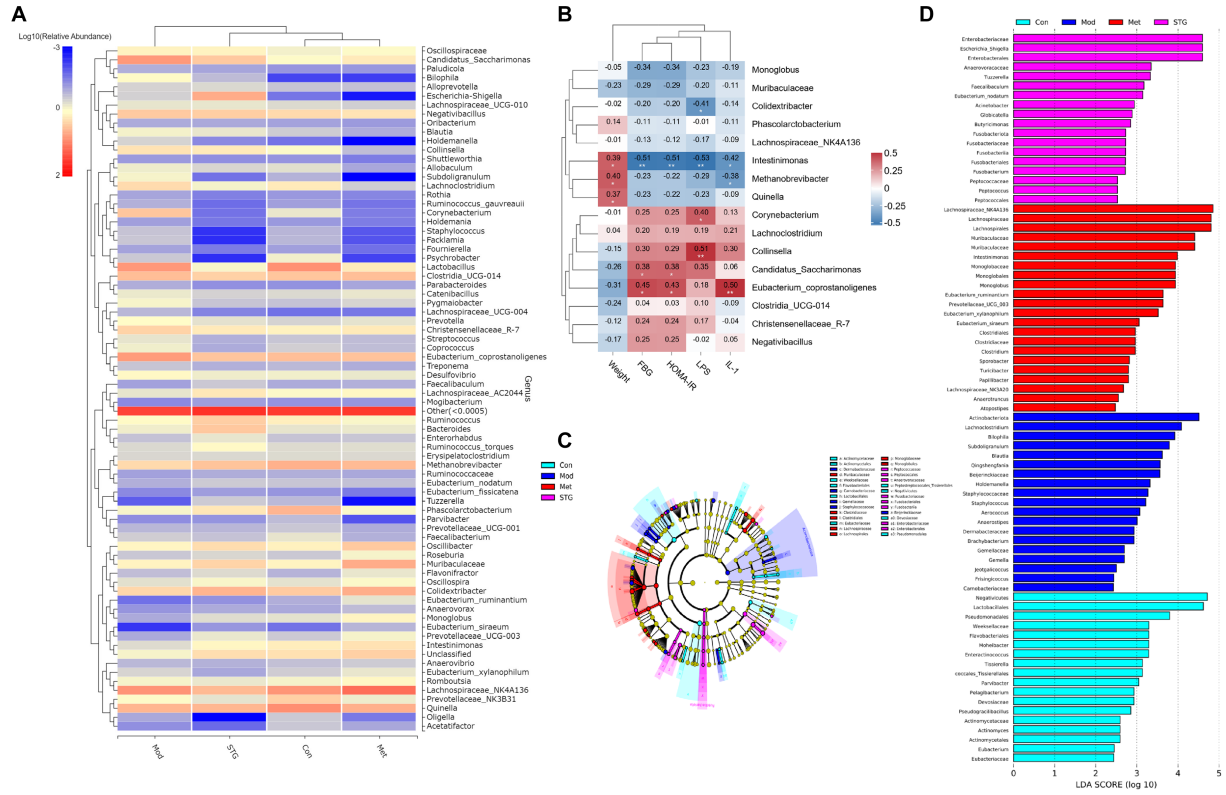

FIGURE 4
Relationships between the gut microbiota at the genus level and baseline data. **(A)** Clustering heatmap of the relative abundance at the genus level. **(B)** Correlation heatmap of the gut microbiota at the genus level with the baseline data. **(C)** The biomarker of gut microbiota via LDA effect size cluster tree. **(D)** The biomarker of gut microbiota via LDA figure. $N = 8$ rats in the four groups. Con, control; Mod, T2DM model; Met, metformin; STG, Shenzhu Tiaopi granule; T2DM, type 2 diabetes mellitus; FBG, fasting blood glucose; HOMA-IR, homeostasis model assessment–insulin resistance; IL-1β, interleukin-1β; LPS, lipopolysaccharide; LDA, linear discriminant analysis. $^{*}p < 0.05$ and $^{**}p < 0.01$.

Lachnospiraceae_NK4A136, *Lachnospiraceae*, *Lachnospirales*, *Muribaculaceae*, and *Muribaculaceae* were significantly enriched in the Met group ($p < 0.05$ or $p < 0.01$). *Enterobacteriaceae*, *Escherichia_Shigella* and *Enterobacterales* were significantly enriched in the STG group ($p < 0.01$), as shown in Figure 4D.

The functional annotation of the gut microflora

KEGG pathway enrichment analysis was performed to obtain 90 pathways at the third level with an abundance ≥0.0025. Moreover, carbohydrate metabolism-related pathways included amino sugar and nucleotide sugar metabolism, starch and sucrose metabolism, glycolysis/gluconeogenesis, pyruvate metabolism, galactose metabolism, the pentose phosphate pathway, fructose and mannose metabolism, glyoxylate and dicarboxylate metabolism, biotin metabolism, butanoate metabolism, pentose and glucuronate interconversions, the citrate cycle (TCA cycle), propanoate metabolism, and ascorbate and aldarate metabolism (Figure 5A). An analysis of different functions was conducted using the Met and STG groups, and pathways with significant differences in abundance ≥0.8 were identified, including secondary bile acid (BA) biosynthesis, riboflavin metabolism, the pentose phosphate pathway, galactose metabolism, the TCA cycle, and biotin metabolism (Figure 5B).

Analysis of metabolites in the ileal contents and their functions

A total of 403 metabolites were identified in HW400. In this study, 289 metabolites were detected, including 4 pyridines, 7 phenylpropanoids, 3 mixed peptides, 2 organic oxides, 33 organic acids, 7 indoles, 1 imidazole, 55 fatty acids, 9 carnitines, 12 carbohydrates, 33 benzene ring-type compounds, 63 amino acids, 59 BAs, and 1 nucleotide. A comparison of the above metabolites revealed that the overall categorization of the Mod group and the Con group was significant. The Met and STG groups were significantly different from the Mod group. The overall categorization of the Met group with the STG group significantly differed from that of the Mod group, as shown in Figure 6A.

The first 20 metabolites with significant differences were screened and included 3 organic acids, 2 fatty acids, 2 carbohydrates, 2 benzene ring-type compounds, 1 amino acid, and 10 BAs ($p < 0.05$ or $p < 0.01$), as shown in Figure 6B. The top 20 differentially abundant metabolites were enriched mainly in phenylalanine and tyrosine metabolism, starch and sucrose metabolism, and BA biosynthesis, as shown in Figure 6C. The KEGG metabolic pathway enrichment analysis revealed that, compared with the Mod group, the STG group was enriched mainly in primary BA biosynthesis, cholesterol metabolism, nicotinate and nicotinamide metabolism, the cAMP signaling pathway, and tryptophan metabolism, among others, as shown in Figure 6D.

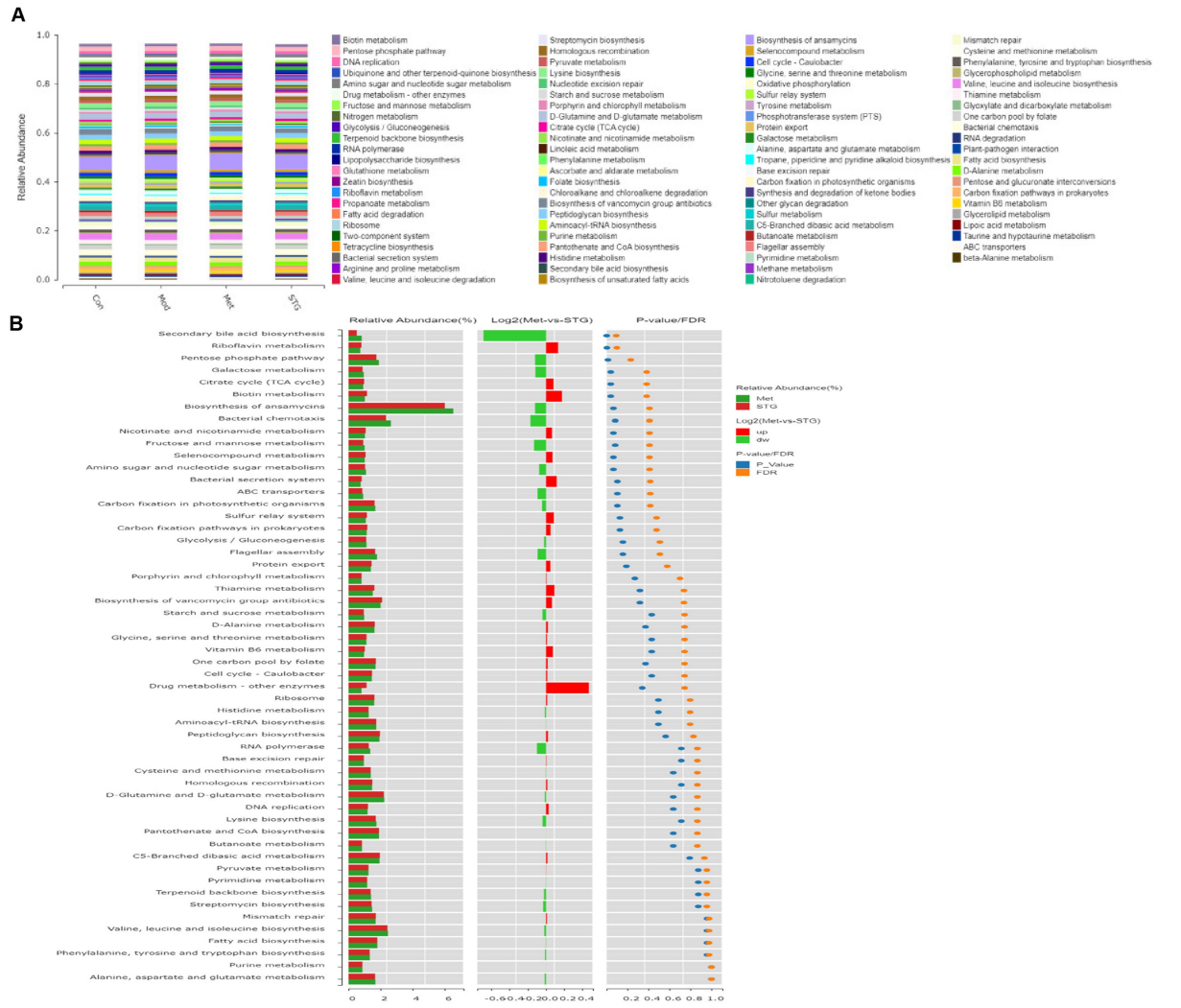

FIGURE 5
Functional annotation of the gut microbiota. **(A)** KEGG pathway functional annotations at the third level. **(B)** Analysis of differences in KEGG pathway functional annotations at the third level. *N* = 8 rats in the four groups. Con, control; Mod, T2DM model; Met, metformin; STG, Shenzhu Tiaopi granule; T2DM, type 2 diabetes mellitus.

Correlation analysis of ileal metabolite levels with baseline data and the gut microbiota

The correlation heatmap revealed that FBG, HOMA-IR and IL-1β levels were significantly positively correlated with 2-deoxyglucose, D-Maltose_and_Alpha-Lactose, dioxolithocholic acid, cholic acid methyl ester, creatine, levulinic acid, alpha-muricholic acid, beta-muricholic acid and glyco-lambda-muricholic acid levels ($p < 0.01$). The LPS level was significantly positively correlated with the glyco-lambda-muricholic acid level ($p < 0.01$), as shown in Figure 7A.

The correlation heatmap showed that creatine and levulinic acid levels were significantly positively correlated with *Corynebacterium* abundance ($p < 0.01$). 23-Norcholic acid diacetate, glyco-lambda-muricholic acid, and creatine levels were significantly positively correlated with *Lachnoclostridium* abundance ($p < 0.01$). 23-Norcholic acid diacetate, glyco-lambda-muricholic acid, alpha-muricholic acid, beta-muricholic acid, dioxolithocholic acid and creatine levels were significantly positively correlated with *Lachnoclostridium* abundance ($p < 0.01$). Glyco-lambda-muricholic acid, cholic acid methyl ester, alpha-muricholic acid, beta-muricholic acid and dioxolithocholic acid levels were significantly negatively correlated with *Intestinimonas* abundance ($p < 0.01$). Moreover, the correlation coefficient between glyco-lambda-muricholic acid and *Intestinimonas* was-0.68, which was the most relevant correlation, as shown in Figure 7B.

Potential biomarkers in the ileal contents

We screened the top three components of the gut microbiota and metabolites that were most strongly correlated with FBG and FIns levels: *Intestinimonas*, *Candidatus_Saccharimonas*, *Eubacterium coprostanoligenes*, 2-deoxyglucose, D-Maltose_and_Alpha-Lactose and glyco-lambda-muricholic acid. The maximum AUC of *Intestinimonas* in the gut microbiota was 0.864. The maximum AUC of D-Maltose_and_Alpha-Lactose was 0.859 for the gut metabolites (Figure 8A). Based on the joint diagnostic analysis of the two highest

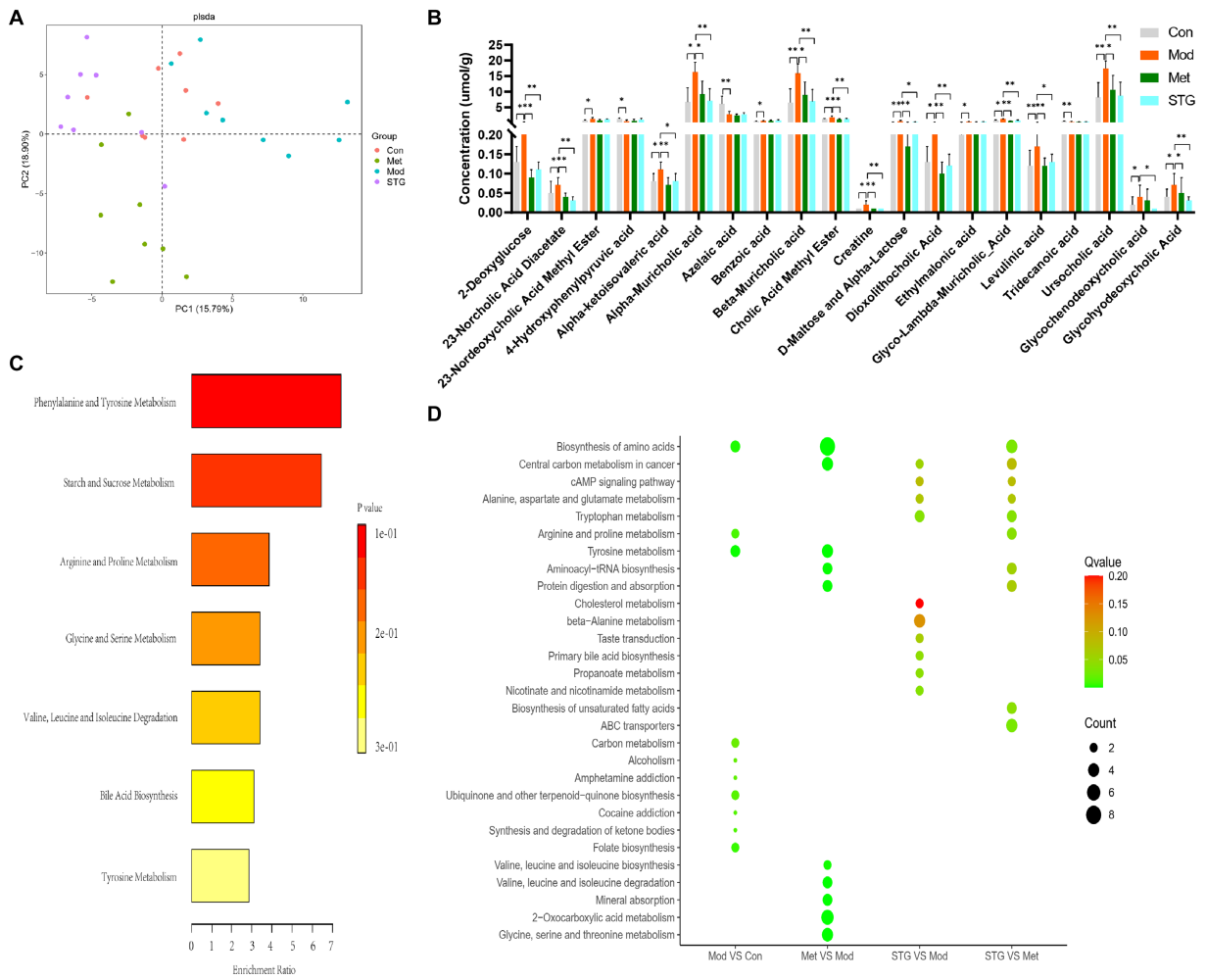

FIGURE 6
Differentially abundant metabolites in the ileal contents and their functions. **(A)** Comparison of the overall classification effect of metabolites in the ileum contents. **(B)** Comparison of differentially abundant metabolites in the ileal contents. **(C)** Metabolic enrichment analysis of differentially abundant metabolites in the ileal contents. **(D)** KEGG metabolic pathway enrichment analysis of differentially abundant metabolites in the ileal contents. $N = 8$ rats in the four groups. Con, control; Mod, T2DM model; Met, metformin; STG, Shenzhu Tiaopi granule; T2DM, type 2 diabetes mellitus. $^{*}p < 0.05$ and $^{**}p < 0.01$.

AUCs, we found that the AUCs of D-Maltose_and_Alpha-Lactose and *Intestinimonas* further increased, with a value of 0.927. These factors may be potential biomarkers for the effect of STG on ameliorating T2DM (Figure 8B).

Discussion

In individuals with T2DM, the body is in a long-term hyperglycemic state, which aggravates impaired glucose uptake and utilization, exacerbates lipolysis, and is prone to negative protein metabolism equilibrium, as observed in rats in the Mod group, resulting in a significant reduction in weight. This result may be related to the fact that the aging stage of Wistar rats is 24 to 30 months, whereas 30-month-old Wistar rats are in a stage of weight gain. No statistically significant difference in the improvement in weight reduction was observed between the Met and STG groups in the present study. Studies by Wachal et al. (2020) revealed that Met also did not significantly ameliorate the reduction in weight in GK rats. This finding may be related to the fact that Met can reduce fat synthesis in the body and cause adverse reactions in the digestive tract (Haddad et al., 2023; Naseri et al., 2023). Huanglian, the main component of STG, can inhibit fatty acid biosynthesis and adipocyte differentiation and reduce visceral fat or upregulate the expression and secretion of growth differentiation factor-15 mRNA in brown fat, which can reduce weight (Urasaki and Le, 2022; Li et al., 2023).

The blood glucose levels of GK T2DM rats in the Mod group were higher than those in the Con group, whereas the blood glucose levels were lower in the STG group. This finding is consistent with our team's previous finding that STG can reduce blood glucose levels (Yang et al., 2023). In GK T2DM rats, a significant difference in FIns levels was not observed among the Con, Mod, Met, and STG groups. Moreover, the HOMA-IR in the Mod group was significantly higher than that in the Con group, indicating the occurrence of insulin resistance in GK rats.

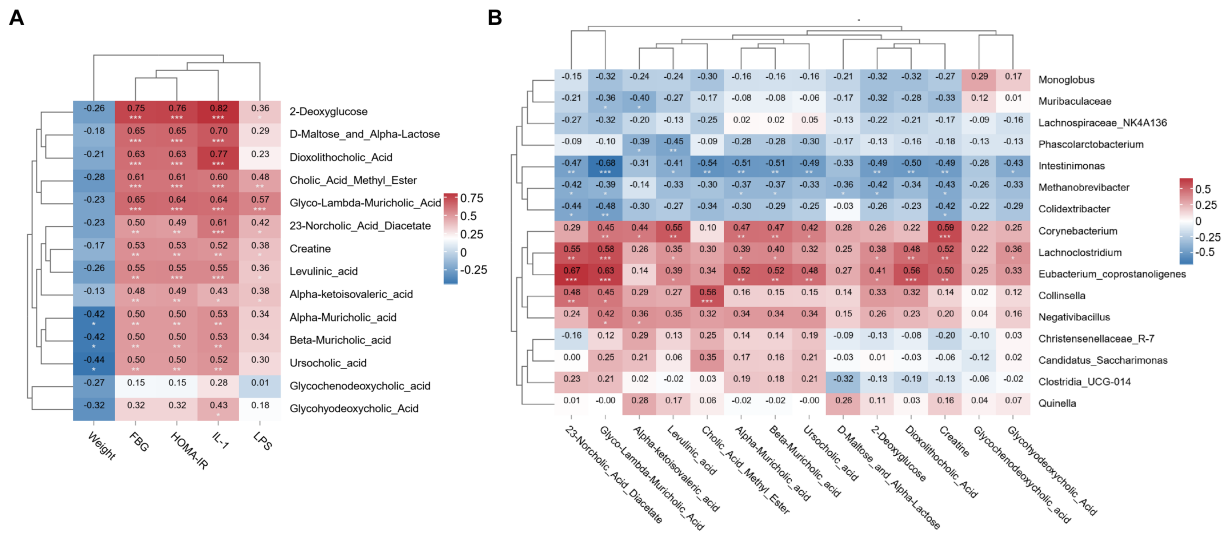

FIGURE 7
Relationships between ileal metabolite and baseline data or gut microbiota. **(A)** Correlation heatmap of the ileal metabolite contents with the baseline data. **(B)** Correlation heatmap of the ileal metabolite contents with the gut microbiota. $N = 8$ rats in the four groups. FBG, fasting blood glucose; HOMA-IR, homeostasis model assessment-insulin resistance; IL-1β, interleukin-1β; LPS, lipopolysaccharide. $^{*}p < 0.05$; $^{**}p < 0.01$; and $^{***}p < 0.001$.

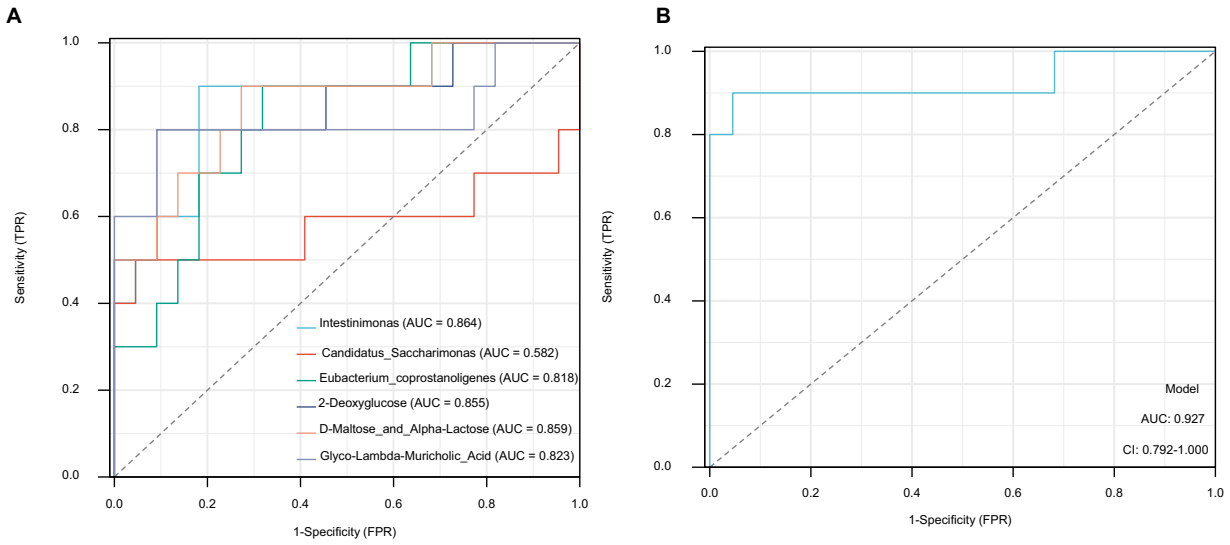

FIGURE 8
Potential biomarkers in the ileal contents. **(A)** The AUCs of the top three components of the gut microbiota and metabolites. **(B)** The AUCs of D-Maltose_and_Alpha-Lactose and *Intestinimonas*. AUC, area under the curve.

This result is consistent with the findings reported by Li et al. (2023) and Skoug et al. (2024). However, in the Met and STG groups, the improvement in the HOMA-IR was significantly reduced.

In the Mod group, the ileum showed a reduction in the length of the intestinal villi, a decrease in the volume of the intestinal crypts, and an increase in the shedding of intestinal epithelial cells, resulting in varying degrees of damage to the integrity of the intestinal epithelium and the intestinal barrier. This phenomenon is basically consistent with the findings of Pereira et al. (2021) and Esteves-Monteiro et al. (2022). Both Met and STG improved the intestinal epithelium and the intestinal barrier. A leaky intestine has attracted attention in individuals with T2DM (Sato et al., 2017). In T2DM patients, intestinal permeability is reduced (Sato et al., 2017). The increased blood levels of LPS may be related to an increase in intestinal permeability. LPS activates Toll-like receptor 4, resulting in chronic low-grade inflammation mediated by cytokines such as interferon-γ, tumor necrosis factor-α and IL-1β (Chen et al., 2021). Furthermore, this inflammation promotes the occurrence of T2DM (Beutler, 2004). ZO-1 is an intestinal tight junction protein that reflects intestinal permeability. Decreased ZO-1 levels indicate some damage to the intestinal barrier (González-Mariscal et al., 2011). Our research revealed the malfunction caused by increasing the amount of LPS in the blood. Moreover, the body may develop an inflammatory response. Elevated levels of IL-1β were also observed in this study. *In vivo*, a significant increase in ZO-1 expression was observed in the Met group

(Rindone et al., 2024). Moreover, we found that Met could decrease the levels of IL-1β and LPS (Balakumar et al., 2018; Deng et al., 2018). Moreover, STG can improve the levels of ZO-1, IL-1β, and LPS to alleviate T2DM.

The abundance of *Intestinimonas* decreased in the Mod group; however, improvements were observed after the Met and STG interventions. Our research revealed that *Intestinimonas* is a potential biomarker for diagnosing diabetes. The results of another study also showed that verbascoside induced an enrichment of *Intestinimonas* to alleviate glucose metabolism disorders (Ran et al., 2023). The development of Alzheimer's disease and T2DM are associated with insulin resistance. The *Monoglobus* abundance decreased in the Mod group; however, improvements were observed after Met and STG interventions. *Monoglobus* are short-chain fatty acid-producing bacteria (Verhaar et al., 2022), and the maintenance of the gut and T2DM are related to short-chain fatty acids (Blaak et al., 2020). *Eubacterium coprostanoligenes* is closely related to T2DM (Tsai et al., 2022; Yin et al., 2022). In this study, this relationship was positively correlated with FBG levels. STG decreased the relative abundance of *Eubacterium coprostanoligenes*. In our study, *Candidatus_Saccharimonas* was positively correlated with FBG. *Candidatus_Saccharimonas* is an opportunistic pathogen. In individuals with diabetes, its abundance is elevated (Ye et al., 2024). This result is consistent with our research findings. The abundance of *Enterobacteriaceae* is higher in T2DM patients (Feng et al., 2022). *Enterobacterales* is negatively associated with T2DM (Hernández-Montoliu et al., 2023). However, STG can effectively regulate the abundances of *Enterobacteriaceae* and *Enterobacterales* to alleviate T2DM.

The abundance of *Muribaculaceae* is abnormal in the T2DM model, and *Muribaculaceae* can migrate to the pancreas, where it causes inflammation and beta cell damage (Yang et al., 2023; Song et al., 2024). The abundance of *Lachnospirales* had a significant negative correlation with T2DM. In this study, Met improved the abundances of *Muribaculaceae* and *Lachnospirales*. This result is different from the impact of STG on the gut microbiota. Based on the predicted function of the gut microbiota, STG may improve glucose levels by affecting metabolic pathways. The pentose phosphate pathway plays an important role in T2DM by regulating the effects of glucose 6-phosphate on glycolysis and gluconeogenesis (Ge et al., 2020). Increased levels of TCA cycle metabolites are a risk factor for T2DM (Guasch-Ferré et al., 2020).

Based on the metabolites detected in the ileal contents, differences were observed in organic acids, benzene ring-type compounds, and BAs. Organic acids have a blood glucose-lowering effect (Jamrozik et al., 2022). Alpha-ketoisovaleric acid is related to T2DM (Fujiwara et al., 2021). We found that the alpha-ketoisovaleric acid content was increased in the Mod group. Both Met and STG improved this change. The ethylmalonic acid content was increased in the Mod group, but another study demonstrated that the ethylmalonic acid level was negatively associated with the HOMA-IR (Liu et al., 2020). The levulinic acid content was higher in the Mod group than in the Con group, and a positive correlation was observed between the levulinic acid content and both FBG levels and the HOMA-IR. Both the Met and STG groups exhibited an improved levulinic acid concentration. In addition, the levulinic acid content was positively correlated with *Corynebacterium*. An increase in *Corynebacterium* abundance can lead to an increased risk of diabetic eye disease and diabetic foot infections (Hartemann-Heurtier and Senneville, 2008; Aoki et al., 2021). 2-Deoxyglucose is a carbohydrate, and its content was positively correlated with FBG levels and the HOMA-IR. The AUC of the potential biomarkers for T2DM was 0.855. This result may be related to decreased 2-deoxyglucose uptake into the intestine (Kobayashi, 2018). This compound inhibits the glycolytic pathway and accelerates gluconeogenesis, leading to an increase in blood glucose levels (Thomas and Lowy, 1992). In a diabetic mouse model, 2-deoxyglucose was shown to affect glycine and serine metabolism (Zhang et al., 2022). This phenomenon was also observed in our study. The glycine level is associated with a decreased risk of incident T2DM (Adeva-Andany et al., 2018). Low systemic serine levels are also emerging as a hallmark of diabetes-related peripheral nerve disorders (Handzlik et al., 2023). In addition, D-maltose and alpha-lactose, which are carbon sources, also have effects on blood glucose levels, similar to 2-deoxyglucose (Wang et al., 2023). Moreover, they can be used for the auxiliary diagnosis of T2DM, and their AUC is 0.859. D-Maltose_and_Alpha-Lactose and *Intestinimonas* can be considered potential candidate biomarkers for T2DM. Glyco-lambda-muricholic acid is a BA and its levels are reportedly increased in chronic kidney disease patients (Wu et al., 2020). In our research, we found that the content of glyco-Lambda-muricholic acid increased in T2DM patients. The cAMP signaling pathway, which regulates glucose homeostasis, has recently been recognized to regulate insulin secretion, glycogen synthesis, gluconeogenesis, etc. (Yang and Yang, 2016). Compared with the Mod group, STG may target the cAMP signaling pathway for the treatment of T2DM. Tryptophan metabolism is strongly related to the onset and progression of T2DM (Sudar-Milovanovic et al., 2022). The serum tryptophan concentration was lower in the T2DM group than in the control group, which was part of the effect of the STG intervention.

BAs are essential physiological agents involved in nutrient absorption, partitioning, metabolism and excretion (Fogelson et al., 2023; Hou et al., 2023). Primary BAs are among the metabolic products of cholesterol breakdown in the liver. Secondary BAs are released from the gallbladder into the intestines, where they are catalyzed and converted by a series of enzymes (Ridlon et al., 2006). Moreover, BAs are also important components maintaining the function of the intestinal mucosa and have regulatory effects on the intestinal mucosal barrier and metabolite function (Zhang et al., 2021; Shi et al., 2023). Previous studies have shown higher total BAs concentrations in patients with T2DM than in healthy individuals, and BA metabolism is closely related to glucose metabolism (Haeusler et al., 2013; Sun et al., 2020). The main BAs associated with BA biosynthesis are beta-muricholic acid, alpha-muricholic acid, glycochenodeoxycholic acid, ursocholic acid, glycohyodeoxycholic acid and dioxolithocholic acid. Wang et al. (2022) reported that differentially abundant metabolites in the faeces of T2DM model rats could also be enriched for BA biosynthesis, and beta-muricholic acid was one of the metabolites. In our research, beta-muricholic acid was considered a potential biomarker for diabetes, and it is closely linked to FBG levels and the HOMA-IR. Elevated glycochenodeoxycholic acid levels may be a risk factor for hepatic steatosis and hepatic fibrosis in T2DM patients (Forlano et al., 2024). Cholic acid methyl ester has potential beneficial effects on T2DM (Mikov et al., 2006). Since GK rats mainly exhibit different degrees of steatosis, these findings are consistent with the results of the present study. Moreover, STG can

decrease the levels of the BAs described above and remodel the metabolism of BAs in the ileal contents to some extent.

Current research shown that an imbalance of intestinal microorganisms and metabolites is a characteristic of T2DM. STG can play a role in reducing blood glucose levels, and underlying mechanism could be related to alleviating this imbalance. A new application of a traditional Chinese medicine for regulating blood glucose levels via effects on the gut microbiota and metabolites has been developed.

Data availability statement

The data presented in the study are deposited in the NCBI repository, accession number: PRJNA1144618.

Ethics statement

The animal studies were approved by the Anhui Chinese Medicine University. The studies were conducted in accordance with the local legislation and institutional requirements. Written informed consent was obtained from the owners for the participation of their animals in this study.

Author contributions

J-DZ: Writing – original draft. Z-HF: Writing – review & editing.

Funding

The author(s) declare that financial support was received for the research, authorship, and/or publication of this article. This study was supported by open bidding for selecting the best candidates for Xin'an Medicine and the Modernization of Traditional Chinese Medicine of IHM (2023CXMMTCM024 and 2023CXMMTCM003), the University Scientific Research Projects of Anhui (2023AH050782), the National Natural Science Foundation of China (82174153), and Anhui provincial quality engineering project for education in the new era (2023gjxslt014) and the Scientific Research Project of Health and Wellness in Anhui Province (AHWJ2023BAc10002).

Conflict of interest

The authors declare that the research was conducted in the absence of any commercial or financial relationships that could be construed as a potential conflict of interest.

Publisher's note

All claims expressed in this article are solely those of the authors and do not necessarily represent those of their affiliated organizations, or those of the publisher, the editors and the reviewers. Any product that may be evaluated in this article, or claim that may be made by its manufacturer, is not guaranteed or endorsed by the publisher.

References

Adeva-Andany, M., Souto-Adeva, G., Ameneiros-Rodríguez, E., Fernández-Fernández, C., Donapetry-García, C., and Domínguez-Montero, A. (2018). Insulin resistance and glycine metabolism in humans. *Amino Acids* 50, 11–27. doi: 10.1007/s00726-017-2508-0

Aoki, T., Kitazawa, K., Deguchi, H., and Sotozono, C. (2021). Current evidence for Corynebacterium on the ocular surface. *Microorganisms* 9, 254–268. doi: 10.3390/microorganisms9020254

Bai, Y., Huang, W., Jiang, X., Xu, W., Li, Y., Wang, Y., et al. (2023). Metabolomic interplay between gut microbiome and plasma metabolome in cardiac surgery-associated acute kidney injury. *Rapid Commun. Mass Spectrom.* 37, 9504–9519. doi: 10.1002/rcm.9504

Bai, L., Li, X., He, L., Zheng, Y., Lu, H., Li, J., et al. (2019). Antidiabetic potential of flavonoids from traditional Chinese medicine: a review. *Am. J. Chin. Med.* 47, 933–957. doi: 10.1142/S0192415X19500496

Balakumar, M., Prabhu, D., Sathishkumar, C., Prabu, P., Rokana, N., Kumar, R., et al. (2018). Improvement in glucose tolerance and insulin sensitivity by probiotic strains of Indian gut origin in high-fat diet-fed C57BL/6J mice. *Eur. J. Nutr.* 57, 279–295. doi: 10.1007/s00394-016-1317-7

Beutler, B. (2004). Inferences, questions and possibilities in toll-like receptor signalling. *Nature* 430, 257–263. doi: 10.1038/nature02761

Blaak, E. E., Canfora, E. E., Theis, S., Frost, G., Groen, A. K., Mithieux, G., et al. (2020). Short chain fatty acids in human gut and metabolic health. *Benef Microbes.* 11, 411–455. doi: 10.3920/BM2020.0057

Chen, Y., and Wang, M. (2021). New insights of anti-hyperglycemic agents and traditional Chinese medicine on gut microbiota in type 2 diabetes. *Drug Des. Devel. Ther.* 15, 4849–4863. doi: 10.2147/DDDT.S334325

Chen, X., Zhang, D., Li, Y., Wang, W., Bei, W., and Guo, J. (2021). NLRP3 inflammasome and IL-1β pathway in type 2 diabetes and atherosclerosis: friend or foe? *Pharmacol. Res.* 173:105885. doi: 10.1016/j.phrs.2021.105885

Deng, J., Zeng, L., Lai, X., Li, J., Liu, L., Lin, Q., et al. (2018). Metformin protects against intestinal barrier dysfunction via AMPKα1-dependent inhibition of JNK signalling activation. *J. Cell. Mol. Med.* 22, 546–557. doi: 10.1111/jcmm.13342

Esteves-Monteiro, M., Menezes-Pinto, D., Ferreira-Duarte, M., Dias-Pereira, P., Morato, M., and Duarte-Araújo, M. (2022). Histomorphometry changes and decreased reactivity to angiotensin II in the ileum and Colon of Streptozotocin-induced diabetic rats. *Int. J. Mol. Sci.* 23, 13233–13250. doi: 10.3390/ijms232113233

Fang, Z., Zhao, J., Shi, G., Shu, Y., Ni, Y., Wang, H., et al. (2014). Shenzhu Tiaopi granule combined with lifestyle intervention therapy for impaired glucose tolerance: a randomized controlled trial. *Complement. Ther. Med.* 22, 842–850. doi: 10.1016/j.ctim.2014.08.004

Feng, Y., Zhu, J., Wang, Q., Cao, H., He, F., Guan, Y., et al. (2022). White common bean extract remodels the gut microbiota and ameliorates type 2 diabetes and its complications: a randomized double-blinded placebo-controlled trial. *Front. Endocrinol.* 13:999715. doi: 10.3389/fendo.2022.999715

Fogelson, K. A., Dorrestein, P. C., Zarrinpar, A., and Knight, R. (2023). The gut microbial bile acid modulation and its relevance to digestive health and diseases. *Gastroenterology* 164, 1069–1085. doi: 10.1053/j.gastro.2023.02.022

Forlano, R., Martinez-Gili, L., Takis, P., Miguens-Blanco, J., Liu, T., Triantafyllou, E., et al. (2024). Disruption of gut barrier integrity and host-microbiome interactions underlie MASLD severity in patients with type-2 diabetes mellitus. *Gut Microbes* 16, 2304157–2304172. doi: 10.1080/19490976.2024.2304157

Fujihara, K., Khin, L., Murai, K., Yamazaki, Y., Tsuruoka, K., Yagyuda, N., et al. (2023). Incidence and predictors of remission and relapse of type 2 diabetes mellitus in Japan: analysis of a nationwide patient registry (JDDM73). *Diabetes Obes. Metab.* 25, 2227–2235. doi: 10.1111/dom.15100

Fujiwara, T., Funatsu, T., and Tsunoda, M. (2021). Fast analysis using pillar array columns: quantification of branched-chain α-keto acids in human plasma samples. *J. Pharm. Biomed. Anal.* 198, 114019–114023. doi: 10.1016/j.jpba.2021.114019

Ge, T., Yang, J., Zhou, S., Wang, Y., Li, Y., and Tong, X. (2020). The role of the pentose phosphate pathway in diabetes and cancer. *Front. Endocrinol.* 11, 365–375. doi: 10.3389/fendo.2020.00365

González-Mariscal, L., Quirós, M., and Díaz-Coránguez, M. (2011). ZO proteins and redox-dependent processes. *Antioxid. Redox Signal.* 15, 1235–1253. doi: 10.1089/ars.2011.3913

Gu, L., Ding, X., Wang, Y., Gu, M., Zhang, J., Yan, S., et al. (2019). Spexin alleviates insulin resistance and inhibits hepatic gluconeogenesis via the FoxO1/PGC-1α pathway in high-fat-diet-induced rats and insulin resistant cells. *Int. J. Biol. Sci.* 15, 2815–2829. doi: 10.7150/ijbs.31781

Guasch-Ferré, M., Santos, J. L., Martínez-González, M. A., Clish, C. B., Razquin, C., Wang, D., et al. (2020). Glycolysis/gluconeogenesis-and tricarboxylic acid cycle-related metabolites, Mediterranean diet, and type 2 diabetes. *Am. J. Clin. Nutr.* 111, 835–844. doi: 10.1093/ajcn/nqaa016

Haddad, F., Dokmak, G., Bader, M., and Karaman, R. (2023). A comprehensive review on weight loss associated with anti-diabetic medications. *Life* 13, 1012–1038. doi: 10.3390/life13041012

Haeusler, R. A., Astiarraga, B., Camastra, S., Accili, D., and Ferrannini, E. (2013). Human insulin resistance is associated with increased plasma levels of 12α-hydroxylated bile acids. *Diabetes* 62, 4184–4191. doi: 10.2337/db13-0639

Handzlik, M. K., Gengatharan, J. M., Frizzi, K. E., McGregor, G. H., Martino, C., Rahman, G., et al. (2023). Insulin-regulated serine and lipid metabolism drive peripheral neuropathy. *Nature* 614, 118–124. doi: 10.1038/s41586-022-05637-6

Hartemann-Heurtier, A., and Senneville, E. (2008). Diabetic foot osteomyelitis. *Diabetes Metab.* 34, 87–95. doi: 10.1016/j.diabet.2007.09.005

Hernández-Montoliu, L., Rodríguez-Peña, M. M., Puig, R., Astiarraga, B., Guerrero-Pérez, F., Virgili, N., et al. (2023). A specific gut microbiota signature is associated with an enhanced GLP-1 and GLP-2 secretion and improved metabolic control in patients with type 2 diabetes after metabolic roux-en-Y gastric bypass. *Front. Endocrinol.* 14:1181744. doi: 10.3389/fendo.2023.1181744

Hou, Y., Zhai, X., Wang, X., Wu, Y., Wang, H., Qin, Y., et al. (2023). Research progress on the relationship between bile acid metabolism and type 2 diabetes mellitus. *Diabetol. Metab. Syndr.* 15, 235–253. doi: 10.1186/s13098-023-01207-6

Hu, L., Zhang, Q., Bai, Y., Hu, G., and Li, J. (2022). Triglyceride-glucose index correlate with telomere length in healthy adults from the National Health and nutrition examination survey. *Front. Endocrinol.* 13, 844073–844082. doi: 10.3389/fendo.2022.844073

Jamrozik, D., Borymska, W., and Kaczmarczyk-Żebrowska, I. (2022). *Hibiscus sabdariffa* in diabetes prevention and treatment-does it work? An evidence-based review. *Foods* 11, 2134–2165. doi: 10.3390/foods11142134

Jia, W., Xie, G. X., and Jia, W. P. (2018). Bile acid–microbiota crosstalk in gastrointestinal inflammation and carcinogenesis. *Nat. Rev. Gastroenterol. Hepatol.* 15, 111–128. doi: 10.1038/nrgastro.2017.119

Kobayashi, S. (2018). Pharmacological mechanisms of boiogito and bofutsushosan in diabetes and obesity models. *Yakugaku Zasshi* 138, 389–403. doi: 10.1248/yakushi.17-00168

Laffel, L. M., Danne, T., Klingensmith, G. J., Tamborlane, W. V., Willi, S., Zeitler, P., et al. (2023). Efficacy and safety of the SGLT2 inhibitor empagliflozin versus placebo and the DPP-4 inhibitor linagliptin versus placebo in young people with type 2 diabetes (DINAMO): a multicentre, randomised, double-blind, parallel group, phase 3 trial. *Lancet Diabetes Endocrinol.* 11, 169–181. doi: 10.1016/S2213-8587(22)00387-4

Li, C., Leng, Q., Li, L., Hu, F., Xu, Y., Gong, S., et al. (2023). Berberine ameliorates obesity by inducing GDF15 secretion by Brown adipocytes. *Endocrinology* 164, 35–60. doi: 10.1210/endocr/bqad035

Li, X., Li, Q., Wu, L., and Wang, Y. (2023). Nebivolol alleviates vascular endothelial insulin resistance by inhibiting endoplasmic reticulum stress. *Int. Heart J.* 64, 283–293. doi: 10.1536/ihj.22-484

Li, J., Yin, Y., Zhang, E., Gui, M., Chen, L., and Li, J. (2023). Peptide deregulated in hypertrophic scar-1 alleviates hypertrophic scar fibrosis by targeting focal adhesion kinase and pyruvate kinase M2 and remodeling the metabolic landscape. *Int. J. Biol. Macromol.* 235, 123809–123821. doi: 10.1016/j.ijbiomac.2023.123809

Liu, X., Yu, J., Zhao, J., Guo, J., Zhang, M., and Liu, L. (2020). Glucose challenge metabolomics implicates the change of organic acid profiles in hyperlipidemic subjects. *Biomed. Chromatogr.* 34, e4815–e4823. doi: 10.1002/bmc.4815

Mikov, M., Fawcett, J. P., Kuhajda, K., and Kevresan, S. (2006). Pharmacology of bile acids and their derivatives: absorption promoters and therapeutic agents. *Eur. J. Drug Metab. Pharmacokinet.* 31, 237–251. doi: 10.1007/BF03190714

Naseri, A., Sanaie, S., Hamzehzadeh, S., Seyedi-Sahebari, S., Hosseini, M. S., Gholipour-Khalili, E., et al. (2023). Metformin: new applications for an old drug. *J. Basic Clin. Physiol. Pharmacol.* 34, 151–160. doi: 10.1515/jbcpp-2022-0252

Peng, Y., Zhang, L., Mok, C. K. P., Ching, J. Y. L., Zhao, S., Wong, M. K. L., et al. (2023). Baseline gut microbiota and metabolome predict durable immunogenicity to SARS-CoV-2 vaccines. *Signal Transduct. Target. Ther.* 8, 373–383. doi: 10.1038/s41392-023-01629-8

Pereira, J. N. B., Murata, G. M., Sato, F. T., Marosti, A. R., Carvalho, C. R. O., and Curi, R. (2021). Small intestine remodeling in male Goto-Kakizaki rats. *Physiol. Rep.* 9, 14755–14770. doi: 10.14814/phy2.14755

Ran, Z., Ju, B., Cao, L., Hou, Q., Wen, L., Geng, R., et al. (2023). Microbiome-metabolomics analysis reveals the potential effect of verbascoside in alleviating cognitive impairment in db/db mice. *Food Funct.* 14, 3488–3508. doi: 10.1039/D2FO03110H

Ridlon, J. M., Kang, D. J., and Hylemon, P. B. (2006). Bile salt biotransformations by human intestinal bacteria. *J. Lipid Res.* 47, 241–259. doi: 10.1194/jlr.R500013-JLR200

Rindone, G. M., Dasso, M. E., Centola, C. L., Sobarzo, C. M., Galardo, M. N., Meroni, S. B., et al. (2024). Effect of metformin on Sertoli cell fatty acid metabolism and blood-testis barrier formation. *Biology* 13:330. doi: 10.3390/biology13050330

Sato, J., Kanazawa, A., and Watada, H. (2017). Type 2 diabetes and bacteremia. *Ann. Nutr. Metab.* 71, 17–22. doi: 10.1159/000479919

Shi, L., Jin, L., and Huang, W. (2023). Bile acids, intestinal barrier dysfunction, and related diseases. *Cells* 12, 1888–1903. doi: 10.3390/cells12141888

Skoug, C., Erdogan, H., Vanherle, L., Vieira, J. P. P., Matthes, F., Eliasson, L., et al. (2024). Density of Sphingosine-1-phosphate receptors is altered in cortical nerve-terminals of insulin-resistant Goto-Kakizaki rats and diet-induced obese mice. *Neurochem. Res.* 49, 338–347. doi: 10.1007/s11064-023-04033-4

Song, Q., Cheng, S. W., Zou, J., Li, K. S. L., Cheng, H., Wai Lau, D. T., et al. (2024). Role of gut microbiota on regulation potential of Dendrobium officinale Kimura & Migo in metabolic syndrome: in-vitro fermentation screening and in-vivo verification in db/db mice. *J. Ethnopharmacol.* 321:117437. doi: 10.1016/j.jep.2023.117437

Sudar-Milovanovic, E., Gluvic, Z., Obradovic, M., Zaric, B., and Isenovic, E. R. (2022). Tryptophan metabolism in atherosclerosis and diabetes. *Curr. Med. Chem.* 29, 99–113. doi: 10.2174/0929867328666210714153649

Sun, Y., Zhu, M., Zhao, H., Ni, X., Chang, R., Su, J., et al. (2020). Serum fibroblast growth factor 19 and Total bile acid concentrations are potential biomarkers of hepatocellular carcinoma in patients with type 2 diabetes mellitus. *Biomed. Res. Int.* 2020, 1–9. doi: 10.1155/2020/1751989

Swann, J. R., Want, E. J., Geier, F. M., Spagou, K., Wilson, I. D., Sidaway, J. E., et al. (2011). Systemic gut microbial modulation of bile acid metabolism in host tissue compartments. *Proc. Natl. Acad. Sci. USA* 108, 4523–4530. doi: 10.1073/pnas.1006734107

Thomas, C. R., and Lowy, C. (1992). Placental transfer and uptake of 2-deoxyglucose in control and diabetic rats. *Metabolism* 41, 1199–1203. doi: 10.1016/0026-0495(92)90009-Y

Tsai, C. Y., Lu, H. C., Chou, Y. H., Liu, P. Y., Chen, H. Y., Huang, M. C., et al. (2022). Gut microbial signatures for glycemic responses of GLP-1 receptor agonists in type 2 diabetic patients: a pilot study. *Front. Endocrinol.* 12:814770. doi: 10.3389/fendo.2021.814770

Urasaki, Y., and Le, T. T. (2022). A composition of phytonutrients for glycemic and weight management. *Nutrients* 14, 3784–3800. doi: 10.3390/nu14183784

Verhaar, B. J. H., Hendriksen, H. M. A., de Leeuw, F. A., Doorduijn, A. S., van Leeuwenstijn, M., Teunissen, C. E., et al. (2022). Gut microbiota composition is related to AD pathology. *Front. Immunol.* 12, 794519–794529. doi: 10.3389/fimmu.2021.794519

Wachal, Z., Bombicz, M., Priksz, D., Hegedűs, C., Kovács, D., Szabó, A. M., et al. (2020). Retinoprotection by BGP-15, a Hydroximic acid derivative, in a type II diabetic rat model compared to Glibenclamide, metformin, and pioglitazone. *Int. J. Mol. Sci.* 21, 2124–2142. doi: 10.3390/ijms21062124

Wang, M., Hu, T., Lin, X., Liang, H., Li, W., Zhao, S., et al. (2023). Probiotic characteristics of *Lactobacillus gasseri* TF08-1: a cholesterol-lowering bacterium, isolated from human gut. *Enzym. Microb. Technol.* 169:110276. doi: 10.1016/j.enzmictec.2023.110276

Wang, L., Wang, Z., Yu, Y., Ren, Z., Jia, Y., Wang, J., et al. (2022). Metabolomics analysis of stool in rats with type 2 diabetes mellitus after single-anastomosis duodenal-ileal bypass with sleeve gastrectomy. *Front. Endocrinol.* 13, 1013959–1013968. doi: 10.3389/fendo.2022.1013959

Wang, N., Zhu, F., Chen, L., and Chen, K. (2018). Proteomics, metabolomics and metagenomics for type 2 diabetes and its complications. *Life Sci.* 212, 194–202. doi: 10.1016/j.lfs.2018.09.035

Wu, I. W., Lee, C. C., Hsu, H. J., Sun, C. Y., Chen, Y. C., Yang, K. J., et al. (2020). Compositional and functional adaptations of intestinal microbiota and related metabolites in CKD patients receiving dietary protein restriction. *Nutrients* 12:2799. doi: 10.3390/nu12092799

Yang, C., Liu, H., Xie, Z., Yang, Q., du, L., and Xie, C. (2023). The protective role of shenqi compound in type 2 diabetes: a comprehensive investigation of pancreatic β-cell function and mass. *Biomed. Pharmacother.* 166, 115287–115301. doi: 10.1016/j.biopha.2023.115287

Yang, X., Wang, Z., Niu, J., Zhai, R., Xue, X., Wu, G., et al. (2023). Pathobionts from chemically disrupted gut microbiota induce insulin-dependent diabetes in mice. *Microbiome* 11:62. doi: 10.1186/s40168-023-01507-z

Yang, H., and Yang, L. (2016). Targeting cAMP/PKA pathway for glycemic control and type 2 diabetes therapy. *J. Mol. Endocrinol.* 57, R93–R108. doi: 10.1530/JME-15-0316

Ye, J., Meng, Q., Jin, K., Luo, Y., and Yue, T. (2024). Phage cocktail alleviated type 2 diabetes by reshaping gut microbiota and decreasing proinflammatory cytokines. *Appl. Microbiol. Biotechnol.* 108:9. doi: 10.1007/s00253-023-12912-7

Yin, Y., Fang, Z., Wu, Y., and You, L. (2021). Effect of Shenzhu Tiaopi granule on hepatic insulin resistance in diabetic Goto-Kakizakirats via liver kinase B1/adenosine 5′-monophosphate/mammalian target of rapamycin signaling pathway. *J. Tradit. Chin. Med.* 41, 107–116. doi: 10.19852/j.cnki.jtcm.2021.01.013

Yin, W., Zhang, S. Q., Pang, W. L., Chen, X. J., Wen, J., Hou, J., et al. (2022). Tang-ping-san decoction remodel intestinal Flora and Barrier to ameliorate type 2 diabetes mellitus in rodent model. *Diabetes Metab. Syndr. Obes.* 15, 2563–2581. doi: 10.2147/DMSO.S375572

Zhang, Y., Gu, Y., Ren, H., Wang, S., Zhong, H., Zhao, X., et al. (2020). Gut microbiome-related effects of berberine and probiotics on type 2 diabetes (the PREMOTE study). *Nat. Commun.* 11, 5015–5026. doi: 10.1038/s41467-020-18414-8

Zhang, Y., Guo, M. Z., Zhao, J. D., Fang, Z. H.. (2023). Analysis of theory and clinical application of treating type 2 diabetes from spleen. *J. Shanxi Univ. Chin. Med.* 24, 1244–1248. doi: 10.19763/j.cnki.2096-7403.2023.11.12

Zhang, H. Y., Tian, J. X., Lian, F. M., Li, M., Liu, W. K., Zhen, Z., et al. (2021). Therapeutic mechanisms of traditional Chinese medicine to improve metabolic diseases via the gut microbiota. *Biomed. Pharmacother.* 133, 110857–110867. doi: 10.1016/j.biopha.2020.110857

Zhang, Y., Wu, X., Xu, M., Yue, T., Ling, P., Fang, T., et al. (2022). Comparative proteomic analysis of liver tissues and serum in db/db mice. *Int. J. Mol. Sci.* 23, 9687–9712. doi: 10.3390/ijms23179687

Zhu, F., Ju, Y., Wang, W., Wang, Q., Guo, R., Ma, Q., et al. (2020). Metagenome-wide association of gut microbiome features for schizophrenia. *Nat. Commun.* 11, 1612–1621. doi: 10.1038/s41467-020-15457-9

Frontiers in Microbiology

Explores the habitable world and the potential of microbial life

The largest and most cited microbiology journal which advances our understanding of the role microbes play in addressing global challenges such as healthcare, food security, and climate change.

Discover the latest Research Topics

See more →

Frontiers

Avenue du Tribunal-Fédéral 34
1005 Lausanne, Switzerland
frontiersin.org

Contact us

+41 (0)21 510 17 00
frontiersin.org/about/contact